Zoosystematics and Evolution

100 (**1**) 2024

PENSOFT

MUSEUM FÜR NATURKUNDE BERLIN

Zoosystematics and Evolution
A Bulletin of Zoology since 1898

Zoosystematics and Evolution

2024. Volume 100. 1 Issue

ISSN: 1435-1935 (print), 1860-0743 (online)
Abbreviated keys title: Zoosyst. Evol.

In Focus

The cover picture shows adult male habitus of *Amphithrax verrucosus* (H. Milne Edwards, 1832) from Barbados. Photo: Nadeshinie Parasram.

See paper of **Parasram N, Santana W, Vallès Y, Windsor AM, Vallès H:** Morphological and molecular support for *Amphithrax verrucosus* (H. Milne Edwards, 1832) and *Amphithrax aculeatus* (Herbst, 1790) (Crustacea, Decapoda, Brachyura) as valid species

Cover design
Pensoft

Publisher

PENSOFT

Zoosystematics and Evolution
A Bulletin of Zoology since 1898

Content of volume **100** (**1**) 2024

Abstract & Indexing Information

Biological Abstracts® (Thompson ISI)
BIOSIS Previews® (Thompson ISI)
Cambridge Scientific Abstracts (CSA/CIG)
Web of Science® (Thompson ISI)
Zoological Record™ (Thompson ISI)

Zoosystematics and Evolution
A Bulletin of Zoology since 1898

Content of volume **100** (**1**) 2024

Zoosyst. Evol. 100 (1) 2024, 1–8 | DOI 10.3897/zse.100.110020

PENSOFT

für Natur MUSEUM FÜR NATURKUNDE BERLIN

A new species of *Ditha* (Pseudoscorpiones, Chthoniidae, Tridenchthoniinae) from the Western Ghats of India, with an identification key for the genus

Kyung-Hoon Jeong[1,2], Danilo Harms[3,4,5], Jithin Johnson[3,6,7]

1 *Seoul National University, 1, Gwanak-ro, Gwanak-gu, Seoul, 08826, Republic of Korea*
2 *National Institute of Biological Resources, Species Diversity Research Division, Environmental Research Complex, Hwangyeong-ro 42, Seo-gu, Incheon, 22689, Republic of Korea*
3 *Museum of Nature Hamburg – Zoology, Leibniz Institute for the Analysis of Biodiversity Change, Martin-Luther-King-Platz 3, Hamburg, 20146, Germany*
4 *Harry Butler Institute, Murdoch University, Murdoch, Western Australia; Australian Museum Research Institute, Australian Museum, Sydney, Australia*
5 *SARChI Chair on Biodiversity Value and Change, Centre for Invasion Biology, University of Venda, Thohoyandou, South Africa*
6 *Sacred Heart College (Autonomous), Thevara, Kerala, 682013, India*
7 *St. Joseph's College (Autonomous), Irinjalakuda, Kerala, 680121, India*

https://zoobank.org/EF0354EC-674D-43F9-B70A-BCB90318DF3C

Corresponding author: Kyung-Hoon Jeong (ds16203@snu.ac.kr)

Academic editor: Pavel Stoev ♦ **Received** 25 July 2023 ♦ **Accepted** 7 September 2023 ♦ **Published** 26 January 2024

Abstract

A new species of the pseudoscorpion genus *Ditha* Chamberlin, 1929, is described from Kerala State, India. A detailed morphological description, diagnostic features, and illustrations of *Ditha* (*Paraditha*) *shivanparaensis* Jeong, Harms & Johnson, **sp. nov.** are provided. The current distribution of all the known *Ditha* species is mapped, and an identification key for the genus is provided.

Key Words

Arachnida, Kerala, montane, morphology, taxonomy

Introduction

Tropical montane cloud forests or 'sholas' of the Western Ghats of India encompass unique ecosystems characterized by their high elevations (>1000 m) and isolated nature. These sholas are considered as isolated 'islands' that are surrounded by the vast ocean of low-altitude forests or grasslands (Robin et al. 2015). The biota of these so-called 'sky islands' provide excellent templates for studying endemism and investigating the factors driving diversification and adaptation in such specialized environments. Pseudoscorpions (order Pseudoscorpiones de Geer, 1778) are one such group of arachnids found in these ecosystems. Globally, ca. 4000 nominal species are described in 25 families, with India hosting ca. 160 described species (WPC 2023). Due to their specific microhabitat preferences and poor dispersal abilities, most leaf-litter dwelling species, particularly those belonging to the family Chthoniidae Daday, 1889, exhibit short-range distributions (Cosgrove et al. 2016; Johnson et al. 2022; Hlebec et al. 2023).

Tridenchthoniinae Balzan, 1892 is a chthoniid subfamily with 71 extant species in 15 genera and one extinct species (*Chelignathus kochii* Menge, 1854). Until recently, it was regarded as a distinct family within the Chthonioidea superfamily (Benavides et al. 2019). It differs from other chthoniid subfamilies in the presence of granulate carapace, spines on both coxa I and II, trichobothria *ib* and *isb* located basally or sub-basally on the chelal hand, and a galea with mul-

tiple ramifications in the juvenile stage (Morikawa 1960; Kennedy 1989). Tridenchthoniinae is divided into two tribes, Tridenchthoniini and Verrucadithini, and they can be distinguished by the shape of the marginal chelal teeth, being relatively acute and distinctly spaced in Verrucadithini, while they are closely contiguous in Tridenchthoniini (Chamberlin and Chamberlin 1945). Tridenchthoniini comprises nine genera; among these, the genus *Ditha* Chamberlin, 1929 is distributed from East Asia to Africa. It includes two subgenera, *Ditha* (*Ditha*) and *Ditha* (*Paraditha*) Beier, 1931, with seven species recorded in each subgenus. The subgenus *Paraditha* comprises seven species: *D. laosana* Beier, 1951, *D. pahangica* Beier, 1955, *D. sumatraensis* (Chamberlin, 1923) and *D. tonkinensis* (Beier, 1951) distributed in Southeast Asia; *D. latimana* (Beier, 1931) and *D. sinuata* (Tullgren, 1901) from Africa; and *D. marcusensis* (Morikawa, 1952) from East Asia (Fig. 1).

Hitherto, only two species of Tridenchthoniinae belonging to the genus *Compsaditha* Chamberlin, 1929 have been reported from India: *Compsaditha indica* Murthy, 1960, and *C. camponota* Sivaraman, 1980. Here, we present the first record of the genus *Ditha* (*Paraditha*) from India and describe a new species from the Southern Western Ghats (Kerala state) of India along with an identification key for the genus *Ditha*.

Materials and methods

The specimens used for this study are lodged in the following institutions: Museum of Nature, Hamburg – Zoology (**ZMH**, formerly Zoological Museum Hamburg) and the Arachnology Division of Sacred Heart College, Thevara, India (**ADSH**). All specimens were initially preserved in 100% ethanol, with DNA extracted from the legs of one paratype female, while the other specimens are stored in 75% ethanol.

All specimens were examined using a Leica M125C stereomicroscope in 75% ethanol. Images were captured using a BK Plus Lab System (Dun, Inc.) equipped with a Canon EOS 7D Mark II camera fitted with a microscopic lens (5X, 10X magnification) using the software CAPTURE ONE PRO 9.3 64 Bit (v.9.3.0.85) and stacked using Zerene Stacker, and a Leica DMC4500 digital camera attached to a Leica M205A stereomicroscope, using the program, LEICA APPLICATION SUITE X (LASX), ver. 3.0.1. LASX was also used for taking the measurements. Mensuration and terminology largely follow Chamberlin (1931), with some minor modifications to the terminology of the trichobothria (Harvey 1992), chelicera (Judson 2007), and appendages (Harvey et al. 2012). Scanning electron micrographs were obtained with a Hitachi TM4000Plus scanning electron micrograph (SEM) system. Illustrations were created using ADOBE ILLUSTRATOR 2023 and edited with ADOBE PHOTOSHOP 2023. The distribution map was made using QGIS 3.22.10. Abbreviations used for chelal trichobothria: ***b*** – basal, ***sb*** – subbasal, ***st*** – subterminal, ***t*** – terminal, ***ib*** – internal basal, ***isb*** – internal subbasal, ***eb*** – external basal, ***esb*** – external subbasal, ***it*** – internal terminal, ***ist*** – internal subterminal, ***et*** – external terminal, ***est*** – external subterminal, ***xs*** – duplex trichobothria; leg segments: ***tr*** – trochanter, ***fe*** – femur, ***pa*** – patella, ***ti*** – tibia, ***mt*** – metatarsus, ***ta*** – tarsus; cheliceral seta: **as** – accessory setae.

Taxonomy

Family Chthoniidae Daday, 1889

Subfamily Tridenchthoniinae (Balzan, 1892)

Remarks. Balzan (1892) proposed the family Tridenchthoniidae to include the species *Tridenchthonius parvulus* Balzan, 1887 from Paraguay which possessed triple galea in the chelicera. However, Hansen (1894) considered this species to be an unusual *Chthonius* and reduced the taxon to the subfamily Tridenchthoniinae. Since then, the taxonomic status of the group has undergone several changes. Chamberlin (1929) in his revised classification scheme for pseudoscorpions, proposed a new subfamily Dithinae Chamberlin, 1929 to include the new genus *Ditha* Chamberlin, 1929. Dithinae chthoniids closely resemble Tridenchthoniinae, except that they include non-galeate forms, but they differ from members of Chthoniinae proper in the characters such as the presence of coxal spines (of single simple type) on coxa I and II and the patella of leg IV being distinctly longer in relation to the femur. Chamberlin (1931) later raised this group to the family status. However, without providing proper justification, Beier (1932) reduced the family to the subfamily status and later to Dithiidae again. However, recognizing Balzan's species *T. parvulus* as a Dithiidae member, Chamberlin and Chamberlin (1945) proposed the family Dithiidae as a junior synonym of Tridenchthoniidae. Finally, in a recent study on pseudoscorpion transcriptomics (Benavides et al. 2019), the group was again reduced to a subfamily within Chthoniidae that now includes Tridenchthoniinae as a subfamily, alongside the Chthoniinae and Lechytiinae.

Genus *Ditha* Chamberlin, 1929

Type species. *Ditha elegans* Chamberlin, 1929.

Diagnosis. The genus *Ditha* can be diagnosed by the following combination of characters: tergites with biseriate setae; carapace with more than 50 setae; trichobothria *st* and *t* more than one areolar diameter apart, and triple galea in the juvenile stage. *Ditha* is divided into two subgenera, *Ditha* (*Ditha*) and *Ditha* (*Paraditha*). The subgenera *Paraditha* and *Ditha* can be differentiated based on the intercoxal tubercle and the number of accessory setae on the cheliceral palm (Beier, 1955). In *Ditha*, the intercoxal tubercle is strongly distinct and 10–12 accessory setae are present on the cheliceral palm, while the intercoxal tubercle is indistinct or even absent in *Paraditha* and only 1–2 accessory seta present on the cheliceral palm.

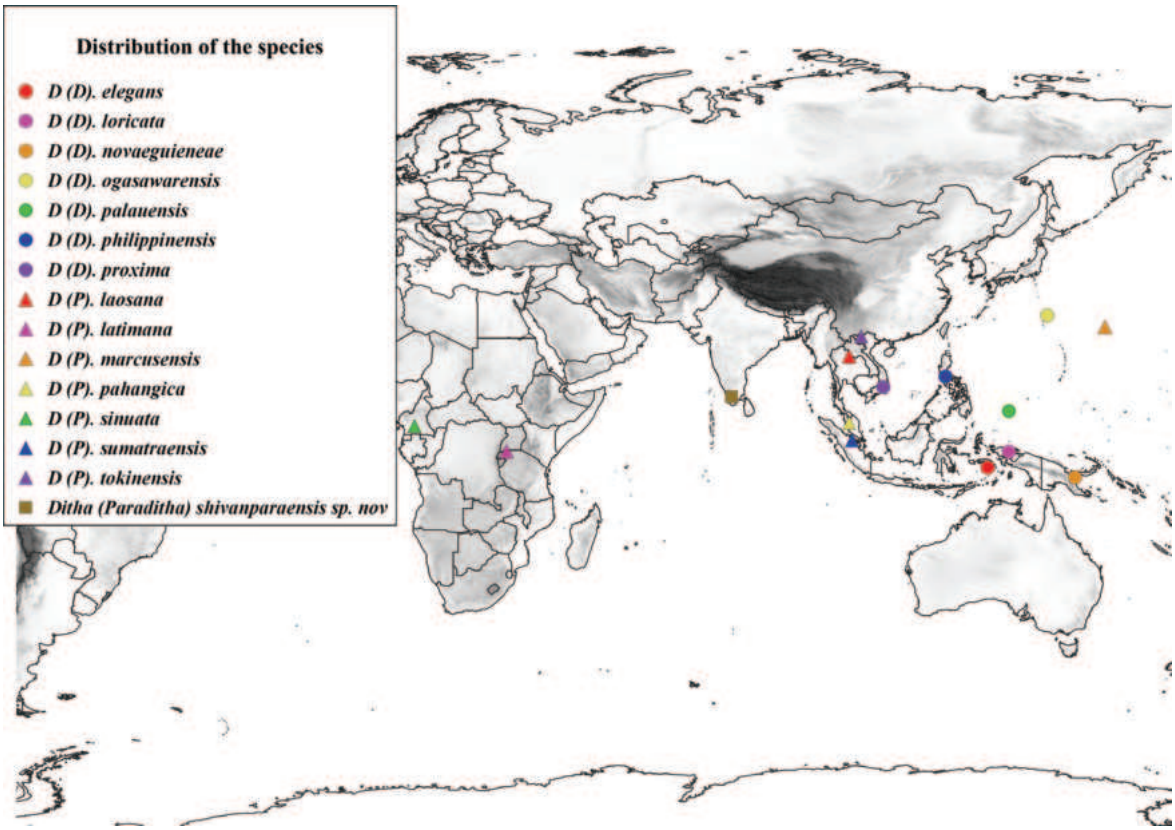

Figure 1. Distribution of the *Ditha* (*Ditha*) and *Ditha* (*Paraditha*) species.

***Ditha* (*Paraditha*) *shivanparaensis* sp. nov.**

https://zoobank.org/879135E3-C951-4A67-9FF8-4233D198E34B

Figs 1–4

Type material. ***Holotype*** (Fig. 2A, B). Female (ADSH PST0001. INDIA: Kerala: Shivanpara, Mathiketan Shola National Park, Kerala, Idukki, 9°58'05.1"N, 77°13'43.5"E, altitude 1072 m, litter sample (sifting and Berlese trap), J. Johnson leg.

Paratypes (Fig. 2C, D): 3 females (ADSH PST0003, ADSH PST0004, ZMH-A0013527) and one male (ADSH PST0002), same data as holotype.

Etymology. This species is named after the hill 'Shivanpara' in the Mathiketan Shola National Park, where all specimens were collected.

Diagnosis. Within the subgenus *Paraditha*, *Ditha shivanparaensis* sp. nov. closely resembles *D. tonkinensis* Beier, 1951 found in Vietnam in having an indistinct intercoxal tubercle between coxa III and IV, and presence of eight setae on the posterior margin of the carapace. However, the new species differs from *D. tonkinensis* and from all other species within the subgenus in having two accessory setae on the cheliceral palm. *Ditha shivanparaensis* sp. nov. also bears similarity to *Ditha* (*Ditha*) *proxima* (Beier, 1951) from Vietnam in terms of having two accessory setae on the cheliceral palm and 45–47 marginal teeth on the movable chelal finger. However, it differs from the latter in possessing 14 setae on the anterior margin of the carapace (as opposed to 10 setae in *D. proxima*) and by the positioning of *st*, i.e., halfway between *sb* and *t* (whereas *st* is much closer to *sb* in *D. proxima*).

Description. Female, adult (holotype, Fig. 2A, B).

Colour. Uniformly orange-brownish, the legs lighter than the body.

Chelicera (Figs 3F, H, 4D, E). Cheliceral palm coarsely granulate and with seven setae (including two accessory setae), movable finger with one seta in medial position and seven marginal teeth, inner margin granulate; fixed finger with seven marginal teeth, the terminal one larger than the others (Fig. 3H); with two dorsal lyrifissures; rallum with ten blades (Figs 3F, 4E); serrula exterior with 16 blades of similar size.

Pedipalp (Figs 3G, 4B, C). Trochanter 1.44 times, femur 3.54 times, patella 1.83 times, chela (with pedicel) 3.79 times, hand 1.51 times longer than broad, movable finger 1.54 times longer than hand. Femur, patella, chela smooth. Fixed chelal finger with six trichobothria, movable finger with four trichobothria, *ib* and *isb* situated basally on the dorsum of the chelal hand; *sb*, *st*, and *t* located separately from *b*; *sb*, *st* and *t* all spaced more than one areolar distance; *st* slightly closer to *sb* than *t*; *eb*, *esb* and *ist* forming a group at basal to subbasal position; *esb* slightly closer to *ist* than *eb*; *est* and *it* positioned at the median on the fixed finger; *et* closely located with *xs*, almost less than one areolar distance (Figs 3G, 4B). Four lyrifissures on the dorsum of fixed chelal finger, one on the basal dorsum of chelal hand. Both fingers with small juxtadentate teeth; fixed finger with 55 triangular and retrorse teeth; movable finger with 47 rounded teeth.

Cephalothorax (Figs 3A, D, E, 4F, G). Carapace 1.04 times longer than broad sub-rectangular; lateral margins almost parallel but slightly wide at the base; coarsely

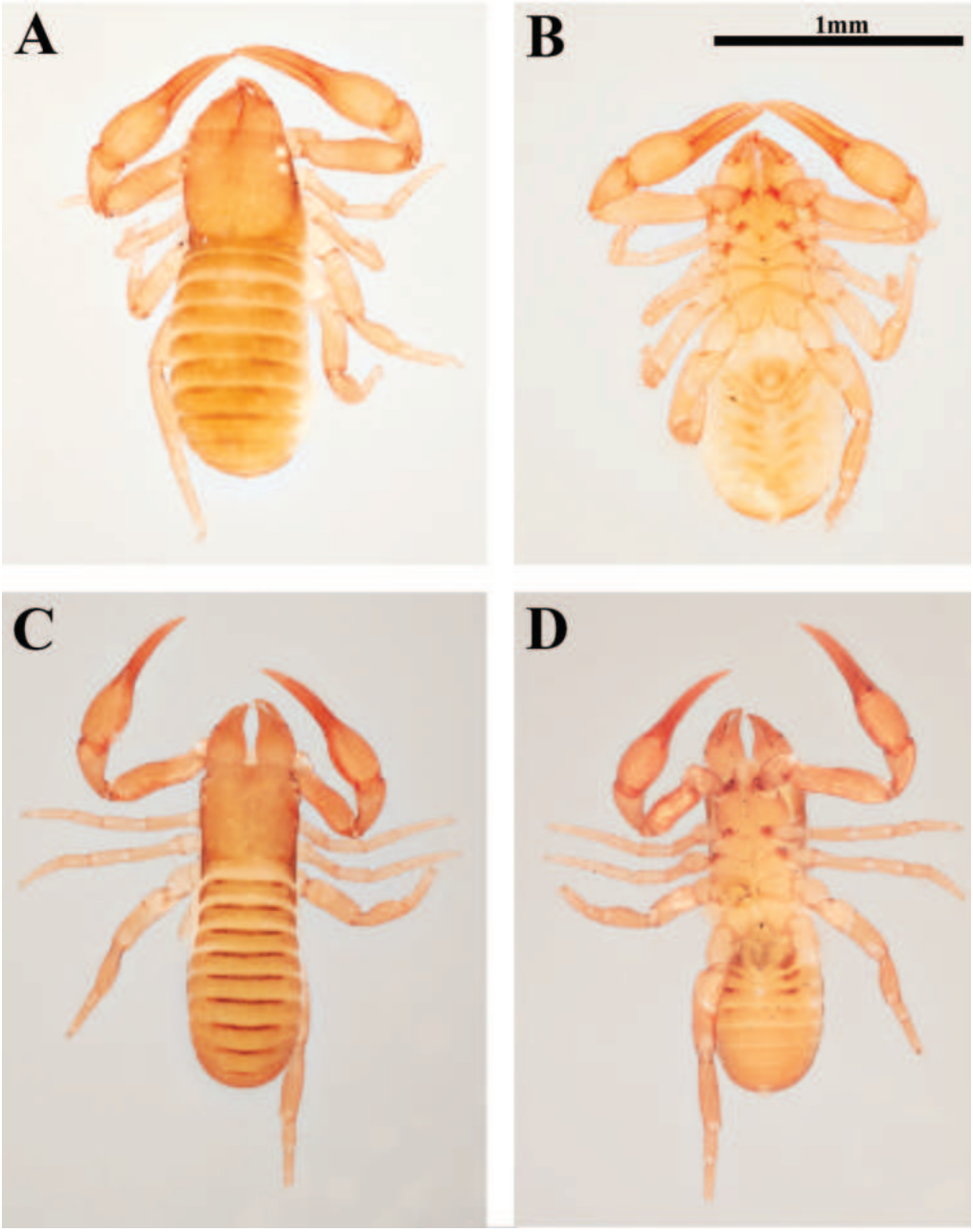

Figure 2. Habitus of *Ditha shivanparaensis* sp. nov. **A.** Female holotype, dorsal view; **B.** Female holotype, ventral view; **C.** Male paratype, dorsal view; **D.** Male paratype, ventral view. Scale bars: 1 mm.

granulate, without furrows; four corneate eyes; anterior margin serrated; epistome small and serrated; with 94 setae; 14 setae on the anterior margin, eight setae on posterior margin; setae short and acuminate; with ten lyrifissures, three each on the sides near the anterior margin, one between each eye, and one on each side situated near the posterior margin (Fig. 3A). Manducatory process with one long, acuminate setae, remainder of maxilla with ten setae; four lyrifissures on the maxilla. Coxal chaetotaxy: 10: 11: 11: 20 (Fig. 3D). Coxa I with ca. 5–6 spines, each spine serrated terminally, and ca. 2–3 spines from one base; coxa II with ca. 5–6 spines (Figs 3E, 4E, F); each spine serrated from the medial. Intercoxal tubercle indistinctly present between coxa III and IV, seta weakly present (Fig. 4F).

***Abdomen*.** Pleural membrane papillostriate, tergites undivided, but sternites III–IV partially divided; setae biseriate and acuminate. Tergal chaetotaxy, 14: 23: 23: 25: 26: 24: 24: 25: 21: 17: 13: 0. Sternal chaetotaxy, 15: 10: 8: 8: 8: 8: 8: 9: 12: 4: 2. Sternite I with 4 setae in the genital opening area.

Legs (Fig. 3B, C). Leg I: trochanter 1.18 times, femur 3.87 times, patella 2.98 times, tibia 2.56 times, tarsus 5.93 times longer than broad, leg IV: trochanter 1.48 times, femur 2.75 times, tibia 3.44 times, metatarsus 2.57 times, tarsus 7.00 times longer than broad; leg IV: trochanter 1.67 times, femur 2.39 times, tibia 3.47 times, metatarsus 2.57 times, tarsus 5.49 times longer than broad. Tarsus of leg IV longer than the metatarsus; arolium undivided and shorter than the claws; pseudotactile seta located basally on leg I patella and medially on leg IV metatarsus.

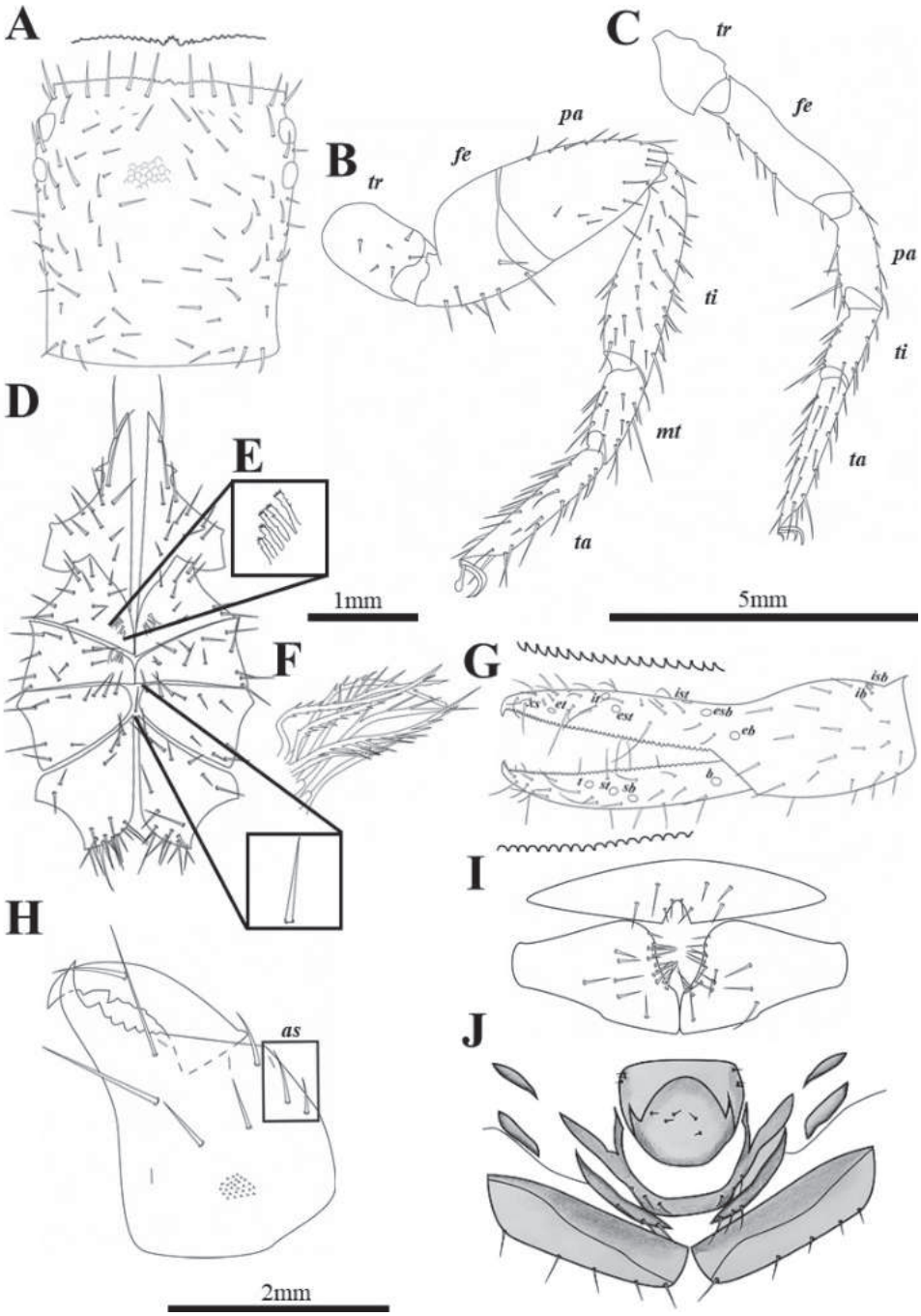

Figure 3. Drawings of *Ditha shivanparaensis* sp. nov. (all paratypes unless mentioned otherwise) **A.** Carapace, dorsal view; **B.** Leg IV; **C.** leg I; **D.** Coxa; **E.** Coxal spines; **F.** Rallum; **G.** Left chela from the lateral; **H.** Cheliceral, dorsal view, two accessory setae in the box; **I.** Male genital area external view; **J.** Female genital area external view (holotype). Scale bars: 0.5 mm (**A**–**D**, **G**); 1 mm (**E**–**F**); 2 mm (**H**–**J**).

Genitalia (Fig. 3J). Typical shape of the genus *Ditha*. 15 setae in the genital opening area, including nine setae on the center of the opening and three setae each on either side of the opening; ten setae on the sternite III; six setae on the anterior part of sternite III; four setae on the posterior region, and two setae each on the part of sternite III.

Dimensions **(in mm).** Body length 1.47; Pedipalp: trochanter 0.22/0.15, femur 0.48/0.13, patella 0.27/0.15, chela (with pedicel) 0.72/0.19, movable finger 0.45, hand 0.29/0.19; Chelicera: total 0.32/0.18, movable finger 0.17; Cephalothorax: Carapace 0.47/0.45, anterior eye 0.005, posterior eye 0.004; Leg I: trochanter 0.13/0.11, femur 0.27/0.07, patella 0.19/0.06, tibia 0.15/0.06, tarsus 0.27/0.05; Leg IV: trochanter 0.16/0.11, femur + patella 0.47/0.17, tibia 0.33/0.10, metatarsus 0.15/0.06, tarsus 0.28/0.04.

Male, adult (paratype, Fig. 2 C, D).

Same as the holotype, except slightly smaller (body length 1.291 mm).

Pedipalp**.** Trochanter 1.46 times, 3.54 times, patella 1.87 times, chela (with pedicel) 3.85 times, hand 1.47 times longer than broad, movable finger 1.56 times lon-

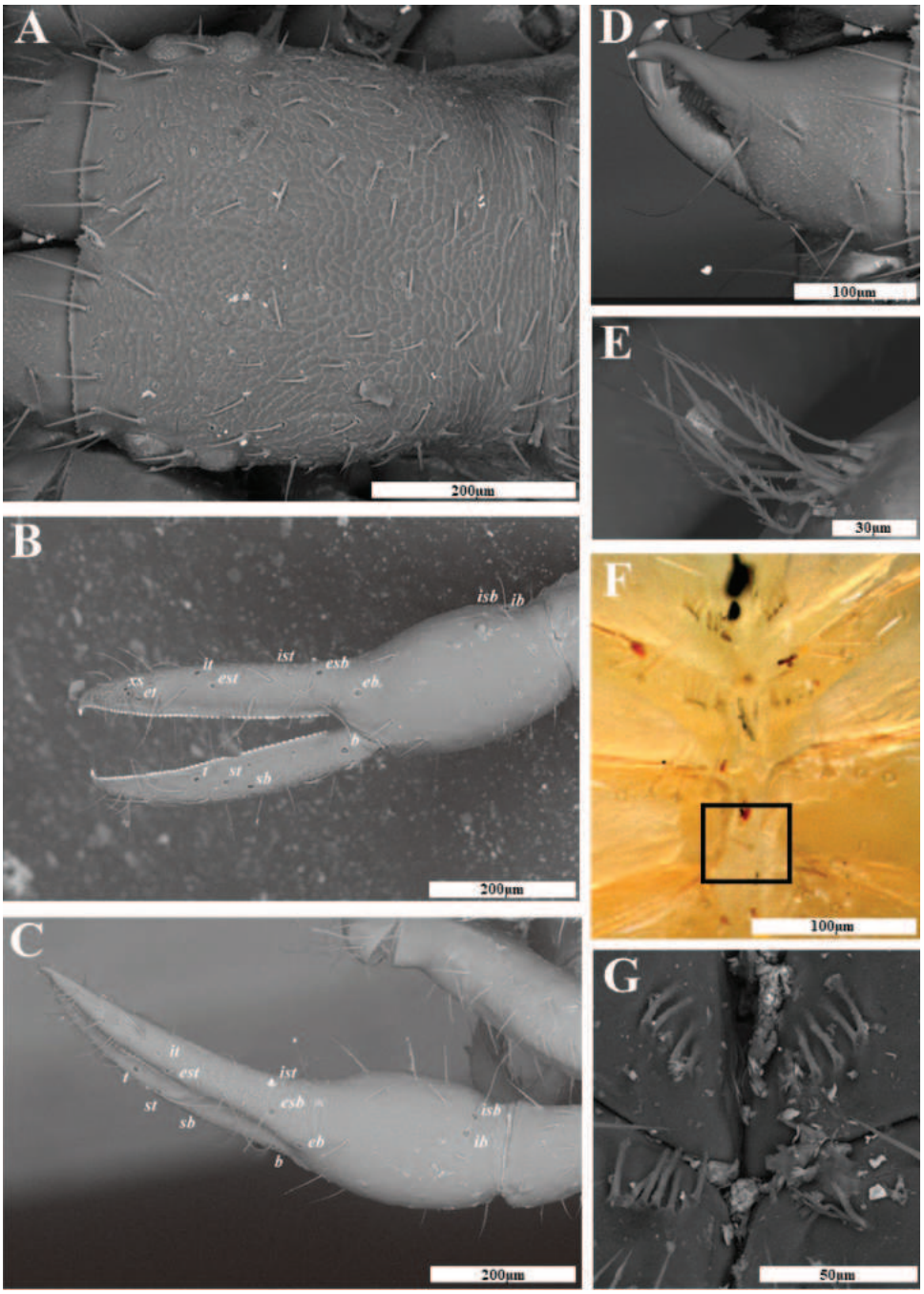

Figure 4. *Ditha shivanparaensis* sp. nov. **A.** Carapace, dorsal view; **B.** Left chela, lateral view; **C.** Left chela, dorsal view; **D.** Cheliceral, dorsal view; **E.** Rallum; **F.** Coxa (intercoxal tubercle in the circle); **G** Coxal spine. Scale bars: 200 μm (**A–C**); 100 μm (**D, F**); 30 μm (**E**); 50 μm (**G**).

ger than hand; fixed finger with 50, movable finger with 48 teeth.

Cephalothorax. Carapace 1.06 times longer than broad; with 92 setae; 14 setae on the anterior margin, eight setae on the posterior margin; Coxal chaetotaxy: 10: 11: 11: 20. Coxa I with ca. 5–6 spines.

Abdomen. Tergal chaetotaxy, 10: 14: 15: 16: 19: 19: 19: 18: 16: 15: 13: 0. Sternal chaetotaxy, 10: 36: 6: 8: 10: 8: 13: 13: 11: 5: 2. Sternite II with nine total setae including six setae near the genital opening, sternite III with 38 total setae including 22 setae near the genital opening.

Legs. Leg I: trochanter 1.33 times, femur 3.65 times, patella 2.92 times, tibia 2.58 times, tarsus 5.80 times longer than broad; leg IV: trochanter 1.67 times, femur 2.39 times, tibia 3.47 times, metatarsus 2.57 times, tarsus 5.49 times longer than broad.

Genitalia (Fig. 3I). Typical shape of the genus *Ditha*. 15 setae in the genital opening area, including nine on the center of the opening and three each on either side of the opening; ten setae on the sternite III; six setae on the anterior part of sternite III; four setae on the posterior region, and two setae each on the part of sternite III.

Dimensions (mm). Body length 1.29. Pedipalp: trochanter 0.19/0.13, femur 0.44/0.12, patella 0.24/0.13, chela (with pedicel) 0.64/0.17, movable finger 0.38, hand 0.24/0.17; Chelicera: total 0.30/0.16, movable finger 0.17; Cephalothorax: Carapace 0.42/0.39, anterior eye 0.005, posterior eye 0.004; Leg I: trochanter 0.12/0.09, femur 0.24/0.07, patella 0.16/0.06, tibia 0.39/0.09, tarsus 0.24/0.04; Leg IV: trochanter 0.18/0.11, femur + patella 0.40/0.17, tibia 0.31/0.09, metatarsus 0.14/0.05, tarsus 0.26/0.05.

Variation of female paratypes (n=2). ***Pedipalp*****.** Trochanter 1.44–1.46 times, femur 3.46–3.68 times, patella 1.85–1.98 times, chela (with pedicel) 3.65–3.74 times, hand 1.48–1.52 times longer than broad, movable finger 1.43–1.44 times longer than hand. Movable finger with 48, fixed finger with 53–54 marginal teeth.

Cephalothorax**.** Carapace 1.04 times longer than broad. 96–100 setae.

Abdomen**.** Tergal chaetotaxy, 13–14: 21–23: 22–24: 24–25: 24–25: 25: 25–26: 23–25: 18: 15–16: 14–15: 0. Sternal chaetotaxy, 10: 10: 8: 7–8: 9–11: 8–10: 8–9: 10: 11–13: 4: 2.

Legs**.** Leg I: trochanter 1.20–1.34 times, femur 3.60–3.93 times, patella 2.61–2.64 times, tibia 2.47–2.77 times, tarsus 5.88–6.08 times longer than broad, leg IV: trochanter 1.59–1.66 times, femur 2.38–2.53 times, tibia 3.40–3.55 times, metatarsus 2.17–2.29 times, tarsus 5.39–6.14 times longer than broad.

Dimensions (mm): Body length 1.33–1.41; Pedipalp: trochanter 0.21–0.22/0.15, femur 0.48–0.51/0.13–0.15, patella 0.28–0.30/0.15, chela 0.71–0.73/0.19–0.20, movable finger 0.41–0.43, hand 0.29–0.30/0.19–0.20; Chelicera: total 0.29–0.31/0.18–0.19, movable finger 0.18–0.19; Cephalothorax: carapace 0.46–0.47/0.45, anterior eye 0.005–0.006, posterior eye 0.004; Leg I: trochanter 0.12–0.13/0.10, femur 0.28/0.07–0.08, patella 0.17–0.19/0.07, tibia 0.14–0.16/0.06, tarsus 0.27/0.04–0.05; Leg IV: trochanter 0.21/0.13, femur + patella 0.43–0.44/0.17–0.18, tibia 0.35–0.37/0.10–0.11, metatarsus 0.14–0.15/0.06–0.07, tarsus 0.27–0.30/0.05.

Distribution. Currently known only from the type locality.

Habitat. The species was collected from moist leaf litter of montane ‘shola’ forests of the Mathiketan Shola National Park and is probably endemic to this mountain, although more field sampling is required to verify this.

Erratum. The sequences with GenBank accession numbers OM792092.1, OM832661.1 and OM876917.1, previously attributed to the genus *Compsaditha* by Johnson et al. (2022), actually belong to the newly discovered species described herein as *Ditha shivanparaensis* sp. nov.

Key to the species of *Ditha*

1	Intercoxal tubercle distinct; 10–12 accessory seta positioned on the cheliceral palm	2, subgenus *Ditha*
–	Intercoxal tubercle indistinct or absent; 1–2 accessory seta positioned on the cheliceral palm	9, subgenus *Paraditha*
2	Cheliceral palm with less than six accessory setae	3
–	Cheliceral palm with more than six accessory setae	4
3	Carapace with less than 100 setae	*D. proxima* (Beier, 1951) (Vietnam)
–	Carapace with more than 100 setae	*D. ogasawarensis* Sato, 1981 (Japan)
4	Carapace with less than 150 setae	5
–	Carapace with more than 150 setae	6
5	12 setae on the anterior margin of the carapace	*D. novaeguineae* Beier, 1965 (Papua New Guinea)
–	14 setae on the anterior margin of the carapace	*D. palauensis* Beier, 1957 (Palau)
6	Tergite I with 12 setae in male	7
–	Tergite I with 21 setae in male	*D. elegans* Chamberlin, 1929 (Indonesia)
7	14 setae on the anterior margin of the carapace	*D. philippinensis* Chamberlin, 1929 (Philippines)
–	16 setae on the anterior margin of the carapace	*D. loricata* Beier, 1965 (Indonesia)
8	Intercoxal tubercle absent	10
–	Intercoxal tubercle indistinct	12
9	Intercoxal tubercle absent	10
–	Intercoxal tubercle indistinct	12
10	Posterior margin of carapace with 8 setae	11
–	Posterior margin of carapace with 14 setae	*D. marcusensis* (Morikawa, 1952) (Japan)
11	Carapace more than 70 setae	*D. pahangica* Beier, 1955 (Malaysia)
–	Carapace fewer than 70 setae	*D. sumatraensis* (Chamberlin, 1923) (Indonesia)
12	Carapace with more than 100 setae	*D. laosana* Beier, 1951 (Laos)
–	Carapace with fewer than 100 setae	13
13	Carapace with more than 70 setae	14
–	Carapace with fewer than 70 setae	*D. sinuata* (Tullgren, 1901) (Cameroon)
14	Pedipalpal femur at least 4 times longer than broad	*D. latimana* (Beier, 1931) (Tanzania)
–	Pedipalpal femur at least 4 times longer than broad	15
15	Chelicera with 1 accessory setae	*D. tonkinensis* Beier, 1951 (Vietnam)
–	Chelicera with 2 accessory setae	*D. shivanparaensis* sp. nov. (India)

Acknowledgements

KHJ thanks Jung-sun Yoo (National Institute for Biological Resources, Korea) for introducing him to Danilo Harms and facilitating his research stay at the Museum of Nature, Hamburg – Zoology. KHJ also extends deep gratitude to his parents, Aekyung Lim and Hyuncheol Jeong for their wholehearted support of his research stay in Hamburg, Germany. JJ thanks the Deutscher Akademischer Austauschdienst (DAAD), Germany for funding his research stay in Germany (No. 57440919, 2019/20). The authors are also grateful to Stephanie F. Loria and Nadine Dupérré (both from Hamburg) for their help with distribution mapping and imaging, respectively, and the forest department of the Indian state of Kerala and the National Biodiversity Authority, Govt. of India (No. NBA/Tech Appl/9/Form B-92/19/19-20/676 dated 20.06.2019) for providing necessary permits for the study. Furthermore, the authors also thank the academic editor and the two reviewers, one anonymous and the other Mark Harvey, for their valuable comments and suggestions that have improved this manuscript.

References

Balzan L (1892) Voyage de M. E. Simon au Venezuela (Décembre 1887–Avril 1888). Arachnides. Chernetes (Pseudoscorpiones). Annales de la Société Entomologique de France 60: 513–552.

Beier M (1932) Pseudoscorpionidea I. Subord. Chthoniinea et Neobisiinea. Das Tierreich 57: i–xx, 1–258. https://doi.org/10.1515/9783111435107.1

Beier M (1955) Pseudoscorpionidea. In: Hanstrom B, Brinck P, Rudebeck G (Eds) South African animal life. Results of the Lund Expedition in 1950–1951. Almquist and Wiksell, Stockholm, 1263–1328.

Benavides LR, Cosgrove JG, Harvey MS, Giribet G (2019) Phylogenomic interrogation resolves the backbone of the Pseudoscorpiones Tree of Life. Molecular Phylogenetics and Evolution 139(106509): 1–14. https://doi.org/10.1016/j.ympev.2019.05.023

Chamberlin JC (1929) A synoptic classification of the false scorpions or chela spinners, with a report on a cosmopolitan collection of the same. Part 1. The Heterosphyronida (Chthoniidae) (Arachnida-Chelonetida). Annals and Magazine of Natural History 4(10): 50–80. https://doi.org/10.1080/00222932908673028

Chamberlin J (1931) The arachnid order Chelonethida. Stanford University Publications, University Series, (Biological. Sciences.) 7: 1–284.

Chamberlin JC, Chamberlin, RV (1945) The genera and species of the Tridenchthoniidae (Dithidae): A family of the arachnid order Chelonethida. Bulletin of the University of Utah, Biological Series 9: 1–67.

Cosgrove JG, Agnarsson I, Harvey MS, Binford GJ (2016) Pseudoscorpion diversity and distribution in the West Indies: Sequence data confirm single island endemism for some clades, but not others. The Journal of Arachnology 44: 257–271. https://doi.org/10.1636/R15-80.1

Hansen HJ (1894) Organs and characters in different orders of arachnids. Entomologiske Meddelelser 4: pl. 2–3.

Harvey MS (1992) The phylogeny and classification of the Pseudoscorpionida (Chelicerata: Arachnida). Invertebrate Systematics 6(6): 1373–1435. https://doi.org/10.1071/IT9921373

Harvey MS, Ratnaweera PB, Udagama PV, Wijesinghe MR (2012) A new species of the pseudoscorpion genus *Megachernes* (Pseudoscorpiones: Chernetidae) associated with a threatened Sri Lankan rainforest rodent, with a review of host associations of Megachernes. Journal of Natural History 46(41–42): 2519–2535. https://doi.org/10.1080/00222933.2012.707251

Hlebec D, Podnar M, Kučinić M, Harms D (2023) Molecular analyses of pseudoscorpions in a subterranean biodiversity hotspot reveal cryptic diversity and microendemism. Scientific Reports 13–(1): 430–444. https://doi.org/10.1038/s41598-022-26298-5

Johnson J, Loria SF, Joseph MM, Harms D (2022) Biogeographical and diversification analyses of Indian pseudoscorpions reveal the Western Ghats as museums of ancient biodiversity. Molecular Phylogenetics and Evolution 175: e107495. https://doi.org/10.1016/j.ympev.2022.107495

Judson ML (2007) A new and endangered species of the pseudoscorpion genus *Lagynochthonius* from a cave in Vietnam, with notes on chelal morphology and the composition of the Tyrannochthoniini (Arachnida, Chelonethi, Chthoniidae). Zootaxa 1627(1): 53–68. https://doi.org/10.11646/zootaxa.1627.1.4

Kennedy CMA (1989) *Pycnodithella harveyi*, a new Australian species of the Tridenchthoniidae (Pseudoscorpionida: Arachnida). Proceedings of the Linnean Society of New South Wales 110: 289–296.

Morikawa K (1960) Systematic studies of Japanese pseudoscorpions. PhD Thesis, Ehime University, Matsuyama, Japan.

Robin VV, Gupta P, Thatte P, Ramakrishnan U (2015) Islands within islands: Two montane palaeo-endemic birds impacted by recent anthropogenic fragmentation. Molecular Ecology 24(14): 3572–3584. https://doi.org/10.1111/mec.13266

WPC (2023) World Pseudoscorpiones Catalog. Natural History Museum Bern. http://wac.nmbe.ch [accessed on 20-July-2023]

Zoosyst. Evol. 100 (1) 2024, 9–14 | DOI 10.3897/zse.100.110105

PENSOFT

für Natur MUSEUM FÜR NATURKUNDE BERLIN

Pilsbrylia, a dextral-shelled door snail from South America (Gastropoda, Clausiliidae)

Rodrigo B. Salvador[1], Abraham S. H. Breure[2,3,4]

1 *The Arctic University Museum of Norway, UiT – The Arctic University of Norway, Lars Thørings veg 10, 9006, Tromsø, Norway*

2 *Royal Belgian Institute of Natural Sciences, Rue Vautier 29, 1000, Brussels, Belgium*

3 *Invertebrate Division, Department of Life Sciences, Natural History Museum, Cromwell Road, South Kensington, SW7 5BD, London, UK*

4 *Naturalis Biodiversity Center, Darwinweg 2, 2333 CR, Leiden, Netherlands*

https://zoobank.org/98538B32-8A69-40E9-85CE-1421B8C60E4E

Corresponding author: Rodrigo B. Salvador (salvador.rodrigo.b@gmail.com)

Academic editor: Frank Köhler ♦ **Received** 26 July 2023 ♦ **Accepted** 3 September 2023 ♦ **Published** 26 January 2024

Abstract

The land snail genus *Pilsbrylia* Hylton Scott, 1952 has been recently shown to not belong to the superfamily to which it was originally assigned (i.e., the Orthalicoidea), instead pointing out a relationship with the Clausilioidea. In this study, we included the type species of the genus in a multi-marker molecular phylogenetic framework to reassess its family-level classification. Our results show that *Pilsbrylia* belongs to family Clausiliidae (known as 'door snails') and more specifically, to subfamily Peruiniinae. This family is unique among stylommatophorans for consisting almost exclusively of animals with sinistral (left-handed) shells, whilst *Pilsbrylia* has a "typical" dextral shell.

Key Words

chirality, Eupulmonata, Orthalicoidea, Peruiniinae, Stylommatophora

Introduction

The South American genus *Pilsbrylia* Hylton Scott, 1952 contains three species, which inhabit areas in southern Brazil and northern Argentina (Simone 2018): *Pilsbrylia paradoxa* Hylton Scott, 1952 (the type species), *P. hyltonae* Fernández & Rumi, 1980, and *P. dalli* Simone, 2018 (Fig. 1). Members of this genus have high-spired and narrow shells and the shell aperture bears a number of teeth and lamellae. The shells are morphologically similar to the members of family Cyclodontinidae (which was formerly part of Odontostomidae; see Salvador et al. 2023 for the revised classification within superfamily Orthalicoidea), in particular to members of genera such as *Clessinia* Doering, 1875 and *Cyclodontina* H. Beck, 1837. Thus, since its description, *Pilsbrylia* has been classified in that family (e.g., Hylton Scott 1952; Breure 1974; Fernández and Rumi 1980; Schileyko 1999; Cuezzo et al. 2013; Simone 2018).

The molecular phylogenetic study of Breure and Romero (2012) showed that *Pilsbrylia* did not belong in Cyclodontinidae and those authors proposed the genus was instead the sister taxon to all other Orthalicoidea. A more recent phylogenetic study (Salvador et al. 2023), showed that *Pilsbrylia* did not belong in Orthalicoidea at all, being instead related to the Clausiliidae, or door snails. That was a surprising result, considering that the door snails typically have sinistral shells (i.e., a shell that "coils" counter-clockwise or, when seen with its aperture facing the observer and the spire top pointing upwards, a shell whose aperture is on the left-hand side).

Furthermore, the two branches of Clausiliidae present in the Americas are restricted to the Caribbean (subfamily Neniinae) and northwest South America (subfamily Peruiniinae) (Uit de Weerd and Gittenberger 2013). Thus, the genus *Pilsbrylia* is rather geographically removed from the family's range.

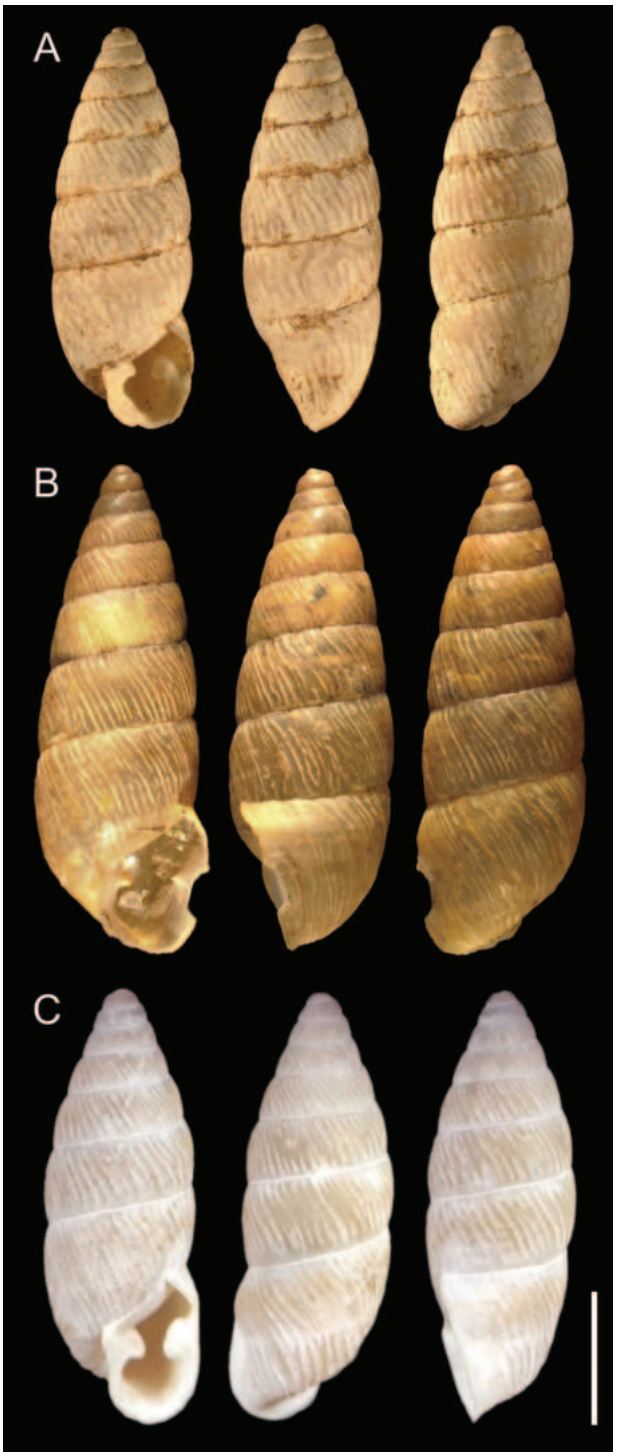

Figure 1. Shells of the three known species of *Pilsbrylia* in apertural, lateral, and dorsal views. **A.** *P. paradoxa*, holotype MLP-Ma 11337 (Museo de La Plata, Argentina); **B.** *P. hyltonae*, lectotype MLP-Ma 3991-1; **C.** *P. dalli*, holotype MZSP 133161 (Museu de Zoologia da Universidade de São Paulo, Brazil). Scale bar: 5 mm.

In the present study we include *Pilsbrylia* in a phylogenetic framework of the Clausiliidae to test if it really belongs to this family and, if so, assess how it is related to other South American door snails.

Materials and methods

DNA sequences of *Pilsbrylia paradoxa* used in previous Orthalicoidea-focused studies (Breure and Romero 2012; Salvador et al. 2023) were used for the present analysis. They are available on GenBank under accession numbers JF514745 (28S) and JF514687 (H3) and stem from a voucher specimen previously housed in the collection of the Instituto Miguel Lillo, Tucumán, Argentina (registration number IFML-MOLL BD316, collected in northern Argentina, Salta province, km 1650 of Salta-Jujuy highway) but now housed in the Instituto de Biodiversidad Neotropical (IBN) of the Universidad Nacional de Tucumán, Argentina. No further specimen of *Pilsbrylia* spp. preserved in ethanol and suitable for DNA extraction could be found in the present study.

The sequences of *P. paradoxa* were included in the phylogenetic framework for the family Clausiliidae established in the study of Uit de Weerd and Gittenberger (2013). That study included a reasonable sample of South American (subfamily Neniinae) taxa across two distinct clades (tribes), which enables us to test the phylogenetic position of *Pilsbrylia*. Later molecular phylogenetic studies with Clausiliidae focused on Eurasian taxa (e.g., Hausdorf and Neiber 2022) and data from them was not included here.

A total of 67 species of Clausiliidae, belonging to all subfamilies and almost all tribes, was part of the analysis. Five species were selected as outgroup representing the families Cerionidae, Chondrinidae, Enidae, Rhytididae, and Urocoptidae (data from Uit de Weerd 2008; Uit de Weerd and Gittenberger 2013; Saadi and Wade 2019). A complete list of the species used in the analysis, with locality data and GenBank accession numbers is given in the Suppl. material 1.

Data from three nuclear markers were used in the present phylogenetic analysis, following Uit de Weerd and Gittenberger (2013): partial 28S rRNA gene (ca. 1700 bp), partial H3 (histone 3) gene (ca. 270 bp), and partial H4 (histone 4) gene (ca. 260 bp). Information on primers and PCR protocols can be found in Uit de Weerd and Gittenberger (2013); for *Pilsbrylia*, see Breure and Romero (2012).

The genetic sequences were aligned through the MUSCLE plugin (Edgar 2004) in Geneious Prime (v.2023.0.4, Biomatters Ltd.), using default settings (i.e., optimised for accuracy). The resulting alignments were visually proofed for inconsistencies. The alignment of the 28S marker was run through Gblocks (Talavera and Castresana 2007), using the least restrictive settings, in order to eliminate poorly-aligned or data-deficient positions that could introduce noise into the analysis. The alignments were then concatenated for a single phylogenetic analysis, with each marker being treated as an individual partition.

A Bayesian inference phylogenetic analysis was performed through MrBayes (v.3.2.7; Ronquist et al. 2012) via the CIPRES Science Gateway (v.3.3; Miller et al. 2015). Two concurrent analyses, each with 4 Markov chains of 80 million generations (the first 20% discarded as 'burn-in'), were run with the default priors, nst = 6,

rates = invgamma, temperature parameter = 0.1, sampling every 1,000 generations. Substitution model parameters were unlinked across the markers (28S, H3, and H4). MCMC convergence was assessed using the standard deviation of split frequencies (<0.01) and the potential scale reduction factor PSRF (~1.0), as well as by examining the trace plots (Ronquist et al. 2009).

Results

The concatenated sequences of the three markers (after trimming the 28S marker using Gblocks) contained 2172 bp. The total-evidence tree resulting from the Bayesian analysis contained 73 species (including *Pilsbrylia paradoxa* and the outgroup) and is shown here in simplified format, with the branches of non-immediate interest collapsed (Fig. 2). The full tree can be seen in the Suppl. material 2.

All subfamilies of Clausiliidae are strongly supported (posterior probability PP=1), except for Serrulininae, which is paraphyletic (Fig. 2). As expected in a clade inflated by family-level names, many of the supposed tribes were recovered as para- or polyphyletic (e.g., Cochlodinini, Delimini; Suppl. material 2), as already noted by Uit de Weerd and Gittenberger (2013). When also considering the existence of several monotypic tribes (e.g., Garnieriini, Strumosini), the Clausiliidae would benefit from a clean-up of names on the tribe level, as many could easily be synonymized if supported by further research.

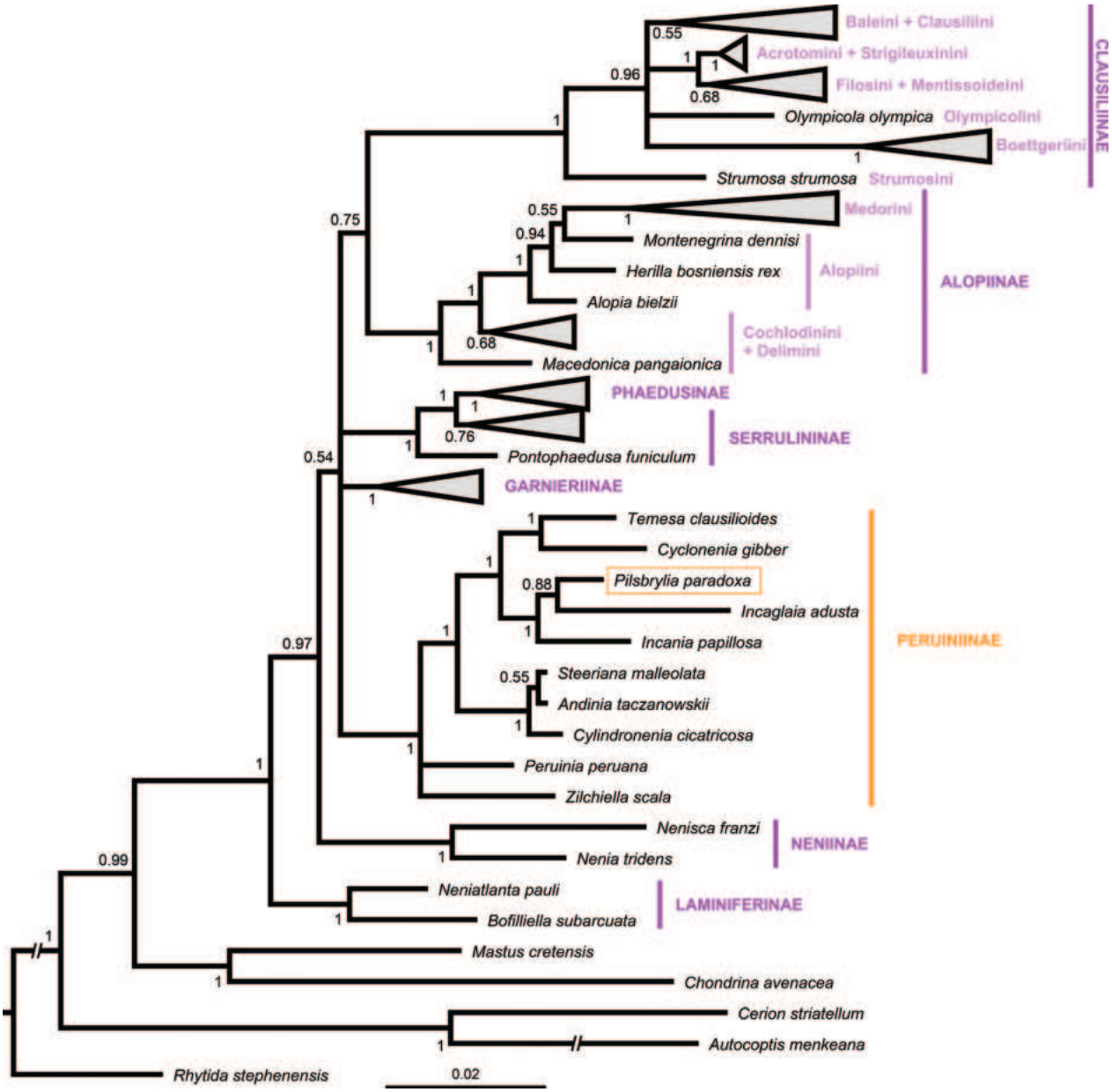

Figure 2. Bayesian inference tree of the Clausilioidea. The crown group is collapsed to facilitate visualization (see Suppl. material 2 for a full view). Posterior probabilities are shown on nodes. Scale bar is substitutions per site.

Considering that our ingroup was identical to that of Uit de Weerd and Gittenberger (2013) – barred the inclusion of *Pilsbrylia paradoxa* – our tree is largely similar to the one presented by those authors. However, a major difference can be observed: while Uit de Weerd and Gittenberger (2013) had the Neniinae as the sister group to all other clausiliids (though unsupported), our tree places the Laminiferinae in that position (Fig. 2). The Laminiferinae are sister to the remaining clausiliids (PP=0.97) and, inside the latter clade, the Neniinae are sister to all others, which are joined in an unsupported polytomy (PP=0.54). This polytomy includes three strongly supported branches (PP=1: Peruiniinae, Garnieriinae, and a clade formed by Phaedusinae and a paraphyletic Serrulininae) and an unsupported branch (PP=0.75) containing the Alopiinae and the Clausiliinae (each PP=1) as sister clades (Fig. 2).

Our taxon of interest, *Pilsbrylia paradoxa*, is included in the Peruiniinae, in a derived position (Fig. 2). It was recovered as the sister taxon to the Peruvian *Incaglaia adusta* (O. Boettger, 1880), although with low support (PP=0.88). Both species are the sister clade to *Incania papillosa* Neubert & Nordsieck, 2005 (PP=1), also from Peru. The relationships within Peruiniinae recovered by our analysis are largely the same as those in Uit de Weerd and Gittenberger (2013), with a single exception: those authors recovered *Zilchiella scala* Neubert & Nordsieck, 2005 and *Peruinia peruana* (Troschel, 1847) as sister taxa (although unsupported), while in the present tree they form a trichotomy with the remaining Peruiniinae (Fig. 2).

Discussion

The results of the present phylogenetic analysis allow the conclusion that *Pilsbrylia* in fact belongs in the family Clausiliidae, more specifically to the South American subfamily Peruiniinae, as expected from a biogeographical perspective.

Pilsbrylia, however, has a much different shell morphology from other members of the Peruiniinae. First of all, the shell is dextral. Dextral shells are rare in Clausiliidae, but are more frequent in subfamily *Alopiinae* (Nordsieck 2007; Páll-Gergely et al. 2019). Within the genera *Alopia* Adams & Adams, 1855 and *Albinaria* Vest, 1867, eniantomorph taxon pairs are known, and dextral lineages have evolved from sinistral ancestors multiple times independently (Fehér et al. 2013; Kornilios et al. 2015). While those shells are usually near mirror images of their congeners or conspecifics, *Pilsbrylia*, on the other hand, presents a shell morphology that is more similar to Cyclodontinidae than to most Clausiliidae, notably by not having a complete peristome (Fig. 1), which justified its previous classification.

Hylton Scott (1952) described the radular and genital anatomy of *P. paradoxa*, the only species in the genus for which anatomical data is available. Notably, that author did not mention a clausilium, which would be a reasonably obvious structure if present (unless it was present as a reduced structure). The single columellar lamella of *Pilsbrylia* spp. only extends about half whorl inside the shell along the columella (Hylton Scott 1952; Simone 2018), which could indicate a reduced or absent clausilium. Clausiliidae have two columellar lamellae that stretch throughout the entire body whorl (Nordsieck 2007, 2015).

Species of the sister genus to *Pilsbrylia* in the present phylogeny, *Incaglaia* Pilsbry, 1949 (Fig. 2), have a typical clausiliid shell morphology. However, members of the next closest genus, *Incania* Poliński, 1922, can exhibit a simplified peristome, reduced lamellae and reduced clausilial apparatus (Neubert and Nordsieck 2005). Notably, some fossil species of European *Ryllia* Munier-Chalmas, 1883 and *Rillyarex* Nordsieck, 1985 have reduced or absent lamellae and a peristome with similar configuration to *Pilsbrylia* spp. (Nordsieck 2015).

Thus, the epithet '*paradoxa*' given to the first species described in this genus reaffirms itself as a very appropriate name: genetically, it is a Clausiliidae, but it does not possess the two typical traits of the family, i.e., a sinistral shell and a clausilial apparatus (or might present it in a reduced state). Nevertheless, the genetic similarity of *Pilsbrylia* with clausiliids is observed across all markers analysed and thus, a fortuitous similarity of a single marker biasing the phylogenetic analysis is unlikely. In view of the present evidence, we conclude that *Pilsbrylia* is a member of Peruiniinae defined by its dextral shell and hypothesize that the simplification of the dextral shell (i.e., aperture and lamellae) is related to the reduction or loss of the clausilium.

The Clausilioidea are considered to have arisen in Europe, as both the extinct Filholiidae and Palaeostoidae, as well as one of the first branches of Clausiliidae (i.e., Laminiferinae; Fig. 2) are from that continent (Nordsieck 2007, 2015; Uit de Weerd and Gittenberger 2013). The Palaeostoidae date back to the Late Cretaceous of western Europe and so does Clausiliidae thanks to the extinct tribe Rillyini Nordsieck, 1985 (Nordsieck 2015).

Still, Clausiliidae has a clear Laurasian component, with Neniinae in the Caribbean and Peruiniinae in South America (Fig. 2) and an origin in the latter cannot be entirely excluded (Uit de Weerd and Gittenberger 2013). It has since become known that the presence of the family Clausiliidae (and purportedly of subfamily Peruiniinae) in South America is equally old. Namely, there is a fragmentary fossil from the Late Cretaceous of Uruguay classified as Clausiliidae indet. (Salvador et al. 2018; Cabrera et al. 2020). The next oldest fossil is *Temesa*? *magalhaesi* (Trindade, 1953) from the Early Eocene of Rio de Janeiro, Brazil (Salvador and Simone 2013; Salvador et al. 2018). The latter species was provisionally assigned to a recent genus, but it likely belongs to a different (and still undescribed) genus, potentially close to the basal node of Peruiniinae.

Conclusion

Considering the present findings, we propose a revised classification of the genus *Pilsbrylia* Hylton Scott, 1952, placing it inside subfamily Peruiniinae of the Clausiliidae. Thus, this extends the known range of this subfamily in South America to the south (Argentina and Uruguay) and to the east (Brazil, Minas Gerais state).

Acknowledgements

We are very grateful to Diego E. Gutierrez Gregoric (MLP), Eugenia S. Oroño (IFML), Fernanda S. Silva (MZSP), M. Gabriela Cuezzo (Universidad Nacional de Tucumán) for the photos of the specimens of *Pilsbrylia*, including the types; and to the reviewers and editor Frank Köhler for their comments. Our study used genetic sequences from previous papers that are freely available in GenBank (Suppl. material 1) and thus, we are very grateful to the authors of those works.

References

Breure ASH (1974) Catalogue of Bulimulidae (Gastropoda, Euthyneura), II. Odontostominae. Basteria 38: 109–127.

Breure ASH, Romero PE (2012) Support and surprises: molecular phylogeny of the land snail superfamily Orthalicoidea using a three-locus gene analysis with a divergence time analysis and ancestral area reconstruction (Gastropoda: Stylommatophora). Archiv für Molluskenkunde 141(1): 1–20. https://doi.org/10.1127/arch.moll/1869-0963/141/001-020

Cabrera F, Martínez S, Verde M (2020) Continental Late Cretaceous gastropod assemblages from Uruguay. Paleoecology, age, and the oldest record of two families and a genus. Historical Biology 32(1): 93–103. https://doi.org/10.1080/08912963.2018.1471478

Cuezzo MG, Miranda MJ, Ovando XMC (2013) Species catalogue of Orthalicoidea in Argentina (Gastropoda: Stylommatophora). Malacologia 56(1 & 2): 135–191. https://doi.org/10.4002/040.056.0210

Edgar RC (2004) MUSCLE: Multiple sequence alignment with high accuracy and high throughput. Nucleic Acids Research 32(5): 1792–1797. https://doi.org/10.1093/nar/gkh340

Fehér Z, Németh L, Nicoara A, Szekeres M (2013) Molecular phylogeny of the land snail genus *Alopia* (Gastropoda: Clausiliidae) reveals multiple inversions of chirality. Zoological Journal of the Linnean Society 167(2): 259–272. https://doi.org/10.1111/zoj.12002

Fernández D, Rumi A (1980) Pilsbrylia hyltonae, nueva especie de pulmonado del Norte argentino (Mollusca Odontostomidae). Neotrópica 26(75): 75–78.

Hausdorf B, Neiber MT (2022) Phylogeny and evolution of the land snail tribe Clausiliini (Gastropoda: Clausiliidae). Molecular Phylogenetics and Evolution 175: 107562. https://doi.org/10.1016/j.ympev.2022.107562

Hylton Scott MI (1952) Nuevos moluscos terrestres del Norte Argentino. Acta Zoológica Lilloana 10: 5–32.

Kornilios P, Stamataki E, Giokas S (2015) Multiple reversals of chirality in the land snail genus *Albinaria* (Gastropoda, Clausiliidae). Zoologica Scripta 44(6): 603–611. https://doi.org/10.1111/zsc.12125

Miller MA, Schwartz T, Pickett BE, He S, Klem EB, Scheuermann RH, Passarotti M, Kaufman S, O'Leary MA (2015) A RESTful API for access to phylogenetic tools via the CIPRES Science Gateway. Evolutionary Bioinformatics Online 11: 43–48. https://doi.org/10.4137/EBO.S21501

Neubert E, Nordsieck H (2005) New South American Clausiliidae from the Collections of the Florida Museum of Natural History (Gastropoda, Clausiliidae, Neniinae). Bulletin of the Florida Museum of Natural History 45(2): 45–62.

Nordsieck H (2007) Worldwide door snails. Hackenheim: ConchBooks.

Nordsieck H (2015) Fossil Clausilioidea in space and time, with special emphasis on Cretaceous and pre-Oligocene Cenozoic Clausiliidae (Gastropoda: Stylommatophora). Archiv für Molluskenkunde 144(1): 83–97. https://doi.org/10.1127/arch.moll/1869-0963/144/083-097

Páll-Gergely B, Szekeres M, Fehér Z, Asami T, Harl J (2019) Evolution of a dextral lineage by left–right reversal in *Cristataria* (Gastropoda, Pulmonata, Clausiliidae). Journal of Zoological Systematics and Evolutionary Research 57(3): 520–526. https://doi.org/10.1111/jzs.12277

Ronquist F, van der Mark P, Huelsenbeck JP (2009) Bayesian phylogenetic analysis using MrBayes. In: Lemey P, Salemi M, Vandamme A-M (Eds) The Phylogenetic Handbook: a practical approach to phylogenetic analysis and hypothesis testing. Cambridge University Press, Cambridge, 210–266. https://doi.org/10.1017/CBO9780511819049.009

Ronquist F, Teslenko M, van der Mark P, Ayres DL, Darling A, Höhna S, Larget B, Liu L, Suchard MA, Huelsenbeck JP (2012) MrBayes 3.2: Efficient Bayesian phylogenetic inference and model choice across a large model space. Systematic Biology 61(3): 539–542. https://doi.org/10.1093/sysbio/sys029

Saadi AJ, Wade CM (2019) Resolving the basal divisions in the stylommatophoran land snails and slugs with special emphasis on the position of the Scolodontidae. Molecular Phylogenetics and Evolution 139: 106529. https://doi.org/10.1016/j.ympev.2019.106529

Salvador RB, Simone LRL (2013) Taxonomic revision of the fossil pulmonate mollusks of Itaboraí Basin (Paleocene), Brazil. Papéis Avulsos de Zoologia 53: 4–56. https://doi.org/10.1590/S0031-10492013000200001

Salvador RB, Cabrera F, Martínez S, Miquel SE, Simone LRL, Cunha CM (2018) Annotated catalogue of the fossil Hygrophila and Eupulmonata (Mollusca: Gastropoda) from South America (Cretaceous – Neogene). Neues Jahrbuch für Geologie und Paläontologie. Abhandlungen 289(3): 249–280. https://doi.org/10.1127/njgpa/2018/0760

Salvador RB, Silva FS, Cavallari DC, Köhler F, Slapcinsky J, Breure ASH (2023) Molecular phylogeny of the Orthalicoidea land snails: Further support and surprises. PLoS ONE 18(7): e0288533. https://doi.org/10.1371/journal.pone.0288533

Schileyko AA (1999) Treatise on Recent terrestrial pulmonate molluscs. Part 3. Partulidae, Aillyidae, Bulimulidae, Orthalicidae, Megaspiridae, Urocoptidae. Ruthenica (suppl. 2): 263–436.

Simone LRL (2018) The presence of the Argentinian genus *Pilsbrylia* in Brazil, with description of a new species (Gastropoda, Odontostomidae). Journal of Conchology 43(1): 13–16.

Talavera G, Castresana J (2007) Improvement of phylogenies after removing divergent and ambiguously aligned blocks from protein sequence alignments. Systematic Biology 56(4): 564–577. https://doi.org/10.1080/10635150701472164

Uit de Weerd DR (2008) Delimitation and phylogenetics of the diverse land-snail family Urocoptidae (Gastropoda: Pulmonata) based on 28S rRNA sequence data: a reunion with *Cerion.* The Journal of Molluscan Studies 74(4): 317–329. https://doi.org/10.1093/mollus/eyn023

Uit de Weerd DR, Gittenberger E (2013) Phylogeny of the land snail family Clausiliidae (Gastropoda: Pulmonata). Molecular Phylogenetics and Evolution 67(1): 201–216. https://doi.org/10.1016/j.ympev.2013.01.011

Supplementary material 1

Table listing all species used in the present analysis, including information on their locality of origin and GenBank accession numbers

Authors: Rodrigo B. Salvador, Abraham S. H. Breure
Data type: xlsx

Link: https://doi.org/10.3897/zse.100.110105.suppl1

Supplementary material 2

Bayesian inference tree of the Clausilioidea showing the complete set of terminal taxa

Authors: Rodrigo B. Salvador, Abraham S. H. Breure
Data type: png
Explanation note: Posterior probabilities are shown on nodes. Scale bar is substitutions per site.

Link: https://doi.org/10.3897/zse.100.110105.suppl2

Zoosyst. Evol. 100 (1) 2024, 15–30 | DOI 10.3897/zse.100.109192

PENSOFT

für Natur MUSEUM FÜR NATURKUNDE BERLIN

Morphological and molecular support for *Amphithrax verrucosus* (H. Milne Edwards, 1832) and *Amphithrax aculeatus* (Herbst, 1790) (Crustacea, Decapoda, Brachyura) as valid species

Nadeshinie Parasram[1], William Santana[2], Yvonne Vallès[1], Amanda M. Windsor[3], Henri Vallès[1]

1 *The University of the West Indies, Cave Hill Campus, Department of Biological and Chemical Sciences, Bridgetown, Barbados*

2 *Museu de Paleontologia Plácido Cidade Nuvens (MPPCN) Universiadade Regional do Cariri (URCA), Crato, CE, Brazil*

3 *Department of Invertebrate Zoology, National Museum of Natural History, Smithsonian Institution, Museum Support Center, Suitland, Maryland, USA*

https://zoobank.org/99E89CD2-C20C-4E0F-8C28-21757110D910

Corresponding author: Nadeshinie Parasram (nadeshinie.parasram@mycavehill.uwi.edu, nadeshinie.parasram@gmail.com)

Academic editor: Sammy De Grave ♦ **Received** 7 July 2023 ♦ **Accepted** 2 November 2023 ♦ **Published** 26 January 2024

Abstract

The large degree of morphological variations, particularly amongst juveniles, has led to inconsistencies in the literature regarding the taxonomic status of *Amphithrax aculeatus* (Herbst, 1790) and *Amphithrax verrucosus* (H. Milne Edwards, 1832). As a result of recent biodiversity sampling initiatives in Barbados, West Indies, multiple specimens of *Amphithrax aculeatus* and *A. verrucosus* have been collected. This has prompted us to undertake a thorough reassessment of their morphological and molecular characteristics. Moreover, morphological differences in the carapace, antennae, chelipeds, pereopods and the male first gonopod (G1) supports *A. aculeatus* and *A. verrucosus* as separate species. Molecular phylogenetic analysis, based on newly-generated sequences of the 12S rRNA, 16S rRNA and ITS-1 genes also shows that *A. verrucosus* is a separate species and sister taxa to *A. aculeatus*. The total number of species within the genus *Amphithrax* is now brought to eleven. However, our molecular analysis also shows that the taxonomic placement of *Amphithrax armatus* (Saussure, 1853) within *Amphithrax* is questionable.

Key Words

Amphithrax, 12S, 16S, ITS-1, Lesser Antilles, Mithracidae

Introduction

The superfamily Majoidea Samouelle, 1819, consists of over 950 species of ecologically and economically important brachyuran crabs (Calado et al. 2003; Guiomar et al. 2007; Hultgren and Stachowicz 2008; Santana et al. 2016). Within this superfamily, the hairy clinging crabs of the genus *Amphithrax* are found dwelling amongst coral rocks and rubble, under sea anemones and in rock crevices in the intertidal zones to subtidal zones of up to 60 m depth (Baeza et al. 2010). They are found in the tropics and subtropical regions (Windsor and Felder 2017) and are especially abundant in nearshore rubble and shallow-water (0–4 m depth) marine habitats of Barbados (Parasram et al. 2023). Current taxonomy supports ten species in *Amphithrax* Windsor & Felder, 2017, nine of which have an Amphiamerican distribution and one, *Amphithrax caboverdianus* (Türkay, 1986), which is found in the eastern Atlantic. However, taxonomic disparity exists within the literature regarding the identity of hairy clinging crabs and this is largely due to the variability in size, shape, larval and adult forms within this genus. In that regard, the relationship and taxonomic status of *Amphithrax aculeatus* (Herbst, 1790) and its presently considered junior subjective synonym, *Amphithrax verrucosus* (H. Milne Edwards, 1832) remains controversial.

Amphithrax aculeatus was originally described as *Cancer aculeatus* by Herbst in 1790. Later, in 1816,

Latreille described the genus *Mithrax* and designated *Cancer aculeatus* Herbst, 1790 as its type species. After that, H. Milne Edwards, in 1832, described *Mithrax verrucosus*, based on syntypes collected from the Antilles, specifically from Martinique. Subsequent research by Desbonne and Schramm (1867) identified both *M. aculeatus* and *M. verrucosus* in samples collected in Guadeloupe. This period also saw the establishment of *Mithrax trispinosus* Kingsley, 1879 from Florida, albeit based on an exceptionally small specimen. The type for this species was later reported as lost by Rathbun (1925). Further, Rathbun, in 1892, described *Mithrax pilosus* from specimens collected in the Bahamas and, in a subsequent study in 1901, described *Mithrax plumosus* from Puerto Rico.

The early 20th century was marked by Rathbun's taxonomic revisions, which had a significant influence on the genus's classification. In her 1901 work, she proposed a synonymy between *M. pilosus* and *M. aculeatus*, treating the latter as a junior synonym of the former. Furthermore, in her 1925 work, she designated both *M. trispinosus* and *M. plumosus* as junior synonyms of *M. verrucosus*. However, Rathbun provided no explanation for these taxonomic changes.

The latter half of the 20th century saw a continuation of these taxonomic debates. Researchers such as Williams (1984) included *Mithrax verrucosus* in their findings for Florida. In parallel, Powers (1977), Abele and Kim (1986) and Wagner (1990) asserted the validity of both *M. pilosus* and *M. verrucosus*. Wagner's study stood out for emphasising the ontogenetic shifts in morphology and he highlighted that juveniles of the two species were morphologically more similar than their adult counterparts.

Ng et al. (2008: 123) corrected the precedence of *Mithrax aculeatus* over *M. pilosus* set by Rathbun, stating that the lectotype specimen of *Cancer aculeatus* Herbst, 1790, is probably a conspecific of *M. pilosus*. They further clarified the synonymic relationship between *C. aculeatus* Fabricius, 1793 and *C. aculeatus* Herbst, 1790 and retained both *Mithrax aculeatus* and *M. verrucosus* as valid species.

More recently, molecular approaches to taxonomy have become central to species delineation. Based on molecular evidence from three mitochondrial (12S, 16S, COI) and two nuclear genes (18S, H3), Windsor and Felder (2014) placed *M. verrucosus* as a junior synonym of *M. aculeatus*. Later, Windsor and Felder (2017) made some amendments to their previous work (Windsor and Felder 2014) and established the now accepted genus *Amphithrax* Windsor & Felder, 2017 to accommodate several species belonging to *Mithrax* Latrielle, 1816, including *Amphithrax aculeatus* (Herbst, 1790) and *Amphithrax verrucosus* (H. Milne Edwards, 1832). Windsor and Felder (2014) reported that the carapace shape and texture in large specimens of *A. verrucosus* closely matches the illustration of *C. aculeatus* by Herbst (1790, pl. 19, fig. 104).

In more recent studies, Carmona-Suárez and Poupin (2016) and Poupin (2018) have revisited the classification of *A. aculeatus* and *A. verrucosus*. Based on morphological characters, they proposed the separate classification of *A. aculeatus* and *A. verrucosus*, arguing for both species to retain their distinct status, a rationale followed by Parasram et al. (2023) in their brachyuran crabs' inventory of Barbados. Thus, the present study attempts to resolve the taxonomic status and phylogenetic relationship between *A. aculeatus* and *A. verrucosus* by using an integrative approach that incorporates both morphological and new molecular evidence.

Materials and methods

Sample collection and preservation

A total of sixty-two (62) specimens of *Amphithrax aculeatus* (24) and *A. verrucosus* (38) were collected from nearshore rubble and shallow subtidal habitats (~ 4 m depth) on the west and south coasts of the island of Barbados, West Indies (Fig. 1A, B). They were collected by hand, with the aid of hand nets and with cage crab traps (Fig. 1C). Collected specimens were transported to the laboratory, euthanised by freezing, and preserved in 70% ethanol. Specimens collected during this study are stored at the Barbados Laboratory of Systematic Zoology (BLSZ). A stereomicroscope (Olympus SZ7, Model #: SZ2-ILST) was used to examine specimens and fresh (after briefly freezing) and preserved specimen images were taken with a Nikon D3300 DSLR camera equipped with a 55 mm super macro lens and with a Toupcam full HD microscope camera (Model #: XCZM, Series HDMI 1080 P) mounted on the Olympus SZ7 microscope. Measurements of the carapace width (CW) and carapace length (CL) were taken with a vernier caliper with an accuracy of 0.01 mm.

Taxonomic classification

Information regarding the synonym, geographic distribution, material examined, and general remarks are included for each species. The morphological terminology follows that of Rathbun (1925) and Davie et al. (2015a). Taxonomic classification mostly follows that of Ng et al. (2008) and Davie et al. (2015b), but Guinot (1967), Manning and Chace (1990), Guinot and Tavares (2003) and Windsor and Felder (2014, 2017) were also considered.

Additional abbreviations used in the text are: **CW** = carapace width (measured dorsally at the widest point of the carapace, including lateral spines); **CL** = carapace length (measured from the bottom of the rostral sinus to the posterior margin of the carapace). Measurements for some studied specimens were not taken; **Idem** = The aforementioned locality; ♂ = male; ♀ = female; **juv.** = juveniles; **ovig.** = ovigerous females; **G1** = male first gonopod; **cm** = centimetre; **mm** = millimetre; **m** = metre; **fig./figs** = figure/s; **tab.** = table; **vol.** = volume; **BI** = Bayesian Inference; **ML** = Maximum Likelihood;

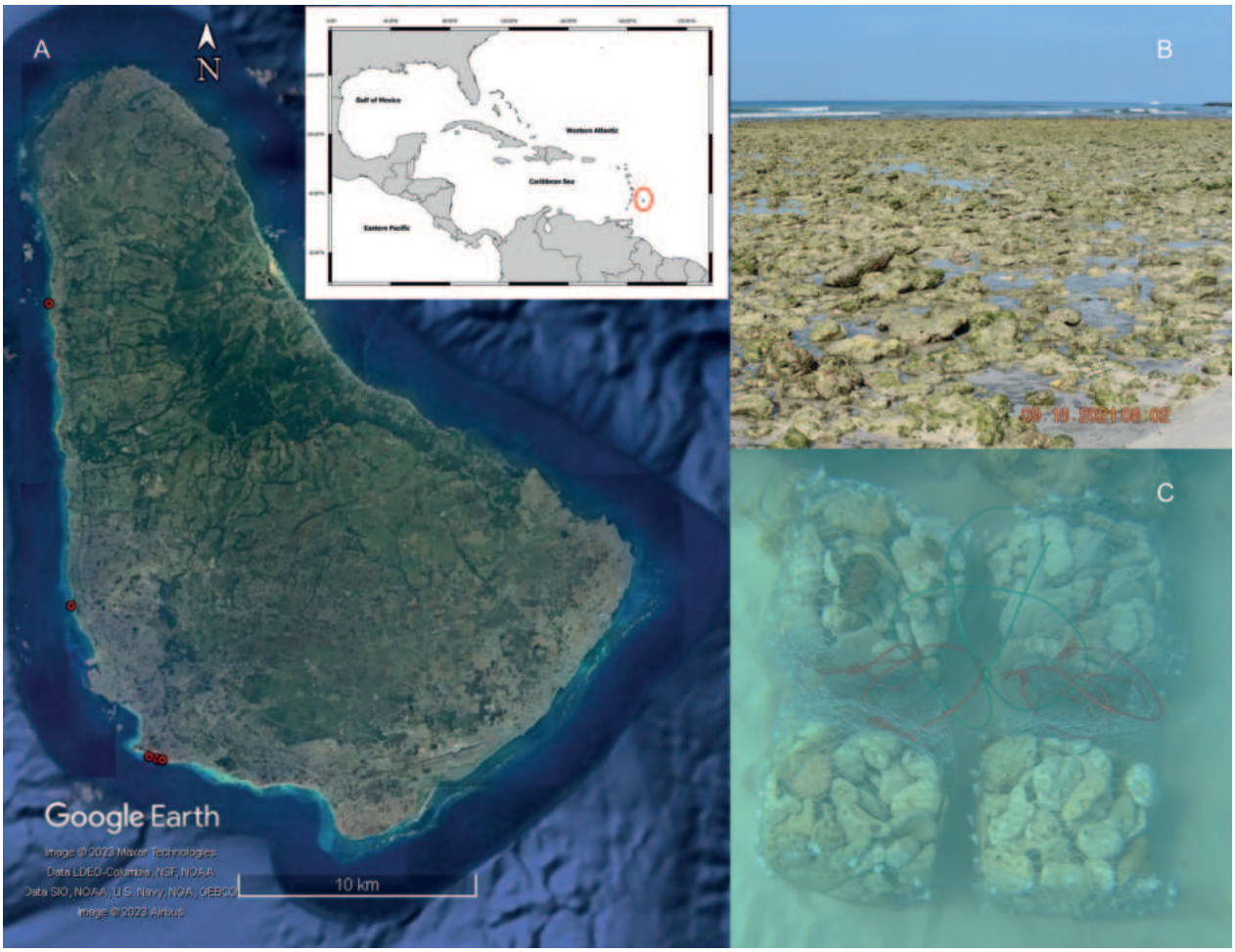

Figure 1. A. Map of Barbados with sampling locations during this study and position of Barbados (red circle) within the Caribbean region; **B.** Nearshore rubble habitat (exposed at low tide); **C.** A cluster of cage crab traps in subtidal habitat. Photos: Nadeshinie Parasram.

SEM = Scanning Electron Microscope; **Pp** = Posterior Probability. Specimens examined are deposited in the Barbados Laboratory of Systematic Zoology, University of the West Indies, Barbados (**BLSZ**); Coleção de Crustáceos do Departmento de Biologia – Faculdade de Filosofia, Ciências e Letras de Ribeirão Preto, Universidade de São Paulo, Brazil (**CCDB**); Grupo de Investigación en Carcinología, Escuela de Ciencias Aplicadas de Mar, Núcleo Nueva Esparta, Universidade de Oriente (**GIC**); Museum of Comparative Zoology, Harvard University (**MCZ**); Muséum national d'Histoire naturelle, France (**MNHN**); Museu de Zoologia da Universidade de São Paulo, Brazil (**MZUSP**); National Museum of Marine Biology and Aquarium, Taiwan (**NMMBA**); University of Louisiana at Lafayette Zoological Collection, USA (**ULLZ**); National Museum of Natural History, Smithsonian Institution, USA (**USNM**); Museum für Naturkunde Berlin, Germany (**ZMB**).

DNA extraction, PCR, and sequencing

Muscle tissue was extracted from the ambulatory legs and chelipeds from 10 specimens each of *A. aculeatus* and *A. verrucosus* and total genomic DNA was extracted from the fresh muscle tissue using the ZYMO Quick-DNA Miniprep DNA extraction kits (catalogue # D3025), following the manufacturer's instructions. The tissue lysis stage was modified to incubate the muscle tissue in Proteinase K for one hour instead of the three hours suggested by the protocol, as this provided better results. Partial sequences of the two mitochondrial (12S rRNA, 16S rRNA) and one nuclear (ITS-1) genes were amplified with the following primers 12Sai/12Sbi (Palumbi et al. 1991), 16SF/16SR (Hultgren and Stachowicz 2008), and SP-1-3'/SP-1-5'138 (Chu et al. 2001).

Polymerised chain reactions (PCR) were carried out in 25 µl volumes with concentrations as follows: 12.5 µl (2X) Master Mix (Applied Biosystem), 0.5 µl (10 µM) of each primer, 6.5 µl of nuclease free water and 5 µl of template DNA. PCR amplifications for each gene were as follows: for 12S, initial denaturation of 2 min, followed by 35 cycles of denaturation for 30 s at 94 °C, annealing for 30 s at 55 °C, extension for 1 min at 72 °C and a final extension for 7 min at 72 °C; for 16S, initial denaturation of 2 min, followed by 35 cycles of denaturation 30 s at 94 °C, annealing for 30 s at 52 °C, extension for 1 min at 72 °C and a final extension for 5 min at 72 °C; and

for ITS-1, initial denaturation of 3 min, followed by 35 cycles of denaturation for 0.15 s at 94 °C, annealing for 0.45 s at 57 °C, extension for 1 min at 72 °C and a final extension for 10 min at 72 °C. Amplified PCR products were visualised on 2% agarose gels and PCR amplicons were sent to Macrogen (Seoul, Republic of Korea) for bi-directional sequencing.

Phylogenetic analysis

Sequences obtained by this study for *A. aculeatus* and *A. verrucosus* were combined with those from Baeza et al. (2010), Windsor and Felder (2014) and Assugeni et al. (2016) which are available on GenBank. Locality information and GenBank accession numbers for all taxa included in the molecular analysis are provided in Table 1. The sequences obtained by our study were checked for quality and trimmed of both forward and reverse primers using the programme BioEdit v.7.2.5. Consensus sequences were generated in Geneious Prime 2023.0.4 (https://www.geneious.com/). Multiple sequence alignment was performed on individual datasets for each gene (12S, 16S and ITS-1) using the MAFFT FFT-NS-1 (Katoh and Standley 2013) alignment algorithm and final alignments were checked manually for presence of incongruence and/or gaps.

Alignments for the 12S, 16S and ITS-1 genes were concatenated in Geneious Prime and phylogenetic trees were constructed using maximum likelihood (ML) and Bayesian inference (BI) methods on the concatenated loci. ML analyses were conducted by RAxML v.8.2.11 (Randomized Accelerated Maximum Likelihood; Stamatakis 2014) implemented in Geneious Prime and MEGA11 (Tamura et al. 2021). Likelihood parameters followed the General Time Reversible model with a gamma distribution (GTR+G) and branch confidence of tree topology was assessed using 1,000 bootstrap replicates.

In RAxML, we used the '-f a -x 1' algorithm option and RAxML estimated all free parameters. In MEGA11, we used the default settings for likelihood parameters with partial deletion of gaps in the alignment. BI analysis of Posterior Probability (Pp) was conducted on the concate-

Table 1. Taxa included in the phylogenetic analysis with locality, catalogue number, and GenBank accession numbers. Newly-sequenced specimens are highlighted in bold. GMx, Gulf of Mexico; water body names preceded by N, S, E or W to indicate northern, southern, eastern, or western, respectively; –, no sequence identifier available.

Taxon name	Locality	Catalogue No.	GenBank Accession Nos.		
			12S	16S	ITS-1
Amphithrax aculeatus	W Atlantic, Barbados	**BLSZ 222**	**OR267308**	**OR267299**	**–**
	W Atlantic, Barbados	**BLSZ 223**	**OR267309**	**OR267300**	**–**
	W Atlantic, Barbados	**BLSZ 267**	**OR267311**	**OR267302**	**OR260473**
	W Atlantic, Barbados	**BLSZ 268**	**OR267312**	**OR267303**	**–**
	W Atlantic, Barbados	**BLSZ 252**	**OR267310**	**OR267301**	**OR260472**
Amphithrax armatus	E Pacific, Taiwan	NMMBCD 4083	–	MG281843	–
Amphithrax caboverdianus	E Atlantic, Cape Verde Island	ULLZ 11711	KF453086	KF452982	–
Amphithrax braziliensis	S Atlantic, Brazil	CCDB_BRA 5060	–	MF178237.1	–
Amphithrax hemphilli	Caribbean, Belize	ULLZ 9150	KF453133	KF453024	–
Amphithrax verrucosus	Caribbean, Panamá	ULLZ 13596	–	MK971519.1	–
	W Atlantic, Florida	ULLZ 4534	KF453096	KF452993	–
	Caribbean, Belize	ULLZ 9148	KF453131	KF453022	–
Amphithrax verrucosus	W Atlantic, Barbados	**BLSZ 226**	**OR267313**	**OR267304**	**–**
	W Atlantic, Barbados	**BLSZ 228**	**OR267134**	**OR267305**	**OR260474**
	W Atlantic, Barbados	**BLSZ 265**	**OR267316**	**OR267307**	**–**
	W Atlantic, Barbados	**BLSZ 250**	**OR267315**	**OR267306**	**OR260475**
Amphithrax verrucosus	W Atlantic, Venezuela	MOBR-C-1529	–	GQ438765	–
	W Atlantic, Venezuela	MOBR-C-1529	–	GQ438766	–
Hemus cristulipes	E GMx, Florida	ULLZ 5783	KF453100	KF452995	–
Hemus magalae	E Pacific, Panamá	USNM 1149374	KF453144	KF453034	–
Maguimithrax spinosissimus	Caribbean, Belize	ULLZ 6981	KF453130	KF453021	–
Mithraculus cinctimanus	Caribbean, Belize	ULLZ 12248	KF453091	KF452988	–
Mithraculus coryphe	Caribbean, Belize	ULLZ 9223	KF453135	KF453026	–
Mithraculus sculptus	W Atlantic, Florida	ULLZ 8774	GU144526	GU144539	–
Mithrax hispidus	W Atlantic, Florida	ULLZ 8619	GU144532	GU14450	–
Omalacantha antillensis	W Atlantic, Florida	ULLZ 5663	KF453099	KF452994	–
Omalacantha bicornutus	Caribbean, Belize	ULLZ 7077	KF453116	KF453008	–
Thoe puella	Caribbean, Colombia	ULLZ 9227	KF453136	KF453027	–
	W Atlantic, Florida	ULLZ 4533	KF453095	KF452992	–
Outgroup taxa					
Libinia emarginata	N GMx, Louisiana	ULLZ 10344	KF453078	KF452974	–
Maja brachydactyla	E Atlantic, Spain	ULLZ 11425	KF453082	KF452978	–

nated loci using MrBayes (plugin v.3.2.6: Huelsenbeck and Ronquist 2001) implemented in Geneious Prime. In MrBayes, the gamma category was set to four, with four heated MCMC of 1,100,000 generations, sampling every 200th tree and a burn-in of 10%; all other parameters remained free. ML and BI analysis were also performed on individual datasets of the 12S, 16S and ITS-1 genes (see supplementary material S1). The resulting best tree generated for the concatenated dataset was used to reflect phylogeny.

Results

Phylogenetic analysis

Our study generated new sequences for both *A. aculeatus* and *A. verrucosus* from specimens collected in Barbados. These sequences, along with sequences available from GenBank, were used to determine the taxonomic status of *A. verrucosus* and to establish its phylogenetic relationship with *A. aculeatus*. All three genes (12S rRNA, 16S rRNA and ITS-1) were successfully amplified and the phylogenetic analysis consisted of 31 terminals (including outgroup taxa, Table 1) that represents eight genera and 18 species. In total 1,408 base pairs (excluding primer regions) were aligned: 418 bp for 12S, 437 bp for 16S and 553 bp for ITS-1. Tree topologies were congruent with both Bayesian Inference (BI) and maximum Likelihood (ML) analyses and, as both ML and BI analyses resulted in similar topologies, only the BI tree is shown with ML bootstrap and BI support values are depicted on nodes (Fig. 2).

Amphithrax forms a monophyletic group with the Western Atlantic species *A. hemphilli* (Rathbun, 1892)

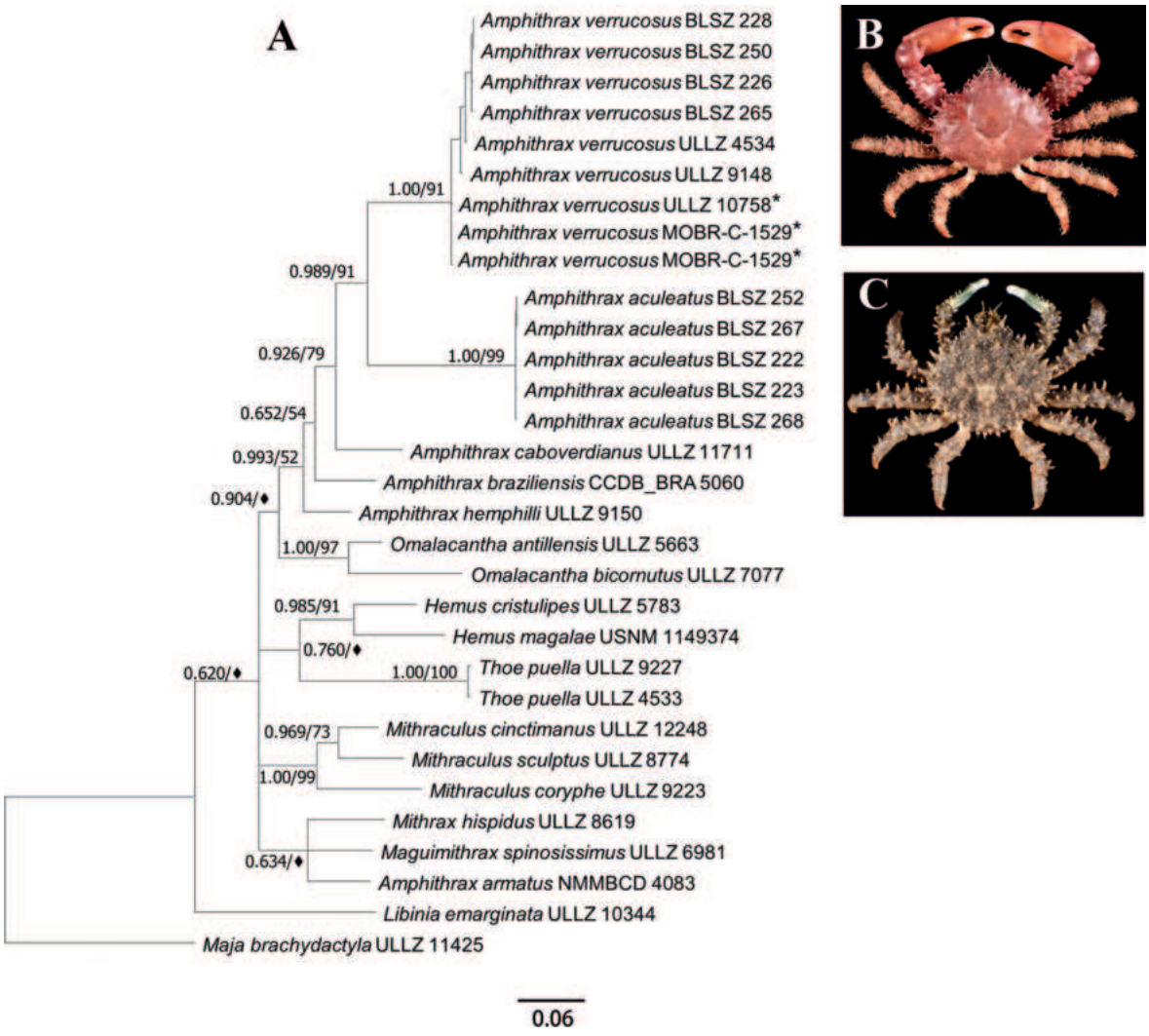

Figure 2. A. BI molecular phylogenetic tree for *Amphithrax verrucosus*, *A. aculeatus* and other selected species within the family Mithracidae MacLeay, 1838. Based on GTR+G nucleotide substitution model on the concatenated dataset for two mitochondrial (12S, 16S) and one nuclear (ITS-1) genes, represented as a maximum likelihood phylogram with Bayesian posterior probabilities and maximum likelihood bootstrap values (black diamond = ≤ 50% support, * = 16S sequences only). Note: ULLZ's 9148 and 4534, of Windsor and Felder (2014) and 13596 all re-identified as *Amphithrax verrucosus* (H. Milne Edwards, 1832); **B.** *Amphithrax verrucosus* (H. Milne Edwards, 1832), male (CW: 40.7 mm; CL: 29.5 mm), Barbados (BLSZ 218); **C.** *Amphithrax aculeatus* (Herbst, 1790), juvenile female (CW: 53.8 mm; CL: 44.0 mm), Barbados (BLSZ 217).

at the basal position. *Amphithrax verrucosus* is well supported (ML = 91%, Pp = 0.989) as a separate species and sister taxa to *A. aculeatus*. All specimens previously identified by Windsor and Felder (2014) as *A. aculeatus* (ULLZ 9148 and 4534) and an additional specimen from the ULLZ collection (ULLZ 13596) were reidentified as *A. verrucosus* based on the morphological examination and the sequences from Barbados (see supplementary material). The phylogenetic tree shows divergence of sequences from ULLZ (4534, 9148, 13596) and MO-BR-C-1529. *Omalacantha* Streets, 1871 is identified as a sister clade to *Amphithrax*, with a high BI support value (ML ≤ 50%, Pp = 0.904). This result is also congruent with that of Ng et al. (2018: fig. 5) where *Omalacantha* forms a sister clade to *Amphithrax*.

Our phylogenetic results show *A. armatus* forming a clade with *Maguimithrax* Klompmaker, Portell, Prueter & Tucker, 2015, and *Mithrax* Latreille, 1816, and not with *Amphithrax*, but the support for this relationship is very low [(ML ≤ 50%, Pp = 0.634) (Fig. 2)].

Systematics

Family Mithracidae MacLeay, 1838
Genus *Amphithrax* Windsor & Felder, 2017

Amphithrax aculeatus (Herbst, 1790)

Figs 2C, 3A–D, 5A, C, D, 6A–D

Cancer aculeatus Herbst, 1790: 248, pl. XVIII, fig. B, pl. XIX, fig. 104 [type-locality: Americas (probably between Florida and Venezuela); holotype (ZMB Herbst 0134) and paralectotype (ZMB Herbst 0079) in Berlin Museum]. — Desmarest (1825: 151).

Cancer spinipes Herbst, 1790: 241, pl. XVII, fig. 94 [type locality: probably West Indies; type: probably lost]. — Desmarest (1825: 151).

Mithrax aculeatus — H. Milne Edwards 1832: class 7; 1834–1840: 321; Schomburgk 1848: 65; Stimpson 1860: 188; Desbonne and Schramm 1867: 5; A. Milne-Edwards 1875: 102; Ng et al. 2008: 120; Windsor and Felder 2014: 163, figs 3G, 4H.

Mithrax pilosus Rathbun, 1892: 262, pl. 39 [type-locality: Abaco Island, Bahamas; holotype (USNM 16299) and paratypes (USNM 16299) in National Museum of Natural History, Washington, D.C.]. — Rathbun 1901: 66; 1921: 83; Nutting 1919: 75; Rodríguez 1980: 287; Abele and Kim 1986: 47, 522 fig. c; Wagner 1990: 25–29, figs 28–31; Carmona-Suárez and Poupin 2016: 373, fig. 6H.

Mithrax (*Mithrax*) *aculeatus* — Young, 1900: 90.

Mithrax (*Mithrax*) *pilosus* — Rathbun, 1925: 394, pl. 138, fig. 3; 1933: 29; Powers 1977: 57; Lira et al. 2013: 55, tab.1.

Amphithrax aculeatus — Windsor & Felder, 2017: 1; Poupin 2018: 192–193, fig. 210; Questel 2019: 16, unnumbered figure; Parasram et al. 2023: 20, fig. 9B.

Material examined. Type material. Paralectotype of *Cancer aculeatus* Herbst, 1790: Americas • dry carapace only, ZMB Herbst 79. Holotype of *Mithrax pilosus* Rathbun, 1982: Bahamas, Abaco Island, Albatross Research Vessel • ♂ (CW: 30.0; CL: 28.0 mm) (USNM 16299), 26°27'59.99"N, 77°04'60.00"W. Paratypes: Idem, 2 ♂♂, 1 juv. ♀ (CW: 29.0; 29.0; 19.0; mm; CL: 26.0; 26.0; 18.0 mm) (USNM 16299).

Additional material. Puerto Rico, Playa de Ponce, Lighthouse Reef • 1 ♂, 1 juv. ♂ (CW: 23.0; 9.0 mm; CL: 21.0; 9.0 mm) (USNM 24091), 18°00'39"N, 66°41'14"W. St. Croix, Christiansted Harbour • 1 ♀ (CW: 42 mm; CL: 35 mm) (USNM 72827), 17°44'47.9004"N, 64°42'11.5236"W. Virgin Islands, St. Croix, Buck Island, 1 ♂ (CW: 28 mm; CL: 25 mm) (USNM 73318), 17°47'14"N, 64°37'15"W. Guadeloupe, Anse Babin, KARUBENTHOS 2012 • 1 ♂ (MNHN-IU-2013-5929), 16°20'26.9988"N, 61°31'32.9988"W. Barbados • 1 ♂ (CW: 105.0 mm; CL: 87.0 mm) (USNM 1519303), 13°04'30.73"N, 59°36'12.49"W. Palm Court, St. Michael • 3 ♂♂, 1 juv. ♀ (CW: 10.0; 11.0; 11.4; 53.8 mm; CL: 11.0; 12.0; 44.0 mm) (BLSZ 217), nearshore rubble, 13°04'30.73"N, 59°36'12.49"W. Idem, 1 ♂, (CW: 37.0 mm; CL: 32.0 mm) (BLSZ 331). Idem, 1 juv. ♀, (CW: 34.4 mm; CL: 30.0 mm) (BLSZ 220). Idem, 1 juv. ♀, (CW: 33.4 mm; CL: 30.0 mm) (BLSZ 221). Idem, 1 ♂ (CW: 32.0 mm; CL: 28.0 mm) (BLSZ 222). Idem, 1 juv. ♀ (CW: 28.0 mm; CL: 24.0 mm) (BLSZ 223). Idem, 1 juv. ♀ (CW: 34.0 mm; CL: 29.0 mm) (BLSZ 267). Idem, 1 juv., ♀ (CW: 16.2 mm; CL: 16.0 mm) (BLSZ 268). Drill Hall, St. Michael • 1 juv. ♀, 1 ♂ (CW: 29.6; 24.7 mm; CL: 26.0, 21.0 mm) (BLSZ 120), nearshore rubble, 13°04'36.30"N, 59°36'26.63"W. Idem, 3 ♂♂, (CW: 12.4;12.5; 7.8 mm; CL: 13.0; 14.0; 9.6 mm) (BLSZ 129). Idem, 1 juv., ♀ (CW: 13.0 mm; CL: 13.3 mm) (BLSZ 252). Idem, 3 ♂♂, 1 juv., ♀ (CW: 22.5; 10.3; 10.4; 11.0 mm; CL: 20.0; 10.0; 10.0; 11.0 mm) (BLSZ 269). Schooner Bay, St. James • 2 ♂♂, 1 ♀ (CW: 10.6; 30.5; 40.5 mm; CL: not taken) (MZUSP 40878, 40884), nearshore rubble, 13°14'48.24"N, 59°38'40.90"W.

Diagnosis. Carapace with acute spines dorsally, mainly in gastric, branchial, cardiac regions. Third antennal segment with long spine distolaterally, distinctly visible dorsally. Chelipeds slender; carpus with strong, sharp spines. Palm of chela with 4–5 spines on the upper margin. Propodus of pereopods with two to four spines on the proximal half. Carapace olive green to brown in colour.

Remarks. Herbst (1790: 248) referred to *Cancer aculeatus* as a "very rare American crab", but *Amphithrax aculeatus* is very abundant in Barbados. It is possible that the Herbst assessment of the rarity of this species is due to sampling biases (methodology used and sampling time), which resulted in a small number of specimens collected and deposited to the Berlin Museum (Tavares and Mendonça 2022).

In the same work, Herbst (1790) described *Cancer spinipes*, and both its description and figure resemble *A. verrucosus*. However, Windsor and Felder (2014) selected the lectotype of *Cancer aculeatus* Herbst, 1790 as the neotype for *Cancer spinipes* Herbst, 1790, establishing these names as objective synonyms. Due to lack of material for *Cancer spinipes* Herbst, 1790, we have opted

to maintain its status as a synonym of *A. aculeatus*. This decision is based on the need for nomenclatural consistency in the absence of more definitive data. While Herbst (1790) did not specify any locality for *Cancer spinipes*, which he referred to as a "Chinese crab" in the description (Herbst 1790: 241 "Der Schild dıefer chinesischen Krabbe ift herzförmig"), Desmarest (1825) cited both *Cancer spinipes* and *Cancer aculeatus* as originating from the East Indies. We believe that this is a labelling mistake (common at that time) given that both species are endemic to the Western Atlantic.

Amphithrax aculeatus can be separated from *A. verrucosus* by: (i) the carapace densely setose, forming a velvet-like cover in both juvenile and adult specimens (Figs 3A, B, 5C, 6 A–D) (vs. carapace almost without setae in fully developed specimens, few setae concentrated laterally; in juveniles, carapace interspace with long and short dark setae, not forming a velvet-like cover in *A. verrucosus*; Figs 4A, B, 5B, 6 E–H); (ii) anterolateral margins of the carapace with six spines, excluding the orbital spine, where the first, second and third anterolateral spines are accompanied by an accessory spine (Figs 3A, 6A, D) (vs. anterolateral and posterior margins of the carapace with six to eight spines, excluding the orbital spine, where the first and second anterolateral spine are accompanied by accessory spines in *A. verrucosus*; Figs 4A, 6E, G); (iii) third antennal segment with long spine distolaterally, distinctly visible dorsally (Fig. 3B) (vs. third antennal segment with short spine distolaterally, not visible dorsally in *A. verrucosus*; Fig. 4B); (iv) chelipeds slender in adults, carpus with several strong, acute spines and palm of chela with four or five spines on the upper margins (Figs 3A, 6A, C) (vs. chelipeds more massive, especially in adult males, carpus without spines dorsally, with one to three blunt teeth on the inner margin, and palm of chela smooth; Figs 4A, 6E, G); (v) propodus of pereopods with two to four spines on the proximal half (vs. propodus of pereopods without spines in *A. verrucosus*); (vi) third maxilliped covered with short setae (vs. third maxilliped without setae in *A. verrucosus*); (vii) dorsal surface of pleon in males and females are covered in small thick setae (vs. dorsal surface of pleon in males and females without setae in *A. verrucosus*; (viii) G1 long, slender, dorsoventrally flattened, with the proximal third slightly curved towards mesial line, lateral margin with pappose setae at the base; tip triangular with rounded mesial lobe (Fig. 3C, D) (vs. G1 long, robust, slightly dorsoventrally flattened, with the proximal third slightly curved towards mesial line, lateral margin with pappose setae from base to distal third of shaft, tip V-shaped, with fold just below tip in *A. verrucosus*; Fig. 4C, D; see also Wagner (1990) and Lianos et al. (2021); (ix) dorsal and ventral surfaces of live specimens are olive green to brown in colour with whitish fingers of chela (Figs 3A, 6A–C) (vs. dorsal surface of live specimens predominantly maroon in colour and mixed with white spots on ventral surface, in ventral view, only tips of fingers are white in *A. verrucosus*; Figs 4A, 6E–H). It is worth pointing out that Wagner's (1990: 27, fig. 30) illustration of an *Mithrax pilosus* G1 is that of a young specimen of *A. aculeatus*.

Ontogenetic intraspecific variations in *A. aculeatus* from juveniles to adults are: spines on the carapace, carpus, and pereiopods become larger and more acute, but can be broken in the larger individuals. In some juvenile specimens, the gastric region of the carapace has more sparse setae than other regions and the dorsal surface also has the presence of flattened granules, five spines on anterolateral margins, with small and blunt accessory spines. In contrast, adults have the dorsal and ventral surface of the cephalothorax covered in short tuft setae, which has the appearance of a velvet mat; the granules on dorsal surface of the carapace develop into spines; anterolateral margins with six spines that are accompanied with well-developed accessory spines that are spiniform in shape. The palm of chelipeds in juveniles can have one to four spines, while in adults, the palm has three to six spines.

Parasram et al. (2023) reported *Amphithrax aculeatus* being found in close association with *A. verrucosus*, *Mithraculus coryphe* (Herbst, 1801), *M. forceps* A. Milne-Edwards, 1875, *Eriphia gonagra* (Fabricius, 1781) and *Pachygrapsus transversus* (Gibbes, 1850). Specimens of *A. aculeatus* were collected by hand and with caged crab traps on the west and south coasts of Barbados. *Amphithrax aculeatus* females collected in Barbados are generally larger than males (see material examined). No sexually mature females were found.

Due to the recurrent misidentifications between *A. aculeatus* and *A. verrucosus* in literature, determining the geographic distribution for these species has proved to be challenging. Nevertheless, based on the morphological characteristics provided by some authors, it seems that *A. aculeatus* has a more restricted geographic range, which encompasses the insular Caribbean. For instance, most of the material examined by Rathbun (1925: 395, Fig. 5) (under the name *Mithrax pilosus*) was collected from Caribbean islands, except for two specimens (one male and one female) from Venezuela. The first mention of these specimens was made by von Martens (1872: 82), but this could be a labelling mistake since Caracas is not a coastal city. These specimens were deposited in the Berlin Museum. In addition, A. Milne-Edwards (1875: 103) also mentioned two specimens of *A. aculeatus* collected in Vera Cruz, Mexico by M. Brémond. Contacting both ZMB and MNHN was not successful in locating these materials, therefore, these specimens are herein classified under *A. verrucosus*, given the prevalence of this species in Central America.

As a result of Windsor and Felder's (2014) revision, multiple collections modified their taxonomic records to align with *A. aculeatus*, which resulted in the renaming of many specimens previously identified as *A. verrucosus* (see USNM and MNHN online catalogues). Based on our re-examination of the literature and materials

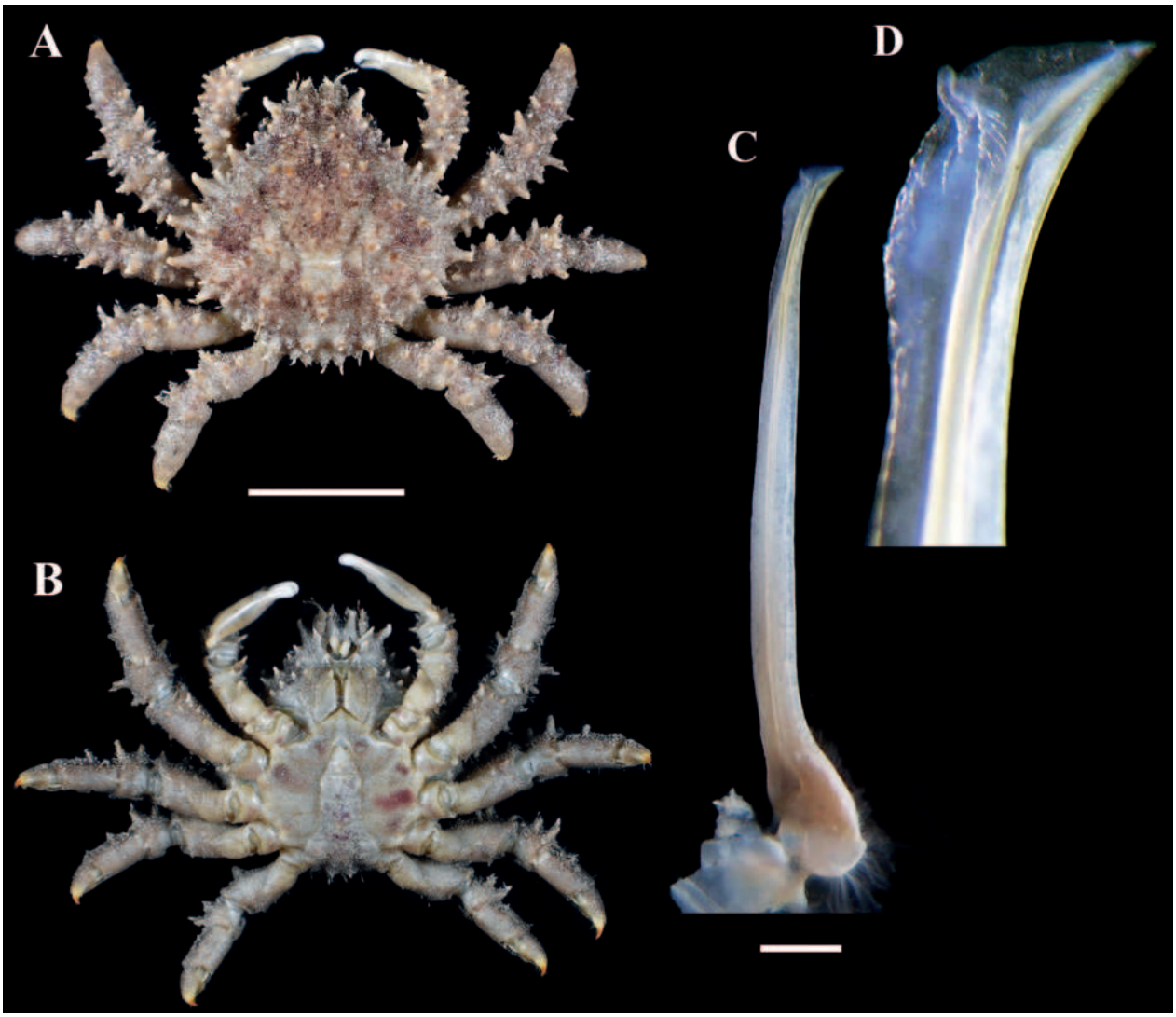

Figure 3. *Amphithrax aculeatus* (Herbst, 1790) adult male (BLSZ 331). **A.** Habitus, dorsal; **B.** Ventral view, locality: Barbados; **C.** Pleonal view of right G1 (BLSZ 222); **D.** Distal third of the right G1. Scale bars: 20 mm (**A, B**); 10 mm (**C**). Photos: Nadeshinie Parasram.

from different localities, we proposed the following update range for the two species: *A. aculeatus* is island endemic with a northern limit of Florida (Tortugas) and a southern limit of Barbados, whereas *A. verrucosus* has a northern limit of USA (South Carolina) and a southern limit of Brazil.

Colouration. In its natural habitat, the carapace of *A. aculeatus* exhibits an olive green to brown hue; but the carapace could be spotted with large beige spots (MNHN-IU-2013-5929) especially in younger individuals. The chelipeds are predominantly green (darker or lighter) with black spots on the palm, fingers are whitish (Figs 3A, 6 A–D). Pereopods are brown (light to dark) or green.

Distribution. Western Atlantic: USA (Florida, Dry Tortugas), Bahamas, Cuba, Puerto Rico, British Virgins Islands, St. Thomas, St. Croix, St. Martin, St. Barthélemy, Antigua, Guadeloupe, Martinique, and Barbados (Stimpson 1860; Rathbun 1925; Carmona-Suárez and Poupin 2016; Poupin 2018; present study).

Amphithrax verrucosus (H. Milne Edwards, 1832)

Figs 2B, 4A–D, 5B, 6E–H

Mithrax verrucosus H. Milne Edwards, 1832: 11, pl. 4 [type-locality: Martinique; type probably in MNHN]. — Schomburgk 1848: 65; Stimpson 1860: 187; Desbonne and Schramm 1867: 6; A. Milne-Edwards 1875: 102; Miers 1886: 86; Rathbun 1897: 9; 1921: 83; 1924: 20; Nutting 1919: 77; Rodriguez 1980: 287; Abele and Kim 1986: 47, 524 fig. c, d; Wagner 1990: 29–32, figs 32–35; Melo 1996: 239, unnumbered fig.; Ng et al. 2008: 120; Alves et al. 2012: 943, fig. 3C; Carmona-Suárez and Poupin 2016: 373, fig. 6I.

Mithrax verrucosus variety — Rathbun 1898: 259.

Mithrax (*Mithrax*) *verrucosus* — Young 1900: 93; Rathbun 1925: 400, pl. 144; 1933: 30; Boone 1927: 39; Williams 1965: 255, figs 235, 245B; 1984: 336, figs 271, 275c; Coelho and Ramos 1972: 215; Collins and Morris 1976: 119, pl. 17, fig. 7, pl. 18, figs 5–7; Powers 1977: 58; Keith 1985: 259, fig. 5E.

Mithrax plumosus Rathbun, 1901: 67 [type-locality: Puerto Real, Puerto Rico; holotype in USNM 23775].

Amphithrax aculeatus — Assugeni et al. 2017: 1630, tab. 1; Mantelatto et al. 2020: 39; Lianos et al. 2021: 1–19, figs 1, 11; Ortiz 2022: 34, fig. 14C (not *Cancer aculeatus* Herbst, 1790).

Amphithrax verrucosus — Poupin 2018: 193, fig. 211; Questel 2019: 16, unnumbered figure; Parasram et al. 2023: 21, fig. 9D.

Material examined. **Type material.** Holotype of *Mithrax plumosus* Rathbun, 1901: Puerto Rico, Port Real, Vieques, Fish Hawk Expedition • 1 ovig., ♀ (CW: 37.0 mm; CL: 29.0 mm) (USNM 23775), 18°7'29.8956"N, 65°26'31.6428"W.

Additional material. USA, Florida, Big Pine Key • 3 ♂♂, 3 ♀♀, 3 ovig. ♀♀ (USNM 14030), 24°40'11.514"N, 81°21'14.2884"W. Florida • 8 ♂♂, 3 ovig. ♀♀ (MCZ 353), 27°59'39.8472"N, 81°45'36.9144"W. Idem, 1 ♂, 1 juv. ♀ (MCZ unnumbered), 27°59'39.8472"N, 81°45'36.9144"W. Idem, 1 juv. ♀ (CW: 34.0 mm; CL: 20.0 mm) (ULLZ 4534), 27°59'39.8472"N, 81°45'36.9144"W. Idem, 1 ♂ (ULLZ 13956), 27°59'39.8472"N, 81°45'36.9144"W. Idem, Florida Keys • 1 ovig. ♀ (CW: 56.0 mm; CL: 42.0 mm) (ULLZ 15294), 24°41'29.0472"N, 81°11'22.8552"W. Idem, Big Pine Key • 1 ♂ (ULLZ 11924), 24°40'11.514"N, 81°21'14.2884"W. Idem, Loggerhead Key • 1 ♂ (CW: 67.0 mm; CL: 53.0 mm) (ULLZ 11736), 24°63'23.745"N, 82°92'06.767"W. Idem, Dry Tortugas • 1 ♂ (USNM 69068), 24°62'82"N, 82°87'32"W. Belize, Carrie Bow Cay Reef • 1 ♂ (CW: 10.0 mm; CL: 8.0 mm) (ULLZ 9148), 17°29'51.77"N,

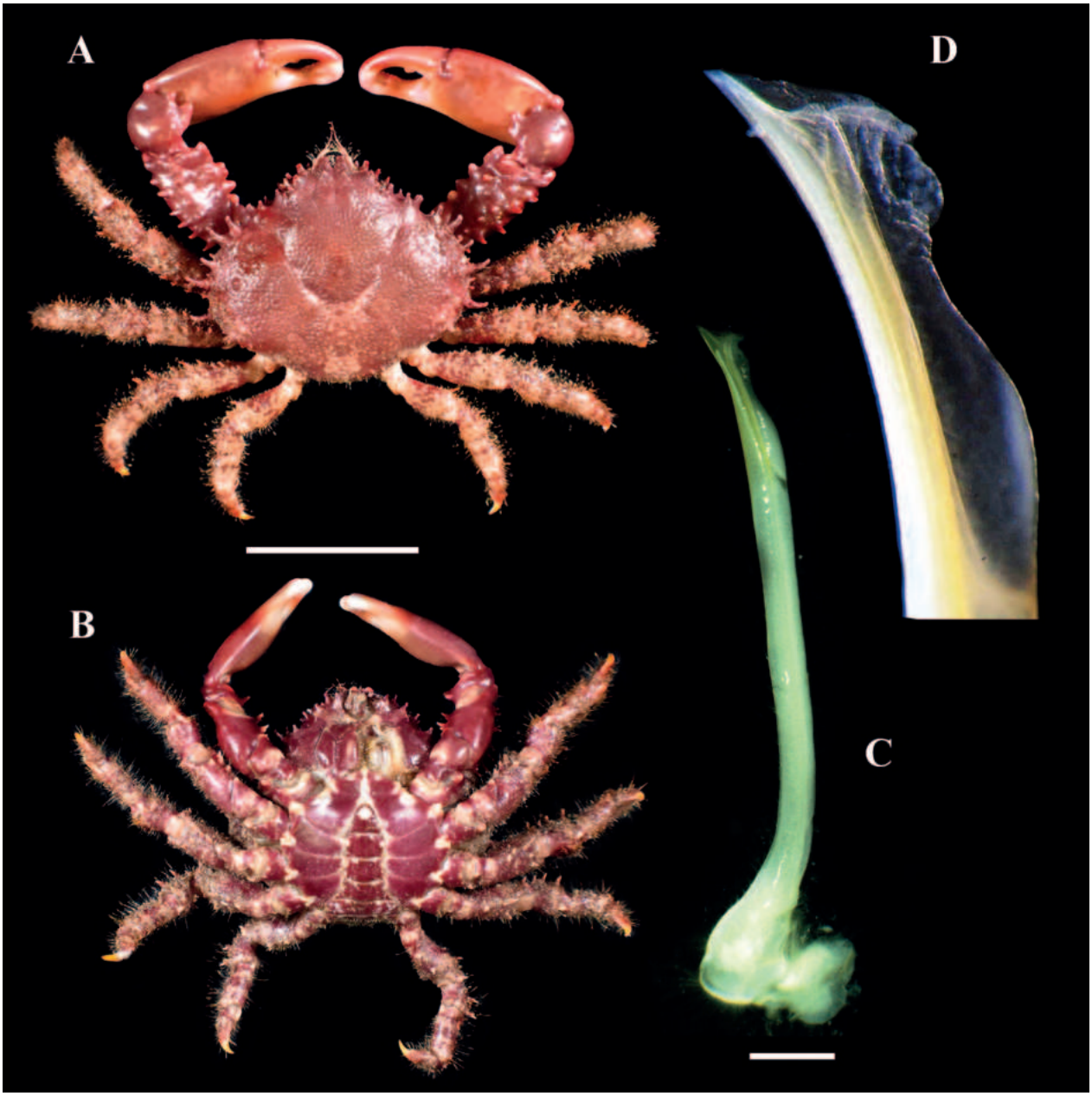

Figure 4. *Amphithrax verrucosus* (H. Milne Edwards, 1832) adult male (BLSZ 218). **A.** Habitus, dorsal; **B.** Ventral view, locality: Barbados; **C.** Pleonal view of left G1 (BLSZ 228); **D.** Distal third of left G1. Scale bars: 20 mm (**A, B**); 10 mm (**C**). Photos: Nadeshinie Parasram.

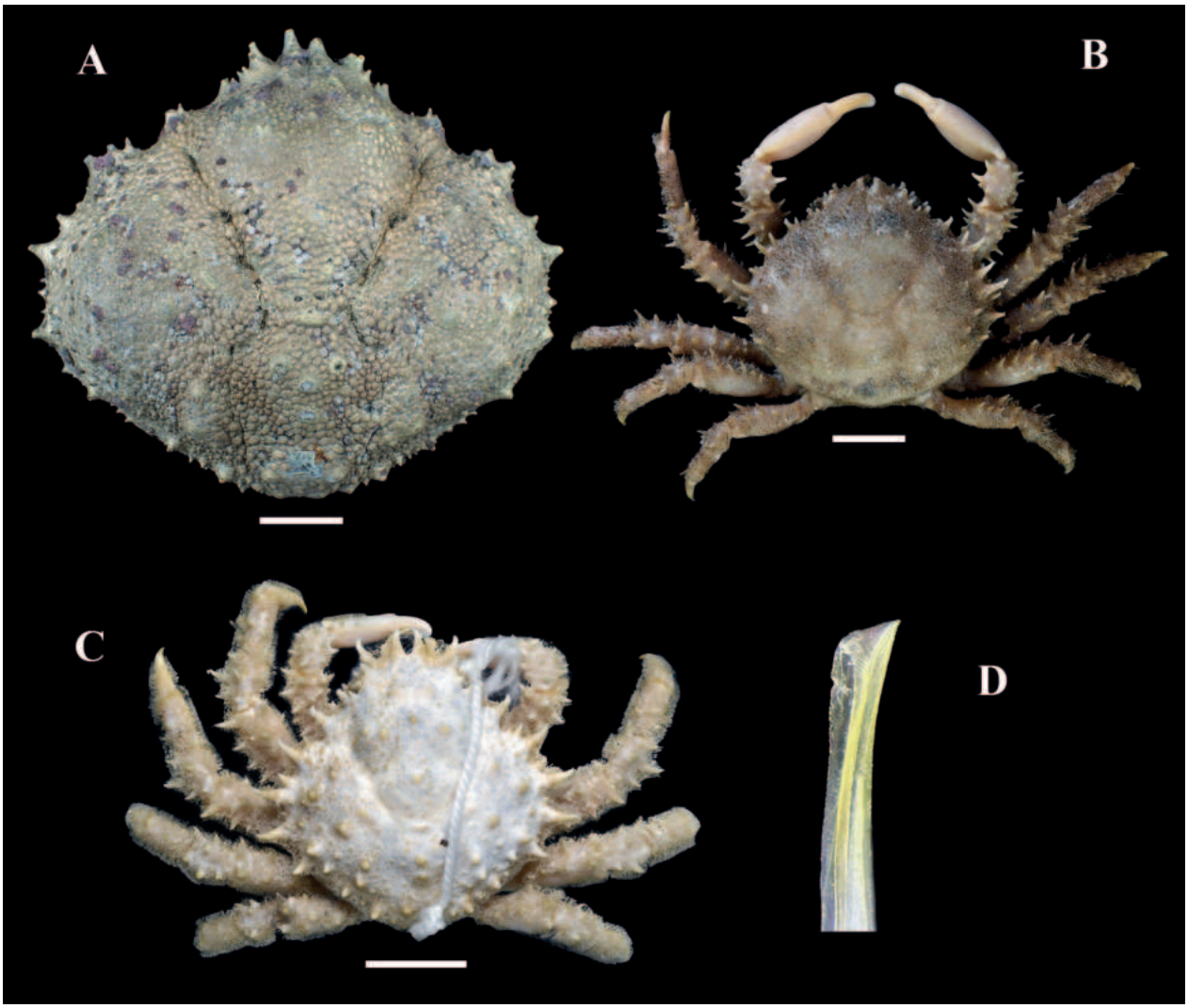

Figure 5. Type specimens. **A.** Paralectotype of *Cancer aculeatus*, Herbst, 1790, dry preserved carapace without setae and with most of the spines broken (ZMB Herbst 79), locality: Antilles; **B.** Holotype of *Mithrax plumosus* Rathbun, 1901 (USNM 23775), ovig. female (CW: 37.0 mm; CL: 29.0 mm), locality: Puerto Rico; **C.** Holotype of *Mithrax pilosus* Rathbun, 1892, setae on carapace removed (USNM 16299), male (CW: 30.0 mm; CL: 28.0 mm), locality: Bahamas; **D.** Distal third of the right G1 of the holotype of *Mithrax pilosus* (USNM 16299) in pleonal view. Photos: **A** Kristina von Rintelen. **B, C, D** Amanda Windsor.

88°11'11.95"W. Honduras, Swan Island • 1 ♂ (USNM 15074). Guadeloupe, Pointe Baham, MADIBENTHOS • 1 ♂ (MNHN-IU-2016-10018), 14°24'42.9984"N, 60°50'4.9956"W. Martinique, Point Jacob, MADIBENTHOS • 1 ♀ (MNHN-IU-2017-10364), 14°36'8.0028"N, 60°48'57.996"W. Barbados, Palm Court, St. Michael • 1 ♀ (CW: 31.6 mm; CL: 24.0 mm) (BLSZ 225). Idem, 1 ovig. ♀ (CW: 26.2 mm; CL: 22.0 mm) (BLSZ 227), nearshore rubble, 13°04'30.73"N, 59°36'12.49"W. Idem, 1 ♂ (CW: 26.7 mm; CL: 22.0 mm) (BLSZ 228). Idem, 1 ♀ (CW: 31.4 mm; CL: 24.5 mm) (BLSZ 328). Idem, 1 juv. ♀ (CW: 12.4 mm; CL: 12.0 mm) (BLSZ 332). Idem, 1 ♂ (CW: 24.5 mm; CL: 23.0 mm) (BLSZ 229). Idem, 1 ♀ (CW: 30.2 mm; CL: 25.6 mm) (BLSZ 251). Idem, 1 ♂ (CW: 21.1 mm; CL: 18.2 mm) (BLSZ 226). Drill Hall, St. Michael • 3 ♀, 1 ♂ (CW: 27.1; 11.3; 5.3 mm; CL: 22.0; 12.5; 6.0) (BLSZ 123), nearshore rubble, 13°04'36.30"N, 59°36'26.63"W. Idem, 1 ♀ ovig., (CW: 26.4 mm; CL: 27.5 mm) (BLSZ 266). Idem, 1 ♂ (CW: 27.2 mm; CL: 22.0 mm) (BLSZ 265). Idem, 1 ♂ (CW: 35.1 mm; CL: 27.4 mm) (BLSZ 250). Idem, 1 ovig., ♀ (CW: 31.6 mm; CL: 25.7 mm) (BLSZ 249). Idem, 12 ♂♂, 3 ♀♀, 2 juv., ♀♀ (CW: 7.5 mm; 14.3 mm; 16.6 mm; 22.0 mm; 14.2 mm; 13.6 mm; 23.5 mm; 8.5 mm; 22.0 mm; 15.2 mm; 15.0 mm; 20.3 mm; 24.0 mm; 25.7 mm; 17.4 mm; 20.0 mm; 15.0 mm; CL: 7.0 mm; 13.1 mm; 15.0 mm; 18.4 mm; 12.6 mm; 12.7 mm; 19.1 mm; 7.0 mm; 19.0 mm; 14.8 mm; 14.0 mm; 17.0 mm; 20.0 mm; 21.0 mm; 20.5 mm; 17.0 mm;13.6 mm) (BLSZ 278). Batts Rock, St. Michael • 1 ♂ (CW: 26.7 mm; CL: 21.5 mm) (BLSZ 165) subtidal, 13°08'04.81"N, 59°38'12.30"W. Idem, 1 ♂ (CW: 40.5 mm; CL not taken) (MZUSP 40921). Coconut Court, Christ Church • 2 ♂♂, 1 ♀, 1 ovig., ♀ (CW: 16.7 mm; 6.0 mm; 15.5 mm; 20.0 mm; CL: 15.5 mm; 6.4 mm; 14.7 mm; 22.8 mm) (BLSZ 211), nearshore rubble, 13°04'31.59"N, 59°36'13.78"W. Trinidad and Tobago, Chacachacare, Rusts Bay • 1 ♂ (CW: 42.0 mm; CL: 33.0 mm) (USNM

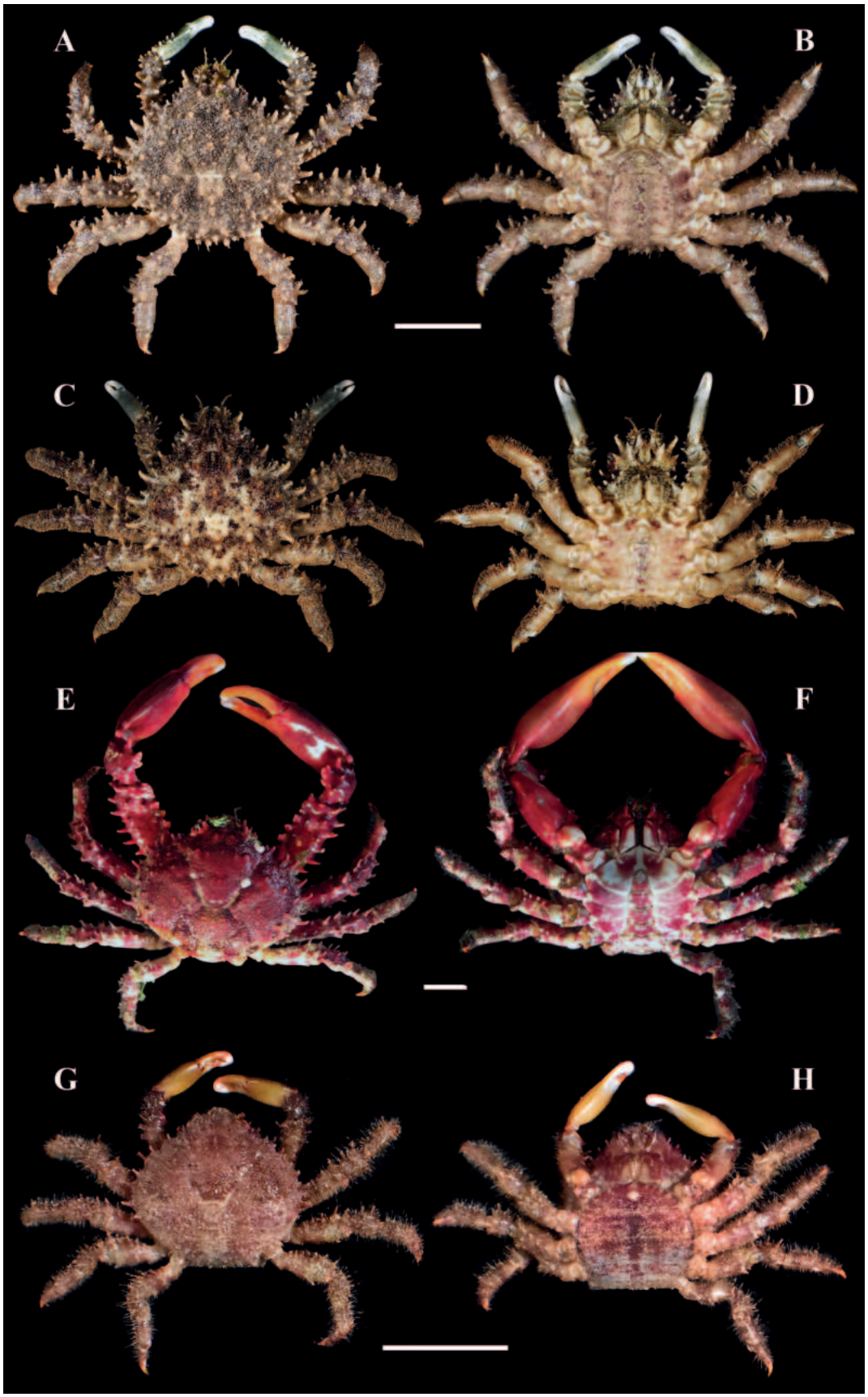

Figure 6. Colour in life. Young female of *Amphithrax aculeatus* (Herbst, 1790) (BLSZ 217), Barbados. **A.** Habitus dorsal view; **B.** Ventral view. Adult male of *Amphithrax aculeatus* (Herbst, 1790) (MNHN-IU-2013-5929), Guadeloupe; **C.** Habitus, dorsal view; **D.** Ventral view. Adult male of *Amphithrax verrucosus* (H. Milne Edwards, 1832) (GIC 072), Venezuela; **E.** Habitus, dorsal view; **F.** Ventral view. Female of *Amphithrax verrucosus* (H. Milne Edwards, 1832) (BLSZ 328), Barbados; **G.** Habitus, dorsal view; **H.** Ventral view. Scale bars: 20 mm. Photos: **A, B, G, H.** Nadeshinie Parasram. **C, D.** Joseph Poupin. **E, F.** William Santana.

137759), 10°40'59.99"N, 61°44'59.99"W. Venezuela, Isla de Coche, Bajo Culebra • 2 ♀♀, 3 ♂♂ (GIC 072), 10°46'21.59"N, 63°56'24.59"W. Idem, 1 ♂ (LSZ 012), 10°46'21.59"N, 63°56'24.59"W. Isla de Cubagua • 1 ♂, 1 ♀ (LSZ 012), 10°49'4.79"N, 64°10'34.20"W. Brazil, Rio Grande do Norte, Atoll das Rocas • 1 ♂ (MZUSP 15323), 3°51'59.99"N, 33°48'59.99"W. Idem, 1 ♂ (MZUSP 24761), 3°51'59.99"N, 33°48'59.99"W. Idem, 2 ♂ (MNRJ 15609), 3°51'59.99"N, 33°48'59.99"W. Idem, 3 ♂♂, 1 ovig., ♀ (MNRJ 4782), 3°51'59.99"N, 33°48'59.99"W. São Paulo, Ilha Vitória • 3 ♂♂ (MZUSP 16708), 20°19'9.98"N, 40°20'16.01"W.

Diagnosis. Dorsal surface of carapace uniformly covered with closely-set granules of irregular size; there are a few blunt tubercles on the gastric, branchial and cardiac regions; spines are only present in the lateral margins. In fully developed males chelipeds massive, carpus dorsally smooth with few blunt, short tubercles dorsolaterally in some specimens, strong teeth on inner margins and the palm of the cheliped is smooth. Propodi of pereopods are without spines, but have the presence of long and short dark setae. Carapace is predominantly maroon in colour.

Remarks. Much of the ambiguity surrounding *A. aculeatus* and *A. verrucosus* originated when Rathbun described *Mithrax pilosus* and *M. plumosus* (Rathbun 1892, 1901; Fig. 5B, C). These descriptions were based on small specimens, which naturally appear more similar than their fully matured counterparts. Additionally, Windsor and Felder (2014) based their decision on very small juvenile specimens, mistakenly identified as *A. aculeatus* (see Suppl. material 2 in supplementary material and phylogenetic section of this work). Despite the similarities observed in younger specimens, the distinct morphological characteristics presented should suffice to prevent any further confusion between the two species.

The G1 of *A. verrucosus* was described in detail by Lianos et al. (2021) under the name *A. aculeatus* and by Wagner (1990) as *Mithrax verrucosus* (see also remark section for *A. aculeatus*).

Ontogenetic intraspecific variations in *A. verrucosus* from juveniles to adults are: juvenile specimens have short and long setae that are evenly distributed on the carapace, cheliped and third maxillipeds, while adults have much less setae or are devoid of setae in these regions. Some very small specimens may have few spines on the carapace, especially on branchial regions. Anterolateral margins with six to eight spines on juveniles, whereas adults have eight spines. Younger specimens and females with strong short spines dorsally on the carpus of the cheliped, which are not present in fully developed adults, remaining only inner carpal spines. The carapace spines on the branchial region, along with the spines dorsally on carpus in young specimens may have led some authors to confuse *A. verrucosus* with *A. aculeatus*. It is important to note that even in very small specimens, the palm of the cheliped and the propodus of pereopods in *A. verrucosus* lack spines. *Amphithrax verrucosus* is very abundant in Barbados as well and specimens were collected by hand and with caged crab traps on the west and south coasts of Barbados. Parasram et al. (2023), reported *Amphithrax verrucosus* as being found in close association with *A. aculeatus*, *Mithraculus coryphe* (Herbst, 1801), *Mithraculus forceps* A. Milne-Edwards, 1875, *Eriphia gonagra* (Fabricius, 1781) and *Pachygrapsus transversus* (Gibbes, 1850). Females of this species are generally smaller than males (see materials examined). Ovigerous females were collected in June and September 2021.

Colouration. Colour in life for *A. verrucosus* is carapace predominantly maroon and maroon mixed with white spots on ventral surface. Some specimens are more brownish, with light spots on the carapace (MNHN-IU-2016-10018) and some adult females have a light brown carapace (MNHN-IU-2017-10364). The chelipeds range from a dark maroon, greenish-brown to a lighter brown hue; in ventral view, only the tip of the fingers is whitish (Figs 4A, 6 E–H) (see also fig. 3G of Windsor and Felder (2014).

Distribution. Western Atlantic: USA (South Carolina to Florida), Gulf of Mexico, Cuba, Jamaica, Puerto Rico, Virgin Islands, St. Maarten, Honduras, Antigua, Belize, Guadeloupe, Isla de Aves, Martinique, Barbados, Grenada, Trinidad and Tobago, Bonaire, Curaçao, Aruba, Colombia, Venezuela, and Brazil, from Fernando de Noronha to São Paulo (Rathbun 1925; Carmona-Suárez and Poupin 2016; Poupin 2018; present study).

Discussion

Windsor and Felder (2014) recommended that *A. verrucosus* should be regarded as a junior subjective synonym of *A. aculeatus* citing substantial intraspecific morphological variation as the basis for their assertion. However, their comparisons were constrained by the limited number of specimens, all misidentified and they heavily relied on the original illustration from Herbst (1790). Upon thorough examination of comprehensive comparative materials, the morphological and molecular data detailed herein advocates for the recognition of *Amphithrax aculeatus* and *A. verrucosus* as distinct species.

Wagner (1990) was the first to study the G1 of *A. aculeatus* (as *Mithrax pilosus*) and *A. verrucosus* (as *Mithrax verrucosus*) showing the differences between both species. Our findings align with Wagner's (1990) observations. On the other hand, Windsor and Felder (2014) overlooked these nuanced disparities when synonymising the two species. This oversight may shed light on the subsequent conflation of *A. verrucosus* with *A. aculeatus*, especially given the pronounced differentiation in the G1 of each species.

Specimens of *A. aculeatus* are a close match to the plate of *Cancer aculeatus* by Herbst (1790) and *Mithrax pilosus* by Rathbun (1892) (Figs 3, 5A, C, D), whereas specimens of *A. verrucosus* resemble the plate of *Mithrax verrucosus* by H. Milne Edwards (1832) and *Mithrax plumosus* by Rathbun (1901) (Figs 4, 5B). Windsor and Felder's (2014: figs 3G, 4H) images of habitus and third maxilliped of a presumed *A. aculeatus* specimen are, in fact, a specimen of *A. verrucosus* (see Figs 4A, D, 6E–H in the present work).

Although the phylogenetic analysis performed supports the monophyly of the genus *Amphithrax*, the ML shows low support for this topology in contrast with the BI analysis (ML = 52%, Pp = 0.99). Nevertheless, the molecular separation of *A. aculeatus* and *A. verrucosus* as two different species and sister taxa is well supported and, in our phylogenetic tree, both species occupy distinct phylogenetic clusters (Fig. 2). Additionally, the divergence observed in ULLZ 13596 and MOBR-C-1529 can be attributed solely to the presence of 16S sequence alone in the dataset, no 12S or ITS-1 sequences being available for these specimens. A similar scenario is observed for ULLZ 4534 and 9148, where the divergence of these sequences in the phylogenetic tree is solely due to 12S and 16S sequences in the dataset. Our study presents the first molecular data for *A. aculeatus* and, additionally, we also provide ITS-1 sequences for *A. verrucosus*, thereby contributing valuable molecular insights for both species. The phylogenetic analysis of Windsor and Felder (2014) contained sequence data from *A. verrucosus* (see Suppl. material 2), which they misidentified as *A. aculeatus*. Our phylogenetic analysis was based on sequence data from both *A. aculeatus* and *A. verrucosus*. The inclusion of both species in our in our study produced different results than those obtained by Windsor and Felder (2014). *Amphithrax* in its majority is an Amphiamerican genus, with only *A. caboverdianus* found exclusively in the eastern Atlantic. The phylogenetic results are consistent with the conclusions drawn by Windsor and Felder (2014) and Ng et al. (2018) with *A. caboverdianus* occupying a basal position to *A. aculeatus* and *A. verrucosus* with relatively high support (ML = 79%, Pp = 0.926).

The phylogenetic analysis suggests that the taxonomic assignment of *Amphithrax armatus* within the *Amphithrax* is questionable. *Amphithrax armatus* aligns with species of *Maguimithrax* and *Mithrax*; however, the support for this relationship is low. Ng et al. (2018) also questioned the placement of *A. armatus* in *Amphithrax*, based on their morphological and phylogenetic analysis, which shows a close phylogenetic relationship of *A. armatus* to *Ala* Lockington, 1877 and *Nonala* Windsor & Felder, 2014. Nevertheless, the overall morphology of the carapace, third maxilliped and G1 of species within *Ala* and *Nonala* are very different when compared to *A. armatus*. Given that our phylogenetic analysis encompasses only sequences from 12S and 16S and lacks representatives from *Ala* and *Nonala*, this might account for the discrepancies observed between our study and Ng et al. (2018) results.

Windsor and Felder (2014) commented on the wide degree of morphological variations seen in *Amphithrax* and mentioned the possible removal of some species of *Amphithrax*. Although our study indicates that *A. armatus* may not belong to *Amphithrax*, we have opted to retain its classification for the time being as suggested by Ng et al. (2018). It is important to note that our study did not encompass a comprehensive revision of the entire *Amphithrax*. Therefore, to address these questions definitively, further-in-depth analysis of all species of *Amphithrax* incorporating both molecular and morphological evidence, as indicated by our results, is necessary. These suggestions were also mentioned by Windsor and Felder (2014) and Ng et al. (2018).

Conclusions

Our study underscores the importance of employing an approach that incorporates both morphology and molecular analysis in biodiversity research. We also emphasise the importance of utilising morphological characters such as the G1 in Brachyura for species identification in taxonomic studies.

Based on the evidence provided, we proposed a taxonomic revaluation, elevating *A. verrucosus* from junior subjective synonym to valid species status. This would bring the total number of species in the genus *Amphithrax*, *sensu stricto* to 11: *A. aculeatus*, *A. armatus*, *A. bellii* (Gerstaecker, 1857), *A. besnardi* (Melo, 1990), *A. braziliensis* (Rathbun, 1892), *A. caboverdianus*, *A. clarionensis* (Garth, 1940), *A. hemphilli* (Rathbun, 1892), *Amphithrax leucomelas* (Desbonne, in Desbonne & Schramm, 1867), *A. tuberculatus* (Stimpson, 1860), and *A. verrucosus* (H. Milne Edwards, 1832).

Additionally, the information provided in our study contributes to the existing body of data (morphological and molecular) that can be valuable for future taxonomic investigations within the superfamily Majoidea and biodiversity research in Caribbean Island hotspots.

Acknowledgements

We are indebted to Dr. Angela Fields for assistance with specimen collection. The authors would like to thank Mr. Kirk Mayers, Dr. Darren Brown and Ms. Kim Ashby for their assistance with laboratory equipment. We thank Professor Julia Horrocks for reviewing an earlier draft of this MS. We are also thankful to Ms. Tassia Turini, Dr. Jessica Colavite, Laira Lianos, Michelle Mollemberg and other members of the LSZ Laboratory in Brazil for their assistance with the Barbados material and Professor Marcos Tavares and his team at the Museum of University of São Paulo, Brazil, for their assistance with the cataloguing of brachyuran crab specimens from Barbados. We would also like to thank Dr. Laure Corbari, Professor Joseph Poupin and Dr. Kristina von Rintelen from MNHN and ZMB, respectively, for their assistance with type specimens. NP is especially thankful for the support and guidance from Dr. Angela Alleyne and Professor Julia Horrocks. Funding for this research was provided by the University of the West Indies, Cave Hill Campus, via two Campus Research Awards to NP. WS thanks the following grants: Fundação Cearense de Apoio ao Desenvolvimento Científico e Tecnológico (FUNCAP) (#PV1-0187-00033.01.00/21 and #6647309/2017) and Conselho Nacional de Desenvolvimento Científico e Tecnológico (CNPq) for financial support (PQ2 #315185/2020-1). This work greatly benefited from the comments of the reviewers Bee Yan Lee (Na-

tional University of Singapore), Darryl Felder (University of Louisiana at Lafayette), Marcos Tavares (University of São Paulo) and the subject editor Sammy De Grave (Oxford University Museum of Natural History).

References

Abele LG, Kim W (1986) An Illustrated Guide to the Marine Decapod Crustaceans of Florida (Vol. 8). Florida Department of Environemtal Regulation, Technical Series, 760 pp.

Alves DFR, Barros-Alves SP, Cobo VJ, Lima DJM, Fransozo A (2012) Checklist of the brachyuran crabs (Crustacea: Decapoda) in the rocky subtidal of Vitória Archipelago, southeast coast of Brazil. Check List 8(5): 940–950. https://doi.org/10.15560/8.5.940

Assugeni CO, Magalhaes T, Tudge CC, Bolanos J, Mantelatto FL, Zara FJ (2016) Spermiotaxonomy of the spider crabs Mithracidae (MacLeay, 1838): Integrative analyses based on morphological and molecular data. National Library of Medicne National Center for Biotechnology Information, 107 pp. https://repositorio.unesp.br/bitstream/handle/11449/151086/assugeni_co_me_svic_int.pdf?sequence=6&isAllowed=y

Assugeni CO, Magalhães T, Bolanos JA, Tudge CC, Mantelatto FL, Zara FJ (2017) Ultrastructure of spermatozoa of spider crabs, family Mithracidae (Crustacea, Decapoda, Brachyura): Integrative analyses based on morphological and molecular data. Journal of Morphology 278(12): 1628–1646. https://doi.org/10.1002/jmor.20737

Baeza AJ, Bolaños JA, Fuentes S, Hernandez JE, Lira C, López R (2010) Molecular phylogeny of enigmatic Caribbean spider crabs from the Mithrax–Mithraculus species complex (Brachyura: Majidae: Mithracinae): ecological diversity and a formal test of genera monophyly. Journal of the Marine Biological Association of the United Kingdom 90(4): 851–858. https://doi.org/10.1017/S0025315409991044

Boone L (1927) Crustacea from Tropical East American Seas. Scientific Results of the First Oceanographic Expedition of the "Pawnee" 1925 (Vol. 1). 147 pp.

Calado R, Lin J, Rhyne AL, Ricardo A, Narciso L (2003) Marine Ornamental Decapods–Popular, Pricey, and Poorly Studied. Journal of Crustacean Biology 23(4): 963–973. https://doi.org/10.1651/C-2409

Carmona-Suárez, Poupin J (2016) Majoidea crabs from Guadeloupe Island, with a documented list of species for the Lesser Antilles (Crustacea, Decapoda, Brachyura, Majoidea). Zoosystema 38: 353–387. https://doi.org/10.5252/z2016n3a5

Chu K, Li C, Ho H (2001) The first internal transcribed spacer (ITS-1) of ribosomal DNA as a molecular marker for phylogenetic and population analyses in Crustacea. Marine Biotechnology 3(4): 355–361. https://doi.org/10.1007/s10126001-0014-5

Coelho PA, Ramos MDA (1972) A constituição e a distribuição da fauna de decápodos do litoral leste da América do Sul entre as latitudes de 5°N e 39°S. Trabalhos Oceanograficos da Universidade Federal de Pernambuco 13(1): 133–236. https://doi.org/10.5914/tropocean.v13i1.2555

Collins JSH, Morris SF (1976) Tertiary and Pleistocene crabs from Barbados and Trinidad. Palaeontology 19: 107–131.

Cruz-Castaño N, Campos N, Hernando (2003) Los cangrejos Araña (Decapoda: Brachyura: Majoidea) del Caribe colombiano. Biota Colombiana 4: 261–269. https://www.redalyc.org/pdf/491/49140208.pdf

Davie PJF, Guinot D, Ng PKL (2015a) Anatomy and functional morphology of Brachyura. In: Castro P, Davie PJF, Guinot D, Schram FA, von Vaupel Klein JC (Eds) Treatise on Zoology-Anatomy, Taxonomy, Biology The Crustacea. Brill, Boston, 11–163. https://doi.org/10.1163/9789004190832_004

Davie PJF, Guinot D, Ng PKL (2015b) Systematics and classification of Brachyura. In: Treatise on Zoology-Anatomy, Taxonomy, Biology The Crustacea, Volume 9 Part C. Brill, 1049–1130. https://doi.org/10.1163/9789004190832_021

Desbonne I, Schramm A (1867) Crustacés de la Guadeloupe, d'apres un manuscrit du Docteur Isis Desboonne comparé avec les échantillons de Crustacés de sa collection et les dernieres publications de MM. Henri de Saussure et William Stimpson. Premiere partie. Brachyures. Imprimerie de Government, Bass-Terre, 60 pp. https://doi.org/10.5962/bhl.title.10000

Desmarest AG (1825) Considérations générales sur la classe des Crustacés, et description des espèces de ces animaux, qui vivent dans la mer, sur les côtes, ou dans les eaux douces de la France. Paris and Strasbourg, Paris, 446 pp. https://doi.org/10.5962/bhl.title.39846

García YLD, Capote AJ (2015) List of marine crabs (Decapoda: Anomura and Brachyura) of shallow littoral of Santiago de Cuba, Cuba. Check List 11: e1601. https://doi.org/10.15560/11.2.1601

Guinot D (1967) Recherches préliminaires sur les groupements naturels chez les Crustacés Décapodes Brachyoures. III. A propos des affinités des genres Dairoides Stebbing et Daira de Haan. Bulletin du Museum National d'Histoire Naturelle, Paris, ser 2 39(2): 345–374.

Guinot D, Tavares M (2003) A new subfamilial arrangement for the Dromiidae de Haan, 1833, with diagnoses and descriptions of new genera and species (Crustacea, Decapoda, Brachyura). Zoosystema 25: 43–129.

Guiomar R, González-Gurriarán E, Fernández L, Benhalima K, Ribes E (2007) Ovarian maturation of the multi-spawning spider crab *Maja brachydactyla* (Decapoda: Majidae) with special reference to yolk formation. Marine Biology 152(2): 383–394. https://doi.org/10.1007/s00227-007-0688-y

Herbst JFW (1782–1804) Versuch einer Naturgeschichte der Krabben und Krebse, nebst einer systematischen Beschereibung ihrer verschiedenen Arten (Vol. 3(4)), Berlin and Stralsund, 274 pp. [271–226, 271–216 pp.] https://doi.org/10.5962/bhl.title.62813

Huelsenbeck JP, Ronquist F (2001) MRBAYES: Bayesian inference of phylogenetic trees. Bioinformatics 17(8): 754–755. https://doi.org/10.1093/bioinformatics/17.8.754

Hultgren KM, Stachowicz JJ (2008) Molecular phylogeny of the brachyuran crab superfamily Majoidea indicates close congruence with trees based on larval morphology. Molecular Phylogenetics and Evolution 48(3): 986–996. https://doi.org/10.1016/j.ympev.2008.05.004

Jarquín-González J, Valdez-Moreno M, Rosas-Luis R (2022) An approach to the diversity of Achelata and Brachyura (Crustacea, Decapoda) from the Southern Mexican Caribbean. Diversity 14(8): 1–12. https://doi.org/10.3390/d14080649

Katoh K, Standley MD (2013) MAFFT Multiple Sequence Alignment Software Version 7: Improvements in Performance and Usability. Molecular Biology and Evolution 30(4): 772–780. https://doi.org/10.1093/molbev/mst010

Keith D (1985) Shallow-water and terrestrial brachyuran crabs of Roatan and the Swan Islands, Honduras. Sarsia 70(4): 251–278. https://doi.org/10.1080/00364827.1985.10419681

Kingsley JS (1879) Notes on North American Decapoda. Proceedings of the Boston Society of Natural History 20: 145–160. https://publikationen.ub.uni-frankfurt.de/frontdoor/index/index/year/2009/docId/11679

Klompmaker AA, Portell RW, Klier AT, Prueter V, Tucker AL (2015) Spider crabs of the Western Atlantic with special reference to fossil and some modern Mithracidae. PeerJ 3: e1301. https://doi.org/10.7717/peerj.1301

Lianos L, Mollemberg M, Zara J Fernando, Tavares M, Santana W (2021) SEM studies on first and second gonopod morphology in Mithracidae (Decapoda: Brachyura). Naupilus 29: 1–19. https://doi.org/10.1590/2358-2936e2021039

Lira C, Fernández D, Bolaños J, Hernández G, Hernández-Ávila I (2013) Contribuciones al conocimiento de la biodiversidad de crustáceos Decápodos de Venezuela. I. Primeros registros de *Macrocoeloma concavum* Miers 1886 y *Microphrys interruptus* Rathbun 1920 (Brachyura: Majoidea: Majidae). Boletín del Centro de Investigaciones Biológicas 47: 47–62.

Manning RB, Chace FA (1990) Decapod and stomatopod Crustacea from Ascension Island, South Atlantic Ocean. Smithsonian Contributions to Zoology 503: 1–91. https://doi.org/10.5479/si.00810282.503

Mantelatto FL, Tamburus AF, Magalhães T, Buranelli RC, Terossi M, Negri M, Castilho AL, Costa RC, Zara FJ (2020) Checklist of decapod crustaceans from the coast of the São Paulo state (Brazil) supported by integrative molecular and morphological data: III. Infraorder Brachyura Latreille, 1802. Zootaxa 4872(1): 1–108. https://doi.org/10.11646/zootaxa.4872.1.1

Martens von E (1872) Uber kubanische Crustaceen nach den Sammlungen Dr. J. Gundlach's. Archiv fur Naturgeschichte 38: 77–147. [+257+258, pls. 144–145.]

McLay CL (2020) Camouflage by the masking crab, *Notomithrax ursus* (Herbst, 1788) (Decapoda: Brachyura: Majidae): is it a decorator or a dressmaker? The Journal of Crustacean Biology 40: 673–683. https://doi.org/10.1093/jcbiol/ruaa076

Melo GAS (1996) Manual de Identificação dos Brachyura (Caranguejos e Siris) do Litoral Brasileiro. Plêiade, São Paulo, 603 pp.

Miers EJ (1886) Report on the Brachyura Collected by H.M.S. "Challenger" during the Years 1873–1876. Report on the Scientific results of the Voyage of H.M.S. "Challenger" during the Years 1873–76. Zoology 17(49): 1–362.

Milne-Edwards H (1832) Observations sur les Crustacés du genre *Mithrax*. Magasin de Zoologie 2(7): 1–5.

Milne-Edwards A (1873–1881) Études sur les xiphosures et les crustacés de la région mexicaine. Mission scientifique au Mexique et dans l'Amérique centrale, recherches zoologiques, sous la direction de M. Milne Edwards (Vol. 1), Imprimerie nationale, Paris, 368 pp. https://doi.org/10.5962/bhl.title.119681

Milne Edwards H (1834–1840) Histoire naturelle des Crustacés, comprenant l'anatomie, la physiologie et la classification de ces animaux (Vols 1–3), Roret, Paris, (1) 468, (462) 532, (463) 638 pp.

Ng PKL, Guinot D, Davie PJF (2008) Systema Brachyurorum: Part I. An annotated checklist of extant brachyuran crabs of the world. The Raffles Bulletin of Zoology 17: 1–286.

Ng PKL, Ho P-H, Lin C-W, Yang C-H (2018) The first record of an eastern Pacific invasive crab in Taiwanese waters: *Amphithrax armatus* (Saussure, 1853) (Brachyura: Majoidea: Mithracidae), with notes on the taxonomy of the genus. Journal of Crustacean Biology 38(2): 198–205. https://doi.org/10.1093/jcbiol/rux109

Nutting CC (1919) Barbados-Antigua expedition; narrative and preliminary report of a zoological expedition from the University of Iowa to the Lesser Antilles under the auspices of the Graduate College. Vol. VIII,University of Iowa Studies in Natural History, Iowa City, 244 pp. https://doi.org/10.5962/bhl.title.12289

Ortiz M (2022) Illustrated keys for the clasification of the Cuban marine and estuarine crabs (Malacostraca: Brachyura) II. Revista de Investigaciones Marinas 42: 21–37. https://doi.org/10.5281/zenodo.7407423

Palumbi S, Martin S, Romano S, McMillian W, Stice L, Grabowski G (1991) Simple Fool's Guide to PCR. Department of Zoology and Kewalo Marine Laboratory, University of Hawaii, Honolulu, 45 pp.

Parasram N, William S, Vallès H (2023) Checklist of the shallow-water marine Brachyura (Crustacea: Decapoda) of Barbados, West Indies. Zootaxa 5314: 001–062. https://doi.org/10.11646/zootaxa.5314.1.1

Poupin J (2018) Les Crustacés décapodes des Petites Antilles: Avec de nouvelles observations pour Saint-Martin, la Guadeloupe et la Martinique. Publications scientifiques du Muséum National d'histoire Naturelle, Paris.

Powers LW (1977) A catalogue and bibliography to the crabs (Brachyura) of the Gulf of Mexico. Contributions in Marine Science 20: 1–90.

Questel K (2019) Les Crabes et Anomoures de Saint-Barthélemy (Vol. 5).

Rathbun MJ (1892) Catalogue of the crabs of the family Periceridae in the U. S. National Museum. Proceedings of the United States National Museum 15: 231–277. [pls, 228–240.] https://doi.org/10.5479/si.00963801.15-901.231

Rathbun MJ (1897) List of the Decapod Crustacea of Jamaica. Annales of the Institute of Jamaica 1: 1–46.

Rathbun MJ (1898) The Brachyura of the biological expedition to the Florida Keys and the Bahamas in 1893. Bulletin from the Laboratories of Natural History. State University of Iowa 4: 250–294.

Rathbun MJ (1901) The Brachyura and Macrura of Porto Rico. US Fish Commission Bulletin for 1900 2: 1–137.

Rathbun MJ (1925) The spider crabs of America. Bulletin – United States National Museum 129(129): 1–613. https://doi.org/10.5479/si.03629236.129.i

Rathbun MJ (1933) Brachyuran crabs of Porto Rico and the Virgin Islands. Scientific survey of Porto Rico and the Virgin Islands 15: 5–121. https://doi.org/10.5962/bhl.title.10214

Rodríguez G (1980) Crustáceos Decápodos de Venezuela. Instituto Venezolano de Investigaciones Científicas, Caracas, 494 pp.

Santana W, Colavite J, Bolaños J, Hernández E, Canepa M (2016) Morphology of the larval stages of *Pitho aculeata* (Gibbes, 1850) (Crustacea, Brachyura, Majoidea) and its implications on the taxonomic position of the genus. Marine Biology Research 12(8): 854–863. https://doi.org/10.1080/17451000.2016.1209524

Schomburgk RH (1848) History of Barbados. London, 776 pp. https://doi.org/10.1080/03745485809496118

Stamatakis A (2014) RAxML version 8: A tool for phylogenetic analysis and post-analysis of large phylogenies. Bioinformatics 30(9): 1312–1313. https://doi.org/10.1093/bioinformatics/btu033

Stimpson W (1860) Notes on North American crustacea, in the Museum, of the Smithsonian Institution, No. II. Annals of the Lyceum of Natural History of New York 7: 177–246. [pls. II +V.] https://doi.org/10.1111/j.1749-6632.1862.tb00153.x

Tamura K, Stecher G, Kumar S (2021) MEGA11: Molecular Evolutionary Genetic Analysis Version 11. Molecular Biology and Evolution 38(7): 3022–3027. https://doi.org/10.1093/molbev/msab120

Tavares M, Mendonça JJB (2022) Brachyuran crabs (Crustacea, Decapoda) from the remote oceanic Archipelago Trindade and Martin Vaz, South Atlantic Ocean. Zootaxa 1(5146): 1–129. https://doi.org/10.11646/zootaxa.5146.1.1

Wagner HP (1990) The genera *Mithrax* Latreille, 1818 and *Mithraculus* White, 1847 (Crustacea: Brachyura: Majidae) in the western Atlantic Ocean. Zoölogische Verhandelingen 264(1): 1–65.

Wicksten MK (1993) A review and a model of decorating behavior in spider crabs (Decapoda, Brachyura, Majidae). Crustaceana 64: 314–325. https://doi.org/10.1163/156854093X00667

Williams AB (1965) Marine decapod crustaceans of the Carolinas. Fishery Bulletin of the Fish and Wildlife Service 65: 1–298.

Williams AB (1984) Shrimps, Lobsters, and Crabs of the Atlantic Coast of the Eastern United States, Maine to Florida. Smithsonian Institution Press, Washington, 550 pp.

Windsor AM, Felder DL (2014) Molecular phylogenetics and taxonomic reanalysis of the family Mithracidae MacLeay (Decapoda: Brachyura: Majoidea). Invertebrate Systematics 28(2): 145–173. https://doi.org/10.1071/IS13011

Windsor AM, Felder DL (2017) Corrigendum to: Molecular phylogenetics and taxonomic reanalysis of the family Mithracidae MacLeay (Decapoda: Brachyura: Majoidea). Invertebrate Systematics 31(2): 232–232. https://doi.org/10.1071/IS13011_CO

Young CG (1900) The Stalk-Eyed Crustacea of British Guiana, West Indies, and Bermuda. J M Watkins, London, 514 pp. https://doi.org/10.5962/bhl.title.10670

Zhang J, Kapli P, Pavlidis P, Stamatakis A (2013) A general species delimitation method with applications to phylogenetic placements. Bioinformatics 29: 2869–2876. https://doi.org/10.1093/bioinformatics/btt499

Supplementary material 1

Phylogenetic trees of individual datasets of 12S, 16S, and ITS-1 genes

Authors: Nadeshinie Parasram, William Santana, Yvonne Vallès, Amanda Windsor, Henri Vallès

Data type: tif

Explanation note: ML reconstruction for individual datasets of 12S, 16S and ITS-1 genes, represented as a maximum likelihood phylogram with maximum likelihood bootstrap values and Bayesian posterior probability (black diamond = ≤ 50% support).

Link: https://doi.org/10.3897/zse.100.109192.suppl1

Supplementary material 2

Specimens used in the molecular analysis of Windsor and Felder (2014), which were erroneously identified as *Amphithrax aculeatus* (Herbst, 1790)

Authors: Nadeshinie Parasram, William Santana, Yvonne Vallès, Amanda M. Windsor, Henri Vallès

Data type: tif

Explanation note: Habitus, dorsal view of carapace of *Amphithrax verrucosus* (H. Milne Edwards, 1832). A ULLZ 4534, juvenile female (CW: 34.0 mm; CL: 20.0 mm), locality: Florida Keys; B ULLZ 9148, juvenile male (CW: 10.0 mm; CL: 8.0 mm), locality: Belize; C ULLZ 10758, juvenile female (CW: 15.0 mm; CL: 13.0 mm), locality: Panama. Scale bar: 20 mm. Photos: Amanda Windsor.

Link: https://doi.org/10.3897/zse.100.109192.suppl2

Zoosyst. Evol. 100 (1) 2024, 31–48 | DOI 10.3897/zse.100.113049

PENSOFT

für Natur MUSEUM FÜR NATURKUNDE BERLIN

Additions to the knowledge on the genus *Phintella* Strand, 1906 (Araneae, Salticidae, Chrysillini) from India

Puthoor Pattammal Sudhin[1], John T. D. Caleb[2], Souvik Sen[1]

1 *Zoological Survey of India, Prani Vigyan Bhawan, M-Block, New Alipore, Kolkata – 700053, West Bengal, India*

2 *Department of Anatomy, Saveetha Medical College & Hospital, Saveetha Institute of Medical and Technical Sciences, Saveetha University, Chennai 602105, Tamil Nadu, India*

https://zoobank.org/486B29D0-88E9-465B-B70F-96FF3CBEDD26

Corresponding author: Souvik Sen (sensouvik07@gmail.com)

Academic editor: Danilo Harms ♦ **Received** 20 September 2023 ♦ **Accepted** 8 November 2023 ♦ **Published** 26 January 2024

Abstract

Four new species of the chrysilline genus *Phintella* – *P. dentis* **sp. nov.** (♂♀), *P. handersoni* **sp. nov.** (♂♀), *P. luna* **sp. nov.** (♀) and *P. rajbharathi* **sp. nov.** (♂) – are described from India. Additionally, the unknown female of *Phintella platnicki* Sudhin, Sen & Caleb, 2023 is described and new distributional data are provided for this species. Notes on the type locality and distribution of *P. accentifera* (Simon, 1901) are provided along with clarification on the identity of other non-type materials. Detailed morphological descriptions, illustrations and a distributional map are also given.

Key Words

China, distribution, jumping spider, new species, taxonomy, type locality, Vietnam

Introduction

The jumping spider genus *Phintella* Strand, 1906, is one of the most diverse genera in the tribe Chrysillini which currently accommodates 71 described species, of which 14 have been described/reported from India (Caleb and Sankaran 2023). The members are small, adorned with colourful scales and are distributed in the African, Palaearctic and Oriental Regions (World Spider Catalog 2023). Several new species were described in the past decade from East, South and Southeast Asia: 16 species from China (Barrion et al. 2013; Lei and Peng 2013; Huang et al. 2015; Cao et al. 2016; Li et al. 2019; Wang and Li 2020), three from India (Prajapati et al. 2021; Sudhin et al. 2023), two from Sri Lanka (Kanesharatnam and Benjamin 2019) and one from Vietnam (Hoang et al. 2023). While studying unidentified jumping spider collections from recent surveys across various locations in India, we recognised four new *Phintella* species. The paper thus aims to provide: (1) detailed descriptions of four new *Phintella* species from India; (2) first description of the female of *P. platnicki* Sudhin, Sen & Caleb, 2023 and update of its distribution in India; (3) clarify the identity of previously misidentified species under *P. vittata* (C.L. Koch, 1846) and *P. accentifera* (Simon, 1902) from India, China and Vietnam; and (4) provide notes on the type locality and distribution of *P. accentifera*.

Material and methods

A total of 42 *Phintella* specimens (17 ♂ and 25 ♀) preserved in 70% ethanol were studied and observed under a Leica M205A stereomicroscope. All measurements are given in millimetres (mm). Lengths of pedipalp and leg segments are given as follows: total [femur, patella, tibia, metatarsus (except for pedipalp), tarsus]. The description of colouration is based on alcohol-preserved specimens. The micrographic images were captured with a Flexacam C3 camera and processed using extended focus montage LAS X software. The description standard and style follows Sudhin et al. (2023). The distribution map was

prepared using the online mapping software SimpleMappr (Shorthouse 2010). The specimens are kept in the National Zoological Collections of the Zoological Survey of India (NZC-ZSI), Kolkata, India.

Abbreviations used in the text and figures are as follows: **ALE** – anterior lateral eye, **AME** – anterior median eye, **C** – cymbium, **CD** – copulatory duct, **CO** – copulatory opening, **do** – dorsal, **E** – embolus, **FD** – fertilisation duct, **LP** – lamellar process, **pl** – prolateral, **PLE** – posterior lateral eye, **PME** – posterior median eye, **plv** – prolateral ventral, **rl** – retrolateral, **RTA** – retrolateral tibial apophysis, **rlv** – retrolateral ventral, **SC** – scapum, **v** – ventral, **WLS** – Wildlife Sanctuary.

Taxonomy

Family Salticidae Blackwall, 1841
Tribe Chrysillini Simon, 1901

Genus *Phintella* Strand, 1906

Type species. *Telamonia bifurcilinea* Bösenberg & Strand, 1906.

***Phintella dentis* Sudhin, Caleb & Sen, sp. nov.**
https://zoobank.org/7C8320F0-A01B-4C97-B6FA-39F1DB73DA06
Figs 1A–H, 2A–D, 4A–D, 14

Type material. ***Holotype*** ♂. INDIA: Karnataka, Shimoga District, Mookambika Wildlife Sanctuary, 13°42'24"N, 75°3'17"E, 629 m elev., 07.xii.2022, P.P. Sudhin coll. (NZC-ZSI-8369/18). ***Paratype***: 1♀, same data as holotype (NZC-ZSI-8370/18).

Diagnosis. The male copulatory organ of *P. dentis* sp. nov. is most similar to that of *P. jaleeli* Kanesharatnam & Benjamin, 2019, from which it can be distinguished by the following combination of characters: RTA robust without basal minute teeth (relatively narrower with basal minute teeth in *P. jaleeli*); embolus long and narrower, with the distal tip directed at 12 o'clock position in ventral view (short and robust with the distal tip directed at 1 o'clock position in *P. jaleeli*) (cf. Figs 2A, B, 4A, B with figs 31D, E and 33A, B in Kanesharatnam and Benjamin (2019)). The female genitalia of *P. dentis* sp. nov. is most similar to that of *P. caledoniensis* Patoleta, 2009 from which it can be easily distinguished by the small copulatory openings, relatively short copulatory ducts and bilobed spermathecae (cf. Figs 2C, D, 4C, D with figs 6–7 in Patoleta (2009)).

Description. Male (Holotype, NZC-ZSI-8369/18) (Figs 1A–C, G, 2A, B, 4A, B): Measurements: body length 4.26; carapace length 1.93, width 1.66; abdomen length 2.22, width 1.17. Ocular area length 1.44, width 1.23. Eye diameters: AME 0.51, ALE 0.23, PME 0.06, PLE 0.24. Eye interdistances: AME–AME 0.01, ALE–AME 0.02, ALE–ALE 1.03, ALE–PLE 0.53, PLE–PLE 1.11, PME–PME 1.18, PME–PLE 0.23. Clypeus height 0.15. Length of chelicera 0.47. Measurement of palp and legs: palp 1.57 [0.60, 0.21, 0.16, 0.60], leg I 4.01 [1.36, 0.62, 0.96, 0.67, 0.40], II 3.16 [1.03, 0.43, 0.74, 0.58, 0.38], III 3.71 [1.10, 0.48, 0.77, 0.86, 0.50], IV 4.23 [1.31, 0.44, 0.99, 0.96, 0.53]. Leg formula: 4132. Leg setation: femur I–III pl 1 rl 1 do 3, IV pl 1 rl 2 do 3; patella III–IV rl 1; tibia I plv 4 rlv 2, II pl 2 rl 2, III pl 1 rl 2 rlv 2, IV pl 2 rl 3 rlv 1; metatarsus I plv 2 rlv 2, II pl 1 rl 1 plv 2 rlv 2, III pl 2 rl 2 plv 2 rlv 3, IV pl 2 rl 2 plv 1 rlv 2. Carapace oval, high, sloping posteriorly, reddish-brown, covered with short white setae, margin of carapace with black lines (Fig. 1A); anterior region of thorax with a transverse diamond-shaped yellow-brown area behind eye field (Fig. 1A); eye field brown; eye bases black; AMEs surrounded by pale yellow setae (Fig. 1G). Clypeus short, reddish-brown, covered with white setae (Fig. 1G). Chelicerae small, sub-vertical, slightly diverging, reddish-brown, inner frontal face with tooth-like outgrowth, situated closer to base (Fig. 1B); chelicerae retromargin with two stout teeth with wide bases, arranged closely and transversely. Endites light brown, scopulate, with pale yellow inner margins; distal tip with beak-like curve (Fig. 1B). Labium light brown, distally pale yellow, covered with setae (Fig. 1B). Sternum oval, truncated anteriorly, pale yellow, with reddish-brown margins (Fig. 1B). Abdomen oval, narrowing posteriorly, pale yellow, laterally with longitudinal white stripes formed of white setae (Fig. 1A); lateral region dark brown (Fig. 1C); venter light brown, laterally with longitudinal white stripes and medially with a pair of yellowish dotted lines (Fig. 1B). Leg I brown with yellow metatarsi and tarsi (Fig. 1C), patella and tibia ventrally provided with brown setae; other leg articles pale yellow (Fig. 1C). Palps yellow-brown (Fig. 2A, B); RTA stout, directed anteriorly, wide at base, narrowing distally, tip slightly bent ventrally (Figs 2B, 4B); cymbium elongate oval, covered with long setae (Figs 2A, B, 4A, B); tegulum nearly rectangular with small U-shaped posterior lobe (Figs 2A, 4A); sperm duct visible on the retrolateral shoulder of tegulum (Figs 2A, 4A); embolus relatively long, situated anterior to bulbus, narrowing towards tip (Figs 2A, 4A).

Female (Paratype) (Figs 1D–F, H, 2C, D, 4C, D): Measurements: body length 4.63; carapace length 1.99, width 1.72; abdomen length 2.70, width 1.46. Ocular area length 1.26, width 1.50. Eye diameters: AME 0.48, ALE 0.25, PME 0.04, PLE 0.23. Eye interdistances: AME–AME 0.06, ALE–AME 0.05, ALE–ALE 1.01, ALE–PLE 0.58, PLE–PLE 1.07, PME–PME 1.16, PME–PLE 0.27. Clypeus height 0.16. Length of chelicera 0.65. Measurement of palp and legs: palp 1.43 [0.48, 0.16, 0.28, 0.51], leg I 4.84 [1.50, 0.66, 1.27, 0.84, 0.57], II 4.10 [1.35, 0.55, 0.92, 0.75, 0.53], III 4.44 [1.39, 0.67, 0.84, 1.03, 0.51], IV 4.92 [1.49, 0.55, 1.18, 1.16, 0.54]. Leg formula: 4132. Leg setation: femur I–IV pl 1 do 3; tibia I plv 4 rlv 4, II plv 3 rlv 3; metatarsus I plv 2 rlv 2, II pl 1 plv 2 rlv 2, III–IV pl 1 rl 1. In all details as male, except the following: carapace dark brown (Fig. 1D); eye field black,

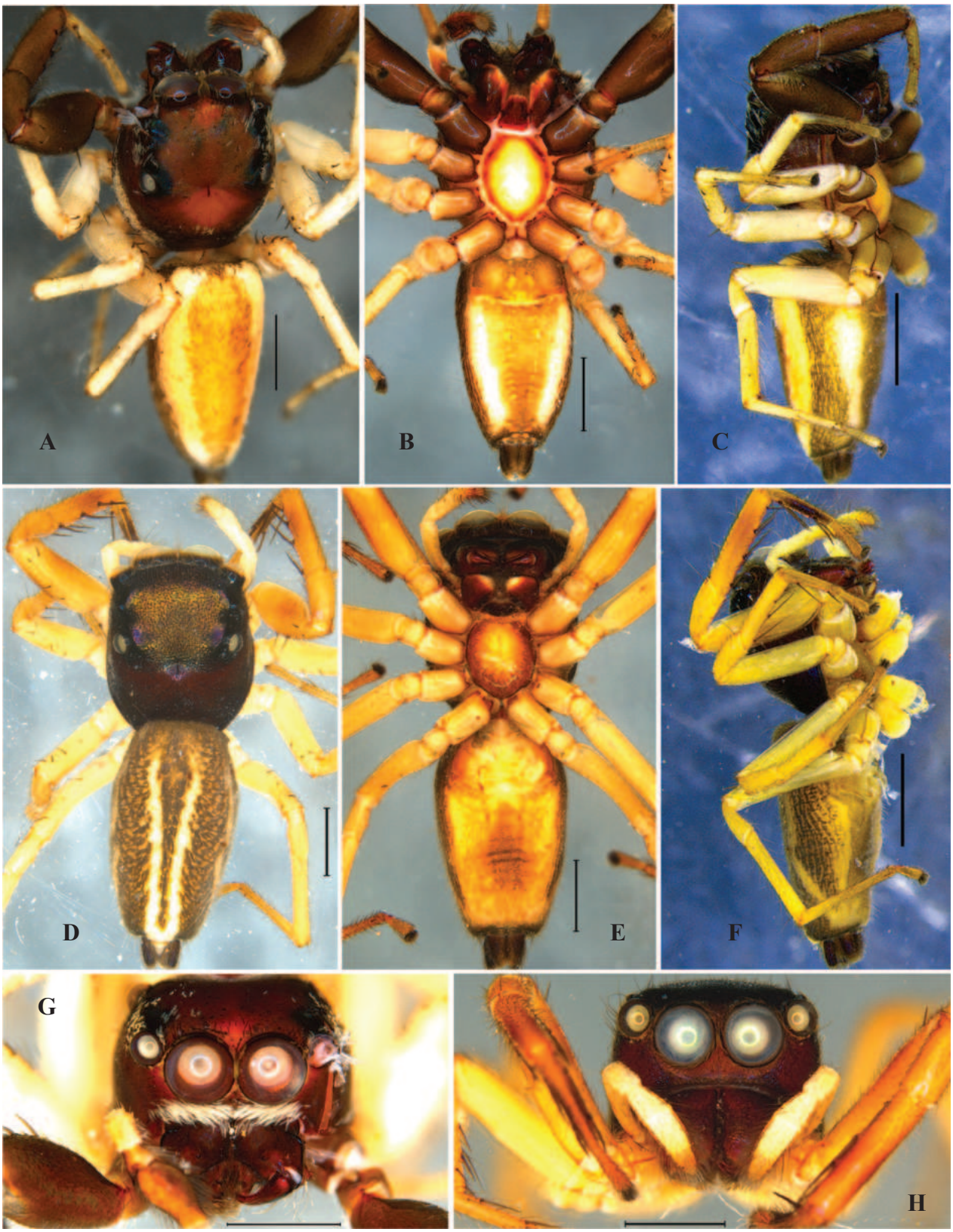

Figure 1. *Phintella dentis* sp. nov. **A.** Male, dorsal view; **B.** Same, ventral view; **C.** Same, lateral view; **D.** Female, dorsal view; **E.** Same, ventral view; **F.** Same, lateral view; **G.** Male, frontal view; **H.** Female, frontal view. Scale bars: 1 mm (**A–H**).

middle region decorated with shiny golden yellow patch (Fig. 1D); clypeus red-brown (Fig. 1H); chelicerae vertical, not diverging, reddish-brown, without any modification; cheliceral promargin with two teeth and retromargin with a single tooth; endites yellowish-brown, without any modifications (Fig. 1E); labium brown (Fig. 1E); sternum nearly round, yellowish-brown with darker sides, margin with dark brown lines (Fig. 1E); abdomen brown

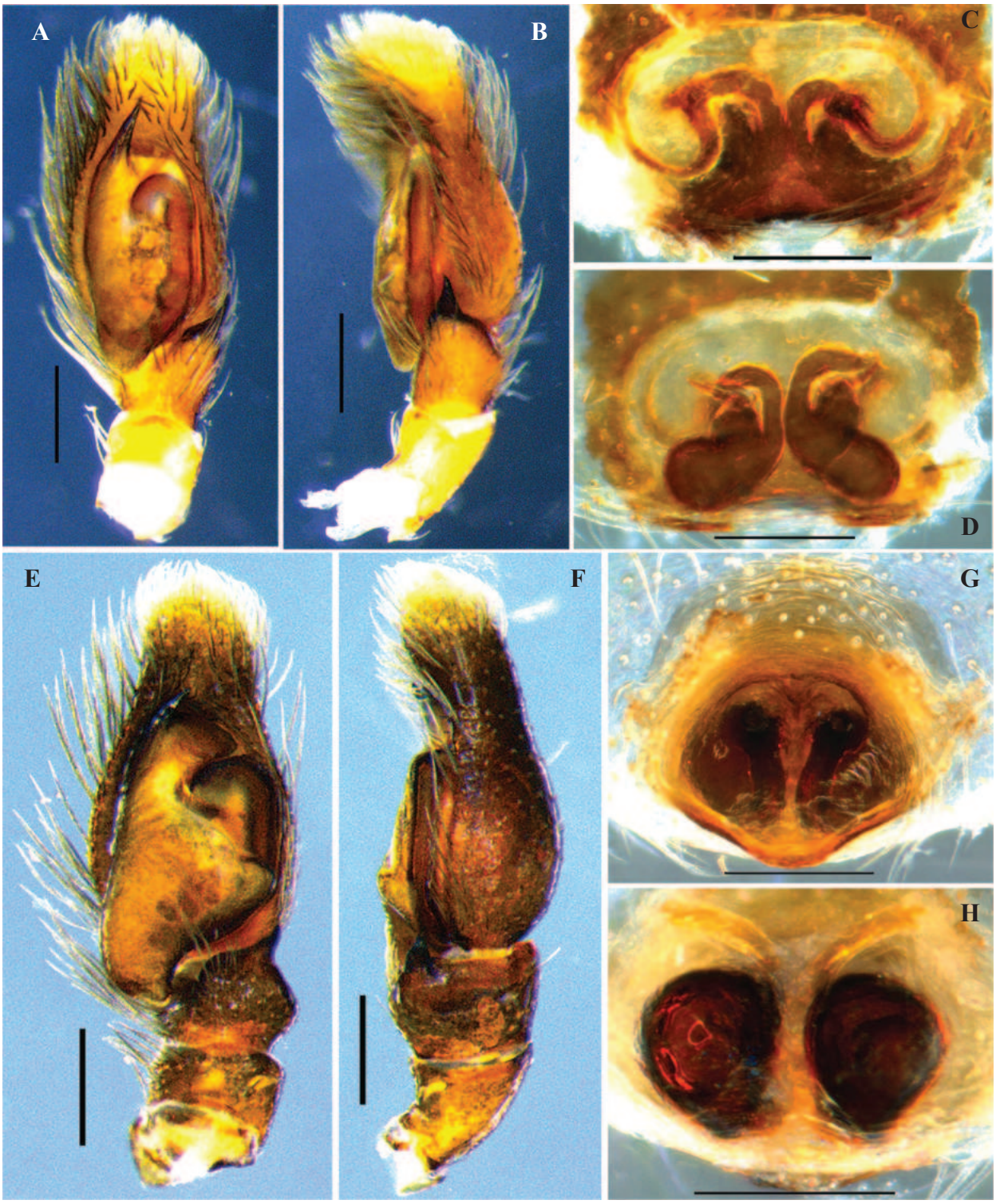

Figure 2. *Phintella dentis* sp. nov. (**A–D**) and *Phintella handersoni* sp. nov. (**E–H**). **A, E.** Left male palp, ventral view; **B, F.** Same, retrolateral view; **C, G.** Female epigyne, ventral view; **D, H.** Vulva, dorsal view. Scale bars: 0.2 mm (**A–H**).

with yellow patches, medially with two closely-arranged U-shaped pale yellow stripes extending longitudinally from below anterior margin to posterior end (Fig. 1D); abdomen dorso-laterally with thin yellow stripes, bending, moving to ventral margin and terminating just before spinnerets (Fig. 1F); abdomen lateral sides brown with thin yellow streaks (Fig. 1F); venter pale yellow with light brown middle region (Fig. 1E). Epigyne simple, moderately sclerotised, wider than long (Figs 2C, 4C); copulatory openings small, widely separated from each other, situated antero-laterally (Figs 2C, 4C); copulatory ducts long, relatively narrow, sclerotised, anteriorly curved, leading posteriorly and connected to anterior part of spermathecae (Figs 2C, D, 4C, D); spermathecae bilobed, posterior lobe large and oval shaped, anterior lobe small and hump-shaped (Figs 2D, 4D); fertilisation ducts

orientated anterolaterally, located at the anterior region of spermathecae (Figs 2D, 4D).

Etymology. The species name is a noun in apposition originating from the Latin word '*dentis*', meaning tooth and referring to the presence of a tooth-like outgrowth on the frontal face of the male chelicerae.

Distribution. Known only from the type locality in Karnataka, India (Fig. 14).

Phintella handersoni Sen, Sudhin & Caleb, sp. nov.

https://zoobank.org/CE3DD031-4FE5-4E09-BEDA-E34E7E24C038
Figs 2E–H, 3A–H, 4E–H, 14

Phintella accentifera: Żabka 1985: 428, figs 430–434, 452 (♀); Xie, 1993: 358, figs 6–7 (♀); Peng et al. 1993: 150, figs 515–517 (♀); Song et al. 1999: 537, figs 307H, 327R (♀); Tyagi et al. 2019: supplement, figs S2.53 (♀); Peng 2020: 294, figs 209a-c (♀); Sudhin et al. 2023: 87, figs 24–27 (♀) (all misidentified).

Phintella suavis: Żabka 1985: 427, figs 426–429, 451 (♂); Peng et al. 1993: 160, figs 560–564; Song et al. 1999: 539, figs 308M-N (♂); Peng 2020: 307, figs 220a-e (♂) (all misidentified).

Type material. ***Holotype*** ♂. INDIA: Meghalaya, Ri Bhoi District, Anderson Tea Estate, 25°47'42"N, 91°53'03"E, 810 m elev., 13.iii.2023, S. Sen & P.P. Sudhin coll. (NZC-ZSI-8313/18). ***Paratype***: 1♀, same data as holotype (NZC-ZSI-8371/18).

Diagnosis. *P. handersoni* sp. nov. is most similar to *Phintella accentifera* (Simon, 1901) in having the similar palpal and epigynal morphology, but it can be distinguished by the following combination of characters: abdominal pattern with dark brown and pale yellow transverse bands (without transverse bands, but with mid-dorsal chevron markings in *P. accentifera*); RTA conical and directed apically in retrolateral view (curved and directed ventrad in *P. accentifera*); tegulum with large lobe-like lamellar process (almost triangular in *P. accentifera*); embolus directed at 2 o'clock position in ventral view (3 o'clock position in *P. accentifera*); epigyne with distinct postero-medial protrusion (without any posterior projection in *P. accentifera*); copulatory ducts relatively narrow (broad in *P. accentifera*) (cf. Figs 2E–H, 3A, D, 4E–H with fig. 156 in Prószyński (1984) and figs 4.28A, D, E, G, I and J in Luong (2017)).

Description. Male (Holotype, NZC-ZSI-8313/18) (Figs 2E–F, 3A–C, G, 4E, F): Measurements: body length 3.72; carapace length 1.73, width 1.43; abdomen length 1.72, width 1.12. Ocular area length 1.05, width 1.21. Eye diameters: AME 0.41, ALE 0.22, PME 0.08, PLE 0.21. Eye interdistances: AME–AME 0.02, ALE–AME 0.03, ALE–ALE 0.83, ALE–PLE 0.53, PLE–PLE 0.89, PME–PME 0.98, PME–PLE 0.21. Clypeus height 0.22. Length of chelicera 0.78. Measurement of palp and legs: palp 1.69 [0.65, 0.21, 0.17, 0.66], leg I 3.67 [1.07, 0.59, 0.87, 0.78, 0.36], II 3.44 [1.13, 0.46, 0.78, 0.64, 0.43], III 4.01 [1.28, 0.47, 0.86, 0.91, 0.49], IV 4.41 [1.40, 0.46, 1.03, 1.05, 0.47]. Leg formula: 4312. Leg setation: femur I–II pl 1 rl 1 do 3, III pl 1 rl 3 do 3, IV pl 1 rl 2 do 3; patella III–IV rl 1; tibia I pl 2 plv 4 rlv 4, II pl 2 rl 2 plv 4 rlv 4, III–IV pl 2 rl 2 plv 2 rlv 2; metatarsus I pl 1 rl 1 plv 2 rlv 2, II–III pl 2 rl 2 plv 2 rlv 2, IV pl 3 rl 3 plv 1 rlv 1. Carapace oval, high, sloping posteriorly, dark brown, anterior of thorax with a transverse diamond-shaped yellowish area behind eye field, margin of carapace with narrow black lines (Fig. 3A); eye field dark brown, anterior row of eyes encircled with pale yellow setae (Fig. 3G). Clypeus low, covered with silvery white setae (Fig. 3G). Chelicerae long, subvertical, diverging, yellowish-brown (Fig. 3G), promargin with two teeth and retromargin with a single tooth. Endites brown, scopulate, margins with narrow black lines (Fig. 3B). Labium brown, with paler tip, distally with dark brown setae (Fig. 3B). Sternum oval, anteriorly flat, dark brown with yellow dots, covered with white setae, lateral sides with more setae (Fig. 3B). Abdomen oval, dark brown, medially and posteriorly with transverse yellow bands (Fig. 3A); abdomen posteriorly with recurved yellow dotted lines and laterally with yellow and dark brown brick line patterns (Figs 3A, C); venter pale yellow medially with a light brown longitudinal band (Fig. 3B). Spinnerets pale yellow, covered with black setae. Legs brown, proximal region of metatarsus I, femora III and IV, metatarsi and tarsi II-IV pale yellow; all femora, patellae and tibiae covered with metallic lustrous setae, I-II with more lustrous setae. Palp brown (Fig. 2E, F); patella and tibia distal region with long black dorsal setae (Fig. 2E, F); tibia and patella covered with black setae (Fig. 2E, F); RTA short, stout, anteriorly directed, wide at base, slightly narrowing distally, tip slightly bent ventrally (Figs 2F, 4F); cymbium elongate oval, covered with long brown setae (Figs 2E, F, 4E, F); tegulum with well-developed posterior lobe (Figs 2E, 4E); lamellar process large, almost cone-shaped (Figs 2E, 4E); tegulum with conspicuous retrolateral shoulder, sperm duct visible at this shoulder (Figs 2E, 4E); embolus short, situated anterior to bulbus, narrowing tip directed at 2 o'clock position in ventral view (Figs 2E, 4E).

Female (Paratype) (Figs 2G, H, 3D–F, H, 4G, H): Measurements: body length 4.24; carapace length 1.68, width 1.32; abdomen length 2.15, width 1.67. Ocular area length 1.01, width 1.22. Eye diameters: AME 0.46, ALE 0.23, PME 0.04, PLE 0.23. Eye interdistances: AME–AME 0.03, ALE–AME 0.05, ALE–ALE 0.88, ALE–PLE 0.57, PLE–PLE 1.06, PME–PME 1.13, PME–PLE 0.27. Clypeus height 0.08. Length of chelicera 0.56. Measurement of palp and legs: palp 1.31 [0.47, 0.16, 0.25, 0.43], leg I 2.77 [0.87, 0.36, 0.68, 0.54, 0.32], II 2.65 [0.88, 0.38, 0.57, 0.50, 0.32], III 3.21 [1.02, 0.39, 0.65, 0.73, 0.42], IV 3.73 [1.17, 0.40, 0.85, 0.87, 0.44]. Leg formula: 4312. Leg setation: femur I–III pl 2 rl 1 do 3, IV pl 1 rl 1 do 3; patella III–IV rl 1; tibia I pl 1 rl 1 plv 2 rlv 2, II pl 2 rl 1 plv 3 rlv 3, III–IV pl 2 rl 3 plv 2 rlv 1; metatarsus I pl 1 rl 1 plv 2 rlv 2, II pl 2 rl 2 plv 3 rlv 3, III pl 2 rl 2 plv 3 rlv 3, IV pl 3 rl 3 plv 1 rlv 1. In all details as male, except the following: eye field black (Fig. 3D); chelicerae small, vertical, yellowish-brown with darker dorsal side

Figure 3. *Phintella handersoni* sp. nov. **A.** Male, dorsal view; **B.** Same, ventral view; **C.** Same, lateral view; **D.** Female, dorsal view; **E.** Same, ventral view; **F.** Same, lateral view; **G.** Male, frontal view; **H.** Female, frontal view. Scale bars: 1 mm (**A–H**).

(Fig. 3H); endites dark brown with pale yellow inner tips (Fig. 3E); labium dark brown (Fig. 3E); abdomen light brown with faint medial transverse band (Fig. 3D); venter with prominent, lens-shaped longitudinal median brown band (Fig. 3E). Epigyne wider than long, sclerotised, with wide, curved posterior margin (Figs 2G, 4G);

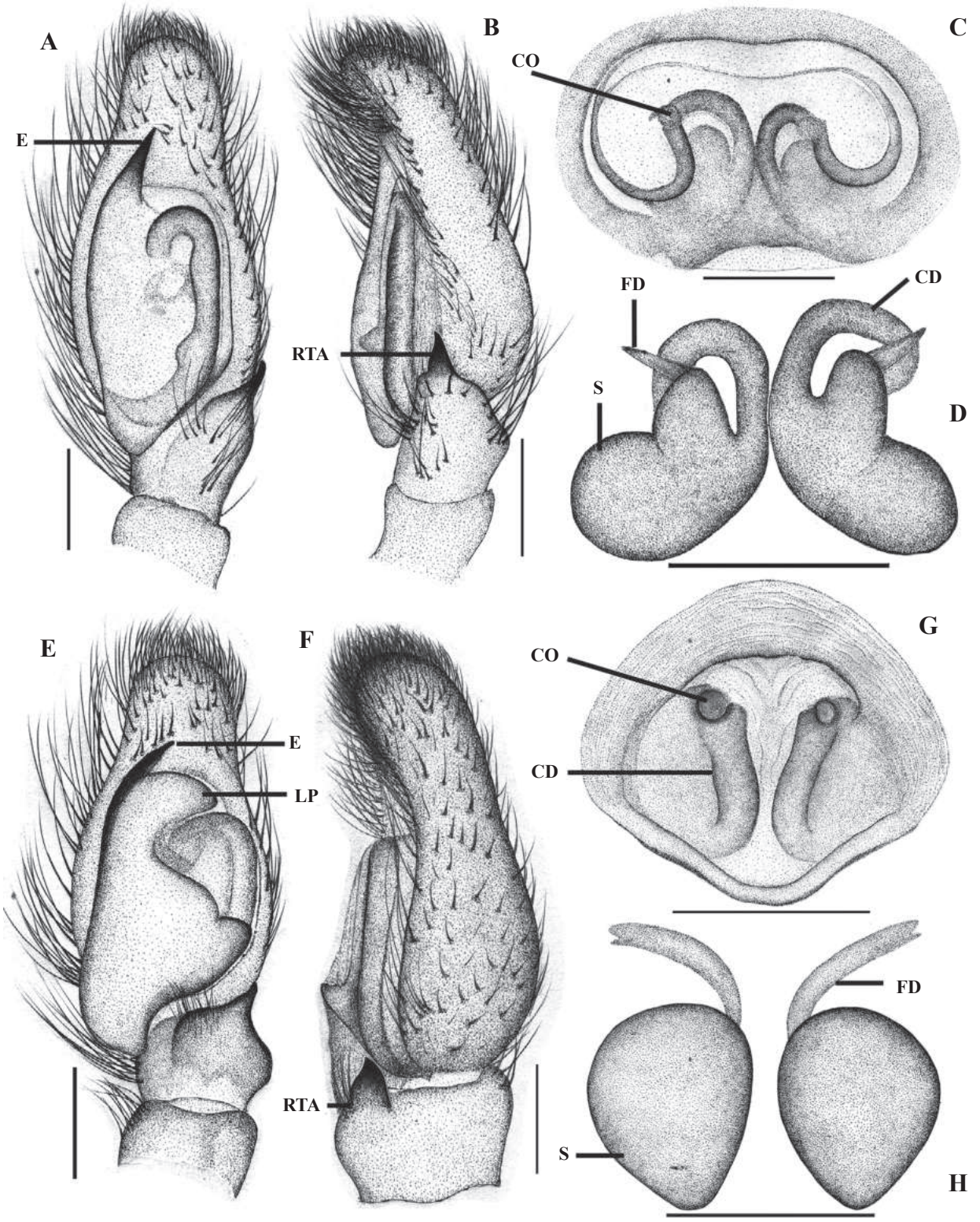

Figure 4. *Phintella dentis* sp. nov. (**A–D**) and *Phintella handersoni* sp. nov. (E–H). **A, E.** Left male palp, ventral view; **B, F.** Same, retrolateral view; **C, G.** Female epigyne, ventral view; **D, H.** Vulva, dorsal view. Scale bars: 0.2 mm (**A–H**).

copulatory openings round, separated from each other, situated anterior region of epigyne (Figs 2G, 4G); copulatory ducts highly sclerotised, slightly curved, extending posteriorly and entering at posterior part of spermathecae (Figs 2G, 4G); spermathecae nearly pear-shaped, separated from each other (Figs 2H, 4H); fertilisation ducts long, orientated anterolaterally, located at anterior region of spermathecae (Figs 2H, 4H).

Etymology. The species is named after the late Handerson Syiemlieh, the owner of the tea estate from where the type series was collected.

Distribution. India (Assam, Manipur, Meghalaya) (Fig. 14), China and Vietnam.

Remarks. Since both sexes were collected together in this study, it was possible for us to determine the identity as we compared them with previous illustrations and with those of the type images (Luong 2017) of both *P. accentifera* and *P. suavis*. The general colour pattern of the female which was earlier identified as *P. accentifera* did not match with the type, thus leading us to re-verify all previous illustrations. On the other hand, it was concluded that *P. suavis* was a synonym of *P. vittata* (Luong 2017: 104). We agree with Luong's conclusion on the synonymy, based on the images of the type specimens; however, that decision has not been made formally yet. Based on these observations, we concluded that this species was misidentified earlier and each sex was assigned to different names by previous scientists. Żabka (1985) illustrated the male as *P. suavis* and the female as *P. accentifera* from Vietnam. This was followed by Chinese (Peng et al. 1993; Xie 1993; Song et al. 1999; Peng 2020) and Indian authors (Tyagi et al. 2019; Sudhin et al. 2023). Two females from Assam (Tyagi et al. 2019: GenBank accession numbers MK392820 and MK392821) and two females from Manipur (Sudhin et al. 2023) were misidentified as *P. accentifera*.

Simon (1901) does not provide the exact locality for *P. accentifera* (Simon, 1901); however, mentions, "et dans les espèces des montagnes de l'Inde, *T. accentifera* E. Sim.," ("and in the species of the mountains of India, *T. accentifera* E. Sim.," – Simon, (1901: 548)). Luong (2017) examined the syntypes of *P. accentifera* deposited in the Muséum national d'Histoire naturelle, Paris and precisely designated the lectotype, based on a specimen from Kodaikanal (a hill station in South India) from the vial No. 10254. Nevertheless, the designation of lectotype and paralectotypes has not yet been formally published. Nevertheless, based on the information from the original description of Simon (1901) and the type label (Luong 2017: fig. 4.28K), the type locality of *P. accentifera* is, thus, Kodaikanal in Tamil Nadu, India. *P. accentifera* (Simon, 1901) is presently confined to its type locality in South India.

Phintella luna Sudhin, Sen & Caleb, sp. nov.

https://zoobank.org/08B77287-5B14-4BE9-BFE3-2E69D999BD4F

Figs 5A–E, 6A, B, 14

Phintella vittata Tyagi et al., 2019: supplement, figs S3.29–30 (♀ misidentified).

Type material. ***Holotype*** ♀. INDIA: West Bengal, Nadia District, Kalyani, 22°59'6.54"N, 88°26'0.06"E, 17.ix.1969, D. Sinharny coll. (NZC-ZSI-6559/18); ***Paratype*****:** 1♀, Andhra Pradesh, East Godavari District, Kittukuru, 17°19'16.5"N, 82°2'26.55"E, 05.xii.2021, D. Jaiswal coll. (NZC-ZSI-8374/18).

Diagnosis. *P. luna* sp. nov. is similar to *Phintella vittata* (C.L. Koch, 1846) in having the similar body colour patterns and female genitalia with well-developed epigynal scape and rounded spermathecae, but it can be distinguished by the following characters: epigyne with straight anterior epigynal border (arched in *P. vittata*); copulatory ducts gently curved, U-shaped and relatively longer (straight, converging posteriorly, V-shaped in *P. vittata*) (cf. Figs 5D, 6A with Figs 12G, 13C).

Description. Female (Holotype, NZC-ZSI-6559/18) (Figs 5A–E, 6A, B): Measurements: body length 2.92; carapace length 1.24, width 1.07; abdomen length 1.60, width 1.25. Ocular area length 0.82, width 0.94. Eye diameters: AME 0.35, ALE 0.18, PME 0.03, PLE 0.16. Eye interdistances: AME–AME 0.02, ALE–AME 0.02, ALE–ALE 0.73, ALE–PLE 0.37, PLE–PLE 0.77, PME–PME 0.81, PME–PLE 0.17. Clypeus height 0.06. Length of chelicera 0.43. Measurement of palp and legs: palp 1.18 [0.43, 0.15, 0.20, 0.40], leg I 2.37 [0.76, 0.34, 0.55, 0.44, 0.28], II 2.13 [0.76, 0.23, 0.52, 0.36, 0.26], III 2.77 [0.89, 0.30, 0.60, 0.67, 0.31], IV 3.23 [1.02, 0.32, 0.75, 0.78, 0.36]. Leg formula: 4312. Leg setation: femur I–IV pl 1 rl do 3; patella III–IV rl 1; tibia I pl 1 plv 3 rlv 3, II pl 2 rl 2 plv 2 rlv 2 III pl 1 rl 1 plv 2 rlv 1, IV pl 1 rl 2 plv 1 rlv 1; metatarsus I pl 1 rl 1 plv 2 rlv 2, II pl 2 rl 2 plv 2 rlv 2, III–IV pl 2 rl 2 plv 1 rlv 1. Carapace oval, sloping posteriorly, light yellowish-brown, with few black patches and stripes (Fig. 5A); eye bases black (Fig. 5A), anterior eyes surrounded by pale white setae. Clypeus low, light yellowish-brown. Chelicerae small, vertical, yellow-brown, promargin with two teeth and retromargin with a single tooth. Endites pale yellow, scopulate, margins with narrow reddish-brown lines (Fig. 5B). Labium pale yellow, distally with few light brown setae (Fig. 5B). Sternum yellowish-brown, with pale yellow posterior sides (Fig. 5B). Abdomen oval, pale yellow with light brown anterior region, medially with a dark brown transverse band and posterior tip with a dark brown patch (Fig. 5A). Venter pale yellow without any prominent markings (Fig. 5B). Legs pale yellow. Epigyne nearly round, moderately sclerotised, posterior region with well-developed epigynal scape (Figs 5D, 6A); copulatory openings small, widely separated from each other, situated antero-laterally (Figs 5D, 6A); copulatory ducts comparatively long, gently curved and connected to anterior region of spermathecae (Figs 5D, 6A); spermathecae nearly round, separated from each other (Figs 5E, 6B); fertilisation duct long, orientated laterally, located at anterior region of spermathecae (Figs 5E, 6B).

Male. Unknown.

Etymology. The specific epithet is noun in apposition, referring to the curved, crescent-like copulatory ducts ('luna' in Latin for the moon). We also take this occasion to mark the successful landing of the spacecraft Chandrayaan-3 close to the South Pole of the moon for the first time during the third Indian lunar expedition.

Distribution. India: West Bengal, Andhra Pradesh, and Gujarat (Tyagi et al. 2019) (Fig. 14).

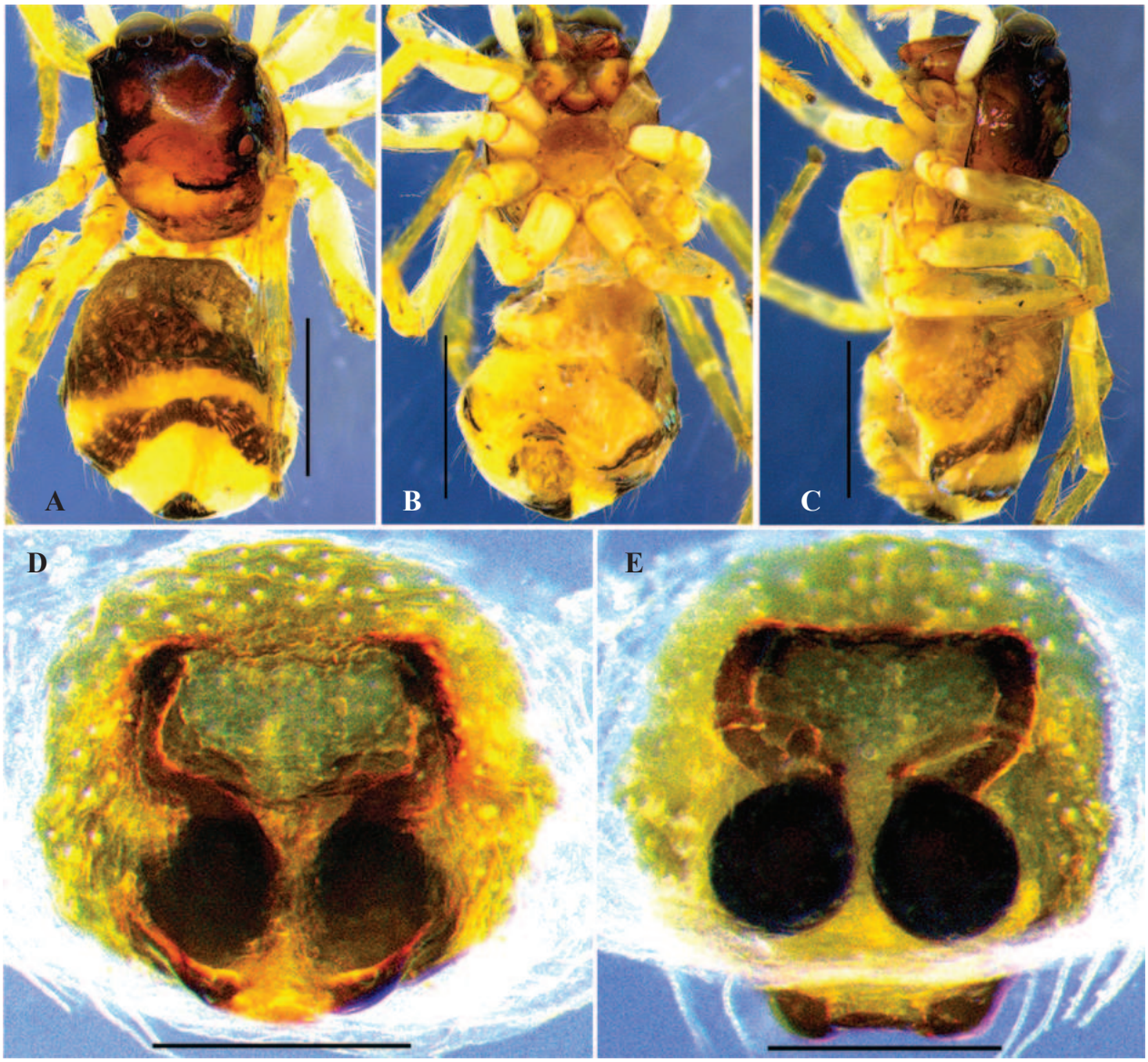

Figure 5. *Phintella luna* sp. nov. **A.** Female, dorsal view; **B.** Same, ventral view; **C.** Same, lateral view; **D.** Female epigyne, ventral view; **E.** Vulva, dorsal view. Scale bars: 0.5 mm (**A–C**); 0.2 mm (**D–E**).

Remarks. A specimen previously identified as *P. vittata* from Gujarat (Tyagi et al. 2019) has been listed here as belonging to this species. The epigyne of this specimen has a longitudinal groove on the ventral surface, present at the mid-line just below the spermathecae. The spermathecae are also comparatively wider than the type illustrated here. The scape is similar to that of the holotype of *Salticus ranjitus* Tikader, 1967 (a synonym of *Phintella vittata*) (cf. fig. S3.29 in Tyagi et al. (2019) with Fig. 13C herein).

***Phintella rajbharathi* Caleb, Sudhin & Sen, sp. nov.**

https://zoobank.org/8FF8C587-E536-44E9-BD1F-9D4995FE3E1F

Figs 6C, D 7A–D, 8A–G, 14

Type material. ***Holotype*** ♂. INDIA: Tamil Nadu, Coimbatore, 10°59'49.71"N, 76°59'8.27"E, 415 m elev., 19.vi.2022, Raj Bharathi coll. (NZC-ZSI-8375/18).

Diagnosis. *P. rajbharathi* sp. nov. can be easily distinguished from those of all other *Phintella* species by the morphology of the tibial apophyses: ventral apophysis relatively short and thin and thorn-like, dorsal apophysis small and hump-shaped (Figs 6D, 8G).

Description. Male (Holotype, NZC-ZSI-8375/18) (Figs 6C, D, 7A–D, 8A–G): Measurements: body length 3.99; carapace length 1.84, width 1.72; abdomen length 2.15, width 1.17. Ocular area length 0.95, width 1.38. Eye diameters: AME 0.44, ALE 0.23, PME 0.07, PLE 0.22. Eye interdistances: AME–AME 0.02, ALE–AME 0.03, ALE–ALE 0.92, ALE–PLE 0.56, PLE–PLE 1.03, PME–PME 1.13, PME–PLE 0.23. Clypeus height 0.04. Length of chelicera 0.52. Measurement of palp and legs: palp 1.71 [0.64, 0.25, 0.18, 0.64], leg I 5.17 [1.60, 0.97, 1.19, 1.00, 0.41], II 3.21 [0.98, 0.58, 0.62, 0.69, 0.34], III 3.82 [1.23, 0.54, 0.74, 0.93, 0.38], IV 4.31 [1.31, 0.57, 0.93, 1.09, 0.41]. Leg formula: 1432. Leg setation: femur

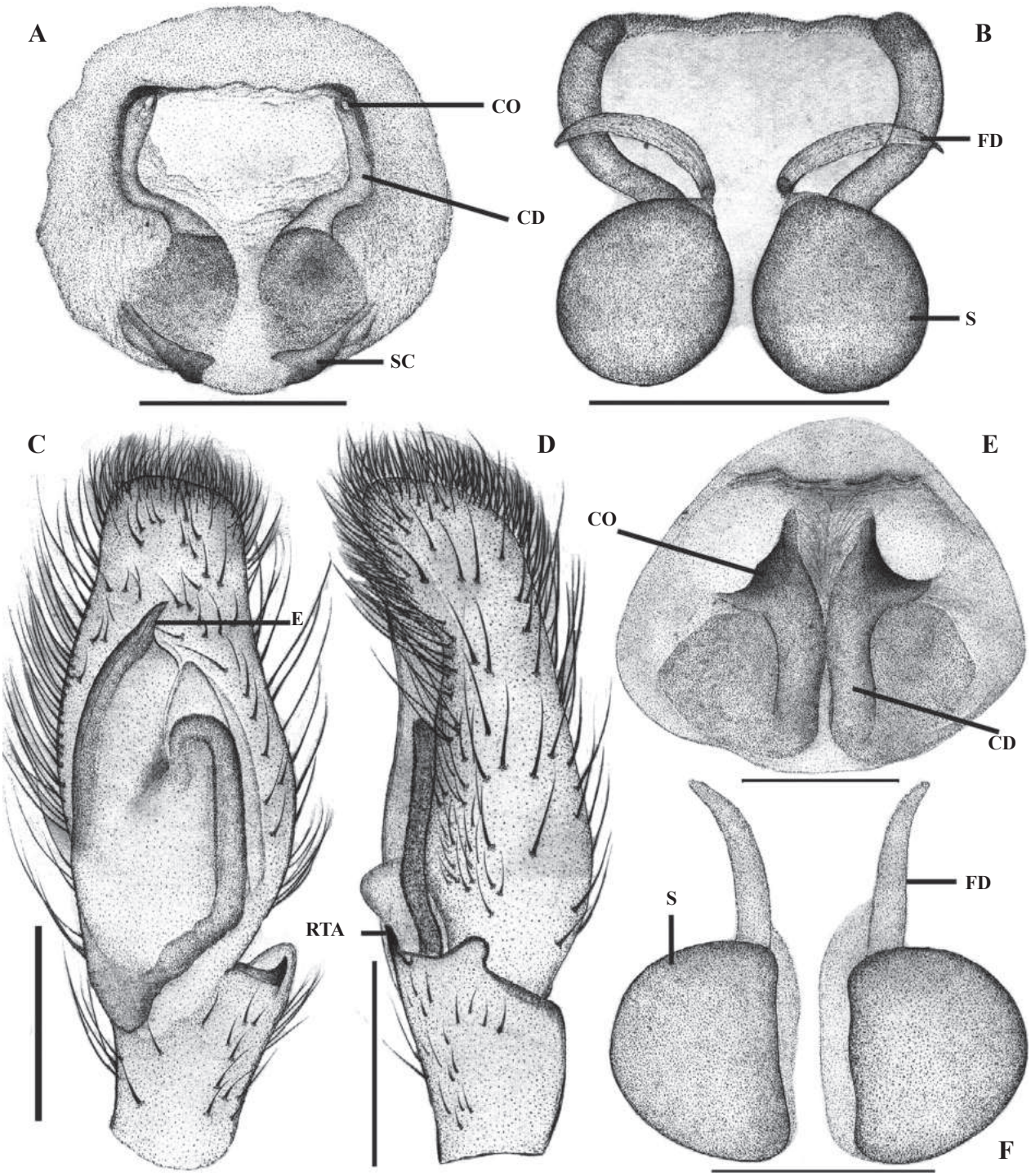

Figure 6. *Phintella luna* sp. nov. (**A, B**), *Phintella rajbharathi* sp. nov. (**C, D**) and *Phintella platnicki* Sudhin, Sen & Caleb, 2023 (**E, F**). **A, E.** Female epigyne, ventral view; **B, F.** Vulva, dorsal view; **C.** Left male palp, ventral view; **D.** Same, retrolateral view. Scale bars: 0.2 mm (**A, B, E, F**); 0.25 mm (**C, D**).

I pl 1 do 3, II–III pl 1 rl 1 do 3, IV pl 2 rl 1 do 3; patella III–IV rl 1; tibia plv 4 rlv 2, II plv 2 rlv 2, III pl 1 rl 2 rlv 2, IV pl 2 rl 3 rlv 1; metatarsus I plv 2 rlv 2, II pl 1 rl 1 plv 2 rlv 2, III pl 2 rl 2 plv 2 rlv 3, IV pl 2 rl 2 plv 2 rlv 2. Carapace oval, high, sloping posteriorly, pale yellowish-brown, covered with brown setae (Fig. 8A); carapace margin with narrow brown lines; eye field densely covered with pale yellow setae, eye bases black, anterior eyes surrounded by pale yellow setae (Fig. 8A, D). Clypeus low, light yellowish-brown, covered with a row of medium-sized light brown setae (Fig. 8D). Chelicerae subvertical, slightly diverging, light yellow to brown, dorsally with a conspicuous bump near fang base (Fig. 8D); promargin with two teeth, one stout with wide base and other small, retromargin with a single tooth with wide base; chelicerae ventrally with a widely curved ridge (Fig. 8E).

Figure 7. *Phintella rajbharathi* sp. nov. **A.** Male, dorsal view; **B.** Same, lateral view; **D, E**. Same, frontal view. Photo credit **A–D**: Raj Bharathi.

Endites scopulate, light yellowish-brown with paler inner sides, margins with black lines (Fig. 8B). Labium yellow brown, with paler tip, distally with light brown setae; with a vertical ridge extending from base to mid-region and a tooth-like bump above it (Fig. 8B). Sternum oval, anteriorly flat, yellow, with light brown margin (Fig. 8B). Abdomen elongate oval, narrowing posteriorly, yellow, laterally with brown longitudinal stripes extending along entire length of abdomen (Fig. 8A,C); venter pale white without any prominent markings (Fig. 8B). Spinnerets light brown with paler tips, covered with light brown setae. Leg I brown with pale yellow metatarsi and tarsi; leg I ventral region provided with short and stout macrosetae; other leg articles pale yellow. Palp yellowish-brown (Figs 8F, G); tibia with two RTA, ventral one short, thin and dorsal one like a hump (Figs 6D, 8G); cymbium elongate oval, covered with long brown setae (Figs 6C, D, 8F–G); posterior lobe small, straight, directed posteriorly with blunt end (Figs 6C, 8F); tegulum with small conical protuberance retrolaterally, sperm duct visible at this shoulder (Figs 6C, 8F); embolus short, situated anterior to bulbus, tip directed at 1 o'clock position in ventral view (Figs 6C, 8F).

Female. Unknown

Etymology. The species is named after the collector of the holotype – Raj Bharathi. The name is treated as a noun in apposition.

Distribution. Known only from the type locality (Fig. 14).

Phintella platnicki Sudhin, Sen & Caleb, 2023

Figs 6E–F, 9A–H, 10A–D, 11A–H, 14

Phintella platnicki Sudhin, Sen & Caleb, 2023: 76, figs 16–23 (♂, examined).

Type material. ***Holotype*** male from INDIA: Tamil Nadu: Salem, Yercaud (10°46′13.95″N, 78°12′6.37″E), 18.x.2019, J. Thilak coll. (NZC-ZSI-7352/18).

Material examined. INDIA: Karnataka: Mookambika Wildlife Sanctuary, Kodachadri, 14♀♀ & 8♂♂, 13°51'25.51"N, 74°52'2.03"E, 1330 m elev., 01.xii.2022, P. P. Sudhin coll. (NZC-ZSI-8376/18). Kerala: Idukki, Kuttikkanam, 7♀♀ & 6♂♂, 9°33'38.44"N, 77°1'2.99"E, 1106 m elev., 24.i.2023, P. Girish Kumar coll. (NZC-ZSI-8377/18).

Diagnosis. The female epigyne of *P. platnicki* Sudhin, Sen & Caleb, 2023, is most similar to that of *Phintella nilgirica* Prószyński, 1992, from which it can be easily distinguished by the broad, funnel-shaped copulatory openings (relatively small and round in *P. nilgirica*) and parallel copulatory ducts (separated, sub-parallel in *P. nilgirica*) (cf. Figs 6E, F, 11C, D, G, H with figs 61–62 in Prószyński (1992)). For the diagnosis of male, see Sudhin et al. (2023).

Description. Male. See Sudhin et al. (2023)

Female (NZC-ZSI-8376-77/18) (Figs 6E, F, 9A–H, 10A–D, 11A–H): Measurements: body length 5.64;

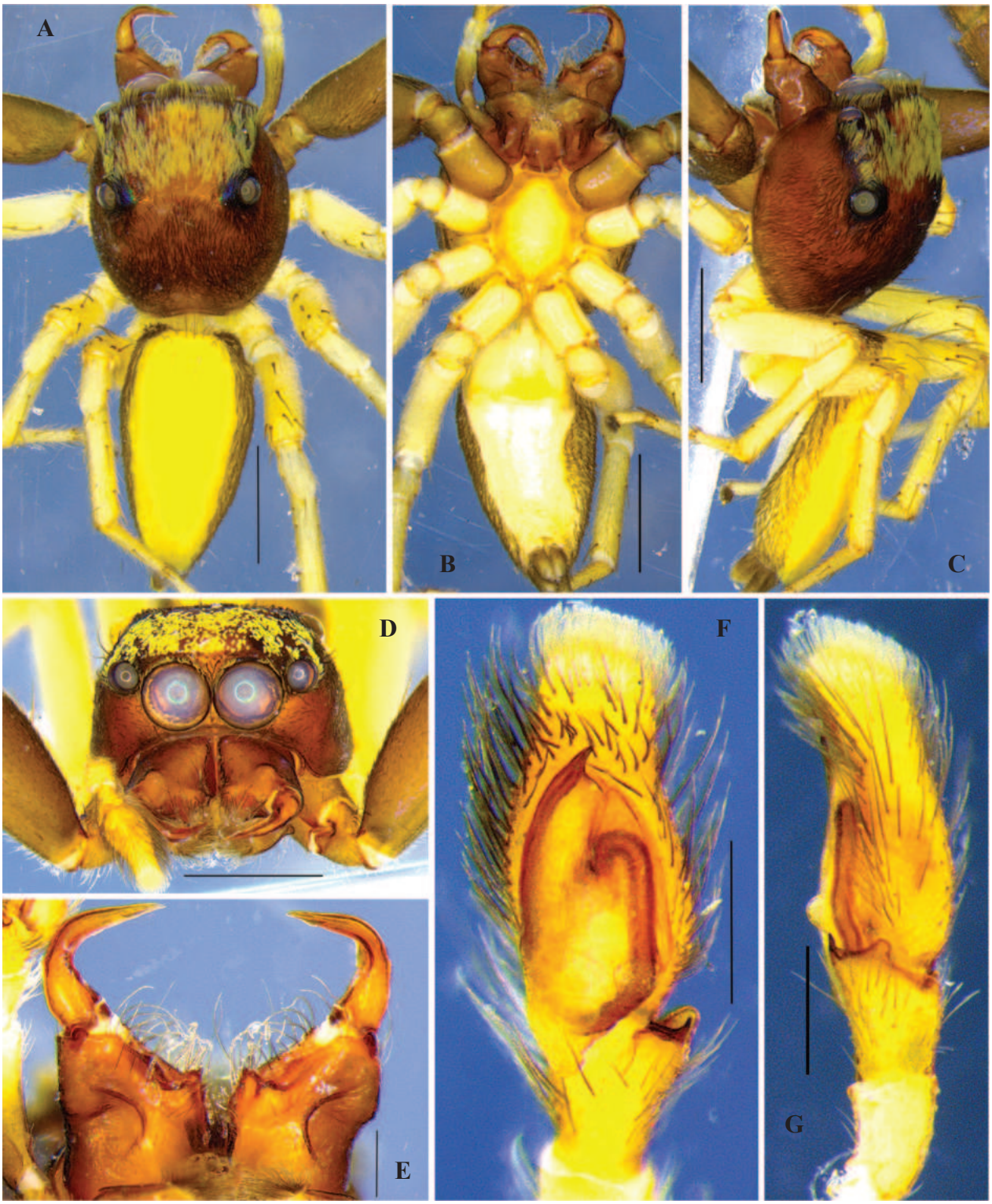

Figure 8. *Phintella rajbharathi* sp. nov. **A.** Male, dorsal view; **B.** Same, ventral view; **C.** Same, lateral view; **D.** Same, frontal view; **E.** Chelicerae, ventral view; **F.** Left male palp, ventral view; **G.** Same, retrolateral view. Scale bars: 1 mm (**A–C**); 0.8 mm (**D**); 0.3 mm (**E**); 0.25 mm (**F, G**).

carapace length 2.09, width 1.52; abdomen length 3.05, width 1.31. Ocular area length 0.95, width 1.31. Eye diameters: AME 0.42, ALE 0.23, PME 0.04, PLE 0.20. Eye interdistances: AME–AME 0.04, ALE–AME 0.03, ALE–ALE 0.89, ALE–PLE 0.50, PLE–PLE 0.98, PME–PME 1.08, PME–PLE 0.20. Clypeus height 0.20. Length of chelicera 0.72. Measurement of palp and legs: palp 1.80 [0.64, 0.22, 0.34, 0.60], leg I 3.81 [1.16, 0.60, 0.87, 0.70, 0.48], II 3.59 [1.17, 0.51, 0.79, 0.66, 0.46], III 4.24 [1.39, 0.45, 0.85, 0.93, 0.62], IV 5.12 [1.57, 0.63, 1.13, 1.24, 0.55]. Leg formula: 4312. Leg setation: femur I pl 1 do 3, II– III pl 1 rl 1 do 3, IV rl 1 do 3;

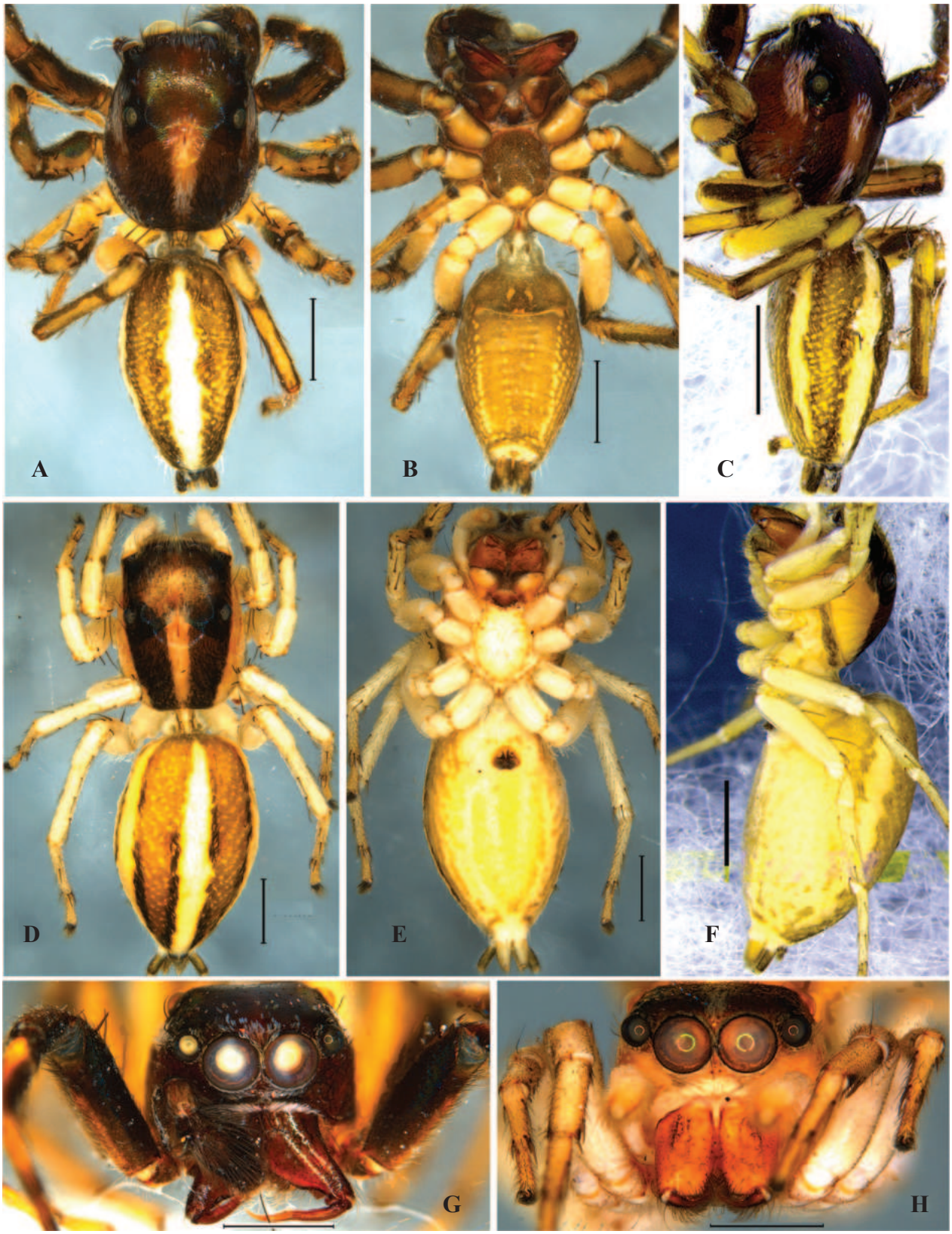

Figure 9. *Phintella platnicki* Sudhin, Sen & Caleb, 2023, from Karnataka. **A.** Male, dorsal view; **B.** Same, ventral view; **C.** Same, lateral view; **D.** Female, dorsal view; **E.** Same, ventral view; **F.** Same, lateral view; **G.** Male, frontal view; **H.** Female, frontal view. Scale bars: 1 mm (**A–H**).

patella III–IV rl 1; tibia I–II pl 2 rl 1 plv 4 rlv 4, III pl 2 rl 2 plv 1 rlv 1, IV pl 2 rl 3 plv 2 rlv 1; metatarsus I–II pl 1 rl 1 plv 2 rlv 2, II pl 2 rl 2 plv 2 rlv 2, III pl 2 rl 2 plv 1 rlv 2, IV pl 3 rl 3 plv 1 rlv 2. Carapace oval, high, sloping posteriorly, pale yellow, covered with short pale white and dark brown setae (Fig. 9D); thoracic region

Figure 10. *Phintella platnicki* Sudhin, Sen & Caleb, 2023, from Kerala. **A.** Male, dorsal view; **B.** Female, dorsal view; **C.** Male, frontal view; **D.** Female, frontal view. Scale bars: 1 mm (**A–D**).

dorsally with two broad dark brown longitudinal stripes (Fig. 9D); margin of carapace with narrow black lines; eye field pale yellow to brown, eye bases black, anterior eyes surrounded by pale yellow orbital setae (Fig. 9D, H). Clypeus low, pale yellow, covered with pale white setae (Fig. 9H). Chelicerae small, yellowish-brown (Fig. 9H), promargin with two teeth and retromargin with a single tooth. Endites pale yellow to yellow, scopulate (Fig. 9E). Labium light-brown, with paler tip, distally with dark brown setae (Fig. 9E). Sternum oval, pale white (Fig. 9E). Abdomen elongate oval, narrowing posteriorly, pale yellow, dorsally with a pair of broad lateral longitudinal light brown bands extending along entire length (Fig. 9D); abdomen lateral sides with irregular light brown longitudinal streaks and patches (Fig. 9F); venter pale yellow, medially with broad light brown longitudinal band and sides with irregular light brown patches (Fig. 9E). Spinnerets light brown. Legs pale yellow with black pro- and retrolateral mottling on proximal and distal areas of tibiae I and distal areas of tibiae II. Epigyne simple, moderately sclerotised, nearly apple-shaped, covered with white setae (Figs 6E, 11C, G); copulatory openings broad, funnel-shaped, anterolaterally orientated (Figs 6E, 11C, G); copulatory ducts long, highly sclerotised, slightly curved anteriorly, running parallel along mid-longitudinal axis and then connected to posterior part of spermathecae (Figs 6E, 11C, G); spermathecae highly sclerotised, nearly semi-circular in shape, separated from each other (Figs 6F, 11D, H); fertilisation ducts long, orientated anteriorly, located at anterior region of spermathecae (Figs 6F, 11D, H).

Distribution. India: Type locality – Tamil Nadu. New records from Karnataka and Kerala (Fig. 14).

Variation. Both sexes of the species have been collected from new localities in south India. Darker and lighter forms have been found in the collections and the variation in the colour pattern of the female have also been illustrated in Figs 9A–H, 10A–D, 11A–H.

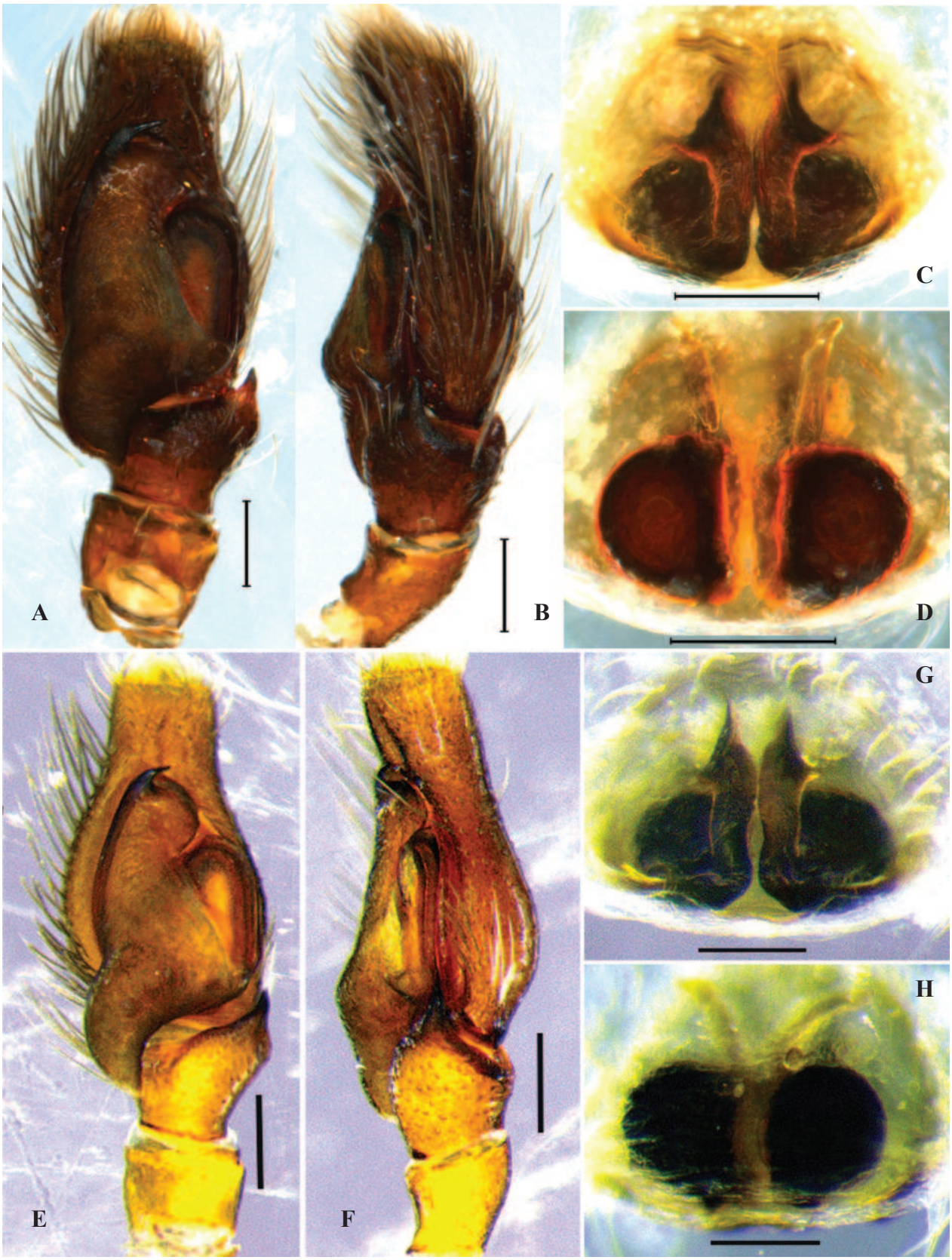

Figure 11. *Phintella platnicki* Sudhin, Sen & Caleb, 2023, from Karnataka (**A–D**) and from Kerala (**E–H**). **A, E.** Left male palp, ventral view; **B, F.** Same, retrolateral view; **C, G.** Female epigyne, ventral view; **D, H.** Vulva, dorsal view. Scale bars: 0.2 mm (**A–F**); 0.1 mm (**G–H**).

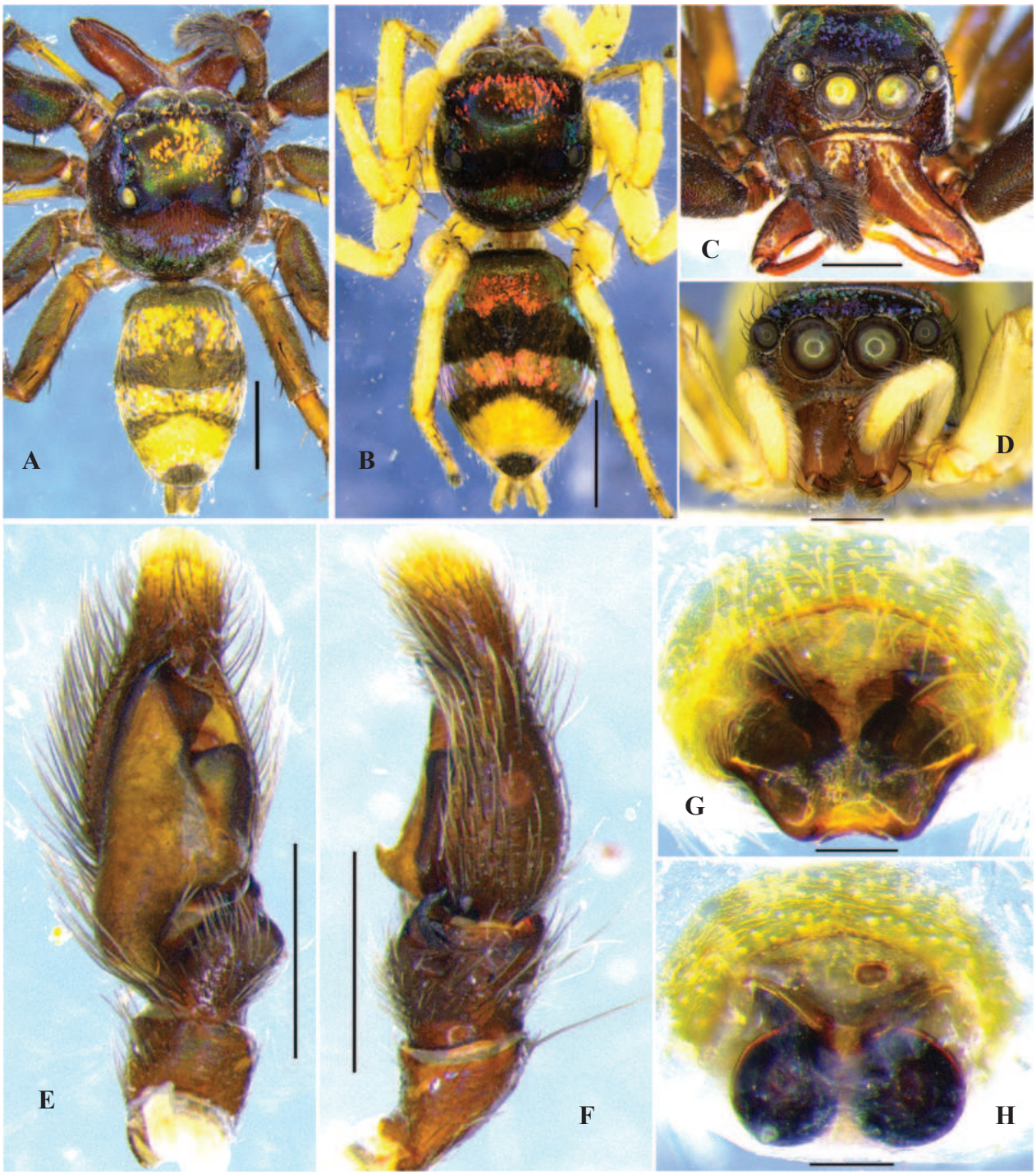

Figure 12. *Phintella vittata* (C. L. Koch, 1846). **A.** Male, dorsal view; **B.** Female, dorsal view; **C.** Male, frontal view; **D.** Female, frontal view; **E.** Left male palp, ventral view; **F.** Same, retrolateral view; **G.** Female epigyne, ventral view; **H.** Vulva, dorsal view. Scale bars: 1 mm (**A, B**); 0.5 mm (**C–F**); 0.1 mm (**G–H**).

Discussion

The present work deals with the description of four new species of the genus *Phintella* Strand, 1906 from India. With the addition of these new species, the total number of *Phintella* species known in India increases from 14 to 18 (Caleb and Sankaran 2023). India has the second highest number of *Phintella* species ever recorded in a single country after China (World Spider Catalog 2023). Sudhin et al. (2023) observed that Indian *Phintella* species are mainly reported from the southern and eastern regions of the country, except for *P. cholkei* Prajapati, Kumbhar, Caleb, Sanap & Kamboj, 2021 and *P. vittata* (C. L. Koch, 1846), both of which occur in the western region. In the present study, *P. dentis* sp. nov., *P. handersoni* sp. nov., *P. rajbharathi* sp. nov. and *P. platnicki* Sudhin, Sen & Caleb, 2023 are reported from the southern or eastern regions of the country, while *P. luna* sp. nov. is being reported from both the western and eastern regions (Fig. 14). However, the exact diversity and distribution of

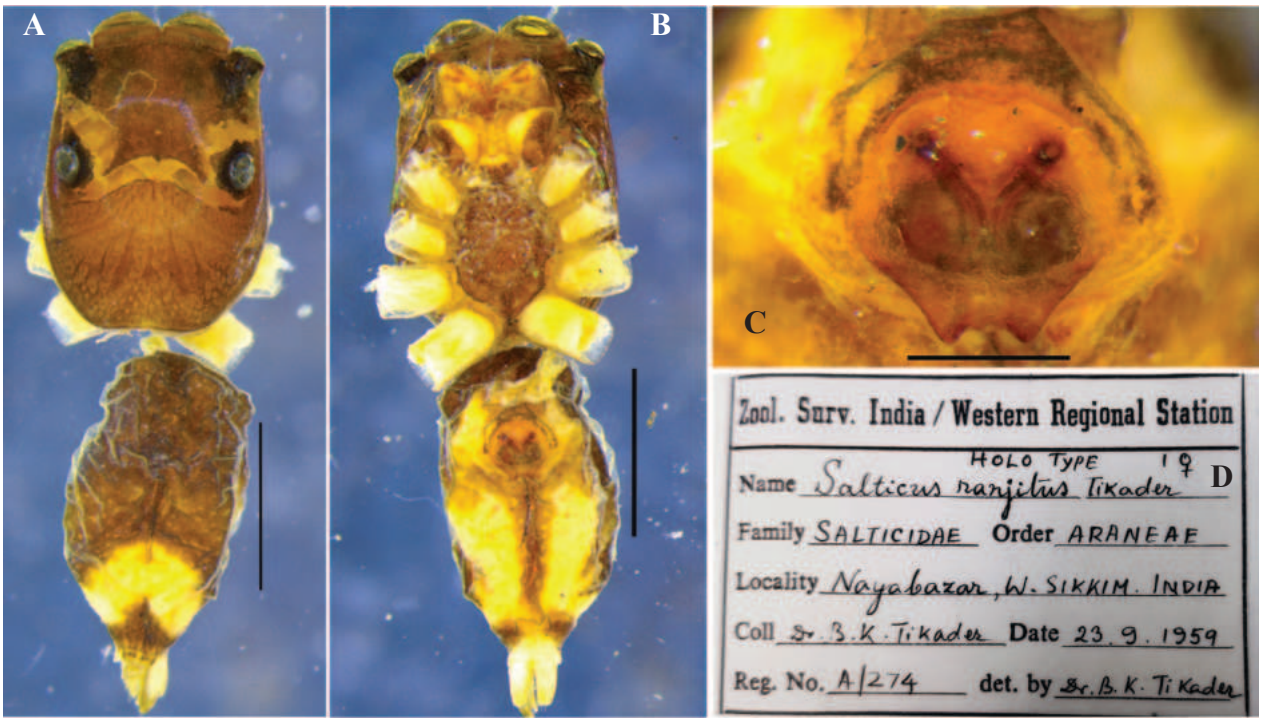

Figure 13. *Phintella vittata* (C. L. Koch, 1846) (Holotype of *Salticus ranjitus* Tikader, 1967). **A.** Female, dorsal view; **B.** Same, ventral view; **C.** Female, epigyne, ventral view. Scale bars: 1 mm (**A, B**); 0.25 mm (**C**).

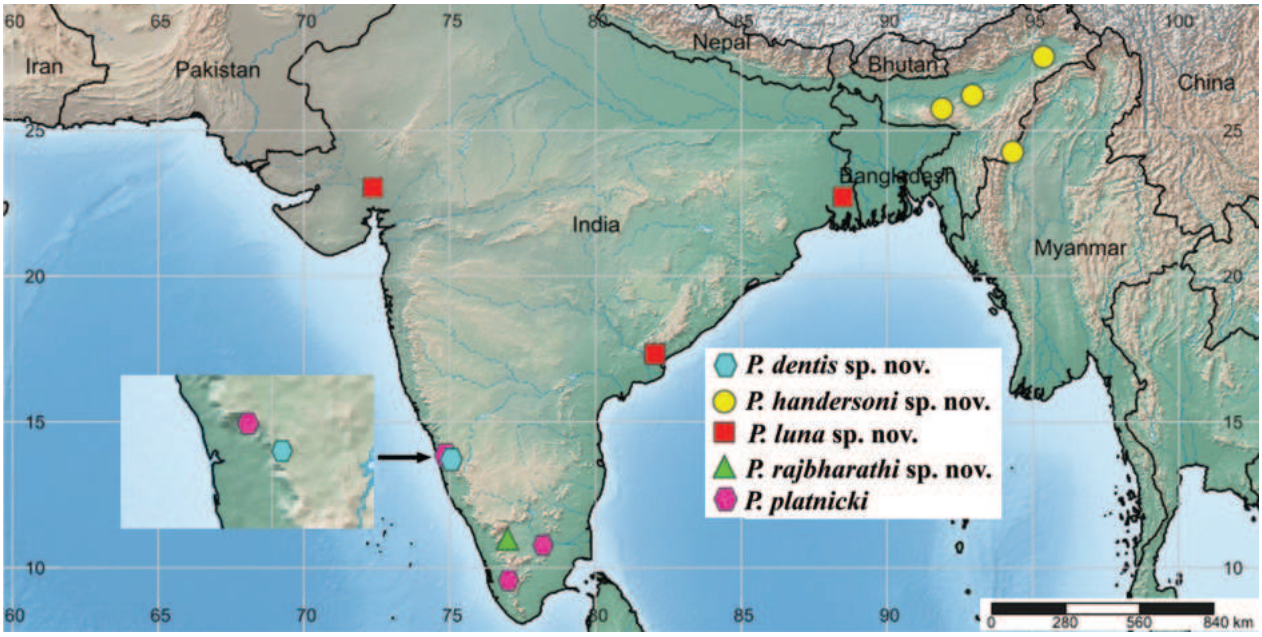

Figure 14. Distributional map of *Phintella* species dealt in this study.

the genus in India remains unclear and must await more comprehensive surveys covering underexplored areas particularly the central and northern regions in India.

Acknowledgements

The authors are grateful to Dr Dhriti Banerjee, Director of the Zoological Survey of India for providing necessary facilities for completing this work. John Caleb thanks Dr Deepak Nallaswamy Veeraiyan the Director of Academics, SIMATS, Saveetha University, Chennai for necessary permissions to carry out the work. We are thankful for the support extended by Dr V. D. Hegde, Officer-in-Charge of Zoological Survey of India, Western Ghat Regional Centre, Kozhikode, Dr K. A Subramanian, Officer-in-Charge of Zoological Survey of India, Southern Regional Centre, Chennai and Dr Deepa Jaiswal, Officer-in-Charge of Zoological Survey of India, Freshwater Biology Regional Centre, Hyderabad. We are grateful to Mr. Nathanael P A Newmai and Mr. Marbakynsai Marbaniang, Shillong, Meghalaya for their support during the survey. We thank the

Chief Conservator of Forest and Chief Wildlife Warden, Karnataka and Kerala State Forest Departments for providing necessary permission and support during the surveys. Thanks to Chandan Bera for his curatorial assistance. We extend our heartfelt thanks to the editor Dr Danilo Harms (Germany) and the two reviewers, Dr Galina N. Azarkina (Russia) and Dr Tamás Szűts (Hungary) for their constructive comments and suggestions on the manuscript.

References

Barrion AT, Barrion-Dupo ALA, Catindig JLA, Villareal MO, Cai D, Yuan QH, Heong KL (2013) New species of spiders (Araneae) from Hainan Island, China. UPLB Museum Publications in Natural History 3: 1–103. https://doi.org/10.5281/zenodo.269136

Caleb JTD, Sankaran PM (2023) Araneae of India. Version 2023. http://www.indianspiders.in [accessed on 13 September 2023]

Cao Q, Li SQ, Żabka M (2016) The jumping spiders from Xishuangbanna, Yunnan, China (Araneae, Salticidae). ZooKeys 630: 43–104. https://doi.org/10.3897/zookeys.630.8466

Hoang QD, Tran HPT, Vu TB, Pham PT (2023) A new species and a new record of the jumping spider genus *Phintella* Strand, 1906 (Araneae: Salticidae) from the Central Highlands of Vietnam. Bonn Zoological Bulletin 72(1): 145–150. https://doi.org/10.20363/BZB-2023.72.1.145

Huang Y, Wang C, Peng XJ (2015) Five new species of *Phintella* Strand, 1906 (Araneae: Salticidae) from the Wuling Mountains, China. ZooKeys 514: 25–42. https://doi.org/10.3897/zookeys.514.9159

Kanesharatnam N, Benjamin SP (2019) Multilocus genetic and morphological phylogenetic analysis reveals a radiation of shiny South Asian jumping spiders (Araneae, Salticidae). ZooKeys 839: 1–81. https://doi.org/10.3897/zookeys.839.28312

Lei H, Peng XJ (2013) Five new species of the genus *Phintella* (Araneae: Salticidae) from China. Oriental Insects 47(1): 99–110. https://doi.org/10.1080/00305316.2013.783747

Li Q, Wang LY, Zhang ZX, Chen HM (2019) Two new spider species (Arachnida, Araneae) from Fanjingshan National Nature Reserve, Guizhou, China. Journal of Guangxi Normal University (Natural Science Edition) 36(4, 2018): 119–123.

Luong PTH (2017) Taxonomic revision of Vietnamese species of the genus *Phintella* Strand (Araneae, Salticidae). Doctoral Thesis, Tokyo, 176 pp. https://core.ac.uk/download/pdf/235010666.pdf [accessed on 11 August 2023]

Patoleta B (2009) Description of a new species of *Phintella* Strand in Bösenberg et Strand, 1906 from New Caledonia (Araneae: Salticidae). Genus 20: 539–543.

Peng XJ (2020) Fauna Sinica, Invertebrata 53, Arachnida: Araneae: Salticidae. Science Press, Beijing, 612 pp.

Peng XJ, Xie LP, Xiao XQ, Yin CM (1993) Salticids in China (Arachniuda: Araneae). Hunan Normal University Press, 270 pp.

Prajapati DA, Kumbhar SB, Caleb JTD, Sanap RV, Kamboj RD (2021) Description of two new species of the tribe Chrysillini Simon, 1901 from India (Araneae: Salticidae). Arthropoda Selecta 30(2): 230–238. https://doi.org/10.15298/arthsel.30.2.10

Prószyński J (1984) Atlas rysunków diagnostycznych mniej znanych Salticidae (Araneae). Zeszyty Naukowe Wyższej Szkoły Rolniczo-Pedagogicznej w Siedlcach 2: 1–177.

Prószyński J (1992) Salticidae (Araneae) of the Old World and Pacific Islands in several US collections. Annales Zoologici, Warszawa 44: 87–163.

Shorthouse DP (2010) SimpleMappr, an online tool to produce publication-quality point maps. http://www.simplemappr.net [Accessed 11 August 2023]

Simon E (1901) Histoire naturelle des araignées. Deuxième édition, tome second. Roret, Paris, 381–668 pp.

Song DX, Zhu MS, Chen J (1999) The spiders of China. Hebei Science and Technology Publishing House, Shijiazhuang, 640 pp.

Sudhin PP, Sen S, Caleb JTD (2023) New species and records in the genus *Phintella* Strand, 1906 (Araneae: Salticidae, Chrysillini) from India. Arthropoda Selecta 32(1): 80–88. https://doi.org/10.15298/arthsel.32.1.07

Tyagi K, Kumar V, Kundu S, Pakrashi A, Prasad P, Caleb JTD, Chandra K (2019) Identification of Indian spiders through DNA barcoding: cryptic species and species complex. Scientific Reports 9(14033): 1–13. [+Supplement] https://doi.org/10.1038/s41598-019-50510-8

Wang C, Li SQ (2020) Seven new species of jumping spiders (Araneae: Salticidae) from Xishuangbanna, China. ZooKeys 968: 43–69. https://doi.org/10.3897/zookeys.968.55047

WSC (2023) World Spider Catalog. Version 23.5. Natural History Museum Bern. http://wsc.nmbe.ch [accessed on 13 September 2023]

Xie LP (1993) New records of Salticidae from China (Arachnida: Araneae). Acta Scientiarum Naturalium Universitatis Normalis Hunanensis 16: 358–361.

Żabka M (1985) Systematic and zoogeographic study on the family Salticidae (Araneae) from Viet-Nam. Annales Zoologici, Warszawa 39: 197–485.

Zoosyst. Evol. 100 (1) 2024, 49–59 | DOI 10.3897/zse.100.113707

PENSOFT

für Natur MUSEUM FÜR NATURKUNDE BERLIN

First occurrence of the genus *Pleurobranchaea* Leue, 1813 (Pleurobranchida, Nudipleura, Heterobranchia) in British waters, with the description of a new species

Martina Turani[1], Leila Carmona[2,3], Peter J. Barry[4], Hayden L. Close[4], Ross Bullimore[4], Juan Lucas Cervera[2,3]

1 *Department of Natural History, University Museum, University of Bergen, Bergen, Norway*
2 *Departamento de Biología, Facultad de Ciencias del Mar y Ambientales, Campus de Excelencia Internacional del Mar (CEI•MAR), Universidad de Cádiz, Av. República Saharaui, s/n, 11510 Puerto Real, Spain*
3 *Instituto Universitario de Investigación Marina (INMAR), Campus de Excelencia Internacional del Mar (CEI•MAR), Universidad de Cádiz, Av. República Saharaui, s/n, 11510 Puerto Real, Spain*
4 *Centre for Environment Fisheries and Aquaculture Science (CEFAS), Lowestoft, Suffolk, UK*

https://zoobank.org/579ED8AF-40E7-4FE4-A8AF-ED87567D5DCC

Corresponding author: Leila Carmona (leila.carmona@uca.es)

Academic editor: M. Glaubrecht ♦ **Received** 5 October 2023 ♦ **Accepted** 28 November 2023 ♦ **Published** 26 January 2024

Abstract

In the north-eastern Atlantic and Mediterranean Sea, the pleurobranchid genus *Pleurobranchaea* Leue, 1813 is represented by two species, *Pleurobranchaea meckeli* (Blainville, 1825) and *Pleurobranchaea morosa* (Bergh, 1892). The former is a well-known species distributed from northern Spain to Senegal and the Mediterranean Sea, while the second is a poorly-described species. In this contribution, species delimitation analyses (ABGD and COI/16S *p*-distances) identified a third undescribed *Pleurobranchaea* species from samples collected in south-western UK waters and the Gulf of Cadiz (SW Spain). This new species, *Pleurobranchaea britannica* **sp. nov.**, is also supported by several morphological synapomorphies. The British specimens constitute the first occurrence of the genus *Pleurobranchaea* in UK waters.

Key Words

Atlantic Ocean, Gulf of Cadiz, Mediterranean Sea, molluscan diversity, *Pleurobranchaea britannica*, Pleurobranchaeidae, southwest UK, systematics

Introduction

The family Pleurobranchaeidae Pilsbry, 1896 was established for heterobranchs, characterised by an oval body, broad oral veil, rolled rhinophores and variable colours. Members of this family have a bipinnate gill in the middle of the right side, which may or may not be covered by the mantle (García-Gomez and Cervera 2011). The latter character led to their inclusion together with the Umbraculida (Order Notaspidea). However, phylogenetic analyses, based on morphological and molecular data (Martynov and Schrödl 2009; Göbbeller and Klussmann-Kolb 2010), demonstrated that the Pleurobranchaeidae should be considered as a separate group. Under an alternative classification scheme, Wägele and Willan (2000) introduced the Nudipleura to unite Pleurobranchoidea and Nudibranchia. Some characteristics the Nudipleura have in common are: the loss of the shell, the presence of papillae on the notum, a hermaphroditic reproductive system with simultaneous maturation of the gametes and obligate cross-fertilisation involving copulation.

Members of the Pleurobranchaeidae are active hunters of invertebrates and typically inhabit sedimentary substrates. The family is ubiquitous and they can be

found from the intertidal zone to the circalittoral. The family is considered monophyletic and comprises three genera: *Pleurobranchaea* Leue, 1813, *Euselenops* Pilsbry, 1896 and *Pleurobranchella* Thiele, 1925. The genus *Pleurobranchaea* constitutes 15 valid species (Alvim et al. 2014; MolluscaBase 2023a) that inhabit temperate or tropical waters across a wide geographical range (Muniain et al. 2007; Alvim et al. 2014). The type species of the genus, *Pleurobranchaea meckeli* (Blainville, 1825), is the only well-known species from European waters (Bergh 1897; Vayssière 1901; Marcus and Gosliner 1984). This species has been recorded in many localities from the Mediterranean Sea, as well as in several localities around the Atlantic Iberian coasts, Madeira, Canary Islands, Azores (Cervera et al. 2004) and Cape Verde Archipelago (Vayssière 1901). Marcus and Gosliner (1984) described two additional species of *Pleurobranchaea*, based on preserved material collected from Turkey, Israel (*P. notmec*) and Algiers (*P. vayssierei*). However, Cervera and Garcia-Gomez (1988), following Willan (pers. comm.), considered both names to be junior synonyms of *P. meckeli*. Bergh (1892) described *P. morosa* from a single specimen collected from the Pico-Faial Channel (Azores) at 130 m depth. No further records are attributed to this second species, since Marcus and Gosliner (1984) did not include *P. morosa* in their review of the Pleurobranchaeidae due to its insufficient description.

The northernmost record of *Pleurobranchaea* in the eastern Atlantic had been from northern Spain (Cervera et al. 2004), but recent bottom trawls conducted along the English Channel in 2018 and 2019, as well as in the Gulf of Cadiz (SW Iberian Peninsula) in 2020 collected specimens of an unknown pleurobranchid with an external appearance slightly different from *Pleurobranchaea meckeli.* During the surveys, the collected specimens were initially considered as a different morphotype of *P. meckeli*, but a detailed examination of the external and internal anatomy revealed marked differences from all other species of the genus. Subsequently, a phylogenetic analysis, based on two mitochondrial (cytochrome-oxidase subunit I and 16SrRNA) and one nuclear (Histone 3) marker, in conjunction with species delimitation analyses, supported the status of this morphotype as a new and previously undescribed species, which is formally described in the present paper.

Materials and methods

Taxon sampling and molecular data

Fourteen specimens of an undescribed species of *Pleurobranchaea* were collected during two different campaigns in southern England (Fig. 1A) and one in the Gulf of Cadiz (Fig. 1B). The surveys in the Western Channel and Celtic Sea occurred during the 2018 and 2019 Centre for Environment, Fisheries and Aquaculture Science (CEFAS) Quarter One South West EcoSystem (Q1SWECOS) surveys. This survey series used two commercially rigged 4 m beam trawls with 80 mm cod-end mesh, with one of the trawls fitted with a 40 mm liner to facilitate the collection of epibenthic species. The bathymetric range covered by the trawls was approximately 20–200 m. The survey conducted by the Instituto Español de Oceanografía (IEO-CSIC) in the Gulf of Cadiz, offshore between Faro and Cadiz was collected by beam trawl of 190 cm and the effective height was 60 cm above the bottom with a duration of 15 min.

The material collected in these campaigns was deposited either in the Natural History Museum of London (NHM) or in the National Museum of Natural Sciences of Madrid (MNCN) (see Table 1). Twenty-four specimens of three different species (11 *Pleurobranchaea meckeli*, 4 *P. maculata* and 14 of the new species) were sequenced in this study to obtain partial sequences of two mitochondrial (cytochrome-oxidase subunit I or COI and 16SrRNA or 16S) and one nuclear (Histone 3 or H3) markers.

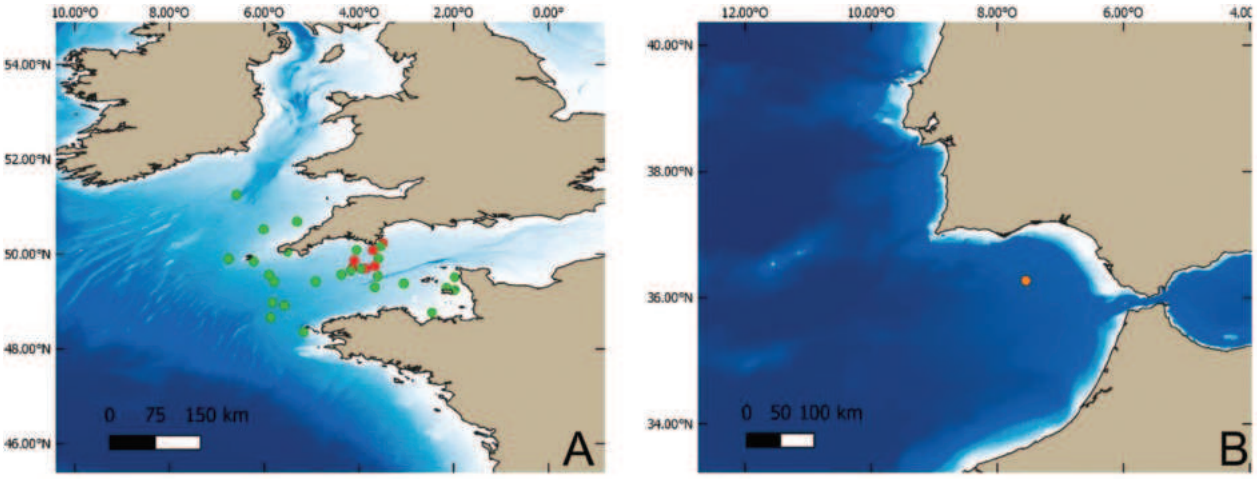

Figure 1. Sampling stations where *Pleurobranchaea britannica* sp. nov. material was collected. **A.** The map on the left shows the south of England: the red dots refer to the 2018 campaign and the green dots to the 2019 campaign; **B.** The map on the right shows part of Spain and the orange dot is where samples were collected in 2019.

Additionally, sequences of these genes from ten closely-related pleurobranchid taxa were added from GenBank, including two additional species of *Pleurobranchaea* (*P. californica* and *P. inconspicua*) and *Bathydoris aioca* (Er. Marcus and Ev. Marcus, 1962), *Bathydoris clavigera* (Thiele, 1912) and *Berthella plumula* (Montagu, 1803) as outgroups (Table 1).

Morphological analysis

The samples were stored in 95%–100% ethanol to allow DNA extraction. Two specimens were dissected by dorsal incision. The internal morphology of the reproductive system was examined and drawn using a Leica Wild M8 dissection microscope. The buccal bulb was removed and placed in a 10% sodium hydroxide (NaOH) solution for three days until the radulae and jaws were cleaned of the surrounding tissue. The radula and jaws were then rinsed in demineralised water and rinsed at least twice with 96% ethanol before drying. Clean radulae and jaws were mounted on SEM stubs with dissection pins and coated with gold for examination with a Nova NanoSEM scanning electron microscope (SEM) at the Central Services of Scientific and Technological Research (SC-ICYT) unit of the University of Cadiz.

DNA extraction and amplification

Genomic DNA was extracted from foot tissue of specimens using the DNeasy Blood & Tissue Kits of Qiagen (Qiagen, Inc., Valencia, Ca., USA) and stored in extraction buffer at –20 °C prior to amplification. Partial sequences of H3 were amplified by polymerase chain reaction (PCR) using the universal primers H3F and H3R (Colgan et al. 2000), while universal and specific primers or their combination were used for the COI and 16S (Table 2).

Table 1. List of species used for this study including sample locality, voucher numbers and GenBank accession numbers.

Species	Locality	Voucher numbers	GenBank accession numbers		
			COI	16S	H3
Berthella plumula (Montagu, 1803)	Ballyhenry Is., Northern Ireland, UK	CASIZ 193034	MK542770	MK542742	MK542803
Prodoris clavigera Thiele, 1912	South Shetland I., Elephant I., Antartica	CASIZ 167553	JX274106	JX274067	KP940463
Bathydoris aioca Er. Marcus & Ev. Marcus, 1962	California	CPIC 01053	KP153283	KP153249	KP153316
Pleurobranchaea maculata Quoy & Gaimard, 1832	Auckland, New Zealand	–	JN675223	–	–
Pleurobranchaea maculata	Auckland, New Zealand	–	JN675222	–	–
Pleurobranchaea maculata	Auckland, New Zealand	–	JN675221	–	–
Pleurobranchaea maculata	Auckland, New Zealand	–	JN675220	–	–
Pleurobranchaea californica MacFarland, 1966	California	–	–	FJ917440	–
Pleurobranchaea inconspicua Bergh, 1897	Patagonia, Argentine, Atlantic Ocean	MNCN 15.05/94846	–	OR723442	OR715121
Pleurobranchaea meckeli (Blainville, 1825)	Blanes, Spain, Mediterranean Sea	–	AY345026	–	–
Pleurobranchaea meckeli	Blanes, Spain, Mediterranean Sea	–	–	–	EF133470
Pleurobranchae meckeli 005	Castellaneta Marina, Italy, Mediterranean Sea	MNCN 15.05/94841	–	OR723434	OR715119
Pleurobranchaea meckeli 006	Castellaneta Marina, Italy, Mediterranean Sea	MNCN 15.05/94842	OR687335	OR723435	OR715118
Pleurobranchaea meckeli 008	Gulf of Cadiz, Spain, Atlantic Ocean	MNCN 15.05/94843	OR687340	OR723441	OR715116
Pleurobranchaea meckeli 010	Gulf of Cadiz, Spain, Atlantic Ocean	MNCN 15.05/94844	OR687336	OR723436	OR715117
Pleurobranchaea meckeli 016	Laayoun, Morocco, Atlantic Ocean	MNCN 15.05/94845	OR687341	OR723437	–
Pleurobranchaea meckeli 21.1	Gulf of Cadiz, Spain, Atlantic Ocean	MNCN 15.05/94837	OR687337	OR723438	OR715120
Pleurobranchaea meckeli 21.2	Gulf of Cadiz, Spain, Atlantic Ocean	MNCN 15.05/94838	OR687339	OR723440	OR715115
Pleurobranchaea meckeli 21.3	Gulf of Cadiz, Spain, Atlantic Ocean	MNCN 15.05/94839	OR687338	OR723439	OR715114
Pleurobranchaea meckeli 22.1	Gulf of Cadiz, Spain, Atlantic Ocean	MNCN 15.05/94840	OR807509	–	–
Pleurobranchaea britannica sp. nov. 17.1	Southwest of England	NHMUK 20230086	OR687348	OR723452	OR715123
Pleurobranchaea britannica sp. nov. 17.2	Southwest of England	NHMUK 20230087	OR687349	OR723446	OR715122
Pleurobranchaea britannica sp. nov. 17.3	Southwest of England	NHMUK 20230085	OR687351	OR723453	OR715124
Pleurobranchaea britannica sp. nov. 17.4	Southwest of England	NHMUK 20230088/1	OR687347	OR723444	OR715125
Pleurobranchaea britannica sp. nov. 18.1	Southwest of England	MNCN 15.05/200180	–	OR723447	–
Pleurobranchaea britannica sp. nov. 18.2	Southwest of England	NHMUK 20230089	–	–	OR715126
Pleurobranchaea britannica sp. nov. 18.3	Southwest of England	NHMUK 20230090	–	–	OR715127
Pleurobranchaea britannica sp. nov. 18.4	Southwest of England	NHMUK 20230091	–	–	OR715128
Pleurobranchaea britannica sp. nov. 20.1	Gulf of Cadiz, Spain, Atlantic Ocean	MNCN 15.05/200181	OR687345	OR723448	OR715132
Pleurobranchaea britannica sp. nov. 20.2	Gulf of Cadiz, Spain, Atlantic Ocean	MNCN 15.05/200182	OR687343	OR723449	OR715133
Pleurobranchaea britannica sp. nov. 20.3	Gulf of Cadiz, Spain, Atlantic Ocean	MNCN 15.05/200183	OR687346	OR723450	OR715129
Pleurobranchaea britannica sp. nov. 20.4	Gulf of Cadiz, Spain, Atlantic Ocean	MNCN 15.05/200184	OR687342	OR723451	OR715130
Pleurobranchaea britannica sp. nov. 20.5	Gulf of Cadiz, Spain, Atlantic Ocean	MNCN 15.05/200185	OR687344	OR723445	OR715134
Pleurobranchaea britannica sp. nov. 20.6	Gulf of Cadiz, Spain, Atlantic Ocean	MNCN 15.05/200186	OR687350	OR723443	OR715131

Table 2. List of primers used for this study.

Gene	Primer ID	Sequence (5'to-3')	Annealing Temperature (°C)	Source
COI	LCO1490 (F)	GGTCAACAAATCATAAAGATATTGG	50	Folmer et al. (1994)
	HCO2198 (R)	TAAACTTCAGGGTGACCAAAAATCA	50	Folmer et al. (1994)
	Pluero26F (F)	GAGTTGGGGACTTCAGGAGC	46	This study
	Pluro526R (R)	AATAGCCCCCGCCAATACTG	46	This study
	jgLCO1490 (F)	TITCIACIAAYCAYAARGAYATTGG	50	This study
	jgHCO2198 (R)	TAIACYTCIGGRTGICCRAARAAYCA	50	This study
16S	Sar-L (F)	CGCCTGTTTATCAAAAACAT	52	Palumbi (1996)
	Sbr-H (R)	CCGGTCTGAACTCAGATCACGT	52	Palumbi (1996)
	F52 (F)	ATAGCCGCGGTACTTTGACC	55	This study
	R384 (R)	AGTCCAACATCGAGGTCACA	55	This study
H3	H3F (F)	ATGGCTCGTACCAAGCAGAGVGC	58	Colgan et al. (1998)
	H3R (R)	ATATCCTTRGGCATRATRGTGAC	58	Colgan et al. (1998)

Reactions took place in a total volume of 25 µl including 2 µl of template DNA, 1 µl of both forward and reverse primers (10 µM), 2.5 µl of dNTP (2 mM), a gene-dependent amount of magnesium chloride (25 mM), 0.25 µl of Qiagen DNA polymerase (5 u/µl), 5 µl of "Q-solution" (5×) and 2.5 µl of Qiagen buffer (10×; Qiagen Taq PCR Core Kit cat. no. 201225). Magnesium chloride ($MgCl_2$) amounts were 4.5 µl for COI and 16S and 3 µl for H3. The COI fragment was amplified with initial denaturation step for 1 min at 95 °C, followed by 35 cycles of 30 s at 95 °C, an annealing step for 30 s at 52 °C (universal primer) or 50–46 °C (specific primer) and 30 s at 72 °C. A final extension step for 3 min at 72 °C was added to ensure extension. For 16S, the thermal cycle profile began with denaturation for 1 min at 95 °C, followed by 35 cycles of 30 s at 95 °C, 16 s at 52 °C (universal primer) or 16 s at 55 °C (specific primer) and 30 s at 72 °C, with a final extension step for 3 min at 72 °C. Finally, the H3 amplification was performed with an initial denaturation for 2 min at 95 °C, followed by 40 cycles of 30 s at 94 °C, an annealing step for 30 s at 58 °C and 1 min at 72 °C, with a final extension step at 72 °C for 7 min. A negative control (no template) was included in each reaction. PCR products were visualised by electrophoresis on a 2% agarose gel and those viable were purified and amplified in both directions by Macrogen Inc. All new sequences obtained were deposited in GenBank.

Nucleotide sequence alignment and phylogenetic reconstruction

All DNA chromatograms were assembled and edited using Geneious version 10.0.9 (http://www.geneious.com, Kearse et al. 2012). The sequences were aligned with MAFFT v.7.402 server (Katon and Standley 2013) using the L-INS-i iterative refinement algorithm via the CIPRES Portal Science Gateway (Miller et al. 2010). The alignments were further optimised by eye using AliView (Larsson 2014) and trimmed to 328 bp (H3), 658 bp (COI) and 450 bp (16S). These partitions were subsequently concatenated with FASconCAT-G v.1.0, resulting in 1436 bp alignment. Pairwise uncorrected *p*-distances between each available taxon were conducted for the COI and 16S gene using PAUP v.4.0 (Swofford 2002).

The best model of evolution was determined with jModelTest 2.1.10 (Darriba et al. 2012). The model identified with the Akaike Information Criterion (AIC) (Akaike 1998) was the Tamura-Nei model (TrN+G) for H3 and the general time-reversible model (GTR+G) for COI and 16S. Phylogenetic analyses were conducted under two optimal criteria: Maximum Likelihood (ML) and Bayesian Inference (BI). The ML phylogenetic trees were inferred using RAxML v.8.2.12 (Stamatakis 2014) under the GTRGAMMA model. Node support was assessed with rapid bootstrap analysis with 1000 replicates. Analysis stopped the search for bootstrap after 100 replicates with the autoMRE-based bootstopping criterion. Values ≥ 70% were interpreted as significant nodal support (Hillis and Bull 1993).

Bayesian Inference analyses were conducted using MrBayes v.3.2.7 (Ronquist et al. 2012). Two runs were performed in parallel with four independent MCMC chains (one heated, three cold) and default priors. The analyses were run for 5,000,000 generations, saving a tree every 1000 generations and discarding the first 1250 trees of each analysis as "burn-in." Nodal support was estimated as posterior probabilities (PP), with values ≥ 90% taken as significant (Huelsenbeck and Rannala 2004).

Species delimitation analyses

Species delimitation analyses involved two methods: (a) the Automatic Barcode Gap Discovery (ABGD; Puillandre et al. 2012), through a simple distance matrix, based on the COI and 16S genes (generated in MEGA v.7.0.18) as input file under default intra- and interspecific priors (pmin = 0.001; pmax = 0.10) in 10 steps and with a relative gap width of 1.5; (b) a pairwise genetic distance matrix, based on the COI sequences generated in PAUP v.4.0 (Swofford 2002).

Results

Systematics

Superorder Nudipleura Wägele & Willan, 2000
Order Pleurobranchida Gray, 1827
Superfamily Pleurobranchoidea Gray, 1827
Family Pleurobranchaeidae Pilsbry, 1896
Genus *Pleurobranchaea* Leue, 1813

***Pleurobranchaea britannica* sp. nov.**
https://zoobank.org/81238088-87DA-4163-81F8-06AEB3ADDCAA

Material examined. ***Holotype:*** NHMUK 20230085, 18 mm preserved length, (49°54'5.306"N, 6°45'7.056"W), southern England, 103 m depth, Apr 2019. ***Paratypes:*** NHMUK 20230087, 19 mm preserved length, (49°35'59.389"N, 4°39'48.485"W) southwest England, 91.98 m depth, Mar 2018; NHMUK 20230086, 18 mm preserved length, (49°42'13.429"N, 4°6'28.514"W) southwest England, 81.12 m depth, Mar 2018; NHMUK 20230091, 22 mm preserved length, (50°5'10.929"N, 3°41'34.436"W) southwest England, 68.94 m depth, Mar 2018; MNCN 15.05/200180, 24 mm preserved length, (50°2'41.978"N, 4°3'33.805"W) southwest England, 75.69 m depth, Mar 2018, dissected specimen; NHMUK 20230090, 18 mm preserved length, (49°54'5.306"N, 6°45'7.056"W), southwest England, 103 m depth, Apr 2019; NHMUK 20230089, 19 mm preserved length, (49°54'5.306"N, 6°45'7.056"W), southwest England, 103 m depth, Apr 2019; NHMUK 20230088/1, 20 mm preserved length, (49°54'5.306"N, 6°45'7.056"W), southwest England, 103 m depth, Apr 2019, dissected specimen; MNCN 15.05/200181, 7 mm preserved length, (36°16'19.56"N, 7°32'52.8"W) Gulf of Cadiz, 555 m depth, Feb 2020; MNCN 15.05/200182, 8 mm preserved length, (36°16'19.56"N, 7°32'52.8"W) Gulf of Cadiz, 555 m depth, Feb 2020; MNCN 15.05/200183, 11 mm preserved length, (36°16'19.56"N, 7°32'52.8"W) Gulf of Cadiz, 555 m depth, Feb 2020; MNCN 15.05/200184, 10 mm preserved length, (36°16'19.56"N, 7°32'52.8"W) Gulf of Cadiz, 555 m depth, Feb 2020; MNCN 15.05/200185, 11 mm preserved length, (36°16'19.56"N, 7°32'52.8"W) Gulf of Cadiz, 555 m depth, Feb 2020; MNCN 15.05/200186, 9 mm preserved length, (36°16'19.56"N, 7°32'52.8"W) Gulf of Cadiz, 555 m depth, Feb 2020. ***Additional material*:** MNCN 15.05/94837, 41 mm preserved length, (36°16'19.56"N, 7°32'52.8"W) Gulf of Cadiz, 555 m depth, Mar 2020; MNCN 15.05/94838, 43 mm preserved length, (36°16'19.56"N, 7°32'52.8"W) Gulf of Cadiz, 555 m depth, Mar 2020; MNCN 15.05/94839, 48 mm preserved length, (36°16'19.56"N, 7°32'52.8"W) Gulf of Cadiz, 555 m depth, Mar 2020; MNCN 15.05/94840, 42 mm preserved length, (36°16'19.56"N, 7°32'52.8"W) Gulf of Cadiz, 555 m depth, Mar 2020.

Diagnosis. Body oval, large, translucent with a minute cream/ochre pigmentation. Some specimens with opaque white specks irregularly spread all over mantle, oral veil, gill and posterior region of the foot not covered by the mantle. Rhinophores with dark spots on the front and white ones on the back. Gill bipinnate, with 15–18 pairs of pinnules and smooth rachis. Caudal spur absent. Outermost radular teeth bicuspid. Seminal receptacle short; bursa copulatrix at the end of the vagina and directly fused to it.

Description. ***External morphology*** (Fig. 2). Body oval and large, with a rough mantle forming irregular polygons delimited by shallow grooves (Fig. 2A, B). Base colour translucent with a minute cream to ochre pigmentation, which may not always be present. Opaque white specks might appear irregularly spread all over mantle, oral veil, gill and posterior region of the foot not covered by the mantle. Speckles density variable. Viscera partially visible through mantle in lighter individuals. Posterior part of foot round with no caudal spur (Fig. 2A). Moreover, no pedal gland was observed. Sole patterned. Anterior part of rhinophores brown and posterior covered with close white dots (Fig. 2A). Oral veil with trapezoid shape and fused with mantle where rhinophores are inserted. Veil front edge not smooth, but slightly irregular. Some specimens with series of white specks at veil corners. Gill located on the right side of the body, clearly visible and not covered by the mantle. Gill bipinnate, with 15–18 pairs of pinnules and smooth rachis. Gill with same base colour, white grains almost always present and variable in density, being visible on rachis and pinnules. Genital openings in front of gill and nephropore, clearly visible since it is covered by a circular fleshy papilla, which may have white dots. Anus opens above the 6th and 7th pinnule of the gill.

Internal anatomy (Figs 3, 4) Radula almost rectangular with no rachidian teeth. Radular formulae are: 35 × (53–50).0.(53–50) (NHMUK 20230088/2); 33 × (54–56).0.(54–56) (MNCN15.05/200180) (Fig. 3A). All teeth with two long and blade-shaped cusps. The outermost cusp is larger, while the one facing the centre of the radula is smaller and sometimes covered by the next tooth. Innermost teeth slightly more elongated and with finer tips, while outermost teeth with rounder tip (Fig. 3B). Jaws elongated. Anterior part of jaw elements hexagonal, hand-shaped, with 4 to 9 denticles along anterior edge. The jaw elements have a depression in the middle (Fig. 3C, D).

Reproductive system (Fig. 4) begins with the hermaphroditic duct which first widens into the ampulla and thereafter narrows and divides into two parts: one entering the prostate gland and the other continuing to oviduct. The prostate gland is composed of small and pyramidal-shaped papillae. Exiting from prostate, vas deferens entering the penial sac, anchored by a retractor muscle to the inner body wall. Inside the sac, penis relatively straight, with a couple of twists, but not coiled and apparently not cuticularised. The oviduct

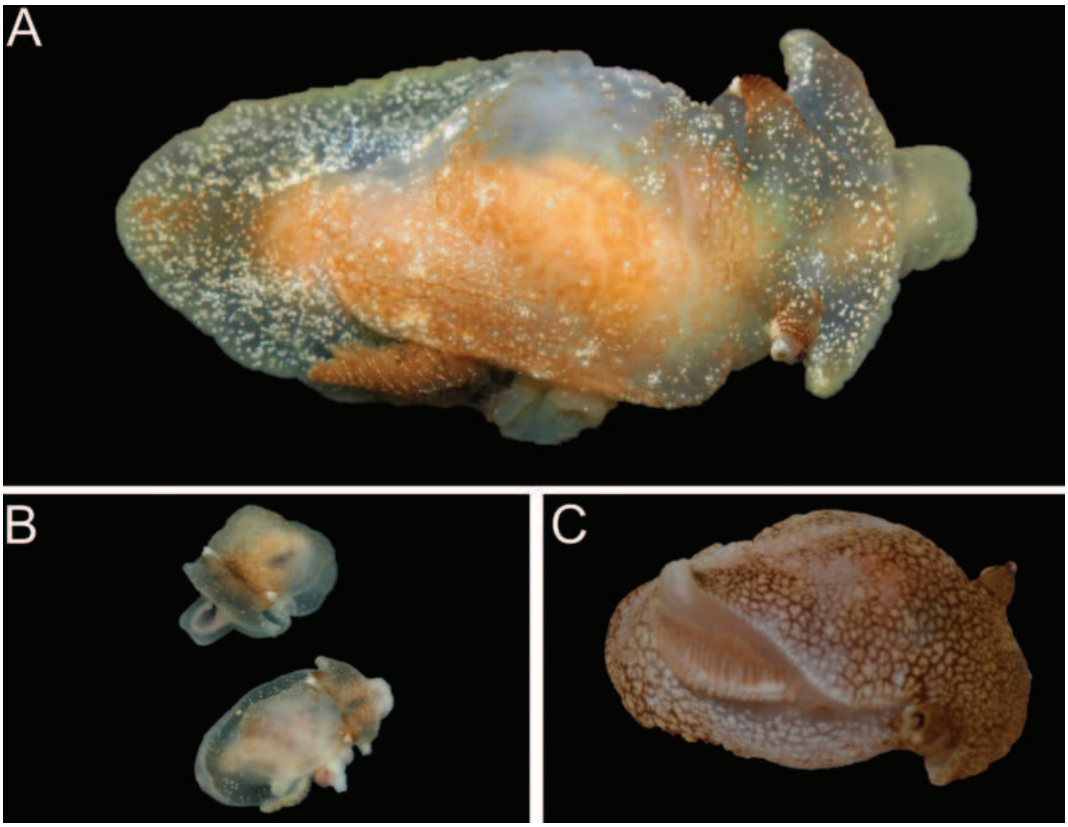

Figure 2. A. Living specimens of *Pleurobranchaea britannica* sp. nov. collected on Survey CEND 0518, southwest England. Photo by Ross Bullimore (NHMUK 20230085); **B.** Two young individuals of *P. britannica* sp. nov. from the Gulf of Cadiz, Spain (MNCN 15.05/200181; MNCN 15.05/200182); **C.** Specimen of *P. meckeli* from Morocco, Mediterranean Sea (MNCN 15.05/94845).

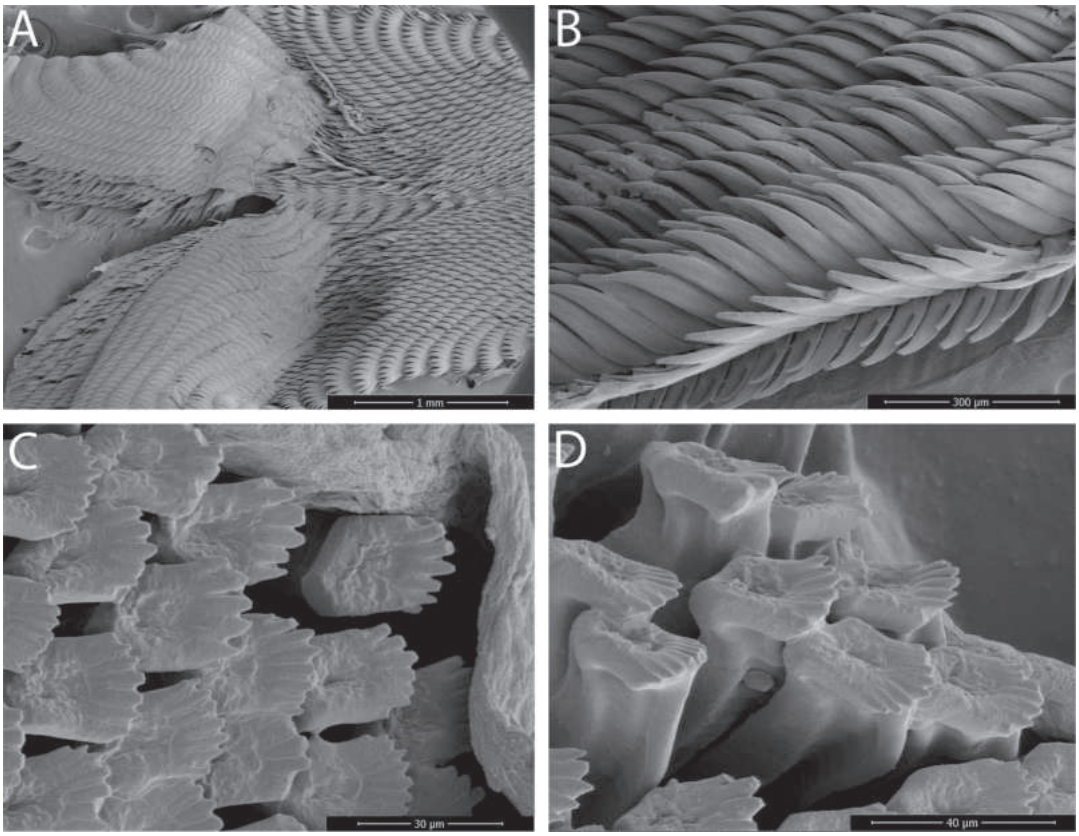

Figure 3. *Pleurobranchaea britannica* sp. nov. Scanning electron micrographs of radula and jaw. **A.** Complete radula (MNCN15.05/200180); **B.** Lateral teeth of radula (MNCN15.05/200180); **C.** View from above of the anterior part of the jaw (MNCN15.05/200180); **D.** Lateral view of the anterior part of the jaw (MNCN15.05/200180).

widens slightly forming a bilobed seminal receptacle, narrowing before entering laterally into the muscular vagina. Copulatory bursa spherical, placed at the distal end of vagina. Copulatory bursa not very muscular, its wall being delicate and thinner than the vagina's. Female gland and vagina join laterally, very close to the female orifice. There are two different genital openings: the opening closest to the nephropore is the female one, the further one is male.

Etymology. The species name in Latin refers to the British waters where this species was initially found.

Distribution. The species has been found in a number of locations in the southwest of UK waters and the Gulf of Cadiz, see Fig. 1, but we hypothesise that it could probably be distributed throughout the Atlantic coast of Spain, Portugal and France up to the southwest approaches to the English Channel.

Type locality and habitat. South-western England (see Fig. 1A). Collected from a range of depths (70–110 m) and a range of substrates that include areas of mosaic rock and mixed sediments and areas of muddier sediments.

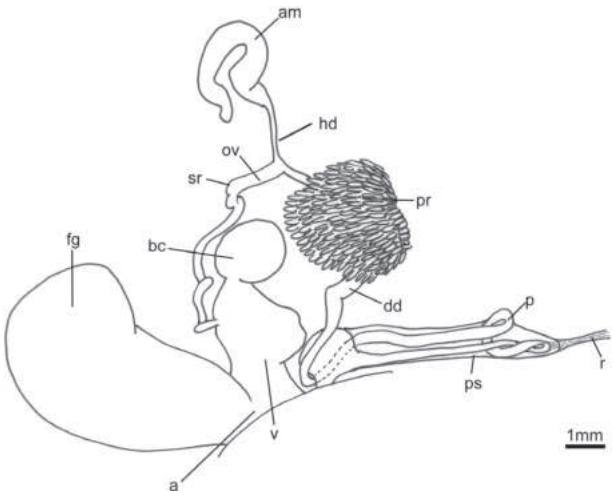

Figure 4. *Pleurobranchaea britannica* sp. nov. Reproductive system (NHMUK 20230088/5). Abbreviations: a – atrium; am – ampulla; bc – bursa copulatrix; dd – deferent duct; fg – female gland; hd – hermaphroditic duct; ov – oviduct; p – penis; pr – prostate; r – retractor muscle; ps – penis sac; sr – seminal receptacle; v – vagina.

Phylogenetic analysis

We obtained 17 sequences for COI, 20 for 16S and 21 for H3 genes. The combined data set (COI+H3+16S) provided better resolution than the COI, 16S and H3 separately. Fig. 5 shows the phylogenetic hypothesis based on the combined dataset (COI+H3+16S) constructed by Bayesian Inference (BI). The topology of the Maximum Likelihood (ML) tree was very similar to that obtained by BI (former not shown). All the sequences of the new species clustered in a single, well-supported clade (PP = 1; BS = 88), included in a broader well-supported clade (PP =1; BS = 80) together with *Pleurobranchaea inconspicua*, *P. maculata* and *P. californica*. All the specimens of *Pleurobranchaea meckeli* clustered in a different and maximum supported clade (PP =1; BS = 100) including the remaining species of *Pleurobranchaea* we analysed.

Uncorrected *p*-distances (%) between *P. britannica* sp. nov. and the species *P. maculata* and *P. meckeli* ranged from 12.7% to 18.3%, respectively (Table 3).

The ABGD species delimitation analysis recovered three putative species, based on the COI gene with both Jukes-Cantor (JC69) and Kimura (K80) parameters, while for the 16S alignment retrieved four putative species. These differences are due to the fact that sequences of *P. inconspicua* and *P. californica* were not available for COI, whereas for 16S, there were no data for *P. maculata*.

Table 3. Maximum and minimum COI gene pairwise uncorrected *p*-distances (%).

Species	*P. meckeli*	*P. maculata*
P. meckeli		
P. maculata	16.2–17.5	
P. britannica sp. nov.	16.3–18.3	12.7–13.9

Discussion

Our analyses support, from both the molecular and morphological approaches, the existence of *Pleurobranchaea britannica* sp. nov. as a distinct species. The geographical range of this species and that of *P. meckeli* partially overlap, but they can be distinguished by both external and internal characters. Externally, the new species lacks a caudal spur and has a transparent cream-coloured base with variation in the density of white spots and the mottled or "net" pattern which can be darker or lighter. *Pleurobranchaea meckeli* exhibits a conspicuous caudal spur and has a brown net pattern all over the body (Fig. 2A). Furthermore, the colour pattern of the rhinophores of *P. britannica* is characteristic with dark spots on the front and white spots on the back, respectively. Other differences between *P. meckeli* and *P. britannica* are summarised in the Appendix 1. This Appendix also includes the main differences between the known species from the Atlantic Ocean and Mediterranean Sea. For example, we also observed differences in the radula formula and the outermost teeth which are bicuspid in *P. britannica*, while they are unicuspid in *P. meckeli*. In the reproductive system, we can find several clear differences: the seminal receptacle of *P. meckeli* is larger than in *P. britannica* and, therefore, easier to observe. The bursa copulatrix in *P. meckeli* is not directly connected to the vagina, but with a small tube that connects the two structures. In the new species, the bursa copulatrix is located at the end of the vagina, directly connected with it. Another difference can be observed in the structure of the penis since, in *P. meckeli*, it performs various loops within the penal sac, while in *P. britannica*, it does not.

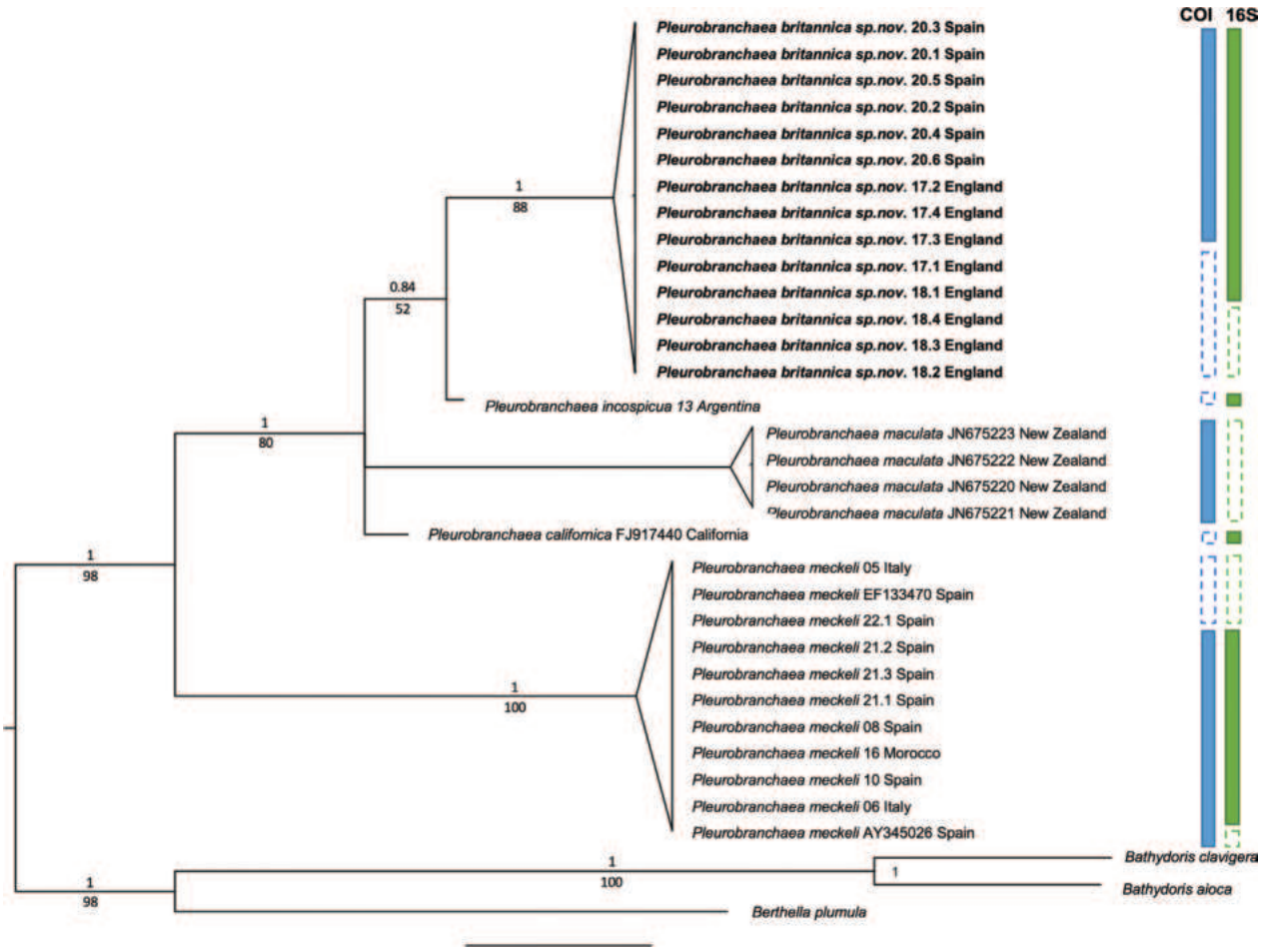

Figure 5. Phylogenetic hypothesis of *Pleurobranchaea* systematics, based on concatenated dataset (COI+16S+H3) inferred by Bayesian analysis. Significant support values are given as BI posterior probabilities (below branch) and ML bootstrap percentages (above branch). Rectangles are automatic barcode gap discovery for the COI and 16S dataset. White rectangles indicate the lack of those sequences in the alignment.

Pleurobranchaea britannica sp. nov. does not correspond to the poor descriptions of other animals currently accepted as synonyms of *P. meckeli* (see MolluscaBase (2023b)). For example, *Pleurobranchaea dellechiaii* Véran y, 1846 has a minimal external description, but the mantle has red dots even after death, which are not present in the new species. *Pleurobranchaea notmec* Marcus, Ev. and Gosliner 1984 has a caudal spur, absent in *P. britannica* and the penis is much longer (as in *P. meckeli*) compared to the new species. *Pleurobranchaea vayssierei* Marcus, Ev. and Gosliner 1984 also has a caudal spur and an elongated penis wrapped in the penal sac, but the vagina is long and quite narrow unlike *P. britannica* which has a wide vagina which connects the bursa copulatrix to the outside. Those last two names (*P. notmac* and *P. vayssierei*) were proposed from preserved material without any information provided of the living individuals' colouration.

All these morphological and anatomical differences which separate *P. britannica* sp. nov. as a standalone species are supported by our genetic data. In fact, individuals identified as *P. britannica* form a single well-supported taxon (PP = 1; BS = 88), which is also separate from *P. meckeli*, the geographically closest species. To date, the only European (excluding the Azores) species of the genus *Pleurobranchaea meckeli*, has not been recorded further north than Iberian coasts. Therefore, *P. britannica* represents the first record of the genus *Pleurobranchaea* in British waters and the second valid species from European seas.

Acknowledgements

We thank the survey scientists and crew of "RV Cefas Endeavour" their help for the collection of the specimens of the new species from the English Channel. Likewise, Carlos Farias (Spanish Institute of Oceanography, IEO) donated the material of *Pleurobranchaea britannica* n. sp. and *P. meckeli* from the Gulf of Cadiz collected during several IEO oceanographic campaigns ARSA. This study has been partially supported by the project 'Desentrañando la diversidad criptica en las regiones Lusitánica y Mediterránea: Heterobranquios marinos (Mollusca), Sílidos (Annelida) y Caprélidos (Arthropoda, Pancrustacea) como casos de estudio' funded by the University of Cadiz (PR2018-039) to J. L. Cervera.

References

Akaike H (1998) Information Theory and an Extension of the Maximum Likelihood Principle. In: Parzen E, Tanabe K, Kitagawa G (Eds) Selected Papers of Hirotugu Akaike. Springer Series in Statistics. Springer, New York, NY, 199–213. https://doi.org/10.1007/978-1-4612-1694-0_15

Alvim J, Simone LRL, Pimenta AD (2014) Taxonomic review of the genus *Pleurobranchaea* (Gastropoda: Pleurobranchoidea) from Brazil, with description of a new species. The Journal of Molluscan Studies 80(5): 604–623. https://doi.org/10.1093/mollus/eyu063

Bergh LSR (1892) Résultats des Campagnes Scientifiques accomplies sur son yacht par Albert Ier Prince Souverain de Monaco.

Bergh LSR (1897) Malacologische Untersuchungen 5. In: Semper C (Ed.) Reisen im Archipel der Philippinen 7, 4 Abt., 1 Absch., Die Pleurobranchiden 1–2. Wiesbaden Kreidel's Verlag, 1–115.

Cervera JL, Garcia-Gomez JC (1988) Estudio anatomico de *Pleurobranchaea meckeli* Blainville, 1825 (Mollusca: Opistobranchia: Notaspidea). Arquivos do Museu Bocage 1(6): 71–90. [nova serie]

Cervera JL, Calado G, Gavaia C, Malaquías MAE, Templado J, Ballesteros M, García Gómez JC, Megina C (2004) An annotated and updated checklist of the opisthobranchs (Mollusca: Gastropoda) from Spain and Portugal (including islands and archipelagos). Boletín del Instituto Español de Oceanografía 20(1–4): 1–122.

Colgan DJ, McLauchlan A, Wilson GDF, Livingston S, Edgecombe GD, Macaranas J, Cassis G, Gray MR (1998). Histone H3 and U2 snRNA sequences and arthropod molecular evolution. Australian Journal of Zoology 46: 419–437. https://doi.org/10.1071/ZO98048

Colgan DJ, Ponder WF, Eggler PE (2000) Gastropod evolutionary rates and phylogenetic relationships assessed using partial 28S rDNA and histone H3 sequences. Zoologica Scripta 29(1): 23–63. https://doi.org/10.1046/j.1463-6409.2000.00021.x

Darriba D, Taboada G, Doallo R, Posada D (2012) jModelTest 2: More models, new heuristics and parallel computing. Nature Methods 9(8): 772. https://doi.org/10.1038/nmeth.2109

Folmer O, Black M, Hoeh W, Lutz R, Vrijenhoek R (1994) DNA primers for amplification of mitochondrial cytochrome c oxidase subunit I from diverse metazoan invertebrates. Molecular Marine Biology and Biotechnology 3(5): 294–299.

García-Gómez JC, Cervera JL (2011) Familia Pleurobranchidae. In: Gofas S, Moreno D, Salas C (Coords) Moluscos marinos de Andalucía. Málaga: Servicio de Publicaciones e Intercambio Científico, Universidad de Málaga, 456–459.

Göbbeller K, Klussmann-Kolb A (2010) Out of Antarctica? – New insights into the phylogeny and biogeography of the Pleurobranchomorpha (Mollusca, Gastropoda). Molecular Phylogenetics and Evolution 55(3): 996–1007. https://doi.org/10.1016/j.ympev.2009.11.027

Hillis DM, Bull JJ (1993) An empirical test of bootstrapping as a method for assessing confidence in phylogenetic analysis. Systematic Biology 42(2): 182–192. https://doi.org/10.1093/sysbio/42.2.182

Huelsenbeck JP, Rannala B (2004) Frequentist properties of Bayesian posterior probabilities of phylogenetic trees under simple and complex substitution models. Systematic Biology 53(6): 904–913. https://doi.org/10.1080/10635150490522629

Katon K, Standley DM (2013) MAFFT Multiple Sequence Alignment Software Version 7: Improvements in Performance and Usability. Molecular Biology and Evolution 30(4): 772–780. https://doi.org/10.1093/molbev/mst010

Kearse M, Moir R, Wilson A, Stones-Havas S, Cheung M, Sturrock S, Buxton S, Cooper A, Markowitz S, Duran C, Thierer T, Ashton B, Meintjies P, Drummond A (2012) Geneious Basic: An integrated and extendable desktop software platform for the organization and analysis of sequence data. Bioinformatics (Oxford, England) 28(12): 1647–1649. https://doi.org/10.1093/bioinformatics/bts199

Larsson A (2014) AliView: A fast and lightweight alignment viewer and editor for large datasets. Bioinformatics (Oxford, England) 30(22): 3276–3278. https://doi.org/10.1093/bioinformatics/btu531

Marcus EDB-R, Gosliner TM (1984) Review of the family Pleurobranchaeidae (mollusca, Opisthobranchia). Annals of the South African Museum 93(1): 1–41.

Martynov AV, Schrödl M (2009) The new Arctic side-gilled sea slug genus *Boreoberthella* (Gastropoda, Opisthobranchia): Pleurobranchoidean systematics and evolution revisited. Polar Biology 32(1): 53–70. https://doi.org/10.1007/s00300-008-0503-3

Miller MA, Pfeiffer W, Schwartz T (2010) Creating the CIPRES Science Gateway for inference of large phylogenetic trees" in Proceedings of the Gateway Computing Environments Workshop, 1–8. https://doi.org/10.1109/GCE.2010.5676129

MolluscaBase [Eds] (2023a) MolluscaBase. Pleurobranchaea Leue, 1813. World Register of Marine Species https://www.marinespecies.org/aphia.php?p=taxdetails&id=138363 [Accessed on 2023-11-17]

MolluscaBase [Eds] (2023b) MolluscaBase. *Pleurobranchaea meckeli* (Blainville, 1825). World Register of Marine Species. https://www.marinespecies.org/aphia.php?p=taxdetails&id=140818 [Accessed on 2023-11-17]

Muniain C, Ardila NE, Cervera JL (2007) *Pleurobranchaea inconspicua* Bergh, 1897 (Opisthobranchia: Pleurobranchidae): Redescription and distribution from Argentina and Colombia. Bonner Zoologische Beitrage 55: 291–300.

Palumbi SR (1996) Nucleic acids II: The polymerase chain reaction. In: Hillis DM, Moritz C, Mable BK (Eds) Molecular systematics. Sinauer Associates, Inc, 205–247.

Puillandre N, Lambert A, Brouillet S, Achaz G (2012) ABGD, Automatic Barcode Gap Discovery for primary species delimitation. Molecular Ecology 21(8): 1864–1877. https://doi.org/10.1111/j.1365-294X.2011.05239.x

Ronquist F, Teslenko M, van der Mark P, Ayres DL, Darling A, Höhna S, Larget B, Liu L, Suchard MA, Huelsenbeck JP (2012) MrBayes 3.2: Efficient Bayesian Phylogenetic Inference and Model Choice Across a Large Model Space. Systematic Biology 61(3): 539–542. https://doi.org/10.1093/sysbio/sys029

Stamatakis A (2014) RaxML version 8: A tool for phylogenetic analysis and post-analysis of large phylogenies. Bioinformatics (Oxford, England) 30(9): 1312–1313. https://doi.org/10.1093/bioinformatics/btu033

Swofford DL (2002) PAUP*. Phylogenetic Analysis Using Parsimony (*and Other Methods). Version 4.0b10. Sin. Assoc.

Vayssière A (1901) Monographie de la famillie des Pleurobranchidés (deusiéme et derniére partie). Annales des Sciences Naturelles (Zoologie) 12: 22–75.

Wägele H, Willan RC (2000) On the phylogeny of the Nudibranchia. Zoologial Journal of the Linnean Society 130: 83–181. https://doi.org/10.1111/j.1096-3642.2000.tb02196.x

Appendix 1

Table A1. Summary of diagnostic features of species of *Pleurobranchaea*.

Species	Radula	Inner and outermost tooth	Mantle and foot	Caudal Spur	Pedal gland	Jaw (denticles on jaw elements)	Rinophores	Veil	Gill	Seminal receptacle	Vagina and bursa copulatrix	Penis	Genital opening	Distribution	References
P. agassizii (Bergh, 1897)	32 x 98.0.98	Bicuspid, but 17 outermost unicuspid	–	Present	–	4–8	–	–	32 pinnules	A single bulge	–	Muscular without cuticle	–	Western Atlantic: Florida, Great Bahama Bank, Gulf of Mexico	Marcus and Gosliner (1984); Alvim et al. (2014)
P. bubala (Maecus and Gosliner, 1984)	35 x 100.0.100	Bicuspid, 20–30 outmost teeth unicuspid	Mantle extends over the foot on both sides; pattern of dark brown pigment and irregular whitish blotches	Absent	Present	4–14 rarely more than 10	–	A row of small tubercles	26 pinnules, smooth rachis	–	Long glandular vagina and bilobed bursa copulatrix	The stylet is similar to that of *P. tarda*	Protruding, with flap on hind border	From Atlantic coast of Cape Península to Inhaca, Mozambique	Marcus & Gosliner (1984); Alvim et al. (2014)
***P. britannica* sp. nov.**	**36 × 59–58.0.59–58**	**Bicuspid, outmost tiny secondary cusp**	**Mantle not covering foot; translucent or cream base colour, irregular white spots**	**Absent**	**Absent**	**4–9**	**Rolled and pointed, are separate; the anterior part of the tip is brown and the posterior is covered with white dots**	**Trapezoid shape and is fused with the mantle, irregular front edge**	**15–18** pinnules, **bipinnate, smooth rachis**	**Slightly bilobed**	**At the distal end of muscular vagina is the spherical copulatory bursa**	**Not cuticularised penis is relatively straight, with a couple of twists**	**Covered by a circular fleshy papilla**	**Atlantic coast of Spain, Portugal and France up to the English Channel**	
P. gela (Er. Marcus and Ev. Marcus, 1966)	42 × 57.0.57	Bicuspid, sometimes	Black foot sole with light	–	Present	8–14	–	–	18–26 pinnules	Bilobed or trilobed	Small, rounded bursa copulatrix	Well–developed crest along cuticular translucent stylet, coiling five to six times	With dorsal flap	West Africa	Marcus and Gosliner (1984); Alvim et al. (2014)
P. inconspicua (Bergh, 1897)	30 X 64.0.64	Bicuspid, sometime s tiny secondary cusp or unicuspid	Mantle is reduced, not covering foot; translucent white, with reticulate pattern of brown lines and white dots	Present	Present	5–11	Smooth, translucent brown with some whitish stains, It is fused with the mantle	Broad with singular row of sensory papillae along the anterior edge	20–26 pinnules, unipennate rachis	Bilobed	Large rounded bursa copulatrix and muscular vagina	Cuticular stylet, translucent white, coiling 10–11 times; Penis large, cylindrical, sometimes projecting	Surrounded by fold with triangular papilla	Northern Brazil, Western Atlantic, Mediterranean, West Africa	Marcus and Gosliner (1984); Muniain, Ardila, Cervera (2006); Alvim et al. (2014); WoRMS (2023)

Species	Radula	Inner and outermost tooth	Mantle and foot	Caudal Spur	Pedal gland	Jaw (denticles on jaw elements)	Rinophores	Veil	Gill	Seminal receptacle	Vagina and bursa copulatrix	Penis	Genital opening	Distribution	References
P. meckeli (Leue, 1813)	46 × 71.0.71	Bicuspid, 1–5 outermost unicuspid	Mantle is smaller than the foot; brown or dark grey crosslinked variable, background colour is cream, but sometimes there are white areas	Present	Present	–	As long as the tentacles, blunt, cylindrical	Irregular front edge and with pointed ends; row of papillae, the sides of the veil produced into a pointed cephalic tentacle with split sides	23–25 pinnules, bipinnate, alternate knobs on rachis	Globular	Vagina elongated and connected at the end with a round bursa copulatrix	Elastic cuticular stylet with a high crest, stylet coiled 6–10 times	Surrounded by thick fold	Mediterranean, Atlantic, including Azores, Cape Verde Islands	Marcus and Gosliner (1984); García-Gómez et al. (2011); Alvim et al. (2014)
P. morosa (Bergh, 1892)	37 × 70–68.0.68– 70	–	–	–	Present	5–7	–	–	15 pinnules	–	–	–	–	Azores	Bergh (1892)
P. obesa (Verrell, 1882)	31–34×75–90.0.75–90	Bicuspid, the outermost is unicuspid	Mantle is smooth, swollen extending far out over the foot	Present	Present	Variable number of denticles	Smooth	A single row of papillae	26–35 pinnules, smooth rachis	Lobate and glandular	Vagina and bursa copulatrix are large	Cuticular stylet present	–	North-western Atlantic	Bergh, (1892); Marcus and Gosliner (1984); Alvim et al. (2014)
P. spiroporphyra (Alvim, Simon & Pimenta, 2014)	30–32 × 40–44.0.40–44	Bicuspid with smaller tiny cusp	Mantle margin reduced, not covering foot, mantle with tiny flap at end of gill	Present	Present	1–5	Rolled, separated	Broad, thin, connected to head region; deep notch in apical third or quarter of oral tentacles; several large rounded papillae forming one row	17–23 pinnules, unipinnate, tuberculated rachis	Many enlargements	–	Penis large, cylindrical; cuticular stylet with 12–14 coils	Surrounded by thick fold, with triangular papillae	Rio de Janeiro	Alvim et al .(2014); WoRMS (2023)
P. tarda (Verrill, 1880)	70.0.70	Bicuspid, six outermost unicuspid	Smooth mantle and about the same size as foot	Sometime there is a short spur	Present	5–7	Typical for the genus	Tubercles	20–30 pinnules, Tuberculated	Ciliated and serial	Vagina is short and wide	Cuticular stylet present	With or without flap	Western and south-eastern Atlantic: from Martha's Vineyard to south of Cuba; from Angola to Agulhas Bank	Vayssiere (1901); Marcus and Gosliner (1984); Alvim et al. (2014)

Zoosyst. Evol. 100 (1) 2024, 61–68 | DOI 10.3897/zse.100.113243

PENSOFT

für Natur MUSEUM FÜR NATURKUNDE BERLIN

A new species of land snail, *Xanthomelon amurndamilumila*, from the North East Isles off Groote Eylandt (= Ayangkidarrba), Gulf of Carpentaria, Australia (Stylommatophora, Camaenidae)

Frank Köhler[1], Richard C. Willan[2], Adam J. Bourke[3], Paul Barden[4], Michael Shea[1]

1 *Australian Museum Research Institute, 1 William Street, Sydney, New South Wales 2010, Australia*
2 *Museum and Art Gallery of the Northern Territory, GPO Box 4646, Darwin, Northern Territory 0801, Australia*
3 *EcoScience NT, 29 Ostermann Street, Coconut Grove, Darwin, Northern Territory 0810, Australia*
4 *Ecological Management Services Pty Ltd., P.O. Box 580, Coolum Beach, Queensland 4573, Australia*

https://zoobank.org/7DDF83B6-257E-4AAE-B21A-ECFA2DA1B13E

Corresponding author: Frank Köhler (frank.koehler@australian.museum)

Academic editor: T. von Rintelen ♦ **Received** 25 September 2023 ♦ **Accepted** 3 December 2023 ♦ **Published** 26 January 2024

Abstract

This paper introduces *Xanthomelon amurndamilumila* **sp. nov.**, a newly-discovered land snail species inhabiting the North East Isles, offshore from Groote Eylandt (= Ayangkidarrba), north-western Gulf of Carpentaria, in the Northern Territory, Australia. Specimens of this species were first collected during the 2021 Bush Blitz expedition to Groote Eylandt, a large offshore archipelago previously unexplored for land snails. The taxonomic status of the new species was established through a comprehensive analysis of comparative morphology and mitochondrial genetics: *X. amurndamilumila* forms a maximally supported clade closely related to *X. arnhemense* and is characterised by a unique combination of morphological characteristics, including smaller shell size, distinctive sculpture of collabral ridges and specific features of its reproductive anatomy. The genetic divergence and phylogenetic relationships suggest historical isolation. While the discovery of *X. amurndamilumila* **sp. nov.** enriches our understanding of land snail diversity in the Northern Territory, its conservation status is of concern on North East Island because of habitat degradation caused by feral deer.

Key Words

distribution, Gastropoda, Helicoidea, Pulmonata, taxonomy

Introduction

The genus *Xanthomelon* E. von Martens, 1860 comprises several species of Australian camaenid land snail, typically characterised by their large, globose shells of mostly uniform yellowish-brown to ochre colour. The distribution of this genus encompasses the Australian Monsoon Tropics as well as eastern Queensland. Of the 11 currently accepted species of *Xanthomelon*, five occur in the 'Top End' of the Northern Territory, according to the latest revision of the genus (Köhler and Burghardt 2016). These species exhibit varying degrees of morphological distinctive characteristics, including some that are highly similar with one another and have distributional ranges that vary from narrow to wide. It is a testament to our rather poor knowledge of land snails in the 'Top End' generally that two of these five species have been described only a few years ago. *Xanthomelon darwinense* was only described in the 21st century (Köhler and Burghardt 2016), even though it occurs in the Territories' capital, Darwin and is readily distinguished from most other congeners by its much smaller size. This species has a narrow distribution in and around Darwin and is currently known only from two separate locations.

In contrast, *X. arnhemense* Köhler & Burghardt, 2016 has a wide distribution, encompassing most of

Arnhem Land. However, this species had also remained unrecognised for at least a century due to its highly cryptic nature, even though specimens are well represented in museum collections. However, shells of *X. arnhemense* are indistinguishable from those of its close ally, *X. interpositum* Iredale, 1938. Indeed, these two species can be distinguished only through comparative reproductive anatomy or genetics. The previously-poor documentation of *Xanthomelon* is but one example of how the scarcity of modern systematic studies impairs the documentation of the Territories' land snail fauna to this day. The recent discovery of another undescribed species of land snail in the Northern Territory, *Parglogenia cobourgensis* Köhler & Shea, 2022, which had been overlooked for centuries due to its externally cryptic shell, is another example illustrating our slow progress towards a more complete documentation of the land snail fauna of the Northern Territory (Köhler and Shea 2022).

The presumably still incomplete knowledge of Australian land snails also hampers our ability to manage and conserve the fauna that has already been described. Indeed, Willan et al. (2009) showed that four species of *Torresitrachia* Iredale, 1939 described in 2009, which are endemic to the Daly Basin Bioregion and have very limited distribution ranges, are under threat of extinction due to the impact of changed fire regimes and the transformation of native savannah by introduced grasses.

To remedy the lack of documentation of biotic patterns throughout the Northern Territory, more systematic studies are urgently needed that employ contemporary methods and analyse evidence from multiple sources of information to reliably identify and delimit species. Oftentimes, new species may be discovered when understudied museum samples are examined, especially by using novel scientific techniques. *Parglogenia cobourgensis* and *Xanthomelon arnhemense* are two such species that were discovered in museum collections. Secondly, new discoveries may be made in hitherto under-surveyed areas.

In the present study, we examine newly-collected samples of a presumed new species that were collected on small islets offshore from Groote Eylandt, which were never surveyed for land snails previously. The specimens examined here were first collected in 2021 during the Bush Blitz expedition to Groote Eylandt that aimed to close a pre-existing survey gap for multiple groups of organisms through a targeted survey (Willan and Bourke 2022).

Preliminarily identified in the field by one of us (RCW) as a putative new species of *Xanthomelon*, we here employ comparative morphology and mitochondrial genetics to resolve its taxonomic status. To ensure an accurate taxonomic assessment, we compare all new data collected on this putative new species with the current knowledge of the *Xanthomelon* species in the 'Top End' as summarised in the latest systematic revision by Köhler and Burghardt (2016).

Materials and methods

The present study is based on samples collected on North East Island (= Amburrkba) and Hawk Island (= Ayangkijirumanja) in the Gulf of Carpentaria during the Bush Blitz on Groote Eylandt conducted in 2021. Additional specimens were collected in 2022 on Lane Island (= Milyekaluwakba) and also on Hawk Island (Fig. 1).

Most of the specimens have been deposited in the malacological collection of the Museum and Art Gallery of the Northern Territory in Darwin (**NTM**). Supplementary specimens have been deposited in the malacological collection of the Australian Museum in Sydney (**AM**).

Material was collected by hand while conducting visual searches of habitats on North East Island, the largest of the North East Isles. Living specimens were fixed and preserved in 95% ethanol. Shells were photographed and reproductive anatomy was studied using a binocular microscope with drawing mirror. Height of shell (**H**) and diameter (**D**) of fully mature shells as recognised by a finished apertural lip were measured with callipers precise to 0.1 mm and shell whorls were counted as described by Köhler (2011).

Genomic DNA was extracted from small pieces of foot muscle using a QIAGEN DNA extraction kit for animal tissue following the standard procedure of the manual. Fragments of two mitochondrial genes, 16S rRNA (16S) and cytochrome c oxidase subunit 1 (COI), were amplified by PCR using the primer pairs 16Scs1 (5′-AAACATACCTTTTGCATAATGG-3′) (Chiba 1999) and 16Sbd1 (5′-CTGAACTCAGATCATGTAGG-3′) (Sutcharit et al. 2007) and L1490 (5′-GGTCAACAAATCATAAAGATATTGG-3′) and H2198 (5′-TAAACTTCAGGGTGACCAAAAAATCA-3′) (Folmer et al. 1994), respectively. Reactions were performed with an annealing step of 60 s at 55 °C for 16S and at 50 °C for COI with elongation times of 90 and 60 s, respectively. PCR fragments were purified with ExoSAP (Affymetrix) and both strands were cycle sequenced by use of the PCR primers. Chromatograms were merged into one sequence contig using Sequencher (Gene Codes Corporation. Ann Abor) and misreads were manually corrected where necessary. New sequences have been deposited in GenBank under the accession numbers OR610390-OR610392 and OR612298-OR612302. For the phylogenetic analyses, we built a sequence dataset by incorporating all available GenBank sequences of *Xanthomelon* (16S and COI). The 16S sequences were aligned using the online version of MAFFT (version 7.4) (Katoh et al. 2002) available at http://mafft.cbrc.jp/alignment/server/ by employing the iterative refinement method E-INS-i. The final sequence alignments of 16S and COI were concatenated into one partitioned dataset. Two partitions were designated, one for each gene fragment. Phylogenetic relationships were estimated by employing a Maximum Likelihood-based method of tree reconstruction (ML) using IQ-TREE v. 2.3 (Nguyen et al. 2015). We used the integrated ModelFinder (Kalyaanamoorthy et al. 2017) to identify the

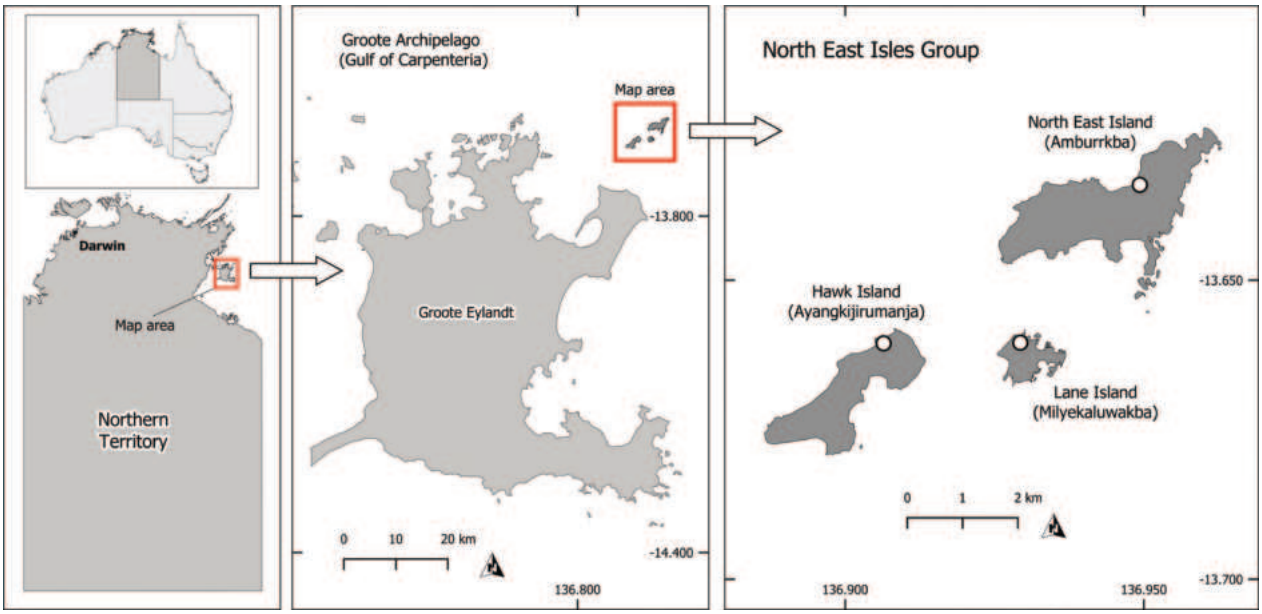

Figure 1. Map of the North East Isles off Groote Eylandt, Arnhem Land, Northern Territory. Specimens of *Xanthomelon amurndamilumila* sp. nov. have been found on North East Island as well as Hawk and Lane Islands. Small circles indicate sampling sites.

best-fit models of sequence evolution for each sequence partition. We employed Ultrafast Bootstrap Approximation (Minh et al. 2013) to estimate the statistical branch support of the best Maximum Likelihood tree.

Abbreviations used: **16S** = 16S rRNA; **COI** = cytochrome c oxidase subunit 1; **H** = shell height; **D** = shell diameter; **SD** = standard deviation.

Results

Mitochondrial phylogenetics

The concatenated sequence dataset of COI and 16S contained sequences from 79 individuals representing all the presently known *Xanthomelon* species (i.e. *X. arnhemense*, *X. darwinense* Köhler & Burghardt, 2016, *X. distractum* Iredale, 1938, *X. durvillii* (Hombron & Jacquinot, 1840), *X. interpositum*, *X. jannellei* (Le Guillou, 1842), *X. magnidicum* Iredale, 1938, *X. obliquirugosum* (E. A. Smith, 1894), *X. pachystylum* (L. Pfeiffer, 1845), *X. saginatum* Iredale, 1938) and five individuals of the presumed new species of *Xanthomelon* from the North East Isles (i.e. two from North East Island and three from Lane Island). In addition, we included *Quistrachia leptogramma* (L. Pfeiffer, 1846) as the outgroup to root the tree. This taxon was selected because *Qusitrachia* is the sister group of *Xanthomelon* in the phylogeny of north-western Australian Camaenidae (Köhler and Criscione 2015).

The COI sequences had a length of 655 bp and the 16S alignment consisted of 797 base pairs. Several samples missed either a COI or a 16S sequence, but all species were represented by individuals with complete sampling of both markers. ModelTest identified the General Time Reversible model with a gamma distributed rates (GTR+G+I) as the best-fit model of sequence evolution for both the COI and 16S sequences.

The Maximum Likelihood phylogram revealed all sequences of the putatively new species formed a maximally supported clade in a maximally supported sister group relationship with *X. arnhemense* (Fig. 2).

Uncorrected p-distances in COI ranged from 0.9% to 1.5% (average: 1.2%) amongst sequences of the putative new species (i.e. intraspecific genetic differentiation) and from 7.9% to 10.4% (average: 8.8%) between sequences of the putative new species and *X. arnhemense* (i.e. interspecific genetic differentiation). For comparison, the intraspecific p-distances in *X. arnhemense* ranged from 2.3 to 7.5% (on average 4.8%).

Comparative morphology

The putative new species from the North East Isles differed from most congeners in having relatively strong collabral ribs on the shell. Collabral ribs are also present in *X. durvillii* and *X. arnhemense*, but are considerably weaker in development. We measured 75 specimens of the putative new species (54 from North East Island, 12 from Hawk Island, 9 from Lane Island) and found that the shells on average were significantly smaller than *Xanthomelon* shells from the closest land mass, which is mainland Groote Eylandt (= *X. arnhemense*; see Köhler and Burghardt (2016)) (Fig. 3). Shells of the putative new species measured between 13.6 and 21.5 mm in height (mean = 17.7 mm, SD = 2.1) and between 15.5 and 24.2 mm in diameter (mean = 19.6, SD = 1.9). By contrast, 25 shells of *X. arnhemense* from mainland Groote Eylandt were between 19.1 and 37.1 mm (mean = 28.8 mm, SD = 4.7) high and between 21.6 and 39.5 mm (mean = 30.2 mm, SD = 4.8) wide (Fig. 3).

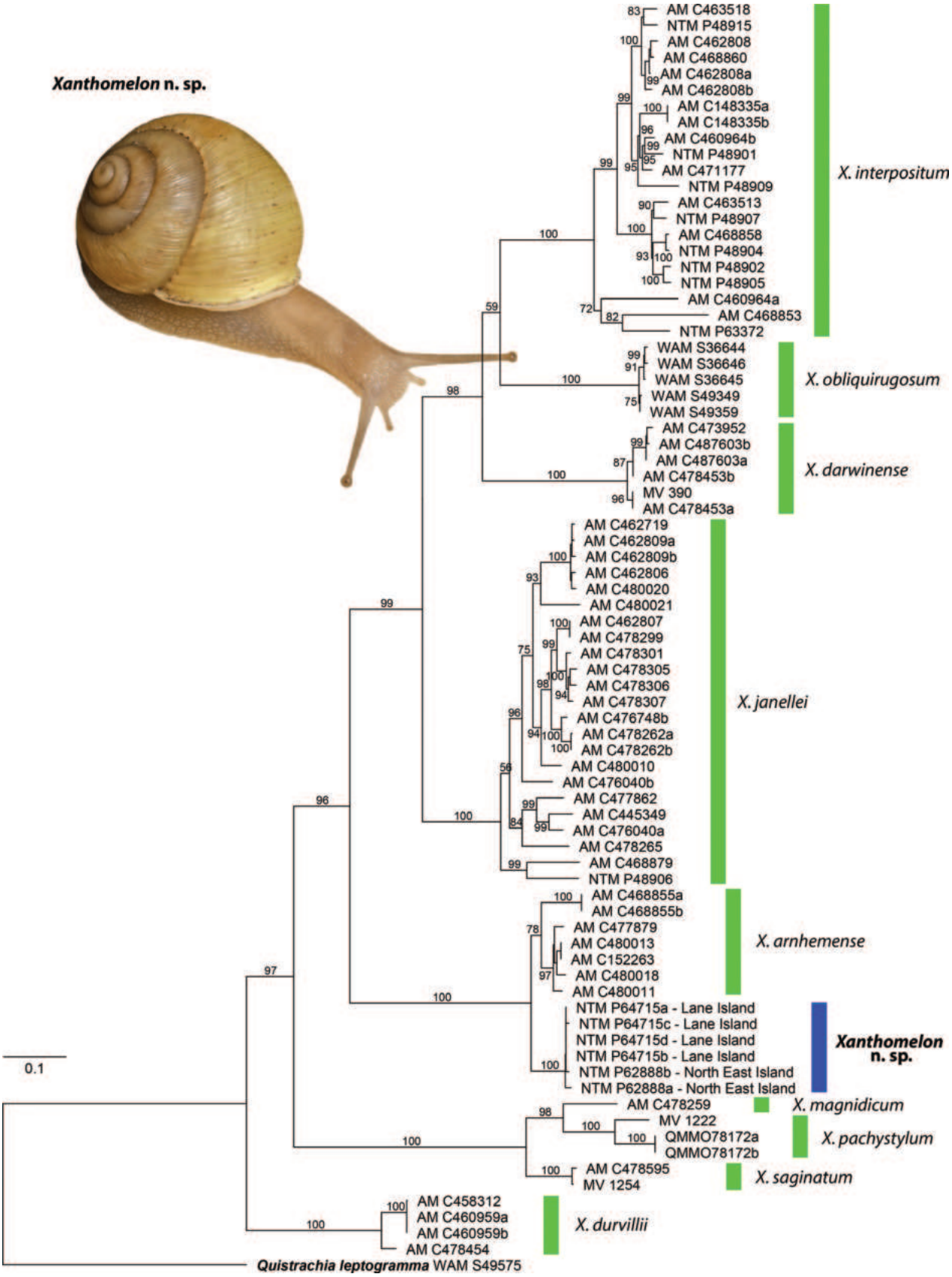

Figure 2. Maximum Likelihood phylogram based on analysis of a concatenated alignment of partial 16S and COI sequences using IQ-Tree. Numbers on branches indicate nodal support by 10,000 ultrafast bootstrap replicates. Sequences of *Quistrachia leptogramma* were used to root this tree. Scale bar indicating modelled evolutionary distance of 10%.

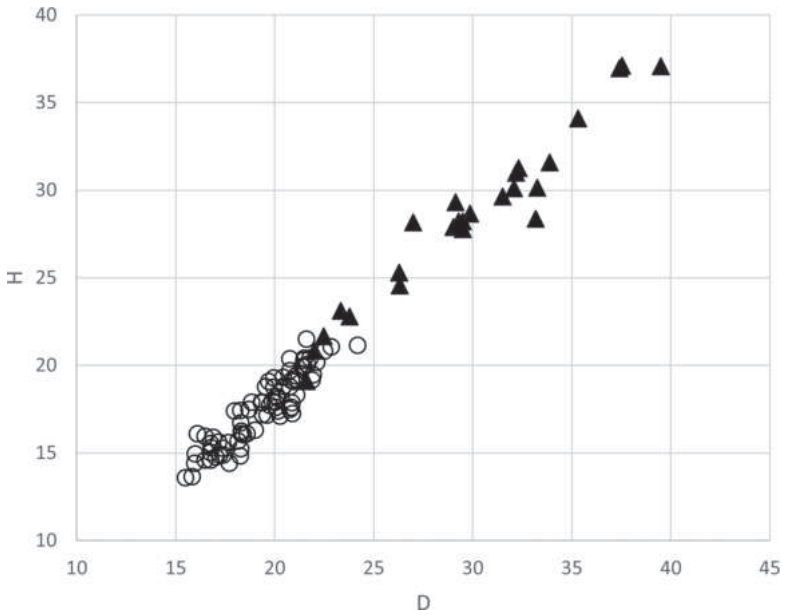

Figure 3. Shell size comparison between the putative new species (circles) and *X. arnhemense* from adjacent Groote Eylandt (full triangles) by plotting shell height (H) against shell diameter (D).

The reproductive anatomy of two specimens from North East Island was examined and found to differ significantly from the reproductive anatomy of *X. durvillii*, *X. interpositum* and *X. darwinense* as depicted by Köhler & Burghardt (2016: fig. 6A-C). Amongst other features, all these species differed most noticeably in having a long epiphallus (1.5 to 3 times longer than penis). By contrast, the epiphallus in specimens from the North East Isles is much shorter relative to the length of the penis (approx. 0.75 of penis length). Both *X. jannellei* and *X. arnhemense* have a similar configuration of reproductive organs, particularly lacking a well-developed epiphallus (i.e. epiphallus shorter than penis; see Köhler & Burghardt (2016: fig. 6D-E). Of these two species, *X. jannellei* is distinguished from the other two species in having a densely pustulated apical portion of the inner penial wall, a feature which is not exhibited by *X. arnhemense* or the putative new species. Indeed, the putative new species and *X. arnhemense* do not differ notably in their reproductive anatomy.

Taxonomic description

***Xanthomelon amurndamilumila* sp. nov.**

https://zoobank.org/37DE5E77-7A67-4069-98C2-9FEA941205C8

Type locality. Australia • Northern Territory, Groote Eylandt (= Ayangkidarrba), North East Isles, North East Island (= Amburrkba), 13°38'13.2"S, 136°56'34.5"E.

Holotype NTM P.65134 (1 preserved specimen, dissected, shell broken; Fig. 4), from type locality, coll. A.J. Bourke, 18 June 2021.

Paratypes NTM P.62888 (14 preserved specimens; Fig. 5B), AM C.548628 (4 preserved specimens), from type locality, coll. A.J. Bourke, 18 June 2021.

Additional (non-type) specimens examined. North East Isles, North East Island (= Amburrkba), NTM P.62774 (59 dried shells), coll. R.C. Willan & A.J. Bourke, 18 June 2021; NTM P.62904 (23 dried shells), coll. R.C. Willan & A.J. Bourke, 18 June 2021; North East Isles, Lane Island (= Milyekaluwakba), NTM P.64715 (4 dried shells), coll. P. Barden, 15 November 2022, NTM P.64717 (7 dried shells), coll. P. Barden, 15 November 2022; North East Isles, Hawk Island (= Ayangkijirumanja), NTM P.62775 (14 dried shells), coll. R.C. Willan & A.J. Bourke, 22 June 2021, P.64716 (1 dried shell), coll. P. Barden, 15 November 2022.

Description. ***Shell*** (Fig. 5). Comparatively small for genus (H = 13.6–21.5 mm, D = 15.5–24.2 mm), broadly conical to almost globose in shape, with moderately elevated spire (H/D = 0.81–0.99). Teleoconch entirely covered with well-developed collabral ridges. Whorls with well-rounded periphery, weakly shouldered below well-incised suture. Last whorl rapidly descending just behind aperture; apertural lip thick, slightly reflected, white, parietal wall calloused. Umbilicus narrow, open, partly concealed by reflected columellar lip; collabral ribs ornamented with very small pustules inside umbilical cavity. Shell colour uniform, light brown.

Reproductive anatomy (Fig. 4). Penis rather thick, uncoiled, slightly bent, with short epiphallus (shorter than penis), embedded in thin semi-transparent penial sheath; vagina short, thick; bursa copulatrix thick, comparatively short, with bulbous head, extending up to half of spermoviduct; vas deferens thick; proximal part of penial wall thickened, inner penial wall proximally with two smooth pilasters and several strongly developed oblique accessory pilasters, distally with dense pustulation (based on dissections of two specimens).

Etymology. The specific name for this new species of land snail, *amurndamilumila*, comes directly from the

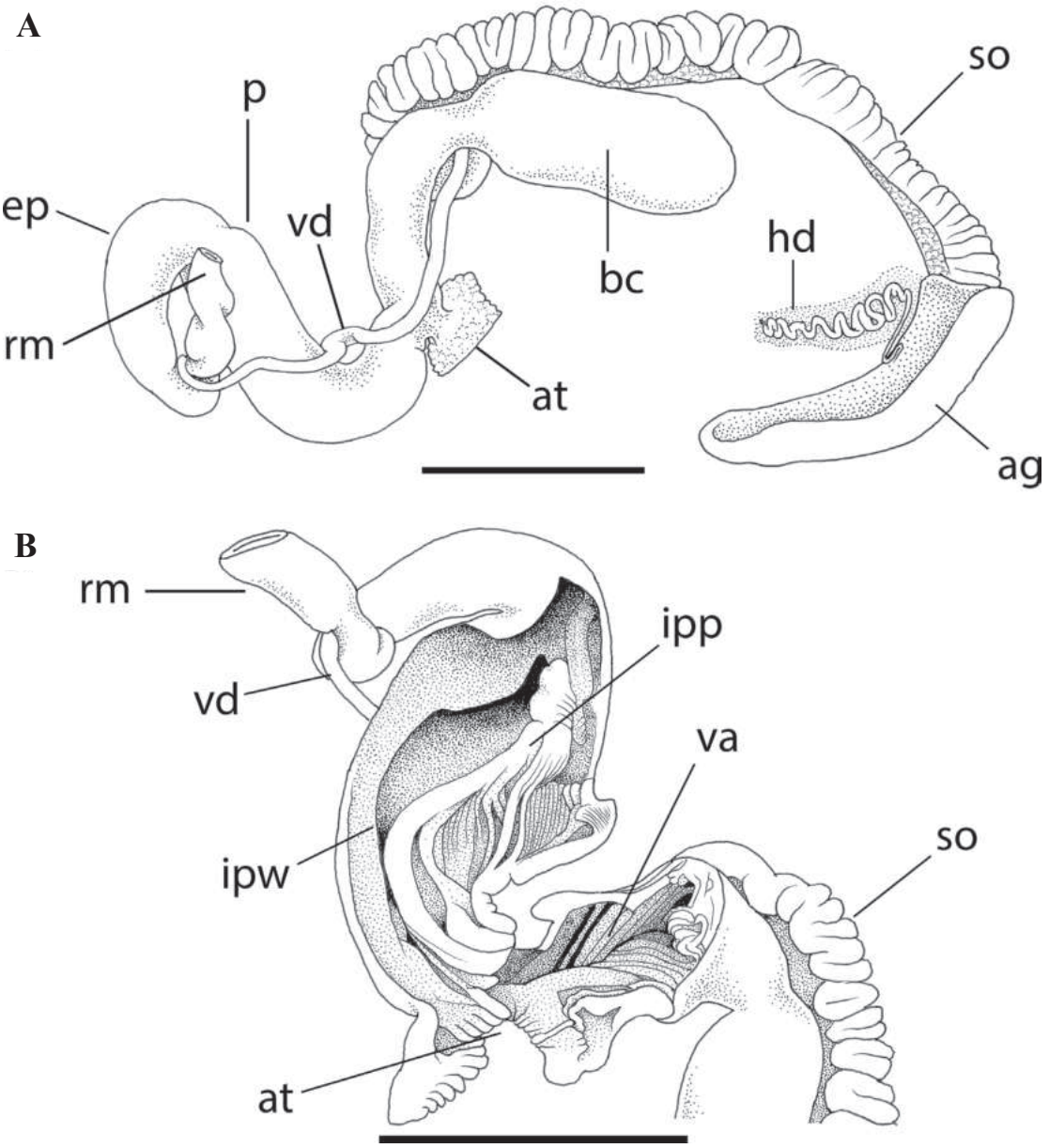

Figure 4. Reproductive anatomy of *Xanthomelon amurndamilumila* sp. nov., based on dissection of the holotype NTM P.65134. **A** Genital system; **B** Penial interior. Abbreviations used: ag, albumen gland; at, atrium; bc, bursa copulatrix; ep, epiphallus; hd, hermaphroditic duct; ipp, penial wall pilasters, ipw, inner penial wall; p, penis; rm, retractor muscle, so, spermoviduct; va, vagina; vd, vas deferens. Scale bars: 5 mm.

Amamalya Ayakwa language spoken by the Anindilyakwa Aboriginal people living on Groote Eylandt and Bickerton Island in the Gulf of Carpentaria. The word, which was provided by the Groote Eylandt Language Centre in consultation with the authors of this paper, means bumpy or corrugated (as in a sheet of corrugated iron) and it is a reference to the regular collabral ribs that ornament the shell. According to the Groote Eylandt Language Centre, the official pronunciation of the word is a-murn-DA-muhluh-muhla. The name is intended as a noun in apposition. Incidentally, *Xanthomelon arnhemense*, which is the cognate species living on mainland Groote Eylandt, has the Anindilyakwa name of yimurnderrma (pers. comm. P. Barden).

Comparative remarks. *Xanthomelon amurndamilumila* differs from other congeners in the Northern Territory by having well-developed collabral ridges (absent in *X. interpositum*, *X. darwinense* and *X. jannellei*), smaller shell size (larger shells in *X. arnhemense*, *X. durvillii* and *X. interpositum*) and in relative length of the epiphallus (1.5–5 times longer than penis in *X. durvillii*, *X. arnhemense* and *X. interpositum*). Furthermore, *X. jannellei* differs by having an extensive field of pustules on the apical half of the inner penial wall (refer to comparative morphology above for details and to Köhler and Burghardt (2016) for descriptions of other species).

Distribution. Known to occur only on the three islands comprising the North East Isles – North East Island

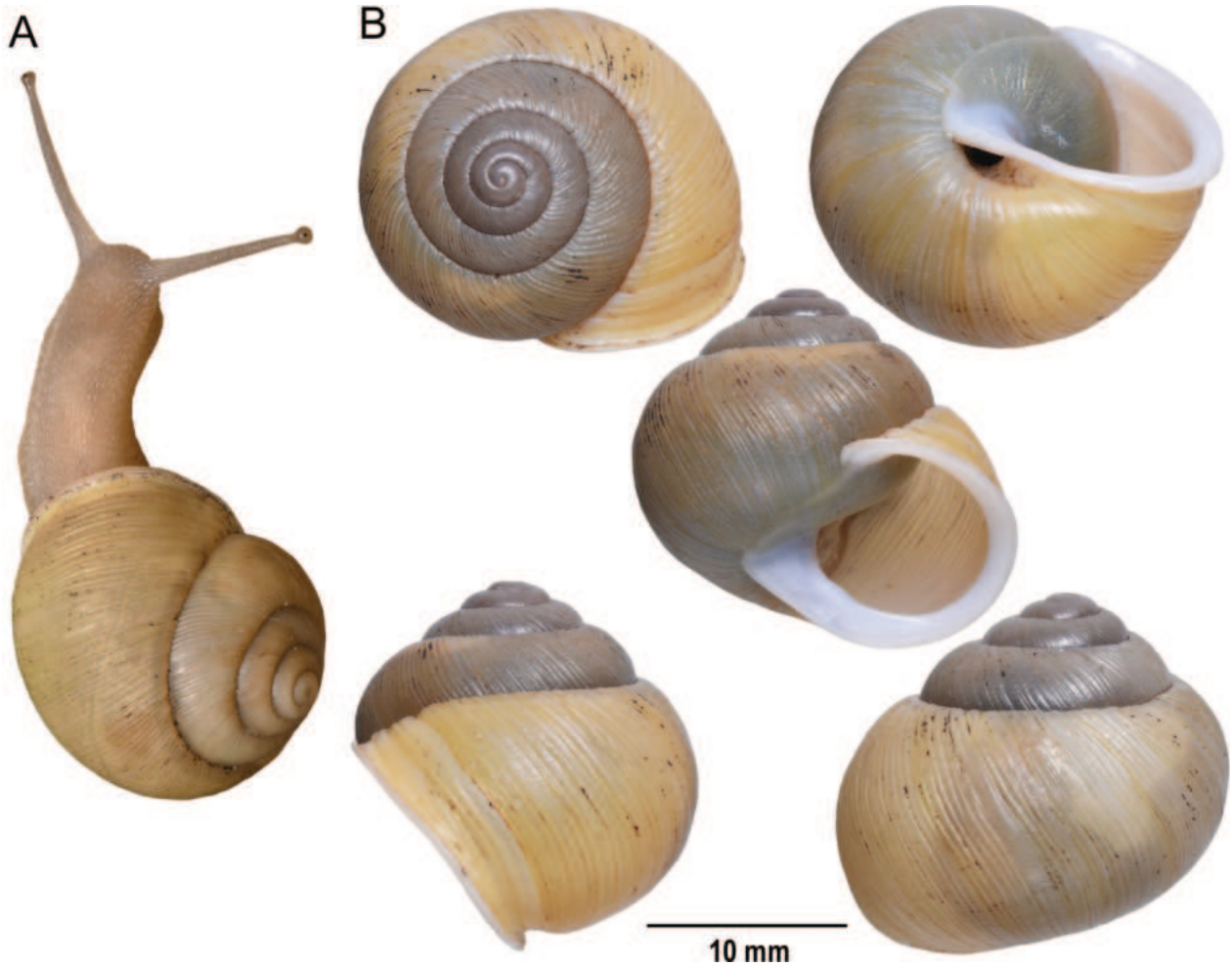

Figure 5. Shell morphology of *Xanthomelon amurndamilumila* sp. nov. **A** Living specimen from North East Island, not to scale; **B** Paratype NTM P.62888. Scale bar: 10 mm.

itself (= Amburrkba), Hawk Island (= Ayangkijirumanja) and Lane Island (= Milyekaluwakba) (Fig. 1).

Threatening processes. The presence of thousands of long dead *Xanthomelon* shells scattered on the surface across North East Island suggests deleterious changes in vegetation have occurred sometime during the last 100 years. Current inspection of North East Island shows that it is heavily damaged through over-browsing by feral Javan Rusa Deer (*Rusa timorensis*) (Willan and Bourke 2022). This over-browsing and habitat destruction puts *Xanthomelon amurndamilumila* potentially at risk of extinction on that island.

Discussion

The mitochondrial phylogeny revealed that the putative new *Xanthomelon* species on the North East Isles is most closely related to *X. arnhemense*, which occurs on Groote Eylandt, the large land mass closest to the North East Isles (Fig. 1). In fact, both species are sister species forming a single clade in the mitochondrial phylogeny of *Xanthomelon* (Fig. 2). The genetic divergence between both species (p-distances of on average 8.8% in COI) is consistent with the amount of interspecific genetic divergence found in this genus (between 14.5% and 19.1%; Köhler and Burghardt (2016)), although perhaps at the lower end of the range. This genetic distance supports the conclusion that there has been a considerable duration of evolutionary isolation of the populations on the North East Isles and that there is no evidence for contemporary genetic exchange between them and *X. arnhemense* on Groote Eylandt.

The largely identical reproductive anatomy is testimony to the close phylogenetic relationship between both species. We hypothesise that the putative new species likely diverged from *X. arnhemense* because of peripatric speciation after an historical event of long-distance dispersal from mainland Groote Eylandt, but that there has been little if any genetic exchange between the two of them subsequently. That both species now form a sister pair of clades in the mtDNA phylogeny shows that there has been a sufficiently long period of isolation to allow any pre-existing ancestral polymorphisms to sort out.

However, comparative morphology provides the strongest arguments for the recognition of the *Xanthomelon* species presently living on the North East Isles as an independent species. The North East Isles species is characterised by several unique features, which distinguish

it from any other species of *Xanthomelon*, including *X. arnhemense* (refer to taxonomic description for details).

The close relationship of both species is also evident from their closely similar reproductive anatomy. However, the significant differences in shell size and sculpture in combination with substantial amounts of mitochondrial variation between both taxa are indicative of the existence of largely distinct gene pools in both forms, hence indicative of the distinct species status of the North East Isles species.

We conclude that molecular and morphological data support the conclusion that the *Xanthomelon* snails from the North East Isles indeed represent a distinct species or an evolutionarily distinct entity, that has a distinct gene pool (as expressed in a consistently distinct morphology) and with a high probability of lacking genetic admixture with *X. arnhemense* (as expressed in substantial mitochondrial differentiation).

Acknowledgements

Fieldwork on the North East Isles was conducted as part of the Bush Blitz Groote Eylandt 2021 expedition. Firstly, we thank the Anindilyakwa Traditional Owners of the North East Isles – Freda Wurramarrba and her four sons, Fabian, Ishmael, Hamilton and Veron – for allowing us on-to their land to collect molluscs. We also thank the Anindilyakwa Land and Sea Rangers, specifically, Katie Oxenham and Dan Keynes, for co-ordinating access to the North East Isles during the Bush Blitz survey. Lastly, we are indebted to Kirsten Eden (Indigenous Protected Areas Operations Co-ordinator, Groote Eylandt Language Centre) for organising the collaboration with Traditional Owners and other Anindilyakwa elders that resulted in the selection of the species' name. Vince Kessner's opinion that this taxon constitutes a new species of *Xanthomelon* is greatly appreciated.

All the specimens were collected under CDU Animal Ethic Approval 20013 – Fauna Surveys and Monitoring in the Anindilyakwa Protected Area. Thanks go to two reviewers, John Stanisic and Bernhard Hausdorf, for their constructive comments, which helped to improve the quality of this article.

References

Chiba S (1999) Accelerated evolution of land snails *Mandarina* in the oceanic Bonin Islands: Evidence from mitochondrial DNA sequences. Evolution; International Journal of Organic Evolution 53(2): 460–471. https://doi.org/10.2307/2640782

Folmer O, Black M, Hoeh W, Lutz R, Vrijenhoek R (1994) DNA primers for amplification of mitochondrial cytochrome c oxidase subunit I from diverse metazoan invertebrates. Molecular Marine Biology and Biotechnology 3: 294–299.

Kalyaanamoorthy S, Minh BQ, Wong TKF, von Haeseler A, Jermiin LJ (2017) ModelFinder: Fast model selection for accurate phylogenetic estimates. Nature Methods 14(6): 587–589. https://doi.org/10.1038/nmeth.4285

Katoh K, Misawa K, Kuma K, Miyata T (2002) MAFFT: A novel method for rapid multiple sequence alignment based on fast Fourier transform. Nucleic Acids Research 30(14): 3059–3066. https://doi.org/10.1093/nar/gkf436

Köhler F (2011) The camaenid species of the Kimberley Islands, Western Australia (Stylommatophora: Helicoidea). Malacologia 54(1–2): 203–406. https://doi.org/10.4002/040.054.0108

Köhler F, Burghardt I (2016) Cryptic diversity in a widespread land snail: Revision of the genus *Xanthomelon* E. von Martens, 1860 from the Australian Monsoon Tropics (Pulmonata, Camaenidae). Zoologica Scripta 45(2): 127–144. https://doi.org/10.1111/zsc.12144

Köhler F, Criscione F (2015) A molecular phylogeny of camaenid land snails from north-western Australia unravels widespread homoplasy in morphological characters (Gastropoda, Helicoidea). Molecular Phylogenetics and Evolution 83: 44–55. https://doi.org/10.1016/j.ympev.2014.11.009

Köhler F, Shea M (2022) A new cryptic species of land snail from the Northern Territory, Australia (Stylommatophora, Camaenidae, *Parglogenia*). Zoosystematics and Evolution 98(2): 427–433. https://doi.org/10.3897/zse.98.93851

Minh BQ, Nguyen MA, von Haeseler A (2013) Ultrafast approximation for phylogenetic bootstrap. Molecular Biology and Evolution 30(5): 1188–1195. https://doi.org/10.1093/molbev/mst024

Nguyen L-T, Schmidt HA, von Haeseler A, Minh BQ (2015) IQ-TREE: A fast and effective stochastic algorithm for estimating Maximum-Likelihood phylogenies. Molecular Biology and Evolution 32(1): 268–274. https://doi.org/10.1093/molbev/msu300

Sutcharit C, Asami T, Panha S (2007) Evolution of whole-body enantiomorphy in the tree snail genus *Amphidromus*. Journal of Evolutionary Biology 20(2): 661–672. https://doi.org/10.1111/j.1420-9101.2006.01246.x

Willan RC, Bourke A (2022) Groote Eylandt Bush Blitz Molluscs. 16 pp. In [Editor]: Department of Climate Change, Energy, the Environment and Water [DEW]. Groote Eylandt, Northern Territory 2021: Bush Blitz Expedition Report. Department of Climate Change, Energy, the Environment and Water, Canberra, CC BY 4.0.

Willan RC, Köhler F, Kessner V, Braby MF (2009) Description of four new species of limestone-associated *Torresitrachia* land snails (Mollusca: Pulmonata: Camaenidae) from the Katherine District of the Northern Territory, with comments on their conservation. The Beagle. Beagle 25: 87–102. https://doi.org/10.5962/p.287452

Zoosyst. Evol. 100 (1) 2024, 69–85 | DOI 10.3897/zse.100.112778

PENSOFT

für Natur MUSEUM FÜR NATURKUNDE BERLIN

Population variation of *Diapoma pampeana* (Characiformes, Characidae, Stevardiinae) from an isolated coastal drainage in Uruguay, with new records: comparing morphological and molecular data

James Anyelo Vanegas-Ríos[1], Wilson Sebastián Serra Alanís[2,3], María de las Mercedes Azpelicueta[1], Thomas Litz[4], Luiz Roberto Malabarba[5]

1 *División Zoología Vertebrados, Facultad de Ciencias Naturales y Museo, Unidades de Investigación Anexo Museo, Gabinete 104, CONICET, UNLP, La Plata, Buenos Aires, Argentina*

2 *Sección Ictiología, Departamento de Zoología, Museo Nacional de Historia Natural, Montevideo, Uruguay*

3 *Centro Universitario Regional del Este (CURE) Sede Rocha, Rocha, Uruguay*

4 *Friedhofstr. 8, 88448 Attenweiler, Germany*

5 *Laboratório de Ictiologia, Departamento de Zoologia, Universidade Federal do Rio Grande do Sul (UFRGS), Av. Bento Gonçalves, 9500, 91501-970 Porto Alegre, RS, Brazil*

https://zoobank.org/BAC6CFC9-E0EC-459A-9A7B-18F0A5F71D68

Corresponding author: James Anyelo Vanegas-Ríos (anyelovr@fcnym.unlp.edu.ar)

Academic editor: Nicolas Hubert ♦ **Received** 20 September 2023 ♦ **Accepted** 8 December 2023 ♦ **Published** 26 January 2024

Abstract

Diapoma pampeana was recently described to occur in the upper Negro basin in Uruguay and Brazil. An isolated population tentatively identified as *D. pampeana* from the Pando stream, a perturbed coastal drainage in Uruguay, is studied and compared under the light of morphological and molecular data to test if there is evidence to consider it as a separate species. New geographical records for the species are presented and included in the comparisons. The specimens analyzed were pooled into four groups: Pando, Santa Lucía, Middle Negro and Upper Negro. We analyzed 32 morphological characters using statistical procedures and recovered a COI-based phylogeny of different populations of *D. pampeana* to test if they may represent different species. Size-corrected PCA revealed that the Pando and Upper Negro groups are greatly diverging in both morphometric and meristic data along PC1 (mainly by the snout to dorsal-fin origin, dorsal to adipose-fin origins, number of longitudinal scales and predorsal scales). This deviating pattern was also obtained in a cluster analysis. The Santa Lucía and Middle Negro groups were found to be intermediate morphotypes. In contrast, molecular analyses revealed that the Pando and Upper Negro specimens resemble genetically and, thus, are placed together in the Neighbor-joining and Bayesian topologies, as part of a monophyletic *Diapoma*. We proposed that the Pando population, despite its deviating morphology observed, can be classified as *D. pampeana*. Therefore, this population constitutes a remarkable example of an isolated population that is morphologically divergent but genetically similar to the geographically most distant conspecific population.

Key Words

Body shape variation, integrative taxonomy, Neotropical fish, phylogeny, size-corrected PCA

Introduction

The Neotropical fish genus *Diapoma* Cope, 1894 is a member of the tribe Diapomini, which is one of the largest monophyletic groups within the Stevardiinae with ~ 135 relatively small-sized species (no more than 100 mm SL) (Thomaz et al. 2015; Mirande 2019; Ferreira et al. 2021; Ito et al. 2022; Fricke et al. 2023). *Diapoma* is recognized as a monophyletic group based on molecular data and combined evidence (Thomaz et al. 2015; Mirande 2019; Ito et al. 2022).

To date, this genus includes sixteen valid species that are distributed along different river drainages in Argentina, Brazil, Paraguay and Uruguay, mainly within the Rio de la Plata basin. Five species are known from the Paraná-Paraguay system, *D. guarani* (Mahnert & Géry, 1987) (several streams flowing into the Paraná basin in the border region between Alto Paraná, Paraguay and Misiones, Argentina), *D. obi* (Casciotta, Almirón, Piálek & Rícan, 2012) (some tributaries from the Paranay-Guazú drainage and the Moreno stream in Misiones, Argentina), *D. nandi* Vanegas-Ríos, Azpelicueta & Malabarba, 2018 (the Piray-Miní stream in Misiones, Argentina), the recently described *D. potamohadros* Ito, Carvalho, Pavanelli, Vanegas-Ríos & Malabarba, 2022 (endemic from the Rio Iguazú basin in Argentina and Brazil) and *D. terofali* (Géry, 1964) (the Rio Luján and other streams flowing into the Rio de la Plata basin in Buenos Aires, Argentina) (Mahnert and Géry 1987; Menezes and Weitzman 2011; Casciotta et al. 2012; Vanegas-Ríos et al. 2018; Ito et al. 2022). The Rio Uruguay basin is the water body that possesses the greater number of *Diapoma* species registered so far (seven spp.), *D. alegretense* (Malabarba & Weitzman, 2003) (the Rio Ibicuí system in Rio Grande do Sul, Brazil, and Laguna Redonda in Artigas, Uruguay), *D. guarani* (Barragem Sanchuri in Rio Grande do Sul, Brazil), *D. lepiclastum* (Malabarba, Weitzman & Casciotta, 2003) (from the Rio Pelotas and Rio Canoas to the Lageado União stream in Brazil, and in the eastern region of Misiones, Argentina), *D. pampeana* Ito, Carvalho, Pavanelli, Vanegas-Ríos & Malabarba, 2022 (the upper Rio Negro basin in Brazil and Uruguay), *D. pyrrhopteryx* Menezes & Weitzman, 2011 (the Rio Pelotas basin in Rio Grande do Sul, Brazil, and the Pepirí Iguazú basin in Misiones, Argentina), *D. terofali* (streams flowing into the Rio Uruguay system in Río Grande do Sul, Brazil, and in Artigas and Cerro Largo, Uruguay), and *D. uruguayense* (Messner, 1962) (tributaries of the Rio Uruguay in the border region between Argentina, Uruguay, and Brazil, and from the headwaters of the Rio Negro) (Malabarba and Weitzman 2003; Zarucki et al. 2010; Menezes and Weitzman 2011; Thomaz et al. 2015; Almirón et al. 2016). Four species have been recorded for the Laguna dos Patos basin and the coastal drainages of south Brazil, *D. dicropotamicum* (Malabarba & Weitzman, 2003) (northern tributaries of the Rio Jacuí from the Serra Geral formation), *D. itaimbe* (Malabarba & Weitzman, 2003) (Tramandaí, Mampituba, Araranguá river basins, southern coast of Brazil), *D. speculiferum* Cope, 1894, *D. thauma* Menezes & Weitzman, 2011 (tributaries of the Rio Jacuí basin, Rio Grande do Sul, Brazil) and *D. tipiaia* (Malabarba & Weitzman, 2003). Finally, *D. alburnum* (Hensel, 1870) is the most widely distributed species occurring in the Uruguay (e.g. the Rio Queguay basin), Paraná (the Río Gualeguay basin), Laguna dos Patos (e.g. the Rio Jacuí system) basins and coastal drainages of southern Brazil (Malabarba 1983; Malabarba and Weitzman 2003; Protogino and Miquelarena 2012; Paullier et al. 2019).

Diapoma pampeana, recently described from the upper Rio Negro basin, reaches 35 mm SL and can be differentiated from all its congeners by a combination of characters, mainly from body pigmentation (Ito et al. 2022), including the presence of: a narrow and conspicuous black line along the horizontal septum, never forming a wide lateral stripe; a longitudinal black stripe extending posteriorly on the middle caudal-fin rays; and a small black blotch, restricted to the base of the middle caudal-fin rays.

We found specimens that potentially could be identified as *D. pampeana* from the Pando stream, a coastal drainage flowing into the Rio de la Plata estuary in Uruguay, based on the resemblance of the humeral mark, midlateral stripe, and caudal-fin pigmentation. The possible presence of this species in the Pando stream caught our attention because the preliminary morphometric data obtained were somewhat incongruent with the data reported in the description by Ito et al. (2022), and because no congener has been recorded in this area so far (Malabarba and Weitzman 2003; Menezes and Weitzman 2011; Gurdek and Acuña-Plavan 2017). This small drainage, which is located in the middle of urban and agricultural areas, has been greatly modified and affected by anthropogenic factors such as pollution, industrial activities, and urban waste originated from anthropogenic actions (Echevarría et al. 2011; Achkar et al. 2012; Gutiérrez et al. 2015; Muniz et al. 2019) and is considered of great importance, among other reasons, because its sub-estuarine mouth plays a role in the breeding and nursery for grounds of fish (Defeo et al. 2009; Acuña et al. 2017; Muniz et al. 2019).

There are several studied cases in which species previously considered as distributed in the Rio Uruguay drainage and Atlantic river coastal drainages have been separated in two different species [e.g. *Parapimelodus nigribarbis* (Boulenger, 1889) vs. *P. valenciennis* (Lütken, 1874), see Lucena et al. (1992); *Pimelodus pintado* Azpelicueta, Lundberg & Loureiro, 2008 vs. *P. maculatus* Lacepède, 1803, see Azpelicueta et al. (2008); *Bunocephalus erondinae* Cardoso, 2010 vs. *B. doriae* Boulenger, 1902, see Cardoso (2010); *Pseudocorynopoma stanleyi* Malabarba, Chuctaya, Hirschmann, Oliveira & Thomaz, 2020 vs. *P. doriae* Perugia, 1891, see Malabarba et al. (2021)]. So, the present study aims to carry out a morphological (mainly morphometric and meristic data) and COI-based comparison between the population of *D. pampeana* from the Rio Negro basin, a tributary of the lower Rio Uruguay, and the population tentatively identified as *D. pampeana* from the Pando stream, that empties directly in the Atlantic Ocean. We expect to test if there is evidence to consider these isolated populations as separate species or to treat them as a single species, describing any intraspecific variation between them. Additionally, a recent examination of specimens of *Diapoma* at Museo Nacional de Historia Natural, Montevideo (MHNM), revealed two lots of individuals similar to *D. pampeana* in the body shape and meristic data from the Yi and Santa Lucía river basins (as fixed in 10% formalin, DNA extraction was unavailable). Consequently, they were included in the morphological analyses to enhance the comparisons and are also presented as new records.

Materials and methods

Specimens were collected in the Pando stream (permission No. 202/717/04, DINARA, Uruguay) between 2003 and 2004. They were fixed in formalin 10% and preserved in alcohol 70%. Some of them, which were preserved originally in ethanol 96%, were rehydrated before being preserved and catalogued as the others. Additional studied specimens of *D. pampeana* and comparative species are deposited in the following institutions: MACN-ict, MLP, MHNG, MHNM, UFRGS, and UNMDP (abbreviations according to Sabaj 2020).

Morphological analysis

Measurements and other counts were taken following Fink and Weitzman (1974), with the modifications presented by Ito et al. (2022). Twenty-two measurements were taken point to point with a digital caliper under a stereomicroscope and are expressed as percentages of standard length (SL) or head length (HL) for units of the head. Specimens were cleared and stained (c&s) following Taylor and Dyke (1985). The total number of vertebrae was counted in c&s specimens. Those counts included the first preural centrum plus the first ural centrum (PU1 + U1) counted as one element and all four vertebrae of the Weberian apparatus.

The specimens from the Pando stream were compared with type specimens of *D. pampeana* from the Rio Negro basin under different statistical procedures. Additionally, the specimens presumably belonging to *D. pampeana* from the Yi and Santa Lucía river basins in Uruguay were only processed in the morphological analyses because they were not suitable for DNA extraction. To facilitate comparisons, a morphometric data matrix that included all of these specimens was pooled into groups (based on geographic drainages) as follows: Pando (n = 17), Santa Lucía (Canelón Grande, n = 2), Middle Negro (Yi, n = 15), and Upper Negro (several localities, n = 35). Nearly all the specimens analyzed in all groups were adults, except for a few immature specimens that were also added in the comparisons (excluding the bone hooks, no morphometric or meristic differences were observed between them and the respective adults). This dataset was analyzed using the "allometric vs. standard" procedure (Elliott et al. 1995), under which the allometric coefficients are calculated concerning a standard (reference, such as overall length) measurement (each variable is regressed onto this after log-transformation). The size-corrected morphometric dataset was analyzed using a principal component analysis (PCA), based on the covariance matrix. For the PCA, the number of significant principal components (PCs) was decided by two criteria: the broken-stick model (Frontier 1976) and the scree plot method (Cattel 1966). To compare the dissimilarity between the groups associated with the size-corrected morphometric data, a hierarchical cluster analysis was performed using Ward's method (Ward 1963) and Euclidean distances, under 1000 bootstrap replicates. Missing values in measurements (e.g. some fin rays were broken in a few individuals) were imputed from predictor values obtained under maximum likelihood from the EM algorithm (Dempster et al. 1977; Pigott 2001) using 500 iterations. For the morphometric data, confidence intervals of 95% were calculated using 9000 bootstraps.

Meristic data showing slightly different patterns between the Pando group and the other groups were analyzed using a PCA on the root-squared transformed values and the correlation matrix (Quinn and Keough 2002) (outliers that could not be reexamined in the specimens were omitted and the mean was imputed for missing data). To illustrate the distinctive patterns within the Pando group, we used Tukey box plots for the variables, which provide a clearer representation of the observed variability. When it comes to counts, both mean and mode values are reported, and they are separated by a slash.

For those analyses, normality was tested using a Shapiro–Wilk statistic (W) in each case ($\alpha < 0.05$) and data were log-transformed when needed to better approximate to a multivariate normality. Statistical procedures were carried out in PAST 4.12 (Hammer et al. 2001), IBM SPSS Statistics 26.0 (IBM 2019), and GraphPad Prism 9.4.1 (GraphPad Software, San Diego, CA, USA).

Molecular analysis

The mitochondrial cytochrome c oxidase subunit I gene (COI) was obtained from two specimens from the Pando stream. DNA extraction and polymerase chain reaction (PCR) were carried out following the standard COI protocols (Ivanova et al. 2006; Rosso et al. 2012), under different sets of primer cocktails for fishes (Ivanova et al. 2007).

In total each amplification reaction produced a volume of 12.375 µL from 2 µL of DNA template, 6.25 µL of 10% trehalose, 2 µL of molecular biology grade water, 1.25 µL of 10× reaction buffer, 0.625 µL of MgCl2 (50 µM), 0.0625 µL of dNTP (10 mM), 0.0625 µL of each primer (10 µM) and 0.0625 µL of Invitrogen's Platinum Taq. polymerase (5 U µL−1). The amplification conditions consisted of 2 min at 95 °C, followed by 35 cycles at 94 °C for 30 s, at 52 °C for 40 s and at 72 °C for 1 min, and ended at 72 °C for 10 min. E-Gels (Invitrogen) were used to check the amplification success. The COI gene was sequenced in Macrogen (Korea) and IGEVET-UNLP (Argentina). Sequence chromatograms were edited using BioEdit 7.2.5 (Hall 1999).

For comparative purposes, in addition to the newly generated sequences, 72 COI sequences were selected from representative specimens of the valid species of *Diapoma* (except *D. nandi*) (Ito et al. 2022) and genera closely related to it (detailed later herein) that are available in GenBank and Barcode of Life database (BOLD, available at http://www.boldsystems.org) (accession numbers for all sequences analyzed are provided in Suppl. material 1). The COI sequences were aligned with MUSCLE (1000 iterations) (Edgar 2004) and generated as a data matrix

partitioned by the first three codon positions in MEGA 11.0.13 (Tamura et al. 2021). The COI dataset was uploaded to Zenodo (https://doi.org/10.5281/zenodo.8361520).

To analyze the phylogenetic placement of the specimens from the Pando stream through different methods, the COI data matrix was analyzed by the phylogenetic procedures and conditions described hereafter. Modeltest-NG (Darriba et al. 2019) was used for selecting the best-fit nucleotide substitution model available for each procedure (and computational package) based on the partitioned alignment when necessary. The AIC and BIC statistical criteria were explored, but the latter was used to choose the best model among the candidate models. The neighbor-joining (NJ) tree (10000 bootstrap) was constructed based on the Tajima+Nei model with rates gamma-distributed as implemented in Mega. Bayesian analyses were conducted in MRBAYES 3.2.2 (Ronquist et al. 2012) using two runs, each with four Markov chains, which ran for 60 million generations (25% discarded as burn-in, sampling a tree every 3000 generations) under the models SYM+I (position 1), F81 (position 2) and HKY+G (position 3). Tracer 1.7.2 (Rambaut et al. 2018) was used to evaluate the results of the MRBAYES analyses from each run (ESS values and lnL plots). The trees were visualized and prepared with FIGTREE 1.4.4 (Rambaut 2018). The CIPRES portal (Miller et al. 2010) was used to run the following computational programs: MODELTEST-NG and MRBAYES 3.2.2. The outgroup was composed of species from *Bryconamericus* Eigenmann, 1907, *Hypobrycon* Malabarba & Malabarba, 1994, *Nantis* Mirande, Aguilera & Azpelicueta, 2006, *Odontostoechus* Gomes, 1947, *Piabarchus* Myers, 1928, and *Piabina* Reinhardt, 1867, genera that have been considered in preceding studies (Ferreira et al. 2011; Mirande 2019; Ito et al. 2022) to be closely related to *Diapoma* (trees were rooted in *Piabina* species when required). Additionally, to compare the interspecific and within-species variability, the uncorrected pairwise genetic distances (gamma distributed and pairwise deletion) were calculated in MEGA 11.0.13 (Tamura et al. 2021).

To examine the potential variability associated with polymorphism between the Pando and Upper Negro specimens, despite the limited number of samples available, the specimens of *D. pampeana* in the COI data matrix were pooled into the two respective groups using DNASP 6.12.03 software (Rozas et al. 2017) to calculate the polymorphism sites, nucleotide diversity (π) (Nei and Li 1979), net (Da) and absolute (Dxy) divergences (Nei 1987), and to generate the haplotypes set including invariant sites and gaps. POPART (Leigh and Bryant 2015) was used to construct a haplotype network using a median-joining algorithm and default settings.

Results

Based on the comparisons carried out (detailed below), we confirmed that the examined specimens from the Pando stream (Figs 1, 2A, B), Santa Lucía system (Fig. 2C), and middle Rio Negro basin (Fig. 2E) correspond to new records of *D. pampeana*, which extend its distribution to the southwest from the upper Negro basin (in straight-line distances: ~ 200 km to Middle Negro, ~ 280 km to Santa Lucía, and ~ 290 km to Pando) (Fig. 3). The list of examined specimens of *D. pampeana* is presented in Table 1.

Morphological comparisons

The measurements of the examined specimens are summarized in Table 2. Comparing the morphometric data between the Pando group and the other groups, discrete differences between the ranges obtained were not detected. Some tendencies based on the mean in some measurements, with partially overlapping ranges, were observed. The distance between the snout and dorsal-fin origin tended to be slightly longer in the Pando, Santa Lucía and Middle Negro groups than in the Upper Negro group (53.5–58.2% SL, mean = 55.7%±1.4 in Pando; 54.2–55.7% SL, mean 54.9%±1.1 in Santa Lucía; 54.2–57.6% SL, mean = 55.8%±1.0 in Middle Negro vs. 49.0–56.2% SL, mean = 52.7%±1.7 in Upper Negro). The Pando group presented a slightly smaller distance between the dorsal- and adipose-fin origins compared to the Upper Negro group (30.4–34.8% SL, mean = 33.0%±1.1 vs. 33.0–39.9% SL, mean = 37.1%±1.4), but almost similar to the other groups (33.6–34.4 & SL, mean = 34.0±0.6 in Santa Lucía; 32.0–36.1% SL, mean = 33.9%±1.0 in Middle Negro, respectively). In other measurements, as the caudal peduncle length and snout length, the Pando group tended to show greater mean values as follow (Pando, Santa Lucía, Middle Negro and Upper Negro, respectively): for caudal peduncle length 12.1–14.6% SL, mean = 13.6%±0.7; 12.1–13.4% SL, mean = 12.8±0.9; 12.5–15.0% SL, mean = 13.4%±0.6; 8.9–13.4% SL, mean = 11.3%±1.0; and for snout length 19.3–22.3% HL, mean = 21.0%±0.8; 21.5–21.6% HL, mean = 21.5%±0.1; 20.1–22.1% HL, mean = 20.8%±0.6; 16.3–22.1% HL, mean = 19.1%±1.6.

Based on the consensus between the scree plot method and broken-stick model (Suppl. material 2), to ensure that did not discard biologically pertinent data, four eigenvector elements were selected in the PCA on the size-corrected data, which accounted for 70.7% of the total variance (Suppl. material 3; Fig. 4A, B). Along the first axis in the PC1 vs. PC2 plot (Fig. 4A: explained 53.2% of the total variance), the Pando group was almost fully differentiated from the Upper Negro group, but overlapped with the majority of the specimens of the Santa Lucía and Middle Negro groups. In the PC3 vs. PC4 plot (Fig. 4B explained 17.6% of total variance), the groups appeared to overlap, and there was no clear distinction between them. PC1 was most heavily loaded by the following measurements (Fig. 4A, Table 3): negatively by the snout to dorsal-fin origin (-0.5), snout to anal-fin origin (-0.3), caudal peduncle length (-0.3), snout to pelvic-fin origin (-0.2), and caudal peduncle depth (-0.2); and positively by the dorsal- to adipose-fin origins (0.5) dorsal fin to caudal-fin base (0.2), dorsal-fin length (0.2), and anal-fin base length (0.2). PC2 was most influenced by positive variables such

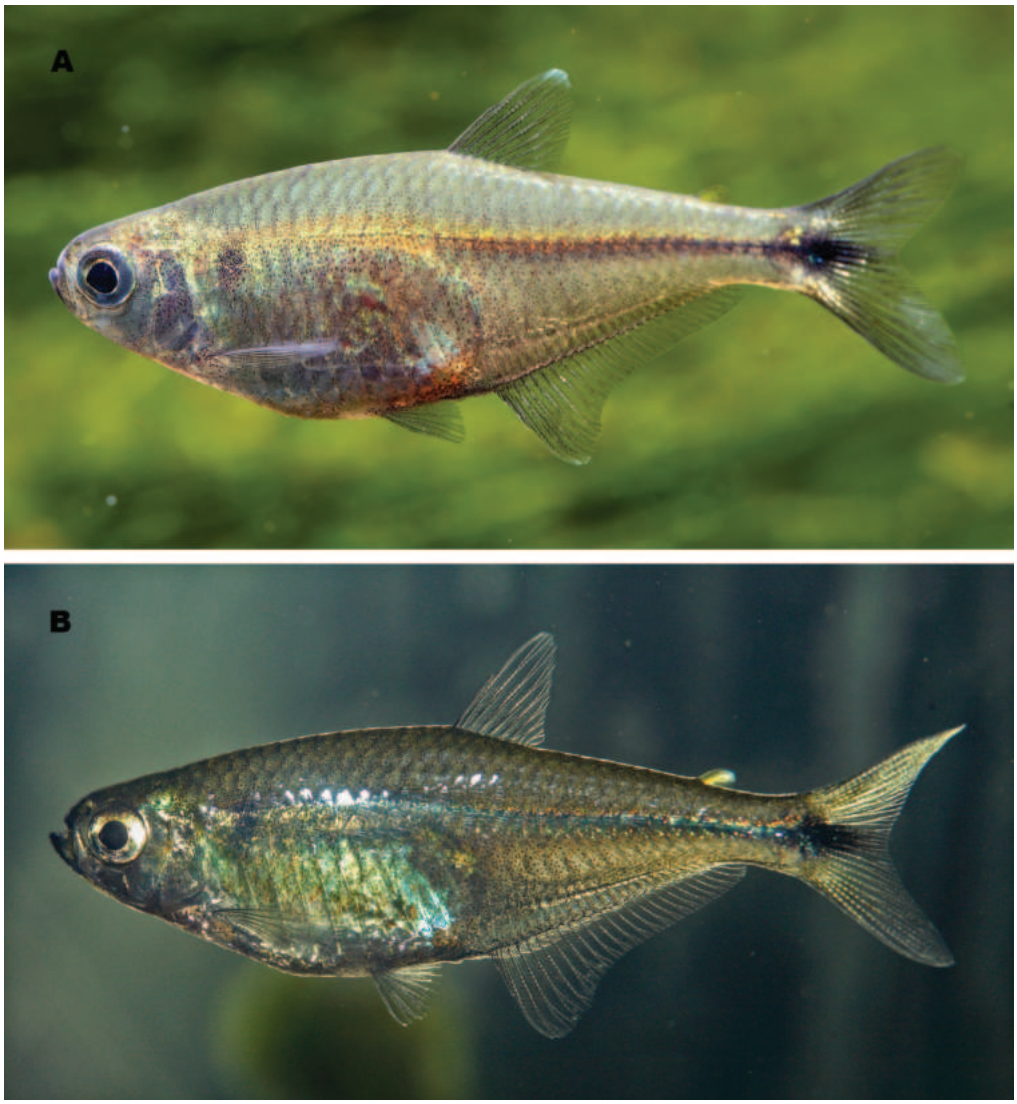

Figure 1. Coloration in life of *D. pampeana* (**A, B**) from the Pando stream, Canelones Uruguay. Photo by J. Pfleiderer.

Table 1. New records and material examined of *D. pampeana*. n = number of examined specimens. Group names corresponds with those described in the text. Accession numbers: OR533516* and OR533515**.

Group	n	SL (mm)	Catalog number	Country	Locality	Latitude/Longitude	Remarks
Santa Lucía	1	31.3	MHNM 1125	Uruguay	Canelones, Rio Santa Lucía basin, Canelón Grande stream	34°29'14.00"S, 56°20'33.61"W	
Santa Lucía	1	28.9	MHNM 1189	Uruguay	Canelones, Rio Santa Lucía basin, Canelón Grande stream	34°29'14.70"S, 56°20'34.54"W	
Pando	2	33.6–33.9	MHNM 812	Uruguay	Canelones, Cañada de Ramos, Pando, Pando stream	34°43'39.01"S, 55°56'39"W	
Pando	1	30.6	MLP 14443	Uruguay	Canelones, Cañada de Ramos, Pando, Pando stream	34°44'19.2"S, 55°56'27"W	
Pando	3	22.2–25.3	MLP 11444*	Uruguay	Canelones, Cañada de Ramos, Pando, Pando stream	34°42'12"S, 55°56'42.6"W	
Pando	10	25.3–34.8	MLP 11445	Uruguay	Canelones, Cañada de Ramos, Pando, Pando stream	34°44'19.2"S, 55°56'27"W	1 c&s: 28.7 mm SL
Pando	1	25.2	UNMDP 5219**	Uruguay	Canelones, Cañada de Ramos, Pando, Pando stream	34°42'12"S, 55°56'42.6"W	
Middle Negro	28	19.6–29.8	MHNM 4018	Uruguay	Durazno, marginal lagoon to Río Yi, Estancias del Lago	33°21'47.16"S, 56°35'23.43"W	15 fully measured
Upper Negro	10	25.9–33.6	UFRGS 8119	Uruguay	Cerro Largo, small stream at Route 26, ca. 59 km from Melo, between Sauce creek and Fraile Muerto creek	32°17'39"S, 54°44'59"W	
Upper Negro	2	27.4–28.7	UFRGS 8120	Uruguay	Tacuarembó, Rio Tacuarembó, at Route 26, Villa Ansina	31°58'33"S, 55°28'13"W	
Upper Negro	1	24.3	UFRGS 8121	Uruguay	Rivera, Mazangano Bridge at Route 44	32°06'33"S, 54°40'08.6"W	
Upper Negro	11	27.2–32.0	UFRGS 8122	Uruguay	Rivera, lateral puddles and Corrales creek, affluent of Rio Tacuarembó, Route 27	31°23'26"S, 55°15'14"W	3 c&s: 30.4–31.5 mm SL
Upper Negro	5	27.3–29.1	UFRGS 8123	Uruguay	Tacuarembó, Caraguatá creek, tributary to Rio Tacuarembó, Route 26, Las Toscas	32°09'29"S, 55°01'27"W	
Upper Negro	1	25.1	UFRGS 8429	Brazil	Rio Grande do Sul, Bagé, road between Aceguá and Bagé, Rio Negro	31°28'37"S, 54°08'20"W	
Upper Negro	10	25.9–33.6	UFRGS 8464	Brazil	Rio Grande do Sul, Bagé, road between Aceguá and Bagé, BR-153, Cinco Saltos creek, affluent of Rio Negro	31°36'53"S, 54°08'42"W	
Upper Negro	1	29.6	UFRGS 28705	Brazil	Rio Grande do Sul, Bagé, road between Aceguá and Bagé, BR-153, Cinco Saltos creek, affluent of Rio Negro	31°36'53"S, 54°08'42"W	holotype

Figure 2. Extern morphology of studied specimens of *Diapoma pampeana*. **A.** MLP 11443, male, 30.6 mm SL, Uruguay, Pando Stream; **B.** MLP 11445, female, 35.1 mm SL, Uruguay, Pando Stream; **C.** MHNM 1125, female, 31.3 mm SL, Uruguay, Canelón Grande Stream; **D.** MHNM 4018, male, 29.8 mm SL, Uruguay, marginal lagoon to Rio Yi; **E.** MHNM 4018, female, 29.3 mm SL, Uruguay, marginal lagoon to Rio Yi. Photographs of the specimens from the Upper Negro are available in Ito *et al*. (2022). Scale bar: 1 mm.

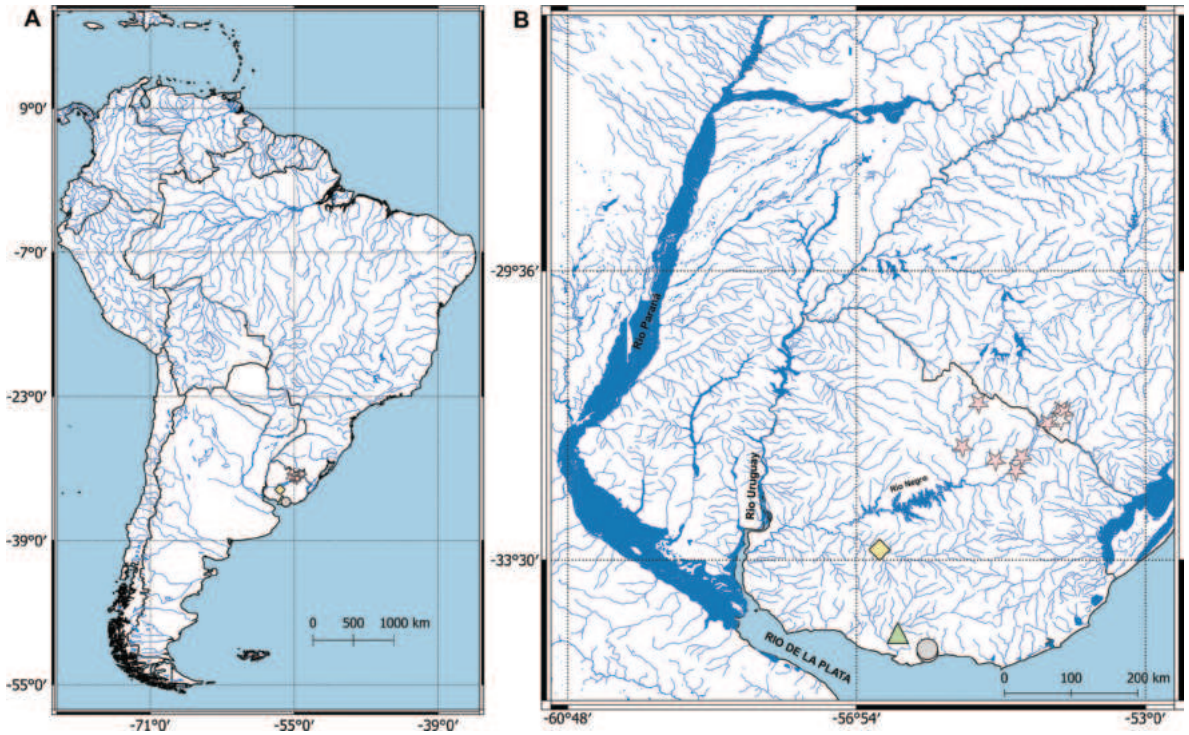

Figure 3. Geographic distribution of *Diapoma pampeana*. **A.** View within South America; **B.** View within Brazil and Uruguay. All studied specimens from the Pando (Circle), Santa Lucía (triangle), Yi (diamond), and Upper Negro (star; holotype represented by not-filled pattern) are depicted. Other records presented by Ito et al. (2022) are also included.

Table 2. Comparative morphometric data obtained in the specimens studied of *D. pampeana*. SD = standard deviation; n = number of examined specimens; CI = confidence interval. Group names corresponds with those described in the text.

	Pando (n = 17)			Santa Lucía (n = 2)			Middle Negro (n = 15)			Upper Negro (n = 35)		
	Range	Mean±SD	CI95%	Range	Mean±SD	CI95%	Range	Mean±SD	CI95%	Range	Mean±SD	CI95%
Standard Length (mm)	22.2–35.1	28.9±3.8	27.1; 30.6	28.9–31.3	30.1±1.7	28.9; 31.3	23.3–29.8	26.6±1.7	25.8; 27.4	25.1–33.6	29.4±2.2	28.7; 30.1
Percents of SL (%)												
Depth at dorsal-fin origin	29.5–34.7	31.7±1.4	31.1; 32.4	30.1–32.2	31.1±1.5	30.1; 32.2	29.6–33.4	31.5±1.3	30.9; 32.1	27.7–33.7	30.9±1.2	30.5; 31.3
Snout to dorsal-fin origin	53.5–58.2	55.7±1.4	55.1; 56.4	54.2–55.7	54.9±1.1	54.2; 55.7	54.2–57.6	55.8±1.0	55.4; 56.3	49.0–56.2	52.7±1.7	52.3; 53.3
Snout to pectoral-fin origin	24.7–27.3	26.2±0.9	25.8; 26.6	25.2–26.2	25.7±0.7	25.2; 26.2	25–28.3	26.4±0.8	26.0; 26.8	23.2–27.5	25.1±0.9	24.8; 25.4
Snout to pelvic-fin origin	44.1–47.8	46.5±1.0	46.1; 47.0	44.7–45.0	44.9±0.2	44.7; 45.0	44.3–48.2	45.8±1.0	45.3; 46.3	41.9–47	44.9±1.2	44.5; 45.3
Snout to anal-fin origin	56.6–62.1	59.9±1.5	59.3; 60.7	57.9–58.5	58.2±0.4	57.9; 58.5	56.6–60.6	58.7±1.2	58.2; 59.3	53.8–60.6	58.3±1.5	57.8; 58.8
Distance between dorsal- and adipose-fin origins	30.4–34.8	33.0±1.1	32.5; 33.5	33.6–34.4	34.0±0.6	33.6; 34.4	32.0–36.1	33.9±1.0	33.4; 34.4	33.0–39.9	37.1±1.4	36.6; 37.5
Dorsal fin to caudal-fin base	46.4–49.0	47.7±0.9	47.3; 48.1	45.5–48.6	47.1±2.2	45.5; 48.6	46.1–49.7	48.2±1.3	47.6; 48.9	45.9–54.8	49.0±1.9	48.2; 49.3
Dorsal-fin length	20.7–24.8	23.0±0.9	22.6; 23.5	23.2–24.0	23.6±0.6	23.2; 24.0	22.7–25.1	23.9±0.7	23.6; 24.3	22.7–27.0	24.6±1.2	24.2; 25.0
Dorsal-fin base length	9.7–12.8	11.1±0.7	10.7; 11.4	10.4–12.2	11.3±1.3	10.4; 12.2	10.5–11.9	11.0±0.4	10.8; 11.3	10.1–14.0	11.7±0.9	11.4; 12.0
Pectoral-fin length	21.6–25.0	23.1±1.0	22.6; 23.6	22.2–23.2	22.7±0.7	22.2; 23.2	20.9–24.4	22.6±0.9	22.2; 23.1	21.9–25.8	23.8±0.9	23.5; 24.1
Pelvic-fin length	11.1–14.7	13±0.9	12.5; 13.4	12.2–12.3	12.2±0.1	12.2; 12.3	11.2–13.7	12.6±0.8	12.2; 13.0	12.0–15.7	13.9±0.9	13.5; 14.2
Anal-fin base length	30.2–37.0	33.5±1.8	32.7; 34.3	31.4–35.1	33.3±2.6	31.4; 35.1	31.7–34.3	33.0±0.9	32.5; 33.4	32.1–36.6	34.5±1.3	34.0; 34.9
Caudal peduncle depth	8.6–11.6	10.1±0.7	9.8; 10.4	10.5–10.7	10.6±0.2	10.5; 10.7	9.6–11.0	10.4±0.4	10.2; 10.7	7.8–10.0	9.0±0.5	8.8; 9.2
Caudal peduncle length	12.1–14.6	13.6±0.7	13.3; 13.9	12.1–13.4	12.8±0.9	12.1; 13.4	12.5–15.0	13.4±0.6	13.1; 13.7	8.9–13.4	11.3±1.0	11.0; 11.6
Head length	21.9–25.4	23.7±0.9	23.3; 24.1	21.7–22.9	22.3±0.9	21.7; 22.9	22.5–25.3	23.5±0.8	23.1; 23.9	21.3–25.2	23.1±0.9	22.8; 23.3
Percents of HL (%)												
Snout length	19.3–22.3	21.0±0.8	20.7; 21.4	21.5–21.6	21.5±0.1	21.5; 21.6	20.1–22.1	20.8±0.6	20.5; 21.1	16.3–22.1	19.1±1.6	18.6; 19.7
Horizontal eye length	38.8–45.0	42.1±1.6	41.4; 42.9	41.8–42.8	42.3±0.7	41.8; 42.8	40.2–44.5	42.3±1.3	41.7; 42.9	39.5–46.8	43.5±1.6	43.0; 44.1
Postorbital head length	36.7–42.8	39.2±2.1	38.2; 40.1	38.3–40.2	39.3±1.3	38.3; 40.2	35.4–40.0	38.0±1.3	37.3; 38.6	35.6–43.1	39.2±1.9	38.5; 39.8
Least interorbital width	30.1–36.0	33.3±1.8	32.5; 34.1	34.2–34.9	34.5±0.5	34.2; 34.9	28.8–35.9	33.4±1.8	32.6; 34.3	28.6–38.7	32.2±1.9	31.6; 32.8
Upper jaw length	32.8–44.5	36.5±2.9	35.1; 37.8	39.1–39.9	39.5±0.6	39.1; 39.9	32.7–37.1	35.3±1.4	34.7; 36.1	32.4–39.1	35.7±1.8	35.1; 36.3
Dentary length	37.1–46.4	40.3±2.4	39.1; 41.3	39.1–39.8	39.4±0.5	39.1; 39.8	37.7–42.8	40.3±1.6	39.5; 41.0	36.5–42.2	38.9±1.6	38.3; 39.4

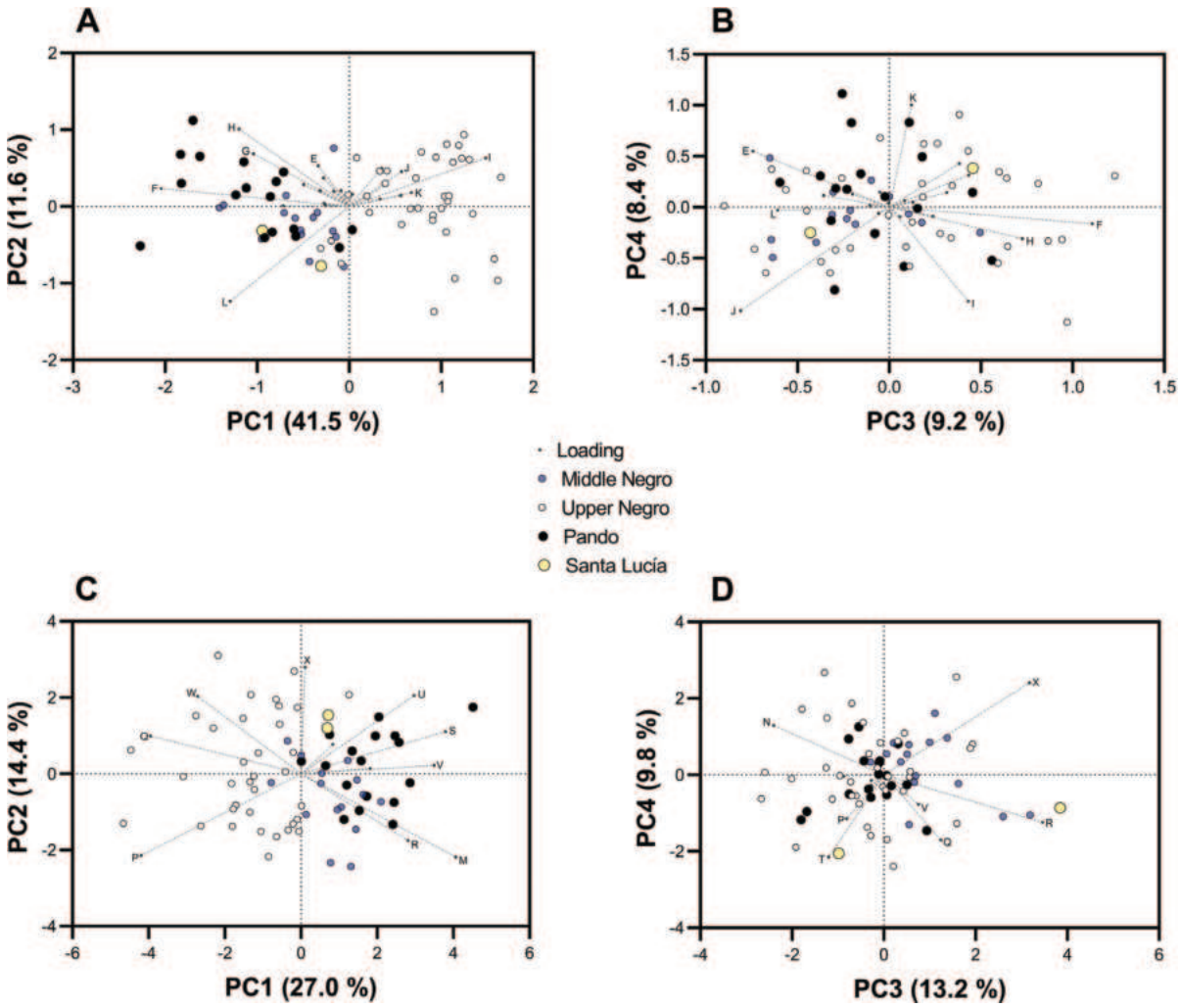

Figure 4. Most discriminant axes obtained from the PCA analyses performed using morphometric and meristic data of studied specimens of *Diapoma pampeana* (in each plot, the loadings are scaled to 90% of the PC scores). Size-corrected measurements: **A.** PC1 *vs.* PC2 plot; **B.** PC3 *vs*. PC4 plot. Meristic data; **C.** PC1 *vs.* PC2 plot; **D.** PC3 vs. PC4 plot. Only these variables that most loaded the components are indicated as follows: E- depth at dorsal-fin origin; F- snout to dorsal-fin origin; G- snout to pelvic-fin origin; H- Snout to anal-fin origin; I- distance between dorsal- and adipose-fin origins; J- dorsal fin to caudal-fin base; K- anal-fin base length; L- caudal peduncle length; M- longitudinal scales; N- lateral-line scales; P- scales between lateral line-dorsal origin; Q- scales between lateral line-pelvic origin; R- circumpeduncular scales; S- predorsal scales; T- number of branched anal-fin rays; U- gill rakers on upper limb of branchial arch; V- gill rakers on lower limb of branchial arch; W- number of maxillary teeth; X- number of dentary teeth.

as the snout to anal-fin origin (0.3), depth at dorsal-fin origin (0.2), snout to pelvic-fin origin (0.2), and distance between the dorsal- and adipose-fin origins (0.2). PC3 was most affected by the dorsal fin to caudal-fin base (-0.3), whereas PC4 was most strongly loaded by the anal-fin base (0.3).

The cluster analysis showed that the four groups analyzed were distributed into two large clusters (most bootstrap values were below 50). All the specimens of the Upper Negro group (except three) were almost completely separated from the Pando, Santa Lucía, and Middle Negro groups. In contrast, the specimens of the Pando group were not clustered separately, but were instead mixed mainly with the specimens of the Santa Lucía and Middle Negro groups (Suppl. material 4).

The comparative results obtained in the meristic data are presented in Table 4. The first four components (explained 64.4% of the total variance, Suppl. material 3) were chosen as significant to analyze the variation in the meristic data, following the same criteria used for the morphometric data (Fig. 4C, D; Suppl. material 2). The Pando group was slightly differentiated from the Upper Negro group along the horizontal axis in the PC1 vs. PC2 plot (accounted for 41.3% of the total variance, Fig. 4C), but overlapped almost completely with the other groups. In the PC3 vs. PC4 plot (explained 23.0% of the total variance, Fig. 4D), the Pando group was not separately distributed from the other groups along the axes. PC1 was most strongly influenced by the number of longitudinal scales (0.7) and predorsal scales (0.7) (Fig. 4C, Table 3). PC2 was strongly loaded by the number of dentary (0.7) and maxillary (0.5) teeth, and number of gill rakers on the upper limb of the first branchial arch (0.5) (Table 3). PC3 was mainly influenced by the number of pored lateral-line scales (-0.7), whereas PC4 was greatly affected by the number of branched anal-fin rays (-0.7). Tukey

Table 3. Loadings obtained from the PCA analyses using morphometric and meristic data. Percentages of variance are reported.

Variables	Components			
	1	2	3	4
Morphometric data:	41.5%	11.6%	9.2%	8.4%
Depth at dorsal-fin origin	-0.1	0.2	-0.2	0.2
Snout to dorsal-fin origin	-0.5	0.1	0.1	0.0
Snout to pectoral-fin origin	-0.1	0.1	0.0	0.0
Snout to pelvic-fin origin	-0.2	0.2	0.0	0.0
Snout to anal-fin origin	-0.3	0.3	0.1	-0.1
Distance between dorsal- and adipose-fin origins	0.5	0.2	0.1	-0.2
Dorsal fin to caudal-fin base	0.2	0.1	-0.3	-0.2
Dorsal-fin length	0.2	0.0	0.1	0.1
Dorsal-fin base length	0.1	0.0	-0.1	0.0
Pectoral-fin length	0.1	0.1	0.0	0.0
Pelvic-fin length	0.1	0.1	0.1	0.1
Anal-fin base length	0.2	0.1	0.0	0.3
Caudal peduncle depth	-0.2	0.0	-0.1	0.0
Caudal peduncle length	-0.3	0.0	-0.2	0.0
Head length	-0.1	0.1	0.0	0.0
Snout length	-0.1	0.0	0.0	0.0
Horizontal eye length	0.0	0.0	0.0	0.0
Postorbital head length	0.0	0.1	0.0	0.0
Least interorbital width	-0.1	0.0	0.0	0.0
Upper jaw length	0.0	0.1	0.0	0.0
Lower jaw length	-0.1	0.1	0.0	0.0
Meristic data:	27.0%	14.4%	13.2%	9.8%
Longitudinal scales	0.7	-0.4	0.1	-0.1
Lateral-line scales	0.3	0.0	-0.7	0.0
Scales between lateral line-dorsal origin	-0.6	-0.4	-0.2	-0.4
Scales between lateral line-pelvic origin	-0.6	0.2	0.2	-0.5
Circumpeduncular scales	0.5	-0.3	0.6	-0.4
Predorsal scales	0.7	0.3	-0.1	0.0
Branched anal-fin rays	0.2	0.2	-0.4	-0.7
Gill rakers upper limb of branchial arch	0.5	0.5	-0.3	0.0
Gill rakers lower limb of branchial arch	0.6	0.1	0.1	-0.2
Maxillary teeth	-0.4	0.5	-0.1	-0.1
Dentary teeth	0.0	0.7	0.5	0.1

box plots of counts that most affected PCA and were most distinctive for the Pando group are presented in Suppl. material 5. The multivariate analyses performed on the morphometric and meristic data converged in coincident results that, despite having overlap between some individuals, showed the population from the Pando stream to be somewhat distinctive morphologically from the specimens from the upper Rio Negro basin. The number of vertebrae of the Pando group was observed within the range of variation of the Upper Negro group (34 vs. 34–35).

The pigmentation pattern observed in the Pando group (Figs 1, 2A, B) was similar to that found in the Upper Negro groups (Ito et al. 2022: figs 1–3), mainly characterized by the vertically enlarged humeral spot, the narrow and conspicuous black line along the horizontal septum of body (in some specimens of the Pando group, it was observed to be somewhat silvery), the longitudinal black stripe extending posteriorly on the middle caudal-fin rays, and the presence of a small black blotch, restricted to the base of the middle caudal-fin rays. The specimens of the Middle Negro group (Fig. 2D, E) were observed to be similarly pigmented as the other groups, except for the caudal-fin blotch, which was not completely extended along the middle rays in some specimens. The examined specimens of the Santa Lucía group were found slightly faded (Fig. 2C), but some pigmentation characters of *D. pampeana* as those aforementioned were found to be present.

Molecular comparisons

The genetic variation seen, based on the Tajima-Nei distance between the Pando specimens and the specimens from the upper Negro basin of *D. pampeana* were found to be very low or nearly zero (≤ 0.002), even when bootstrapped (10000). In the NJ topology (Fig. 5), the two specimens of the Pando stream analyzed were placed together with the remaining specimens of *D. pampeana* from the upper Negro basin and, particularly, as closely related to one specimen of that basin than between each other (Fig. 5). The Bayesian topology showed that *D. pampeana* was more related to *D. guarani* and *D. obi* within a common clade with *D. potamohadros* and *D. tipiaia* (Fig. 6). In both the Bayesian and NJ trees, the analyzed specimens of *Diapoma* from the Pando stream were strongly placed together in the same clade with the specimens of *D. pampeana*. The general pattern of interrelationships among the *Diapoma* species was found to be almost similar between both methods. The uncorrected pairwise mean distance obtained for *D. pampeana* ranged from 3.5 to 7.6% (Suppl. material 6: the lowest value with *D. obi* and the highest value with *D. itaimbe*). The intraspecific variation of *D. pampeana* was observed to be varying from 0 to 0.2%. Only one specimen of the Upper Negro group (UFRGS

Table 4. Comparative meristic data obtained for the studied specimens of *D. pampeana*. SD = standard deviation; n = number of examined specimens. Mean and mode values are reported. Group names corresponds with those described in the text.

	Pando			Santa Lucía			Middle Negro			Upper Negro		
	Range	Mean/ Mode±SD	n	Range	Mean/ Mode±SD	n	Range	Mean/ Mode±SD	n	Range	Mean/ Mode±SD	n
Longitudinal scales	35–38	36.9/37±0.9	17	35–37	36.0/N/A±1.4	2	35–39	37.0/36±1.1	15	32–37	35.1/36±1.2	35
Lateral-line scales	7–9	7.8/7±0.8	17	5–8	6.5/N/A±2.1	2	5–8	6.7/7±1.0	15	5–9	7.3/8±1.0	35
Scales between lateral line-dorsal origin	5–5	5.0/5±0.0	17	5–5	5.0/N/A±0.0	2	5–5	5.0/5±0.0	15	5–6	5.6/6±0.5	35
Scales between lateral line-pelvic origin	4–5	4.1/4±0.2	17	5–5	5.0/N/A±0.0	2	4–5	4.1/4±0.4	15	4–5	4.5/4±0.5	34
Circumpeduncular scales	14–15	14.1/14±0.3	15	15	N/A	1	14–15	14.3/14±0.5	15	11–15	13.0/13±0.9	35
Predorsal scales	12–15	13.6/13±0.8	17	14–15	14.5/N/A±0.7	2	11–13	12.3/12±0.6	15	10–14	12.3/12±0.8	35
Branched anal-fin rays	21–26	23.4/23±1.4	17	22–26	24.0/N/A±2.8	2	21–25	22.8/23±1.1	15	21–25	22.8/22±1.1	35
Gill rakers upper limb of branchial arch	7–10	8.3/8±0.8	14	7	N/A	1	7–8	7.5/7±0.5	15	6–9	7.1/7±0.9	34
Gill rakers lower limb of branchial arch	14–18	14.9/14±1.2	14	15	N/A	1	14–15	14.3/14±0.5	15	13–15	13.9/14±0.8	35
Maxillary teeth	1–3	1.6/2±0.6	15	2	N/A	1	1–2	1.3/1±0.5	15	1–4	2.1/3±0.9	34
Dentary teeth	7–11	8.8/9±1.1	15	12	N/A	1	7–11	9.0/9±1.0	15	6–14	9.0/9±1.3	35

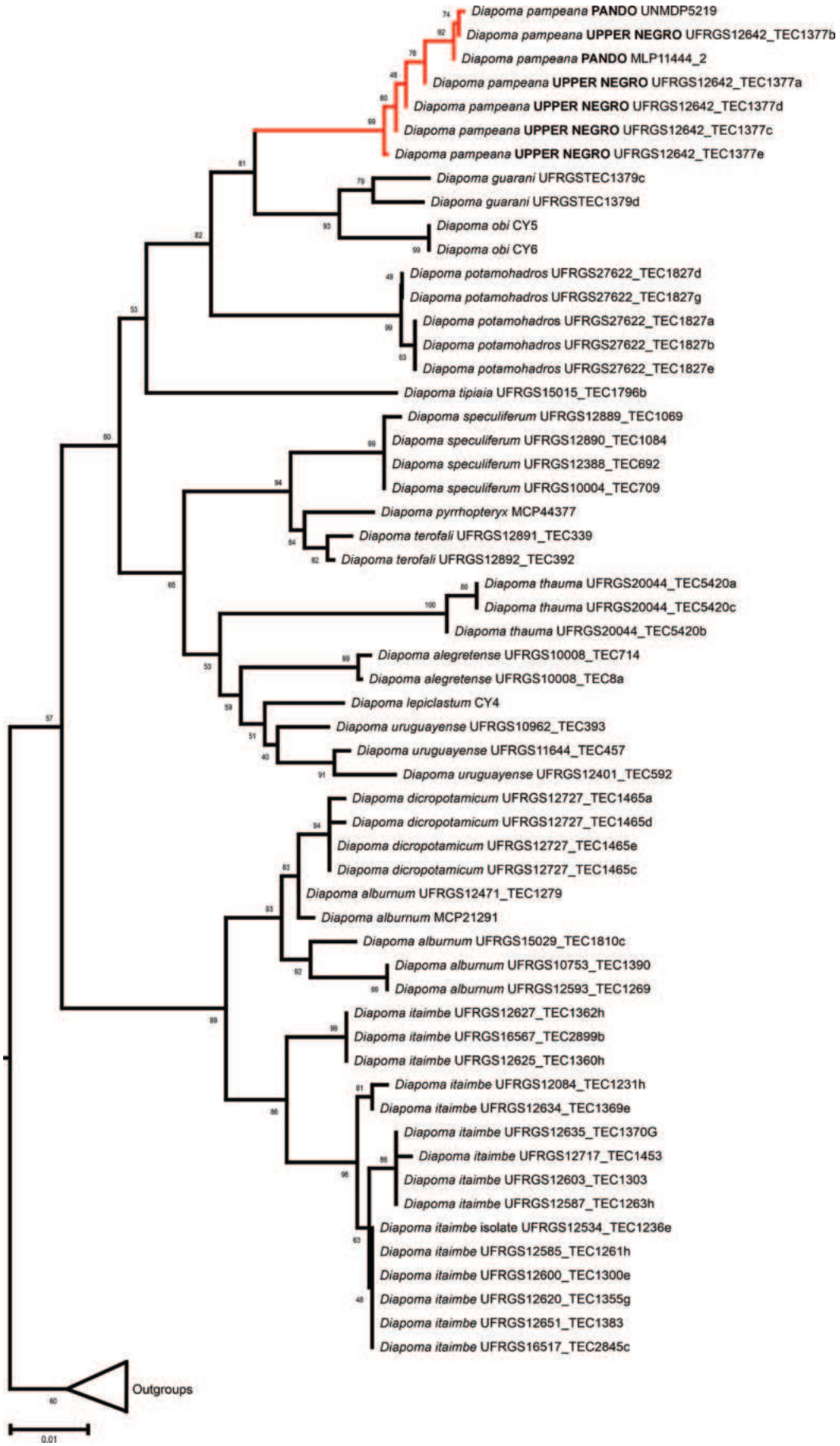

Figure 5. Neighbor-Joining topology of analyzed *Diapoma* specimens based on Tamura-Nei model and COI sequence data. Bootstrap values (10000 replicates) are shown below the branches. SBL = 0.783.

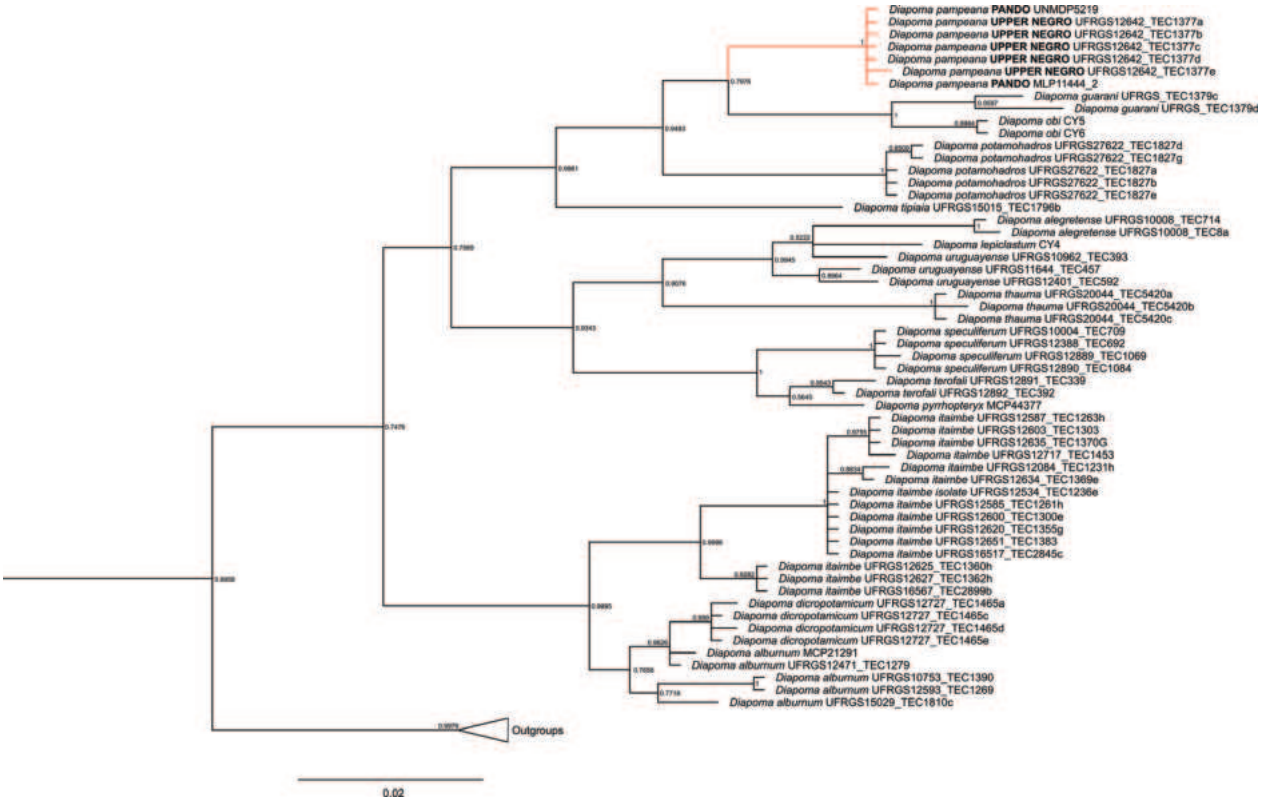

Figure 6. Bayesian topology of phylogenetic relationships among the analyzed *Diapoma* species (comparing specimens of *D. pampeana* from the Pando stream and Upper Negro basin) based on COI sequence data. Numbers at nodes correspond to posterior probabilities.

12642: TEC1377e) showed the greater p-distance (0.2%) in each comparison with the other specimens analyzed of *D. pampeana* (Suppl. material 6).

In the polymorphism analysis comparing the Pando and Upper Negro specimens, 728 sites were analyzed (381: invariable; 347: with gaps or missing data), resulting in one polymorphic site (singleton) and two haplotypes (Hd = 0.286; variance = 0.034; standard deviation = 0.196). In general, the nucleotide diversity was extremely low (π = 0.00095; θ = 0.00107; k = 0.286) for the samples analyzed. No variation was found within the Pando samples (π = 0.00000; k = 0.000). For the Upper Negro samples, only one polymorphic site (monomorphic in the Pando samples) was found and, thus, their diversity was slightly greater (π = 0.00105; k = 0.400). There were no observed shared mutations between these two populations. Regarding the divergence between the populations compared, the values obtained were low (Dxy = 0.00052; Da = 0.00000). The haplotype network showed a simple structure of two groups without well-defined geographic structure and in which one of them was mixed (Suppl. material 7).

Comparative examined material

Diapoma alburnum: UFRGS 13309, 11, 33.4–56.0 mm SL. *Diapoma guarani*: MHNG 2366.99, holotype, 31.7 mm SL. *Diapoma lepiclastum*: MACN-ict 9682, 47, 29.3–42.0 mm SL. *Diapoma obi*: MLP 11312, 3, 29.5–35.6 mm SL. MACN-ict 9560, holotype, 52.6 mm SL. *Diapoma uruguayense*, MACN-ict 9681, 7, 31.6–34.6 mm SL.

Discussion

The stevardiine species *D. pampeana* was recently described from several localities along the Rio Negro basin in Brazil and Uruguay (Ito et al. 2022). The freshwater fish fauna from the Pando stream is mainly known from studies focused on estuarine-influenced coastal waters (Plavan et al. 2010; Gurdek and Acuña-Plavan 2017). Although the body coloration was similar between the specimens of the Pando and Upper Negro groups, the former showed a striking morphometric and meristic divergence from the latter. Additionally, the intraspecific variation between the Pando and Upper Negro populations became much more subtle when compared with specimens from geographically intermediate areas such as the Santa Lucía and Middle Negro basins (*i.e.* the specimens of these groups were slightly more similar to each other in the morphometric and meristic data than to the specimens of the Upper Negro). Frequently, in morphological comparisons using multivariate methods, the populations exhibiting major differences in body shape correspond with those morphotypes that are located at the farthest distance geographically from the others (Lazzarotto et al. 2017; Vanegas-Rios et al. 2019; Rodrigues-Oliveira et al. 2023). In consequence, the analyzed specimens of *D. pampeana* may be responding to a gradual pattern of divergence associated with spatial segregation, often observed in widespread species (Lazzarotto et al. 2017; Arroyave et al. 2019; Vanegas-Rios et al. 2019; Rodrigues-Oliveira et al. 2023).

In the morphological comparisons performed herein, the Pando group was greatly differentiated in the size-corrected PCA from the Upper Negro group along PC1, which was mainly influenced by the following distances: snout to dorsal-fin origin, snout to anal-fin origin, dorsal- and adipose-fin origins, and caudal peduncle length (Fig. 4A). Some measurements such as the snout to dorsal-fin origin, snout to anal-fin origin, snout to pelvic-fin origin, distance between the dorsal- and pectoral-fin origins, head length, snout length, and eye diameter have been found to be taxonomically informative to discriminate among *Diapoma* species (Malabarba and Weitzman 2003; Vanegas-Ríos et al. 2018; Ito et al. 2022). Based on the meristic data, these groups were also found to be slightly divergent from each other along PC1. For this component, some main counts defining the variability were the number of longitudinal scales and predorsal scales (Table 3, Fig. 4C). Usually, the range is used as the main indicator to define the limits of the morphological variation among species in measurements or counts (Garavello et al. 1992; Aguirre et al. 2016; Lazzarotto et al. 2017; Arroyave et al. 2019; Vanegas-Rios et al. 2019; Malabarba et al. 2021). The main dilemma for defining these limits appears when data have varied degrees of overlapping between populations of study.

Further statistical procedures are used as a complement to test if diverging tendencies in morphometric data are, or are not, significant (Lazzarotto et al. 2017; Arroyave et al. 2019; Vanegas-Rios et al. 2019; Rodrigues-Oliveira et al. 2023). For instance, it is frequently found that subtle or moderate intraspecific differences in body shape result in being statistically significant, but it may be also associated with the degree of sensitivity involved in pairwise tests (e.g. means). Recently, the statistical potential behind morphometrically divergent patterns has been used to propose subspecies within gymnotids (Craig et al. 2017). Such criterion is not commonly used in modern ichthyology, so that the erection of infraspecific categories can be considered unnecessary to understand the intraspecific variation (e.g. clines) (Kottelat 1998; Kullander 1999). In the case of the Pando group, it seems unjustified to propose a new infraspecific category under the light of the current evidence described from morphological data, even more when it is geographically isolated and its phenotypic variation is described and contextualized in the present contribution. In a similar case, geographically isolated coastal river populations of *D. itaimbe* that showed a statistically significant difference in overlapping ranges of anal-fin ray counts were treated as structured isolated populations instead of separate species (Malabarba and Weitzman 2003; Hirschmann et al. 2015).

When the discriminative tendencies are striking, as occurred here between the Pando and Upper Negro groups, including additional independent evidence, such as DNA data, can help to support the conclusion. The COI marker has played an important role in resolving taxonomic questions in freshwater fishes (Pereira et al. 2013). In general, comparative studies using COI and morphology are dealing with cryptic species, species complexes or populations with slight morphological variations (under a context of geographic isolation) (Serrano et al. 2019; Garavello et al. 2021; Guimarães et al. 2021; Malabarba et al. 2021; Aguilera et al. 2022). The phylogenetic signal of the COI marker within *Diapoma* has been studied and used to propose intraspecific and interspecific limits, as well as new species (Casciotta et al. 2012; Hirschmann et al. 2015; Ito et al. 2022). However, the use of this marker by itself for recognizing species (e.g. as single locus without morphological or cytogenetic support) has its own methodological limits, and it is especially important to have this into account when dealing with complex groups of species or populations (Castro Paz et al. 2014; García-Melo et al. 2019; Klimov et al. 2019; Silva-Santos et al. 2023). This may imply that in some cases there is no guarantee of complete interspecific delimitation (e.g. Castro Paz et al. 2014).

The phylogenetic comparison performed using the COI marker of all known species of *Diapoma* (except *D. nandi* from the Paraná basin) recovered the Pando group as part of *D. pampeana*. It also demonstrates that the recognition of the Pando group as separate would make *D. pampeana* paraphyletic (Fig. 5: NJ topology). The variability of the p-distances calculated for the Pando group were observed to be lower than the average congeneric values (0–0.2% vs. 1.3–8.0%), as it has been often reported in other characids (Pereira et al. 2011b; García-Melo et al. 2019; Silva-Santos et al. 2023). Furthermore, the mean genetic distances were 3.5% and 4.3% between *D. pampeana* and its closest related species (*D. obi* and *D. guarani*, respectively). The intraspecific values obtained for *D. pampeana* are within the conspecific variation reported in species of other characid groups such as *Astyanax* (from the Rio Paraguaçu basin, mean = 0–1.7%); *Hyphessobrycon* Durbin, 1908 (from the Amazon basin, mean = 0–8.9%), and some stevardiines (*Bryconamericus*, *Eretmobrycon* Fink, 1976, *Hemibrycon* Günther, 1864, *Knodus* Eigenmann, 1911, and *Piabina*: 0–1.9%) (Pereira et al. 2011b; Castro Paz et al. 2014; García-Melo et al. 2019; Silva-Santos et al. 2023). In barcoding studies, 2% threshold limit (at least 10 times the average conspecific values) has been used as the cutoff divergence value for delimiting species or molecular operational taxonomic units (Hebert et al. 2004; Ward 2009). However, an alternative threshold value of 1% has been considered for studying species complexes (Hubert et al. 2008; Pereira et al. 2011a; Silva-Santos et al. 2023). Therefore, these threshold values should be cautiously evaluated for each case in particular.

The results obtained from the exploratory analysis using haplotype, allowed us to detect the potential presence of two haplotypes that were separated by a single mutational change. Additionally, the Pando group presented the same haplotype as the Upper Negro group, which again reinforces the great resemblance between both groups. Additionally, no well-defined lineages were detected in the molecular comparisons. However, this needs to be further investigated so that within *Diapoma*, for instance, it has been found that *D. itaimbe* forms populations with well-defined structural lineages associated with a coastal biographic pattern (Hirschmann et al. 2015). The recognition of species as

separately evolving metapopulation lineages is a unifying concept in defining species (De Queiroz 2007), and so far, we have no support from molecular data to separate the Pando group from *D. pampeana*.

Freshwater fishes have limited their ability to disperse across brackish, marine or terrestrial barriers, being biologically restricted to water bodies after their formation, and thus, the disjunct geographic range associated with species and populations across several basins might be explained by river captures or dispersal favored by temporary connections (Albert and Reis 2011; Thomaz et al. 2017; Camelier et al. 2018; Cassemiro et al. 2023). These potential explanations would be plausible for testing in *D. pampeana* if its distribution was really widespread along most coastal drainages in Uruguay, as our findings suggest.

Conclusion

We concluded that the specimens from the Pando stream, despite the morphological divergence observed, can be classified as *D. pampeana*. We supported our decision based on the following arguments: 1) the deviations found on the morphometric and meristic data (e.g. PCA) are not enough to erect a new species and, as consequence, the intraspecific variability is increased; 2) the specimens of the Pando group were similarly pigmented as the specimens of the Upper Negro group (sharing the same diagnostic pattern on the humeral mark, midlateral stripe, and caudal-fin pigmentation); 3) the COI-based phylogenetic procedures supported the placement of the Pando group within the genetic variation of the Upper Negro group (typical distribution of *D. pampeana*); and 4) based on the genetic distances, the Pando group was found to be genetically similar to the Upper Negro group, with p-distances (0–0.2%) being lower than the mean distances obtained between each congener (1.3–8.0%). Additionally, the present work also confirmed the presence of *D. pampeana* in the Yi (Middle Negro basin) and Santa Lucía river basins, based on morphological evidence. Although it was not possible to separate species, our results provide new information that can be further appreciated. For instance, it has been proposed that diverging populations can represent separate evolutionarily significant units, which should be conserved (Moritz 1994; de J. May-Itzá et al. 2012; Stockwell et al. 2013; Berger et al. 2018). The geographic range of *D. pampeana* seems to be incompletely understood and might be more widely represented along the Rio Negro basin and other coastal drainages in Uruguay (Fig. 3, Suppl. material 8). Future studies may bring new insights into the population variation of the species and other phylogeographic patterns if more specimens and new localities are analyzed. The Pando population of *D. pampeana* constitutes a remarkable example of an isolated population that is morphologically divergent (in the morphometric and meristic data) from the geographically most distant conspecific population (upper Rio Negro basin), but that shares a high degree of genetic resemblance with it.

Acknowledgments

We thank the following institutions and museums for their assistance and support: G. Chiaramonte (MACN-ict); Sonia Fisch-Muller and Rafael Covain (MHNG); D. Nadalin, Jorge R. Casciotta and Adriana E. Almirón (MLP); C. Lucena (MCP), Priscila M. Ito and Juliana M. Wingert (UFRGS). The authors are grateful for the financial support provided by FONCyT (BID-PICT 2019–02419 and PIBBA 0654CO to JAVR). We are indebted to Juan José Rosso, Matías Delpiane, and Juan Martín Díaz de Astarloa (IIMyC-UNMDP), and C. Bruno and G. Giovambattista (IGEVET-UNLP) for their assistance with the DNA procedures. Nicolas Tizio (Fundación Unidos por Naturaleza), J. Pfleiderer, and F. M. Frias helped with photographs. This paper benefited from valuable suggestions and comments of anonymous reviewers, W. Costa, and F. Araújo.

References

Achkar M, Domínguez A, Pesce F (2012) Cuenca del Río Santa Lucía-Uruguay. Aportes para la discusión ciudadana. Montevideo.

Acuña A, Muñoz N, Gurdek R, Machado I, Severi V (2017) Inter-estuarine and temporal patterns of the fish assemblage of subtropical subestuaries along the Río de la Plata coast (Uruguay). Brazilian Journal of Oceanography 65(2): 173–186. https://doi.org/10.1590/s1679-87592017131106502

Aguilera G, Terán GE, Mirande JM, Alonso F, Chumacero GM, Cardoso Y, Bogan S, Faustino-Fuster DR (2022) An integrative approach method reveals the presence of a previously unreported species of *Imparfinis* Eigenmann and Norris 1900 (Siluriformes: Heptapteridae) in Argentina. Journal of Fish Biology 101(5): 1248–1261. https://doi.org/10.1111/jfb.15197

Aguirre WE, Navarrete R, Malato G, Calle P, Loh MK, Vital WF, Valadez G, Vu V, Shervette VR, Granda JC (2016) Body shape variation and population genetic structure of *Rhoadsia altipinna* (Characidae: Rhoadsiinae) in southwestern Ecuador. Copeia 104(2): 554–569. https://doi.org/10.1643/CG-15-289

Albert JS, Reis RE (2011) Historical Biogeography of Neotropical Freshwater Fishes. University of California Press, California, 388 pp. https://doi.org/10.1525/9780520948501

Almirón A, Casciotta J, Říčanová S, Dragová K, Piálek L, Říčan R (2016) First record of *Diapoma pyrrhopteryx* Menezes & Weitzman, 2011 (Characiformes: Characidae) from freshwaters of Argentina. Ichthyological Contributions of Peces Criollos 40: 1–3.

Arroyave J, Martinez CM, Stiassny MLJ (2019) DNA barcoding uncovers extensive cryptic diversity in the African long-fin tetra *Bryconalestes longipinnis* (Alestidae: Characiformes). Journal of Fish Biology 95: 379–392. https://doi.org/10.1111/jfb.13987

Azpelicueta MM, Lundberg JG, Loureiro M (2008) *Pimelodus pintado* (Siluriformes: Pimelodidae), a new species of catfish from affluent rivers of Laguna Merín, Uruguay, South America. Proceedings of the Academy of Natural Sciences of Philadelphia 157(1): 149–162. https://doi.org/10.1635/0097-3157(2008)157[149:PPSPAN]2.0.CO;2

Berger C, Štambuk A, Maguire I, Weiss S, Füreder L (2018) Integrating genetics and morphometrics in species conservation–A case study on the stone crayfish, *Austropotamobius torrentium*. Limnologica 69: 28–38. https://doi.org/10.1016/j.limno.2017.11.002

Camelier P, Menezes NA, Costa-Silva GJ, Oliveira C (2018) Molecular and morphological data of the freshwater fish *Glandulocauda melanopleura* (Characiformes: Characidae) provide evidences of river captures and local differentiation in the Brazilian Atlantic Forest. PLOS ONE 13(3): e0194247. https://doi.org/10.1371/journal.pone.0194247

Cardoso AR (2010) *Bunocephalus erondinae*, a new species of banjo catfish from southern Brazil (Siluriformes: Aspredinidae). Neotropical Ichthyology 8(3): 607–613. https://doi.org/10.1590/S1679-62252010000300005

Casciotta J, Almirón A, Piálek L, Říčan O (2012) *Cyanocharax obi*, a new species (Characiformes: Characidae) and the first record of the genus from tributaries of the río Paraná basin, Argentina. Zootaxa 3391(1): 39–51. https://doi.org/10.11646/zootaxa.3391.1.3

Cassemiro FAS, Albert JS, Antonelli A, Menegotto A, Wüest RO, Cerezer F, Coelho MTP, Reis RE, Tan M, Tagliacollo V, Bailly D, da Silva VFB, Frota A, da Graça WJ, Ré R, Ramos T, Oliveira AG, Dias MS, Colwell RK, Rangel TF, Graham CH (2023) Landscape dynamics and diversification of the megadiverse South American freshwater fish fauna. Proceedings of the National Academy of Sciences of the United States of America 120(2): e2211974120. https://doi.org/10.1073/pnas.2211974120

Castro Paz FP, Batista Jd S, Porto JIR (2014) DNA Barcodes of Rosy Tetras and Allied Species (Characiformes: Characidae: *Hyphessobrycon*) from the Brazilian Amazon Basin. PLOS ONE 9(5): e98603. https://doi.org/10.1371/journal.pone.0098603

Cattel R (1966) The scree test for the number of factors. Multivariate Behavioral Research 1: 245–276. https://doi.org/10.1207/s15327906mbr0102_10

Craig JM, Crampton WGR, Albert JS (2017) Revision of the polytypic electric fish *Gymnotus carapo* (Gymnotiformes, Teleostei), with descriptions of seven subspecies. Zootaxa 4318(3): 401–438. https://doi.org/10.11646/zootaxa.4318.3.1

Darriba D, Posada D, Kozlov AM, Stamatakis A, Morel B, Flouri T (2019) ModelTest-NG: A new and scalable tool for the selection of DNA and protein evolutionary models. Molecular Biology and Evolution 37(1): 291–294. https://doi.org/10.1093/molbev/msz189

May-Itzá W de J, Quezada-Euán JJG, Ayala R, De La Rúa P ((2012) Morphometric and genetic analyses differentiate Mesoamerican populations of the endangered stingless bee *Melipona beecheii* (Hymenoptera: Meliponidae) and support their conservation as two separate units. Journal of Insect Conservation 16: 723–731. https://doi.org/10.1007/s10841-012-9457-4

De Queiroz K (2007) Species concepts and species delimitation. Systematic Biology 56(6): 879–886. https://doi.org/10.1080/10635150701701083

Defeo O, Horta S, Carranza A, Lercari D, de Álava A, Gómez J, Martínez G, Lozoya JP, Celentano E (2009) Hacia un Manejo Ecosistémico de Pesquerías. Áreas Marinas Protegidas en Uruguay. Facultad de Ciencias-UNDECIMAR, Montevideo, 122 pp.

Dempster AP, Laird NM, Rubin DB (1977) Maximum likelihood from incomplete data via the EM algorithm. Journal of the Royal Statistical Society, Series B, Methodological 39(1): 1–38. https://doi.org/10.1111/j.2517-6161.1977.tb01600.x

Echevarría L, Gómez A, Lale M, López R, Nieto P, Pereyra G (2011) Plan de manejo costero integrado del tramo de costa A° Solís Chico –A° Solís Grande. In: Conde D (Ed) Manejo Costero Integrado en Uruguay: ocho ensayos interdisciplinarios Centro Interdisciplinario para el Manejo Costero Integrado del Cono Sur, Montevideo, 123–152.

Edgar RC (2004) MUSCLE: Multiple sequence alignment with high accuracy and high throughput. Nucleic Acids Research 32(5): 1792–1797. https://doi.org/10.1093/nar/gkh340

Elliott NG, Haskard K, Koslow JA (1995) Morphometric analysis of orange roughy (*Hoplostethus atlanticus*) off the continental slope of southern Australia. Journal of Fish Biology 46: 202–220. https://doi.org/10.1111/j.1095-8649.1995.tb05962.x

Ferreira KM, Menezes NA, Quagio-Grassioto I (2011) A new genus and two new species of Stevardiinae (Characiformes: Characidae) with a hypothesis on their relationships based on morphological and histological data. Neotropical Ichthyology 9(2): 281–298. https://doi.org/10.1590/S1679-62252011000200005

Ferreira KM, Mirande JM, Quagio-Grassiotto I, Santana JCO, Baicere-Silva CM, Menezes NA (2021) Testing the phylogenetic hypotheses of Stevardiinae Gill, 1858 in light of new phenotypic data (Teleostei: Characidae). Journal of Zoological Systematics and Evolutionary Research 59(8): 2060–2085. https://doi.org/10.1111/jzs.12517

Fink WL, Weitzman SH (1974) The so-called Cheirodontin fishes of Central America with descriptions of two new species (Pisces: Characidae) Smithsonian Contributions to Zoology 172: 1–45. https://doi.org/10.5479/si.00810282.172.

Fricke R, Eschmeyer WN, Van der Laan R (2023) Eschmeyer's Catalog of Fishes: genera, species, references. http://researcharchive.calacademy.org/research/ichthyology/catalog/fishcatmain.asp [accessed 1 December.2023]

Frontier S (1976) Etude de la dècroissance des valeurs propres dans une analyse en composantes principales: comparaison avec le modèle du bâton brisé. Journal of Experimental Marine Biology and Ecology 25: 67–75. https://doi.org/10.1016/0022-0981(76)90076-9

Garavello JC, Dos Reis SF, Strauss RE (1992) Geographic variation in *Leporinus friderici* (Bloch) (Pisces: Ostariophysi: Anostomidae) from the Paraná-Paraguay and Amazon River basins. Zoologica Scripta 21(2): 197–200. https://doi.org/10.1111/j.1463-6409.1992.tb00320.x

Garavello JC, Ramirez JL, de Oliveira AK, Britski HA, Birindelli JLO, Galetti Jr PM (2021) Integrative taxonomy reveals a new species of Neotropical headstanding fish in genus *Schizodon* (Characiformes: Anostomidae). Neotropical Ichthyology 19(4): e210016. https://doi.org/10.1590/1982-0224-2021-0016

García-Melo JE, Oliveira C, Da Costa Silva GJ, Ochoa-Orrego LE, Garcia Pereira LH, Maldonado-Ocampo JA (2019) Species delimitation of neotropical Characins (Stevardiinae): Implications for taxonomy of complex groups. PLOS ONE 14(6): e0216786. https://doi.org/10.1371/journal.pone.0216786

Guimarães KL, Rosso JJ, Souza MF, Díaz de Astarloa JM, Rodrigues LR (2021) Integrative taxonomy reveals disjunct distribution and first record of *Hoplias misionera* (Characiformes: Erythrinidae) in the Amazon River basin: morphological, DNA barcoding and cytogenetic considerations. Neotropical Ichthyology 19(2): e200110. https://doi.org/10.1590/1982-0224-2020-0110

Gurdek R, Acuña-Plavan A (2017) Temporal dynamics of a fish community in the lower portion of a tidal creek, Pando sub-estuarine system, Uruguay. Iheringia. Série Zoologia 107(0): e2017003. https://doi.org/10.1590/1678-4766e2017003

Gutiérrez JM, Villar S, Acuña Plavan A (2015) Micronucleus test in fishes as indicators of environmental quality in subestuaries of the Río de la Plata (Uruguay). Marine Pollution Bulletin 91(2): 518–523. https://doi.org/10.1016/j.marpolbul.2014.10.027

Hall TA (1999) BioEdit: A User-Friendly Biological Sequence Alignment Editor and Analysis Program for Windows 95/98/NT. Nucleic Acids Symposium Series. Oxford University Press, 95–98.

Hammer Ø, Harper DAT, Ryan PD (2001) PAST: Paleontological statistics software package for education and data analysis. Palaeontologia Electronica 4: 1–9.

Hebert PDN, Stoeckle MY, Zemlak TS, Francis CM (2004) Identification of Birds through DNA Barcodes. PLOS Biology 2(10): e312. https://doi.org/10.1371/journal.pbio.0020312

Hirschmann A, Malabarba LR, Thomaz AT, Fagundes NJR (2015) Riverine habitat specificity constrains dispersion in a Neotropical fish (Characidae) along Southern Brazilian drainages. Zoologica Scripta 44(4): 374–382. https://doi.org/10.1111/zsc.12106

Hubert N, Hanner R, Holm E, Mandrak NE, Taylor E, Burridge M, Watkinson D, Dumont P, Curry A, Bentzen P, Zhang J, April J, Bernatchez L (2008) Identifying Canadian Freshwater Fishes through DNA Barcodes. PLOS ONE 3(6): e2490. https://doi.org/10.1371/journal.pone.0002490

IBM (2019) IBM SPSS Statistics for Windows, Version 26.0. IBM Corp, Armonk, NY.

Ito PMM, Carvalho TP, Pavanelli CS, Vanegas-Ríos JA, Malabarba LR (2022) Phylogenetic relationships and description of two new species of *Diapoma* (Characidae: Stevardiinae) from the La Plata River basin. Neotropical Ichthyology 20(1): e210115. https://doi.org/10.1590/1982-0224-2021-0115

Ivanova NV, Dewaard JR, Hebert PDN (2006) An inexpensive, automation-friendly protocol for recovering high-quality DNA. Molecular Ecology Notes 6: 998–1002. https://doi.org/10.1111/j.1471-8286.2006.01428.x

Ivanova NV, Zemlak TS, Hanner RH, Hebert PDN (2007) Universal primer cocktails for fish DNA barcoding. Molecular Ecology Notes 7: 544–548. https://doi.org/10.1111/j.1471-8286.2007.01748.x

Klimov PB, Skoracki M, Bochkov AV (2019) Cox1 barcoding versus multilocus species delimitation: validation of two mite species with contrasting effective population sizes. Parasites & Vectors 12: 1–8. https://doi.org/10.1186/s13071-018-3242-5

Kottelat M (1998) Systematics, species concepts and the conservation of freshwater fish diversity in Europe. The Italian Journal of Zoology 65(sup1): 65–72. https://doi.org/10.1080/11250009809386798

Kullander SO (1999) Fish species – how and why. Reviews in Fish Biology and Fisheries 9(4): 325–352. https://doi.org/10.1023/A:1008959313491

Lazzarotto H, Barros T, Louvise J, Caramaschi EP (2017) Morphological variation among populations of *Hemigrammus coeruleus* (Characiformes: Characidae) in a Negro River tributary, Brazilian Amazon. Neotropical Ichthyology 15: e160152. https://doi.org/10.1590/1982-0224-20160152

Leigh JW, Bryant D (2015) popart: full-feature software for haplotype network construction. Methods in Ecology and Evolution 6: 1110–1116. https://doi.org/doi.org/10.1111/2041-210X.12410

Lucena CA, Malabarba LR, Reis RE (1992) Resurrection of the neotropical pimelodid catfish *Parapimelodus nigribarbis* (Boulenger), with a phylogenetic diagnosis of the genus *Parapimelodus* (Teleoastei: Siluriformes). Copeia 1992(1): 138–146. https://doi.org/10.2307/1446545

Mahnert V, Géry J (1987) Deux nouvelles espèces du genre *Hyphessobrycon* (Pisces, Ostariophysi, Characidae) du Paraguay: *H. guarani* n. sp. et *H. procerus* n. sp. Bonner Zoologische Beitrage 38: 307–314.

Malabarba LR (1983) Redescrição e discussao da posição taxonômica de *Astyanax hasemani* Eigenmann, 1914 (Teleostei, Characidae). Comunicações do Museu de Ciências da PUCRS. Serie Zoologica 14: 177–199.

Malabarba LR, Weitzman SH (2003) Description of new genus with six new species from southern Brazil, Uruguay and Argentina, with a discussion of a putative characid clade (Teleostei: Characiformes: Characidae). Comunicações do Museu de Ciências e Tecnologia da PUCRS. Série Zoologia 16: 67–151.

Malabarba LR, Chuctaya J, Hirschmann A, de Oliveira EB, Thomaz AT (2021) Hidden or unnoticed? Multiple lines of evidence support the recognition of a new species of *Pseudocorynopoma* (Characidae: Corynopomini). Journal of Fish Biology 98(1): 219–236. https://doi.org/10.1111/jfb.14572

Menezes NA, Weitzman SH (2011) A systematic review of *Diapoma* (Teleostei: Characiformes: Characidae: Stevardiinae: Diapomini) with descriptions of two new species from southern Brazil. Papéis Avulsos de Zoologia 51(5): 59–82. https://doi.org/10.1590/S0031-10492011000500001

Miller MA, Pfeiffer W, Schwartz T (2010) Creating the CIPRES Science Gateway for inference of large phylogenetic trees. 2010 Gateway Computing Environments Workshop (GCE), 8 pp. https://doi.org/10.1109/GCE.2010.5676129

Mirande JM (2019) Morphology, molecules and the phylogeny of Characidae (Teleostei, Characiformes). Cladistics 35(3): 282–300. https://doi.org/10.1111/cla.12345

Moritz C (1994) Defining 'Evolutionarily Significant Units' for conservation. Trends in Ecology & Evolution 9: 373–375. https://doi.org/https://doi.org/10.1016/0169-5347(94)90057-4

Muniz P, Venturini N, Brugnoli E, Gutiérrez JM, Acuña A (2019) Chapter 30 – Río de la Plata: Uruguay. In: Sheppard C (Ed.) World Seas: An Environmental Evaluation (2nd edn.). Academic Press, 703–724. https://doi.org/10.1016/B978-0-12-805068-2.00036-X

Nei M (1987) Molecular Evolutionary Genetics. Columbia University Press, New York, 514 pp. https://doi.org/10.7312/nei-92038

Nei M, Li WH (1979) Mathematical model for studying genetic variation in terms of restriction endonucleases. Proceedings of the National Academy of Sciences of the United States of America 76(10): 5269–5273. https://doi.org/10.1073/pnas.76.10.5269

Paullier S, Bessonart J, Brum E, Loureiro M (2019) Lista de especies de peces de la cuenca del Río Queguay, Río Uruguay bajo. Boletin de la Sociedad Zoológica del Uruguay 28: 66–78. https://doi.org/10.26462/28.2.3

Pereira LHG, Maia GMG, Hanner R, Foresti F, Oliveira C (2011a) DNA barcodes discriminate freshwater fishes from the Paraíba do Sul River Basin, São Paulo, Brazil. Mitochondrial DNA 22(sup1): 71–79. https://doi.org/10.3109/19401736.2010.532213

Pereira LHG, Pazian MF, Hanner R, Foresti F, Oliveira C (2011b) DNA barcoding reveals hidden diversity in the Neotropical freshwater fish *Piabina argentea* (Characiformes: Characidae) from the Upper Paraná Basin of Brazil. Mitochondrial DNA 22(sup1): 87–96. https://doi.org/10.3109/19401736.2011.588213

Pereira LHG, Hanner R, Foresti F, Oliveira C (2013) Can DNA barcoding accurately discriminate megadiverse Neotropical freshwater fish fauna? BMC Genetics 14(1): 1–20. https://doi.org/10.1186/1471-2156-14-20

Pigott TD (2001) A review of methods for missing data. Educational Research and Evaluation 7(4): 353–383. https://doi.org/10.1076/edre.7.4.353.8937

Plavan AA, Passadore C, Gimenez LJ (2010) Fish assemblage in a temperate estuary on the uruguayan coast: Seasonal variation and

environmental influence. Brazilian Journal of Oceanography 58(4): 299–314. https://doi.org/10.1590/S1679-87592010000400005

Protogino LC, Miquelarena AM (2012) *Cyanocharax alburnus* (Hensel, 1870) (Characiformes: Characidae): First distribution record in Argentina. Check List 8(3): 581–583. https://doi.org/10.15560/8.3.581

Quinn GP, Keough MJ (2002) Experimental desing and data analysis for biologist. Cambrigde University Press, Cambrigde.

Rambaut A (2018) FigTree: Tree figure drawning tool. 1.4.4 ed, Institute of Evolutionary Biology, University of Edinburgh.

Rambaut A, Drummond AJ, Xie D, Baele G, Suchard MA (2018) Posterior summarization in bayesian phylogenetics using Tracer 1.7. Systematic Biology 67(5): 901–904. https://doi.org/10.1093/sysbio/syy032

Rodrigues-Oliveira IH, Kavalco KF, Pasa R (2023) Body shape variation in the Characid *Psalidodon rivularis* from São Francisco river, Southeast Brazil (Characiformes: Stethaprioninae). Acta Zoologica 104(3): 345–354. https://doi.org/10.1111/azo.12415

Ronquist F, Teslenko M, van der Mark P, Ayres DL, Darling A, Höhna S, Larget B, Liu L, Suchard MA, Huelsenbeck JP (2012) MrBayes 3.2: Efficient Bayesian phylogenetic inference and model choice across a large model space. Systematic Biology 61(3): 539–542. https://doi.org/10.1093/sysbio/sys029

Rosso JJ, Mabragaña E, González Castro M, Díaz de Astarloa JM (2012) DNA barcoding Neotropical fishes: Recent advances from the Pampa Plain, Argentina. Molecular Ecology Resources 12(6): 999–1011. https://doi.org/10.1111/1755-0998.12010

Rozas J, Ferrer-Mata A, Sánchez-DelBarrio JC, Guirao-Rico S, Librado P, Ramos-Onsins SE, Sánchez-Gracia A (2017) DnaSP 6: DNA Sequence Polymorphism Analysis of Large Data Sets. Molecular Biology and Evolution 34(12): 3299–3302. https://doi.org/10.1093/molbev/msx248

Sabaj MH (2020) Codes for natural history collections in ichthyology and herpeteology. Copeia 108(3): 593–669. https://doi.org/10.1643/ASIHCODONS2020

Serrano ÉA, Melo BF, Freitas-Souza D, Oliveira MLM, Utsunomia R, Oliveira C, Foresti F (2019) Species delimitation in Neotropical fishes of the genus *Characidium* (Teleostei, Characiformes). Zoologica Scripta 48(1): 69–80. https://doi.org/10.1111/zsc.12318

Silva-Santos R, de Barros Machado C, Zanata AM, Camelier P, Galetti Jr PM, Domingues de Freitas P (2023) Molecular characterization of *Astyanax* species (Characiformes: Characidae) from the upper Paraguaçu River basin, a hydrographic system with high endemism. Neotropical Ichthyology 21(2): e230032. https://doi.org/10.1590/1982-0224-2023-0032

Stockwell CA, Heilveil JS, Purcell K (2013) Estimating divergence time for two evolutionarily significant units of a protected fish species. Conservation Genetics 14(1): 215–222. https://doi.org/10.1007/s10592-013-0447-1

Tamura K, Stecher G, Kumar S (2021) MEGA11: Molecular Evolutionary Genetics Analysis Version 11. Molecular Biology and Evolution 38(7): e30223027. https://doi.org/10.1093/molbev/msab120

Taylor WR, Dyke GCV (1985) Revised procedures for staining and clearing small fishes and other vertebrates for bone and cartilage study. Cybium 9: 107–119.

Thomaz AT, Arcila D, Ortí G, Malabarba LR (2015) Molecular phylogeny of the subfamily Stevardiinae Gill, 1858 (Characiformes: Characidae): classification and the evolution of reproductive traits. BMC Evolutionary Biology 15(1): e146. https://doi.org/10.1186/s12862-015-0403-4

Thomaz AT, Malabarba LR, Knowles LL (2017) Genomic signatures of paleodrainages in a freshwater fish along the southeastern coast of Brazil: Genetic structure reflects past riverine properties. Heredity 119(4): 287–294. https://doi.org/10.1038/hdy.2017.46

Vanegas-Ríos JA, Azpelicueta MM, Malabarba LR (2018) A new species of *Diapoma* (Characiformes, Characidae, Stevardiinae) from the Rio Paraná basin, with an identification key to the species of the genus. Journal of Fish Biology 93(5): 830–841. https://doi.org/10.1111/jfb.13786

Vanegas-Rios JA, Britzke R, Mirande JM (2019) Geographic variation of *Moenkhausia bonita* (Characiformes: Characidae) in the rio de la Plata basin, with distributional comments on *M. intermedia*. Neotropical Ichthyology 17(1): e170123. https://doi.org/10.1590/1982-0224-20170123

Ward Jr JH (1963) Hierarchical grouping to optimize an objective function. Journal of the American Statistical Association 58(301): 236–244. https://doi.org/10.1080/01621459.1963.10500845

Ward RD (2009) DNA barcode divergence among species and genera of birds and fishes. Molecular Ecology Resources 9(4): 1077–1085. https://doi.org/10.1111/j.1755-0998.2009.02541.x

Zarucki M, González-Bergonzoni I, Teixeira-de-Mello F, Duarte A, Serra S, Quintans F, Loureiro M (2010) New records of freshwater fish for Uruguay. Check List 6(2): 1–4. https://doi.org/10.15560/6.2.191

Supplementary material 1

All COI sequences analyzed in the present work

Authors: James Anyelo Vanegas-Ríos, Wilson Sebastián Serra Alanís, María de las Mercedes Azpelicueta, Thomas Litz, Luiz Roberto Malabarba

Data type: xlsx

Link: https://doi.org/10.3897/zse.100.112778.suppl1

Supplementary material 2

Scree plots obtained from the morphometric and meristic data analyzed

Authors: James Anyelo Vanegas-Ríos, Wilson Sebastián Serra Alanís, María de las Mercedes Azpelicueta, Thomas Litz, Luiz Roberto Malabarba

Data type: pdf

Link: https://doi.org/10.3897/zse.100.112778.suppl2

Supplementary material 3

Total variance accounted for the PCA performed for the morphometric and meristic data

Authors: James Anyelo Vanegas-Ríos, Wilson Sebastián Serra Alanís, María de las Mercedes Azpelicueta, Thomas Litz, Luiz Roberto Malabarba
Data type: pdf

Link: https://doi.org/10.3897/zse.100.112778.suppl3

Supplementary material 4

Cluster analysis (Ward's method) of size-corrected morphometric data of analyzed specimens of *Diapoma pampeana*

Authors: James Anyelo Vanegas-Ríos, Wilson Sebastián Serra Alanís, María de las Mercedes Azpelicueta, Thomas Litz, Luiz Roberto Malabarba
Data type: tif

Link: https://doi.org/10.3897/zse.100.112778.suppl4

Supplementary material 5

Tukey box plot of most distinctive meristic data observed in analyzed specimens of *Diapoma pampeana*

Authors: James Anyelo Vanegas-Ríos, Wilson Sebastián Serra Alanís, María de las Mercedes Azpelicueta, Thomas Litz, Luiz Roberto Malabarba
Data type: pdf

Link: https://doi.org/10.3897/zse.100.112778.suppl5

Supplementary material 6

Uncorrected pairwise genetic distances using the COI data matrix

Authors: James Anyelo Vanegas-Ríos, Wilson Sebastián Serra Alanís, María de las Mercedes Azpelicueta, Thomas Litz, Luiz Roberto Malabarba
Data type: xlsx

Link: https://doi.org/10.3897/zse.100.112778.suppl6

Supplementary material 7

Haplotype network of the COI data analyzed of *D. pampeana*

Authors: James Anyelo Vanegas-Ríos, Wilson Sebastián Serra Alanís, María de las Mercedes Azpelicueta, Thomas Litz, Luiz Roberto Malabarba
Data type: pdf

Link: https://doi.org/10.3897/zse.100.112778.suppl7

Supplementary material 8

Table of coordinates used

Authors: James Anyelo Vanegas-Ríos, Wilson Sebastián Serra Alanís, María de las Mercedes Azpelicueta, Thomas Litz, Luiz Roberto Malabarba
Data type: xlsx

Link: https://doi.org/10.3897/zse.100.112778.suppl8

Zoosyst. Evol. 100 (1) 2024, 87–99 | DOI 10.3897/zse.100.112557

PENSOFT

MUSEUM FÜR NATURKUNDE BERLIN

The trouts of the Marmara and Aegean Sea drainages in Türkiye, with the description of a new species (Teleostei, Salmonidae)

Davut Turan[1], Esra Bayçelebi[1], Sadi Aksu[2], Münevver Oral[1]

1 *Recep Tayyip Erdogan University, Faculty of Fisheries and Aquatic Sciences, 53100 Rize, Turkiye*

2 *Eskişehir Osmangazi University, Vocational School of Health Services, 26040, Eskişehir, Turkiye*

https://zoobank.org/6AF795D4-BBB3-402A-AAAB-1DD5AE61E435

Corresponding author: Münevver Oral (munevver.oral@erdogan.edu.tr)

Academic editor: Nicolas Hubert ♦ **Received** 11 September 2023 ♦ **Accepted** 8 December 2023 ♦ **Published** 26 January 2024

Abstract

The taxonomic status of native trout species of the Marmara and Aegean Sea drainages is evaluated and three species, *Salmo duhani*, *S. coruhensis* and *S. brunoi* **sp. nov.**, are recognized. *Salmo brunoi*, a new species, is described from the Nilüfer River, a tributary of the Susurluk River. It is distinguished by a general brownish body color in life; few black spots (fewer than 60) on the body, generally scattered on the back and the upper part of the flank, rarely in the median part; few (fewer than 40) and small (smaller than pupil) red spots on the body, scattered on the median part and lower half of the flank; a number of black and red spots not increasing with size in both sexes; a long adipose fin (adipose-fin height 8–9% SL); a short distance between adipose-fin and caudal-fin (12–14% SL); and a short anal fin (anal-fin height 12–15% SL). *Salmo brunoi* **sp. nov.** is separated from the rest of the Marmara and Aegean trouts of Anatolia based on genome-wide distributed 187.385 unlinked SNP markers. According to the best of the authors' knowledge, whole genome data is used for the first time here to characterize a new species of trout.

Key Words

Anatolia, biodiversity, freshwater fish, *Salmo*, taxonomy

Introduction

Salmo trutta Linnaeus, 1758 (brown trout) has long been considered a species widely distributed throughout Europe, reaching the Atlas Range southwards (Morocco, Algeria) and the upper Amu Darya drainage in Afghanistan eastwards (Kottelat and Freyhof 2007).

Anatolia has a high level of species richness and endemism and thus has been classified as a European biodiversity hotspot (Kosswig 1955; Durand et al. 2002; Şekercioğlu et al. 2011), and salmonids are no exception with a high level of endemism in the area (Bardakçı et al. 2006). As it is conveniently located at the intersection of three major biodiversity hotspots, namely: Caucasian, Mediterranean and Irano-Anatolia, Türkiye harbors a high genetic and morphological diversity across a wide range of taxa (Noroozi et al. 2019). So far, the rich diversity of Anatolian trouts has been mostly revealed by the examination of morphological characters (Tortonese 1955; Behnke 1968; Turan et al. 2010, 2011, 2012, 2014a, 2014b, 2017, 2021, 2022; Turan and Bayçelebi 2020; Turan and Aksu 2021) and more recently based on the joint use of genetic and morphological characters (Turan et. al. 2010, 2020, 2021; Kaya, 2020). With these comprehensive studies, there are seventeen *Salmo* species naturally distributed in Türkiye. These are: *Salmo abanticus* Tortonese, 1954 (Lake Abant), *Salmo araxensis* Turan, Kottelat & Kaya, 2022 (Aras River), *Salmo ardahanensis* Turan, Kottelat & Kaya, 2022 (upper drainages of Kura River), *Salmo baliki T*uran, Aksu, Oral, Kaya & Bayçelebi, 2021 (upper drainages of Murat River, Euphrates drainage), *Salmo chilo* Turan, Kottelat & Engin, 2012 (Ceyhan River), *Salmo coruhensis* Turan, Kottelat & Engin, 2010 (the streams and rivers from the Turkish Black Sea coast and Marmara drainages), *Salmo duhani* Turan & Aksu, 2021 (Gönen Stream, south western Marmara

drainage) *Salmo euphrataeus* Turan, Kottelat & Engin, 2014 (Karasu River, northern Euphrates drainage), *Salmo fahrettini* Turan, Kalayci, Bektaş, Kaya & Bayçelebi, 2020 (Karasu River, northern Euphrates drainage), *Salmo kottelati* Turan, Doğan, Kaya & Kanyılmaz, 2014 (Alakır Stream, Mediterranean drainage), *Salmo labecula* Turan, Kottelat & Engin, 2012 (lower drainages of Seyhan River), *Salmo munzuricus* Turan, Kottelat & Kaya, 2017 (Munzur Stream, northern Euphrates drainage), *Salmo murathani* Turan, Kottelat & Kaya, 2022 (Aras River), *Salmo okumusi* Turan, Kottelat & Engin, 2014 (Tohma and Göksu streams, western Euphrates drainage), *Salmo opimus* Turan, Kottelat & Engin, 2012 (Alara Stream, Mediterranean drainage), *Salmo platycephalus* Behnke, 1968 (upper drainages of Seyhan River), *Salmo rizeensis* Turan, Kottelat & Engin, 2010 (Turkish Black Sea coast) and *Salmo tigridis* Turan, Kottelat & Bektaş, 2011 (Tigris River) (Turan et al. 2022). Of these, nine species (*S. abanticus*, *S. araxensis*, *S. ardahanensis*, *S. coruhensis*, *S. duhani*, *S. euphrataeus*, *S. fahrettini*, *S. murathani*, *S. rizeensis*) belong to the Danubian lineage, while *S. tigridis* belongs to the Tigris lineage and the remaining species belong to the Adriatic lineage.

A previous phylogenetic study of the brown trout based on mitochondrial DNA sequences revealed five major brown trout evolutionary lineages including AD (Adriatic origin), AT (Atlantic), DA (Danubian), MA (Marmaratus), and ME (Mediterranean) (Bernatchez 2001). Subsequently, new lineages were described from Spain as Duero (DU; Suárez et al. 2001), from Türkiye as TI (Tigris; Sušnik et al. 2005; Bardakçı et al. 2006), from Morocco as Dades (Snoj et al. 2011), from Northern Africa (Tougard et al. 2018). A molecular study of the brown trout populations inhabiting the Marmara Sea drainages (*S. coruhensis* and *S. duhani*) placed them in the DA lineage (Bardakci et al. 2006).

Next-generation sequencing (NGS) technologies have revolutionized genomic research, enabling the identification of a massive number of genome-wide markers in a single reaction (Metzker 2010; Goodwin et al. 2016; McCombie et al. 2019). Advances have dramatically reduced the cost while providing high-quality sequence data. NGS has been extensively used in aquatic species, including population structure analysis (Segherloo et al. 2021), genetic linkage map construction (Leitwein et al. 2017), quantitative trait locus mapping for economically important traits (Palaiokostas et al. 2013, 2015) and improving the quality of reference genome assemblies (Lien et al. 2016; Hansen et al. 2021).

Based on current knowledge, only two valid species, namely *Salmo coruhensis* and *S. duhani*, inhabit the rivers flowing to the Marmara Sea. *Salmo coruhensis* is distributed in the drainages of the Southern Black Sea and the northern part of the Marmara drainages [Elmalı Stream (İznik Lake drainage) and Kurtköy Stream]. *Salmo duhani* is restricted to the upper part of Gönen Stream, the southern drainage of the Marmara Sea. During the present study, additional populations of *Salmo* were discovered in the Nilüfer River (another drainage of the Marmara Sea) and cannot be reliably assigned to one of the two known species from the area. To determine their taxonomic status, we compared their morphological characters and genome-wide molecular data to other known *Salmo* species in the area. In addition, the status of the *Salmo* populations from the Ayazma Stream is reexamined here. Our comparisons indicate that *Salmo* populations from the Nilüfer River correspond to a distinct and undescribed species belonging to the DA lineage.

Materials and methods

The fieldwork followed the guidelines of the Local Ethics Committee of RTE University related to the use of animals in scientific experiments with a permit reference number of 2014/72. Samples were collected from the streams Aras, Ericek and Deliçay, drainages of the Marmara Sea and western Türkiye (Fig. 1). These are known to be the uppermost tributaries of the Nilüfer River. Specimens were captured using an electrofishing device (Samus 1000) and euthanized using tricaine methanesulphonate solution (MS-222). Subsequently, fin clips were collected from one of the pelvic fins and placed into 96% ethanol for subsequent molecular work. Finally, specimens were fixed in a 4% formaldehyde solution in a vertical position. These specimens were deposited at the FFR, Zoology Museum of the Faculty of Fisheries, Recep Tayyip Erdogan University, Rize (Sabaj 2020) FSJF, Fischsammlung J. Freyhof, Berlin for detailed morphologic analysis.

Abbreviations: **SL**: Standard length; **HL**: Head length.

Morphological analyses

The study by Turan et al. (2010) was used as a guideline for morphometric analysis. All measurements were carried out in the form of a point-to-point approach (projections were not used) using a dial calliper calibrated to 0.01 mm. Specific to the present study, the last two branched rays articulating on a single pterygiophore in the anal and dorsal fins were counted as "1½".

Comparison material

All materials are from Türkiye except *Salmo labrax.*

***Salmo abanticus*:** FFR 3163, 7,77–272 mm SL; Bolu prov.: outlet of Abant Lake, 40.5737°N, 31.2957°E.

***Salmo ardahanensis*:** FFR 3164, 10, 154–217 mm SL; Ardahan prov.: stream Toros, Kura River drainage, 41.1000°N, 42.4333°E.—FFR 3107, 4, 156–192; FFR 3167, 2, 155–182 mm SL; Ardahan prov.: stream Alabalık, Kura River drainage, 41.0500°N, 42.3666°E.—FFR 3110, 4, 67–118 mm SL; Ardahan prov.: stream Karaman at Aşıkzülal, Kura River drainage, 41.4166°N, 42.6500°E.—FFR 3136, 16, 99–185 mm SL; Ardahan prov.: stream Kınavur at Çataldere, Kura River drainage, 41.1833°N, 42.6000°E.

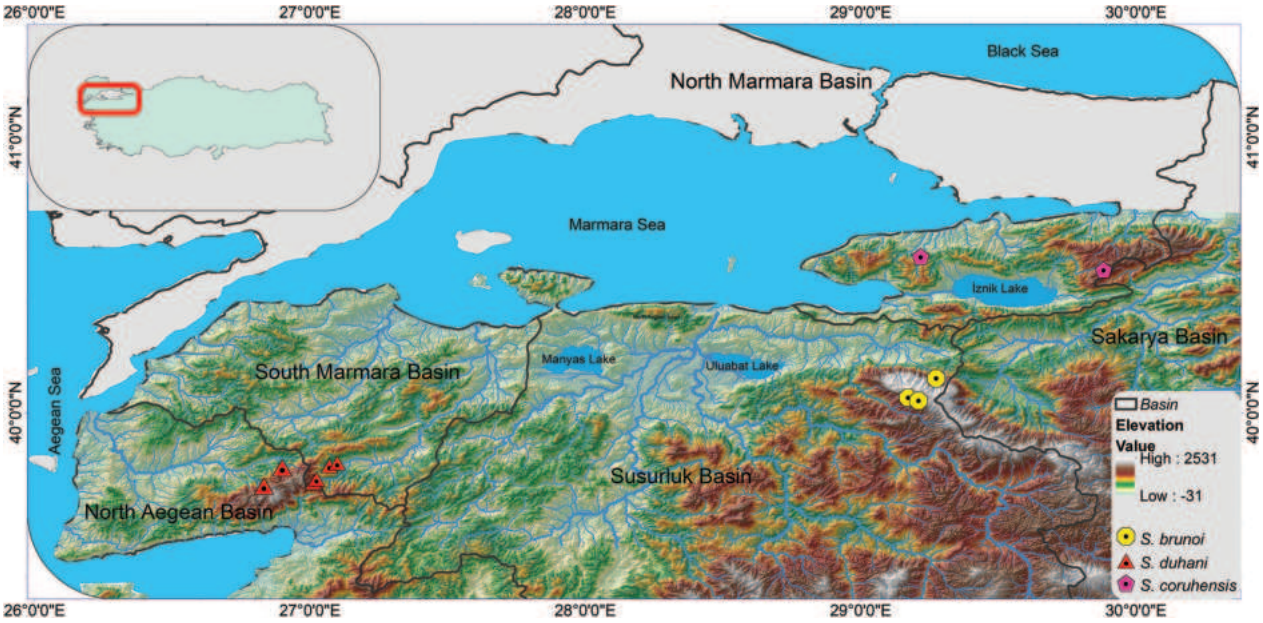

Figure 1. Distributions of *Salmo* in Marmara and Aegean Sea basins.

***Salmo araxensis*:** FFR 3114, 12, 116–201 mm SL; Kars prov.: Susuz district Kayalık stream, a tributary of Kars stream, Aras River drainage, 40.8166°N, 43.1166°E.—FFR 3115, 15, 93–237 mm SL; Kars prov.: Susuz district: Porsuklu (Akçalı) stream, a tributary of Kars stream, Aras River drainage, 40.8000°N, 43.1833°E.—FFR 3118, 6, 95–132 mm SL; Kars prov.: Sarıkamış district: Boyalı stream, a tributary of Kars stream, Aras River drainage, 40.4333°N, 42.5666°E.—FFR 3144, 16, 87–265 mm SL; Kars prov.: Susuz district: İncilipınar stream, a tributary of Kars stream, Aras River drainage, 40.8166°N, 43.0666°E.

***Salmo baliki*:** FFR 3234, 6, 132–276 mm SL; Ağrı prov.: stream Sinek a tributary of Murat River at Taşlıçay, 39.7587°N, 43.4644°E.—FFR 3205, 3, 175–267 mm SL; Ağrı prov.: a tributary of Murat River 39.7307°N,43.4818°E.

***Salmo chilo*:** FFR 3055, 23, 65–235 mm SL; Sivas prov.: stream Akdere at Gürün, Ceyhan River drainage, 38.6088°N, 36.8962°E.

***Salmo coruhensis*:** FFR 3004, 16, 95–240 mm SL; Artvin prov.: stream Osmaniye at Karaosmaniye village, 41.4689°N, 41.5105°E.—FFR 3011, 11, 90–189 mm SL; Artvin prov.: stream Hopa at Çavuslu village, 41.4509°N, 41.7001°E.—FFR 3021, 25, 90–520 mm SL; Rize prov.: stream Fırtına at Çat village 40.8653°N, 40.9311°E.—FFR 3022, 9,95–228 mm SL; Rize prov.: stream Kendirli at Kalkandere District on road to Kendirli village, İyidere drainage 40.9373°N, 40.4320°E.—FFR 3023, 13, 120–450 mm SL; Rize prov.: stream Iyidere (Ikizdere) at Güneyce 40.8219°N, 40.4765°E.—FFR 3024, 13, 115–330 mm SL; Artvin prov.: stream Dörtkilise at Tekkale village, Çoruh River, 40.7877°N, 41.4946°E.—FFR 3025, 13, 80–550 mm SL; Erzurum prov.: stream Çayırbası (Kırık) at Kırık village, Çoruh River, 40.2904°N, 40.8097°E.—FFR 3026, 6, 160–290 mm SL; Erzurum prov.: stream Büyük at Büyükköy village, Çoruh River, 40.4452°N, 40.8513°E.—FFR 3027, 6, 130–420 mm SL; Rize prov.: stream Veliköy at Veliköy village, 41.0332°N, 40.6145°E.—FFR 3029, 6, 130–220 mm SL; Rize prov.: stream Bozukkale at Bozukkale village, 41.0543°N, 40.6297°E.—FFR 3030, 6, 80–170 mm SL; Rize prov.: stream Çaglayan at Çaglayan district 40.9230°N, 40.4452°E.—FFR 3031, 6, 190–265 mm SL; Bayburt prov.: stream Ölçer at Ölçer village, Çoruh River, 40.5147°N, 40.5609°E.—FFR 3032, 16, 70–310 mm SL; Rize prov.: stream Sögütlü at Sögutlü village, about 5 km west of Çayeli, 41.0659°N, 40.6526°E.—FFR 3033, 16, 110–210 mm SL; Bayburt prov.: stream Kurtbogazı at Kurtbogazı village, Çoruh River, 40.1883°N, 40.5033°E.—FFR 3034, 16, 70–210 mm SL; Gümüşhane prov.: stream Harşit at Yağmurdere, 40.5746°N, 39.8645°E.—FFR 3035, 9, 160–450 mm SL; Sivas prov.: stream Gemin at Camili, Yeşıırmak River drainage, 40.0619E 38.0536N.—FFR 3037, 10, 90–380 mm SL; Erzurum prov.: stream Pehlivanlı at Pehlivanlı village, tributary of Tortum, Çoruh River, 40.5176°N, 41.4780°E.—FFR 3041, 10, 115–250 mm SL; Trabzon prov.: stream Solaklı at Taskıran village 40.6722°N, 40.2568°E.—FFR 3042, 6, 95–117 mm SL; Rize prov.: stream Sarayköy at Sarayköy village, 41.0190°N, 40.3807°E.—FFR 3043, 5, 130–229 mm SL; Artvin prov.: stream Barhal at Sarıgöl village, Çoruh River, 40.9744°N, 41.4184°E.—FFR 3043, 9, 110–223 mm SL; Rize prov.: stream Derepazarı at Derepazarı 41.0237°N, 40.4293°E.—FFR 3044, 6, 100–250 mm SL; Rize prov.: stream Iyidere at Iyidere 40.9676°N, 40.3778°E.—FFR 3045, 7, 150–450 mm SL; Rize prov.: stream Fırtına at Çamlıhemsin 41.0517°N, 41.0032°E.—FFR3046, 5, 10–280 mm SL; Rize prov.: stream Limanköy at Limanköy village, 41.0714°N, 40.7121°E.

***Salmo duhani*:** FFR 3184, 15, 95–287 mm SL; Çanakkale prov.: stream Zeytinli about 9 km east of Kazdağı National Park, 39.750°N, 27.017°E, 28.11.2006. –FFR 3185, 14, 85–170 mm SL; Çanakkale prov.: stream Zeytinli, 39.749°N, 27.015°E.—FFR 3186, 12, 108–160 mm SL; Çanakkale prov.: stream Zeytinli 39.759°N, 27.021°E.—FFR 3194, 10, 62–122 mm SL; Çanakkale prov.: stream Kocaçayı, 12 km west of Kalkım, 39.804°N, 27.071°E.—FFR 3195, 15, 93–275 mm SL; Çanakkale prov.: stream Kocaçayı at Yenice, 39.817°N, 27.099°E.

***Salmo euphrataeus*:** FFR 1220, 24, 80–260 mm SL; Erzurum prov.: stream Kuzgun, a tributary of Karasu Stream, Euphrates River drainage, 40.2198°N, 41.1051°E.—FFR 1255, 25, 88–230 mm SL; Erzurum prov.: stream Şenyurt at Şenyurt, a tributary of Karasu Stream, Euphrates River, 40.1830°N, 41.5037°E.—FFR 1223, 5, 122–222 mm SL; Erzurum prov.: stream Sırlı, a tributary of Karasu Stream, Euphrates River, 40.2183°N, 41.1010°E.—FFR 1269, 8, 117–198 mm SL; Erzurum prov.: stream Kuzgun, Euphrates River, 40.2198°N, 41.1050°E.

***Salmo fahrettini*:** FFR 3232, 20, 134–227 mm SL; Erzurum prov.: stream Ömertepesuyu at Palandöken 39.7958°N, 40.9444°E.—FFR 3233, 5, 126–194 mm SL; Erzurum prov.: stream Tekke at Palandöken, 39.8197°N, 41.1516°E.

***Salmo kottelati*:** FFR 3181, 21, 98–210 mm SL; Antalya prov.: stream Alakır at Altınyaka, 36.5608°N, 30.3428°E.—FFR 3182, 16, 98–176 mm SL; Antalya prov.: stream Alakır at Altınyaka, 36.5608°N, 30.3428°E.

***Salmo labecula*:** FFR 3057, 4, 103–237 mm SL; Niğde prov.: stream Ecemiş at Çamardı, Seyhan River drainage, 37.8253°N, 34.9902°E.—FFR 3058, 5, 142–241 mm SL; Isparta prov.: stream Kartoz at Aşağıyaylabel, Köprüçay drainage, 37.5532°N, 31.3070°E.—FFR 3059, 5, 140–184 mm SL;Antalya prov.: stream Zindan at Aksu, Köprüçay drainage, 37.8064°N, 31.0734°E.

***Salmo labrax*:** FSJF 396, 6, 107–147 mm SL; Ukraine: Ula–Uzev River; N. Bogustkaya, A. Neseka, J. Bohlen & J. Freyhof, 12 June 2002.—FSJF 10, 6, 102–160 mm SL; Russia: Crasnodar prov.: Khosta River; J. Freyhof, 19July 2002.

***Salmo munzuricus*:** FFR 3162, 17, 127–270 mm SL; Tunceli prov.: stream Munzur at Koyungölü, 39.3472°N, 39.1341°E.—FFR 3147, 8, 146–320 mm SL; stream Munzur at Koyungölü, 39.3461°N, 39.1316°E.

***Salmo murathani*:** FFR 3121, 18, 60–233 mm SL; Kars prov.: Keklik stream [a tributary of Kars stream], Sarıkamış district, Aras River drainage, 40.2833°N, 42.6500°E.—FFR 3117, 22, 95–192 mm SL; FFR 3113, 17, 91–206; Kars prov.: Keklik stream [a tributary of Kars stream] Sarıkamış district, Aras River drainage, 40.2500°N, 42.6666°E.—FFR 3120, 10, 69–163 mm SL, Kars prov.: Maksutçuk stream [a tributary of Kars stream], Aras River drainage, 40.5333°N, 42.8666°E.—FFR 3108, 14, 90–186 mm SL; Ardahan prov.: Çıldır Lake, Aras River drainage 41.0500°N, 43.3166°E.—FFR 3228, 23, 95–241 mm SL; Kars prov.: Arpaçay stream [a tributary of Kars stream] Arpaçay district, Aras River drainage 40.9000°N, 43.1666°E.—FFR 3229, 8, 110–156 mm SL; Kars prov.: Keklik stream [a tributary of Kars stream] Sarıkamış District, Aras River drainage, 40.2833°N, 42.6500°E.

***Salmo okumusi*:** FFR 1254, 10, 75–202 mm SL; Malatya prov.: stream Sürgü, Euphrates River drainage, 37.9975°N, 37.9583°E.—FFR 125, 10, 129–169 mm SL; Sivas prov.: stream Gökpınar, a tributary of Tohma stream, Euphrates River, 38.6600°N, 37.3089°E.—FFR 1256, 10, 68–280 mm SL; Sivas prov.: stream Gökpınar, Euphrates River, 38.6600°N, 37.3089°E.—FFR 124, 2, 149–175 mm SL; Kahramanmaraş prov.: stream Göksu 4 km north of Düzbağ, Euphrates River, 37.8331°N, 37.4756°E.

***Salmo opimus*:** FFR 3048, 12, 118–180 mm SL; Antalya prov.: stream Alara at Gündoğmuş, 36.7921°N, 31.9749°E.—FFR 3049, 20, 115–186; Kahramanmaraş prov.: stream Göçüksu at Kömürköy, Ceyhan River drainage, 38.1447°N, 36.5630°E.—FFR 3050, 4, 175–210 mm SL; Kahramanmaras prov.: drainage of stream Tekir at Tekir, Ceyhan River drainage, 37.8767°N, 36.6058°E.—FFR 3051, 9, 90–300 mm SL; Kahramanmaras prov.: stream Fırnız at Fırnız, Ceyhan River drainage, 37.7591°N, 36.6983°E.

***Salmo platycephalus*:** FFR 972, 7, 145–184 mm SL; Kayseri prov.: Pınarbası stream at Pınarbası district, Seyhan River drainage.—FFR 1260, 10, 137–237 mm SL; Kayseri prov.: Pınarbası Stream at Pınarbası district, Seyhan River drainage.

***Salmo rizeensis*:** FFR 3001, 15, 90–220 mm SL; Erzurum prov.: stream Ovit (2) [Kan] at Ovit mountain, Çoruh River, 40.5887°N, 40.8583°E.—FFR 3002, 10, 114–245 mm SL; Trabzon prov.: stream Degirmen at Çosandere village, 40.7512°N, 39.5908°E.—FFR 3003, 12, 112–230 mm SL; Trabzon prov.: stream Solaklı at Demirkapı village, 40.7586°N, 40.5913°E.—FFR 3005, 13, 111–220 mm SL; Rize prov.: stream Çağlayan at Gürcüdüzü plateau 41.1905°N, 41.3086°E.—FFR 3006, 18, 95–226 mm SL; Rize prov.: stream Sehitlik at Sehitlik village, 41.1407°N, 40.9828°E.—FFR 3007, 12, 90–118 mm SL; Rize prov.: stream Çayeli at Kaptanpasa village, 40.958°N, 40.7794°E.—FFR 3008, 18, 91–198 mm SL; Rize prov.: stream Fırtına at Tunca village, 41.1259°N, 41.1310°E.—FFR 3009, 10, 110–240 mm SL; Rize prov.: stream Taşlıdere at Pasaçur village; 40.8837°N, 40.5796°E.—FFR 3010, 9, 110–240 mm SL; Rize prov.: stream Taslıdere at Kangel village, 40.9453°N, 40.6642°E.—FFR 3011, 7, 100–180 mm SL; Rize prov.: stream Erenler at Erenler village, 41.0914°N, 40.8298°E.—FFR 3012, 7, 88–237 mm SL; Artvin prov.: stream Dörtkilise at Tekkale Village, Çoruh River, 40.7800°N, 41.5098°E.—FFR 3013, 12, 75–167 mm SL; Artvin prov.: Çifteköprü stream at Cankurtaran mountain, Çoruh River, 41.3844°N, 41.5691°E.—FFR 3014, 7, 112–201 mm SL; Artvin prov.: stream Kapisre at Kücükköy village, 41.2753°N,

41.3755°E.—FFR 3015, 9, 113–228 mm SL; Bayburt prov.: stream Kop at Kop Mountain, Çoruh River, 40.0654°N, 40.4331°E.—FFR 3016, 9, 113–221 mm SL; Erzurum prov.: stream Yağlı at Yaglı village, Çoruh River, 40.3643°N, 41.0728°E.—FFR 3017, 12, 112–223 mm SL; Erzurum prov.: stream Büyük at Büyükdere plateau, Çoruh River drainage, 40.5698°N, 40.7140°E.—FFR 3018, 16, 145–224 mm SL; Gümüşhane prov.: stream Akbulak at Akbulak village, Yesilırmak River drainage, 40.281462°N, 39.0896°E.—FFR 3019, 10, 122–221 mm SL; Kütahya prov.: stream Sefaköy at Domaniç, Sakarya River drainage, 39.8426°N, 29.6706°E.—FFR 3020, 10, 111–119 mm SL; Kütahya prov.: Çatalalıç Stream at Domaniç, Sakarya River, 39.8600°N, 29.6291°E.—FFR 3036, 10, 130–170 mm SL; Rize prov.: stream Ikizdere at Anzer plateau, 40.5926°N, 40.5148°E.—FFR 3038b, 7, 130–170 mm SL; Rize prov.: stream Çiftekavak at Ortapazar village, 40.9959°N, 40.4851°E.—FFR 3039a, 14, 120–200 mm SL; Rize prov.: stream Fırtına at Elevit Plateau, 40.8471°N, 41.0151°E.—FFR 3038a, 1, 250 mm SL; Erzurum prov.: stream Ovit (2) [Kan] at Ovit mountain, Çoruh River, 40.5735°N, 40.8634°E.—FFR 3039b, 10, 90–238 mm SL; Rize prov.: stream Ovit at Ovit mountain, Iyidere drainage, 40.6361°N, 40.8214°E.—FFR 3040, 14, 90–190 mm SL; Erzurum prov.: stream Merekum at Merekum, Çoruh River, 40.5527°N, 41.4592°E.

***Salmo tigridis*:** FFR 1253, 9, 136–227 mm SL; Van prov.: stream Çatak, Tigris River, 38.0077°N, 43.0652°E.

Samples

In total, 71 samples fixed in formalin were investigated morphologically (see Paratypes section) and tissue samples were collected from two specimens of the new species, *S. brunoi*, originating from Bursa, Uludağ, Aras Stream, Türkiye. In total, 12 samples were examined for genetic analysis including 2 specimens of new species *S. brunoi* from Bursa, Uludağ, Aras Stream, 1 specimen of *Salmo coruhensis*, collected from Bursa, İznik, Sığırhisar village and 3 specimens of *Salmo coruhensis* from Sultaniye Stream, Kartepe, İzmit, 3 specimens of *Salmo pelagonicus* collected from Çanakkale, Bayramiç, Ayazma Stream and 3 specimens of *S. duhani* taken from the type locality, in Çanakkale, Yenice, Kalkım. In addition to Anatolian samples, globally recognized *Salmo* lineages were included as references in the genetic analyses. From these references 3 specimens of Danubian lineage samples included in the genetic analysis (1 specimen provided from the Kuban River, Russia, has been treated as *S. labrax* based on Turan et al. (2014b) who have previously reported the distribution of the species from the northwest Caucasia in Russia to the Danube River and 2 specimens from the Sevan River, Armenia were treated as *S. ischchan* (thus Danubian reference). The rest of the reference samples included 2 specimens from *S. marmaratus* from Svenica and Trebuscica in Slovenia; 3 specimens from Atlantic fish origin of Babeau hatchery in France (unidentified species), 2 specimens of *S. obtusirostris* from Studenčica in Bosna and Herzegovina, 3 specimens of Adriatic lineage samples (unidentified species) from Alfios and Kalamos in Greece and 1 specimen from Ohrid-Drin-Skadar in Albania, respectively.

DNA extraction, ddRADseq library preparation and NGS sequencing

Total genomic DNA extraction was carried out on a KingFisher Flex DNA extraction robot (Thermo Fisher Scientific, France) following the manufacturer's instructions. DNA quality was assessed on 0.8% agarose gels and DNA quantity was estimated using a NanoDrop 2000 (Thermo Fisher Scientific, France). High molecular weight genomic DNA samples were further assessed using Qubit (Thermo Fisher Scientific, France) BR assay for the final quantification of double-stranded DNA prior to ddRADseq library construction. The library construction was performed following the original ddRADseq protocol by Peterson et al. (2012) with slight modifications detailed by Leitwein et al. (2016) and Oral (2023). Genomic DNA was doubled-digested using *EcoRI* and *MspI* enzymes. Fragmented DNA was then individually barcoded using adaptors. Samples were pooled and processed into single tubes following adaptor ligation. Purified and size-selected fragments (c. 300–700 bp) were then enriched for 15 PCR cycles. The amplified library was quantified using NanoDrop spectrometry and Qubit fluorimetry and the size distribution of the library was further assessed on a Fragment Analyzer (Advanced Analytical Technologies, France). The ddRADseq library was sequenced on an Illumina NovaSeq platform with paired-end reads of 150 base pairs.

Bioinformatic data analysis

The initial quality control of the raw data files was carried out using FastQC (Andrews 2010; Babraham BioInformatics). Reads of low quality (Phred score < 30), missing restriction sites and/or involving ambiguous barcodes were removed. Retained reads were then processed using Stacks v2.55 (Catchen et al. 2013) for demultiplexing based on their barcodes, restriction enzymes and cleaned with ProcessRadtags (-c -r -q --renz_1 ecoRI --renz_2 mspI). Cleaned reads were mapped against the *Salmo trutta* reference genome (accession number: GCA_901001165.2; Hansen et al. 2021) with BWA-mem2 v2.1 (-k 19 -c 500 -O 0,0 -E 2,2 -T 0 -R) (Li and Durbin 2010) and samtools v1.11 (-Sb -q 1 -F 4 -F 256 -F 2048). Then gstacks (--max-clipped 0.01) was run with a minimum number of 2 populations where a locus must be present (-p 2), a minimum 20% of individuals in a population (-r 0.2), a maximum observed heterozygosity of 60% (--max-obs-het 0.6), a minimum allele frequency of 1% (--min-maf 0.01) and a single representative of each overlapping site (--ordered-export).

Once variants were collected following the steps above mentioned, they were filtered with vcftools v0.1.16 (Danecek et al. 2011). First, we focused on individuals, removing those with more than 20% of missing data. Second, we filtered SNPs according to the sequencing depth, missing data, frequency and number of alleles per site (--minDP 4 --minGQ 30 --max-missing 0.4 --min-alleles 2 -max-alleles 2 --maf 0.01). Finally, we removed SNPs that were in high linkage disequilibrium using 11_extract_unlinked_snps_genome.py (diff_threshold=0.5 and max_distance=50) from stacks_workflow v2.62 (https://github.com/enormandeau/stacks_workflow). Bioinformatics analyses were performed with the support of LDgenX (www.ldgenx.com) and only a subset of these data was used in the present study.

Population structure analysis

We performed ADMIXTURE and Principal Component Analysis (PCA) on filtered and unlinked SNPs. ADMIXTURE v.1.3.0 (Alexander et al. 2009) was used to estimate individual cluster memberships. ADMIXTURE provides an estimation of individual ancestry proportion for K groups and the number of different groups was explored from 1 to 12. Based on the cross-validation procedure, the best K with the lowest cross-validation error was detected as 9. Q-values estimated by ADMIXTURE were used to produce bar plots with R v 4.2.1 (R Core Team 2015).

Alongside the ADMIXTURE analysis, the unlinked SNPs of 12 individuals from the Marmara Aegean basin were further investigated using PCA calculated with PLINK 1.9 (Chang et al. 2015). PCA was conducted to determine the population structure and the first two components of the PCA were plotted using R v 4.2.1.

Results

***Salmo brunoi* sp. nov.**

https://zoobank.org/6AB6FDA0-37BF-49D8-8A74-BE2FCED9212F

Figs 2–4

Type material. *Holotype*: FFR 3243, 175 mm SL; Türkiye, Bursa prov.: stream Aras, a tributary of Nilüfer River, 40.0536°N, 29.1722°E.

***Paratypes*:** FFR 3216, 188–153 mm SL; same data as holotype.—FFR 3213, 7, 142–195 mm SL;—FFR 3215, 7, 142–195 mm SL; Türkiye, Bursa prov.: stream Deliçay at Kestel, 40.1241°N, 29.2737°E.—FFR 3211, 18, 93–180 mm SL; —FFR 3217, 12, 85–153 mm SL; Türkiye, Bursa prov.: stream Ericek at Osmangazi, 40.0426°N, 29.2098°E.

Diagnosis. *Salmo brunoi* is distinguished from all the species of *Salmo* in Türkiye and adjacent areas by the combination of the following characters: a small size (known maximum size 187 mm SL); body brownish in life; one black spot in postorbital and suborbital areas, greater than the pupil; two to four black spots on the opercle, approximately smaller than the pupil; black spots on the body few (fewer than 60), approximately equal to the pupil, ocellated, scattered on the back and the upper part of the flank (missing in the predorsal area); red spots few (fewer than 40), smaller than the pupil, irregularly shaped, surrounded by an irregularly shaped narrow ring, organized in two to four irregular longitudinal rows; number of black and red spots not increasing with size; anal fin short (12–15% SL in males, 12–14 in females), adipose fin large (adipose fin height 8–9% SL in males and females), short distance between adipose fin and caudal fin bases (13–14% SL in males, 12–14% in females).

Description. The general appearance is shown in Figs 2, 3, live images are in Fig. 4, morphometric data are in Table 1. Body moderately deep, compressed laterally, its depth smaller than head length. The dorsal profile is slightly arched, and the head is short, upper profile slightly convex on the interorbital area and the snout in males and markedly convex on both interorbital areas and the snout in females. Mouth large in males, small in females, terminal or slightly subterminal in males, subterminal in females. Tip of lower jaw slightly curved upwards, pointed, with a slightly developed process at symphysis in males larger than 160 mm SL. Maxilla somewhat long, with a length of 10–12% SL, reaching beyond the posterior margin of the eye in males larger than 140 mm SL and only reaching the posterior margin of the eye in females. Snout somewhat short, with a pointed tip in males, rounded in females. Adipose fin long, height about 8–9% SL in males and in females. Known maximum size 195 mm SL.

Dorsal fin with 3–4 unbranched and 8–10 branched rays, its distal margin convex. Pectoral fin with 1 unbranched and 11–13 branched rays, its external margin slightly convex. Pelvic fin with 1 unbranched and 7–8 branched rays, its external margin convex. Anal fin with 3 unbranched and 7–9 branched rays, its distal margin convex anteriorly and concave posteriorly. The caudal fin deeply emarginated in specimens less than 120 mm SL, slightly emarginated or truncated in specimens larger than 140 mm SL, lobes slightly pointed. Lateral line with 108–122 scales; 23–32 scale rows between dorsal fin origin and lateral line; 16–23 scale rows between anal fin origin and lateral line; 14–18 scale rows between origin of the adipose fin and lateral line. Gill rakers 15–18 on the first gill arch.

Coloration. In life: General body color brownish or light brownish. Back and flank brownish and belly yellowish. Red spots conspicuously organized in two to four irregular longitudinal rows on the median part of the body and half of the lower part of the flank. Conspicuously black spots in postorbital and suborbital areas. Black spots roundish, scattered on back and upper part of flank. Pectoral, pelvic and anal fins yellowish, dorsal and anal fins yellowish or light brownish. Adipose fin with reddish margin (see Fig. 4).

Figure 2. *Salmo brunoi*, FFR 3243, holotype, 175 mm SL, male; Türkiye: stream Aras, a tributary of Nilüfer River.

Figure 3. *Salmo brunoi*, from top: FFR 3216, paratypes, 137 mm SL, male; 105 mm SL, female; Türkiye: stream Aras, a tributary of Nilüfer River.

In formalin: The general coloration of freshly preserved specimens dark brown on the back and upper part of the flank, brownish on the lower part of the flank and yellowish on the belly. One black spot in postorbital and suborbital areas, greater than the pupil; two to four black spots on the opercle, approximately smaller than the pupil. Black spots on the body few (fewer than 60), approximately equal to the pupil, ocellated, commonly scattered on the back and the upper part of the flank (missing in the predorsal area) and rarely median part of the flank; no black spot on top of the head. Red spots few (fewer than 40), small (smaller than the pupil), irregularly shaped, surrounded by an irregularly shaped narrow ring, organized in two to four irregular longitudinal rows on the median part of the body and half of the lower part of the flank. The number of black and red spots on the flanks do not increase with size. Dorsal fin gray, with two or three rows of black spots (smaller than pupil) and one or two rows of red spots (smaller than pupil). Caudal fin dark gray; pectoral, anal and pelvic fins grayish. Adipose fin plain grayish, rarely one or two red spots on its posterior edge (Figs 2,3). Eleven to thirteen parr marks on the body, distinct in specimens up to about 195 mm SL.

Distribution and habitat. *Salmo brunoi* sp. nov. inhabits clear and swift-flowing water, with a substrate consisting of gravel and pebbles. The observed material for this species has been collected from streams Aras, Deliçay and Ericek, drainages of Nilüfer River (Fig. 1).

Conservation status. According to the First Author's (DT) observations, *Salmo brunoi* sp. nov. is under the influence of overfishing. Besides fresh consumption, trout oil is a widely preferred natural remedy, particularly for the treatment of rheumatism, muscle, and joint pains among local people (Turan et al. 2006). Therefore, the

Table 1. Morphometry of *Salmo brunoi* (holotype, FFR 3243; paratypes FFR 3215, n=6, and FFR 3216, n=8). The calculations include the holotype.

	Holotype	Paratypes			
Sex	**male**	**male**	**SD**	**female**	**SD**
Number of specimens		**n=6**		**n=8**	
Standard length (mm)	**175**	**112–179**		**110–153**	
In percentage of standard length		**Range (mean)**		**Range (mean)**	
Head length	29.6	26.1–29.6 (27.7)	1.3	24.8–26.9 (26.0)	0.7
Predorsal length	49.6	47.1–49.6 (48.7)	0.8	44.2–48.4 (47.1)	1.4
Prepelvic length	55.9	53.8–55.9 (54.8)	0.8	52.7–55.5 (53.8)	1.0
Preanal length	73.6	73.2–75.0 (74.3)	0.7	73.3–75.7 (74.2)	1.0
Body depth at dorsal-fin origin	24.8	22.1–25.3 (23.8)	0.4	19.9–24.3 (21.6)	1.3
Body depth at anal-fin origin	19.2	16.2–19.3 (17.7)	1.1	16.1–17.8 (16.8)	0.6
Depth of caudal peduncle	10.9	9.9–10.9 (10.1)	0.3	8.8–10.0 (9.4)	0.4
Length of caudal peduncle	17.0	15.5–18.0 (16.6)	0.9	15.3–17.8 (17.0)	0.8
Distance between adipose- and caudal-fins	14.0	12.6–14.4 (13.5)	0.6	11.5–13.6 (12.6)	0.7
Body width at anal-fin origin	9.0	7.1–10.4 (8.9)	1.3	7.0–9.9 (9.0)	1.0
Length of dorsal-fin base	9.0	12.2–14.5 (13.3)	0.9	12.7–13.8 (13.1)	0.5
Height of dorsal fin	19.4	16.3–19.5 (17.6)	1.2	15.2–17.1 (16.2)	0.7
Length of pectoral fin	14.1	15.9–20.1 (18.0)	1.6	16.3–18.5 (17.3)	0.8
Length of adipose-fin base	3.7	2.9–4.1 (3.6)	0.5	2.8–4.8 (3.8)	0.4
Height of adipose fin	8.6	8.0–9.2 (8.4)	0.5	7.8–8.5 (8.1)	0.2
Length of pelvic fin	19.4	12.1–15.3 (13.4)	1.6	11.9–14.4 (13.1)	0.9
Height of anal fin	13.4	12.1–14.7 (13.4)	1.2	11.9–14.4 (13.1)	0.9
Length of anal-fin base	10.7	9.3–12.2 (10.4)	0.9	8.3–11.6 (10.3)	1.2
Length of upper caudal-fin lobe	19.9	12.9–17.6 (15.6)	1.6	15.4–17.7 (16.3)	0.9
Length of median caudal-fin rays	14.3	10.9–14.7 (13.0)	1.4	10.8–14.0 (12.4)	1.1
Length of lower caudal-fin lobe	14.7	14.0–18.0 (16.2)	1.6	15.2–18.5 (16.6)	1.1
Snout length	8.8	6.7–8.7 (7.7)	0.8	6.6–7.4 (7.0)	0.3
Distance between nasal openings	4.8	4.0–5.6 (4.9)	0.5	4.0–4.8 (4.4)	0.2
Eye diameter	6.1	5.2–7.0 (6.0)	0.6	5.4–6.6 (5.8)	0.4
Interorbital width	8.4	7.3–8.4 (7.8)	0.4	7.0–8.0 (7.5)	0.3
Head depth through eye	13.4	11.2–13.4 (12.5)	0.8	11.5–13.4 (12.8)	0.6
Head depth at nape	17.5	15.0–17.7 (16.3)	0.4	16.1–17.9 (16.9)	0.7
Length of maxilla	12.0	9.5–12.0 (10.5)	0.9	8.5–9.7 (9.2)	0.5
Maximum height of maxilla	2.5	2.6–3.7 (3.1)	0.3	2.6–3.8 (3.1)	0.4
Width of mouth gape	9.7	7.9–11.0 (9.2)	1.0	8.0–9.3 (8.7)	0.4
Length of mouth gape	16.6	12.2–16.7 (14.0)	1.6	12.0–13.2 (12.6)	0.5

species is in high demand. Given the highly restricted distribution of *S. brunoi* sp. nov. to a very limited area (only three streams), and considering the above mentioned socio-economic interest, this species is likely to be under a serious threat. Thus, there is a need for the species to be conserved under international legislation.

Comparison with other *Salmo* species. *Salmo brunoi* sp. nov. differs from the other species of trout recorded from Marmara, Aegean and Black Sea basins (*S. duhani*, *S. coruhensis*, *S.abanticus*, *S. rizeensis* and *S. labrax*) by having a shorter anal fin in females (12–14% SL, vs. 14–20), a longer adipose fin in females (adipose fin height 8–9% SL, vs. 4–8) and males (8–9% SL, vs. 4–8, except *S. coruhensis*), a shorter distance between adipose fin and caudal fin bases in females (12–14% SL, vs. 14–17, except *S. duhani*) and males (13–14% SL, vs. 15–17 in *S. labrax*, 14–16 in *S. rizeensis*, 14–16 in *S. duhani*, except *S. abanticus* and *S. coruhensis*). *Salmo brunoi* further differs from *S. abanticus*, *S. coruhensis* and *S. labrax* by the brownish body color in life (vs. silvery). *Salmo brunoi* further differs from *S. abanticus* and *S. coruhensis* by fewer black spots on the body in adult males (fewer than 60, vs. more than 80), whose number does not increase with size (vs. number increasing with size). *Salmo brunoi* further differs from *S. duhani* by having fewer black spots on the back and flank in females (fewer than 60, vs. more than 80). *Salmo brunoi* is further distinguished from *S. abanticus* by the presence of red spots on the body in all sizes (vs. absent in specimens larger than about 200 mm SL) and black spots circular (vs. polygonal).*Salmo brunoi* is further distinguished from *S. labrax* by having a shorter predorsal distance in males (47–50% SL, vs. 46–47), a slenderer body in males (body depth at anal fin origin 16–19% SL, vs. 19–21) and a slenderer caudal peduncle in females (9–10% SL, vs. 10–11). *Salmo brunoi* is further distinguished from *S. rizeensis* by having a slenderer caudal peduncle in females (9–10% SL, vs. 10–11).

The new species, *Salmo brunoi*, *is* also distinguished from *S. ardahanensis* by having fewer gill rakers on

Figure 4. *Salmo brunoi*, from top: not preserved, ~145 mm SL, male; not preserved, ~150 mm SL, female; Türkiye: stream Aras, a tributary of Nilüfer River.

the outer side of the first gill arch (15–18, vs. 19–21), no black spots on the top of the head (vs. small black spots). It further differs from *S. ardahanensis* by having a smaller distance between adipose and caudal fins in females (12–14% SL, vs. 14–17) and a shorter anal fin in males (12–15%SL, vs. 15–18). In males of *Salmo brunoi*, anal and adipose fins do not reach the caudal fin base (vs. reaching in specimens larger than 200 mm SL) and the interorbital area is convex (vs.flat straight).

Salmo brunoi is further distinguished from *Salmo murathani* by having fewer black spots on flank and back in adult specimens (fewer than 60, vs. more than 66); one black spot behind eye (larger than pupil); 2–4 spots on preopercle and opercle (vs. 4–15); black spots scattered on back (missing in predorsal area), the upper part of flank, sometimes a few black spots below lateral line behind head (vs. black spots scattered on back, the middle and upper part of the flank and the anterior part of the lower flank in males) black spots few (34–47), restricted to the back and upper part of flank in females smaller than about 210 mm SL). It further differs from *S. murathani* by having a smaller distance between adipose and caudal fins in females (12–14% SL, vs. 15–17) and a shorter anal fin in females (12–14% SL, vs. 14–18) and a slenderer caudal peduncle depth in females (9–10% SL, vs. 10–12).

Salmo brunoi is distinguished from *Salmo araxensis* by having a longer maxilla in males (10–12% SL, vs. 9–10), a shorter anal fin (12–15% SL in males, 12–14 in females, vs. 15–18 in males, 14–18 in females), a slenderer caudal peduncle in females (9–10% SL, vs.10–12) and a smaller distance between adipose and caudal fins in females (12–14% SL, vs. 14–17).

Salmo brunoi is distinguished from *S. fahrettini* by having the general body color brownish in life (vs. silvery); fewer black spots on the body (fewer than 60, vs. more than 80); black spots on the back (missing on the predorsal area) and upper part of flank, sometimes a few below lateral line behind the head (vs. black spots scattered on back, middle and upper part of flank and anterior part of lower half of flank); their number not increasing with size (vs. their number increasing with size); fewer red spots on body (fewer than 40, vs. more than 70 in adult specimens), their number not increasing with size (vs. increasing with size); a longer maxilla in males (length 10–12% SL, vs. 9–10); a longer adipose fin in males (8–9% SL vs. 3–8); a smaller distance between adipose and caudal fins in females (12–14% SL, vs. 15–18) and a shorter anal fin in females (12–14% SL, vs. 15–17).

Salmo brunoi is distinguished from *S. euphrataeus* by having a smaller distance between adipose and caudal fins in males (13–14% SL, vs. 14–16), a slenderer caudal peduncle in females (9–10% SL, vs.10–12), a shorter anal fin in females (12–14% SL, vs. 16–19), and the adipose fins do not reach the caudal fin base (vs. reaching in specimens larger than 200 mm SL).

Salmo brunoi is distinguished from *S. platycephalus*, *S. chilo*, *S. labecula*, *S. kottelati*, *S. opimus*, all from streams draining to the Mediterranean and *S. okumusi*,

S. munzuricus and *S. baliki* from Euphrates River, by having a smaller distance between adipose and caudal fins in males (12–14% SL, vs. 14–19), a slenderer caudal peduncle in females (9–10% SL, vs.10–13), a shorter anal fin (12–15% SL, vs.15–21, except *S. labecula* and *S. munzuricus*) and fewer gill rakers on first gill arch (15–18, vs. 18–25, except *S. munzuricus* and *S. balıki*). *Salmo brunoi* is further differs from *S. platycephalus*, *S. chilo*, *S. labecula*, *S. kottelati* and *S. opimus*, by the absence of four dark bands on the flank (vs. presence). It further differs from *S. munzuricus* by having a smaller adipose in males (8–9% SL, vs. 9–12) and a longer maxilla in males (10–12% SL, vs. 8–10). It further differs from *S. platycephalus* by the presence of red spots on flank (vs. absent in specimens larger than about 70 mm SL) also differs from *S. labecula* by the presence of red spots on flank in all size (vs. absent in specimens larger than about 70 mm SL).

Salmo brunoi differs from *S. tigridis* by having fewer scale rows between the dorsal fin origin and the lateral line (23–32, vs. 32–35); fewer scale rows between the end of the adipose fin base and the lateral line (14–18, vs. 19–20), a slenderer caudal peduncle depth 9–11% SL, vs. 12–13).

Sexual dimorphism. The maxillary length in males is longer than that of females (10–12% SL in males, 9–10 in females). The length of mouth gape in males is longer than that of females (12–17% SL, 12–13). The snout of the male is more pointed than that of the female.

Etymology. The species is named after Dr. Bruno Guinand (University of Montpellier, ISEM, France) for his valuable contribution to *Salmo* population genomics research.

ddRAD loci and SNP calling

In total, an average of thirteen million raw reads were generated per individual with a mean sequence depth of 30. Sequences with a missingness index higher than 20% were removed from the dataset. Once filtered according to sequencing depth, missing data, frequency and number of alleles, a total of 215k SNPs were retrieved. More than 187k unlinked SNPs within the 50 bp window were used for downstream population analysis.

Interference of ADMIXTURE and PCA analysis

The ADMIXTURE program identified 9 separate clusters. In the reference lineages, the Danubian (DA) cluster was placed in two groups of which DA-1 (*S. labrax*) separated from DA-2 and DA-3 (*S. ischchan*) corresponding to the origin and the geographic basin. The rest of the reference *Salmo* species including *S. obtusirostris* and *S. marmaratus* clustered separately, as expected. Similarly, *S. brunoi* sp. nov., generated a separate cluster from the rest of the Marmara and Aegean trout of Anatolia. The only exception was observed in *Salmo duhani*, which individuals clustered together (K=9; Fig. 5; see Discussion for detailed explanation).

The 187,385 unrelated SNPs for each of the 12 individuals from the Marmara Aegean basin were used for PCA. The analysis results indicated 3 clusters of which the first cluster included DA reference samples originated from Armenia as *S. ischchan*, the second cluster included *S. brunoi* and *S. coruhensis* clustered with *S.labrax* from Russia and the third cluster included *S. duhani* and that of *S.pelagonicus* (see discussion). The first two components of PCA represented 29.31% and 21.39% of the variance among individuals.

Discussion

Up until the present study, three species of trout have been reported from the Marmara and Aegean Sea drainages: *S. duhani* (Gönen Stream-Marmara Sea drainage), *S. coruhensis* (Elmalı and Kurtköy streams, İznik and Sapanca Lake drainages) and *S. pelagonicus* (Ayazma Stream; Karamenderes drainage, Aegean Sea drainage). In the present study, our molecular data (Q values, 0.99992, 0.9992 respectively for *S. pelagonicus* and *S. duhani*, Fig. 5) showed that trout samples from Gönen Stream (Marmara Sea drainage) largely overlapped in genetic diversity of 187,385 genome-wide SNP markers with those of Ayazma Stream samples (Aegean Sea drainage). Turan and Bayçelebi, (2020) reported Ayazma samples as *Salmo pelagonicus*. Indeed, *Salmo pelagonicus* was originally described from Mountain Brooks in Macedonia (Karaman, 1938). Although Turan and Bayçelebi, (2020) compared specimens from the Ayazma stream with 3 photographs of *S. pelagonicus* from the Aliakmon River in Greece, these authors did not compare the Ayazma population with that of the type locality for *S. pelagonicus* from Macedonia. Later, Turan and Aksu (2021) described *Salmo duhani* from Gönen Stream and gave a few morphological differences between *S. duhani* and *S. pelagonicus*. For example, *Salmo duhani* is distinguished from *S. pelagonicus* by having fewer lateral-line scales (115–121, vs. 109–115), a shorter maxilla in males (8–10% SL, vs. 10–11) and a slenderer body in males (body depth at dorsal–fin origin 20–23% SL, vs. 23–27). Taking all into account; the distance, geographic barriers between Macedonia and Ayazma stream, Türkiye and our molecular data; here, we treated this species as *S. duhani*. Furthermore, bases on our present results, *Salmo duhani* needs to be rediagnosed by considering all samples (Gönen ve Ayazma streams) in future studies.

In the present study, 187,385 unlinked SNP loci shared among the populations were analysed to provide support our recognition of a distinct species. Results provided evidence that *S. brunoi* sp. nov. separates from other *Salmo* species that inhabit adjacent basins (Figs 5, 6).

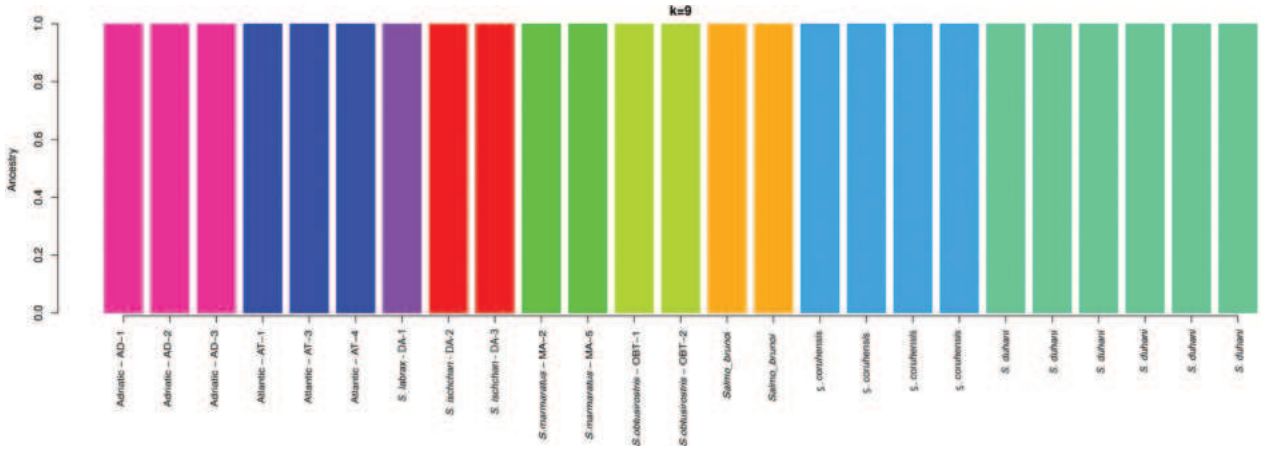

Figure 5. Bar plots of the individuals ancestry generated by ADMIXTURE v.1.3.0 using 187,385 unlinked SNPs. Vertical lines represent each individual and color-code defines the ancestry origin with k= 9 groups. Reference trout specimens are: Adriatic (AD), Atlantic (AT) and Danubian (DA) lineage (originates from two different locations), *Salmo marmaratus* and *S. obtusirostris*.

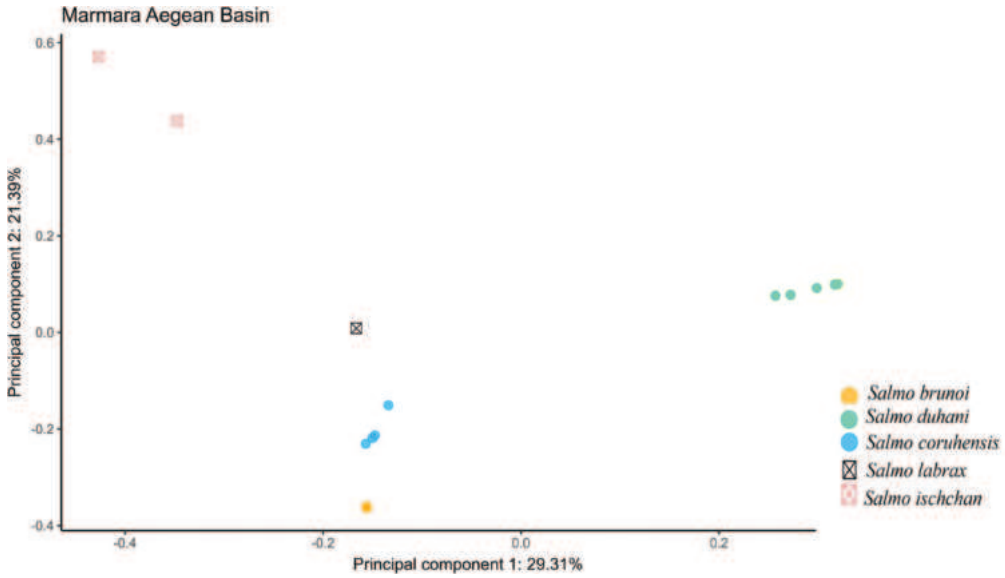

Figure 6. Principal Component Analysis (PCA) plot using 187,385 unlinked SNPs. Rectangular symbols represent the Danubian (DA) lineage reference, whereas circles indicate trout specimens used in the study. Colors represent the *Salmo coruhensis* and *S. duhani* specimens.

Author Contributions

DT conceptualized and conceived the idea. EB carried out morphometric measurements under the guidance of DT. SA carried out the fieldwork. MO performed genetic wet-lab work and data analysis and provided funding acquisition. The draft was written primarily by DT and all authors have read, edited and agreed with the final version.

Acknowledgements

This work was financially supported by the Scientific Research Project Units of Recep Tayyip Erdogan University (Project ID: FBA-2022-1355). MO has received a post-doctoral research grant from The Scientific and Technical Research Council of Türkiye, TÜBITAK-BIDEB-2219, at ISEM (University of Montpellier, France). Supplementary funding by the OSU OREME (Univ. Montpellier) for sequencing was appreciated. The wet lab work of the present study was carried out at the GenSeq facility of the University of Monpellier (https://www.labex-cemeb.org/en/genotyping-sequencing-genseq) and sequencing at the MGX platforms (Montpellier, France), respectively. GenSeq is supported by the Laboratoire d'Excellence (LabEx) CeMEB and by ANR "Investissements d'Avenir" program (ANR-10-LABX-04-01). MGX acknowledges financial support from the France Génomique National infrastructure, funded as part of ANR "Investissement d'Avenir" (ANR-10-INBS-09). The bioinformatic analysis benefited from support by K. Belkhir (MBB), M. Leitwein and E. Delpuech from the LDgenX.

Therefore, the authors would like to express their sincere appreciation to ISEM and especially to the 'Biodiversité et Evolution Marine' team for enabling access to laboratories to conduct the research. Additionally, we thank J. Freyhof for the specimen loan from FSJF, Fischsammlung, Berlin.

References

Alexander DH, Novembre J, Lange K (2009) Fast model-based estimation of ancestry in unrelated individuals. Genome Research 19(9): 1655–1664. https://doi.org/10.1101/gr.094052.109

Andrews S (2010) FastQC: a quality control tool for high throughput sequence data. http://www.bioinformatics.babraham.ac.uk/projects/fastqc

Bardakci F, Degerli N, Ozdemir O, Basıbuyuk BB (2006) Phylogeography of the Turkish brown trout *Salmo trutta* L.: Mitochondrial DNA PCR-RFLP variation. Journal of Fish Biology 68(A): 36–55. https://doi.org/10.1111/j.0022-1112.2006.00948.x

Behnke RJ (1968) A new subgenus and species of trout *Salmo* (*Platysalmo*) *platycephalus*, from south-central Turkey with comments on the classification of the subfamily Salmoninae. Mitteilungen aus dem Hamburgischen Zoologischen Museum und Institut 66: 1–15.

Bernatchez L (2001) The evolutionary history of brown trout (*Salmo trutta* L.) inferred from phylogeographic, nested clade, and mismatch analyses of mitochondrial DNA variation. Evolution; International Journal of Organic Evolution 55(2): 351–379. https://doi.org/10.1111/j.0014-3820.2001.tb01300.x

Catchen J, Hohenlohe PA, Bassham S, Amores A, Cresko WA (2013) Stacks: An analysis tool set for population genomics. Molecular Ecology 22(11): 3124–3140. https://onlinelibrary.wiley.com/doi/10.1111/mec.12354

Chang CC, Chow CC, Tellier LC, Vattikuti S, Purcell SM, Lee JJ (2015) Second-generation PLINK: Rising to the challenge of larger and richer datasets. GigaScience 4(7): 7. https://doi.org/10.1186/s13742-015-0047-8

Danecek P, Auton A, Abecasis G, Albers CA, Banks E, DePristo MA, Handsaker RE, Lunter G, Marth GT, Sherry ST, McVean G, Durbin R (2011) The variant call format and VCFtools. Bioinformatics (Oxford, England) 27(15): 2156–2158. https://doi.org/10.1093/bioinformatics/btr330

Durand JD, Tsigenopoulos CS, Ünlü E, Berrebi P (2002) Phylogeny and Biogeography of the Family Cyprinidae in the Middle East Inferred from Cytochrome b DNA– Evolutionary Significance of This Region. Molecular Phylogenetics and Evolution 22(1): 91–100. https://doi.org/10.1006/mpev.2001.1040

Goodwin S, McPherson J, McCombie W (2016) Coming of age: Ten years of next-generation sequencing technologies. Nature Reviews. Genetics 17(6): 333–351. https://doi.org/10.1038/nrg.2016.49

Hansen T, Fjelldal PG, Lien S, Smith M, Corton C, Oliver K, Skelton J, Betteridge E, Doulcan J, Fedrigo O, Mountcastle J, Jarvis E, McCartey A, Chow W, Howe K, Torrance J, Wood J, Sims Y, Haggerty L, Challis R, Threlfall J, Mead D, Durbin R, Blaxter M (2021) The genome sequence of the brown trout, *Salmo trutta* Linnaeus 1758. Wellcome Open Research 6: 108. https://doi.org/10.12688/wellcomeopenres.16838.1

Karaman S (1938) Beitrag zur Kenntnis der Süßwasserfische Jugoslaviens. (Salmoniden, l. Teil.). Glasnik Skopskog Nauchnog Drustva [Glasnik -- Bulletin de la Société Scientifique de Skopje] v 18: 131–139.

Kaya C (2020) The first record and origin of *Salmo trutta* populations established in the upper Tigris river and Lake Van basin (Teleostei: Salmonidae). Journal of Anatolian Environmental and Animal Sciences 5(3): 366–372. https://doi.org/10.35229/jaes.777575

Kosswig C (1955) Zoogeography of the Near East. Systematic Biology 4(2): 49–73. https://doi.org/10.2307/sysbio/4.2.49

Kottelat M, Freyhof J (2007) Handbook of European freshwater fishes. Kottelat, Cornol & Freyhof, Berlin, 660 pp. https://www.nhbs.com/handbook-of-european-freshwater-fishes-book

Leitwein M, Gagnaire PA, Desmarais E, Guendouz S, Rohmer M, Berrebi P, Guinand B (2016) Genome-wide nucleotide diversity of hatchery-reared Atlantic and Mediterranean strains of brown trout *Salmo trutta* compared to wild Mediterranean populations. Journal of Fish Biology 89(6): 2717–2734. https://doi.org/10.1111/jfb.13131

Leitwein M, Guinand B, Pouzadoux J, Desmarais E, Berrebi P, Gagnaire PA (2017) A dense brown trout (*Salmo trutta*) linkage map reveals recent chromosomal rearrangements in the Salmo genus and the impact of selection on linked neutral diversity. G3 Genes|Genomes|Genetic 7: 1365–1376. https://doi.org/10.1534/g3.116.038497

Li H, Durbin R (2010) Fast and accurate long-read alignment with Burrows-Wheeler transform. Bioinformatics 26: 5 589–595. https://doi.org/10.1093/bioinformatics/btp698

Lien S, Koop BF, Sandve SR, Miller JR, Kent MP, Nome T, Hvidsten TR, Leong JS, Minkley DR, Zimin A, Grammes F, Grove H, Gjuvsland A, Walenz B, Hermansen RA, Schalburg KV, Rondeau EB, Genova AD, Samy JKA, Vik JO, Vigeland MD, Caler L, Grimholt U, Jentoft S, Våge DI, Jong P, Moen T, Baranski M, Palti Y, Smith DR, Yorke JA, Nederbragt AJ, Klunderud AT, Jakobsen AS, Jiang X, Fan D, Hu Y, Liberles DA, Vidal R, Iturra P, Jones SJM, Jonassen I, Maass A, Omholt SW, Davidson WS (2016) The Atlantic salmon genome provides insights into rediploidization. Nature 6020(7602): 200–205. https://doi.org/10.1038/nature17164

McCombie WR, McPherson JD, Mardis ER (2019) Next-Generation Sequencing Technologies. Cold Spring Harbor Perspectives in Medicine 9(11): 11. https://doi.org/10.1101/cshperspect.a036798

Metzker M (2010) Sequencing technologies – the next generation. Nature Reviews. Genetics 11(1): 31–46. https://doi.org/10.1038/nrg2626

Noroozi J, Zare G, Sherafati M, Mahmoodi M, Moser D, Asgarpour Z, Schneeweiss GM (2019) Patterns of endemism in Turkey, the meeting point of three global biodiversity hotspots, based on three diverse families of vascular plants. Frontiers in Ecology and Evolution 7: 444247. https://doi.org/10.3389/fevo.2019.00159

Oral M (2023) A cost effective alternative method to ddRADseq library construction during size selection. Su Ürünleri Dergisi 40(1): 20–26. https://doi.org/10.12714/egejfas.40.1.03

Palaiokostas C, Bekaert M, Davie A, Cowan ME, Oral M, Taggart JB, Gharbi K, McAndrew BJ, Penman DJ, Migaud H (2013) Mapping the sex determination locus in the Atlantic halibut (*Hippoglossus hippoglossus*) using RAD sequencing. BMC Genomics 14(1): 566. https://doi.org/10.1186/1471-2164-14-566

Palaiokostas C, Bekaert M, Taggart JB, Gharbi K, McAndrew BJ, Chatain B, Penman DJ, Vandeputte M (2015) A new SNP-based vision of the genetics of sex determination in European sea bass (*Dicentrarchus labrax*). Genetics, Selection, Evolution. 47(1): 1–68. https://doi.org/10.1186/s12711-015-0148-y

Peterson BK, Weber J, Kay EH, Fisher HS, Hoekstra HE (2012) Double digest RADseq: An inexpensive method for *de novo* SNP discovery and genotyping in model and non-model species. PLoS ONE 7(5): e37135. https://doi.org/10.1371/journal.pone.0037135

R Core Team (2015) R: A Language and Environment for Statistical Computing, R Foundation for Statistical Computing, Vienna, Austria. https://www.R-project.org/

Sabaj MH (2020) Codes for natural history collections in ichthyology and herpetology. Copeia 08(3): 593–669. https://doi.org/10.1643/ASIHCODONS2020

Segherloo IH, Freyhof J, Berrebi P, Ferchaud AL, Geiger M, Laroche J, Levin BA, Normandeau E, Bernatchez L (2021) A genomic perspective on an old question: *Salmo trouts* or *Salmo trutta* (Teleostei: Salmonidae)? Molecular Phylogenetics and Evolution 162: 107204. https://doi.org/10.1016/j.ympev.2021.107204

Snoj A, Marić S, Bajec SS, Berrebi, Janjani S, Schöffmann J (2011) Phylogeographic structure and demographic patterns of brown trout in North-West Africa Molecular Phylogenetics and Evolution 61(1): 203–211. https://doi.org/10.1016/j.ympev.2011.05.011

Şekercioğlu ÇH, Anderson S, Akçay E, Bilgin R, Can OA, Semiz G, Tavşanoğlu C, Yokes MB, Soyumert A, İpekdal K, Sağ IK, Yücel M, Dalfes HN (2011) Turkey's globally important biodiversity in crisis. Biological Conservation 144(12): 2752–2769. https://doi.org/10.1016/j.biocon.2011.06.025

Suárez J, Bautista J, Almodóvar A, Machordom A (2021) Evolution of the mitochondrial control region in Palaearctic brown trout (*Salmo trutta*) populations: The biogeographical role of the Iberian Peninsula. Heredity 87(2): 198–206. https://doi.org/10.1046/j.1365-2540.2001.00905.x

Sušnik S, Schöffmann J, Weiss S (2005) Genetic verification of native brown trout from the Persian Gulf (Catak Cay River, Tigris basin). Journal of Fish Biology 67(3): 879–884. https://doi.org/10.1111/j.0022-1112.2005.00780.x

Tortonese E (1955) The trouts of Asiatic Turkey. Publications of the Hydrobiological Research Institute. University of Istanbul B 2(1): 1–25.

Tougard C, Justy F, Guinand B, Douzery EJP, Berrebi P (2018) *Salmo macrostigma* (Teleostei, Salmonidae): Nothing more than a brown trout (*S. trutta*) lineage? Journal of Fish Biology 93(2): 302–310. https://doi.org/10.1111/jfb.13751

Turan D, Aksu S (2021) A New Trout Species from Southern Marmara Sea Drainages (Teleostei: Salmonidae). Journal of Anatolian Environmental and Animal Sciences 2(2): 232–239. https://doi.org/10.35229/jaes.903810

Turan D, Bayçelebi E (2020) First Record of *Salmo pelagonicus* Karaman, 1938 (Teleostei: Salmonidae) in the Karamenderes River, Turkey. Journal of Anatolian Environmental and Animal Sciences 4(4): 551–555. https://doi.org/10.35229/jaes.777776

Turan H, Yalçın K, Sönmez G (2006) Balık Etinin Besin Değeri ve İnsan Sağlığındaki Yeri. Ege Journal of Fisheries and Aquatic Sciences 23(3): 505–508.

Turan D, Kottelat M, Engin S (2010) Two new species of trouts, resident and migratory, sympatric in streams of northern Anatolia (Salmoniformes: Salmonidae). Ichthyological Exploration of Freshwaters 20: 333–364. [(2009 [2010])] https://www.pfeil-verlag.de/wp-content/uploads/2015/05/ief20_4_06.pdf

Turan D, Kottelat M, Bektaş Y (2011) *Salmo tigridis*, a new species of trout from the Tigris River, Turkey (Teleostei: Salmonidae). Zootaxa 2993(1): 23–33. https://doi.org/10.11646/zootaxa.2993.1.2

Turan D, Kottelat M, Engin S (2012) The trouts of the Mediterranean drainages of southern Anatolia, Turkey, with description of three new species (Teleostei: Salmonidae). Ichthyological Exploration of Freshwaters 23: 219–236. https://scholarbank.nus.edu.sg/handle/10635/128706

Turan D, Kottelat M, Engin S (2014a) Two new species of trouts from the Euphrates drainage, Turkey (Teleostei: Salmonidae). Ichthyological Exploration of Freshwaters 24(3): 275–287.

Turan D, Doğan E, Kaya C, Kanyılmaz M (2014b) *Salmo kottelati*, a new species of trout from Alakır Stream, draining to the Mediterranean in southern Anatolia, Turkey (Teleostei, Salmonidae). ZooKeys 462: 135–151. https://doi.org/10.3897/zookeys.462.8177

Turan D, Kottelat M, Kaya C (2017) *Salmo munzuricus*, a new species of trout from the Euphrates River drainage, Turkey (Teleostei: Salmonidae). Ichthyological Exploration of Freshwaters 28: 55–63.

Turan D, Kalayci G, Bektaş Y, Kaya C, Bayçelebi E (2020) A new species of trout from the northern drainages of Euphrates River, Turkey (Salmoniformes: Salmonidae). Journal of Fish Biology 96(6): 1454–1462. https://doi.org/10.1111/jfb.14321

Turan D, Aksu İ, Oral M, Kaya C, Bayçelebi E (2021) Contribution to the trout of Euphrates River, with description of a new species, and range extension of *Salmo munzuricus* (Salmoniformes, Salmonidae). Zoosystematics and Evolution 97(2): 471–482. https://doi.org/10.3897/zse.97.72181

Turan D, Kaya C, Kottelat M (2022) The trouts of the upper Kura and Aras rivers in Turkey, with descriptions of three new species (Teleostei: Salmonidae). Zootaxa 5150(1): 43–64. https://doi.org/10.11646/zootaxa.5150.1.2

Zoosyst. Evol. 100 (1) 2024, 101–110 | DOI 10.3897/zse.100.113467

PENSOFT

für Natur MUSEUM FÜR NATURKUNDE BERLIN

Description of a new species of *Phoxinus* from the Ergene River (Aegean Sea Basin) in Türkiye (Actinopterygii, Leuciscidae)

Esra Bayçelebi[1], İsmail Aksu[1], Davut Turan[1]

1 *Recep Tayyip Erdogan University, Faculty of Fisheries and Aquatic Sciences, 53100 Rize, Turkiye*

https://zoobank.org/3D001C5D-C528-4CB4-BFE3-D1C0880DBB29

Corresponding author: Esra Bayçelebi (doganeesra@gmail.com)

Academic editor: N. Hubert ♦ **Received** 29 September 2023 ♦ **Accepted** 21 December 2023 ♦ **Published** 26 January 2024

Abstract

Phoxinus radeki, a new species, is described from the Ergene River (Aegean Sea Basin). It is distinguished from *Phoxinus* species in Türkiye and the adjacent area by having the scales of the breast, scaled but separated unscaled area anteriorly, short dark rectangular blotches along the lateral line between the lateral line and belly yellowish in both males and females, body depth dorsal fin origin 16–21% SL, caudal peduncle depth 8–10% SL. Additionally, molecular results demonstrated that the new species differed from its closest congeners with a mean genetic distance value of 3.08% (min. 2.82–max. 3.29) and moderately support values in cytochrome *b* (Cyt *b*) gene partial sequences (1064 bp.). Further, the species delimitation analysis identified the new species as a single MOTU independent of other *Phoxinus* species.

Key Words

Cyt *b*, Freshwater fish, minnows, taxonomy

Introduction

The genus *Phoxinus* Rafinesque, 1820 is widely distributed in the Palaearctic region, from the Ebro drainage in Spain eastward to the Anadyr and Amur drainages in Russia and China (basins of the Atlantic, North and Baltic Seas, the Arctic and the northern Pacific Ocean) (Kottelat 2007; Vucić et al. 2018; Bogutskaya et al. 2023; Turan et al. 2023). The fish of the genus *Phoxinus* belong to the family Leuciscidae and are commonly known as minnows. These small freshwater fish are also found in various freshwater habitats, including streams, rivers, lakes, and ponds, in various environments (Banarescu 1992; Kottelat and Freyhof 2007). *Phoxinus* species are typically small fish, with most species reaching lengths of only a few centimeters. They are omnivorous, feeding on various small aquatic invertebrates, algae and plant matter (Billard 1997). Some species of *Phoxinus* are popular among aquarium enthusiasts due to their small size and attractive coloration Froese and Pauly (2023).

All European minnows were previously identified as *Phoxinus phoxinus* (Linnaeus 1758). With the development of molecular and morphological techniques, numerous *Phoxinus* species' designations as synonyms of *P. phoxinus* (such as the list of synonyms published by Kottelat 2007) started to be questioned (Palandačić et al. 2015, 2017, 2020; Vucić et al. 2018; Bogutskaya et al. 2019, 2023; Denys et al. 2020; Turan et al. 2023). The first study on this was by Kottelat (2007), who described three species from Greece and southern France. Following are some studies: Four new *Phoxinus* species were described by Bianco and De Bonis (2015) from Italy and the Western Balkans. Molecular evidence points to a multispecies *Phoxinus* (Cyprinidae) complex in the Western Balkan Peninsula, as reported by Palandačić et al. (2015). Moreover, Vucić et al. (2018) investigated The Western Balkans' distribution of Eurasian minnow. Again, Palandačić et al. (2017) used molecular information in their taxonomic investigations to assign *Phoxinus* species to genetic lineages. The latest studies, *P. krkae* Bogutskaya et al. (2019), described a new minnow from Croatia and initially identified it as a molecular clad and Palandačić et al. (2020) researched museum collections to help with the genetic evaluation of species introductions in freshwater fishes (Cyprinidae: *Phoxinus* species complex): European minnows through time. In 2020, Denys et al. (2020) revised

Phoxinus in France and described two new species (Teleostei, Leuciscidae) and also created zones of coloration in *Phoxinus*. Finally, Turan et al. (2023) described a new species from Türkiye. Presently, the minnows of the genus *Phoxinus* include about 25 species (Eschmeyer et al. 2023; Froese and Pauly 2023; Turan et al. 2023). The geography of Türkiye has become the hub for diversifying many species and taxa currently recognized. Recent genetic-based studies on this topic demonstrate Türkiye's contribution to the planet's biodiversity (Geiger et al. 2014; Bektaş et al. 2019, 2020). Despite this rich biodiversity, the genus *Phoxinus* does not have a wide distribution in Türkiye.

The genus is represented by three species in Türkiye: *Phoxinus abanticus*, *P. colchicus*, *P. strandjae*. Ergene populations in the Thrace (in Türkiye) were defined as *Phoxinus strandjae* in previous studies (Çiçek et al. 2023; Özuluğ et al. 2023). These populations have never been studied in detail and we were able to collect them from six different places. Here, based on the morphological characters and a molecular data set, we describe a new *Phoxinus* species from the Ergene, a tributary of the Meriç River, Aegean Sea Basin, Türkiye.

Materials and methods

Fish sampling and measurements

Fish were collected by Samus 1000 pulsed DC electro-fishing equipment, at thirty-five sampling sites carried out between 2006 and 2017. After anaesthesia, specimens were fixed in 5% formaldehyde and stored in 70% ethanol or directly fixed in 96% ethanol. Measurements were made with a dial calliper and recorded to 0.1 mm. All measurements were made point to point. Methods for counts and measurements follow Kottelat and Freyhof (2007). Standard length (SL) was measured from the tip of the upper lip to the end of the hypural complex. The length of the caudal peduncle was measured from behind the base of the last anal-fin ray to the end of the hypural complex, at mid-height of the caudal-fin base. The last two branched rays articulating on a single pterygiophore in the dorsal and anal fins were counted as "1½". lts body measurements were standardized by individuals' SL, and the measurements taken from the head region were standardized by individuals' head length.

The map in Fig. 1 was created using the Qgis software, version 3.22, available at http://diva-gis.org. Occurrence data in the map (Fig. 1) are based on the authors' material. The drawings were made using a Wacom Intuos comıc brand drawing tablet, Adobe ıllustrator and Adobe Photoshop programs (Fig. 7).

Abbreviations used: SL, standard length. **HL**, Head length. **SD**, standard deviation, Collection codes: **FFR**, Recep Tayyip Erdogan University Zoology Museum of the Faculty of Fisheries, Rize.

DNA isolation, amplification and sequencing

Total DNA from ethanol-preserved tissue of *Phoxinus* specimens was isolated with the DNeasy Blood & Tissue Kit (Qiagen, Hilden, Germany) following the manufacturer's instructions. The Cytochrome *b* (Cyt *b*) gene of vertebrate mitochondrial DNA was amplified using the primers AlbCF (5′-CAACTACAAGAACATGGCAAGCC-3′) and AlbCR (5′-CTTCGGATTACAAGACCGATGC-3′) described by Bektas et al. 2019. The PCR protocol and thermocycler conditions were performed according to

Figure 1. Distribution of *Phoxinus* species in the Aegean and Black Sea basins and Abant Lake.

Turan et al. (2023). PCR products were purified using the QIAquick PCR Purification Kit (Qiagen, Hilden, Germany), and both directional sequencing of PCR products was performed with the same primers used for amplification at Macrogen Europe using an ABI PRISM 3730×1 Genetic Analyser and a BigDye Terminator 3.1 cycle sequencing ready reaction kit (Applied Biosystem).

Molecular data analyses

The Cyt *b* gene of seven specimens five specimens of stream Buyukdere and two specimens of stream Ahmetbey) from the type locality of the newly identified species was sequenced for molecular comparison. First, the chromatograms of the raw Cyt *b* sequences were examined with the program Bioedit 7.2.5 (Hall 1999) and the detected errors were manually edited. The sequences were then matched with reference data stored in this database using nBLAST (Basic Local Alignment Search Tool) on GenBank. In order to determine the phylogenetic position of the new species and to calculate the sequence difference, the reference Cyt *b* sequences of the topotype samples of the congener species were downloaded from the Genbank. In the absence of sequences of topotype samples of congeners taxa, correct sequences considered representative of the species were included (Also see the "Material used in molecular genetic analysis" section).

All sequences were aligned using the CLUSTAL-W method (Thompson et al. 1994), trimmed from the ends and converted to FASTA file. The final data set had 1064 nucleotide positions without insertion and deletion. Also, the sequences were translated into protein sequence, and the stop codon was not determined. The interspecific genetic distances were calculated based on the uncorrected *p*-distance in MEGA X version (Kumar et al. 2018). Phylogenetic relationships between the species were estimated using maximum likelihood (ML) algorithm in MEGA X program and the bayesian (BI) algorithm in MrBayes v3.2.1 program (Ronquist et al. 2012). ML tree was generated based on the GTR+I+G model such that the best-fit evolution model was selected by the Akaike information criterion (AIC) in jModeltest 0.1.1 (Posada 2008). The ML tree was generated with 1000 bootstrap replicates to estimate the phylogenetic relationships of the mtDNA lineages. BI tree was generated according to the GTR+I+G model that the best-fit evolution model was selected by the Bayesian Information Criterion (BIC) in jModelTest 0.1.1. For BI, analyses were run for 1×10^6 generations with Metropolis coupled Monte Carlo Markov Chains (MCMC) sampled every 1000 generations. A conservative 25% of the trees were discarded as burn-in. To root the all phylogenetic tree, the authors used *Alburnoides fasciatus*, *Alburnus alburnus*, *Squalius cephalus* and *Rhynchocypris lagowskii* (GenBank accession numbers: MK860065, Bektaş et al. 2019; MT394745, Bektaş et al. 2020; JQ652365, Dubut et al. 2012; MG806688, Schönhuth et al. 2018, respectively) as out-groups.

The species delimitation analysis was carried out using ASAP (Assemble Species by Automatic Partitioning; Puillandre et al. 2012) method based on Cyt *b* data. To implement the ASAP method, we used the Kimura 2-parameter (K2P) distances and transition/transversion ratio (R:7.2) settings at the web address https://bioinfo.mnhn.fr/abi/public/asap/. The transition/transversion ratio (R) for the Cyt *b* data was calculated in MEGA X software.

Results

Molecular data analyses

We used molecular methods to test the validity of the new species, *Phoxinus radeki*, identified in this study. The Cyt *b* gene data of the new species were deposited at NCBI (OR552423–OR552429) and its first genetic record was created. In order to determine the phylogenetic position of the new species, we included the morphologically valid European *Phoxinus* species in our dataset and reconstructed phylogenies with ML and BI methods. Almost similar topologies emerged in the results of both methods, and the genus *Phoxinus* was monophyletic in both. The new species was moderately supported by both methods (BI: 0.55; ML: 72% Fig. 8). The phylogenetic analysis placed the new species as the sister species of *P. abanticus*.

The results based on genetic distance demonstrated that *Phoxinus strandjae* was the closest neighbor species to the new species with a mean *p*-distance of 3.08% (min. 2.82–max. 3.29%), while the most distant species was *P. fayollarum* with a mean *p*-distance of 8.73% (min. 8.46–max. 8.83%).

The species delimitation analysis according to the ASAP method based on Cyt *b* data identified 15 MOTUs (molecular operational taxonomic units) for 15 morphologically valid *Phoxinus* species. This result had the best ASAP score of 1.0 (p = 0.01) at a threshold distance of 0.017644. The new species, *P. radeki*, formed a single MOTU independent of other *Phoxinus* species.

***Phoxinus radeki* sp. nov.**

https://zoobank.org/1AECCBFE-F5AB-4E2D-916B-29582D7A98DA

Figs 2–4

Materials examined. *Holotype*. FFR 2327, 54 mm SL; Türkiye: Kırklareli prov.: stream Büyükdere about 6 km west of Pınarhisar, 41.6337, 27.5994.

***Paratypes*.** FFR 2301, 12, 45–71 mm SL. –FFR 2304, 20, 42–68 mm SL; –FFR 2314, 19, 38–46 mm SL; same data as holotype. –FFR 2320, 22, 44–60 mm SL; Türkiye: Kırklareli prov.: stream Poyralı about 5 km west of Pınarhisar, 41.6172, 27.5909. –FFR 2311, 1, 49 mm SL; Türkiye: Kırklareli prov.: stream Ahmetbey at Soğurcak, 41.6345, 27.6540. –FFR 2326, 26, 44–65 mm SL; Türkiye: Tekirdağ prov.: Ergene River at Saray, 41.4257, 27.9131.

Figure 2. *Phoxinus radeki* FFR 2327: holotype, 54 mm SL, male; Türkiye: Ergene River.

Figure 3. *Phoxinus radeki* FFR 2326, from top: paratypes, 57–55 mm standard length (SL), possible males; Türkiye: Ergene River.

Genetic material. FFR-DNA-Ph42-43-44-45-46; Türkiye: Kırklareli prov.: stream Büyükdere about 6 km west of Pınarhisar, 41.6337, 27.5994 (GenBank accession numbers: OR552425–OR552426–OR552427–OR552428–OR552429). –FFR-DNA-Ph31-32; Türkiye: Kırklareli prov.: stream Ahmetbey at Soğurcak, 41.6345, 27.6540 (GenBank accession numbers: OR552423–OR552424).

Diagnosis. *Phoxinus radeki* is distinguished from the *Phoxinus* species (*P. strandjae*, *P. abanticus*) in adjacent basins as below. It is immediately distinguished from species *P. strandjae* by body color and pattern (not spawning period and immediately after fixation). *Phoxinus radeki* has short dark rectangular blotches along the lateral line. The area between the lateral line and belly is yellowish in both males and females. There are irregularly-shaped black spots on the upper part of the flank and no dark stripes on the middle part of the flank in males. *Phoxinus strandjae* (Fig. 5) has bars reaching from the dorsal to below the lateral line, hyaline between the lateral line and belly in females, blackish in males and no black spots on the upper part of the flank. It further differs from *P. strandjae* by the scales of the breast. *Phoxinus radeki* has breast scaled but separated unscaled area anteriorly, *P. strandjae* has breast scaled connected or scales not connected anteriorly (Fig. 7).

Phoxinus radeki is distinguished from species *P. abanticus* by the presence of scales on the breast in males (vs. absent, Fig. 7), a slenderer body (body depth dorsal fin origin 16–21% SL vs. 22–25) and a slenderer caudal peduncle (8–10% SL vs. 11–13). It further differs from *P. abanticus* by having more lateral line scales (75–96 vs.60–69).

Description. The general appearance is shown in Figs 2–4, and morphometric data are given in Table 1. The maximum size is 71 mm SL. Body depth at dorsal-fin origin 16%–21% SL.The dorsal body profile more convex than the ventral profile. The head short, its length 24%–27% SL, upper profile straight or slightly convex on the interorbital area and convex on the snout. The snout short and its upper profile markedly convex. The mouth terminal to slightly subterminal, the upper lip not projecting or slightly projecting beyond the tip of the lower lip. The corner of the mouth reaches to level with the lower margin of the eye or pupil.

Lateral line complete, with 75–96 scales, and almost reaching to caudal-fin base; 9–15 scale rows between lateral line and dorsal-fin origin; and 6–9 scale rows between lateral line and anal-fin origin. Dorsal fin with three simple 7½ branched rays, outer margin straight or slightly convex. Pectoral-fin with 16–18 rays, outer margin convex. Pelvic fin with seven to eight branched rays, outer margin convex. Anal fin with three simple 6½–7½ branched rays, outer margin straight or convex. The caudal fin, deeply forked.

Coloration (Not spawning period and immediately after fixation): A short dark rectangular blotch along the lateral line, between the lateral line and belly yellowish in both males and females, irregularly shaped black spots on the upper part of the flank and no dark stipe or very faintly marked narrow stripe on the middle part of flank in males. Dorsal and caudal fins slightly gray or hyaline, pectoral, pelvic and anal fins hyaline (except for some individuals). In some specimens often 10–14 short brownish bars over-imposed on the stripe. Black spot in the middle of the caudal-fin base.

Sexual dimorphism. Males with stronger and longer pectoral fins, and nuptial tubercles on the head, in both species.

Figure 4. *Phoxinus radeki* FFR 2311, from top: paratypes, 46 mm SL, male; 55 mm SL female; Türkiye: Stream Ahmetbey.

Figure 5. *Phoxinus strandjae* FFR 2312, from top: 62 mm SL male; 62 mm SL female; Türkiye: Rezve River.

Etymology. The species is named for Radek Sanda (Prague) for his contribution to the knowledge of the ichthyofaunal of Europe. A noun in genitive, indeclinable.

Distribution. *Phoxinus radeki* is presently known from the Ergene River (Ageaen Sea Basin) (Fig. 1). It inhabits the cold, well-oxygenated waters of fast-flowing mountain streams and large lowland rivers. A transboundary river known as Meriç-Ergene (Maritsa, Evros) serves as a border between Türkiye, Greece, and Bulgaria. It starts in Bulgaria and flows through Türkiye, where it forms a 203 km-long border with Greece. It is the longest river in the Balkan Region. Before flowing into the Aegean Sea, the river passes through Greece. Bulgaria (upstream), Türkiye (downstream), and Greece (downstream) are the three riparian nations in the basin. The remaining 35% of its catchment area is divided into 28% and 7% within the borders of Türkiye and Greece, respectively, while the remaining 65% of its catchment area is contained within the boundaries of Bulgaria. The border between Türkiye and Greece is formed by a piece of the Meriç River's lower course, while the remaining portion flows in Türkiye. The river emerges into the Aegean Sea from Saros. (https://floodmerg.tarimorman.gov.tr/en/meric-ergene-river-basin). It is known that after the entry of the Ergene River into the system, the water quality of the Meriç River decreased seriously and this situation adversely affected the biota (Elipek et al. 2010; Güher et al. 2011; Tokatlı 2020).

Discussion

Until 2023, only two *Phoxinus* species were known in Türkiye which are *P. colchicus* from Çoruh River (southeast of the Black Sea basin) and *P. strandjae* from the coastal rivers southwest of the Black Sea basin in Thrace region and Lake Sapanca drainage (Geiger et al. 2014; Bayçelebi et al. 2015; Saç and Özuluğ 2015; Sarı et al. 2019). Most recently, Turan et al. (2023) described *P. abanticus* from the Lake Abant drainage. The morphological characters of *Phoxinus radeki* that distinguish it from *P. abanticus* and *P. strandjae* species are given in the identification section. In addition, *Phoxinus radeki* is distinguished from *P. strymonicus*, which is distributed in the Aegean basin, by having fewer scale rows between anal-fin origin and lateral line (7–9 vs.10–13) and a slenderer caudal peduncle (8–10% SL vs. 10–12 Fig. 6). It further differs from *P. strymonicus* by scales of breast. *Phoxinus radeki* has breast scaled but separated unscaled area anteriorly, while *P. colchicus* and *P. strymonicus* have breast scaled and scaled area connected anteriorly.

The COI marker has been frequently used to identify many vertebrate and invertebrate species (Hebert et al. 2003; Hubert et al. 2008, 2015; Geiger et al. 2014). This gene region was preferred in *Phoxinus* species in previous studies, but it was observed that it was less successful in species delimitation for this genus compared to the Cyt *b* gene (Palandačić et al. 2015, 2017, 2020; Vucić et al. 2018; Corral-Lou et al. 2019). Especially within the genus *Phoxinus*, genetic differences based on COI between neighboring species appear to be lower compared to the Cyt *b* gene. (Palandačić et al. 2015, 2017, 2020). Therefore, we performed our analyses based on the Cyt *b* gene.

The findings of analyses based on the mitogenome's Cyt *b* gene proved that it diverged from valid European *Phoxinus* species and developed an independent lineage from them, supporting the morphometric findings.

Figure 6. *Phoxinus strymonicus*, NMP6V88934–88954, from top: 64 mm SL male; 62 mm SL female; Bulgaria: Strymon River.

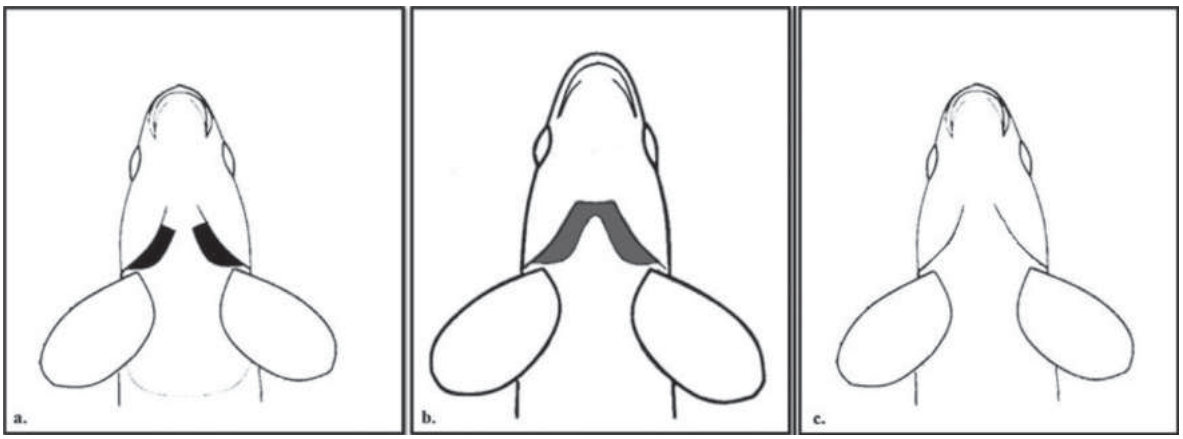

Figure 7. Breast scale shape of a. *Phoxinus radeki*,b. *P. strandjae* and c. *P. abanticus*.

The genetic characterization of the new species was carried out in the current investigation, and its first genetic record was created. This could be important for upcoming research on the genus *Phoxinus*. With the initial data of type samples, inaccurate identifications can be avoided. Previous investigations have evaluated the effectiveness of the mtDNA Cyt *b* gene in identifying genetic lineages in the genus *Phoxinus*, and those investigations have produced positive outcomes (Palandačić et al. 2015, 2017, 2020; Vucić et al. 2018; Corral-Lou et al. 2019; Turan et al. 2023). Furthermore, our findings agreed with those of previous investigations (Palandačić et al. 2015, 2017, 2020; Vucić et al. 2018; Corral-Lou et al. 2019; Turan et al. 2023).

Comparative material

Materials examined are already listed by Turan et al. (2023), except the materials listed below:

Phoxinus strymonicus NMP6V88934-88954, 17, 42–66 mm SL; Bulgaria: Elešnica River, upstream of Vaksevo Strymon River basin, 42.1364, 22.8521.

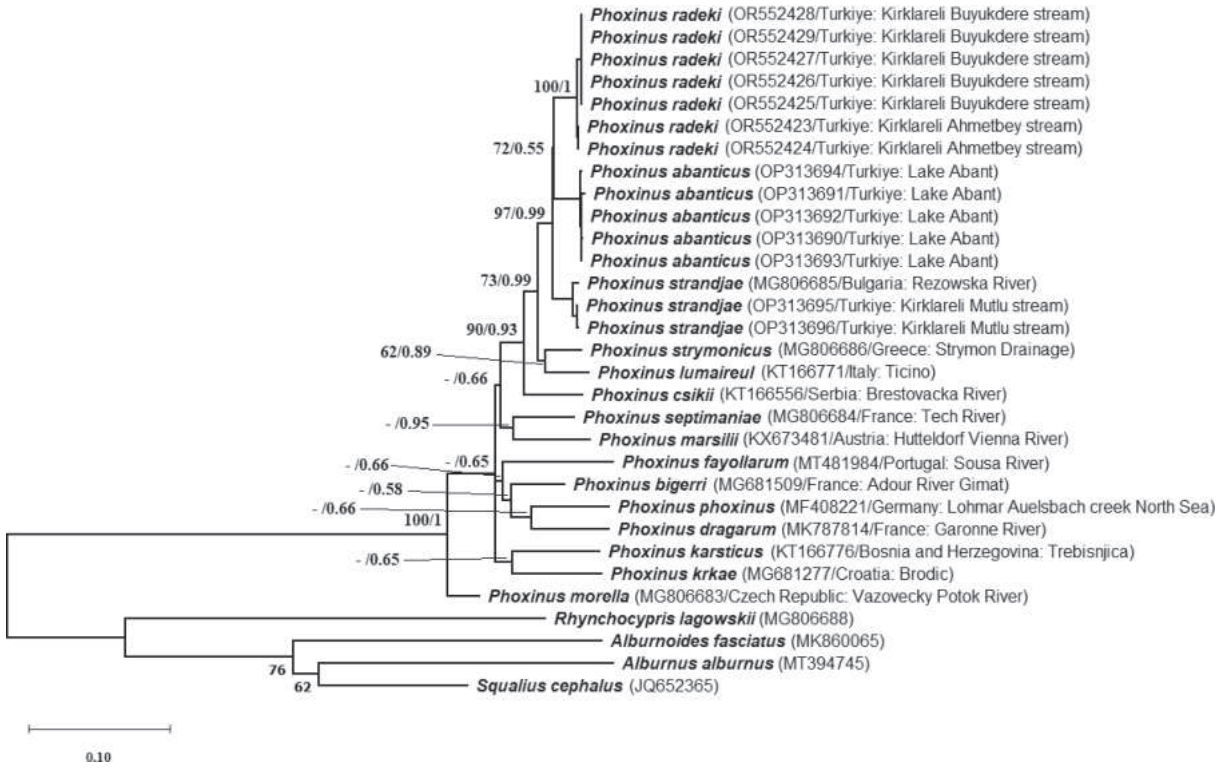

Figure 8. Maximum Likelihood (ML) phylogenetic tree reconstructed based on the Cyt *b* gene. ML and BI methods yielded the same topologies, and therefore only the ML tree is indicated. The bootstrap values of ML and posterior probability values of BI are indicated on nodes (ML/BI). The bootstrap and posterior probability values are indicated above nodes on tree if 50% and 0.5 or higher.

Table 1. Morphometry of *Phoxinus radeki* and *P. strymonicus* species. Mean values are given in parentheses.

	***P. radeki* n=38**			***P. strymonicus* n=19**	
	Aegean Sea			**Aegean Sea**	
	Ergene River			**Strymon River**	
	Range	**SD**	**H**	**Range**	**SD**
Standard length (mm)	46–61		54	47–64	
In per cent of standard length					
Head length	24.4–26.7 (25.7)	0.07	25.5	23.9–28.3 (25.8)	0.12
Body depth at dorsal-fin origin	16.0–21.1 (18.8)	0.11	19.4	18.8–21.6 (20.0)	0.08
Caudal peduncle depth	8.1–10.2 (9.2)	0.05	9.9	9.7–12.0 (10.7)	0.05
Head $width_1$ (ant. margin of the eye)	30.4–39.9 (36.2)	0.20	39.6	31.6–49.7 (38.3)	0.04
Head $width_2$ (post. margin of the eye)	47.7–55.2 (50.6)	0.16	51.0	38.6–57.6 (51.5)	0.48
Head $width_3$ (at opercle)	48.8–58.1 (53.3)	0.26	57.0	46.2–64.6 (57.2)	0.40
Head $depth_1$ at the interorbital region	44.2–53.1 (48.9)	0.21	53.1	40.7–60.1 (50.4)	0.46
Head $depth_2$ (at occiput)	57.6–69.8 (64.1)	0.28	67.7	56.9–72.0 (64.5)	0.39
Eye diameter	20.6–30.5 (25.2)	0.20	26.7	24.7–31.7 (27.6)	0.19
Snout length	25.1–32.4 (29.0)	0.19	29.7	22.3–31.6 (28.1)	0.27
Interorbital width	23.9–30.1 (27.6)	0.16	28.7	27.1–42.7 (32.6)	0.43
Snout width at nostrils	24.6–35.9 (31.2)	0.23	29.8	26.4–39.0 (32.1)	0.36
Snout depth at nostrils	25.6–35.6 (30.9)	0.23	35.6	30.1–42.9 (36.2)	0.34
Predorsal length	52.2–57.7 (55.0)	0.11	54.0	52.3–57.0 (54.3)	0.15
Prepelvic length	44.0–50.2 (46.6)	0.16	44.5	41.3–46.8 (44.6)	0.16
Preanal length	61.8–67.1 (64.2)	0.13	62.3	58.2–65.0 (62.0)	0.20
Pectoral-fin origin to anal fin	36.7–44.0 (41.0)	0.19	39.7	37.7–44.6 (41.0)	0.20
Pectoral-fin origin to pelvic fin	19.4–27.2 (23.1)	0.18	21.3	19.7–25.1 (22.3)	0.19
Pelvic-fin origin to anal fin	16.3–20.7 (17.8)	0.09	17.1	16.4–22.1 (18.6)	0.12
Caudal peduncle length	22.7–28.0 (25.3)	0.12	25.5	22.4–28.6 (26.1)	0.14
Dorsal fin height	17.0–24.3 (20.7)	0.14	21.7	17.9–23.3 (21.3)	0.15
Pectoral-fin length	16.7–22.3 (19.3)	0.15	20.7	15.6–23.4 (18.2)	0.17
Pelvic-fin length	13.1–19.6 (15.3)	0.14	16.6	13.0–17.5 (15.3)	0.13
Anal-fin length	18.9–23.2 (20.4)	0.11	22.1	16.2–21.0 (18.9)	0.13
Upper caudal-fin lobe	19.1–24.4 (21.8)	0.12	20.9	21.3–26.1 (23.6)	0.12

Material used in molecular genetic analysis

***Phoxinus abanticus*:** FFR-DNA-Ph26-27-28-29-30; Türkiye: Bolu prov., Lake Abant, 40.6647, 31.4250 (GenBank accession numbers: OP313690–OP313691–OP313692–OP313693–OP313694; Topotype samples; Turan et al. 2023).

***P. strandjae*:** FFR-DNA-Ph34-36; Türkiye: Kırklareli prov.: stream Mutlu (Rezve), 41.9422, 27.6202 (GenBank accession numbers: OP313695–OP313696; Topotype samples; Turan et al. 2023). – Bulgaria: Rezowska River (GenBank accession number: MG806685; Topotype sample; Schönhuth et al. 2018).

***P. strymonicus*:** Greece: Strymon Drainage (GenBank accession number: MG806686; Topotype sample; Schönhuth et al. 2018).

***P. csikii*:** Serbia: Brestovacka River (GenBank accession number: KT166556; Palandačić et al. 2015).

***P. septimaniae*:** France: Tech River (GenBank accession number: MG806684; Schönhuth et al. 2018).

***P. lumaireul*:** Italy: Ticino, Po River (GenBank accession number: KT166771; Topotype sample; Palandačić et al. 2015).

***P. marsilii*:** Austria: Hutteldorf Vienna River (GenBank accession number: KX673481; Topotype sample; Ramler et al. 2016).

***P. bigerri*:** France: Adour River Gimat (GenBank accession number: MG681509; Topotype sample; Vucić et al. 2018).

***P. karsticus*:** Bosnia and Herzegovina: Trebisnjica (GenBank accession number: KT166776; Topotype sample; Palandačić et al. 2015).

***P. phoxinus*:** Germany: Lohmar Auelsbach creek North Sea (GenBank accession number: MF408221; Palandačić et al. 2017).

***P. morella*:** Czech Republic: Vazovecky Potok River (GenBank accession number: MG806683; Topotype sample; Schönhuth et al. 2018).

***P. krkae*:** Croatia: Brodic (GenBank accession number: MG681277; Topotype sample; Vucić et al. 2018).

***P. fayollarum*:** Portugal: Sousa River (GenBank accession number: MT481984; Garcia-Raventós et al. 2020).

***P. dragarum*:** France: Garonne River (MK787814; Topotype sample; Corral-Lou et al. 2019).

Acknowledgements

We are pleased to thank Jörg Freyhof (Berlin) and Radek Sanda (Prague) for the loan of comparative material. We are also grateful to Hazel Baytasoglu (Rize) for producing the drawing (Fig. 7).

References

Banarescu P (1992) Zoogeography of fresh waters (Vol. II). Distribution and dispersal of freshwater animals in North America and Eurasia. AULA-Verlag, Wiesbaden.

Bayçelebi E, Turan D, Japoshvili B (2015) Fish fauna of Çoruh river and two first record for Turkey. Turkish Journal of Fisheries and Aquatic Sciences 15: 783–794. https://doi.org/10.4194/1303-2712-v15_4_01

Bektaş Y, Aksu I, Kaya C, Baycelebi E, Atasaral S, Ekmekci FG, Turan D (2019) Phylogeny and phylogeography of the genus *Alburnoides* (Teleostei, Cyprinidae) in Turkey based on mitochondrial DNA sequences. Mitochondrial DNA, Part A, DNA Mapping, Sequencing, and Analysis 30(7): 794–805. https://doi.org/10.1080/24701394.2019.1664493

Bektaş Y, Aksu I, Kaya C, Baycelebi E, Küçük F, Turan D (2020) Molecular systematics and phylogeography of the genus *Alburnus* Rafinesque, 1820 (Teleostei, Leuciscidae) in Turkey. Mitochondrial DNA, Part A, DNA Mapping, Sequencing, and Analysis 31(7): 273–284. https://doi.org/10.1080/24701394.2020.1791840

Bianco PG, De Bonis S (2015) A taxonomic study on the genus *Phoxinus* (Acthinopterigy, Cyprinidae) from Italy and western Balkans with description of four new species: *P. ketmaieri*, *P. karsticus*, *P. apollonicus* and *P. likai*. In: Bianco PG, de Filippo G (Eds) Researches on Wildlife Conservation (Vol. 4). IGF publications.

Billard R (1997) Les Poissons d'eau Douce des Rivières de France. Identification, Inventaire et Répartition des 83 Espèces. Lausanne, Delachaux & Niestlé, 192 pp.

Bogutskaya NG, Jelic D, Vucic M, Jeli M, Diripasko OA, Stefanov T, Klobucar G (2019) Description of a new species of *Phoxinus* from the upper Krka River (Adriatic Basin) in Croatia (Actinopterygii: Leuciscidae), first discovered as a molecular clade. Journal of Fish Biology 96(2): 378–393. https://doi.org/10.1111/jfb.14210

Bogutskaya NG, Diripasko OA, Palandačić A (2023) Novel data support validity of *Phoxinus chrysoprasius* (Pallas, 1814)(Actinopterygii, Leuciscidae). European Journal of Taxonomy 861: 1–20. https://doi.org/10.5852/ejt.2023.861.2061

Çiçek E, Sungur S, Fricke R, Seçer B (2023) Freshwater lampreys and fishes of Türkiye; an annotated checklist, 2023. Turkish Journal of Zoology 47(6): 324–468. https://doi.org/10.55730/1300-0179.3147

Corral-Lou A, Perea S, Aparicio E, Doadrio I (2019) Phylogeography and species delineation of the genus *Phoxinus* Rafinesque, 1820 (Actinopterygii: Leuciscidae) in the Iberian Peninsula. Journal of Zoological Systematics and Evolutionary Research 57(4): 926–941. https://doi.org/10.1111/jzs.12320

Denys GPJ, Dettaï A, Persat H, Daszkiewicz P, Hautecoeur M, Keith P (2020) Revision of *Phoxinus* in France with the description of two new species (Teleostei, Leuciscidae). Cybium 44: 205–237. https://doi.org/10.26028/cybium/2020-443-003

Dubut V, Fouquet A, Voisin A, Costedoat C, Chappaz R, Gilles A (2012) From Late Miocene to Holocene: processes of differentiation within the *Telestes* genus (Actinopterygii: Cyprinidae). PLOS ONE 7(3): e34423. https://doi.org/10.1371/journal.pone.0034423

Elipek BÇ, Arslan N, Kirgiz T, Öterler B, Güher H, Özkan N (2010) Analysis of benthic macroinvertebrates inrelation to environmental variables of Lake Gala, a National Park of Turkey. Turkish Journal of Fisheries and Aquatic Sciences 10: 235–243. https://doi.org/10.4194/trjfas.2010.0212

Eschmeyer WN, Fricke R, van der Laan R [Eds] (2023) Catalog of fishes: genera, species, references. https://researcharchive.calacademy.org/research/ichthyology/catalog/fishcatmain.asp [Electronic version accessed 06.06.2023]

Froese R, Pauly D (2023) FishBase. World Wide Web electronic publication. https://www.fishbase.org [July 2023]

Garcia-Raventós A, Martins FMS, Teixeira A, Sousa RG, Froufe E, Varanda S, Lopes-Lima M, Beja P, Filipe AF (2020) Origin and history of *Phoxinus* (Cyprinidae) introductions in the Douro Basin (Iberian Peninsula): an update inferred from genetic data. Biological Invasions 22: 2409–2419. https://doi.org/10.1007/s10530-020-02279-5

Geiger MF, Herder F, Monaghan MT, Almada V, Barbieri R, Bariche M, Berrebi P, Bohlen J, Casal-Lopez M, Delmastro GB, Denys GPJ, Dettai A, Doadrio I, Kalogianni E, Kärst H, Kottelat M, Kovačić M, Laporte M, Lorenzoni M, Marčić Z, Özuluğ M, Perdices A, Perea S, Persat H, Porcelotti S, Puzzi C, Robalo J, Šanda R, Schneider M, Šlechtová V, Stoumboudi M, Walter S, Freyhof J (2014) Spa tial heterogeneity in the Mediterranean Biodiversity Hotspot affects barcoding accuracy of its freshwater fishes. Molecular Ecology Resources 14: 1210–1221. https://doi.org/10.1111/1755-0998.12257

Güher H, Erdoğan S, Kırgız T, Elipek BÇ (2011) The Dynamics of zooplankton in National Park of Lake Gala (Edirne-Turkey). Acta Zoologica Bulgarica 63: 157–168.

Hall TA (1999) BioEdit: A user–friendly biological sequence alignment editor and analysis program for Windows 95/98/NT. Nucleic Acids Symposium Series 41: 95–98.

Hebert PDN, Cywinska A, Ball SL, deWaard JR (2003) Biological identifications through DNA barcodes. Proceedings. Biological Sciences 270(1512): 313–321. https://doi.org/10.1098/rspb.2002.2218

Hubert N, Hanner R, Holm E, Mandrak NE, Taylor E, Burridge M, Watkinson D, Dumont P, Curry A, Bentzen P, Zhang J, April J, Bernatchez L (2008) Identifying Canadian freshwater fishes through DNA barcodes. PLOS ONE 3(6): 2490–e2490. https://doi.org/10.1371/journal.pone.0002490

Hubert N, Wibowo A, Busson F, Caruso D, Sulandari S, Nafiqoh N, Pouyaud L, Rüber L, Avarre JC, Herder F, Hanner R, Keith P, Hadiaty RK (2015) DNA barcoding Indonesian freshwater fishes: Challenges and prospects. DNA Barcodes 3(1): 144–169. https://doi.org/10.1515/dna-2015-0018

Kottelat M (2007) Three new species of *Phoxinus* from Greece and southern France (Teleostei: Cyprinidae). Ichthyological Exploration of Freshwaters 18: 145–162.

Kottelat M, Freyhof J (2007) Handbook of European Freshwater Fishes. Kottelat, Cornol and Freyhof, Berlin, [xiv +] 646 pp.

Kumar S, Stecher G, Li M, Knyaz C, Tamura K (2018) MEGA X: Molecular evolutionary genetics analysis across computing platforms. Molecular Biology and Evolution 35(6): 1547–1549. https://doi.org/10.1093/molbev/msy096

Özuluğ M, Gaygusuz Ö, Gaygusuz ÇG, Kaya N, Saç G (2023) Fishes Encountered in the Turkish Thrace River Systems (Northwestern Part of Turkey). Inland Water Biology 16: 341–356. https://doi.org/10.1134/S1995082923020165

Palandačić A, Bravničar J, Zupančič P, Šanda R, Snoj A (2015) Molecular data suggest a multispecies complex of *Phoxinus* (Cyprinidae) in the Western Balkan Peninsula. Molecular Phylogenetics and Evolution 92: 118–123. https://doi.org/10.1016/j.ympev.2015.05.024

Palandačić A, Naseka A, Ramler D, Ahnelt H (2017) Contrasting morphology with molecular data: An approach to revision of species complexes based on the example of European (Cyprinidae). BMC Evolutionary Biology 17(1): e184. https://doi.org/10.1186/s12862-017-1032-x

Palandačić A, Kruckenhauser L, Ahnelt H, Mikschi E (2020) European minnows through time: Museum collections aid genetic assessment of species introductions in freshwater fishes (Cyprinidae: *Phoxinus* species complex). Heredity 124(3): 410–422. https://doi.org/10.1038/s41437-019-0292-1

Posada D (2008) jModelTest: Phylogenetic model averaging. Molecular Biology and Evolution 25(7): 1253–1256. https://doi.org/10.1093/molbev/msn083

Puillandre N, Modica MV, Zhang Y, Sirovich L, Boisselier MC, Craud C, Holford M, Samadi S (2012) Large-scale species delimitation method for hyperdiverse groups. Molecular Ecology 21(11): 2671–2691. https://doi.org/10.1111/j.1365-294X.2012.05559.x

Ramler D, Palandačić A, Delmastro GB, Wanzenböck J, Ahnelt H (2016) Morphological divergence of lake and stream *Phoxinus* of Northern Italy and the Danube basin based on geometric morphometric analysis. Ecology and Evolution 7(2): 572–584. https://doi.org/10.1002/ece3.2648

Ronquist F, Teslenko M, van Van der Mark P, Ayres DL, Darling A, Höhna S, Larget B, Liu L, Suchard MA, Huelsenbeck JP (2012) MrBayes 3.2: Efficient Bayesian phylogenetic inference and model choice across a large model space. Systematic Biology 61(3): 539–542. https://doi.org/10.1093/sysbio/sys029

Saç G, Özulug M (2015) New data on the distribution and conservation status of *Phoxinus strandjae* (Teleostei: Cyprinidae). Ichthyological Exploration of Freshwaters 25: 381–383.

Sarı HM, İlhan A, Saç G, Özuluğ M (2019) Fish fauna of Yıldız Mountains (North-Eastern Thrace, Turkey). Ege Journal of Fisheries and Aquatic Sciences, 36(1): 65–73. https://doi.org/10.12714/egejfas.2019.36.1.08

Schönhuth S, Vukić J, Šanda R, Yang L, Mayden RL, Schönhuth (2018) Phylogenetic relationships and classification of the Holarctic family Leuciscidae (Cypriniformes: Cyprinoidei). Molecular Phylogenetics and Evolution 127: 781–799. https://doi.org/10.1016/j.ympev.2018.06.026

Thompson JD, Higgins DG, Gibson TJ (1994) CLUSTAL W: Improving the sensitivity of progressive multiple sequence alignment through sequence weighting, position-specific gap penalties and weight matrix choice. Nucleic Acids Research 22(22): 4673–4680. https://doi.org/10.1093/nar/22.22.4673

Tokatlı C (2020) Ergene Nehir Havzası Su Kalitesinin Çok Değişkenli İstatistik Analizler Kullanılarak Değerlendirilmesi. LimnoFish. 6(1): 38–46. https://doi.org/10.17216/limnofish.524036

Turan D, Bayçelebi E, Özuluğ M, Gaygusuz Ö, Aksu İ (2023) *Phoxinus abanticus*, a new species from the Lake Abant drainage in Türkiye (Teleostei: Leuciscidae). Journal of Fish Biology 102(5): 1157–1167. https://doi.org/10.1111/jfb.15371

Vucić M, Jelić D, Žutinić P, Grandjean F, Jelić M (2018) Distribution of Eurasian minnows (*Phoxinus*: Cypriniformes) in the western Balkans. Knowledge and Management of Aquatic Ecosystems 419: 1–11. https://doi.org/10.1051/kmae/2017051

Zoosyst. Evol. 100 (1) 2024, 111–118 | DOI 10.3897/zse.100.115692

PENSOFT

für Natur MUSEUM FÜR NATURKUNDE BERLIN

Molecular characterization and phylogenetic position of the giant deep-sea oyster *Neopycnodonte zibrowii* Gofas, Salas & Taviani, 2009

Matteo Garzia[1], Daniele Salvi[1]

1 *Department of Health, Life & Environmental Sciences - University of L'Aquila,Via Vetoio snc, 67100 L'Aquila-Coppito, Italy*

https://zoobank.org/7DB92668-7DCA-4F0D-B6AB-8C74C3EC6B89

Corresponding author: Daniele Salvi (danielesalvi.bio@gmail.com)

Academic editor: M. Glaubrecht ♦ **Received** 13 November 2023 ♦ **Accepted** 3 January 2024 ♦ **Published** 26 January 2024

Abstract

The giant deep-sea oyster *Neopycnodonte zibrowii* Gofas, C. Salas & Taviani, 2009 is a keystone deep-sea habitat builder species. Discovered about fifteen years ago in the Azores, it has been described and assigned to the genus *Neopycnodonte* Fischer von Waldheim, 1835 based on morphological features. In this study, we generated DNA sequence data for both mitochondrial (COI and 16S) and nuclear (ITS2 and 28S) markers based on the holotype specimen of *N. zibrowii* to establish a molecular phylogenetic framework for the systematic assessment of this species and to provide a reliable (i.e., holotype-based) reference sequence set for multilocus DNA barcoding approaches. Molecular data provide compelling evidence that the giant deep-sea oyster is a distinct species, rather than a deep-water ecophenotype of *Neopycnodonte cochlear* (Poli, 1795), with extremely high genetic divergence from any other gryphaeid. Multilocus phylogenetic analyses place the giant deep-sea oyster within the clade "*Neopycnodonte*/*Pycnodonte*" with closer affinity to *N. cochlear* rather than to *P. taniguchii* Hayami & Kase, 1992, thus supporting its assignment to the genus *Neopycnodonte*. Relationships within this clade are not well supported because mitochondrial variation is inflated by saturation that eroded phylogenetic signal, implying an old split between taxa within this clade. Finally, the set of reference barcode sequences of *N. zibrowii* generated in this study will be useful for a wide plethora of barcoding applications in deep-sea biodiversity surveys. Molecular validation of recent records of deep-sea oysters from the Atlantic Ocean and the Mediterranean Sea will be crucial to clarify the distribution of *N. zibrowii* and assess the phenotypic variation and ecology of this enigmatic species.

Key Words

Azores, DNA sequences, Gryphaeidae, holotype, molecular systematics, Mollusca, multilocus phylogeny, Natural History Museum

Introduction

Deep-sea is the Earth's largest biome but it is still one of the most underexplored regions (Ramirez-Llodra et al. 2010). Deep-sea biodiversity is mostly unknown due to the extreme environmental conditions that limits sampling capabilities (Rogers et al. 2015; Sinniger et al. 2016; Woodall et al. 2018). Along with advances in exploration technologies (Feng et al. 2022), new molecular technologies such as high-throughput sequencing and the molecular identification of multiple species in environmental DNA (eDNA metabarcoding; Taberlet et al. 2012) have boosted deep-sea biodiversity assessments (Guardiola et al. 2016; Everett and Park 2018). However, the low number of reference sequences taxonomically validated in online repository databases (e.g. GenBank) limits the identifications of MOTUs (Molecular Operational Taxonomic Unit), thus reducing the taxonomic resolution of eDNA studies (Ruppert et al. 2019). Studies using an integrative taxonomic approach − combining molecular, morphological and environmental data − on new deep-sea taxa have been carried out in several groups of organisms, such as Anthozoa (López-González et al. 2022), Mollusca (Xu et al. 2019), and some others (Silva et al. 2016; Błażewicz et al. 2019). However, while molecular data are still not available for a great portion of known

deep-sea biodiversity, deep-sea exploration has continued, contributing to the discovery of new benthic ecosystems and associated communities. Therefore, there is a great need to constantly improve with reliable reference sequences the taxonomic coverage of deep-sea taxa in repository databases.

In this study, we focused on a keystone deep-sea habitat builder species discovered about fifteen years ago in the Azores Archipelago: the giant deep-sea oyster *Neopycnodonte zibrowii* Gofas, C. Salas & Taviani, 2009 (Gryphaeidae Vialov, 1936) (Wisshak et al. 2009b). This reef-forming oyster was first observed during a submersible dive along the Faial Channel (480–500 meter depth) (Wisshak et al. 2009b). Deep-sea reefs of *N. zibrowii* are built by both stacked living and dead specimens on vertical rocky substrate of seamounts, escarpments and in canyons (Beuck et al. 2016), and host peculiar deep-sea communities. Benthic associations between *N. zibrowii* and the cyrtocrinid *Cyathidium foresti* Cherbonnier & Guille, 1972 have been documented in the Atlantic Ocean (Wisshak et al. 2009a), and between *N. zibrowii* and cold-water corals in both the Atlantic Ocean (Van Rooij et al. 2010) and the Mediterranean Sea (Taviani et al. 2017, 2019). Recently, new records and observations on *N. zibrowii* in the Atlantic Ocean allowed updating its ecology and distribution (Beuck et al. 2016). The giant deep-sea oyster has been meticulously described in terms of external morphology, microstructures of shell and anatomy (Wisshak et al. 2009b). The systematic placement of this species in the genus *Neopycnodonte* was based on morphological characteristics such as the circular muscle scar, the enlarged vermiculate chomata (see 'neopycnodontine chomata' in Harry 1985) and the vesicular structures in the inner shell layer. *Neopycnodonte zibrowii* is morphologically different from the only extant congeneric species *Neopycnodonte cochlear* (Poli, 1795) in several characters such as the shell architecture and outline, the absence of the resilifer bulge in the latter species and the shape and thickness of the vesicular microstructures. On the other hand, 15 years on from its discovery, molecular data are still not available for this species, thus limiting the assessment of its phylogenetic position and systematic placement.

The taxonomic assessment of oysters based on morphology can be challenging due to a high shell variability and a low number of diagnostic characters (Lam and Morton 2006; Raith et al. 2015; Salvi et al. 2021). Molecular data have a key role in species delimitation and taxonomic identification of oyster species (Lam and Morton 2003; Bieler et al. 2004; Kirkendale et al. 2004; Al-Kandari et al. 2021; Salvi et al. 2022) and would provide compelling evidence that the giant deep-sea oyster *N. zibrowii* is a distinct species rather than a deep-water ecophenotype of *N. cochlear* (Wisshak et al. 2009b).

In this study, we generated DNA sequence data of the giant deep-sea oyster *N. zibrowii* for both mitochondrial and nuclear markers based on the holotype and performed a multilocus phylogenetic analyses to establish its relationships with other gryphaeids. The main aims of this study are to provide: (i) a molecular phylogenetic framework for the systematic assessment of the giant deep-sea oyster, and (ii) a reliable (i.e., holotype-based) reference sequence set for multilocus DNA barcoding approaches.

Materials and methods

Specimens and sequence data gathering

We gathered tissue samples for molecular analyses from museum collections and by field collection. The holotype of *N. zibrowii* (MNHN-IM-2000-20888) and the specimen of *Hyotissa numisma* (Lamarck, 1819) (MNHN-IM-2013-13700) are deposited at the National Museum of Natural History (MNHN) of Paris, while the specimen of *Pycnodonte taniguchii* Hayami & Kase, 1992 (UF 280382) is preserved in the collection of Florida Museum of Natural History (FLMNH). *Neopycnodonte cochlear* (OS239) was collected during scuba diving off the coast of Civitavecchia (nearby Rome, Italy) and stored in pure ethanol. Total genomic DNA was extracted from adductor muscles following standard high-salt protocols (Sambrook et al. 1989). We amplified two mitochondrial − cytochrome oxidase subunit I (COI) and 16S rRNA (16S) − and two nuclear − 28S rRNA (28S) and ITS2 rRNA (ITS2) − gene fragments by polymerase chain reaction (PCR). Primers and conditions used for the amplification are reported in Table 2. Sequencing of PCR products was carried out by the company Genewiz® (https://www.genewiz.com), using the same primers employed for amplification. Sequences generated from these specimens were complemented with sequences obtained from GenBank for additional gryphaeid species. Localities and GenBank accession numbers of sequences used for molecular analyses are shown in Table 1. GenBank sequences were selected in order to minimise the use of chimeric sequences in concatenated alignments (i.e., sequences of different gene fragments obtained from different voucher specimens), therefore whenever possible for each species we selected mitochondrial (COI and 16S) and nuclear (28S and ITS2) sequences from the same voucher. Three specimens (*Hyotissa hyotis* #2, *Hyotissa imbricata* and *N. cochlear* #1) have GenBank sequences from different vouchers (chimeric concatenated sequences). We validated the taxonomic identification of each of these vouchers based on single-gene NJ trees. First, we built four single-gene datasets (COI, 16S, 28S and ITS2) including all the sequences of Gryphaeidae species in GenBank and our sequences. Then for each marker we selected GenBank sequences that clustered within the same clade of conspecific vouchers we sequenced (*H. hyotis* #1 and *N. cochlear* #1) or that have a congruent phylogenetic placement among the four single-gene datasets (*H. imbricata*) (results not shown).

Table 1. Details on the species and DNA sequence data used in this study. Asterisks indicate specimens sequenced in this study. GenBank data are as follows: [1]: Matsumoto 2003; [2]: Matsumoto and Hashimoto unpublished; [3]: Kirkendale et al. 2004; [4]: Plazzi and Passamonti 2010; [5]: Kim et al. 2009; [6]: Plazzi et al. 2011; [7]: Li et al. unpublished; [8]: Ren et al. 2016; [9]: Salvi et al. 2014; [10]: Ip et al. 2022.

Specimen	Locality	Genbank accession number			
		COI	16S	28S	ITS2
Hyotissa hyotis #1	Madagascar	GQ166583[6]	GQ166564[6]	–	–
Hyotissa hyotis #2	Singapore (COI); Maldives (16S and ITS2)	OM946450[10]	LM993886[8]	–	LM993876[9]
Hyotissa imbricata	Japan: Okinawa (COI and ITS2); China: Beibu Bay (16S and 28S)	AB076917[1]	KC847136[7]	KC847157[7]	AB102758[2]
Hyotissa numisma #1	Guam	–	AY376598[4]	AF137035[3]	–
Hyotissa numisma #2 *	Papua New Guinea: Rempi Area	–	PP070396	PP070400	–
Neopycnodonte cochlear #1	Italy: Mediterranean Sea (COI, 16S and ITS2)	JF496772[6]	JF496758[6]	–	LM993878[9]
Neopycnodonte cochlear #2 *	Italy: Civitavecchia	PP069758	PP070397	PP070401	PP074322
Neopycnodonte zibrowii *	Azores: Faial Channel	PP069759	PP070398	PP070402	PP074323
Pycnodonte taniguchii #1	Japan: Okinawa	AB076916[1]	–	AB102759[2]	–
Pycnodonte taniguchii #2 *	Indonesia: Sulawesi Island	PP069760	PP070399	PP070403	PP082050
Magallana gigas (outgroup)	Japan (COI, 16S and 28S); South Korea (ITS2)	KJ855241[8]	KJ855241[8]	AB102757[2]	EU072458[5]

Table 2. Primers used in this study: forward primers are listed above and reverse primers below. For the COI and ITS2 gene fragments we designed new primers specific to Ostreoidea Rafinesque, 1815, and we used the following PCR cycling conditions: denaturation step: 94 °C / 3 min; 35 cycles of: 94 °C / 60 s, T° annealing (COI: 49 °C; ITS2: 50 °C) / 60 s, 72 °C / 60 s; final extension: 10 min at 72 °C.

Gene	Primer	Sequence	Reference	Notes
COI	MolI-F	5′ – ATAATYGGNGGNTTTGGNAAYTG – 3′	This study	Dr Zuccon D. (MNHN), pers. comm.
	osHCO998-R	5′ – ACRGTIGCIGCICTRAARTAAGCICG – 3′		Salvi et al., in prep
16S	16Sar-L	5′ – CGCCTGTTTATCAAAAACAT – 3′	Salvi et al. (2010)	
	16Sbr-H	5′ – CCGGTCTGAACTCAGATCAC – 3′		
28S	D1F-OS	5′ – GAGACTACGCCCTGAACTTAAGCAT – 3′	This study	
	D6R-OS	5′ – GCTATCCTGAGGGAAACYTCAGAGG – 3′	Salvi et al. (2022)	
ITS2	its3d-OS	5′ – GGGTCGATGAAGARCGCAGC – 3′	This study	Modified from Oliverio and Mariottini (2001)
	its4r-OS	5′ – CCTAGTTAGTTTCTTTTCCTGC – 3′		

Phylogenetic analyses

Newly generated sequences for each marker were used as query in BLAST searches (blastn algorithm) using default settings to evaluate contaminants and to confirm the identification of the specimens from family to species level. Multiple sequence alignments of each marker were performed with MAFFT v.7 (Katoh et al. 2019) using the G-INS-I iterative refinement algorithm for the COI and the E-INS-i iterative refinement algorithm for the rRNA markers. GBlocks (Castresana 2000) was used to remove poorly aligned and ambiguous position of the hypervariable regions of the rRNA alignments using a relaxed selection of blocks (Talavera and Castresana 2007). Single-gene alignments were concatenated using the software SequenceMatrix (Vaidya et al. 2011).

Phylogenetic relationships were inferred using Maximum Likelihood (ML) and Bayesian Inference (BI) methods. We used the oyster *Magallana gigas* (Thunberg, 1793) as outgroup based on previous phylogenetic studies (Tëmkin 2010; Plazzi et al. 2011). ML analyses were performed in the W-IQ-TREE web server v.1.6.12 [http://iqtree.cibiv.univie.ac.at/; (Trifinopoulos et al. 2016)] based on a partitioned substitution model. For each gene partition, the best substitution model was calculated by the ModelFinder module (Kalyaanamoorthy et al. 2017) using an edge-linked model and the BIC criterion (COI: TPM2u+F+G4; 16S: HKY+F+G4; 28S: TN+F+G4; ITS2: K2P+G4). ML analysis was performed with 1,000 pseudo-replicates of ultrafast bootstrapping [uBS; (Minh et al. 2013)]. Bayesian analyses (BA) were carried out with MrBayes v.3.2.7 (Ronquist et al. 2012), using the substitution models selected by ModelFinder for each gene partition. We ran two Markov chains of two million generations each, with a sample frequency of 200 generations. Convergence of the runs (ESS values > 200) were checked with Tracer 1.7 (Rambaut et al. 2018) after a burn-in of 25%. Nodal support was estimated as Bayesian posterior probability (BPP). FigTree v.1.4.4 (http://tree.bio.ed.ac.uk/software/figtree/) was used to visualize both ML and BI trees.

Genetic divergence between species at each marker (COI, 16S, 28S and ITS2) were calculated using both uncorrected genetic distance (*p*-distance) and genetic distance corrected under the Kimura 2-paramer model (K2P-distance) using the software Mega11 and the option "*Compute Between Groups Mean Distance*" (Tamura et al. 2021).

Results

BLAST searches using mitochondrial sequences (COI and 16S) of the newly sequenced specimens of *H. numisma*, *N. cochlear* and *P. taniguchii* confirmed the taxonomic identifications of these species (sequence identity of 99–100%). BLAST searches using the mitochondrial sequences generated from the holotype of *N. zibrowii* recovered as best hits sequences belonging to Gryphaeidae species (COI: sequence identity of 73.2%/72.5%/73.1% with GenBank sequences of *Hyotissa* sp./*Neopycnodonte* sp./*Pycnodonte* sp. respectively; 16S: sequence identity of 87.3%/87.5% with GenBank sequences of *Hyotissa* sp./*Neopycnodonte* sp. respectively). This confirms the lack of contamination during the amplification and the affiliation of this species to Gryphaeidae.

The concatenated dataset included 2409 positions (COI: 455, 16S: 449, 28S: 1078, ITS2: 427 positions) and among the 828 variable positions 436 were phylogenetically informative (i.e., parsimony informative). Maximum likelihood and Bayesian trees show two main clades: one including *Hyotissa* species (uBS = 95; BPP = 1), and the other one including *Pycnodonte* and *Neopycnodonte* species (uBS = 83; BPP = 0.94) (Fig. 1). *Neopycnodonte zibrowii* is nested within the second clade with a sister relationship with *N. cochlear* (uBS = 56; BPP = 0.72), whereas *P. taniguchii* is sister to *Neopycnodonte* species.

The COI genetic distances (K2P/*p*-distance) between *N. zibrowii* and *N. cochlear* and between *N. zibrowii* and *P. taniguchii* are respectively 35.8%/28.2% and 35%/27.6% (Table 3). The 16S genetic distances (K2P/*p*-distance) between *N. zibrowii* and either *N. cochlear* or *P. taniguchii* are 13.5%/12.1% (Table 3). The mean interspecific genetic distances (K2P/*p*-distance) among the six gryphaeid species are 33.7% ± 4.6% / 26.8% ± 3% at the COI and 15.5% ± 4.6%/13.7% ± 3.7% at the 16S. The 28S genetic distances (K2P/*p*-distance) between *N. zibrowii* and *N. cochlear* and between *N. zibrowii* and *P. taniguchii* are respectively 2.5%/2.4% and 9%/8.4% (Table 4). The ITS2 genetic distances (K2P/*p*-distance) between *N. zibrowii* and *N. cochlear* and between *N. zibrowii* and *P. taniguchii* are respectively 15.8%/14.9% and 38.2%/29.6% (Table 4). The mean interspecific genetic distances (K2P/*p*-distance) among the six gryphaeid species are 5.5% ± 2.5% / 5.1% ± 2.2% at the 28S and 27.4% ± 16.8% / 22.0% ± 11.9% at the ITS2.

Discussion

Benthic organisms such as oysters, with extensive phenotypic variation and few diagnostic characters, are prone to misidentification in morphological assessments. The utility of molecular characters for taxonomic identification

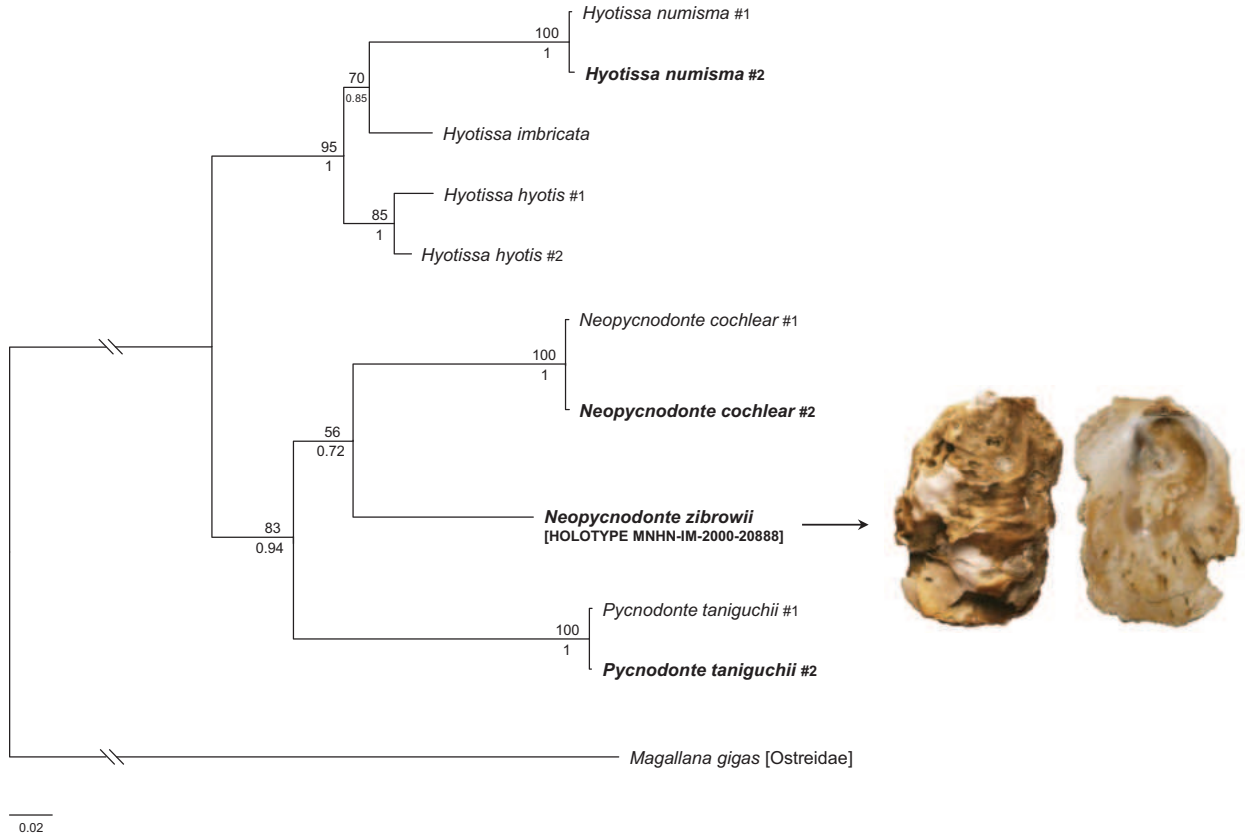

Figure 1. Bayesian phylogenetic tree of six Gryphaeidae species based on COI, 16S, 28S and ITS2 markers. Nodal supports indicate the values of uBS (upper) and the BPP (lower). The tree is rooted with *Magallana gigas* which belongs to the sister family Ostreidae Rafinesque, 1815. Specimens sequenced in this study are highlighted in bold.

Table 3. Mean genetic distance based on COI (lower triangular matrix) and 16S (upper triangular matrix) DNA sequences, calculated using the K2P model (first value) and uncorrected (*p*-distance: value inside brackets). The COI and 16S dataset are composed by 2 sequences for each species, except for *N. zibrowii* (one sequence for each marker), *H. imbricata* (one COI and one 16S sequence) and *P. taniguchii* (one 16S sequence), see Table 1; n. a.: not available.

	Neopycnodonte zibrowii	***Neopycnodonte cochlear***	***Pycnodonte taniguchii***	***Hyotissa hyotis***	***Hyotissa numisma***	***Hyotissa imbricata***
Neopycnodonte zibrowii	–	13.5% (12.1%)	13.5% (12.1%)	15.1% (13.4%)	23.5% (19.9%)	14.9% (13.3%)
Neopycnodonte cochlear	35.8% (28.2%)	–	11.2% (10.3%)	15.5% (13.8%)	22.9% (19.5%)	14.9% (13.4%)
Pycnodonte taniguchii	35.0% (27.6%)	35.4% (28.1%)	—	14.9% (13.3%)	22.3% (19.0%)	14.2% (12.7%)
Hyotissa hyotis	33.3% (26.7%)	39.6% (30.5%)	32.7% (26.5%)	–	15.6% (13.9%)	5.3% (5.1%)
Hyotissa numisma	n. a.	n. a.	n. a.	n. a.	–	15.1% (13.6%)
Hyotissa imbricata	34.0% (27.2%)	37.0% (28.8%)	31.8% (25.8%)	22.4% (19.1%)	n. a.	–

Table 4. Mean genetic distance based on 28S (lower triangular matrix) and ITS2 (upper triangular matrix) DNA sequences, calculated using the K2P model (first value) and uncorrected (*p*-distance: value inside brackets). The 28S and ITS2 dataset are composed by 2 sequences for each species, except for *N. zibrowii* (one sequence for each marker), *H. hyotis* (one ITS2 sequence and no 28S sequence), *N. cochlear* (one 28S sequence) and *P. taniguchii* (one ITS2 sequence), see Table 1. The ITS2 sequence of *H. imbricata* was not used for genetic distance calculation because it was too short; n. a.: not available.

	Neopycnodonte zibrowii	***Neopycnodonte cochlear***	***Pycnodonte taniguchii***	***Hyotissa hyotis***	***Hyotissa numisma***	***Hyotissa imbricata***
Neopycnodonte zibrowii	–	15.8% (14.9%)	38.2% (29.6%)	23.8% (20.4%)	n. a.	n. a.
Neopycnodonte cochlear	2.5% (2.4%)	–	43.5% (33.0%)	20.9% (19.4%)	n. a.	n. a.
Pycnodonte taniguchii	9.0% (8.4%)	4.4% (4.2%)	–	48.4% (35.4%)	n. a.	n. a.
Hyotissa hyotis	n. a.	n. a.	n. a.	–	n. a.	n. a.
Hyotissa numisma	6.8% (6.5%)	4.4% (4.2%)	7.3% (6.9%)	n. a.	–	n. a.
Hyotissa imbricata	6.8% (6.5%)	4.6% (4.4%)	7.7% (6.3%)	n. a.	1.2% (1.2%)	–

and systematic assessment of these organisms cannot be overstated and has been proven over and over by studies on true oysters (Lam and Morton 2006; Raith et al. 2015; Salvi et al. 2021), pearl oysters (Cunha et al. 2011), tree oysters (Garzia et al. 2022) as well as gryphaeid oysters (Li et al. 2023). Conchological convergence, phenotypic plasticity, and the occurrence of cryptic species make molecular taxonomic validation of new oyster species necessary to accurately estimate the diversity of these taxa.

Our molecular phylogenetic results clearly demonstrate that *N. zibrowii* is a distinct species with extremely high genetic divergence from any other gryphaeid at all the markers analysed (Tables 3, 4). *Neopycnodonte zibrowii* is nested within the clade "*Neopycnodonte*/*Pycnodonte*" with closer affinity to *N. cochlear* rather than *P. taniguchii* (Fig. 1), and thus supporting its assignment to the genus *Neopycnodonte* Fischer von Waldheim, 1835 based on morphological features (Wisshak et al. 2009b). Phylogenetic relationships within this clade are not well-supported, like in a previous phylogenetic study including *N. cochlear* and *P. taniguchii* and based on COI and 28S markers (Li et al. 2021). However, the extended dataset of our study improved nodal support and allowed us to clarify the source of phylogenetic uncertainty. Indeed, at both mitochondrial markers, values of pairwise genetic distance between *N. cochlear* / *N. zibrowii* / *P. taniguchii* are similar and remarkably high (COI: 35.0–35.8%; 16S: 11.2–13.5%); whereas at nuclear markers the genetic distance between *P. taniguchii* and *N. zibrowii* is two-three times higher than between the latter and *N. cochlear* (Table 4). Such a pattern suggests that mitochondrial variation is inflated by saturation that eroded phylogenetic signal, implying an old split between taxa within this clade. Wisshak et al. (2009b) highlighted a low number of morphological and ecological differences between the genus *Neopycnodonte* and *Pycnodonte* Fischer von Waldheim, 1835 and pointed out the need for a systematic revision of the genera. Our results highlight that nuclear data will have a key role in further systematic assessment of these genera.

The availability of taxonomically validated reference sequence is a premise for DNA barcoding and metabarcoding approaches for large-scale, fast, and cost-effective molecular taxonomic identification (Hebert et al. 2003; Moritz and Cicero 2004; Schindel and Miller 2005; Salvi et al. 2020). The mitochondrial COI and 16S are the most common markers in DNA barcoding studies on Ostreidae and Gryphaeidae (Lam and Morton 2003, 2004, 2006; Kirkendale et al. 2004; Liu et al. 2011; Hsiao et al. 2016; Salvi et al. 2021). However, also nuclear rRNA markers such as 28S (Mazón-Suástegui et al. 2016) and ITS2 (Salvi et al. 2014; Salvi and Mariottini 2017) have proven useful for molecular taxonomic identification of oysters. Moreover, rRNA markers are frequently selected as target genes in eDNA metabarcoding projects (Ruppert et al. 2019). In this respect, the set of four reference (holotype-based) barcode sequences of *N. zibrowii* provided in this study will be useful for a wide plethora of barcoding applications in deep-sea biodiversity surveys. During the last decade, deep-sea oysters from a mounting number of regions across the Atlantic Ocean and the Mediterranean Sea have been morphologically identified as *N. zibrowii*: from Bay of Biscay (Van Rooij et al. 2010), Gulf of Cadiz (Gofas et al. 2010), Celtic Sea (Johnson et al. 2013), Angola and Mauritania (Beuck et al. 2016), southern Sardinia (Taviani et al. 2017), Sicilian Channel (Rueda et al. 2019) and Gulf of Naples (Taviani et al. 2019). Molecular validation of these records will be crucial to clarify the distribution of *N. zibrowii* and assess the phenotypic variation and ecology of this enigmatic species. Finally, given the high prevalence of cryptic species in oysters, it is not unlikely that future molecular assessments of deep-sea oysters will disclose new species.

Acknowledgements

The authors wish to thank Philippe Bouchet (Muséum National d'Histoire Naturelle, Paris) and Serge Gofas (Universidad de Málaga) for the access to holotype material, Paolo Mariottini for the specimen of *Neopycnodonte cochlear* and to Gustav Paulay (FLMNH) for the specimens of *Pycnodonte taniguchii*. MG is supported by the SYNTHESYS Project "Synthesys FR-TAF Call3_040" at The Muséum National d'Histoire Naturelle (MNHN, Paris) and the research grant of the Symposium in honour of Philippe Bouchet (World Congress of Malacology 2022 - LMU Munich). This work is part of the PhD thesis of MG under the supervision of DS ("Health and Environmental Sciences" PhD Program, University of L'Aquila).

References

Al-Kandari M, Oliver PG, Salvi D (2021) Molecular and morphological systematics of a new, reef forming, cupped oyster from the northern Arabian Gulf: *Talonostrea salpinx* new species. ZooKeys 1043: 1–20. https://doi.org/10.3897/zookeys.1043.66992

Beuck L, Aguilar R, Fabri MC, Freiwald A, Gofas S, Hebbeln D, López Correa M, Ramos A, Ramil F, Sánchez F, Taviani M, Wienberg C, Wisshak M, Zibrowius H (2016) Biotope characterisation and compiled geographical distribution of the deepwater oyster *Neopycnodonte zibrowii* in the Atlantic Ocean and Mediterranean Sea. In: Centro Oceanográfico de Vigo. http://www.repositorio.ieo.es/e-ieo/handle/10508/10677

Bieler R, Mikkelsen PM, Lee T, Foighil DÓ (2004) Discovery of the Indo-Pacific oyster *Hyotissa hyotis* (Linnaeus, 1758) in the Florida Keys (Bivalvia: Gryphaeidae). Molluscan Research 24(3): 149–159. https://doi.org/10.1071/MR04013

Błażewicz M, Jóźwiak P, Jennings RM, Studzian M, Frutos I (2019) Integrative systematics and ecology of a new deep-sea family of tanaidacean crustaceans. Scientific Reports 9(1): 18720. https://doi.org/10.1038/s41598-019-53446-1

Castresana J (2000) Selection of conserved blocks from multiple alignments for their use in phylogenetic analysis. Molecular Biology and Evolution 17(4): 540–552. https://doi.org/10.1093/oxfordjournals.molbev.a026334

Cunha RL, Blanc F, Bonhomme F, Arnaud-Haond S (2011) Evolutionary patterns in pearl oysters of the genus *Pinctada* (Bivalvia: Pteriidae). Marine Biotechnology (New York, N.Y.) 13(2): 181–192. https://doi.org/10.1007/s10126-010-9278-y

Everett MV, Park LK (2018) Exploring deep-water coral communities using environmental DNA. Deep-sea Research, Part II, Topical Studies in Oceanography 150: 229–241. https://doi.org/10.1016/j.dsr2.2017.09.008

Feng J-C, Liang J, Cai Y, Zhang S, Xue J, Yang Z (2022) Deep-sea organisms research oriented by deep-sea technologies development. Science Bulletin 67(17): 1802–1816. https://doi.org/10.1016/j.scib.2022.07.016

Garzia M, Furfaro G, Renda W, Rosati A-M, Mariottini P, Giacobbe S (2022) Mediterranean spreading of the bicolor purse oyster, *Isognomon bicolor*, and the chicken trigger, *Malleus* sp., vs. the Lessepsian prejudice. Mediterranean Marine Science 23(4): 777–788. https://doi.org/10.12681/mms.29218

Gofas S, Rueda JL, Salas C, Díaz-Del-Río V (2010) A new record of the giant deep-sea oyster *Neopycnodonte zibrowii* in the Gulf of Cadiz (south-western Iberian Peninsula). Marine Biodiversity Records 3: e72. https://doi.org/10.1017/S1755267210000618

Guardiola M, Wangensteen OS, Taberlet P, Coissac E, Uriz MJ, Turon X (2016) Spatio-temporal monitoring of deep-sea communities using metabarcoding of sediment DNA and RNA. PeerJ 4: e2807. https://doi.org/10.7717/peerj.2807

Harry HW (1985) Synopsis of the supraspecific classification of the living oysters (Gryphaeidae and Ostreidae). The Veliger 28: 121–158.

Hebert PDN, Cywinska A, Ball SL, deWaard JR (2003) Biological identifications through DNA barcodes. Proceedings. Biological Sciences 270(1512): 313–321. https://doi.org/10.1098/rspb.2002.2218

Hsiao S-T, Chuang S-C, Chen K-S, Ho P-H, Wu C-L, Chen CA (2016) DNA barcoding reveals that the common cupped oyster in Taiwan is the Portuguese oyster *Crassostrea angulata* (Ostreoida; Ostreidae), not *C. gigas*. Scientific Reports 6(1): 34057. https://doi.org/10.1038/srep34057

Ip YCA, Chang JJM, Oh RM, Quek ZBR, Chan YKS, Bauman AG, Huang D (2022) Seq' and ARMS shall find: DNA (meta)barcoding of Autonomous Reef Monitoring Structures across the tree of life uncovers hidden cryptobiome of tropical urban coral reefs. Molecular Ecology 32(23): 6223–6242. https://doi.org/10.1111/mec.16568

Johnson MP, White M, Wilson A, Würzberg L, Schwabe E, Folch H, Allcock AL (2013) A vertical wall dominated by *Acesta excavata* and *Neopycnodonte zibrowii*, part of an undersampled group of deep-sea habitats. PLoS ONE 8(11): e79917. https://doi.org/10.1371/journal.pone.0079917

Kalyaanamoorthy S, Minh BQ, Wong TKF, von Haeseler A, Jermiin LS (2017) ModelFinder: Fast model selection for accurate phylogenetic estimates. Nature Methods 14(6): 587–589. https://doi.org/10.1038/nmeth.4285

Katoh K, Rozewicki J, Yamada KD (2019) MAFFT online service: Multiple sequence alignment, interactive sequence choice and visualization. Briefings in Bioinformatics 20(4): 1160–1166. https://doi.org/10.1093/bib/bbx108

Kim W-J, Lee J-H, Kim K-K, Kim Y-O, Nam B-H, Kong H-J, Jung H-T (2009) Genetic relationships of four Korean oysters based on RAPD and nuclear rDNA ITS sequence analyses. The Korean Journal of Malacology 25: 41–49.

Kirkendale L, Lee T, Baker P, Ó Foighil D (2004) Oysters of the Conch Republic (Florida Keys): A molecular phylogenetic study of *Parahyotissa mcgintyi*, *Teskeyostrea weberi* and *Ostreola equestris*. Malacologia 46: 309–326.

Lam K, Morton B (2003) Mitochondrial DNA and morphological identification of a new species of Crassostrea (Bivalvia: Ostreidae) cultured for centuries in the Pearl River Delta, Hong Kong, China. Aquaculture (Amsterdam, Netherlands) 228: 1–13. https://doi.org/10.1016/S0044-8486(03)00215-1

Lam K, Morton B (2004) The oysters of Hong Kong (Bivalvia: Ostreidae and Gryphaeidae). The Raffles Bulletin Of Zoology 52: 11–28.

Lam K, Morton B (2006) Morphological and mitochondrial-DNA analysis of the Indo-West Pacific rock oysters (Ostreidae: *Saccostrea* species). The Journal of Molluscan Studies 72(3): 235–245. https://doi.org/10.1093/mollus/eyl002

Li C, Kou Q, Zhang Z, Hu L, Huang W, Cui Z, Liu Y, Ma P, Wang H (2021) Reconstruction of the evolutionary biogeography reveal the origins and diversification of oysters (Bivalvia: Ostreidae). Molecular Phylogenetics and Evolution 164: 107268. https://doi.org/10.1016/j.ympev.2021.107268

Li F, Liu H, Heng X, Zhang Y, Fan M, Wang S, Liu C, Gu Z, Wang A, Yang Y (2023) The complete mitochondrial genome of *Hyotissa sinensis* (Bivalvia, Ostreoidea) indicates the genetic diversity within Gryphaeidae. Biodiversity Data Journal 11: e101333. https://doi.org/10.3897/BDJ.11.e101333

Liu J, Li Q, Kong L, Yu H, Zheng X (2011) Identifying the true oysters (Bivalvia: Ostreidae) with mitochondrial phylogeny and distance-based DNA barcoding. Molecular Ecology Resources 11(5): 820–830. https://doi.org/10.1111/j.1755-0998.2011.03025.x

López-González PJ, Drewery J, López-González PJ, Drewery J (2022) When distant relatives look too alike: A new family, two new genera and a new species of deep-sea *Umbellula*-like sea pens (Anthozoa, Octocorallia, Pennatulacea). Invertebrate Systematics 36(3): 199–225. https://doi.org/10.1071/IS21040

Matsumoto M (2003) Phylogenetic analysis of the subclass Pteriomorphia (Bivalvia) from mtDNA COI sequences. Molecular Phylogenetics and Evolution 27(3): 429–440. https://doi.org/10.1016/S1055-7903(03)00013-7

Mazón-Suástegui JM, Fernández NT, Valencia IL, Cruz-Hernández P, Latisnere-Barragán H (2016) 28S rDNA as an alternative marker for commercially important oyster identification. Food Control 66: 205–214. https://doi.org/10.1016/j.foodcont.2016.02.006

Minh BQ, Nguyen MAT, von Haeseler A (2013) Ultrafast Approximation for Phylogenetic Bootstrap. Molecular Biology and Evolution 30(5): 1188–1195. https://doi.org/10.1093/molbev/mst024

Moritz C, Cicero C (2004) DNA Barcoding: Promise and Pitfalls. PLOS Biology 2(10): e354. https://doi.org/10.1371/journal.pbio.0020354

Oliverio M, Mariottini P (2001) Contrasting morphological and molecular variation in *Coralliophila meyendorffii* (Muricidae, Coralliophilinae). The Journal of Molluscan Studies 67(2): 243–246. https://doi.org/10.1093/mollus/67.2.243

Plazzi F, Passamonti M (2010) Towards a molecular phylogeny of Mollusks: Bivalves' early evolution as revealed by mitochondrial genes. Molecular Phylogenetics and Evolution 57(2): 641–657. https://doi.org/10.1016/j.ympev.2010.08.032

Plazzi F, Ceregato A, Taviani M, Passamonti M (2011) A Molecular Phylogeny of Bivalve Mollusks: Ancient Radiations and Divergences as Revealed by Mitochondrial Genes. PLoS ONE 6(11): e27147. https://doi.org/10.1371/journal.pone.0027147

Raith M, Zacherl DC, Pilgrim EM, Eernisse DJ (2015) Phylogeny and Species Diversity of Gulf of California Oysters (Ostreidae) Inferred from Mitochondrial DNA. American Malacological Bulletin 33(2): 263–283. https://doi.org/10.4003/006.033.0206

Rambaut A, Drummond AJ, Xie D, Baele G, Suchard MA (2018) Posterior Summarization in Bayesian Phylogenetics Using Tracer 1.7. Systematic Biology 67(5): 901–904. https://doi.org/10.1093/sysbio/syy032

Ramirez-Llodra E, Brandt A, Danovaro R, De Mol B, Escobar E, German CR, Levin LA, Martinez Arbizu P, Menot L, Buhl-Mortensen P, Narayanaswamy BE, Smith CR, Tittensor DP, Tyler PA, Vanreusel A, Vecchione M (2010) Deep, diverse and definitely different: Unique attributes of the world's largest ecosystem. Biogeosciences 7(9): 2851–2899. https://doi.org/10.5194/bg-7-2851-2010

Ren J, Hou Z, Wang H, Sun M-A, Liu X, Liu B, Guo X (2016) Intraspecific variation in mitogenomes of five Crassostrea species provides insight into oyster diversification and speciation. Marine Biotechnology (New York, N.Y.) 18(2): 242–254. https://doi.org/10.1007/s10126-016-9686-8

Rogers A, Brierley A, Croot P, Cunha M, Danovaro R, Devery C, Hoel AH, Ruhl H, Sarradin P-M, Trevisanut S, van den Hove S, Vieira H, Visbeck M, Mcdonough N, Donaldson K, Larkin K (2015) Delving Deeper: Critical challenges for 21st century deep-sea research.

Ronquist F, Teslenko M, van der Mark P, Ayres DL, Darling A, Höhna S, Larget B, Liu L, Suchard MA, Huelsenbeck JP (2012) MrBayes 3.2: Efficient Bayesian Phylogenetic Inference and Model Choice Across a Large Model Space. Systematic Biology 61(3): 539–542. https://doi.org/10.1093/sysbio/sys029

Rueda JL, Urra J, Aguilar R, Angeletti L, Bo M, García-Ruiz C, González-Duarte MM, López E, Madurell T, Maldonado M, Mateo-Ramírez Á, Megina C, Moreira J, Moya F, Ramalho LV, Rosso A, Sitjà C, Taviani M (2019) 29 Cold-Water Coral Associated Fauna in the Mediterranean Sea and Adjacent Areas. In: Orejas C, Jiménez C (Eds) Mediterranean Cold-Water Corals: Past, Present and Future: Understanding the Deep-Sea Realms of Coral. Coral Reefs of the World. Springer International Publishing, Cham, 295–333. https://doi.org/10.1007/978-3-319-91608-8_29

Ruppert KM, Kline RJ, Rahman MS (2019) Past, present, and future perspectives of environmental DNA (eDNA) metabarcoding: A

systematic review in methods, monitoring, and applications of global eDNA. Global Ecology and Conservation 17: e00547. https://doi.org/10.1016/j.gecco.2019.e00547

Salvi D, Mariottini P (2017) Molecular taxonomy in 2D: a novel ITS2 rRNA sequence-structure approach guides the description of the oysters' subfamily Saccostreinae and the genus *Magallana* (Bivalvia: Ostreidae). Zoological Journal of the Linnean Society 179: 263–276. https://doi.org/10.1111/zoj.12455

Salvi D, Bellavia G, Cervelli M, Mariottini P (2010) The analysis of rRNA sequence-structure in phylogenetics: An application to the family Pectinidae (Mollusca: Bivalvia). Molecular Phylogenetics and Evolution 56(3): 1059–1067. https://doi.org/10.1016/j.ympev.2010.04.025

Salvi D, Macali A, Mariottini P (2014) Molecular Phylogenetics and Systematics of the Bivalve Family Ostreidae Based on rRNA Sequence-Structure Models and Multilocus Species Tree. PLoS ONE 9: e108696. https://doi.org/10.1371/journal.pone.0108696

Salvi D, Berrilli E, D'Alessandro P, Biondi M (2020) Sharpening the DNA barcoding tool through a posteriori taxonomic validation: The case of *Longitarsus* flea beetles (Coleoptera: Chrysomelidae). PLoS ONE 15(5): e0233573. https://doi.org/10.1371/journal.pone.0233573

Salvi D, Berrilli E, Garzia M, Mariottini P (2021) Yet Another Mitochondrial Genome of the Pacific Cupped Oyster: The Published Mitogenome of *Alectryonella plicatula* (Ostreinae) Is Based on a Misidentified *Magallana gigas* (Crassostreinae). Frontiers in Marine Science 8: 741455. https://doi.org/10.3389/fmars.2021.741455

Salvi D, Al-Kandari M, Oliver PG, Berrilli E, Garzia M (2022) Cryptic Marine Diversity in the Northern Arabian Gulf: An Integrative Approach Uncovers a New Species of Oyster (Bivalvia: Ostreidae), *Ostrea oleomargarita*. Journal of Zoological Systematics and Evolutionary Research 2022: e7058975. https://doi.org/10.1155/2022/7058975

Sambrook J, Fritsch EF, Maniatis T (1989) Molecular cloning: a laboratory manual. Cold Spring Harbor Laboratory Press, Cold Spring Harbor, New York.

Schindel DE, Miller SE (2005) DNA barcoding a useful tool for taxonomists. Nature 435(7038): 17. https://doi.org/10.1038/435017b

Silva CF, Shimabukuro M, Alfaro-Lucas JM, Fujiwara Y, Sumida PYG, Amaral ACZ (2016) A new *Capitella* polychaete worm (Annelida: Capitellidae) living inside whale bones in the abyssal South Atlantic. Deep-sea Research, Part I, Oceanographic Research Papers 108: 23–31. https://doi.org/10.1016/j.dsr.2015.12.004

Sinniger F, Pawlowski J, Harii S, Gooday AJ, Yamamoto H, Chevaldonne P, Cedhagen T, Carvalho G, Creer S (2016) Worldwide analysis of sedimentary DNA reveals major gaps in taxonomic knowledge of deep-sea benthos. Frontiers in Marine Science 3: 92. https://doi.org/10.3389/fmars.2016.00092

Taberlet P, Coissac E, Hajibabaei M, Rieseberg LH (2012) Environmental DNA. Molecular Ecology 21(8): 1789–1793. https://doi.org/10.1111/j.1365-294X.2012.05542.x

Talavera G, Castresana J (2007) Improvement of Phylogenies after Removing Divergent and Ambiguously Aligned Blocks from Protein Sequence Alignments. Kjer K, Page R, Sullivan J (Eds) Systematic Biology 56: 564–577. https://doi.org/10.1080/10635150701472164

Tamura K, Stecher G, Kumar S (2021) MEGA11: Molecular Evolutionary Genetics Analysis Version 11. Molecular Biology and Evolution 38(7): 3022–3027. https://doi.org/10.1093/molbev/msab120

Taviani M, Angeletti L, Canese S, Cannas R, Cardone F, Cau A, Cau AB, Follesa MC, Marchese F, Montagna P, Tessarolo C (2017) The "Sardinian cold-water coral province" in the context of the Mediterranean coral ecosystems. Deep-sea Research, Part II, Topical Studies in Oceanography 145: 61–78. https://doi.org/10.1016/j.dsr2.2015.12.008

Taviani M, Angeletti L, Cardone F, Montagna P, Danovaro R (2019) A unique and threatened deep water coral-bivalve biotope new to the Mediterranean Sea offshore the Naples megalopolis. Scientific Reports 9(1): 3411. https://doi.org/10.1038/s41598-019-39655-8

Tëmkin I (2010) Molecular phylogeny of pearl oysters and their relatives (Mollusca, Bivalvia, Pterioidea). BMC Evolutionary Biology 10(1): 342. https://doi.org/10.1186/1471-2148-10-342

Trifinopoulos J, Nguyen L-T, von Haeseler A, Minh BQ (2016) W-IQ-TREE: A fast online phylogenetic tool for maximum likelihood analysis. Nucleic Acids Research 44(W1): W232–W235. https://doi.org/10.1093/nar/gkw256

Vaidya G, Lohman DJ, Meier R (2011) SequenceMatrix: Concatenation software for the fast assembly of multi-gene datasets with character set and codon information. Cladistics 27(2): 171–180. https://doi.org/10.1111/j.1096-0031.2010.00329.x

Van Rooij D, De Mol L, Le Guilloux E, Wisshak M, Huvenne VAI, Moeremans R, Henriet J-P (2010) Environmental setting of deep-water oysters in the Bay of Biscay. Deep-sea Research, Part I, Oceanographic Research Papers 57(12): 1561–1572. https://doi.org/10.1016/j.dsr.2010.09.002

Wisshak M, Neumann C, Jakobsen J, Freiwald A (2009a) The 'living-fossil community' of the cyrtocrinid *Cyathidium foresti* and the deep-sea oyster *Neopycnodonte zibrowii* (Azores Archipelago). Palaeogeography, Palaeoclimatology, Palaeoecology 271(1–2): 77–83. https://doi.org/10.1016/j.palaeo.2008.09.015

Wisshak M, López Correa M, Gofas S, Salas C, Taviani M, Jakobsen J, Freiwald A (2009b) Shell architecture, element composition, and stable isotope signature of the giant deep-sea oyster *Neopycnodonte zibrowii* sp. n. from the NE Atlantic. Deep-sea Research. Part I, Oceanographic Research Papers 56(3): 374–407. https://doi.org/10.1016/j.dsr.2008.10.002

Woodall LC, Andradi-Brown DA, Brierley AS, Clark MR, Connelly D, Hall RA, Howell KL, Huvenne VAI, Linse K, Ross RE, Snelgrove P, Stefanoudis PV, Sutton TT, Taylor M, Thornton TF, Rogers AD (2018) A multidisciplinary approach for generating globally consistent data on mesophotic, deep-pelagic, and bathyal biological communities. Oceanography (Washington, D.C.) 31(3): 76–89. https://doi.org/10.5670/oceanog.2018.301

Xu T, Feng D, Tao J, Qiu J-W (2019) A new species of deep-sea mussel (Bivalvia: Mytilidae: Gigantidas) from the South China Sea: Morphology, phylogenetic position, and gill-associated microbes. Deep-sea Research, Part I, Oceanographic Research Papers 146: 79–90. https://doi.org/10.1016/j.dsr.2019.03.001

Zoosyst. Evol. 100 (1) 2024, 119–128 | DOI 10.3897/zse.100.116611

PENSOFT

für Natur MUSEUM FÜR NATURKUNDE BERLIN

Two new species of the congrid eel genus *Ariosoma* (Anguilliformes, Congridae, Bathymyrinae) from Indian waters

Paramasivam Kodeeswaran[1,2], Ayyathurai Kathirvelpandian[1], Dipanjan Ray[3], Anil Mohapatra[4], Thipramalai Thangappan Ajith Kumar[1], Chelladurai Raghunathan[5], Uttam Kumar Sarkar[1]

1 *ICAR-National Bureau of Fish Genetic Resources, Lucknow, Uttar Pradesh 226 002, India*
2 *Faculty of Fisheries Science, Kerala University of Fisheries and Ocean Studies, Kochi 682 506, India*
3 *Bajkul Milani Mahavidyalaya, Kismat Bajkul, Purba Medinipur, West Bengal 721 655, India*
4 *Estuarine Biology Regional Centre, Zoological Survey of India, Gopalpur-on-Sea, Ganjam, Odisha 761 002, India*
5 *Zoological Survey of India, New Alipore, Kolkata 700 053, India*

https://zoobank.org/FD307F80-4B3E-41E1-9283-E5C93C17C399

Corresponding author: Thipramalai Thangappan Ajith Kumar (ttajith87@gmail.com)

Academic editor: Nalani Schnell ♦ **Received** 30 November 2023 ♦ **Accepted** 10 January 2024 ♦ **Published** 26 January 2024

Abstract

Two new species have been described from Indian waters, based on the materials collected from Kochi coast, Arabian Sea, Gulf of Mannar and West Bengal coast along the Bay of Bengal. *Ariosoma gracile* **sp. nov.** is described, based on five specimens collected from the landings at Kalamukku Fishing Harbour, Arabian Sea. The new species is characterised by longer tail, 55.3–58.7% TL; dorsal-fin origin above pectoral-fin base; no dark or whitish bands on dorsal surface of head, ventral extremities of lower jaw and mid-portion with minute dark pigmentation patch; anus positioned well before the middle of total length; SO canal with 4 pores; 0 or 3 pores on ST canal; pre-dorsal vertebrae 9; pre-anal vertebrae 49–54; total vertebrae 140–142. *Ariosoma gracile* **sp. nov.** is closely related to *Ariosoma dolichopterum* and *Ariosoma emmae* by sharing similar morphometrics and pre-anal vertebral counts. However, it differs by having more total pores (132–135 vs. 121–129 in *A. dolichopterum*, 123–126 in *A. emmae*); fewer pre-anal pores (43–46 vs. 47–51 in *A. dolichopterum*, 50–53 in *A. emmae*); more pre-dorsal pores (9 vs. 5–9 in *A. dolichopterum*, 4–6 in *A. emmae*). Another new species, *Ariosoma kannani* **sp. nov.** is described on the basis of two specimens (157–171 mm TL) from Gulf of Mannar and one specimen (201 mm TL) collected from Shankarpur Fish Landing Centre, West Bengal. This species is similar to *Ariosoma megalops*, but readily differs by having smaller eyes, smaller interorbital distance and exhibits 10.8% genetic divergence from *A. megalops* from the Taiwan waters.

Key Words

Arabian Sea, Bathymyrinae, Bay of Bengal, new eel, systematics

Introduction

The congrid eel genus, *Ariosoma* Swainson, 1838, includes 38 valid species (Fricke et al. 2023). The genus *Ariosoma* along Indian waters was known only by two species till 2021 (Roy et al. 2021). Then, extensive sampling efforts and integrative taxonomic approaches resulted in the description and documentation of an additional six species from the Indian waters (Roy et al. 2021; Kodeeswaran et al. 2021, 2022a, 2022b, 2023; Ray et al. 2022) and also Kodeeswaran et al. (2021) mentioned the existence of a few more undescribed species along the Indian waters. Following sampling along the southern coasts of India, several specimens of an unknown congrid eel were encountered as trawl by-catch, with one unidentified specimen also being collected from the northern part of the Bay of Bengal. Subsequent comparison with existing species from Indian waters suggested that the presently collected specimens were undescribed. Here, we describe two new species of *Ariosoma* from Indian

waters, based on the meristic and morphometric details with the support of molecular analyses.

Materials and methods

Sampling, morphometric and meristic analyses

Eel samples were collected from different landing centres along the India coast viz. Kalamukku Fishing Harbour (9°59'N, 76°14'E), off Kerala coast, west coast of India, Arabian Sea and Rameshwaram Fish Landing Centre (9°16'N, 79°18'E), Tamil Nadu, Gulf of Mannar, east coast of India, Bay of Bengal and Shankarpur Fish Landing Centre, West Bengal, Bay of Bengal, India. Fresh photographs were taken with a Canon 80D Digital Single-Lens Reflex camera (EF-S 18–135mm f/3.5-f/5.6 IS USM Kit Lens) and a small portion of muscle and pectoral fin-clips were incised and preserved in 99.9% ethanol for phylogenetic analyses. Collected specimens were preserved in 10% formaldehyde for taxonomical studies and deposited in the National Fish Museum and Repository of the ICAR–National Bureau of Fish Genetic Resources (NBFGR), Lucknow, India and Estuarine Biology Regional Centre (EBRC), Zoological Survey of India, Gopalpur-on-Sea, Odisha, India.

Morphometric measuring and meristic counting follow Smith and Kanazawa (1977) and Smith (1989) using a Digimatic caliper with accuracy to 0.1 mm. Vertebral counting follow Böhlke (1982) with the help of digital radiographs. Head pores abbreviations are: IO, infraorbital; POM, pre-opercular-mandibular; SO, supraorbital; ST, supratemporal. Details of the comparative material are listed in the "Comparative material examined" section.

Molecular analyses

The DNA isolation, PCR cycle conditions and mtDNA gene amplifications were done, based on the methods followed in Kodeeswaran et al. (2021; 2022a). The obtained PCR products were sent out for sequencing with outsources. Newly-generated sequences were edited and aligned manually using clustalW Multiple alignments implemented in BioEdit version 5.0.9 (Hall 1999) with other sequences retrieved from the public domain (GenBank). Pair-wise distance, nucleotide diversity, nucleotide composition and transition transversion bias (R) were estimated using the Kimura 2 parameter (K2P) model in MEGA X (Kumar et al. 2018). The Maximum Likelihood (ML) phylogenetic tree was reconstructed using IQ-TREE software v.1.6.12 (Nguyen et al. 2015) with the best-fit model: HKY+F+I+G4 chosen according to the BIC score: 8550.210 using ModelFinder (Kalyaanamoorthy et al. 2017) with ultrafast bootstrap (1000 bootstrap replicates) (UFBoot) (Hoang et al. 2018) and the tree diagram was constructed aided by the Interactive Tree Of Life v.5 (Letunic and Bork 2021). *Japonoconger proriger* (MF956462) and *Uroconger lepturus* (ON799405) sequences were used as outgroups for reconstructing the phylogenetic tree.

Comparative materials examined

***Ariosoma albimaculatum*.** NBFGR/CONAALB, holotype, (487 mm TL); paratypes (nine specimens), NBFGR/CONAALB.1–9 (5: 305–401 mm TL), collected from deep-sea trawl by-catch, Colachel Fishing Harbour, off Kanyakumari, Arabian Sea.

***Ariosoma bengalense*.** F12898, holotype (304 mm TL), collected from Petua Ghat, West Bengal, India from the depth of 168 m; EBRC/ZSI/F12899, paratype (216 mm TL), data same as holotype.

***Ariosoma gnanadossi*.** ZSI F7146/2, holotype (283 mm TL), collected from the depth of 250 m, off Madras, east coast of India, Bay of Bengal.

***Ariosoma indicum*.** NBFGR/CONAIND, holotype (362 mm TL); NBFGR/CONAIND.1–2 (2: 355–371 mm TL), EBRC/ZSI/F13597 (2: 337–438 mm TL); NBFGR/CONAIND.3–9 (7: 335–433 mm TL) taken with holotype, all collected from Kalamukku Fishing Harbour, Kochi, Arabian Sea. EBRC/ZSI/F13604 (7: 223–356 mm TL) non-types, collected from Digha Mohana, West Bengal, Bay of Bengal.

***Ariosoma majus*.** EBRC/ZSI/F 11528 (2 specimens: 246–290 mm TL) collected from Deshpran Fishing Harbour, West Bengal, east coast of India, Bay of Bengal.

***Ariosoma maurostigma*.** NBFGR/CONAMAUR, holotype (233 mm TL); NBFGR/CONAMAUR.1–3, paratypes, (3: 202–295 mm TL), NBFGR/CONAMAUR.4 (1: 229 mm TL) taken with holotype. NBFGR/CONAMAUR.5 (15: 181–292 mm TL); EBRC/ZSI/F12905, (4: 206–273 mm TL) all collected from Kalamukku Fishing Harbour, Kochi, Arabian Sea.

***Ariosoma melanospilos*.** NBFGR/CONAMEL, holotype (302 mm TL), Colachel Fishing Harbour, southwest coast of India, Indian Ocean. ZSI F 14502/2, paratype (296 mm TL) same collection details as holotype. EBRC/ZSI/F14040, Colachel Fishing Harbour, southwest coast of India, Indian Ocean.

***Ariosoma* sp.** NBFGR/CONATHO, (440 mm TL), Thoothukudi Fishing Harbour, southeast coast of India, Bay of Bengal.

Results

***Ariosoma gracile* Kodeeswaran, Kathirvelpandian, Mohapatra, Kumar & Sarkar, sp. nov.**

https://zoobank.org/757F2921-E865-4B92-B363-F7C90DB2E241

Figs 1a, 2a, 3, 4, Table 1

Proposed common name: Slender Conger eel

Type material. *Holotype*. NBFGR/CONACOM, 241 mm TL, collected from deep-sea trawl by-catch, Kalamukku Fishing Harbour, off Kerala coast, Arabian Sea, 9°59'N, 76°14'E, P. Kodeeswaran, 19 February 2021.

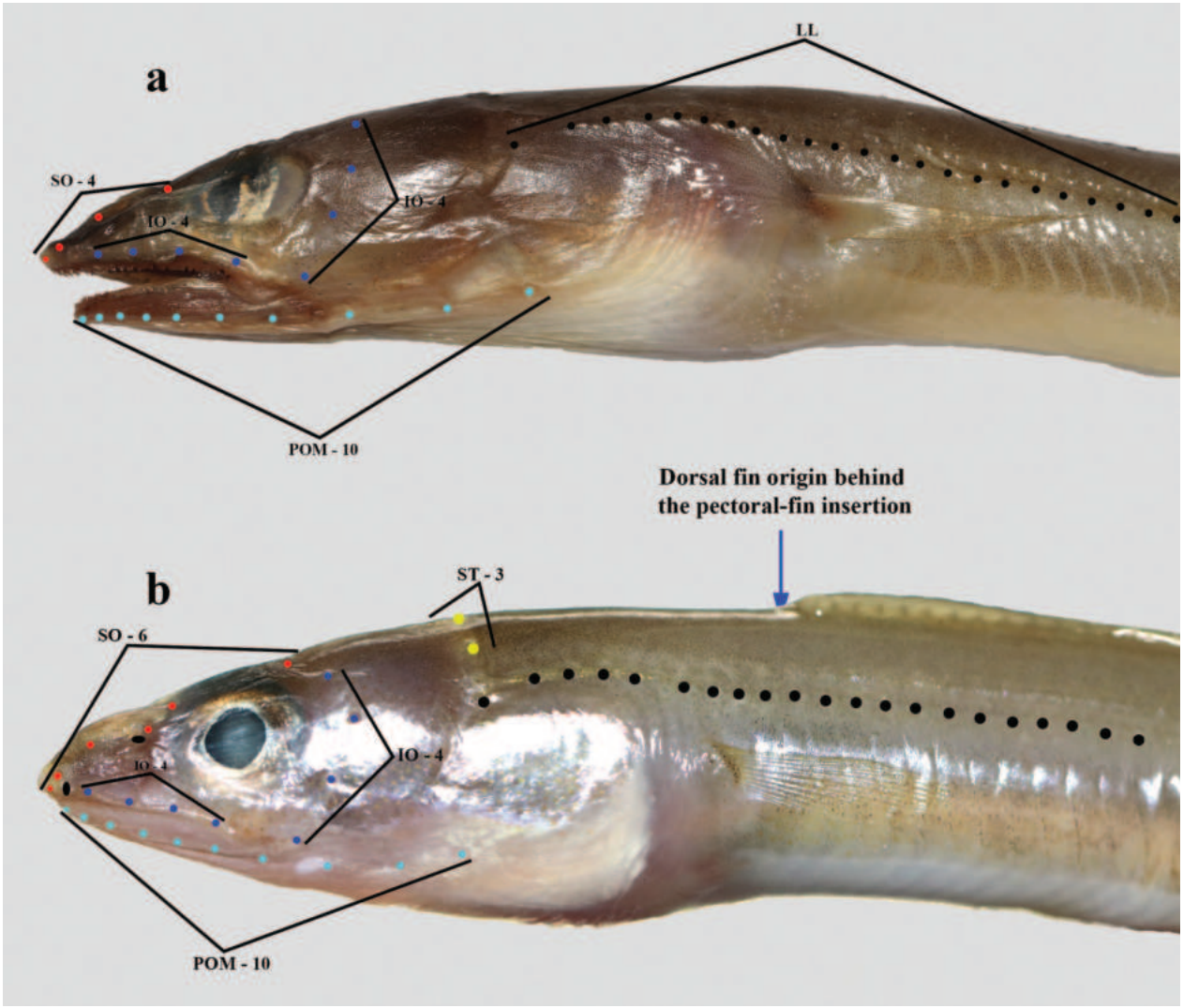

Figure 1. Image showing the head pores and anterior lateral-line pores. **a.** *Ariosoma gracile* sp. nov., NBFGR/CONACOM, holotype (241 mm TL); **b.** *Ariosoma kannani* sp. nov., NBFGR/CONAKAN, holotype, (171 mm TL).

***Paratypes*.** NBFGR/CONACOM.1–2, (2:197–199 mm TL) and EBRC/ZSI/F15709 (2: 206–221 mm TL) taken with holotype.

Diagnosis. A medium-sized slender eel species of *Ariosoma* distinguished from all other species by the following combination of characters: position of anus well-before middle of total length, pre-anal length 43.7% (41.3–44.7%) of TL; tail longer, 55.3–58.7% TL; dorsal-fin above pectoral-fin base; no dark or whitish bands on dorsal surface of head, ventral extremities and mid-portion of lower jaw with minute dark pigmentation patch; short vomerine teeth patch with three or four rows of pointed teeth in anterior portion, intermaxillary teeth patch curved, slightly upturned at anterior end, clearly visible when mouth closed, separated from vomerine and maxillary teeth by a definite gap; SO canal with 4 pores; 0 or 3 pores on ST canal; pre-dorsal vertebrae 9 (9); pre-anal vertebrae 48 (49–54); total vertebrae 141 (140–142).

Description (dimensions in mm). Morphometric and meristic data are provided in Table 1. HL 5.9 (5.5–5.7) in TL; pre-anal length 2.3 (2.2); pre-dorsal length 5.7 (5.6–5.8); trunk length 4.9 (4.1–4.6); tail length 1.7 (1.8); and depth at gill opening 18.2 (18.1–23.4). Snout length 5.1 (4.7–5.3) in HL; eye diameter 5.8 (5.4–6.4); interorbital width 9.9 (8.5–14.9); upper jaw 3.4 (3.1–3.6); gill opening width 5.8 (5.6–9.6); interbranchial width 8.8 (8.0–11.3); and pectoral fin 2.9 (2.7–3.7).

Body slender, cylindrical anterior portion, followed by more laterally compressed caudal portion; tip of caudal fin stiff and blunt or conical; anus positioned well-before mid-point of total length, pre-anal length 43.7% (41.3–44.7%) of TL; dorsal-fin origin above pectoral-fin base, above ninth lateral-line pores, confluent with caudal and anal fin. Origin of anal fin just after anus. Pectoral fin developed, with narrow base and pointed distally. Gill opening medium, slightly larger or equal to eye diameter, its upper origin reaching nearly upper half of pectoral-fin base; interbranchial width smaller than gill opening and eye diameter.

Head fairly large 5.9 (5.5–5.7) in TL, snout very short, anteriorly pointed in dorsal view, its length 1.1 (1.1–1.2) times eye diameter, projecting beyond lower jaw; length of snout relatively shorter than lower jaw; fleshy portion of snout projecting anteriorly beyond the end of

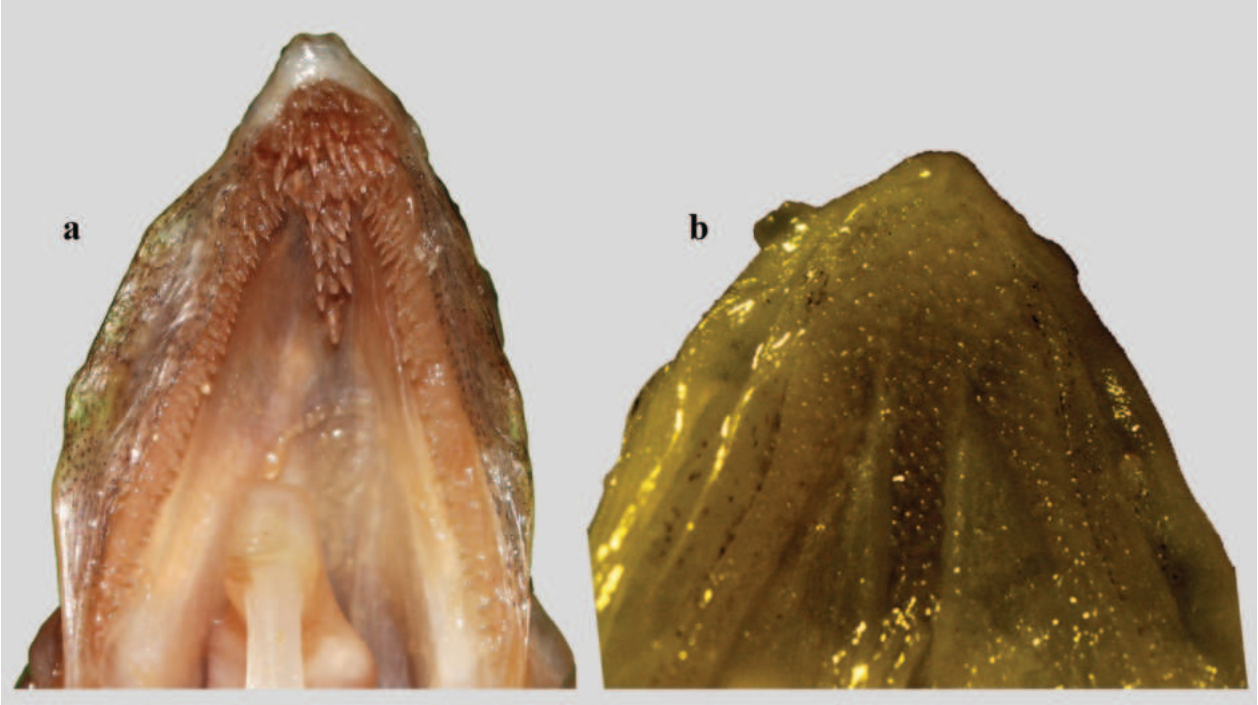

Figure 2. Dentition of upper jaw. **a.** *Ariosoma gracile* sp. nov., NBFGR/CONACOM, holotype (241 mm TL); **b.** *Ariosoma kannani* sp. nov., NBFGR/CONAKAN, holotype, (171 mm TL).

intermaxillary tooth patch; rictus positioned just before middle length of eye. Fairly large tubular anterior nostril at tip of snout and relatively large elliptical pore of posterior nostril in front of mid-eye orbit diameter. Upper and lower jaw with slightly reduced flange. Tongue short and narrow; anterior portion free from mouth with conical or blunt tip.

Lateral-line pores complete; first pore commences moderately at level of supratemporal canal and terminating well before caudal-fin base; 9 (9) pre-dorsal pores; 43 (43–46) pre-anal pores and 132 (132–138) total pores.

Head pores moderate, few pores rather small. SO canal with 4 pores; first (ethmoidal) relatively small, on ventral side of snout tip; second pore medium-sized, in front of anterior nostril; third pore enlarged, on dorsal surface of snout just behind anterior nostril; fourth pore circular and enlarged, no pores in interorbital portion. IO canal with 8 (4+4) pores, first pore large, behind anterior nostril; second pore below posterior end of posterior nostril; third pore below anterior eye-orbit margin; fourth pore at above or slightly before rictus, below mid-eye; fifth pore behind rictus, at posterior margin of eye and 3 pores at infraorbital canal behind eye. POM pores 10; 7 in mandibular section, 6 before rictus and 1 behind rictus; pre-opercular section with 3 pores in a longitudinal row. Small-sized ST pores 0 or 3, (holotype and one paratype does not possess ST pores, 2 specimens with 3 pores and one specimen with 2 pores) (Fig. 3).

Pre-dorsal vertebrae 9 (9); pre-anal vertebrae 48 (49–54); total vertebrae 141 (140–142).

Teeth larger, conical or pointed (no blunt teeth) (Fig. 2a). Curved intermaxillary teeth patch with three or four transverse rows, clearly visible when mouth closed, anterior portion fairly upturned, separated from vomerine and maxillary teeth by a definite gap. Maxillary and mandibular teeth continuous in bands; anterior part of maxillary teeth narrow with three rows, middle portion with two rows, innermost and outermost teeth pointed or conical, followed by uniserial pointed teeth posteriorly. Mandibular teeth wider anteriorly and narrower posteriorly. Vomerine teeth form a short patch, reaching in front of posterior nostril, three or four rows with pointed teeth in anterior portion, followed by four irregular triserial pointed teeth and two conical teeth in a series posteriorly.

Colour (in fresh specimens). Body often bicolour, dark brownish to paler, upper half almost darker and paler ventrally; very minute dark pigmentations irregularly spread over body. Dorsal and anal fin creamy-white with thin black margin; caudal fin dull white with black upper and lower margins (Fig. 1). Head same as body, dorsal surface of head without any dark or whitish bands, extremities of lower jaw under surface and mid-portion with minute dark pigmentation patch (Fig. 4b, c). Eyes bright with dark pupil, surrounded by thick pale golden-yellowish ring. Pectoral fin goldish-yellow (Fig. 4a). Colour in formalin slightly darker than fresh material or almost beige; pectoral fin translucent. Dark pigmentation patch remains on the ventral head.

Distribution. Known from five specimens collected from trawl by-catches landings at Kalamukku Fishing Harbour, off Kerala, south-western Indian coast, Arabian Sea, western Indian Ocean.

Etymology. From the Latin word, '*gracilis* - *gracile*' meaning slender, which denotes the slender-bodied eel.

Figure 3. *Ariosoma gracile* sp. nov., NBFGR/CONACOM, holotype (241 mm TL) fresh colouration. Scale bar: 40 mm.

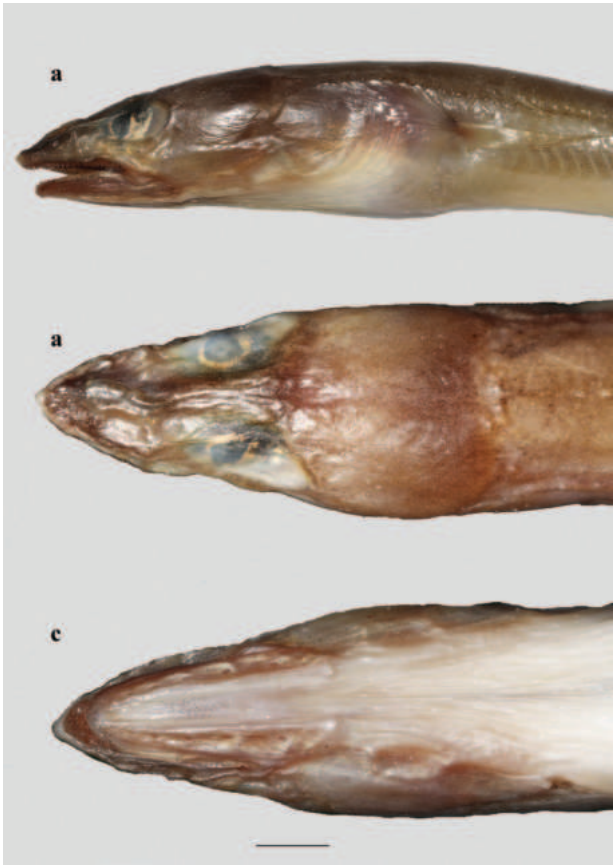

Figure 4. Lateral (**a**); Dorsal (**b**); Ventral (**c**) view of *Ariosoma gracile* sp. nov., NBFGR/CONACOM, 241 mm TL. Scale bar: 10 mm.

Comparisons. *Ariosoma gracile* differs from all the congeners but shares similar morphological characters and overlapping pre-anal vertebrae counts with *Ariosoma dolichopterum* Karmovskaya, 2015 from the South China Sea, off Vietnam and Taiwan and *Ariosoma emmae* Smith & Ho, 2018 from Taiwan waters. *Ariosoma gracile* differs from these congeners by having: 132–135 total pores (vs. 121–129 in *A. dolichopterum*, 123–126 in *A. emmae*); 43–46 pre-anal pores (vs. 47–51 in *A. dolichopterum*, 50–53 in *A. emmae*); 9 pre-dorsal pores (vs. 5–9 in *A. dolichopterum*, 4–6 in *A. emmae*); more total vertebrae (140–142 vs. 129–134 in *A. dolichopterum*, 127–133 in *A. emmae*); trunk 38.5–42.6% TL (vs. 26.6–29.8% TL in *A. dolichopterum*, 28.9–32.7% TL in *A. emmae*); short vomerine tooth patch (vs. long in *A. dolichopterum* and *A. emmae*) (Karmovskaya 2015; Smith et al. 2018).

Ariosoma gracile differs from the Indian water congeners, such as *Ariosoma gnanadossi* Talwar & Mukherjee, 1977, *Ariosoma melanospilos* Kodeeswaran, Jayakumar, Akash, Kumar & Lal, 2021, *Ariosoma albimaculatum* Kodeeswaran, Dhas, Kumar & Lal, 2022 and *Ariosoma* sp. nov. Kodeeswaran et al. (in press) in having fewer total vertebrae (140–142 vs. 161–164 in *A. albimaculatum*; 146 in *A. gnanadossi*; 144–153 in *A. melanospilos*; 162–163 in *Ariosoma* sp. nov.); fewer total pores (132–135 vs. 145 in *A. gnanadossi*; 136–144 in *A. melanospilos*; 148–155 in *Ariosoma* sp. nov.). The new species shares similar vertebral counts with *Ariosoma maurostigma* Kodeeswaran, Mohapatra, Dhinakaran, Kumar & Lal, 2022, but readily differs from the latter by the absence of a dark spot on posterior-dorsal margins of eye orbit (vs. present in *A. maurostigma*); tail longer (55.3–58.7% TL vs. 47.8–54.6% TL); shorter pre-anal length (41.3–44.7% TL vs. 44.0–48.8% SL); fewer SO pores (4 vs. 6). Further, the new species differs from *Ariosoma majus* (Asano, 1958) in having more pre-dorsal pores (9 vs. 6–7 in *A. majus*); fewer pre-anal pores (43–46 vs. 50–53); fewer total pores (132–135 vs. 139–142); smaller depth at gill opening (4.3–5.5% TL vs. 6.7–7.3% TL); fewer SO pores (4 vs. 6). Further, the new species shares overlapping vertebral counts with newly-described sympatric species *Ariosoma indicum* Kodeeswaran, Kathirvelpandian, Acharya, Mohanty, Mohapatra, Kumar & Lal, 2022, but the new species differs from the latter in having shorter pectoral fin (26.8–36.9% HL vs. 37.5–46.7% HL in *A. indicum*); smaller interorbital width (6.7–11.8% HL vs. 11.8–15.7% HL); fewer SO pores (4 vs. 5); ST pores (0 vs. 3); pectoral fin grey (vs. blackish or bicoloured).

The new species differs from the species viz. *Ariosoma anago* (Temminck & Schlegel, 1846), *Ariosoma anale* (Poey, 1860), *Ariosoma fasciatum* (Günther, 1872), *Ariosoma meeki* (Jordan & Snyder, 1900), *Ariosoma howensis* (McCulloch & Waite, 1916), *Ariosoma shiroanago* (Asano, 1958), *Ariosoma coquettei* Smith & Kanazawa, 1977, *Ariosoma kapala* (Castle, 1990), *Ariosoma ophidiophthalmus* Karmovskaya, 1991, *Ariosoma multivertebratum* Karmovskaya, 2004, *Ariosoma sazonovi* Karmovskaya, 2004, and *Ariosoma sereti* Karmovskaya, 2004 and in having fewer total vertebrae (140–142 vs. 143–144 in *A. anago*; 146–150 in *A. anale*; 155–158 in *A. fasciatum*; 144–155 in *A. meeki*; 151–161 in *A. howensis*; 161–162 in *A. shiroanago*; 152–160 in *A. coquettei*; 147 in *A. kapala*; 150–153 in *A. ophidiophthalmus*;

Table 1. Meristic and morphometrics of *Ariosoma gracile* from Arabian Sea and *Ariosoma kannani* from the Gulf of Mannar, Bay of Bengal.

	***Ariosoma gracile* sp. nov.**		***Ariosoma kannani* sp. nov.**	
	Holotype	**Paratypes**	**Holotype**	**Paratypes**
Total length (mm)	241	197–221 (n = 4)	173	157–201 (n = 2)
%TL				
Head length	17.6	17.1–18.2	16.0	16.1
Depth at gill opening	5.0	4.3–5.5	6.4	5.4–6.1
Depth at anus	4.5	3.4–5.0	6.7	6.2–6.3
Width at anus	3.6	3.2–4.0	4.9	4.7–4.9
Pre-dorsal length	17.6	17.2–17.9	18.9	17.5–17.2
Pre-anal length	43.7	41.3–44.7	46.9	46.0–47.2
Trunk length	22.5	20.3–24.4	28.0	28.0–27.9
Tail length	56.3	55.3–58.7	53.1	52.8–54.0
%HL				
Snout length	19.8	18.7–21.4	20.8	17.7–18.1
Eye diameter	17.4	15.7–18.4	21.1	20.7–20.9
Interorbital width	9.6	6.7–11.8	8.9	10.7–8.5
Upper jaw length	29.5	27.6–31.8	29.5	23.7–28.5
Gill opening width	15.4	10.4–18.0	12.8	10.0–10.8
Interbranchial width	10.4	8.8–12.5	21.5	14.4–14.1
Pectoral-fin length	32.9	26.8–36.9	37.0	29.5–37.4
Meristics				
Pre-dorsal vertebrae	9	9	10	10
Pre-anal vertebrae	48	49–52	45	45–48
Total vertebrae	141	140–142	116	118–116
Lateral-line pores				
Pre-dorsal pores	9	9	11	10
Pre-anal pores	43	43–46	45	47
Total pores	132	133–135	110	111–110

183–189 in *A. multivertebratum*; 146–148 in *A. sazonovi*; 168–172 in *A. sereti*; *Ariosoma gracile* differs from *Ariosoma balearicum* (Delaroche, 1809), *Ariosoma megalops* Fowler, 1938, *Ariosoma scheelei* (Strömman, 1896) and *Ariosoma sokotranum* Karmovskaya, 1991 in having more vertebrae (140–142 vs. 121–135 in *A. balearicum*; 114–118 in *A. scheelei*; 136–141 in *A. sokotranum*).

Remarks. The specimens were directly preserved in formalin; hence this could not be included in the molecular analyses.

Ariosoma kannani Kodeeswaran, Kathirvelpandian, Ray, Kumar, Mohapatra & Sarkar, sp. nov.

https://zoobank.org/AF62080E-7DF4-43AE-BF0C-D83C0440E8AA

Figs 1b, 2b, 5, Table 1

Type material. ***Holotype*.** NBFGR/CONAKAN (171 mm TL), Rameshwaram Fish Landing Centre, Tamil Nadu, Gulf of Mannar, east coast of India, Bay of Bengal (9°16'N, 79°18'E), Coll. P. Kodeeswaran and A. Kathirvelpandian, 4 February 2022.

***Paratype*.** EBRC/ZSI/F15710 **(**157 mm TL**)** taken with holotype, EBRC/ZSI/F15711 **(**201 mm TL**),** Shankarpur Fish Landing Centre, West Bengal, Coll. Dipanjan Ray, 10 November, 2021.

Diagnosis. A small-sized slender eel species of *Ariosoma* distinguished from all other species by the following combination of the characters: dorsal-fin origin behind pectoral-fin insertion, pre-anal length 46.0–47.2% of TL, smaller eye, 20.7–21.1% HL, smaller interorbital distance, 8.9–10.7% HL, no distinct bands on head, pre-opercle whitish, teeth on jaw small, pointed, intermaxillary and vomerine teeth continuous, short vomerine tooth patch; SO canal with 6 pores; 3 pores on ST canal; pre-dorsal vertebrae 10 (10); pre-anal vertebrae 45 (45); total vertebrae 116 (118).

Description. Body stout, anterior portion cylindrical, laterally compressed in tail region; caudal fin tip rounded; anus positioned at mid-point of body, pre-anal length 46.0–47.2% of TL; dorsal-fin origin behind pectoral-fin insertion, above tenth to eleventh lateral-line pores. Pectoral-fin developed, with a narrow base and round or blunt distally. Gill opening small, smaller than eye diameter, interbranchial width larger than gill opening and smaller than eye diameter.

Head moderately large 6.0 (5.5) in TL, snout short, anteriorly pointed in dorsal view, its length 1.1 times eye diameter, projecting beyond lower jaw; snout length shorter than lower jaw; fleshy portion of snout projecting anteriorly beyond the end of intermaxillary tooth patch; rictus positioned just behind middle length of eye. Tubular anterior nostril moderate in size at snout tip and posterior nostril relatively large elliptical pore, in front of mid-eye orbit diameter. Upper and lower jaw with reduced flange.

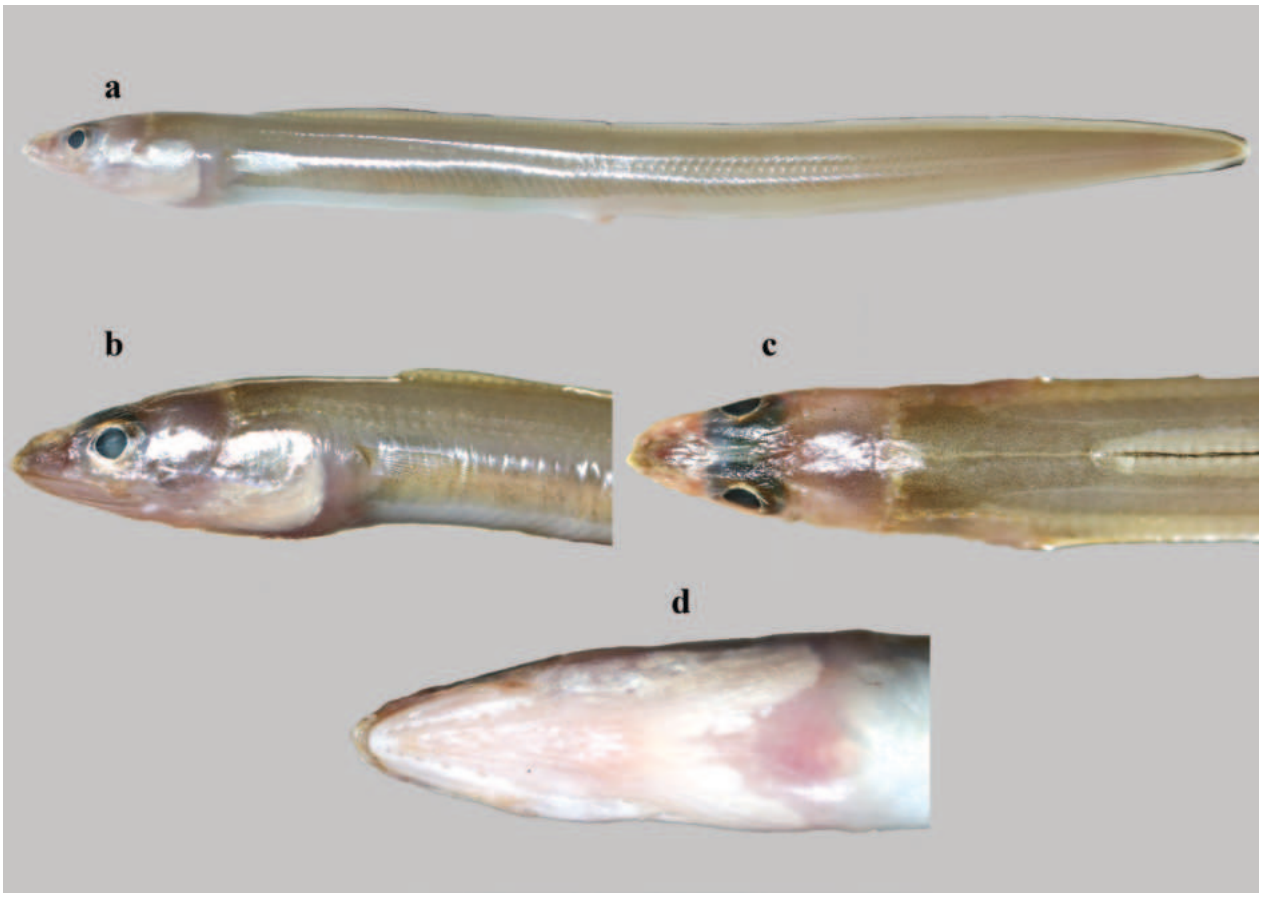

Figure 5. *Ariosoma kannani* sp. nov., NBFGR/CONAKAN, holotype, (171 mm TL). **a.** Lateral view; **b.** Lateral; **c.** Dorsal; **d.** Ventral view of anterior portion of head.

Lateral-line pores complete; first pore commences at level of supratemporal canal and terminates well before base of caudal fin; 10–11 pre-dorsal pores; 45–47 pre-anal pores and 110–111 total pores.

Head pores medium or small. SO canal pores 6; first pore (ethmoidal) smaller, on snout tip; second pore medium, just before anterior nostril; third pore enlarged, on dorsal surface of snout just behind anterior nostril; fourth pore moderate, behind posterior nostril; fifth pore smaller, at anterior interorbital space; sixth pore small at posterior interorbital space. IO canal pores 8 (4+4), first pore moderate, behind anterior nostril; second pore below posterior nostril; third pore below just before orbit eye-orbit margin; fourth pore at slightly before rictus, fifth pore behind rictus and 3 pores at infraorbital canal behind eye. POM pores 10; mandibular section with 7, pre-opercular section with 3 pores in a longitudinal row. ST pores 3, 1 median pore and 1 lateral pore on each side just behind median pore (Fig. 1b).

Teeth on jaws small, pointed; continuous maxillary and intermaxillary teeth; intermaxillary and vomerine teeth continuous; vomerine teeth pointed anteriorly and blunt posteriorly, reach beyond mid-maxillary teeth row (Fig. 2b).

Pre-dorsal vertebrae 10, pre-anal vertebrae 45–48; total vertebrae 116–118.

Colouration. Dorsal body pale brownish; ventral half above anus whitish; dorsal fin margin black; anal fin clear; pre-opercle whitish; head brownish; interorbital region black; pectoral-fin translucent; ventral surface of lower jaw whitish without any black pigmentation (Fig. 5).

Distribution. Indian Ocean: Gulf of Mannar, Bay of Bengal probably widespread in the east coast of India, but rare in catch.

Etymology. The species was named after the late Prof. Dr. L. Kannan, Former Director, CAS in Marine Biology, Annamalai University and Former Vice Chancellor, Thiruvalluvar University for his contribution in Marine Science.

Comparison. *Ariosoma kannani* is closely related to *Ariosoma megalops* from China, Taiwan and Vietnam waters in having the dorsal-fin origin behind the pectoral-fin insertion and similar vertebral counts, but the new species readily differs by having smaller interorbital distance (8.9–10.7% HL vs. 12.1–18.4% HL in *A. megalops*) and smaller mean eye diameter (20.9% HL vs. 22.8–22.9% HL) and the new species show 10.8% genetic divergence from *A. megalops* from the Taiwan waters. The new species shares similar vertebral counts with *Ariosoma scheelei*, a widely distributed species in Indo-West Pacific, but *A. kannani* can be easily distinguished from *A. scheelei* by having fewer POM pores (10 vs. 12 in *A. scheelei*) (Smith et al. 2018) and shows 19.4% genetic differences.

Further, *A. kannani* differs from all the Indian water congeners by having fewer total vertebrae (116–118 vs. 121–164 in others) and dorsal-fin origin behind pectoral-fin insertion (Kodeeswaran et al. 2021, 2022a, 2022b, 2023; Ray et al. 2022).

Molecular analyses

Out of 548 bp studied, conserved and variable sites were found to be 348 bp, 200 bp long, respectively. Amongst variable sites, parsimony informative sites constitute 190 bp, wherein a singleton with 10 bp. The nucleotide composition was found to be A = 26.1%; T = 30%; C = 25.2%; G = 18.7. The transition and transversion bias (R) was documented using substitution patterns and rates were ascertained using the Kimura 2 Parameter model. The obtained R value of 7.48, clearly indicate the sequences of the species used for analyses are delineated in a proper manner. The R value supports the findings of genetic divergence values and phylogenetic tree analyses.

The Maximum Likelihood tree (Fig. 6), obtained using the sequences generated for the new species *Ariosoma kannani* along with other sister species, confirms the species identification as the new species forms a separate cluster and is closely related to the sequences of *Ariosoma megalops* from the Taiwan waters with 10.8% genetic divergence. Further, the new species *A. kannani* exhibits 16.3% distance with the sequences of *Ariosoma kapala*, 17.6% with *A. bowersi*, 18.9% with *A. shiroanago*, 19.2% with *A. balearicum* and 19.3% with *A. anago*.

Discussion

At present, 40 species of the genus *Ariosoma* were described (Fricke et al. 2023 and this study), with at least 74% (31 species) of all species of this genus being described or identified from the Indo-West Pacific, seven species distributed along the Atlantic Ocean and two from the eastern Pacific Ocean (Smith and Kanazawa 1977; Karmovskaya 1991, 2004, 2015, 2018; Shen 1998; Smith et al. 2018; Roy et al. 2021; Kodeeswaran et al. 2021, 2022a, 2022b, 2023; Fricke et al. 2023) and doubtlessly there will be many undescribed species to be discovered. Very few species of the genus *Ariosoma* exhibit an endemic distributional range like a specific locality or around several islands, for example, *Ariosoma bauchotae* Karrer, 1983 collected around western Madagascar (Smith 1989; Fricke et al. 2018); *Ariosoma emmae* Smith

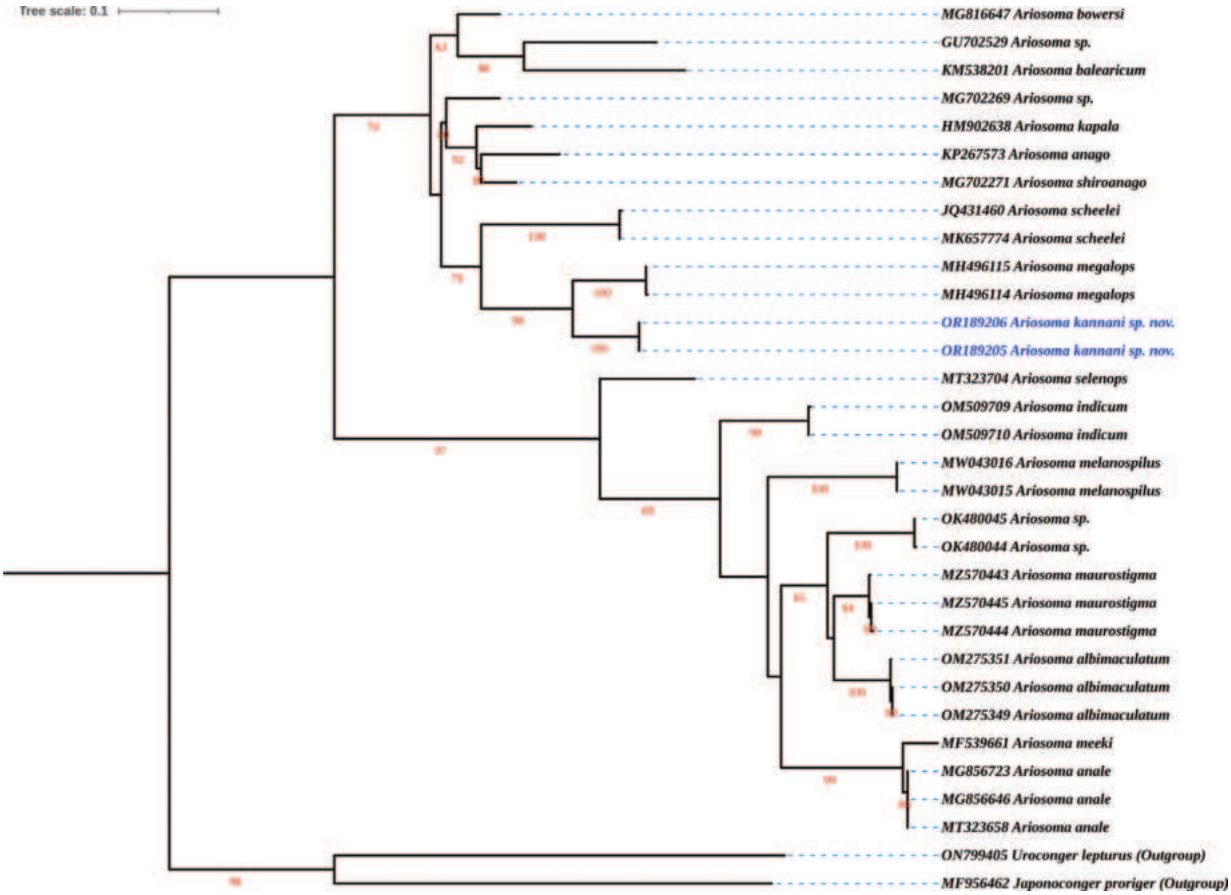

Figure 6. Maximum Likelihood phylogeny tree of the genus *Ariosoma* from analysis of cytochrome c oxidase subunit I gene, including new species, *Ariosoma kannani* collected from the south Indian coast, based on the IQ-Tree. The ML tree was plotted with the HKY+F+I+G4 model using ModelFinder (Kalyaanamoorthy et al. 2017). Each node is labelled with a GenBank accession number and support values (bootstrap probability) are indicated along branches.

& Ho, 2018, known only from Taiwan (Smith et al. 2018); *Ariosoma hemiaspidus* (Wade, 1946), described from the Gulf of California, Mexico (McCosker and Rosenblatt 2010); *Ariosoma mellissii* (Günther, 1870), endemic to Saint Helena, southern-central Atlantic (Smith 2016); *Ariosoma multivertebratum* Karmovskaya, 2004, known only from Marquesas Islands (Karmovskaya 2004; Delrieu-Trottin et al. 2015); *Ariosoma sereti* Karmovskaya, 2004, described only from Hiva Oa Island, Marquesas Islands (Karmovskaya 2004); and *Ariosoma sazonovi* Karmovskaya, 2004, collected and described only from the Philippines (Karmovskaya 2004); these species were known and described only from holotypes or with very few paratypes. Amongst the ten species from Indian waters, *A. majus* was recorded by Roy et al. (2021) along the east coast of India in the Bay of Bengal showing that *A. majus* was widely distributed in the Indo-Pacific. The new species, *Ariosoma kannani* was collected from two different localities from the Bay of Bengal, which might indicate a wider distributional range, but it is rare in landings. Further, *A. indicum* shows a continuous distribution along the coast of the Arabian Sea and Bay of Bengal. The species, *A. albimaculatum* and *A. melanospilos* were previously known only from type locality, but the first author found plenty of specimens in deep-sea trawl landings at Kollam coast, Arabian Sea.

The phylogenetic analyses of this study was based on only one marker due to availability of comparative sequences in public domain. Phylogenetic analyses for most of the species of the genus *Ariosoma* was meagre, hence vast sampling is needed to fulfil the complete genomics of these congrid eel groups. Furthermore, most eels do not possess economic value and are landed mostly as bycatch and sampling on this group was very rare in Indian waters (Kodeeswaran et al. 2021), but extensive sampling is a prerequisite to understand the complete aspects of this conger eel group's biodiversity along the Indian coast. In addition, species in the genus *Ariosoma* dwell in unusual habitats like continental slopes and underwater seamounts (Shen 1998; Karmovskaya 2018) making them rare in landings. Based on our analyses and results, it suggests that future surveys (sampling and collections) will be extended along the entire coast of India including the islands and may reveal many new species which additionally afford detailed insights into the diversity, ecology and evolution of the *Ariosoma* species.

Authors contribution

PK collected, identified, examined the specimens and prepared the manuscript. PK and AK performed molecular analyses and revised the manuscript. AM identified, examined the specimens and revised the manuscript. DR collected and identified specimens from West Bengal. TTA and CR revised the manuscript. UKS provided comprehensive guidance and supported the work. All authors read and approved the final version of the manuscript.

Acknowledgements

The authors acknowledge the Director, ICAR–National Bureau of Fish Genetic Resources (NBFGR), Lucknow, for providing support and encouragement through the Institutional exploration project. AM and CR thank Dr. Dhriti Banerjee, Director, Zoological Survey of India for providing essential working facilities.

References

Asano H (1958) Studies on the conger eels of Japan. I. Description of two new subspecies referable to the genus *Alloconger*. Zoological Magazine Tokyo 67: 191–196.

Böhlke EB (1982) Vertebral formulae for type specimens of eels (Pisces: Anguilliformes). Proceedings of the Academy of Natural Sciences of Philadelphia, 31–49.

Castle PHJ (1990) Two new species of the previously monotypic congrid eel genera *Poeciloconger* and *Macrocephenchelys* from eastern Australia. Records of the Australian Museum 42(2): 119–126. https://doi.org/10.3853/j.0067-1975.42.1990.109

Delaroche FE (1809) Suite du mémoire sur les espèces de poissons observées à Iviça. Observations sur quelques-uns des poissons indiqués dans le précédent tableau et descriptions des espèces nouvelles ou peu connues. Annales du Muséum d'Histoire Naturelle, Paris 13: 313–361. [pls. 20–25]

Delrieu-Trottin E, Williams JT, Bacchet P, Kulbicki M, Mourier J, Galzin R, de Loma TL, Mou-Tham G, Siu G, Planes S (2015) Shore fishes of the Marquesas Islands, an updated checklist with new records and new percentage of endemic species. Check List 11(5): 1758–1758. https://doi.org/10.15560/11.5.1758

Fowler HW (1938) Studies of Hong Kong fishes. No. 3. Hong Kong Naturalist 6: 1–52.

Fricke R, Mahafina J, Behivoke F, Jaonalison H, Léopold M, Ponton D (2018) Annotated checklist of the fishes of Madagascar, southwestern Indian Ocean, with 158 new records. FishTaxa : Journal of Fish Taxonomy 3(1): 1–432.

Fricke R, Eschmeyer WN, Fong JD (2023) Species by Family/Subfamily. Eschmeyer's Catalog of Fishes. http://researcharchive.calacademy.org/research/ichthyology/catalog/SpeciesByFamily.asp [Online Version, Updated 19 August 2023]

Günther A (1870) Catalogue of the Physostomi, containing the families Gymnotidae, Symbranchidae, Muraenidae, Pegasidae, and of the Lophobranchii, Plectognathi, Dipnoi, Ganoidei, Chondropterygii, Cyclostomata, Leptocardii, in the British Museum. Catalogue of the fishes in the British Museum 8: 1–549.

Günther A (1872) Report on several collections of fishes recently obtained for the British Museum. Proceedings of the Zoological Society of London 3: 652–675. [pls. 53–70]

Hall TA (1999) BioEdit: A user-friendly biological sequence alignment editor and analysis program for Windows 95/98/NT. Nucleic Acids Symposium Series 41: 95–98.

Hoang DT, Chernomor O, Von Haeseler A, Minh BQ, Vinh LS (2018) UFBoot2: Improving the ultrafast bootstrap approximation. Molecular Biology and Evolution 35(2): 518–522. https://doi.org/10.1093/molbev/msx281

Jordan DS, Snyder JO (1900) A list of fishes collected in Japan by Keinosuke Otaki, and by the United States steamer Albatross, with descriptions of fourteen new species. Proceedings of the United States National Museum 23(213): 335–380. https://doi.org/10.5479/si.00963801.23-1213.335

Kalyaanamoorthy S, Minh BQ, Wong TK, Von Haeseler A, Jermiin LS (2017) ModelFinder: Fast model selection for accurate phylogenetic estimates. Nature Methods 14(6): 587–589. https://doi.org/10.1038/nmeth.4285

Karmovskaya ES (1991) New species of conger eel (Congridae) from the western Indian Ocean. Voprosy Ikhtiologii 3: 891–897. [In Russian. English translation in Journal of Ichthyology 32:1–8.]

Karmovskaya ES (2004) Benthopelagic bathyal conger eels of families Congridae and Nettastomatidae from the western tropical Pacific, with descriptions of ten new species. Journal of Ichthyology 44(suppl. 1): S1–S32.

Karmovskaya ES (2015) New species of the genus *Ariosoma*, *A. dolichopterum* (Bathymyrinae), from the waters of Central Vietnam. Journal of Ichthyology 55(6): 906–910. https://doi.org/10.1134/S0032945215060077

Karmovskaya ES (2018) On the species composition of eels of the genus *Ariosoma* (Anguilliformes: Congridae) from NhaTrang and Van Phong Bays (South China Sea, Central Vietnam). Journal of Ichthyology 58(4): 455–472. https://doi.org/10.1134/S0032945218040070

Karrer C (1983) Anguilliformes du Canal de Mozambique (Pisces, Teleostei). Faune Tropicale (23): 1–116.

Kodeeswaran P, Jayakumar TKT, Akash S, Kumar TTA, Lal KK (2021) A new species of Congrid eel, *Ariosoma melanospilos* sp. nov., from Indian waters with taxonomic description of *A. dolichopterum* (Congridae: Bathymyrinae). Marine Biodiversity 51(3): 47. https://doi.org/10.1007/s12526-021-01187-8

Kodeeswaran P, Mohapatra A, Dhinakaran A, Ajith Kumar TTP, Lal KK (2022a) A new species of the congrid eel genus *Ariosoma* (Anguilliformes: Congridae) from the Southwest coast of India. Journal of Fish Biology 100(3): 775–782. https://doi.org/10.1111/jfb.14994

Kodeeswaran P, Kathirvelpandian A, Acharya S, Mohanty SR, Mohapatra A, Ajith Kumar TTP, Lal KK (2022b) *Ariosoma indicum* sp. nov., a new species of congrid eel (Anguilliformes: Congridae: Bathymyrinae) from the Indian waters. Journal of Fish Biology 100(6): 1447–1454. https://doi.org/10.1111/jfb.15055

Kodeeswaran P, Dhas D, Ajith Kumar TTP, Lal KK (2023) Description of a new congrid eel, *Ariosoma albimaculata* sp. nov. (Anguilliformes: Congridae), from the southwest coast of India, Arabian Sea. Ichthyological Research 70(2): 233–242. https://doi.org/10.1007/s10228-022-00882-1

Kodeeswaran P, Kathirvelpandian A, Mohapatra A, Ajith Kumar TTP (in press) A new species of the congrid eel genus *Ariosoma* (Teleostei: Anguilliformes: Congridae) from the Southeast coast of India. Bay of Bengal.

Kumar S, Stecher G, Li M, Knyaz C, Tamura K (2018) MEGA X: Molecular Evolutionary Genetics Analysis across computing platforms. Molecular Biology and Evolution 35(6): 1547–1549. https://doi.org/10.1093/molbev/msy096

Letunic I, Bork P (2021) Interactive Tree Of Life (iTOL) v5: An online tool for phylogenetic tree display and annotation. Nucleic Acids Research 49(W1): W293–W296. https://doi.org/10.1093/nar/gkab301

McCosker JE, Rosenblatt RH (2010) The fishes of the Galápagos Archipelago: An update. Proceedings of the California Academy of Sciences 61(2): 167–195.

McCulloch AR, Waite ER (1916) Additions to the fish fauna of Lord Howe Island No. 5. Transactions of the Royal Society of South Australia 40: 437–451.

Nguyen LT, Schmidt HA, Von Haeseler A, Minh BQ (2015) IQ-TREE: A fast and effective stochastic algorithm for estimating maximum-likelihood phylogenies. Molecular Biology and Evolution 32(1): 268–274. https://doi.org/10.1093/molbev/msu300

Poey F (1860) Memorias sobra la historia natural de la Isla de Cuba, acompañadas de sumarios Latinos y extractos en Francés. Tomo 2. La Habana 2: 97–336. https://doi.org/10.5962/bhl.title.2485

Ray D, Acharya S, Khatua T, Roy D, Mohapatra A, Mishra SS (2022) A new species of conger eel, *Ariosoma* (Congridae: Bathymyrinae), from the Bay of Bengal, India. Zootaxa 5165(1): 133–143. https://doi.org/10.11646/zootaxa.5165.1.8

Roy D, Khatua T, Ray D, Mohapatra A (2021) First Report of Conger Eel (Anguilliformes: Congridae) *Ariosoma majus* (Asano, 1958) From Indian Ocean. Thalassas. Thalassas 37(1): 93–96. https://doi.org/10.1007/s41208-020-00284-y

Shen SC (1998) A review of congrid eels of the genus *Ariosoma* from Taiwan, with description of a new species. Zoological Studies-Taipei 37: 7–12.

Smith DG (1989) Family Congridae. In: Böhlke EB (Ed.) Fishes of the Western North Atlantic, Pt 9, 1. Memoir Sears Foundation for Marine Research, New Haven, 460–567.

Smith DG (2016) Miscellaneous groups (Pp. 1590–1613, 1643–1653, 1667–1714). In: Carpenter, De Angelis (Eds) The living marine resources of the Eastern Central Atlantic. Volume 3. Bony fishes part 1 (Elopiformes to Scorpaeniformes). FAO Species Identification Guide for Fishery Purposes, Rome, FAO. v. 3. i–xiv + 1511–2350.

Smith DG, Kanazawa RH (1977) Eight new species and a new genus of congrid eels from the western north Atlantic with redescriptions of *Ariosoma analis*, *Hildebrandia guppyi*, and *Rhechias vicinalis.* Bulletin of Marine Science 27: 530–543.

Smith DG, Ho HC, Huang JF, Chang YH (2018) The congrid eel genus *Ariosoma* in Taiwan (Anguilliformes: Congridae), with description of a new species. Zootaxa 4454(1): 84–106. https://doi.org/10.11646/zootaxa.4454.1.10

Strömman PH (1896) Leptocephalids in the University Zoological Museum at Upsala. Almqvist & Wiksell, Uppsala. 1–53. [pls. 1–5] https://doi.org/10.5962/bhl.title.56320

Swainson W (1838) On the natural history and classification of fishes, amphibians, & reptiles, or monocardian animals. Vol. 1. A. Spottiswoode, London, 368 pp. https://doi.org/10.5962/bhl.title.62140

Talwar PK, Mukherjee P (1977) A note on a new bathypelagic eel, *Ariosoma gnanadossi*, from the Bay of Bengal. The Indian Journal of Animal Sciences 47: 432–434.

Temminck CJ, Schlegel H (1846) Pisces, in Fauna Japonica, Sive Descriptio Animalium Quae in Itinere per Japoniam Suscepto Annis 1823–30 Colle-git, Notis Observationibus et Adumbrationibus Illustravit P.F. de Siebold. Fauna Japonica, Sive Descriptio Animalium Quae in Itinere per Japoniam, Batavia: Lugduni Batavorum, 1846, parts 10–14, 173–269.

Wade CB (1946) Two new genera and five new species of apodal fishes from the eastern Pacific. Allan Hancock Pacific Expeditions 9(7): 181–213.

Zoosyst. Evol. 100 (1) 2024, 129–140 | DOI 10.3897/zse.100.113132

Supplemental re-description of a deep-sea ascidian, *Fimbrora calsubia* (Ascidiacea, Enterogona), with an inference of its phylogenetic position

Naohiro Hasegawa[1], Natsumi Hookabe[2], Yoshihiro Fujiwara[2], Naoto Jimi[3,4], Hiroshi Kajihara[5]

1 *Department of Natural History Sciences, Graduate School of Science, Hokkaido University, Kita 10 Nishi 8 Kitaku, Sapporo, Hokkaido, 060-0810, Japan*
2 *Research Institute for Global Change (RIGC), Japan Agency for Marine-Earth Science and Technology (JAMSTEC), Yokosuka, Kanagawa 237-0061, Japan*
3 *Sugashima Marine Biological Laboratory, Graduate School of Science, Nagoya University, 429-63 Sugashima, Toba, Mie 517-0004, Japan*
4 *Centre for Marine & Coastal Studies, Universiti Sains Malaysia, 11800 USM, Penang, Malaysia*
5 *Faculty of Science, Hokkaido University, Kita 10 Nishi 8 Kitaku, Sapporo, Hokkaido, 060-0810 Japan*

https://zoobank.org/D84B5915-751E-4BAC-BB3A-A45E9282FE29

Corresponding author: Naohiro Hasegawa (hoya.hasegawa.ronbun@gmail.com)

Academic editor: Pavel Stoev ♦ **Received** 22 September 2023 ♦ **Accepted** 11 January 2024 ♦ **Published** 26 January 2024

Abstract

Fimbrora Monniot & Monniot, 1991, a macrophagous ascidian genus within the family Ascidiidae Adams & Adams, 1858, is currently monotypic, represented by *F. calsubia* Monniot & Monniot, 1991, a species previously recorded from the bottom of the South Pacific at depths of 1000–1860 m. The taxonomic status of *Fimbrora* has remained ambiguous because characteristics in its branchial papillae and neural-gland opening are incompletely known in previous studies, while these traits are essential for distinguishing other ascidiid genera. So far, no nucleotide sequence representing *F. calsubia* is available. In this study, we collected a single specimen of *F. calsubia* at a depth of 2027 m, about 400 km off the Pacific coast of Honshu, Japan. This is the deepest record, as well as the first report from the North Pacific, for the species. Our examination indicates that *Fimbrora* is morphologically similar to another ascidiid genus, *Psammascidia* Monniot, 1962, by having only secondary branchial papillae in the pharynx. Our phylogenetic analysis, based on the 18S ribosomal RNA and cytochrome *c* oxidase subunit I genes, along with those of 27 ascidian species available in public databases, showed that *F. calsubia* was more closely related to *Ascidia zara* Oka, 1935, *Phallusia fumigata* (Grube, 1864) and *Phallusia mammilata* (Cuvier, 1815) than to *Ascidia ceratodes* (Huntsman, 1912), *Ascidiella aspersa* (Müller, 1776) and *Ascidiella scabra* (Müller, 1776). Our results also indicated that acquisitions of macrophagous feeding by deep-sea members happened independently at least three times in the evolutionary history of the entire Ascidiacea.

Key Words

bathyal zone, biogeography, Chordata, phylogeny, taxonomy, Tunicata, Urochordata

Introduction

The ascidiid genus *Fimbrora* Monniot & Monniot, 1991a is currently monotypic, consisting of the deep-sea ascidian *Fimbrora calsubia* Monniot & Monniot, 1991a. The taxonomic identity of *Fimbrora* is not fully established because states of some characters used for distinguishing other ascidiid genera are not known for this taxon. Apart from *Fimbrora*, the family Ascidiidae Adams & Adams, 1858 also contains four genera: *Ascidia* Linnaeus, 1767; *Ascidiella* Roule, 1884; *Phallusia* Savigny, 1816; and *Psammascidia* Monniot, 1962. *Fimbrora* is supposed to be distinguished from the other ascidiid genera by having a combination of three characteristics: *i*) the large, cup-shaped oral siphon with thin, uniformly long, and soft lobes, *ii*) two large blood vessels running on the oral-siphon wall and *iii*) macrophagous feeding behaviour (cf. Monniot and Monniot (1991a)). The remaining four

genera are distinguished from each other, based on: *i*) whether primary and/or secondary branchial papillae in the pharynx are present and *ii*) whether accessory openings of the neural gland are present (e.g. Kott (1985); Monniot et al. (1991); Rocha et al. (2012)). However, while the branchial papillae have been reported to be present in *Fimbrora* (Monniot & Monniot, 1991a), whether they are primary and/or secondary was not mentioned in any of the previous literature (Monniot and Monniot 1991a; Monniot 1993; Monniot and López-Legentil 2017); also, the nature of the neural-gland opening (or, whether accessory openings are present) has not been stated in any of these works.

While ascidians are generally suspension feeders that filter food particles, such as phytoplankton, from the surrounding seawater (Millar 1971), 40 species have hitherto been identified as macrophagous, based on their large oral siphons and unciliated pharynges; direct confirmation of this feeding behaviour was made in 10 species by the presence of small crustaceans in their gut contents (Table 1). These macrophagous ascidians exclusively inhabit deep waters below 200 m with one exception, *Oligotrema psammites* Bourne, 1903, which is also distributed up to 90 m (Table 1). In addition to *Fimbrora*, another three ascidian taxa—the family Octacnemidae, Herdman 1888 (with 26 species in 10 genera), as well as the two molgulid genera *Asajirus* Kott, 1989 (with eight species) and *Oligotrema* Bourne, 1903 (with five species)—are known to consist of macrophagous members (Table 1). Previously, certain morphological data suggested that macrophagous feeding amongst ascidians evolved convergently, probably due to difficulty in filter-feeding in the deep sea (Millar 1959). This view was confirmed by the phylogenetic study of Tatián et al. (2011), including two macrophagous taxa, the octacnemid *Megalodicopia* Oka, 1918 and the molgulid *Oligotrema*, but *F. calsubia* has not been represented with any molecular sequence data.

The taxonomy of macrophagous molgulids has experienced twists and turns. Historically, *Asajirus* and *Oligotrema* were once considered by Kott (1989) to comprise the now-abandoned family Hexacrobylidae Seeliger, 1906, for which the monofamilial order Aspiraculata and the mono-order class Sorberacea had been established by Seeliger (1906) and Monniot et al. (1975), respectively. These suprafamilial higher taxa were rejected by Kott (1989), who also noted morphological similarities between Hexacrobylidae and Molgulidae Lacaze-Duthiers, 1877. At another time, Hexacrobylidae was regarded by Monniot and Monniot (1990) to consist of the four genera *Hexacrobylus* Sluiter, 1905a, *Gasterascidia* Monniot & Monniot, 1968, *Sorbera* Monniot & Monniot, 1974 and *Hexadactylus* Monniot & Monniot, 1990, the first three of which were synonymised with *Oligotrema* by Kott (1989) and the last was synonymised with *Asajirus* by Kott (1992). Later, Hexacrobylidae was demonstrated to be a junior synonym of Molgulidae by a molecular phylogenetic analysis supporting the inclusion of *O. lyra* (Monniot & Monniot, 1973) in the latter family (Tatián et al. 2011). Until then, Hexacrobylidae/Aspiraculata/Sorberacea had been occasionally considered valid in certain publications (e.g. Monniot (2001)).

So far, *F. calsubia* has been known from the South Pacific bathyal zone in three publications, based on a total of 13 specimens: three specimens at a depth of 1865 m in New Caledonian waters (Monniot and Monniot 1991a), two specimens at about 1000 m depth in Indonesia (Monniot 1993) and eight specimens at 1000–1200 m depth in Papua New Guinea (Monniot and López-Legentil 2017). Meanwhile, during a biodiversity survey in an off-shore submarine nature conservation area around Nishi-Shichito Ridge in the western North Pacific, a 14th individual of *F. calsubia* was obtained. Here, we provide a morphological re-description and an inference of its molecular phylogenetic position within the class Ascidiacea.

Materials and methods

A single specimen of *F. calsubia* was collected near the south of Hoei Seamount, about 400 km off the Pacific coast of Honshu, Japan (Fig. 1), with a manipulator of the human-occupied vehicle *Shinkai 6500* (Dive No. 1651) during the cruise YK22-17C of the R/V *Yokosuka* (Suppl. material 1, 2). The live animal was photographed with an OM-D E-M1X digital still camera (Olympus, Tokyo, Japan) attached to an M.Zuiko Digital ED 30 mm F3.5 Macro lens (Olympus). Two of the thread-like lobes of the specimen were dissected from the oral siphon; one was preserved in 99% ethanol for DNA extraction, the other in RNAlater (Thermo Fisher Scientific, Waltham, MA, USA) for future analysis; the remaining body was fixed in 10% formalin seawater for morphological observation. For detailed examination, the pharynx was stained with haematoxylin. The voucher specimens have been deposited in the Japan Agency for Marine-Earth Science and Technology (JAMSTEC), Yokosuka, with the catalogue number JAMSTEC No. 111618 for the formalin-fixed specimen, JAMSTEC No. 111619 for the lobe in 99% ethanol and JAMSTEC No. 111620 for the lobe in RNAlater.

Total DNA was extracted using a DNeasy Tissue Kit (Qiagen, Hilden, Germany). For amplification, KOD One PCR Master Mix (TOYOBO, Osaka, Japan) was used. Partial sequences of the 18S rRNA (18S) gene and the mitochondrial cytochrome *c* oxidase subunit I (COI) gene were PCR amplified from the total DNA; the primer pairs 1F/9R (Giribet et al. 1996) and dinF/Nux1R (Brunetti et al. 2017) were used for 18S and COI, respectively. PCRs were performed under the following conditions. For 18S: 94 °C for 2 min; 35 cycles of 94 °C for 45 sec, 52 °C for 50 sec and 72 °C for 90 sec; then 72 °C for 5 min. For COI: 94 °C for 2 min; 35 cycles of 94 °C for 40 sec, 50 °C for 60 sec and 72 °C for 60 sec; then 72 °C for 7 min. Purification of PCR products was conducted by enzymatic reaction with ExoSAP-IT (Applied Biosystem, Waltham, MA, USA). The purified products were

Table 1. List of macrophagous species in Ascidiacea with information about family, species, depth, evidence for macrophagous feeding and references.

Family	Species	Depth (m)	Evidence for macrophagous feeding*	References
Ascidiidae	*Fimbrora calsubia* Monniot & Monniot, 1991	1000–2027	m/c	Monniot and Monniot (1991a), Monniot (1993), Monniot and López-Legentil (2017), present study
Octacnemidae	*Benthascidia michaelseni* Ritter, 1907	399	m	Ritter (1907), Monniot (1998)
	Cibacapsa gulosa Monniot & Monniot, 1983	567	m/c	Monniot and Monniot (1983)
	Cryptia planum Monniot & Monniot, 1985	4930	m/c	Monniot and Monniot (1985a)
	Dicopia antirrhinum Monniot, 1972	600–4300	m/c	Monniot (1972), Monniot and Monniot (1974, 1985a), Sanamyan (2014)
	Dicopia fimbriata Sluiter, 1905	1210	m	Sluiter (1905a), Monniot and Monniot (1991b), Monniot and López-Legentil (2017), Sanamyan and Sanamyan (1999)
	Dicopia japonica Oka, 1913	4526–4609	m	Oka (1913), Millar (1988)
	Kaikoja globosa Monniot, 1998	1978	m	Monniot (1998)
	Kaikoja multitentaculata (Vinogradova, 1975)	4485–4520	m	Vinogradova (1975), Sanamyan and Sanamyan (2002)
	Megalodicopia hians Oka, 1918	200–5325	m/c	Oka (1918), Tokioka (1953), Kott (1969), Nishikawa (1991), Sanamyan (1998), Okuyama et al. (2002), Havenhand et al. (2006)
	Megalodicopia rineharti (Monniot & Monniot, 1989)	695–3970	m	Monniot and Monniot (1989), Sanamyan and Sanamyan (2002)
	Myopegma melanesium Monniot & Monniot, 2003	445–472	m/c	Monniot and Monniot (2003)
	Myopegma midatlantica Monniot, 2011	2087	m	Monniot (2011)
	Octacnemus alatus Monniot & Monniot, 1985	3344	m	Monniot and Monniot (1985b)
	Octacnemus bythius Moseley, 1876	1957–4087	m/c	Moseley (1876), Ritter (1906), Ihle (1935), Millar (1959), Monniot and López-Legentil (2017)
	Octacnemus ingolfi Madsen, 1947	640–4655	m	Madsen (1947), Monniot and Monniot (1973, 1976, 1985a, 1985b, 1985c, 1991b, 2003), Sanamyan (2014)
	Octacnemus kottae Sanamyan & Sanamyan, 2002	3700–3910	m	Sanamyan and Sanamyan (2002)
	Octacnemus vinogradovae Sanamyan & Sanamyan, 1999	5400	m	Sanamyan and Sanamyan (1999)
	Octacnemus zarcoi Monniot & Monniot, 1984	4260–4270	m/c	Monniot and Monniot (1984a), Sanamyan (2014)
	Polyoctacnemus patagoniensis (Metcalf, 1893)	1920	m	Metcalf (1893), Ihle (1935)
	Situla cuculli Monniot & Monniot, 1991	2040	m	Monniot and Monniot (1991b)
	Situla galeata Monniot & Monniot, 1991	1395–4891	m	Monniot and Monniot (1991b), Sanamyan and Sanamyan (1998)
	Situla lanosa Monniot & Monniot, 1973	1800–4990	m	Monniot and Monniot (1973, 1974, 1985a), Sanamyan (2014)
	Situla macdonaldi Monniot & Monniot, 1977	790	m	Monniot and Monniot (1977)
	Situla pelliculosa Vinogoradova, 1969	5035–8400	m	Vinogradova (1969)
	Situla rebainsi Vinogradova, 1975	3700–5651	m	Vinogradova (1975), Sanamyan and Sanamyan (2002)
	Situla rineharti Monniot & Monniot, 1989	695–3680	m	Monniot and Monniot (1989, 1991b)
Molgulidae	*Asajirus arcticus* (Hartmeyer, 1923)	905–1283	m	Hartmeyer (1923)
	Asajirus dichotomus (Monniot & Monniot, 1984)	3550	m	Monniot and Monniot (1984a, 1985a), Kott (1989)
	Asajirus eunuchus (Monniot & Monniot, 1976)	2000–5000	m	Monniot and Monniot (1976)
	Asajirus gulosus (Monniot & Monniot, 1984)	1800–2500	m	Monniot and Monniot (1984a), Kott (1989)
	Asajirus hemisphericus (Monniot & Monniot, 1990)	3680–3740	m	Monniot and Monniot (1990)
	Asajirus indicus (Oka, 1913)	800–5000	m/c	Oka (1913), Hartmeyer (1923), Van Name (1945), Millar (1959, 1970), Kott (1957, 1969, 1989), Monniot (1969, 1971), Monniot and Monniot (1968, 1970, 1973, 1974, 1976, 1982, 1984a, 1984b, 1985a, 1985b, 1990), Sanamyan and Sanamyan (2006), Maggioni et al. (2018, 2022)
	Asajirus ledanoisi (Monniot & Monniot, 1990)	720–4829	m	Monniot and Monniot 1973; 1974; 1977; 1985b; 1990; Sanamyan 2014
	Asajirus ovirarus (Monniot & Monniot, 1990)	820–1900	m	Monniot and Monniot 1990; 2003
	Oligotrema lyra (Monniot & Monniot, 1973)	3360–4680	m/c	Monniot C. and Monniot F. (1973, 1974, 1984b, 1985a, 1990), Kott (1989), Sanamyan and Sanamyan (1999), Sanamyan (2014)
	Oligotrema psammatodes (Sluiter, 1905)	1158	m	Millar (1969), Sluiter (1905a, 1905b), Monniot and Monniot (1990)
	Oligotrema psammites Bourne, 1903	90–4000	m	Bourne (1903), Monniot and Monniot (1990), Monniot (2022), Kott (1992, 2009)
	Oligotrema sandersi (Monniot & Monniot, 1968)	2200–5020	m	Monniot and Monniot (1968, 1970, 1974, 1985a, 1990), Millar (1970), Kott (1989), Sanamyan (2014)
	Oligotrema unigonas (Monniot Monniot, 1974)	2300–5500	m	Monniot and Monniot (1974, 1984b, 1985a, 1985b, 1990), Kott (1989), Sanamyan (2014)

*'m' indicates that the species was judged to be macrophagous, based on morphological characteristics; 'm/c' indicates that gut contents were also observed in addition to morphological features.

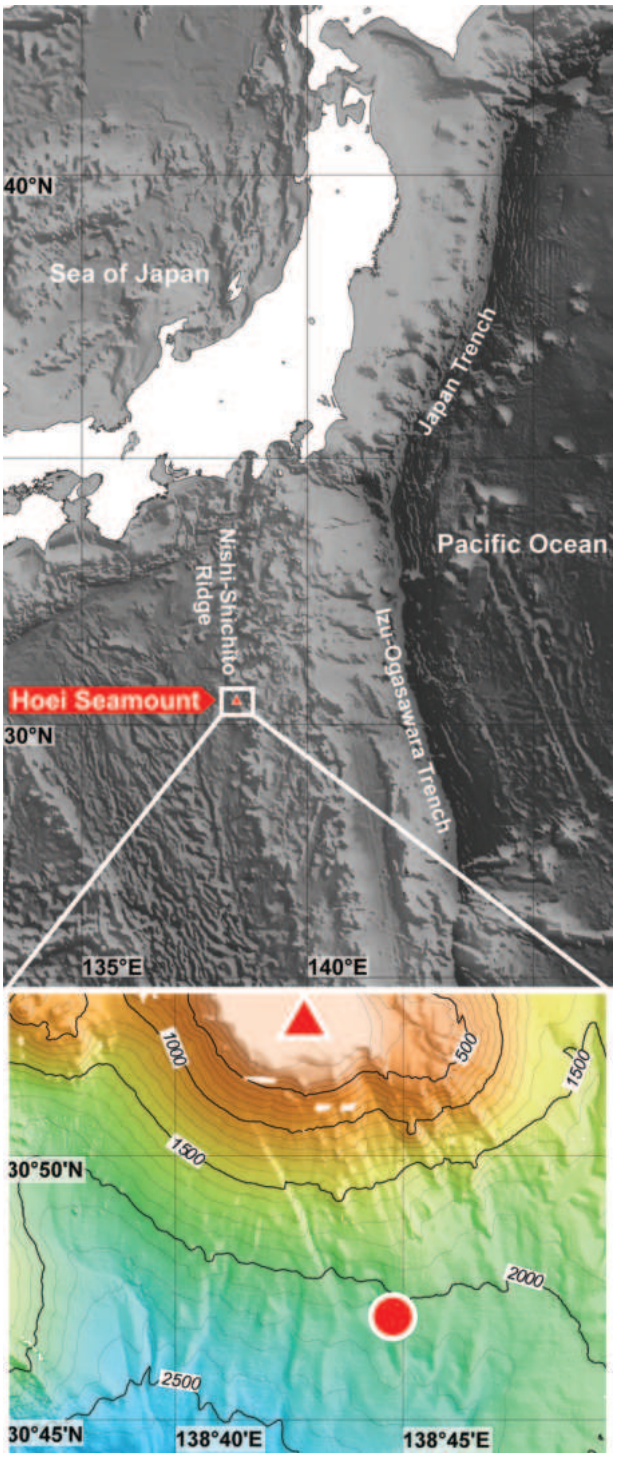

Figure 1. Maps showing the sampling site (red circle), south of Houei Seamount (of which the top is indicated with a red triangle). The images were generated by using GMT 6 (Wessel et al. 2019), based on grid data provided by the General Bathymetric Chart of the Oceans.

sequenced with an ABI BigDye Terminator ver. 3.1 Cycle Sequencing Kit and an ABI 3100 Avant Genetic Analyzer (Applied Biosystem), using the same primer pairs for amplification; for 18S, the internal primers 3F and 5R (Giribet et al. 1996), as well as a2.0 and bi (Whiting et al. 1997), were also used.

For phylogenetic analysis, 18S and COI sequences of 27 ascidian species and those of the lancelet *Branchiostoma floridae* Hubbs, 1922 were downloaded from GenBank (Table 2). The dataset of 18S was aligned using MAFFT ver. 7.310 with *E-INS-I* strategy (Katoh and Standley 2013); the aligned 18S dataset was trimmed by using trimAl ver. 1.4. rev15 with gappyout command (Capella-Gutiérrez et al. 2009). An alignment of COI was obtained by using MEGA X (Kumar et al. 2018) following Hasegawa and Kajihara (2019). Then, the 18S and COI sequences were concatenated on MEGA X (Kumar et al. 2018).

Table 2. The GenBank accession numbers of 18S and COI sequences of *Fimbrora calsubia* Monniot & Monniot, 1991a, as well as 27 ascidian species and the lancelet *Branchiostoma floridae* Hubbs, 1922, used for phylogenetic analysis in this study.

Species	18S	COI
Ascidia ceratodes	L12378	MW872268
Ascidia zara	LC547325	KY235397
Ascidiella aspersa	LC547321	KF886702
Ascidiella scabra	AB811928	MN064599
Botrylloides violaceus	LC432326	LC432331
Chelyosoma siboja	AF165821	AB104867
Ciona robusta	AB013017	MF479417
Ciona savignyi	LC547329	MK512499
Clavelina lepadiformis	JN573225	AY603104
Clavelina meridionalis	FM244840	AM706470
Corella eumyota	FM244846	KU299765
Ecteinascidia herdmanni	FM244847	AY600968
Ecteinascidia turbinata	FM244848	MT873564
Fimbrora calsubia	LC777587	LC777585
Halocynthia roretzi	AB013016	HM151268
Herdmania momus	AF165827	KM411616
Megalodicopia hians	AB075543	AB104866
Molgula manhattensis	L12426	MT873565
Oligotrema lyra	JN565043	–
Perophora japonica	AB499607	MN064600
Perophora viridis	FM244849	OM912740
Phallusia fumigata	FM244844	KF309548
Phallusia mammillata	AF236803	MN064634
Pycnoclavella diminuta	KJ632948	KC017435
Pyura mirabilis	LC432327	LC432332
Styela clava	LC432329	LC432334
Symplegma reptans	AF165826	LS992553
Syncarpa composita	LC432325	LC432330
Branchiostoma floridae	M97571	AB478593

For constructing phylogenetic trees, Bayesian Inference (BI) and Maximum Likelihood (ML) analyses were performed; MrBayes ver. 3.2.6 (Huelsenbeck and Ronquist 2001; Ronquist and Huelsenbeck 2003: Ronquist et al. 2012) for BI and the ultrafast bootstrap method (Hoang et al. 2018) implemented in IQtree (Nguyen et al. 2015) for ML. PartitionFinder ver. 2.1.1 (Lanfear et al. 2016) was used for selecting the best-fit substitution models, which suggested GTR + I + G for 18S and COI first codon position and GTR + G for COI second and third codon positions. For BI, Markov chains were

started from a random tree and run for 10^7 generations; trees were picked up every 100 generations from the chain. Burn-in was set at 25%. The "sumt" command was used for calculating a consensus of trees; the posterior probability (PP) for each node was collected to assess the certainty of the inference. Run convergence was assumed, based on the following values of variables: average standard deviation of split frequencies = 0.002002; average estimated sample size of all parameters > 200; and potential scale reduction factor for all parameters ≤ 1.008. For ML analysis, branch support was calculated with 1000 ultrafast bootstraps (Minh et al. 2013).

Results

Taxonomy and morphology

Order Enterogona
Suborder Phlebobranchia
Family Ascidiidae Adams & Adams, 1858

***Fimbrora calsubia* Monniot & Monniot, 1991a**
Figs 2–4

Fimbrora calsubia Monniot & Monniot, 1991a, p. 384, figs 1–6; Monniot (1993), p. 356; Monniot and López-Legentil (2017), p. 531, figs 1, 2.

New Japanese name. *Yorifusa-boya*, from *yorifusa*, an ornament for kimonos and Japanese accessories and *boya*, a phonological variant of *hoya*, meaning a sea squirt.

Material examined. One individual, JAMSTEC No. 111618, collected by N. Hookabe on 26 September 2022, about 400 km off the Pacific coast of middle Honshu, Japan, 30°47.05'N, 138°44.72'E, at a depth of 2027 m (Fig. 1).

Description. Individual ca. 20 cm in length including oral siphon (Fig. 2A, B). Tunic opaque and gelatinous; blood vessels running on surface of tunic (Fig. 2B); fine warts, each about 0.5 mm in diameter, scattered evenly over entire tunic. Body attached to substrate with its posterior end (Fig. 2A, B). Oral siphon enlarged, ca. 10 cm in diameter; single annular muscle strand running on outer edge of oral siphon; thread-like lobes, 52 in number, tightly arranged to each other on oral-siphon edge; single groove radially arranged on edge of oral siphon between base of each lobe; muscle strand associated to each lobe, running on inner wall of oral-siphon edge from lobe base for ca. 1 cm; beneath inner surface of oral siphon, neural cords radially running from neural ganglion (Fig. 2C). Oral aperture situated 2.5 cm anterior to neural ganglion. Atrial siphon 1.5 cm in diameter; 37 blood vessels longitudinally running on surface of atrial siphon (Fig. 2D).

Body wall attached to tunic on oral siphon, heart and renal vesicles; irregular cavity existing between tunic and body wall; inner surface of tunic covered with epithelial tissue. Neural ganglion situated between oral siphon and atrial siphon. On base of oral siphon, 105 oral tentacles present, each being ca. 8 mm in length. Peripharyngeal band made of single lamina running in a short distance posterior to oral tentacles, forming V-shape posterior to neural gland aperture (Fig. 3A); latter being single in number, almost straight in shape (Fig. 3A) and opening at dorsal tubercle. Pharynx connected by mesenteries to peripharyngeal epithelium; mesenteries 0.5–3.0 mm in diameter (Fig. 3B). Smooth dorsal lamina running along mid-line on ventral side of pharynx (Fig. 3A, B). Longitudinal and transverse vessels running on inner surface of pharynx (Fig. 3C); 6–10 stigmata without lateral cilia per mesh (Fig. 3C). Secondary branchial papillae present on intersections of longitudinal and transverse vessels (Fig. 3C).

Digestive tract positioned on left side of body (Fig. 4A). Oesophagus opening to left side of dorso-posterior part of pharynx. Stomach about 1.5 cm in length, having 10 folds, surrounded with renal vesicles (Fig. 4A); multiple crustaceans (probably copepods) found in stomach lumen (Fig. 4B). Intestinal loop S-shaped, having primary loop and secondary loop; intestine ca. 7 cm in length, ca. 5 mm in diameter (Fig. 4A). Anus smoothly edged, opening close to atrial siphon (Fig. 4A).

Gonad situated proximally on intestinal loop (Fig. 4C). Ovaries surrounded with male testis (Fig. 4C, D). Oviduct and spermiduct running along secondary loop, opening close to anus (Fig. 4A). Eggs contained in ovaries and oviduct, up to 0.2 mm in diameter (Fig. 4D).

Habitat. The animal attached itself to a dead sponge in an area with accumulated sand and mud at a depth of 2027 m, where the water temperature was 1.93 °C (Fig. 2A; Suppl. material 1). It opens the oral aperture in the direction facing the water current (Suppl. material 2). An euplectellid sponge was also found attached to the same substrate. Macrobenthos found around this area included other sponges, octocorals, sandy creeplets, sea anemones and sea lilies.

Molecular phylogeny

The clade consisting of four genera in the family Ascidiidae, i.e. *Ascidia*, *Ascidiella*, *Fimbrora* and *Phallusia*, received high support values (97% bootstrap; 1.00 posterior probability) (Fig. 5). In this clade, *F. calsubia* was most closely related to *Ascidia zara* Oka, 1935, but with less-supported values (53% bootstrap; 0.68 posterior probability). The clade of *Ascidia* + *Fimbrora* + *Phallusia* was sister to the genus *Ascidiella*. The genus *Ascidia* was recovered as a non-monophyletic group.

The three macrophagous ascidians included in this analysis—*F. calsubia*, *Megalodicopia hians* Oka, 1918 and *Oligotrema lyra*—were each positioned differently in the phylogenetic tree. As in previous analyses (Kurabayashi et al. 2003; Tatián et al. 2011), *M. hians* was sister to *Corella eumyota* Traustedt, 1882; *O. lyra* was sister to *Molgula manhattensis* (De Kay, 1843).

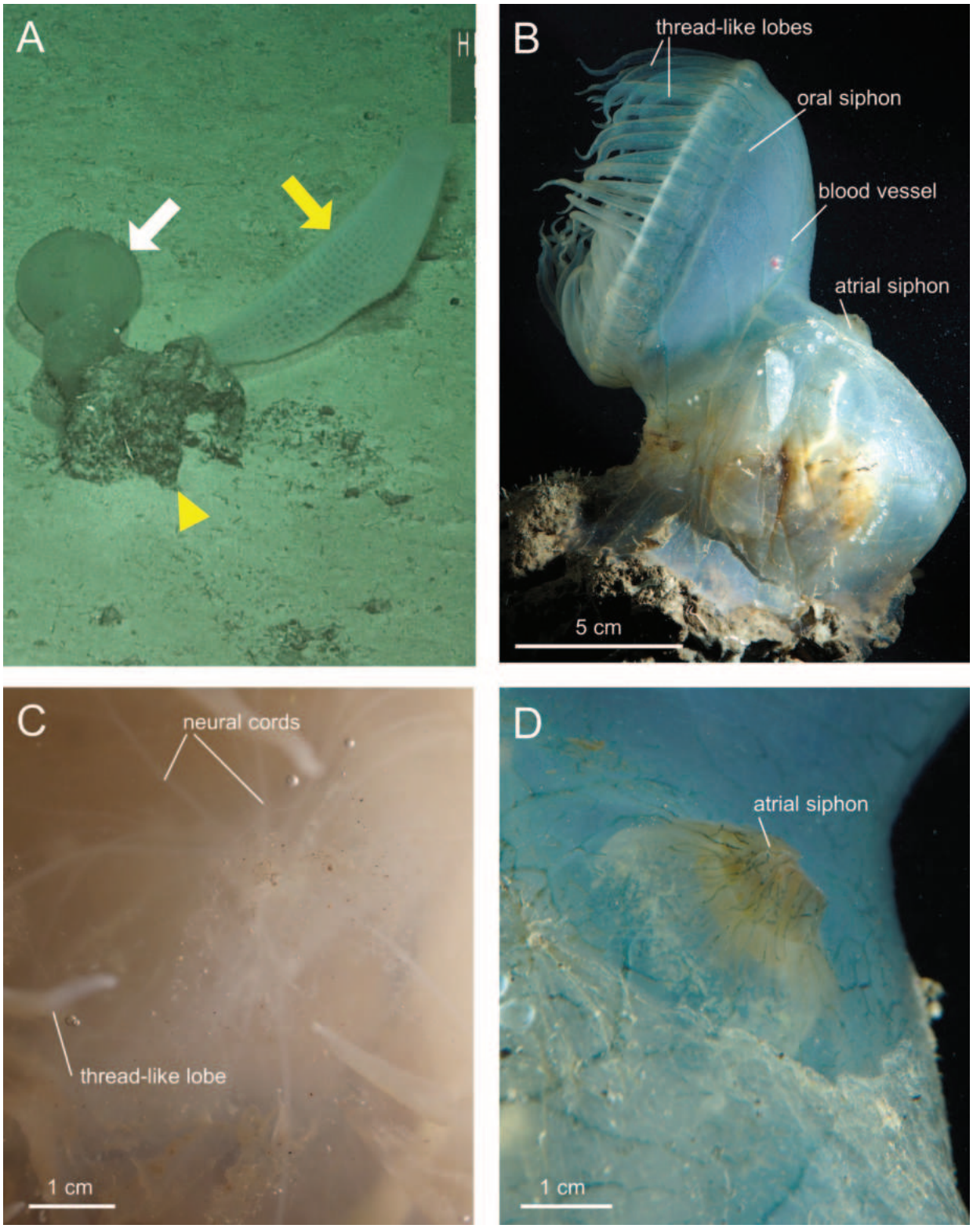

Figure 2. *Fimbrora calsubia* Monniot & Monniot, 1991a, photographs showing external appearance of JAMSTEC No. 111618. **A.** The individual *in situ* (white arrow), attaching to a dead sponge (yellow arrowhead) along with a euplectellid glass sponge (yellow arrow); **B.** Left view in life; **C.** Inner surface of the oral siphon in fixed state; **D.** Enlarged view of atrial siphon in life.

Discussion

Previous studies posited that *Fimbrora* would belong to Ascidiidae (Monniot and Monniot 1991a; Monniot and López-Legentil 2017) and our phylogenetic analysis supported this view. The morphological characteristics that suggested *Fimbrora*'s familial affiliation were the longitudinal vessels having papillae and straight stigmata in the pharynx (Monniot and Monniot 1991a; Monniot

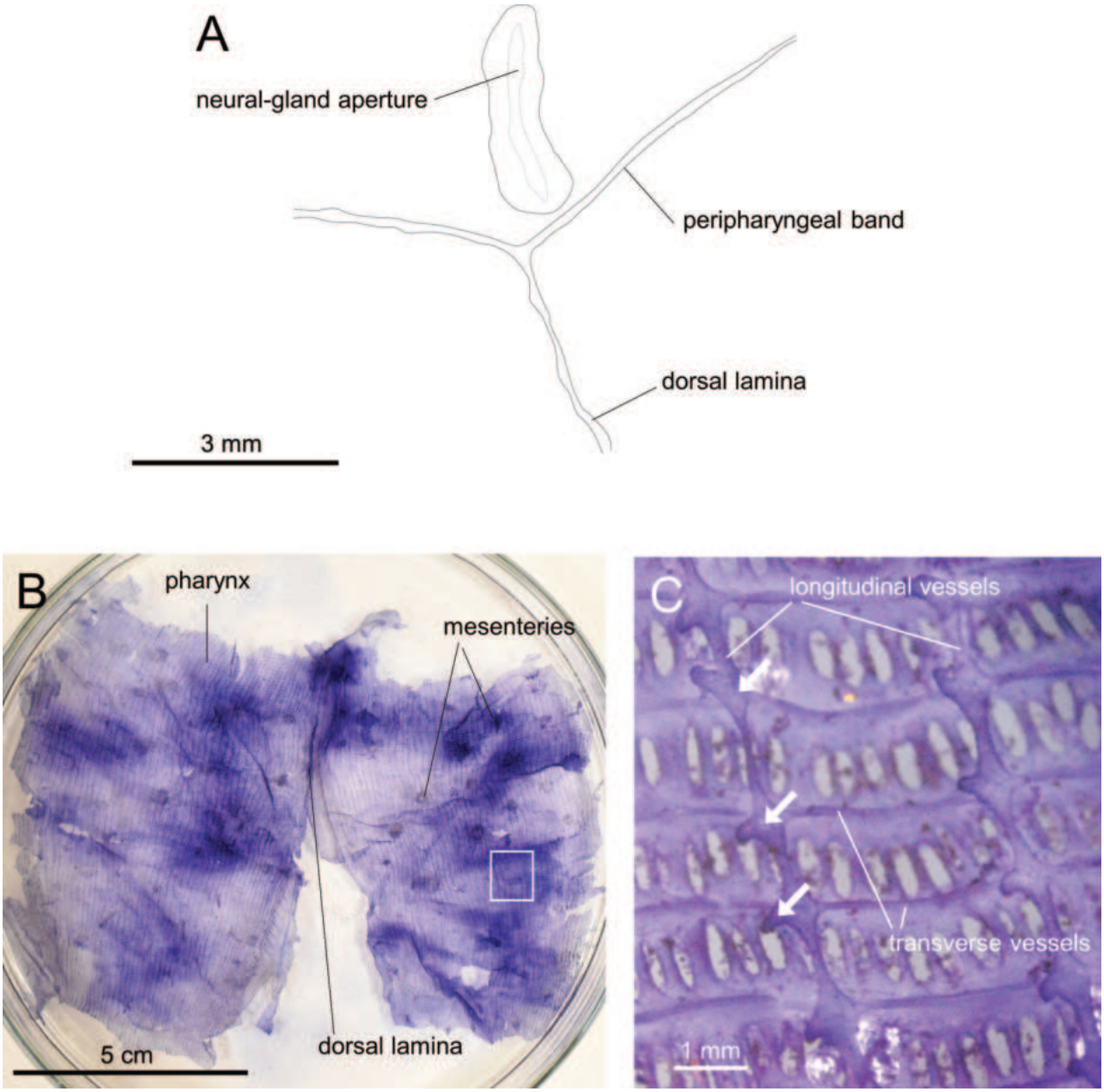

Figure 3. *Fimbrora calsubia* Monniot & Monniot, 1991a (JAMSTEC No. 111618). **A.** Drawing of dissected specimen, showing the shape of neural-gland aperture, peripharyngeal band and dorsal lamina; **B.** Photograph of dissected pharynx cut open from ventral side; **C.** Magnification of the rectangle on B, showing the arrangement of longitudinal vessels, transverse vessels, stigmata and secondary branchial papillae (indicated with arrows).

and López-Legentil 2017), while Monniot and Monniot (1991a) noted the superficial resemblance of the genus with the family Octacnemidae in having an enlarged oral siphon. The phylogenetic position of *Fimbrora* within Ascidiidae was unresolved in our tree (Fig. 5). The more precise phylogenetic position of *Fimbrora* in the family would require the inclusion of additional ascidiid taxa in molecular analyses. One such to-be-included taxa is *Psammascidia*, which shares two characteristics with *Fimbrora*—having secondary branchial papillae on the longitudinal vessels and lacking primary and intermediate branchial papillae (Monniot and Monniot 1973), features that are not found in other ascidiid genera (cf. Kott (1985); Brunetti and Mastrototaro (2017)). Future molecular analyses may reveal the phylogenetic relationship amongst ascidiid species including *Fimbrora*.

Monniot and Monniot (1991a) suggested that *F. calsubia* has a partly carnivorous diet, based on the finding of copepods in its gut contents mixed with unidentified particles, as well as the shape of the oral siphon. The presence of small crustaceans, likely copepods, in the stomach of our specimen supports this assertion. The reports of *F. calsubia* from Indonesia (Monniot 1993) and Papua New Guinea (Monniot and López-Legentil 2017), however, did not provide any information on gut contents in their specimens. In addition to this, the observed

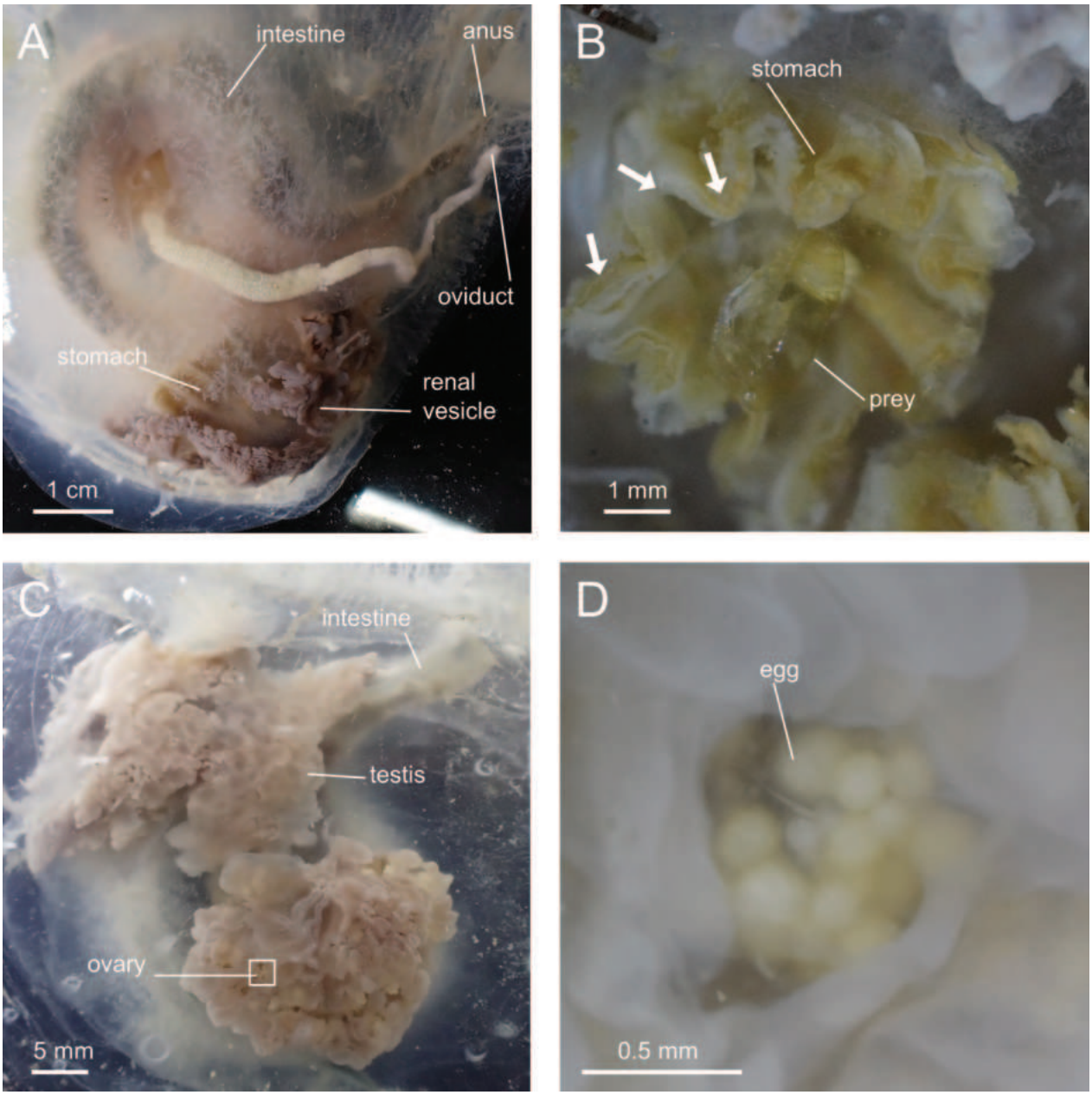

Figure 4. *Fimbrora calsubia* Monniot & Monniot, 1991a (JAMSTEC No. 111618), photographs of fixed specimen. **A.** Sinistero-posterior portion of body, viewed from outside, showing alimentary canal and reproductive system; **B.** Cross section of stomach, showing the prey crustacean (probably a copepod); arrows indicating stomach folds; **C.** Gonads; **D.** Magnification of the rectangle on **C**, showing an ovary containing multiple eggs.

behaviour of *F. calsubia*, where the individual orientates its oral siphon towards the water flow (Suppl. material 2), is similar to the behaviour found in *M. hians* as described by Okuyama et al. (2002). This suggests that *F. calsubia* also utilises water currents for feeding.

While the convergent evolution of macrophagous feeding in *Megalodicopia* and *Oligotrema* has already been revealed by Tatián et al. (2011), our phylogenetic tree clearly shows that *Fimbrora* is also the case: this trait was acquired at least three times independently within the class Ascidiacea (Fig. 5).

The present study expanded the species' known distribution range for about 4000 km northwards, representing the first record of the species from the North Pacific. Our material also represents the deepest record for the species with the known vertical distribution range being about 1000–2000 m (Monniot and Monniot 1991a; Monniot 1993; Monniot and López-Legentil 2017; present study).

Conclusions

We present the first report of *F. calsubia* from the North Pacific. Our molecular phylogenetic analysis suggested that macrophagous feeding was convergently acquired at

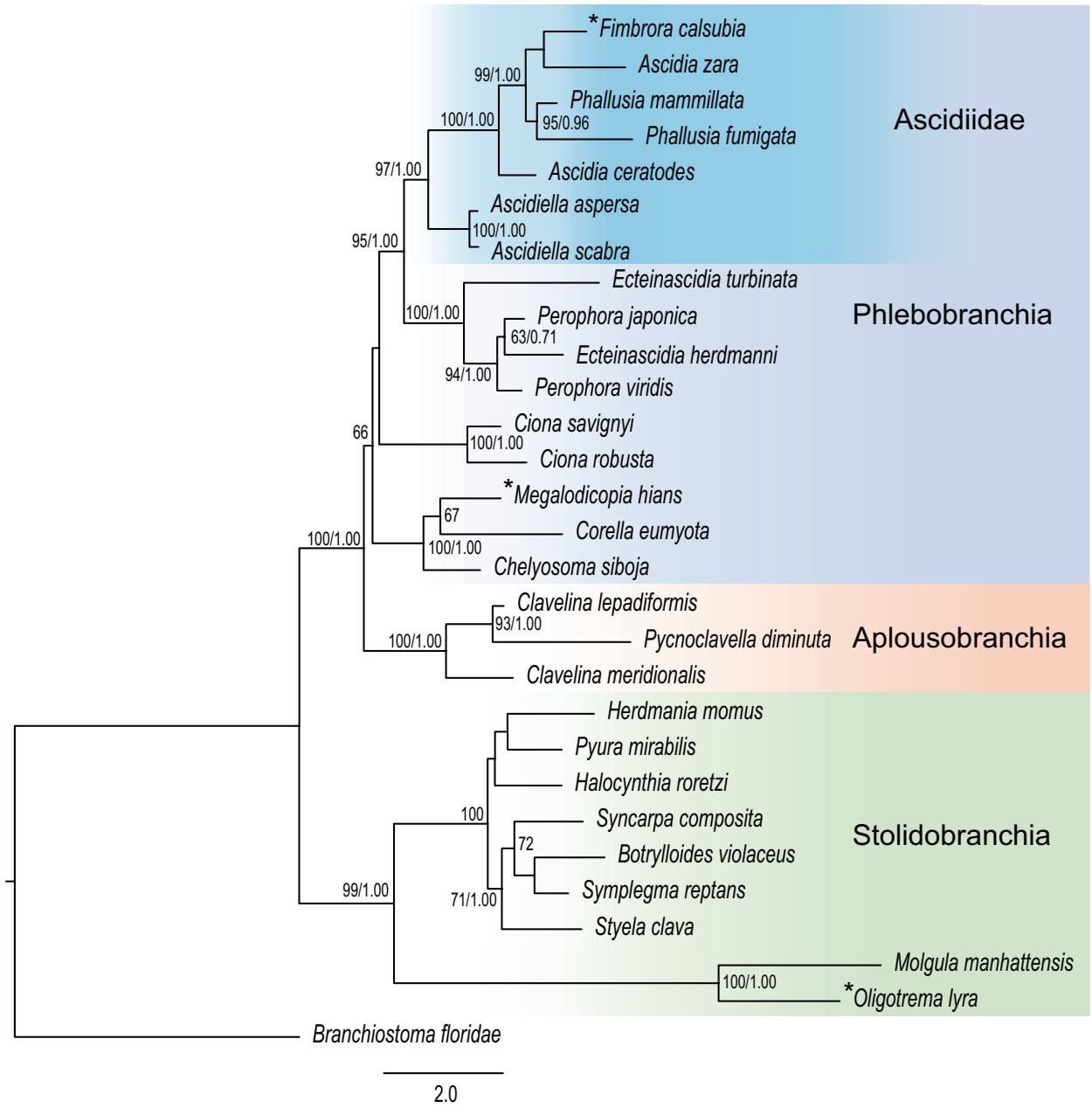

Figure 5. Phylogenetic relationship of 28 ascidian species; a Maximum-Likelihood tree, based on a concatenated dataset consisting of 18S rRNA (1676 bp) and COI (1136 bp) genes. Bootstrap values and posterior probabilities are indicated if they are higher than 60% and 0.70, respectively. Macrophagous species are indicated with an asterisk (*).

least three times independently in Ascidiacea. Our morphological observation indicated a similarity of *Fimbrora* to *Psammascidia* in having secondary papillae and lacking primary and intermediate branchial papillae.

Acknowledgements

We extend our profound gratitude to the captain and crew of the support vessel *Yokosuka*, the commander and operation team of the human-occupied vehicle *Shinkai 6500* and to both Takao Yoshida (JAMSTEC) and Hiroyuki Yokooka (IDEA Inc.) for their invaluable assistance in sample collection. Without the kind support from Kanta Ochiai and Misato Sako (Nagoya University, Sugashima Marine Biological Laboratory) for experimental work, this paper would not have materialised. We are indebted to all the people who donated to NHa through the academic crowd-funding site "academist", especially to Shunji Furukuma, Naoki Hayashi, Miyuki Honda, Hitoki Horie, Sho Hosotani, Yoshiki Iwai, Nami Kenmotsu, Moe, Takehiro Nakamura, Ryoma Nishikawa, Yuichi Sasaki, Tatsuya Shimoyama, Makoto Taniguchi, Daiki Wakita, Takaaki Yonekura, amongst others. NHa received financial support from JST SPRING, Grant Number JPMASP2119. This research was partly performed by the

Environment Research and Technology Development Fund (JPMEERF20S20700) of the Environmental Restoration and Conservation Agency Provided by the Ministry of Environment of Japan. The cruise YK22-17C of the R/V *Yokosuka* was funded by an MPA monitoring project outsourced by the Ministry of the Environment of Japan.

References

Adams H, Adams A (1858) The genera of resent Mollusca; arranged according to their organization. John van Voorst, Paternoster row, London, 661 pp. https://doi.org/10.5962/bhl.title.4772

Bourne GC (1903) *Oligitrema psammites*, a new ascidian belonging to the family Molgulidae. The Quarterly Journal of Microscopical Science 47(1): 233–273. https://doi.org/10.1242/jcs.s2-47.186.233

Brunetti R, Mastrototaro F (2017) Ascidiacea of the European waters. Calderini, Bologna, 447 pp.

Brunetti R, Manni L, Mastrototaro F, Gissi C, Gasparini F (2017) Fixation, description and DNA barcode of a neotype for *Botryllus schlosseri* (Pallas, 1766) (Tunicata, Ascidiacea). Zootaxa 4353(1): 29–50. https://doi.org/10.11646/zootaxa.4353.1.2

Capella-Gutiérrez S, Silla-Martinez JM, Gabaldón T (2009) trimAl: A tool for automated alignment trimming in large-scale phylogenetic analyses. Bioinformatics (Oxford, England) 25(15): 1972–1973. https://doi.org/10.1093/bioinformatics/btp348

Giribet G, Carranza S, Baguña J, Riutort M, Ribera C (1996) First molecular evidence for the existence of a Tardigrada + Arthropoda clade. Molecular Biology and Evolution 13(1): 76–84. https://doi.org/10.1093/oxfordjournals.molbev.a025573

Hartmeyer R (1923) Ascidiacea, part I. Zugleich eine Übersicht über die arktische und boreale Ascidienfauna auf tiergeographischer Grundlage. Ingolf-Expedition 2(6): 1–365.

Hasegawa N, Kajihara H (2019) A redescription of *Syncarpa composita* (Ascidiacea, Stolidobranchia) with an inference of its phylogenetic position within Styelidae. ZooKeys 857: 1–15. https://doi.org/10.3897/zookeys.857.32654

Havenhand JN, Matsumoto GI, Seidel E (2006) *Megalodicopia hians* in the Monterey submarine canyon: Distribution, larval development, and culture. Deep-sea Research. Part I, Oceanographic Research Papers 53(2): 215–222. https://doi.org/10.1016/j.dsr.2005.11.005

Hoang DT, Chernomor O, von Haeseler A, Minh BQ, Vinh LS (2018) UFBoot2: Improving the ultrafast bootstrap approximation. Molecular Biology and Evolution 35(2): 518–522. https://doi.org/10.1093/molbev/msx281

Huelsenbeck JP, Ronquist F (2001) MRBAYES: Bayesian inference of phylogeny. Bioinformatics (Oxford, England) 17(8): 754–755. https://doi.org/10.1093/bioinformatics/17.8.754

Ihle JEW (1935) *Octacnemus*. Handbuch der Zoologie 35(2): 533–544.

Katoh K, Standley DM (2013) MAFFT multiple sequence alignment software version 7: Improvements in performance and usability. Molecular Biology and Evolution 30(4): 772–780. https://doi.org/10.1093/molbev/mst010

Kott P (1957) The sessile Tunicata. The John Murray Expedition 1933–34 10(4): 129–149.

Kott P (1969) Antarctic Ascidiacea. Antarctic Research Series 13: 1–239.

Kott P (1985) The Australian Ascidiacea. Part 1: Phlebobranchia and Stolidobranchia. Memoirs of the Queensland Museum 23: 1–440.

Kott P (1989) The family Hexacrobylidae Seeliger, 1906 (Ascidiacea, Tunicata). Memoirs of the Queensland Museum 27(2): 517–534.

Kott P (1992) The Australian Ascidiacea, supplement 2. Memoirs of the Queensland Museum 32: 621–655.

Kott P (2009) Taxonomic revision of Ascidiacea (Tunicata) from the upper continental slope off north-western Australia. Journal of Natural History 43(31–32): 1947–1986. https://doi.org/10.1080/00222930902993708

Kumar S, Stecher G, Li M, Knyaz C, Tamura K (2018) MEGA X: Molecular Evolutionary Genetics Analysis across computing platforms. Molecular Biology and Evolution 35(6): 1547–1549. https://doi.org/10.1093/molbev/msy096

Kurabayashi A, Okuyama M, Ogawa M, Takeuchi A, Jing Z, Naganuma T, Saito Y (2003) Phylogenetic position of a deep-sea ascidian, *Megalodicopia hians*, inferred from the molecular data. Zoological Science 20(10): 1243–1247. https://doi.org/10.2108/zsj.20.1243

Lacaze-Duthiers H (1877) Histoire des ascidies simples des côtes de France. Deuxième partie: Étude des espèces. Archives de Zoologie Expérimentale et Générale 6: 457–673.

Lanfear R, Frandsen PB, Wright AM, Senfeld T, Calcott B (2016) PartitionFinder 2: New methods for selecting partitioned models of evolution for molecular and morphological phylogenetic analyses. Molecular Biology and Evolution 34(3): 772–773. https://doi.org/10.1093/molbev/msw260

Madsen FJ (1947) *Octacnemus ingolfi* n.sp., an Atlantic representative of peculiar tunicate-family Octacnemidae. Videnskabelige Meddelelser fra Dansk naturhistorisk Forening 110: 31–44.

Maggioni T, Taverna A, Reyna P, Alurralde G, Rimondino C, Tatián M (2018) Deep-sea ascidians (Chordata, Tunicata) from the SW Atlantic: Species richness with descriptions of two new species. Zootaxa 4526(1): 1–28. https://doi.org/10.11646/zootaxa.4526.1.1

Maggioni T, Rimondino C, Taverna A, Reyna P, Largger C, Alurralde G, Calcagno E, Tatián M (2022) Abyssal ascidians (Chordata, Tunicata) from the Weddell Sea, Antarctica, including a new *Styela* species and stomach content identifications. Zootaxa 5093(3): 296–314. https://doi.org/10.11646/zootaxa.5093.3.2

Metcalf MM (1893) Notes upon an apparently new species of *Octacnemus*, a deep sea, Salpa-like tunicate. John Hopkins University Circulars 12(106): 98–100.

Millar RH (1959) Ascidiacea. Galathea Report 1: 189–209.

Millar RH (1969) Ascidiacea: Some further specimens. Galathea Report 10: 91–98.

Millar RH (1970) Ascidians, including specimens from the deep sea, collected by R.V. 'Vema' and now in the American Museum of Natural History. Zoological Journal of the Linnean Society 49(2): 99–159. https://doi.org/10.1111/j.1096-3642.1970.tb00732.x

Millar RH (1971) The biology of ascidians. Advances in Marine Biology 9: 1–100. https://doi.org/10.1016/S0065-2881(08)60341-7

Millar RH (1988) Deep-sea ascidians from the eastern Pacific collected during the Pacific Ocean Biological Survey Program. Journal of Natural History 22(5): 1427–1435. https://doi.org/10.1080/00222938800770851

Minh BQ, Nguyen MAT, von Haeseler A (2013) Ultrafast approximation for phylogenetic bootstrap. Molecular Biology and Evolution 305(5): 1188–1195. https://doi.org/10.1093/molbev/mst024

Monniot C (1969) Ascidies récoltées par la "Thalassa" sur la pente continentale du golfe de Gascogne: (3–12 août 1967). Bulletin du Muséum National d`Histoire Naturelle 41(1): 155–186.

Monniot F (1971) Les Ascidies des grandes profondeurs récoltées par les navires atlantis II et chain, 3e note. Cahiers de Biologie Marine 7: 457–469.

Monniot C (1972) *Dicopia antirrhinum* n.sp. Ascidie de la pente du plateau continental du Golfe de Gascogne. Interprétation nouvelle de la famille des Octacnemidae. Cahiers de Biologie Marine 13: 9–20.

Monniot C (1993) Tunicata: Sur trois espèces d`ascidies bathyales récoltées au cours de la campagne franco-indonésienne Karubar. Mémoires du Museum National d`Histoire Naturelle 158: 355–359.

Monniot C (1998) Abyssal ascidians collected from the proximity of hydrothermal vents in the Pacific Ocean. Bulletin of Marine Science 63(3): 541–558.

Monniot C (2001) Ascidiacea and Sorberacea. In: Costello MJ, Emblow C, White R (Eds) European register of marine species: a check-list of the marine species in Europe and a bibliography of guides to their identification. Muséum national d'histoire naturelle, Paris, 352–355.

Monniot F (2011) A new Octacnemidae (Ascidiacea) from the Mid-Atlantic Ridge. Zootaxa 2864(1): 65–68. https://doi.org/10.11646/zootaxa.2864.1.5

Monniot F (2022) Additional records of bathyal ascidians (Tunicata) from the New Caledonia region. Zootaxa 5195(3): 201–223. https://doi.org/10.11646/zootaxa.5195.3.1

Monniot F, López-Legentil S (2017) Deep-sea ascidians from Papua New Guinea. Zootaxa 4276(4): 529–538. https://doi.org/10.11646/zootaxa.4276.4.5

Monniot C, Monniot F (1968) Les ascidies de grandes profondeurs récoltées par le navire oceanographique american Atlantis 2 (Premiere note). Bulletin de l`Institut Océanographique 67(1379): 1–48.

Monniot C, Monniot F (1970) Les ascidies des grandes profondeurs récoltées par les navires Atlantis, Atlantis II et Chain (2éme note). Deep-Sea Research and Oceanographic Abstracts 17(2): 317–336. https://doi.org/10.1016/0011-7471(70)90024-0

Monniot C, Monniot F (1973) Ascidies abyssales récoltées au cours de la campagne océanographique Biacores par le "Jean Charcot". Bulletin du Muséum National d`Histoire Naturelle 121: 389–475.

Monniot C, Monniot F (1974) Ascidies abyssales de l`Atlantique récoltées par le "Jean Charcot" (Campagnes Nortlante, Walda, Polygas A). Bulletin du Muséum National d`Histoire Naturelle 226: 721–786.

Monniot F, Monniot C (1976) Tuniciers abyssaux du bassin argentin récoltés par l "Atlantis II". Bulletin du Muséum National d`Nistoire Naturelle 387(269): 629–662.

Monniot C, Monniot F (1977) Quelques ascidies abyssales du Sud-Ouest de l'Ocean Indien. Comité National Français des Recherches Antarctiques 42: 305–327.

Monniot C, Monniot F (1982) Some Antarctic deep-sea tunicates in the Smithsonian collections. In: Biology of the Antarctic Seas. 10. Antarctic Research Series 32: 95–130. https://doi.org/10.1029/AR032p0095

Monniot C, Monniot F (1983) Ascidies antarctiques et subantarctiques: Morphologie et biogeographie. Mémoires du Muséum National d`Histoire Naturelle Série A. Zoologie 125: 1–168.

Monniot C, Monniot F (1984a) Tuniciers benthiques récoltées au cours de la campagne Abyplaine au large de Madère. Annales de l`Institut Océanographique 60(2): 129–142.

Monniot C, Monniot F (1984b) Nouvelles Sorberacea (Tunicata) profondes de l'Atlantique Sud et l'Ocean Indien. Cahiers de Biologie Marine 25: 197–215.

Monniot C, Monniot F (1985a) Nouvelles récoltes de tuniciers benthiques profonds dans l`Ocean Atlantique. Bulletin du Muséum National d`Histoire Naturelle. Section A. Zoologie, Biologie, et Écologie Animales A7(1): 5–37. https://doi.org/10.5962/p.285870

Monniot C, Monniot F (1985b) Tuniciers profondes de l'Ocean Indien: Campagnes SAFARI du 'Marion Dufresne'. Bulletin du Muséum National d`Histoire Naturelle. Section A. Zoologie, Biologie, et Écologie Animales A7(2): 279–308. https://doi.org/10.5962/p.287567

Monniot C, Monniot F (1985c) Ascidies profondes au large de Mayotte (Archipel des Comores). Cahiers de Biologie Marine 26(1): 35–52.

Monniot C, Monniot F (1989) Ascidians collected around the Galapagos Islands using the Johnson-Sea-Link research submersible. Proceedings of the Biological Society of Washington 102(1): 14–32.

Monniot C, Monniot F (1990) Revision of the class Sorberacea (benthic tunicates) with descriptions of seven new species. Zoological Journal of the Linnean Society 99(3): 239–290. https://doi.org/10.1111/j.1096-3642.1990.tb00562.x

Monniot C, Monniot F (1991a) Découverte d`une nouvelle lignée évolutive chez les ascidies de grande profondeur: Une Ascididae carnivore. Comptes Rendus de l`Académie des Sciences, Série 3. Sciences de la Vie 312: 383–388.

Monniot C, Monniot F (1991b) Tunicata: Peuplement d`ascidies profondes en Nouvelle-Caledonie. Diversite des strategies adaptives. Mémoires du Muséum National d`Histoire Naturelle, Série A. Zoologie 151: 357–448.

Monniot F, Monniot C (2003) Ascidies de la pente externe et bathyales de l'ouest Pacifique. Zoosystema 25(4): 681–749.

Monniot C, Monniot F, Gaill F (1975) Les Sorberacea: Une nouvelle classe des tuniciers. Archives de Zoologie Expérimentale et Générale 116: 77–122.

Monniot C, Monniot F, Laboute P (1991) Coral reef ascidians of New Caledonia. ORSTOM, Paris, 247 pp.

Moseley HN (1876) On two new forms of deep-sea ascidians, obtained during the voyage of H.M.S. "Challenger". Transactions of the Linnean Society of London, 2nd Series. Zoology : Analysis of Complex Systems, ZACS 1: 287–294. https://doi.org/10.1111/j.1096-3642.1877.tb00443.x

Nguyen LT, Schmidt HA, von Haeseler A, Minh BQ (2015) IQ-TREE: A fast and effective stochastic algorithm for estimating maximum-likelihood phylogenies. Molecular Biology and Evolution 32(1): 268–274. https://doi.org/10.1093/molbev/msu300

Nishikawa T (1991) The ascidians of the Japan Sea. II. Publications of the Seto Marine Biological Laboratory 35(1–3): 25–170. https://doi.org/10.5134/176172

Oka A (1913) Zur Kenntnis der zwei aberranthen Ascidiengattungen *Dicopia* Sluit. und *Hexacrobylus* Sluit. Zoologischer Anzeiger 43: 1–10.

Oka A (1918) *Megalodicopia hians* n.g., n.sp., eine sehr merkwurdig Ascidie aus dem japanischen Meere. Annotationes Zoologicae Japonenses 9(4): 399–406.

Okuyama M, Saito Y, Ogawa M, Takeuchi A, Jing Z, Naganuma T, Hirose E (2002) Morphological studies on the bathyal ascidian, *Megalodicopia hians* Oka, 1918 (Octacnemidae, Phlebobranchia), with remarks on feeding and tunic morphology. Zoological Science 19(10): 1181–1189. https://doi.org/10.2108/zsj.19.1181

Ritter WE (1906) *Octacnemus*. Bulletin of the Museum of Comparative Zoology at Harvard College 46(13): 233–252.

Ritter WE (1907) The ascidians collected by the United States Fisheries Bureau steamer Albatross on the coast of California during the summer of 1904. University of California Publications in Zoology 4(1): 1–52. https://doi.org/10.5962/bhl.title.1573

Rocha RM, Zanata TB, Moreno TR (2012) Keys for the identification of families and genera of Atlantic shallow water ascidians. Biota Neotropica 12(1): 270–302. https://doi.org/10.1590/S1676-06032012000100022

Ronquist F, Huelsenbeck JP (2003) MRBAYES 3: Bayesian phylogenetic inference under mixed models. Bioinformatics (Oxford, England) 19(12): 1572–1574. https://doi.org/10.1093/bioinformatics/btg180

Ronquist F, Teslenko M, van der Mark P, Ayres DL, Darling A, Höhna S, Larget B, Liu L, Suchard MA, Huelsenbeck JP (2012) MRBAYES 3.2: Efficient Bayesian phylogenetic inference and model selection across a large model space. Systematic Biology 61(3): 539–542. https://doi.org/10.1093/sysbio/sys029

Sanamyan K (1998) Ascidians from the north-western Pacific region. 5. Phlebobranchia. Ophelia 49(2): 97–116. https://doi.org/10.1080/00785326.1998.10409376

Sanamyan K (2014) Deep-sea fauna of European seas: An annotated species check-list of benthic invertebrates living deeper than 2000 m in the seas bordering Europe. Ascidiacea. Zoologia Bespozvonocnyh 11(1): 13–24. https://doi.org/10.15298/invertzool.11.1.04

Sanamyan K, Sanamyan N (1998) Some deep-water ascidians from the NW Pacific (Tunicata: Ascidiacea). Zoosystematica Rossica 7(2): 209–214.

Sanamyan K, Sanamyan N (1999) Some benthic Tunicata from the southern Indo-Pacific Ocean. Journal of Natural History 33(12): 1835–1876. https://doi.org/10.1080/002229399299761

Sanamyan K, Sanamyan N (2002) Deep-water ascidians from the south-western Atlantic (RV Dmitry Mendeleev, cruise 43 and Academic Kurchatov, cruise 11). Journal of Natural History 36(3): 305–359. https://doi.org/10.1080/00222930010004232

Sanamyan K, Sanamyan N (2006) Deep-water ascidians (Tunicata, Ascidiacea) from the northern and western Pacific. Journal of Natural History 40(5–6): 307–344. https://doi.org/10.1080/00222930600628416

Seeliger O (1906) Tunicata: Mantelthiere. Klassen und Ordnungen des Tierreichs 3(Suppl. 68–80): 1041–1280.

Sluiter CP (1905a) Zwei merkwurdige Ascidien von der Siboga-Expedition. Tijdschrift der Nederlandsche Dierkundige Vereeniging 9(2): 325–327.

Sluiter CP (1905b) Die Tunicaten der Siboga-Expedition. Supplement zu der I Abteilung: Die socialen und holosomen Ascidien. Siboga-Expeditie 56a: 129–139.

Tatián M, Lagger C, Demarchi M, Mattoni C (2011) Molecular phylogeny endorses the relationship between carnivorous and filter-feeding tunicates (Tunicata, Ascidiacea). Zoologica Scripta 40(6): 603–612. https://doi.org/10.1111/j.1463-6409.2011.00493.x

Tokioka T (1953) Ascidians of Sagami Bay. Iwanami Shoten, Tokyo, 315 pp.

Van Name WG (1945) The north and south American ascidians. Bulletin of the American Museum of Natural History 84: 1–476.

Vinogradova NG (1969) On the finding of a new aberrant ascidian in the ultrabyssal of the Kuril-Kamchatka Trench. Bulletin de la Société des Naturalistes de Moscou. Section Biologique 74(3): 27–43.

Vinogradova NG (1975) On the discovery of two new species of an aberrant deep-water ascidiacean genus *Situla* in the South-Sandwich trench. Trudy Instituta Oceanologii 103: 289–306.

Wessel P, Luis JF, Uieda L, Scharroo R, Wobbe F, Smith WHF, Tian D (2019) The Generic Mapping Tools version 6. Geochemistry, Geophysics, Geosystems 20(11): 5556–5564. https://doi.org/10.1029/2019GC008515

Whiting MF, Carpenter JC, Wheeler QD, Wheeler WC (1997) The Strepsiptera problem: Phylogeny of the holometabolous insect orders inferred from 18S and 28S ribosomal DNA sequences and morphology. Systematic Biology 46(1): 1–68. https://doi.org/10.1093/sysbio/46.1.1

Supplementary material 1

Video 1. A close encounter with the deep-sea ascidian

Authors: Naohiro Hasegawa, Natsumi Hookabe, Yoshihiro Fujiwara, Naoto Jimi, Hiroshi Kajihara

Data type: mov

Explanation note: Video of the moment the specimen was discovered at a depth of 2027 m.

Link: https://doi.org/10.3897/zse.100.113132.suppl1

Supplementary material 2

Video 2. Grabbing the ascidian with the manipulator of *Shinkai 6500*

Authors: Naohiro Hasegawa, Natsumi Hookabe, Yoshihiro Fujiwara, Naoto Jimi, Hiroshi Kajihara

Data type: mov

Explanation note: Video of the moment the specimen used in this study was collected by *Shinkai 6500*.

Link: https://doi.org/10.3897/zse.100.113132.suppl2

Zoosyst. Evol. 100 (1) 2024, 141–154 | DOI 10.3897/zse.100.116601

PENSOFT

MUSEUM FÜR NATURKUNDE BERLIN

A new species of krait of the genus *Bungarus* (Squamata, Elapidae) from Ratchaburi Province, western Thailand

Akrachai Aksornneam[1], Attapol Rujirawan[1,2], Siriporn Yodthong[3], Yik-Hei Sung[4], Anchalee Aowphol[1,2]

1 *Animal Systematics and Ecology Speciality Research Unit, Department of Zoology, Faculty of Science, Kasetsart University, Bangkok 10900, Thailand*

2 *Biodiversity Center, Kasetsart University, Bangkok 10900, Thailand*

3 *Department of Biological Science, Faculty of Science, Ubon Ratchathani University, Ubon Ratchathani 34190, Thailand*

4 *School of Allied Health Sciences, University of Suffolk, 19 Neptune Quay, Ipswich, IP4 1QJ, UK*

https://zoobank.org/F31FC865-868E-4A74-8C4D-52DE7C37FF49

Corresponding author: Anchalee Aowphol (fsciacl@ku.ac.th)

Academic editor: Justin Bernstein ♦ **Received** 30 November 2023 ♦ **Accepted** 15 January 2024 ♦ **Published** 30 January 2024

Abstract

We described a new species of elapid snake genus *Bungarus* from the Tenasserim Mountain Range in Ratchaburi Province, western Thailand. *Bungarus sagittatus* sp. nov. can be distinguished from all congeners by having the combination of 15 dorsal scale rows; 215–217 ventral scales; 48–56 undivided subcaudal; prefrontal suture 2.4–2.6 times length of internasal suture; anterior chin shields larger than posterior chin shields; head of adult uniform black while juvenile black with small dim white patches on temporal and parietal areas; dorsal body black, with 25–31 white narrow bands, white and black bands at midbody covering 1.5–3.0 and 4.5–6.0 vertebral scales, respectively; dorsal body black bands not intruding ventrals or intruding ventrals less than 0.5 times of width of outer dorsal scales; ventral surface of body immaculate white; ventral side of tail white with a row of dark brown triangular patches on middle pointing posteriorly; tail relatively long, tail length/total length 0.140–0.143. Genetically, the new species has uncorrected pairwise divergences of ≥ 8.29% of the mitochondrial cytochrome *b* from other *Bungarus* species. Currently, the new species is only known from the type locality.

Key Words

biodiversity, snake, Southeast Asia, systematics, Tenasserim

Introduction

The kraits, genus *Bungarus* Daudin, 1803, are a group of highly venomous snakes in the family Elapidae, with 17 recognized species that are distributed across Asia, from Southeast Asia and China, westwards through the South Asia to Iran (Smith 1943; Slowinski 1994; Abtin et al. 2014; Ahsan and Rahman 2017; Chen et al. 2021; Uetz et al. 2023). In Thailand, five species are currently reported, including *B. candidus* (Linnaeus, 1758), *B. fasciatus* (Schneider, 1801), *B. flaviceps* Reinhardt, 1843, *B. slowinskii* Kuch, Kizirian, Nguyen, Lawson, Donnelly & Mebs, 2005 and *B. wanghaotingi* Pope, 1928 (Smith 1943; Taylor 1965; Cox 1991; Leviton et al. 2003, 2008; Das 2010; Cox et al. 2012, 2018; Smits and Hauser 2019; Chen et al. 2021). Among the members of the genus *Bungarus*, the species with black-and-white crossbands are some of the most taxonomically confusing groups due to their highly similar color patterns and morphological characteristics (Pope 1928; Leviton et al. 2003, 2008; Xie et al. 2018; Chen et al. 2021; Yuan et al. 2022). Recently, Chen et al. (2021) investigated the taxonomic status of the *B. candidus*/*multicinctus*/*wanghaotingi* complex (black-and-white banded kraits) from China and some parts of Southeast Asia using the multiple lines of evidence (mitochondrial DNA, external morphology and cranial osteology). The combination of molecular phylogeny and morphological data supported the validity of three species in the complex (*B. candidus*, *B. multicinctus* and *B. wanghaotingi*) and uncovered a new species, *B. suzhenae* Chen, Shi, Vogel,

Ding & Shi, 2021 from Yunnan Province, China (Chen et al. 2021). Yuan et al. (2022) also investigated the molecular phylogeny of *B. multicinctus* Blyth, 1861 in Hong Kong and verified the occurrence of *B. multicinctus* and *B. wanghaotingi*.

Khao (mountain) Krachom is part of Tenasserim Mountain Range that is located at Suan Phueng District, Ratchaburi Province, western Thailand. The area lies on the Thai–Myanmar border and contains a variety of forest habitats ranging from 200 meters to more than 1,100 meters in elevation (The Office of Her Royal Highness Princess Maha Chakri Sirindhorn's Projects 2005; Pawangkhanant et al. 2018; Grismer et al. 2020b; Phutthai et al. 2021). Recently, several new species of herpetofauna were described from the area (e.g., Pawangkhanant et al. 2018; Grismer et al. 2020a, 2020b, 2021; Poyarkov et al. 2020, 2022; Suwannapoom et al. 2021), indicating a high diversity of herpetofauna.

During our field surveys in 2022, specimens of black-and-white banded *Bungarus* were collected from Suan Phueng District, Ratchaburi Province in western Thailand. These specimens closely resemble *B. candidus*/*multicinctus*/*wanghaotingi* complex in color pattern. The combination of morphological and molecular analyses revealed that the Ratchaburi specimens differed from all recognized *Bungarus* species. Thus, we herein describe it as a new species.

Methods

Sampling

Three *Bungarus* samples were collected during field surveys by hand and pitfall trap from Khao Krachom, Suan Phueng District, Ratchaburi Province from, May to June 2022 (Fig. 1). Geographical coordinates with elevation of

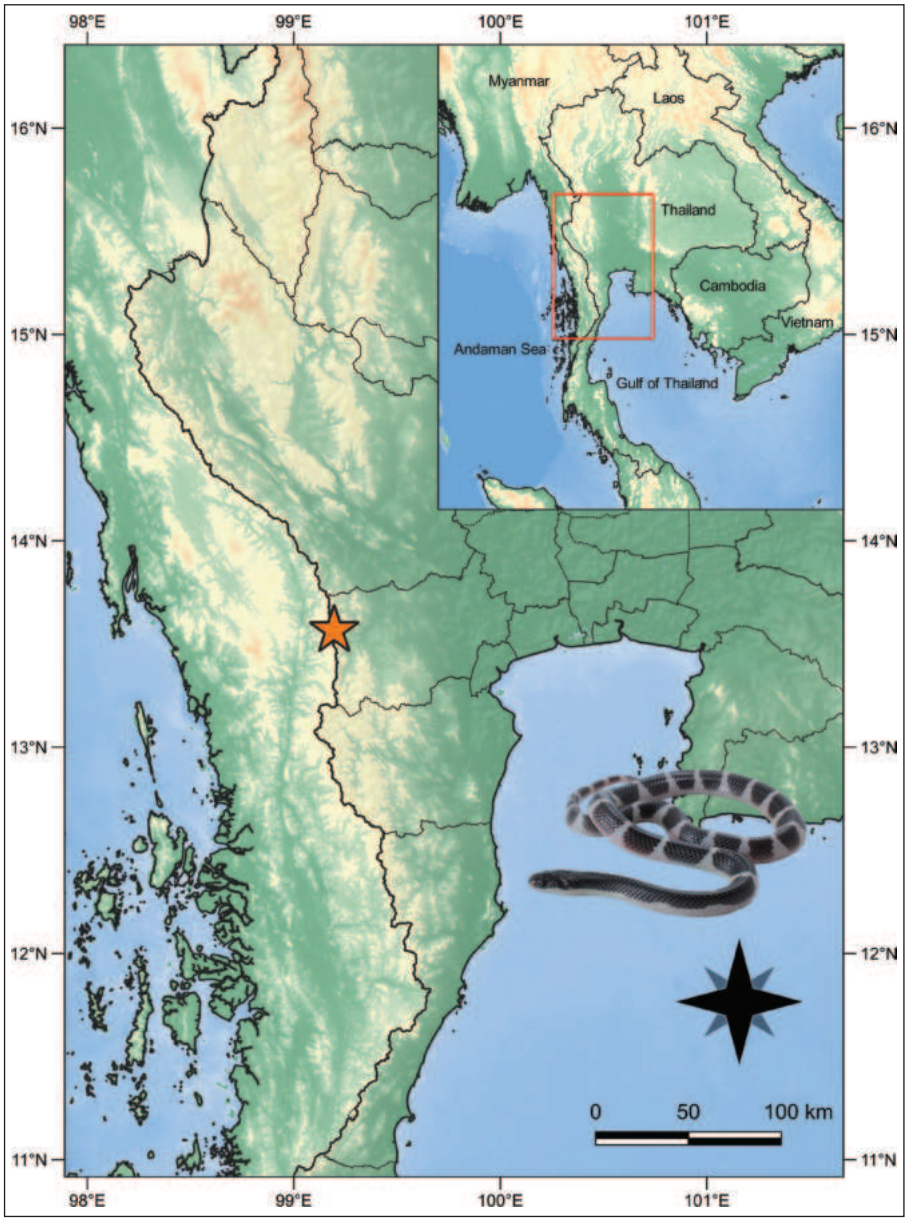

Figure 1. Map showing the type locality of *Bungarus sagittatus* sp. nov. (orange star) in Khao Krachom, Suan Phueng District, Ratchaburi Province.

each specimen were collected using a Garmin GPSMAP 64st. Ambient air temperature and relative humidity were collected with Kestrel 4000 Weather Meter. The specimens were humanely euthanized using tricaine methanesulfonate (MS-222) solution (Simmons 2015). Liver tissue was immediately cut from a euthanized individual, preserved in 95% ethyl alcohol, and stored at -20 °C for genetic analysis. Voucher specimens were then initially fixed in 10% formaldehyde solution and later transferred to 70% ethyl alcohol for long-term preservation. All type series and tissue samples were deposited in herpetological collection of Zoological Museum, Kasetsart University, Bangkok, Thailand (ZMKU). An additional specimen was examined at herpetological collection of the Rabbit in the Moon Foundation (RIM), Suan Phueng District, Ratchaburi Province.

DNA extraction and PCR amplification

We extracted genomic DNA from liver tissue of three individuals of *Bungarus* from Ratchaburi Province (Suppl. material 1) using the DNeasy (Qiagen, German) Blood and Tissue Kit according to manufacturer's protocol. A 1,041 base pairs of mitochondrial cytochrome *b* (cyt *b*) was amplified by the polymerase chain reaction (PCR), using the light strand primer L14910 (5'-AACCACCGTTGTACATCAACT-3') and heavy strand primer H16064 (5'-CTTTGGCTTACAAGAACAATGCTTTA-3') (Burbrink et al. 2000). PCR conditions were as follows: initial denaturation at 95 °C for 2 min, followed by a second denaturation at 95 °C for 40 s, annealing at 57 °C for 25 s, followed by a cycle extension at 72 °C for 15 s, for 35 cycles with a final extension at 72 °C for 2 min. PCR amplifications were carried out in a Mastercycler® nexus gradient thermocycler (Eppendorf SE, Germany). Amplified PCR products were run on a 1.5% agarose gel and viewed with a Molecular Imager® Gel Doc™ XR system (Bio-Rad Laboratories, USA) to confirm the PCR amplification. PCR products were purified using a QIAquick PCR Purification Kit (Qiagen, Germany). PCR products were sequenced in both forward and reverse directions using the same amplifying primers at Biobasic Asia Inc. (Singapore) on an ABI 3730XL automatic sequencer (Applied Biosystems, CA, USA). Bidirectional sequences were visually checked and edited in Geneious Prime 2022.2.1 (Biomatters, Ltd, Auckland, New Zealand). The protein-coding region of cyt *b* was translated to amino acids and checked to confirm the lack of premature termination codons. All new sequences were deposited in GenBank under accession numbers PP131180 to PP131182 (Suppl. material 1).

Phylogenetic analyses

Additional homologous cyt *b* sequences from 43 individuals of *Bungarus* species and the outgroups were downloaded from GenBank, based on previous *Bungarus* studies (Kuch et al. 2005; Xie et al. 2018; Biakzuala et al. 2021b, 2023; Chen et al. 2021) (Suppl. material 1). *Naja naja* (Linnaeus, 1758) and *Elapsoidea sundevallii* Smith, 1848 were selected as outgroups to root the tree following Xie et al. (2018) and Chen et al. (2021). The three newly generated *Bungarus* sequences and GenBank dataset were aligned using the MUSCLE alignment function (Edgar 2004) with default setting in Geneious Prime 2022.2.1 (Biomatters, Ltd, Auckland, New Zealand). The aligned dataset was partitioned into three partitions (1st–3th cyt *b* codon positions). We used ModelFinder (Kalyaanamoorthy et al. 2017) to identify the best-fit model of sequence evolution for each partition as determined by the Bayesian Information Criterion (BIC). The best-fit evolutionary models were TIM2+F+G4, TN+F+G4 and TN+F+I+G4 for cyt *b* codon position 1, 2, and 3, respectively.

Maximum Likelihood (ML) and Bayesian Inference (BI) were used to estimate phylogenetic relationships. The ML analysis was conducted using the IQ-TREE 1.6.12 web server available at "http://iqtree.cibiv.univie.ac.at" (Trifinopoulos et al. 2016) with 1,000 bootstrap replicates using the ultrafast bootstrap analysis (Minh et al. 2013; Hoang et al. 2018). The BI analysis was carried out using MrBayes v3.2 (Ronquist et al. 2012) on CIPRES Science Gateway V. 3.3 (Miller et al. 2010) with default prior setting. Two independent runs, each with three heated and one cold chain, were performed using Metropolis-coupled Markov Chain Monte Carlo (MCMC). The MCMC chains were run for 10,000,000 generations, with trees sampled every 1,000 generations, and the first 25% of each run was discarded as burn-in. Stationarity was evaluated by ensuring that effective sample sizes (ESS) exceeded 200 for all parameters in Tracer v. 1.7 (Rambaut et al. 2018). Nodal support for ML and BI was quantified using Ultrafast bootstrap support values (UFB) and Bayesian posterior probabilities (BPP), respectively. UFB values ≥ 95 and BPP ≥ 0.95 are considered highly supported (Huelsenbeck and Ronquist 2001; Wilcox et al. 2002; Minh et al. 2013). The phylogenetic trees from the ML and BI analyses were visualized and edited using FigTree v. 1.4.4 (http://tree.bio.ed.ac.uk/software/figtree/). Uncorrected pairwise sequence divergences (*p*-distances) were calculated in MEGA 11 (Tamura et al. 2021) using the pairwise deletion option to remove gaps and missing data from the alignment prior to analysis.

Morphological analyses

Morphological measurements were taken with digital calipers to the nearest 0.1 mm (except SVL and TaL, which were measured to the nearest 1 mm). The morphological characters and abbreviations used were modified from the previous studies of the genus *Bungarus* (Slowinski 1994; Kuch et al. 2005; Chen et al. 2021). The following morphometric and meristic characters were recorded: snout–vent length (SVL); tail length (TaL); head length (HL), from the tip of snout to the posterior edge of mouth; head width (HW), the widest part of head; head height (HH), the highest part of head in vertical; eye diameter (ED), the

horizontal length of eye ball; distance between eyes (DE), was measured from the margin of upper eye contacting supraocular to opposite side; the length of internasal suture (IS), the length of suture between left and right internasal scales; the length of prefrontal suture (PS), the length of suture between left and right prefrontal scales; supralabials (SL); infralabials (IL); dorsal scale rows (DSR), were counted at one head length behind the angle of jaw, at midbody, and at one head length before the cloaca; ventral scales (VS), were counted following Dowling (1951); and subcaudals (SC). The number of white bands on dorsal body (BB) and white bands on tail (TB) were counted, while incomplete white bands were counted as one.

Comparative morphological data from other species of *Bungarus* were obtained from the original descriptions and literature (Boulenger 1890, 1897; Wall 1907, 1908; Pope 1928; Smith 1943; Biswas and Sanyal 1978; Slowinski 1994; Leviton et al. 2003; Kuch et al. 2005; Faiz et al. 2010; Cox et al. 2012, 2018; Chanhome 2013; Abtin et al. 2014; Knierim et al. 2017; Luu and Ha 2018; Xie et al. 2018; Smits and Hauser 2019; Biakzuala et al. 2021b; Chen et al. 2021) (Suppl. material 3).

Results

The final alignment of cyt *b* contained 1,137 characters of 46 taxa (44 individuals of *Bungarus* and two individuals of the outgroup species). The standard deviation of split frequencies among the four Bayesian runs was 0.003186 and the ESS values of all parameters were greater than or equal to 6,531. The best tree in ML analysis had a maximum likelihood value of -6,833.101. The ML and BI analyses recovered trees with similar topologies (Fig. 2). The three Ratchaburi samples formed a strongly supported monophyletic lineage (100 UFB, 1.00 BPP) and nested within the genus *Bungarus*. The Ratchaburi population was a strongly supported sister lineage (97 UFB,

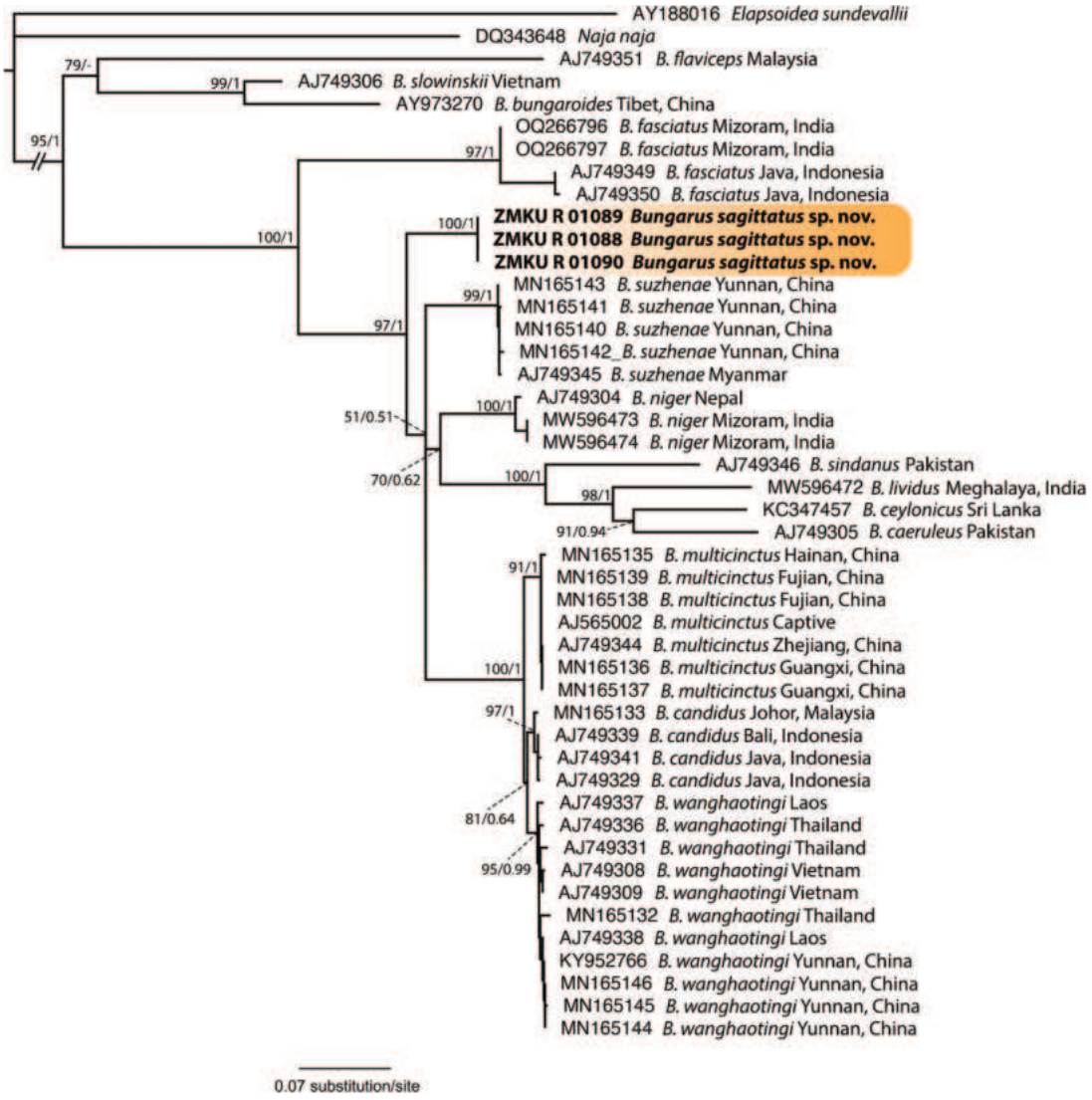

Figure 2. The best tree resulting from Maximum Likelihood analysis of 1,137 aligned characters of the mitochondrial cytochrome *b* gene of *Bungarus* species. Nodal support is indicated by Ultrafast bootstrap (UFB) values and Bayesian posterior probabilities (BPP), respectively. GenBank accession numbers and locality data for sequenced samples are provided in Suppl. material 1.

1.00 BPP) to a clade containing *B. caeruleus* (Schneider, 1801), *B. candidus*/*multicinctus*/*wanghaotingi* complex, *B. ceylonicus* Günther, 1864, *B. lividus* Cantor, 1839, *B. niger* Wall, 1908, *B. sindanus* Boulenger, 1897 and *B. suzhenae*. However, the relationships among the Indian subcontinent clade (*B. caeruleus*, *B. ceylonicus*, *B. lividus*, *B. niger* and *B. sindanus*), *B. candidus*/*multicinctus*/*wanghaotingi* complex clade and *B. suzhenae* were not resolved representing as a polytomy. Uncorrected pairwise genetic divergences (*p*-distances) among *Bungarus* species ranged from 1.77–20.46% (Suppl. material 2). The uncorrected *p*-distances between Ratchaburi population and all other *Bungarus* species ranged from 8.29–19.42%, being most similar to *B. suzhenae* and most distant to *B. bungaroides* (Cantor, 1839). The uncorrected *p*-distances within the Ratchaburi population were 0.00%.

Taxonomic hypotheses

The samples of *Bungarus* from Suan Phueng District, Ratchaburi Province, western Thailand differed from congeners in mtDNA and morphological comparisons (see below). Based on these corroborated lines of support, we hypothesize that this population represents a distinct species, which is described as a new species below.

Taxonomy

***Bungarus sagittatus* sp. nov.**

https://zoobank.org/F19C3493-FA00-4F4A-A9B1-4A39B5C5FF0A

Figs 3–5

Type material. ***Holotype*** (Fig. 3). ZMKU R 01089, adult female collected from Thailand, Ratchaburi Province, Suan Phueng District, Suan Phueng Subdistrict, Khao Krachom (13°33'57"N, 99°11'43"E, 834 m elevation), on 15 May 2022 by Akrachai Aksornneam, Mali Naiduangchan, Kritsada Rungrot, Purinut Numuan, Suphap Sisuk and Goe Wongdee.

Paratypes (Figs 4, 5A–D). ZMKU R 01088 (subadult female) bear the same locality data as the holotype. ZMKU R 01090 (juvenile) collected from Thailand, Ratchaburi Province, Suan Phueng District, Suan Phueng Subdistrict, Khao Krachom (13°33'41"N, 99°12'18"E, 619 m elevation), on 15 June 2022, by Akrachai Aksornneam and Naka Taou.

Referred specimen (Fig. 5E, F). RIM00012 (subadult male) collected from Thailand, Ratchaburi Province, Suan Phueng District, Suan Phueng Subdistrict, Khao Krachom (13°34'53"N, 99°10'43"E, 987 m elevation), on 16 April 2021, by Parinya Pawangkhanant and Boontorn Wongdee.

Diagnosis. *Bungarus sagittatus* sp. nov. is assigned to the genus *Bungarus* by its recovered phylogenetic position and having enlarged, hexagonal-shaped, midbody vertebrae scales (Smith 1943; Slowinski 1994). This species can be distinguished from other species of *Bungarus* by the following combination of characters: 15–15–15 dorsal scale rows; 215–217 ventral scales; 48–56 undivided subcaudal; prefrontal suture 2.4–2.6 times length of internasal suture; anterior chin shields larger than posterior chin shields; head of adult uniform black while juvenile black with small dim white patches on temporal and parietal areas; dorsal surface of body black, with 25–31 white narrow bands, white and black bands at midbody covering 1.5–3.0 and 4.5–6.0 vertebral scales, respectively; dorsal black bands of body not intruding ventrals or intruding ventrals less than 0.5 times of width of outer dorsal scales; ventral surface immaculate white; ventral side of tail white with a row of dark brown triangular patches on middle pointing posteriorly; tail relatively long, tail length/total length = 0.140–0.143.

Description of holotype. Adult female. Head length 19.9 mm, head width 16.8 mm; head height 10.7 mm, head 1.2 times longer than wide, distance between eyes 9.2 mm. Body length (SVL) 791 mm; tail incomplete, 132 mm; total length 923 mm.

Body scalation. Dorsal scales smooth, in 15–15–15 rows; vertebral scales enlarged, hexagonal, largest at midbody, wider than long. Ventrals 216, preventrals 3, anterior edge of first ventral starting at level of oral rictus. Cloacal plate undivided. Subcaudals 48 undivided, tail incomplete.

Head. Head scales smooth. Λ-shaped rostral visible from above 1.6 times wider than tall. Nasal large, divided into one irregular quadrilateral-shaped prenasal and one crescent-shaped postnasal on both side; prenasal and postnasal bordered by internasal and first supralabial; prenasal contacted with rostral; postnasal surrounded by prefrontal, preocular and second supralabial. External nares large, vertically oval-shaped, about half size of eye diameter. Preoculars 1/1 (left/right) hexagonal-shaped, bordered by orbit, supraocular, prefrontal, postnasal, second and third supralabials. Two internasals, 1.03 times wider than long, surrounded by rostral, prenasal, postnasal and prefrontal. Prefrontals large, 1.06 times wider than long, prefrontals suture length 2.6 times of internasals suture. Frontal shield-shaped, pointing backward to parietals, 1.3 times longer than wide, bordered by prefrontals, supraoculars and parietals; anterior suture of frontal pointed toward prefrontal suture. Supraocular 1/1 small, 1.6 times longer than wide, in contact with preocular, orbit, upper postocular, parietal, frontal and prefrontal. Parietals large and long, 2 times longer than wide, 1.6 times longer than frontal length; left parietal anteriorly and laterally bordered by frontal, supraocular, upper postocular, anterior temporal and upper posterior temporal; right parietal anteriorly and laterally bordered by frontal, supraocular, upper postocular, lower postocular, anterior temporal and upper posterior temporal; posterolateral margins of parietals bordered by 1/1 enlarged elongate scales that anteriorly contact upper posterior temporals; posteriormost extensions of parietals pointed, divided by one of three small dorsal scales bordering posterior end of parietals. Eyes small, oval-shaped, horizontal diameter 2.6 mm, vertical diameter 2.3 mm. Postoculars 2/2, relatively small with one-third size of

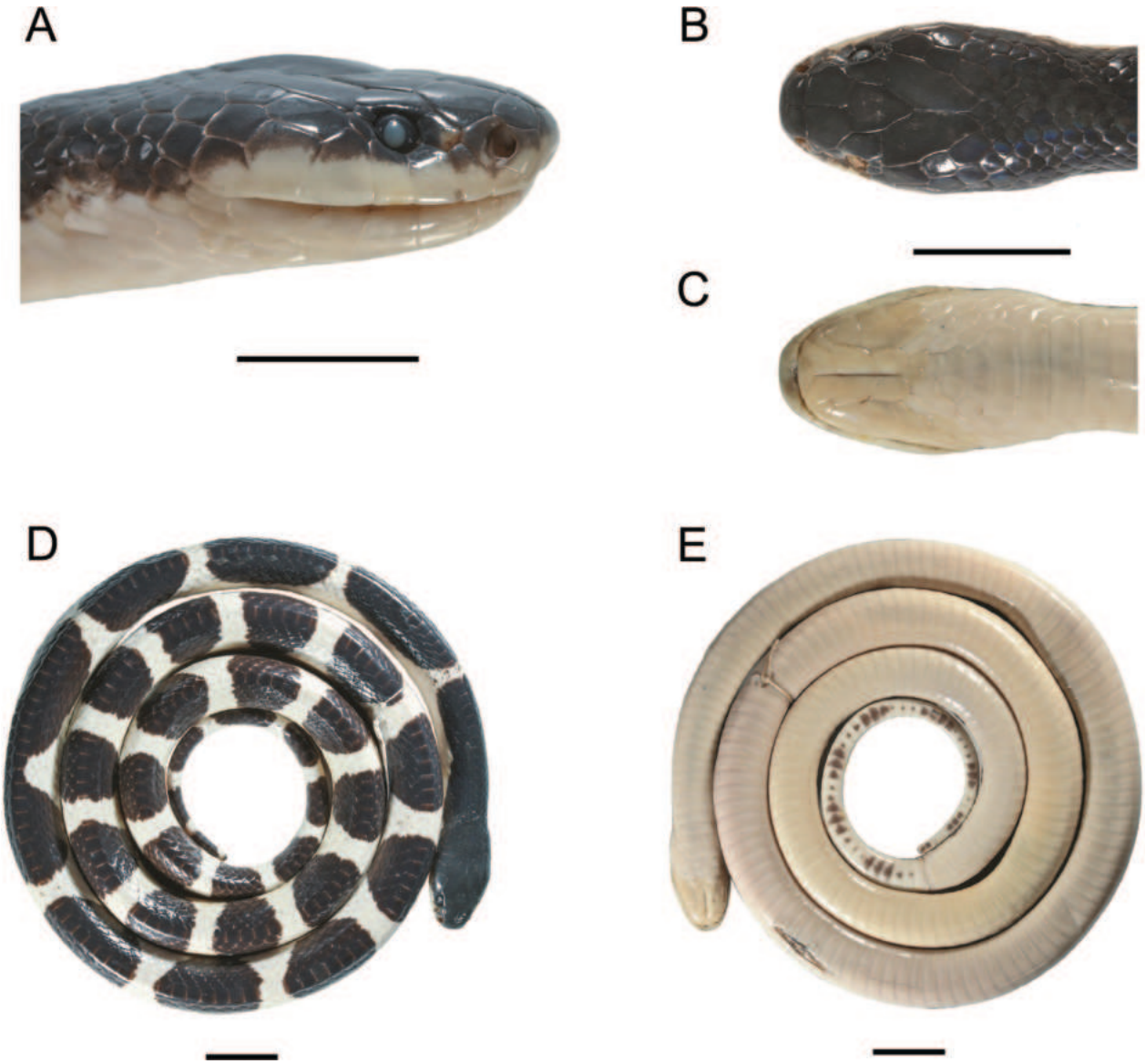

Figure 3. Holotype of *Bungarus sagittatus* sp. nov. (ZMKU R 01089) in preservation. **A.** Lateral view; **B.** Dorsal view and **C.** Ventral view; **D.** Dorsal view; **E.** Ventral view. Scale bars: 20 mm.

preoculars; on right side, lower postocular bordered by orbit, fourth and fifth supralabials, anterior temporal, parietal and upper postocular; on left side, lower postocular bordered by orbit, fourth and fifth supralabials, anterior temporal and upper postocular; on right side, upper postocular bordered by orbit, lower postocular, parietal and supraocular; on left side, upper postocular bordered by orbit, lower postocular, anterior temporal, parietal and supraocular. Anterior temporals 1/1, long and subhexagonal-shaped, 1.6 times longer than wide; right anterior temporal bordered by lower postocular, fifth and sixth supralabials, lower posterior temporal, upper posterior temporal and parietal; left anterior temporal bordered by upper postocular, lower postocular, fifth and sixth supralabials, lower posterior temporal, upper posterior temporal and parietal. Posterior temporals 2/2 surrounded by parietals, anterior temporals, sixth and seventh supralabials and dorsal scales. Supralabials 7/7, the third and fourth supralabials touching lower margin of orbit; first supralabials small, subtriangular, 1.2 times wider than height; other supralabials in different pentagonal shapes; second supralabials height pentagonal-shaped, larger than the first, 1.8 times higher than wide; the third supralabial larger than first, second and fourth supralabials, 1.3 times higher than wide; fourth supralabials with 1.5 times higher than wide; fifth and sixth supralabials are two largest, both height equal to width, but fifth supralabials wider at lower part while the sixth supralabials is wider at the upper part; seventh supralabials is the third largest, 1.2 times higher than wide. Mental triangular-shaped, 1.4 times shorter than width of rostral, in contact with first infralabials, mental groove distinct. Infralabials 7/7, first infralabials pentagonal-shaped, long and narrow, 1.6 times longer than wide, in contact behind the mental and anterior chin shields; second infralabials square-shaped, one-third size of the first, 2.1 times longer than wide, in contact with anterior chin

Figure 4. Paratypes in life showing the variation in different age class. **A.** Subadult female (ZMKU R 01088); **B.** Juvenile (ZMKU R 01090).

shields; the third infralabials enlarged, in contact with anterior chin shields, 1.1 times longer than wide; the fourth is largest infralabial, pentagonal shaped, in contact with anterior and posterior chin shields, 1.2 times longer than wide; fifth infralabials in form of a square, half size of the fourth, 1.2 times longer than wide; the sixth is widest infralabial, 1.9 times wider than long; seventh infralabials is smallest, 1.4 times wider than long. Anterior chin shields larger than posterior chin shields; anterior chin shield suture 2 times the length of the posterior chin shield suture; posterior chin shields bordered by anterior chin shields, fourth infralabials, 2/2 sublabials and three gulars. Three gulars between first ventral and posteriormost extension of posterior chin shield; one gular and three preventrals between first ventral and suture of posterior chin shields.

Coloration in preservative. Dorsal surface and lateral sides of head, including upper part of supralabial, upper part of rostral uniform black; lower part of head, including portions of lower supralabials and rostral to ventral head uniform creamy white. Dorsal body black with 26 white crossbands (the fifth band incomplete). Some white bands on the body scattered with few dark spots, most bands nearly immaculate creamy white. The white bands cover 0.5 to 2.0 times vertebral scales (average 1.5 ± 0.4, n = 26; 1.5 vertebral scales at midbody), bands widening on flanks before merging with the immaculate creamy white ventral scales. The first white band starts at 16th ventral, 11 vertebral scales between first and second bands and five vertebral scales between 25th and 26th bands. A dark spot is present at the junction between white bands and ventral scales at midbody positions. Black bands on body wide, covering 6.0 vertebral scales at midbody positions, generally not intruding white ventral scales; some bands slightly intruding ventral scales less than 0.5 times width of outer lateral dorsal scales.

Dorsal surface of tail black with eight creamy white bands on dorsal part, covering 1.0–1.5 times of vertebral scales. Ventral surface of tail creamy white with a row of dark brown triangular patches pointing posteriorly at the middle of subcaudals, starting from second subcaudal to the tip of tail.

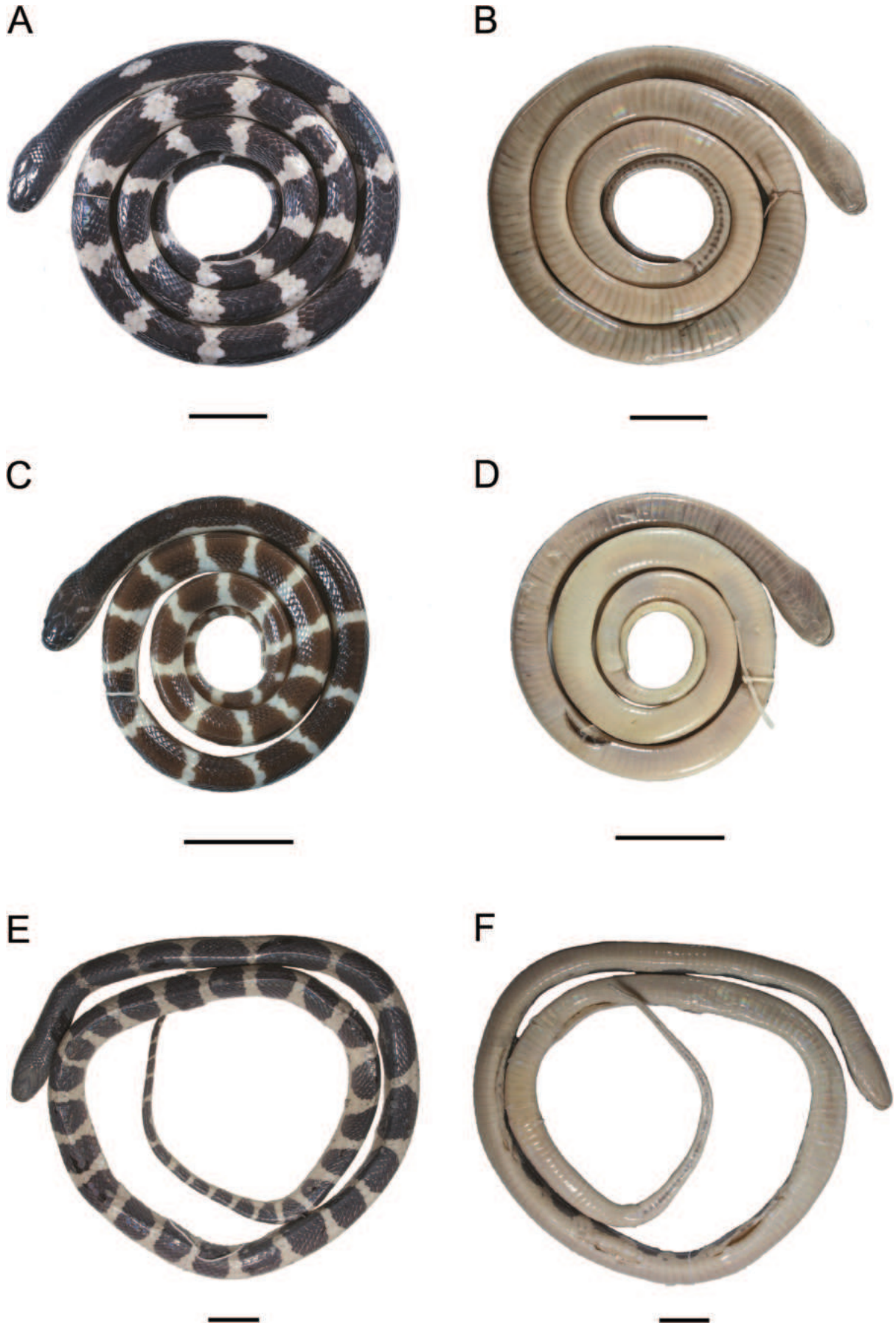

Figure 5. Paratypes and referred specimen in preservation. **A.** Dorsal and **B.** Ventral view of subadult female (ZMKU R 01088); **C.** Dorsal and **D.** Ventral view of juvenile (ZMKU R 01090); **E.** Dorsal and **F.** Ventral view of subadult male (RIM00012). Scale bars: 20 mm.

Variation. Paratypes and referred specimens closely resemble the holotype in general aspects of morphology and color pattern. First and second white bands on dorsum of ZMKU R 01090 (juvenile) are disconnected. In ZMKU R 01088 (subadult female), the first white band on dorsum is disconnected; the second and third are incompletely connected on lateral side of body. Twentieth white band on dorsum of RIM00012 (subadult male) is incomplete (present only on left side). Juvenile (ZMKU R 01090) head black with small dim white patches on temporal and parietal areas. A row of dark brown triangular patches on ventral surface of tail in juvenile is indistinct. Other variations in measurements, meristics and color pattern among the type series and referred specimen are shown in Table 1.

Etymology. The specific epithet *sagittatus* is derived from *sagittata* (L.) meaning arrow and in reference to the dark triangular shape on subcaudals which resembles a barbed arrow.

Distribution. *Bungarus sagittatus* sp. nov. is currently known from type locality: Khao Krachom, Suan Phueng District, Ratchaburi Province. The area is part of Tenasserim Mountain Range, which lies on Thai-Myanmar borderline.

Ecology. Most observations of *Bungarus sagittatus* sp. nov. occurred at night, three specimens (ZMKU R 01088, ZMKU R 01089 and RIM00012) were collected in hill evergreen forest (834 m to 987 m elevation; Fig. 6) between 2050 and 2210 h with air temperature 24.1 °C and relative humidity 91.7%. One juvenile (ZMKU R 01090) was collected in a pitfall trap at daytime in mixed deciduous forest (619 m elevation). One subadult (not collected) was found swallowing an adult scincid lizard, *Scincella reevesii* (Gray, 1839), on forest floor in hill evergreen forest (1,049 m elevation) on 6 November 2022 at 2154 h (Fig. 7).

The new species was found sympatrically with other snake species such as *Ahaetulla prasina* (Boie, 1827), *Boiga cyanea* (Duméril, Bibron & Duméril, 1854), *Coelognathus flavolineatus* (Schlegel, 1837), *Gonyosoma oxycephalum* (Boie, 1827), *Lycodon ophiophagus* Vogel, David, Pauwels, Sumontha, Norval, Hendrix, Vu & Ziegler, 2009, *Ptyas carinata* (Günther, 1858), *Rhabdophis chrysargos* (Schlegel, 1837), *Psammodynastes pulverulentus* (Boie, 1827), *Pareas carinatus* Wagler, 1830, *Argyrophis diardii* (Schlegel, 1839), *Naja kaouthia* Lesson, 1831, *Bungarus flaviceps*, *Ophiophagus hannah* (Cantor, 1836) and *Trimeresurus* cf. *popeiorum* Smith, 1937.

Comparison. *Bungarus sagittatus* sp. nov. is distinguished from all other *Bungarus* by a combination of morphological and color pattern characteristics (see Suppl. material 3). *Bungarus sagittatus* sp. nov. differed from *B. andamanensis* Biswas & Sanyal, 1978 by having 215–217 ventral scales (vs. 192–197); 48–56 subcaudals (vs. 45–47); TaL/TL 0.140–0.143 (vs. 0.156–0.161); 25–31

Table 1. Descriptive measurement (millimeters), meristics (left/right) and color pattern of *Bungarus sagittatus* sp. nov. Morphological abbreviations are defined in Methods.

Character	ZMKU R 01089	ZMKU R 01088	ZMKU R 01090	RIM00012
Sex	Female	Subadult female	Juvenile	Subadult male
Type	Holotype	Paratype	Paratype	Referred specimen
Measurement				
SVL	791	550	300	710
TaL	132	92	49	118
HL	19.9	15.0	10.2	17.8
HW	16.8	11.2	8.1	12.6
HH	10.7	7.0	5.5	9.0
ED	2.6	2.1	1.8	2.1
DE	9.2	6.7	4.6	7.4
IS	1.6	1.2	0.8	1.3
PS	4.1	2.9	1.9	3.2
Tal/TL	0.143	0.143	0.140	0.143
PS/IS	2.56	2.42	2.38	2.46
Meristics				
SL	7/7	7/7	7/7	7/7
IL	7/7	7/7	7/7	7/7
DSR	15/15/15	15/15/15	15/15/15	15/15/15
VS	216	215	216	217
SC	48	53	56	55
BB	26	25	25	31
TB	8	7	11	12
Color pattern				
Black bands intruding ventrals	Yes	No	No	No
Head color	Uniform black	Black with small dim white patches	Black with small dim white patches	Uniform black
Vertebral scales covered by white bands at midbody	1.5 scales	3.0 scales	1.5 scales	1.5 scales
Vertebral scales covered by black bands at midbody	6.0 scales	5.5 scales	6.0 scales	4.5 scales

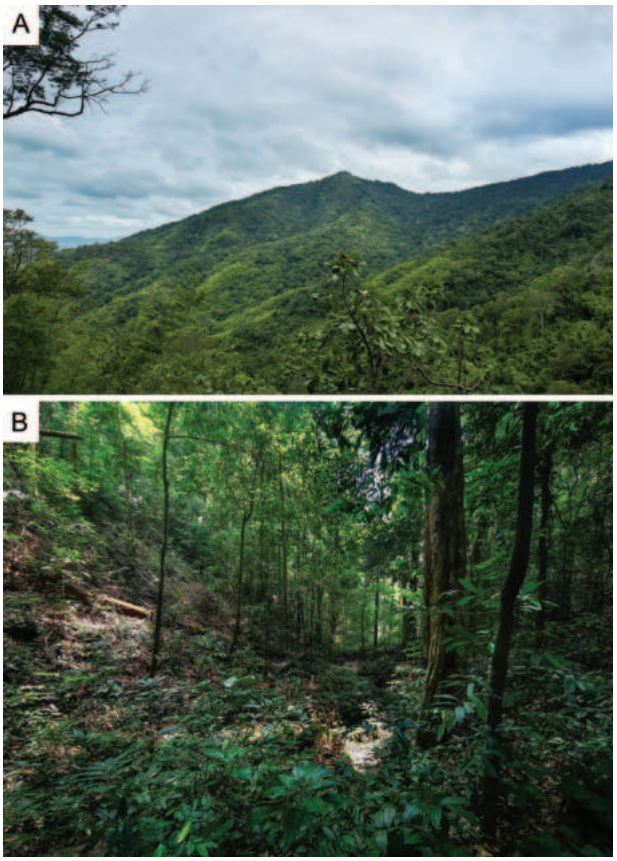

Figure 6. Habitat of *Bungarus sagittatus* sp. nov. **A.** Macrohabitat at Khao Laem Summit (1,130 m elevation), Khao Krachom, Suan Phueng District, Ratchaburi Province; **B.** Hill evergreen forest at 1,000 m elevation.

Figure 7. Feeding behavior of *Bungarus sagittatus* sp. nov. (not collected) on smooth skink (*Scincella reevesii*) from the type locality, in hill evergreen forest at 1,049 m elevation. Red arrows indicate the tail part of skink.

narrow white body bands (vs. 39–47 yellow or white bands mottled with brown); head uniform black (vs. head brown chocolate); and ventral surface of body immaculate white (vs. anterior and margin of ventral scales tinged with brown).

Bungarus sagittatus sp. nov. differed from *B. bungaroides* by having 215–217 ventral scales (vs. 220–237); TaL/TL 0.140–0.143 (vs. 0.114–0.130); subcaudals undivided (vs. divided); dorsal body with 25–31 narrow white bands (vs. 46–60 narrow white bands consisting of small white spots); dorsal body with larger black bands covering 4.5–6.0 vertebral scales at midbody (vs. 3.0–4.5 vertebral scales); and ventral surface of body immaculate white (vs. blackish with irregular yellowish white pattern).

Bungarus sagittatus sp. nov. differed from *B. caeruleus* (Schneider, 1801) by having TaL/TL 0.140–0.143 (vs. 0.111); 25–31 narrow white body bands (vs. 29–65 white bands); and white bands not in pairs (vs. white bands in pairs).

Bungarus sagittatus sp. nov. differed from *B. candidus* by having prefrontal suture length 2.4–2.6 times of internasal suture (vs. 1.4–2.4 times); TaL/TL 0.140–0.143 (vs. 0.112–0.130); white bands on dorsal body covering 1.5–3.0 vertebral scales at midbody (vs. 3.0–5.0 vertebral scales); black bands on dorsal body covering 4.5–6.0 vertebral scales at midbody (vs. 3.0–5.0 vertebral scales); dorsal body black bands not intruding ventrals or intruding ventrals less than 0.5 times of width of outer dorsal scales (vs. 1.0–2.0 times); adult head uniform black (vs. temporal area and lateral neck stained white); juvenile head black with small dim white patches on temporal and parietal areas (vs. creamy white head); and ventral surface of tail creamy white with a row of dark brown triangular patches on middle (vs. broad dark crossbars).

Bungarus sagittatus sp. nov. differed from *B. ceylonicus* by having 215–217 ventral scales (vs. 219–235); 48–56 subcaudals (vs. 33–40); 25–31 narrow white body bands (vs. 15–21 narrow white bands); TaL/TL 0.140–0.143 (vs. 0.087); and ventral surface of body immaculate white (vs. broad dark crossbands).

Bungarus sagittatus sp. nov. differed from *B. fasciatus* by having 48–56 subcaudals (vs. 23–39); TaL/TL 0.140–0.143 (vs. 0.074–0.096); dorsal body and tail black with narrow white bands (vs. broad yellow and black bands); ventral surface of body immaculate white (vs. yellow and black bands); dorsal body black bands not intruding ventrals or intruding ventrals less than 0.5 times of width of outer dorsal scales (vs. black bands encircling ventrals); and ventral surface of tail creamy white with a row of dark brown triangular patches on middle (vs. yellow and black bands).

Bungarus sagittatus sp. nov. differed from *B. flaviceps* by having 15 dorsal scale rows (vs. 13 rows); dorsal body and tail black with narrow white bands (vs. body black with or without light vertebral and paraventral stripes, tail bright red); and head uniform black (vs. head red).

Bungarus sagittatus sp. nov. differed from *B. lividus* by having vertebral scales distinctly enlarged (vs. slightly enlarged on the anterior body); 48–56 subcaudals (vs. 35–43); TaL/TL 0.140–0.143 (vs. 0.118); and dorsal body black with narrow white bands (vs. black without bands).

Bungarus sagittatus sp. nov. differed from *B. magnimaculatus* Wall & Evans, 1901 by having 48–56 subcaudals (vs. 40–48); TaL/TL 0.140–0.143 (vs. 0.115);

and 25–31 narrow white body bands (vs. 11–14 broad white bands).

Bungarus sagittatus sp. nov. differed from *B. multicinctus* by having 25–31 white bands on dorsal body (vs. 31–50); black bands on dorsal body covering 4.5–6.0 vertebral scales at midbody (vs. 3.0–4.0 vertebral scales); dorsal body black bands not intruding ventrals or intruding ventrals less than 0.5 times of width of outer dorsal scales (vs. 1.2–2.0 times); ventral surface of body immaculate white (vs. white with dense brown pigments); and ventral surface of tail creamy white with a row of dark brown triangular patches on middle (vs. dense black bands and patches).

Bungarus sagittatus sp. nov. differed from *B. niger* by having dorsal body black with mostly complete narrow white bands (vs. body bands absent); and ventral surface of tail creamy white with a row of dark brown triangular patches on middle (vs. immaculate white).

Bungarus sagittatus sp. nov. differed from *B. percicus* Abtin, Nilson, Mobaraki, Hosseini & Dehgannejhad, 2014 by having 15 dorsal scale rows (vs. 17); 215–217 ventral scales (vs. 236–238); TaL/TL 0.140–0.143 (vs. 0.127–0.134); loreal scale absent (vs. present); and dorsal body black with mostly complete narrow white bands (vs. black with light triangular-shaped crossbars, ending in pairs of rectangular whitish dots or crossbars along the vertebral area).

Bungarus sagittatus sp. nov. differed from *B. sindanus* by having 15 dorsal scale rows (vs. 17); 215–217 ventral scales (vs. 220–237); and dorsal body black with mostly complete narrow white bands (vs. black with white bands formed by series of white spots).

Bungarus sagittatus sp. nov. differed from *B. slowinskii* by having 215–217 ventral scales (vs. 225–230); 48–56 subcaudals (vs. 33–41); TaL/TL 0.140–0.143 (vs. 0.120); subcaudals undivided (vs. divided); ventral surface of body immaculate white (vs. black bands encircling with irregular yellowish white pattern); and ventral surface of tail creamy white with a row of dark brown triangular patches on middle (vs. black bands encircling with irregular yellowish white pattern).

Bungarus sagittatus sp. nov. differed from *B. suzhenae* by having prefrontal suture 2.4–2.6 times of internasal suture (vs. 2.7–3.4 times); 215–217 ventral scales (vs. 220–229); 25–31 narrow white body bands (vs. 26–38); head of juvenile black with small dim white patches on temporal and parietal areas (vs. uniform black head); and ventral surface of tail creamy white with a row of dark brown triangular patches on middle (vs. immaculate white or with small brown dots).

Bungarus sagittatus sp. nov. differed from *B. walli* Wall, 1907 by having 15 dorsal scale rows (vs. 17); 215–217 ventral scales (vs. 198–207); and dorsal body black with mostly complete narrow white bands (vs. black with white bands formed by series of white spots).

Bungarus sagittatus sp. nov. differed from *B. wanghaotingi* by having TaL/TL 0.140–0.143 (vs. 0.114–0.132); dorsal body black bands not intruding ventrals or intruding ventrals less than 0.5 times of width of outer dorsal scales (vs. 0.5–1.5 times); head of juvenile black with small dim white patches on temporal and parietal areas (vs. light brown); and ventral surface of tail creamy white with a row of dark brown triangular patches on middle (vs. a row of small light brown dots on middle).

Discussion

The combination of phylogenetic and morphological analyses revealed that the populations of *Bungarus* from Ratchaburi Province should be recognized as a distinct species, which is described here as *Bungarus sagittatus* sp. nov. Based on general morphology and color pattern, *Bungarus sagittatus* sp. nov. superficially resembles the members of the *B. candidus*/*multicinctus*/*wanghaotingi* complex, but phylogenetic analyses revealed that the new species is not closely related to those species. Moreover, the new species has high uncorrected pairwise divergences based on cyt *b* gene (≥ 8.29%) from other *Bungarus* species whereas members of the *B. candidus*/*multicinctus*/*wanghaotingi* complex have uncorrected pairwise divergences of 1.6–3.3% (in Chen et al. 2021) and 1.8–3.1% (this study; Suppl. material 2).

In this study, the new species was observed preying on scincid lizard, *Scincella reevesii*, which revealed that the new species could prey on other reptiles or non-snake prey animals e.g., amphibians, rodents or birds (not strictly on snakes) as reported in other *Bungarus* species (see Knierim et al. 2017; Luu and Ha 2018; Biakzuala et al. 2019a, 2019b, 2021a; Mohalik et al. 2019; Pandey et al. 2020; Hong et al. 2021; Hruaia et al. 2023; Subba et al. 2023). The ecology and natural history of this species should be further investigated. Furthermore, the report on their venom composition is still lacking. Since kraits are recognized as highly venomous snakes, this data is needed for snake bite management and development of effective antivenom (Fry et al. 2003; Sunagar et al. 2021; Talukdar et al. 2023).

Bungarus sagittatus sp. nov. is currently known only from the lowland hill forest at 600 meters to over 1,000 meters elevation in Khao Krachom, Suan Phueng District, Ratchaburi Province, western Thailand. Additional field surveys in the Tenasserim Range including Thai-Myanmar border and examination of museum specimens are needed to investigate the geographic range of the new species. Description of *Bungarus sagittatus* sp. nov. brings the total number of *Bungarus* to 18 species (Chen et al. 2021; Uetz et al. 2023). The discovery of this new *Bungarus* species and recent studies from Tenasserim Range highlight that this area is a potential stronghold for amphibians and reptiles, and also act as an important herpetofaunal exchange (dispersal) between Indochina and Sundaland in the past (see Grismer et al. 2017, 2020a; Suwannapoom et al. 2018).

Acknowledgements

This research is funded by Kasetsart University through the Graduate School Fellowship Program and National

Research Council of Thailand (NRCT). AR and AA were supported by Office of the Permanent Secretary, Ministry of Higher Education, Science, Research and Innovation (RGNS 64-038). The research protocol was approved by Institutional Animal Care and Use Committee, Kasetsart University (ACKU65-SCI-032). We thank the Rabbit in the Moon Foundation, Charnchai Bindusen, Juthamas Wangaryattawanich and Suthep Kraithep (Suan Phueng Nature Education Park initiated by Her Royal Highness Princess Maha Chakri Sirindhorn) for supporting this research. Parinya Pawangkhanant, Mali Naiduangchan, Pattarawich Dawwrueng and Kawin Jiaranaisakul for their assistance and useful suggestions. Bangroh Taou, Naka Taou, Goe Wongdee, Pree Wongdee, Boontorn Wongdee, Krarok Wongdee, Suphap Sisuk, Cherd Manora, Kritsada Rungrot and Purinut Numuan assisted the fieldwork. Lal Biakzuala and Evan S.H. Quah improved the manuscript.

References

Abtin E, Nilson G, Mobaraki A, Hosseini AA, Dehgannejhad M (2014) A new species of krait, *Bungarus* (Reptilia, Elapidae, Bungarinae) and the first record of that genus in Iran. Russian Journal of Herpetology 21(4): 243–250.

Ahsan MF, Rahman MM (2017) Status, distribution and threats of kraits (Squamata: Elapidae: *Bungarus*) in Bangladesh. Journal of Threatened Taxa 9(3): 9903–9910. https://doi.org/10.11609/jott.2929.9.3.9903-9910

Biakzuala L, Lalrinsanga, Lalremsanga HT, Romalsawma, Vanlalhrima, Laltlanchhuaha H (2019a) *Bungarus fasciatus* (banded krait). Diet. Herpetological Review 50(4): 797.

Biakzuala L, Lalrinsanga, Lalremsanga HT, Romalsawma, Vanlalhrima, Sailo V, Laltlanchhuaha H (2019b) *Bungarus niger* (greater black krait). Diet and elevation. Herpetological Review 50(4): 797–798.

Biakzuala L, Malsawmtluanga M, Lalremsanga HT (2021a) Ophiophagy by banded krait (*Bungarus fasciatus*) exposed by a road kill. Taprobanica 10(2): 127. https://doi.org/10.47605/tapro.v10i2.262

Biakzuala L, Purkayastha J, Rathee YS, Lalremsanga HT (2021b) New data on the distribution, morphology, and molecular systematics of two venomous snakes, *Bungarus niger* and *Bungarus lividus* (Serpentes: Elapidae), from north-east India. Salamandra (Frankfurt) 57(2): 219–228.

Biakzuala L, Lalremsanga HT, Santra V, Dhara A, Ahmed MT, Mallick ZB, Kuttalam S, Amarasinghe AAT, Malhotra A (2023) Molecular phylogeny reveals distinct evolutionary lineages of the banded krait, *Bungarus fasciatus* (Squamata, Elapidae) in Asia. Scientific Reports 13(2061): 2061. https://doi.org/10.1038/s41598-023-28241-8

Biswas S, Sanyal DP (1978) A new species of krait of the genus *Bungarus* Daudin, 1803 (Serpentes: Elapidae) from the Andaman Island. Journal of the Bombay Natural History Society 75: 179–183.

Boulenger GA (1890) The fauna of British India, including Ceylon and Burma. Reptilia and Batrachia. Taylor & Francis, London, 541 pp. https://doi.org/10.5962/bhl.title.100797

Boulenger GA (1897) A new krait from Sind (*Bungarus sindanus*). Journal of the Bombay Natural History Society 11: 73–74.

Burbrink FT, Lawson R, Slowinski JB (2000) Mitochondrial DNA phylogeography of the polytypic North American rat snake (*Elaphe obsoleta*): A critique of the subspecies concept. Evolution; International Journal of Organic Evolution 54(6): 2107–2118. https://doi.org/10.1554/0014-3820(2000)054[2107:MDPOTP]2.0.CO;2

Chanhome L (2013) Reproduction of the red-headed krait (*Bungarus flaviceps*) in captivity. Tropical Natural History 13(1): 59–63.

Chen ZN, Shi SC, Vogel G, Ding L, Shi JS (2021) Multiple lines of evidence reveal a new species of krait (Squamata, Elapidae, *Bungarus*) from Southwestern China and Northern Myanmar. ZooKeys 1025: 35–71. https://doi.org/10.3897/zookeys.1025.62305

Cox MJ (1991) The snakes of Thailand and their husbandry. Krieger Publishing Company, 526 pp.

Cox MJ, Hoover MF, Chanhome L, Thirakupt K (2012) The snakes of Thailand. Chulalongkorn University Museum of National History, Bangkok, Thailand, 845 pp.

Cox MJ, Hoover MF, Chanhome L, Thirakupt K, Pongcharoen C (2018) A field guide to the venomous snakes of mainland ASEAN nations. Parbpim Limited Partnership, Bangkok, Thailand, 82 pp.

Das I (2010) A field guide to the reptiles of Thailand and South-east Asia. New Holland Publishers, 376 pp.

Dowling HG (1951) A proposed standard system of counting ventrals in snakes. British Journal of Herpetology 1: 97–99.

Edgar RC (2004) MUSCLE: Multiple sequence alignment with high accuracy and high throughput. Nucleic Acids Research 32(5): 1792–1797. https://doi.org/10.1093/nar/gkh340

Faiz A, Ghose A, Ahsan F, Rahman R, Amin R, Hassan MU, Chowdhury AW, Kuch U, Rocha T, Harris JB, Theakston RDG, Warrell DA (2010) The greater black krait (*Bungarus niger*), a newly recognized cause of neuro-myotoxic snake bite envenoming in Bangladesh. Brain 133(11): 3181–3193. https://doi.org/10.1093/brain/awq265

Fry BG, Winkel KD, Wickramaratna JC, Hodgson WC, Wüster W (2003) Effectiveness of snake antivenom: Species and regional venom variation and its clinical impact. Journal of Toxicology: Toxin Reviews 22(1): 23–34. https://doi.org/10.1081/TXR-120019018

Grismer LL, Wood Jr PL, Aowphol A, Cota M, Grismer MS, Murdoch ML, Aguilar C, Grismer JL (2017) Out of Borneo, again and again: biogeography of the stream toad genus *Ansonia* Stoliczka (Anura: Bufonidae) and the discovery of the first limestone cave-dwelling species. Biological Journal of the Linnean Society, Linnean Society of London 120(2): 371–395. https://doi.org/10.1111/bij.12886

Grismer LL, Yushchenko PV, Pawangkhanant P, Naiduangchan M, Nazarov RA, Orlova VF, Suwannapoom C, Poyarkov NA (2020a) A new species of *Hemiphyllodactylus* Bleeker (Squamata; Gekkonidae) from Peninsular Thailand that converges in morphology and color pattern on *Pseudogekko smaragdinus* (Taylor) from the Philippines. Zootaxa 4816(2): 171–190. https://doi.org/10.11646/zootaxa.4816.2.2

Grismer LL, Yushchenko PV, Pawangkhanant P, Nazarov RA, Naiduangchan M, Suwannapoom C, Poyarkov NA (2020b) A new species of *Cnemaspis* Strauch (Squamata: Gekkonidae) of the *C. siamensis* group from Tenasserim Mountains, Thailand. Zootaxa 4852(5): 547–564. https://doi.org/10.11646/zootaxa.4852.5.3

Grismer LL, Suwannapoom C, Pawangkhanant P, Nazarov RA, Yushchenko PV, Naiduangchan M, Le MD, Luu VQ, Poyarkov NA (2021) A new cryptic arboreal species of the *Cyrtodactylus brevipalmatus* group (Squamata: Gekkonidae) from the uplands of western Thailand. Vertebrate Zoology 71: 723–746. https://doi.org/10.3897/vz.71.e76069

Hoang DT, Chernomor O, von Haeseler A, Minh BQ, Vinh LS (2018) UFBoot2: Improving the ultrafast bootstrap approximation. Molec-

ular Biology and Evolution 35(2): 518–522. https://doi.org/10.1093/molbev/msx281

Hong Z, Anuar S, Grismer LL, Quah ESH (2021) Preliminary report on the herpetofaunal diversity of Batu Hampar Recreational Forest, Kedah, Malaysia. Check List 17(3): 791–814. https://doi.org/10.15560/17.3.791

Hruaia V, Tochhawng L, Laltlanchhuaha H, Decemson HT, Lalremsanga HT, Biakzuala L (2023) *Bungarus niger* (greater black krait). Diet. Herpetological Review 54(1): 131–132.

Huelsenbeck JP, Ronquist F (2001) MRBAYES: Bayesian inference of phylogenetic trees. Bioinformatics (Oxford, England) 17(8): 754–755. https://doi.org/10.1093/bioinformatics/17.8.754

Kalyaanamoorthy S, Minh BQ, Wong TKF, von Haeseler A, Jermiin LS (2017) ModelFinder: Fast model selection for accurate phylogenetic estimates. Nature Methods 14(6): 587–589. https://doi.org/10.1038/nmeth.4285

Knierim T, Barnes CH, Hodges C (2017) *Bungarus fasciatus* (banded krait). Diet/scavenging. Herpetological Review 48(1): 204–205.

Kuch U, Kizirian D, Truong NQ, Lawson R, Donnelly MA, Mebs D (2005) A new species of krait (Squamata: Elapidae) from the red river system of northern Vietnam. Copeia 2005(4): 818–833. https://doi.org/10.1643/0045-8511(2005)005[0818:ANSOKS]2.0.CO;2

Leviton AE, Wogan GOU, Koo MS, Zug GR, Lucas RS, Vindum JV (2003) The dangerously venomous snakes of Myanmar illustrated checklist with keys. Proceedings of the California Academy of Sciences 54(24): 407–462.

Leviton AE, Zug GR, Vindum JV, Wogan GOU (2008) Handbook to the dangerously venomous snakes of Myanmar. California Academy of Sciences, 122 pp.

Luu VQ, Ha NV (2018) *Bungarus fasciatus* (banded krait). Diet. Herpetological Review 49(3): 543.

Miller MA, Pfeiffer W, Schwartz T (2010) Creating the CIPRES Science Gateway for inference of large phylogenetic trees. In: 2010 Gateway Computing Environments Workshop (GCE), 1–8. https://doi.org/10.1109/GCE.2010.5676129

Minh BQ, Nguyen MAT, von Haeseler A (2013) Ultrafast approximation for phylogenetic bootstrap. Molecular Biology and Evolution 30(5): 1188–1195. https://doi.org/10.1093/molbev/mst024

Mohalik RK, Sahu SB, Arif M, Kar NB (2019) *Bungarus caeruleus* (common krait). Coloration and diet. Herpetological Review 50(1): 150–151.

Pandey DP, Bhattarai P, Piya RC (2020) Food spectrum of common kraits (*Bungarus caeruleus*): An implication for snakebite prevention and snake conservation. Journal of Herpetology 54(1): 87–96. https://doi.org/10.1670/18-054

Pawangkhanant P, Poyarkov NA, Duong TV, Naiduangchan M, Suwannapoom C (2018) A new species of *Leptobrachium* (Anura, Megophryidae) from western Thailand. PeerJ 6: e5584. https://doi.org/10.7717/peerj.5584

Phutthai T, Thananthaisong T, Daonurai K, Srisom P, Suddee S, Hughes M (2021) *Begonia sirindhorniana* (Begoniaceae) a new species from Thailand. Thai Forest Bulletin 49(2): 201–205. https://doi.org/10.20531/tfb.2021.49.2.07

Pope CH (1928) Four new snakes and a new lizard from South China. American Museum Novitates 325: 1–4.

Poyarkov NA, Pawangkhanant P, Gorin VA, Juthong W, Suwannapoom C (2020) A new species of miniaturised narrow-mouth frog of the genus *Microhyla* Tschudi, 1838 (Amphibia: Anura: Microhylidae) from northern Tenasserim, Thailand. Journal of Natural History 54(23–24): 1525–1558. https://doi.org/10.1080/00222933.2020.1804005

Poyarkov NA, Nguyen TV, Pawangkhanant P, Yushchenko PV, Brakels P, Nguyen LH, Nguyen HN, Suwannapoom C, Orlov N, Vogel G (2022) An integrative taxonomic revision of slug-eating snakes (Squamata: Pareidae: Pareineae) reveals unprecedented diversity in Indochina. PeerJ 10: e12713. https://doi.org/10.7717/peerj.12713

Rambaut A, Drummond AJ, Xie D, Baele G, Suchard MA (2018) Posterior summarization in Bayesian phylogenetics using Tracer 1.7. Systematic Biology 67(5): 901–904. https://doi.org/10.1093/sysbio/syy032

Ronquist F, Teslenko M, van der Mark P, Ayres DL, Darling A, Höhna S, Larget B, Liu L, Suchard MA, Huelsenbeck JP (2012) MrBayes 3.2: Efficient Bayesian phylogenetic inference and model choice across a large model space. Systematic Biology 61(3): 539–542. https://doi.org/10.1093/sysbio/sys029

Simmons JE (2015) Herpetological collecting and collections management, 3rd ed. Society for the Study of Amphibians and Reptiles Herpetological Circular No. 42. Salt Lake City, UT, 191 pp.

Slowinski JB (1994) A phylogenetic analysis of *Bungarus* (Elapidae) based on morphological characters. Journal of Herpetology 28(4): 440–446. https://doi.org/10.2307/1564956

Smith MA (1943) The fauna of British India, Ceylon and Burma, including the whole of the Indo-Chinese Sub-Region. Reptilia and Amphibia. Vol. 3 (Serpentes). Taylor and Francis, London, 583 pp.

Smits T, Hauser S (2019) First record of the krait *Bungarus slowinskii* Kuch, Kizirian, Nguyen, Lawson, Donelly and Mebs, 2005 (Squamata: Elapidae) from Thailand. Tropical Natural History 19(2): 43–50.

Subba A, Luitel S, Rai TP, Limbu KP (2023) Bizarre record: Banded krait, (*Bungarus fasciatus*) (Schneider 1801), feeding on other krait species. Reptiles & Amphibians : Conservation and Natural History 30(1): e18661. https://doi.org/10.17161/randa.v30i1.18661

Sunagar K, Khochare S, Laxme RRS, Attarde S, Dam P, Suranse V, Khaire A, Martin G, Captain A (2021) A wolf in another wolf's clothing: Post-genomic regulation dictates venom profiles of medically-important cryptic kraits in India. Toxins 13(69): 69. https://doi.org/10.3390/toxins13010069

Suwannapoom C, Sumontha M, Tunprasert J, Ruangsuwan T, Pawangkhanant P, Korost DV, Poyarkov NA (2018) A striking new genus and species of cave-dwelling frog (Amphibia: Anura: Microhylidae: Asterophryinae) from Thailand. PeerJ 6: e4422. https://doi.org/10.7717/peerj.4422

Suwannapoom C, Grismer LL, Pawangkhanant P, Naiduangchan M, Yushchenko PV, Arkhipov DV, Wilkinson JA, Poyarkov NA (2021) Hidden tribe: a new species of stream toad of the genus *Ansonia* Stoliczka, 1870 (Anura: Bufonidae) from the poorly explored mountainous borderlands of western Thailand. Vertebrate Zoology 71: 763–779. https://doi.org/10.3897/vz.71.e73529

Talukdar A, Malhotra A, Lalremsanga HT, Santra V, Doley R (2023) *Bungarus fasciatus* venom from eastern and north-east India: Venom variation and immune cross-reactivity with Indian polyvalent antivenoms. Journal of Proteins and Proteomics 14: 61–76. https://doi.org/10.1007/s42485-022-00104-2

Tamura K, Stecher G, Kumar S (2021) MEGA11: Molecular evolutionary genetics analysis version 11. Molecular Biology and Evolution 38(7): 3022–3027. https://doi.org/10.1093/molbev/msab120

Taylor EH (1965) The serpents of Thailand and adjacent waters. The University of Kansas Science Bulletin 4: 609–1096.

The Office of Her Royal Highness Princess Maha Chakri Sirindhorn's Projects (2005) Model scheme: the Suan Phueng Nature Education Park, initiated by Her Royal Highness Princess Maha Chakri Sirindhorn, Suan Phueng District, Ratchaburi Province, 2000–2004 (in Thai), 30 pp.

Trifinopoulos J, Nguyen LT, von Haeseler A, Minh BQ (2016) W-IQTREE: A fast online phylogenetic tool for maximum likelihood analysis. Nucleic Acids Research 44(W1): W232–W235. https://doi.org/10.1093/nar/gkw256

Uetz P, Freed P, Hosek J (2023) The reptile database. https://reptile-database.org [accessed 5 July 2023]

Wall F (1907) A new krait from Oudh (*Bungarus walli*). Journal of the Bombay Natural History Society 17: 608–611.

Wall F (1908) A popular treatise of the common Indian snakes. Journal of the Bombay Natural History Society 18: 711–735.

Wilcox TP, Zwickl DJ, Heath TA, Hillis DM (2002) Phylogenetic relationships of the dwarf boas and a comparison of Bayesian and bootstrap measures of phylogenetic support. Molecular Phylogenetics and Evolution 25(2): 361–371. https://doi.org/10.1016/S1055-7903(02)00244-0

Xie Y, Wang P, Zhong G, Zhu F, Liu Q, Che J, Shi L, Murphy RW, Guo P (2018) Molecular phylogeny found the distribution of *Bungarus candidus* in China (Squamata: Elapidae). Zoological Systematics 43(1): 109–117.

Yuan FL, Prigge TL, Sung YH, Dingle C, Bonebrake TC (2022) Two genetically distinct yet morphologically indistinct *Bungarus* species (Squamata, Elapidae) in Hong Kong. Current Herpetology 41(1): 114–124. https://doi.org/10.5358/hsj.41.114

Supplementary material 1

Samples used in the molecular analyses

Authors: Akrachai Aksornneam, Attapol Rujirawan, Yik-Hei Sung, Siriporn Yodthong, Anchalee Aowphol

Data type: pdf

Explanation note: Samples used in the molecular analyses, including their locality, voucher number and GenBank accession number.

Link: https://doi.org/10.3897/zse.100.116601.suppl1

Supplementary material 2

Mean (minimum-maximum) percentages of uncorrected pairwise sequence divergences (*p*-distances) of *Bungarus* species compared to *Bungarus sagittatus* sp. nov.

Authors: Akrachai Aksornneam, Attapol Rujirawan, Yik-Hei Sung, Siriporn Yodthong, Anchalee Aowphol

Data type: pdf

Explanation note: Mean (minimum-maximum) percentages of uncorrected pairwise sequence divergences (*p*-distances) of *Bungarus* species compared to *Bungarus sagittatus* sp. nov., based on 1,137 aligned characters of the mitochondrial cytochrome *b* gene. Intraspecific p-distances are in bold font. Key: NA = data unavailable or not applicable.

Link: https://doi.org/10.3897/zse.100.116601.suppl2

Supplementary material 3

Diagnostic morphological and color pattern characteristics distinguishing *Bungarus sagittatus* sp. nov. from other *Bungarus* species

Authors: Akrachai Aksornneam, Attapol Rujirawan, Yik-Hei Sung, Siriporn Yodthong, Anchalee Aowphol

Data type: pdf

Explanation note: Diagnostic morphological and color pattern characteristics distinguishing *Bungarus sagittatus* sp. nov. from other *Bungarus* species. Key: / = data unavailable or not applicable. Morphological abbreviations are defined in Methods.

Link: https://doi.org/10.3897/zse.100.116601.suppl3

Zoosyst. Evol. 100 (1) 2024, 155–166 | DOI 10.3897/zse.100.118675

PENSOFT

für Natur MUSEUM FÜR NATURKUNDE BERLIN

Updated taxonomy and new insights into the evolutionary relationships of the genus *Sporonchulus* Cobb, 1917 (Nematoda, Mononchida) after the study of two Vietnamese species

Tam T. T. Vu[1,2], Anh D. Nguyen[1,2], Thi Mai Linh Le[1,2], Reyes Peña-Santiago[3]

1 *Institute of Ecological and Biological Resources, Vietnam Academy of Sience and Technology, 18 Hoang Quoc Viet, Cau Giay, Hanoi, Vietnam*
2 *Graduate University of Science and Technology, Vietnam Academy of Science and Technology, 18 Hoang Quoc Viet, Cau Giay, Hanoi, Vietnam*
3 *Departamento de Biología Animal, Biología Vegetal y Ecología, Universidad de Jaén, Campus "Las Lagunillas" s/n, Edificio B3, 23071- Jaén, Spain*

https://zoobank.org/DA6152E1-3DDF-402B-999F-E4024F916D36

Corresponding author: Tam T. T. Vu (vtam7572@gmail.com)

Academic editor: Pavel Stoev ♦ **Received** 12 January 2024 ♦ **Accepted** 6 February 2024 ♦ **Published** 15 February 2024

Abstract

Two known species of the genus *Sporonchulus*, namely *S. ibitiensis* and *S. vagabundus*, collected from natural areas of Vietnam, are characterized, including descriptions and illustrations of both species, as well as SEM observations and molecular (18S-, 28S rDNA) analyses of *S. ibitiensis*. The identity of the two species is discussed, with detailed comparison with previously known populations. The taxonomy of the genus is updated, presenting a diagnosis, list of species, key to their identification, and a compendium of their main morphometrics. An integrative analysis, combining morphological data with a cladistic approach and the first molecular study for a representative of *Sporonchulus*, better supports a narrow relationship of this genus with Mononchidae than with Mylonchulidae members, however further research should be conducted to elucidate its phylogeny.

Key Words

Description, molecular analysis, morphology, phylogeny, 18S, 28S-rDNA

Introduction

Mononchs, the members of the nematode order Mononchida, are an interesting taxon due to their wide geographical distribution and their role as active predators. Their 47 valid genera and 432 valid species (Hodda 2022) dwell in all kind of continental, both soil and freshwater, habitats in the six continents, even Antarctica. They are comparatively large nematodes, often ranging from 1 to 3 mm long, show a very active predatory behaviour toward other nematodes, including cannibalism, and play an important role in feeding relationships of nematode assemblages. Ahmad and Jairajpuri (2010) provided an excellent monograph devoted to their morphology and taxonomy, which still is the best reference for a general overview of the group.

The genus *Sporonchulus* is a rare mononchid taxon, with only four valid species, that, however, display a Pantropical distribution, recorded in Neotropics, Africa and Indomalayan region (Ahmad and Jairajpuri 2010). Originally proposed by Cobb (1917) as a subgenus of *Mononchus* Bastian, 1865 with *M.* (*S.*) *dentatus* Cobb, 1917 as its type and only species, its rank was raised to genus level by Andrássy (1958). Taxonomy of *Sporonchulus* was studied by different authors (Mulvey 1963; Jairajpuri 1971; Andrássy 1993; Ahmad and Jairajpuri 2010) and its position in Mononchida tree was a matter of some controversy. Thus, Jairajpuri (1969) created the subfamily Sporonchulinae, within the family Mylonchulidae Jairajpuri, 1969, to include the genera *Granonchulus* Andrássy, 1958, *Judonchulus* Andrássy, 1958, *Prionchuloides* Mulvey, 1963 and *Sporonchulus* Cobb, 1917.

This idea was followed in subsequent major contributions co-authored by the same author (Jairajpuri and Khan 1982; Ahmad and Jairajpuri 2010). Nevertheless, other authors (Andrássy 1976, 1993, 2009; Zullini and Peneva 2006) did not accept Jairajpuri's scheme, did not recognise Sporonchulinae as a valid taxon, and considered all its genera as members of Mononchinae Filipjev, 1934 in Mononchidae Filipjev, 1934. These authors provided morphological evidence in favour of their proposals, but no molecular analyses were available to support them. Besides, Loof (2006) stated (p. 308) that "this genus is in need of revision".

The occurrence of *Sporonchulus* in Vietnam is not reported so far. Nevertheless, a population of *Sporonchulus ibitiensis* (Carvalho, 1951) Andrássy, 1958 was collected in the course of a general nematological survey conducted to explore the mononchid diversity of natural enclaves of the country, and fresh specimens were therefore available for sequencing. Besides, the revision of the material previously identified as *Actus conoidus* Dhanachand, Romoni & Pramodini, 2006 by Vu (2017) has revealed that it belongs to *S. vagabundus* Jairajpuri, 1971. Thus, this contribution aims to provide a morphological characterisation of the Vietnamese specimens of the mentioned above species, to carry out the first molecular study of a representative of the genus, to discuss their evolutionary relationships and to provide its updated taxonomy.

Materials and methods

Sampling, extraction and processing of nematodes

Three females of *S. vagabundus*, previously deposited at Department of Nematology, Institute of Ecology and Biological Resources (IBSR), Vietnamese Academy of Sciences and Technology (VAST), Hanoi, Vietnam, were available for study. Four females of *S. ibitiensis* obtained from soil samples were collected in a natural forest at Tram Tau town, Yen Bai Province and Du Gia Natural Reserve, Ha Giang Province (Vietnam). Nematodes were extracted using a modified Baermann funnel technique (Southey 1986), heat killed, fixed in TAF solution (Southey 1986) for morphological observations or in a DESS mixture (Yoder et al. 2006) for molecular analyses. Then, specimens were transferred to anhydrous glycerol (Seinhorst 1959, 1962), and mounted on glass slides for their observation with light microscopy. Nematodes were measured and photographed using an Eclipse 80i microscope (Nikon, Tokyo, Japan) with differential interference contrast optics, a drawing tube (camera lucida) and a DS digital camera. Line drawings were made from taken photomicrographs, after processing with Adobe Photoshop CS8. Morphometrics include Demanian indices and other measurements and ratios, some of them presented in a separate table; meanwhile, others form part of the literal description of the species. All measurements were recorded in µm, except body length in mm. After filming and taking pictures, selected specimens were submitted for molecular studies. SEM photographs were taken using SEM PRISMA E according to Abolafia (2015) at VAST. Pictures were edited using Adobe Photoshop CC2018.

DNA extraction, polymerase chain reaction (PCR) and sequencing

Nematode DNA of *S. ibitiensis* was extracted from a single individual as described by Holterman et al. (2006) and DNA extracts were stored at –20° until used as PCR template. The D2-D3 expansion segment of 28S rDNA and 18S were amplified using the forward D2A (5′–ACAAGTACCGTGGGGAAAGTTG–3′) and reverse D3B (5′–TCGG AAGGAACCAGCTACTA–3′) primers (Subbotin et al. 2006) and primers 18S (18F: 5'-TCTAGAGCTAATACATGCAC-3'/18R: 5'-TACGGAAACCTTGTTACGAC-3'). All PCR reactions contained 12,5 µl Hot start green PCR Master Mix (2×) (Promega, USA), 1 µl of the forward and reverse primer (10 µM each), the 3 µl DNA template and sterile Milli-Q water to 25 µl of the total volume. All PCR reactions were performed in SimpliAmp Thermal cycler (Thermo Fisher scientific) as follows: an initial denaturation step at 95 °C for 4 min, followed by 40 cycles at 95 °C for 30 s, 54 °C for 30 s and 72 °C for 60s with a final incubation for 5 min at 72 °C. Amplicons were visualised under UV illumination after Simply safe gel staining and gel electrophoresis. Purified PCR products were sent to Apical Scientific Company for sequencing (Selangor, Malaysia). After sequencing the obtained rDNA sequences fragments were deposited in GenBank under the following accession numbers: OQ377123 (18S) and OQ377128 (28S).

Phylogenetic analyses

For exploring phylogenetic relationships, analyses were based on 18S and 28S rDNA. The newly obtained sequences were manually edited using Chromas 2.6.6 (Technelysium, Queensland, 110 Australia) and aligned with other sequences available in GenBank using ClustalW alignment tool implemented in the MEGA11 (Kumar et al. 2021). Poorly aligned regions at extremes were removed from the alignments using MEGA7. The best fit model of nucleotide substitution used for the phylogenetic analysis was statistically selected using jModelTest 2.1.10 (Darriba et al. 2012). The phylogenetic tree was generated with the Bayesian inference method using MrBayes 3.2.6 (Ronquist et al. 2012). The analysis under the generalised time reversible and invariant sites and gamma distribution (GTR + I + G) model was initiated with a random starting tree and run with the Markov chain Monte Carlo (Larget and Simon 1999) for 1×10^6 generations. The tree was visualised and saved with FigTree 1.4.4 (Rambaut 2018).

Results

Descriptions of species

Sporonchulus ibitiensis (Carvalho, 1951) Andrássy, 1958

Mononchus ibitiensis Carvalho, 1951. Syn.
Sporonchuloides ibitiensis (Carvalho, 1951) Mohandas & Prabhoo, 1982.

Material examined. Four females from one location, in good state of preservation.

Morphometrics. See Table 1.

Description. Female. Moderately slender to slender (*a* = 28–34) nematodes of medium size, 1.09–1.37 mm long. Body cylindrical, slightly tapering towards the anterior end and more appreciably towards the posterior extremity as the tail is conical. Upon fixation, habitus strongly curved ventrad, C- to G-shaped. Cuticle smooth when observed with LM, but showing very fine transverse striation under SEM, two-layered, 1 µm thick at anterior region, 1.5 µm in midbody and 1.5–2 µm on tail. Lip region almost continuous with the adjoining body, 2.0–2.2 times as wide as high and one-half to two-thirds (53–67%) of body diameter at neck base, with totally fused lips and weakly protruding papillae; SEM observations (Fig. 1D): oral field comparatively small, with almost hexagonal oral aperture surrounded by six perioral liplets, labial papillae button-like, prominent, cephalic papillae also button-like, but visibly smaller than labial ones. Amphid fovea small, goblet-like, located at 10–11 µm from the anterior end, its aperture a short transverse slit 3–3.5 µm long, occupying up to one sixth (12–16%) of lip region diameter. Vestibulum 4.5–5.5 µm long. Buccal cavity up to twice (1.8–1.9 times) as long as wide, 1.1–1.3 times longer than lip region diameter: vertical (anterior) plates somewhat convergent at their anterior and posterior ends, their walls 1–1.5 µm thick, horizontal (posterior or basal) plates visibly oblique, with foramina, dorsal tooth apex situated at anterior third of buccal cavity (68–74% from the base), anterior subventral plates bearing each two irregular rows of small teeth with decreasing size from the base till the level of dorsal tooth. Anterior end of pharynx embracing the basal part of buccal cavity, gland nuclei obscure except S_2N = 81–85%. Nerve ring located at 92–101 µm or *ca* one-third (31–36%) of the total neck length. Pharyngo-intestinal junction non-tuberculate, 14–18 × 8.5–10 µm. Genital system diovarian, with small and equally developed branches occupying 6–13% of body length: ovaries comparatively large, 50–146 µm long, with oocytes first arranged in several rows and then in only one row; genital tract very short and poorly differentiated, oviduct 35–48 µm long or 1.0–1.2 body diameters, ***pars dilatata oviductus*** not enlarged, uterus 17–33 µm long or 0.5–0.7 body diameters, both separated by an indistinct weak sphincter; vagina 11 µm long, extending inwards to one-third (34%) of body diameter, ***pars proximalis*** 6.5 × 1.5 µm, ***pars refringens*** with two drop-shaped or somewhat trapezoidal sclerotized pieces 2.5 × 2.5 µm and a combined width of 5 µm, ***pars distalis*** 1.5 µm, vulva a transverse slit. Rectum 0.8–1.0 times the anal body diameter long. Tail conical with finely rounded tip, regularly curved ventrad, with poorly developed glands and lacking a terminal spinneret (Figs 1, 2).

Table 1. Main morphometrics of two *Sporonchulus* species found in Vietnam. Measurements in µm except L in mm.

Species	*S. ibitiensis*	*S. vagabundus*
n	**4♀♀**	**3♀♀**
Character		
L	1.26 ± 0.12 (1.09–1.37)	1.27–1.41
a	29.9 ± 2.8 (28–34)	34–39
b	4.1 ± 0.2 (3.8–4.2)	4.6–4.8
c	24.0 ± 1.5 (22–25)	23–25
c'	2.2 ± 0.0 (2.1–2.2)	2.4–2.5
V	60.4 ± 0.9 (60–62)	57–59
Lip region diameter	24.1 ± 1.9 (21–26)	20–21,
Buccal cavity length	27.3 ± 0.5 (27–28)	22–23
Buccal cavity width	14.5 ±1.7 (12–16)	11.5–12.5
Dorsal tooth apex (%)	71.6 ± 2.8 (68–74)	73–75
Neck length	293 ± 13 (284–302)	278–293
Body diameter at neck base	35.5 ± 4.9 (32–39)	34–36
midbody	42.8 ±7.3 (32–48)	33–40
anus	24.8 ± 3.3 (21–29)	22–24
Distance vulva – ant. end	761 ± 64 (674–824)	748–806
Rectum length	21.0 ± 3.8 (16–24)	20–23
Tail length	52.8 ± 6.7 (46–62)	53–60

Male. Not found.

Molecular characterization. After sequencing and editing, two sequences were obtained for phylogenetic analyses: one full length 18S rDNA with 1591 bp length (GenBank accession N° OQ377123) and one nearly 745 bp length D2D3 of LSU rRNA (28S) (GenBank accession OQ377128).

Locality and habitat. Vietnam, Yen Bai Province, Tram Tau town (coordinates 21°50'18"N, 104°44'22"E, altitude 930 m) and Ha Giang Province, Du Gia Natural Reserve, (coordinates 22°43'18"N, 105°11'38"E, altitude 780 m) where the nematodes were found in soil around the roots of forest trees.

Voucher specimens. Permanent slides are stored at the Department of Nematology, Institute of Ecology and Biological Resources, VAST, Hanoi, Vietnam.

Remarks. Present description provides new data and illustrations of *S. ibitiensis*, especially useful for comparative purposes. General morphology of Vietnamese females very well fits that of type specimens and other known populations (Mulvey 1963; Mulvey and Jensen 1967; Lordello 1970; Chaves and Geraert 1977; Mohandas and Prabhoo 1979; Jairajpuri and Khan 1982; Chaves 1990; Loof 2006; Tahseen et al. 2013; Perichi et al. 2021) of the species. Nevertheless, their morphometrics need further analysis. Table 1 shows the most relevant measurements and ratios of females herein studied; meanwhile, Table 2 includes those available from the literature. Especially relevant is the variation observed in buccal cavity length (18–34 µm), an unusually wide range in mononchid species. Actually, Vietnamese specimens display 26–28 µm long buccal cavity, totally comparable or

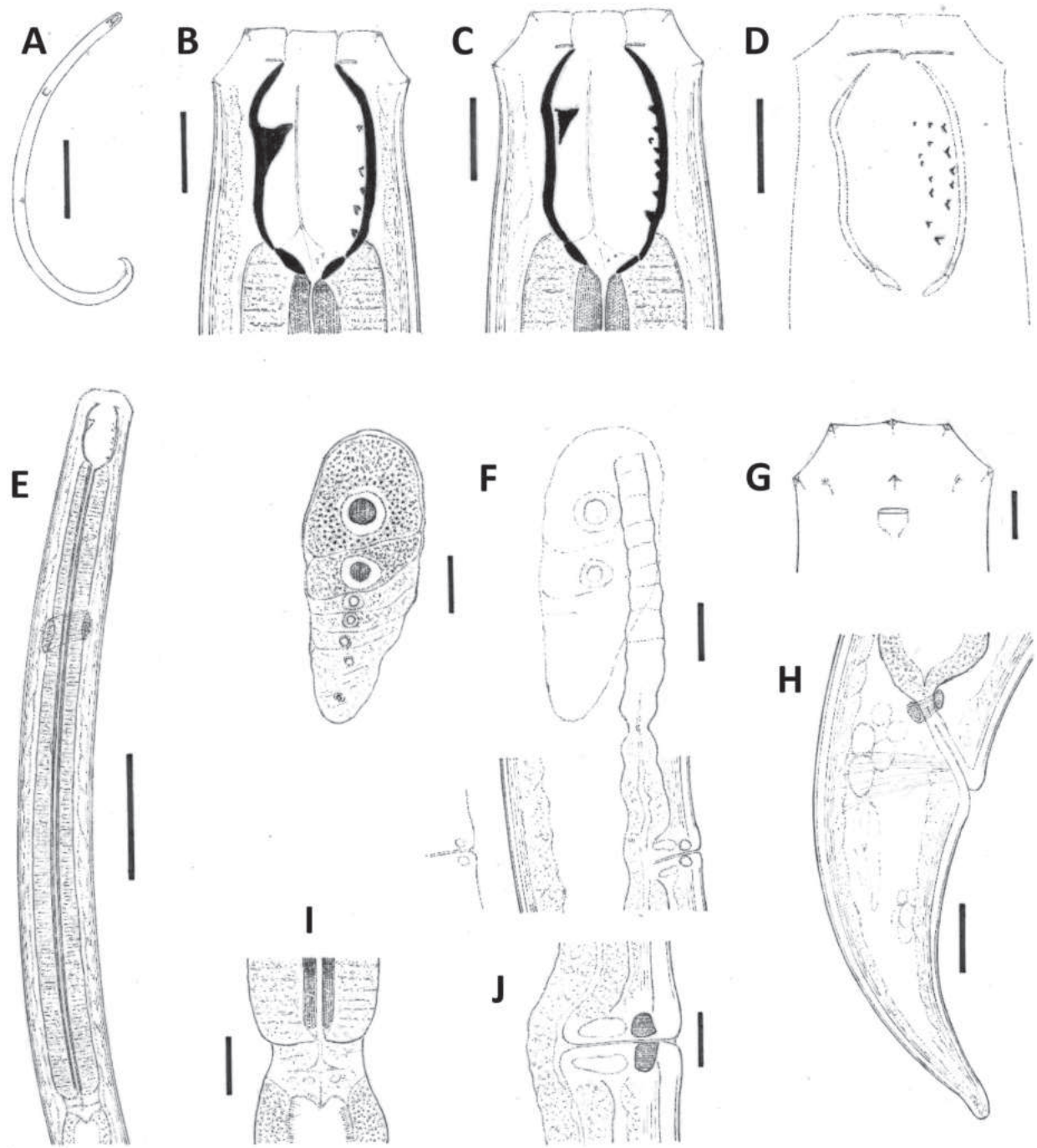

Figure 1. *Sporonchulus ibitiensis* (Carvalho, 1951) Andrássy, 1958 (Female). **A.** Entire; **B–D.** Anterior body region, lateral median (**B, C**) and lateral submedian (**D**) view; **E.** Neck region; **F.** Anterior genital branch; **G.** Anterior body region, lateral surface view; **H.** Caudal region; **I.** Pharyngo-intestinal junction; **J.** Vagina. Scale bars: 200 µm (**A**); 10 µm (**B–D, F, H, I**); 50 µm (**E**); 5 µm (**G, J**).

with appreciably overlapping ranges to those reported for Afrotropical (Mulvey and Jensen 1967; Chaves and Geraert 1977) and Indomalayan (Mulvey 1963; Mohandas and Prabhoo 1979; Jairajpuri and Khan 1982; Loof 2006) populations, but they differ from some South American specimens (Carvalho 1951; Chaves 1990), 25–33 vs 18–23 µm, indeed a remarkable difference that might be the result of a biogeographical pattern with two tentative species or subspecies. Nevertheless, a doubt persists over the true identity of several of these populations, which should be resolved before proposing any taxonomical change. Thus, South American females recorded by Carvalho (1951) and Chaves (1990) were not characterised enough for a comparative analysis. The two Brazilian females studied by Lordello (1970) showed 23 and 27.5 µm long buccal cavity. Chaves and Geraert (1977) studied three females from the former Zaire characterised by bearing a terminal subdorsal pore, which might be a remarkable distinguishing trait. Besides, two (more recent) contributions (Tahseen et al. 2013; Perichi et al. 2021) raise more uncertainties. On the one hand, Tahseen et al. (2013) studied only one Indian female with 22 µm long buccal cavity, which suggests that the species might display more variation in Indomalayan range than previously re-

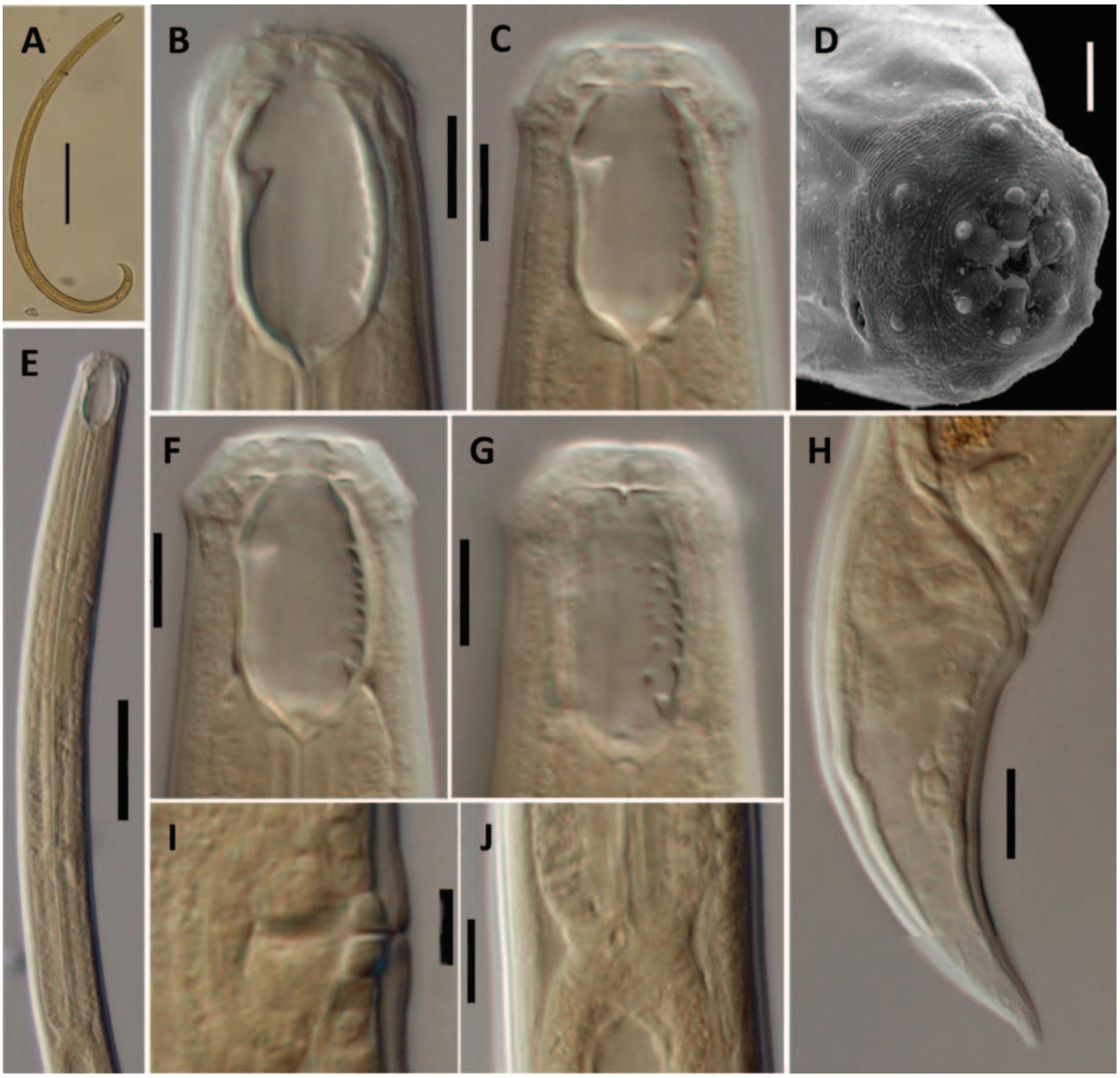

Figure 2. *Sporonchulus ibitiensis* (Carvalho, 1951) Andrássy, 1958 (Female, LM). **A.** Entire; **B, C, F, G.** Anterior body region, lateral median (**B, C**) and lateral submedian (**F, G**) view; **C.** Lip region (SEM), in face view; **E.** Neck region; **H.** Caudal region. **I.** Vagina; **J.** Pharyngo-intestinal junction. Scale bars: 200 µm (**A**); 10 µm (**B, C, F, G, H, J**); 5 µm (**D, I**); 50 µm (**E**).

ported. On the other hand, Perichi et al. (2021) described two Venezuelan populations whose buccal cavities display very wide variation in their length (27–33 and 24–34 µm) and with appreciable difference in their lip region width (26–30 and 20–27 µm, respectively).

Sporonchulus vagabundus Jairajpuri, 1971

Material examined. Three females from one location, in good state of preservation.

Morphometrics. See Table 1.

Description. Female. Moderately slender to slender (a = 28–35) of medium size, 1.27–1.41 mm long. Body cylindrical, slightly tapering towards the anterior end and more appreciably towards the posterior extremity as the tail is conical. Upon fixation, habitus strongly curved ventrad, C- to G-shaped. Cuticle smooth, two-layered, 1 µm thick at anterior region, 1–1.5 µm in midbody and 2 µm on tail. Lip region almost continuous with the adjoining body, 2.1–2.5 times as wide as high and hardly more than one-half (53%) of body diameter at neck base, with totally fused lips and weakly protruding papillae. Amphid fovea small, goblet-like, located at 8–10 µm from the anterior end, its aperture a short transverse slit 3 µm long, occupying less than one-sixth (14–15%) of lip region diameter. Vestibulum 5 µm long. Buccal cavity up to twice (1.8–1.9 times) as long as wide, hardly longer (1.1 times) than lip region diameter: vertical (anterior) plates somewhat convergent at their anterior and posterior ends, their walls 1–1.5 µm thick, horizontal (posterior or basal) plates visibly oblique, with foramina, dorsal tooth apex situated at three-fourths of buccal cavity (74–75% from the base), anterior subventral plates bearing each two irregular rows

Table 2. Compilation of main morphometrics of *Sporonchulus* species. Measurements in µm except L in mm.

Character / Species	n	L	a	b	c	V	c'	lrd	bcl	neck	abd	tail	spic	vm	country	Ref.[1]
S. coronatus	3♀♀	1.07–1.40	17–22	3.3–4.0	20–26	60–66	?	?	28	?	?	?	–	–	Brazil	1, 2
S. dentatus	♀	1.1	31*	3.7*	20*	62	2.6*	29*	33*	297*	21*	55*	–	–	Brazil	3
	♀	1.1–1.3	30–31*	4.0*	18–19*	61	2.3*	25–30	31–36	272–231*	22–26*	60–71	–		Mauritius	4
	♀	1.25	30	3.9	19	62	?	?	34	321*	?	65	–	–	Venezuela	2
?	♀♀	1.14–1.15	26–27	3.4	21–23	62–64	2.1*	?	32–34	330–335	?	49–55	–	–	Brazil	5
?	♀♀[2]	1.1–1.5	26–30	3.4–3.9	19–23	62–64	2.0–2.5	?	32–35	?	?	?	–	–	Several	6
S. Ibitiensis	♀	1.4	24	4	23*	60	2.5*	23*	18*	350*	24	60	–	–	Brazil	7
	♀	1.2	30	3.9	24	63	2.6*	?	25	308*	19*	50	–	–	Sri Lanka	2
	5♀♀	1.1–1.4	28–36	3.9–4.3	21–23	57–63	?	?	27–28	?	?	52–62	–	–	Nigeria	8
	3♀♀	1.01–1.05	23–25	3.0	17–21	57–60	2.3*	25*	26	?	20*	47*	–	–	Zaire	9
	2♀♀	0.99, 1.37	21, 26	3.4, 3.9	20, 26	71, 61	?	?	23, 27	291, 344	?	49, 53	–	–	Brazil	5
	21♀♀	1.24–1.43	20–28	3.9–4.4	23–28	59–63	1.7–2.1	22–28	28–30	?	?	47–60	–	–	India	10, 11
	4♂♂	1.18–1.28	27–30	3.8–4.0	23–24	–	1.6–1.7	22–28	30–31	?	?	52–54	30–35	11–12		
	8♀♀	0.95–1.12	25–32	3.5–4.2	17–19	58–60	2.1–2.7	19–23	21–23	210–237	?	49–64	–	–	Argentina	12
	30♀♀	1.26–1.73	24–34	3.8–5.0	20–27	58–64	1.8–3.1	20–28	26–33	299–396	21–33	53–78	–	–	Malaysia	13
	♀	1.10	27	4.0	20	61	2.0	22	22	272	27	57	–	–	India	14
	11♀♀[2]	1.0–1.5	22–33	3.4–5.2	17–28	59–63	1.4–2.3	20–30	24–34	?	24–30	36–57	–	–	Venezuela	15
	4♀♀	1.09–1.37	28–34	3.8–4.2	22–25	60–62	2.1–2.2	21–26	27–28	284–302	21–29	46–62	–	–	Vietnam	16
S. vagabundus	3♀♀[2]	1.26–1.34	28–36	4.2–4.6	22–25	58–61	2.0	19–21	21–22	280–319*	?	53–58	–	–	India	17
?	♀♀[2]	1.2–1.8	22–32	3.7–4.8	21–27	51–63	2.0–2.5	22–27	22–27	?	?	50–79	–	–	India	11
?	10♀♀[2]	0.91–1.09	20–29	3.6–4.2	19–22	59–64	1.7–2.4	20–23	24–27	232–297	22–28	45–55	–	–	India	14
	3♀♀	1.27–1.41	34–39	4.6–4.8	23–25	57–59	2.4–2.5	20–21	22–23	278–293	22–24	53–60	–	–	Vietnam	16

[1]References: 1 – Carvalho (1956). 2 – Mulvey (1963). 3 – Cobb (1917). 4 – Williams (1958). 5 – Lordello (1970). 6 – Ahmad and Jairajpuri (2010). 7 – Carvalho (1951). 8 – Mulvey and Jensen (1967). 9 – Chaves and Geraert (1977). 10 – Mohandas and Prabhoo (1979). 11 – Jairajpuri and Khan (1982). 12 – Chaves (1990). 13 – Loof (2006). 14 – Tahseen *et al.* (2013). 15 – Perichi *et al.* (2021). 16 – Present paper. 17 – Jairajpuri (1971).

[2]Morphometrics of specimens collected from two or more locations.

* Values calculated from literal description and/or other morphometrics.

? = Either populations whose identity raises some doubt (see text) or morphometrics not available from the corresponding reference.

of small teeth with decreasing size from the base till the level of dorsal tooth. Anterior end of pharynx embracing the basal part of buccal cavity, gland nuclei obscure. Nerve ring located at 93–101 µm or *ca* one-third (34–36%) of the total neck length. Pharyngo-intestinal junction non-tuberculate, 15 × 8–9 µm. Genital system diovarian, with small and equally developed branches occupying 6–7% of body length: ovaries comparatively large, 50–56 µm long, with oocytes first arranged in several rows and then in only one row; genital tract very short: oviduct 40–57 µm long or 1.1–1.4 body diameters, consisting of a small distal part and a well-developed ***pars dilatata***, sphincter hardly perceptible, uterus a simple tube 17–21 µm or 0.4–0.5 body diameters; vagina 11–12 µm long, extending inwards to less than one-third (29–30%) of body diameter, ***pars proximalis*** 5.5–6.5 × 1.5–2 µm, ***pars refringens*** with two trapezoidal sclerotized pieces 2.5 × 2 µm and a combined width of 4.5–5.5 µm, ***pars distalis*** 0.5–1.5 µm, vulva a transverse slit. Rectum as long as anal body diameter long. Tail conical with finely rounded tip, regularly curved ventrad, with distinct caudal glands leading to a visible ampulla with terminal spinneret 2.5 µm long (Figs 3, 4).

Male. Not found.

Locality and habitat. Vietnam, Quang Ninh Province, Bach Long Vi Island, where the nematodes were collected in soil around the roots of a natural forest.

Voucher specimens. Permanent slides are stored at the Department of Nematology, Institute of Ecology and Biological Resources, VAST, Hanoi, Vietnam.

Remarks. As mentioned in the introductory section, these specimens were originally described as *A. conoidus* by Vu (2017). Nevertheless, their general morphology and morphometrics are almost identical to those provided by Jairajpuri (1971) for the type material of *S. vagabundus*, with no appreciable difference. This species is very similar to *S. ibitiensis*, but the study of Vietnamese specimens of both species have revealed some relevant differences. Morphologically, *S. vagabundus* females show a more developed ***pars dilatata oviductus*** and bear distinct caudal glands that, most importantly, lead to appreciable terminal ampulla and spinneret (vs ampulla and spinneret absent). Morphometrically (Table 1), *S. vagabundus* shows a much shorter buccal cavity (22–23 vs 27–28 µm). Although these differences are based on the comparison of only a few specimens, they seem significant enough to separate both species.

Jairajpuri's (1971) original description and Vietnamese specimens herein studied are regarded as the basic material for the characterization of this species and for comparative purposes. Other references should be taken with more caution due to some uncertainties. Jairajpuri and Khan (1982) provided data of specimens with excessively large ranges of some relevant morphometrics (for instance, L = 1.2–1.8 mm, buccal cavity 22–27 µm), which might belong to more than one species. Tahseen et al. (2013) studied two Indian populations with smaller general size (body length 0.91–1.09 mm), and some inconsistences in their description (for instance, buccal cavity 1.4–1.6 times wider than long according to literal description, but 24–27 × 11–13 µm after the morphometrics provided in their Table 1, and buccal cavity similar-sized after their morphometrics (25–27 and 24–26 µm long), but appreciably different according to Figs 1A, 2A and their corresponding scales.

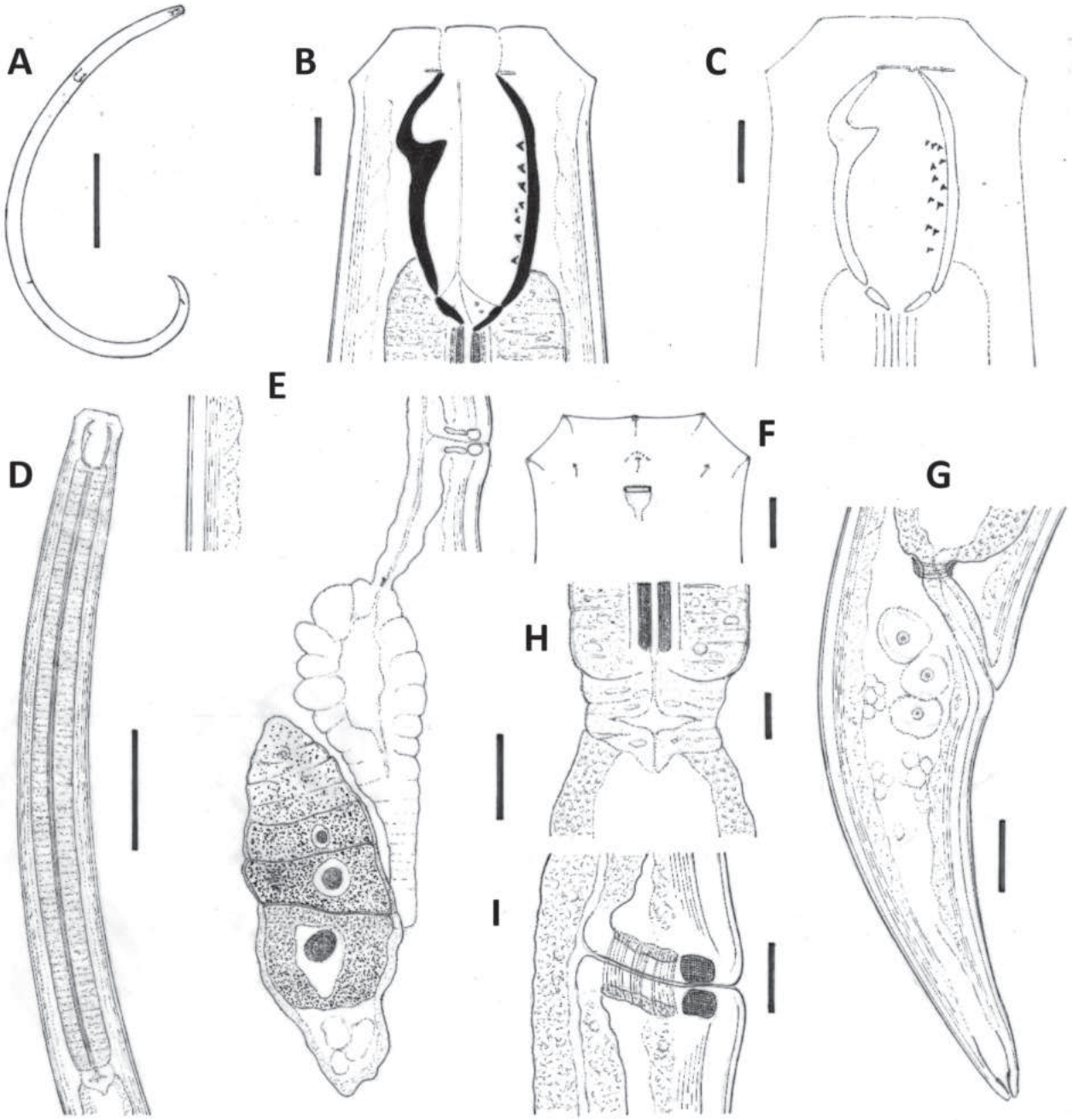

Figure 3. *Sporonchulus vagabundus* Jairajpuri, 1971 (Female). **A.** Entire; **B, C.** Anterior body region, lateral median view; **D.** Neck region; **E.** Posterior genital branch; **F.** Anterior body region, lateral surface view; **G.** Caudal region; **H.** Pharyngo-intestinal junction; **I.** Vagina. Scale bars: 200 µm (**A**); 5 µm (**B, C, F, G, H**); 50 µm (**D**); 10 µm (**E, G**).

Evolutionary relationships of *Sporonchulus* Cobb, 1917

The study of Vietnamese females of *S. ibitiensis* and *S. vagabundus* confirms at least two remarkable morphological features with evolutionary projection: the absence of tubercles at their pharyngo-intestinal junction and, most important, its buccal cavity, very similar to that found in Mononchidae members. Thus, the buccal cavity consists of more or less parallel, convergent at their both ends, vertical (anterior) plates, and visibly oblique horizontal (posterior) plates. Besides, the dorsal tooth, located at the anterior third of buccal cavity, shows an almost horizontal plane anterior margin, very slightly forward directed. This design significantly differs from that observed in Mylonchulidae, with the vertical and basal plates more distinctly converging at their posterior ends than at their anterior ends, the whole cavity becoming V-shaped, and the dorsal tooth conspicuously forwards directed, its anterior margin appearing visibly concave. The mylonchulid pattern is herein interpreted as derived (apomorphic) compared to the more primitive (plesiomorphic) mononchid (Mononchidae) pattern.

Unfortunately, the GenBank database does not include any representative of *Sporonchulus*, therefore the first sequences of both 18S and 28S rDNA are herein provid-

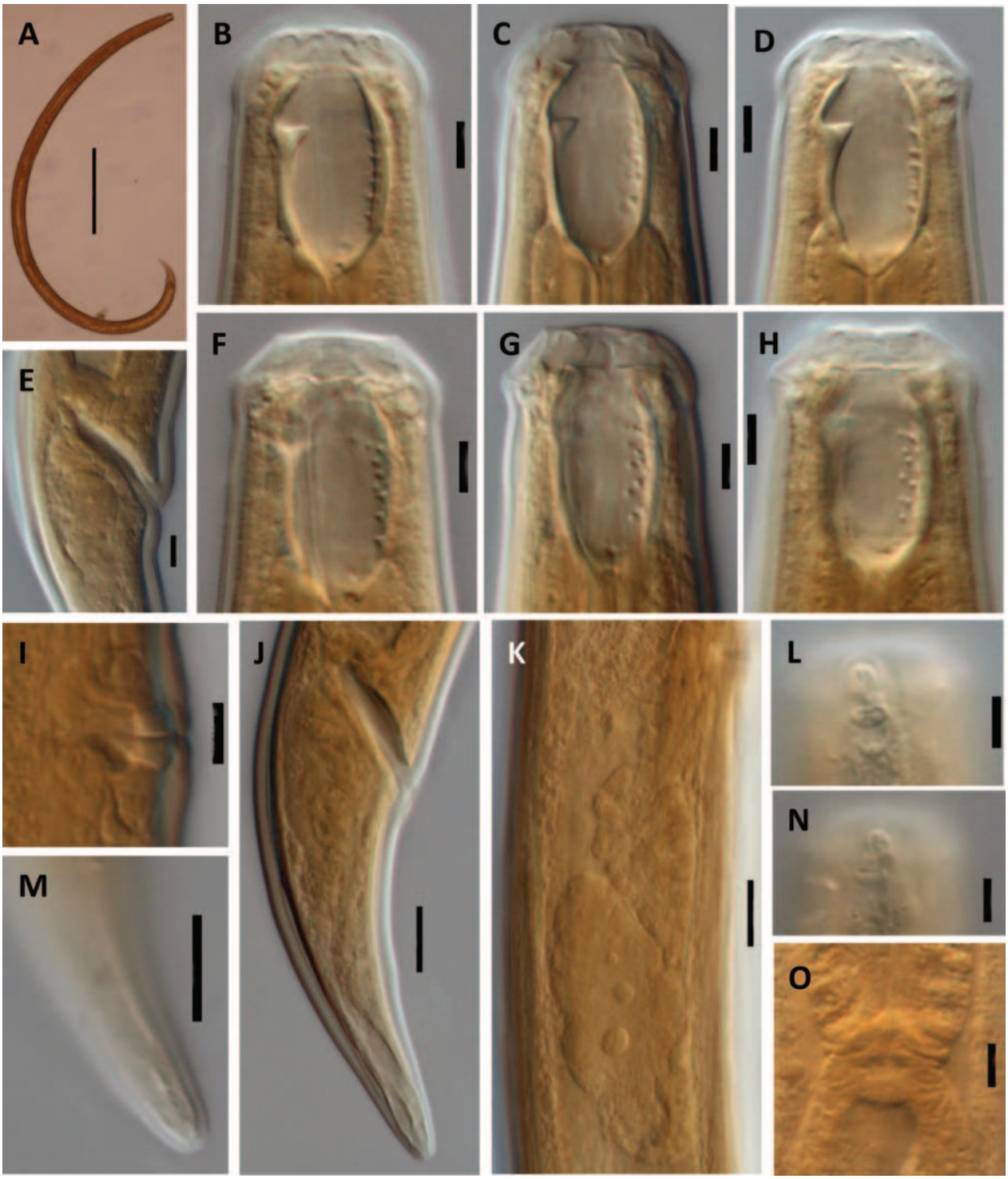

Figure 4. *Sporonchulus vagabundus* Jairajpuri, 1971 (Female, LM). **A.** Entire; **B–D.** Anterior body region, lateral median view; **E.** Caudal glands; **F–H.** Anterior body region, lateral submedian view; **I.** Vagina; **J.** Caudal region; **K.** Posterior genital branch; **L, N.** Anterior body region, lateral surface view; **M.** Detail of caudal region tip; **O.** Pharyngo-intestinal junction. Scale bars: 200 µm (**A**); 5 µm (**B–I, L, N, O**); 10 µm (**J, K, M**).

ed. The results of their analyses are presented in the trees shown in Figs 5, 6, respectively. A BLAST search for matches to the partial 18S rDNA sequence revealed 99% similarity to *Actus* sequences, 97–98% to *Miconchus* sp., 96.6% to *Iotonchulus*, 96% to several *Mylonchulus* sequences, etc. 28S rDNA sequence is 98% similar to that of *Actus*, 94–95% to *Coomansus*, *Parkellus* and *Prionchulus*, 93–94% to *Anatonchus*, 86–88% to *Mylonchulus*, etc. Both trees display a different main branching of Mononchina representatives. 18S tree presents *Mononchus* sequences (Mononchidae, Mononchinae) forming part of a totally supported (100%) clade that is the sister group of the re-

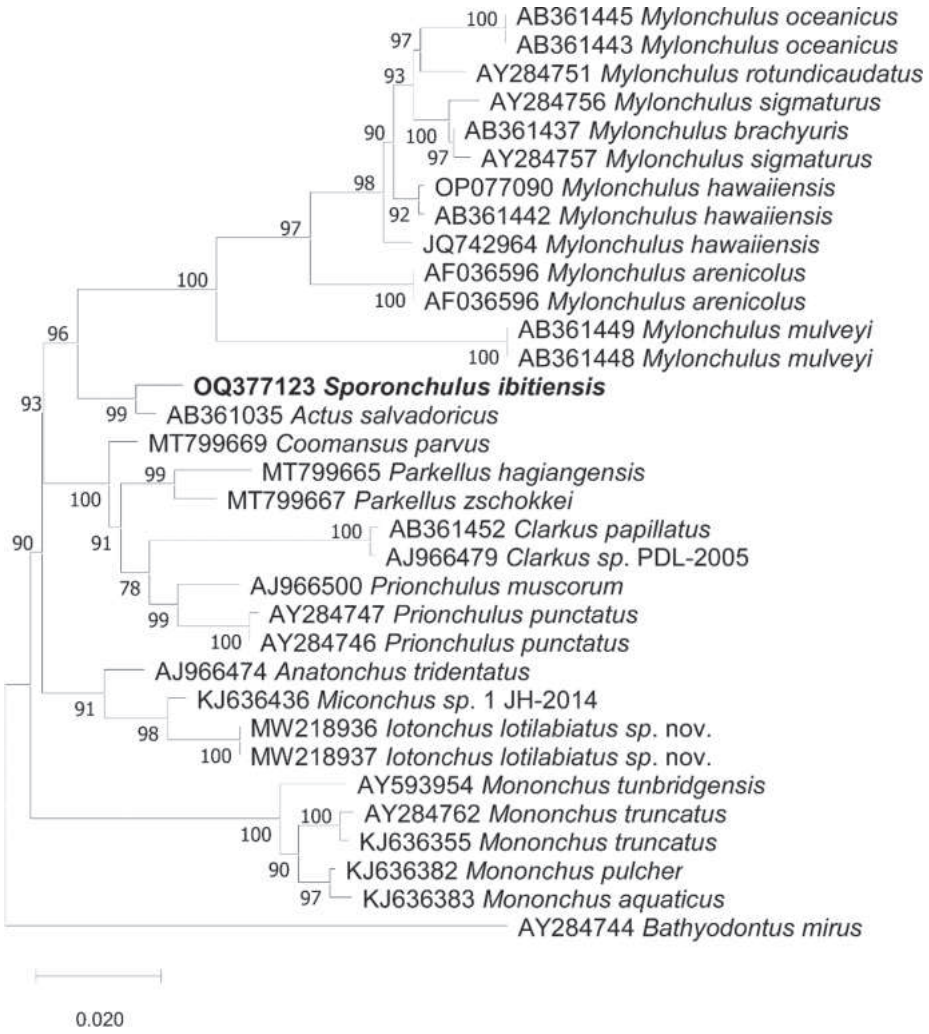

Figure 5. Bayesian Inference tree from the newly sequenced *Sporonchulus ibitiensis* (Carvalho, 1951) Andrássy, 1958 based on sequences of the 18S rDNA region. Bayesian posterior probabilities (%) are given for each clade. Scale bar shows the number of substitutions per site.

maining members of the suborder, all of them components of another, highly supported (98%) clade. Conversely, 28S tree presents *Mylonchulus* sequences (Mylonchulidae, Mylonchulinae) forming a maximally supported clade, which is the sister group of the remaining taxa included in another, maximally supported clade. It is remarkable that neither of these two trees confirms the traditional (morphological) division of Mononchina into two superfamilies, namely Anatonchoidea and Mononchoidea, a system accepted for several decades (Jairajpuri 1969; Jairajpuri and Khan 1982; Andrássy, 1976, 1993, 2009), which did not obtain confirmation when the first molecular analyses, focused on SSU rDNA (Holterman et al. 2006, 2008; Olia et al. 2008; van Megen et al. 2009), were available. Regarding the position of *Sporonchulus* sequences in Mononchida tree, both trees significantly differ in their topology. Thus, 18S tree shows *Sporonchulus* sequence as part of a highly supported (99%) clade also including *Actus salvadoricus*, this clade being the sister group of a maximally supported (100%) *Mylonchulus* clade, both clades grouped in a less supported major (96%) clade. These results argued in favour of the monophyly of Sporonchulinae and of its inclusion in the family Mylonchulidae. Conversely, in LSU tree the *Sporonchulus* sequence is included in a weakly supported (85%) large clade together with *Mononchus* sequences, which is the sister group of a maximally supported clade including all the sequences belonging to Anatonchoidea genera (*Anatonchus*, *Iotonchus*, *Miconchus*, *Parahadronchus*).

As mentioned in the introductory section, the position of *Sporonchulus* and Sporonchulinae was a matter of some controversy. Several authors (Andrássy 1976, 1993, 2009; Zullini and Peneva 2006) claimed they belonged to Mononchidae. This hypothesis is herein morphologically supported. Conversely, molecular analyses do not agree about the position of *Sporonchulus* sequences (see above), but 28S tree provides better resolution in the main branching of Mononchina, with *S. ibitiensis* sequence forming part of the large clade which is the sister group of *Mononchus* clade, thus supporting the results derived from morphological analysis. Although a further study should be conducted to clarify the subject, the belonging of *Sporonchulus* and Sporonchulinae to Mononchidae is herein tentatively accepted.

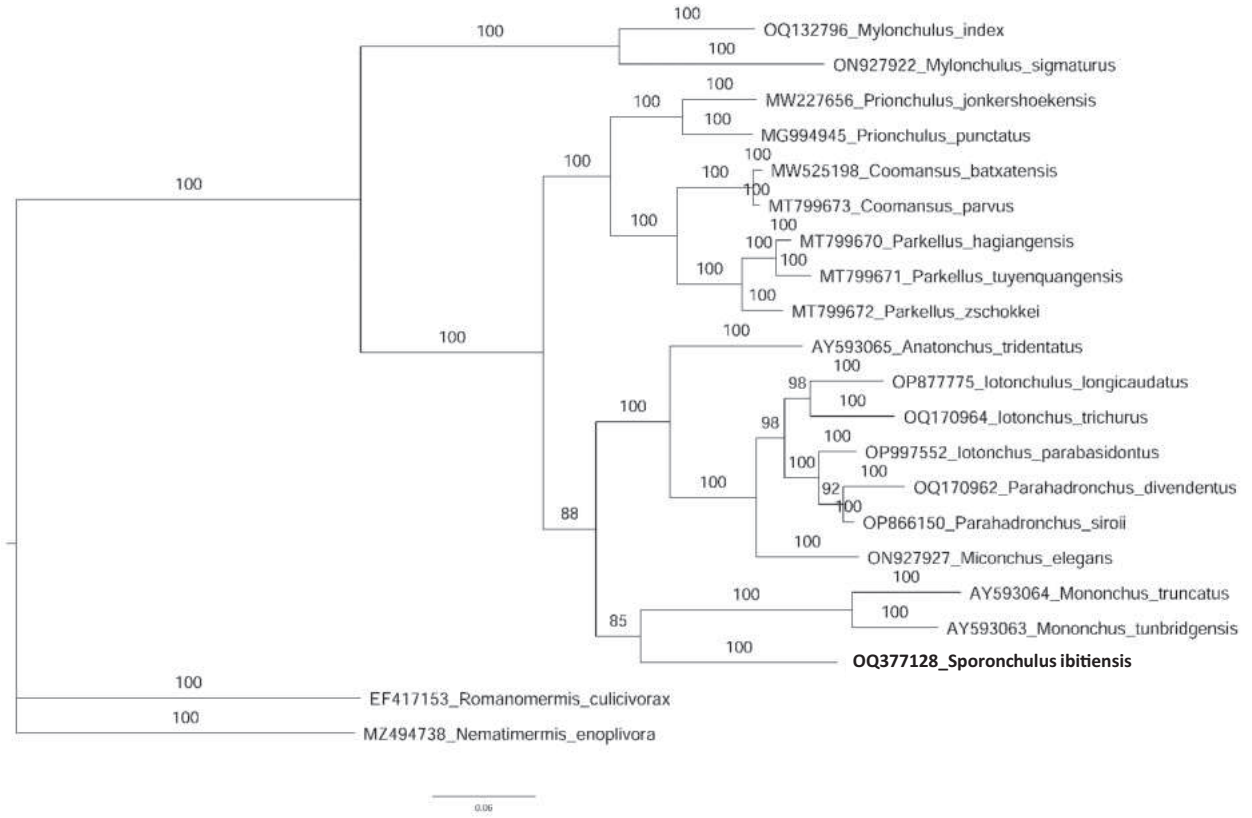

Figure 6. Bayesian Inference tree from the newly sequenced *Sporonchulus ibitiensis* (Carvalho, 1951) Andrássy, 1958 based on sequences of the 28S rDNA region. Bayesian posterior probabilities (%) are given for each clade. Scale bar shows the number of substitutions per site.

Taxonomy of *Sporonchulus* Cobb, 1917

***Sporonchulus* Cobb, 1917**

= *Sporonchuloides* Mohandas & Prabhoo, 1982, syn. by Andrássy (1993).

Historical outline. Cobb (1917) proposed the subgenus *Sporonchulus* under the genus (*Mononchus*) to accommodate three new species, namely *M.* (*S.*) *decurrens*, *M.* (*S.*) *dentatus* (type) and *M.* (*S.*) *recessus*, and characterized it by the presence of irregularly arranged denticles opposed to the dorsal tooth. Andrássy (1958) raised the rank of *Sporonchulus* to generic level, regarded *M. ibitiensis* Carvalho, 1951 and *M. coronatus* Carvalho, 1956 as members of *Sporonchulus*, and transferred *M.* (*S.*) *decurrens* to *Granonchulus*, and *M.* (*S.*) *recessus* to *Judonchulus*. Since then, the taxonomy of the genus has been a matter of some controversy. Goodey (1963) follows Andrássy's ideas. Mulvey (1963) listed five species, recovering *S. recessus* and describing a new species, *S. minutus*. Jairajpuri (1971) added a sixth species, *S. vagabundus*, and noted that the genus consisted of two groups of species, but he did not propose any nomenclatorial change. Jairajpuri and Khan (1982) included only four species (*coronatus*, *dentatus*, *ibitiensis* and *vagabundus*), a scheme accepted in subsequent contributions (Andrássy 1993, 2009; Ahmad and Jairajapuri 2010).

Mohandas and Prabhoo (1982) created the genus *Sporonchuloides* to transfer two *Sporonchulus* species, namely *ibitiensis* (type) and *coronatus*, with "at least two (of their denticles) arranged in longitudinal ribs", meanwhile retained under *Sporonchulus* three species: *dentatus*, *recessus* and *vagabundus*. Moreover, *Sporonchuloides* was classified under Mononchidae instead of under Mylonchulidae. Nevertheless, Andrássy (1993) discussed the identity of this genus and concluded that the denticles of *S. ibitiensis* were "not arranged along ribs", and regarded *Sporonchuloides* as identical and a junior synonym of *Sporonchulus*.

Diagnosis. Mononchidae. Sporonchulinae. Small- to medium-sized nematodes, 0.95–1.78 mm long. Cuticle two-layered. Lip region almost continuous with the adjoining body, with fused lips. Buccal cavity with slightly convergent vertical plates and visibly oblique transverse plates, dorsal tooth situated at the anterior third of the cavity, each vertical subventral plate bearing two irregular rows of small teeth, ca 24 in total. Pharyngo-intestinal junction lacking tubercles. Female genital system diovarian or mono-opistho-ovarian, with poorly differentiated genital tract, distinct ***pars refringens vaginae*** and a transverse vulva. Tail conical, regularly curved ventrad, with variably developed caudal glands and terminal spinneret. Males very rare, with dorylaimid spicule and 11–12 shortly spaced ventromedian supplements without hiatus.

Separation from its relatives. Within Sporonchulinae, and by having dorsal tooth located at the anterior third of buccal cavity, *Sporonchulus* resembles the genera *Granonchulus* and *Actus* Baqri & Jairajpuri, 1974. It can be distinguished from *Granonchulus* in the absence (vs presence)

of a transverse row of denticles on the vertical subventral plates at level of the dorsal tooth, and small teeth arranged in four (two on each plate) irregular longitudinal rows (vs teeth scattered, not distinctly arranged in longitudinal rows) on the vertical subventral plates. From *Actus* in bearing higher number of subventral teeth (ca 24 vs ca 10) arranged into four (vs two) irregular longitudinal rows, two rows per subventral plate (vs only one row per plate).

Type species:

***S. dentatus* Cobb, 1917**
= *Mononchus* (*Sporonchulus*) *dentatus* Cobb, 1917

Other species:

***S. coronatus* (Carvalho, 1956) Andrássy, 1958**
= *Mononchus coronatus* Carvalho, 1956
= *Sporonchuloides coronatus* (Carvalho, 1956) Mohandas & Prabhoo, 1982

***S. ibitiensis* (Carvalho, 1951) Andrássy, 1958**
= *Mononchus ibitiensis* Carvalho, 1951
= *Sporonchuloides ibitiensis* (Carvalho, 1951) Mohandas & Prabhoo, 1982

***S. vagabundus* Jairajpuri, 1971**

Key to species

1 Female genital system mono-opistho-ovarian ..... *Sporonchulus coronatus*
– Female genital system diovarian 2
2 *Pars dilatata oviductus* well-developed. Caudal glands conspicuous, with terminal aperture at tail end .....*S. vagabundus*
– *Pars dilatata oviductus* hardly appreciable. Caudal glands and their aperture inconspicuous 3
3 Larger buccal cavity, 32–35 µm long..... *S. dentatus*
– Smaller buccal cavity, up to 30 µm long, only exceptionally more..... *S. ibitiensis*

Table 2 compiles the main morphometrics of known populations of *Sporonchulus* species for comparative purposes.

Acknowledgements

The Spanish author (RPS) deeply appreciates the invitation, support and reception of the Department of Nematology, Institute of Ecology and Biological Resources (IBSR), Vietnamese Academy of Sciences and Technology (VAST), Hanoi, Vietnam, to visit its lab and to participate in the project "Developing the first-class research team on the discovery of diversity and application potential of hymenopterans, myriapods and soil nematodes in the limestone mountains of north-eastern Vietnam" grant number NCXS01.04/23-25.

The authors would like to thank Dr. Tran, Duc Luong (Institute of Ecology and Biological Resources, VAST) for supporting the value of SEM photographs.

The work is supported by the Vietnam Academy of Science and Technology (VAST) under the project NCXS01.04/23-25 "Developing the first-class research team on the discovery of diversity and application potential of hymenopterans, myriapods and soil nematodes in the limestone mountains of north-eastern Vietnam".

References

Abolafia J (2015) A low-cost technique to manufacture a container to process meiofauna for scanning electron microscopy. Microscopy Research and Technique 78(9): 771–776. https://doi.org/10.1002/jemt.22538

Ahmad W, Jairajpuri MS (2010) Mononchida. The predatory soil nematodes. Nematology Monographs and Perspectives, n° 7. E.J. Brill. Leiden, the Netherlands, 298 pp. https://doi.org/10.1163/ej.9789004174641.i-298

Andrássy I (1958) Über das System der Mononchiden (Mononchidae Chitwood, 1937; Nematoda). Annales Historico-Naturales Musei Nationalis Hungarici 50: 151–171.

Andrássy I (1976) Evolution as a basis for the systematization of nematodes. Pitman Publ. Ltd. London, 288 pp.

Andrássy I (1993) A taxonomic review of the family Mononchidae (Nematoda). Acta Zoologica Hungarica 39: 13–60.

Andrássy I (2009) Free-living nematodes of Hungary. III. Pedozoologica Hungarica n° 5. Hungarian Natural History Museum. Budapest, Hungary, 608 pp.

Baqri QH, Jairajpuri MS (1974) Studies on Mononchida. V. The mononchs of El Salvador with descriptions of two new genera. Nematologica 19(1973): 326–333.

Bastian HC (1865) Monograph on the Anguillulidae, free nematoids, marine, land, and freshwater; with descriptions of 100 new species. Transactions of the Linnean Society of London 25(2): 73–184. https://doi.org/10.1111/j.1096-3642.1865.tb00179.x

Carvalho JC (1951) Uma nova espécie de *Mononchus* (Nematoda, Mononchidae). Bragantia 11(1–3): 51–54. https://doi.org/10.1590/S0006-87051951000100007

Carvalho JC (1956) *Mononchus coronatus* n. sp. (Nematoda, Mononchidae). Revista do Instituto Adolfo Lutz 16: 151–153.

Chaves E (1990) Mononchida (Nematoda) from Argentina. Nematologica 36(1–4): 181–193. https://doi.org/10.1163/002925990X00149

Chaves E, Geraert E (1977) Observations sur quelques Mononchides et Dorylaimides du Camerun et du Zaïre. Revue de Zoologie Africaine 91: 766–780.

Cobb NA (1917) The mononchs (*Mononchus* Bastian, 1865). A genus of free-living predatory nematodes. Soil Science 3(5): 431–486. https://doi.org/10.1097/00010694-191705000-00004

Darriba D, Taboada GL, Doallo R, Posada D (2012) jModelTest 2: more models, new heuristics and parallel computing. Nature Methods 9: 772. https://doi.org/10.1038/nmeth.2109

Dhanachand C, Romoni H, Pramodini M (2006) Two new species of mononch (Nematoda: Mononchida) from soil around the rhizosphere of bamboo from Manipur. Iranian Journal of Nematology 36: 32–36.

Filipjev IN (1934) The classification of free-living nematodes and their relation to parasitic nematodes. Smithsonian Miscellaneous Collections 89: 1–63.

Goodey JB (1963) Soil and freshwater nematodes, 2nd edn. London, UK, Methuen, 544 pp.

Holterman M, Wurff A, Elsen S, Megen H, Bongers T, Holovachov O, Bakker J, Helder J (2006) Phylum-Wide analysis of SSU rDNA reveals deep Phylogenetic relationships among nematodes and accelerated evolution toward crown clades. Molecular Biology and Evolution 23(9): 1792–1800. https://doi.org/10.1093/molbev/msl044

Holterman M, Rybarczyk K, Elsen S, Megen H, Mooyman P, Peña Santiago R, Bongers T, Bakker J, Helder J (2008) A ribosomal DNA-based framework for the detection and quantification of stress-sensitive nematode families in terrestrial habitats. Molecular Ecology Resources 8: 23–34. https://doi.org/10.1111/j.1471-8286. 2007.01963.x

Hodda M (2022) Phylum Nematoda: a classification, catalogue and index of valid genera, with a census of valid species. Zootaxa 5114(1): 001–289. https://https://doi.org/10.11646/zootaxa.5114.1.1

Jairajpuri MS (1969) Studies on Mononchida of India. I. The genera *Hadronchus*, *Iotonchus* and *Miconchus* and a revised classification of Mononchida, new order. Nematologica 15(4): 557–581. https://doi.org/10.1163/187529269X00894

Jairajpuri MS (1971) Studies on Mononchida of India. IV. The genera *Sporonchulus*, *Bathyodontus* and *Oionchus*. Nematologica 17(3): 407–412. https://doi.org/10.1163/187529271X00639

Jairajpuri MS, Khan WU (1982) Predatory nematodes (Mononchida). New Delhi, India. Associated Publishing, 131 pp.

Kumar S, Stecher G, Tamura K (2021) MEGA 11: Molecular Evolutionary Genetics Analysis version 11.0. Molecular Biology and Evolution 38(7): 3022–3027. https://doi.org/10.1093/molbev/msab120

Larget B, Simon DL (1999) Markov chain Monte Carlo algorithms for the bayesian analysis of phylogenetic trees. Molecular Biology and Evolution 16(6): 750–759. https://doi.org/10.1093/oxfordjournals.molbev.a026160

Loof PAA (2006) Mononchina (Dorylaimida) from Western Malaysia. Nematology 8(2): 287–310. https://doi.org/10.1163/156854106777998737

Lordello LGE (1970) Pesquisas sobre nematoides da familia Mononchidae encontrados no Brasil. Anais Escola Superior de Agricultura 'Luiz de Queiroz' 17: 15–48. https://doi.org/10.1590/S0071-12761970000100002

Megen H, van Den Elsen S, Holterman M, Karssen G, Mooyman P, Bongers T, Holovachov O, Bakker J, Helder J (2009) A phylogenetic tree of nematodes based on about 1200 full length small subunit ribosomal DNA sequences. Nematology 11(6): 927–950. https://doi.org/10.1163/156854109X456862

Mohandas C, Prabhoo NR (1979) New predatory nematodes of the genus *Iotonchus* (Iotonchidae, Mononchida) from the soils of Kerala (India). Proceedings of the Indiana Academy of Sciences 88(6): 433–440. https://doi.org/10.1007/BF03179124

Mohandas C, Prabhoo NR (1982) On a new genus, *Sporonchuloides*, with notes on *Sporonchulus* (Cobb, 1917) Pennak, 1953. (Mononchida: Nematoda). Records of the Zoological Survey of India 79(3–4): 359–362. https://doi.org/10.26515/rzsi/v79/i3-4/1981/161732

Mulvey RH (1963) The Mononchidae: a family of predaceous nematodes. V. Genera *Sporonchulus*, *Granonchulus* and *Prionchuloides* n. gen. (Enoplida: Mononchidae). Canadian Journal of Zoology 41(5): 763–774. https://doi.org/10.1139/z63-048

Mulvey RH, Jensen HJ (1967) The Mononchidae of Nigeria. Canadian Journal of Zoology 45(5): 667–727. https://doi.org/10.1139/z67-084

Olia M, Ahmad W, Araki M, Minaka N, Oba H, Okada H (2008) *Actus salvadoricus* Baqri & Jairajpri (Mononchida: Mylonchulidae) from Japan with comment on the phylogenetic position of the genus *Actus* based on 18S rDNA. Japanese Journal of Nematology 38: 57–69. https://doi.org/https://doi.org/10.3725/jjn.38.57

Perichi G, Lugo Z, Crozzoli R, Aguirre Y, Melero N (2021) Morphobiometric data of *Chitwoodius coffeae* and of some mononchids (Nematoda: Enoplea from Venezuela. Revista de la Facultad de Agronomía 47: 24–38.

Rambaut A (2018) Figtree, a graphical viewer of phylogenetic trees. https://github.com/rambaut/figtree/releases/tag/v1.4.4

Ronquist F, Teslenko M, van der Mark P, Ayres DL, Darling A, Höhna S, Larget B, Liu L, Suchard MA, Huelsenbeck JP (2012) MrBayes 3.2: Efficient Bayesian phylogenetic inference and model choice across a large model space. Systematic Biology 61(3): 539–542. https://doi.org/10.1093/sysbio/sys029

Seinhorst JW (1959) A rapid method for the transfer of nematodes from fixative to anhydrous glycerine. Nematologica 4(1): 67–69. https://doi.org/10.1163/187529259X00381

Seinhorst JW (1962) On the killing, fixation and transferring to glycerine of nematodes. Nematologica 8(1): 29–32. https://doi.org/10.1163/187529262X00981

Southey JF (1986) Laboratory methods for work with plant and soil nematodes. London: Her Majesty' Stationery Office, 202 pp.

Subbotin SA, Sturhan D, Chizhov VN, Vovlas N, Baldwin JG (2006) Phylogenetic analysis of Tylenchida Thorne, 1949 as inferred from D2 and D3 expansion fragmants of the 28S rDNA gen sequences. Nematology 8(3): 455–474. https://doi.org/10.1163/156854106778493420

Tahseen Q, Asif M, Musaquim M, Ahlawat S, Bert W (2013) Descriptions of ten known species of the superfamily Mononchoidea (Mononchida: Nematoda) from North India with a detailed account on their variations. Zootaxa 3646: 301–335. https://doi.org/10.11646/zootaxa.3646.4.1

Vu TTT (2017) Occurrence of the genus *Actus* (Mononchida: Mylonchulidae) in Vietnam. Sinh Hoc 39(3): 264–269. https://doi.org/10.15625/0866-7160/v39n3.9269

Williams JR (1958) Studies on the nematode soil fauna of sugar cane fields in Mauritius. I. The genus *Mononchus* (Trilobidae, Enoplida). Mauritius Sugar Industry Research Institute, Occasional Paper 1: 1–13.

Yoder M, De Ley IT, King I, Mundo-Ocampo M, Mann J, Blaxter M, Poiras L, De Ley P (2006) DESS: A versatile solution for preserving morphology and extractable DNA of nematodes. Nematology 8(3): 367–376. https://doi.org/10.1163/156854106778493448

Zullini A, Peneva V (2006) Order Mononchida. In: Eyualem-Abebe, Andrássy I, Traunspurger W (Eds) Freshwater nematodes: ecology and taxonomy. Wallingford, UK, CABI Publishing, 468–496. https://doi.org/10.1079/9780851990095.0468

Zoosyst. Evol. 100 (1) 2024, 167–182 | DOI 10.3897/zse.100.114016

PENSOFT

für Natur MUSEUM FÜR NATURKUNDE BERLIN

Integrative description of a new species of *Dugesia* (Platyhelminthes, Tricladida, Dugesiidae) from southern China, with its complete mitogenome and a biogeographic evaluation

Ying Zhu[1], JiaJie Huang[1], Ronald Sluys[2], Yi Liu[1], Ting Sun[1], An-Tai Wang[1], Yu Zhang[1,3]

1 *Shenzhen Key Laboratory of Marine Bioresource and Eco-environmental Science, College of Life Science and Oceanography, Shenzhen University, Shenzhen, Guangdong, China*

2 *Naturalis Biodiversity Center, P.O. Box 9517, 2300 RA Leiden, Netherlands*

3 *Guangdong Engineering Research Center for Marine Algal Biotechnology, College of Life Sciences and Oceanography, Shenzhen University, Shenzhen, Guangdong, China*

https://zoobank.org/808B9FAB-975D-4A59-8D9F-18E7F4A176D3

Corresponding author: Yu Zhang (biozy@szu.edu.cn)

Academic editor: Pavel Stoev ♦ **Received** 13 October 2023 ♦ **Accepted** 10 January 2024 ♦ **Published** 16 February 2024

Abstract

A new species of freshwater flatworm of the genus *Dugesia* from Guangdong Province in China is described through an integrative approach, including molecular and morphological data, as well as mitochondrial genome analysis. The new species, *Dugesia ancoraria* Zhu & Wang, **sp. nov.**, is characterised by: (a) a highly asymmetrical penis papilla, provided with a hunchback-like dorsal bump; (b) a short duct between seminal vesicle and ejaculatory duct; and (c) a postero-ventral course of the ejaculatory duct, which opens to the exterior at the subterminal, ventral part of the penis papilla. The molecular phylogenetic tree obtained from the concatenated dataset of four DNA markers (18S rDNA, ITS-1, 28S rDNA, COI) facilitated determination of the phylogenetic position of the new species, which shares a sister-group relationship with a small clade, comprising *D. notogaea* Sluys & Kawakatsu, 1998 from Australia and *D. bengalensis* Kawakatsu, 1983 from India. The circular mitogenome of the new species is 17,705 bp in length, including 12 protein coding genes, two ribosomal genes, and 22 transfer RNAs. Via analysis of gene order of mitochondrial genomes, the presently available pattern of mitochondrial gene rearrangement in the suborder Continenticola is discussed.

Key Words

biogeography, *Dugesia*, mitogenome, molecular phylogeny, taxonomy

Introduction

The distributional range of freshwater planarians of the genus *Dugesia* Girard, 1850 covers a large part of the Old World and Australia (cf. Sluys and Riutort 2018, fig. 13B). The historical biogeography of the genus has attracted the attention of planarian specialists for already a good number of years (cf. Sluys et al. 1998 and references therein), culminating in the most recent analysis, which could make use of a time-calibrated phylogenetic tree (Solà et al. 2022).

From the approximately 110 known species of *Dugesia*, thus far only 12 species have been recorded from China, namely, *D. japonica* Ichikawa & Kawakatsu, 1964; *D. ryukyuensis* Kawakatsu, 1976; *D. sinensis* Chen & Wang, 2015; *D. umbonata* Song & Wang, 2020; *D. semiglobosa* Chen & Dong, 2021; *D. majuscula* Chen & Dong, 2021; *D. circumcisa* Chen & Dong, 2021; *D. verrucula* Chen & Dong, 2021; *D. constrictiva* Chen & Dong, 2021; *D. gemmulata* Sun & Wang, 2022; *D. adunca* Chen & Sluys, 2022; and *D. tumida* Chen & Sluys, 2022. The present study adds a new species of *Dugesia* to

the Chinese fauna by describing it through an integrative approach, involving morphological, molecular phylogenetic and mitogenomic analyses. Among these methods, morphological characters, especially the anatomy of the copulatory apparatus, form the main source for the description and identification of the new species.

Since the mitogenome is characterized by strict gene homology and uniparental inheritance without recombination, and contains genes that evolve at different rates, mitochondrial gene order is considered as a strong genetic marker for resolving the phylogenetic position of new species (Rosa et al. 2017). Unfortunately, mitochondrial genomic information on freshwater planarians is still highly limited. Therefore, we expanded our taxonomic study by including also the sequencing and annotation of the complete mitogenome of the new species *Dugesia ancoraria* Zhu & Wang, sp. nov. and compare its gene order with that of other species in the suborder Continenticola Carranza et al., 1998 for which such information is currently available from GenBank.

Materials and methods

Sample collection and culturing

Specimens were collected from a narrow artificial canal running from Wenshan lake in Shenzhen city, Guangdong Province, China (22°31'55"N, 113°56'21"E) on 10 May 2021 (Fig. 1). A 200-μm-mesh sieve was used to collect *Cladophora* algae, to which the worms were attached. The contents of the mesh sieve were washed into a bucket using habitat water, and then transported to the laboratory of Shenzhen University for further analysis and culturing. The flatworms were reared in a glass aquarium (21 cm × 15 cm; depth 18 cm) at room temperature (23–26 °C). The culture was aerated, and the flatworms were fed daily with *Daphnia*.

DNA extraction, amplification, sequencing and phylogenetic analysis

After starvation for three days, total DNA was extracted from three sexual individuals using the E.Z.N.A.™ Mollusc DNA Isolation Kit (Omega, Norcross, GA, USA). Four gene fragments, namely 18S ribosomal gene (18S rDNA), 28S ribosomal gene (28S rDNA), ribosomal internal transcribed spacer-1 (ITS-1), and cytochrome C oxidase subunit I (COI), were amplified by polymerase chain reaction (PCR). We used 2×Taq Plus Master Mix II (Vazyme, China) to amplify 18S rDNA, 28S rDNA, ITS-1, and COI. Primers used for amplification and the PCR protocol are listed in Table 1. Forward and reverse DNA strands were determined by Sanger sequencing either at BGI (Guangzhou, China) or TsingKe Biotech (Beijing, China). All new sequences have been uploaded to GenBank, NCBI (Table 2).

To determine the phylogenetic position of the new species within the genus *Dugesia*, we generated datasets consisting of marker gene sequences (18S rDNA, 28S rDNA, ITS-1, and COI; see Table 2) of the new species *Dugesia ancoraria* and available sequences of other *Dugesia* species from GenBank, NCBI, as well as two outgroup species, viz., *Recurva postrema* Sluys & Solà, 2013 (ITS-1 sequence not available in GenBank, NCBI), and *Schmidtea mediterranea* (Benazzi, Baguñà, Ballester, Puccinelli & del Papa, 1975).

Nuclear ribosomal markers were aligned with MAFFT (online version 7: MAFFT alignment and NJ / UPGMA phylogeny (cbrc.jp), Katoh et al. 2017) using the E-INS-i algorithm, while mitochondrial coding gene COI was aligned by MASCE v2.03 (Ranwez et al. 2018). In order to check for the absence of stop codons, COI sequences were translated into amino acids by ORFFINDER in NCBI, applying genetic code 9 before alignment, after which regions of ambiguous alignments were removed by Gblocks v0.91b (Talavera and Castresana 2007), using the same parameters as specified in Li et al. (2019). For ribosomal DNA, sequences were excluded by ClipKIT (Steenwyk et al. 2020) with kpic-gappy mode to keep parsimony-informative and constant sites and to remove highly gappy sites. Final length of the alignments was 693 base pairs (bp) for COI, 1,388 bp for 18S rDNA, 1,383 bp for 28S rDNA, and 591 bp for ITS-1. To ensure sequences' validity, the substitution saturation test (Xia et al. 2003; Xia and Lemey 2009) in DAMBE6 software (Xia 2017) was used to evaluate the nucleotide substitution saturation of four datasets, followed by the assembly of a multi-gene concatenated dataset (with the order 18S rDNA–28S rDNA–ITS-1–COI), using SequenceMatrix v1.8 (Vaidya et al. 2011). Sequences that were shorter or not available in GenBank were completed with "-". We used PartitionFinder2 (Lanfear et al. 2017) to evaluate the best-fit evolution models by estimating independent models of molecular evolution for subsets of sites that were deemed to have evolved in similar ways.

Table 1. Primer sequences used for PCR amplification.

Gene	Primer	Sequence (5'-3')	Reference	PCR protocol
COI	COIEFMF	Forward: GGW GGK TTT GGW AAW TG		94 °C 5 min, 35× (94 °C 50 s,
	COIRSong	Reverse: GWG CAA CAA CAT ART AAG TAT CAT		50 °C 45 s, 72 °C 45 s); 72 °C 7 min
ITS-1	ITS9F	Forward: GTA GGT GAA CCT GCG GAA GG	Baguñà et al. 1999	98 °C 5 min, 30× (98 °C 30 s,
	ITSR	Reverse: TGC GTT CAA ATT GTC AAT GAT C		46 °C 45 s, 72 °C 30 s); 72 °C 7 min
18S rDNA	18S 1F	Forward: TAC CTG GTT GAT CCT GCC AGT AG	Carranza et al. 1996	94 °C 5 min, 40× (95 °C 50 s,
	18S 9R	Reverse: GAT CCT TCC GCA GGT TCA CCT AC		50 °C 45 s, 72 °C 50 s); 72 °C 7 min
28S rDNA	28S 1F	Forward: TAT CAG TAA GCG GAG GAA AAG	Álvarez-Presas et al. 2008	94 °C 5 min, 40× (94 °C 50 s,
	28S 6R	Reverse: GGA ACC CCT TCT CCA CTT CAG T		52 °C 45 s, 72 °C 50 s); 72 °C 7 min

Table 2. GenBank accession numbers of sequences for species taxa used in the phylogenetic analyses.

Species	COI	ITS–1	18S rDNA	28S rDNA
Recurva postrema	KF308763	–	KF308691	MG45274
Schmidtea mediterranea	JF837062	AF047854	U31085	MG457267
Dugesia adunca	OL505739	OL527659	–	–
D. aenigma	KC006968	KC007043	KF308698	–
D. aethiopica	KY498845	KY498785	KY498822	KY498806
D. afromontana	KY498846	KY498786	KY498823	KY498807
*D. ancoraria1**	OR326966	OR296750	OR198141	OR225689
*D. ancoraria2**	OR326967	OR296751	OR198142	OR225690
*D. ancoraria3**	OR326968	OR296752	OR198143	OR225691
D. arabica	OL410620	OK587374	OK646637	OK491342
D. arcadia	KC006969	KC007047	KF308694	OK491318
D. ariadnae	JN376142	KC007049	OK646636	OK491317
D. aurea	MK712632	MK713027	–	MK712523
D. batuensis	KF907819	KF907816	OK646630	KF907823
D. benazzii	FJ646977, FJ646933	MK713037	OK646628	MK712509
D. bengalensis	–	FJ646897	–	–
D. bifida	KY498851	KY498791	KY498843	KY498813
D. bijuga	MH119630	–	MH113806	–
D. circumcisa	MZ147041	MZ146782	–	–
D. constrictiva	MZ871766	MZ869023	–	–
D. corbata	MK712637	MK713029	–	MK712525
D. cretica	KC006974	KC007055	KF308697	–
D. damoae	KF308768	KC007057	OK646619	OK491310
D. deharvengi	KF907820	KF907817	–	KF907817
D. effusa	KF308780	KC007058	OK646618	OK491311
D. elegans	KC006985	KC007063	KF308695	OK491313
D. etrusca	MK712651	FJ646898	OK646617	OK491312
D. gemmulata	OL632201	–	–	–
D. gibberosa	KY498857	KY498803	KY498842	KY498819
D. gonocephala	FJ646941, FJ646986	FJ646901	DQ666002	DQ665965
D. granosa	OL410634	KY498795	KY498833	KY498816
D. hepta	MK712639	MK713035	OK646612	MK712512
D. ilvana	FJ646989, FJ646944	FJ646903	OK646608	OK491334
D. improvisa	KF308774	KC007065	KF308696	OK491304
D. japonica	AB618487	FJ646906	D83382	DQ665966
D. liguriensis	MK712645	FJ646907	OK646615	OK491353
D. majuscula	MW533425	MW533591	–	–
D. malickyi	KF308750	KC007069	OK646585	OK491294
D. naiadis	KF308757	OK587343	OK646581	OK491293
D. notogaea	FJ646993, FJ646945	FJ646908	KJ599713	KJ599720
D. parasagitta	KF308739	KC007073	OK646577	–
D. pustulata	MH119631	OK587366	MH113807	OK491355
D. ryukyuensis	AB618488	FJ646910	AF050433	DQ665968
D. sagitta	KC007006	KC007085	OK646567	OK491320
D. semiglobosa	MW525210	MW526992	–	–
D. sicula	KF308797	FJ646915	KF308693	DQ665969
D. sigmoides	KY498849	KY498789	KY498827	KY498811
D. sinensis	KP41592	–	–	–
D. subtentaculata	MK712561	MK712995	AF013155	MK712493
D. tubqalis	OM281843	OK587337	OK646555	OK491285
D. tumida	OL505740	OL527709	–	–
D. umbonata	MT176641	MT177211	MT177214	MT177210
D. vilafarrei	MK712648	MK712997	OM281820	MK712511
D. verrucula	MZ147040	MZ146760	–	–

*this study.

Phylogenetic trees were constructed by Maximum Likelihood (ML) and Bayesian Inference (BI) methods. For ML, standard bootstrap analysis with 1,000 replications was performed by IQ-TREE v1.6.2 (Nguyen et al. 2015). BI was performed in MrBayes v3.2.6 (Ronquist et al. 2012) with two simultaneous runs of one cold and three hot chains. Each run for the concatenated dataset was performed for 1,000,000 generations, sampling every 1,000 generations. We checked the resulting parameter file of each run in TRACER v1.7.1 (Rambaut et al. 2018) to ensure that the effective sample size (ESS) values of each parameter were above 200.

Mitochondrial DNA extraction, amplification, sequencing and phylogenetic analysis

After having been starved for three days, the mitochondrial DNA of an asexual specimen of *D. ancoraria* was extracted (due to absence of sexual specimens at that time) using Animal mitochondrial DNA column extraction kit (PCR Grade; BioLebo Technology, Beijing China), followed by amplification of mitochondrial DNA using a REPLI-g Midi Kit (QIAGEN, Hilden, Germany). We compared the COI gene of the three sexual individuals with that of the asexual individual for mitochondrial extraction via megablast and, thus, found that they were perfectly identical. Paired-end sequencing was conducted on the Illumina Hiseq 2500 platform (BGI, Guangzhou, China). The mitogenome sequences were assembled using MitoFinder (Allio et al. 2020). The functional regions of these genes were annotated and verified according to Huang et al. (2022). However, both MITOS (online version: MITOS Web Server (uni-leipzig.de), Bernt et al. 2013) and tRNAscan-SE (Lowe and Chan 2016;) failed to annotate trnT in the mitogenome of *D. ancoraria*. Therefore, trnT was identified manually on the basis of homology comparisons with other species in the family Dugesiidae Ball, 1974. Seven species belonging to Dugesiidae, five to Geoplanidae Stimpson, 1857, and two species belonging to Planariidae Stimpson, 1857 were chosen for the construction of the mitochondrial tree (Table 3). As outgroup taxon we used the maricolan species *Obrimoposthia wandeli* (Hallez, 1906), which is a member of Uteriporidae Diesing, 1862 (Table 3). Multiple sequences alignments (MSA) for protein coding genes (PCGs) and ribosomal genes were carried out using MASCE v2.03, which translates the nucleotides to amino acids before alignment. Hereafter, MSAs were trimmed by Gblocks v0.91b. Substitution saturation tests for each PCG were performed using DAMBE6. Subsequently, SequenceMatrix v1.8 was used to combine the alignments. The best-fit model for each PCG was selected by PartitionFinder2. ML analysis was conducted by IQ-TREE v1.6.2. For BI, MrBayes v3.2.6 was applied with 2,000,000 generations, sampling every 2,000 generations. Gene rearrangement scenarios including reversals, transpositions, reverse transpositions, reversal and tandem-duplication-random-losses (TDRL) among all species were analysed using the software CREx (Bernt et al. 2007) on the CREx web server (http://www.pacosy.informatik.uni-leipzig.de/crex) based on common intervals.

Histology

For the morphological analysis, the flatworms were starved for three days prior to the preparation of histological sections according to procedures described by Song et al. (2020). Briefly, histological sections were made at intervals of 6 μm and were stained with modified Cason's Mallory-Heidenhain stain solution (see Yang et al. 2020). Hereafter, slides were mounted onto glass slides with neutral balsam (Yuanye Biotechnology, Shanghai, China) and sealed with a coverslip. Preparations registered with PLA codes were deposited in the Institute of Zoology, Chinese Academy of Sciences (IZCAS), while histological slides registered with RMNH.VER. codes will be deposited at Naturalis Biodiversity Center, Leiden, The Netherlands.

Abbreviations used in the figures

au: auricle; **bc**: bursal canal; **ca**: common atrium; **cb**: copulatory bursa; **cm**: circular muscle; **d**: diaphragm; **db**: distal bulge; **du**: duct; **e**: eye; **ed**: ejaculatory duct; **esv**: extension seminal vesicle; **go**: gonopore; **hb**: hunchback bump; **ie**: inner epithelium; **lm**: longitudinal muscle; **lod**: left oviduct; **lvd**: left vas deferens; **ma**: male atrium; **od**: oviduct; **oe**: outer epithelium; **ov**: ovary; **pg**: penis glands; **ph**: pharynx; **pp**: penis papilla; **rod**: right oviduct; **rvd**: right vas deferens; **sg**: shell glands; **sv**: seminal vesicle.

Results

Molecular phylogeny

The phylogenetic trees obtained by BI and ML from the concatenated dataset (with the order 18S rDNA–28S rDNA–ITS-1–COI) showed similar topologies and supported nodes (Fig. 2). In this tree, the terminals for *D. ancoraria* grouped together and did not group with any other species of *Dugesia* included in our molecular analysis. It is noteworthy that the new species *D. ancoraria* formed a well-supported clade with *D. notogaea* Sluys & Kawakatsu, 1998 and *D. bengalensis* Kawakatsu, 1972 (Fig. 2, 100% bootstrap [bs] in ML; Suppl. material 1, 1.00 posterior probability [pp] in BI). *Dugesia notogaea* is an Australian species, while *D. bengalensis* inhabits a

Table 3. Species and corresponding GenBank accession numbers of mitochondrial genomes used for mitochondrial analysis.

Species	GenBank	Species	GenBank
Amaga expatria	MT527191	*Obama* sp.	NC026978
Bipalium kewense	NC045216	*Obrimoposthia wandeli*	NC050050
Crenobia alpina	KP208776	*Parakontikia ventrolineata*	MT081960
*Dugesia ancoraria**	OR400685	*Phagocata gracilis*	KP090060
Dugesia japonica	NC016439	*Platydemus manokwari*	MT081580
Dugesia constrictiva	OK078614	*Schmidtea mediterranea*	JX398125
Dugesia ryukyuensis	AB618488		

*this study.

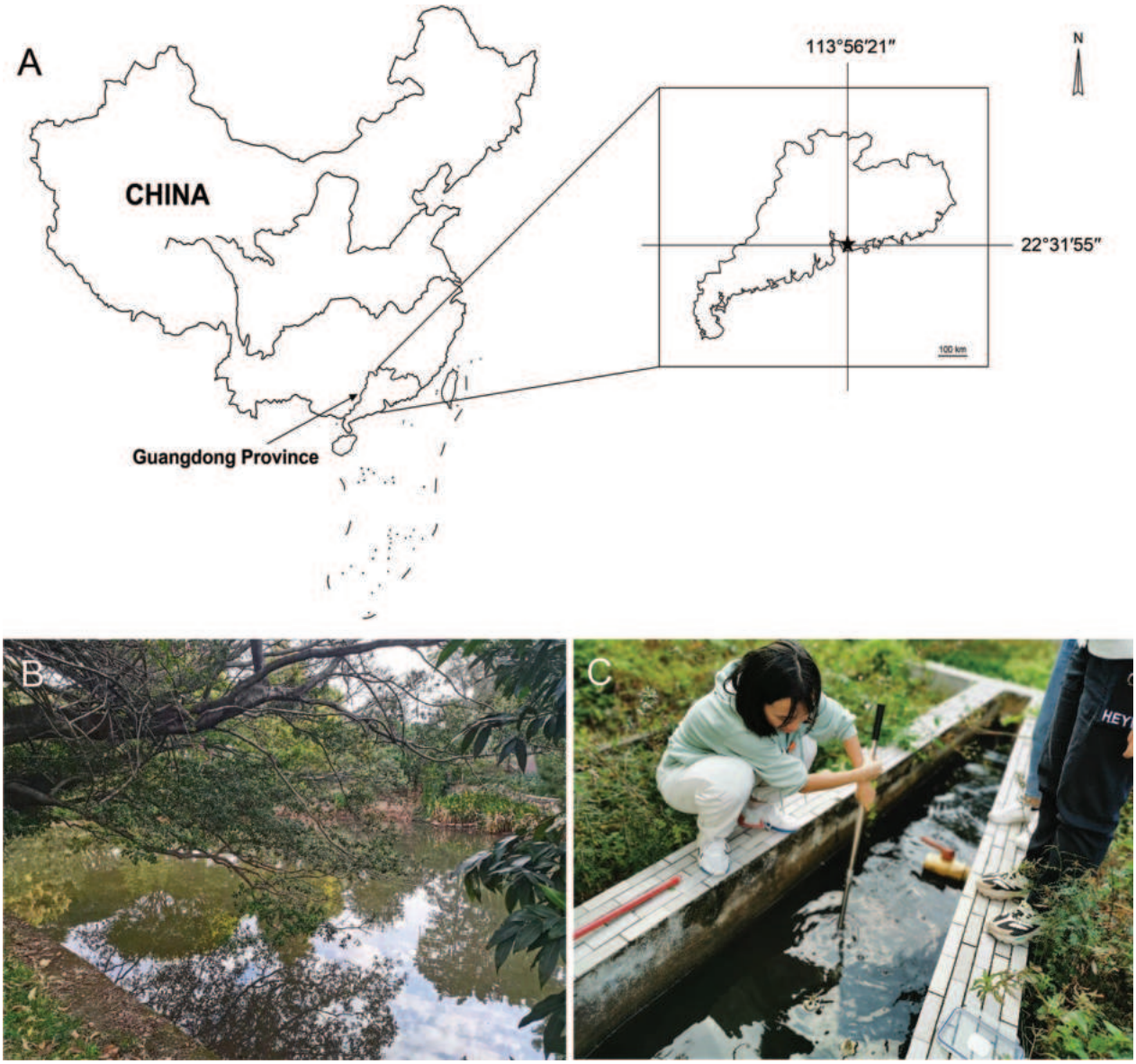

Figure 1. Locality and habitat of *Dugesia ancoraria*. **A.** Sampling locality in Guangdong Province, China; **B, C.** Habitat at sampling locality.

portion of India. As suggested by the high support value (99% bs; 1.00 pp), these three species are closely related and share a sister-group relationship with *D. adunca* Chen & Sluys, 2022 from Guangxi province. Then, these four species are supported as sister to a small clade composed of *D. ryukyuensis* Kawakatsu, 1976 and *D. batuensis* Ball, 1970 (96% bs; 1.00 pp).

Mitochondrial genome

The complete, circular mitochondrial genome of *Dugesia ancoraria* is 17,705 bp in length, and includes 12 of the 13 protein-coding genes of mitochondrial genomes (atp8 was not found), two ribosomal RNA (rRNA) genes, and 22 transfer RNA (tRNA) genes, which are arranged as follows: *cox1-E-nad6-nad5-S2-D-R-cox3-I-Q-K-atp6-V-nad1-W-cox2-P-nad3-A-nad2-M-H-F-rrnS-L1-Y-G-S1-rrnL-L2-T-C-N-cob-nad4l-nad4*. GC content is 23.77%, while a positive GC skew ([G-C]/[G+C] = 0.323) indicated the occurrence of more Gs than Cs (Fig. 3).

Both the ML and BI trees obtained from 12 protein coding genes (PCGs) have highly supported clades, excepting one node with a bootstrap support lower than 70%. Since the topologies of the ML and BI trees are basically identical, we integrated them into one phylogenetic tree. In the integrated tree, *Crenobia alpina* (Dana, 1766) and *Phagocata gracilis* (Haldeman, 1840) together form a clade that shares a sister-group relationship with a clade that is composed of two smaller clades, one comprising land planarians (Geoplanidae) and the other constituted by dugesiid freshwater planarians (Dugesiidae). The latter family forms a well-supported monophyletic group, in which *D. ancoraria* is sister to *D. ryukyuensis* with high support values (100% bs; 1.00 pp) (Fig. 4).

Figure 2. Maximum likelihood phylogenetic tree topology inferred from the concatenated dataset (18S rDNA, ITS-1, 28S rDNA and COI). Numbers at nodes indicate support values (bootstrap/ posterior probability). Asterisks (*) indicate support values lower than 50% bs/0.50 pp, or posterior probability not applicable to this node, because of different topologies of trees generated by BI and ML methods. Scale bar: substitutions per site.

The gene order of rRNAs, PCGs and tRNAs of *D. ancoraria* and other species used in our phylogenetic analysis are shown in Fig. 4. Some tRNAs absent in previous publications, such as those from *Platydemus manokwari* de Beauchamp, 1963 and *Parakontikia ventrolineata* (Dendy, 1892), had been successfully annotated using MITOS (Bernt et al. 2013). Our results show that the orders of PCGs and ribosomal genes are conserved among species belonging to the triclad suborder Continenticola and are arranged as follows: cox1-nad6-nad5-cox3-atp6-nad1-cox2-nad3-nad2-rrnS-rrnL-cob-nad4l-nad4. In contrast, the order of tRNAs is highly variable. Within the cluster of Dugesiidae species, *D. ancoraria* shares an identical gene order with *D. constrictiva.* An analysis of gene order rearrangements with CREx suggests that only one transposition (trnN) occurred from *D. ancoraria* to *D. ryukyuensis* and also one transposition (trnE) from *D. ryukyuensis* to *D. japonica*. Except for a transposition of trnE, a tandem-duplication-random-loss (TDRL) event is required for the transformation from *D. japonica* to *Schmidtea mediterranea* (Benazzi et al., 1975). With respect to the Geoplanidae, *Amaga expatria* Jones & Sterrer, 2005 and *Obama* sp. share the same gene order. Besides a transposition of trnF, a transposition of trnM and trnH linkage is needed to go from *C. alpina* to *Bipalium kewense* Moseley, 1878. Two inverse transpositions, namely trnL2 and trnT, occurred from *Bipalium kewense* to *Obama* sp. and *Amaga expatria*, and from *Obama* sp. to *Platydemus manokwari*, resulting in almost the same gene order shared by *B. kewense* and *P. manokwari*, with the only exception being the position of trnC (Fig. 4).

Systematic account

Order Tricladida Lang, 1884
Suborder Continenticola Carranza, Littlewood, Clough, Ruiz-Trillo, Baguñà & Riutort, 1998
Family Dugesiidae Ball, 1974
Genus *Dugesia* Girard, 1850

***Dugesia ancoraria* Zhu & Wang, sp. nov.**
https://zoobank.org/137337E1-0D52-4288-A3A3-7E8C80241A74

Material examined. *Holotype*: PLA-0251, a narrow artificial canal of Wenshan lake, Shenzhen city, Guangdong Province, China, 22°31'55"N, 113°56'21"E, 10 May 2021, coll. MY Xia and co-workers, sagittal sections on 14 slides.

***Paratypes*:** PLA-0252, ibid., sagittal sections on 12 slides; PLA-0253, ibid., transverse sections on 35 slides; RMNH.VER.21525.1, ibid., sagittal sections on 12 slides.

Habitat. Specimens were collected from a narrow artificial canal running from Wenshan lake (22°31'55"N,

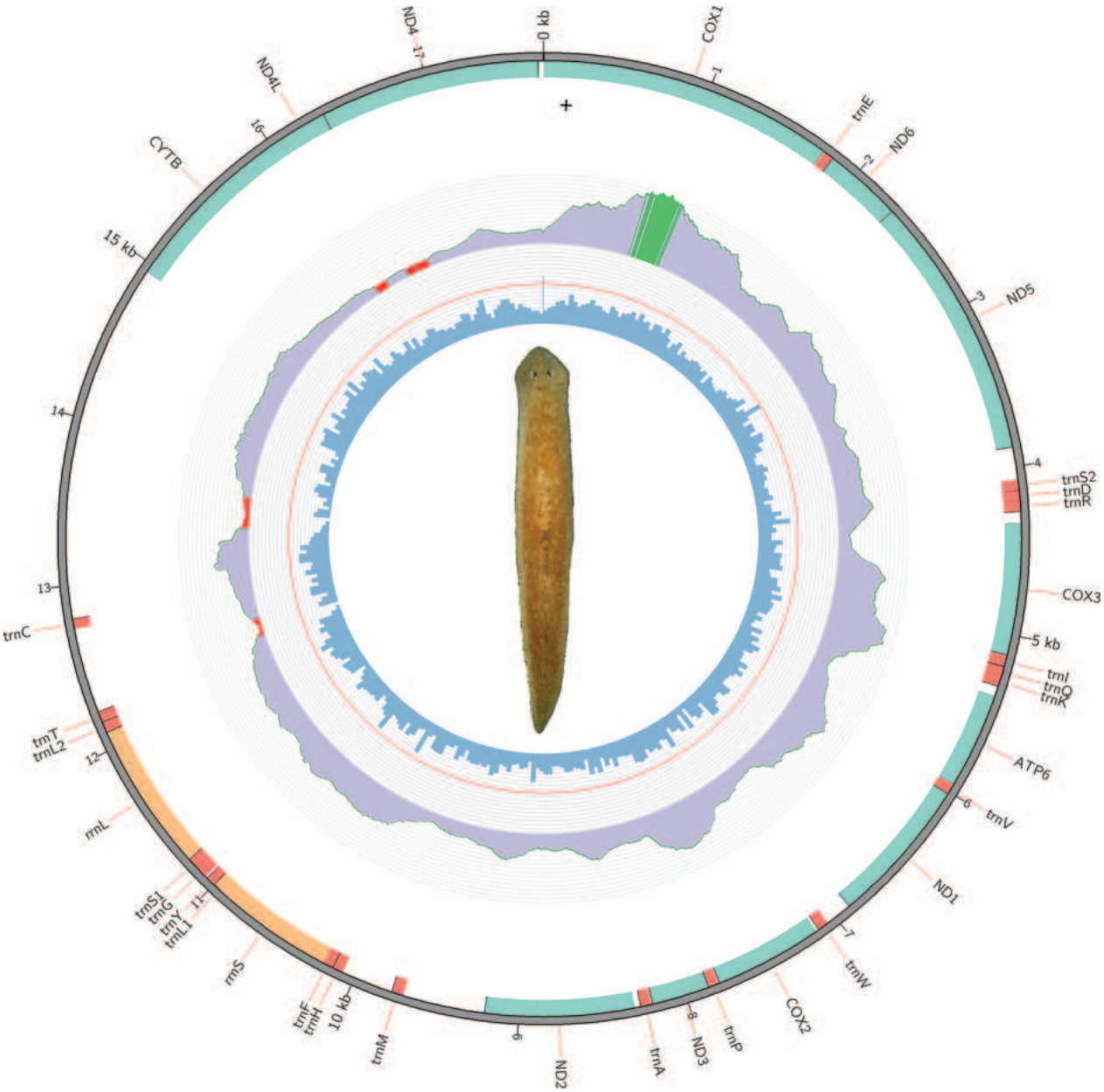

Figure 3. Arrangement of the mitochondrial genome of *Dugesia ancoraria*. Outer circle: annotation of genes, with protein-coding genes, ribosomal RNAs and transfer RNAs represented by cyan, orange, and red, respectively. Intermediate circle: sequencing coverage, with green colour indicating coverage greater than 95% average coverage. Inner circle, with the blue colour indicating GC content and the thin orange circle indicating 50% of GC content. The picture in the middle represents an individual of *D. ancoraria*.

113°56'21"E), which is located in Shenzhen city, Guangdong Province, China (Fig. 1A). The animals were collected from *Cladophora* algae, as well as the stone wall of the canal, which had a water depth of 20–30 cm; water temperature was about 23 °C. Thirty specimens were collected, none of which was sexually mature. However, after six months of rearing under laboratory conditions, about 20 specimens eventually attained sexual maturity.

Diagnosis. *Dugesia ancoraria* is characterised by the following characters: highly asymmetrical penis papilla, provided with a hunchback-like dorsal bump; vasa deferentia opening symmetrically into the mid-lateral section of the more or less ellipsoidal seminal vesicle, which may give rise to a narrow dorsal extension; long and narrow duct connecting seminal vesicle with small diaphragm; ejaculatory duct with a subterminal opening through the ventral surface of the penis papilla; asymmetrical oviducal openings, with the right oviduct opening into a section of the bursal canal that bends ventrally to communicate with the common atrium; the left oviduct opens into the bursal canal at the point where the latter meets the common atrium.

Etymology. The specific epithet is derived from Latin adjective *ancorarius*, of the anchor, and alludes to the penis papilla, which has a hunchback-shape, reminiscent of an anchor, more or less.

Description. Sexualized specimens measured 8.43–9.11 mm in length and 1.13–1.18 mm in width (n = 4;

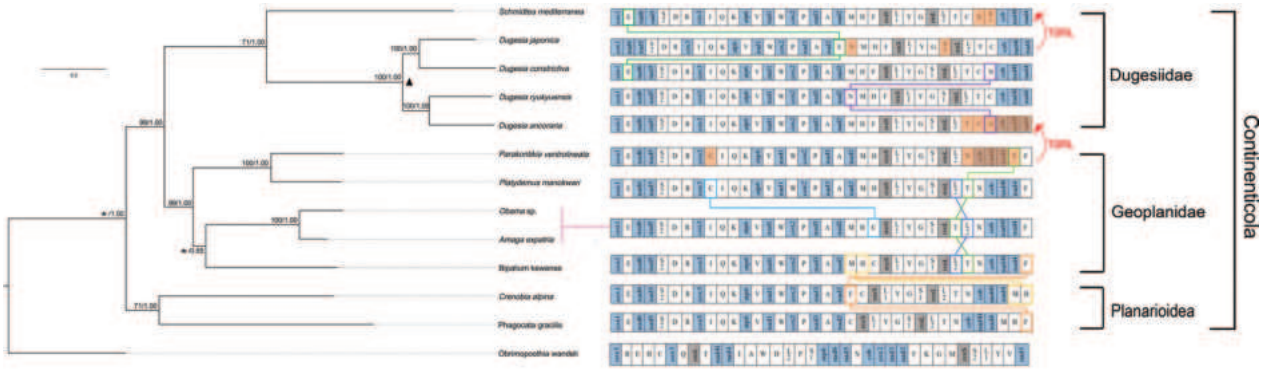

Figure 4. Possible mechanisms of mitochondrial gene rearrangement in Continenticola estimated using CREx, with reference to phylogenetic relationships. On the left-hand side, phylogenetic tree obtained from Maximum likelihood and Bayesian analysis of the concatenated dataset for the protein-coding and rRNA genes within mitochondrial genomes; numbers at nodes indicate support values (pp/bs); Asterisks (*) indicate that bootstrap is not applicable to these nodes because of different topologies of trees generated by BI and ML methods. Pink lines connect species that share the same gene order. On the right-hand side, changes of gene order in mitochondrial genomes in several species of triclad; protein-coding genes in blue, tRNA genes in white, rRNA genes in grey; lines with different colours indicate transpositions of different genes; red lines indicate tandem duplication random loss (TDRL) events between species, while the orange colour indicates where TDRL events occurred.

Fig. 5A, B). Head of low triangular shape with blunt auricles. At the level of the auricles there is a pair of black, bean-shaped eyes, located in pigment-free areas. The distance between the eyes and the lateral body margin is about 0.36–0.46 mm, while the size of the eyecups varies between 210–230 µm. Each eyecup contains numerous retinal cells.

The ground colour of the dorsal surface is brown, dotted with dark brown and white specks; ventral surface much paler than dorsal surface; the body margin is pale (Fig. 5A, B).

The cylindrical pharynx is positioned at about 1/2 of the body and measures about 1/5 of the total body length; the mouth opening is situated at the posterior end of the pharyngeal pocket. The musculature of the pharynx consists of an outer, subepithelial layer of circular muscle, followed by a layer of longitudinal muscle, while the inner musculature is composed of a thick, subepithelial layer of circular muscle, followed by 2–3 layers of longitudinal muscle. The gonopore is situated at about 1/5 of the length of the body, as measured from the posterior body margin (Fig. 5D).

The globular ovaries are located at 1/6 – 1/7 of the distance between the brain and the root of pharynx. From the ovaries, the nucleated oviducts run ventrally in a caudal direction and open separately and asymmetrically into the female reproductive apparatus. Posterior to the gonopore, the right oviduct turns antero-medially and then opens into a section of the bursal canal that bends ventrally to communicate with the common atrium. The left oviduct opens into the bursal canal at the point where the latter meets the common atrium. (Figs 6A, 9B).

A large sac-shaped copulatory bursa is situated immediately behind the pharyngeal pocket and occupies the entire dorso-ventral space; it is lined with a layer of vacuolated, nucleated cells (Figs 6B, 9B). From the bursa, the bursal canal runs in a caudal direction dorso-laterally to the male copulatory apparatus. At the level of the gonopore, the bursal canal curves rather sharply downwards, thus giving rise to a more or less vertically oriented section that opens through the dorsal wall of the common atrium (Figs 6C, 9B).

The bursal canal is lined by a nucleated, columnar glandular epithelium, which is underlain with a layer of longitudinal muscles, followed by 1–4 layers of circular muscles. Along the ventral coat of muscle, ectal reinforcement is present in the form of a single layer of longitudinal muscle running from about the opening of the canal into the common atrium to about 1/3 of the length of the bursal canal (Fig. 9B). Shell glands discharge their cyanophil secretion into the most ventral section of the vertically running portion of the bursal canal, with some glands even discharging into the common atrium (Figs 6B, C, 9B).

The large, near-globular testicular follicles are situated dorsally and extend posteriorly from a short distance behind the brain to well beyond the copulatory apparatus. The male atrium comprises most of the dorso-ventral space of the body (Figs 6A, 9A, B). The large and oval-shaped penis bulb is composed of intermingled longitudinal and circular muscle fibres. The penis papilla has a more or less oblique, postero-ventral orientation or even a vertical orientation, and has a striking shape (Figs 6A, 9A). The papilla is markedly asymmetrical as a result of the course of ejaculatory duct, which opens to the exterior through the postero-ventral wall of the penis papilla. Furthermore, near its root, the papilla has a dorsal bump, which gives it a hunchback appearance (Figs 6A, 9A). The degree of development of this dorsal bump differs between specimens. In the holotype it is highly developed (Fig. 6A), while in paratype PLA-0104 it is somewhat smaller, albeit still well-developed (Fig. 8A), but in paratype PLA-0102 the bump is practically absent (Fig. 7A).

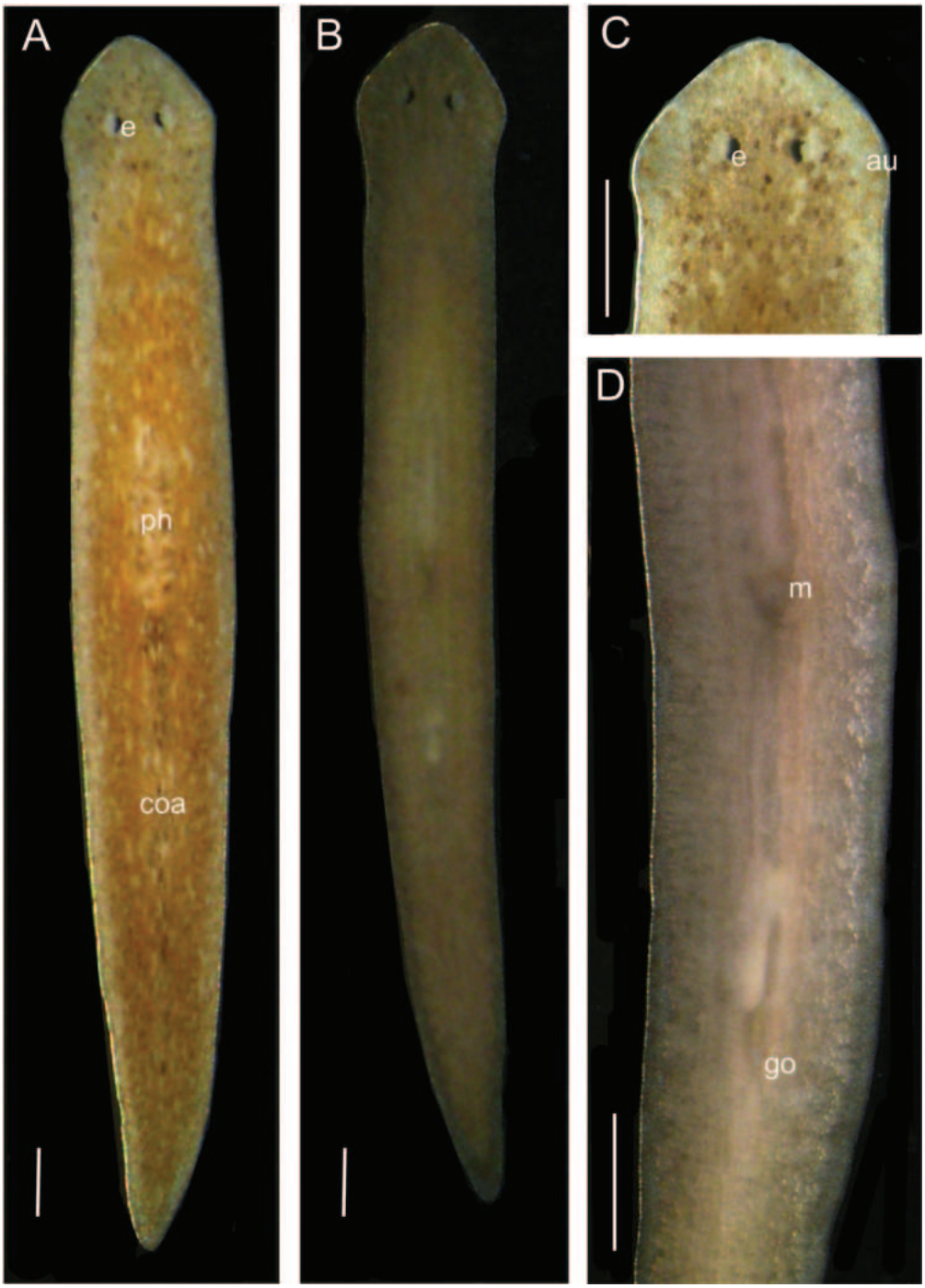

Figure 5. External morphology of *Dugesia ancoraria*. **A.** Living sexual animal in dorsal view; **B.** Living sexual animal in ventral view; **C.** Anterior end, dorsal view; **D.** Ventral view of rear end, showing pharynx, mouth and gonopore. Scale bars: 500 μm.

In addition, the asymmetrical appearance of the penis papilla is enhanced by the fact that the distal portion of the dorsal lip of the papilla gives rise to another bulge, which may be swollen or drawn-out to a greater or lesser extent. In paratype RMNH.VER.21525.1, it is a rather long-drawn bulge (Fig. 8A), whereas in the holotype and paratype PLA-0102 it is more rounded (Fig. 7A). The papilla is covered by a thin, nucleated epithelium, which is underlain with a well-developed, subepithelial layer of circular muscle, followed by a layer of longitudinal muscle at the ventral root.

The vasa deferentia have expanded to form spermiducal vesicles that are packed with sperm. At the level of the penis bulb, the ducts recurve, while decreasing in diameter, run postero-medially for some distance and, thereafter, recurve anteriad before opening separately into the mid-lateral portion of the seminal vesicle (Figs 6A, 9A, B). The vesicle has a more or less ellipsoidal shape, while its dorsal wall may form a narrow extension, which was present in all specimens examined, excepting paratype RMNH.VER.21525.1. The seminal vesicle is lined by a ciliated, nucleated epithelium. A long and narrow duct connects

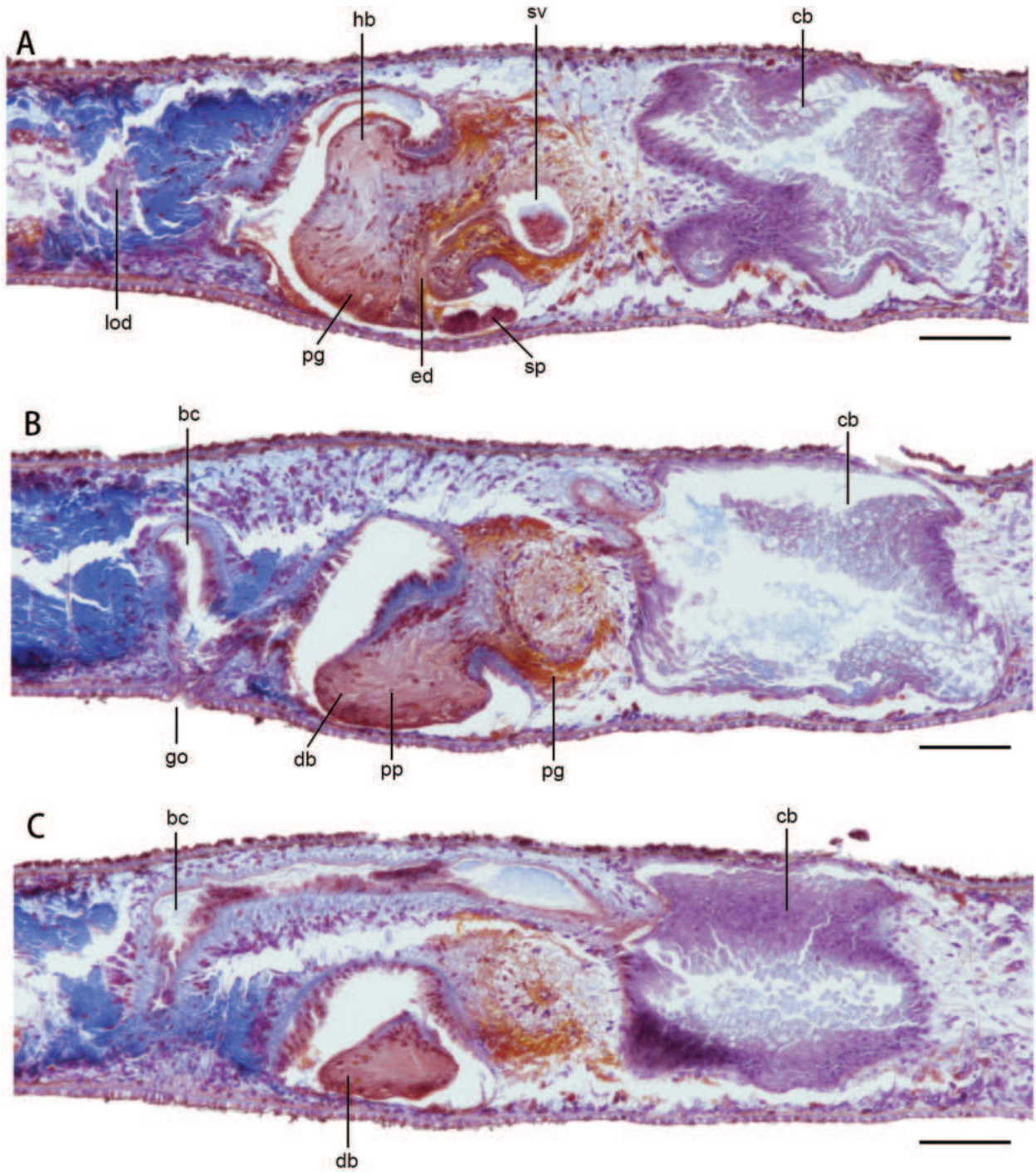

Figure 6. *Dugesia ancoraria*, holotype PLA-0101, sagittal sections, anterior to the right. **A.** Photomicrograph showing copulatory bursa, ejaculatory duct, penis papilla, and seminal vesicle; **B.** Photomicrograph showing copulatory bursa, bursal canal, and gonopore; **C.** Photomicrograph showing copulatory bursa, and bursal canal. Scale bars: 100 μm.

the seminal vesicle with the small diaphragm, which communicates with the ejaculatory duct. The diaphragm receives the abundant secretion of erythrophil penial glands. From the diaphragm, the ejaculatory duct curves strongly postero-ventrally to open subterminally through the ventral epithelium of the penis papilla, thus giving rise to a highly asymmetrical papilla with a large dorsal lip and a small ventral lip (Figs 6A, 9A). Particularly the blunt tip of the dorsal lip of the penis papilla is penetrated by the numerous openings of orange-staining glands.

The male atrium is lined by a nucleated epithelium. The dorsal part of the male atrium is surrounded by a layer of circular muscle, followed by 1–2 layers of longitudinal muscle, while a subepithelial layer of circular muscle, followed by a layer of longitudinal muscle constitutes the musculature on the ventral part of the atrium. The male atrium communicates with the common atrium via a broad opening. The common atrium is lined with a nucleated epithelium, which is underlain by 2–3 layers of circular muscle (Figs 6A, 9).

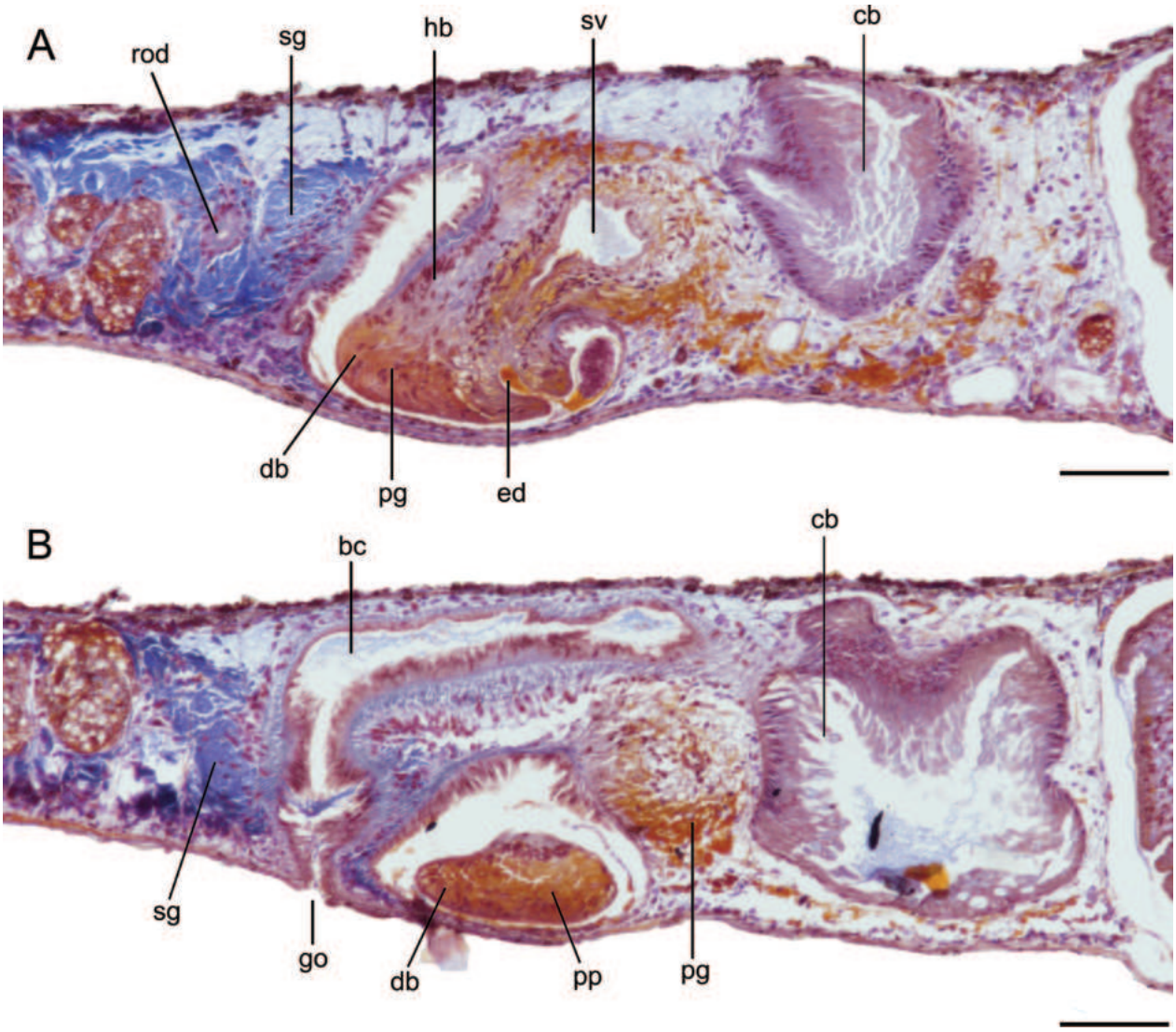

Figure 7. *Dugesia ancoraria*, paratype PLA-0102, sagittal sections. **A.** Photomicrograph showing ejaculatory duct, penis papilla, and seminal vesicle; **B.** Photomicrograph showing copulatory bursa, bursal canal, and gonopore. Scale bars: 100 μm.

Discussion

Molecular phylogeny and biogeography

In our phylogenetic tree (Fig. 2), the terminals for *D. ancoraria* grouped together, while they did not group with any other species of *Dugesia* included in our molecular analysis. Thus, the molecular analysis already suggested that *D. ancoraria* concerns a new species of *Dugesia*, which was supported by the morphological study (see below).

In the phylogenetic trees obtained from the concatenated dataset (Fig. 2), the sister-group relationship between *D. ancoraria* on the one hand and *D. notogaea* and *D. bengalensis* on the other hand is consistent and is supported by high bootstrap values, strongly suggesting that these three species form a monophyletic group. It is noteworthy that *D. ancoraria* from southern China, shares only a distant relationship to other *Dugesia* species from China, including *D. constrictiva*, *D. verrucula*, *D. majuscula*, *D. circumcisa*, *D. semiglobosa*, *D. umbonata*, *D. gemmulata* and *D. tumida*, but is most closely related to *D. notogaea* from Australia and *D. bengalensis* from India. The clade comprising *D. ancoraria*, *D. notogaea* and *D. bengalensis* shares a sister-group relationship with *D. adunca*, then is sister to a small clade comprising *D. ryukyuensis* from Japan and *D. batuensis* from peninsular Malaysia, and then further clusters with *D. deharvengi*, which is basically in agreement with the results of Chen et al. (2022). However, according to Liu et al. (2022), *D. deharvengi* shares a sister-group relationship with *D. notogaea* first, and then clusters with a group comprising *D. ryukyuensis* and *D. batuensis*, which could be due to the absence in the species phylogeny of the COI sequence of *D. bengalensis*. Actually, in the phylogenetic tree generated solely on COI sequences, *D. adunca* shared a sister-group relationship with *D. deharvengi*, albeit with low support, while *D. ryukyuensis* and *D. batuensis* clustered with a clade consisting of *D. majuscula*, *D. verrucula*, *D. constrictiva* and *D. tumida* with very low support (data not shown here), instead of clustering with *D. notogaea* and *D. bengalensis*,

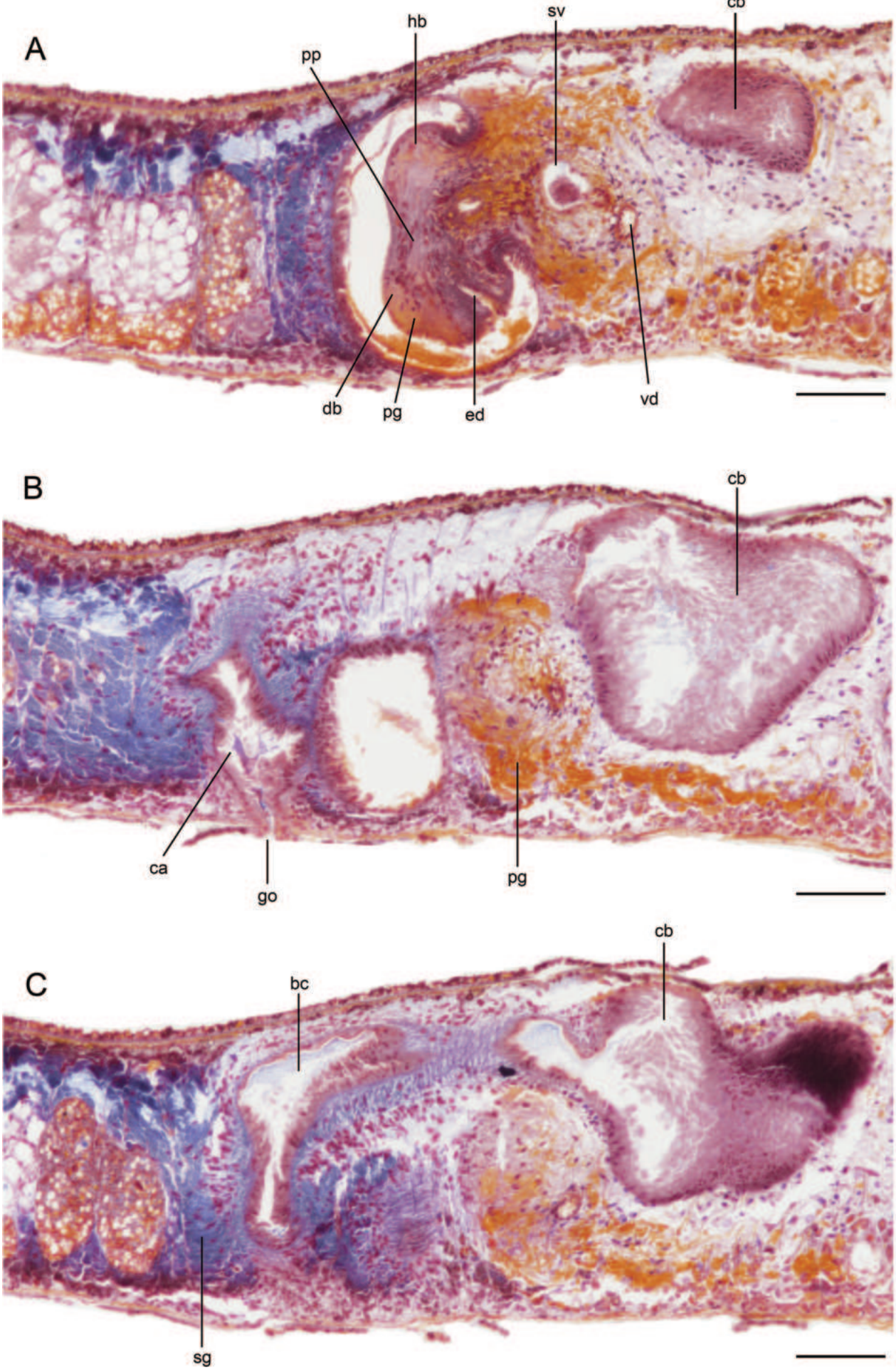

Figure 8. *Dugesia ancoraria*, paratype RMNH.VER.21525.1, sagittal sections. **A.** Photomicrograph showing ejaculatory duct, penis papilla, and seminal vesicle; **B.** Photomicrograph showing copulatory bursa, common atrium, and gonopore; **C.** Photomicrograph showing copulatory bursa, and bursal canal. Scale bars: 100 µm.

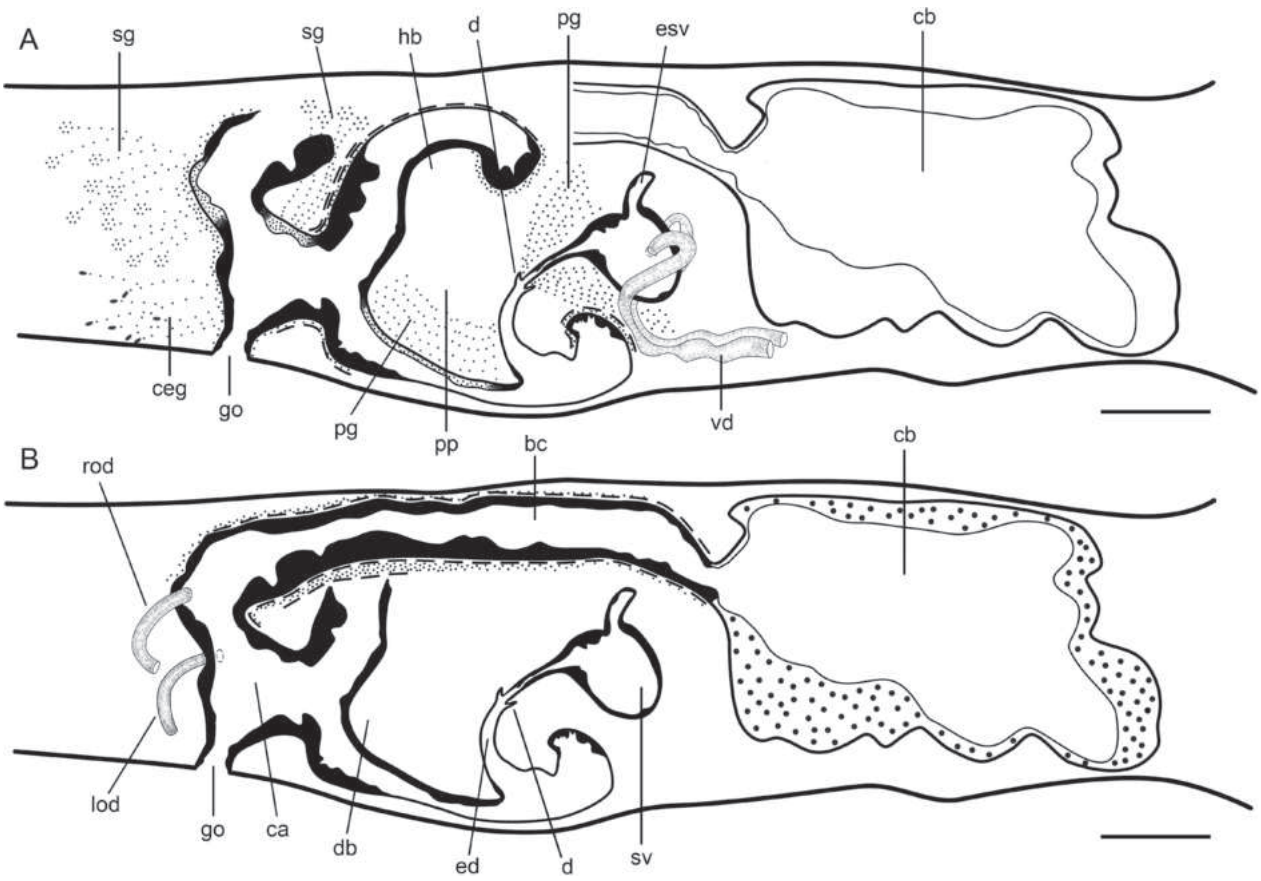

Figure 9. *Dugesia ancoraria*, Sagittal reconstruction of the copulatory apparatus of the holotype. **A.** Male copulatory apparatus; **B.** Female copulatory apparatus. Scale bars: 100 μm.

as in concatenation-based analyses. Furthermore, since different genes may exhibit highly variable rates of evolution, phylogenies inferred from single genes, with only limited evolutionary information, are often inconsistent. Altogether, our results suggested that concatenation-based analyses resulted in more resolved phylogenetic trees.

With respect to the geographical distribution within China of other species of *Dugesia*, in relation to the distribution of *D. ancoraria*, the following should be noted. *Dugesia japonica* has a wide distribution, as it has been reported from the eastern, southern and northern regions of China, while the remaining 11 species are found only in southern China. Among these species, *D. semiglobosa* and *D. majuscula* were documented in Hainan province, *D. circumcisa* and *D. adunca* in Guangxi province, with these two provinces being relatively close to the locality of *D. ancoraria* in Guangdong. *Dugesia tumida* and *D. sinensis* occur also in Guangdong Province, while they share only a very distant relationship with the new species *D. ancoraria*. Other species, like *D. umbonata*, were found in Jiangsu province and *D. gemmulata* in Guizhou. Although these two species are geographically far distant from each other, they share a close relationship.

The close relationship between Chinese *D. ancoraria* and Australian *D. notogaea*, with the latter being the sister-species of Malaysian *D. bengalensis*, is interesting from a historical biogeographic perspective. This pattern of relationships basically agrees with that uncovered by Solà et al. (2022), in which *D. notogaea* also fell into an Asian clade, including specimens from China, Malaysia, Thailand, Japan, and Indonesia. These authors surmised that this pointed to anthropochore dispersal of *Dugesia* from Asia to Australia, as they considered Wallace's Line to indicate an unsurmountable biological barrier for natural arrival of the genus in Australia (see also Ali and Heaney 2022). Excluding unlikely jump dispersal, earlier hypotheses that *Dugesia* naturally spread from Southeast Asia to Australia (Sluys et al. 1998) foundered on the paleogeographical evolution of the Indo-Australian archipelago. According to paleogeographical reconstructions, the river systems of Asia on the one hand and those of Australia/New Guinea on the other hand have never been in contact, not even during the Pleistocene when the sea level was much lower (Sluys et al. 2007). Nevertheless, the distribution of *Dugesia* is repeated by the equally remarkable distribution in Asia and Australasia of portions of the camaenid land snails (Scott 1997; Cuezzo 2003), while the earliest nautiloids from Australia share major characteristics with Asiatic species (Stait and Burrett 1987). Evidently, similarity in these distributional patterns does not imply that they originated during the same period in geological history. Future studies on *Dugesia* from China and the Indo-Australian archipelago would be very interesting, as these may shed light on the biogeographic history of the region.

Annotation of trnT

In our mitogenome analysis, trnT was the only tRNA that could not be automatically annotated by MITOS. However, through translating nucleotides of 12 PCGs to amino acid with Expacy (http://web.expasy.org/translate/), 63 sites of threonine, which is coded by ACN, were found. These results thus support the existence of trnT, which is required for the reading of the triplet of the genetic code (ACN). Therefore, we annotated trnT manually, based on homology comparisons with other species in the family Dugesiidae. Specifically, we aligned the complete mitogenome of *D. ancoraria* with three species belonging to family Dugesiidae, namely *D. japonica*, *D. ryukyuensis* and *D. constrictiva* and found a homologous sequence (60 bp) among these five species, which is particularly conserved at 5' end (AGAA) and 3' end (TTCTT). In addition, the position of trnT of all reported species belonging to Dugesiidae is very conserved and is situated between trnL2 and trnC. Interestingly, the putative trnT in *D. ancoraria* is also located between trnL2 and trnC, providing another line of evidence in support of the annotation. Furthermore, we predicted the secondary structure of trnT manually and presented this through RNAalifold WebServer (http://rna.tbi.univie.ac.at/cgi-bin/RNAWebSuite/RNAfold.cgi) and were surprised to find that the predicted result is not a typical cloverleaf structure with an absence of the DHU stem. By comparing the free energy between the two predicted structures, we found that the free energy with DHU stem (-1.20 kcal/mol) is higher than the one without DHU stem (-4.50 kcal/mol). The absence of the DHU stem in trnT also occurred in several other species of Tricladida, such as *Dugesia japonica*, *D. ryukyuensis*, *Crenobia alpina*, *Obama* sp. and *Schmidtea mediterranea.* (Sakai and Sakaizumi 2012; Solà et al. 2015; Ross et al. 2016). To the best of our knowledge, *P. gracilis* is the only Tricladida species reported to possess trnT with a DHU loop. Therefore, absence of the DHU stem in trnT could be a common phenomenon among species of the Tricladida.

Mitochondrial gene order of suborder Continenticola

In addition, some common features can be discovered in the mitochondrial gene order of the investigated species. Among the five species of Geoplanidae, locations of trnT are variable, in that transpositions of trnT occur in each of two adjacent species in the mitogenome tree, from *B. kewense* to *P. ventrolineata*. Besides, trnF is located at 3' downstream of nad4, with the only exception being *Crenobia alpina*. The gene rearrangement of the maricolan *Obrimoposthia wandeli* differs considerably from species belonging to the suborder Continenticola. Therefore, transformation of gene order in *O. wandeli* to species of the Continenticola may require multiple rearrangements, including reversals, transpositions, and TDRL. Similarly, several TDRL events are required to go from the Geoplanoidea gene order to those of the Dugesiidae species. It is also noteworthy that two species (*D. ancoraria* and *D. constrictiva*) with identical mitochondrial gene order occur in two separate clades. Since gene rearrangements appear to be rare events that may not arise independently in separate lineages (Boore 1999), it is likely that the ancestor of *Dugesia* (indicated by a triangle in Fig. 4) may have had a pattern identical to that of *D. ancoraria* and *D. constrictiva*, implying that in the course of evolutionary history only a transposition of trnE occurred in *D. japonica* as well as transposition of trnN in *D. ryukyuensis*. However, the small number of species for which mitogenomic datasets are currently available, make it presently impossible to test this hypothesis.

Morphological comparisons

A highly asymmetrical penis papilla with both a proximal as well as distal dorsal bumps is the most characteristic feature of *Dugesia ancoraria*. Similar bumps are known only from *D. gibberosa* Stocchino & Sluys, 2017. However, in *D. gibberosa* the penis papilla has a different, ventro-caudal orientation, while its ejaculatory duct opens terminally at the tip of the papilla, in contrast to the subterminal opening in *D. ancoraria*. Moreover, in *D. gibberosa* the bursal canal is surrounded by a very thick layer of circular muscle, while its ectal reinforcement extends more than halfway along the bursal canal. In contrast, the bursal canal musculature in *D. ancoraria* is thinner and the ectal reinforcement weakly developed. Furthermore, *D. ancoraria* and *D. gibberosa* are far removed from each other in the phylogenetic tree (Fig. 2), thus corroborating their separate taxonomic status.

Our molecular analyses, particularly the concatenated dataset, showed that *D. ancoraria* shares a sister-group relationship with Australian *D. notogaea* and Malaysian *D. bengalensis*. Morphologically, all three species have an asymmetrical penis papilla, with the dorsal lip being thicker than ventral lip, and a duct between seminal vesicle and ejaculatory duct. In addition, *D. ancoraria* and *D. notogaea* share the condition in which the oviducts open asymmetrically into the bursal canal. However, there are also clear differences between these three species. For example, in *D. bengalensis* and *D. ancoraria*, the ejaculatory duct has a subterminal opening at the tip of the penis papilla, whereas *D. notogaea* exhibits a terminal opening. In *D. bengalensis* and *D. notogaea*, the vasa deferentia open through the postero-lateral roof of the seminal vesicle, whereas in *D. ancoraria* the ducts open into the mid-lateral portion of the vesicle.

Although *D. gibberosa* is the only other species with two clear dorsal bumps on the penis papilla, there are a number of *Dugesia* species that deserve some comparison with *D. ancoraria*, viz., *D. astrocheta* Marcus, 1958, *D. austroasiatica* Kawakatsu, 1985, and *D. tamilensis* Kawakatsu, 1980. *Dugesia astrocheta* has a clear, proximal hunchback bump on its very asymmetrical penis

papilla, while there is also some indication of a distal bump or bulge (cf. Sluys 2007, fig. 4A). But even when there is indeed such a distal bulge, the species differs in other details from *D. ancoraria*. For example, in *D. ancoraria* there is a relatively long duct interposed between the seminal vesicle and the diaphragm, whereas this duct is virtually absent in *D. astrocheta*. In *D. austroasiatica* there seems to be a rather flexible distal bulge on the dorsal lip of the penis papilla that receives the secretion of glands (cf. Kawakatsu et al. 1986, fig. 3). Apart from the absence of the hunchback, proximal penial bump in *D. austroasiatica*, there are also other differences which signal that it differs from *D. ancoraria*. For example, in the latter the oviducts open asymmetrically into the bursal canal, whereas *D. austroasiatica* has symmetrical oviducal openings. The penis papilla of *D. tamilensis* resembles that of *D. ancoraria* in that it is highly asymmetrical, with the ejaculatory duct opening also at the postero-ventral wall of the papilla, while its dorsal lip is provided also with a distal bulge. However, in this species the oviducts also open symmetrically into the bursal canal, in contrast to the asymmetrical oviducal openings in *D. ancoraria*.

Acknowledgements

This study was supported by grants from Cultivation of Guangdong College Students' Scientific and Technological Innovation ("Climbing Program" Special Funds; grant no. pdjh2023b0449), China Undergraduate Training Program for Innovation and Entrepreneurship (grant no. S202210590072) and the Shenzhen University Innovation Development Fund (grant no. 2021258), as well as grants from the Scientific and Technical Innovation Council of Shenzhen Government (grant nos. jcyj20210324093412035 and kcxfz20201221173404012) and Special Program of Key Sectors in Guangdong Universities (grant no. 2022ZDZX4040). We are grateful to Meng-yu Xia for assistance with sample collection.

References

Ali JR, Heaney LR (2022) Alfred R. Wallace's enduring influence on biogeographical studies of the Indo-Australian archipelago. Journal of Biogeography 50(1): 32–40. https://doi.org/10.1111/jbi.14470

Allio R, Schomaker-Bastos A, Romiguier J, Prosdocimi F, Nabholz B, Delsuc F (2020) MitoFinder: Efficient automated large-scale extraction of mitogenomic data in target enrichment phylogenomics. Molecular Ecology Resources 20(4): 892–905. https://doi.org/10.1111/1755-0998.13160

Bernt M, Merkle D, Ramsch K, Fritzsch G, Perseke M, Bernhard D, Schlegel M, Stadler PF, Middendorf M (2007) CREx. inferring genomic rearrangements based on common intervals. Bioinformatics (Oxford, England) 23(21): 2957–2958. https://doi.org/10.1093/bioinformatics/btm468

Bernt M, Donath A, Juhling F, Externbrink F, Florentz C, Fritzsch G, Putz J, Middendorf M, Stadler PF (2013) MITOS: Improved de novo metazoan mitochondrial genome annotation. Molecular Phylogenetics and Evolution 69(2): 313–319. https://doi.org/10.1016/j.ympev.2012.08.023

Boore JL (1999) Animal mitochondrial genomes. Nucleic Acids Research 27(8): 1767–1780. https://doi.org/10.1093/nar/27.8.1767

Chen GW, Wang L, Wu F, Sun XJ, Dong ZM, Sluys R, Yu F, Yu-wen YQ, Liu DZ (2022) Two new species of *Dugesia* (Platyhelminthes, Tricladida, Dugesiidae) from the subtropical monsoon region in Southern China, with a discussion on reproductive modalities. BMC Zoology 7(25): 1–20. https://doi.org/10.1186/s40850-022-00127-8

Cuezzo MG (2003) Phylogenetic analysis of the *Camaenidae* (Mollusca: Stylommatophora) with special emphasis on the American taxa. Zoological Journal of the Linnean Society 138(4): 449–476. https://doi.org/10.1046/j.1096-3642.2003.00061.x

Huang JJ, Liao YY, Li WX, Li JY, Wang AT, Zhang Y (2022) The complete mitochondrial genome of a marine triclad *Miroplana shenzhensis* (Platyhelminthes, Tricladida, Maricola). Mitochondrial DNA. Part B, Resources 7(6): 927–929. https://doi.org/10.1080/23802359.2022.2079102

Katoh K, Rozewicki J, Yamada KD (2017) Mafft online service: Multiple sequence alignment, interactive sequence choice and visualization. Briefings in Bioinformatics 20(4): 1160–1166. https://doi.org/10.1093/bib/bbx108

Kawakatsu M, Takai M, Oki I, Tamura S, Aoyagi M (1986) A note on an introduced species of freshwater planarian, *Dugesia austroasiatica* Kawakatsu, 1985, collected from culture ponds of *Tirapia mossambica* in Saga City, Kyûshû, Japan (Turbellaria, Tricladida, Paludicola). Bulletin of Fuji Women's College no. 24, ser. II: 87–94.

Lanfear R, Frandsen PB, Wright AM, Senfeld T, Calcott B (2017) PartitionFinder 2: New methods for selecting partitioned models of evolution for molecular and morphological phylogenetic analyses. Molecular Biology and Evolution 34(3): 772–773. https://doi.org/10.1093/molbev/msw260

Li WX, Sluys R, Vila-Farré M, Chen JJ, Yang Y, Li SF, Wang AT (2019) A new continent in the geographic distribution of the genus *Oregoniplana* (Platyhelminthes: Tricladida: Maricola), its rediscovery in South Africa and its molecular phylogenetic position. Zoological Journal of the Linnean Society 187(1): 82–99. https://doi.org/10.1093/zoolinnean/zlz013

Liu Y, Song XY, Sun ZY, Li WX, Sluys R, Li SF, Wang AT (2022) Addition to the known diversity of Chinese freshwater planarians: Integrative description of a new species of *Dugesia* Girard, 1850 (Platyhelminthes, Tricladida, Dugesiidae). Zoosystematics and Evolution 98(2): 233–243. https://doi.org/10.3897/zse.98.83184

Lowe TM, Chan PP (2016) tRNAscan-SE On-line: Search and Contextual Analysis of Transfer RNA Genes. Nucleic Acids Research 44(W1): W54–W57. https://doi.org/10.1093/nar/gkw413

Nguyen LT, Schmidt HA, Haeseler A, Minh BQ (2015) IQ-TREE: A fast and effective stochastic algorithm for estimating maximum-likelihood phylogenies. Molecular Biology and Evolution 32(1): 268–274. https://doi.org/10.1093/molbev/msu300

Rambaut A, Drummond AJ, Xie D, Baele G, Suchard MA (2018) Posterior summarisation in Bayesian phylogenetics using Tracer 1.7. Systematic Biology 67(5): 901–904. https://doi.org/10.1093/sysbio/syy032

Ranwez V, Douzery EJP, Cambon C, Chantret N, Delsuc F (2018) MACSE v2: Toolkit for the alignment of coding sequences accounting for frameshifts and stop codons. Molecular Biology and Evolution 35(10): 2582–2584. https://doi.org/10.1093/molbev/msy159

Ronquist F, Teslenko M, Van der Mark P, Ayres DL, Darling A, Höhna S, Larget B, Liu L, Suchard MA, Huelsenbeck JP (2012) MrBayes 3.2: Efficient Bayesian phylogenetic inference and model choice across a large model space. Systematic Biology 61(3): 539–542. https://doi.org/10.1093/sysbio/sys029

Rosa MT, Oliveira DS, Loreto ELS (2017) Characterization of the first mitochondrial genome of a catenulid flatworm: *Stenostomum leucops* (Platyhelminthes). Journal of Zoological Systematics and Evolutionary Research 55(2): 98–105. https://doi.org/10.1111/jzs.12164

Ross E, Blair D, Guerrero-Hernández C, Alvarado AS (2016) Comparative and transcriptome analyses uncover key aspects of coding and long noncoding RNAs in flatworm mitochondrial genomes. G3 Genes|Genomes|Genetics 6(5): 1191–1200. https://doi.org/10.1534/g3.116.028175

Sakai M, Sakaizumi M (2012) The complete mitochondrial genome of *Dugesia japonica* (Platyhelminthes; Order Tricladida). Zoological Science 29(10): 672–680. https://doi.org/10.2108/zsj.29.672

Scott B (1997) Biogeography of the *Helicoidea* (Mollusca: Gastropoda: Pulmonata): land snails with a Pangean distribution. Journal of Biogeography 24(4): 399–407. https://doi.org/10.1111/j.1365-2699.1997.00106.x

Sluys R (2007) Annotations on freshwater planarians (Platyhelminthes Tricladida Dugesiidae) from the Afrotropical Region. Tropical Zoology 20(2): 229–257.

Sluys R, Riutort M (2018) Planarian diversity and phylogeny. In: Rink JC (Ed.) Planarian Regeneration: Methods and Protocols. Methods in Molecular Biology, vol 1774, Humana Press, Springer Science+Business Media, New York, 1–56. https://doi.org/10.1007/978-1-4939-7802-1_1

Sluys R, Kawakatsu M, Winsor L (1998) The genus *Dugesia* in Australia, with its phylogenetic analysis and historical biogeography (Platyhelminthes, Tricladida, Dugesiidae). Zoologica Scripta 27(4): 273–289. https://doi.org/10.1111/j.1463-6409.1998.tb00461.x

Sluys R, Grant LJ, Blair D (2007) Freshwater planarians from artesian springs in Queensland, Australia (Platyhelminthes, Tricladida, Paludicola). Contributions to Zoology 76(1): 9–19. https://doi.org/10.1163/18759866-07601002

Solà E, Álvarez-Presas M, Frías-López C, Littlewood DTJ, Rozas J, Riutort M (2015) Evolutionary analysis of mitogenomes from parasitic and free-living flatworms. PLoS ONE 10(3): 1–20. https://doi.org/10.1371/journal.pone.0120081

Solà E, Leria L, Stocchino GA, Bagherzadeh R, Balke M, Daniels SR, Harrath AH, Khang TF, Krailas D, Kumar B, Li MH, Maghsoudlou A, Matsumoto M, Naser N, Oben B, Segev O, Thielicke M, Tong X, Zivanovic G, Riutort M (2022) Three dispersal routes out of Africa: The puzzling biogeographical history in freshwater planarians. Journal of Biogeography 49(7): 1219–1233. https://doi.org/10.1111/jbi.14371

Song XY, Li WX, Sluys R, Huang SX, Li SF, Wang AT (2020) A new species of *Dugesia* (Platyhelminthes, Tricladida, Dugesiidae) from China, with an account on the histochemical structure of its major nervous system. Zoosystematics and Evolution 96(2): 431–447. https://doi.org/10.3897/zse.96.52484

Stait B, Burrett C (1987) Biogeography of Australian and Southeast Asian Ordovician nautiloids. In: McKenzie GD (Ed.) Gondwana Six: Stratigraphy, Sedimentology and Paleontology. Washington DC: American Geophysical Union, 21–28. https://doi.org/10.1029/GM041p0021

Steenwyk JL, Buida TJ III, Li Y, Shen XX, Rokas A (2020) ClipKIT: A multiple sequence alignment trimming software for accurate phylogenomic inference. PLoS Biology 18(12): 1–17. https://doi.org/10.1371/journal.pbio.3001007

Talavera G, Castresana J (2007) Improvement of phylogenies after removing divergent and ambiguously aligned blocks from protein sequence alignments. Systematic Biology 56(4): 564–577. https://doi.org/10.1080/10635150701472164

Vaidya G, Lohman DJ, Meier R (2011) SequenceMatrix: Concatenation software for the fast assembly of multi-gene datasets with character set and codon information. Cladistics 27(2): 171–180. https://doi.org/10.1111/j.1096-0031.2010.00329.x

Xia X (2017) DAMBE6: New tools for microbial genomics, phylogenetics, and molecular evolution. The Journal of Heredity 108(4): 431–437. https://doi.org/10.1093/jhered/esx033

Xia X, Lemey P (2009) Assessing substitution saturation with DAMBE. In: Lemey P, Salemi M, Vandamme A (Eds) The phylogenetic handbook: a practical approach to phylogenetic analysis and hypothesis testing. Cambridge University Press, Cambridge, 615–630. https://doi.org/10.1017/CBO9780511819049.022

Xia X, Zheng X, Salemi M, Chen L, Wang Y (2003) An index of substitution saturation and its application. Molecular Phylogenetics and Evolution 26(1): 1–7. https://doi.org/10.1016/S1055-7903(02)00326-3

Yang Y, Li JY, Sluys R, Li WX, Li SF, Wang AT (2020) Unique mating behavior, and reproductive biology of a simultaneous hermaphroditic marine flatworm (Platyhelminthes, Tricladida, Maricola). Invertebrate Biology 139(1): 1–10. https://doi.org/10.1111/ivb.12282

Supplementary material 1

Bayesian inference phylogenetic tree topology

Authors: Ying Zhu, JiaJie Huang, Ronald Sluys, Yi Liu, Ting Sun, An-Tai Wang, Yu Zhang

Data type: docx

Explanation note: Bayesian inference phylogenetic tree topology inferred from the concatenated dataset (18S rDNA, IT-1, 28S DNA and COI). Numbers at nodes indicate support values (posterior probability). Scare bar: substitutions per site.

Link: https://doi.org/10.3897/zse.100.114016.suppl1

Zoosyst. Evol. 100 (1) 2024, 183–197 | DOI 10.3897/zse.100.113850

PENSOFT

MUSEUM FÜR NATURKUNDE BERLIN

A new species of *Zhangixalus* (Anura, Rhacophoridae) from Yunnan, China

Yuanqiang Pan[1,2], Mian Hou[3], Guohua Yu[1,2], Shuo Liu[4]

1 *Key Laboratory of Ecology of Rare and Endangered Species and Environmental Protection, Guangxi Normal University, Ministry of Education, Guilin 541004, China*

2 *Guangxi Key Laboratory of Rare and Endangered Animal Ecology, College of Life Science, Guangxi Normal University, Guilin 541004, China*

3 *College of Continuing (Online) Education, Sichuan Normal University, Chengdu 610068, Sichuan, China*

4 *Kunming Natural History Museum of Zoology, Kunming Institute of Zoology, Chinese Academy of Sciences, Kunming 650223, China*

https://zoobank.org/FB7E03EC-A2BB-4C9C-9896-20E53A2667DB

Corresponding authors: Guohua Yu (yugh2018@126.com); Shuo Liu (liushuo@mail.kiz.ac.cn)

Academic editor: Umilaela Arifin ♦ **Received** 8 October 2023 ♦ **Accepted** 30 January 2024 ♦ **Published** 20 Februarry 2024

Abstract

We described herein *Zhangixalus yunnanensis* **sp. nov.**, a new treefrog species from central and western Yunnan, China, which had previously been confused with *Z. nigropunctatus*, based on morphological and molecular evidence. Our phylogenetic analyses revealed that the new species is sister to the clade of *Z. nigropunctatus* and *Z. melanoleucus* with strong support (100% and 73% for BI and ML, respectively). Our morphological analysis suggested that *Z. yunnanensis* **sp. nov.** is distinctly different from all known congeners by the combination of the following morphological characters: black blotches on body flank and hind-limb, medium body size (SVL31.3–36.0 mm in males and 47.6–48.6 mm in females), head wider than long, iris yellowish-brown, dorsum uniformly green, vocal sac external, throat black, webbing greyish and fingers webbed one third and toes webbed half. Additionally, we revealed that the specimens ROM 38011 (Sa Pa, Vietnam) and VNMN 4099 (Son La, Vietnam) are neither *Z. dorsoviridis* nor *Z. nigropunctatus*, but probably represent one or two cryptic species of *Zhangixalus* pending further morphological and molecular data. Including the new species described herein, the genus *Zhangixalus* currently comprises 42 species, 30 of which are distributed in China with 11 species known from Yunnan. Amongst different zoogeographic regions in Yunnan, south-eastern Yunnan has the highest diversity of *Zhangixalus*, followed by western Yunnan and southern Yunnan. More studies are required to clarify the species diversity of this genus based on multiple lines of evidence (e.g. morphological and molecular data).

Key Words

cryptic species, treefrog, *Zhangixalus*, *Zhangixalus nigropunctatus*

Introduction

The treefrog genus *Zhangixalus* Li, Jiang, Ren & Jiang, 2019, recently removed from *Rhacophorus* Kuhl & Van Hasselt, 1822 *sensu lato* and recognised as a distinct genus, is characterised by medium-to-large body size, absence of dermal folds along limbs, absence of tarsal projections and usual green dorsal colouration (Jiang et al. 2019). The genus is distributed widely in South, East and Southeast Asia and currently contains 41 species (Frost 2023). In China, 29 species of *Zhangixalus* have been recorded to date, 10 of which are distributed in Yunnan: *Z. burmanus* (Andersson, 1939), *Z. dorsoviridis* (Bourret, 1937), *Z. duboisi* (Ohler, Marquis, Swan & Grosjean, 2000), *Z. feae* (Boulenger, 1893), *Z. franki* Ninh, Nguyen, Orlov, Nguyen & Ziegler, 2020, *Z. nigropunctatus* (Liu, Hu & Yang, 1962), *Z. omeimontis* (Stejneger, 1924), *Z. pachyproctus* Yu, Hui, Hou, Wu, Rao & Yang, 2019, *Z. puerensis* (He, 1999) and *Z. smaragdinus* (Blyth, 1852) (AmphibiaChina 2023).

Amongst others, the taxonomy of *Zhangixalus nigropunctatus* is confusing. This species was originally

described from western Guizhou, China (Weining and Shuicheng) by Liu et al. (1962) and, afterwards, was recorded from Yunnan (Longling, Longchuan, Yingjiang, Qiaojia, Pingbian, Jinping) (Yang 1991; Zhao and Yang 1997; Fei 1999; Fei et al. 2005, 2009, 2010; Yang and Rao 2008; Yu et al. 2008), Hunan, and Anhui (Fei 1999; Fei et al. 2005, 2009, 2010). Orlov et al. (2001) considered that *Z. nigropunctatus* is closely allied with *Z. dorsoviridis* based on the descriptions of the former and, therefore, noted that *Z. nigropunctatus* was possibly a synonym of *Z. dorsoviridis*. Yu et al. (2009) revealed that *Z. nigropunctatus* from Pingbian did not group together with topotypes of *Z. nigropunctatus*, indicating that misidentification may be involved within *Z. nigropunctatus*. Li et al. (2012a) revealed that both *Z. nigropunctatus* and *Z. dorsoviridis* did not form a monophyletic group. They found that *Z. nigropunctatus* from the type locality and Longling formed clade II with a sample of *Z. dorsoviridis* (ROM 38011) from Sa Pa, northern Vietnam and this clade was closely related to *Z. chenfui* (Liu, 1945). Meanwhile, *Z. nigropunctatus* from Jinping and Pingbian grouped into clade I with another sample of *Z. dorsoviridis* from Sa Pa (ROM 38015; see fig. 1 of Li et al. (2012a)). Based on morphological evidence, Li et al. (2012a) referred clade II to true *Z. nigropunctatus* and referred clade I to *Z. dorsoviridis*. This finding implies that previous records of *Z. nigropunctatus* from Jinping and Pingbian belong to *Z. dorsoviridis* (Zhang et al. 2011) and that *Z. nigropunctatus* is distributed in northern Vietnam. However, Mo et al. (2016) revealed that the sample ROM 38011 was distantly related to *Z. nigropunctatus* and it was sister to *Z. pinglongensis* (Mo, Chen, Liao & Zhou, 2016), indicating that the record of *Z. nigropunctatus* in northern Vietnam may be misidentified. In addition, Pan et al. (2017) revealed that *Z. nigropunctatus* recorded from the Dabie Mountains of Anhui Province represents an independent species and named it as *Z. zhoukaiyae* (Pan, Zhang & Zhang, 2017).

During our recent field surveys in central Yunnan, China, specimens of a treefrog species resembling *Zhangixalus nigropunctatus* were collected from Xinping County. Amphibian diversity in Yunnan is still poorly understood. In recent years, a number of new amphibian species have been reported from Yunnan, China (e.g. Gan et al. (2020); Du et al. (2022); Wang et al. (2022a); Tang et al. (2023a, 2023b)). Considering the taxonomic history of *Z. nigropunctatus* and the status of amphibian diversity in Yunnan, we sequenced our newly-collected treefrogs from Yunnan to confirm their identity. Our phylogenetic analyses recovered these specimens as a distinct lineage and are sister to the clade composed of *Z. nigropunctatus* and *Z. melanoleucus* Brakels, Nguyen, Pawangkhanant, Idiiatullina, Lorphengsy, Suwannapoom & Poyarkov, 2023. Furthermore, our morphological examination suggested that this lineage differs from *Z. nigropunctatus*, *Z. melanoleucus* and other members of *Zhangixalus* by a series of characters. Herein, we officially describe this lineage as a new species of *Zhangixalus*.

Materials and methods

Sampling

This study was carried out in accordance with the ethical guidelines issued by the Ethics Committee of Guangxi Normal University. Field surveys were conducted in July 2019 and April 2020 at Xinping County, Yunnan, China (Fig. 1) and a total of nine treefrog specimens were collected during the surveys. Specimens were photographed, euthanised, fixed and then stored in 75% ethanol. Liver tissues were preserved in 99% ethanol. Specimens were deposited at Guangxi Normal University (**GXNU**).

Phylogenetic analysis

Total genomic DNA was extracted from liver tissues stored in 99% ethanol. A fragment encoding mitochondrial 12S rRNA, $tRNA^{val}$ and 16S rRNA genes was amplified and sequenced using the primers and protocols of Yu et al. (2019). Seven samples were newly sequenced and all new sequences have been deposited in GenBank under Accession Nos. PP177446 and PP187265–PP187270 (Table 1). Additionally, 43 homologous sequences of other *Zhangixalus* species and outgroups were obtained from GenBank (Table 1). *Theloderma albopunctatum* (Liu & Hu, 1962), *Rhacophorus rhodopus* Liu & Hu, 1960 and *Leptomantis gauni* (Inger, 1966) were included in the data as outgroups.

Sequences were aligned using MUSCLE with default parameters in MEGA v.7.0 (Kumar et al. 2016). Uncorrected pairwise distances (using 16S rRNA sequences) between species were calculated in MEGA v.7.0. The best substitution model was selected using the corrected Akaike Information Criterion (AICc) in jModelTest v.2.1.10 (Darriba et al. 2012). Bayesian Inference was performed in MrBayes v.3.2.6 (Ronquist et al. 2012) under the selected substitution model (GTR + I + G). Two runs were performed simultaneously with four Markov chains starting from a random tree. The chains were run for 3,000,000 generations and sampled every 100 generations. The first 25% of the sampled tree was discarded as burn-in after the standard deviation of split frequencies of the two runs was less than 0.01. The remaining trees were then used to create a consensus tree and to estimate Bayesian posterior probabilities (BPPs). In addition, a Maximum Likelihood (ML) analysis was conducted in raxmlGUI v.2.0 (Edler et al. 2021) with 1000 rapid bootstrap replicates. The node was considered strongly supported with BPP $\geq$ 0.95 and bootstrap value $\geq$ 70 (Huelsenbeck and Hillis 1993; Leaché and Reeder 2002).

Morphology

Morphometric data were taken using electronic digital calipers to the nearest 0.1 mm. Morphological terminology

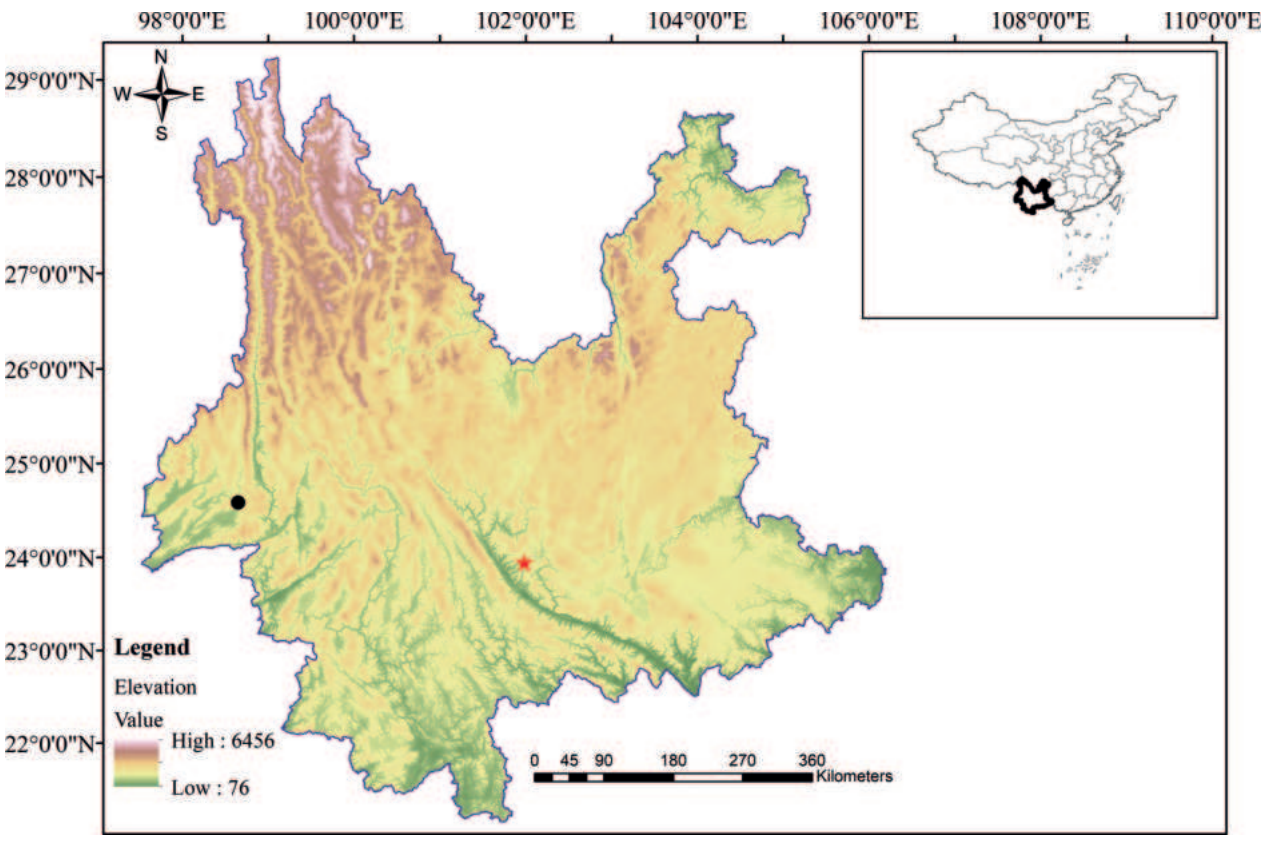

Figure 1. Known distribution sites of *Zhangixalus yunnanensis* sp. nov. in Yunnan, China. The red star represents the type locality of the new species. The map was generated using ArcMap v.10.2 (ESRI Inc.).

followed Yu et al. (2019). Measurements included: snout-vent length (SVL, from tip of snout to vent); head length (HL, from tip of snout to rear of jaws); head width (HW, width of head at its widest point); snout length (SL, from tip of snout to anterior corner of eye); internarial distance (IND, distance between nares); interorbital distance (IOD, minimum distance between upper eyelids); upper eyelid width (UEW, maximum width of upper eyelid); eye diameter (ED, diameter of exposed portion of eyeball); distance between nostril and eye (DNE, from nostril to anterior border of eye); tympanum diameter (TD, the greater of tympanum vertical and horizontal diameters); forearm and hand length (FHL, from elbow to tip of third finger); tibia length (TL, distance from knee to heel); foot length (FL, from proximal end of inner metatarsal tubercle to tip of fourth toe); and length of foot and tarsus (TFL, from tibiotarsal joint to tip of fourth toe). Webbing formula followed Myers and Duellman (1982).

Comparative morphological data of other *Zhangixalus* species were taken from their original descriptions or re-descriptions (Boulenger 1892; Stejneger 1907; Inger 1947; Liu et al. 1962; Lue et al. 1994, 1995; He 1999; Ohler et al. 2000; Harvey et al. 2002; Matsui and Panha 2006; Rao et al. 2006; Bordoloi et al. 2007; Chou et al. 2007; Fei et al. 2009, 2010; Zhang et al. 2011; Li et al. 2012b; Mo et al. 2016; Liu et al. 2017; Pan et al. 2017; Yu et al. 2019; Nguyen et al. 2020; Ninh et al. 2020; Brakels et al. 2023). Multivariate principal component analysis (PCA) was conducted in SPSS v.17.0 (SPSS Inc.), based on the correlation matrix of size-standardised measurements (all measurements divided by SVL) of adult males. Scatter plots of the scores of the first two factors of PCA were used to examine the differentiation between the new species and its closest relatives revealed by phylogenetic analyses (*Z. nigropunctatus* and *Z. melanoleucus*). Differences in quantitative characters of adult males between these three species were also evaluated with t-tests in SPSS. In these analyses, Levene's test was also performed for each character to test for equality of variances. Specimens of *Z. nigropunctatus* were collected from the type locality and data for *Z. melanoleucus* were retrieved from Brakels et al. (2023).

Results

Phylogenetic relationship

The obtained sequence alignment was 1971 bp. Phylogenetic analyses revealed that the specimens from Xinping, Yunnan form a distinct clade with two individuals previously identified as *Z. nigropunctatus* (KIZ Rao3494 and KIZ Rao3496; Li et al. (2012a)) from Longling, Yunnan. This clade was recovered as sister to the clade consisting of *Z. nigropunctatus* from the type locality and *Z. melanoleucus* with strong support (Fig. 2). The genetic distances between the novel lineage and other *Zhangixalus* species ranged from 4.8% to 13.9% in 16S rRNA sequences and the distances

Table 1. Species used for phylogenetic analyses in this study (*Z.* = *Zhangixalus*).

Species	Voucher No.	Locality	Accession No.
Theloderma albopunctatum	ROM 30246	Vietnam	AF458148
Rhacophorus rhodopus	SCUM 060692L	Mengyang, Yunnan, China	EU215531
Leptomantis gauni	FMNH 273928	Sarawak, Malaysia	JX219456
Zhangixalus dulitensis	BORNEENSIS09087	Borneo, Malaysia	AB847123
Z. pachyproctus	KIZ 090148	Puer, Yunnan, China	MN613222
Z. smaragdinus	KIZ 20160298	Yingjiang, Yunnan, China	MN613219
Z. dennysi	ROM 30249	Vietnam	AF458139
Z. feae	SCUM 050642W	Hekou, Yunnan, China	EU215544
Z. chenfui	SCUM 060404L	Mt. Omei, Sichuan, China	EU215534
Z. jodiae	VNMN 07122	Vietnam	LC545595
Zhangixalus sp.	ROM 38011	Sa Pa, Lao Cai, Vietnam	JX219427
	VNMN 4099	Son La, Vietnam	LC010577
Z. dorsoviridis	ROM 38015	Sa Pa, Lao Cai, Vietnam	JX219423
	Rao060821200	Jinping, Yunnan, China	JX219424
	YN080446	Pingbian, Yunnan, China	JX219425
	Rao060821199	Pingbian, Yunnan, China	JX219426
	KIZ 060821287	Jinping, Yunnan, China	EF564563
Z. yaoshanensis	NHMG150408	Jinxiu, Guangxi, China	MG322122
Z. pinglongensis	NHMG201002011	Shiwandashan, Guangxi, China	KU170684
Z. nigropunctatus	KIZ07061001	Weining, Guizhou, China	EU924623
	GZ070658	Weining, Guizhou, China	JX219430
	SCUM 070657L	Weining, Guizhou, China	EU215533
	GXNU YU000361	Weining, Guizhou, China	PP187265
	GXNU YU000362	Weining, Guizhou, China	PP187266
	GXNU YU000363	Weining, Guizhou, China	PP187267
Z. yunnanensis sp. nov.	GXNU YU20160340	Xinping, Yunnan, China	PP187268
	GXNU YU20160268	Xinping, Yunnan, China	PP187269
	GXNU YU20160267	Xinping, Yunnan, China	PP187270
	Rao3494	Longling, Yunnan, China	JX219429
	Rao3496	Longling, Yunnan, China	JX219428
Z. moltrechti	SCUM 061106L	Lianhuachi, Taiwan, China	EU215543
Z. schlegelii	-	Hiroshima, Japan	AB202078
Z. arboreus	TTU-R-11748	Japan	AF458142
Z. puerensis	SCUM 060649L	Puer, Yunnan, China	EU215542
Z. dugritei	SCUM 051001L	Baoxing, Sichuan, China	EU215541
Z. hui	Li01	Zhaojue, Sichuan, China	JN688878
Z. hongchibaensis	CIB 097687	Wuxi, Chongqing, China	JN688883
Z. hungfuensis	SCUM 060425L	Wenchuan, Sichuan, China	EU215538
Z. minimus	KIZ 061214YP	Mt. Dayao, Guangxi, China	EU215539
Z. burmanus	SCUM 060614L	Mt. Gaoligong, Yunnan, China	EU215537
Z. franki	VNMN 011687	Ha Giang, Vietnam	LC548746
Z. duboisi	SCUM 061104L	Pingbian, Yunnan, China	EU215536
Z. omeimontis	SCUM 0606137L	Pengxian, Sichuan, China	EU215535
Z. zhoukaiyae	AHU-RhaDB-120428	Jinzhai, Anhui, China	KU601502
	HM05293	Anhui, China	PP177446
Z. lishuiensis	YPX47792	Lishui, Zhejiang, China	KY653720
Z. melanoleucus	BEI 01010	Phou Samsoum Mt., Xiengkhoang, Laos	OQ305233
	ZMMU A-7781	Phou Samsoum Mt., Xiengkhoang, Laos	OQ305234
	BEI 01011	Phou Samsoum Mt., Xiengkhoang, Laos	OQ305235
	AUP 02507	Phou Samsoum Mt., Xiengkhoang, Laos	OQ305236

between the novel lineage, *Z. nigropunctatus* and *Z. melanoleucus* ranged from 5.1%–5.5% (Suppl. material 1).

Additionally, KIZ 060821287 and ROM 38011, two samples previously identified as *Z. nigropunctatus* by Yu et al. (2008) and Li et al. (2012a), respectively, were not grouped together with topotypes of *Z. nigropunctatus*. KIZ 060821287 was nested within the clade of *Z. dorsoviridis* from the type locality (Sa Pa, Lao Cai, Vietnam) and Yunnan and this clade was sister to the clade of *Z. lishuiensis* and *Z. zhoukaiyae*. ROM 38011 was sister to the lineage of nominal *Z. dorsoviridis* from Son La, Vietnam (VNMN 4099) and the two together were sister to the clade of *Z. yaoshanensis* (Liu & Hu, 1962) and *Z. pinglongensis* with strong support (98% for BI and 83% for ML; Fig. 2).

Morphometric analysis

Morphometric data are summarised in Table 2. Three measurements (FHL, TFL and FL) were not included in PCA analysis because they were not available for *Z. melanoleucus*. We retained the first two principal components that accounted for 66.99% of the total variance (Table 3). Loadings for PC1, which accounted for 45.21% of the

Table 2. Measurements of *Zhangixalus yunnanensis* sp. nov. (1–9), *Z. nigropunctatus* (10–17) and *Z. melanoleucus* (18–21). Specimens of *Z. nigropunctatus* were collected from the type locality (Weining, Guizhou) and data of *Z. melanoleucus* were obtained from Brakels et al. (2023).

ID	Voucher no.	Sex	SVL	HL	HW	SL	IND	IOD	UEW	ED	TD	DNE	FHL	TL	TFL	FL
1	GXNU YU20160267	M	31.3	9.7	11.4	4.9	4.0	4.0	2.8	3.5	1.9	2.2	17.3	13.3	21.8	14.9
2	GXNU YU20160268	M	34.0	11.1	12.6	5.3	4.0	4.0	3.2	4.0	2.1	2.2	16.9	13.0	21.6	14.8
3	GXNU YU20160269	M	35.4	11.5	12.5	5.5	4.1	4.1	3.4	4.1	2.1	2.2	18.7	14.5	23.2	15.7
4	GXNU YU20160335	F	48.6	15.1	18.0	7.2	5.6	5.6	4.2	4.9	2.9	3.0	25.5	20.0	32.5	22.5
5	GXNU YU20160336	M	35.3	11.2	13.6	5.4	4.3	4.3	3.5	4.3	2.3	2.2	18.3	14.3	23.5	15.5
6	GXNU YU20160337	M	35.6	11.6	12.9	5.3	4.2	4.2	3.2	4.3	2.2	2.1	18.3	13.9	22.4	15.1
7	GXNU YU20160338	M	34.4	11.3	12.9	5.3	4.3	4.5	3.3	4.1	2.2	2.3	18.1	14.9	22.9	15.6
8	GXNU YU20160340	M	36.0	11.8	13.9	5.5	4.3	4.3	3.6	4.3	2.3	2.2	18.5	14.3	23.5	16.2
9	GXNU YU20160355	F	47.6	14.4	17.2	6.8	5.8	5.7	4.1	5.0	2.9	2.9	25.5	20.5	33.2	23.3
10	KIZ25362	F	39.4	13.2	13.7	5.9	4.2	5.0	3.1	4.1	2.7	2.8	22.1	17.1	27.7	19.0
11	KIZ25367	F	43.7	13.0	13.8	6.1	4.2	4.8	3.0	4.3	2.8	2.8	22.7	17.1	27.5	20.0
12	KIZ25369	M	31.7	11.2	11.4	4.8	3.2	3.7	2.4	3.7	2.2	2.3	16.4	12.8	20.6	14.7
13	KIZ25370	M	33.6	11.5	12.0	5.1	3.4	3.9	2.7	3.9	2.3	2.3	17.4	12.9	21.4	15.8
14	KIZ25372	M	34.8	11.7	12.5	5.1	3.7	4.1	2.6	4.0	2.4	2.4	17.1	13.5	21.6	15.6
15	KIZ25373	M	34.1	11.9	12.1	4.9	3.7	4.0	2.7	3.9	2.5	2.3	18.6	13.4	21.9	15.2
16	KIZ25374	M	34.7	11.7	11.8	5.3	3.3	3.8	2.9	3.6	2.3	2.5	16.8	13.3	21.1	15.4
17	KIZ25375	M	33.2	11.8	11.3	5.1	3.4	4.0	2.7	3.7	2.2	2.2	16.5	11.9	20.4	14.3
18	BEI 01010	M	35.0	13.6	13.3	6.1	4.3	4.7	3.2	4.6	2.3	2.4	-	14.7	-	-
19	BEI 01011	M	34.4	12.6	12.2	5.8	4.2	4.1	3.0	4.2	1.9	2.0	-	14.0	-	-
20	ZMMU A-7781	M	36.3	13.3	13.4	6.1	4.4	4.8	3.1	4.7	2.2	2.6	-	14.3	-	-
21	AUP 02507	M	34.4	12.0	12.0	5.4	4.2	4.2	3.1	4.1	1.9	2.4	-	13.8	-	-

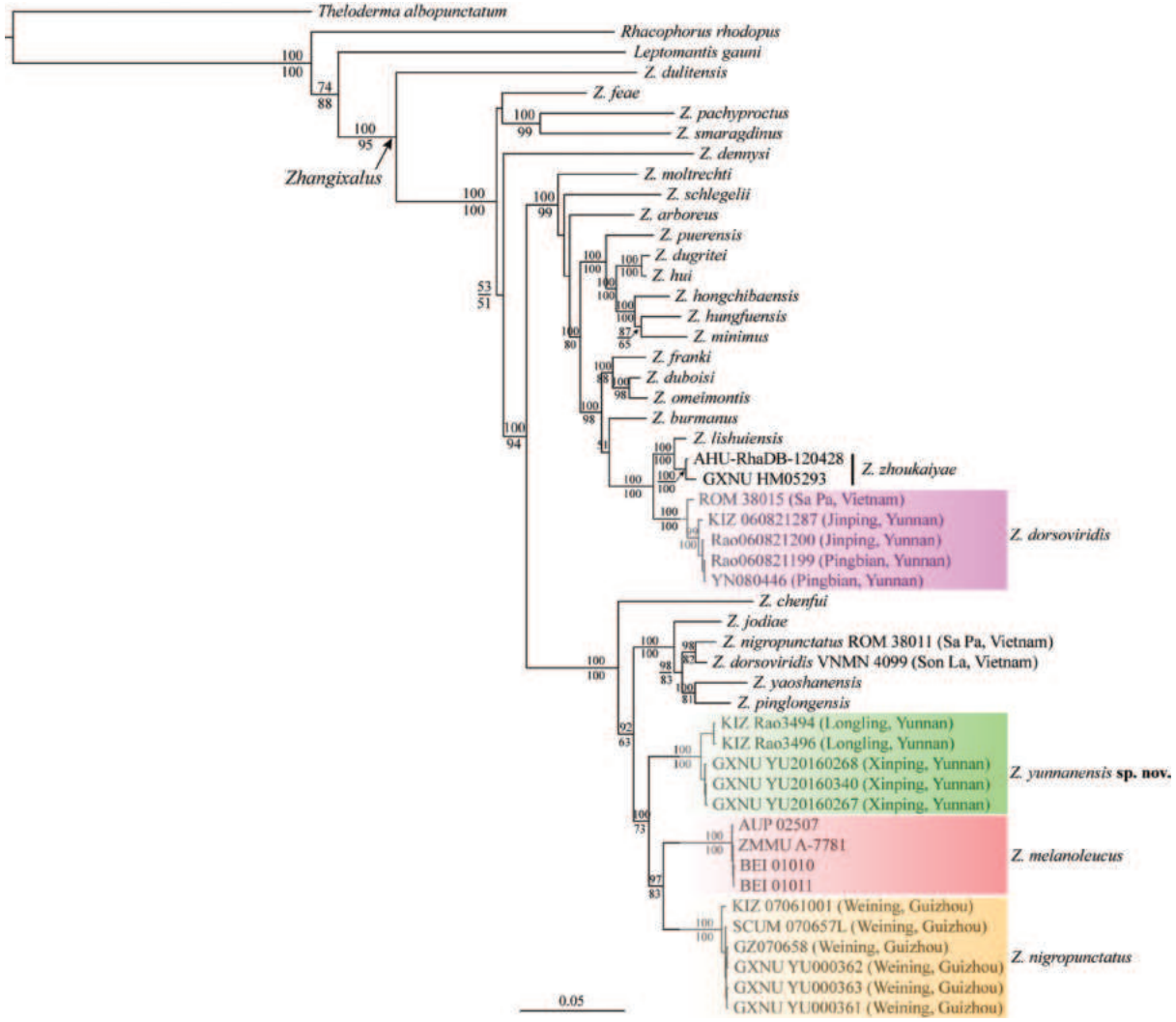

Figure 2. Bayesian phylogram of *Zhangixalus* inferred from mitochondrial 12S-tRNA-16S sequences. Numbers above and below branches are Bayesian posterior probabilities and ML bootstrap values (only values above 50% are shown), respectively.

total variance, were most heavily loaded on internarial distance (IND) and Loadings for PC2, which accounted for 21.78%, were most heavily loaded on head length (HL). Differentiation was found along both the PC1 and PC2 axis between the specimens from Xinping and *Z. nigropunctatus* from the type locality and differentiation was also found along the PC2 axis between the specimens from Xinping and *Z. melanoleucus* (Fig. 3). The results of PCA analysis revealed distinct morphometric differences in head length and internarial distance between the specimens from Xinping and *Z. nigropunctatus* from the type locality, as well as in head length between the specimens from Xinping and *Z. melanoleucus*. Moreover, the t-tests demonstrated that male specimens from Xinping differed significantly ($p < 0.05$) from male topotypes of *Z. nigropunctatus* in HL, HW, IND, UEW, TD, DNE and TFL (Table 4) and differed significantly ($p < 0.05$) from *Z. melanoleucus* in HL, SL, UEW and ED (Table 5). Additionally, the new lineage is distinguishable from its congeners by body size and the combination of texture and colouration pattern. Therefore, on the basis of the above molecular and morphological evidence, we officially describe them as a new species of the genus *Zhangixalus*.

Table 3. Factor loadings of first two principal components of 10 size-adjusted male morphometric characteristics of *Zhangixalus yunnanensis* sp. nov., *Z. nigropunctatus* and *Z. melanoleucus*.

Character	PC1	PC2
Eigenvalue	4.521	2.178
% variation	45.214%	21.778%
HL (head length)	0.124	**0.898**
HW (head width)	0.708	-0.185
SL (snout length)	0.698	0.527
IND (internarial distance)	**0.926**	-0.208
IOD (interorbital distance)	0.778	0.402
UEW (width of upper eyelid)	0.713	-0.571
ED (eye diameter)	0.801	0.363
TD (tympanum diameter)	-0.577	0.192
DNE	-0.323	0.596
TL (tibia length)	0.685	-0.072

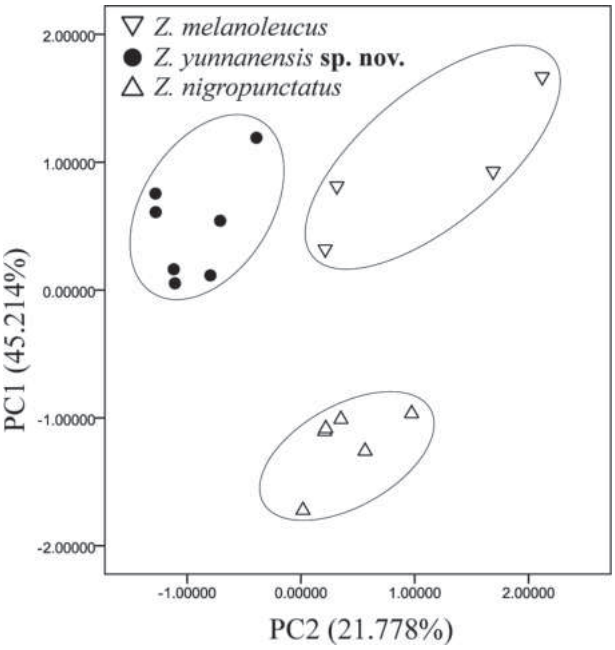

Figure 3. Scatterplot of principal components 1 and 2 of size-adjusted male morphometric data of *Z. yunnanensis* sp. nov., *Z. nigropunctatus* and *Z. melanoleucus*.

Taxonomic account

***Zhangixalus yunnanensis* sp. nov.**

https://zoobank.org/742755AC-423C-4080-8568-8E7D34700F36

Figs 4–6

Yunnan tree Frog/ Yún Nán Shù Wā (云南树蛙)

Type material. *Holotype*: GXNU YU20160340, adult male, collected on 20 April 2020 by Guohua Yu from Mopan Mountain, Xinping County, Yunnan Province, China (23°56'06"N, 102°01'18"E, 2443 m a.s.l.).

***Paratypes*:** GXNU YU20160267–20160269, three adult males, collected on 14 July 2019 from the type locality by Guohua Yu; GXNU YU20160336–20160338,

Table 4. Summary statistics of male specimens (mean ± standard deviation) and results of the *t*-test between the *Z. yunnanensis* sp. nov. (n = 7) and *Z. nigropunctatus* (n = 6) from the type locality. The *t*-test was performed on the size-adjusted data, except SVL. * = $p < 0.05$, ** = $p < 0.01$.

Character	Mean ± SD (n = 7)	Mean ± SD (n = 6)	Levene's test		t-test	
	Z. yunnanensis sp. nov.	*Z. nigropunctatus*	F	*p*-value	t	*p*-value
SVL	34.6 ± 1.6	33.7 ± 1.2	0.370	0.555	1.129	0.283
HL	0.323 ± 0.0068	0.346 ± 0.0082	0.793	0.392	-5.420	0.000**
HW	0.371 ± 0.0122	0.352 ± 0.0092	0.388	0.546	3.144	0.009**
SL	0.154 ± 0.0026	0.150 ± 0.0039	2.043	0.181	2.117	0.058
IND	0.121 ± 0.0043	0.102 ± 0.0047	0.016	0.902	7.350	0.000**
IOD	0.122 ± 0.0056	0.116 ± 0.0037	1.862	0.200	1.956	0.076
UEW	0.095 ± 0.0041	0.079 ± 0.0034	0.297	0.597	7.468	0.000**
ED	0.118 ± 0.0034	0.113 ± 0.0049	0.519	0.486	2.266	0.045*
TD	0.062 ± 0.0021	0.069 ± 0.0026	0.010	0.921	-4.966	0.000**
DNE	0.064 ± 0.0038	0.069 ± 0.0025	1.169	0.303	-3.008	0.012*
FHL	0.522 ± 0.0171	0.509 ± 0.0226	0.925	0.357	1.146	0.276
TL	0.406 ± 0.0182	0.385 ± 0.1508	0.556	0.472	2.246	0.046*
FL	0.446 ± 0.0164	0450 ± 0.0143	0.029	0.868	-0.517	0.615
TFL	0.657 ± 0.0223	0.629 ± 0.0167	0.086	0.775	2.576	0.026*

Table 5. Summary statistics of male specimens (mean ± standard deviation) and results of the *t*-test between the *Z. yunnanensis* sp. nov. (n = 7) and *Z. melanoleucus* (n = 4) from the type locality. The *t*-test was performed on the size-adjusted data, except SVL. * = $p < 0.05$, ** = $p < 0.01$.

Character	Mean ± SD (n = 7)	Mean ± SD (n = 4)	Levene's test		t-test	
	Z. yunnanensis sp. nov.	*Z. melanoleucus*	F	*p*-value	t	*p*-value
SVL	34.6 ± 1.6	35.0 ± 0.9	0.856	0.379	-0.515	0.619
HL	0.323 ± 0.0068	0.368 ± 0.0163	1.420	0.264	-6.502	0.000**
HW	0.371 ± 0.0122	0.363 ± 0.0141	0.239	0.637	0.968	0.358
SL	0.154 ± 0.0026	0.167 ± 0.0072	3.050	0.115	-4.491	0.002**
IND	0.121 ± 0.0043	0.122 ± 0.0007	8.056	0.019	-0.773	0.467
IOD	0.122 ± 0.0056	0.127 ± 0.0074	1.342	0.276	-1.359	0.207
UEW	0.095 ± 0.0041	0.089 ± 0.0027	0.751	0.409	2.753	0.022*
ED	0.118 ± 0.0034	0.126 ± 0.0058	4.303	0.068	-2.737	0.023*
TD	0.062 ± 0.0021	0.059 ± 0.0050	6.278	0.034	1.211	0.300
DNE	0.064 ± 0.0038	0.067 ± 0.0061	0.836	0.384	-1.107	0.297
TL	0.406 ± 0.0182	0.406 ± 0.0110	1.215	0.299	0.057	0.956

three adult males, collected on 20 April 2020 by Guohua Yu from the type locality; and two adult females (GXNU YU20160335 and YU20160355), collected on 20 April 2020 by Guohua Yu from the type locality.

Etymology. The species epithet is named for Yunnan, China, where the species was collected. We suggest the English common name "Yunnan tree frog" and the Chinese common name "Yún Nán Shù Wā (云南树蛙)".

Diagnosis. The new treefrog species is assigned to *Zhangixalus* by the presence of intercalary cartilage between terminal and penultimate phalanges of digits, Y-shaped distal end of terminal phalanx, tips of digits expanded into large discs bearing circum-marginal grooves, and vomerine teeth present, dermal folds along limbs not significant, tarsal projections absent, green dorsa colouration and medium body size (Jiang et al. 2019). Phylogenetically, the new species is nested within the genus *Zhangixalus* with strong support (100% for BI and 73% for ML).

Zhangixalus yunnanensis sp. nov. can be distinguished from its congeners by a combination of the following characters: 1) body size medium (SVL 31.3–36.0 mm [34.6 ± 1.6, n = 7] in males and 47.6–48.6 mm [48.1 ± 0.71, n = 2] in females); 2) head wider than long; 3) iris yellowish-brown; 4) tibiotarsal articulation reaching posterior corner of eye; 5) IND/SVL 11.6%–12. 8% (12.1% ± 0.0043, n =7) in males; 6) HL/SVL 31.0%–32.8% (32.3% ± 0.0068, n = 7) in males; 7) UEW/SVL 8.9%–10.00% (9.5% ± 0.0041, n = 7) in males; 8) dorsum uniformly green; 9) black blotches in axilla, groin and posterior part of thigh; 10) vocal sac external, single; 11) throat black; 12) webbing greyish; and 13) fingers webbing formula I2–2II2–3III2–2IV and toes webbing formula I2–2II1.5–2.5III2–3IV3–1.5V.

Description of holotype. Adult male, body robust, size small (SVL 36.0 mm); HL (11.8 mm) 84.9% of HW (13.9 mm); snout rounded, sloping in profile, protruding beyond margin of lower jaw in ventral view; snout (SL 5.5 mm) longer than eye (ED 4.3 mm); canthus rostralis blunt; lore region oblique, slightly concave; nostril oval, slightly protuberant, located at the middle between snout tip and eye; IND (4.3 mm) equal to IOD and wider than UEW (3.6 mm); pineal spot absent; pupil oval, horizontal; tympanum distinct (TD 2.3 mm), rounded, slightly greater than half of ED, nearly equal to the distance between eye and nostril (DNE 2.2 mm); supratympanic fold distinct, curves from posterior edge of eye to insertion of arm; vomerine teeth in two oblique series touching inner front edge of choanae, separated by space almost equal to length of each series; choanae oval; tongue attached anteriorly and notched posteriorly; single external vocal sac, with a sac slit opening on floor of mouth at each corner.

Relative length of fingers I < II < IV < III; tips of all fingers expanded into discs with circum-marginal grooves; nuptial pad present on first finger; fingers webbed one third, webbing formula I2–2II2–3III2–2IV; lateral fringe on free edge of all fingers; subarticular tubercles prominent and rounded, formula 1, 1, 2, 2; supernumerary tubercles present; inner metacarpal tubercle large, ovoid, outer metacarpal tubercle smaller in size, flattened; white dermal fringe along outer edge of forearm present, not well developed.

Hind limbs relatively short, heels do not meet when legs positioned at right angle to body; tibiotarsal articulation reaching posterior margin of eye; relative length of toes I < II < V < III < IV; tibia (TL 14.3 mm) 39.7% of body size, shorter than foot (FL16.2 mm); tips of toes expanded into discs with circum-marginal grooves, smaller than finger discs; toes webbed, webbing formula I2–2II1.5–2.5III2–3IV3–1.5V; subarticular tubercles prominent and rounded, formula 1, 1, 2, 3, 2; supernumerary tubercles present; inner metatarsal tubercle oval, prominent; outer metatarsal tubercle absent; white dermal fringe along outer edge of tibia, tarsus and fifth toe.

Dorsal surface of body and head smooth; dorsolateral folds absent; throat smooth; chest, belly and ventral surface of thigh granular; a few white warts around vent.

Colouration in life. Iris yellowish-brown with dark wash; dorsal surface green; side of head and tympanic region green; lower part of flanks cream mottled with greyish-brown; throat black; venter and chest cream-white mottled with yolk yellow; limbs dorsally green and ventrally light yellow; anterior and posterior of thigh light yellow; large black blotches in axilla, groin and posterior

Figure 4. Views of the holotype (GXNU YU20160340) in life and in preservative. Photos by Guohua Yu.

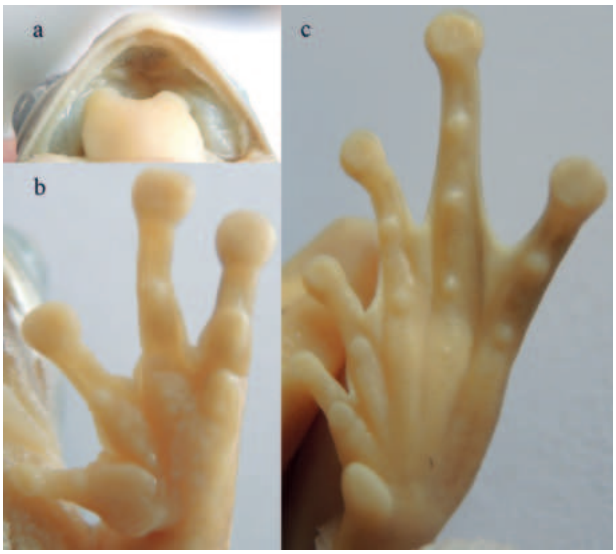

Figure 5. Views of vomerine teeth, hand and foot of the holotype. Photos by Guohua Yu.

part of thigh; white fringes along outer edge from elbow to the fourth finger and from tibiotarsal articulation to the fifth toe; webbing between fingers and toes grey; dorsal surface of discs greyish-brown.

Colouration in preservative. Dorsal surface violet; lower part of flanks and ventral surface of body and limbs white.

Sexual dimorphism. The new species is sexually dimorphic with females being distinctly larger than males (Table 2) and having no vocal sac and nuptial pad. Males have external single subgular vocal sac and light yellow nuptial pad on base of finger I.

Morphological variation. The colour pattern varied amongst individuals. The paratype GXNU YU20160267 has no black blotches on both anterior and posterior parts of the thigh (Fig. 6a, b). The holotype (GXNU YU20160340) and two paratypes (GXNU YU20160267 and GXNU YU20160338) have no black blotches on tibia and tarsal, paratypes GXNU YU20160268 and

GXNU YU20160269 have black blotches on tarsal, but have none on tibia and the other four paratypes (GXNU YU20160355, YU20160336, YU20160335 and YU20160337) have black blotches on both tibia and tarsal. The two specimens from Longling have no black blotches on tibia and tarsal. Dorsal surfaces are uniformly green in all types with the exception of GXNU YU20160335, which has small yellow spots scattered on the dorsal surface of the body and limbs (Fig. 6c). In addition, colouration of the new species in life can vary as day period and microhabitat change; dorsum is lighter nocturnally than during the day, with dorsal surfaces appearing light to dark green.

Distribution and ecology. The new species is currently known from the type locality (Mt. Mopan, Xinping, Yunnan) and Longling, Yunnan, China. Breeding was observed from April to July at the type locality. In April, adult males assembled and called on ground beside permanent pools (Fig. 7a) and the eggs were laid in white foam nests deposited in mud near the pool (Fig. 7b); in mid-July, sparse calls of this species were heard. *Zhangixalus puerensis* and *Hyla anectans* (Jerdon, 1870) were found at the same site. The Jinping and Pingbian populations previously recorded as *Z. nigropunctatus* have been re-assigned into *Z. dorsoviridis* (Li et al. 2012a) and we confirmed that the sample KIZ 060821287, which was collected from Jinping and identified as *Z. nigropunctatus* (Yu et al., 2008), also belongs to *Z. dorsoviridis*. Considering that Longchuan and Yingjiang are close to Longling, the populations previously recorded as *Z. nigropunctatus* from Longchuan and Yingjiang of Yunnan probably belong to the new species pending more data.

Comparison. Phylogenetically, the new species is closely related to *Zhangixalus nigropunctatus* and *Z. melanoleucus*. *Zhangixalus yunnanensis* sp. nov. can be distinguished from *Z. nigropunctatus*, with which the new species has previously been confused, by yellowish-brown iris (vs. yellowish-gold; Fig. 8 and Table 6), head obviously wider than long (vs. head width nearly equal to head length), tibiotarsal articulation reaching posterior corner of eye (vs. reaching posterior edge of tympanum), wider internarial space (mean IND/SVL in males 12.1% ± 0.0043 [11.6%–12.8%, n = 7] vs. 10.2% ± 0.0047 [9.51%–10.85%, n = 6]), longer hind-limb (mean TFL/SVL in males 65.7% ± 0.0223 [62.92%–69.65%, n = 7] vs. 62.9% ± 0.0167

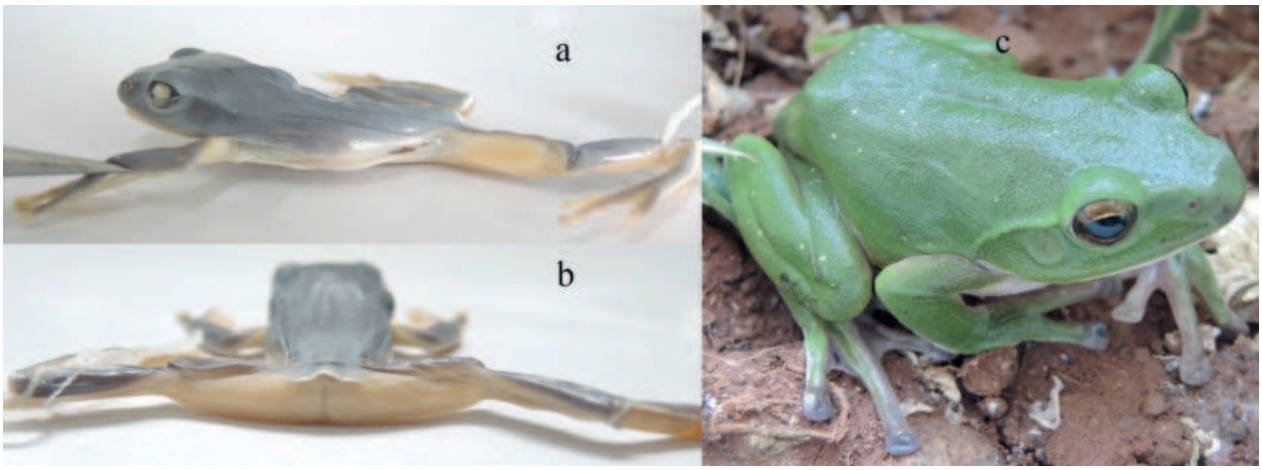

Figure 6. Views of the paratype GXNU YU20160267 in preservative (**a, b**) and the paratype GXNU YU20160335 in life. Photos by Guohua Yu.

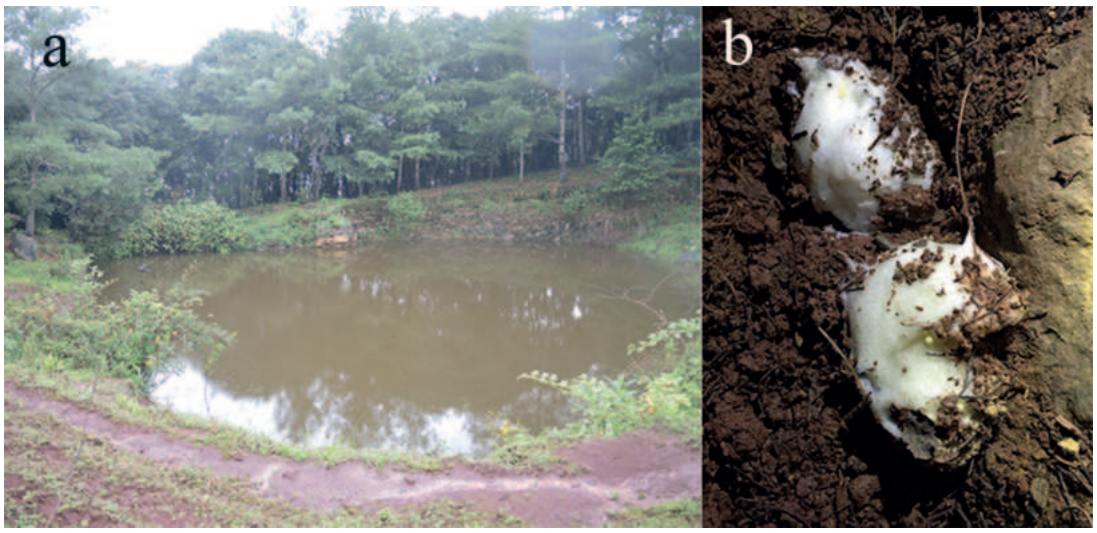

Figure 7. Habitat of the new species at the type locality (**a**) and foam nests of the new species (**b**). Photos by Guohua Yu.

Table 6. Morphological comparison between the new species and congeners of *Zhangixalus*. Characters are: ① dorsum colour: 0 = solid green or green with a few small light spots, 1 = green mottled with brown, 2 = green mottled with black, 3 = brownish; ② black blotches in axilla, groin and thigh: 0 = present, 1 = absent; ③ vocal sac: 0 = external, 1 = internal, 2 = absent; ④ throat: 0 = blackish, 1 = not blackish; ⑤ development of finger web: 0 = webbed one third, 1 = webbed half, 2 = entirely webbed, 3 = rudimentary; ⑥ development of toe web: 0 = webbed half, 1 = entirely webbed, 2 = webbed 2/3, 3 = webbed 1/3. "?" means unknown.

Species	Body size		①	②	③	④	⑤	⑥	Webbing color	Iris color
	Male	Female								
Z. yunnanensis sp. nov.	31.3–36.0	47.6–48.6	0	0	0	0	0	0	greyish	yellowish-brown
Z. achantharrhena	36.5–40.6	47.1	2	1	0	1	1	2	mottled red and green	dull red edged with silvery white
Z. chenfui	33–41	46–55	0	1	0	1	0	0	pale brownish-yellow	reddish-orange
Z. dorsoviridis	31.3–42.4	37.9–42.8	0	0	1	1	0	0	greyish-brown	orange red
Z. dulitensis	38.4–39.7	?	1	1	?	1	2	1	webbing between outer two toes red	reddish
Z. hungfuensis	30.8–36.8	45.5	0	1	0	1	0	0	greyish	greenish
Z. jarujini	33.7–40.0	41.5–46.1	3	1	1	1	0	1	reddish-orange	yellow
Z. jodiae	34.8–39.8	?	0	0	0	1	0	0	cream with black blotches	silver
Z. leucofasciatus	35–48.2	?	0	1	?	1	2	1	greyish black or greyish-purple	yellowish
Z. lishuiensis	34.2–35.8	45.9	0	1	1	1	0	0	golden yellow	yellow
Z. melanoleucus	34.4–36.3	53.7	0	0	0	0	0	2	cream with black blotches	reddish-orange
Z. minimus	21.3–33.0	31.7–38.3	0	1	0	0	3	3	grey mottled with dark blotches	yellowish-gold
Z. moltrechti	36.3–42.4	44.7–54.6	0	0	0	1	1	1	orange red spotted with black	red or red brown
Z. nigropunctatus	32.0–37.0	44.0–45.0	0	0	0	0	3	0	greyish	yellowish-gold
Z. pinglongensis	32.0–38.5	?	0	0	0	1	1	1	tangerine	silver
Z. puerensis	35.5–41.1	52.0–55.2	1	0	0	0	0	0	grey mottled with dark blotches	yellowish-gold
Z. schlegelii	32–43	43–53	0	0	1	1	1	2	purple	yellowish-gold
Z. suffry	38.5–52.9	31.5–61.0	0	1	?	1	2	1	orange red	yellowish-gold
Z. taipeianus	30.4–37.9	39.1–43.0	0	1	0	1	3	1	yellow	yellowish-gold
Z. wui	35.2–38.2	48.6	1	0	1	1	3	3	greyish-brown	yellowish-gold
Z. yaoshanensis	31.6–36.4	49.2–51.1	0	1	0	1	3	1	greyish	pale yellowish-gold
Z. zhoukaiyae	27.9–37.1	42.1–44.7	0	0	0	1	1	2	greyish	golden-yellow
Z. amamiensis	45–56	65–76	0	0	1	1	0	1	purple	greenish
Z. arboreus	42–60	59–82	0	0	1	1	1	1	purple	reddish
Z. arvalis	39.0–46.4	59.5–64	0	1	0	1	1	0	pink	yellow
Z. aurantiventris	47.8–53.9	?	0	1	1	1	1	2	orange-red	pale yellow
Z. burmanus	54–72	66–82	1	0	1	1	0	2	dull brown	greenish
Z. dennysi	68–92	83–109	0	1	1	1	1	1	brown	yellowish-gold
Z. duboisi	>61.5	?	1	0	2	1	1	2	black and white	dark gold
Z. dugritei	41.5–45.4	57.7–64.3	1	0	0	1	1	2	black and grey	yellowish-brown
Z. feae	86–111	68–116	0	1	1	1	2	1	green	green-gold
Z. franki	77.9–85.8	?	1	1	?	1	2	1	grey	bronze
Z. hongchibaensis	46.5–49.7	55.3	1	0	1	1	3	3	grey	yellowish-brown
Z. hui	40–45.4	?	1	0	0	1	3	3	black and grey	reddish-brown
Z. omeimontis	52.0–65.5	70.0–79.5	1	0	1	1	1	1	yellowish	yellowish-gold
Z. owstoni	42–51	?	0	0	1	1	1	2	yellow	yellowish-gold mottled with silver
Z. pachyproctus	73.4–78.2	102.4	0	1	1	1	2	1	pale blue black	bronze
Z. prasinatus	44.8–58.5	63.9–66.9	0	0	0	1	1	1	purple	yellowish-gold
Z. prominanus	50.5–51.3	?	1	1	?	1	1	1	red	reddish
Z. smaragdinus	76.3–79.6	?	0	1	1	1	2	1	blue black	yellowish-gold
Z. viridis	41–54	52–68	0	0	1	1	1	2	red	yellow
Z. yinggelingensis	43.0–43.4	?	0	0	?	1	0	0	red	silver

Figure 8. Irises of the new species (**a.** Photo by Guohua Yu), *Z. nigropunctatus* (**b.** Photo by Guohua Yu) and *Z. melanoleucus* (**c.** reproduced from Brakels et al. (2023)).

[60.8%–65.0%, n = 6]), shorter head (mean HL/SVL in males 32.3% ± 0.0068 [31.0%–32.8%, n = 7] vs. 34.6% ± 0.0082 [33.6%–35.5%, n = 6]), wider upper eyelid (mean UEW/SVL in males 9.5% ± 0.0041 [8.9%–10.0%, n = 7] vs. 7.9% ± 0.0034 [7.5%–8.4%, n = 6]), wider head (mean HW/SVL 37.1% ± 0.0122 [35.3%–38.6%, n = 7] vs. 35.2% ± 0.0092 [34.0%–36.0%, n = 6]), smaller tympanum (mean TD/SVL 6.2% ± 0.0021 [5.9%–6.5%, n = 7] vs. 6.9% ± 0.0026 [6.6%–7.3%, n = 6]) and smaller DNE (mean DNE/SVL 6.4% ± 0.0038 [5.9%–7.0%, n = 7] vs. 6.9% ± 0.0025 [6.7%–7.3%, n = 6]) (Tables 1, 4; Fig. 3); and from *Z. melanoleucus* by yellowish-brown iris (vs. reddish-orange; Fig. 8), shorter head (mean HL/SVL in males 32.3% ± 0.0068 [1.0%–32.8%, n = 7] vs. 36.8% ± 0.0163 [34.9%–38.9%, n = 4]), shorter snout (mean SL/SVL in males 15.4% ± 0.0026 [14. 9%–15.7%, n = 7] vs. 16.7% ± 0.0072 [15.7%–17.4%, n = 4]), wider upper eyelid (mean UEW/SVL in males 9.5% ± 0.0041 [8.9%–10.0%, n = 7] vs. 8.9% ± 0.0027 [8.5%–9.1%, n = 4]) and smaller eye (mean ED/SVL 11.8% ± 0.0034 [11.2%–12.2%, n = 7] vs. 12.6% ± 0.0058 [11.9%–13.1%, n = 4]) (Fig. 3; Table 5).

In body size, besides *Zhangixalus nigropunctatus* and *Z. melanoleucus*, the new species is relatively similar to *Z. achantharrhena* (Harvey, Pemberton & Smith, 2002), *Z. chenfui*, *Z. dorsoviridis*, *Z. dulitensis* (Boulenger, 1892), *Z. hungfuensis* (Liu & Hu, 1961), *Z. jarujini* (Matsui & Panha, 2006), *Z. jodiae* (Nguyen, Ninh, Orlov, Nguyen & Ziegler, 2020), *Z. leucofasciatus* (Liu & Hu, 1962), *Z. lishuiensis* (Liu, Wang & Jiang, 2017), *Z. minimus* (Rao, Wilkinsonand & Liu, 2006), *Z. moltrechti* (Boulenger, 1908), *Z. pinglongensis*, *Z. puerensis*, *Z. schlegelii* (Günther, 1858), *Z. suffry* (Bordoloi, Bortamuli & Ohler, 2007), *Z. taipeianus* (Liang & Wang, 1978), *Z. wui* (Li, Liu, Chen, Wu, Murphy, Zhao, Wang & Zhang, 2012), *Z. yaoshanensis* and *Z. zhoukaiyae* (Table 4). The new species can be easily distinguished from *Z. achantharrhena*, *Z. dulitensis*, *Z. jarujini*, *Z. puerensis* and *Z. wui* by dorsum uniformly green (vs. green with black and white spots in *Z. achantharrhena*, yellowish-green with a few purplish dots on head and back and a purplish line round snout in *Z. dulitensis*, brownish with dark marking in *Z. jarujini*, green with many reddish-brown blotches edged with dark brown in *Z. puerensis* and dark yellowish-brown to light green with numerous light-brown spots in *Z. wui*); from *Z. achantharrhena*, *Z. chenfui*, *Z. dulitensis*, *Z. hungfuensis*, *Z. jarujini*, *Z. leucofasciatus*, *Z. lishuiensis*, *Z. minimus*, *Z. suffry*, *Z. taipeianus* and *Z. yaoshanensis* by having black blotches in axilla, groin and posterior part of thigh (vs. absent); from *Z. dorsoviridis*, *Z. jarujini*, *Z. lishuiensis*, *Z. schlegelii* and *Z. wui* by vocal sac external (vs. internal); from *Z. achantharrhena*, *Z. chenfui*, *Z. dorsoviridis*, *Z. dulitensis*, *Z. hungfuensis*, *Z. jarujini*, *Z. jodiae*, *Z. leucofasciatus*, *Z. lishuiensis*, *Z. moltrechti*, *Z. pinglongensis*, *Z. schlegelii*, *Z. suffry*, *Z. taipeianus*, *Z. wui*, *Z. yaoshanensis* and *Z. zhoukaiyae* by throat black (vs. bright yellow in *Z. achantharrhena*, purplish flesh in *Z. chenfui*, yellow in *Z. dorsoviridis* and *Z. taipeianus*, cream in *Z. hungfuensis* and *Z. jarujini*, greyish in *Z. jodiae* and *Z. yaoshanensis*, white in *Z. dulitensis*, *Z. leucofasciatus*, *Z. lishuiensis*, *Z. moltrechti* and *Z. zhoukaiyae*, white with slightly grey background in *Z. pinglongensis*, cream-white in *Z. schlegelii* and *Z. suffry* and creamy-white with greyish-brown blotches in *Z. wui*); from *Z. achantharrhena*, *Z. chenfui*, *Z. dulitensis*, *Z. jarujini*, *Z. jodiae*, *Z. lishuiensis*, *Z. minimus*, *Z. moltrechti*, *Z. pinglongensis*, *Z. puerensis*, *Z. schlegelii*, *Z. suffry* and *Z. taipeianus* by webbing greyish (vs. having red colour in *Z. achantharrhena*, *Z. dulitensis*, *Z. jarujini*, *Z. moltrechti*, *Z. pinglongensis* and *Z. suffry*, pale brownish-yellow in Z. *chenfui*, mottled with black blotches in *Z. jodiae*, *Z. minimus* and *Z. puerensis*, purple in *Z. schlegelii* and yellow in *Z. lishuiensis* and *Z. taipeianus*); from *Z. achantharrhena*, *Z. dulitensis*, *Z. leucofasciatus*, *Z. moltrechti*, *Z. suffry*, *Z. taipeianus* and *Z. zhoukaiyae* by fingers webbed one third and toes webbed half (vs. fingers webbed half in *Z. achantharrhena*, *Z. leucofasciatus* and *Z. zhoukaiyae*, fingers entirely webbed in *Z. dulitensis*, fingers webbed half and toes webbed entirely in *Z. moltrechti*, fingers webbed entirely and toes webbed fully in *Z. suffry* and toes webbed entirely in *Z. taipeianus*); and from *Z. achantharrhena*, *Z. chenfui*, *Z. dorsoviridis*, *Z. dulitensis*, *Z. jodiae*, *Z. moltrechti* and *Z. pinglongensis* by iris yellowish-brown (vs. dull red, edged with silvery-white in *Z. achantharrhena*, orange-red in *Z. chenfui* and *Z. dorsoviridis*, reddish in *Z. dulitensis*, silver in *Z. jodiae* and *Z. pinglongensis* and red or reddish-brown in *Z. moltrechti*). The new species further differs from *Z. hungfuensis* and *Z. wui* by nuptial pad present on first finger (vs. present on fingers I and II), from *Z. jodiae* by lacking orange blotches in the groin, thigh and ventral side of the tibia (vs. present) and from *Z. pinglongensis* by black blotches on flank and hind-limb being fewer in number and discontinuous (vs. a number of black blotches united to be reticular).

The new species is distinguishable from *Zhangixalus amamiensis* (Inger, 1947), *Z. arboreus* (Okada & Kawano, 1924), *Z. arvalis* (Lue, Lai & Chen, 1995), *Z. aurantiventris* (Lue, Lai & Chen, 1994), *Z. burmanus*, *Z. dennysi* (Blanford, 1881), *Z. duboisi*, *Z. dugritei* (David, 1872), *Z. feae*, *Z. franki*, *Z. hongchibaensis* (Li, Liu Chen, Wu, Murphy, Zhao, Wang & Zhang, 2012), *Z. hui* (Liu, 1945), *Z. omeimontis*, *Z. owstoni* (Stejneger, 1907), *Z. pachyproctus*, *Z. prasinatus* (Mou, Risch & Lue, 1983), *Z. prominanus* (Smith, 1924), *Z. smaragdinus*, *Z. viridis* (Hallowell, 1861) and *Z. yinggelingensis* (Chou, Lau & Chan, 2007) by smaller body size (Table 4). Moreover, the new species can be easily distinguished from *Z. burmanus*, *Z. duboisi*, *Z. dugritei*, *Z. hongchibaensis*, *Z. hui*, *Z. omeimontis* and *Z. prasinatus* by dorsal surface uniformly green and no brown stripe along canthus rostralis and supratympanic fold (vs. dorsal surface green with brown blotches and a brown stripe along canthus rostralis and supratympanic fold or dorsum green with brown stripe along canthus rostralis and supratympanic fold); from *Z. amamiensis*, *Z. arboreus*, *Z. aurantiven-*

tris, *Z. burmanus*, *Z. dennysi*, *Z. feae*, *Z. hongchibaensis*, *Z. omeimontis*, *Z. owstoni*, *Z. pachyproctus*, *Z. smaragdinus*, *Z. viridis* and *Z. yinggelingensis* by external vocal sac (vs. internal vocal sac); and from *Z. arvalis*, *Z. aurantiventris*, *Z. dennysi*, *Z. feae*, *Z. franki*, *Z. pachyproctus*, *Z. prominanus* and *Z. smaragdinus* by having black blotches in axilla, groin and anterior and posterior part of thighs (vs. absent).

Discussion

Zhangixalus nigropunctatus has been recorded widely in central and south-western China (e.g. Fei (1999); Fei et al. (2009, 2010)) and north-western Vietnam (Orlov et al. 2012; Li et al. 2012a). However, previous phylogenetic analyses revealed that records of this species actually involve multiple misidentified populations (Yu et al. 2009; Li et al. 2012a; Mo et al. 2016; Pan et al. 2017). In this study, based on molecular and morphological evidence, we revealed that the Xinping population represents a novel lineage of the genus *Zhangixalus* and previous records of *Z. nigropunctatus* from Longling, Yunnan belong to it. This result supports the viewpoint of Dufresnes and Litvinchuk (2022) that some populations assigned to *Z. nigropunctatus* in Yunnan represent a cryptic species and further improves our understanding of the taxonomy and distribution of *Z. nigropunctatus* complex.

With the Longling population transferred into *Z. yunnanensis* sp. nov., there are three records of *Z. nigropunctatus* left in Yunnan, China according to Yang and Rao (2008) and Fei et al. (2010), including Longchuan, Yingjiang and Qiaojia Counties (Fig. 9). Geographically, Longchuan and Yingjiang are very close to Longling, while Qiaojia is closer to the type locality of *Z. nigropunctatus* (Weining, Guizhou) than to the known distribution of the new species. Therefore, we presume that the populations of nominal *Z. nigropunctatus* in Longchuan and Yingjiang likely also belong to the new species and the Qiaojia population probably belongs to true *Z. nigropunctatus* pending further data.

In addition to the new species described here, we found that the taxonomy of the samples ROM 38011 and VNMN 4099 needs further investigation. The specimen ROM 38011 was collected from Sa Pa, Vietnam and initially identified as *Z. dorsoviridis* (Orlov et al. 2001). However, it obviously differs from other individuals of *Z. dorsoviridis* from Sa Pa (e.g. ROM 38015) by having a darkened vocal sac instead of yellow (Orlov et al. 2001). Li et al (2012a) found that phylogenetically ROM 38011 is closer to *Z. nigropunctatus* than to other samples of *Z. dorsoviridis* and transferred it into *Z. nigropunctatus*. Orlov et al. (2012) also listed *Z. nigropunctatus* as a member of Vietnamese rhacophorid frogs. However, Mo et al. (2016) recovered the specimen ROM 38011 as sister to *Z. pinglongensis*. The specimen VNMN 4099 was collected from Son La, Vietnam and was included as single representative of *Z. dorsoviridis* in Nguyen et al. (2014). In this study, we revealed that these two samples are sister to each other. Moreover, the clade formed by these two samples did not cluster together with the clade containing topotypes of *Z. nigropunctatus* or the clade containing the topotype of *Z. dorsoviridis*; instead, it is sister to the clade comprised of *Z. pinglongensis* and *Z. yaoshanensis*

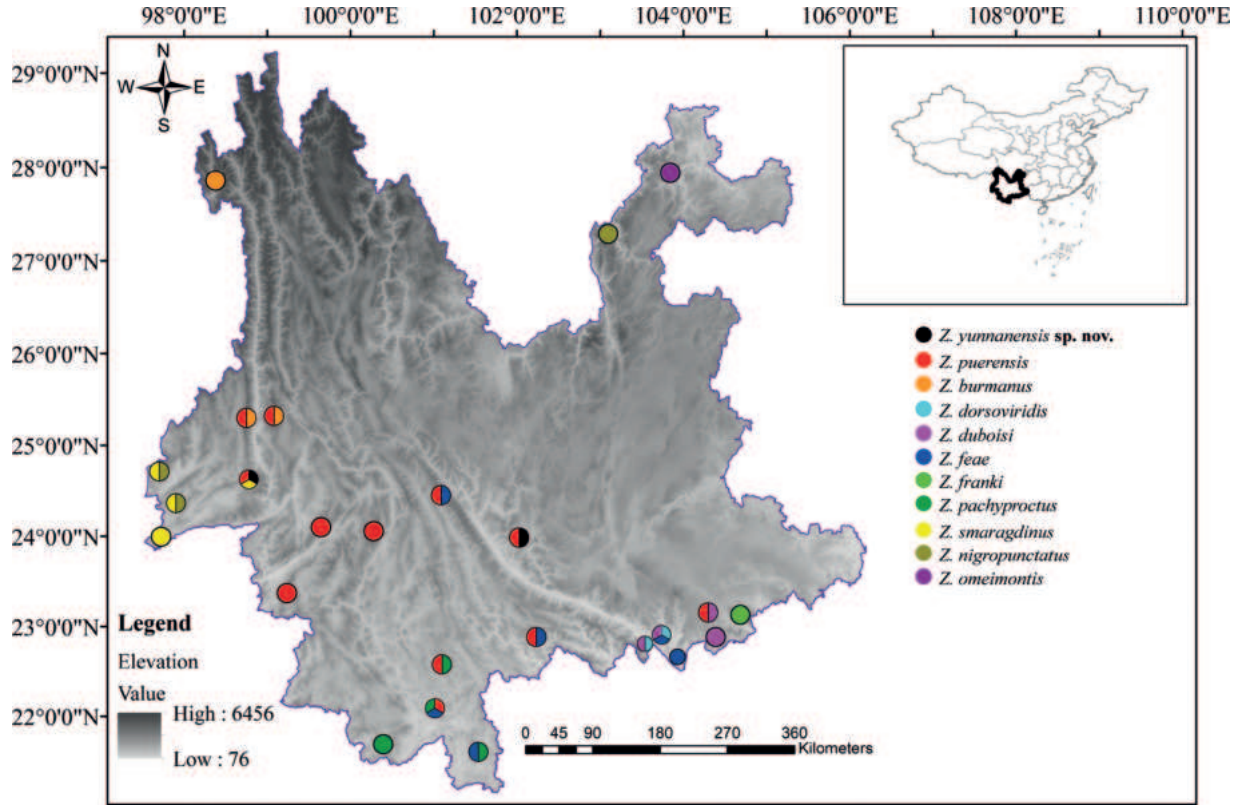

Figure 9. Geographic distribution of *Zhangixalus* species in Yunnan, China. The map was generated using ArcMap v.10.2 (ESRI Inc.).

with strong support. These findings suggest that probably ROM 38011 and VNMN 4099 are neither *Z. nigropunctatus* nor *Z. dorsoviridis*, but potentially represent one or two distinct species pending further morphological and molecular data. Consequently, the presumption of Poyarkov et al. (2021) that records of *Z. nigropunctatus* from Vietnam are a misidentification with *Z. dorsoviridis* remains debatable. Geographically, the collection site of ROM 38011 (Sa Pa, Vietnam) is adjacent to Yunnan, China. Therefore, it could be expected that this potential cryptic species will also be found in Yunnan.

Including the new species described here, the genus *Zhangixalus* now contains 42 described species. Amongst these, 30 species are distributed in China and 11 species are known in Yunnan. Yunnan is a mountainous region with an extremely diverse topography and climate, which supports an extremely rich biodiversity and shapes different zoogeographic regions. Generally, six zoogeographic regions were recognised in Yunnan, namely North-western Hengduan Mountains (NHM), Western Hills of Yunnan (WHY), Tropical Hills of Southern Yunnan (THSY), South-eastern Hills of Yunnan (SHY), Northern and Central Yunnan Plateau (NCYP) and North-eastern Hills of Yunnan (NHY) and the three southern zoogeographic regions (WHY, THSY and SHY) located at the northern edge of tropic Asia have the highest overall diversity (Yang and Rao 2008; Wang et al. 2022b). Rhacophorids are conservative in their preferences to ecoregions since they primarily inhabit tropical and subtropical moist broadleaf forests ecoregions (Ellepola and Meegaskumbura 2023). Accordingly, in Yunnan, most members of the genus *Zhangixalus* are distributed in southern, south-eastern and western Yunnan, with the exceptions of *Z. omeimontis* and *Z. nigropunctatus* (Fig. 9). Amongst the three zoogeographic regions, south-eastern Yunnan has the highest diversity of *Zhangixalus* (six species, namely *Z. franki*, *Z. duboisi*, *Z. puerensis*, *Z. dorsoviridis*, *Z. feae* and *Z. yunnanensis* sp. nov.), followed by western Yunnan (five species including *Z. smaragdinus*, *Z. burmanus*, *Z. puerensis*, *Z. yunnanensis* sp. nov. and the doubtful records of *Z. nigropunctatus* in Longchuan and Yingjiang) and southern Yunnan (three species, namely *Z. pachyproctus*, *Z. puerensis* and *Z. feae*) in order (Fig. 9).

Recently, Dufresnes and Litvinchuk (2022) considered *Zhangixalus hui* as a synonym of *Z. dugritei*, noted that *Z. lishuiensis* is likely conspecific with *Z. zhoukaiyae* and *Z. duboisi* is likely conspecific with *Z. omeimontis* and suggested that *Z. schlegelii* covers additional cryptic species just based on genetic divergence at 16S sequences. In this study, we also revealed low genetic divergence between these sister species at the 16S rRNA gene (1.4% between *Z. lishuiensis* and *Z. zhoukaiyae*, 1.4% between *Z. duboisi* and *Z. omeimontis* and 0.4% between *Z. hui* and *Z. dugritei*; Suppl. material 1). However, we consider that the taxonomic rearrangements of Dufresnes and Litvinchuk (2022) should be treated with caution at the present time because they did not consider morphological data and other genetic factors (e.g. hybridisation and incomplete lineage sorting) that possibly lead to the low divergence between these sister species. For instance, *Z. duboisi* has no vocal sac according to its original description (Ohler et al. 2000), but *Z. omeimontis* has an internal single subgular vocal sac (Fei et al. 2010). Therefore, we consider that more studies are required to resolve these taxonomic confusions and clarify the species diversity of the genus *Zhangixalus*, based on multiple lines of evidence (e.g. morphological and molecular data).

Acknowledgements

Thanks go to Jian Zang for his help with the field surveys. This work was supported by the National Natural Science Foundation of China (32060114), Guangxi Natural Science Foundation Project (2022GXNSFAA035526) and the Key Laboratory of Ecology of Rare and Endangered Species and Environmental Protection (Guangxi Normal University), Ministry of Education (ERESEP2022Z04) and Guangxi Key Laboratory of Rare and Endangered Animal Ecology, Guangxi Normal University (19-A-01-06).

References

AmphibiaChina (2023) The database of Chinese amphibians. Kunming Institute of Zoology (CAS), Kunming, Yunnan, China. https://www.Amphibiachina.org [Accessed 4 October 2023.]

Andersson LG (1939) ["1938"] Batrachians from Burma collected by Dr. R. Malaise, and from Bolivia and Ecuador collected by Dr. C. Hammarlund. Arkiv för Zoologi. Stockholm 30(23): 1–24.

Blanford WT (1881) On a collection of reptiles and frogs chiefly from Singapore. Proceedings of the Zoological Society of London 1881(1): 215–226. https://doi.org/10.1111/j.1096-3642.1881.tb01281.x

Blyth E (1852) Report of Curator, Zoological Department. Journal of the Asiatic Society of Bengal 21: 341–358.

Bordoloi S, Bortamuli T, Ohler A (2007) Systematics of the genus *Rhacophorus* (Amphibia, Anura): Identity of red-webbed forms and description of a new species from Assam. Zootaxa 1653(1): 1–20. https://doi.org/10.11646/zootaxa.1653.1.1

Boulenger GA (1892) An account of the reptiles and batrachians collected by Mr. C. Hose on Mt. Dulit, Borneo. Proceedings of the Zoological Society of London 1892: 505–508.

Boulenger GA (1893) Concluding report on the reptiles and batrachians obtained in Burma by Signor L. Fea dealing with the collection made in Pegu and the Karin Hills in 1887–88. Annali del Museo Civico di Storia Naturale di Genova (Serie 2) 13: 304–347.

Boulenger GA (1908) Descriptions of a new frog and a new snake from Formosa. Annals and Magazine of Natural History (Series 8) 2: e221. https://doi.org/10.1080/00222930808692472

Bourret R (1937) Notes herpétologiques sur l'Indochine française. XIV. Les batraciens de la collection du Laboratoire des Sciences Naturelles de l'Université. Descriptions de quinze especes ou variétés nouvelles. Annexe au Bulletin Général de l'Instruction Publique. Hanoi 1937: 5–56.

Brakels P, Nguyen TV, Pawangkhanant P, Idiiatullina S, Lorphengsy S, Suwannapoom C, Poyarkov NA (2023) Mountain jade: A

new high-elevation microendemic species of the genus *Zhangixalus* (Amphibia: Anura: Rhacophoridae) from Laos. Zoological Research 44: 374–379. https://doi.org/10.24272/j.issn.2095-8137.2022.382

Chou WH, Lau MW, Chan BPL (2007) A new treefrog of the genus *Rhacophorus* (Anura: Rhacophoridae) from Hainan Island, China. The Raffles Bulletin of Zoology 55: 157–165.

Darriba D, Taboada GL, Doallo R, Posada D (2012) jModelTest 2: More models, new heuristics and parallel computing. Nature Methods 9(8): e772. https://doi.org/10.1038/nmeth.2109

David A (1872) ["1871"] Rapport adressé a MM. les Professeurs-Administráteurs du Museum d'histoire naturelle. Nouvelles Archives du Muséum d'Histoire Naturelle 7: 75–100.

Du LY, Wang J, Liu S, Yu GH (2022) A new cryptic species in the *Theloderma rhododiscus* complex (Anura, Rhacophoridae) from China-Vietnam border regions. ZooKeys 1099: 123–138. https://doi.org/10.3897/zookeys.1099.80390

Dufresnes C, Litvinchuk SN (2022) Diversity, distribution and molecular species delimitation in frogs and toads from the Eastern Palaearctic. Zoological Journal of the Linnean Society 195(3): 695–760. https://doi.org/10.1093/zoolinnean/zlab083

Edler D, Klein J, Antonelli A, Silvestro D (2021) RaxmlGUI 2.0: A graphical interface and toolkit for phylogenetic analyses using RAxML. Methods in Ecology and Evolution 12(2): 373–377. https://doi.org/10.1111/2041-210X.13512

Ellepola G, Meegaskumbura M (2023) Diversification and biogeography of Rhacophoridae – a model testing approach. Frontiers in Ecology and Evolution 11: e1195689. https://doi.org/10.3389/fevo.2023.1195689

Fei L (1999) Atlas of Amphibians of China. Henan Publishing House of Science and Technology, Zhengzhou.

Fei L, Ye CY, Jiang JP, Xie F, Huang YZ (2005) An Illustrated Key to Chinese Amphibians. Sichuan Publishing House of Science and Technology, Chengdu.

Fei L, Hu SQ, Ye CY, Huang YZ (2009) Fauna Sinica. Amphibia (Vol. 3). Anura Ranidae. Science Press, Beijing.

Fei L, Ye CY, Jiang JP (2010) Colored Atlas of Chinese Amphibians. Sichuan Publishing House of Science and Technology, Chengdu.

Frost DR (2023) Amphibian Species of the World: an Online Reference. Version 6.2. American Museum of Natural History, New York. https://amphibiansoftheworld.amnh.org/index.php [Accessed at 4 October 2023.]

Gan YL, Yu GH, Wu ZJ (2020) A new species of the genus *Amolops* (Anura: Ranidae) from Yunnan, China. Zoological Research 41(2): 188–193. https://doi.org/10.24272/j.issn.2095-8137.2020.018

Günther ACLG (1858) Neue Batrachier in der Sammlung des britischen Museums. Archiv für Naturgeschichte 24: 319–328. https://doi.org/10.5962/bhl.part.5288

Hallowell E (1861) ["1860"] Report upon the Reptilia of the North Pacific Exploring Expedition, under command of Capt. John Rogers, U.S. N. Proceedings. Academy of Natural Sciences of Philadelphia 12: 480–510.

Harvey MB, Pemberton AJ, Smith EN (2002) New and poorly known parachuting frogs (Rhacophoridae: *Rhacophorus*) from Sumatra and Java. Herpetological Monograph 16(1): 46–92. https://doi.org/10.1655/0733-1347(2002)016[0046:NAPKPF]2.0.CO;2

He XR (1999) A new species of the family Rhacophoridae from Yunnan–*Polypedates puerensis*. Sichuan Journal of Zoology 18: 99–100.

Huelsenbeck JP, Hillis DM (1993) Success of phylogenetic methods in the four-taxon case. Systematic Biology 42(3): 247–264. https://doi.org/10.1093/sysbio/42.3.247

Inger RF (1947) Preliminary survey of the amphibians of the Riukiu islands. Fieldiana. Zoology 32: 297–352. https://doi.org/10.5962/bhl.title.2991

Inger RF (1966) The systematics and zoogeography of the Amphibia of Borneo. Fieldiana. Zoology 52: 1–402. https://doi.org/10.5962/bhl.title.3147

Jerdon TC (1870) Notes on Indian herpetology. Proceedings of the Asiatic Society of Bengal 1870: 66–85.

Jiang D, Jiang K, Ren J, Wu J, Li J (2019) Resurrection of the genus *Leptomantis*, with description of a new genus to the family Rhacophoridae (Amphibia: Anura). Asian Herpetological Research 10: 1–12.

Kuhl H, Van Hasselt JC (1822) Uittreksels uit breieven van de Heeren Kuhl en van Hasselt, aan de Heeren C. J. Temminck, Th. van Swinderen en W. de Haan. Algemeene Konst-en Letter-Bode 7: 99–104.

Kumar S, Stecher G, Tamura K (2016) MEGA7: Molecular evolutionary genetics analysis version 7.0 for bigger datasets. Molecular Biology and Evolution 33(7): 1870–1874. https://doi.org/10.1093/molbev/msw054

Leaché AD, Reeder TW (2002) Molecular systematics of the eastern fence lizard (*Sceloporus undulatus*): A comparison of parsimony, likelihood, and Bayesian approaches. Systematic Biology 51(1): 44–68. https://doi.org/10.1080/106351502753475871

Li JT, Li Y, Murphy RW, Rao DQ, Zhang YP (2012a) Phylogenetic resolution and systematics of the Asian tree frogs, *Rhacophorus* (Rhacophoridae, Amphibia). Zoologica Scripta 41(6): 557–570. https://doi.org/10.1111/j.1463-6409.2012.00557.x

Li JT, Liu J, Chen YY, Wu JW, Murphy RW, Zhao EM, Wang YZ, Zhang YP (2012b) Molecular phylogeny of treefrogs in the *Rhacophorus dugritei* species complex (Anura: Rhacophoridae), with descriptions of two new species. Zoological Journal of the Linnean Society 165(1): 143–162. https://doi.org/10.1111/j.1096-3642.2011.00790.x

Liang YS, Wang CS (1978) A new tree frog *Rhacophorus taipeianus* (Anura: Rhacophoridae) from Taiwan (Formosa). Quarterly Journal of the Taiwan Museum 31: 185–202.

Liu CC (1945) New frogs from West China. Journal of the West China Border Research Society 15: 28–44. [Series B]

Liu CC, Hu SQ (1960) ["1959"] Preliminary report of Amphibia from southern Yunnan. Acta Zoologica Sinica 11: 508–538.

Liu CC, Hu SQ (1961) Tailless Amphibians of China. Science Press, Beijing.

Liu CC, Hu SQ (1962) A herpetological report of Kwangsi. Acta Zoologica Sinica 14(Supplement): 73–104. https://doi.org/10.1080/00845566.1962.10396361

Liu CC, Hu SQ, Yang FH (1962) Preliminary report of Amphibia from western Kweichow. Acta Zoologica Sinica 14: 381–392.

Liu BQ, Wang YF, Jiang K, Chen HM, Zhou JJ, Xu JN, Wu CH (2017) A new treefrog species of the genus *Rhacophorus* Found in Zhejiang, China (Anura: Rhacophoridae). Chinese Journal of Zoology 52: 361–372.

Lue KY, Lai JS, Chen SL (1994) A new species of *Rhacophorus* (Anura: Rhacophoridae) from Taiwan. Herpetologica 50: 303–308.

Lue KY, Lai JS, Chen SL (1995) A new species of *Rhacophorus* (Anura: Rhacophoridae) from Taiwan. Journal of Herpetology 29(3): 338–345. https://doi.org/10.2307/1564982

Matsui M, Panha S (2006) A new species of *Rhacophorus* from eastern Thailand (Anura: Rhacophoridae). Zoological Science 23(5): 477–481. https://doi.org/10.2108/zsj.23.477

Mo YM, Chen WC, Liao X, Zhou SC (2016) A new species of the genus *Rhacophorus* (Anura: Rhacophoridae) from southern China. Asian Herpetological Research 7: 139–150.

Mou YP, Risch JP, Lue KY (1983) *Rhacophorus prasinatus*, a new tree frog from Taiwan, China (Amphibia, Anura, Rhacophoridae). Alytes 2: 154–162.

Myers CW, Duellman WE (1982) A new species of *Hyla* from Cerro Colorado, and other tree frog records and geographical notes from western Panama. American Museum Novitates 2752: 1–32.

Nguyen TT, Matsui M, Eto K, Orlov NL (2014) A preliminary study of phylogenetic relationships and taxonomic problems of Vietnamese *Rhacophorus* (Anura: Rhacophoridae). Russian Journal of Herpetology 21(4): 274–280.

Nguyen TT, Ninh HT, Orlov NL, Nguyen TQ, Ziegler T (2020) A new species of the genus *Zhangixalus* (Amphibia: Rhacophoridae) from Vietnam. Journal of Natural History 54(1–4): 257–273. https://doi.org/10.1080/00222933.2020.1754484

Ninh HT, Nguyen TT, Orlov NL, Nguyen TQ, Ziegler T (2020) A new species of the genus *Zhangixalus* (Amphibia: Rhacophoridae) from Vietnam. European Journal of Taxonomy 688(688): 1–8. https://doi.org/10.5852/ejt.2020.688

Ohler A, Marquis O, Swan SR, Grosjean S (2000) Amphibian biodiversity of Hoang Lien Nature Reserve (Lao Cai Province, northern Vietnam) with description of two new species. Herpetozoa 13: 71–87.

Okada Y, Kawano U (1924) On the ecological distribution of two new varieties of *Rhacophorus* in Japan. Zoological Magazine 36: 104–109. [144–153.]

Orlov NL, Lathrop A, Murphy RW, Ho CT (2001) Frogs of the family Rhacophoridae (Anura: Amphibia) in the northern Hoang Lien Mountains (Mount Fan Si Pan, Sa Pa District, Lao Cai Province), Vietnam. Russian Journal of Herpetology 8: 17–44.

Orlov NL, Poyarkov NA, Vassilieva AB, Ananjeva NB, Nguyen TT, Sang NN, Geissler P (2012) Taxonomic notes on rhacophorid frogs (Rhacophorinae: Rhacophoridae: Anura) of southern part of Annamite Mountains (Truong Son, Vietnam), with description of three new species. Russian Journal of Herpetology 19(1): 23–64.

Pan T, Zhang Y, Wang H, Wu J, Kang X, Qian L, Li K, Zhang Y, Chen J, Rao D, Jiang JP, Zhang B (2017) A New Species of the Genus *Rhacophorus* (Anura: Rhacophoridae) from Dabie Mountains in East China. Asian Herpetological Research 8: 1–13.

Poyarkov NA, Nguyen TV, Popov ES, Geissler P, Pawangkhanant P, Neang T, Suwannapoom C, Orlov NL (2021) Recent progress in taxonomic studies, biogeographic analysis, and revised checklist of amphibians of Indochina. Russian Journal of Herpetology 28(3A): 1–110. https://doi.org/10.30906/1026-2296-2021-2лес8-3A-1-110

Rao DQ, Wilkinson JA, Liu HN (2006) A new species of *Rhacophorus* (Anura: Rhacophoridae) from Guangxi Province, China. Zootaxa 1258: 17–31.

Ronquist F, Teslenko M, van der Mark P, Ayres DL, Darling A, Höhna S, Larget B, Liu L, Suchard MA, Huelsenbeck JP (2012) MrBayes 3.2: Efficient Bayesian phylogenetic inference and model choice across a large model space. Systematic Biology 61(3): 539–542. https://doi.org/10.1093/sysbio/sys029

Smith MA (1924) Two lizards and a new tree frog from the Malay Peninsula. Journal of the Federated Malay States Museums 11: 183–186.

Stejneger L (1907) Herpetology of Japan and adjacent territory. Bulletin – United States National Museum 58: 1–557. https://doi.org/10.5479/si.03629236.58.i

Stejneger L (1924) Herpetological novelties from China. Occasional Papers of the Boston Society of Natural History 5: 119–121.

Tang SJ, Sun T, Liu S, Luo SD, Yu GH, Du LN (2023a) A new species of cascade frog (Anura: Ranidae: *Amolops*) from central Yunnan, China. Zoological Letters 9(1): 1–15. https://doi.org/10.1186/s40851-023-00214-9

Tang SJ, Liu S, Yu GH (2023b) A new species of *Nanorana* (Anura: Dicroglossidae) from northwestern Yunnan, China, with comments on the taxonomy of *Nanorana arunachalensis* and *Allopaa*. Animals 13(21): e3427. https://doi.org/10.3390/ani13213427

Wang J, Li J, Du LY, Hou M, Yu GH (2022a) A cryptic species of the *Amolops ricketti* species group (Anura, Ranidae) from China-Vietnam border regions. ZooKeys 1112: 139–159. https://doi.org/10.3897/zookeys.1112.82551

Wang K, Lyu ZT, Wang J, Qi S, Che J (2022b) The updated checklist and zoogeographic division of the reptilian fauna of Yunnan Province, China. Biodiversity Science 30(4): e21326. https://doi.org/10.17520/biods.2021326

Yang DT (1991) The Amphiba-Fauna of Yunnan. China Forestry Publishing House, Beijing.

Yang DT, Rao DQ (2008) Amphibia and Reptilia of Yunnan. Yunnan Science and Technology Press, Kunming.

Yu GH, Rao DQ, Yang JX, Zhang MW (2008) Phylogenetic relationships among Rhacophorinae (Rhacophoridae, Anura, Amphibia), with an emphasis on the Chinese species. Zoological Journal of the Linnean Society 153(4): 733–749. https://doi.org/10.1111/j.1096-3642.2008.00404.x

Yu GH, Rao D, Zhang MW, Yang JX (2009) Re-examination of the phylogeny of Rhacophoridae (Anura) based on mitochondrial and nuclear DNA. Molecular Phylogenetics and Evolution 50(3): 571–579. https://doi.org/10.1016/j.ympev.2008.11.023

Yu GH, Hui H, Hou M, Wu ZJ, Rao DQ, Yang JX (2019) A new species of *Zhangixalus* (Anura: Rhacophoridae), previously confused with *Zhangixalus smaragdinus* (Blyth, 1852). Zootaxa 4711(2): 275–292. https://doi.org/10.11646/zootaxa.4711.2.3

Zhang J, Jiang K, Hou M (2011) *Rhacophorus dorsoviridis* Bourret, a new record of family Rhacophoridae to China. Acta Zootaxonomica Sinica 36(4): 986–989.

Zhao EM, Yang DT (1997) Amphibians and Reptiles of the Hengduan Mountains Region. Science Press, Beijing.

Supplementary material 1

Genetic distances between *Zhangixalus* species estimated from 16S sequences

Authors: Yuanqiang Pan, Mian Hou, Guohua Yu, Shuo Liu
Data type: xls

Link: https://doi.org/10.3897/zse.100.113850.suppl1

Zoosyst. Evol. 100 (1) 2024, 199–221 | DOI 10.3897/zse.100.116759

PENSOFT

MUSEUM FÜR NATURKUNDE BERLIN

A survey of *Pholcus* spiders (Araneae, Pholcidae) from the Qinling Mountains of central China, with descriptions of seven new species

Lan Yang[1], Chang Fu[1], Yaxuan Zhang[1], Qiaoqiao He[1], Zhiyuan Yao[1]

1 *College of Life Science, Shenyang Normal University, Shenyang 110034, Liaoning, China*

https://zoobank.org/1149D05E-7AF5-43D9-A18F-C58157F9A36C

Corresponding authors: Qiaoqiao He (heqq@synu.edu.cn); Zhiyuan Yao (yaozy@synu.edu.cn)

Academic editor: Danilo Harms ♦ **Received** 3 December 2023 ♦ **Accepted** 13 February 2024 ♦ **Published** 26 February 2024

Abstract

We report 18 spider species of the genus *Pholcus* Walckenaer, 1805 from a survey in the Qinling Mountains of central China. They belong to four species groups and include seven species new to science: *Pholcus jiaozuo* Yang & Yao, **sp. nov.** (♂♀) in the *taishan* species group; *P. luonan* Yang & Yao, **sp. nov.** (♂♀), *P. luoyang* Yang & Yao, **sp. nov.** (♂♀), *P. lushan* Yang & Yao, **sp. nov.** (♂♀), *P. shangluo* Yang & Yao, **sp. nov.** (♂♀), *P. weinan* Yang & Yao, **sp. nov.** (♂♀) and *P. yuncheng* Yang & Yao, **sp. nov.** (♂♀) in the *yichengicus* species group. Detailed diagnoses, descriptions, photomicroscopy images and DNA barcodes of all new species are provided. Our study will make a significant contribution to understanding species diversity and zoogeography of the region.

Key Words

Biodiversity, daddy-long-legs, DNA barcode, morphology, taxonomy

Introduction

The family Pholcidae C.L. Koch, 1850 is a highly diverse group of spiders, with 97 extant genera and 1,937 extant species (WSC 2023). It has a wide distribution and occupies a variety of habitats, for example, in buildings, on rock walls, in caves (or at cave entrance ecotones), in leaf litter, on the underside of leaves and in webs between trunks and twigs of trees (Huber 2005, 2011; Yao and Li 2010, 2012, 2013; Yao et al. 2015, 2016). The genus *Pholcus* Walckenaer, 1805 is the most diverse genus in the family and one of the largest in Araneae Clerck, 1757, with 389 described species placed in 21 species groups (Huber 2011; Huber et al. 2018; WSC 2023). It is mainly distributed in the Palaearctic, Oriental, Afrotropical and Australasian Realms (WSC 2023).

China exhibits the highest species diversity of the genus *Pholcus*. To date, 169 species have been recorded in China, which represent 43% of the genus (WSC 2023). Recently, a series of surveys of *Pholcus* have been carried out in northern China and a large number of new species have been reported. For instance, a wide-ranging expedition to the Changbai Mountains in 2020 recorded 27 species of *Pholcus*, including 13 new species (Lu et al. 2021; Yao et al. 2021; Zhao et al. 2023a). Another investigation in the Yanshan-Taihang Mountains in 2021 recorded 36 *Pholcus* species, of which 14 species were new to science (Lu et al. 2022a, b). In 2022, *Pholcus* spiders were collected for the first time during an expedition to the Lüliang Mountains and the study identified one known species and eight new species (Zhao et al. 2023b).

The Qinling Mountain range represents a major geographical dividing line between the temperate zone and the subtropical zone of China, as well as between the Palaearctic and Oriental zoogeographic realms. It is home to many iconic wild animals, such as giant pandas and golden monkeys. For invertebrates, nearly 8,000 species of insects have been recorded in the Qinling Mountains (Yang 2018). However, reports on spiders from the Qinling Mountains are relatively few and the species diversity has not been systematically investigated.

The present study focuses on species diversity of the genus *Pholcus* from the Qinling Mountains. Previously, 14 species of *Pholcus* have been recorded in this region according to a series of previously published papers

(e.g. Zhang and Zhu (2009); Yao and Li (2012); Dong et al. (2016); WSC (2023)). We undertook a systematic investigation there in 2022 (Fig. 1) and the aim is to reveal the species diversity.

Materials and methods

All specimens were collected by Z Yao, L Yang and L Zhang. Specimens were examined and measured with a Leica M205 C stereomicroscope. Left male palps were photographed. Epigynes were photographed before dissection. Vulvae were photographed after treating them in a 10% warm solution of potassium hydroxide (KOH) to dissolve soft tissues. Images were captured with a Canon EOS 750D wide zoom digital camera (24.2 megapixels) mounted on the stereomicroscope mentioned above and assembled using Helicon Focus v. 3.10.3 image stacking software (Khmelik et al. 2005). All measurements are given in millimetres (mm). Leg measurements are shown as: total length (femur, patella, tibia, metatarsus, tarsus). Leg segments were measured on their dorsal side. The distribution map was generated with ArcGIS v. 10.2 (ESRI Inc.). The specimens studied are deposited in the College of Life Science, Shenyang Normal University (SYNU) in Liaoning, China and the Institute of Applied Ecology, Chinese Academy of Sciences (IAECAS) in Liaoning, China.

Terminology and taxonomic descriptions follow Huber (2011) and Yao et al. (2015, 2021). The following abbreviations are used: **a** = appendix, **aa** = anterior arch, **ALE** = anterior lateral eye, **AME** = anterior median eye, **b** = bulb, **da** = distal apophysis, **dp** = distal process, **ds** = dorsal spine, **dt** = distal teeth, **e** = embolus, **fa** = frontal apophysis, **kn** = knob, **L/d** = length/diameter ratio, **mb** = median branch, **pa** = proximo-lateral apophysis, **PME** = posterior median eye, **pp** = pore plate, **pda** = prolatero-distal apophysis, **pr** = procursus, **pra** = proximal apophysis, **psa** = prolatero-subdistal apophysis, **pse** = prolatero-subdistal edge, **pss** = prolatero-subdistal sclerite, **pvp** = prolatero-ventral protuberance, **rb** = retrolateral branch, **rda** = retrolatero-distal apophysis, **rdb** = retrolatero-distal branch, **rma** = retrolatero-median apophysis, **rpa** = retrolatero-proximal apophysis, **sb** = subdistal branch, **sc** = sclerite, **u** = uncus, **va** = ventral apophysis, **vp** = ventral protuberance, **vsa** = ventro-subdistal apophysis.

DNA barcode sequences of new species were obtained. A partial fragment of the mitochondrial cytochrome oxidase subunit I (COI) gene was targeted using the following primers: forward: LCO1490 (5'-GGTCAACAAATCATAAAGATATTGG-3') and reverse: HCO2198 (5'-TAAACTTCAGGGTGACCAAAAAATCA-3') (Folmer et al. 1994). Additional information on extraction, amplification and sequencing procedures is provided in Yao et al. (2016).

Results

A total of 18 species were identified, including seven new species. A list of known species is provided in Table 1 and descriptions of all the new species are provided below. In addition, one species, *P. bidentatus* Zhu, Zhang, Zhang & Chen, 2005, is recorded from the Qinling Mountains for the first time. Of the 14 previously recorded species from

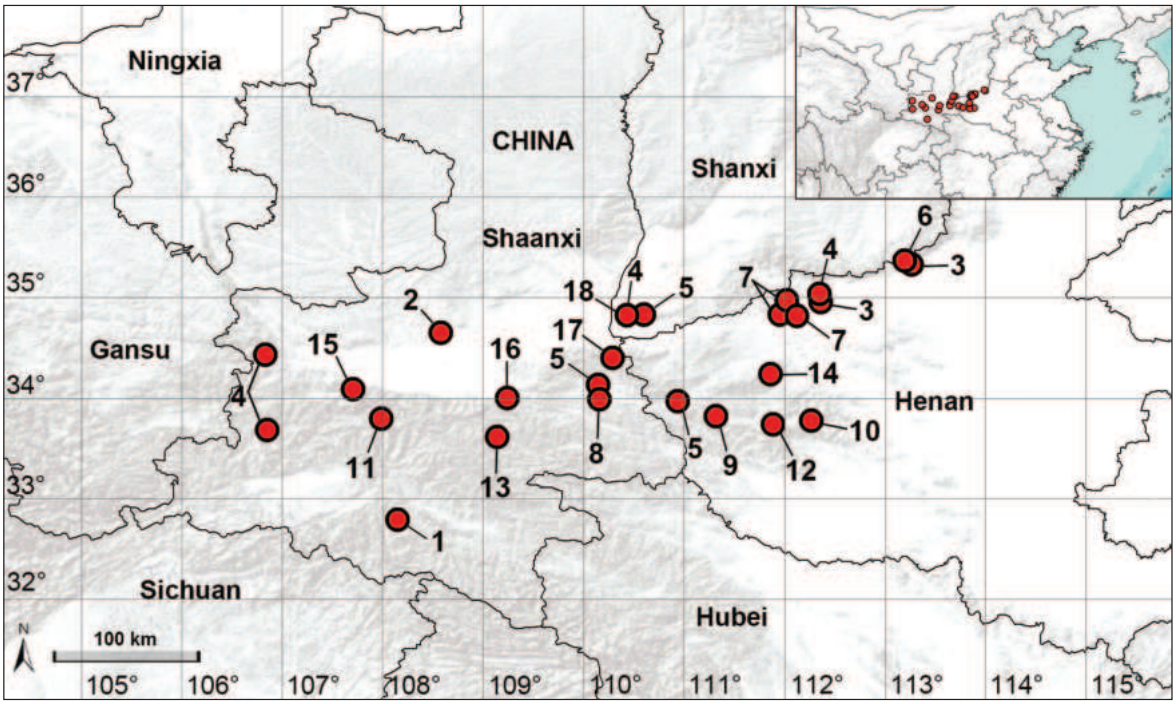

Figure 1. Distribution records of *Pholcus* spiders from the Qinling Mountains in this study. The *bidentatus* group: **1** *P. bidentatus*; the *crypticolens* group: **2** *P. jingyangensis*, **3** *P. langensis*, **4** *P. manueli*, **5** *P. zichyi*; the *taishan* group: **6** *P. jiaozuo* sp. nov., **7** *P. yugong*; the *yichengicus* group: **8** *P. luonan* sp. nov., **9** *P. luoyang* sp. nov., **10** *P. lushan* sp. nov., **11** *P. ovatus*, **12** *P. parayichengicus*, **13** *P. shangluo* sp. nov., **14** *P. songxian*, **15** *P. taibaiensis*, **16** *P. tangyuensis*, **17** *P. weinan* sp. nov., **18** *P. yuncheng* sp. nov.

the Qinling Mountains, we identified ten from our collection. We did not find four previously recorded species of the region, *P. paralinzhou* Zhang & Zhu, 2009, *P. henanensis* Zhu & Mao, 1983, *P. harveyi* Zhang & Zhu, 2009 and *P. lingguanensis* Yao & Li, 2016. All the identified species are endemic to the Qinling Mountains, except three widely-distributed species *P. bidentatus*, *P. manueli* Gertsch, 1937 and *P. zichyi* Kulczyński, 1901. One DNA barcode sequence was obtained from each new species and all sequences are deposited in GenBank. The voucher numbers, GenBank accession numbers and other related information are given in Table 2. Our study significantly increases the number of known spider species in the Qinling Mountains and will make a significant contribution to the understanding of species diversity of the region, as well as zoogeography.

Table 1. Information of the 11 known species collected and identified.

Species	Voucher code	Collection locality
bidentatus group		
P. bidentatus	2♂ (SYNU-Ar00083F–84F) 2♀ (SYNU-Ar00085F–86F)	**Shaanxi***, Ankang, Shiquan County, Yundou Town, Hanjiang Yanxiangdong Scenic Spot, 32°47.75'N, 108°8.93'E, 393 m elev., 24/07/2022
crypticolens group		
P. jingyangensis	2♂ (SYNU-Ar00087F–88F) 2♀ (SYNU-Ar00089F–90F)	**Shaanxi**, Xianyang, Jingyang County, Wangqiao Town, Zhangjiashan Reservoir, 34°39.08'N, 108°34.58'E, 440 m elev., 01/08/2022
P. langensis	2♂ (SYNU-Ar00091F–92F) 2♀ (SYNU-Ar00093F–94F)	**Henan**, Jiyuan, Dayu Town, 34°57.62'N, 112°21.55'E, 373 m elev., 15/07/2022
	1♂ (SYNU-Ar00095F) 1♀ (SYNU-Ar00096F)	**Henan**, Jiaozuo, Xiuwu County, Xicun Town, 35°19.85'N, 113°15.97'E, 276 m elev., 14/07/2022
P. manueli	1♂ (SYNU-Ar00097F) 1♀ (SYNU-Ar00098F)	**Henan***, Jiyuan, Dayu Town, 35°2.52'N, 112°20.62'E, 443 m elev., 15/07/2022
	1♂ (SYNU-Ar00099F) 1♀ (SYNU-Ar00100F)	**Shanxi**, Yuncheng, Yongji, Shuiyukou Village, Shentan Grand Canyon Scenic Spot, 34°49.50'N, 110°25.72'E, 529 m elev., 20/07/2022
	2♀ (SYNU-Ar00101F–02F)	**Shaanxi**, Hanzhong, Liuba County, Liuhou Town, 33°41.27'N, 106°50.80'E, 1187 m elev., 27/07/2022
	1♂ (SYNU-Ar00103F) 1♀ (SYNU-Ar00104F)	**Shaanxi**, Baoji, Chencang District, Pingtou Town, Jiulongshan Scenic Spot, 34°25.93'N, 106°49.98'E, 1082 m elev., 28/07/2022
P. zichyi	1♂ (SYNU-Ar00105F) 1♀ (SYNU-Ar00106F)	**Henan**, Sanmenxia, Lushi County, Shuanglongwan Town, 33°58.30'N, 110°56.22'E, 580 m elev., 18/07/2022
	1♂ (SYNU-Ar00107F) 1♀ (SYNU-Ar00108F)	**Shanxi***, Yuncheng, Yongji, Wulaofeng Scenic Spot, Dabaiyu Village, 34°50.18'N, 110°36.05'E, 522 m elev., 20/07/2022
	1♂ (SYNU-Ar00109F) 1♀ (SYNU-Ar00110F)	**Shaanxi***, Shangluo, Luonan County, Chengguan Street, Liuwan Village, 34°8.13'N, 110°8.62'E, 893 m elev., 20/07/2022
taishan group		
P. yugong	2♂ (SYNU-Ar00111F–12F) 2♀ (SYNU-Ar00113F–14F)	**Henan**, Sanmenxia, Mianchi County, Rencun Town, Honghuawo Village, 34°50.20'N, 111°57.22'E, 725 m elev., 16/07/2022
	2♂ (SYNU-Ar00115F–16F) 1♀ (SYNU-Ar00117F)	**Henan**, Luoyang, Xin'an County, Qingyaoshan Town, Longtan Grand Canyon Scenic Spot, 34°58.48'N, 112°1.27'E, 336 m elev., 16/07/2022
	1♂ (SYNU-Ar00118F) 1♀ (SYNU-Ar00119F)	**Henan**, Luoyang, Xin'an County, Shisi Town, 34°49.43'N, 112°7.43'E, 370 m elev., 16/07/2022
yichengicus group		
P. ovatus	1♂ (SYNU-Ar00120F) 1♀ (SYNU-Ar00121F)	**Shaanxi**, Xi'an, Zhouzhi County, Banfangzi Town, 33°48.02'N, 107°59.08'E, 1165 m elev., 31/07/2022
P. parayichengicus	2♂ (SYNU-Ar00122F–23F) 2♀ (SYNU-Ar00124F–25F)	**Henan**, Luoyang, Song County, Baiyunshan Scenic Spot, 33°44.63'N, 111°52.97'E, 830 m elev., 17/07/2022
P. songxian	2♂ (SYNU-Ar00126F–27F) 2♀ (SYNU-Ar00128F–29F)	**Henan**, Luoyang, Song County, Tianchishan Scenic Spot, 34°14.35'N, 111°51.72'E, 810 m elev., 17/07/2022
P. taibaiensis	3♂ (SYNU-Ar00130F–32F) 3♀ (SYNU-Ar00133F–35F)	**Shaanxi**, Baoji, Mei County, Yingtou Town, Haopingsi Temple, 34°5.32'N, 107°42.33'E, 1101 m elev., 30/07/2022
P. tangyuensis	2♂ (SYNU-Ar00136F–37F) 3♀ (SYNU-Ar00138F–40F)	**Shaanxi**, Xi'an, Lantian County, Tangyu Town, Tangyuhu Forest Park, Laoaogou Village, 34°0.03'N, 109°14.43'E, 898 m elev., 31/07/2022

* indicates new provincial records.

Table 2. Voucher specimen information.

New species	Voucher code	GenBank accession number	Sequence length	Collection locality
P. jiaozuo sp. nov.	W215	PP082960	626 bp	**Henan**, Jiaozuo, Xiuwu County
P. luonan sp. nov.	W257	PP082965	626 bp	**Shaanxi**, Shangluo, Luonan County
P. luoyang sp. nov.	W242	PP082962	626 bp	**Henan**, Luoyang, Luanchuan County,
P. lushan sp. nov.	W237	PP082961	626 bp	**Henan**, Pingdingshan, Lushan County
P. shangluo sp. nov.	W260	PP082966	626 bp	**Shaanxi**, Shangluo, Zhashui County
P. weinan sp. nov.	W252	PP082964	626 bp	**Shaanxi**, Weinan, Tongguan County
P. yuncheng sp. nov.	W251	PP082963	626 bp	**Shanxi**, Yuncheng, Yongji

Taxonomic accounts

Family Pholcidae C.L. Koch, 1850
Subfamily Pholcinae C.L. Koch, 1850

Genus *Pholcus* Walckenaer, 1805

Type species. *Aranea phalangioides* Fuesslin, 1775.

Pholcus taishan species group

This species group was recognised by Huber (2011). It currently includes ten species and is distributed in central China (Huber 2011; Peng and Zhang 2011). A new species, *P. jiaozuo* sp. nov., is described below.

Pholcus jiaozuo Yang & Yao, sp. nov.

https://zoobank.org/A8DC2A11-B767-4FCA-A23C-487F8BFE22C3
Figs 2, 3

Type material. ***Holotype*** ♂ (SYNU-Ar00363) and ***paratypes*** 2♂ (SYNU-Ar00364, IAECAS-Ar00365Y) 3♀ (SYNU-Ar00366–67, IAECAS-Ar00368Y), **China**, **Henan**, Jiaozuo, Xiuwu County, Qinglongxia Scenic Spot (35°22.05'N, 113°11.77'E, 820 m elev.), 14/07/2022.

Etymology. The specific name refers to the type locality and is a noun in apposition.

Diagnosis. The new species resembles *P. henanensis* Zhu & Mao, 1983 (Yao and Li 2012: 18, figs 77A–D, 78A–B) by having similar male chelicerae, bulbal apophyses and epigyne (Fig. 3A, C, D), but can be distinguished by prolatero-subdistal sclerite of procursus laterally curved (Fig. 2C vs. laterally flat), by procursus with distal membranous process (Fig. 2C vs. absent), by retrolatero-distal apophysis of procursus distally pointed in prolateral view (Fig. 2C vs. distally blunt) and by wavy vulval anterior arch (Fig. 3B vs. arch-shaped).

Description. Male (***holotype***). Total length 5.38 (5.58 with clypeus), carapace 1.66 long, 1.88 wide, opisthosoma 3.72 long, 1.66 wide. Leg I: 39.95 (10.25, 0.79, 9.85, 16.31, 2.75), leg II: 28.15 (7.88, 0.72, 6.95, 10.96, 1.64), leg III: 20.28 (5.90, 0.66, 4.84, 7.63, 1.25), leg IV: 26.12 (7.76, 0.67, 6.67, 9.52, 1.50); tibia I L/d: 62. Eye interdistances and diameters: PME–PME 0.26, PME 0.17, PME–ALE 0.04, AME–AME 0.04, AME 0.10. Sternum width/length: 1.25/0.86. Habitus as in Fig. 3E, F. Carapace yellowish, with brown radiating marks and marginal brown bands; ocular area yellowish, with median and lateral brown bands; clypeus and sternum yellowish, with brown marks. Legs yellowish, but dark brown on patellae and whitish on distal parts of femora and tibiae, with darker rings on subdistal parts of femora and proximal and subdistal parts of tibiae. Opisthosoma yellowish, with dorsal and lateral spots. Chelicerae (Fig. 3D) with pair of proximo-lateral apophyses and pair of distal apophyses. Palp as in Fig. 2A, B; trochanter with long (8 times longer than wide), retrolatero-proximally strongly bulged ventral apophysis; femur with small retrolatero-proximal apophysis and distinct ventral protuberance; tibia with prolatero-ventral protuberance; procursus (Fig. 2C, D) simple proximally, but complex distally, with raised prolatero-subdistal membranous edge, curved prolatero-subdistal sclerite, distal membranous process, sclerotised retrolatero-distal apophysis and two strong dorsal spines; uncus (Fig. 3C) distally widened, with proximal apophysis and distal scaly edge; appendix (Fig. 3C) hooked, with distal teeth; embolus (Fig. 3C) weakly sclerotised, with some indistinct transparent distal projections. Retrolateral trichobothrium on tibia I at 5% proximally; legs with short vertical setae on tibiae, metatarsi and tarsi; tarsus I with 38 distinct pseudosegments.

Female (***paratype***). Similar to male, habitus as in Fig. 3G, H. Total length 5.00 (5.19 with clypeus), carapace 1.52 long, 1.70 wide, opisthosoma 3.48 long, 1.60 wide; tibia I: 8.05; tibia I L/d: 50. Eye interdistances and diameters: PME–PME 0.21, PME 0.14, PME–ALE 0.04, AME–AME 0.03, AME 0.08. Sternum width/length: 1.03/0.80. Clypeus brown. Epigyne (Fig. 3A) nearly triangular, laterally slightly sclerotised, with knob developed into long scape (10 times longer than wide). Vulva (Fig. 3B) with wavy, posteriorly sclerotised anterior arch and pair of elliptic pore plates.

Variation. Tibia I in two paratype males: 9.55, 10.50. Tibia I in the other two paratype females: 7.95, 8.25.

Habitat. Underside of overhang on rocky cliffs in the mountain area.

Distribution. China (Henan, type locality; Fig. 1).

Pholcus yichengicus species group

This species group was recognised by Huber (2011). It currently includes 44 species and is widely distributed in central and southern China, as well as Thailand (Huber 2011; Zhu et al. 2018; Lan et al. 2020). Six new species are described below.

Pholcus luonan Yang & Yao, sp. nov.

https://zoobank.org/4A9F4DB6-3FF3-46D9-8131-3BAD55918638
Figs 4, 5

Type material. ***Holotype*** ♂ (SYNU-Ar00369) and ***paratypes*** 1♂ (IAECAS-Ar00370Y) 2♀ (SYNU-Ar00371, IAECAS-Ar00372Y), **China**, **Shaanxi**, Shangluo, Luonan County, Beikuanping Town, Hanziping Village (33°59.67'N, 110°9.28'E, 1105 m elev.), 21/07/2022.

Etymology. The specific name refers to the type locality and is a noun in apposition.

Diagnosis. The new species resembles *P. tangyuensis* Yao & Li, 2016 (Dong et al. 2016: 30, figs 21A–D,

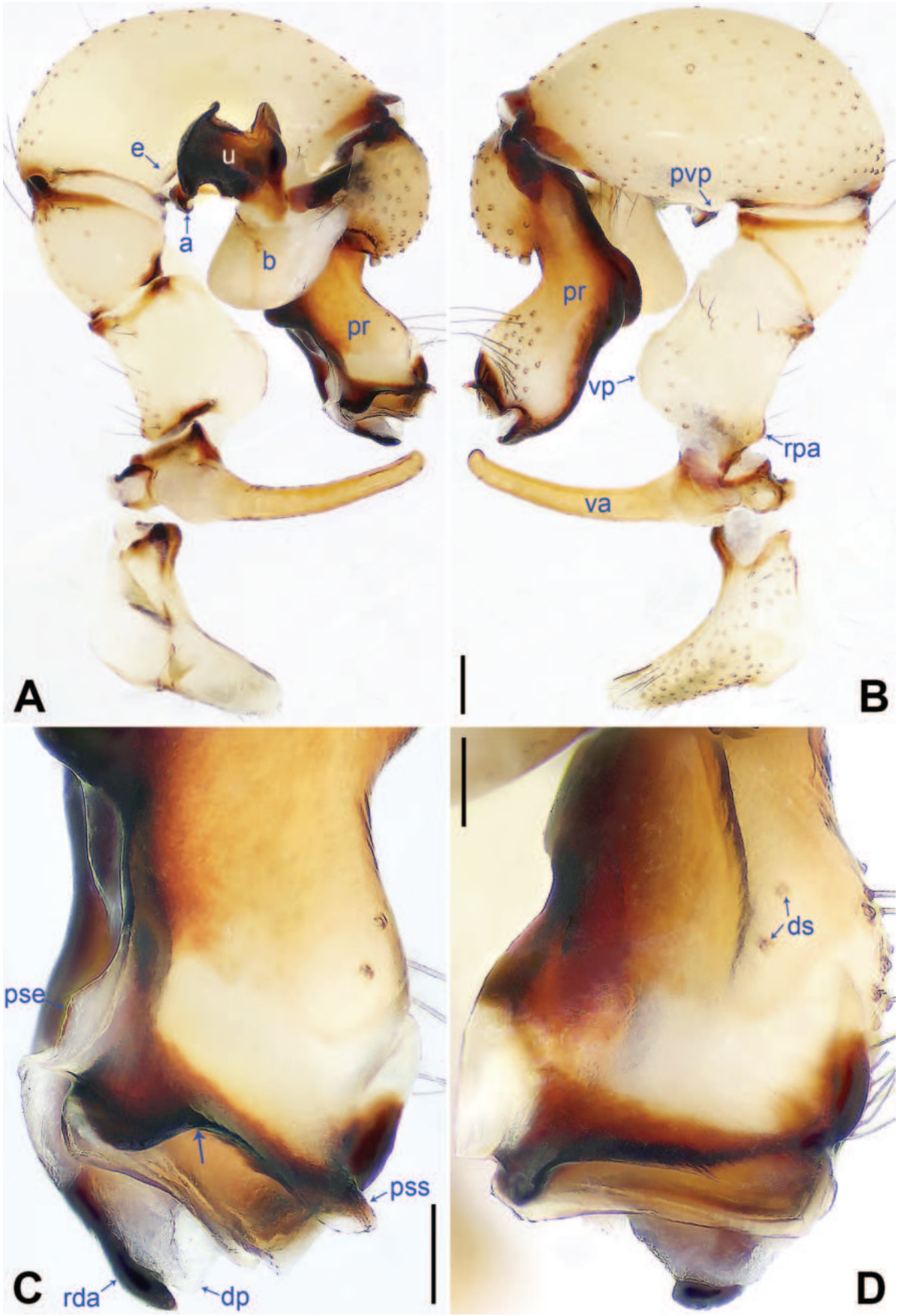

Figure 2. *Pholcus jiaozuo* sp. nov., holotype male **A, B.** Palp (**A.** Prolateral view; **B.** Retrolateral view); **C, D.** Distal part of procursus (**C.** Prolateral view, arrow points at curved part of sclerite; **D.** Dorsal view). Scale bars: 0.20 mm (**A, B**); 0.10 mm (**C, D**).

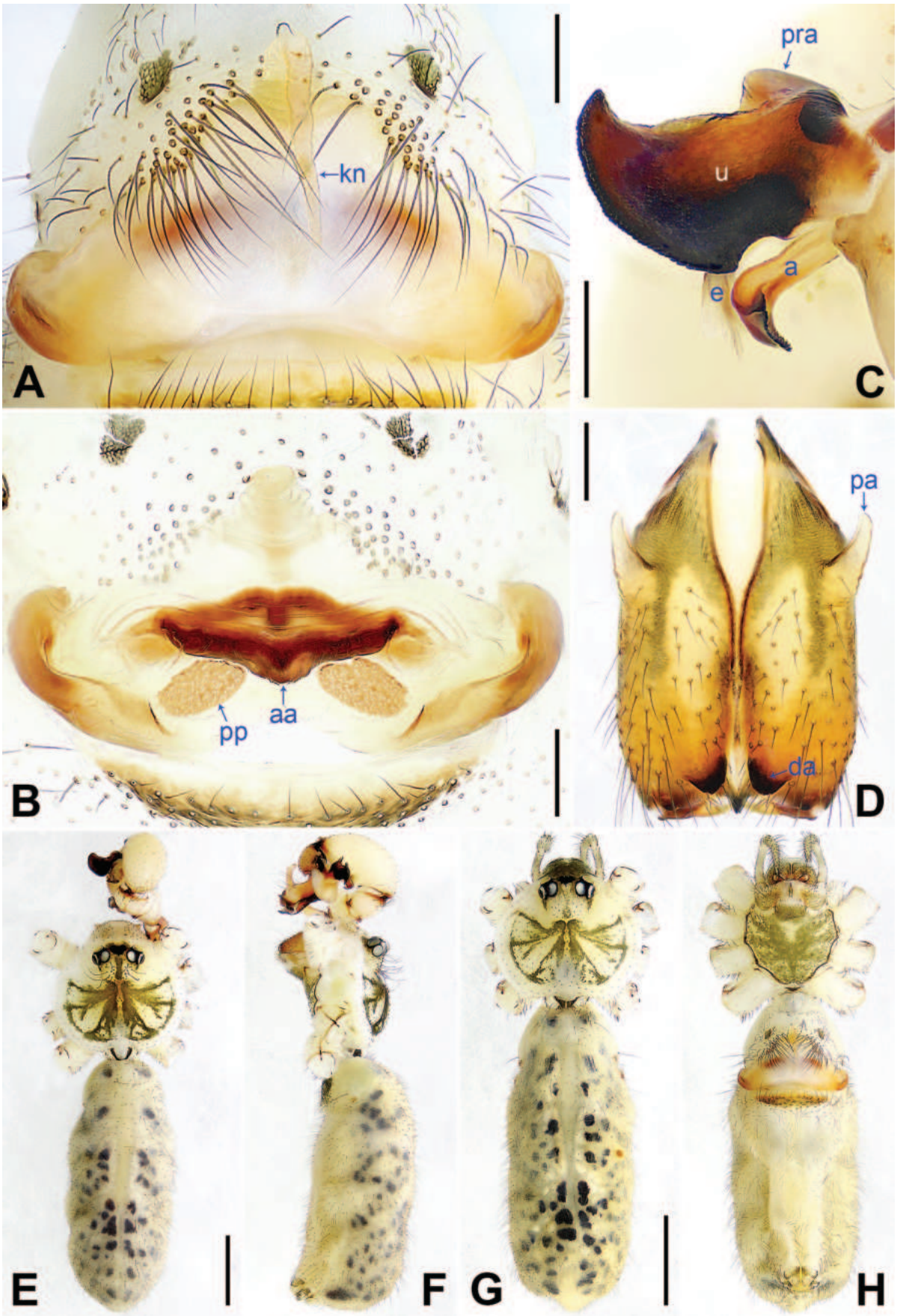

Figure 3. *Pholcus jiaozuo* sp. nov., holotype male (**C–F**) and paratype female (**A, B, G, H**) **A.** Epigyne, ventral view; **B.** Vulva, dorsal view; **C.** Bulbal apophyses, prolateral view; **D.** Chelicerae, frontal view; **E–H.** Habitus (**E, G.** Dorsal view; **F.** Lateral view; **H.** Ventral view). Scale bars: 0.20 mm (**A–D**); 1.00 mm (**E–H**).

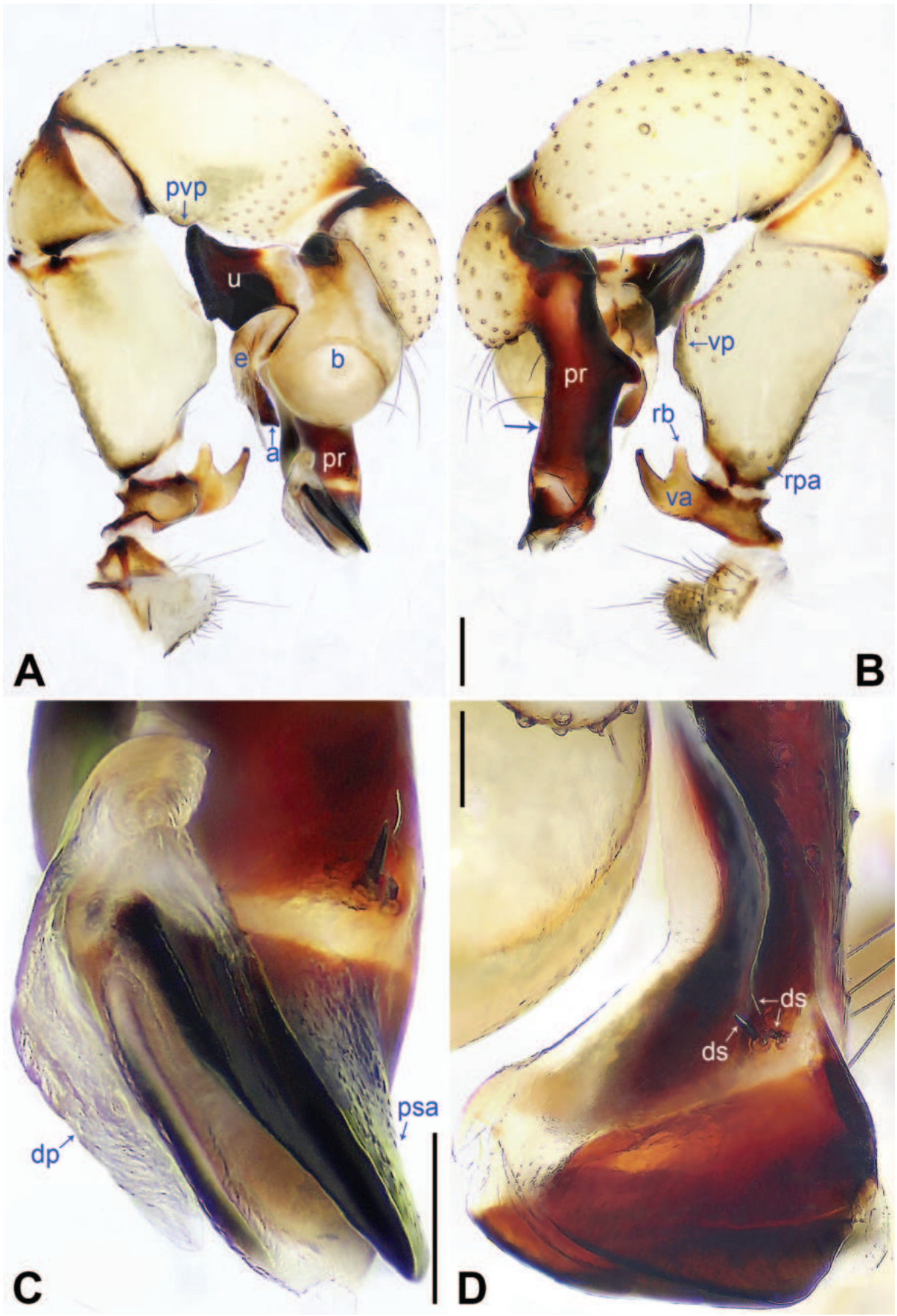

Figure 4. *Pholcus luonan* sp. nov., holotype male **A, B.** Palp (**A.** Prolateral view; **B.** Retrolateral view, arrow points at dorso-median part of procursus); **C, D.** Distal part of procursus (**C.** Prolateral view; **D.** Dorsal view). Scale bars: 0.20 mm (**A, B**); 0.10 mm (**C, D**).

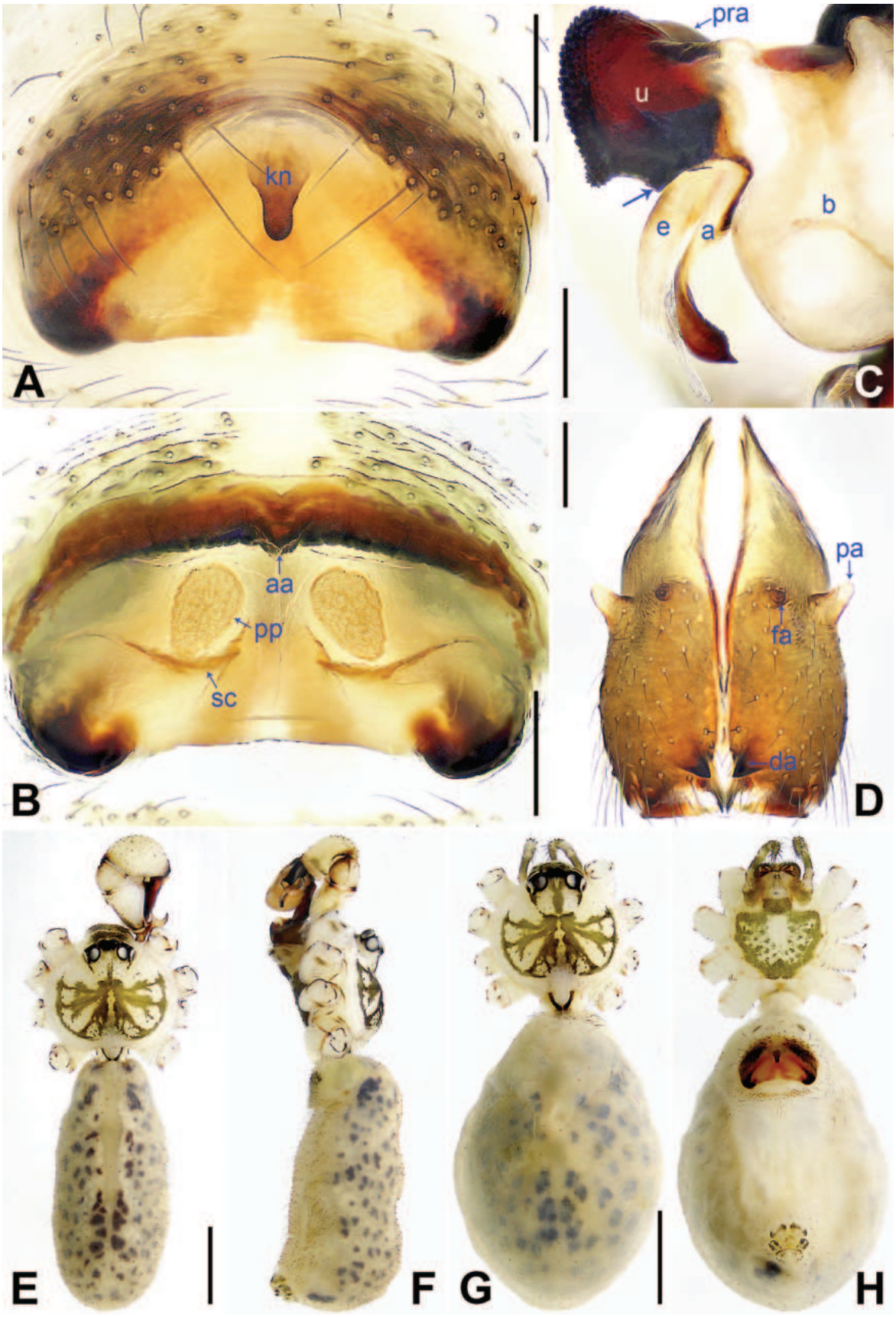

Figure 5. *Pholcus luonan* sp. nov., holotype male (**C–F**) and paratype female (**A, B, G, H**) **A.** Epigyne, ventral view; **B.** Vulva, dorsal view; **C.** Bulbal apophyses, prolateral view (arrow points at latero-median protrusion); **D.** Chelicerae, frontal view; **E–H.** Habitus (**E, G.** Dorsal view; **F.** Lateral view; **H.** Ventral view). Scale bars: 0.20 mm (**A–D**); 1.00 mm (**E–H**).

22A–H) by having similar male chelicerae and epigyne (Fig. 5A, D), but can be distinguished by dorso-median part of procursus not protruding (Fig. 4B vs. protruding), by male palpal trochanteral apophysis with distinct retrolateral branch (Fig. 4B vs. indistinct projection), by uncus latero-medially strongly protruding (Fig. 5C vs. latero-proximally slightly protruding), by appendix without branch (Fig. 5C vs. present) and by vulval pore plates nearly elliptic (anteriorly wide and posteriorly narrow, Fig. 5B vs. nearly round).

Description. Male (***holotype***). Total length 4.92 (5.06 with clypeus), carapace 1.56 long, 1.78 wide, opisthosoma 3.36 long, 1.56 wide. Legs I and II missing, leg III: 17.78 (5.19, 0.61, 4.10, 6.80, 1.08), leg IV: 24.87 (7.92, 0.65, 5.83, 9.12, 1.35). Eye interdistances and diameters: PME–PME 0.26, PME 0.17, PME–ALE 0.06, AME–AME 0.06, AME 0.12. Sternum width/length: 1.16/0.94. Habitus as in Fig. 5E, F. Carapace yellowish, with brown radiating marks and marginal brown bands; ocular area yellowish, with median and lateral brown bands; clypeus brown; sternum yellowish, with brown marks. Legs yellowish, but dark brown on patellae and whitish on distal parts of femora and tibiae, with darker rings on subdistal parts of femora and proximal and subdistal parts of tibiae. Opisthosoma yellowish, with dorsal and lateral spots. Chelicerae (Fig. 5D) with pair of proximo-lateral apophyses, pair of distal apophyses with two teeth each and pair of frontal apophyses. Palp as in Fig. 4A, B; trochanter with long (3 times longer than wide) ventral apophysis bearing distinct retrolateral branch; femur with small retrolatero-proximal apophysis and distinct ventral protuberance; tibia with prolatero-ventral protuberance; procursus (Fig. 4C, D) simple proximally, but complex distally, with raised prolatero-subdistal membranous edge bearing distal membranous process, sclerotised prolatero-subdistal apophysis and two strong and one slender dorsal spines; uncus (Fig. 5C) latero-medially protruding, with proximal apophysis and distal scaly edge; appendix (Fig. 5C) curved, with distal scales; embolus (Fig. 5C) weakly sclerotised, with some indistinct transparent distal projections. Legs with short vertical setae on tibiae, metatarsi and tarsi.

Female (***paratype***). Similar to male, habitus as in Fig. 5G, H. Total length 4.70 (4.80 with clypeus), carapace 1.38 long, 1.45 wide, opisthosoma 3.32 long, 2.31 wide; tibia I: 6.04; tibia I L/d: 48. Eye interdistances and diameters: PME–PME 0.23, PME 0.15, PME–ALE 0.05, AME–AME 0.06, AME 0.11. Sternum width/length: 0.96/0.78. Epigyne (Fig. 5A) nearly triangular, laterally strongly sclerotised, with knob (distally narrowed). Vulva (Fig. 5B) with laterally strongly curved, sclerotised anterior arch, pair of nearly elliptic pore plates (anteriorly wide and posteriorly narrow) and pair of wavy sclerites.

Variation. Tibia I in paratype male: 8.75; tibia I L/d: 58. Retrolateral trichobothrium on tibia I at 6% proximally; tarsus I with 31 distinct pseudosegments. Leg I missing in another female paratype.

Habitat. Underside of overhang on rocky cliffs in the mountain area.

Distribution. China (Shaanxi, type locality; Fig. 1).

Pholcus luoyang Yang & Yao, sp. nov.

https://zoobank.org/4EF6B12F-2ADC-42CF-A45A-E3172BC7D3D7

Figs 6, 7

Type material. ***Holotype*** ♂ (SYNU-Ar00373) and ***paratypes*** 2♂ (SYNU-Ar00374, IAECAS-Ar00375Y) 2♀ (SYNU-Ar00376, IAECAS-Ar00377Y), **China**, **Henan**, Luoyang, Luanchuan County, Jiaohe Town, Tianhe Grand Canyon Scenic Spot (33°49.43'N, 111°18.82'E, 1140 m elev.), 18/07/2022.

Etymology. The specific name refers to the type locality and is a noun in apposition.

Diagnosis. The new species resembles *P. songxian* Zhang & Zhu, 2009 (Yao and Li 2012: 32, figs 159A–D, 160A–C) by having similar male chelicerae and epigyne (Fig. 7A, D), but can be distinguished by prolatero-distal apophysis of procursus curved (Fig. 6C vs. flat), by uncus narrow, distally pointed (Fig. 7C vs. wide, distally blunt), by appendix with subdistal branch (Fig. 7C vs. median branch), by vulval anterior arch medially sclerotised (Fig. 7B vs. entirely sclerotised) and by vulval pore plates long elliptic (length/width ratio: 5, Fig. 7B vs. elliptic and length/width ratio: 2).

Description. Male (***holotype***). Total length 4.44 (4.55 with clypeus), carapace 1.41 long, 1.66 wide, opisthosoma 3.03 long, 1.34 wide. Leg I: 34.83 (8.95, 0.69, 8.85, 14.10, 2.24), leg II: 23.67 (6.75, 0.66, 5.76, 9.04, 1.46), leg III: 15.75 (4.95, 0.61, 3.95, 5.10, 1.14), leg IV: 22.22 (6.65, 0.62, 5.65, 7.95, 1.35); tibia I L/d: 63. Eye interdistances and diameters: PME–PME 0.20, PME 0.16, PME–ALE 0.04, AME–AME 0.05, AME 0.11. Sternum width/length: 1.06/0.81. Habitus as in Fig. 7E, F. Carapace yellowish, with brown radiating marks and marginal brown bands; ocular area yellowish, with median and lateral brown bands; clypeus brown; sternum yellowish, with brown marks. Legs yellowish, but dark brown on patellae and whitish on distal parts of femora and tibiae, with darker rings on subdistal parts of femora and proximal and subdistal parts of tibiae. Opisthosoma yellowish, with dorsal and lateral spots. Chelicerae (Fig. 7D) with pair of proximo-lateral apophyses, pair of distal apophyses with two teeth each and pair of frontal apophyses. Palp as in Fig. 6A, B; trochanter with long (4 times longer than wide) ventral apophysis bearing retrolatero-distal branch; femur with small retrolatero-proximal apophysis and distinct ventral protuberance; tibia with prolatero-ventral protuberance; procursus (Fig. 6C, D) simple proximally, but complex distally, with raised prolatero-subdistal membranous edge bearing distal membranous process, curved sclerotised prolatero-distal

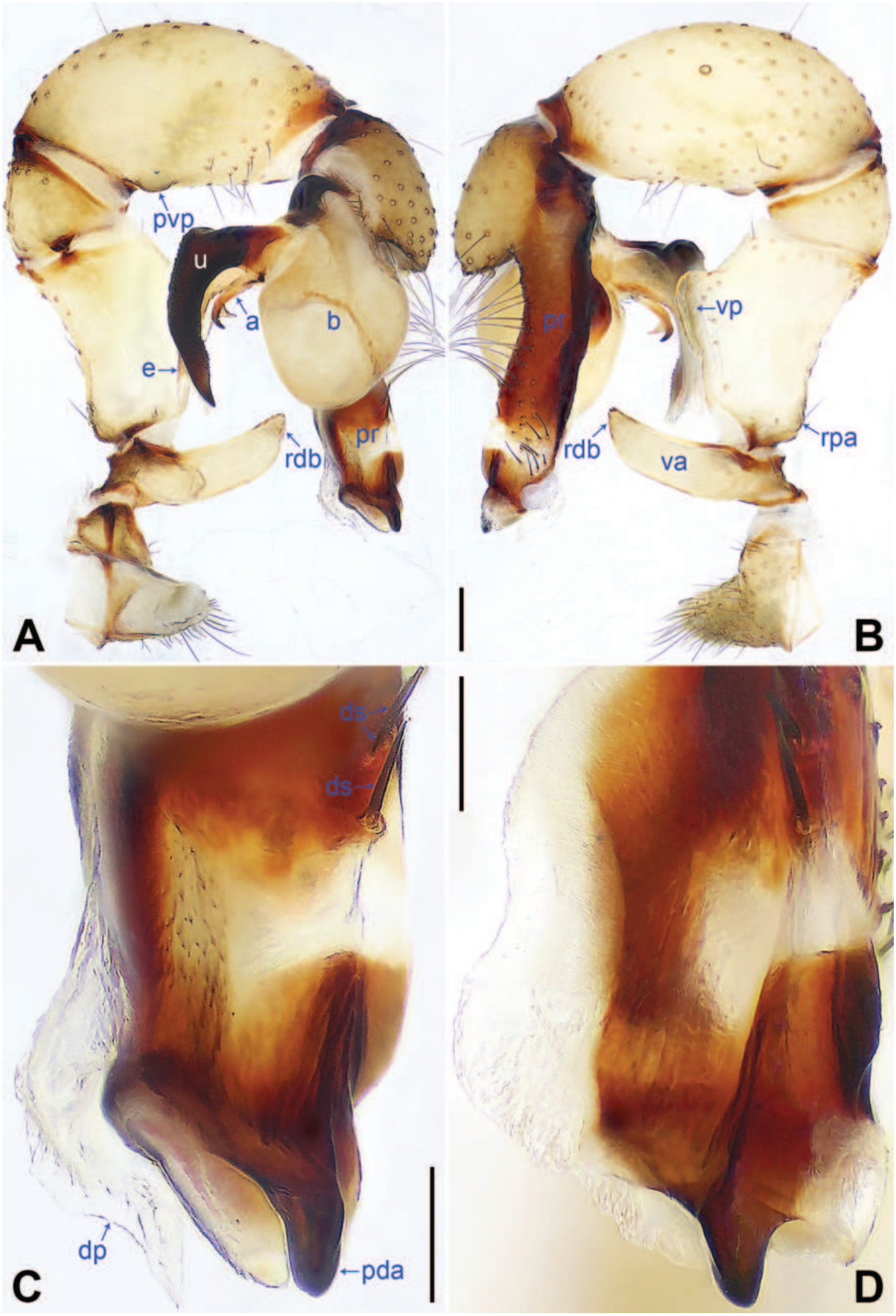

Figure 6. *Pholcus luoyang* sp. nov., holotype male **A, B.** Palp (**A.** Prolateral view; **B.** Retrolateral view); **C, D.** Distal part of procursus (**C.** Prolateral view; **D.** Dorsal view). Scale bars: 0.20 mm (**A, B**); 0.10 mm (**C, D**).

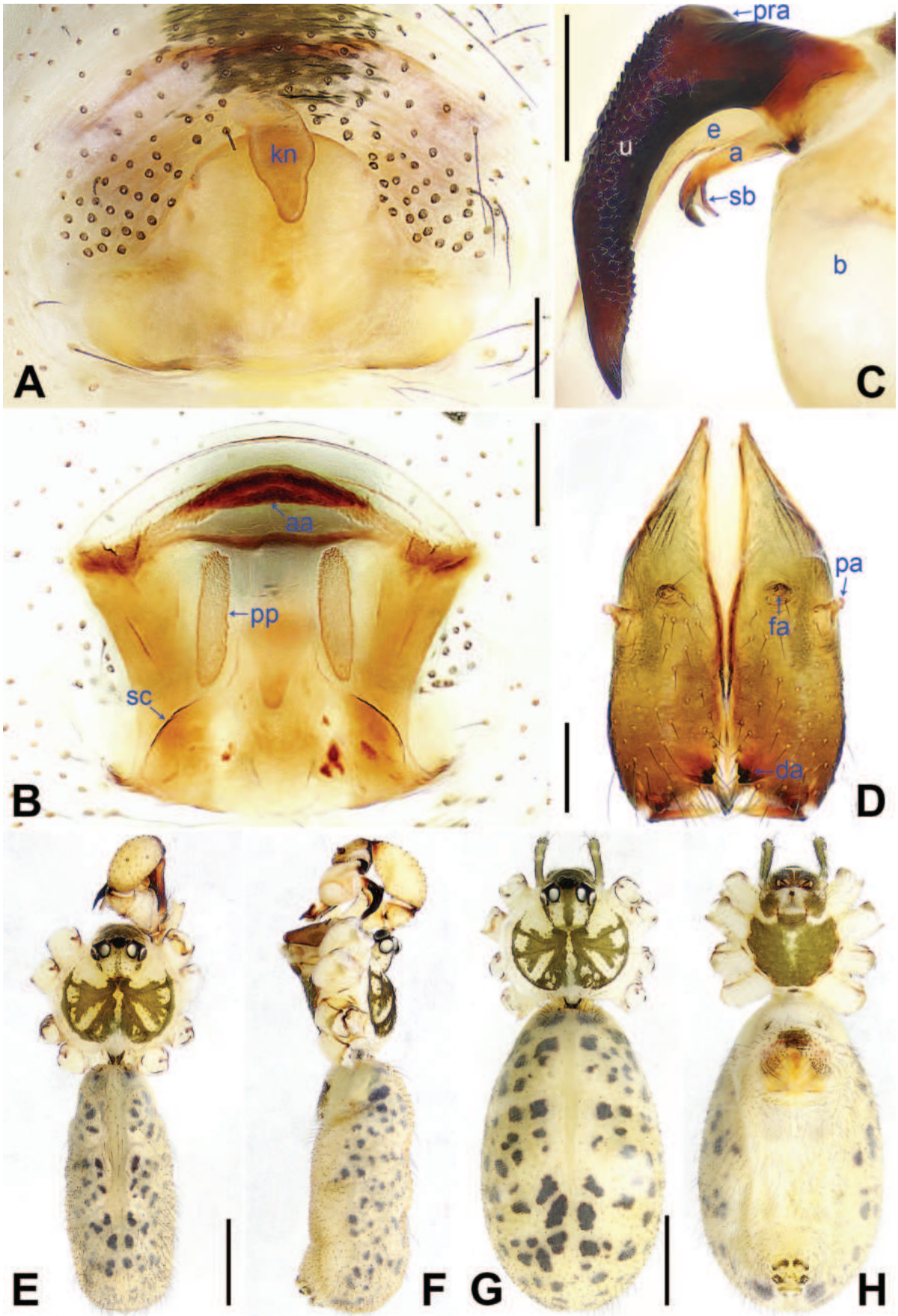

Figure 7. *Pholcus luoyang* sp. nov., holotype male (**C–F**) and paratype female (**A, B, G, H**) **A.** Epigyne, ventral view; **B.** Vulva, dorsal view; **C.** Bulbal apophyses, prolateral view; **D.** Chelicerae, frontal view; **E–H.** Habitus (**E, G.** Dorsal view; **F.** Lateral view; **H.** Ventral view). Scale bars: 0.20 mm (**A–D**); 1.00 mm (**E–H**).

apophysis and two strong and one slender dorsal spines; uncus (Fig. 7C) narrow, distally pointed, with proximal apophysis and scales; appendix (Fig. 7C) hooked, with angular subdistal branch; embolus (Fig. 7C) weakly sclerotised, with some indistinct transparent distal projections. Retrolateral trichobothrium on tibia I at 5% proximally; legs with short vertical setae on tibiae, metatarsi and tarsi; tarsus I with 38 distinct pseudosegments.

Female (***paratype***). Similar to male, habitus as in Fig. 7G, H. Total length 5.00 (5.13 with clypeus), carapace 1.48 long, 1.64 wide, opisthosoma 3.52 long, 2.23 wide; tibia I: 7.05; tibia I L/d: 47. Eye interdistances and diameters: PME–PME 0.20, PME 0.15, PME–ALE 0.04, AME–AME 0.05, AME 0.09. Sternum width/length: 1.03/0.78. Epigyne (Fig. 7A) nearly trapezoid, slightly sclerotised, with wedge-shaped knob. Vulva (Fig. 7B) with curved, medially sclerotised anterior arch, pair of long elliptic pore plates and pair of posterior sclerites.

Variation. Tibia I in two paratype males: 8.78, 9.95. Tibia I in another paratype female: 7.10.

Habitat. Underside of overhang on rocky cliffs in the mountain area.

Distribution. China (Henan, type locality; Fig. 1).

Pholcus lushan Yang & Yao, sp. nov.

https://zoobank.org/E2C38327-FB2F-44E8-AADA-48C370724414

Figs 8, 9

Type material. ***Holotype*** ♂ (SYNU-Ar00378) and ***paratypes*** 1♂ (IAECAS-Ar00379Y) 2♀ (SYNU-Ar00380, IAECAS-Ar00381Y), **China**, **Henan**, Pingdingshan, Lushan County (33°46.72'N, 112°16.03'E, 743 m elev.), 17/07/2022.

Etymology. The specific name refers to the type locality and is a noun in apposition.

Diagnosis. The new species resembles *P. parayichengicus* Zhang & Zhu, 2009 (Yao and Li 2012: 29, figs 140A–D, 141A–C) by having similar male chelicerae and epigyne (Fig. 9A, D), but can be distinguished by distal membranous process of procursus wide (Fig. 8C vs. narrow), by ventro-subdistal apophysis of procursus spine-shaped (Fig. 8C vs. hooked), uncus latero-medially strongly protruding (Fig. 9C vs. latero-proximally slightly protruding) and by vulval anterior arch nearly half-round and posteriorly sclerotised (Fig. 9B vs. crescent-shaped and entirely sclerotised).

Description. Male (***holotype***). Total length 5.06 (5.19 with clypeus), carapace 1.54 long, 1.73 wide, opisthosoma 3.52 long, 1.43 wide. Leg I: 38.44 (9.81, 0.69, 9.60, 15.96, 2.38), leg II: 26.47 (7.44, 0.64, 6.47, 10.32, 1.60), leg III: 18.94 (5.58, 0.60, 4.55, 6.99, 1.22), leg IV: 26.04 (7.29, 0.62, 6.41, 10.26, 1.46); tibia I L/d: 60. Eye interdistances and diameters: PME–PME 0.23, PME 0.16, PME–ALE 0.06, AME–AME 0.05, AME 0.10. Sternum width/length: 1.10/0.88. Habitus as in Fig. 9E, F. Carapace yellowish, with brown radiating marks and marginal brown bands; ocular area yellowish, with lateral brown bands; clypeus brown; sternum yellowish, with brown marks. Legs yellowish, but dark brown on patellae and whitish on distal parts of femora and tibiae, with darker rings on subdistal parts of femora and proximal and subdistal parts of tibiae. Opisthosoma yellowish, with dorsal and lateral spots. Chelicerae (Fig. 9D) with pair of proximo-lateral apophyses, pair of distal apophyses with two teeth each and pair of frontal apophyses. Palp as in Fig. 8A, B; trochanter with long (4 times longer than wide), retrolaterally strongly bulged ventral apophysis; femur with small retrolatero-proximal apophysis and distinct ventral protuberance; tibia with prolatero-ventral protuberance; procursus (Fig. 8C, D) simple proximally, but complex distally, with raised prolatero-subdistal membranous edge bearing distal membranous process, sclerotised prolatero-subdistal apophysis, sclerotised retrolatero-distal apophysis, spine-shaped ventro-subdistal apophysis and three strong and one slender dorsal spines; uncus (Fig. 9C) latero-medially protruding, with proximal apophysis and distal scaly edge; appendix (Fig. 9C) hooked, with angular median branch; embolus (Fig. 9C) weakly sclerotised, with some indistinct transparent distal projections. Retrolateral trichobothrium on tibia I at 6% proximally; legs with short vertical setae on tibiae, metatarsi and tarsi; tarsus I with 42 distinct pseudosegments.

Female (***paratype***). Similar to male, habitus as in Fig. 9G, H. Total length 4.60 (4.75 with clypeus), carapace 1.47 long, 1.62 wide, opisthosoma 3.13 long, 1.58 wide; tibia I: 7.45; tibia I L/d: 47. Eye interdistances and diameters: PME–PME 0.22, PME 0.15, PME–ALE 0.06, AME–AME 0.04, AME 0.08. Sternum width/length: 1.05/0.73. Ocular area with median and lateral brown bands. Epigyne (Fig. 9A) nearly trapezoid, laterally strongly sclerotised, with wedge-shaped knob. Vulva (Fig. 9B) with nearly half-round, posteriorly sclerotised anterior arch and pair of anteriorly blunt and posteriorly pointed pore plates.

Variation. Leg I missing in paratype male. Tibia I in another paratype female: 7.30.

Habitat. Underside of overhang on rocky cliffs in the mountain area.

Distribution. China (Henan, type locality; Fig. 1).

Pholcus shangluo Yang & Yao, sp. nov.

https://zoobank.org/5BC2B733-B7D9-46A3-8A97-0F807A231E99

Figs 10, 11

Type material. ***Holotype*** ♂ (SYNU-Ar00382) and ***paratypes*** 1♂ (IAECAS-Ar00383Y) 3♀ (SYNU-Ar00384–85, IAECAS-Ar00386Y), **China**, **Shaanxi**, Shangluo, Zhashui County, Jiutianshan Scenic Spot (33°36.93'N, 109°8.45'E, 878 m elev.), 22/07/2022.

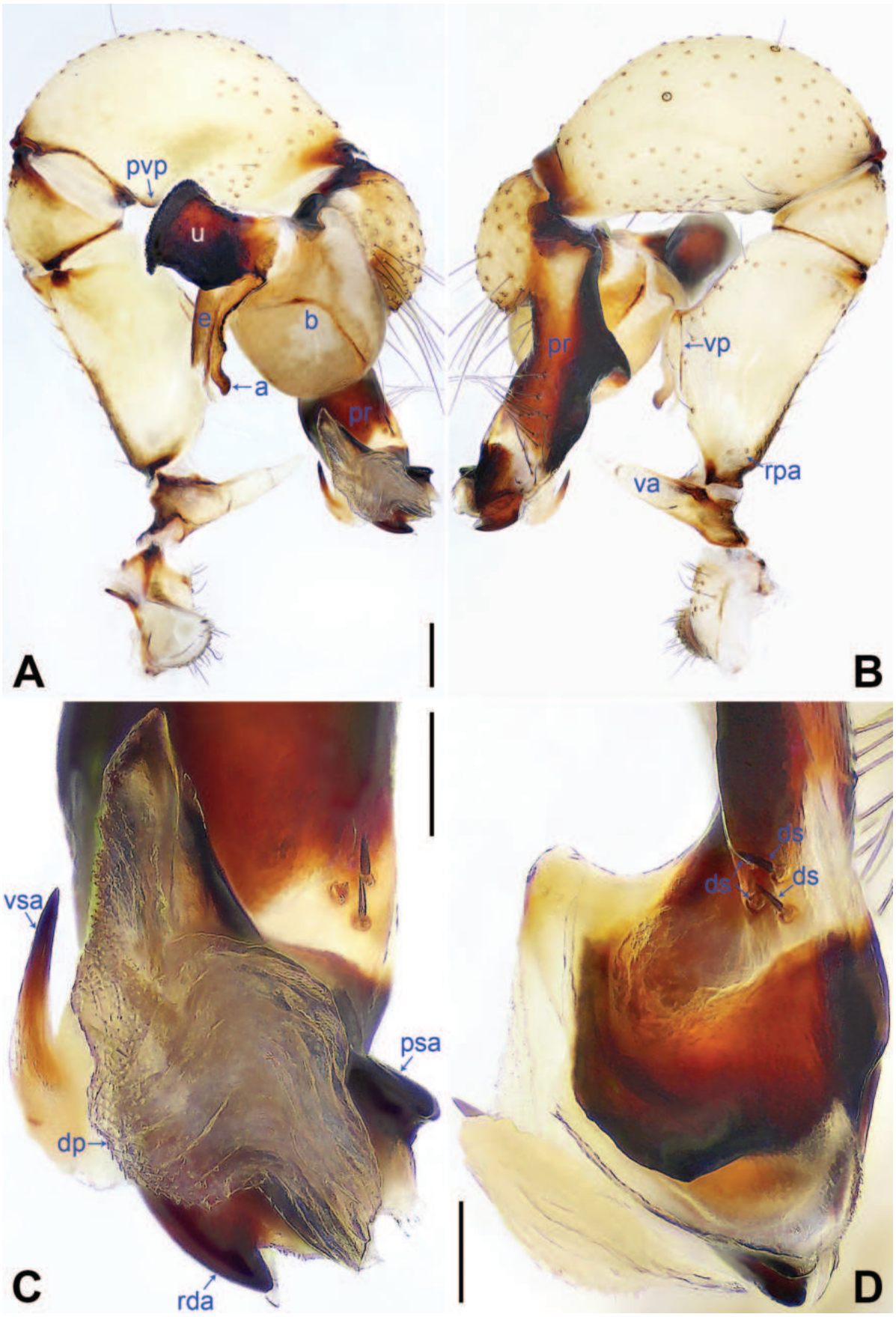

Figure 8. *Pholcus lushan* sp. nov., holotype male **A, B.** Palp (**A.** Prolateral view; **B.** Retrolateral view); **C, D.** Distal part of procursus (**C.** Prolateral view; **D.** Dorsal view). Scale bars: 0.20 mm (**A, B**); 0.10 mm (**C, D**).

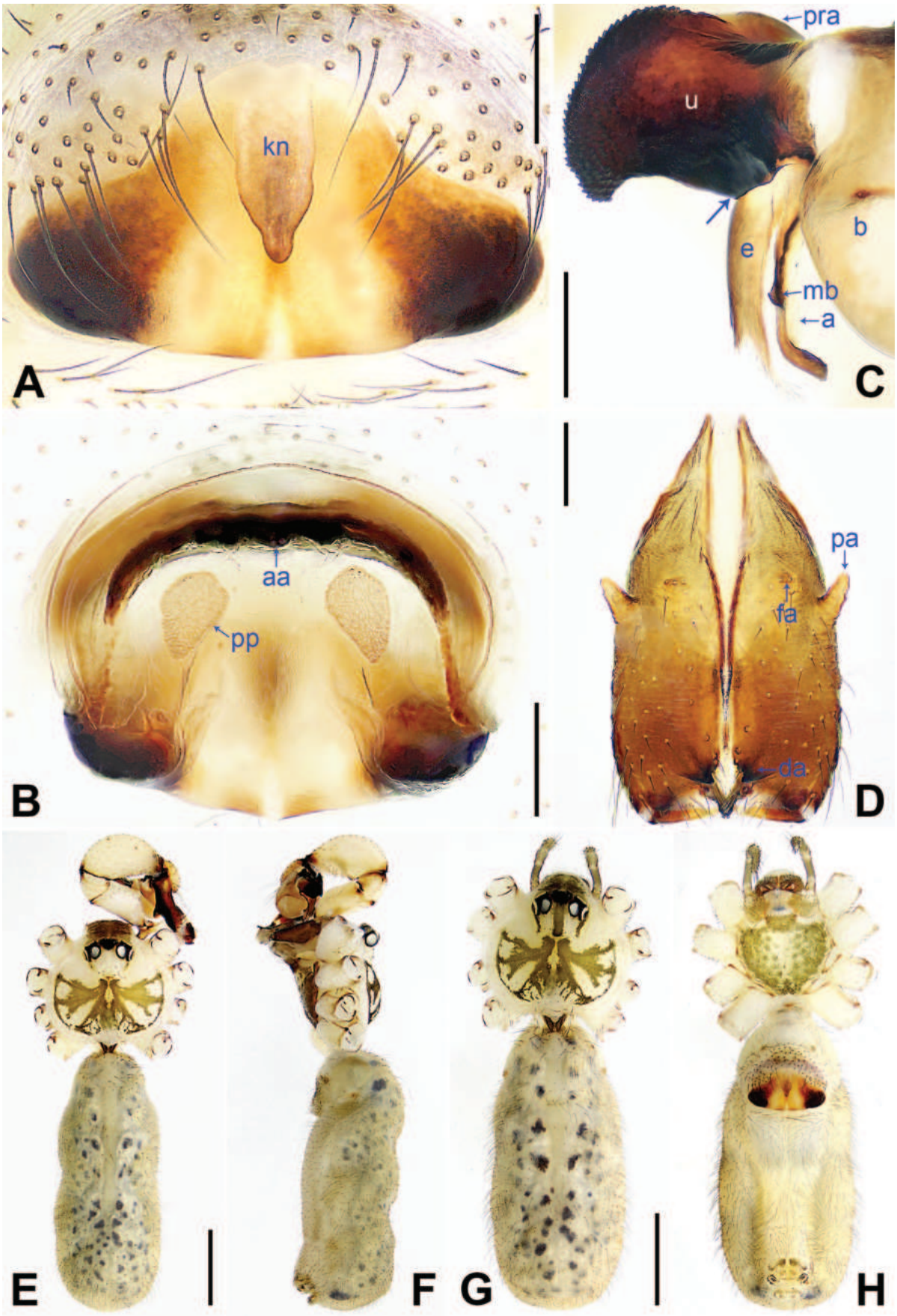

Figure 9. *Pholcus lushan* sp. nov., holotype male (**C–F**) and paratype female (**A, B, G, H**) **A.** Epigyne, ventral view; **B.** Vulva, dorsal view; **C.** Bulbal apophyses, prolateral view (arrow points at latero-median protrusion); **D.** Chelicerae, frontal view; **E–H.** Habitus (**E, G.** Dorsal view; **F.** Lateral view; **H.** Ventral view). Scale bars: 0.20 mm (**A–D**); 1.00 mm (**E–H**).

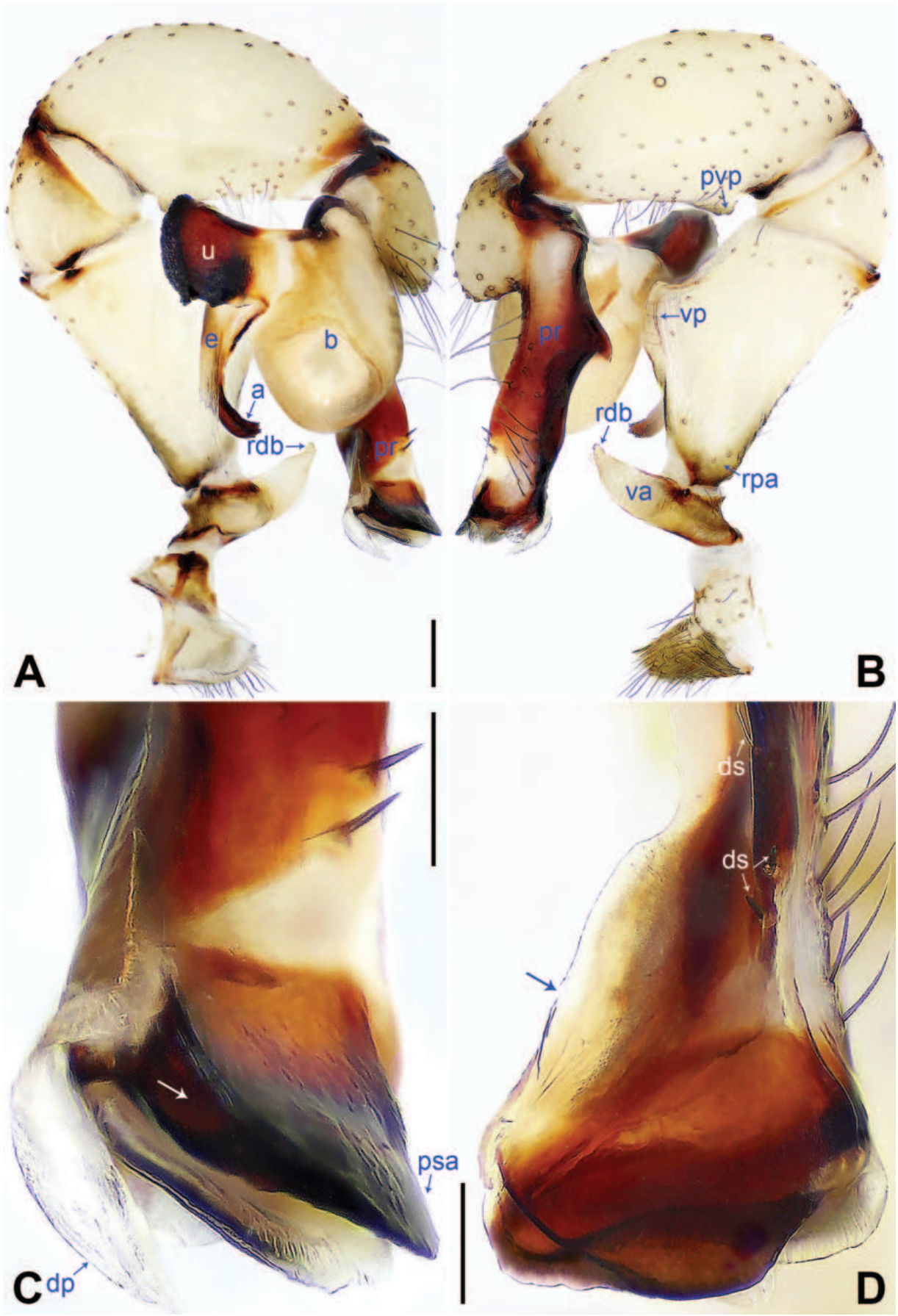

Figure 10. *Pholcus shangluo* sp. nov., holotype male **A, B.** Palp (**A.** Prolateral view; **B.** Retrolateral view); **C, D.** Distal part of procursus (**C.** Prolateral view, arrow points at thick part; **D.** Dorsal view, arrow points at straight part). Scale bars: 0.20 mm (**A, B**); 0.10 mm (**C, D**).

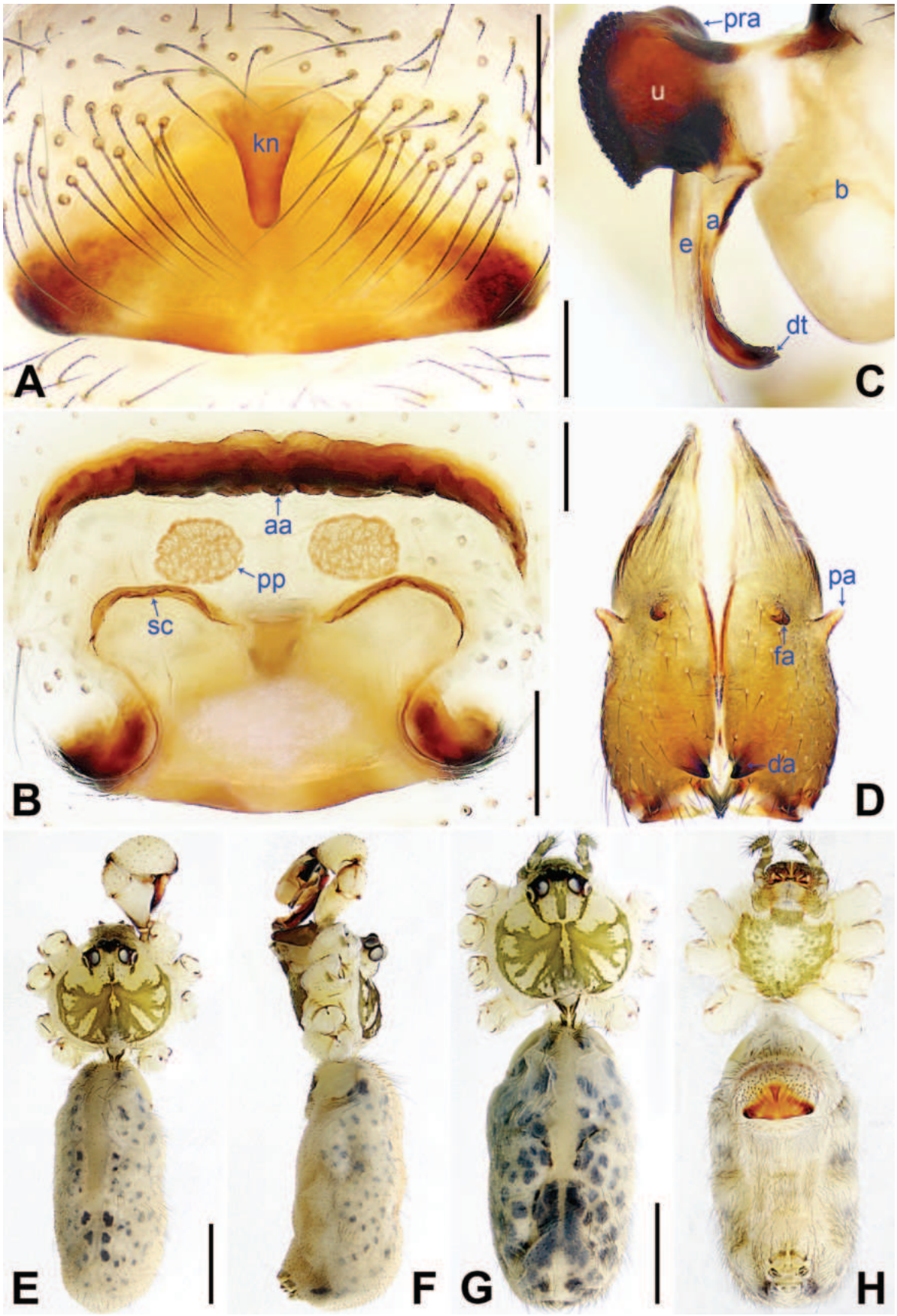

Figure 11. *Pholcus shangluo* sp. nov., holotype male (**C–F**) and paratype female (**A, B, G, H**) **A.** Epigyne, ventral view; **B.** Vulva, dorsal view; **C.** Bulbal apophyses, prolateral view; **D.** Chelicerae, frontal view; **E–H.** Habitus (**E, G.** Dorsal view; **F.** Lateral view; **H.** Ventral view). Scale bars: 0.20 mm (**A–D**); 1.00 mm (**E–H**).

Etymology. The specific name refers to the type locality and is a noun in apposition.

Diagnosis. The new species resembles *P. huberi* Zhang & Zhu, 2009 (Yao and Li 2012: 19, figs 83A–D, 84A–C) by having similar male chelicerae, uncus and epigyne (Fig. 11A, C, D), but can be distinguished by prolatero-subdistal apophysis of procursus proximally thick (Fig. 10C vs. thin), by prolatero-subdistal membranous edge of procursus laterally straight (Fig. 10D vs. latero-medially strongly curved), by male palpal trochanteral apophysis with retrolatero-distal branch (Fig. 10A, B vs. male palpal trochanteral apophysis retrolatero-medially strongly bulged, with retrolatero-median branch), by appendix with distal teeth (Fig. 11C vs. absent) and by vulval anterior arch laterally strongly curved (Fig. 11B vs. C-shaped).

Description. Male (***holotype***). Total length 4.68 (4.90 with clypeus), carapace 1.44 long, 1.66 wide, opisthosoma 3.24 long, 1.50 wide. Leg I: 36.43 (9.55, 0.73, 9.05, 14.74, 2.36), leg II: 24.19 (7.05, 0.68, 5.95, 9.17, 1.34), leg III: 17.65 (5.15, 0.62, 4.20, 6.60, 1.08), leg IV: 23.71 (6.90, 0.65, 5.83, 9.05, 1.28); tibia I L/d: 60. Eye interdistances and diameters: PME–PME 0.24, PME 0.17, PME–ALE 0.06, AME–AME 0.07, AME 0.12. Sternum width/length: 1.08/0.86. Habitus as in Fig. 11E, F. Carapace yellowish, with brown radiating marks and marginal brown bands; ocular area yellowish, with median and lateral brown bands; clypeus brown; sternum yellowish, with brown marks. Legs yellowish, but dark brown on patellae and whitish on distal parts of femora and tibiae, with darker rings on subdistal parts of femora and proximal and subdistal parts of tibiae. Opisthosoma yellowish, with dorsal and lateral spots. Chelicerae (Fig. 11D) with pair of proximo-lateral apophyses, pair of distal apophyses with two teeth each and pair of frontal apophyses. Palp as in Fig. 10A, B; trochanter with long (3 times longer than wide) ventral apophysis bearing retrolatero-distal branch; femur with small retrolatero-proximal apophysis and distinct ventral protuberance; tibia with prolatero-ventral protuberance; procursus (Fig. 10C, D) simple proximally, but complex distally, with raised prolatero-subdistal membranous edge bearing distal membranous process, sclerotised prolatero-subdistal apophysis and two strong and one slender dorsal spines; uncus (Fig. 11C) with proximal apophysis and distal scaly edge; appendix (Fig. 11C) curved, with distal teeth; embolus (Fig. 11C) weakly sclerotised, with some indistinct transparent distal projections. Retrolateral trichobothrium on tibia I at 5% proximally; legs with short vertical setae on tibiae, metatarsi and tarsi; tarsus I with 36 distinct pseudosegments.

Female (***paratype***). Similar to male, habitus as in Fig. 11G, H. Total length 4.35 (4.52 with clypeus), carapace 1.38 long, 1.53 wide, opisthosoma 2.97 long, 1.58 wide; tibia I: 7.45; tibia I L/d: 53. Eye interdistances and diameters: PME–PME 0.19, PME 0.15, PME–ALE 0.05, AME–AME 0.05, AME 0.11. Sternum width/length: 1.02/0.80. Epigyne (Fig. 11A) nearly triangular, laterally strongly sclerotised, with cone-shaped knob. Vulva (Fig. 11B) with laterally strongly curved, sclerotised anterior arch, pair of nearly round pore plates and pair of C-shaped sclerites.

Variation. Tibia I in paratype male: 9.15. Tibia I in the other two paratype females: 7.15, 7.60.

Habitat. Underside of overhang on rocky cliffs in the mountain area.

Distribution. China (Shaanxi, type locality; Fig. 1).

Pholcus weinan Yang & Yao, sp. nov.

https://zoobank.org/A06698F6-1451-4E17-A61E-AB7559B2C6D1

Figs 12, 13

Type material. ***Holotype*** ♂ (SYNU-Ar00387) and ***paratypes*** 1♂ (IAECAS-Ar00388Y) 3♀ (SYNU-Ar00389–90, IAECAS-Ar00391Y), **China**, **Shaanxi**, Weinan, Tongguan County, Kuishudian Village (34°24.17'N, 110°17.05'E, 1214 m elev.), 20/07/2022.

Etymology. The specific name refers to the type locality and is a noun in apposition.

Diagnosis. The new species resembles *P. parayichengicus* Zhang & Zhu, 2009 (Yao and Li 2012: 29, figs 140A–D, 141A–C) by having similar male chelicerae, bulbal apophyses and epigyne (Fig. 13A, C, D), but can be distinguished by procursus without distal apophysis (Fig. 12C vs. with angular distal apophysis), by male palpal trochanteral apophysis without retrolateral branch (Fig. 12B vs. present), by epigynal knob column-shaped (Fig. 13A vs. wedge-shaped), by vulval anterior arch eyebrow-shaped (Fig. 13B vs. crescent-shaped) and by vulval pore plates elliptic (Fig. 13B vs. anteriorly wide and posteriorly narrow).

Description. Male (***holotype***). Total length 5.44 (5.58 with clypeus), carapace 1.76 long, 1.98 wide, opisthosoma 3.68 long, 1.80 wide. Leg I: – (10.32, 0.79, 10.19, 17.18, –), leg II: 28.79 (7.80, 0.77, 7.15, 11.54, 1.53), leg III: 20.78 (5.83, 0.68, 5.13, 8.01, 1.13), leg IV: 27.10 (7.75, 0.70, 6.95, 10.32, 1.38); tibia I L/d: 58. Eye interdistances and diameters: PME–PME 0.26, PME 0.13, PME–ALE 0.05, AME–AME 0.07, AME 0.11. Sternum width/length: 1.28/0.94. Habitus as in Fig. 13E, F. Carapace yellowish, with brown radiating marks and marginal brown bands; ocular area yellowish, with lateral brown bands; clypeus brown; sternum yellowish, with brown marks. Legs yellowish, but dark brown on patellae and whitish on distal parts of femora and tibiae, with darker rings on subdistal parts of femora and proximal and subdistal parts of tibiae. Opisthosoma yellowish, with dorsal and lateral spots. Chelicerae (Fig. 13D) with pair of proximo-lateral apophyses, pair of distal apophyses with two teeth each and pair of frontal apophyses. Palp as in Fig. 12A, B; trochanter with long (4 times longer than wide), retrolatero-proximally

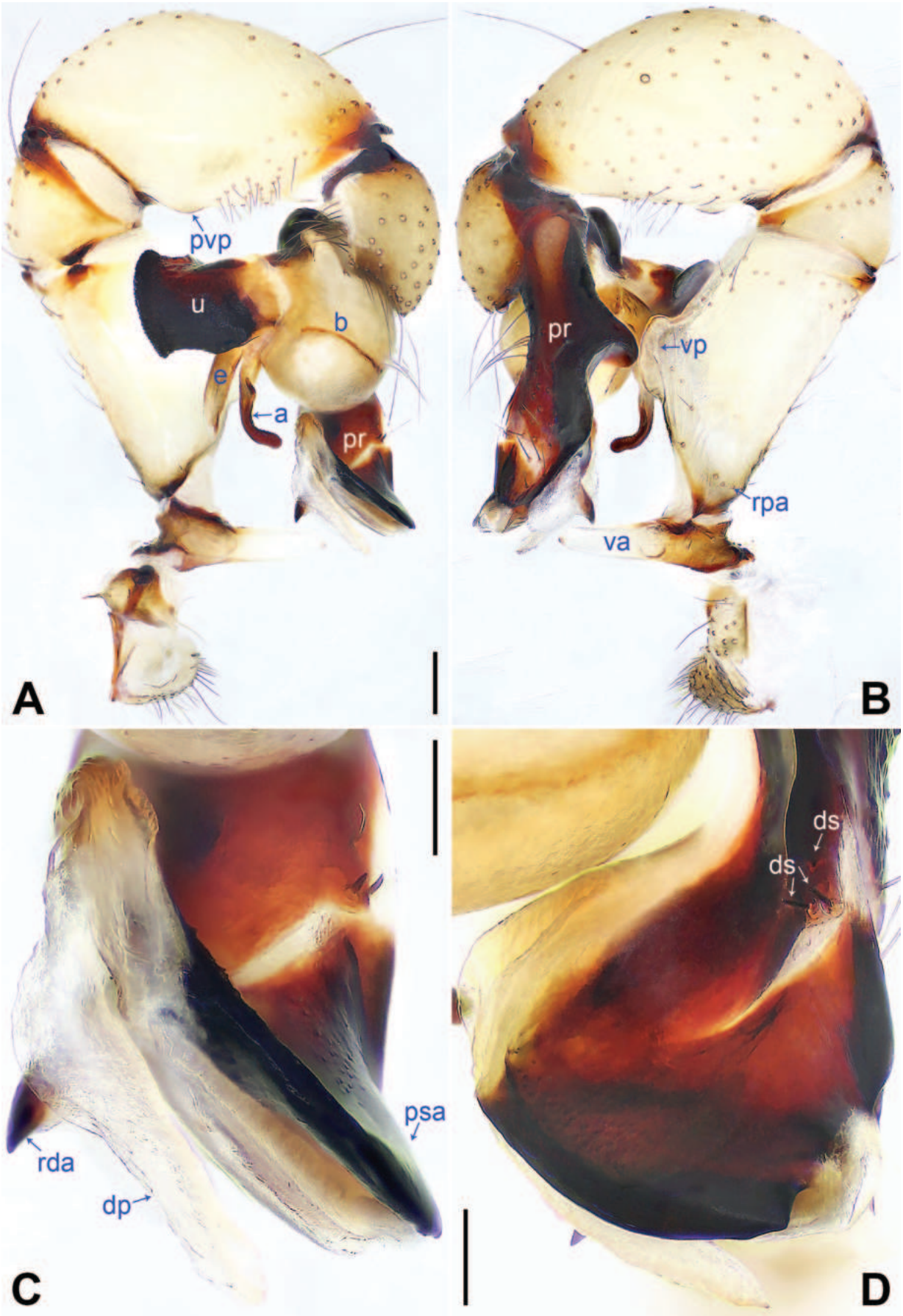

Figure 12. *Pholcus weinan* sp. nov., holotype male **A, B.** Palp (**A.** Prolateral view; **B.** Retrolateral view); **C, D.** Distal part of procursus (**C.** Prolateral view; **D.** Dorsal view). Scale bars: 0.20 mm (**A, B**); 0.10 mm (**C, D**).

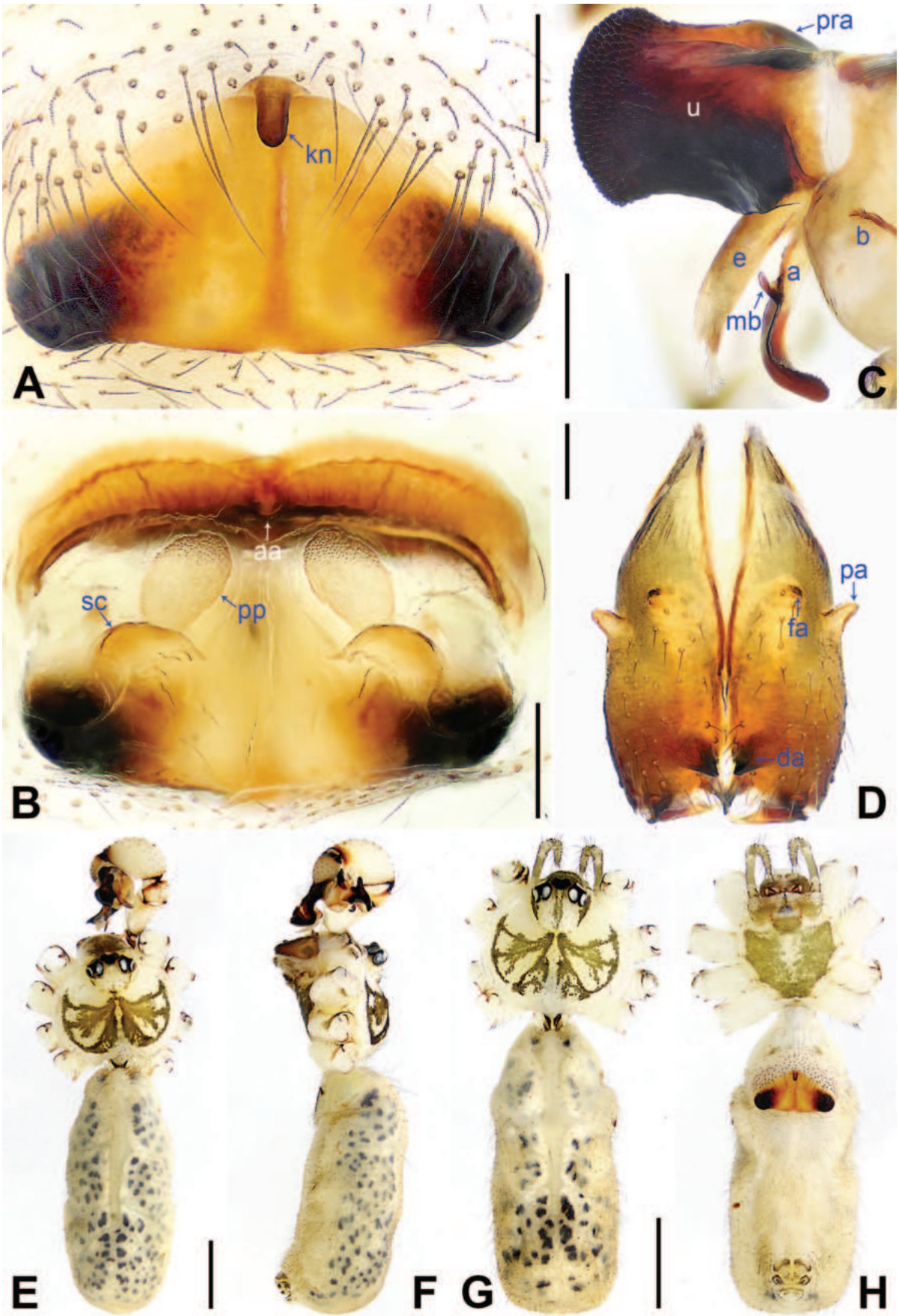

Figure 13. *Pholcus weinan* sp. nov., holotype male (**C–F**) and paratype female (**A, B, G, H**) **A.** Epigyne, ventral view; **B.** Vulva, dorsal view; **C.** Bulbal apophyses, prolateral view; **D.** Chelicerae, frontal view; **E–H.** Habitus (**E, G.** Dorsal view; **F.** Lateral view; **H.** Ventral view). Scale bars: 0.20 mm (**A–D**); 1.00 mm (**E–H**).

strongly bulged ventral apophysis; femur with small retrolatero-proximal apophysis and distinct ventral protuberance; tibia with prolatero-ventral protuberance; procursus (Fig. 12C, D) simple proximally, but complex distally, with raised prolatero-subdistal membranous edge bearing distal membranous process, sclerotised prolatero-subdistal apophysis, pointed sclerotised retrolatero-distal apophysis and two strong and one slender dorsal spines; uncus (Fig. 13C) latero-medially contracted, with proximal apophysis and distal scaly edge; appendix (Fig. 13C) hooked, with curved median branch and distal teeth; embolus (Fig. 13C) sclerotised, with some indistinct transparent distal projections. Retrolateral trichobothrium on tibia I at 5% proximally; legs with short vertical setae on tibiae and metatarsi.

Female (***paratype***). Similar to male, habitus as in Fig. 13G, H. Total length 4.76 (4.90 with clypeus), carapace 1.56 long, 1.78 wide, opisthosoma 3.20 long, 1.43 wide; tibia I: 7.45; tibia I L/d: 47. Eye interdistances and diameters: PME–PME 0.21, PME 0.14, PME–ALE 0.06, AME–AME 0.05, AME 0.09. Sternum width/length: 1.10/0.80. Ocular area with median and lateral brown bands. Epigyne (Fig. 13A) nearly triangular, laterally strongly sclerotised, with column-shaped knob. Vulva (Fig. 13B) with eyebrow-shaped, sclerotised anterior arch, pair of elliptic pore plates and pair of nearly half-round sclerites.

Variation. Tibia I in paratype male: 9.29. Tibia I in the other two paratype females: 6.45, 7.45.

Habitat. Underside of overhang on rocky cliffs in the mountain area.

Distribution. China (Shaanxi, type locality; Fig. 1).

Pholcus yuncheng Yang & Yao, sp. nov.

https://zoobank.org/FEB41C4F-6B7C-4822-B322-C24C35AE9A7B

Figs 14, 15

Type material. ***Holotype*** ♂ (SYNU-Ar00392) and ***paratypes*** 2♂ (SYNU-Ar00393, IAECAS-Ar00394Y) 3♀ (SYNU-Ar00395–96, IAECAS-Ar00397Y), **China**, **Shanxi**, Yuncheng, Yongji, Shuiyukou Village, Shentan Grand Canyon Scenic Spot (34°49.50'N, 110°25.72'E, 529 m elev.), 20/07/2022.

Etymology. The specific name refers to the type locality and is a noun in apposition.

Diagnosis. The new species resembles *P. lushan* sp. nov. by having similar male chelicerae and bulbal apophyses (Fig. 15C, D), but can be distinguished by procursus without ventro-subdistal apophysis (Fig. 14C vs. with spine-shaped ventro-subdistal apophysis, Fig. 8C), by procursus with small pointed distal apophysis (Fig. 14C vs. large angular distal apophysis, Fig. 8C), by male palpal trochanteral apophysis with retrolatero-median apophysis (Fig. 14B vs. absent, Fig. 8B), by epigynal plate posteriorly straight (Fig. 15A vs. curved, Fig. 9A), by vulval anterior arch laterally strongly curved (Fig. 15B vs. nearly half-round, Fig. 9B) and by vulval pore plates nearly round (Fig. 15B vs. anteriorly blunt and posteriorly pointed, Fig. 9B).

Description. Male (***holotype***). Total length 5.35 (5.51 with clypeus), carapace 1.59 long, 1.84 wide, opisthosoma 3.76 long, 1.60 wide. Leg I: 40.99 (10.64, 0.81, 10.38, 16.47, 2.69), leg II: 29.19 (8.21, 0.79, 7.18, 11.28, 1.73), leg III: 20.69 (6.15, 0.70, 5.06, 7.63, 1.15), leg IV: 28.40 (8.14, 0.77, 7.12, 10.83, 1.54); tibia I L/d: 59. Eye interdistances and diameters: PME–PME 0.25, PME 0.18, PME–ALE 0.07, AME–AME 0.06, AME 0.11. Sternum width/length: 1.24/1.02. Habitus as in Fig. 15E, F. Carapace yellowish, with brown radiating marks and marginal brown bands; ocular area yellowish, with indistinct median band; clypeus and sternum yellowish, with brown marks. Legs yellowish, but dark brown on patellae and whitish on distal parts of femora and tibiae, with darker rings on subdistal parts of femora and proximal and subdistal parts of tibiae. Opisthosoma yellowish, with dorsal and lateral spots. Chelicerae (Fig. 15D) with pair of proximo-lateral apophyses, pair of distal apophyses with two teeth each and pair of frontal apophyses. Palp as in Fig. 14A, B; trochanter with long (4 times longer than wide) ventral apophysis bearing retrolatero-median apophysis; femur with small retrolatero-proximal apophysis and distinct ventral protuberance; tibia with prolatero-ventral protuberance; procursus (Fig. 14C, D) simple proximally, but complex distally, with raised prolatero-subdistal membranous edge bearing distal membranous process, sclerotised prolatero-subdistal apophysis, pointed distal apophysis and two strong dorsal spines; uncus (Fig. 15C) latero-medially contracted, with proximal apophysis and distal scaly edge; appendix (Fig. 15C) hooked, with curved median branch and distal teeth; embolus (Fig. 15C) weakly sclerotised, with some indistinct transparent distal projections. Retrolateral trichobothrium on tibia I at 5% proximally; legs with short vertical setae on tibiae, metatarsi and tarsi; tarsus I with 35 distinct pseudosegments.

Female (***paratype***). Similar to male, habitus as in Fig. 15G, H. Total length 4.97 (5.13 with clypeus), carapace 1.53 long, 1.66 wide, opisthosoma 3.44 long, 1.66 wide; tibia I: 7.56; tibia I L/d: 54. Eye interdistances and diameters: PME–PME 0.22, PME 0.16, PME–ALE 0.06, AME–AME 0.06, AME 0.10. Sternum width/length: 1.06/0.84. Ocular area with median and lateral brown bands; clypeus brown. Epigyne (Fig. 15A) nearly triangular, laterally strongly sclerotised, with wedge-shaped knob. Vulva (Fig. 15B) with laterally strongly curved, posteriorly sclerotised anterior arch, pair of nearly round pore plates and pair of C-shaped sclerites.

Variation. Tibia I in two paratype males: 8.97, 10.96. Tibia I in the other two paratype females: 8.27, 8.33.

Habitat. Underside of overhang on rocky cliffs in the mountain area.

Distribution. China (Shanxi, type locality; Fig. 1).

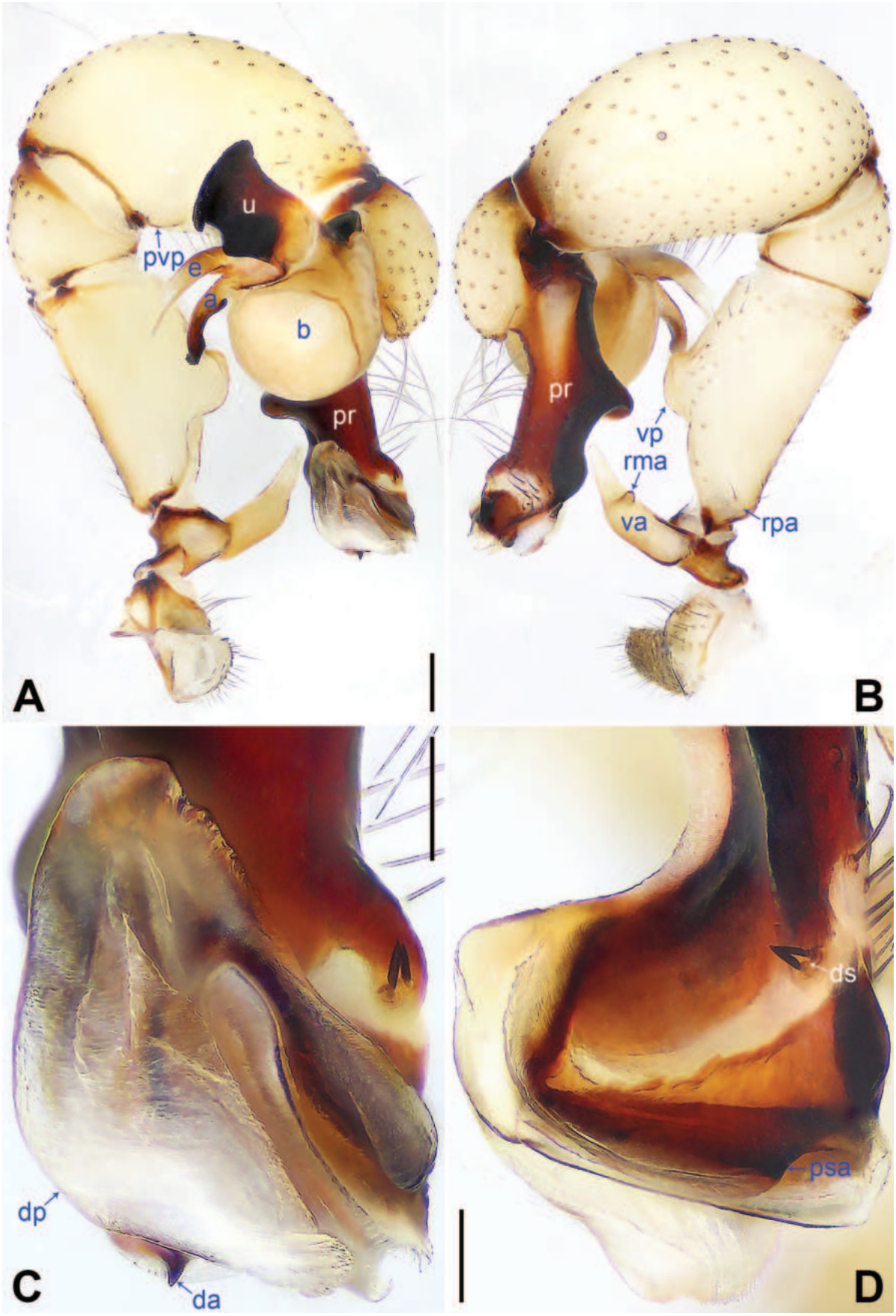

Figure 14. *Pholcus yuncheng* sp. nov., holotype male **A, B.** Palp (**A.** Prolateral view; **B.** Retrolateral view); **C, D.** Distal part of procursus (**C.** Prolateral view; **D.** Dorsal view). Scale bars: 0.20 mm (**A, B**); 0.10 mm (**C, D**).

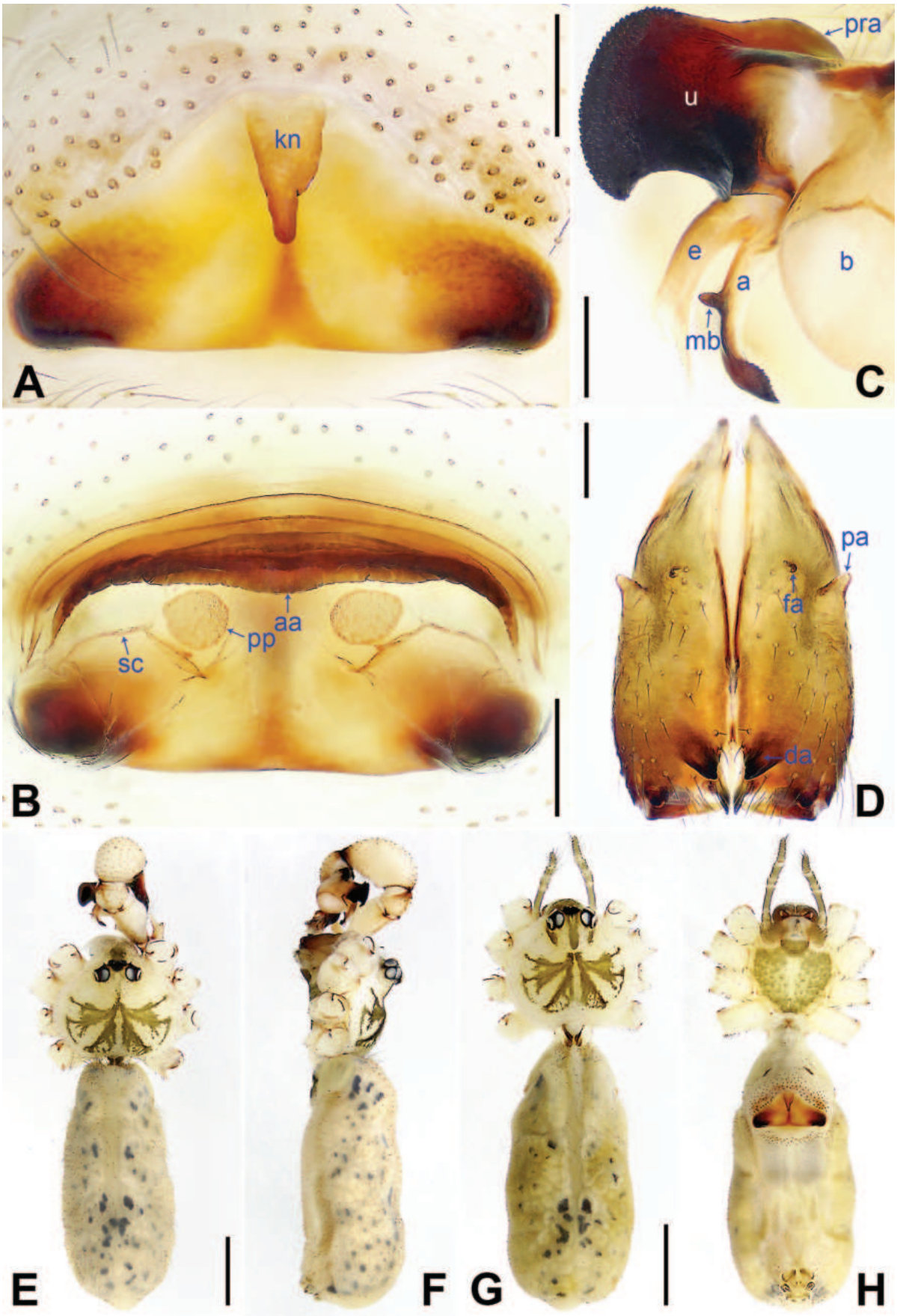

Figure 15. *Pholcus yuncheng* sp. nov., holotype male (**C–F**) and paratype female (**A, B, G, H**) **A.** Epigyne, ventral view; **B.** Vulva, dorsal view; **C.** Bulbal apophyses, prolateral view; **D.** Chelicerae, frontal view; **E–H.** Habitus (**E, G.** Dorsal view; **F.** Lateral view; **H.** Ventral view). Scale bars: 0.20 mm (**A–D**); 1.00 mm (**E–H**).

Acknowledgements

The manuscript benefits greatly from comments by Danilo Harms, Yanfeng Tong and two anonymous reviewers. We thank Joseph KH Koh (Singapore) and Jinzhong Fu (Canada) for their suggestions and language editing. This study is supported by the Science & Technology Fundamental Resources Investigation Program of China (2023FY100200) and the National Natural Science Foundation of China (NSFC-32170461, 31872193).

References

Dong T, Zheng G, Yao Z, Li S (2016) Thirteen new species of the spider genus *Pholcus* Walckenaer, 1805 (Araneae: Pholcidae) from China. Zootaxa 4170(1): 1–40. https://doi.org/10.11646/zootaxa.4170.1.1

Folmer O, Black M, Hoeh W, Lutz R, Vrijenhoek R (1994) DNA primers for amplification of mitochondrial cytochrome c oxidase subunit I from diverse metazoan invertebrates. Molecular Marine Biology and Biotechnology 3(5): 294–299.

Huber BA (2005) High species diversity, male-female coevolution, and metaphyly in Southeast Asian pholcid spiders: The case of *Belisana* Thorell 1898 (Araneae, Pholcidae). Zoologica 155: 1–126.

Huber BA (2011) Revision and cladistic analysis of *Pholcus* and closely related taxa (Araneae, Pholcidae). Bonner Zoologische Monographien 58: 1–509.

Huber BA, Eberle J, Dimitrov D (2018) The phylogeny of pholcid spiders: A critical evaluation of relationships suggested by molecular data (Araneae, Pholcidae). ZooKeys 789: 51–101. https://doi.org/10.3897/zookeys.789.22781

Khmelik VV, Kozub D, Glazunov A (2005) Helicon Focus 3.10.3. https://www.heliconsoft.com/heliconsoftproducts/helicon-focus/ [accessed on 2 October 2023]

Lan T, Yao Z, Zheng G, Li S (2020) Two new species of the spider genus *Pholcus* Walckenaer, 1805 (Araneae: Pholcidae) from Guizhou and Guangxi, China. Zootaxa 4758(2): 360–368. https://doi.org/10.11646/zootaxa.4758.2.9

Lu Y, Yang F, He Q (2021) *Pholcus maxian* sp. nov., the fifth endemic spider species of *Pholcus phungiformes* species-group (Araneae: Pholcidae) at the border between Jilin, China and North Korea. Biodiversity Data Journal 9: e72464 [1–7]. https://doi.org/10.3897/BDJ.9.e72464

Lu Y, Chu C, Zhang X, Li S, Yao Z (2022a) Europe vs. China: *Pholcus* (Araneae, Pholcidae) from Yanshan-Taihang Mountains confirms uneven distribution of spiders in Eurasia. Zoological Research 43(4): 532–534 [& Suppl. 1–78]. https://doi.org/10.24272/j.issn.2095-8137.2022.103

Lu Y, Yao Z, He Q (2022b) A new species of *Pholcus yichengicus* species-group (Araneae, Pholcidae) from Hebei Province, China. Biodiversity Data Journal 10: e81800 [1–7]. https://doi.org/10.3897/BDJ.10.e81800

Peng Y, Zhang F (2011) Two new species of the genus *Pholcus* (Araneae: Pholcidae) from Taihang Mountains, China, with first report of the female of *Pholcus oculosus*. Entomologica Fennica 22(2): 78–84. https://doi.org/10.33338/ef.84546

WSC (2023) World Spider Catalog. Version 24.5. Natural History Museum Bern. http://wsc.nmbe.ch [accessed on 12 November 2023]

Yang X [editor in chief] (2018) Insect Fauna of the Qinling Mountains (12 Volumes). World Publishing Corporation.

Yao Z, Li S (2010) Pholcid spiders of the genus *Khorata* Huber, 2005 (Araneae: Pholcidae) from Guangxi, China. Zootaxa 2594(1): 1–79. https://doi.org/10.11646/zootaxa.2594.1.1

Yao Z, Li S (2012) New species of the spider genus *Pholcus* (Araneae: Pholcidae) from China. Zootaxa 3289(1): 1–271. https://doi.org/10.11646/zootaxa.3289.1.1

Yao Z, Li S (2013) New and little known pholcid spiders (Araneae: Pholcidae) from Laos. Zootaxa 3709(1): 1–51. https://doi.org/10.11646/zootaxa.3709.1.1

Yao Z, Pham DS, Li S (2015) Pholcid spiders (Araneae: Pholcidae) from northern Vietnam, with descriptions of nineteen new species. Zootaxa 3909(1): 1–82. https://doi.org/10.11646/zootaxa.3909.1.1

Yao Z, Dong T, Zheng G, Fu J, Li S (2016) High endemism at cave entrances: a case study of spiders of the genus *Uthina*. Scientific Reports 6: 35757 [1–9 & Suppl. 1–52]. https://doi.org/10.1038/srep35757

Yao Z, Wang X, Li S (2021) Tip of the iceberg: species diversity of *Pholcus* spiders (Araneae, Pholcidae) in the Changbai Mountains, northeast China. Zoological Research 42(3): 267–271 [& Suppl. 1–60]. https://doi.org/10.24272/j.issn.2095-8137.2021.037

Zhang F, Zhu M (2009) A review of the genus *Pholcus* (Araneae: Pholcidae) from China. Zootaxa 2037(1): 1–114. https://doi.org/10.11646/zootaxa.2037.1.1

Zhao F, Jiang T, Yang L, He Q, Zheng G, Yao Z (2023a) Pholcid spiders of the *Pholcus phungiformes* species-group (Araneae, Pholcidae) from Liaoning Province, China: An overview, with description of a new species. ZooKeys 1156: 1–14. https://doi.org/10.3897/zookeys.1156.98331

Zhao F, Yang L, Zou Q, Ali A, Li S, Yao Z (2023b) Diversity of *Pholcus* spiders (Araneae: Pholcidae) in China's Lüliang Mountains: an integrated morphological and molecular approach. Insects 14(4): 364 [1–34]. https://doi.org/10.3390/insects14040364

Zhu K, Yao Z, Bai X, Li S (2018) Five new species of the spider genus *Pholcus* Walckenaer, 1805 (Araneae: Pholcidae) from China and Thailand. Zootaxa 4377(2): 235–253. https://doi.org/10.11646/zootaxa.4377.2.5

Zoosyst. Evol. 100 (1) 2024, 223–231 | DOI 10.3897/zse.100.115564

PENSOFT

für Natur MUSEUM FÜR NATURKUNDE BERLIN

Relationships and description of a new catfish species from Chapada Diamantina, the northernmost record of *Trichomycterus s.s.* (Siluriformes, Trichomycteridae)

Wilson J. E. M. Costa[1], Caio R. M. Feltrin[1], José L. O. Mattos[1], Axel M. Katz[1]

1 *Laboratory of Systematics and Evolution of Teleost Fishes, Institute of Biology, Federal University of Rio de Janeiro, Rio de Janeiro, Brazil*

https://zoobank.org/0E463E5B-8BE7-49F9-98E7-B170F18CDC6B

Corresponding author: Wilson J. E. M. Costa (wcosta@acd.ufrj.br)

Academic editor: Nicolas Hubert ♦ **Received** 9 November 2023 ♦ **Accepted** 7 February 2024 ♦ **Published** 6 March 2024

Abstract

Psammocambeva exhibits the largest geographical distribution amongst the subgenera of *Trichomycterus s.s.*, with its present northernmost represented by *Trichomycterus tete*, endemic to the upper Rio de Contas Basin in the Chapada Diamantina Region, north-eastern Brazil. Herein, we describe a new species recently collected in the Chapada Diamantina Region, but in the Rio Paraguaçu Basin, about 100 km north of the area inhabited by *T. tete*. A molecular phylogeny using one nuclear and two mitochondrial genes (2430 bp) supported the new species as sister to *T. tete*; both species are distinguished by colour patterns, morphometric data, relative position of dorsal and anal fins and osteological character states. The clade comprising the new species and *T. tete*, endemic to the semi-arid Caatinga biogeographical province, is supported as sister to a clade comprising species from the Rio Doce and Rio Paraíba do Sul Basins, in the Atlantic Forest biogeographical province. This study corroborated the Chapada Diamantina Region, a well-known mountainous biodiversity centre, as an important centre of endemism for trichomycterid catfishes.

Key Words

Caatinga, molecular phylogeny, mountain biodiversity, osteology, Rio Paraguaçu

Introduction

The Trichomycterinae (hereafter trichomycterines) are the most common fish group in South American mountainous regions (Costa 2021). In eastern and north-eastern Brazilian highlands, trichomycterines are represented by the genus *Trichomycterus* Valenciennes, 1832, which in its strict sense (i.e. *Trichomycterus s.s.*) is a well-supported clade, which is sister to a clade containing the genera *Cambeva* Katz, Barbosa, Mattos & Costa, 2018 and *Scleronema* Eigenmann, 1917 (Katz et al. 2018). *Trichomycterus s.s.* includes the type species of the genus, *Trichomycterus nigricans* Valenciennes, 1832 and others about 80 species, in six subgenera (Costa 2021). Amongst these subgenera, *Psammocambeva* Costa, 2021, presently including 35 nominal species, exhibits the largest geographical distribution and is the only one occurring in north-eastern Brazil (Costa 2021; Vilardo et al. 2023). *Psammocambeva* is well-supported in molecular phylogenies, but it is not diagnosable by unique morphological character states, with species positioning being determined mainly by molecular phylogenies, besides the absence of synapomorphic osteological characteristics of other genera and, exceptionally, by the presence of derived osteological characteristics that are shared by groups of species within *Psammocambeva* (Costa 2021; Costa et al. 2022, 2023).

The present northernmost record for *Psammocambeva*, as well as for *Trichomycterus s.s.*, is *Trichomycterus tete* Barbosa & Costa, 2011, endemic to the Rio de Contas Basin, southern Chapada Diamantina, north-eastern Brazil (Barbosa and Costa 2011). Recently, one of us (CRMF) collected another species of *Psammocambeva* in the Chapada Diamantina, but in the Rio Paraguaçu Basin, about 100 km north of the area inhabited by *T. tete* in the Rio de

Contas Basin. The objectives of the present study are to conduct a phylogenetic analysis to investigate the positioning of the new species and to present a formal description.

Materials and methods

Field studies were approved by ICMBio (Instituto Chico Mendes de Conservação da Biodiversidade; permit number: 38553-13) and field methods by the Ethics Committee for Animal Use of Federal University of Rio de Janeiro (permit number: 065/18). Euthanasia, fixation, preparation for morphological studies and conservation followed methods of our previous studies on trichomycterine systematics (e.g. Costa et al. (2023)). In lists of specimens, C&S indicates cleared and stained specimens for osteological analyses and DNA indicates specimens directly fixed and preserved in absolute ethanol. Geographical names followed Portuguese terms used in the region. Specimens were deposited in the Instituto de Biologia, Universidade Federal do Rio de Janeiro (UFRJ). Comparative material is listed in Costa et al. (2022, 2023). Methods to take and express morphometric and meristic data, morphological terminology, selection of described and illustrated osteological structures and sequence of morphological characters used in the species description are according to our previous studies on *Psammocambeva* (Costa et al. 2022, 2023).

Proceedings for DNA extraction, amplification and sequencing, reading and interpretation of sequencing chromatograms and sequences annotation were according to our previous studies on systematics of *Psammocambeva* (e.g. Costa et al. (2023)).

Primers for PCR reactions for the three genes used in the analysis, the mitochondrial genes cytochrome b (CYTB) and cytochrome c oxidase I (COX1) and the nuclear encoded gene recombination activating 2 (RAG2), were the same used in other studies on *Psammocambeva* (e.g. Costa et al. (2023)). The concatenated molecular data matrix comprised 2430 bp (COX1 521 bp, CYTB 1088 bp, RAG2 821 bp). Parameters for PCR reactions and thermal profile of PCR protocol were the same used in Costa et al. (2023). The sequencing reaction thermal profile was 35 cycles of 30 s at 95 °C, 30 s at 55 °C and 1.5 min at 73 °C. GenBank accession numbers are provided in Table 1.

Terminal taxa for the phylogenetic analyses comprised the new species and 22 species of *Psammocambeva* representing all included lineages. Outgroups were four congeners representing other subgenera of *Trichomycterus s.s.*, two species of the clade *Cambeva* plus *Scleronema*, the sister group of *Trichomycterus s.s.*, one species of a distantly related trichomycterine genus, two species representing other Trichomycteridae subfamilies and one species of the Nematogenyidae, the sister group of Trichomycteridae. Alignment of individual gene datasets was made with the Clustal W algorithm (Chenna et al. 2003) implemented in MEGA 11 (Tamura et al. 2021). The optimal partition scheme and the best-fit evolutive models (Table 2) were calculated using the PartitionFinder 2.1.1 (Lanfear et al. 2016) software, based on the Corrected Akaike Information Criterion. Bayesian Inference was performed with MrBayes 3.2.7a (Ronquist et al. 2012), using two independent Markov Chain Monte Carlo (MCMC) runs with 5 × 107 generations; sampling frequency of every 1000 generations; Tracer 1.7.2 (Rambaut et al. 2018) for evaluation of convergence of the MCMC chains, attainment of the stationary phase, effective sample size adequacy and determination of the burn-in percentage; and 25% burn-in to calculate Bayesian posterior probabilities. Maximum Likelihood (ML) was performed using IQ-TREE 2.2.0 (Minh et al. 2020), with node support estimated through both ultrafast bootstrap (Hoang et al. 2018) and traditional bootstrap (Felsenstein 1985), with 1000 replicates for each one.

Table 1. Species used in the phylogenetic analyses and respective GenBank accession numbers.

	COX1	CYTB	RAG2
Nematogenys inermis	KY857952	–	KY858182
Trichogenes longipinnis	MK123682	MK123704	MF431117
Microcambeva ribeirae	MN385807	OK334290	MN385832
Ituglanis boitata	MK123684	MK123706	MK123758
Scleronema minutum	MK123685	MK123707	MK123759
Cambeva barbosae	MK123689	MK123713	MN385820
Trichomycterus itatiayae	MW671552	MW679291	OL779233
Trichomycterus nigricans	MN813005	MK123723	MK123765
Trichomycterus albinotatus	MN813007	MK123716	MN812990
Trichomycterus brasiliensis	MK123691	MK123717	MK123763
Trichomycterus travassosi	MK123701	MK123730	OL752425
Trichomycterus alterrnatus	OQ357886	OQ355710	OQ400957
Trichomycterus pantherinus	MK123697	MK123725	MN812989
Trichomycterus goeldii	MT435136	MT436453	MT446427
Trichomycterus jacupiranga	OL764372	OL779234	OL779232
Trichomycterus pradensis	MN813003	MK123726	MN812988
Trichomycterus melanopygius	OQ357896	OQ355720	OQ400967
Trichomycterus auroguttatus	MT435135	MT436452	OP699434
Trichomycterus saquarema	OP698258	OP688464	OP688470
Trichomycterus macrophthalmus	OL741727	OL752426	OL752421
Trichomycterus astromycterus	ON036881	OK652453	OK652448
Trichomycterus altipombensis	OP698260	OP688466	OP688472
Trichomycterus puriventris	OP698259	OP688465	OP688471
Trichomycterus mimosensis	OQ357893	OQ355719	OQ400966
Trichomycterus longibarbatus	OQ357895	OQ355718	OQ400965
Trichomycterus gasparinii	OR354437	OR356032	OQ400962
Trichomycterus vinnulus	ON036819.1	OK652452	OK652449
Trichomycterus barrocus	OQ357889	OQ355713	OQ400959
Trichomycterus ipatinga	OQ357892	OQ355716	OQ400963
Trichomycterus illuvies	OQ357894	OQ355717	OQ400964
Trichomycterus tete	OL741729	MH620966	–
Trichomycterus diamantinensis	OR435278	OR438925	OR438926
Trichomycterus caudofasciatus	–	MK123719	MK123764

Table 2. Best-fitting partition schemes and evolutive models.

Partition	Base pairs	Evolutive Model
COX1 1st	174	GTR+I
COX1 2nd	174	F81
COX1 3rd	173	GTR+G
CYTB 1st	363	K80+I+G
CYTB 2nd	363	HKY+I
CYTB 3rd	362	GTR+G
RAG2 1st	455	K80+I+G
RAG2 2nd	274	GTR+G
RAG2 3rd	273	K80+G

Results

Phylogenetic analyses

The phylogenetic analyses generated identical trees (Fig. 1), in which the new species is highly supported as sister to *T. tete*, the only other species of *Trichomycterus* endemic to the Chapada Diamantina.

Taxonomic accounts

Trichomycterus (*Psammocambeva*) *diamantinensis* sp. nov.

https://zoobank.org/2E7E0C0D-2FC6-452B-95EF-8931787C2D73

Figs 2, 3, 4A–C, Table 3

Type material. ***Holotype.*** Brazil • 1 ex., 82.2 mm SL; Bahia State: Palmeiras Municipality: Vale do Capão District: Rio da Bomba, tributary of Rio Preto, Rio Santo Antônio drainage, Rio Paraguaçu Basin; 12°39'35"S, 41°29'14"W; about 980 m a.s.l.; 15 May 2023; C. R. M. Feltrin, R. dos Santos-Junior, and G. L. Canella, leg; UFRJ 13688.

Paratypes. Brazil • 3 ex. (DNA), 39.7–60.5 mm SL; collected with holotype; UFRJ 13686; • 3 ex. (C&S), 49.4–70.0 mm SL; collected with holotype; UFRJ 13689; • 2 ex., 27.1 and 79.6 mm SL; collected with holotype; UFRJ 13690.

Diagnosis. *Trichomycterus diamantinensis* is distinguished from all other species of *Psammocambeva* by having a unique colour pattern of adult specimens consisting of a faint brown stripe along the lateral mid-line of trunk, overlapped by a great concentration of rounded light brown spots in a more superficial layer of skin (vs. never a similar colour pattern). *Trichomycterus diamantinensis* also differs from its hypothesised sister species and the only other species of the CD-clade, *T. tete*, by having the anal-fin origin at a vertical posterior to the dorsal-fin base (vs. through the posterior portion of the dorsal-fin base), a longer nasal barbel, its tip posteriorly reaching the opercular patch of odontodes (vs. reaching area between the orbit and the opercular patch of odontodes), 39 or 40 vertebrae (vs. 36 or 37), a deeper body (body depth 14.0–17.3% SL vs. 12.5–13.2%), a deeper caudal peduncle (caudal peduncle depth 11.5–12.9% SL vs. 9.7–10.8%), a wider body (body width 11.2–12.3% SL vs. 7.3–9.0%), a wider head (head width 83.1–89.3% of head length vs. 68.7–77.5%), the anal-fin origin at a vertical through the centrum of the 25th vertebra (vs. 22nd or 23rd vertebra), the sesamoid supraorbital slender, without a lateral process (Fig. 4A; vs. with a lateral expansion, often forming a distinctive process, Fig. 4D), a relatively wider metapterygoid and quadrate (Fig. 4B vs. Fig. 4E) and a minute ventral middle foramen of the parurohyal (Fig. 4C; vs. broad, Fig. 4F).

Description. ***General morphology.*** Morphometric data are in Table 3. Body moderately slender, head and trunk excluding caudal peduncle with dorsal profiles slightly convex, and ventral profile nearly straight, dorsal and ventral profiles of caudal peduncle approximately straight. Greatest body depth at vertical just anterior to pelvic-fin base. Trunk subcylindrical anteriorly, compressed posteriorly. Anus and urogenital papilla at vertical through dorsal-fin origin or just posterior to it. Head subtrapezoidal in dorsal view, snout profile slightly convex. Eye relatively small, dorsally positioned in head, nearer snout margin than opercle. Posterior nostril located nearer anterior nostril than orbital rim. Tip of maxillary barbel posteriorly reaching between posterior limit of interopercular patch of odontodes and pectoral-fin base, rictal barbel reaching posterior portion of interopercular patch of odontodes and tip of nasal barbel reaching opercular patch of odontodes. Mouth subterminal. Jaw teeth pointed, slightly curved, arranged in irregular rows. Premaxillary teeth 45–50, dentary teeth 44–50. Odontodes conical, elongate; opercular odontodes arranged in irregular transverse rows, interopercular odontodes arranged in irregular longitudinal rows. Opercular odontodes 17–19, interopercular odontodes 38–42. Branchiostegal rays 7.

Dorsal and anal fins subtriangular, anterior and posterior margins slightly convex. Total dorsal-fin rays 12 (iii + II + 7), total anal-fin rays 10 (iii + II + 5); anal-fin origin at vertical just posterior to dorsal-fin base end. Dorsal-fin origin at vertical through centrum of 20th vertebra; anal-fin origin at vertical through centrum of 25th vertebra. Pectoral fin subtriangular in dorsal view, posterior margin slightly convex, first pectoral-fin ray terminating in filament, its length about 25% of pectoral-fin length without filament. Total pectoral-fin rays 8 (I + 7). Pelvic fin subtruncate, its posterior extremity not reaching urogenital papilla, at vertical through dorsal-fin origin or immediately posterior to it. Pelvic-fin bases medially in close proximity. Total pelvic-fin rays 5 (I + 4). Caudal fin truncate. Total principal caudal-fin rays 13 (I + 11 + I),

Table 3. Morphometric data of *Trichomycterus diamantinensis* sp. nov.

	Holotype	Paratypes (n=4)
Standard length (SL)	70.0	49.4–79.6
Percentage of standard length		
Body depth	14.0	14.9–17.3
Caudal peduncle depth	11.5	11.6–12.9
Body width	11.2	11.5–12.3
Caudal peduncle width	5.1	4.1–5.5
Pre-dorsal length	63.7	62.6–64.3
Pre-pelvic length	59.3	58.3–61.0
Dorsal-fin base length	10.0	10.6–11.6
Anal-fin base length	8.1	8.0–10.3
Caudal-fin length	17.0	14.6–16.5
Pectoral-fin length	14.1	12.8–13.3
Pelvic-fin length	8.9	9.4–9.6
Head length	19.7	18.5–20.8
Percentage of head length		
Head depth	48.8	51.4–55.3
Head width	84.0	83.1–89.3
Snout length	42.7	39.7–44.0
Interorbital width	26.0	26.4–29.9
Pre-orbital length	12.2	14.2–15.6
Eye diameter	13.1	12.2–16.9

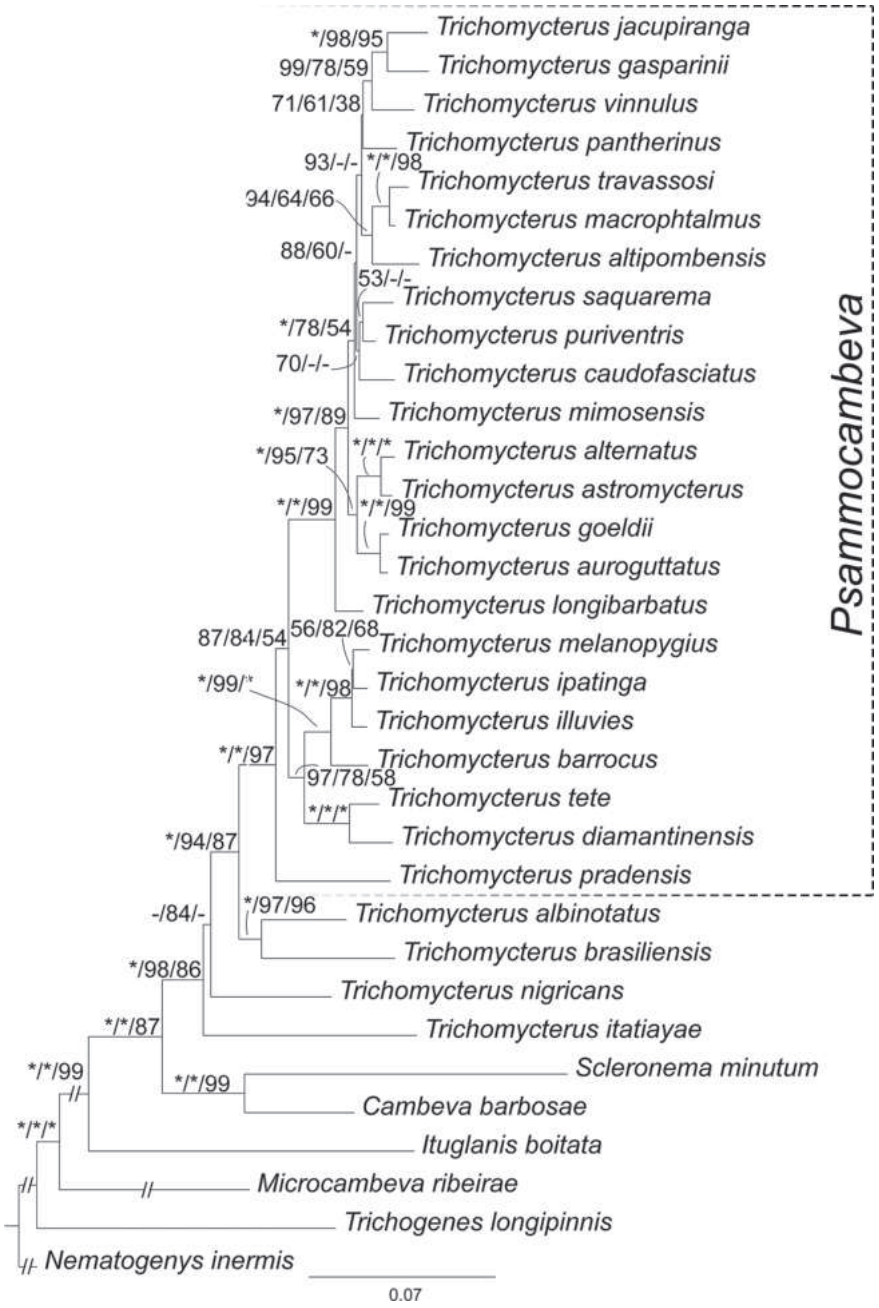

Figure 1. Bayesian Inference topology calculated using MrBayes 3.2.7a for 33 taxa. The dataset comprised two mitochondrially encoded genes (COI, CYTB) and one nuclear gene (RAG2), with a total of 2430 bp. The numbers above branches indicate Bayesian posterior probabilities from the Bayesian Inference analysis and the ultrafast bootstrap and regular bootstrap values from the Maximum Likelihood analyses, respectively, separated by a bar. Asterisks (*) indicate maximum support values and dashes (-) indicate values below 50.

total dorsal procurrent rays 17 or 18 (xvi–xvii + I), total ventral procurrent rays 13 or 14 (xii–xiii + I).

***Latero-sensory system*.** Supraorbital canal, posterior section of infraorbital canal and postorbital canal continuous. Supraorbital sensory canal with 3 paired pores: s1, adjacent to medial margin of anterior nostril; s3, adjacent and just posterior to medial margin of posterior nostril and s6, at transverse line through posterior half of orbit; s6 pore about equidistant from its symmetrical homologous s6 pore than orbit. Infraorbital sensory canal with 2 segments. Anterior infraorbital canal with 2 pores: i1, at transverse line through anterior nostril and i3, at transverse line just anterior to posterior nostril. Posterior infraorbital canal with two pores: i10, adjacent to ventral margin of orbit and i11, posterior to orbit. Postorbital canal with 2 pores: po1, at vertical line above posterior portion of interopercular patch of odontodes, and po2, at vertical line above posterior portion of opercular patch of odontodes. Lateral line of trunk with 2 pores just posterior to head.

Osteology (Fig. 4A–C). Anterior margin of mesethmoid nearly straight, mesethmoid cornu rod-shaped,

Figure 2. *Trichomycterus* (*Psammocambeva*) *diamantinensis* sp. nov., UFRJ 13688, holotype, 82.2 mm SL: **A.** Left lateral view; **B.** Dorsal view; **C.** Ventral view.

tip rounded. Lacrimal oval, its largest length about one third of sesamoid supraorbital length. Sesamoid supraorbital narrow, rod-like, longer than premaxilla largest length. Premaxilla sub-rectangular in dorsal view, slightly tapering laterally. Maxilla boomerang-shaped, slender, slightly shorter than premaxilla, with minute posterior process. Autopalatine sub-rectangular in dorsal view when excluding posterolateral process, its shortest width about half autopalatine length, lateral and medial margins weakly concave. Latero-posterior process of autopalatine triangular, its length about two thirds of autopalatine length excluding anterior cartilage. Metapterygoid subtriangular, deeper than long, with distinctive posterior projection; anterior margin weakly bent, posterior margin slightly sinuous. Quadrate robust, dorsoposterior outgrowth in close proximity to hyomandibular outgrowth. Hyomandibula long, anterior outgrowth with small concavity on dorsal margin. Opercle moderately elongate, opercular odontode patch slender, its depth about half length of dorsal articular facet of hyomandibula; dorsal process of opercle short and blunt. Interopercle long, its longitudinal length about three fourths of hyomandibula longitudinal length. Preopercle compact, without ventral expansion. Parurohyal robust, lateral process relatively elongate, sharply pointed. Parurohyal head well-developed, with minute anterolateral paired process. Middle parurohyal foramen small, its largest length about one fourth of distance between anterior margin of parurohyal and anterior insertion of posterior process. Posterior parurohyal process long, slightly longer than distance between anterior margin of parurohyal and anterior insertion of posterior process. Vertebrae 39 or 40. Ribs 13. Two dorsal hypural plates, corresponding to hypurals 4 + 5 and 3, respectively; single ventral hypural plate corresponding to hypurals 1 and 2 and parhypural.

Colouration in alcohol (Figs 2, 3). Dorsum and flank brownish-grey, lighter ventrally, with faint brown stripe along lateral mid-line of trunk, overlapped by great concentration of rounded light brown spots extending over flank and dorsum in more superficial layer of skin. Dorsum

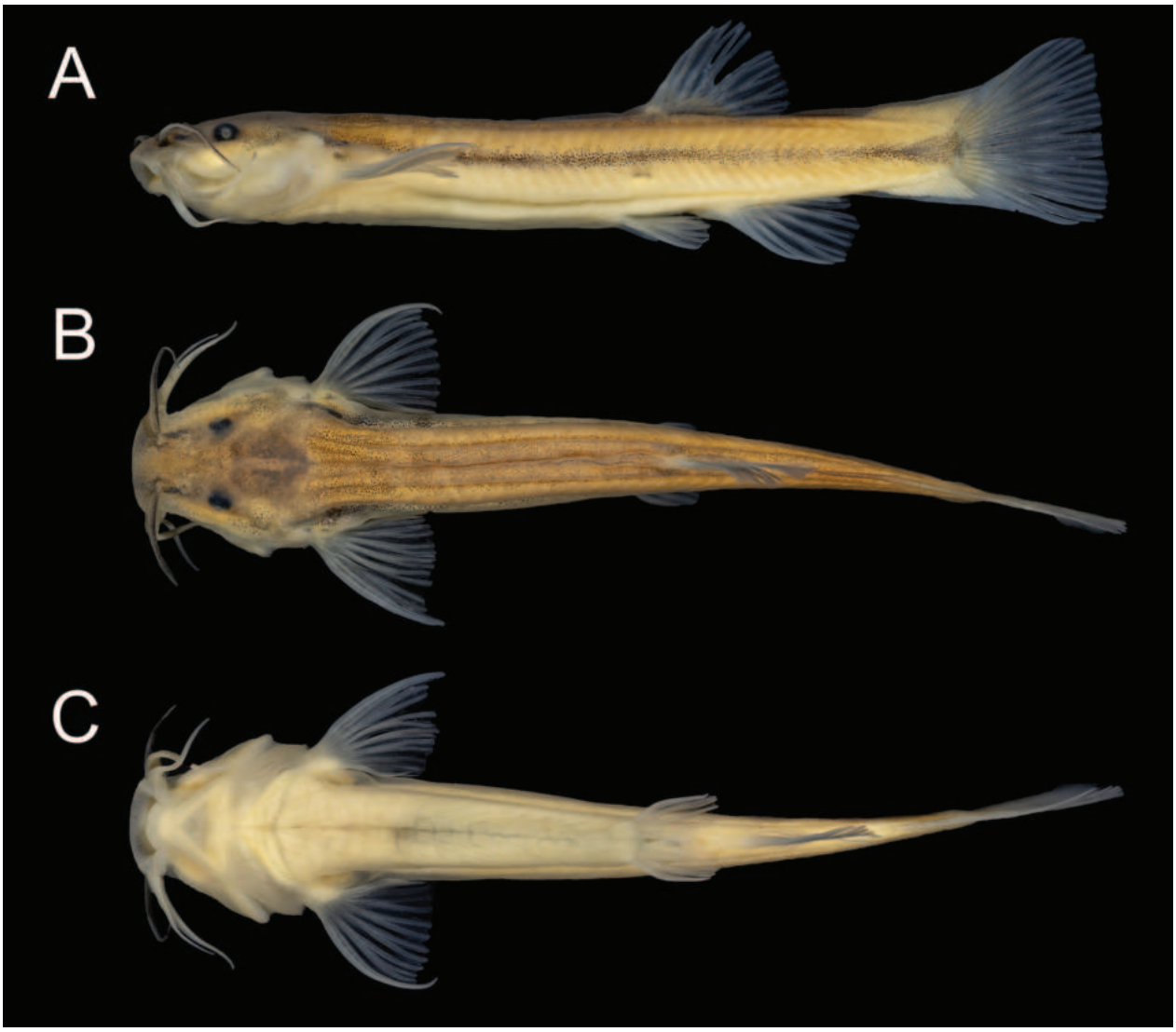

Figure 3. *Trichomycterus* (*Psammocambeva*) *diamantinensis* sp. nov., UFRJ 13690, paratype, 27.1 mm SL: **A.** Left lateral view; **B.** Dorsal view; **C.** Ventral view.

light brown with yellowish-grey with mid-dorsal row of small brown spots between nape and dorsal-fin origin. Dorsal and lateral portions of head brownish-grey with brown spots. Ventral surface of head and trunk white. Jaws and barbels brown. Fins hyaline, with faint brown spots on basal portion of unpaired and pectoral fins. Smallest specimen (27.1 mm SL) with flank pale yellow and narrow black stripe along lateral mid-line, which becomes paler and diffuse and overlapped by brown spots in larger specimens.

Distribution and habitat. *Trichomycterus diamantinensis* is presently known only from the type locality, the Rio da Bomba, a tributary of the Rio Preto, Rio Santo Antônio drainage, Rio Paraguaçu Basin (Fig. 5). Rio da Bomba at the type locality is a dark-coloured small river, about 15 m wide and about 1 m at deepest places, with dense riparian forest in the river banks (Fig. 6). Specimens of *T. diamantinensis* were found amongst small and medium-sized loose stones, with diameters ranging from 1 cm to 50 cm, approximately, in shallow (about between 5 and 50 cm) and fast-flowing places, with the presence of mosses, algae and fallen leaves composing the microhabitats. They were collected both in shaded and fully sun-exposed places.

Etymology. The name *diamantinensis* is an allusion to the occurrence of the new species in the Chapada Diamantina, north-eastern Brazil.

Discussion

The present description of *T. diamantinensis* expands the distribution of *Trichomycterus s.s.* about 100 km to north, consisting of the first record of the genus for the Rio Paraguaçu Basin, an important fluvial system of north-eastern Brazil, with a surface area about 54,900 km2. A previous record of the occurrence of *Trichomycterus* further north in north-eastern Brazil by Sarmento-Soares et al. (2011), in the Rio Itapicuru Basin, was actually due to a misplacement of the species *Ituglanis payaya* (Sarmento-Soares, Zanata & Martins-Pinheiro, 2011), as discussed by Costa

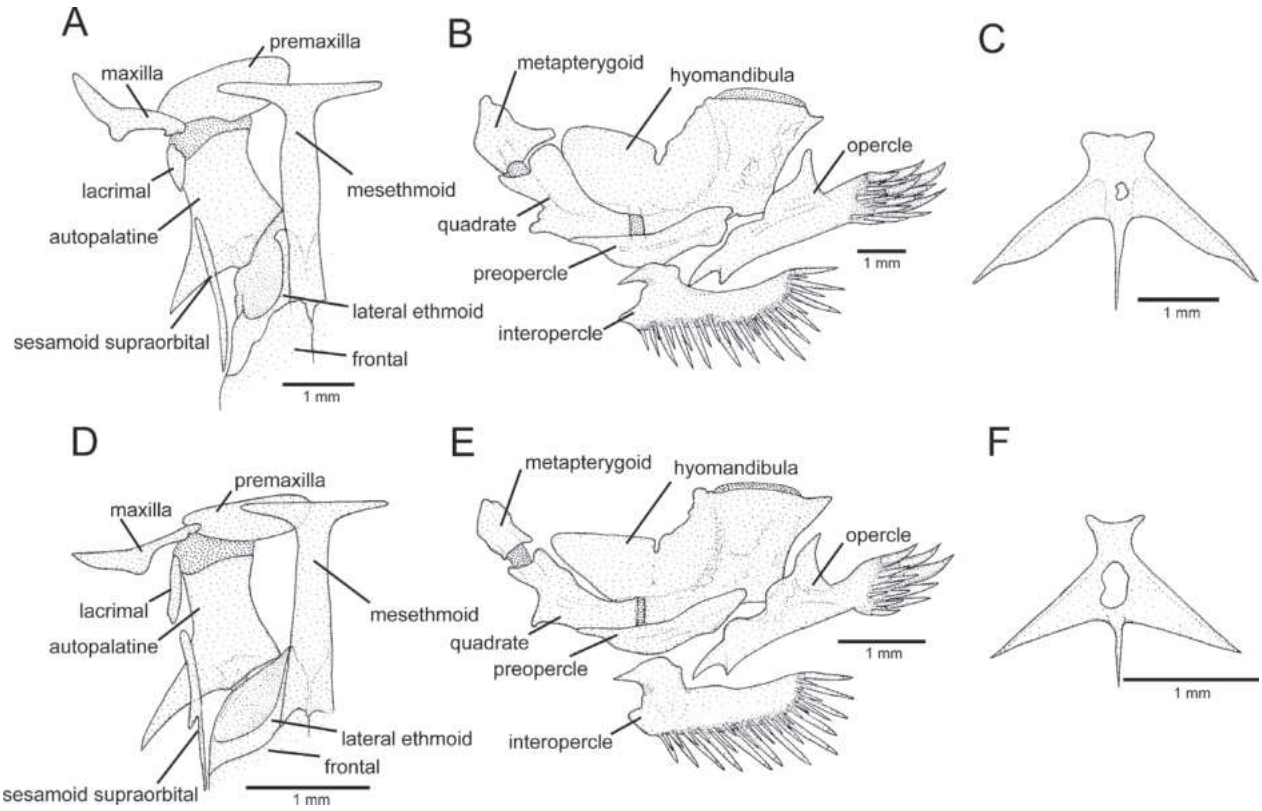

Figure 4. Osteological structures of **A–C.** *Trichomycterus diamantinensis* sp. nov.; **D–F.** *T. tete*. **A, D.** Mesethmoidal region and adjacent structures, left and middle portions, dorsal view; **B, E.** Left jaw suspensorium and opercular series, lateral view; **C, F.** Parurohyal, ventral view. Larger stippling represents cartilaginous areas.

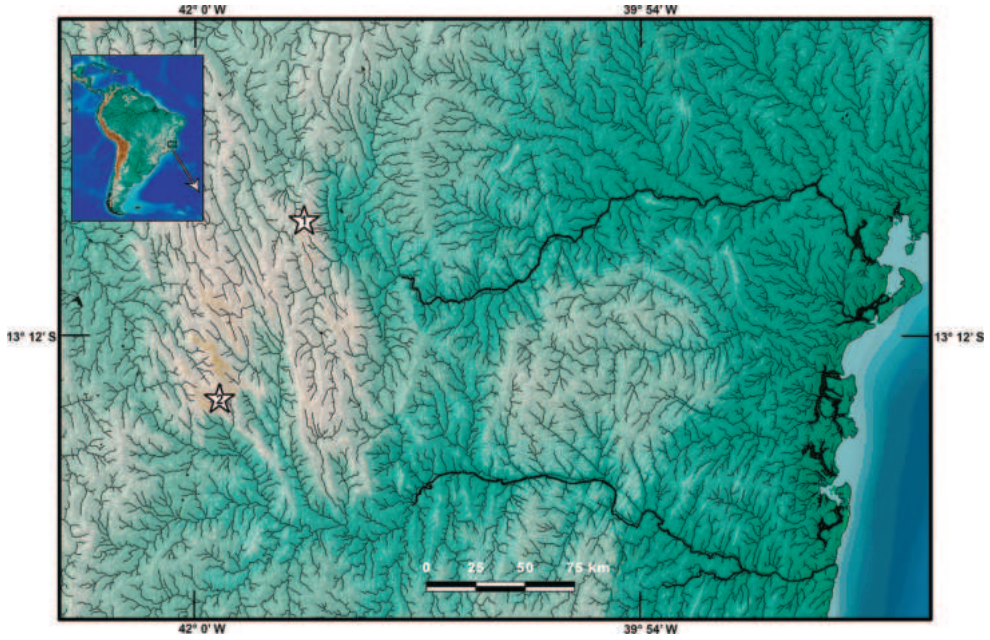

Figure 5. Map of geographical distribution of: **1.** *Trichomycterus diamantinensis* sp. nov. and **2.** *T. tete*.

et al. (2021). No species of *Trichomycterus s.s.* was found during our field studies in the Rio Itapicuru Basin.

This study supported a clade endemic to the Chapada Diamantina Region, in the semi-arid Caatinga biogeographical province (sensu Morrone (2006)), comprising *T. diamantinensis* from the Rio Paraguaçu Basin and *T. tete* from the Rio de Contas Basin (Fig. 1). No other species of *Trichomycterus s.s.* is known to occur in the Caatinga. The analysis indicated that the clade comprising *T. diamantinensis* and *T. tete* is sister to a well-supported clade including species endemic to the Rio Doce Basin, in the Atlantic Forest biogeographical province: *Trichomyc-*

Figure 6. Rio da Bomba at the type locality of *Trichomycterus diamantinensis* sp. nov.

terus barrocus Reis & de Pinna, 2022, *Trichomycterus illuvies* Reis & de Pinna, 2022, *Trichomycterus ipatinga* Reis & de Pinna, 2022 and *Trichomycterus melanopygius* Reis, dos Santos, Britto, Volpi & de Pinna, 2020. Recent molecular data indicated that *Trichomycterus brucutu* Reis & de Pinna, 2022 from the Rio Doce Basin is also a member of this group (Vilardo et al. 2023), here named as the *Psammocambeva* beta-clade. Our molecular studies in progress and molecular data presented in Reis and de Pinna (2022) support *Trichomycterus tantalus* Reis & de Pinna, 2022 also from the Rio Doce Basin as closely related to *T. ipatinga* and *T. melanopygius*. *Trichomycterus tantalus* is distinguishable from *Trichomycterus largoperculatus* Costa & Katz, 2022, a species endemic to the Rio Paraíba do Sul Basin, south-eastern Brazil, not available for molecular analyses, only by minor morphological features (i.e. odontode counts) and both species share river migrating habits (Costa and Katz 2022; Reis and de Pinna 2022). Thus, available evidence indicates that *T. largoperculatus* and *T. tantalus* are also members of the *Psammocambeva* beta-clade. On the other hand, the present study supports *Trichomycterus pradensis* Sarmento-Soares, Martins-Pinheiro, Aranda & Chamon, 2005, a species occurring in coastal river basins of north-eastern Brazil (Sarmento-Soares et al. 2005), as distantly related to the *Psammocambeva* beta-clade. Relationships of other nominal species morphologically similar and occurring in areas close to the distribution area of *T. pradensis* (e.g. *Trichomycterus bahianus* Costa, 1992, *Trichomycterus itacambirussu* Triques & Vono, 2004, *Trichomycterus jequitinhonhae* Triques & Vono, 2004 and *Trichomycterus landinga* Triques & Vono, 2004) are still unknown.

The colour pattern of adult specimens of *T. diamantinensis*, comprising dark pigmentation occurring in two layers of the skin, with a faint brown stripe along the lateral mid-line of the trunk at an internal layer, overlapped by a great concentration of rounded light brown spots at a more external layer (Fig. 2), immediately distinguishes this species from all other congeners of *Psammocambeva*. In *T. tete*, its hypothesised sister species, the colour pattern consists of dark pigmentation arranged in a single layer, forming round spots separated by broad interspaces (Barbosa and Costa 2011: fig. 1). However, juvenile specimens below about 30 mm SL of both species (Fig. 3), share an identical colour pattern, in which the flank is pale yellow with a narrow black stripe along the longitudinal mid-line, possibly corroborating sister group relationships, since no other species of *Psammocambeva* has a similar colour pattern in juvenile specimens. In the distantly-related *Trichomycterus saquarema* Costa, Katz, Vilardo & Amorim, 2022, in addition to a broad black stripe along the lateral mid-line, there is another stripe on the dorsal part of the flank (Costa et al. 2022: fig. 14C), thus considered a non-homologous condition.

The sources of the Rio Paraguaçu are located in the Chapada Diamantina, a well-known mountainous biodiversity centre with numerous endemic plants (Giulietti et al. 1997). The present study corroborates the Chapada Diamantina as an important centre of endemism for trichomycterid catfishes. In addition to *T. diamantinensis* and *T. tete*, endemic trichomycterids include the whole subfamily Copionodontinae (de Pinna 1992), two species of the trichomycterine genus *Ituglanis* Costa & Bockmann, 1993 (Campos-Paiva and Costa 2007; Costa et al. 2021) and one species of the sarcoglanidine genus *Ammoglanis* Costa, 1994 (Costa et al. 2020).

Acknowledgements

We are grateful to Ronaldo dos Santos-Junior and Gustavo L. Canella for assistance during field studies. Instituto Chico Mendes de Conservação da Biodiversidade provided collecting permits. Thanks are also due to Felipe Ottoni and Valter Azevedo-Santos for comments and suggestions. This work was partially supported by Conselho Nacional de Desenvolvimento Científico e Tecnológico (CNPq; grant 304755/2020-6 to WJEMC) and Fundação Carlos Chagas Filho de Amparo à Pesquisa do Estado do Rio de Janeiro (FAPERJ; grant E-26/201.213/2021 to WJEMC, E-26/202.005/2020 to AMK and E-26/202.327/2018 to JLM). This study was also supported by CAPES (Finance Code 001) through Programa de Pós-Graduação em Biodiversidade e Biologia Evolutiva /UFRJ and Programa de Pós-Graduação em Genética/UFRJ.

References

Barbosa MA, Costa WJEM (2011) Description of a new species of the catfish genus *Trichomycterus* (Teleostei: Siluriformes: Trichomycteridae) from the rio de Contas basin, northeastern Brazil. Vertebrate Zoology 61(3): 307–312. https://doi.org/10.3897/vz.61.e31157

Campos-Paiva RM, Costa WJEM (2007) *Ituglanis paraguassuensis* sp. n. (Teleostei: Siluriformes: Trichomycteridae): a new catfish from the rio Paraguaçu, northeastern Brazil. Zootaxa 1471(1): 53–59. https://doi.org/10.11646/zootaxa.1471.1.5

Chenna R, Sugawara H, Koike T, Lopez R, Gibson TJ, Higgins DG, Thompson JD (2003) Multiple sequence alignment with the Clustal series of programs. Nucleic Acids Research 31(13): 3497–3500. https://doi.org/10.1093/nar/gkg500

Costa WJEM (2021) Comparative osteology, phylogeny and classification of the eastern South American catfish genus *Trichomycterus* (Siluriformes: Trichomycteridae). Taxonomy 1(2): 160–191. https://doi.org/10.3390/taxonomy1020013

Costa WJEM, Katz AM (2022) A new catfish of the genus *Trichomycterus* from the Rio Paraíba do Sul Basin, south-eastern Brazil, a supposedly migrating species (Siluriformes, Trichomycteridae). Zoosystematics and Evolution 98: 13–21. https://doi.org/10.3897/zse.98.72392

Costa WJEM, Mattos JLO, Santos ACA (2020) *Ammoglanis multidentatus*, a new miniature sand-dwelling sarcoglanidine catfish with unique osteological features from northeastern Brazil (Siluriformes: Trichomycteridae). Vertebrate Zoology 70: 61–67. https://doi.org/10.26049/VZ70-1-2020-04

Costa WJEM, Mattos JLO, Katz AM (2021) Phylogenetic position of *Trichomycterus payaya* and examination of osteological characters diagnosing the Neotropical catfish genus *Ituglanis* (Siluriformes: Trichomycteridae). Zoological Studies (Taipei, Taiwan) 60: 43. https://doi.org/10.6620/ZS.2021.60-43

Costa WJEM, Mattos JL, Vilardo PJ, Amorim PF, Katz AM (2022) Perils of underestimating species diversity: revisiting systematics of *Psammocambeva* catfishes (Siluriformes: Trichomycteridae) from the Rio Paraíba do Sul Basin, south-eastern Brazil. Taxonomy 2(4): 491–523. https://doi.org/10.3390/taxonomy2040032

Costa WJEM, Mattos JL, Barbosa MA, Vilardo PJ, Katz AM (2023) High endemism in an endangered biodiversity hotspot: phylogeny, taxonomy and distribution patterns of catfishes of the *Psammocambeva* alpha-clade (Siluriformes: Trichomycteridae) from the Rio Doce basin, Brazil. Fishes 8(10): 474. https://doi.org/10.3390/fishes8100474

de Pinna MCC (1992) A new subfamily of Trichomycteridae (Teleostei, Siluriformes), lower loricarioid relationships and a discussion on the impact of additional taxa for phylogenetic analysis. Zoological Journal of the Linnean Society 106(3): 175–229. https://doi.org/10.1111/j.1096-3642.1992.tb01247.x

Felsenstein J (1985) Confidence limits on phylogenies: An approach using the bootstrap. Evolution; International Journal of Organic Evolution 39(4): 783–791. https://doi.org/10.2307/2408678

Giulietti AM, Pirani JR, Harley RM (1997) Espinhaço Range region, eastern Brazil. In: Davis SD, Heywood VH, Herrera-Macbryde O, Villa-Lobos J, Hamilton AC (Eds) Centres of plant diversity: a guide and strategy for their conservation. IUCN Publication Unit, Cambridge, 397–404.

Hoang DT, Chernomor O, von Haeseler A, Minh BQ, Vinh LS (2018) UFBoot2: Improving the ultrafast bootstrap approximation. Molecular Biology and Evolution 35(2): 518–522. https://doi.org/10.1093/molbev/msx281

Katz AM, Barbosa MA, Mattos JLO, Costa WJEM (2018) Multigene analysis of the catfish genus *Trichomycterus* and description of a new South American trichomycterine genus (Siluriformes, Trichomycteridae). Zoosystematics and Evolution 94(2): 557–566. https://doi.org/10.3897/zse.94.29872

Lanfear R, Frandsen PB, Wright AM, Senfeld T, Calcott B (2016) PartitionFinder 2: New methods for selecting partitioned models of evolution for molecular and morphological phylogenetic analyses. Molecular Biology and Evolution 34: 772–773. https://doi.org/10.1093/molbev/msw260

Minh BQ, Schmidt HA, Chernomor O, Schrempf D, Woodhams MD, von Haeseler A, Lanfear R (2020) IQ-TREE 2: New models and efficient methods for phylogenetic inference in the genomic era. Molecular Biology and Evolution 37(5): 1530–1534. https://doi.org/10.1093/molbev/msaa015

Morrone JJ (2006) Biogeographic areas and transition zones of Latin America and the Caribbean islands based on panbiogeographic and cladistic analyses of the entomofauna. Annual Review of Entomology 51(1): 467–494. https://doi.org/10.1146/annurev.ento.50.071803.130447

Rambaut A, Drummond AJ, Xie D, Baele G, Suchard MA, Rambaut A, Drummond AJ, Xie D, Baele G, Suchard MA (2018) Posterior summarisation in Bayesian phylogenetics using Tracer 1.7. Systematic Biology 67(5): 901–904. https://doi.org/10.1093/sysbio/syy032

Reis VJC, de Pinna MCC (2022) Diversity and systematics of *Trichomycterus* Valenciennes 1832 (Siluriformes: Trichomycteridae) in the Rio Doce Basin: iterating DNA, phylogeny and classical taxonomy. Zoological Journal of the Linnean Society 197(2): 344–441. https://doi.org/10.1093/zoolinnean/zlac018

Ronquist F, Teslenko M, Van der Mark P, Ayres DL, Darling A, Höhna S, Larget B, Liu L, Suchard MA, Huelsenbeck JP (2012) MrBayes 3.2: Efficient Bayesian phylogenetic inference and model choice across a large model space. Systematic Biology 61(3): 539–542. https://doi.org/10.1093/sysbio/sys029

Sarmento-Soares LM, Martins-Pinheiro RF, Aranda AT, Chamon CC (2005) *Trichomycterus pradensis*, a new catfish from southern Bahia coastal rivers, northeastern Brazil (Siluriformes: Trichomycteridae). Ichthyological Exploration of Freshwaters 16: 289–302.

Sarmento-Soares LM, Zanata AM, Martins-Pinheiro RF (2011) *Trichomycterus payaya*, new catfish (Siluriformes: Trichomycteridae) from headwaters of rio Itapicuru, Bahia, Brazil. Neotropical Ichthyology 9(2): 261–271. https://doi.org/10.1590/S1679-62252011000200003

Tamura K, Stecher G, Kumar S (2021) MEGA11: Molecular Evolutionary Genetics Analysis Version 11. Molecular Biology and Evolution 38(7): 3022–3027. https://doi.org/10.1093/molbev/msab120

Vilardo PJ, Katz AM, Costa WJEM (2023) Phylogeny and historical biogeography of neotropical catfishes *Trichomycterus* (Siluriformes: Trichomycteridae) from eastern Brazil. Molecular Phylogenetics and Evolution 186: 107836. https://doi.org/10.1016/j.ympev.2023.107836

Zoosyst. Evol. 100 (1) 2024, 233–253 | DOI 10.3897/zse.100.110133

A new species of terrestrial foam-nesting frog of the *Adenomera simonstuarti* complex (Anura, Leptodactylidae) from white-sand forests of central Amazonia, Brazil

Bryan da Cunha Martins[1], Alexander Tamanini Mônico[2], Cianir Mendonça[1], Silionamã P. Dantas[1], Jesus R. D. Souza[1], James Hanken[3], Albertina Pimentel Lima[2], Miquéias Ferrão[1,3,4,5]

1 *Programa de Pós-graduação em Zoologia, Instituto de Ciências Biológicas, Universidade Federal do Amazonas, Manaus, Amazonas, Brazil*
2 *Instituto Nacional de Pesquisas da Amazônia, Manaus, Amazonas, Brazil*
3 *Museum of Comparative Zoology, Harvard University, Cambridge, Massachusetts, USA*
4 *Programa de Pós-graduação em Biodiversidade Animal, Instituto de Ciências Biológicas, Universidade Federal de Goiás, Goiânia, Goiás, Brazil*
5 *Centro Nacional de Pesquisa e Conservação de Répteis e Anfíbios, Instituto Chico Mendes de Conservação da Biodiversidade, Goiânia, Goiás, Brazil*

https://zoobank.org/1F8E43AD-2A15-4244-AA77-F914D3BFAF2F

Corresponding author: Miquéias Ferrão (uranoscodon@gmail.com)

Academic editor: Pedro Taucce ♦ **Received** 27 July 2023 ♦ **Accepted** 14 February 2024 ♦ **Published** 7 March 2024

Abstract

By using integrative taxonomy, we describe a new species of terrestrial foam-nesting frog of the genus *Adenomera* from white-sand forests of the Rio Negro Sustainable Development Reserve, Central Amazonia, Brazil. Within the *A. andreae* clade, the new species belongs to the *A. simonstuarti* complex where it is sister to the lineage from the lower Juruá River. The new species is assigned to the genus *Adenomera* by having adult SVL smaller than 34.1 mm, by its lack of fringing and webbing between toes and by the absence of spines on the thumb of adult males. It differs from other *Adenomera* by the following combination of characters: antebrachial tubercle absent; toe tips flattened or slightly flattened, with visible expansions; nearly solid, dark-coloured stripe on underside of forearm; single-note advertisement call; notes formed by 11–21 incomplete pulses; call duration varying between 100 and 199 ms; fundamental frequency 1,765–2,239 Hz; dominant frequency 3,448–4,349 Hz; and endotrophic tadpoles with spiracle present and labial teeth absent. Over the last decade, we have inventoried many permanent sampling modules in ombrophilous forests in the Manaus Region and in the Purus-Madeira interfluve, but the new species was found only in the white-sand forest from West Negro-Solimões Interfluve. *Adenomera* **sp. nov.** may be endemic to, or at least a specialist in, this environment.

Key Words

campina, *campinarana*, integrative taxonomy, tadpoles, West Negro-Solimões Interfluve

Introduction

Leptodactylid frogs of the genus *Adenomera* Steindachner, 1867 comprise 30 described species distributed throughout South America east of the Andes (Frost 2024). The taxonomic history of this genus is very complex and, over the last 50 years, numerous systematic studies have reviewed its taxonomic validity, phylogenetic position and species diversity (Heyer 1973, 1974; Frost et al. 2006; Pyron and Wiens 2011; de Sá et al. 2014). The genus was originally described by Steindachner (1867) to accommodate a single species, *A. marmorata*. Later, Lutz (1930) synonymised the genus with *Parvulus*, a subgenus of *Leptodactylus* Fitzinger, 1826, but Parker (1932) soon gave priority to the name *Adenomera* and elevated it as a subgenus of *Leptodactylus*. Four decades later, *Adenomera* was resurrected by Heyer (1974) to accommodate taxa of the *Leptodactylus marmoratus* species group.

To avoid paraphyly of *Leptodactylus* rendered by *Vanzolinius* Heyer, 1974, Frost et al. (2006), supported by evidence from Heyer (1998) and Kokubum and Giaretta (2005), declared *Adenomera* a synonym of *Lithodytes* Fitzinger, 1843 and the latter taxon a synonym (subgenus) of *Leptodactylus*. Based on molecular data, Pyron and Wiens (2011) recovered *Adenomera* as sister to *Lithodytes* and this clade as sister to *Leptodactylus*. The authors also removed the two former taxa from the synonymy with *Leptodactylus*. The sister relationship between *Adenomera* and *Lithodytes* was corroborated by de Sá et al. (2014) through a total evidence analysis, which recovered the clade comprising the two genera as sister to the one grouping *Hydrolaetare* and *Leptodactylus*. Fouquet et al. (2014) performed a comprehensive phylogenetic analysis and recovered eight major clades within *Adenomera*: *A. lutzi* clade, *A. heyeri* clade, *Adenomera* sp. I clade, *A. andreae* clade, *A. marmorata* clade, *A. thomei* clade, *A. martinezi* clade and *A. hylaedactyla* clade. However, Carvalho et al. (2021) recovered *Adenomera* sp. I as *A. juikitam* and, based on acoustic, morphologic and genetic data, concluded that *A. juikitam* instead belongs to the *A. heyeri* clade.

The genus *Adenomera* displays a high prevalence of morphologically cryptic species (e.g. Angulo and Icochea (2010); Carvalho and Giaretta (2013a); Carvalho et al. (2020a); Zaracho et al. (2023)). Some species also show high levels of intraspecific polymorphism (e.g. Cassini et al. (2020)) and congeneric sympatry and syntopy are common; up to three species may occur in the same region (e.g. Carvalho et al. (2021)). These factors make species delimitation in *Adenomera* challenging. Nevertheless, 15 of the 30 currently recognised species were described in the last 10 years (Frost 2024) and several candidate species still await formal description (Fouquet et al. 2014). The massive advance in the taxonomy of *Adenomera* has been made possible by the use of integrative taxonomy (Carvalho et al. 2019a, 2019c). In particular, despite morphological crypsis, advertisement calls are markedly divergent amongst species and represent a powerful source of reliable diagnostic characters (Angulo and Icochea 2010; Carvalho and Giaretta 2013a, b; Carvalho et al. 2019c, 2021).

The *Adenomera andreae* clade comprises four described species—*A. andreae* (Müller, 1923); *A. chicomendesi* Carvalho, Angulo, Kokubum, Barrera, Souza, Haddad & Giaretta, 2019; *A. guarayo* Carvalho, Angulo, Barrera, Aguilar-Puntriano & Haddad, 2020; and *A. simonstuarti* (Angulo & Icochea, 2010)—and two candidate species, *Adenomera* sp. D and *Adenomera* sp. T (Fouquet et al. 2014). While the *A. andreae* clade is restricted to Amazonia, none of the nominal species has a restricted geographic distribution. *Adenomera andreae* shows the widest range, being distributed throughout Amazonia (Carvalho et al. 2019c), while *A. chicomendesi* and *A. guarayo* are widely distributed in south-western Amazonia (Carvalho et al. 2019a, 2020a). *Adenomera simonstuarti* is distributed in western and south-western Amazonia (Carvalho et al. 2020b).

Adenomera simonstuarti was described from Peruvian Amazonia, based on morphological and acoustic data of four males and two females (Angulo and Icochea 2010). Subsequently, Fouquet et al. (2014) reported that the species was more widespread than previously thought, also occurring in Venezuela, Ecuador and Brazil (States of Acre and Amazonas). They also suggested the existence of more than one species hidden under the name *A. simonstuarti* (Fouquet et al. 2014, appendix S2a). Recently, Carvalho et al. (2020b) sequenced additional specimens from Brazil referred to as *A. simonstuarti* and their delimitation analysis recovered eight lineages within this name (hereafter, the *A. simonstuarti* complex). They also re-described the species' advertisement call, based on recordings from the type locality in Peru and an additional locality in the upper Juruá River Basin (Acre, Brazil). Based on molecular, morphological and bioacoustic data, Carvalho et al. (2020b) recognised their lineage 3 as *A. simonstuarti* sensu stricto. They also identified the other lineages as putative new species, pending confirmation with additional data (e.g. acoustic and morphologic data).

Poorly sampled environments in Amazonia usually harbour undocumented biodiversity of anurans (Ferrão et al. 2016; Vacher et al. 2020). Physiognomies comprising the white-sand ecosystems (hereafter, WSE) exemplify such environments (Adeney et al. 2016). The WSE occupies an area of 5% of the Amazonia and comprises two main physiognomies in Brazil: *campina*—open environments characterised as patches of grasslands or scrublands (canopy < 7 m) on a matrix of exposed sandy soil; and *campinarana*—closed-canopy, forested environments characterised by thin-trunked trees of low stature (canopy < 20 m) (Anderson 1981; Ferreira 2009; Adeney et al. 2016). Despite the increasing interest in WSE organisms (Capurucho et al. 2013; Fine and Baraloto 2016; Vicentini 2016; Lamarre et al. 2016; Borges et al. 2016; Fraga et al. 2018; Gonella et al. 2020), studies of anurans from WSE are rare. The few such studies recently published show that WSE represents a source of poorly known and new species of anurans, many of which appear to be specialists in or endemic to these environments (Carvalho et al. 2019a; Ferrão et al. 2019, 2022; Mônico et al. 2023).

In the present study, we sampled an unreported lineage of the *Adenomera simonstuarti* complex from the white-sand forests of Central Amazonia and, by using integrative taxonomy, describe it as a new species.

Methods

Sampling

Fieldwork was conducted between 2019 and 2023 in three long-term ecological research sites (RAPELD) in the Rio Negro Sustainable Development Reserve (hereafter, RDS Rio Negro), Municipality of Iranduba, State of Amazonas, Brazil (Fig. 1). Modules are located near km 18 (3°06'33.6"S, 60°40'29.0"W; 73 m above sea level

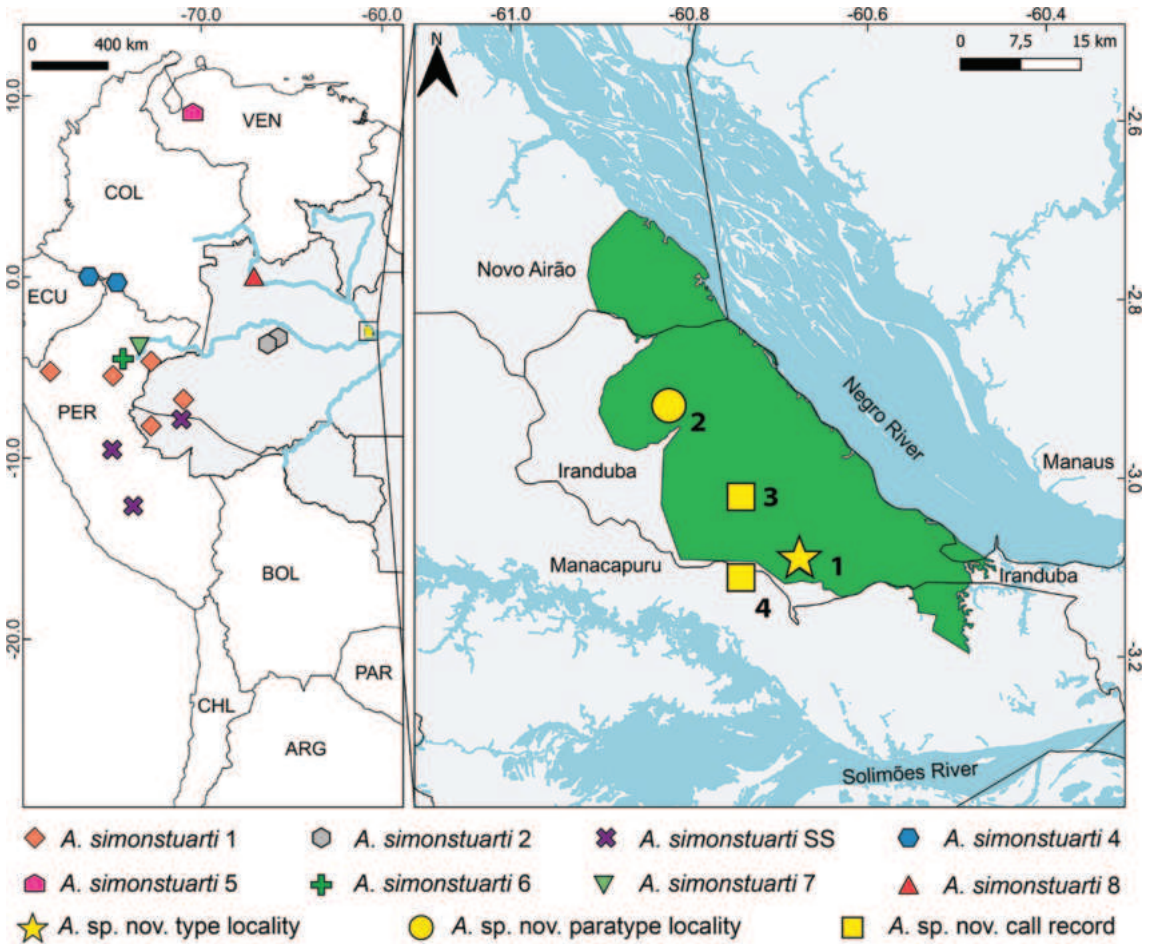

Figure 1. Geographic distribution of the *Adenomera simonstuarti* species complex (left) and a detailed view of the geographic distribution of the new species in central Amazonia, Amazonas, Brazil (right). Green area: Rio Negro Sustainable Development Reserve. Numbers: permanent sampling modules at (1) km 18, (2) km 26 and (3) km 50 along the AM-352 highway; (4) Vale da Benção Community, Ramal do 25, Manacapuru. South American countries: ARG, Argentina; BOL, Bolivia; CHL, Chile; COL, Colombia; ECU, Ecuador; PAR, Paraguay; PER, Peru; VEN, Venezuela.

[hereafter [a.s.l.]), km 26 (3°03'31.0"S, 60°45'42.0"W; 73 m a.s.l.) and km 50 (2°50'10.0"S, 60°50'20.0"W; 19 m a.s.l.) of the AM-352 highway. Adults were euthanised with 2% aqueous benzocaine topical solution, fixed in 10% neutral-buffered formalin and preserved in 70% ethanol. Before fixation, tissue samples of each specimen were collected and stored in 100% ethanol. Tadpoles were collected from two foam nests in the calling site of two uncollected males near the sampling module at km 18. They were euthanised as described above, fixed and preserved in 5% neutral-buffered formalin. Adults were deposited in the herpetological collections of the Instituto Nacional de Pesquisas da Amazônia (**INPA-H**; Manaus, Brazil), Museu Paraense Emílio Goeldi (**MPEG**; Belém, Brazil) and Museu de Zoologia da Universidade de Campinas (**ZUEC-AMP**; Campinas, Brazil); tadpoles were deposited at **INPA-H**.

Advertisement calls of six males of the new species (INPA-H 44867 [holotype], MPEG 44649, INPA-H 44868–69, MPEG 44652 and INPA-H 44877) were recorded with a Sennheiser K6/ME66 unidirectional microphone (Sennheiser, Germany) coupled to a Marantz PMD660 digital recorder (Kanagawa, Japan) and with a Sony PCM-D50 digital recorder with built-in microphone. Recordings were stored in wav files with a sampling rate of 44.1 kHz and sample size of 16 bits. The microphone was positioned 50–100 cm from the calling male. Air temperature during all recordings was 25 °C. Recordings were deposited in the Neotropical Jacques Vielliard sound repository of the University of Campinas (**FNJV;** Campinas, Brazil) under accession numbers FNJV 59561–66.

To facilitate interspecific comparisons, 16 specimens and the advertisement calls of six males of *Adenomera simonstuarti* sensu stricto were collected and recorded, respectively, at Unidade de Gestão Ambiental Acurauá, Municipality of Tarauacá, State of Acre, Brazil. A specimen from this locality (INPA-H 40967) was included in the phylogenetic inference of Carvalho et al. (2020b) and nests with samples of *A. simonstuarti* sensu stricto from Peru and male advertisement calls of the Acre population match with those in the original description by Angulo and Icochea (2010). All males of the Acre population were found in the field by their vocalisation, ensuring that we collected the target species.

Morphology

The description of external morphology of adults of the new species is based on 21 males and five females. Sex was determined through direct assessment of sexual characters: the presence of vocal slits, vocal sac and a fleshy ridge on the snout tip in males and absence in females. Maturity was determined, based on breeding behaviour in males (calling activity) and examination of secondary sexual characters in females (mature oocytes visible through the belly skin). The following 16 morphometric measurements (Watters et al. 2016) were taken to the nearest 0.1 mm using digital calipers and an ocular micrometer coupled to a stereomicroscope: snout-vent length (**SVL**), head length (**HL**), head width (**HW**), snout length (**SL**), eye-nostril distance (**EN**), eye diameter (**ED**), interorbital distance (**IOD**) internarial distance (**IND**), tympanum diameter (**TD**), upper arm length (**UAL**), hand length (**HAL**), forearm length (**FLL**), thigh length (**THL**), tibia length (**TL**), foot length (**FL**) and tarsus length (**TSL**). Toe tip development (character states) follows Heyer (1973). Snout shape follows Heyer et al. (1990). Terminology for other morphological characters follows Carvalho et al. (2020a). We follow the colour catalogue of Köhler (2012): colour names are italicised; cc, colour code. Repeated colours do not repeat codes. See Suppl. material 1: table S1 for morphometric raw data.

The larval developmental stage was determined according to Gosner (1960). The following morphometric measurements were taken with a micrometer coupled to a stereomicroscope from 10 tadpoles at stages 35 (n = 7) and 41 (n = 3): total length (**TL**), body length (**BL**), tail length (**TAL**), maximum tail height (**MTH**), tail muscle height (**TMH**), tail muscle width (**TMW**), inter-nostril distance (**IND**) and interorbital distance (**IOD**) (Altig and McDiarmid 1999); body height (**BH**), body width at spiracle level (**BW**), eye-nostril distance (**END**), eye diameter (**ED**) and oral-disc width (**ODW**) (Lavilla and Scrocchi 1986); body width at eye level (**HW**) (Lima et al. 2015); and vent-tube length (**VTL**) (Lins et al. 2018). Morphological description is based on seven tadpoles at stage 35. Terminology and diagnostic characters follow Altig and McDiarmid (1999) and Schulze et al. (2015).

Vocalisation

Description of the advertisement call and the following acoustic parameters follow Carvalho et al. (2019a) and Köhler et al. (2017): call duration (**CD**), notes per call (**NpC**), note duration (**ND**), note repetition rate (**NrR**) note rise time (**NrT**), pulses per note (**PpN**), pulse duration (**PD**; measured for the first, central and last pulses of each note), pulse repetition rate (**PrR**), dominant frequency (**DF**), fundamental frequency (**FF**) and frequency modulation (**FM**). See Suppl. material 1: table S2 for bioacoustic raw data.

Calls were analysed with Raven 1.5.1 (Bioacoustics Research Program 2014) configured as follows: Hamming window (size = 20 ms), filter bandwidth 65 Hz, overlap 90%, hop size 2 ms and Discrete Fourier Transform 1,024 samples. The dominant frequency and rise time were measured with the peak frequency and peak time relative functions. Figures were produced in R platform (R Core Team 2021) with the packages seewave 2.1.0 (Sueur et al. 2008) and tuneR 1.3.2 (Ligges et al. 2017). Seewave was set as follows: Hamming window, Fast Fourier Transform 256 points, overlap 90%.

Molecular phylogenetics

Genomic DNA was extracted from tissues of four specimens of the new species using a Wizard genomic DNA Purification Kit (Promega Corp., Madison, WI, USA) according to the manufacturer's protocol. Fragments of cytochrome c oxidase subunit I (COI) were amplified through polymerase chain reaction (PCR) using the primers CHmL4 (5'-TYTCWACWAAYCAYAAAGAY-ATCGG-3') and CHmR4 (5'-ACYTCRGGRTGRC-CRAARAATCA-3') (Che et al. 2012). Reaction conditions were: 60 s at 94 °C followed by 35 cycles of 94 °C (20 s), 50 °C (50 s) and 72 °C (90 s) and final extension of 10 min at 72 °C. The final volume of the PCR reaction was 15 µl and contained 0.6 µl of 50 mM $MgCl_2$, 1.2 µl of 10 mM dNTPs (2.5 mM each dNTP), 1.5 µl of tampon 10× (75 mM Tris HCl, 50 mM KCl, 20 mM $(NH_4)_2SO_4$), 0.5 µl of each primer (10 µM), 9.55 µl of ddH_2O, 0.15 µl of 1 U Taq DNA Polymerase and 1 µl of DNA (30–50 ng/µl).

The PCR products were purified using Exonuclease I and Thermosensitive Alkaline Phosphatase (Thermo Fisher Scientific, Waltham, MA, USA). Subsequent sequencing reactions were performed using standard protocols of the Big Dye™ Terminator Kit (Applied Biosystems, Waltham, USA). We used an automated sequencer ABI Prism 3130 (ThermoFisher Scientific, Waltham, USA) to sequence the amplicons. Sequences were edited with Geneious 5.3.4 (Kearse et al. 2012). Newly-generated sequences are deposited in the online repository GenBank under accession numbers OQ974333–36.

To infer phylogenetic relationships, we inserted the generated sequences into a dataset containing sequences retrieved from GenBank (Suppl. material 1: table S3). Our dataset contains the genes cytochrome b (Cytb), cytochrome c oxidase subunit I (COI), recombination activating gene 1 (RAG1) and pro-opiomelanocortin C. These sequences represent all species of the *Adenomera andreae* clade, including all known lineages of *A. simonstuarti*, as well as *Adenomera* sp. D and *Adenomera* sp. T (Fouquet et al. 2014; Carvalho et al. 2020b) and species belonging to the other six clades (Suppl. material 1: table S3). *Lithodytes lineatus* was used to root the tree. To align sequences of each gene, we used the MAFFT online server following default parameters under the G-INS-i strategy. The final matrix was concatenated in Geneious 5.3.4 and comprises 53 terminals and 3,293 base pairs (bp) (667 for Cytb, 657 for COI, 1,422 for RAG1 and 547 for POMC).

We divided the dataset considering first, second and third codon positions for each protein-coding gene and we used PartitionFinder 2.1.1 (Lanfear et al. 2017) under

the corrected Akaike Information Criterion (AICc) to infer partition schemes and evolutionary models. The best evolutionary models for partitions in the concatenated matrix were TIM+G for Cytb 1st and COI 3rd positions; SYM+I+G for Cytb 2nd position; GTR+I+G for Cytb 3rd position; TRNEF+I+G for COI 1st position; F81+I+G for COI 2nd position; TRN+I+G for RAG1 1st and 2nd positions; GTR+G for RAG1 3rd and POCM 1st positions; TVM+I+G for POMC 2nd position; and GTR+I for POMC 3rd position. Phylogenetic relationships were reconstructed through Maximum Likelihood (ML) using IQTREE (Nguyen et al. 2015) implemented in the online server http://iqtree.cibiv.univie.ac.at/ (Trifinopoulos et al. 2016). Clade support was estimated with 10,000 ultrafast bootstrap replicates (Hoang et al. 2018) using 5,000 maximum iterations, 3,000 replicates and a minimum correlation coefficient of 0.99. Lineage numbering within the *A. simonstuarti* species complex follows Carvalho et al. (2020b), except by *A. simonstuarti* 3, which is referred to as *A. simonstuarti* sensu stricto (SS) in the present study.

Based on COI alignment, we calculated pairwise genetic distances (uncorrected p-distance and Kimura two-parameter distance; Kimura (1980)) between the new species and closely related taxa of the *A. simonstuarti* species complex using MEGA 6 (Tamura et al. 2013). Mean distances are presented as in the main text, minimum–maximum values in the Suppl. material 1: table S4.

Morphometric analysis

Due to the phenotypic similarity between *A. simonstuarti* sensu stricto and the new species, we performed a Principal Component Analysis (PCA) associated with a Multivariate Analysis of Variance (MANOVA) to test for a statistical difference between the morphometric multidimensional spaces of each species. Analysis was performed only for males due to the low number of females collected for *A. simonstuarti* sensu stricto. The same 16 morphometric measurements taken from the new species were also taken from 14 adult males of *A. simonstuarti*. To perform morphometric PCA, we transformed the raw data into 15 morphometric ratios: HL/SVL, HW/SVL, SL/SVL, END/SVL, IND/SVL, ED/SVL, IOD/SVL, TD/SVL, FAL/SVL, UAL/SVL, HAL/SVLL, TL/SVL, FL/SVL, THL/SVL and TAL/SVL. The PCA and MANOVA were run using the functions prcomp and manova of the package stats 4.1 (R Core Team 2021); an ellipse representing the standard errors of points in the graphic representation of PCA was drawn using the function ordiellipse of the package vegan 2.5-7 (Oksanen et al. 2020) with parameter kind set as *se*. See Suppl. material 1: table S1 for morphometric measurements of *Adenomera* sp. nov. and *A. simonstuarti* sensu stricto.

Interspecific morphological comparisons

Succinct morphological comparisons of adults were made with all 30 nominal congeners but detailed morphological and acoustic comparisons were restricted to species of the *Adenomera andreae* clade (*A. andreae* [Müller, 1923]; *A. chicomendesi* Carvalho, Angulo, Kokubum, Barrera, Souza, Haddad & Giaretta, 2019; *A. guarayo* Carvalho, Angulo, Barrera, Aguilar-Puntriano & Haddad, 2020; and *A. simonstuarti*) and species distributed in Amazonia (*A. amicorum* Carvalho, Moraes, Lima, Fouquet, Peloso, Pavan, Drummond, Rodrigues, Giaretta, Gordo, Neckel-Oliveira & Haddad, 2021; *A. aurantiaca* Carvalho, Moraes, Lima, Fouquet, Peloso, Pavan, Drummond, Rodrigues, Giaretta, Gordo, Neckel-Oliveira & Haddad, 2021; *A. glauciae* Carvalho, Simões, Gagliardi-Urrutia, Rojas-Runjaic, Haddad and Castrovejo-Fisher, 2020; *A. gridipappi* Carvalho, Moraes, Lima, Fouquet, Peloso, Pavan, Drummond, Rodrigues, Giaretta, Gordo, Neckel-Oliveira & Haddad, 2021; *A. heyeri* Boistel, Massary & Angulo, 2006; *A. hylaedactyla* (Cope, 1868); *A. inopinata* Carvalho, Moraes, Lima, Fouquet, Peloso, Pavan, Drummond, Rodrigues, Giaretta, Gordo, Neckel-Oliveira & Haddad, 2021; *A. kayapo* Carvalho, Moraes, Lima, Fouquet, Peloso, Pavan, Drummond, Rodrigues, Giaretta, Gordo, Neckel-Oliveira & Haddad, 2021; *A. lutzi* Heyer, 1975; *A. martinezi* (Bokermann, 1956); *A. phonotriccus* Carvalho, Giaretta, Angulo, Haddad & Peloso, 2019; and *A. tapajonica* Carvalho, Moraes, Lima, Fouquet, Peloso, Pavan, Drummond, Rodrigues, Giaretta, Gordo, Neckel-Oliveira & Haddad, 2021). Larval comparisons were made with all nominal species for which tadpoles are described (*A. andreae*, *A. guarani*, *A. hylaedactyla*, *A. marmorata*, *A. saci* and *A. thomei*), except for *A. bokermanni* because the tadpole described for it might correspond to another species (Carvalho and Giaretta 2013b). Comparisons were made based on published data (i.e. taxonomic descriptions, re-descriptions and revisions), except the one for *Adenomera simonstuarti*, which is based on direct analysis of specimens (Appendices 1, 2).

Results

Phylogenetic relationships and genetic distances

Individuals of *Adenomera* sp. nov. nest together as a new monophyletic lineage (bootstrap support = 100) within the *A. simonstuarti* species complex (sensu Carvalho et al. (2020b)), which nests within the *A. andreae* clade (Fig. 2). The new species is sister to the lineage *A. simonstuarti* 2 from the lower Juruá River in Brazil. Clades representing *A. simonstuarti* 2 and *Adenomera* sp. nov. are the shallowest within the species complex; the average p-distance for COI between them equals 2.9% (2.5–3.3%) (Table 1; Suppl. material 1: table S4). Peruvian and Brazilian individuals of *A. simonstuarti* sensu stricto are recovered as sister to the clade comprising *A. simonstuarti* 1, *A. simonstuarti* 2 and *Adenomera* sp. nov. Genetic p-distance between the new species and *A. simonstuarti* sensu stricto averages 5.2% (4.3–5.9%).

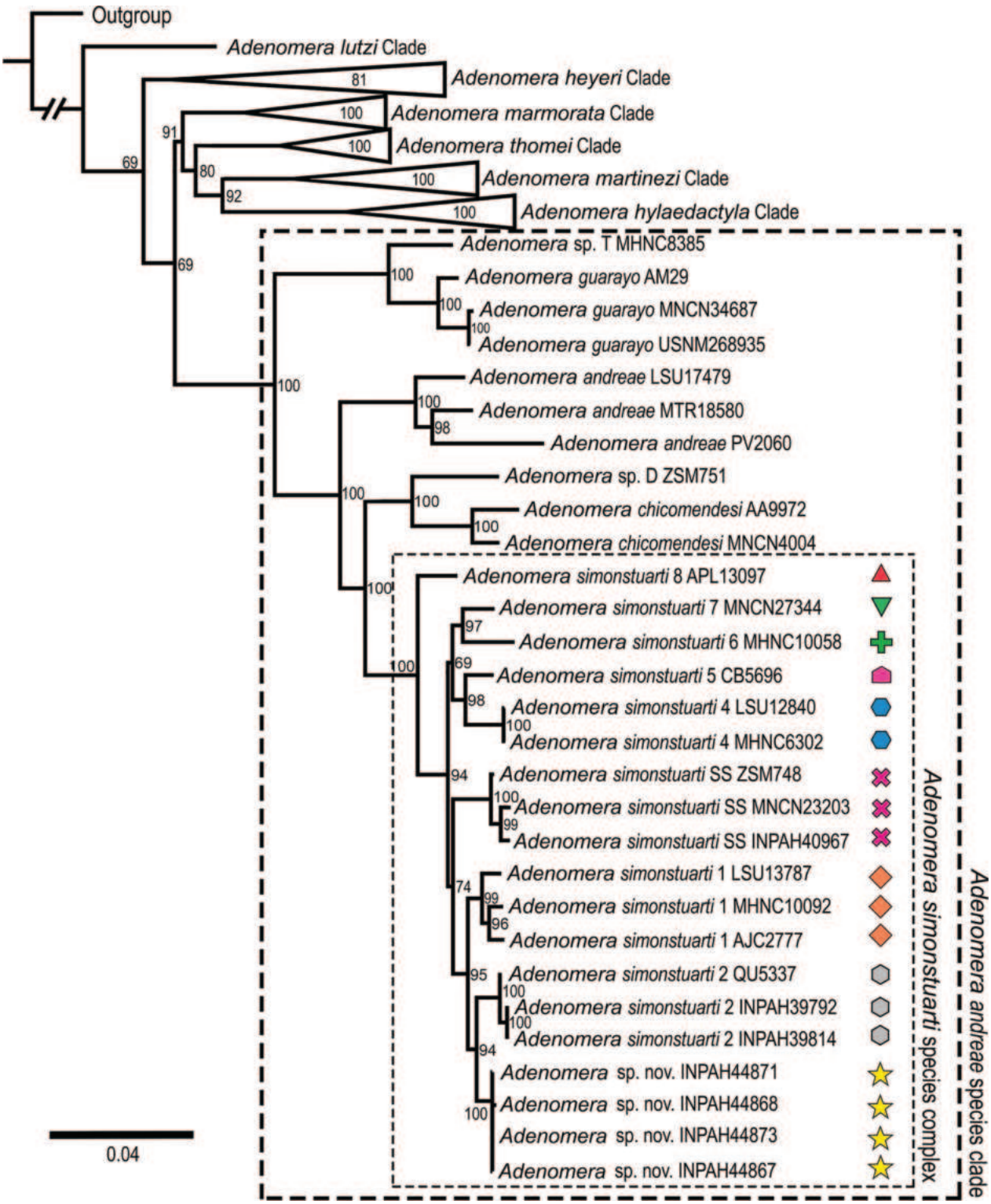

Figure 2. Phylogenetic relationships of the *Adenomera andreae* species clade with a focus on the *A. simonstuarti* species complex. Maximum Likelihood values are inferred from sequence data for Cytb, COI, RAG1 and POMC genes. Lineage numbering within *A. simonstuarti* species complex follows Carvalho et al. (2020b), except for *A. simonstuarti* sensu stricto (SS). Species names are followed by the corresponding museum voucher numbers. Symbols are as in Fig. 1.

Morphometric analysis

The first two principal components (PCs) of morphometric PCA explained ~ 53% of data variance. Spaces occupied by *Adenomera* sp. nov. and *A. simonstuarti* SS are significantly different (Pillai = 0.286, df = 32, $p = 0.004$) and do not overlap (Fig. 3). The three morphometric ratios that contribute most of the variation along PC1 are END/SVL, ED/SVL and DSL/SVL. See Table 2 for data regarding other PCA variables.

Table 1. Average pairwise genetic distances (%) between lineages of the *Adenomera simonstuarti* species complex and related species of the *A. andreae* clade. Interspecific uncorrected p-distances (lower diagonal) and Kimura 2-parameter distances (upper diagonal) are based on a fragment of the COI gene. Intraspecific p-distances are shown along the diagonal in bold. See Supplementary file 4 for minimum and maximum values.

	Species	1	2	3	4	5	6	7	8	9	10	11	12	13	14
1	*Adenomera* sp. nov. (n = 4)	0.3	4.0	3.0	5.5	5.7	5.1	5.5	5.6	7.1	13.8	13.9	17.5	14.0	16.9
2	*A. simonstuarti* 1 (n = 3)	3.9	2.1	3.7	5.7	6.1	5.2	6.7	4.6	7.1	14.0	14.4	16.7	14.2	18.1
3	*A. simonstuarti* 2 (n = 3)	2.9	3.6	0.4	5.5	7.0	5.6	6.1	5.5	7.5	14.6	14.4	17.1	14.1	17.3
4	*A. simonstuarti* SS (n = 3)	5.2	5.4	5.2	0.8	5.4	5.0	5.4	5.3	7.4	13.6	14.8	16.7	14.0	18.0
5	*A. simonstuarti* 4 (n = 2)	5.4	5.8	6.5	5.1	0.0	4.1	7.5	5.7	7.7	14.5	14.0	15.7	14.5	17.1
6	*A. simonstuarti* 5 (n = 1)	4.9	4.9	5.3	4.8	3.9	NA	6.2	3.9	7.3	13.8	15.1	16.6	13.5	17.3
7	*A. simonstuarti* 6 (n = 1)	5.2	5.8	5.8	5.2	7.0	6.2	NA	6.1	6.9	14.1	14.4	17.6	14.7	17.6
8	*A. simonstuarti* 7 (n = 1)	5.4	4.4	5.2	5.0	5.4	3.8	5.8	NA	6.7	15.5	14.7	16.6	15.0	19.5
9	*A. simonstuarti* 8 (n = 1)	6.6	6.7	7.0	6.9	7.2	6.9	6.5	6.4	NA	13.0	12.6	16.5	14.1	17.3
10	*A. andreae* (n = 3)	12.3	12.5	12.9	12.2	12.9	12.3	12.6	13.7	11.7	6.6	15.3	17.0	12.8	16.1
11	*A. chicomendesi* (n = 2)	12.4	12.8	12.8	13.1	12.5	13.3	12.8	13.0	11.4	13.4	4.9	19.2	10.3	19.4
12	*A. guarayo* (n = 3)	15.2	14.6	14.9	14.6	13.9	14.5	15.2	14.5	14.5	14.9	16.6	2.7	17.9	8.8
13	*Adenomera* sp. D (n = 1)	12.4	12.6	12.5	12.4	12.8	12.0	12.9	13.1	12.5	11.5	9.4	15.6	NA	17.9
14	*Adenomera* sp. T (n = 1)	14.0	15.7	15.1	15.6	14.9	15.1	15.3	16.8	15.1	14.2	16.7	8.2	15.6	NA

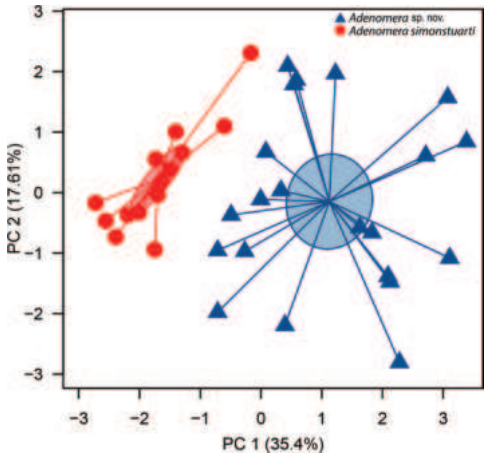

Figure 3. Morphometric Principal Component Analysis. Analyses were based on 15 morphometric ratios of 21 males of *Adenomera* sp. nov. and 14 males of *A. simonstuarti* sensu stricto. Ellipse represents the standard error with 95% confidence interval.

Table 2. Loadings of 15 morphometric and 9 bioacoustic ratios on the respective first principal components. Values were generated from data for 21 males of *Adenomera* sp. nov. and 14 males of *A. simonstuarti* sensu stricto.

Variables	PC 1	PC 2
HL/SVL	0.480	0.697
HW/SVL	0.378	0.777
SL/SVL	0.732	-0.325
END/SVL	0.845	-0.355
IND/SVL	0.348	0.168
ED/SVL	0.743	-0.112
IOD/SVL	0.720	0.145
TD/SVL	0.199	-0.420
FAL/SVL	0.571	-0,152
UAL/SVL	-0.174	-0.046
HAL/SVL	0.097	0.009
TL/SVL	0.099	-0.118
FL/SVL	-0.041	0.172
THL/SVL	-0.165	-0.051
TSL/SVL	0.448	-0.215

Taxonomic account

Order Anura Fischer von Waldhein, 1813
Family Leptodactylidae Werner, 1896
Subfamily Leptodactylinae Werner, 1896
Genus *Adenomera* Steindachner, 1867

***Adenomera albarena* sp. nov.**

https://zoobank.org/0FAB2CE9-3291-453D-8C58-E092BD288DCA

Tables 3, 4, Figs 4–7, 9B–D

Chresonymy. *Adenomera* gr. *heyeri* (Lima et al. 2021).

Type material. *Holotype*. INPA-H 44867, an adult male collected at km 26 of the AM-352 highway, Rio Negro Sustainable Development Reserve (03°05'35"S, 60°40'36"W; 76 m a.s.l.), Municipality of Iranduba, State of Amazonas, Brazil, on 11 December 2020 by M. Ferrão, A. P. Lima and W. E. Magnusson.

***Paratypes*.** Twenty-four adults collected at the same locality as the holotype; eight males MPEG 44649, INPA-H 44868–73 and ZUEC-AMP 25694 collected on 11 December 2020 by M. Ferrão, A. P. Lima and W. E. Magnusson; four females INPA-H 44874–75, ZUEC-AMP 25695 and MPEG 44650 collected on 10 December 2021 by M. Ferrão, A. P. Lima and B. Martins; four males INPA-H 44876–77 and MPEG 44651–52 collected on 11 December 2021 by M. Ferrão, A. P. Lima and B. Martins; four males INPA-H 44878–80 and ZUEC-AMP 25696 collected on 12 December 2021 by M. Ferrão, A. P. Lima and B. Martins; a male INPA-H 44881 collected on 19 January 2022 by B. Martins; a male INPA-H 44882 collected on 3 February 2022 by B. Martins; a male ZUEC-AMP 25697 and a female INPA-H 44883 collected on 14 May 2022 by B. Martins. One adult male INPA-H 44885, collected at km 50 of the AM-352 Highway, Rio Negro Sustainable Development Reserve (2°50'10.0"S, 60°50'20.0"W), Municipality of Iranduba, State of Amazonas, Brazil, on 12 January 2023 by B. Martins.

Table 3. Morphometric measurements of the type series of *Adenomera albarena* (Rio Negro Sustainable Development Reserve, Iranduba, Amazonas, Brazil) and *A. simonstuarti* sensu stricto (Tarauacá, Acre, Brazil). Values depict average, standard deviation and range. Abbreviation: SS, sensu stricto. Trait acronyms are explained in the text. * Holotype included.

	Adenomera albarena			*Adenomera simonstuarti* SS	
Trait	**Holotype**	**Males (n = 21)***	**Females (n = 5)**	**Males (n = 14)**	**Females (n = 2)**
SVL	22.9	21.9 ± 0.5 (21.2–23.0)	23.7 ± 0.9 (22.1–24.3)	24.9 ± 0.7 (23.9–26.4)	24.4 ± 2.0 (23.0–25.8)
HL	8.4	7.9 ± 0.3 (7.4–8.4)	8.1 ± 0.4 (7.4–8.5)	8.9 ± 0.3 (8.2–9.4)	8.5 ± 0.5 (8.1–8.8)
HW	8.5	8.1 ± 0.3 (7.6–8.7)	8.4 ± 0.6 (7.6–9)	9.2 ± 0.3 (8.7–9.7)	9.2 ± 0.6 (8.7–9.6)
SL	3.8	3.5 ± 0.2 (3.3–3.9)	3.4 ± 0.3 (2.9–3.8)	3.8 ± 0.2 (3.5–4.0)	3.4 ± 0.5 (3.1–3.8)
EN	2.0	2.0 ± 0.1 (1.9–2.2)	2.3 ± 0.2 (2.0–2.5)	2.0 ± 0.1 (2.0–2.2)	2.0 ± 0.4 (1.8–2.3)
IND	2.4	2.3 ± 0.1 (2.0–2.4)	2.3 ± 0.1 (2.1–2.5)	2.6 ± 0.1 (2.5–2.7)	2.5 ± 0.1 (2.4–2.5)
ED	2.4	2.5 ± 0.1 (2.2–2.7)	2.6 ± 0.2 (2.3–2.8)	2.3 ± 0.2 (2.1–2.6)	2.3 ± 0.1 (2.2–2.4)
IOD	5.4	5.4 ± 0.2 (5.0–5.8)	5.6 ± 0.4 (4.9–5.9)	5.8 ± 0.2 (5.6–6.3)	5.6 ± 0.2 (5.4–5.7)
TD	1.4	1.4 ± 0.1 (1.2–1.5)	1.4 ± 0.1 (1.2–1.5)	1.5 ± 0.1 (1.3–1.8)	1.5 ± 0.1 (1.5–1.6)
FAL	4.7	4.5 ± 0.3 (4.0–5.0)	5.1 ± 0.5 (4.7–6)	5.0 ± 0.3 (4.7–5.8)	5.1 ± 0.3 (5.1–5.6)
UAL	4.4	4.1 ± 0.4 (3.1–4.8)	4.6 ± 0.5 (4.1–5.4)	5.0 ± 0.3 (4.5–5.5)	5.3 ± 0.3 (5.1–5.6)
HAL	4.9	4.5 ± 0.2 (4.0–4.9)	4.7 ± 0.2 (4.5–4.9)	5.2 ± 0.2 (4.8–5.6)	5.1 ± 0.4 (4.8–5.3)
TL	9.5	9.7 ± 0.5 (8.9–10.8)	10.9 ± 0.2 (10.5–11.1)	11.1 ± 0.6 (10.0–12.1)	11.4 ± 0.4 (11.1–11.6)
FL	10.5	10.0 ± 0.4 (9.5–10.7)	10.7 ± 0.3 (10.5–11.2)	11.5 ± 0.5 (10.5–12.2)	11.6 ± 0.6 (11.2–12.0)
THL	9.4	9.2 ± 0.3 (8.9–10)	9.7 ± 0.8 (8.4–10.2)	10.8 ± 0.7 (9.8–11.8)	11.1 ± 0.6 (10.6–11.5)
TSL	5.5	5.6 ± 0.3 (5.0–6.2)	6.1 ± 0.2 (5.9–6.5)	6.2 ± 0.4 (5.5–6.8)	6.2 ± 0.5 (5.8–6.5)

Etymology. The specific epithet *albarena* is formed by the combination of two Latin words: "alba" (white) and "arena" (sand). This is a reference to the white-sand forests of central Amazonia, the distinctive environment inhabited by this species.

Vernacular names. White-sand terrestrial foam-nesting frog (English), rana terrestre de arena blanca (Spanish) and rãzinha da areia branca (Portuguese).

Diagnosis. The species *Adenomera albarena* is recognised by the following combination of characters. (1) Medium size (adult male SVL = 21.2–23.0 mm, n = 21; adult female SVL 22.1–24.3, n = 5); (2) snout of males subovoid in dorsal view and acuminate in lateral view; (3) absence of antebrachial tubercle; (4) toe tips moderately to fully expanded (character states C, D sensu Heyer (1973)); (5) throat in males with condensed melanophores near the jaw and scattered melanophores on the central portion; 6) nearly solid dark-coloured stripe present on the underside of the forearm; (7) Advertisement call composed of a single pulsed note; (8) notes formed by 11–21 pulses; (9) pulses incomplete; (10) dominant frequency 3,448–4,349 Hz; (11) dominant frequency coinciding with the second harmonic; (12) Endotrophic tadpoles; (13) with labial teeth absent; (13) spiracle present; and (14) internarial distance 44–52% of IOD.

Interspecific comparisons. *Adenomera albarena* differs from all congeners, except *A. simonstuarti* by having a nearly solid dark-coloured stripe on the underside of the forearm (Heyer 1973, 1975; Kwet and Angulo 2002; Almeida and Angulo 2006; Kok et al. 2007; Kwet 2007; Angulo and Reichle 2008; Berneck et al. 2008; Kwet et al. 2009; Angulo and Icochea 2010; Carvalho and Giaretta 2013a, 2013b; Carvalho et al. 2019a, 2019b, 2019c, 2019d, 2020a, 2020c, 2021; Cassini et al. 2020; Zaracho et al. 2023).

Amongst Amazonian congeners, adult male *Adenomera albarena* have SVL 21.2–23.0 mm, which is smaller than *A. glauciae* (SVL 27.6–30.4; Carvalho et al. (2020b)), *A. gridipappi* (SVL 25.4–27.7 mm; Carvalho et

Table 4. Spectral and temporal parameters of the advertisement calls of *Adenomera albarena* and *A. simonstuarti* sensu stricto. Values depict average, standard deviation and range. Symbols: *, same values of call duration because the call is composed of only one note; **, measured by Carvalho et al. (2020b) from calls at the type locality in Cusco, Peru and Tarauacá, Brazil; ***, dominant frequency correspond to the first harmonic in *A. simonstuarti* and to the second harmonic in the new species. Abbreviation: SS, sensu stricto. Trait acronyms are described in the main text.

Call traits	***Adenomera albarena* (n = 6)**	***A. simonstuarti* SS (n = 6)**	***A. simonstuarti* SS (n = 2)****
CD (ms)	142 ± 19.0 (100–199), n = 148	4,700 ± 1,400 (1,800–7,000), n = 93	800–6,500
ND (ms)	142 ± 19.0 (100–199), n = 148*	64 ± 10 (40–93), n = 93	57–79
NpC	1 ± 0 (1–1), n = 148	22.4 ± 6.5 (9–33), n = 93	4–30
NrT (%)	28.4 ± 19.9 (2–73), n = 90	50 ± 14 (16–76), n = 93	13–73
NrR	0.8 ± 0.15 (0.6–1.2), n = 30	4.8 ± 0.3 (4.3–5.4), n = 30	4.6 ± 0.1 (4.5–4.9)
PpN	14.8 ± 1.9 (11–21), n = 148	3.4 ± 0.7 (2–6), n = 93	2–3
PD (ms)	10 ± 3.3 (4–23), n = 444	26.4 ± 6.4 (10–53), n = 192	10–53
PrR	107 ± 9.7 (94–138), n = 60	53 ± 8.7 (37–78), n = 30	–
FF (Hz)	1,986 ± 0.1 (1,765–2,239), n = 148***	3,987 ± 0.16 (3,617–4,263), n = 93***	3596–4156***
DF (Hz)	3,899 ± 1.3 (3,448–4,349), n = 148***	1,991 ± 0.05 (1,851–2,224), n = 93***	1,873–2,046***
FM (Hz)	273.8 ± 238.1 (-173–861), n = 90	261.7 ± 119.7 (-173–517), n = 93	43–301

al. (2021)), *A. lutzi* (SVL 25.7–33.5 mm; Kok et al. (2007)) and *A. simonstuarti* (SVL 23.4–26.2 mm; Angulo and Icochea (2010); Carvalho et al. (2020b); present study), but larger than *A. kayapo* (SVL 17.5–21.0 mm; Carvalho et al. (2021)). *Adenomera albarena* has a snout rounded in dorsal view, which differs from *A. martinezi* (snout pointed in dorsal view; Carvalho & Giaretta (2013b)). The absence of an antebrachial tubercle distinguishes *A. albarena* from *A. amicorum*, *A. aurantiaca*, *A. cotuba*, *A. glauciae*, *A. gridipappi*, *A. inopinata*, *A. kayapo*, *A. lutzi*, *A. tapajonica* and *A. phonotriccus* (antebrachial tubercle present; Kok et al. (2007); Carvalho and Giaretta (2013b), Carvalho et al. (2019b, 2020c, 2021)). *Adenomera albarena* has toe tips moderately to fully expanded (states C and D, sensu Heyer (1973)), which differs from *A. cotuba*, *A. hylaedactyla* and *A. martinezi* (toe tips pointed to poorly expanded, states A and B, respectively; Carvalho et al. (2019c); Carvalho and Giaretta (2013a, 2013b)). *Adenomera albarena* differs from *A. heyeri* by having white ventral colouration (yellow colouration; Carvalho et al. (2021)). Although *A. albarena* differs morphologically from *A. andreae*, *A. chicomendesi* and *A. guarayo* only by having a nearly solid dark-coloured stripe on the underside of the forearm (absence in *A. andreae*, *A. chicomendesi* and *A. guarayo*; Carvalho et al. (2019a, 2019b, 2019c)), it also differs acoustically from these species (see below).

The advertisement call of *Adenomera albarena* is composed of incomplete pulses, which differs from *A. aurantiaca*, *A. guarayo*, *A. inopinata* and *A. phonotriccus* (complete pulses; Carvalho et al. (2019b, 2020a, 2021)). Amongst those with incomplete pulses, calls of *A. albarena* sp. nov. differ from *A. amicorum*, *A. glauciae*, *A. gridipappi* and *A. simonstuarti* sensu stricto by having a single note (multi-note calls; Angulo and Icochea (2010); Carvalho et al. (2020b, 2021)). *Adenomera albarena* has calls composed of 11–21 pulses, which differ from *A. amicorum* (4–10 pulses; Carvalho et al. (2021)), *A. andreae* (3–10 pulses; Carvalho et al. (2019c)), *A. chicomendesi* (22–35 pulses; Carvalho et al. (2019a)), *A. gridipappi* (2–4 pulses; Carvalho et al. (2021)), *A. heyeri* (4–12 pulses; Carvalho et al. (2021)), *A. hylaedactyla* (4–10 pulses; Carvalho et al. (2019c)), *A. tapajonica* (3–5 pulses; Carvalho et al. (2021)), *A. glauciae* (unpulsed; Carvalho et al. (2020b)) and *A. simonstuarti* sensu stricto (2–6 pulses; this study). *Adenomera albarena* has a dominant frequency of 3,448–4,349 Hz, which differs from *A. kayapo* (4,570–4,990 Hz; Carvalho et al. (2021)) and *A. simonstuarti* sensu stricto (1,851–2,224 Hz; this study). The dominant frequency of *Adenomera albarena* sp. nov. is placed in the second harmonic, which differs from *A. simonstuarti* sensu stricto (dominant frequency in the fundamental harmonic).

Lack of labial teeth distinguishes tadpoles of *Adenomera albarena* from exotrophic tadpoles of *A. guarani*, *A. saci* and *A. thomei* (present in all mentioned species; De la Riva (1995); Almeida and Angulo (2006); Carvalho and Giaretta (2013a)). Endotrophic tadpoles of *A. albarena* differ from those of *A. hylaedactyla* and *A. andreae* by the presence of a spiracle (absent in all mentioned species; Menin et al. (2009); Menin and Rodrigues (2013)); from *A. marmorata* by an internarial distance 44–52% of IOD (IND/IOD = 74%; Heyer et al. (1990)).

Description of the holotype. Adult male (Figs 4A, B, C, 5A, C). Dorsal skin glandular, warty on flank. Dorsolateral fold indistinct. Sacral region, dorsal surface of tibia and posterior surface of tarsus with white-tipped tubercles. Vertebral stripe in sacral region. Throat, belly and ventral surface of limbs smooth. Pair of lumbar glands. Posterior surface of thigh with a pair of paracloacal glands. Snout subovoid in dorsal view and acuminate in profile. Nostril closer to the snout tip than to the eye and orientated dorsolaterally; fleshy ridge on the snout tip. Eye nostril distance 83% of eye diameter, eye diameter equals internarial distance. Head wider than long. Internarial distance > 25% of head width. Canthus rostralis defined; loreal region slightly concave. Triangular interorbital blotch. Tympanum distinct, nearly 60% of eye diameter; black-coloured supratympanic fold well developed, extending from posterior corner of eye to base of arm. Postcommissural gland ovoid. Subgular vocal sac; vocal slits present. Vomerine teeth in two straight rows posterior to choanae and arranged in transverse series parallel to choanae. Tongue lanceolate (sensu Duellman (1970)) and free behind. Relative finger lengths IV < I ≈ II < III; fringes or webbing on fingers absent; finger tips rounded, slightly expanded, but without disc; inner metacarpal tubercle elliptical; outer metacarpal tubercle rounded; distinct rounded greyish subarticular tubercles on the underside of fingers; supernumerary tubercles rounded; antebrachial tubercle absent. Elliptical axillary gland. Tibia slightly longer than thigh (TL/THL = 1.01). Relative toe lengths I < II < V < III < IV; toe tips flattened or slightly flattened, with visible expansions (character states C and D, sensu Heyer (1973)); fringes or webbing absent; inner metatarsal tubercle elliptical; outer metatarsal tubercle rounded. Tarsal fold from the inner metatarsal tubercle extends 2/3 of tarsus length. Subarticular tubercles elliptical or rounded, supernumerary tubercles rounded.

Colour of the holotype in life. Snout tip ***Cinnamon-drab*** (cc 50), with a fleshy ridge ***Pale neutral grey*** (cc 296). Blotches on upper and lower lips ***Light sky blue*** (cc 191). Postcommissural gland with melanophores. Tympanum ***Dark carmine*** (cc 61) at its edge and ***Buff*** (cc 5) in the centre. Supratympanic fold ***Vandyke brown*** (cc 281). Thoracic dorsal surface of body ***Prout's brown*** (cc 47); lumbar region ***Cinnamon-drab*** with white-tipped tubercles. Interorbital region ***Sepia*** (cc 286). Flank ***Dark spectrum yellow*** (cc 78). Triangular blotch ***Sepia***. Dorsal surface of forelimbs ***Tawny*** (cc 60) with ***Raw umber*** (cc 280) blotches. Dorsal surface of hind-limbs ***True cinnamon*** (cc 260) with transverse ***Raw umber*** bars. Vertebral stripe in sacral region ***Medium chrome orange*** (cc 75).

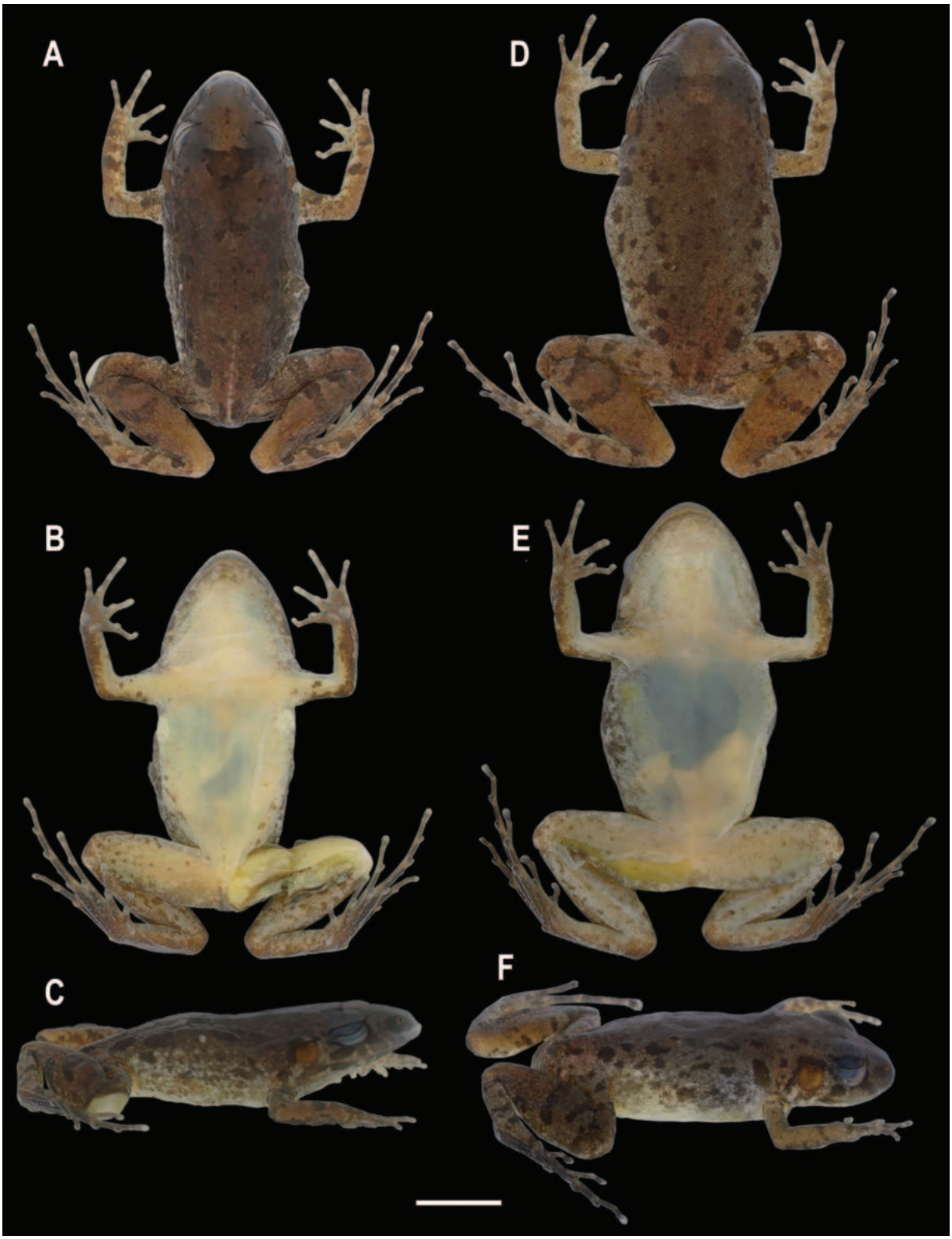

Figure 4. Male holotype and female paratype of *Adenomera albarena*. **A–C.** Male holotype, INPA-H 44867; **D–F.** Female paratype INPA-H 44875. Scale bar: 5 mm.

Paracloacal region and lumbar glands ***Sepia***. Throat ***Pale mauve*** (cc 204) with low density of melanophores around the jaw; belly ***Light buff*** (cc 2) and chest and underside of limbs the same colour as throat. Underside of forearm with ***Dark greyish-olive*** (cc 275) nearly solid stripe. Palm of hand, sole of foot, digits and subarticular tubercles almost completely covered with melanophores. Metatarsal, proximal and medial phalanx have a ***Fuscous*** (cc 283) ventral stripe, which is not present in distal phalanx and toe tip.

Figure 5. Ventral views of the hands and feet of *Adenomera albarena*. **A, C.** Male holotype INPA-H 44867; **B, D.** Female paratype, INPA-H 44875. Scale bars: 5 mm.

Colour of the holotype in preservative*.** See Figs 4A–C, 5A, C. Iris ***chrome orange (colour code [cc] 74). Snout tip ***Pale neutral grey*** (cc 296), as well as the fleshy ridge. Blotches on upper and lower lips ***Pale neutral grey***. Postcommissural gland with melanophores. Tympanum ***Dark grey*** (cc 45). Supratympanic fold ***Vandyke brown*** (cc 281). Thoracic dorsal surface of body ***Hair brown*** (cc 277); lumbar region ***Cinnamon-drab*** (cc 50) with white-tipped tubercles. Interorbital region ***Sepia*** (cc 279). Flank ***Pale buff*** (cc 1). Triangular

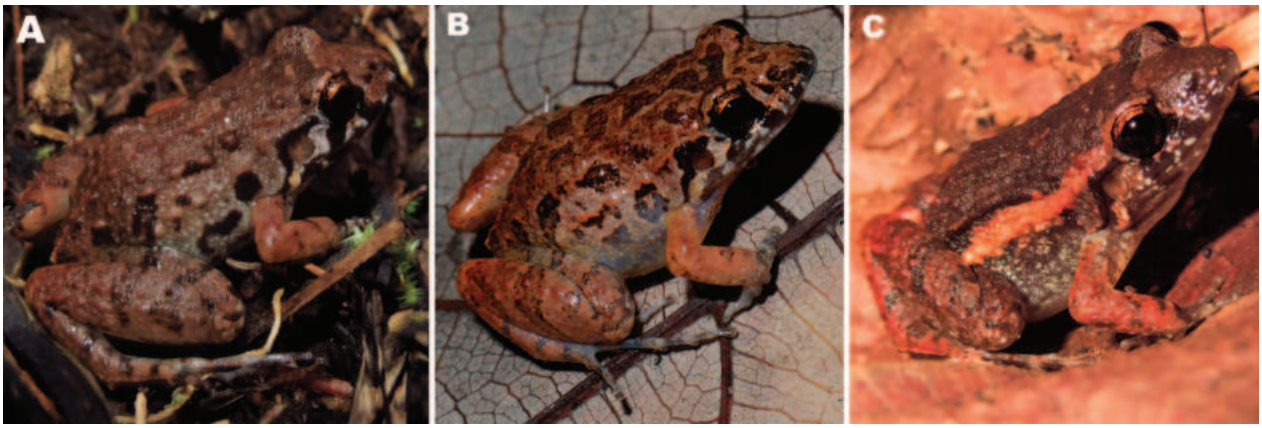

Figure 6. Three dorsal colour patterns of *Adenomera albarena* in life. **A.** Dark blotches few or absent; **B.** Many dark blotches; and C. Dorsolateral stripe. Unvouchered specimens.

interorbital blotch ***Dark greyish-brown*** (cc 284). Dorsal surface of forelimbs ***Pale buff*** (cc 1) with ***Drab*** (cc 19) blotches. Dorsal surface of hind-limbs ***Tawny olive*** (cc 17); transverse bars ***Sepia*** with white-tipped tubercles. Vertebral stripe ***Pale buff*** in sacral region. Paracloacal region and lumbar glands ***Sepia***. Throat ***Light buff*** (cc 2) with melanophores and a greater density around the jaw; belly ***Light buff*** and chest and underside of limbs pale ***Pinkish buff*** (cc 3). Underside of forearm with nearly solid ***Brownish-olive*** (cc 276) stripe. Palm of hand, sole of foot, digits and subarticular tubercles almost completely covered with melanophores. Stripe in metatarsal and proximal and medial phalanx ***Fuscous*** (cc 283) (Figs 5C, D).

Intraspecific variation. Morphometric variation of the new species is summarised in Table 3. The type series shows three dorsal colour patterns: dark blotches few or absent (Figs 6A, 7A); many dark blotches (Figs 6B, 7D); and a dorsolateral stripe (Figs 6C, 7G). Sixty-eight percent of the type series (including the holotype) has the first pattern, 20% have many dark blotches and only 12% have a dorsolateral stripe. A sacral stripe is present in 64% of specimens. About 52% of paratypes have a toe tip shape in stage D (sensu Heyer (1973)), while 48% have an intermediate shape, stages C or D. All individuals have a triangular mark on the head (Fig. 6), which is less visible in individuals that lack dorsal blotches. Texture of the dorsum varies from rough to smooth, with few to many glandules. Throat and belly show slight variation in melanophore density (Fig. 7B, E, H).

Advertisement call. The advertisement call of *Adenomera albarena* consists of a single note with partially fused pulses. Pulse number varies from 11 to 21; pulse duration from 4 to 23 ms; and pulse repetition rate from 94 to 138 pulses per second. Note duration varies from 100 to 199 ms and note repetition rate from 0.6 to1.2 notes per minute. The fundamental frequency of the note coincides with the first harmonic and varies from 1,765 to 2,239 Hz; the dominant frequency varies from 3,746 to 4,349 Hz and corresponds to the second harmonic (Table 4; Fig. 8).

Table 5. Morphometric measurements (mm) of 10 tadpoles of *Adenomera albarena* from Rio Negro Sustainable Development Reserve, Iranduba, Amazonas, Brazil. Trait acronyms are defined in the text; n, sample size.

Traits	Stage 35 (n = 7)	Stage 41 (n = 3)
BH	3.08 ± 0.15 (2.94–3.34)	2.50 ± 0.00 (2.50–2.50)
BL	5.63 ± 0.21 (5.40–6.00)	5.13 ± 0.15 (5.00–5.30)
BW	3.40 ± 0.13 (3.19–3.56)	2.79 ± 0.12 (2.66–2.88)
ED	0.60 ± 0.04 (0.56–0.67)	0.67 ± 0.04 (0.63–0.71)
END	0.38 ± 0.02 (0.35–0.40)	0.40 ± 0.03 (0.38–0.43)
HW	2.77 ± 0.12 (2.58–2.88)	2.58 ± 0.09 (2.50–2.68)
IND	0.76 ± 0.03 (0.70–0.79)	0.75 ± 0.09 (0.67–0.84)
IOD	1.63 ± 0.08 (1.54–1.73)	1.65 ± 0.11 (1.54–1.76)
MTH	2.67 ± 0.12 (2.48–2.80)	2.12 ± 0.04 (2.08–2.16)
ODW	1.03 ± 0.04 (0.96–1.09)	0.89 ± 0.05 (0.85–0.95)
TAL	9.23 ± 0.78 (7.80–10.10)	9.17 ± 0.35 (8.80–9.50)
TL	14.86 ± 0.91 (13.30–16.10)	14.30 ± 0.35 (13.90–14.50)
TMH	1.66 ± 0.07 (1.55–1.75)	1.04 ± 0.07 (1.00–1.13)
TMW	1.25 ± 0.08 (1.14–1.35)	1.18 ± 0.04 (1.14–1.22)
VTL	0.76 ± 0.11 (0.63–0.95)	0.74 ± 0.11 (0.63–0.86)

Tadpole. Body elliptical in dorsal and ventral views, globular in lateral view (Fig. 9A–C); BH 86–96% and 51–58% of BW and BL, respectively (Table 5). Body length 36–41% of TL, with a well-marked constriction in the postorbital region (Fig. 9A) that is more pronounced in dorsal than ventral view and less marked in some tadpoles. Snout rounded in dorsal and lateral views; eye-nostril distance 6–7% of BL. Internarial region convex; internarial distance 44–52% of IOD. Nostrils small, rounded, located and directed anterolaterally; visible in lateral view, poorly visible in dorsal view; closer to snout than to eyes. Border of external nares without fleshy marginal rim; border smooth, slightly below the level of marginal region. Eyes large, diameter 34–39% and 139–190% of IOD and END, respectively; located laterally, but directed anterolaterally. Interorbital region slightly concave; interorbital distance 46–50% of BW. Spiracle very small, single, sinistral; directed posterodorsally, located immediately above the edge of the lateral body surface at the level

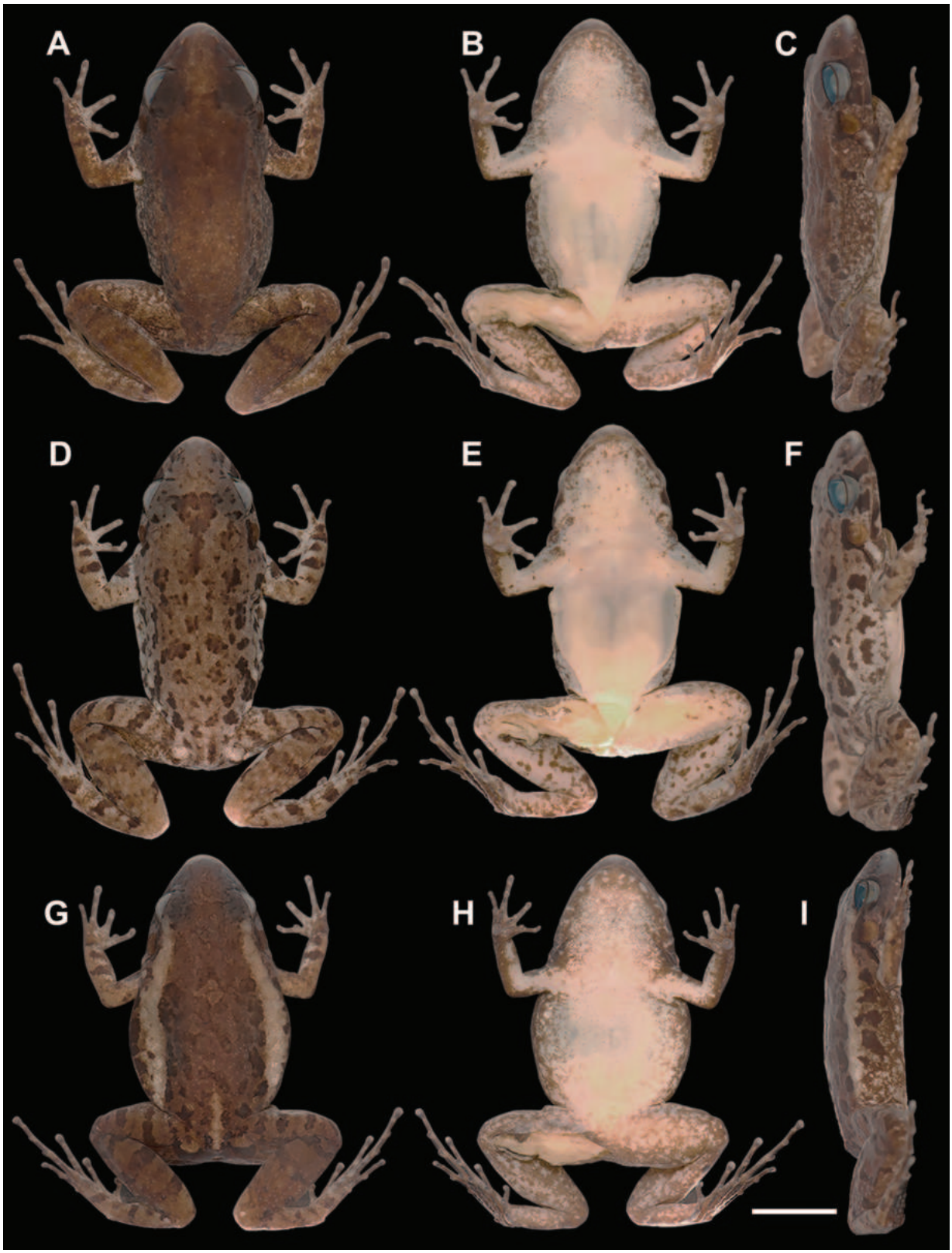

Figure 7. Dorsal, ventral and lateral views of the three colour patterns of *Adenomera albarena* in preservative. Paratypes: **A–C.** (INPA-H 44869, male); **D–F.** (INPA-H 44870, male) and **G–I** (INPA-H 44877, male). Photographs: L. R. Mendonça. Scale bar: 5 mm.

of the hind-limb insertion; poorly visible in dorsal and lateral views. Spiracular opening elliptical; aperture small, narrower than spiracle width, inner wall fused to the body wall. Widely coiled intestines positioned ventrally, perpendicular to main body axis, concealing other internal organs. Vent tube medial with sinistral displacement; comma-shaped, directed upwards; opening very small, rounded, directed dorsally; mostly free

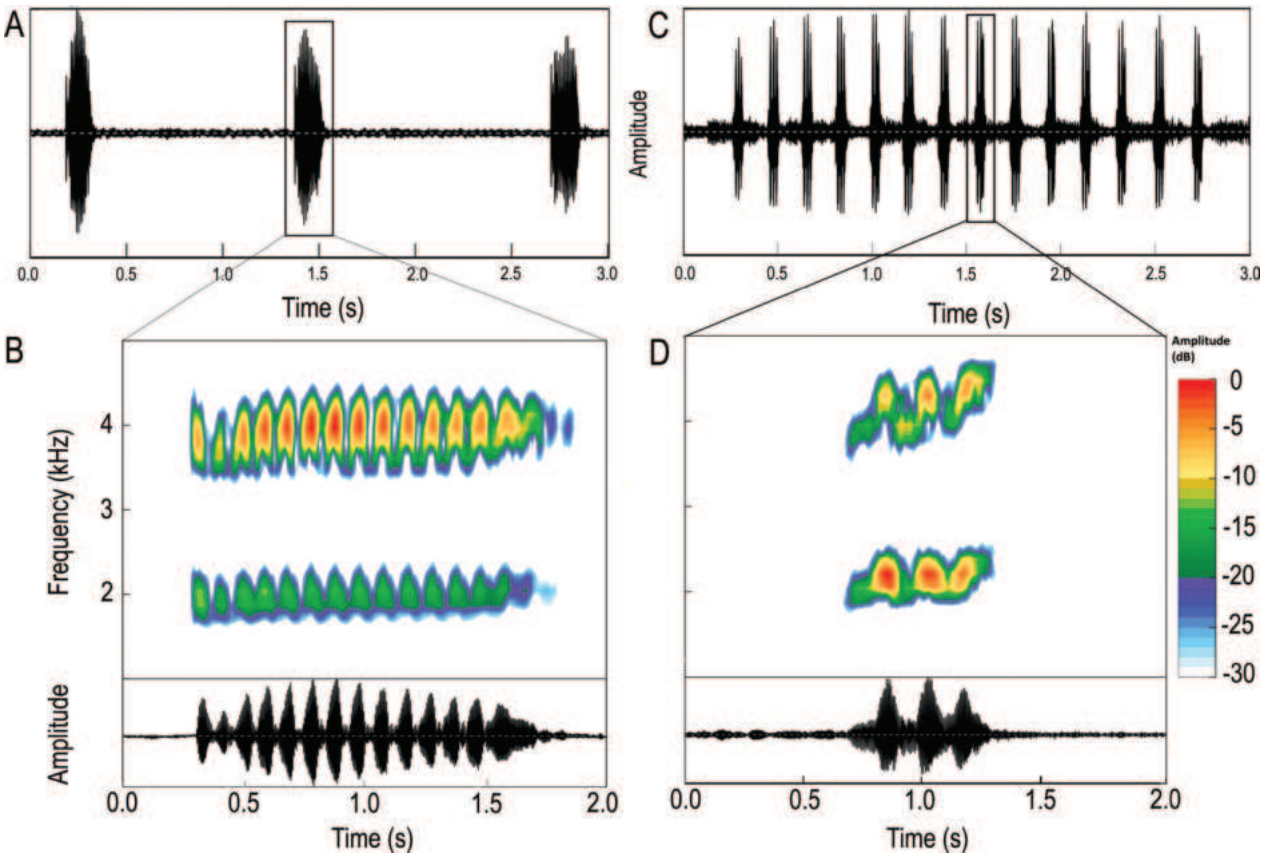

Figure 8. Advertisement call of *Adenomera albarena* (**A, B**) and *A. simonstuarti* sensu stricto (**C, D**). **A, B.** INPA-H 44876 (FNJV 59564), Rio Negro Sustainable Development Reserve, Iranduba, Amazonas, Brazil. **C, D.** INPA-H 44904 (FNJV 59568), Tarauacá, Acre, Brazil.

from the ventral fin, dorsal wall attached only near the body junction. Tail moderately long, length 142–178% and 59–64% of BL and TL, respectively; low, maximum tail height 83–94% of BH; tip rounded. Musculature moderately robust with strongly acuminate tip, which reaches the tail tip; higher than wide near the tail-body junction, tail muscle width 70–79% of TMH; tail muscle height 43–49% of MTH. Dorsal fin external margin slightly convex, originating from posterior third of body; higher than body, slightly higher than ventral fin, with maximum height at its central portion. Ventral fin external margin poorly arched; maximum height at mid-tail; same height as or shorter than body. Oral disc small, ODW 29–33% of BW; unemarginated; located and directed anteroventrally (Fig. 9D). Upper and lower labium present; upper labium with 4–6 short, rounded papillae on lateral region, interleaved by a large medial gap, but arranged in a straight line; posterior labium projected posteriorly, with 3–6 short rounded papillae laterally, interleaved by a medial gap, but arranged in a straight line; anterior gap larger than posterior. Submarginal papillae absent. Jaw sheath keratinised only at the external borders; upper jaw sheath arch-shaped, lower jaw sheath V-shaped. Serrations on each sheath extend its entire length. Labial teeth absent; two labial ridges on the upper labium and three on the lower, formulae 2(2)/3(1).

In preservative, dorsal surface of body brown; anterior half of body darker and with more melanophores than posterior half, with very fine translucent vermiculation on posterior half. Dorsal hind-limbs translucent with numerous melanophores. Tail mostly translucent grey, brown at the tail/body junction; caudal musculature whitish-grey; fins translucent grey; small melanophores on the caudal musculature. Vent tube translucent grey. Ventral surface of body translucent grey with numerous melanophores anteriorly; posterior portion translucent, except for lateral regions, which are light brown.

Distribution, habitat and natural history. *Adenomera albarena* is known only from the white-sand ecosystems between West Negro and the Solimões Rivers, specifically in the RDS Rio Negro and nearby localities, Municipalities of Iranduba and Manacapuru, Amazonas, Brazil, where these ecosystems are dominant (Figs 1, 10A). Two other species of *Adenomera* occur in sympatry: *A. hylaedactyla* and *A. andreae.* Although these species occur in the same region, their habitat is not the same; *A. andreae* mainly inhabits non-flooded forests, while *A. hylaedactyla* occurs in open areas. On the other hand, *Adenomera albarena* inhabits white-sand forests subject to flooding regimes close to streams. At the type locality, *A. andreae* and the new species occur in syntopy at the border between forests subject to flooding regimes and those that do not flood.

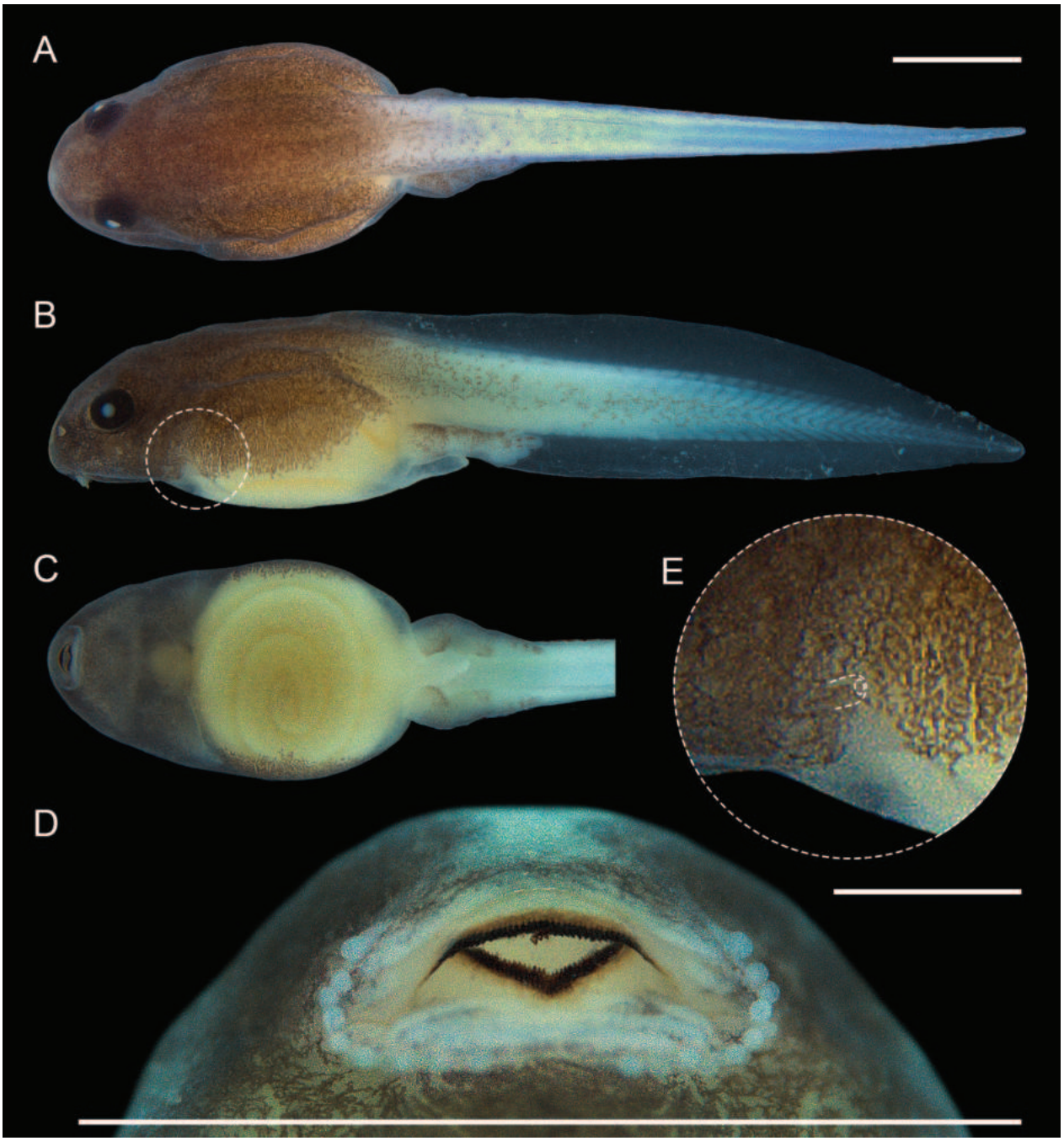

Figure 9. Preserved tadpole of *Adenomera albarena*, Gosner stage 35. Dorsal (**A**), lateral (**B**) and ventral views of the body (**C**) and ventral view of the oral disc (**D**). **E.** Detailed view of the spiracle, with its shape and aperture highlighted by dotted lines. Scale bar: 2 mm (**A–D**); 1 mm (**E**).

Males call from the ground, above or hidden in the leaf litter (Fig. 10B). They start calling at ~ 16:00 h and continue calling until ~ 19:00 h. Isolated individuals sometimes call later, but it is unusual.

Adult males are found easily and juveniles are also not difficult to observe, but females are very secretive (Fig. 10C). Males excavate underground chambers in which foam nests are built and females deposit their eggs (Fig. 10D). The chambers are very difficult to find when they are located under leaf litter amongst the roots of palm trees and ferns.

Conservation. The known geographic distribution of *Adenomera albarena* comprises an area of approximately 150 km^2 within the RDS Rio Negro and nearby localities. Although the species is known only from a small area, it is very common there and likely occurs in other parts of the RDS Rio Negro and, potentially, in the nearby Jaú National Park. Despite its abundance, the new species occurs exclusively in white-sand forests subject to flooding regimes, which are highly vulnerable to anthropogenisation (e.g. from pollution, deforestation, mining, free-ranging livestock, irregular occupation and recreational use

Figure 10. Natural history of *Adenomera albarena*. **A.** Example of the species' habitat; **B.** Unvouchered male vocalising on leaf litter; **C.** Unvouchered female hiding in the leaf litter; **D.** Foam nest, artificially exposed for illustration purpose. Scale bar: ~ 5 mm.

of water). Indeed, several riverine areas in this environment at RDS Rio Negro, including the type locality, have already been impacted by some of these anthropogenic drivers. Long-term monitoring that compares populations between pristine and anthropogenised areas is essential to evaluate whether and how these drivers impact the conservation status of *A. albarena.*

Discussion

For many years, several undescribed species of Amazonian anurans have been erroneously assigned to nominal species that were believed to be geographically widespread (e.g. *Allobates caldwellae* Lima et al. 2020, *Atelopus manauensis* Jorge et al. 2020; *Pristimantis guianensis* Mônico et al. 2022). However, the integration of molecular, acoustic and morphological data has allowed contemporary taxonomists to more accurately delimit and describe such cryptic species (Fouquet et al. 2014; Carvalho et al. 2021; Moraes et al. 2022). Crypsis amongst species of the genus *Adenomera*, combined with their syntopy and sympatry, has been especially challenging, as exemplified by the *A. simonstuarti* species complex. Fouquet et al. (2014) recovered six lineages within this complex (including *A. simonstuarti* sensu stricto). Carvalho et al. (2020b) subsequently considered additional data and delimited eight candidate species. However, none of those candidate species corresponds to the one from RDS Rio Negro that we describe here as a new species. As it is the easternmost taxon within the *A. simonstuarti* complex, this species complex may be more widespread and diverse than previously thought.

Considering the current taxonomic uncertainty of lineages *Adenomera simonstuarti* 1–2 and 4–8, the description of *A. albarena* may introduce taxonomic instability by rendering *A. simonstuarti* as paraphyletic in a few scenarios of species delimitation (e.g. conspecificity of *A. simonstuarti* SS + lineage 1 + lineage 2). In addition to a previous molecular analysis that supports eight candidate species (Carvalho et al. 2020b) and the phenotypic divergence between *A. albarena* and *A. simonstuarti*

SS (present study), Fouquet et al. (2014) document phenotypic divergence between *A. simonstuarti* SS and *A. simonstuarti* 4 (DF 2,830 Hz in *A. simonstuarti* 4 vs. 1,851–2,224 Hz in *A. simonstuarti* SS), which are also distinct from *A. albarena* (DF 3,448–4,349 Hz). Moreover, the slight genetic divergence between *A. albarena* and *A. simonstuarti* 1–2 and the large divergence between them and *A. simonstuarti* SS support the heterospecificity of the two nominal species. A comprehensive taxonomic revision is needed to resolve these taxonomic issues, but it may take decades to complete due to the difficulties in obtaining necessary field samples. On the other hand, solving lineage-by-lineage issues is much less time-consuming and can support conservation planning at the species level across threatened landscapes, such as the white-sand environment (WSE) inhabited by *A. albarena*.

Adenomera albarena is the first species of its genus to be described from a WSE. Although this species is likely a WSE specialist, its known distribution is limited to WSE in the Negro-Solimões interfluve. Other frogs may be specialists in or endemic to WSE in this interfluve, including *Scinax albertinae* (Ferrão et al. 2022), *Pristimantis campinarana* (Mônico et al. 2023) and *Osteocephalus vilarsi* (Ferrão et al. 2019). Moreover, the geographic distributions of two additional candidate species, *Rhinella* aff. *proboscidea* and *Pristimantis* aff. *orcus*, apparently are associated with WSE and limited to the West Negro-Solimões interfluve (unpublished data). The congruence of frog species sharing the same habitat specialisation and pattern of restricted distribution highlights the Jaú Region as an area of endemism within Amazonia (Borges and da Silva 2012).

Two reproductive modes are reported for *Adenomera*: endotrophic tadpoles that complete development entirely in a subterranean foam nest without an exotrophic feeding phase (mode 32, sensu Haddad and Prado (2005)); and exotrophic tadpoles with early developmental stages completed in a subterranean foam nest and later free-living aquatic stages (mode 30, sensu Haddad and Prado (2005)). A spiracle is present in all *Adenomera* with known exotrophic tadpoles (*A. guarani*, *A. saci* and *A. thomei*; Heyer (1973); Almeida and Angulo (2006); Carvalho and Giaretta (2013a); Zaracho and Kokubum (2017); Zaracho et al. (2023)). Amongst species with endotrophic tadpoles, the spiracle is absent in *A. andreae* and *A. hylaedactyla* (Heyer and Silverstone 1969; Kokubum and Sousa 2008; Menin et al. 2009; Menin and Rodrigues 2013) and present in *A. marmorata* (Heyer et al. 1990), *A.* aff. *hylaedactyla* from south-eastern Brazil (Kokubum and Giaretta 2005) and *A. albarena*. The condition of the spiracle differs interspecifically, ranging from a tube free from the body wall in some species to an attached tube in other species. The larval life history and morphological diversity make *Adenomera* an interesting model to investigate the evolution of reproductive features in anurans at small phylogenetic scale. Morphological and behavioural studies of *Adenomera* are urgently required for such evolutionary studies, since tadpoles are known for only a few species.

Amongst the three sympatric species of *Adenomera* living in white-sand environments at RDS Rio Negro, all of them with endotrophic tadpoles, only *A. albarena* inhabits forests subject to flooding and has subterranean foam nests that submerged for at least a few days; flooding habitats are not occupied by *A. andreae* and *A. hylaedactyla*. Hence, the spiracle in *A. albarena* may increase larval survivorship during short flooding periods, enabling the occupancy of flooding habitats by this species. Detailed ecophysiological studies evaluating survival rates in larvae of these three species under distinct flooding conditions are needed to test this hypothesis.

Acknowledgements

We thank William E. Magnusson for fieldwork assistance; Lucas R. Mendonça for photographs; Igor Y. Fernandes and Esteban D. Koch for assistance with phylogenetic analyses; Instituto Nacional de Pesquisas da Amazônia (INPA) for logistic assistance (especially Andressa Viana) and for supporting molecular data acquisition in the Laboratório Temático de Biologia Molecular (LTBM); Ana L.C. Prudente (MEPG), João Sarmento (MPEG), L. Felipe Toledo (ZUEC-AMP, FNJV), Fernanda P. Werneck (INPA-H), Ariane Silva (INPA-H) and Simone Dena (FNJV) for access to collections under their care; Marcelo N. C. Kokubum, Thais H. Condez and Thiago R. de Carvalho for important suggestions regarding an earlier version of this manuscript; Thiago R. de Carvalho for assistance with bioacoustic analysis; Laboratório de Entomologia Sistemática Urbana e Forense (LESUF-INPA; especially Larissa L. de Queiroz) for assistance with photographs of the holotype and a female paratype; the Cornell Lab of Ornithology for providing a free licence for Raven; and Instituto Chico Mendes de Conservação da Biodiversidade/Sistema de Autorização e Informação em Biodiversidade (Process n° 81575-1), Secretaria de Estado do Meio Ambiente (Process SIGED n° 01.01.030101.003202/2021-21) and SEMAPI for collecting permits.

This study was funded by Fundação de Amparo à Pesquisa do Estado do Amazonas (FAPEAM-UNIVERSAL, Edital 002/2018, proc. N° 062.00187/2019; and BIODIVERSA, Edital 007/2021, proc. 001760.2021-00) and by the Brazilian National Council for Scientific and Technological Development (CNPq Universal Grant n°: 401120/2016-3 to A.P.L.). Bryan C. Martins received a Master's Fellowship from FAPEAM (process n°. 008/2021). Albertina P. Lima received a fellowship from FAPEAM (Programa de Produtividade em CT&I – Edital n.° 013/2022). Miquéias Ferrão received an Edward O. Wilson Biodiversity Postdoctoral Fellowship from the Harvard Museum of Comparative Zoology, a fellowship from the David Rockefeller Center for Latin American Studies of Harvard University and a fellowship (PDPG) from Coordenação de Aperfeiçoamento de Pessoal de Nível Superior (CAPES; Proc. 88887.927982/2023-00). Published by a grant from the Wetmore Colles fund.

References

Adeney JM, Christensen NL, Vicentini A, Cohn-Haft M (2016) White-sand ecosystems in Amazonia. Biotropica 48(1): 7–23. https://doi.org/10.1111/btp.12293

Almeida AP, Angulo A (2006) A new species of *Leptodactylus* (Anura: Leptodactylidae) from the state of Espírito Santo, Brazil, with remarks on the systematics of associated populations. Zootaxa 1334(1): 1–25. https://doi.org/10.11646/zootaxa.1334.1.1

Altig R, McDiarmid RW (1999) Body plan: Development and morphology. In: McDiarmid RW, Altig R (Eds) Tadpoles: The Biology of Anuran Larvae. University of Chicago Press, Chicago, IL, 24–51.

Anderson AB (1981) White-sand vegetation of Brazilian Amazonia. Biotropica 13(3): 199–210. https://doi.org/10.2307/2388125

Angulo A, Icochea J (2010) Cryptic species complexes, widespread species and conservation: lessons from Amazonian frogs of the *Leptodactylus marmoratus* group (Anura: Leptodactylidae). Systematics and Biodiversity 8(3): 357–370. https://doi.org/10.1080/14772000.2010.507264

Angulo A, Reichle S (2008) Acoustic signal, species diagnosis, and species concepts: The case of a new cryptic species of *Leptodactylus* (Amphibia, Anura, Leptodactylidae) from the Chapare region, Bolivia. Zoological Journal of the Linnean Society 152(1): 59–77. https://doi.org/10.1111/j.1096-3642.2007.00338.x

Berneck BVM, Costa COR, Garcia PCA (2008) A new species of *Leptodactylus* (Anura: Leptodactylidae) from the Atlantic Forest of São Paulo State, Brazil. Zootaxa 1795(1): 46–56. https://doi.org/10.11646/zootaxa.1795.1.3

Bioacoustics Research Program (2014) Raven Pro: interactive sound analysis software. Version 1.5. Ithaca, New York: The Cornell Lab of Ornithology. https://ravensoundsoftware.com/software/raven-pro [Acessed 05 Jan 2023]

Boistel R, Massary JC, Angulo A (2006) Description of a new species of the genus *Adenomera* (Amphibia, Anura, Leptodactylidae) from French Guiana. Acta Herpetologica 1: 1–14. https://doi.org/10.13128/Acta_Herpetol-1249

Borges SH, da Silva JMC (2012) A new area of endemism for Amazonian birds in the Rio Negro Basin. The Wilson Journal of Ornithology 124(1): 15–23. https://doi.org/10.1676/07-103.1

Borges SH, Cornelius C, Moreira M, Ribas CC, Cohn-Haft M, Capurucho JM, Vargas C, Almeida R (2016) Bird communities in Amazonian white-sand vegetation patches: Effects of landscape configuration and biogeographic context. Biotropica 48(1): 121–131. https://doi.org/10.1111/btp.12296

Capurucho JMG, Cornelius C, Borges SH, Cohn-Haft M, Aleixo A, Metzger JP, Ribas CC (2013) Combining phylogeography and landscape genetics of *Xenopipo atronitens* (Aves: Pipridae), a white sand campina specialist, to understand Pleistocene landscape evolution in Amazonia. Biological Journal of the Linnean Society. Linnean Society of London 110(1): 60–76. https://doi.org/10.1111/bij.12102

Carvalho TR, Giaretta AA (2013a) Bioacoustics reveals two new syntopic species of *Adenomera* Steindachner (Anura: Leptodactylidae: Leptodactylinae) in the Cerrado of central Brazil. Zootaxa 3731(3): 533–551. https://doi.org/10.11646/zootaxa.3731.4.6

Carvalho TR, Giaretta AA (2013b) Taxonomic circumscription of *Adenomera martinezi* (Bokermann, 1956) (Anura: Leptodactylidae: Leptodactylinae) with the recognition of a new cryptic taxon though a bioacoustic approach. Zootaxa 3701(2): 207–237. https://doi.org/10.11646/zootaxa.3701.2.5

Carvalho TR, Angulo A, Kokubum MNC, Barrera DA, de Souza MB, Haddad CFB, Giaretta AA (2019a) A new cryptic species of the *Adenomera andreae* clade from southwestern Amazonia (Anura, Leptodactylidae). Herpetologica 75(3): 233–246. https://doi.org/10.1655/D-18-00049

Carvalho TR, Giaretta AA, Maciel NM, Barrera DA, Aguilar-Puntriano C, Haddad CFB, Kokubum MNC, Menin M (2019b) On the uncertain taxonomic identity of *Adenomera hylaedactyla* (Cope, 1868) and the composite type series of *A. andreae* (Müller, 1923) (Anura, Leptodactylidae). Copeia 107(4): 708–723. https://doi.org/10.1643/CH-19-237

Carvalho TR, Giaretta AA, Angulo A, Haddad CFB, Peloso PLV (2019c) A new Amazonian species of *Adenomera* (Anura: Leptodactylidae) from the Brazilian state of Pará: a tody-tyrant voice in a frog. American Museum Novitates 3919(1): 1–21. https://doi.org/10.1206/3919.1

Carvalho TR, Cassini CS, Taucce PPG, Haddad CFB (2019d) A new, morphologically cryptic species of *Adenomera* closely related to *A. araucaria* from the Atlantic Forest of southern Brazil (Anura, Leptodactylidae). Journal of Herpetology 53(2): 131–143. https://doi.org/10.1670/18-172

Carvalho TR, Angulo A, Barrera DA, Aguilar-Puntriano AC, Haddad CFB (2020a) Hiding in plain sight: A fourth new cryptic species of the *Adenomera andreae* clade (Anura: Leptodactylidae) from southwestern Amazonia. Herpetologica 76(3): 304–314. https://doi.org/10.1655/Herpetologica-D-19-00068.1

Carvalho TR, Moraes LJCL, Angulo A, Werneck FP, Icochea J, Lima AP (2020b) New acoustic and molecular data shed light on the poorly known Amazonian frog *Adenomera simonstuarti* (Leptodactylidae): Implications for distribution and conservation. European Journal of Taxonomy 682(682): 1–18. https://doi.org/10.5852/ejt.2020.682

Carvalho TR, Simões PI, Gagliardi-Urrutia LAG, Rojas-Runjaic FJM, Haddad CFB, Castroviejo-Fisher S (2020c) A new forest-dwelling frog species of the genus *Adenomera* (Leptodactylidae) from northwestern Brazilian Amazonia. Copeia 108(4): 924–937. https://doi.org/10.1643/CH-19-329

Carvalho TR, Moraes LJCL, Lima AP, Fouquet A, Peloso PLV, Pavan D, Drummond LO, Rodrigues MT, Giaretta AA, Gordo M, Neckel-Oliveira S, Haddad CFB (2021) Systematics and historical biogeography of neotropical foam-nesting frogs of the *Adenomera heyeri* clade (Leptodactylidae), with the description of six new Amazonian species. Zoological Journal of the Linnean Society 192(2): 395–433. https://doi.org/10.1093/zoolinnean/zlaa051

Cassini CS, Taucce PPG, Carvalho TR, Fouquet A, Solé M, Haddad CFB, Garcia PCA (2020) One step beyond a broad molecular phylogenetic analysis: Species delimitation of *Adenomera marmorata* Steindachner, 1867 (Anura: Leptodactylidae). PLOS ONE 15(2): e0229324. https://doi.org/10.1371/journal.pone.0229324

Che J, Chen HM, Yang JX, Jin JQ, Jiang K, Yuan ZY, Murphy RW, Zhang YP (2012) Universal COI primers for DNA barcoding amphibians. Molecular Ecology Resources 12(2): 247–258. https://doi.org/10.1111/j.1755-0998.2011.03090.x

De la Riva I (1995) A new reproductive mode for the genus *Adenomera* (Amphibia: Anura: Leptodactylidae): Taxonomic implications for certain Bolivian and Paraguayan populations. Studies on Neotropical Fauna and Environment 30(1): 15–29. https://doi.org/10.1080/01650529509360937

de Sá RO, Grant T, Camargo A, Heyer WR, Ponssa ML, Stanley E (2014) Systematics of the Neotropical genus *Leptodactylus* Fitzinger, 1826 (Anura: Leptodactylidae): phylogeny, the relevance of non-molecular evidence, and species accounts. South American

Journal of Herpetology 9(s1): S1–S128. https://doi.org/10.2994/SAJH-D-13-00022.1

Duellman WE (1970) The hylid frogs of Middle America. Monograph of the Museum of Natural History, University of Kansas 1: 1–428. https://doi.org/10.5962/bhl.title.2835

Ferrão M, Colatreli O, Fraga R, Kaefer IL, Moravec J, Lima AP (2016) High species richness of *Scinax* treefrogs (Hylidae) in a threatened Amazonian landscape revealed by an integrative approach. PLOS ONE 11(11): e0165679. https://doi.org/10.1371/journal.pone.0165679

Ferrão M, Moravec J, Moraes LJCL, Carvalho VT, Gordo M, Lima AP (2019) Rediscovery of *Osteocephalus vilarsi* (Anura: Hylidae): an overlooked but widespread Amazonian spiny-backed treefrog. PeerJ 7: e8160. https://doi.org/10.7717/peerj.8160

Ferrão M, Moravec J, Ferreira AS, Moraes LJCL, Hanken J (2022) A new snouted treefrog of the genus *Scinax* (Anura, Hylidae) from the white-sand forests of central Amazonia. Breviora 573(1): 1–36. https://doi.org/10.3099/0006-9698-573.1.1

Ferreira CAC (2009) Análise comparativa de vegetação lenhosa do ecossistema de campina na Amazônia brasileira. 2009. 277 f. Tese (Doutorado em Biologia Tropical e Recursos Naturais) - Convênio INPA e UFAM, Manaus.

Fine PVA, Baraloto C (2016) Habitat endemism in white-sand forests: Insights into the mechanisms of lineage diversification and community assembly of the Neotropical flora. Biotropica 48(1): 24–33. https://doi.org/10.1111/btp.12301

Fouquet A, Cassini CS, Haddad CFB, Pech N, Rodrigues MT (2014) Species delimitation, patterns of diversification and historical biogeography of the Neotropical frog genus *Adenomera* (Anura, Leptodactylidae). Journal of Biogeography 41(5): 855–870. https://doi.org/10.1111/jbi.12250

Fraga R, Souza E, Santos-Jr AP, Kawashita-Ribeiro RA (2018) Notes on the rare *Mastigodryas moratoi* (Serpentes: Colubridae) in the Brazilian Amazon white-sand forests. Phyllomedusa 17(2): 299–302. https://doi.org/10.11606/issn.2316-9079.v17i2p299-302

Frost DR (2024) Amphibian species of the world: an online reference. Version 6.2 (Accessed on 12 Jan. 2024). Electronic database accessible at https://amphibiansoftheworld.amnh.org/index.php. American Museum of Natural History, New York, USA. https://doi.org/10.5531/db.vz.0001

Frost DR, Grant T, Faivovich J, Bain RH, Haas A, Haddad CFB, de Sá RO, Channing A, Wilkinson M, Donnellan SC, Raxworthy CJ, Campbell JA, Blotto BL, Moler P, Drewes RC, Nussbaum RA, Lynch JD, Green DM, Wheeler WC (2006) The amphibian tree of life. Bulletin of the American Museum of Natural History 297: 1–291. https://doi.org/10.1206/0003-0090(2006)297[0001:TATOL]2.0.CO;2

Gonella PM, Barbosa-Silva RG, Fleischmann AS, Zappi DC, Baleeiro PC, Andrino CO (2020) Hidden biodiversity of Amazonian white-sand ecosystems: Two distinctive new species of *Utricularia* (Lentibulariaceae) from Pará, Brazil. PhytoKeys 169: 75–98. https://doi.org/10.3897/phytokeys.169.57626

Gosner KL (1960) A simplified table for staging anuran embryos and larvae with notes on identification. Herpetologica 16: 183–190. https://www.jstor.org/stable/3890061

Haddad CFB, Prado CPA (2005) Reproductive modes in frogs and their unexpected diversity in the Atlantic Forest of Brazil. Bioscience 55(3): 207–217. https://doi.org/10.1641/0006-3568(2005)055[0207:RMIFAT]2.0.CO;2

Heyer WR (1973) Systematics of the *marmoratus* group of the frog genus *Leptodactylus* (Amphibia, Leptodactylidae). Contributions in Science, Los Angeles County Museum of Natural History 251: 1–50. https://doi.org/10.5962/p.241234

Heyer WR (1974) Relationships of the *marmoratus* species group (Amphibia, Leptodactylidae) within the subfamily Leptodactylinae. Contributions in Science, Los Angeles County Museum of Natural History 253: 1–45. https://doi.org/10.5962/p.241236

Heyer WR (1975) *Adenomera lutzi* (Amphibia: Leptodactylidae), a new species of frog from Guyana. Proceedings of the Biological Society of Washington 88: 315–318. https://biostor.org/reference/65701

Heyer WR (1998) The relationships of *Leptodactylus diedrus* (Anura, Leptodactylidae). Alytes 16: 1–24.

Heyer WR, Silverstone PA (1969) The larva of *Leptodactylus hylaedactylus* (Amphibia, Leptodactylidae). Fieldiana. Zoology 51: 141–145.

Heyer WR, Rand AS, Cruz CAG, Peixoto OL, Nelson CE (1990) Frogs of Boraceia. Arquivos de Zoologia 31: 231–410.

Hoang DT, Chernomor O, Haeseler AV, Minh BQ, Vinh LS (2018) UFBoot2: Improving the ultrafast bootstrap approximation. Molecular Biology and Evolution 35(2): 518–522. https://doi.org/10.1093/molbev/msx281

Jorge RF, Ferrão M, Lima AP (2020) Out of bound: A new threatened harlequin toad (Bufonidae, *Atelopus*) from the outer borders of the Guiana Shield in central Amazonia described through integrative taxonomy. Diversity 12(310): 1–25. https://doi.org/10.3390/d12080310

Kearse M, Moir R, Wilson A, Stones-Havas S, Cheung M, Sturrock S, Buxton S, Cooper A, Markowitz S, Duran C, Thierer T, Ashton B, Meintjes P, Drummond A (2012) Geneious basic: An integrated and extendable desktop software platform for the organization and analysis of sequence data. Bioinformatics 28: 1647–1649. https://doi.org/10.1093/bioinformatics/bts199

Kimura M (1980) A simple method for estimating evolutionary rate of base substitutions through comparative studies of nucleotide sequences. Journal of Molecular Evolution 16(2): 111–120. https://doi.org/10.1007/BF01731581

Köhler G (2012) Color catalogue for field biologists. Herpeton. [ISBN9783936180404]

Köhler J, Jansen M, Rodriguez A, Kok PJR, Toledo LP, Emmrich M, Glaw F, Haddad CFB, Rödel MO, Vences M (2017) The use of bioacoustics in anuran taxonomy: theory, terminology, methods and recommendations for best practice. Zootaxa 4251: 1–124. https://doi.org/10.11646/zootaxa.4251.1.1

Kok PJR, Kokubum MNC, MacCulloch RD, Lathrop A (2007) Morphological variation in *Leptodactylus lutzi* (Anura, Leptodactylidae) with description of its advertisement call and notes on its courtship behavior. Phyllomedusa 6(1): 45–60. https://doi.org/10.11606/issn.2316-9079.v6i1p45-60

Kokubum MNC, Giaretta AA (2005) Reproductive ecology and behaviour of a species of *Adenomera* (Anura, Leptodactylidae) with endotrophic tadpoles: Systematic implications. Journal of Natural History 39(20): 1745–1758. https://doi.org/10.1080/00222930400021515

Kokubum MNC, Sousa MB (2008) Reproductive ecology of *Leptodactylus* aff *hylaedactylus* (Anura, Leptodactylidae) from an open area in northern Brazil. South American Journal of Herpetology 3(1): 15–21. https://doi.org/10.2994/1808-9798(2008)3[15:REOLAH]2.0.CO;2

Kwet A (2007) Bioacoustic variation in the genus *Adenomera* in southern Brazil, with revalidation of *Leptodactylus nanus* Müller, 1922 (Anura: Leptodactylidae). Zoologische Reihe 83: 56–68. https://doi.org/10.1002/mmnz.200600027

Kwet A, Angulo A (2002) A new species of *Adenomera* (Anura, Leptodactylidae) from the Araucaria forest of Rio Grande do Sul (Brazil), with comments on the systematic status of southern populations of the genus. Alytes 20(1–2): 28–43.

Kwet A, Steiner J, Zillikens A (2009) A new species of *Adenomera* (Amphibia: Anura: Leptodactylidae) from the Atlantic rain forest in Santa Catarina, southern Brazil. Studies on Neotropical Fauna and Environment 44(2): 93–107. https://doi.org/10.1080/01650520902901659

Lamarre GPD, Amoretti S, Baraloto C, Bénéluz F, Mesones I, Fine PV (2016) Phylogenetic overdispersion in Lepidoptera communities of Amazonian white-sand forests. Biotropica 48(1): 101–109. https://doi.org/10.1111/btp.12294

Lanfear R, Frandsen PB, Wright AM, Senfeld T, Calcott B (2017) PartitionFinder 2: new methods for selecting partitioned models of Evolution for molecular and morphological phylogenetic analyses. Molecular Biology and Evolution 34: 772–773. https://doi.org/10.1093/molbev/msw260

Lavilla EO, Scrocchi GJ (1986) Mofometría laval de los géneros de Telmatobiinae (Anura: Leptodactylidae) de Argentina y Chile. Physis (Rio de Janeiro, Brazil) 44: 39–43.

Ligges U, Krey S, Mersmann O, Schnackenberg S (2017) tuneR: Analysis of Music and Speech, Version 1.3.2. https://CRAN.R-project.org/package=tuneR [Accessed on 20 November 2023]

Lima AP, Simões PI, Kaefer IL (2015) A new species of *Allobates* (Anura: Aromobatidae) from Parque Nacional da Amazônia, Pará State, Brazil. Zootaxa 3980(4): 501–525. https://doi.org/10.11646/zootaxa.3980.4.3

Lima AP, Ferrão M, Silva DH (2020) Not as widespread as thought: Integrative taxonomy reveals cryptic diversity in the Amazonian nurse frog *Allobates tinae* Melo-Sampaio, Oliveira & Prates, 2018 and description of a new species. Journal of Zoological Systematics and Evolutionary Research 58(4): 1173–1194. https://doi.org/10.1111/jzs.12406

Lins AC, Magalhaes RF, Costa RN, Brandão RA, Py-Daniel TR, Miranda NE, Maciel NM, Nomura F, Pezzuti TL (2018) The larvae of two species of *Bokermannohyla* (Anura, Hylidae, Cophomantini) endemic to the highlands of central Brazil. Zootaxa 4527(4): 501–520. https://doi.org/10.11646/zootaxa.4527.4.3

Lutz A (1930) Segunda memoria sobre especies brasileiras do genero *Leptodactylus*, incluindo outras aliadas. Memorias do Instituto Oswaldo Cruz 23(1): 1–59. https://doi.org/10.1590/S0074-02761930000100001

Menin M, Rodrigues DJ (2013) The terrestrial tadpole of *Leptodactylus andreae* (Anura, Leptodactylidae), a member of the *Leptodactylus marmoratus* species group. Zootaxa 3683(1): 92–94. https://doi.org/10.11646/zootaxa.3683.1.7

Menin M, Almeida AP, Kokubum MNC (2009) Reproductive aspects of *Leptodactylus hylaedactylus* (Anura: Leptodactylidae), a member of the *Leptodactylus marmoratus* species group, with a description of tadpoles and calls. Journal of Natural History 43: 2257–2270. https://doi.org/10.1080/00222930903097707

Mônico AT, Ferrão M, Chaparro JC, Fouquet A, Lima AP (2022) A new species of rain frog (Anura: Strabomantidae: *Pristimantis*) from the Guiana Shield and amended diagnosis of *P. ockendeni* (Boulenger, 1912). Vertebrate Zoology 72: 1035–1065. https://doi.org/10.3897/vz.72.e90435

Mônico AT, Ferrão M, Moravec J, Fouquet A, Lima AP (2023) A new species of *Pristimantis* (Anura: Strabomantidae) from white-sand forests of central Amazonia, Brazil. PeerJ 11: e15399. https://doi.org/10.7717/peerj.15399

Moraes LJCL, Werneck FP, Réjaud A, Rodrigues MT, Prates I, Glaw F, Kok PJR, Ron SR, Chaparro JC, Osorno-Muñoz M, Vechio FD, Recoden RS, Marques-Souza S, Rojas RR, Demay L, Hrbek T, Fouquet A (2022) Diversification of tiny toads (Bufonidae: *Amazophrynella*) sheds light on ancient landscape dynamism in Amazonia. Biological Journal of the Linnean Society. Linnean Society of London 136(1): 1–17. https://doi.org/10.1093/biolinnean/blac006

Nguyen LT, Schmidt AH, von Haeseler A, Minh BQ (2015) IQ-TREE: A fast and effective stochastic algorithm for estimating Maximum-Likelihood phylogenies. Molecular Biology and Evolution 32(1): 268–274. https://doi.org/10.1093/molbev/msu300

Oksanen J, Blanchet FG, Friendly M, Kindt R, Legendre P, McGlinn D, Minchin PR, O'Hara RB, Simpson GL, Solymos P, Stevens MHH, Szoecs E, Wagner H (2020) vegan: Community Ecology Package. R package version 2.5-7. https://CRAN.R-project.org/package=vegan

Parker HW (1932) XXXVII.—The systematic status of some frogs in the Vienna Museum. Annals & Magazine of Natural History 10(58): 341–344. https://doi.org/10.1080/00222933208673582

Pyron RA, Wiens JJ (2011) A large-scale phylogeny of Amphibia including over 2800 species, and a revised classification of extant frogs, salamanders, and caecilians. Molecular Phylogenetics and Evolution 61(2): 543–583. https://doi.org/10.1016/j.ympev.2011.06.012

R Core Team (2021) A language and environment for statistical computing. Vienna: R Foundation for Statistical Computing. http://www.r-project.org [Acessed 25 Nov. 2022]

Schulze A, Jansen M, Köhler G (2015) Tadpole diversity of Bolivia's lowland anuran communities: Molecular identification, morphological characterization, and ecological assignment. Zootaxa 4016(1): 1–111. https://doi.org/10.11646/zootaxa.4016.1.1

Steindachner F (1867) Reise der österreichischen Fregatte Novara um die Erde in den Jahren 1857, 1858, 1859 unter den Befehlen des Commodore B. von Wüllerstorf-Urbair. Pt. 9, Bd. 1, Abt. 4, Zoologischer Theil. Amphibien. Wien: K. K. Hof- und Staatsdruckerei.

Sueur J, Aubin T, Simonis C (2008) Seewave, a free modular tool for sound analysis and synthesis. Bioacoustics 18: 213–226. https://doi.org/10.1080/09524622.2008.9753600

Tamura K, Stecher G, Peterson D, Filipski A, Kumar S (2013) MEGA6: Molecular Evolutionary Genetics Analysis version 6.0. Molecular Biology and Evolution 30(12): 2725–2729. https://doi.org/10.1093/molbev/mst197

Trifinopoulos J, Nguyen LT, von Haeseler A, Minh BQ (2016) W-IQ-TREE: A fast online phylogenetic tool for maximum likelihood analysis. Nucleic Acids Research 44(W1): 232–235. https://doi.org/10.1093/nar/gkw256

Vacher J-P, Chave J, Ficetola FG, Sommeria-Klein G, Tao S, Thébaud C, Blanc M, Camacho A, Cassimiro J, Colston TJ, Dewynter M, Ernst R, Gaucher P, Gomes JO, Jairam R, Kok PJR, Lima JD, Martinez Q, Marty C, Noonan BP, Nunes PMS, Ouboter P, Recoder R, Rodrigues MT, Snyder A, Marques-Souza S, Fouquet A (2020) Large scale DNA-based survey of frogs in Amazonia suggests a vast underestimation of species richness and endemism. Journal of Biogeography 47(8): 1781–1791. https://doi.org/10.1111/jbi.13847

Vicentini A (2016) The evolutionary history of *Pagamea* (Rubiaceae), a white-sand specialist lineage in tropical South America. Biotropica 48(1): 58–69. https://doi.org/10.1111/btp.12295

Watters JL, Cummings ST, Flanagan RL, Siler CD (2016) Review of morphometric measurements used in anuran species descriptions and recommendations for a standardized approach. Zootaxa 4072(4): 477–495. https://doi.org/10.11646/zootaxa.4072.4.6

Zaracho VH, Kokubum MNC (2017) Reproduction and larval morphology of *Adenomera diptyx* (Anura: Leptodactylidae) from the Argentinean humid Chaco and Brazilian Pantanal. Salamandra (Frankfurt) 53: 1–9.

Zaracho VH, Lavilla EO, Carvalho TR, Motte M, Basso NG (2023) Redescription of *Adenomera diptyx* (Boettger, 1885) (Anura, Leptodactylidae) and description of a closely related new species. European Journal of Taxonomy 888: 1–45. https://doi.org/10.5852/ejt.2023.888.2205

Appendix 1

Material examined.

***Adenomera simonstuarti*.** BRAZIL: ACRE: Tarauacá (ZUEC-AMP 25698–700; INPA-H 40967, 44903–12; MPEG 44653–55).

Appendix 2

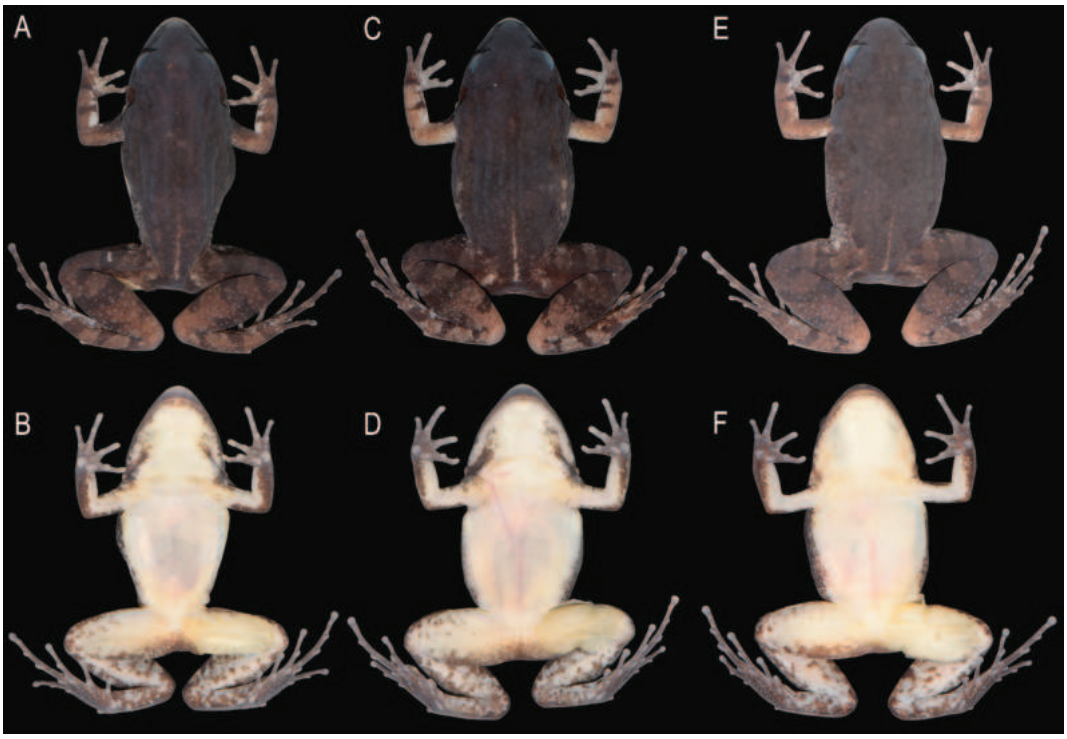

Figure A1. *Adenomera simonstuarti* from the Municipality of Tarauacá, State of Acre, Brazil. Dorsal and ventral views of males (**A–D**) and females (**E–F**). **A, B.** INPA-H 44905, SVL 25.2 mm; **C, D** INPA-H 44912, SVL 24.5 mm; **E, F.** INPA-H 44909, SVL 23.0 mm. Photographs: L. R. Mendonça.

Supplementary material 1

Additional information

Authors: Bryan da Cunha Martins, Alexander Tamanini Mônico, Cianir Mendonça, Silionamã P. Dantas, Jesus R. D. Souza, James Hanken, Albertina Pimentel Lima, Miquéias Ferrão

Data type: xlsx

Explanation note: **table S1.** Morphometric raw data. **table S2.** Bioacoustic raw data. **table S3.** dataset containing sequences retrieved from GenBank. **table S4.** minimum–maximum values of genetic distances.

Link: https://doi.org/10.3897/zse.100.110133.suppl1

Zoosyst. Evol. 100 (1) 2024, 255–277 | DOI 10.3897/zse.100.117968

PENSOFT

MUSEUM FÜR NATURKUNDE BERLIN

A survey of the genus *Orchestina* Simon, 1882 (Araneae, Oonopidae) from Xishuangbanna, China, with descriptions of five new species

Chenxue Song[1], Yanfeng Tong[1], Dongju Bian[2], Shuqiang Li[3]

1 *College of Life Science, Shenyang Normal University, Shenyang 110034, Liaoning, China*

2 *Key Laboratory of Forest Ecology and Management, Institute of Applied Ecology, Chinese Academy of Sciences, Shenyang 110016, China*

3 *Institute of Zoology, Chinese Academy of Sciences, Beijing 100101, China*

https://zoobank.org/03EBDEC5-543B-4E3C-B71B-DB45873BA5D7

Corresponding authors: Yanfeng Tong (tyf68@hotmail.com); Dongju Bian (biandongju@163.com)

Academic editor: Danilo Harms ♦ **Received** 29 December 2023 ♦ **Accepted** 20 February 2024 ♦ **Published** 8 March 2024

Abstract

Five new species and three known species of the genus *Orchestina* Simon, 1882 are recorded from Xishuangbanna, Yunnan Province: *O. clavulata* Tong & Li, 2011 (♂), *O. colubrina* Liu, Henrard & Xu, 2019 (♂♀), *O. concava* Tong & Li, **sp. nov.** (♂), *O. menglun* Tong & Li, **sp. nov.** (♂), *O. subclavulata* Tong & Li, **sp. nov.** (♂), *O. truncatula* Tong & Li, 2011 (♂♀), *O. wengnan* Tong & Li, **sp. nov.** (♂) and *O. xui* Tong & Li, **sp. nov.** (♂♀). The males of *O. colubrina* Liu, Henrard & Xu, 2019 is described for the first time. An identification key to species of the genus *Orchestina* from Xishuangbanna is provided.

Key Words

Asia, goblin spiders, identification key, Orchestininae, taxonomy

Introduction

Xishuangbanna (Fig. 19), located in the south of Yunnan Province, has the best preserved tropical rainforest of China and belongs to the Indo-Burma biodiversity hotspot (Myers 1988). Implementing an "All Species Inventory" of spiders in Xishuangbanna Tropical Botanical Garden (XTBG, 1125-hectare area in total) has increased the spider species from fewer than 50 before 2006 to about 782 by the end of 2021 (Li 2021). Goblin spiders (Oonopidae Simon, 1890) are composed of tiny spiders between 1.0 and 3.0 mm. They have a nearly worldwide distribution, and mainly occur in leaf litter, under bark, and in the tree canopy (Jocqué and Dippenaar-Schoeman 2006; Henrard and Jocqué 2012; Ubick and Dupérré 2017). Currently, 1940 extant described species in 115 genera of oonopid spiders have been recorded in the world (WSC 2024).

The genus *Orchestina* Simon, 1882 is characterized by having an enlarged femur IV with which these species are capable of jumping. The genus is also characterized by having a well-sclerotized sperm duct, six well developed eyes with near H-shaped arrangement, a 4-4-3-3 pattern of raised receptors on the tarsal organs of the legs I–IV, respectively, and by lacking spines on all the legs (Henrard and Jocqué 2012; Platnick et al. 2012; Izquierdo and Ramírez 2017). Currently, 164 extant species have been described, in which 14 species have been recorded from China (Tong and Li 2011; Liu et al. 2016, 2019; Wang et al. 2021; Lin et al. 2024).

The survey of oonopid spiders from Xishuangbanna has started relatively recently. To date, 20 species in 4 genera (*Bannana* Tong & Li, 2015, *Camptoscaphiella* Caporiacco, 1934, *Ischnothyreus* Simon, 1893 and *Opopaea* Simon, 1892) have been recorded from Xishuangbanna (Tong and Li 2015a, b; Sun et al. 2019; Huang et al. 2021; Tong et al.

2021). While studying spiders collected from Xishuangbanna, Yunnan Province, China, we found many *Orchestina* specimens, and belonging to several different species. The present paper aims to provide the descriptions of five new species and three known species from this region.

Materials and methods

The specimens were examined using a Leica M205C stereomicroscope. Details of body parts and measurements were studied under an Olympus BX51 compound microscope. Photos were made with a Canon EOS 750D zoom digital camera (18 megapixels) mounted on an Olympus BX51 compound microscope. Vulvae were cleared in lactic acid. Photos were stacked using Helicon Focus 7.6.1 and processed using Adobe Photoshop 21.1.2. All measurements in the text are given in millimeters. Terminology and taxonomic descriptions follow Henrard and Jocqué (2012) and Tong and Li (2011).

All material studied is deposited in Shenyang Normal University (SYNU) in Shenyang, China.

The following abbreviations are used in the text and figures: **ALE** = anterior lateral eyes; **ARe** = anterior receptaculum; **AUS** = anterior uterine sclerite; **Ex** = dorsolateral extension; **Exc** = excavations; **PLE** = posterior lateral eyes; **PME** = posterior median eyes; **Po** = pocket; **PP** = posterior plate; **Pr** = protrusion; **Se** = serrula; **TO** = triangular outgrowth; **XNNR** = Xishuangbanna National Natural Reserve; **XTBG** = Xishuangbanna Tropical Botanical Garden.

Taxonomy

Family Oonopidae Simon, 1890

Genus *Orchestina* Simon, 1882

Type species. *Schoenobates pavesii* Simon, 1873; gender feminine.

N.B.: considered a senior synonym of *Ferchestina* Saaristo & Marusik, 2004: 52 (type *F. storozhenkoi* Saaristo & Marusik, 2004) by Platnick et al. 2012: 37.

Key to *Orchestina* from Xishuangbanna

O. concava, *O. menglun*, *O. subclavulata* and *O. wengnan* females unknown.

1 Male 2
– Female 9
2 Bulb oval or roughly triangle shaped, embolus base thinner (Figs 7E, F, 12A, B) 3
– Bulb pear-shaped in lateral view, with ventral side strongly protruding proximally, embolus base thicker (e.g., Fig. 1A–C) 4
3 Bulb oval shaped (Fig. 12A, B); chelicerae with distal group of long converging setae (Fig. 10F); tibia I with a group of ventrobasal spines (Fig. 10D) ..... *O. truncatula* Tong & Li, 2011
– Bulb triangle shaped (Fig. 7E, F); chelicerae with distal single long setae (Fig. 2D, F); tibia I without the aforementioned character ..... *O. colubrina* Liu, Henrard & Xu, 2019
4 Palpal tibia distinctly narrower than bulb (Fig. 7A, B) ..... *O. menglun* sp. nov.
– Palpal tibia strongly enlarged, at least as wide as bulb (e.g., Fig. 1A–C) 5
5 Sperm duct with 2 loops in prolateral view (Figs 5A, 14A) 6
– Sperm duct with 3 loops in prolateral view (Figs 1A, 9A, 16A) 7
6 Endites with deep excavations (Figs 4G, 5D) ..... *O. concava* sp. nov.
– Endites without deep excavations (Figs 13G, 14D) ..... *O. wengnan* sp. nov.
7 Embolus with conspicuous dorsal flattened extension and acute tip (Fig. 16A–C) ..... *O. xui* sp. nov.
– Embolus gradually tapered (Figs 1A–D, 9A–C) 8
8 Endites with large triangular outgrowth (Fig. 9D) ..... *O. subclavulata* sp. nov.
– Endites lacking triangular outgrowth (Fig. 1E) ..... *O. clavulata* Tong & Li, 2011
9 Genitalia with posterior plate (PP); anterior uterine sclerite (AUS) with lateral protrusion (Pr) well developed (Fig. 18D) 10
– Genitalia with two dorsolateral extensions (Ex) surrounding anterior uterine sclerite (AUS); AUS with lateral protrusion (Pr) reduced (Figs 3I, 12F) 11
10 Epigaster with two small, dark sclerotized pockets (Fig. 18C) ..... *O. xui* sp. nov.
– Epigaster without two small, dark sclerotized pockets (Tong and Li 2011: fig. 4B) ..... *O. clavulata* Tong & Li, 2011
11 Epigaster with distinctly medial marks in ventral view (Fig. 11G); anterior uterine sclerite (AUS) short, length/width ratio about 1.25 (Fig. 12F) ..... *O. truncatula* Tong & Li, 2011
– Epigaster without distinctly medial marks in ventral view (Fig. 3G); anterior uterine sclerite (AUS) long, length/width ratio about 2.0 (Fig. 3H, I) ..... *O. colubrina* Liu, Henrard & Xu, 2019

Orchestina clavulata Tong & Li, 2011

Fig. 1

Orchestina clavulata Tong & Li, 2011: 38, figs 1C–D, 2B, 3B, 4B, 5D, 7A–F; Tong 2013: 47, figs 26C–D, 27B, 28B, 29B, 30D, 65A–F.

Material examined. 1♂ (SYNU-777), **China, Yunnan**, Mengla Co., Menglun Town, XNNR, fogging, seasonal rainforest, 48 km (21°58.764'N, 101°09.748'E), elev. 1038 m, 10 August 2011, Zheng, Zhao & Gao leg.; 2♂ (SYNU-778), fogging, Lvshilin, limestone monsoon rainforest (21°54.769'N, 101°16.959'E), elev. 599 m, 9 August 2011, Zheng, Zhao & Gao leg.; 2♂ (SYNU-890), fogging, mountaintop secondary rainforest, 55 Km (21°57.987'N, 101°12.167'E), elev. 1038 m, 10 August 2011, Zheng, Zhao & Gao leg.

Type material (examined). ***Paratypes*:** 6♂3♀ (IZCAS Ar 19334), China: Hainan, Lingshui, Diaoluoshan, Plank roadside, 963 m a.s.l., 18°43.631'N, 109°51.939'E, 7 August 2010, leg. G. Zheng.

Diagnosis. This species is most similar to *O. thoracica* Xu, 1987 in having the net-shaped pattern on carapace and the pear-shaped bulb, but can be distinguished by the sperm duct with three loops in prolateral view (Fig. 1A, B; Tong and Li 2011: fig. 7A) vs. two loops in *O. thoracica* (Xu 1987: fig. 11), and by female genitalia without marks (Tong and Li 2011: fig. 4B), vs. with elongate heart-shaped mark in *O. thoracica* (Xu 1987: fig. 9) .

Description. See Tong and Li (2011).

Distribution. China (Hainan, Yunnan).

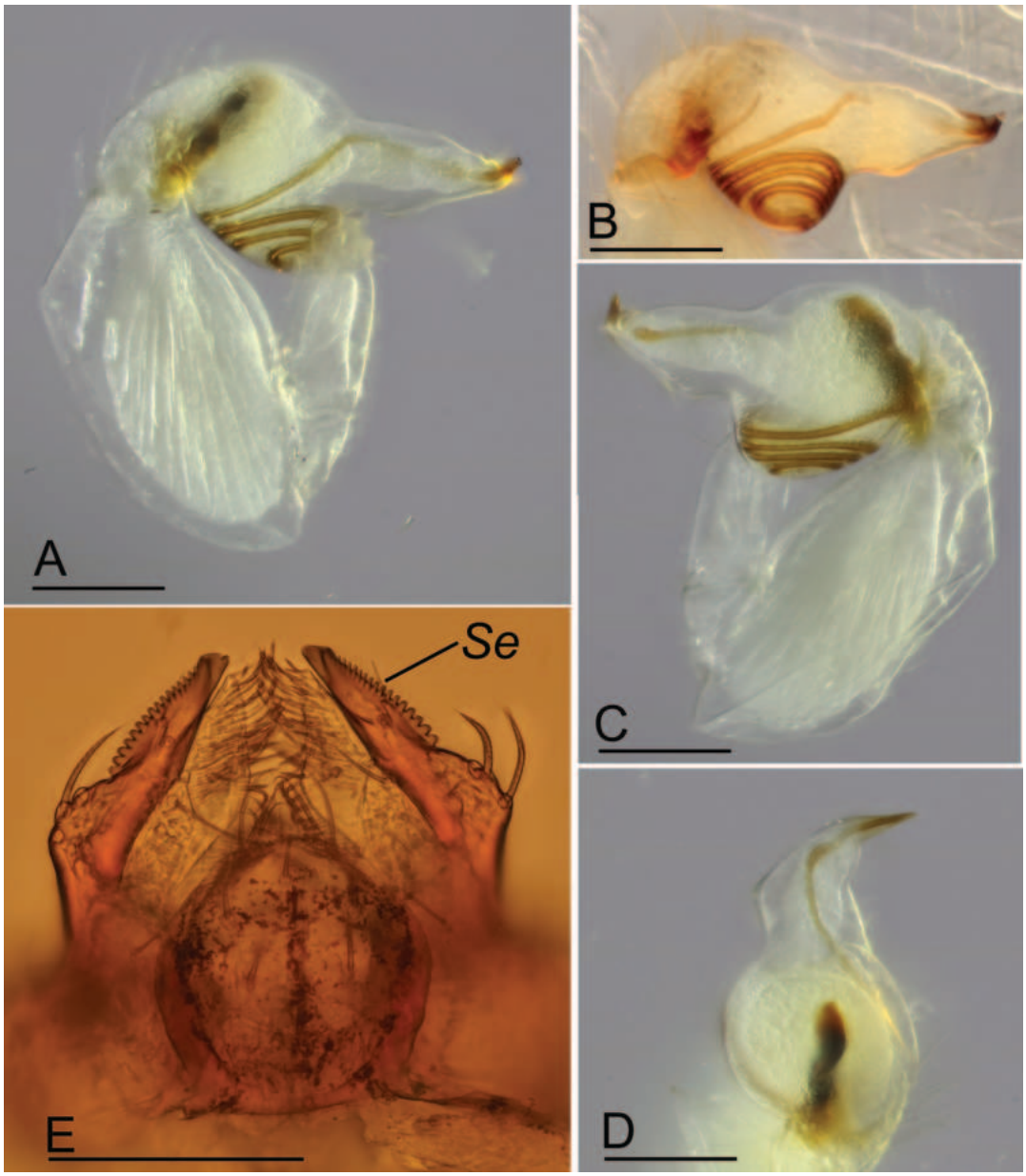

Figure 1. *Orchestina clavulata* Tong & Li, 2011, male (SYNU-777). **A, C, D.** Left palp, prolateral, retrolateral and dorsal views; **B.** Left bulb, prolateral view; **E.** Endites and labium, ventral view. Abbreviation: Se = serrula. Scale bars: 0.1 mm.

Orchestina colubrina **Liu, Henrard & Xu, 2019**
Figs 2, 3, 7E, 7F

Orchestina colubrina Liu, Henrard & Xu, in Liu et al. 2019: 246, figs 10A–H, 11A–F.

Material examined. 1♂ (SYNU-841), **China, Yunnan**, Mengla Co., Menglun Town, XTBG, trunk traps, *Paramichella baillonii* plantation (21°54.772'N,101°16.043'E), elev. 556 m, 16–31 May 2007, Zheng leg.; 1♂1♀ (SYNU-845-846), same data as above; 3♀ (SYNU-847-849), same data as above; 1♂ (SYNU-843), XTBG, Fogging, same locality as above, 18 July 2007, Zheng leg.; 1♂ (SYNU-842), XTBG, fogging, rubber plantation (21°54.463'N,101°15.978'E), elev. 569 m, 21 July 2007, Zheng leg.; 1♂ (SYNU-844), XTBG, trunk traps, rubber plantation (21°55.551'N, 101°16.923'E), elev. 561 m, 1–15 June 2007, Zheng leg.

Type material (unexamined). ***Holotype*** ♀, China, Jiangxi Province: Ji'an City, Jinggangshan County Level City, Ciping Town, Xingzhou Vill., forest, 26.519°N, 114.193°E, 514m, 3.X.2015, Keke Liu, Zeyuan Meng, Lei Zhang, Jianyun Wen and Tianming Wang leg. (OON 75). ***Paratype*****:** 1♀, collected together with the holotype (OON 76).

Diagnosis. Males of *Orchestina colubrina* is similar to *O. multipunctata* Liu, Xiao & Xu, 2016 (female unknown) in having a strongly swollen palpal tibia, the tube-shaped embolus and the same kind of modified setae in the labium, but can be distinguished by the triangle shaped bulb (Fig. 7E, F) vs. drop-shaped (Liu et al. 2016, fig. 8H, I). Females of *O. colubrina* resemble to those of *O. yinggezui* Tong & Li, 2011 in having the long lateral extensions (Ex) surrounding anterior uterine sclerite (AUS), but can be distinguished by the narrow cylindrical sclerite (AUS) having Y-shaped lateral protrusions (Fig. 3H, I), vs. AUS with circular protrusions in *O. yinggezui* (Tong and Li 2011: fig. 5H, 10B).

Description. Male (SYNU-841). Total length 1.33, carapace length 0.72, carapace width 0.48, abdomen length 0.63. Habitus as in Fig. 2A, B. Color in alcohol: pale yellow. Carapace oval, with net-shaped pattern, pars cephalica strongly elevated in lateral view, with rounded posterolateral corners. Clypeus (Fig. 2D, F) margin unmodified, curved downwards in front view, sloping forward in lateral view. Sternum (Fig. 2E) longer than wide, with marginal band of tiny dark spots, surface smooth. Mouthparts (Fig. 2D, F): chelicerae straight, with a single distal long setae; labium rounded, not fused to sternum, anterior margin not indented at middle, with five modified, leaf-shaped setae; endites not strongly sclerotized, without serrula. Abdomen ovoid, with gray ^-shaped pattern. Genitalia (Fig. 7E, F): tibia of palp strongly enlarged, length/width ratio = 1.41, cymbium small; bulb triangle-shaped, about 0.76 times as wide as tibia; tapering apically; sperm duct not strongly sclerotized, barely visible through cuticle; embolus slender, tube-shaped, flattened at tip.

Female (SYNU-846). Same as male except as noted. Body: habitus as in Fig. 3A, B; body length 1.36. Carapace: 0.66 long, 0.51 wide. Clypeus (Fig. 3F): anterior margin straight. Mouthparts: chelicerae shorter; endites simple, with serrula. Abdomen: 0.67 long. Epigaster (Fig. 3G, H): without special external features; internal parts visible through integument. Endogyne (Fig. 3I): with medial cylindrical sclerite (AUS), anterior part of cylindrical sclerite (AUS) with pair of Y-shaped protrusions (Pr); AUS surrounded by narrow hoop (Ex).

Distribution. China (Jiangxi, Yunnan).

Orchestina concava **Tong & Li, sp. nov.**
https://zoobank.org/528FB8F7-E56D-4CDF-9260-EE5CD2C30470
Figs 4, 5

Type material. ***Holotype*****:** ♂ (SYNU-771), **China, Yunnan**, Jinghong City, Menghai Co., Meng'a Town, Wengnan Vill., sifting leaf litter, secondary forest (22°05.020'N, 100°22.086'E), elev. 1118 m, 24 July 2012, Zhao & Chen leg. ***Paratypes*****:** 1♂(SYNU-772),same data as for holotype.

Etymology. The specific name comes from Latin, *concavus*, meaning hollowed, referring to the excavations of male endites.

Diagnosis. The new species is similar to *O. clavulata* in having the strongly swollen palpal tibia and the pear-shaped bulb, but can be distinguished by the endites with deep excavations (Fig. 5D) vs. straight in *O. clavulata* (Fig. 1E) and the sperm duct with two loops in prolateral view (Fig. 5A) vs. three loops in *O. clavulata* (Fig. 1A, B). This new species is also similar to *O. wengnan* sp. nov. in having the pear-shaped bulb and the sperm duct with two loops in prolateral view, but can be distinguished by the endites with deep excavations (Fig. 5D) vs. straight in *O. wengnan* sp. nov. (Fig. 14D).

Description. Male (holotype). Total length 1.29, carapace length 0.63, carapace width 0.46, abdomen length 0.64. Habitus as in Fig. 4A–C. Color in alcohol: carapace yellow, abdomen and legs pale yellow. Carapace oval, with net-shaped pattern, pars cephalica strongly elevated in lateral view, with rounded posterolateral corners. Clypeus (Fig. 4F): margin unmodified, curved downwards in front view, sloping forward in lateral view. Sternum (Fig. 4G) longer than wide, with marginal band and median area of radiating lines, surface smooth; setae sparse, needle-like, evenly scattered, without hair tufts. Mouthparts (Fig. 4F): chelicerae straight, anterior face unmodified; labium rounded, not fused to sternum, anterior margin not indented at middle; endites (Figs 4G, 5D) strongly sclerotized, with triangular outgrowth, outer margin with serrula and excavations. Abdomen ovoid,

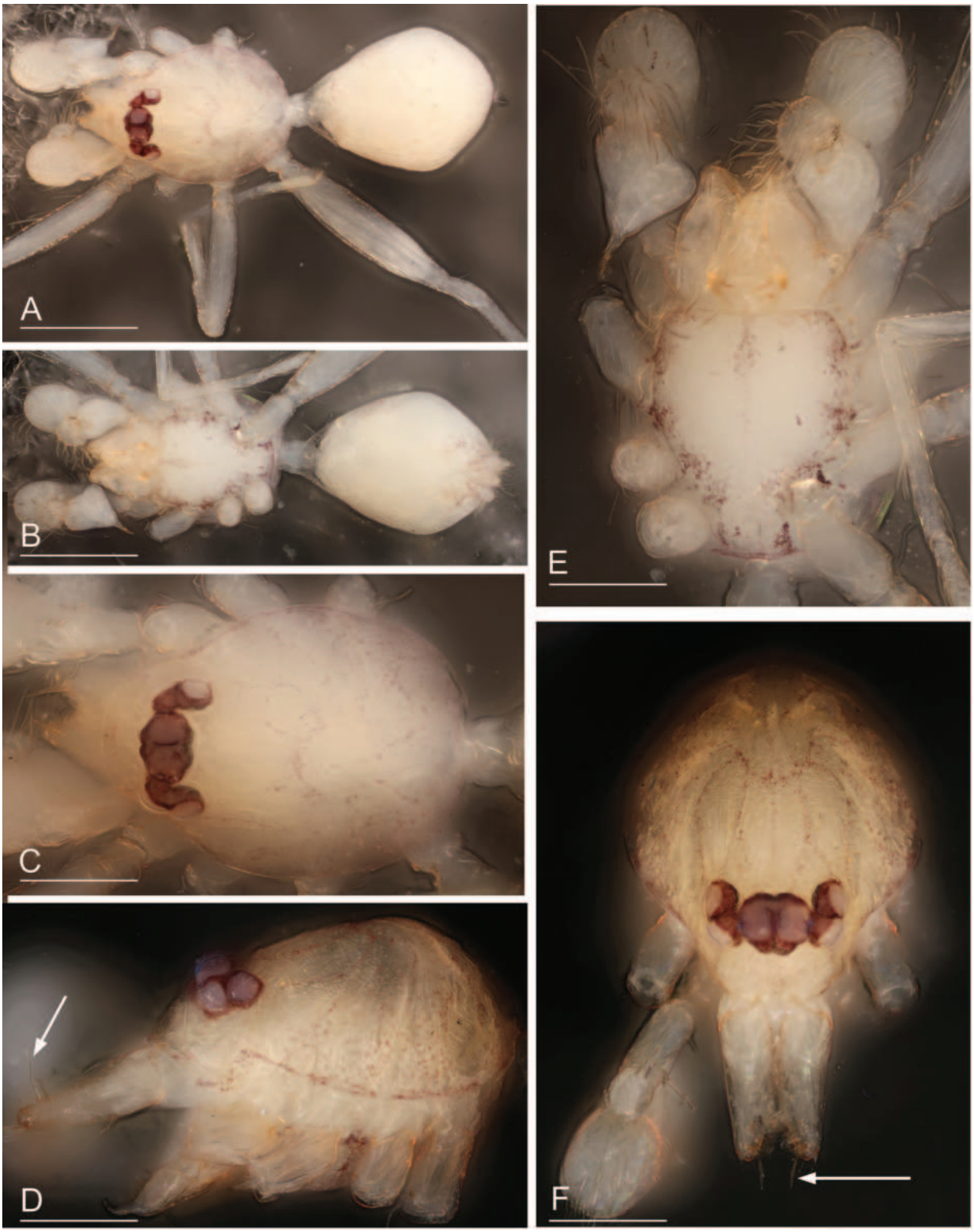

Figure 2. *Orchestina colubrina* Liu, Henrard & Xu, 2019, male (SYNU-841). **A, B.** Habitus, dorsal and ventral views; **C–F.** Prosoma, dorsal, lateral, ventral and anterior views (arrows show the single distal seta). Scale bars: 0.4 mm (**A, B**); 0.2 mm (**C–F**).

with gray ^-shaped pattern. Genitalia (Fig. 5A–C): tibia of palp strongly enlarged, length/width ratio = 1.63, cymbium small; bulb pear-shaped in lateral view, with ventral side strongly protruding proximally, about 0.92 times as wide as tibia; the sperm duct strongly curved with two loops; embolus slender.

Female. Unknown.

Distribution. Known only from the type locality.

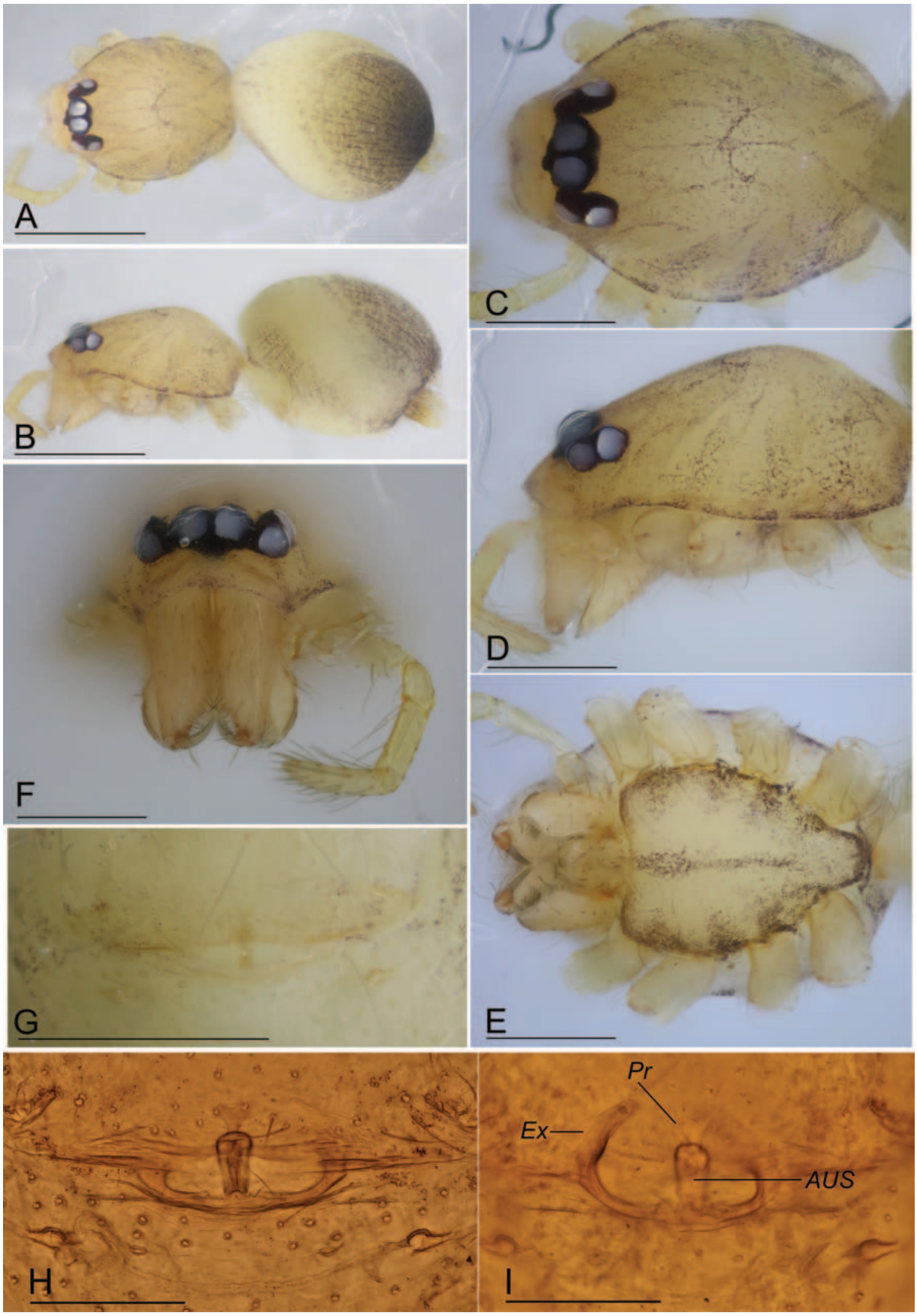

Figure 3. *Orchestina colubrina* Liu, Henrard & Xu, 2019, female (SYNU-846). **A, B.** Habitus, dorsal and lateral views; **C–F.** Prosoma, dorsal, lateral, ventral and anterior views; **G.** Epigaster, ventral view; **H–I.** Endogyne, ventral and dorsal views. Abbreviations: AUS = anterior uterine sclerite; Ex = dorsolateral extension; Pr = protrusion. Scale bars: 0.4 mm (**A, B**); 0.2 mm (**C–G**); 0.1 mm (**H, I**).

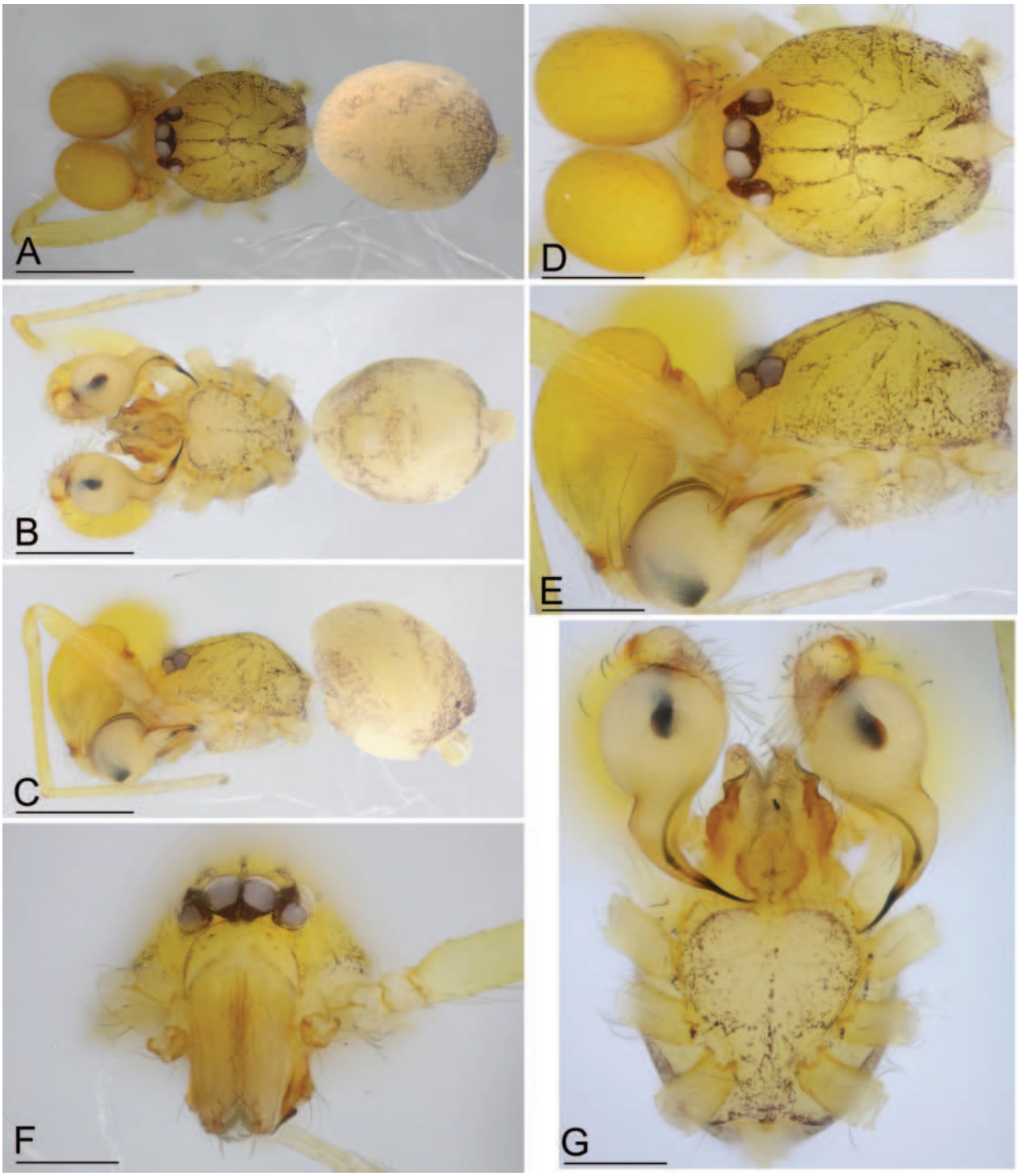

Figure 4. *Orchestina concava* sp. nov., holotype male. **A–C.** Habitus, dorsal, ventral and lateral views; **D–G.** Prosoma, dorsal, lateral, anterior and ventral views. Scale bars: 0.4 mm (**A–C**); 0.2 mm (**D–G**).

***Orchestina menglun* Tong & Li, sp. nov.**

https://zoobank.org/EAD9BEBA-2A52-44BC-A6E8-0BA96462F79A

Figs 6, 7A–D

Type material. ***Holotype*****:** ♂ (SYNU-775), **China, Yunnan**, Mengla Co., Menglun Town, XTBG, fogging, Lvshilin, limestone monsoon rainforest (21°54.617'N, 101°16.843'E), elev. 738 m, 8 August 2011, Zheng, Zhao & Gao leg. ***Paratypes*****:** 7♂ (SYNU-900-906), XTBG, fogging, secondary tropical seasonal moist forest (21°54.607'N, 101°17.005'E), elev. 633 m, 28 July 2007, Zheng leg.

Etymology. The specific name is a noun in apposition taken from the type locality.

Diagnosis. The new species is similar to *O. clavulata* in having the pear-shaped bulb and the net-shaped pattern on carapace, but can be distinguished by the palpal tibia distinctly narrower than bulb

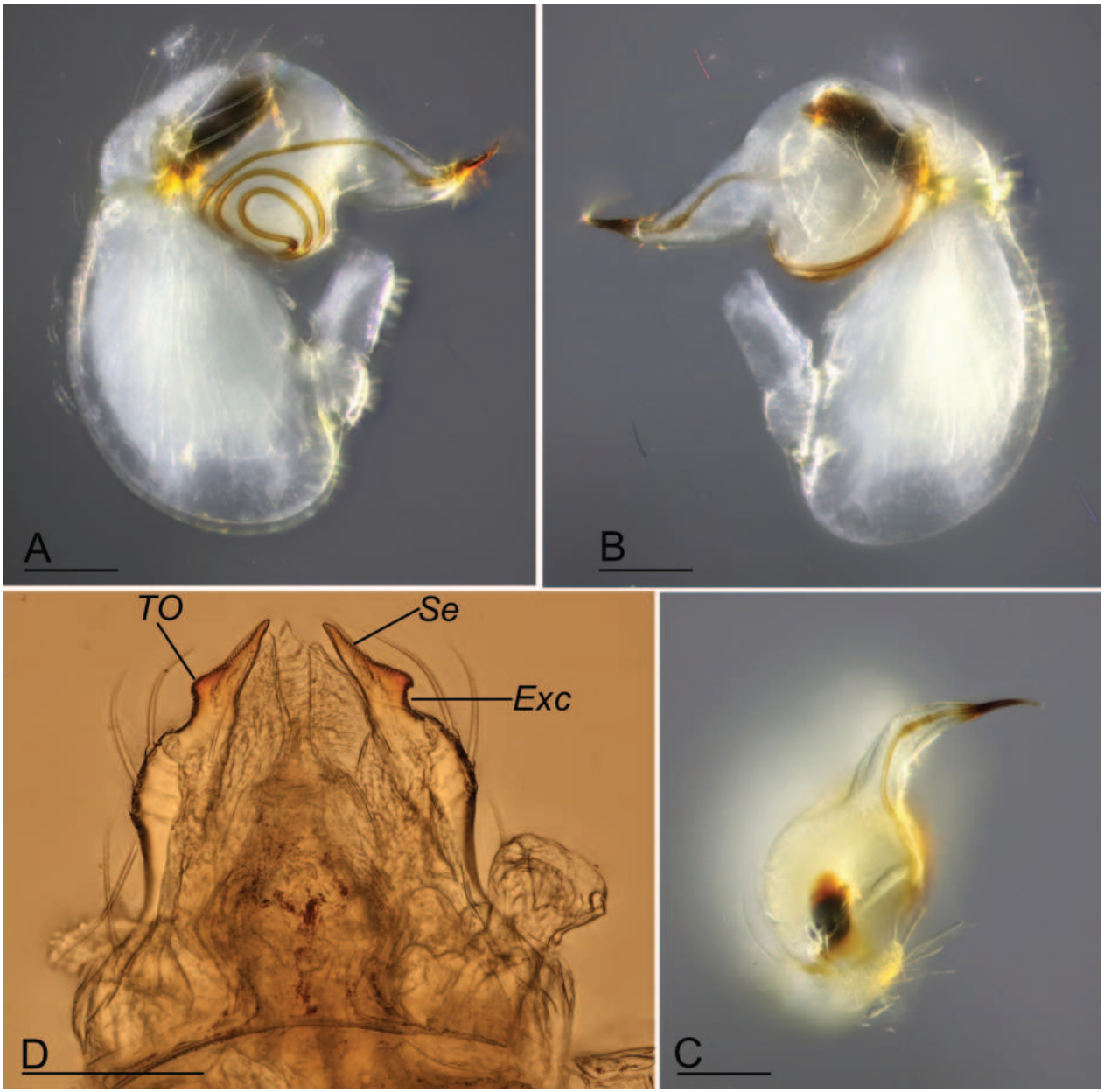

Figure 5. *Orchestina concava* sp. nov., holotype male. **A–C.** Left palp, prolateral, retrolateral and dorsal views; **D.** Endites and labium, ventral view. Abbreviations: Exc = excavations; Se = serrula; TO = triangular outgrowth. Scale bars: 0.1 mm.

(Fig. 7A, B) vs. as wide as bulb in *O. clavulata* (Fig. 1A) and endites not strongly sclerotized, with smoothly curved outer margin (Figs 6G, 7D) vs. strongly sclerotized, with straight outer margin in *O. clavulata* (Fig. 1E).

Description. Male (holotype). Total length 1.18, carapace length 0.61, carapace width 0.42, abdomen length 0.56. Habitus as in Fig. 6A–C. Color in alcohol: pale yellow. Carapace oval, with sepia net-shaped pattern, pars cephalica strongly elevated in lateral view, with rounded posterolateral corners. Clypeus (Fig. 6F) margin unmodified, curved downwards in front view, sloping forward in lateral view. Sternum (Fig. 6G) longer than wide, with marginal band and median area of radiating lines, surface smooth. Mouthparts: chelicerae straight, anterior face unmodified; labium rounded, not fused to sternum, anterior margin not indented at middle; endites (Fig. 7D) not strongly sclerotized, outer margin smoothly curved, with serrula. Abdomen ovoid, with gray ^-shaped pattern. Genitalia (Fig. 7A–C): tibia of palp enlarged, length/width ratio = 1.72, cymbium small; bulb pear-shaped in lateral view, with ventral side strongly protruding proximally, about 1.52 times as wide as tibia; the sperm duct strongly curved with three loops; embolus short.

Female. Unknown.

Distribution. China (Yunnan: Xishuangbanna Tropical Botanical Garden).

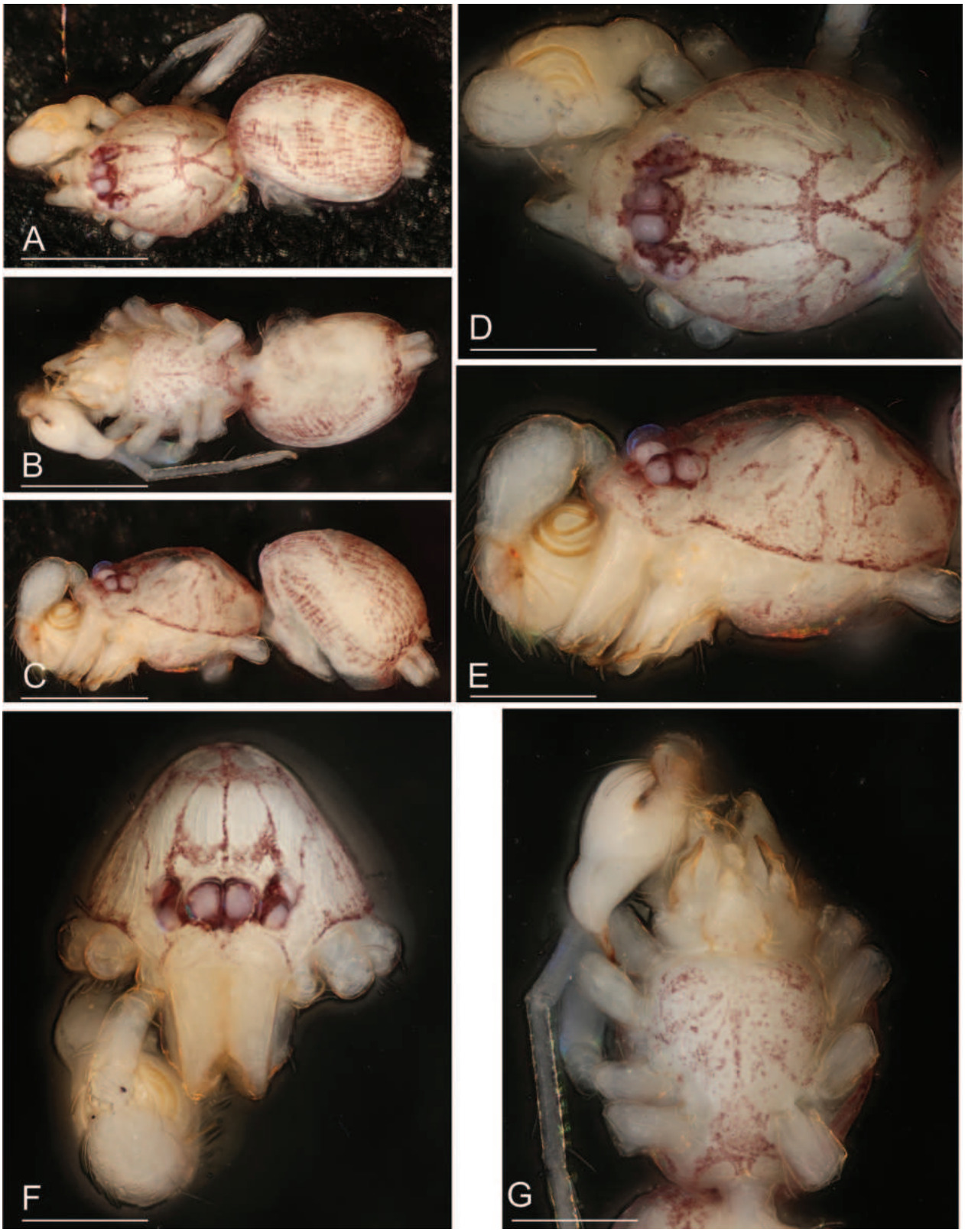

Figure 6. *Orchestina menglun* sp. nov., holotype male. **A–C.** Habitus, dorsal, ventral and lateral views; **D–G.** Prosoma, dorsal, lateral, anterior and ventral views. Scale bars: 0.4 mm (**A–C**); 0.2 mm (**D–G**).

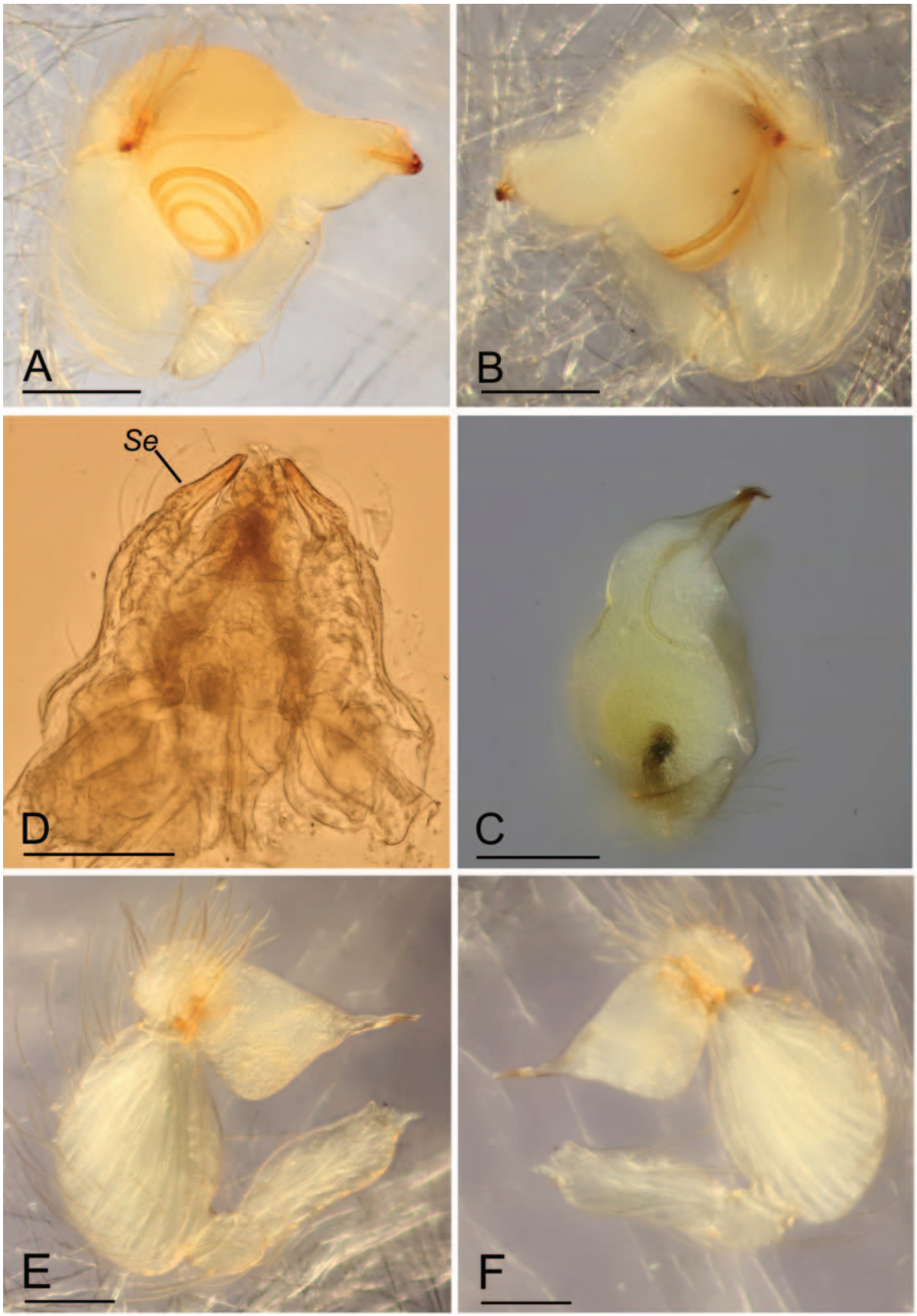

Figure 7. *Orchestina menglun* sp. nov., **A–D**, holotype male; *Orchestina colubrina* Liu, Henrard & Xu, 2019, **E, F,** male (SYNU-841). **A, E.** Left palp, prolateral view; **B, F.** Left palp, retrolateral view; **C.** Left palp, dorsal view; **D.** Endites and labium, ventral view. Abbreviation: Se = serrula. Scale bars: 0.1 mm.

***Orchestina subclavulata* Tong & Li, sp. nov.**

https://zoobank.org/FE9EC909-7177-4E77-A09F-15634499B087

Figs 8, 9

Type material. ***Holotype*:** ♂ (SYNU-776), **China, Yunnan**, Mengla Co., Menglun Town, XNNR, fogging, seasonal rainforest, 55 Km (21°57.953'N, 101°12.305'E), elev. 781 m, 13 August 2011, Zheng, Zhao & Gao leg. ***Paratypes*:** 5♂ (SYNU-819-823), same data as for holotype.

Etymology. The specific name refers to the similarities to *O. clavulata*.

Diagnosis. The new species is similar to *O. clavulata* and *O. menglun* sp. nov. in having the pear-shaped bulb and the net-shaped pattern on carapace, but can be distinguished by the endites with triangular outgrowth (Figs 8G, 9D), vs. without triangular outgrowth in *O. clavulata* (Fig. 1E) and *O. menglun* (Fig. 7D), and the sperm duct overlapped at the margin of bulb (white arrow in Fig. 9A) vs. not overlapped in *O. clavulata* (Fig. 1B) and *O. menglun* (Fig. 7A).

Description. Male (holotype). Total length 0.96, carapace length 0.41, carapace width 0.39, abdomen length 0.48. Habitus as in Fig. 8A–C. Color in alcohol: carapace yellow, abdomen, legs and palp pale yellow. Carapace oval, with net-shaped pattern, pars cephalica strongly elevated in lateral view, with rounded posterolateral corners. Clypeus (Fig. 8F) margin unmodified, curved downwards in front view, rounded forward in lateral view. Sternum (Fig. 8G) longer than wide, pale yellow, with marginal band and median area of radiating lines, surface smooth. Mouthparts: chelicerae elongate, anterior face unmodified; labium elongate, spade-shaped, not fused to sternum, anterior margin not indented at middle; endites (Figs 8G, 9D) strongly sclerotized, with triangular outgrowth, outer margin with serrula. Abdomen ovoid, with ^-shaped pattern. Genitalia (Fig. 9A–C): tibia of palp strongly enlarged, length/width ratio = 1.67, cymbium small; bulb pear-shaped in lateral view, with ventral side strongly protruding proximally, about 0.91 times as wide as tibia; the sperm duct strongly curved with three loops; embolus short, with sub-apical, opaque crest.

Female. Unknown.

Distribution. Known only from the type locality.

***Orchestina truncatula* Tong & Li, 2011**

Figs 10–12

Orchestina truncatula Tong & Li, 2011: 39, figs 1E–F, 2C, 3C–D, 4D, 5E, 8A–F; Tong, 2013: 48, figs 26E–F, 27C, 28C–D, 29D, 30E, 66A–F; Rajoria & Jadhao, 2016: 61, figs 1–5.

Material examined. 2♂ (SYNU-773-774), **China, Yunnan**, Mengla Co., Menglun Town, XTBG, fogging, Lvshilin, limestone monsoon rainforest (21°54.617'N, 101°16.843'E), elev. 738 m, 8 August 2011, Zheng, Zhao & Gao leg.; 1♀ (SYNU-783), sifting leaf litter, Bubang Vill. (21°36.640'N, 101°34.905'E), elev. 823 m, 10 July 2012, Zhao & Chen leg.; **7**♂5♀ (SYNU-874), sifting leaf litter, seasonal rainforest (22°09.765'N, 100°52.553'E), elev. 862 m, 22 July 2012, Zhao & Chen leg.

Type material (examined). ***Holotype*** ♂ (IZCAS Ar 19320), China: Hainan, Baisha, Yinggeling, Yinggezui Protection Station, 693 m a.s.l., 19°03.049'N, 109°33.751'E, 25 August 2010, leg. G. Zheng. ***Paratypes*:** 1 ♂, 1♀ (IZCAS Ar 19319), same data as holotype; 2 ♀ (IZCAS Ar 19318), China: Hainan, Ledong, Jianfengling, 997m a.s.l., 18°44.658'N, 108°50.435'E, 18 August 2010, leg. G. Zheng.

Diagnosis. This species is similar to *O. communis* Henrard & Jocqué, 2012 in the large leaf-shaped setae on the diamond-shaped labium and the group of strong, converging setae on distal part of the male chelicerae, but can be distinguished by the small process at base of male chelicerae (Fig. 10F, G; Tong and Li 2011: fig. 3C, D), vs. without the small process (Henrard and Jocqué 2012: figs 90, 93), and the shape of anterior uterine sclerite (AUS), the length/width ratio about 1.25 (Fig. 12F; Tong and Li 2011: fig. 5E), vs. about 0.6 (Henrard and Jocqué 2012: fig. 104).

Description. See Tong and Li (2011).

Comment. Tong and Li (2011) described this species based on two male and three female specimens from forest canopy of Hainan Island. The present study materials were collected by fogging and sifting leaf litter from Xishuangbanna, Yunnan. Rajoria and Jadhao (2016) reported this species from Melghat region of Maharashtra, India based on a single male specimen. This suggests that *O. truncatula* may be widely distributed in Asia. In addition, tibia I of male with a group of ventrobasal spines (Fig. 10D). This character was overlooked in the original publication.

Distribution. China (Hainan, Yunnan); India.

***Orchestina wengnan* Tong & Li, sp. nov.**

https://zoobank.org/58A0D0E9-CBC1-4742-B1C8-E9436A18A7C3

Figs 13, 14

Type material. ***Holotype*:** ♂ (SYNU-767), **China, Yunnan**, Jinghong City, Menghai Co., Meng'a Town, Wengnan Vill., sifting leaf litter, secondary forest (22°05.020'N, 100°22.086'E), elev. 1118 m, 24 July 2012, Zhao & Chen leg. ***Paratypes*:** 1♂ (SYNU-768), sifting leaf litter, Mandazhai Vill., secondary forest (22°01.702'N, 100°23.697'E), elev. 1188 m, 28 July 2012, Zhao & Chen leg.; 1♂ (SYNU-789), sifting leaf litter, Wengnan Vill., secondary forest (22°04.996'N, 100°22.223'E), elev. 1137 m, 25 July 2012, Zhao & Chen leg.

Etymology. The specific name is a noun in apposition taken from the type locality.

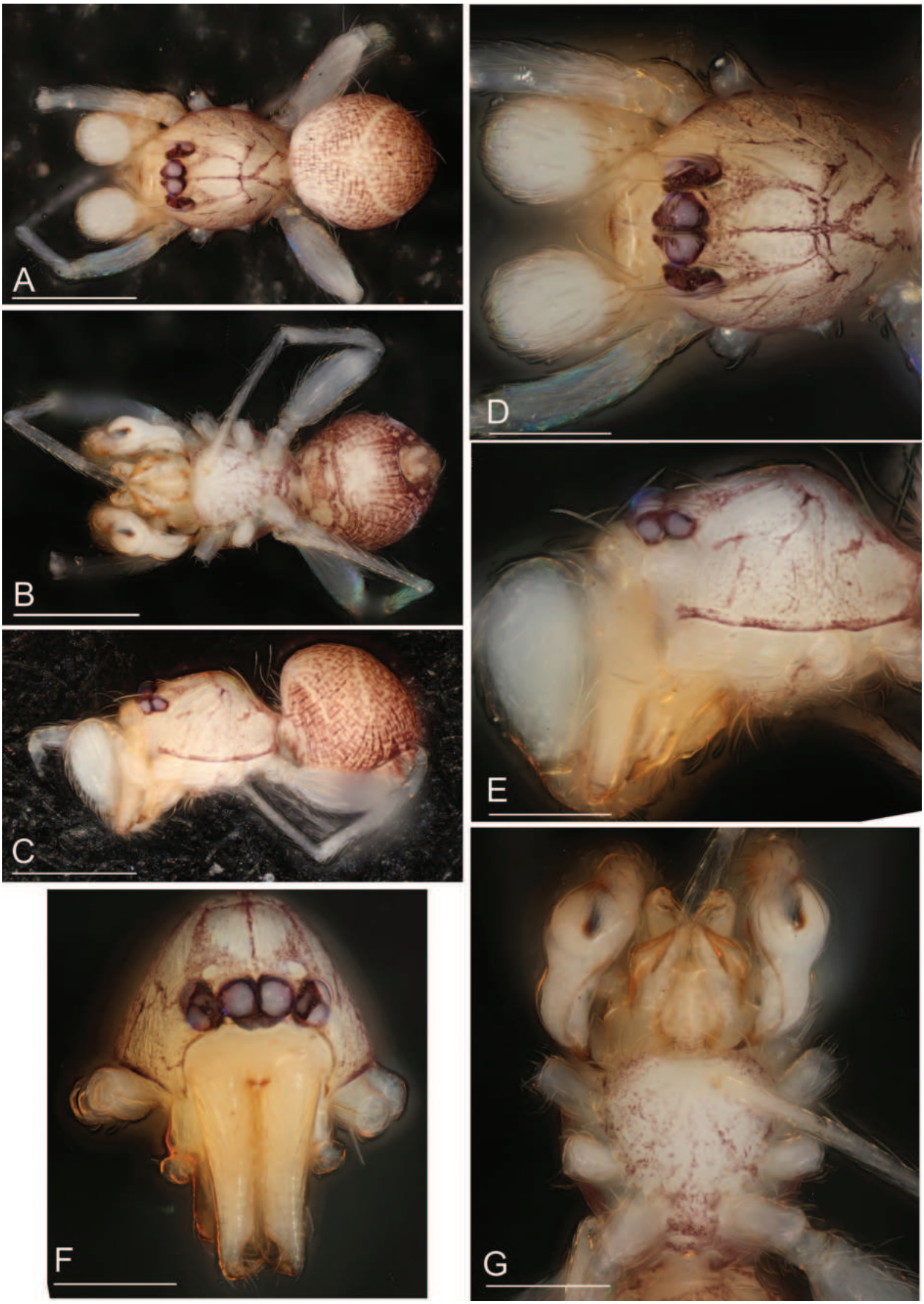

Figure 8. *Orchestina subclavulata* sp. nov., holotype male. **A–C.** Habitus, dorsal, ventral and lateral views; **D–G.** Prosoma, dorsal, lateral, anterior and ventral views. Scale bars: 0.4 mm (**A–C**); 0.2 mm (**D–G**).

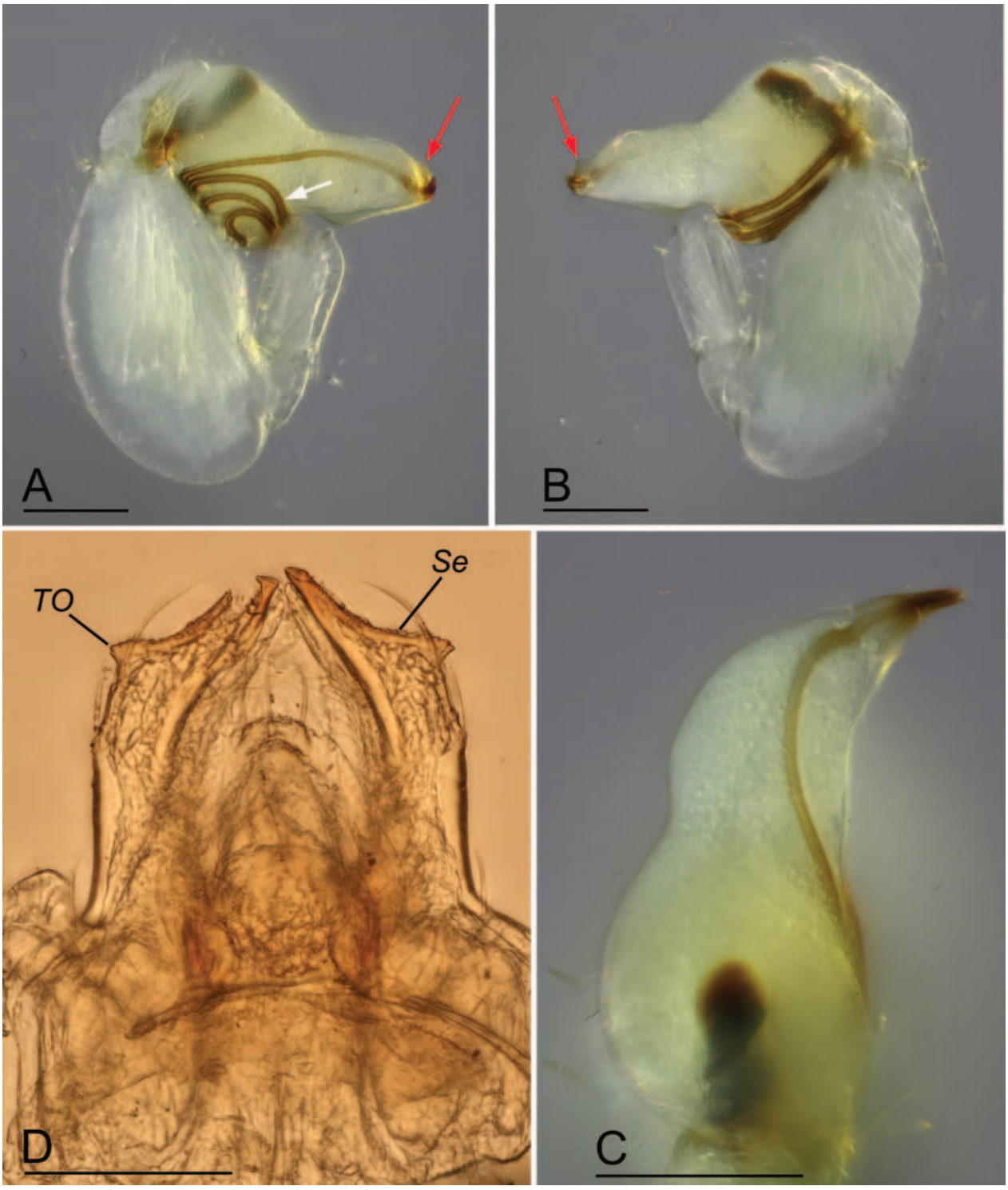

Figure 9. *Orchestina subclavulata* sp. nov., holotype male. **A–C.** Left palp, prolateral, retrolateral and dorsal views, white arrow shows the overlapped sperm duct, red arrow pointing on subapical crest of embolus; **D.** Endites and labium, ventral view. Abbreviations: Se = serrula; TO = triangular outgrowth. Scale bars: 0.1 mm.

Diagnosis. The new species is similar to *O. zhiwui* Liu, Xu & Henrard, 2019 in having median projection of clypeus and the net-shaped pattern on carapace, but can be distinguished by the endites with smoothly outer margin (Fig. 14D) vs. with triangular outgrowth in *O. zhiwui* (Liu et al. 2019: figs 12H,13A; Wang et al. 2021: figs 1H, 2G) and the sperm duct with two loops in prolateral view (Fig. 14A) vs. only half loops (Liu et al. 2019: fig. 13B; Wang et al. 2021: fig. 1I).

Description. Male (holotype). Total length 0.94, carapace length 0.48, carapace width 0.38, abdomen length 0.49. Habitus as in Fig. 13A–C. Color in alcohol: carapace yellow, abdomen and legs pale

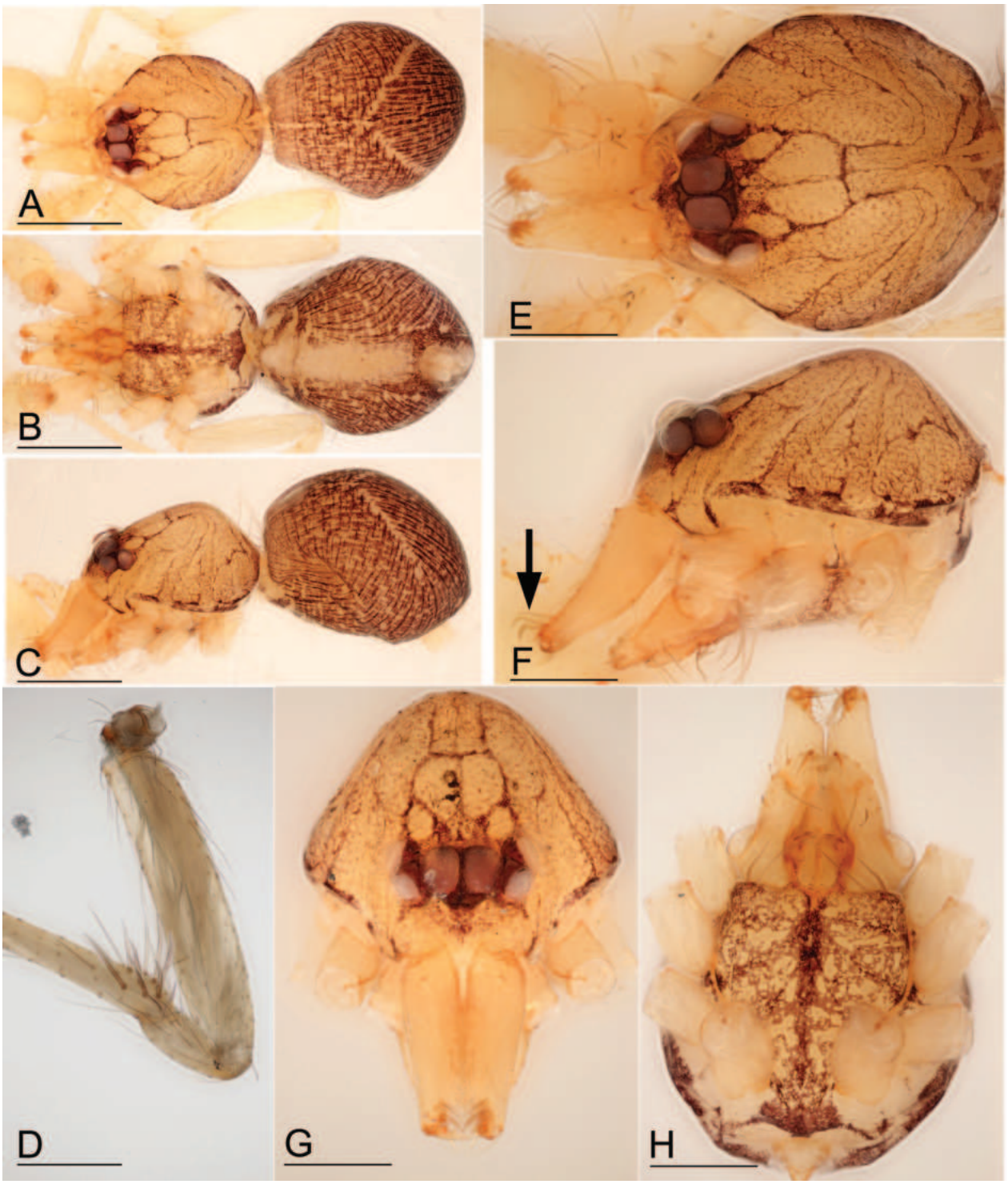

Figure 10. *Orchestina truncatula* Tong & Li, 2011, male (SYNU-773). **A–C.** Habitus, dorsal, ventral and lateral views; **D.** Left leg I, prolateral view; **E–H.** Prosoma, dorsal, lateral, anterior and ventral views, arrow shows the characteristic distal setae. Scale bars: 0.4 mm (**A–C**); 0.1 mm (**D**); 0.2 mm (**E–H**).

yellow. Carapace oval, with net-shaped pattern, pars cephalica strongly elevated in lateral view, with rounded posterolateral corners. Clypeus (Fig. 13F) with a median projection in frontal view, rounded forward in lateral view. Sternum (Fig. 13G) longer than wide, with marginal band and median area of radiating lines, surface smooth. Mouthparts: chelicerae straight, anterior face unmodified; labium rounded, not fused to sternum, anterior margin not indented at middle; endites (Figs 13G, 14D) strongly sclerotized, outer margin with serrula. Abdomen ovoid, with gray ^-shaped pattern. Genitalia (Fig. 14A–C): tibia of palp strongly enlarged, length/width ratio = 1.72, cymbium small; bulb pear-shaped, about 1.0 times as wide

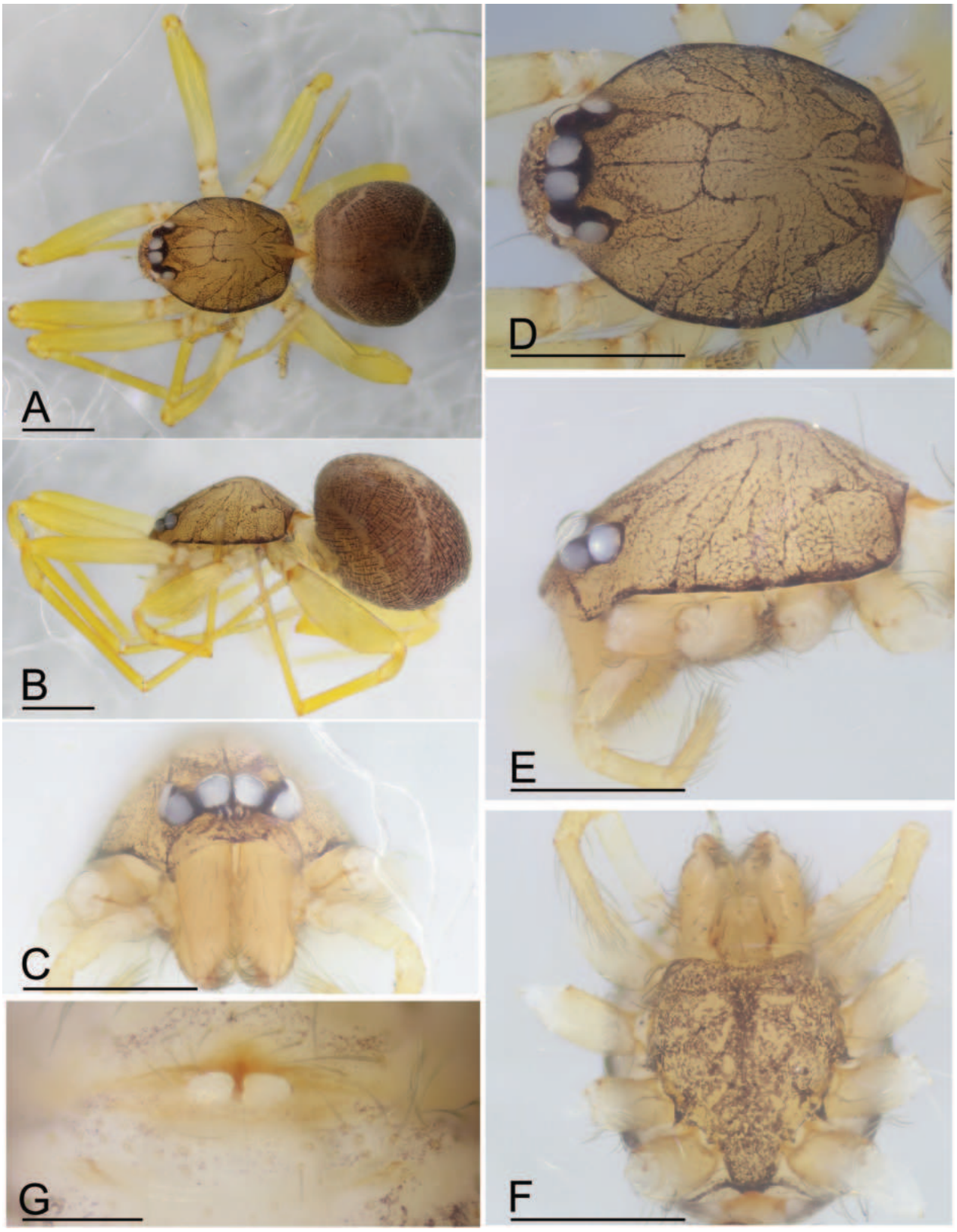

Figure 11. *Orchestina truncatula* Tong & Li, 2011, female (SYNU-783). **A, B.** Habitus, dorsal and lateral views; **C–F.** Prosoma, anterior, dorsal, lateral and ventral views; **G.** Epigaster, ventral view. Scale bars: 0.4 mm (**A–F**); 0.1 mm (**G**).

as tibia, with distal part gradually tapered towards embolus; the sperm duct strongly curved with two loops; embolus short.

Female. Unknown.

Distribution. China (Yunnan: Menghai County, Meng'a Town).

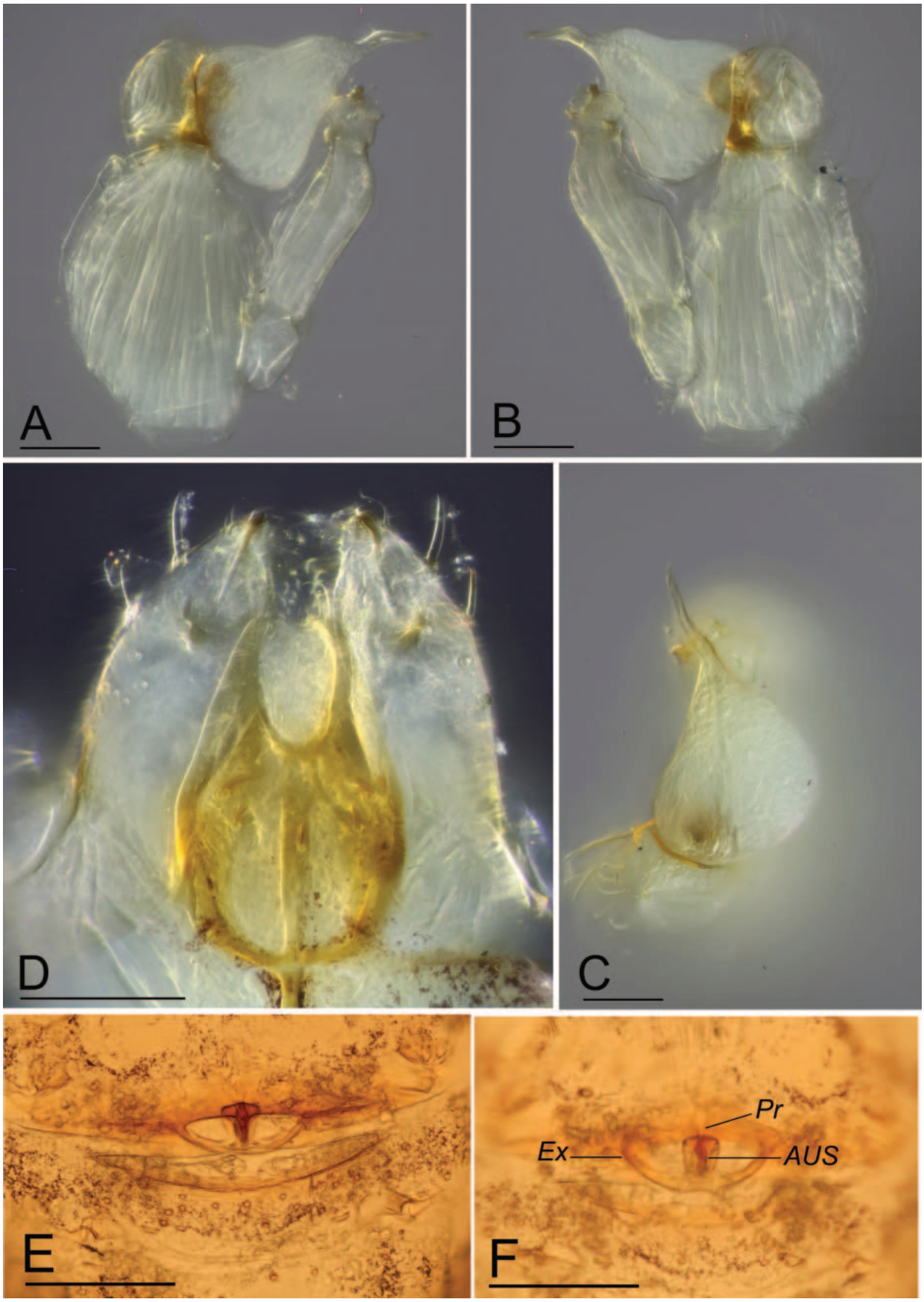

Figure 12. *Orchestina truncatula* Tong & Li, 2011, male (SYNU-773), female (SYNU-783). **A–C.** Left palp, prolateral, retrolateral and dorsal views; **D.** Endites and labium, ventral view; **E, F.** Endogyne, ventral and dorsal views. Abbreviations: AUS = anterior uterine sclerite; Ex = dorsolateral extension; Pr = protrusion. Scale bars: 0.1 mm.

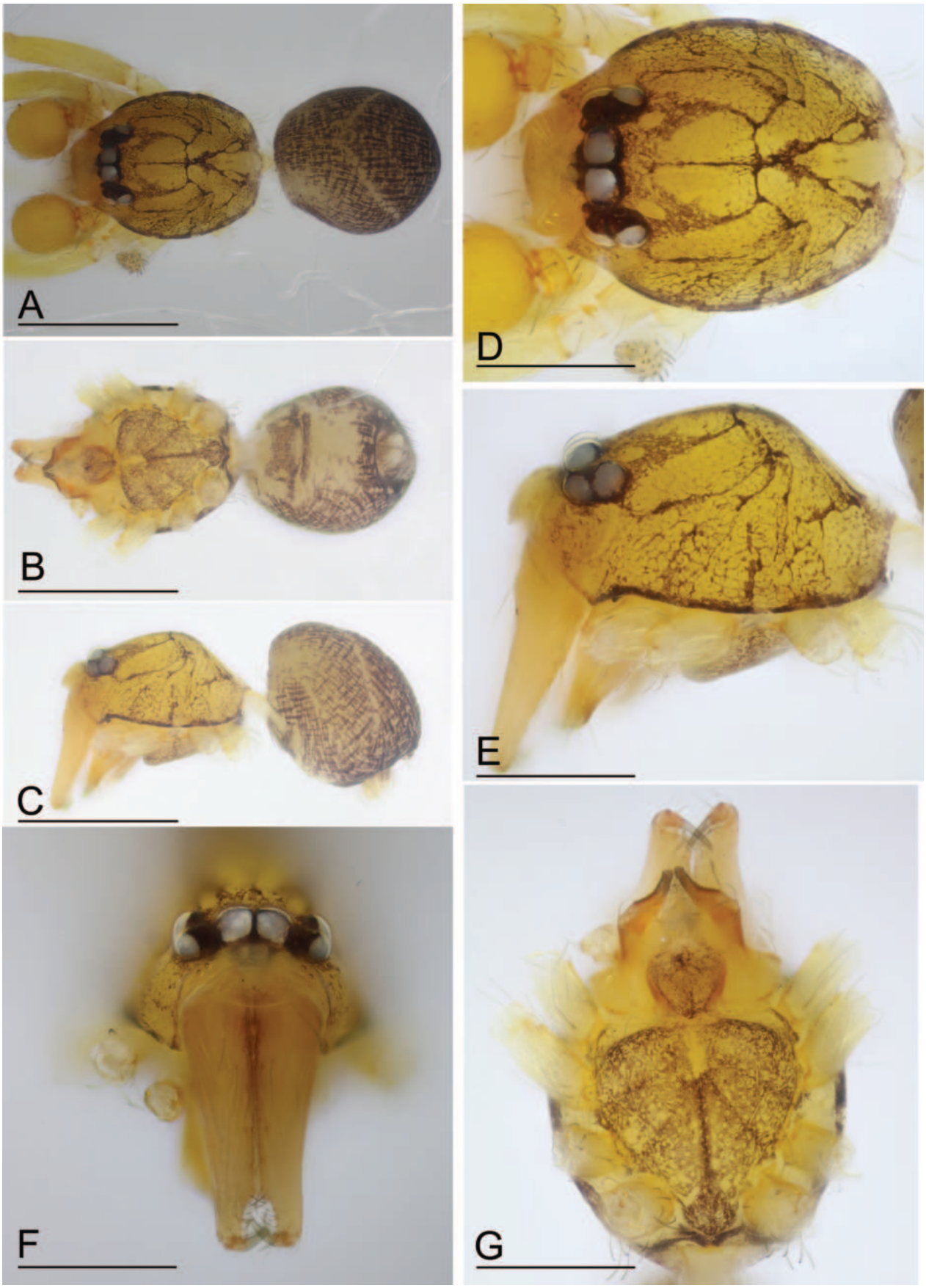

Figure 13. *Orchestina wengnan* sp. nov., holotype male. **A–C.** Habitus, dorsal, ventral and lateral views; **D–G.** Prosoma, dorsal, lateral, anterior and ventral views. Scale bars: 0.4 mm (**A–C**); 0.2 mm **(D–G**).

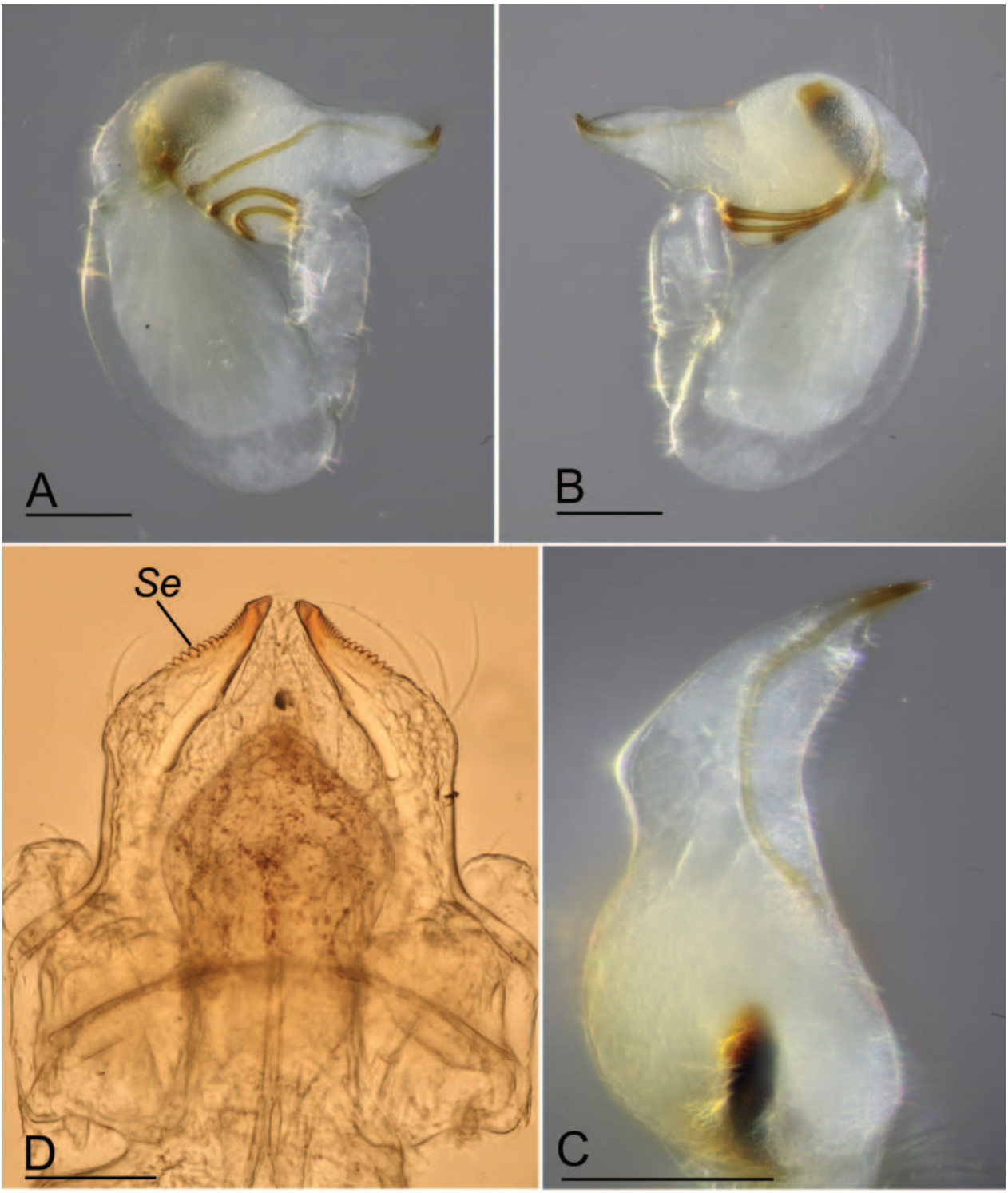

Figure 14. *Orchestina wengnan* sp. nov., holotype male. **A–C.** Left palp, prolateral, retrolateral and dorsal views; **D.** Endites and labium, ventral view. Abbreviation: Se = serrula. Scale bars: 0.1 mm.

***Orchestina xui* Tong & Li, sp. nov.**

https://zoobank.org/B9604684-7F31-4D24-B20E-A90BEB9A2127

Figs 15–18

Type material. ***Holotype*:** ♂ (SYNU-769), **China, Yunnan**, Mengla Co., Menglun Town, XNNR, fogging, mountaintop secondary rainforest, 55 Km (21°57.987'N, 101°12.167'E), elev. 842 m, 18 August 2011, Zheng, Zhao & Gao leg. ***Paratypes*:** 1♂ (SYNU-770), same data as for holotype; 1♂ (SYNU-811), sifting leaf litter, Xiaolongha Vill., seasonal forest (21°24.330'N, 101°37.022'E), elev. 801 m, 30 June 2012, Zhao & Chen leg.; 1♂2♀ (SYNU-790-792), sifting leaf litter, Xiaolongha Vill., secondary forest (21°24.213'N, 101°37.995'E), elev. 834 m, 3 June 2012, Zhao & Chen leg.; 3♂2♀ (SYNU-805-809), XNNR, fogging, valley rainforest, 55 Km (21°57.883'N, 101°12.147'E), elev. 839 m, 15 August 2011, Zheng, Zhao & Gao leg.

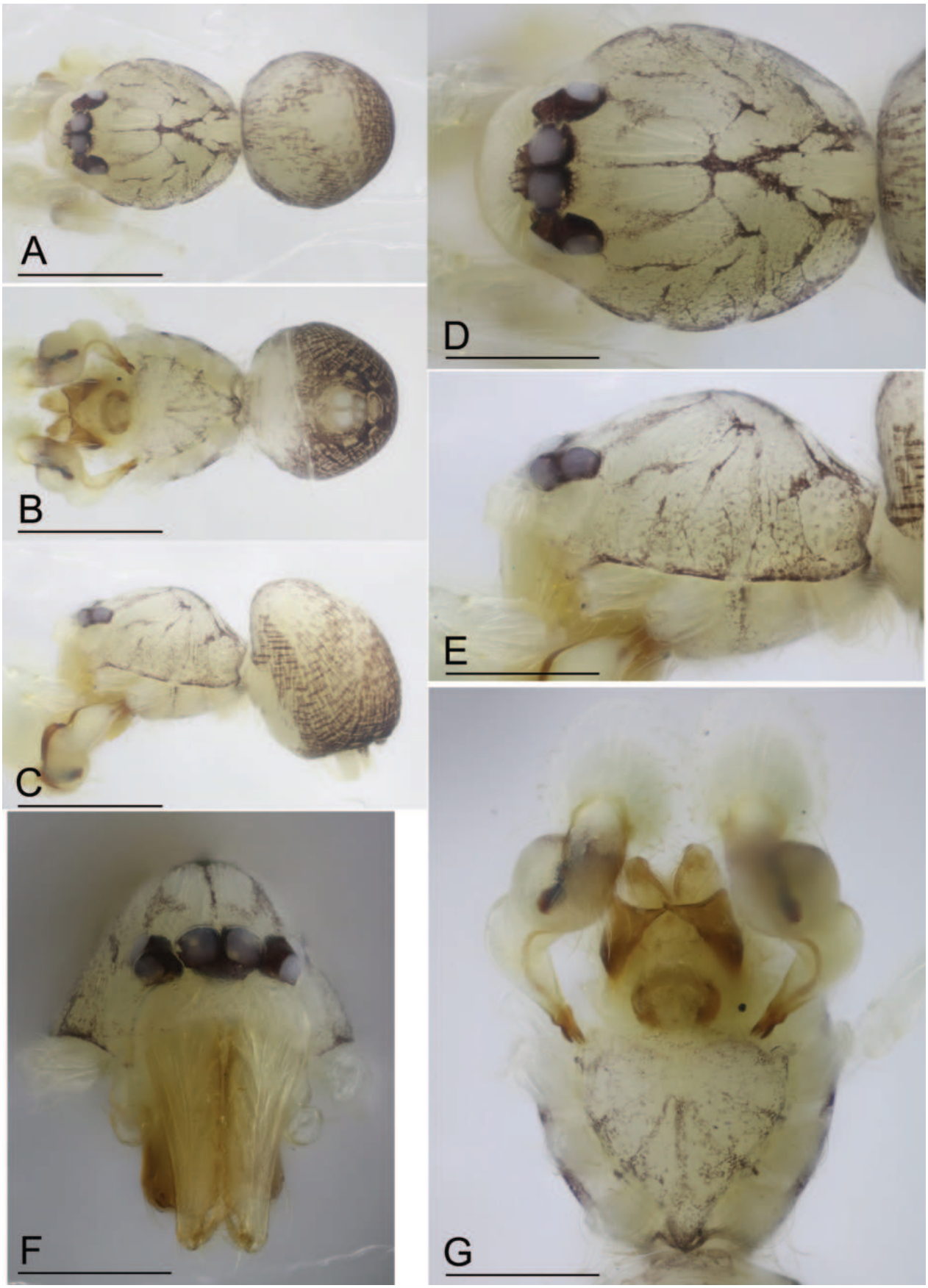

Figure 15. *Orchestina xui* sp. nov., holotype male. **A–C.** Habitus, dorsal, ventral and lateral views; **D–G.** Prosoma, dorsal, lateral, anterior and ventral views. Scale bars: 0.4 mm (**A–C**); 0.2 mm (**D–G**).

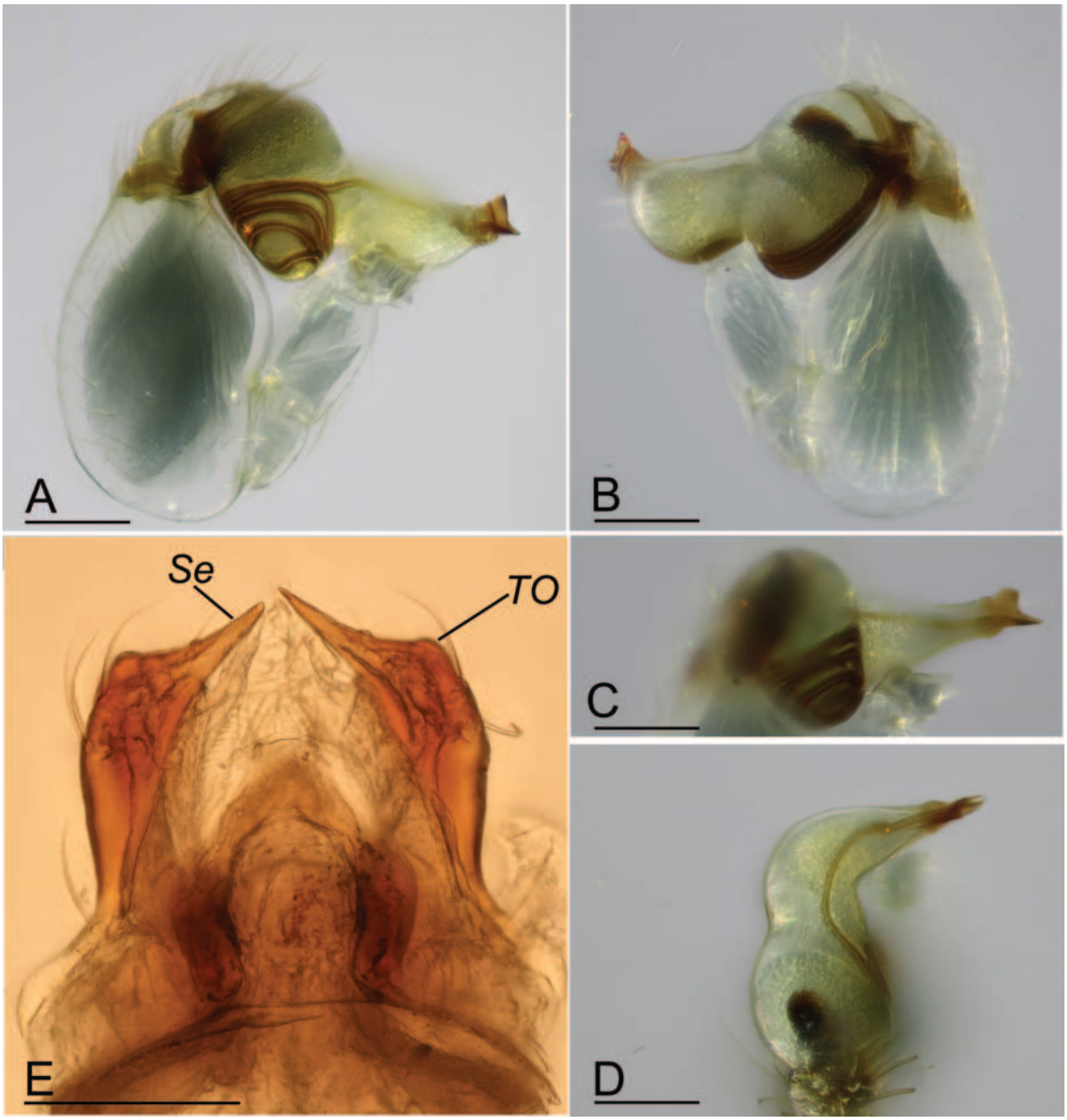

Figure 16. *Orchestina xui* sp. nov., holotype male. **A, B, D.** Left palp, prolateral, retrolateral and dorsal views; **C.** Distal part of bulb, prolateral view; **E.** Endites and labium, ventral view. Abbreviations: Se = serrula; TO = triangular outgrowth. Scale bars: 0.1 mm.

Etymology. The specific name comes from the family name of Mr Yajun Xu, who worked extensively on the Chinese goblin spiders; noun.

Diagnosis. The new species is similar to *O. clavulata* in having the pear-shaped bulb, the net-shaped pattern on carapace and the large posterior plate, but can be distinguished by the endites with large triangular outgrowth (Figs 15G, 16E), vs. straight outer margin in *O. clavulata* (Fig. 1E), the embolus with flattened extension (Fig. 16A–D) vs. gradually narrower in *O. clavulata* (Fig. 1A–D), and the genital area with two small, dark sclerotized pockets (Fig. 18B, C) vs. without sclerotized pockets (Tong and Li 2011: fig. 4B). The new species is also similar to *O. subclavulata* sp. nov. in the shape of male endites, but can be distinguished by the embolus with conspicuous dorsal flattened extension and acute tip (Fig. 16A, B), vs. embolus gradually tapered, with sub-apical, opaque crest (Fig. 9A, B).

Description. Male (holotype). Total length 1.13, carapace length 0.55, carapace width 0.43, abdomen length 0.58. Habitus as in Fig. 15A–C. Color in alcohol: pale yellow. Carapace oval, with net-shaped pattern, pars cephalica strongly elevated in lateral view, with rounded posterolateral corners. Clypeus (Fig. 15F) margin

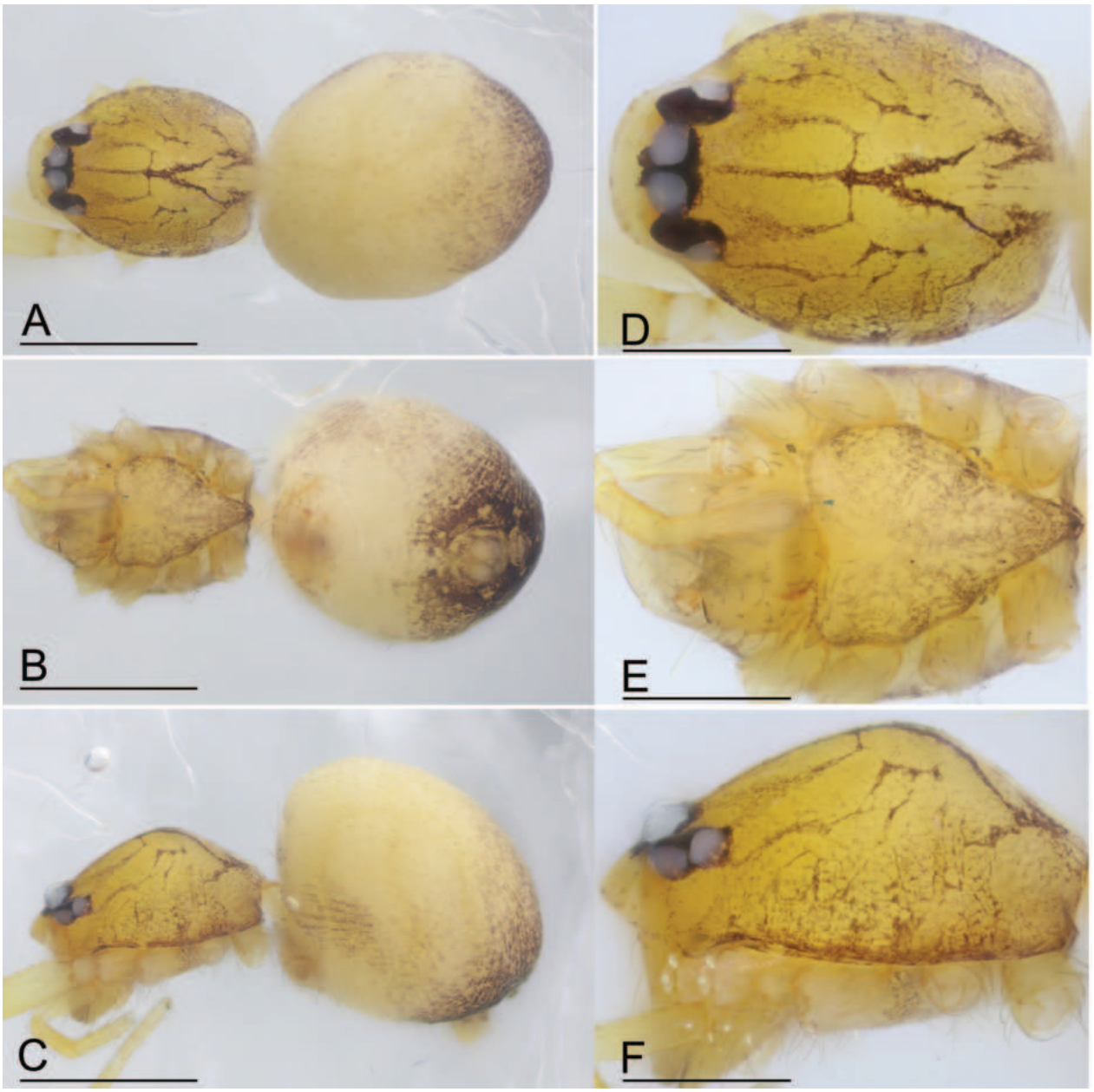

Figure 17. *Orchestina xui* sp. nov., paratype female. **A–C.** Habitus, dorsal, ventral and lateral views; **D–F.** Prosoma, dorsal, ventral and lateral views. Scale bars: 0.4 mm (**A–C**); 0.2 mm (**D–F**).

unmodified, curved downwards in front view, rounded forward in lateral view. Sternum (Fig. 15G) longer than wide, with marginal band and median area of radiating lines, surface smooth. Mouthparts: chelicerae elongate, anterior face unmodified; labium rounded, not fused to sternum, anterior margin not indented at middle; endites (Figs 15G, 16E) strongly sclerotized, with large triangular outgrowth, outer margin with serrula. Abdomen ovoid, with gray ^-shaped pattern. Genitalia (Fig. 16A–D): tibia of palp strongly enlarged, length/width ratio = 1.53, cymbium small; bulb pear-shaped, about 0.88 times as wide as tibia, with distal part gradually tapered towards embolus; the sperm duct strongly curved with three loops; embolus flattened, with acute tip.

Female (SYNU-792). Same as male except as noted. Body: habitus as in Fig. 17A–C; body length 1.18. Carapace: 0.52 long, 0.41 wide. Mouthparts: chelicerae shorter; endites simple, with serrula. Abdomen: 0.67 long. Epigaster (Fig. 18B, C): with two small, dark sclerotized pockets; internal parts visible through integument. Endogyne (Fig. 18D): with stout medial clavate sclerite (AUS), anterior part of cylindrical sclerite (AUS) with pair of lateral protrusions (Pr); anterior receptaculum (ARe) rounded, transparent, slightly longer than AUS; with large posterior plate (PP).

Distribution. China (Yunnan: Mengla County, Menglun Town).

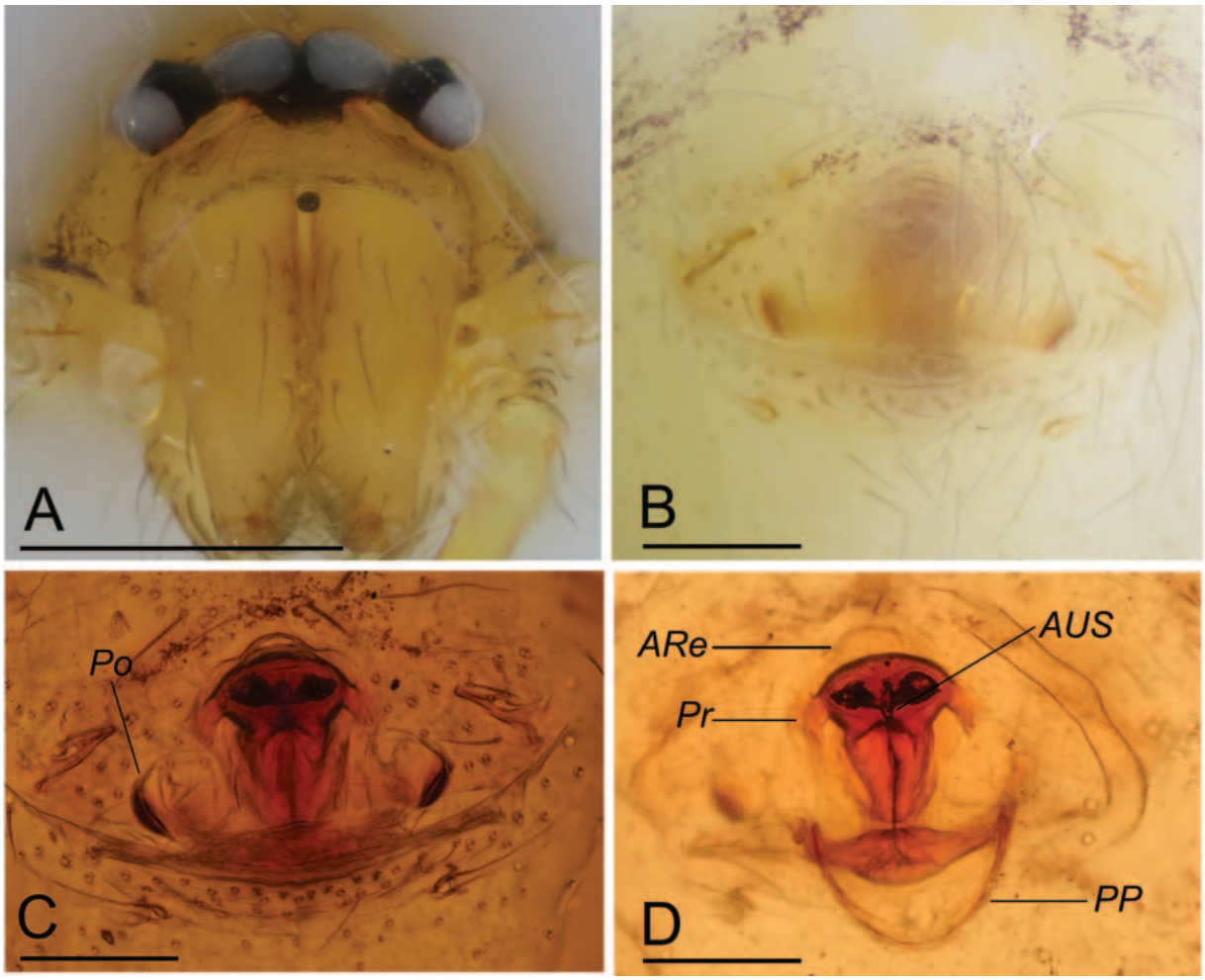

Figure 18. *Orchestina xui* sp. nov., paratype female. **A.** Prosoma, anterior view; **B.** Epigaster, ventral view; **C, D.** Endogyne, ventral and dorsal views. Abbreviations: ARe = anterior receptaculum; AUS = anterior uterine sclerite; Po = pocket; PP = posterior plate; Pr = protrusion. Scale bars: 0.2 mm (**A**); 0.1 mm (**B–D**).

Figure 19. Locality of Xishuangbanna, Yunnan Province, China

Discussion

The genus *Orchestina* is perhaps the dominant group in canopies (Henrard and Jocqué 2012). Occasionally, some of these spiders are also found under bark, in litter, grasses, and suspended litter, and even inside buildings (Izquierdo and Ramírez 2017).

The diversity of *Orchestina* from China is still poorly known. Xu (1987) firstly reported two species from Anhui Province. Both species were collected from leaf litter by hand. Tong and Li (2011) reported six species collected from forest canopy from Hainan Province. Liu et al. (2016, 2019) discovered five species from Hunan and Jiangxi Provinces. All species were collected by sifting leaf litter. Wang et al. (2021) recorded one species from Fenghuang Mountain, Liaoning Province by sifting leaf litter. So far, it is the northernmost locality of *Orchestina* in China. Recently, Lin et al. (2024) reported one species from Chongqing municipality. This species was collected from leaf litter by hand. In the 14 known *Orchestina* species of China, eight species were collected from leaf litter.

As to the eight species of *Orchestina* from Xishuangbanna, *O. concava and O. wengnan* were collected by sifting leaf litter, *O. clavulata*, *O. menglun* and *O. subclavulata* were collected from forest canopy, *O. truncatula* and *O. xui* were collected from leaf litter and forest canopy, and *O. colubrina* was collected by fogging and trunk trap. At least three Chinese species, i.e., *O. colubrina*, *O. truncatula* and *O. xui* were collected from both leaf litter and forest canopy, suggesting that some species of the genus *Orchestina* can occupy a wide variety of habitats.

Acknowledgements

The manuscript benefitted greatly from comments by Arnaud Henrard (Tervuren, Belgium), Yuri M. Marusik (Magadan, Russia), the subject editor Danilo Harms (Hamburg, Germany) and one anonymous referee. This study was supported by the National Natural Science Foundation of China (NSFC-32370479, 31972867).

References

Henrard A, Jocqué R (2012) An overview of Afrotropical canopy-dwelling *Orchestina* (Araneae, Oonopidae), with a wealth of remarkable sexual dimorphic characters. Zootaxa 3284(1): 1–104. https://doi.org/10.11646/zootaxa.3284.1.1

Huang Y, Bian D, Tong Y, Li S (2021) Two new species of the genus *Camptoscaphiella* from Yunnan, China (Araneae, Oonopidae). ZooKeys 1052: 43–53. https://doi.org/10.3897/zookeys.1052.66743

Izquierdo MA, Ramírez MJ (2017) Taxonomic revision of the jumping goblin spiders of the genus *Orchestina* Simon, 1882, in the Americas (Araneae: Oonopidae). Bulletin of the American Museum of Natural History 410: 1–362. https://doi.org/10.1206/0003-0090-410.1.1

Jocqué R, Dippenaar-Schoeman AS (2006) Spider Families of the World. Musée Royal de l'Afrique Central, Tervuren, 336 pp.

Li S (2021) Spiders of Xishuangbanna, China. ZooKeys 1034: 1–236.

Lin Y, Li S, Mo H, Wang X (2024) Thirty-eight spider species (Arachnida: Araneae) from China, Indonesia, Japan and Vietnam. Zoological Systematics 49(1): 4–98.

Liu K, Xiao Y, Xu X (2016) On three new *Orchestina* species (Araneae: Oonopidae) described from China. Zootaxa 4121(4): 431–446. https://doi.org/10.11646/zootaxa.4121.4.4

Liu K, Henrard A, Xiao Y, Xu X (2019) On three new oonopid species from China and the discovery of the male *Orchestina bialata* Liu, Xiao & Xu, 2016 (Araneae: Oonopidae). Zootaxa 4701(3): 235–256. https://doi.org/10.11646/zootaxa.4701.3.2

Myers N (1988) Threatened biotas: "hot spots" in tropical forests. The Environmentalist 8(3): 1–20. https://doi.org/10.1007/BF02240252

Platnick NI, Abrahim N, Álvarez-Padilla F, Andriamalala D, Baehr BC, Baert L, Bonaldo AB, Brescovit AD, Chousou-Polydouri N, Dupérré N, Eichenberger B, Fannes W, Gaublomme E, Gillespie R, Grismado CJ, Griswold CE, Harvey MS, Henrard A, Hormiga G, Izquierdo MA, Jocqué R, Kranz-Baltensperger Y, Kropf C, Ott R, Ramírez MJ, Raven RJ, Rheims CA, Ruiz GRS, Santos AJ, Saucedo A, Sierwald P, Szűts T, Ubick D, Wang XP (2012) Tarsal organ morphology and the phylogeny of goblin spiders (Araneae, Oonopidae), with notes on basal genera. American Museum Novitates 3736(3736): 1–52. https://doi.org/10.1206/3736.2

Rajoria A, Jadhao H (2016) First record of genus *Orchestina* Simon, 1882 in India (Araneae: Oonopidae). Serket = Sarkat 15(1): 60–62.

Sun X, Lin Y, Tong Y, Li S (2019) First report of a new myrmecophile spider (Araneae, Oonopidae) from Xishuangbanna, China. Acta Arachnologica Sinica 28(1): 37–40.

Tong Y (2013) Haplogynae spiders from Hainan, China. Science Press, Beijing, 96 pp. [81 pl.]

Tong Y, Li S (2011) Six new *Orchestina* species from Hainan Island, China (Araneae, Oonopidae). Zootaxa 3061(1): 36–52. https://doi.org/10.11646/zootaxa.3061.1.2

Tong Y, Li S (2015a) Six new species of the genus *Opopaea* Simon, 1891 from Xishuangbanna Rainforest, southwestern China (Araneae: Oonopidae). Zootaxa 3931(1): 41–62. https://doi.org/10.11646/zootaxa.3931.1.3

Tong Y, Li S (2015b) One new genus and two new species of oonopid spiders from Xishuangbanna Rainforest, southwestern China (Araneae, Oonopidae). ZooKeys 494: 1–12. https://doi.org/10.3897/zookeys.494.9183

Tong Y, Sun X, Li S, Bian D (2021) Taxonomic study of the genus *Ischnothyreus* (Araneae, Oonopidae) from Xishuangbanna Rainforest, southwestern China. ZooKeys 1034: 165–197. https://doi.org/10.3897/zookeys.1034.63388

Ubick D, Dupérré N (2017) Oonopidae. In: Ubick D, Paquin P, Cushing P, Roth V (Eds) Spiders of North America: An Identification Manual (2nd edn.). American Arachnological Society, Keene, New Hampshire, 181–182.

Wang Y, Wan N, Tong Y, Marusik YM (2021) On the northernmost *Orchestina* species in China, with a first description of the female of *O. zhiwui* (Araneae, Oonopidae). ZooKeys 1022: 1–11. https://doi.org/10.3897/zookeys.1022.62387

WSC (2024) World Spider Catalog, version 25.0. Natural History Museum Bern. World Spider Catalog. https://doi.org/10.24436/2 [accessed on 19 February 2024]

Xu Y (1987) Two new species of the genus *Orchestina* from Anhui Province, China (Araneae: Oonopidae). Acta Zootaxonomica Sinica 12: 256–259.

Zoosyst. Evol. 100 (1) 2024, 279–289 | DOI 10.3897/zse.100.115633

PENSOFT

MUSEUM FÜR NATURKUNDE BERLIN

Taxonomic study of four closely-related species of the *Pholcus yichengicus* species group (Araneae, Pholcidae) from China's Qinling Mountains: An integrated morphological and molecular approach

Lan Yang[1], Qiaoqiao He[1], Zhiyuan Yao[1]

1 *College of Life Science, Shenyang Normal University, Shenyang 110034, Liaoning, China*

https://zoobank.org/45A26952-6A37-4C42-99D6-DB5E6AD1BCC4

Corresponding author: Qiaoqiao He (heqq@synu.edu.cn); Zhiyuan Yao (yaozy@synu.edu.cn)

Academic editor: Danilo Harms ♦ **Received** 24 November 2023 ♦ **Accepted** 21 February 2024 ♦ **Published** 14 March 2024

Abstract

Four morphologically similar species of the *Pholcus yichengicus* species group, occurring in geographic proximity of China's Qinling Mountains, were recognised, based on morphology and four methods of molecular species delimitation. They comprise two new species, namely *Pholcus ankang* **sp. nov.** and *P. baoji* **sp. nov.** and two previously described species: *P. ovatus* Yao & Li, 2012 and *P. taibaiensis* Wang & Zhu, 1992. Their DNA barcodes were obtained to estimate p-distances and K2P distances. In addition, an identification key for the four closely-related species is presented.

Key Words

Biodiversity, daddy-long-legs spider, identification key, molecular species delimitation, new species

Introduction

The family Pholcidae C.L. Koch, 1850 is a highly diverse group of spiders, with 97 genera and 1,937 species (World Spider Catalog 2023), classified under five subfamilies: Arteminae Simon, 1893, Modisiminae Simon, 1893, Ninetinae Simon, 1890, Pholcinae C.L. Koch, 1850 and Smeringopinae Simon, 1893 (Huber 2011a; Dimitrov et al. 2013; Huber et al. 2018). *Pholcus* Walckenaer, 1805 is the most diverse genus within Pholcinae, with 389 described species belonging to 21 species groups distributed mainly in the Palaearctic, Oriental, Afrotropical and Australasian biogeographic realms (Huber 2011b; Huber et al. 2018; World Spider Catalog 2023).

Bestriding the Palaearctic and Oriental Regions, China harbours a high diversity of *Pholcus* spiders. Recently, a large number of new species of *Pholcus* have been reported from northern China, based on morphological and molecular data. For instance, the extensive 2020 expedition into the Changbai Mountains, at the border between north-eastern China and North Korea, brings the species count of *Pholcus* in the Changbai Mountains to 27 species, including 13 new species (Lu et al. 2021; Yao et al. 2021; Zhao et al. 2023a). The systematic investigation in the Yanshan-Taihang Mountains in northern China in 2021 recorded 36 *Pholcus* species, of which 14 species were new to science (Lu et al. 2022a, b). In 2022, *Pholcus* spiders were collected for the first time during an expedition to the Lüliang Mountains in Shanxi Province, northern China. The study identified one known species and eight new species (Zhao et al. 2023b). So far, 169 species, 43% of the genus, have been recorded in China (World Spider Catalog 2023).

China's Qinling Mountains is generally regarded as a geographical dividing line between northern China and southern China. It straddles the Provinces of Shanxi, Shaanxi and Henan. To date, 14 species of *Pholcus* have been found to be recorded in the Qinling Mountains (Zhang and Zhu 2009; Yao and Li 2012; Dong et al. 2016; World Spider Catalog 2023). This paper identifies four morphologically similar species from the Qinling Mountains (Shaanxi part, Fig. 1), based on

morphological and molecular evidence, including two new species to be described and all belong to the *Pholcus yichengicus* species group.

Materials and methods

Specimens were examined and measured with a Leica M205 C stereomicroscope. Left male pedipalps were photographed. Epigynes were photographed before dissection. Vulvae were illustrated after treating them in a 10% warm solution of potassium hydroxide (KOH) to dissolve soft tissues. Images were captured with a Canon EOS 750D wide zoom digital camera (24.2 megapixels) mounted on the stereomicroscope mentioned above and assembled using Helicon Focus v. 3.10.3 image stacking software (Khmelik et al. 2005). All measurements are given in millimetres (mm). Leg measurements are shown as: total length (femur, patella, tibia, metatarsus, tarsus). Leg segments were measured on their dorsal side. The distribution map was generated with ArcGIS v. 10.2 (ESRI Inc.). The specimens studied are preserved in 75% ethanol and deposited in the College of Life Science, Shenyang Normal University (SYNU) in Liaoning, China.

Terminology and taxonomic descriptions follow Huber (2011b) and Yao et al. (2015, 2021). The following abbreviations are used in the descriptions: **ALE** = anterior lateral eye, **AME** = anterior median eye, **PME** = posterior median eye, **L/d** = length/diameter ratio; used in the illustrations: **a** = appendix, **b** = bulb, **da** = distal apophysis, **e** = embolus, **fa** = frontal apophysis, **pa** = proximo-lateral apophysis, **pp** = pore plate, **pr** = procursus, **u** = uncus.

The mitochondrial gene fragment encoding COI and two nuclear gene fragments encoding H3 and wnt were obtained for 19 samples (Table 1). Primers are listed in Table 2. Two species *Pholcus paralinzhou* and *P. taishan* were selected as outgroups. DNA sequences were checked and edited with BioEdit 7.2.2 (Hall 1999). P-distances and K2P distances from COI were computed using MEGA 5 (Tamura et al. 2011). Phylogenetic trees were constructed using the Maximum Likelihood (ML) method for molecular species delimitation, using both COI and a combined dataset. ML analyses were conducted using RAxML 8.2.9 under a GTRCAT model for all partitions, with 500 rapid bootstrap replicates followed

Table 1. Voucher specimen information.

Species	Voucher code	GenBank accession number			Collection locality
		COI	H3	wnt	
P. ankang sp. nov.	W265	PP082941	PP349964	PP349983	China, Shaanxi, Ankang
	W266	PP082942	PP349965	PP349984	
	W267	PP082943	PP349966	PP349985	
	W268	PP082944	PP349967	PP349986	
	W269	PP082945	PP349968	PP349987	
P. baoji sp. nov.	W270	PP082946	PP349969	PP349988	China, Shaanxi, Baoji
	W271	PP082947	PP349970	PP349989	
	W272	PP082948	PP349971	PP349990	
	W273	PP082949	PP349972	PP349991	
	W274	PP082950	PP349973	PP349992	
P. ovatus	W220	PP082951	PP349955	PP349974	China, Shaanxi, Xi'an
	W221	PP082952	PP349956	PP349975	
	W222	PP082953	PP349957	PP349976	
	W223	PP082954	PP349958	PP349977	
P. taibaiensis	W224	PP082955	PP349959	PP349978	China, Shaanxi, Baoji
	W225	PP082956	PP349960	PP349979	
	W226	PP082957	PP349961	PP349980	
	W227	PP082958	PP349962	PP349981	
	W228	PP082959	PP349963	PP349982	
P. paralinzhou	y046	MW721825	ON375203	ON375294	China, Henan, Jiaozuo
P. taishan	y133	MW721826	ON375204	ON375293	China, Shandong, Taian

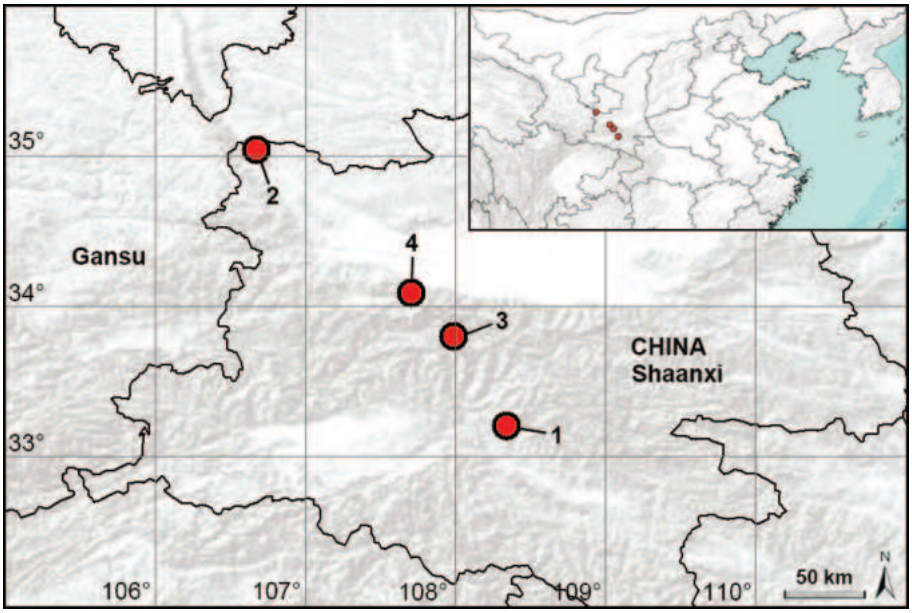

Figure 1. Distribution records of four closely-related species of *Pholcus* from the Qinling Mountains, China. **1.** *Pholcus ankang* sp. nov.; **2.** *P. baoji* sp. nov.; **3.** *P. ovatus*; **4.** *P. taibaiensis*.

Table 2. Primers used for amplification and sequencing.

Gene	Primer	F/R	Sequence 5'–3'	Reference
COI	LCO1490	F	GGTCAACAAATCATAAAGATATTGG	Folmer et al. (1994)
	C1-N-2776	R	GGATAATCAGAATANCGNCGAGG	Vink et al. (2005)
H3	H3af	F	ATGGCTCGTACCAAGCAGACVGC	Colgan et al. (1998)
	H3ar	R	ATATCCTTRGGCATRATRGTGAC	
wnt	Spwgf1	F	GYAAATGCCAYGGWATGTCMGG	Blackledge et al. (2009)
	Spwgr1	R	ACTTGRCAACACCARTGAAAWG	
	Wnt2f	F	CAGTGRAATGTRCARTTG	
	Wnt2r	R	CNGTTCAAACTTGYTGGATG	

by a thorough Maximum Likelihood tree search (Stamatakis 2014). The sequences are deposited in GenBank. For additional information on extraction, amplification and sequencing procedures, see Yao et al. (2016).

We applied four methods for molecular species delimitation. The Automatic Barcode Gap Discovery (ABGD) analyses were conducted using both Jukes–Cantor and Kimura 2-P distance matrices with options: Pmin = 0.001, Pmax = 0.1, Steps = 10, X = 1.0, Nb bins = 20 (Puillandre et al. 2012). The Bayesian implementation of the Poisson Tree Processes (bPTP) analysis was run for 100,000 generations, with a thinning of 100 and burn-in of 0.25 (Zhang et al. 2013). The Generalised Mixed Yule Coalescent (GMYC) analysis was performed under the single threshold model using the R 4.2.2 package SPLITS (R Development Core Team 2023). The phylogenetic tree was converted to an ultrametric format for GMYC analysis using BEAST 1.8.2 (Drummond et al. 2012). Bayesian Phylogenetics and Phylogeography (BPP) requires data from multiple genes and pre-defined candidate species. We used BPP to test the results between the analyses mentioned above. Like Yang (2015), we conducted four different sets of analyses with different values of α and β: $G\theta(2, 1000)$ and $G\tau(2, 2000)$, $G\theta(2, 100)$ and $G\tau(2, 200)$, $G\theta(2, 100)$ and $G\tau(2, 2000)$, $G\theta(2, 1000)$ and $G\tau(2, 200)$. The analyses were performed using the following settings: species delimitation = 1, algorithm = 0, finetune = 5. The reversible-jump MCMC analyses were run for 100,000 generations and sampled every two generations, with 25,000 samples being discarded as burn-in.

Results

We obtained a concatenated alignment of 1767 bp (COI, 1184 bp; H3, 293 bp; wnt, 290 bp). Separate phylogenetic analyses of the individual gene COI and concatenated data found compatible topologies. Fig. 2 presents the phylogenetic tree from the concatenated data. The tree clearly divided the samples into four deeply divergent clades. We defined the four major clades as four candidate species, because the ABGD, GMYC and bPTP analyses unambiguously support their status as separate species and the results were fairly consistent with morphology. We used BPP to validate the four species. The BPP analyses found speciation probabilities of one for all of the nodes tested using all four prior combinations. Furthermore, the smallest p-distance and K2P distance amongst the species is 0.068 and 0.072, respectively (between *P. ovatus* and *P. taibaiensis*) (Table 3). Of the four species, two are new and descriptions are provided below.

Table 3. The average uncorrected p-distances (below diagonal) and K2P distances (above diagonal) amongst the species and the maximum p-distances (on diagonal) within each species.

	P. ankang sp. nov.	*P. baoji* sp. nov.	*P. ovatus*	*P. taibaiensis*
***P. ankang* sp. nov.**	**0.001**	0.099	0.102	0.119
***P. baoji* sp. nov.**	0.092	**0**	0.096	0.102
P. ovatus	0.094	0.090	**0.001**	0.072
P. taibaiensis	0.109	0.095	0.068	**0.001**

Taxonomy

Family Pholcidae C.L. Koch, 1850
Subfamily Pholcinae C.L. Koch, 1850

Genus *Pholcus* Walckenaer, 1805

Type species. *Aranea phalangioides* Fuesslin, 1775

***Pholcus yichengicus* species group**

Diagnosis and description. See Huber (2011b).

Identification key

Note that males and females must be present for this key to work.

1 Sclerotised prolatero-subdistal apophysis of procursus prolatero-proximally strongly widened (figs 134C, 137A in Yao and Li (2012)); raised prolatero-subdistal membranous edge of procursus laterally strongly curved (figs 134D, 137B in Yao and Li (2012)); appendix with slender median branch (branch length/appendix length ratio: 0.5); vulval anterior arch postero-medially strongly protruding (figs 135B, 137D in Yao and Li (2012)) ..... *P. ovatus*

– Sclerotised prolatero-subdistal apophysis of procursus not widened prolatero-proximally (e.g. fig. 169C in Yao and Li (2012)); raised prolatero-subdistal membranous edge of procursus laterally angular or rectangular (e.g. fig. 169D in Yao and Li (2012) and Fig. 5D); appendix with slender median branch (branch length/appendix length ratio: 1 or 0.2) or angular branch; vulval anterior arch not protruding postero-medially (e.g. Fig. 4B) 2

2 Raised prolatero-subdistal membranous edge of procursus laterally rectangular (Fig. 5D); appendix with slender median branch (branch length/appendix length ratio: 1, arrow 2 in Fig. 6C); epigynal plate nearly triangular and posteriorly straight (Fig. 6A); vulval pore plates relatively close to each other (Fig. 6B) ..... *P. baoji* sp. nov.

– Raised prolatero-subdistal membranous edge of procursus laterally angular; epigynal plate posteriorly strongly curved (e.g. Fig. 4A); vulval pore plates widely separated (e.g. Fig. 4B) 3

3 Sclerotised prolatero-subdistal apophysis of procursus not protruding latero-distally (arrow 4 in Fig. 3D); appendix with angular median branch (arrow 2 in Fig. 4C) ..... *P. ankang* sp. nov.

– Sclerotised prolatero-subdistal apophysis of procursus latero-distally protruding (fig. 169D in Yao and Li (2012)); appendix with slender median branch (branch length/appendix length ratio: 0.2) ..... *P. taibaiensis*

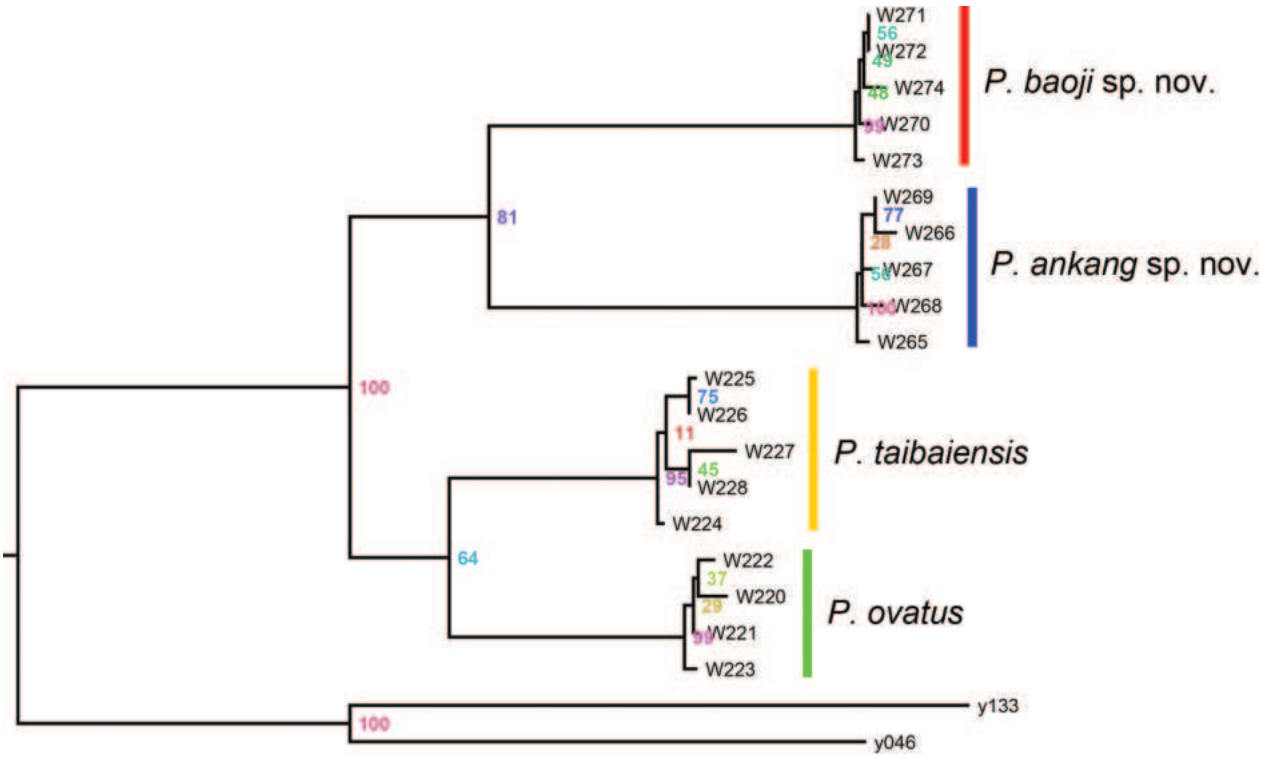

Figure 2. The results of species delimitation conducted by the ABGD, GMYC, bPTP and BPP analyses; different colours of the bars represent the different species (Phylogenetic tree was inferred from ML analysis, bootstrap values are provided at the nodes).

Pholcus ankang sp. nov.

https://zoobank.org/D586922C-E2C7-4C52-BE9F-A9AA9F38BD06

Figs 3, 4

Type material. ***Holotype*** ♂ (SYNU-Ar00398) and ***Paratypes*** 2♂ (SYNU-Ar00399–400) 2♀ (SYNU-Ar00401–02), **China**, **Shaanxi**, Ankang, Shiquan County, Chengguan Town, Guiguling Scenic Spot (33°12.32'N, 108°20.15'E, 1585 m elev.), 24 July 2022, Z. Yao, L. Yang & L. Zhang leg.

Etymology. The specific name refers to the type locality and is a noun in apposition.

Diagnosis. The species resembles *P. baoji* sp. nov. with similar male chelicerae and uncus (Fig. 4C, D), but it can be distinguished by raised prolatero-subdistal membranous edge of procursus laterally angular (arrow 3 in Fig. 3D; laterally rectangular in *P. baoji* sp. nov., arrow 3 in Fig. 5D), by appendix with angular median branch (arrow 2 in Fig. 4C; slender median branch, same length as appendix in *P. baoji* sp. nov., arrow 2 in Fig. 6C), by epigynal plate posteriorly strongly curved (Fig. 4A; posteriorly straight and epigynal plate nearly triangular in *P. baoji* sp. nov., Fig. 6A) and by vulval pore plates widely separated (Fig. 4B; relatively close to each other in *P. baoji* sp. nov., Fig. 6B).

Description. Male (holotype): Total length 5.17 (5.26 with clypeus), carapace 1.53 long, 1.62 wide, opisthosoma 3.64 long, 1.58 wide. Leg I: 39.46 (10.13, 0.66, 9.94, 16.54, 2.19), leg II: 26.96 (7.50, 0.63, 6.79, 10.57, 1.47), leg III: 18.30 (5.38, 0.60, 4.45, 6.79, 1.08), leg IV: 24.35 (7.24, 0.61, 6.03, 9.29, 1.18); tibia I L/d: 70. Eye interdistances and diameters: PME-PME 0.25, PME 0.19, PME-ALE 0.06, AME-AME 0.06, AME 0.15. Sternum width/length: 1.12/0.94. Habitus as in Fig. 4E, F. Carapace yellowish, with brown radiating marks and marginal brown bands; ocular area yellowish, with anterior brown marks; clypeus brown; sternum yellowish, with brown marks. Legs yellowish, but dark brown on patellae and whitish on distal parts of femora and tibiae, with darker rings on subdistal parts of femora and proximal and subdistal parts of tibiae. Opisthosoma yellowish, with dorsal and lateral spots. Chelicerae (Fig. 4D) with pair of

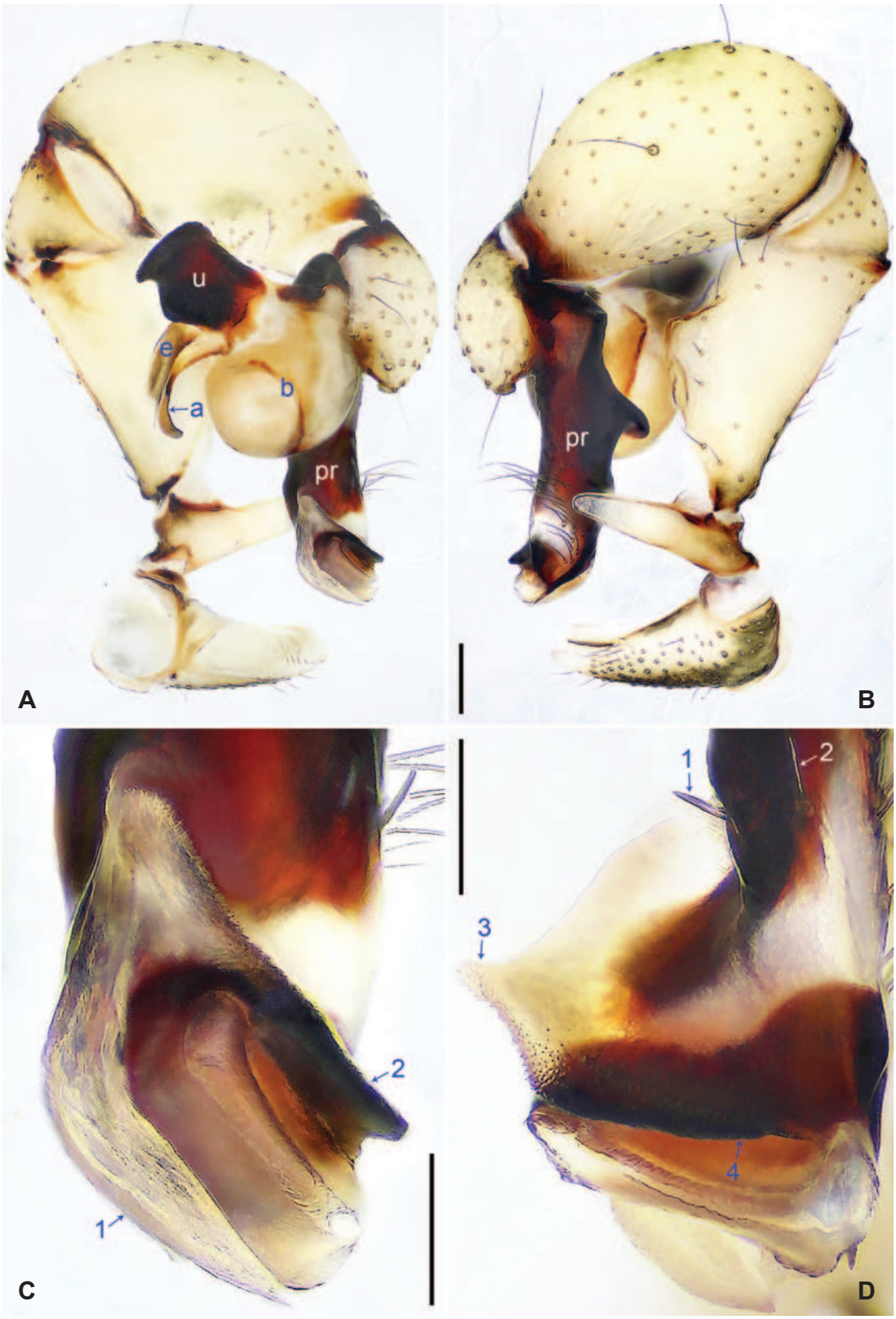

Figure 3. *Pholcus ankang* sp. nov., holotype male **A, B.** Pedipalp (**A.** Prolateral view; **B.** Retrolateral view); **C, D.** Distal part of procursus (**C.** Prolateral view, arrow 1 indicates distal membranous process, arrow 2 indicates sclerotised prolatero-subdistal apophysis; **D.** Dorsal view, arrows 1, 2 indicate dorsal spines, arrow 3 indicates angular part of raised prolatero-subdistal membranous edge, arrow 4 indicates latero-distal part of sclerotised prolatero-subdistal apophysis). Abbreviations: a = appendix, b = bulb, e = embolus, pr = procursus, u = uncus. Scale bars: 0.20 mm (**A, B**); 0.10 mm (**C, D**).

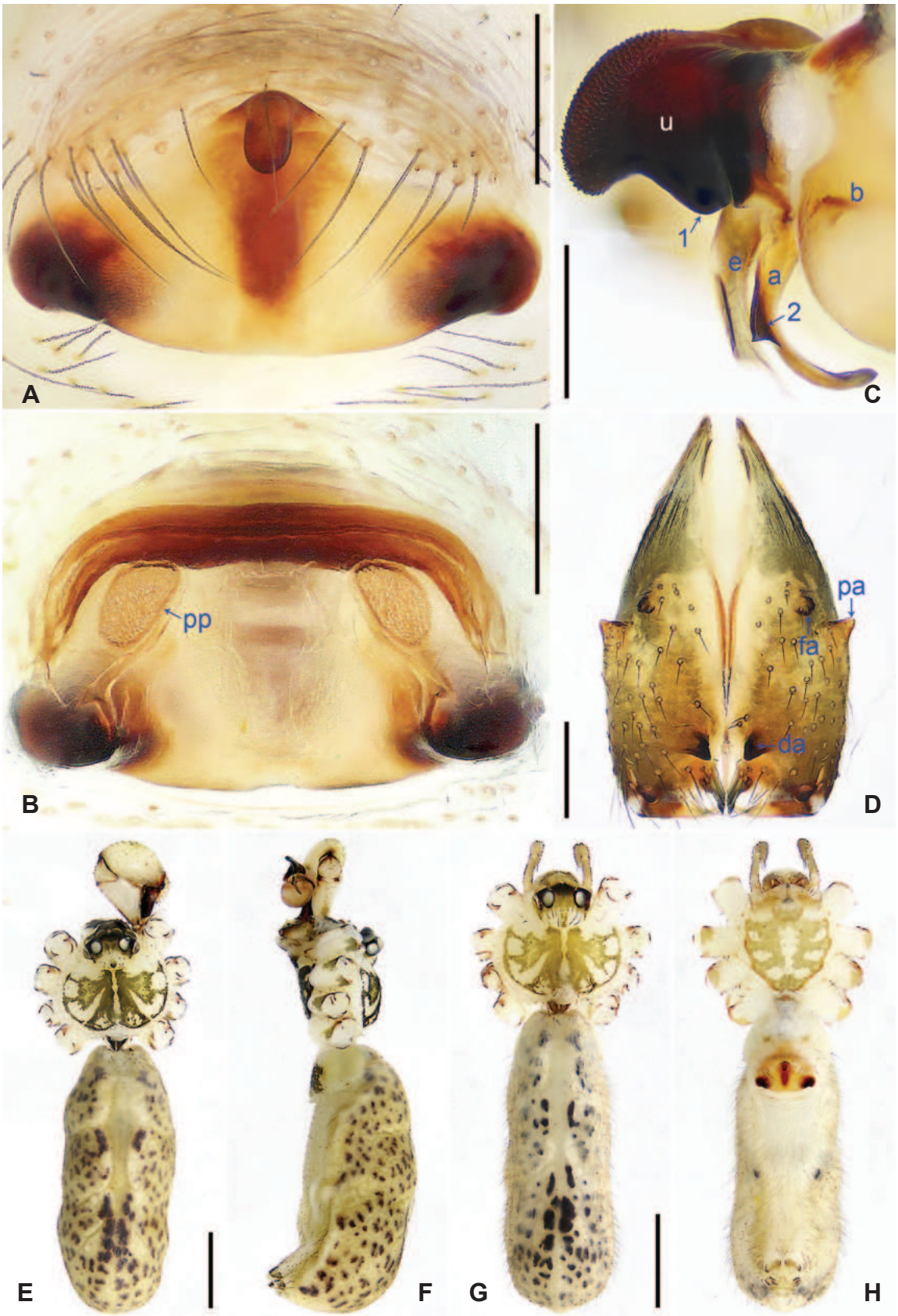

Figure 4. *Pholcus ankang* sp. nov., holotype male (**C–F**) and paratype female (**A, B, G, H**) **A.** Epigyne, ventral view; **B.** Vulva, dorsal view; **C.** Bulbal apophyses, prolateral view, arrow 1 indicates latero-median protrusion, arrow 2 indicates angular median branch; **D.** Chelicerae, frontal view; **E–H.** Habitus (**E, G.** Dorsal view; **F.** Lateral view; **H.** Ventral view). Abbreviations: a = appendix, b = bulb, da = distal apophysis, e = embolus, fa = frontal apophysis, pa = proximo-lateral apophysis, pp = pore plate, u = uncus. Scale bars: 0.20 mm (**A–D**); 1.00 mm (**E–H**).

proximo-lateral apophyses, pair of distal apophyses with two teeth each and pair of frontal apophyses. Pedipalp as in Fig. 3A, B; trochanter with long (longer than wide), retrolaterally strongly bulged ventral apophysis; femur with small retrolatero-proximal apophysis and distinct ventral protuberance; tibia with prolatero-ventral projection; procursus simple proximally, but complex distally, with raised prolatero-subdistal membranous edge bearing distal membranous process (arrow 1 in Fig. 3C), sclerotised prolatero-subdistal apophysis (arrow 2 in Fig. 3C) and two strong dorsal spines (arrows 1 and 2 in Fig. 3D); uncus latero-medially protruding (arrow 1 in Fig. 4C), with proximal apophysis and distal scaly edge; appendix curved, with angular median branch (arrow 2 in Fig. 4C); embolus weakly sclerotised, with some transparent distal projections (Fig. 4C). Retrolateral trichobothrium of tibia I at 7% proximally; legs with short vertical setae on tibiae, metatarsi and tarsi; tarsus I with 38 distinct pseudosegments.

Female (paratype, SYNU-Ar00401): Similar to male, habitus as in Fig. 4G, H. Total length 4.60 (4.75 with clypeus), carapace 1.31 long, 1.44 wide, opisthosoma 3.29 long, 1.22 wide; tibia I: 7.18; tibia I L/d: 51. Eye interdistances and diameters: PME-PME 0.23, PME 0.16, PME-ALE 0.05, AME-AME 0.05, AME 0.13. Sternum width/length: 0.90/0.76. Epigyne (Fig. 4A) posteriorly strongly curved, laterally and medially strongly sclerotised, with column-shaped knob. Vulva (Fig. 4B) with laterally strongly curved, sclerotised anterior arch and pair of nearly elliptic pore plates.

Variation. Tibia I in two paratype males (SYNU-Ar00399–400): 9.04, 9.36. Tibia I in another paratype female (SYNU-Ar00402): 7.12.

Natural history. The species was found on the underside of an overhang on rocky cliffs.

Distribution. China (Shaanxi, type locality; Fig. 1).

Pholcus baoji sp. nov.

https://zoobank.org/EE2818D8-A3D6-4E90-BE29-91278647C486

Figs 5, 6

Type material. ***Holotype*** ♂ (SYNU-Ar00403) and ***Paratypes*** 1♂ (SYNU-Ar00404) 2♀ (SYNU-Ar00405–06), **China**, **Shaanxi**, Baoji, Long County, Xinjichuan Town, Longmendong Scenic Spot (35°2.33'N, 106°40.22'E, 1489 m elev.), 29 July 2022, Z. Yao, L. Yang & L. Zhang leg.

Etymology. The specific name refers to the type locality and is a noun in apposition.

Diagnosis. The species resembles *P. ankang* sp. nov. with similar male chelicerae and uncus (Fig. 6C, D), but it can be distinguished by raised prolatero-subdistal membranous edge of procursus laterally rectangular (arrow 3 in Fig. 5D; laterally angular in *P. ankang* sp. nov., arrow 3 in Fig. 3D), by appendix with slender median branch (same length as appendix, arrow 2 in Fig. 6C; angular median branch in *P. ankang* sp. nov., arrow 2 in Fig. 4C), by epigynal plate nearly triangular and posteriorly straight (Fig. 6A; posteriorly strongly curved in *P. ankang* sp. nov., Fig. 4A) and by vulval pore plates relatively close to each other (Fig. 6B; widely separated in *P. ankang* sp. nov., Fig. 4B).

Description. Male (holotype): Total length 4.96 (5.05 with clypeus), carapace 1.48 long, 1.78 wide, opisthosoma 3.48 long, 1.52 wide. Leg I: 42.86 (10.77, 0.75, 11.15, 17.56, 2.63), leg II: 28.13 (7.82, 0.70, 6.98, 10.96, 1.67), leg III missing, leg IV: 25.71 (7.69, 0.65, 6.28, 9.62, 1.47); tibia I L/d: 70. Eye interdistances and diameters: PME-PME 0.26, PME 0.16, PME-ALE 0.06, AME-AME 0.05, AME 0.12. Sternum width/length: 1.08/0.93. Habitus as in Fig. 6E, F. Carapace yellowish, with brown radiating marks and marginal brown bands; ocular area yellowish, with anterior brown marks; clypeus brown; sternum yellowish, with brown marks. Legs yellowish, but dark brown on patellae and whitish on distal parts of femora and tibiae, with darker rings on subdistal parts of femora and proximal and subdistal parts of tibiae. Opisthosoma yellowish, with dorsal and lateral spots. Chelicerae (Fig. 6D) with pair of proximo-lateral apophyses, pair of distal apophyses with two teeth each and pair of frontal apophyses. Pedipalp as in Fig. 5A, B; trochanter with long (longer than wide), retrolaterally strongly bulged ventral apophysis; femur with small retrolatero-proximal apophysis and distinct ventral protuberance; tibia with prolatero-ventral projection; procursus simple proximally, but complex distally, with raised prolatero-subdistal membranous edge bearing distal membranous process (arrow 1 in Fig. 5C), sclerotised prolatero-subdistal apophysis (arrow 2 in Fig. 5C) and two strong dorsal spines (arrows 1 and 2 in Fig. 5D); uncus latero-medially protruding (arrow 1 in Fig. 6C), with proximal apophysis and distal scaly edge; appendix curved, with slender median branch (same length as appendix, arrow 2 in Fig. 6C); embolus weakly sclerotised, with some transparent distal projections (Fig. 6C). Retrolateral trichobothrium of tibia I at 8% proximally; legs with short vertical setae on tibiae, metatarsi and tarsi; tarsus I with 35 distinct pseudosegments.

Female (paratype, SYNU-Ar00405): Similar to male, habitus as in Fig. 6G, H. Total length 4.75 (4.80 with clypeus), carapace 1.35 long, 1.62 wide, opisthosoma 3.40 long, 1.70 wide; tibia I: 7.10; tibia I L/d: 51. Eye interdistances and diameters: PME-PME 0.22, PME 0.15, PME-ALE 0.06, AME-AME 0.05, AME 0.11. Sternum width/length: 1.01/0.79. Epigyne (Fig. 6A) nearly triangular, laterally and medially strongly sclerotised, with column-shaped knob. Vulva (Fig. 6B) with laterally strongly curved, posteriorly sclerotised anterior arch and pair of nearly elliptic pore plates.

Variation. Tibia I in paratype male (SYNU-Ar00404): 10.44. Tibia I in another paratype female (SYNU-Ar00406): 7.18.

Natural history. The species was found on the underside of an overhang on rocky cliffs.

Distribution. China (Shaanxi, type locality; Fig. 1).

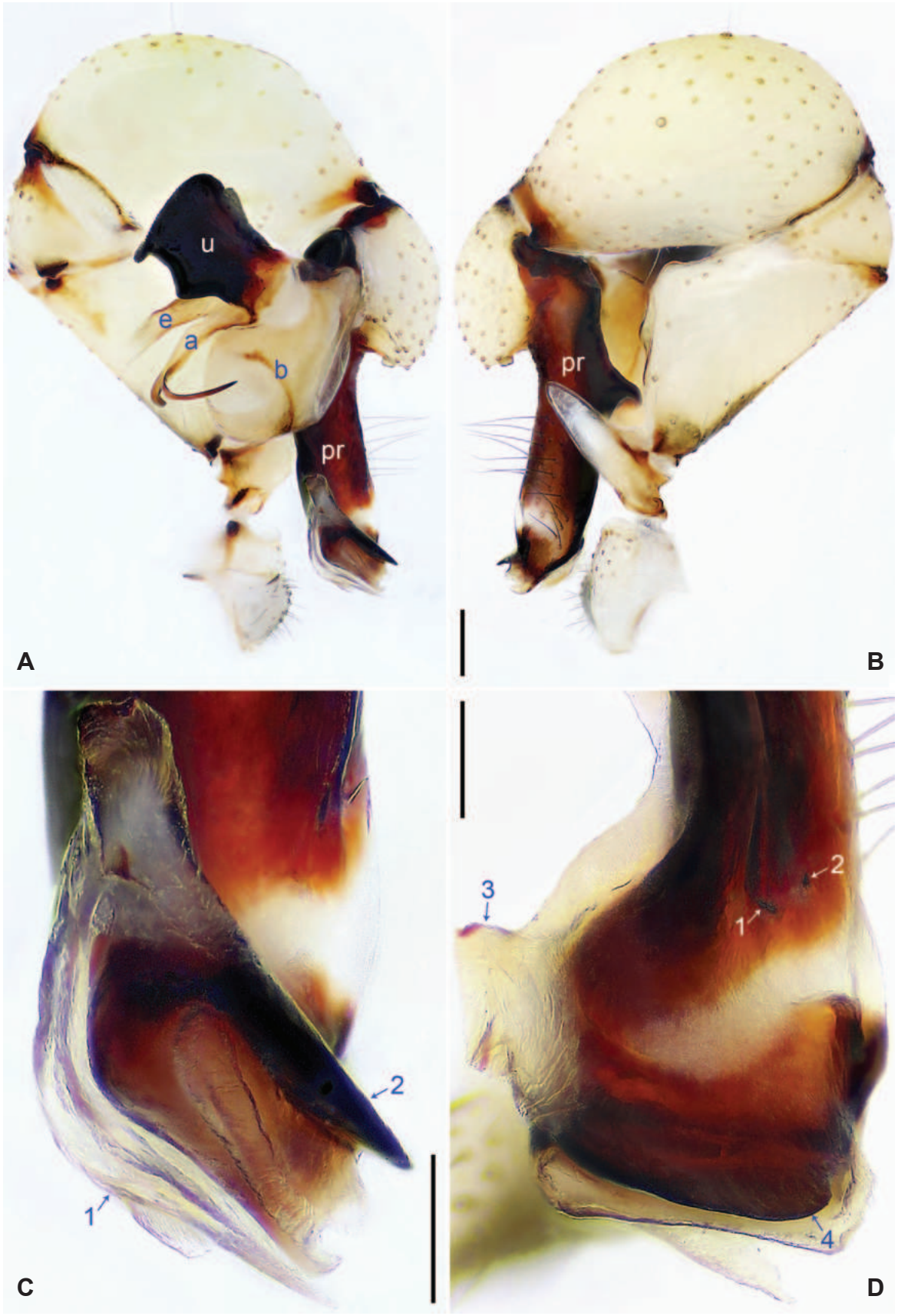

Figure 5. *Pholcus baoji* sp. nov., holotype male **A, B.** Pedipalp (**A.** Prolateral view; **B.** Retrolateral view); **C, D.** Distal part of procursus (**C.** Prolateral view, arrow 1 indicates distal membranous process, arrow 2 indicates sclerotised prolatero-subdistal apophysis; **D.** Dorsal view, arrows 1, 2 indicate dorsal spines, arrow 3 indicates rectangular part of raised prolatero-subdistal membranous edge, arrow 4 indicates latero-distal part of sclerotised prolatero-subdistal apophysis). Abbreviations: a = appendix, b = bulb, e = embolus, pr = procursus, u = uncus. Scale bars: 0.20 mm (**A, B**); 0.10 mm (**C, D**).

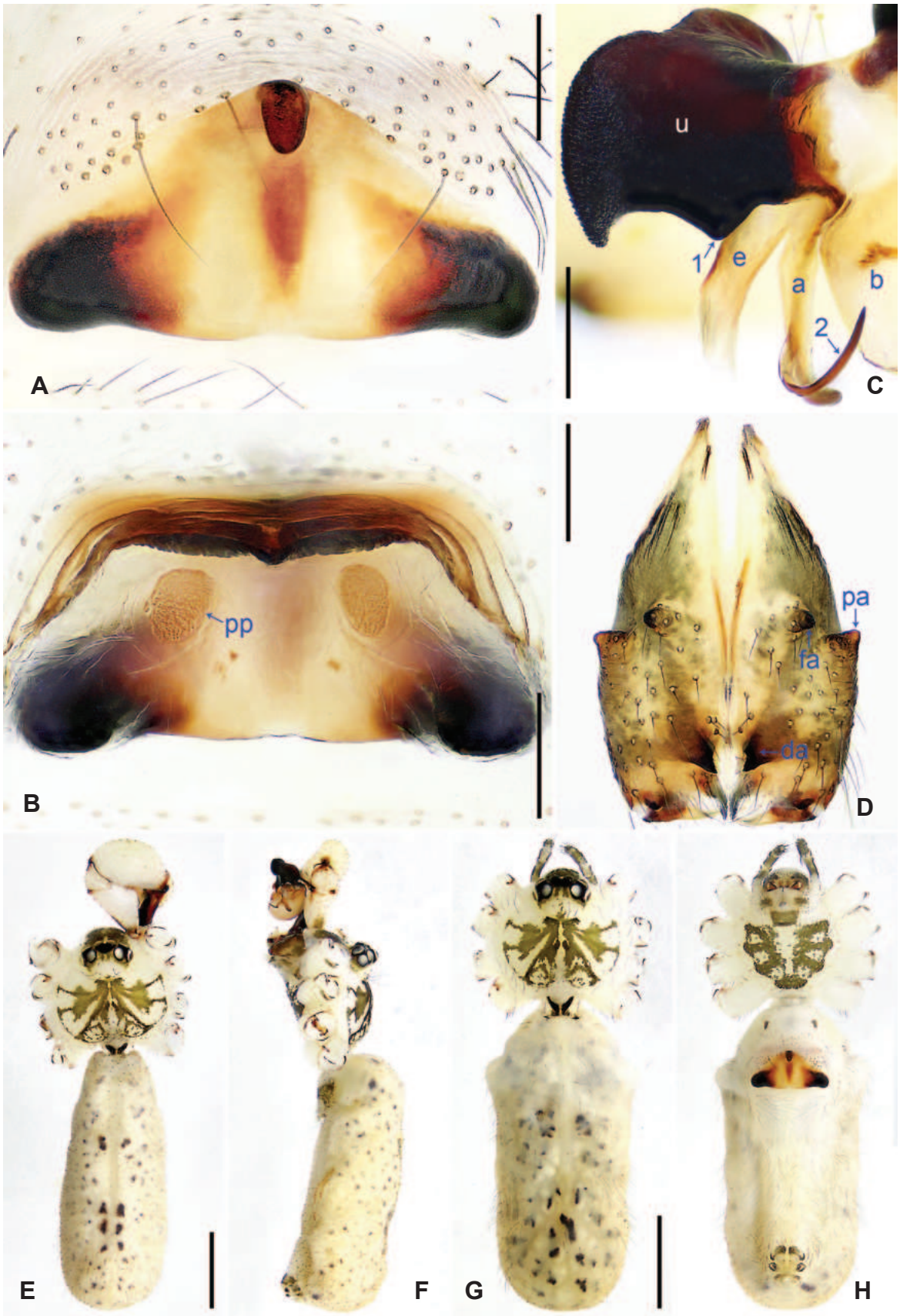

Figure 6. *Pholcus baoji* sp. nov., holotype male (**C–F**) and paratype female (**A, B, G, H**) **A.** Epigyne, ventral view; **B.** Vulva, dorsal view; **C.** Bulbal apophyses, prolateral view, arrow 1 indicates latero-median protrusion, arrow 2 indicates slender median branch; **D.** Chelicerae, frontal view; **E–H.** Habitus (**E, G.** Dorsal view; **F.** Lateral view; **H.** Ventral view). Abbreviations: a = appendix, b = bulb, da = distal apophysis, e = embolus, fa = frontal apophysis, pa = proximo-lateral apophysis, pp = pore plate, u = uncus. Scale bars: 0.20 mm (**A–D**); 1.00 mm (**E–H**).

Pholcus ovatus Yao & Li, 2012

Pholcus ovatus Yao and Li (2012: 28), figs 134A–D, 135A–E, 136A–D, 137A–D.

Material examined. 1♂ (SYNU-Ar00120F) 1♀ (SYNU-Ar00121F), **China**, **Shaanxi**, Xi'an, Zhouzhi County, Banfangzi Town (type locality), roadside of G108 (33°48.02'N, 107°59.08'E, 1165 m elev.), 31 July 2022, Z. Yao, L. Yang & L. Zhang leg.

Diagnosis. The species resembles *P. taibaiensis* Wang & Zhu, 1992 (Yao and Li 2012: 34, figs 169A–D, 170A–C) with similar male chelicerae and epigyne (figs 135A, 136B, C, 137C in Yao and Li (2012)), but it can be distinguished by sclerotised prolatero-subdistal apophysis of procursus prolatero-proximally strongly widened (figs 134C, 137A in Yao and Li (2012); not widened in *P. taibaiensis*, fig. 169C in Yao and Li (2012)), by raised prolatero-subdistal membranous edge of procursus laterally strongly curved (figs 134D, 137B in Yao and Li (2012); laterally angular in *P. taibaiensis*, fig. 169D in Yao and Li 2012), by appendix median branch length/appendix length ratio: 0.5 (figs 134A, 136A in Yao and Li (2012); 0.2 in *P. taibaiensis*, fig. 169A in Yao and Li (2012)) and by vulval anterior arch postero-medially strongly protruding (figs 135B, 137D in Yao and Li (2012); not protruding in *P. taibaiensis*, fig. 170B in Yao and Li (2012)).

Natural history. The species was found on the underside of an overhang on rock cliffs.

Distribution. China (Shaanxi, Fig. 1).

Pholcus taibaiensis Wang & Zhu, 1992

Pholcus taibaiensis Wang and Zhu (1992: 20), figs 1–6. Song, Zhu and Chen (1999: 63), fig. 25I–K. Zhang and Zhu (2009: 90), fig. 52A–I. Huber (2011b: 451), figs 2097–2099, 2124, 2125, 2178–2183, 2185 and 2199. Yao and Li (2012: 34), figs 169A–D, 170A–C.

Material examined. 3♂ (SYNU-Ar00130F–Ar00132F) 3♀ (SYNU-Ar00133F–Ar00135F), **China**, **Shaanxi**, Baoji, Mei County, Yingtou Town, near Haopingsi Temple (type locality) (34°5.32'N, 107°42.33'E, 1101 m elev.), 30 July 2022, Z. Yao, L. Yang & L. Zhang leg.

Diagnosis. The species resembles *P. ovatus* Yao & Li, 2012 (Yao and Li 2012: 28, figs 134A–D, 135A–E, 136A–D, 137A–D) with similar male chelicerae and epigyne (fig. 170A in Yao and Li (2012)), but it can be distinguished by sclerotised prolatero-subdistal apophysis of procursus not widened prolatero-proximally (fig. 169C in Yao and Li (2012); strongly widened in *P. ovatus*, figs 134C, 137A in Yao and Li (2012)), by raised prolatero-subdistal membranous edge of procursus laterally angular (fig. 169D in Yao and Li (2012); laterally strongly curved in *P. ovatus*, figs 134D, 137B in Yao and Li (2012)), by appendix median branch length/appendix length ratio: 0.2 (fig. 169A in Yao and Li (2012); 0.5 in *P. ovatus*, figs 134A, 136A in Yao and Li (2012)) and by vulval anterior arch not protruding postero-medially (fig. 170B in Yao and Li (2012); strongly protruding in *P. ovatus*, figs 135B, 137D in Yao and Li (2012)).

Natural history. The species was found on the underside of an overhang on rocky cliffs.

Distribution. China (Shaanxi, Fig. 1).

Acknowledgements

The manuscript benefits greatly from comments by Danilo Harms, Bernhard Huber, Yanfeng Tong and an anonymous reviewer. Joseph KH Koh checked the English. This study was supported by the Science & Technology Fundamental Resources Investigation Program of China (2023FY100200) and the National Natural Science Foundation of China (NSFC-32170461, 31872193).

References

Blackledge TA, Scharff N, Coddington JA, Szüts T, Wenzel JW, Hayashi CY, Agnarsson I (2009) Reconstructing web evolution and spider diversification in the molecular era. Proceedings of the National Academy of Sciences of the United States of America 106(13): 5229–5234. https://doi.org/10.1073/pnas.0901377106

Colgan DJ, McLauchlan A, Wilson GDF, Livingston SP, Edgecombe GD, Macaranas J, Cassis G, Gray MR (1998) Histone H3 and U2 snRNA DNA sequences and arthropod molecular evolution. Australian Journal of Zoology 6(5): 419–437. https://doi.org/10.1071/ZO98048

Dimitrov D, Astrin JJ, Huber BA (2013) Pholcid spider molecular systematic revisited, with new insights into the biogeography and the evolution of the group. Cladistics 29(2): 132–146. https://doi.org/10.1111/j.1096-0031.2012.00419.x

Dong T, Zheng G, Yao Z, Li S (2016) Thirteen new species of the spider genus *Pholcus* Walckenaer, 1805 (Araneae: Pholcidae) from China. Zootaxa 4170(1): 1–40. https://doi.org/10.11646/zootaxa.4170.1.1

Drummond AJ, Suchard MA, Xie D, Rambaut A (2012) Bayesian Phylogenetics with BEAUti and the BEAST 1.7. Molecular Biology and Evolution 29(8): 1969–1973. https://doi.org/10.1093/molbev/mss075

Folmer O, Black M, Hoeh W, Lutz R, Vrijenhoek R (1994) DNA primers for amplification of mitochondrial cytochrome c oxidase subunit I from diverse metazoan invertebrates. Molecular Marine Biology and Biotechnology 3(5): 294–299.

Hall TA (1999) BioEdit: A user-friendly biological sequence alignment editor and analysis program for Windows 95/98/NT. Nucleic Acids Symposium Series 41: 95–98.

Huber BA (2011a) Phylogeny and classification of Pholcidae (Araneae): An update. The Journal of Arachnology 39(2): 211–222. https://doi.org/10.1636/CA10-57.1

Huber BA (2011b) Revision and cladistic analysis of *Pholcus* and closely related taxa (Araneae, Pholcidae). Bonner Zoologische Monographien 58: 1–509.

Huber BA, Eberle J, Dimitrov D (2018) The phylogeny of pholcid spiders: A critical evaluation of relationships suggested by molecular data (Araneae, Pholcidae). ZooKeys 789: 51–101. https://doi.org/10.3897/zookeys.789.22781

Khmelik VV, Kozub D, Glazunov A (2005) Helicon Focus 3.10.3. https://www.heliconsoft.com/heliconsoft-products/helicon-focus/ [Accessed 1 November 2023]

Lu Y, Yang F, He Q (2021) *Pholcus maxian* sp. nov., the fifth endemic spider species of *Pholcus phungiformes* species-group (Araneae: Pholcidae) at the border between Jilin, China and North Korea. Biodiversity Data Journal 9: e72464 [1–7]. https://doi.org/10.3897/BDJ.9.e72464

Lu Y, Chu C, Zhang X, Li S, Yao Z (2022a) Europe vs. China: *Pholcus* (Araneae, Pholcidae) from Yanshan-Taihang Mountains confirms uneven distribution of spiders in Eurasia. Zoological Research 43(4): 532–534 [& Suppl. 1–78]. https://doi.org/10.24272/j.issn.2095-8137.2022.103

Lu Y, Yao Z, He Q (2022b) A new species of *Pholcus yichengicus* species-group (Araneae, Pholcidae) from Hebei Province, China. Biodiversity Data Journal 10: e81800 [1–7]. https://doi.org/10.3897/BDJ.10.e81800

Puillandre N, Lambert A, Brouillet S, Achaz G (2012) ABGD, Automatic barcode gap discovery for primary species delimitation. Molecular Ecology 21(8): 1864–1877. https://doi.org/10.1111/j.1365-294X.2011.05239.x

R Development Core Team (2023) R Foundation for Statistical Computing. http://www.R-project.org/ [Accessed on 1 November 2023]

Song D, Zhu M, Chen J (1999) The spiders of China. Hebei Science and Technology Publishing House Shijiazhuang, 640 pp.

Stamatakis A (2014) RAxML Version 8: A tool for phylogenetic analysis and post-analysis of large phylogenies. Bioinformatics (Oxford, England) 30(9): 1312–1313. https://doi.org/10.1093/bioinformatics/btu033

Tamura K, Peterson D, Peterson N, Stecher G, Nei M, Kumar S (2011) MEGA5: Molecular evolutionary genetics analysis using maximum likelihood, evolutionary distance, and maximum parsimony methods. Molecular Biology and Evolution 28(10): 2731–2739. https://doi.org/10.1093/molbev/msr121

Vink CJ, Thomas SM, Paquin P, Hayashi CY, Hedin M (2005) The effects of preservatives and temperatures on arachnid DNA. Invertebrate Systematics 19(2): 99–104. https://doi.org/10.1071/IS04039

Wang X, Zhu M (1992) One new species of the genus *Pholcus* from China (Araneae: Pholcidae). Acta Arachnologica Sinica 1(1): 20–22.

World Spider Catalog (2023) World Spider Catalog, Version 24.5. Natural History Museum Bern. http://wsc.nmbe.ch [Accessed 12 November 2023]

Yang Z (2015) The BPP program for species tree estimation and species delimitation. Current Zoology 61(5): 854–865. https://doi.org/10.1093/czoolo/61.5.854

Yao Z, Li S (2012) New species of the spider genus *Pholcus* (Araneae: Pholcidae) from China. Zootaxa 3289(1): 1–271. https://doi.org/10.11646/zootaxa.3289.1.1

Yao Z, Pham DS, Li S (2015) Pholcid spiders (Araneae: Pholcidae) from northern Vietnam, with descriptions of nineteen new species. Zootaxa 3909(1): 1–82. https://doi.org/10.11646/zootaxa.3909.1.1

Yao Z, Dong T, Zheng G, Fu J, Li S (2016) High endemism at cave entrances: a case study of spiders of the genus *Uthina*. Scientific Reports 6: 35757 [1–9 & Suppl. 1–52]. https://doi.org/10.1038/srep35757

Yao Z, Wang X, Li S (2021) Tip of the iceberg: species diversity of *Pholcus* spiders (Araneae, Pholcidae) in the Changbai Mountains, Northeast China. Zoological Research 42(3): 267–271 [& Suppl. 1–60]. https://doi.org/10.24272/j.issn.2095-8137.2021.037

Zhang F, Zhu M (2009) A review of the genus *Pholcus* (Araneae: Pholcidae) from China. Zootaxa 2037(1): 1–114. https://doi.org/10.11646/zootaxa.2037.1.1

Zhang J, Kapli P, Pavlidis P, Stamatakis A (2013) A general species delimitation method with applications to phylogenetic placements. Bioinformatics (Oxford, England) 29(22): 2869–2876. https://doi.org/10.1093/bioinformatics/btt499

Zhao F, Jiang T, Yang L, He Q, Zheng G, Yao Z (2023a) Pholcid spiders of the *Pholcus phungiformes* species group (Araneae, Pholcidae) from Liaoning Province, China: An overview, with description of a new species. ZooKeys 1156: 1–14. https://doi.org/10.3897/zookeys.1156.98331

Zhao F, Yang L, Zou Q, Ali A, Li S, Yao Z (2023b) Diversity of *Pholcus* spiders (Araneae: Pholcidae) in China's Lüliang Mountains: an integrated morphological and molecular approach. Insects 14(4): 364 [1–34]. https://doi.org/10.3390/insects14040364

Zoosyst. Evol. 100 (1) 2024, 291–308 | DOI 10.3897/zse.100.115696

PENSOFT

für Natur MUSEUM FÜR NATURKUNDE BERLIN

Taxonomic revision of *Phoxinus* minnows (Leuciscidae) from Caucasus, with description of a new narrow-ranged endemic species

Oleg N. Artaev[1], Ilya S. Turbanov[1,2,3], Aleksey A. Bolotovskiy[1], Aleksandr A. Gandlin[1,2], Boris A. Levin[1,2]

1 *Papanin Institute for Biology of Inland Waters, Russian Academy of Sciences, Borok, Yaroslavl Region, 152742, Russia*

2 *A.N. Severtsov Institute of Ecology and Evolution, Russian Academy of Sciences, Leninsky prosp., 33, 119071, Moscow, Russia*

3 *Cherepovets State University, Cherepovets, Vologda Region, 162600, Russia*

https://zoobank.org/6FB4D4CA-3C7D-4014-9955-63E23637794C

Corresponding authors: Oleg N. Artaev (artaev@gmail.com); Boris A. Levin (borislyovin@gmail.com)

Academic editor: Nicolas Hubert ♦ **Received** 13 November 2023 ♦ **Accepted** 27 February 2024 ♦ **Published** 20 March 2024

Abstract

Taxonomic revision of *Phoxinus* from the Caucasus revealed two distinct species. One species, *P. colchicus*, was known from eastern drainage of Black Sea, but was recorded also in the middle reach of the Kuban (Sea of Azov basin), for the first time. The Kuban population represents a genetically unique sub-lineage of *P. colchicus*. Its ancestors might have colonized the Kuban system through the event of ancient river capture. Another species inhabits only the Adagum River basin in the lower Kuban and represents a new narrow-ranged endemic species – *Phoxinus adagumicus* sp. nov. According to mtDNA phylogeny (COI and cyt*b*), *P. adagumicus* sp. nov. represents deeply divergent and one of the two early branched lineages of the genus *Phoxinus* being distant to other species (min. *p*-distance = 0.074) including geographical neighbors – *P. chrysoprasius* from Crimean Peninsula and *P. colchicus* from the Caucasus. The new species differs from most *Phoxinus* species by frequently occurring single-row pharyngeal teeth (modal formula 5–4). The narrow geographic range (ca. 55 km in length and 15–20 km in width) and high anthropogenic load on local water systems suggests the new species is under threat and needs protection.

Key Words

Caucasus, DNA barcoding, endemics, freshwater fish, taxonomy

Introduction

Minnows of the genus *Phoxinus* Rafinesque, 1820 are small freshwater fish in the family Leuciscidae Bonaparte, 1835, which prefer rheophilic environment and are widespread in Eurasia from northern Spain eastward to the Anadyr and Amur drainages in Russia and China. Before the implementation of genetic methods to the taxonomy, the genus *Phoxinus* was represented by a few species despite its wide geographic range (Kottelat 1997). Although detailed morphological studies still contribute to identification of new species in *Phoxinus* (Kottelat 2007; Bianco and De Bonis 2015), introduction of genetic methods to *Phoxinus* taxonomy has resulted in a significant increase in the numbers of newly described species, and taxonomic and geographic range revisions (Palandačić et al. 2015, 2017, 2020; Vucić et al. 2018; Denys et al. 2020; Turan et al. 2023). In particular, recent genetic studies have revealed: i) deep genetic divergences within the genus, and ii) presence of numerous yet undescribed species. On the other hand, discovered patterns of genetic diversity do not always correspond to the morphology-based classification (Palandačić et al. 2017).

The Caucasus is a mountainous transcontinental region between the Black and Caspian seas. It is considered a significant Pleistocene refugium and a hotspot (i.e., the Caucasus Biodiversity Hotspot) of endemism for both plants and animals (Gadzhiev et al. 1979; Kolakovskiy 1980;

Nakhutsrishvili et al. 2015; Mahmoudi et al. 2019; Parvizi et al. 2019; Myers et al. 2000; Gandlin et al. 2022), that remains insufficiently studied from an evolutionary standpoint. The freshwater fish fauna of the Caucasus is rich, highly endemic (up to 68%; Naseka 2010), ecologically diverse, important for fisheries, and despite permanent interest is still significantly underexplored (Kuljanishvili et al. 2020). During the last decade, 15 new species have been described from the Caucasus Biodiversity Hotspot: one species from each of the genera *Rhodeus* Agassiz, 1832 (Esmaeili et al. 2020), *Benthophilus* Eichwald, 1831 (Kovačić et al. 2021), *Cobitis* Linnaeus, 1758 (Vasil'eva et al. 2020), and *Gobio* Cuvier, 1816 (Turan et al. 2016); two species from each of the genera *Capoeta* Valenciennes, 1842 (Levin et al. 2019a; Roman et al. 2022) and *Oxynoemacheilus* Bănărescu et Nalbant, 1966 (Çiçek et al. 2018; Freyhof et al. 2021); three species in the genus *Salmo* Linnaeus, 1758 (Turan et al. 2022); and four species in the genus *Ponticola* Iljin, 1927 (Vasil'eva et al. 2015; Eagderi et al. 2020; Zarei et al. 2022a, b; Epitashvili et al. 2023). Species status of some other taxa was re-evaluated (e.g., *Barbus rionicus* Kamensky, 1899 – Levin et al. 2019b; Sevan trout complex *Salmo ischchan* Kessler, 1877 – Levin et al. 2022; *Proterorhinus nasalis* (De Filippi, 1963) – Zarei et al. 2022c), or new species for Caucasus were recorded due to increase of knowledge on the geographic distribution of some species described outside the region — e.g., *Alburnoides samiii* Mousavi-Sabet, Vatandoust & Doadrio, 2015 (Levin et al. 2018).

Minnows of the genus *Phoxinus* are distributed in the western part of the Caucasus, Black and Azov seas drainage and absent in the eastern part of the Caucasus – in the Caspian Sea basin (Berg 1949; Naseka 2010). Widely distributed *P. colchicus* Berg, 1910 is known from the Eastern drainage of Black Sea – from the Chorokh River system in south (Turkey and Georgia) to small rivers nearby Novorossiysk in north (Russia) (ca. 550 km along coastline). The Kuban River basin (Azov Sea drainage) is locally inhabited by the *Phoxinus* sp., whose taxonomy remains ambiguous for a long time. The Kuban species was referred to *P. phoxinus* (Linnaeus, 1758) (Malyatsky 1930; Berg 1949; Sukhanova and Troitskiy 1949; Reshetnikov et al. 2003), but recent molecular studies (Palandačić et al. 2017, 2020) have shown that they form independent phyletic lineages. In addition, the geographic range of the Kuban *Phoxinus* lineage appears to be discontinuous (Artaev et al. 2021). Some populations were found in the system of the Adagum River (50–130 m a.s.l.), a left tributary of Lower Kuban, while others are located in a narrow riverine segment of the Belaya River (280–580 m a.s.l.), a large left tributary of the Kuban River. Therefore, a discontinuous geographic range as well as difference in the altitude of the identified habitats question the taxonomic identity of these populations.

Using an integrative morphological and molecular framework, this study aims to assess and revise the taxonomic diversity and distribution of *Phoxinus* spp. from the Caucasus, with a special focus on the Kuban basin populations.

Materials and methods

Sampling

Fishes were collected by the authors from different localities using frame and seine nets (mesh size 6–8 mm) (Fig. 1; Suppl. material 1). Fishes were euthanized in a solution of clove oil and photographed in an aquarium with artificial lighting using a Nikon D5300 camera (Nikon Corporation, Tokyo, Japan) equipped with a Nikkor 60 mm f/2.8G lens (Nikon Corporation, Tokyo, Japan). Fin clips (pectoral or pelvic) were collected from some specimens (DNA-vouchers) and fixed in 96% ethanol for subsequent DNA extraction in the laboratory. Most of the collected specimens were preserved in 10% formalin (form.), whereas some smaller specimens were preserved in 96% ethanol for molecular analysis. Subsequently, formalin-fixed specimens were washed out in running water and transferred to 70% ethanol for long-term storage.

The types (holotype, part of paratypes), additional and comparative material are deposited in the Fish collection of the Papanin Institute for Biology of Inland Waters of Russian Academy of Sciences, Borok, Russia (**IBIW_FS**); the rest of the paratypes are kept in the Zoological Institute of the Russian Academy of Sciences, Saint Petersburg, Russia (**ZISP**) and the Zoological Museum of the Moscow University, Moscow, Russia (**ZMMU**).

Morphological studies

Morphological analyses included *Phoxinus* spp. materials from fifteen localities (No. 1–2, 4, 6–8, 10, 12, 14, 16–19 and 21–22 on Fig. 1; Suppl. material 1). Morphological methods followed Bogutskaya et al. (2019, 2023). In particular, 28 morphometric measurements (Suppl. material 2), 17 meristic and two qualitative characters (Suppl. material 3), were investigated. Morphological abbreviations of the examined characters are explained in Suppl. material 4. Morphometric measurements were taken from the left side of the body using a digital caliper to the nearest 0.1 mm by one operator for the purposes of consistency, as recommended by Mina et al. (2005). Meristics (except for axial skeleton) and type of breast scalation (Bogutskaya et al. 2019) were assessed using material stained in an ethanol solution of alizarin red S (Taylor and Van Dyke 1985 with modifications), followed by short exposure to 1–2% potassium hydroxide and preservation in 70% ethanol.

Sex was determined by the size of the pectoral fins. External meristics were counted on the left side. The total number of the pectoral and pelvic-fin rays was counted on the left fins. Scales above lateral line were counted between lateral line and base of first unbranched ray of dorsal fin; scales below lateral line were counted between lateral line and base of first unbranched ray of anal fin. In both cases, lateral line scales were not taken into account. The number of anterior gill rakers of the first gill arch

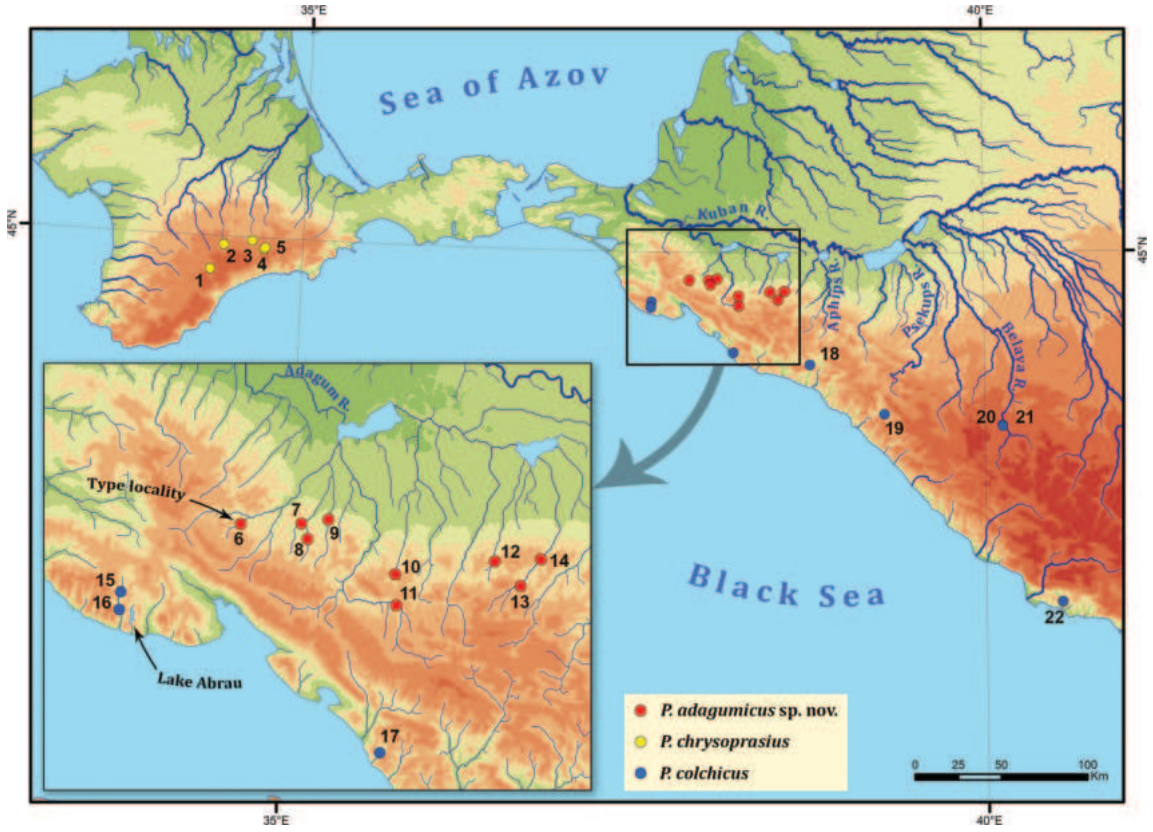

Figure 1. Map of localities of *Phoxinus* spp. sampled for this study. Localities are designated in Suppl. material 1.

was counted on the left and right sides of the specimens. The number of the scale rows was counted on the left and right breast patches and average value was taken according to Bogutskaya et al. (2019). Counts of meristic characters (except for the axial skeleton) and assessment of qualitative characters were done using a MC-2-ZOOM stereomicroscope (Micromed, Saint Petersburg, Russia). Counts of vertebrae and pterygiophores followed Naseka (1996) and Bogutskaya et al. (2019) based on radiographs made by a PRDU (v. II) X-Ray equipment (ELTECH-Med, St. Petersburg, Russia). Images of pharyngeal teeth were taken using a JEOL JSM-6510LV scanning electron microscope (Jeol, Tokyo, Japan).

Measurement indexes were statistically processed in Microsoft Excel. Comparison of multiple samples was carried out using the Kruskal–Wallis test followed by the Dunn's post hoc test with Bonferroni correction [*rstatix* (Kassambara 2020) and *tidyverse* (Wickham et al. 2019) packages in R version 4.3.1 (Ihaka and Gentleman 1996)]. Differences between sexes were tested using the Mann–Whitney U test in Past 4.12b (Hammer and Harper 2001). Principal component analysis (PCA) was performed using the *ggfortify* (Tang et al. 2016) package in R.

Molecular analyses

Molecular analyses included *Phoxinus* spp. samples from thirteen localities (No. 3–11, 15, 17, 20 and 22 on Fig. 1) (Suppl. material 5).

DNA was isolated by salt-extraction (Aljanabi and Martinez 1997) from ethanol-fixed tissues. Two mitochondrial markers were analyzed. Mitochondrial cytochrome *c* oxidase subunit I (COI) barcode region was amplified using M13-tailed primer cocktail: FishF2_t1: 5′-TGT AAA ACG ACG GCC AGT CGA CTA ATC ATA AAG ATA TCG GCA C-3′, FishR2_t1: 5′-CAG GAA ACA GCT ATG ACA CTT CAG GGT GAC CGA AGA ATC AGA A-3′, VF2_t1: 5′-TGT AAA ACG ACG GCC AGT CAA CCA ACC ACA AAG ACA TTG GCA C-3′ and FR1d_t1: 5′-CAG GAA ACA GCT ATG ACA CCT CAG GGT GTC CGA ARA AYC ARA A-3′ (Ivanova et al. 2007). PCR conditions for COI followed protocols from Ivanova et al. (2007). In addition, mitochondrial cytochrome *b* fragment was amplified by PCR using the following primers: GluF: 5′-AACCACCGTTGTATTCAACTACAA-3′ and ThrR: 5′-ACCTCCGATCTTCGGATTACAAGACCG-3′ (Machordom and Doadrio 2001). PCR amplifications were performed using Evrogen ScreenMix-HS under conditions described by Levin et al. (2017).

Sequencing of the PCR products, purified by ethanol and ammonium acetate (3 M) precipitation, was conducted using the Applied Biosystems 3500 DNA sequencer (Thermo Fisher Scientific, USA) with forward sequencing primer M13F 5′-GTA AAA CGA CGG CCA GT-3′ and reverse sequencing primer M13R-pUC 5′- CAG GAA ACA GCT ATG AC-3′ (Geiger et al. 2014).

DNA chromatograms were checked for errors in FinchTV 1.4.0 (Rothgänger et al. 2006), and the DNA

sequences were aligned using the ClustalW algorithm in MEGA7 (Kumar et al. 2016). Phylogenetic analysis was performed on COI (567 bp) and cyt*b* (1089 bp) concatenated sequences. In addition to the 29 newly determined COI and cyt*b* sequences in this study, 294 concatenated sequences of all available *Phoxinus* spp. were mined from the GenBank (derived from the studies of Imoto et al. 2013; Xu et al. 2014; Palandačić et al. 2015, 2017, 2020; Ramler et al. 2016; Schönhuth et al. 2018; and unpublished works). Three outgroups representing genera *Pseudaspius*, *Rhynchocypris*, and *Oreoleuciscus* were selected according to the previous phylogenetic studies (Palandačić et al. 2015, 2020). (Suppl. material 5). Only unique haplotypes were used in downstream phylogenetic analyses.

The Bayesian phylogenetic analysis was performed in a Bayesian statistical framework implemented in BEAST v.1.10.4. (Hill and Baele 2019) with $2^7 \times 10$ MCMC generations (10% burn-in) and parameters sampled every 2000 steps. The substitution models by codon position for Bayesian analysis were selected in PartitionFinder v.2.1.1 (Lanfear et al. 2016) with the greedy algorithm (Lanfear et al. 2012) (Suppl. material 6).

Maximum likelihood phylogenies were inferred using IQ-TREE v.2.2.0 (Nguyen et al. 2015) in PhyloSuite v1.2.3 (Zhang et al. 2020; Xiang et al. 2023) under Edge-linked partition model for 1000 ultrafast (Minh et al. 2013) bootstraps. ModelFinder v.2.2.0 (Kalyaanamoorthy et al. 2017) in PhyloSuite v.1.2.3 was used to select the best-fit partition model (Edge-linked) using AICc criterion (Suppl. material 6).

The average intra-group as well as the average pairwise intergroup *p*-distances using concatenated COI+cyt*b* sequences data set were calculated using the MEGA7 program (Kumar et al. 2016) with 1000 bootstrap replicas.

Results

Phylogenetic placement and genetic distance

Phylogenetic Bayesian tree of the genus *Phoxinus* shows that *Phoxinus adagumicus* sp. nov. has its own cluster representing one of the earliest branches with a position between the earliest branch of *Phoxinus* (*P. tumensis* and *Phoxinus* sp. from Far East) and large clade represented the other species from Europe (Fig. 2). Although ML-tree shows some differences in topology, the early branching of *Phoxinus adagumicus* sp. nov. compared to the most of European species is retained (Suppl. material 7). *Phoxinus adagumicus* sp. nov. shows the lowest genetic distance to *P.* cf. *morella* (Leske, 1774) from basins of the North and Baltic seas and adjacent upper reaches of the Danube (*p*-distance = 0.074±0.006) (Table 1), although it is almost equally close to *P. marsilii* Heckel,

Table 1. Genetic *p*-distances between species or groups of *Phoxinus* spp. for concatenated COI and cyt*b* mtDNA sequences. The averages of interspecies distances are given below diagonal, the standard errors are given above diagonal; the intraspecies divergence is given in a diagonal in bold.

	***P. adagumicus* sp. nov.**	***P. chrysoprasius***	***P. colchicus* (Black Sea)**	***P. colchicus* (Kuban basin)**	***P. csikii* (Clade 5a)**	***P. csikii* (Clade 5b)**	***P. karsticus***	***P. krkae***	***P. lumaireul* (Clade 1a)**	***P. lumaireul* (Clade 1b)**	***P. lumaireul* (Clade 1c)**	***P. lumaireul* (Clade 1d)**	***P. lumaireul* (Clade 1e)**
P. adagumicus sp. nov.	**0.007**	0.007	0.007	0.007	0.006	0.006	0.006	0.007	0.006	0.006	0.006	0.006	0.006
P. chrysoprasius	0.084	**0.001**	0.006	0.006	0.006	0.006	0.006	0.006	0.006	0.006	0.006	0.005	0.006
P. colchicus (Black Sea)	0.089	0.073	**0.005**	0.002	0.007	0.007	0.007	0.006	0.006	0.006	0.006	0.006	0.006
P. colchicus (Kuban basin)	0.091	0.074	0.012	**0.001**	0.007	0.006	0.007	0.006	0.006	0.006	0.006	0.006	0.006
P. csikii (Clade 5a)	0.086	0.072	0.085	0.086	**0.006**	0.003	0.006	0.005	0.005	0.005	0.005	0.005	0.005
P. csikii (Clade 5b)	0.085	0.071	0.084	0.084	0.019	**0.008**	0.006	0.005	0.005	0.005	0.005	0.005	0.005
P. karsticus	0.090	0.073	0.091	0.092	0.074	0.076	**0.003**	0.006	0.005	0.005	0.005	0.005	0.006
P. krkae	0.089	0.071	0.082	0.085	0.063	0.062	0.070	**0.001**	0.005	0.005	0.005	0.005	0.005
P. lumaireul (Clade 1a)	0.081	0.068	0.078	0.078	0.047	0.048	0.073	0.060	**0.007**	0.002	0.002	0.004	0.003
P. lumaireul (Clade 1b)	0.082	0.068	0.079	0.080	0.046	0.047	0.073	0.059	0.021	**0.013**	0.002	0.003	0.003
P. lumaireul (Clade 1c)	0.078	0.068	0.079	0.078	0.047	0.046	0.070	0.058	0.019	0.017	**0.004**	0.003	0.003
P. lumaireul (Clade 1d)	0.083	0.066	0.081	0.081	0.046	0.045	0.070	0.064	0.028	0.028	0.026	**0.004**	0.003
P. lumaireul (Clade 1e)	0.079	0.067	0.079	0.079	0.047	0.046	0.067	0.057	0.026	0.025	0.023	0.022	**0.002**
P. lumaireul (Clade 1f)	0.082	0.064	0.077	0.077	0.043	0.046	0.069	0.059	0.026	0.026	0.025	0.022	0.019
P. marsilii	0.075	0.066	0.074	0.076	0.071	0.071	0.076	0.070	0.071	0.067	0.066	0.071	0.066
P. cf. *morella*	0.074	0.066	0.072	0.070	0.074	0.074	0.071	0.068	0.066	0.068	0.067	0.069	0.062
P. phoxinus	0.086	0.077	0.082	0.084	0.078	0.079	0.080	0.078	0.077	0.075	0.074	0.081	0.074
P. septimaniae	0.086	0.071	0.078	0.078	0.067	0.066	0.073	0.081	0.067	0.066	0.066	0.069	0.064
P. sp. (Amur basin)	0.090	0.079	0.090	0.086	0.090	0.087	0.086	0.082	0.086	0.085	0.084	0.089	0.081
P. sp. (Clade 2)	0.078	0.062	0.077	0.078	0.044	0.045	0.065	0.052	0.041	0.039	0.038	0.041	0.041
P. sp. (Clade 3)	0.081	0.069	0.083	0.083	0.045	0.042	0.069	0.061	0.046	0.046	0.043	0.043	0.043
P. sp. (Clade 4)	0.080	0.067	0.078	0.080	0.043	0.044	0.070	0.056	0.043	0.043	0.041	0.044	0.045
P. sp. (Clade 8)	0.089	0.070	0.079	0.079	0.077	0.075	0.066	0.072	0.070	0.072	0.073	0.075	0.068
P. strandjae	0.077	0.066	0.081	0.081	0.043	0.044	0.069	0.062	0.039	0.036	0.035	0.042	0.040
P. strymonicus	0.081	0.065	0.078	0.078	0.047	0.046	0.072	0.062	0.035	0.038	0.036	0.038	0.040
P. tumensis	0.092	0.076	0.089	0.090	0.075	0.077	0.085	0.082	0.083	0.081	0.084	0.083	0.082

Table 1. Continued.

	P. lumaireul (Clade 1f)	*P. marsilii*	*P.* cf. *morella*	*P. phoxinus*	*P. septimaniae*	*P.* sp. (Amur basin)	*P.* sp. (Clade 2)	*P.* sp. (Clade 3)	*P.* sp. (Clade 4)	*P.* sp. (Clade 8)	*P. strandjae*	*P. strymonicus*	*P. tumensis*
P. adagumicus sp. nov.	0.006	0.005	0.006	0.006	0.006	0.006	0.006	0.006	0.006	0.006	0.006	0.006	0.006
P. chrysoprasius	0.006	0.006	0.006	0.006	0.006	0.006	0.005	0.006	0.006	0.005	0.006	0.006	0.006
P. colchicus (Black Sea)	0.006	0.006	0.006	0.006	0.006	0.006	0.006	0.007	0.006	0.006	0.006	0.006	0.007
P. colchicus (Kuban basin)	0.006	0.006	0.006	0.006	0.006	0.006	0.006	0.006	0.006	0.006	0.006	0.006	0.007
P. csikii (Clade 5a)	0.005	0.006	0.006	0.006	0.006	0.006	0.005	0.005	0.005	0.006	0.005	0.005	0.006
P. csikii (Clade 5b)	0.005	0.006	0.006	0.006	0.005	0.006	0.005	0.005	0.005	0.005	0.005	0.005	0.006
P. karsticus	0.005	0.006	0.006	0.006	0.006	0.006	0.006	0.006	0.006	0.005	0.005	0.006	0.007
P. krkae	0.005	0.006	0.005	0.006	0.006	0.006	0.005	0.006	0.006	0.006	0.005	0.006	0.006
P. lumaireul (Clade 1a)	0.003	0.005	0.006	0.006	0.006	0.006	0.004	0.005	0.005	0.005	0.004	0.004	0.006
P. lumaireul (Clade 1b)	0.003	0.005	0.005	0.006	0.005	0.006	0.004	0.005	0.005	0.005	0.004	0.004	0.006
P. lumaireul (Clade 1c)	0.003	0.005	0.006	0.006	0.006	0.006	0.004	0.005	0.005	0.006	0.004	0.004	0.006
P. lumaireul (Clade 1d)	0.003	0.006	0.006	0.006	0.006	0.006	0.004	0.005	0.005	0.006	0.004	0.005	0.007
P. lumaireul (Clade 1e)	0.003	0.006	0.006	0.006	0.006	0.006	0.005	0.005	0.005	0.005	0.004	0.005	0.006
P. lumaireul (Clade 1f)	**0.000**	0.005	0.006	0.006	0.006	0.006	0.004	0.005	0.005	0.005	0.004	0.004	0.006
P. marsilii	0.067	**0.004**	0.006	0.006	0.006	0.006	0.006	0.006	0.006	0.006	0.006	0.005	0.006
P. cf. *morella*	0.065	0.065	—	0.006	0.006	0.006	0.005	0.006	0.006	0.006	0.006	0.005	0.006
P. phoxinus	0.076	0.072	0.069	**0.001**	0.005	0.006	0.006	0.006	0.006	0.006	0.006	0.006	0.006
P. septimaniae	0.064	0.066	0.064	0.059	**0.003**	0.006	0.006	0.006	0.006	0.005	0.005	0.006	0.007
P. sp. (Amur basin)	0.085	0.078	0.085	0.088	0.085	—	0.006	0.006	0.006	0.006	0.006	0.006	0.006
P. sp. (Clade 2)	0.039	0.066	0.065	0.070	0.068	0.083	**0.004**	0.004	0.004	0.005	0.004	0.004	0.006
P. sp. (Clade 3)	0.044	0.068	0.065	0.075	0.070	0.087	0.036	**0.002**	0.004	0.005	0.004	0.005	0.006
P. sp. (Clade 4)	0.041	0.068	0.066	0.076	0.069	0.086	0.033	0.035	**0.001**	0.006	0.005	0.005	0.006
P. sp. (Clade 8)	0.073	0.073	0.069	0.073	0.069	0.081	0.065	0.067	0.072	**0.001**	0.005	0.006	0.006
P. strandjae	0.037	0.064	0.068	0.072	0.067	0.085	0.035	0.039	0.042	0.067	—	0.004	0.006
P. strymonicus	0.037	0.065	0.063	0.073	0.069	0.086	0.038	0.044	0.041	0.069	0.038	—	0.007
P. tumensis	0.077	0.081	0.079	0.088	0.080	0.073	0.074	0.077	0.075	0.084	0.078	0.079	—

1836 (0.075±0.005) from the Danube basin (Black Sea drainage) and rivers of Baltic Sea basin. The new species is not close in genetics to geographically neighbor species – *P. colchicus* and *P. chrysoprasius* (Pallas, 1814) (Table 1). At the same time, another population of *Phoxinus* sp. from the Kuban basin, inhabiting the middle reach of Belaya basin, is characterized by unique haplotypes and has a minimum distance (0.012±0.002) to *P. colchicus* from the Black Sea basin (Fig. 2) and currently is considered a divergent population of *P. colchicus* (Fig. 2). Intraspecies divergence of *Phoxinus adagumicus* sp. nov. (0.007) is comparable to such in other species (Table 1).

Systematics

Class Actinopterygii Klein, 1885
Order Cypriniformes Bleeker, 1859
Family Leuciscidae Bonaparte, 1835
Genus *Phoxinus* Rafinesque, 1820

Phoxinus adagumicus sp. nov.

https://zoobank.org/67F76C90-DC80-48CE-974B-B4A3DEB39263
Figs 3, 4

Phoxinus phoxinus – Berg 1949: 590 (Khabl, Abin, Shibik, Psebeps rivers and Abrau Lake); Sukhanova and Troitskiy 1949: 154, 164–165 (Khabl, Adagum, Shibik, Abin and Ayuk rivers); Emtyl et al. 1994: 137–141, figs 1–2 (Ayuk and Dyurso rivers); Reshetnikov et al. 2003: 301–302 (Kuban River); Otrishko and Emtyl 2013a: 20 (Kuban River).

Phoxinus phoxinus kubanicum Emtyl et Ivanenko, 2002 *unavailable name*: 90–92, fig. 69 ex Berg 1949 not *P. adagumicus* sp. nov. (Psekups River basin; Aphips, Il, Ubin, Abin, Adagum rivers and Abrau Lake); Otrishko and Emtyl 2013a: 20 (Kuban River).

Phoxinus phoxinus kubanicus [sic] – Karnaukhov 2020: 76–77 (Adagum and Psebeps rivers).

Phoxinus kubanicus [sic] – Otrishko and Emtyl 2013b: 22 (Adagum River); Otrishko and Emtyl 2013c: 69–70 (Adagum, Ubin, Aphips and Ayuk rivers).

Phoxinus colchicus – Kottelat and Freyhof 2007: 226 (southern tributaries of lower Kuban).

Phoxinus sp. – Artaev et al. 2021 (Zybza, Il, Psyzh, Shibik and Neberdjai rivers).

Phoxinus sp. Kuban Clade 19 – Palandačić et al. 2020: figs 1–2 (Kuban River); Bogutskaya et al. 2023: 6, Fig. 2 (Adagum River).

Type material. ***Holotype***, IBIW_FS_385, female, (57.5 SL mm, Genbank Accession numbers OR713923 - COI, PP351730 - cyt*b*), Russia, Krasnodar Krai, Kuban River drainage, Pryamaya Shchel River (Adagum River drainage) upstream Nizhnebakanskaya, 44.8538°N, 37.8417°E, 22 May 2023, I.S. Turbanov leg. ***Paratypes*:** 3 females, 2 males (IBIW_FS_386), SL 45.7–51.1 mm, 3 females, 2 males (ZISP 57031), SL 42.2–51.1 mm, 3 females, 2 males (ZMMU P-24612), SL 45.3–51.7 mm, all from the same locality and date as holotype.

Additional material. Suppl. material 1.

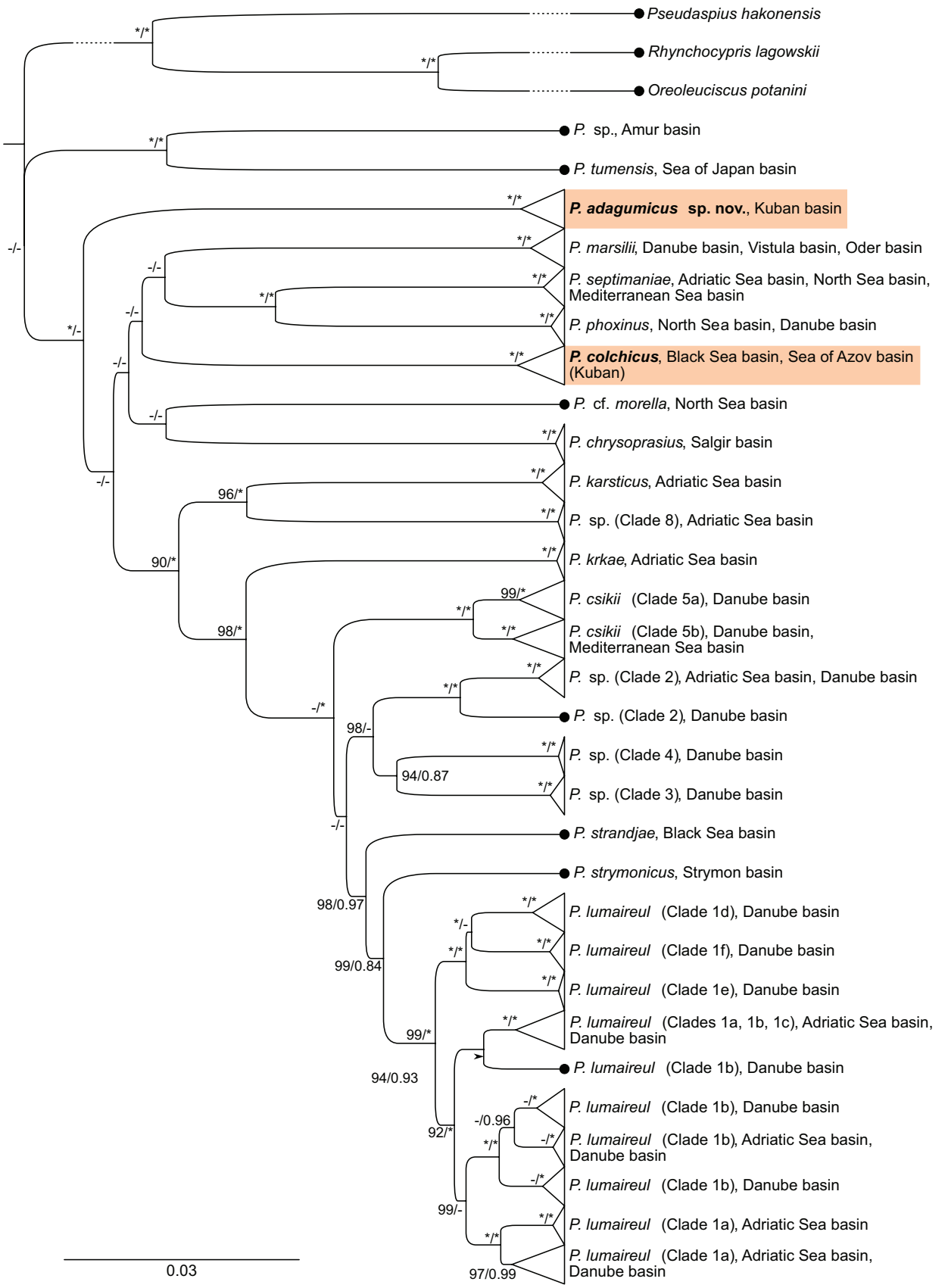

Figure 2. BI consensus tree of concatenated COI and cyt*b* mtDNA sequences representing all available *Phoxinus* species in Genbank combined with our data set. Number of some clades is given according to the study of Palandačić et al. (2020). Species from the Kuban basin are highlighted with color. Bootstrap values/posterior probabilities above 80/0.8 are shown; asterisks represent of 100/1 bootstrap/posterior probabilities values. Scale bar is in expected substitutions per site. The nodes with multiple specimens were collapsed to a triangle, with the horizontal depth indicating the level of divergence within the node.

Figure 3. Holotype of *Phoxinus adagumicus* sp. nov. (IBIW_FS_385): **A.** General appearance of preserved specimen; **B.** Radiograph.

Comparative material. Suppl. material 1.

Material used in the genetic analysis. Suppl. material 5.

Etymology. The new species is named after the Adagum River, left tributary of the lower reach of the Kuban River, where the species occurs; *adagumicus* – an adjective.

Diagnosis. *Phoxinus adagumicus* sp. nov. is distinguished from geographically close species (*P. chrysoprasius* and *P. colchicus*) by the presence and predominance of specimens with single-row pharyngeal teeth on one or both sides and a combination of characters, none of which is unique, as follows: head depth at nape 54.1–64.8% HL (mean 60.5), and head depth through eye 45.3–51.6% HL (mean 48.0); head length 2.7–3.7 (mean 3.1) times caudal peduncle depth in females and 2.7–3.2 (mean 2.9) times in males; body width at dorsal-fin origin 1.4–2 (mean 1.6) times caudal peduncle depth in females and 1.3–1.6 (mean 1.4) times in males; mean number of scale rows on left and right breast patches 3–9 (mean 6.1); scales below lateral line 8–14 (mean 11.8); number of circumpeduncular scales 37–50 (mean 41.5); 3rd–6th type of breast scalation (mode 4th type).

Description. The general appearance of *P. adagumicus* sp. nov. is shown in Figs 3–4. Morphometric measurements for the holotype and type series with level of significance of sex-related differences are given in Table 2; meristic and qualitative characters for specimens from the type locality are given in Table 3. Primary morphological data for specimens from the type locality (holotype, paratypes and additional material) are given in Suppl. material 2; meristic and qualitative characters of *P. adagumicus* sp. nov. and other *Phoxinus* spp. are given in Suppl. material 3; morphometric measurements of *P. adagumicus* sp. nov., *P. chrysoprasius* and *P. colchicus* and their comparison are given in Suppl. material 4.

Morphometrics (Table 2, Suppl. materials 2, 4). The new species has a medium size – the maximum SL is 59.4 mm (male from the Il River). The new species has elongated head – head depth at nape (% HL) (holotype: 62.2, paratypes: 58.5–63.9, add. material 54.1–64.8); and head depth through eye (% HL) (holotype: 49.8, paratypes: 46.4–50.0, add. material 45.3–51.6). Head length 3.0 times caudal peduncle depth in the holotype, 2.8–3.2 in the paratypes, and 2.7–3.7 in the add. material.

Meristics (Table 3, Suppl. material 3). Dorsal fin with 3 (sometimes 2, rarely 4) unbranched and 7½ branched rays. Anal fin with 3 unbranched and 7½ (rarely 6½) branched rays. Pectoral fin with 14–18 rays, often 16–17. Pelvic fin with 8 rays (rarely 7 or 9). Caudal fin with 19 rays (sometimes 18, rarely 20). Number of dorsal procurrent caudal-fin rays 9–13, often 10–12. Number of ventral procurrent caudal-fin rays 7–12, often 9–10.

The most common pharyngeal teeth formulae are 5–4 (n = 11), 5–4.1 (n = 6), 1.5–4 (n = 5) and 1.5–4.1 (n = 7) (Fig. 5, Table 4). Total number of vertebrae in the holotype 41, 39–41 in the paratypes, and 39–42 in the add. material, commonly 40 or 41. Number of abdominal vertebrae in the holotype 22, 22–23 in the paratypes, and 21–24 in the add. material, commonly 22 or 23. Number of caudal vertebrae in the holotype 19, 17–19 in the paratypes, and 16–19 in add. material, commonly 18. Number of predorsal abdominal vertebrae in the holotype 15, 14–15 in the paratypes, and 14–16 in the add. material, commonly 15. Number of anal-fin pterygiophores in front of the first caudal vertebrae in the holotype 3, 3–6 in the paratypes,

Figure 4. Live coloration of *Phoxinus adagumicus* sp. nov. from the Zybza River. Side and ventral views are of the same specimens (IBIW_FS_339). Fish of spawning or post-spawning coloration were caught on 8th May 2022.

and 3–7 in the add. material, commonly 4 or 5. Difference in the number of abdominal and caudal vertebrae in the holotype 3, 3–6 in the paratypes, and 2–7 in the add. material, commonly 4 or 5.

Total number of scales in the lateral series 74–94, mean 84.5. Lateral line incomplete and discontinuous. Relative number of total lateral-line (pored) scales in specimens of 41–57 mm SL varies greatly from 26 to 92%, mean 58.5%. Number of scale rows on breast patches 3–6, commonly 4. Number of circumpeduncular scales 37–44, mean 41.3. Number of scales above lateral line 16–22, mean 18.4. Number of scales below lateral line 9–14, mean 11.8.

Gill rakers (in series from the type locality) on the first left arch 7–8 (mode 8), on the first right arch 7–9 (modes 7, 8, and 9) (Suppl. material 2).

Table 2. Morphometric measurements of *Phoxinus adagumicus* sp. nov. (type series) (primary data see in Suppl. material 2); *p** - difference between females (including the holotype) and males, Mann–Whitney U test: ns ($p > 0.05$), + ($p < 0.05$), ++ ($p < 0.01$).

Characters	Holotype (female)	Females, n=10			Males, n=6			p*
		mean	range	SD	mean	range	SD	
Standard length (SL, in mm)	57.5	48.9	42.2–57.5	3.2	47.1	45.3–51.1	2.5	
In percentage of standard length (% SL)								
Body depth at dorsal-fin origin	20.0	21.1	19.4–23.4	1.3	20.5	19.1–22.2	1.2	ns
Body width at dorsal-fin origin	12.7	13.4	12.6–14.9	0.8	13.5	12.9–14.2	0.5	ns
Minimum depth of caudal peduncle	8.1	8.7	8.0–9.2	0.4	9.5	8.7–10.0	0.6	ns
Caudal peduncle width	8.3	8.6	7.6–10.1	0.7	9.2	8.7–9.7	0.4	ns
Predorsal length	55.2	57.2	55.2–60.5	1.6	55.4	53.9–57.0	1.1	+
Postdorsal length	34.1	33.9	32.9–35.6	0.9	33.0	31.9–34.3	1.0	ns
Prepelvic length	47.3	50.9	47.3–54.8	1.6	49.1	46.6–51.1	1.5	+
Preanal length	65.1	67.9	65.1–70.8	1.3	65.7	63.2–69.1	2.4	ns
Pectoral – pelvic-fin origin length	23.8	25.8	23.8–27.2	1.2	23.7	22.4–24.3	0.7	++
Pelvic – anal-fin origin length	19.0	19.0	17.8–20.7	0.9	18.0	16.5–19.3	1.2	ns
Caudal peduncle length	23.5	21.7	20.1–23.5	1.0	23.1	22.3–24.7	0.8	+
Dorsal-fin base length	11.8	11.8	11.1–12.4	0.5	12.2	11.1–13.1	0.8	ns
Dorsal-fin depth	20.6	20.8	18.8–22.4	1.2	22.2	21.5–23.8	0.9	+
Anal-fin base length	9.2	10.5	9.2–11.5	0.5	10.8	9.6–11.3	0.6	ns
Anal-fin depth	18.6	19.6	17.7–21.3	1.1	21.0	20.5–21.6	0.4	++
Pectoral-fin length	18.3	19.0	17.2–21.9	1.5	21.1	20.1–21.6	0.6	+
Pelvic-fin length	14.1	14.4	12.5–15.9	1.1	16.2	15.1–17.2	0.7	++
Head length (HL)	24.0	26.5	24.0–27.9	0.9	27.4	25.4–28.7	1.3	ns
Head depth at nape	14.9	16.1	14.9–17.1	0.6	16.7	16.2–17.3	0.4	ns
Maximum head width	12.6	13.8	12.6–14.8	0.7	13.9	13.0–14.8	0.7	ns
Snout length	7.7	8.3	7.3–9.4	0.7	8.2	7.4–9.3	0.7	ns
Eye horizontal diameter	6.3	7.2	6.3–7.7	0.3	6.8	6.4–7.1	0.3	+
Interorbital width	8.6	9.1	8.3–10.0	0.5	9.3	8.6–9.9	0.5	ns
In percentage of head length (% HL)								
Maximum head width	52.5	52.0	46.6–54.4	2.8	50.7	45.4–54.9	3.1	ns
Snout length	31.9	31.2	28.9–33.6	1.8	30.0	27.6–32.5	1.8	ns
Head depth at nape	62.2	60.8	58.5–63.0	1.7	61.0	58.5–63.9	2.0	ns
Head depth through eye	49.8	48.2	46.4–50.0	1.5	48.4	47.4–49.2	0.7	ns
Eye horizontal diameter	26.3	27.2	26.3–28.5	0.7	24.9	23.8–25.7	0.7	++
Postorbital distance	51.8	45.6	41.9–51.8	1.8	48.0	46.6–49.2	1.3	ns
Interorbital width	35.8	34.4	31.0–36.7	1.6	34.1	32.1–35.4	1.3	ns
In percentage of caudal peduncle length								
Minimum depth of caudal peduncle	34.3	40.1	34.3–43.8	2.9	41.3	38.1–44.9	3.0	ns
In percentage of body depth								
Head length	120.0	126.0	116.7–139.9	7.9	133.9	128.2–143.4	5.6	+
In percentage of interorbital width								
Eye horizontal diameter	73.4	79.3	71.8–90.1	5.0	73.3	71.0–75.6	1.6	+
Ratios								
Interorbital width/eye horizontal diameter	1.4	1.3	1.1–1.4	0.1	1.4	1.3–1.4	0.0	+
Snout length/eye horizontal diameter	1.2	1.1	1.0–1.2	0.1	1.2	1.1–1.3	0.1	ns
Head depth at nape/eye horizontal diameter	2.4	2.2	2.1–2.4	0.1	2.4	2.3–2.6	0.1	++
Head length/caudal peduncle depth	3.0	3.1	2.8–3.2	0.1	2.9	2.8–3.1	0.1	+
Length of caudal peduncle/caudal peduncle depth	2.9	2.5	2.3–2.9	0.2	2.4	2.2–2.6	0.2	ns
Pectoral fin length/pectoral – pelvic-fin origin distance	0.8	0.7	0.6–0.9	0.1	0.9	0.9–0.9	0.0	++
Predorsal length/head length	2.3	2.2	2.1–2.3	0.1	2.0	1.9–2.1	0.1	++
Body width at dorsal-fin origin/caudal peduncle depth	1.6	1.5	1.4–1.7	0.1	1.4	1.3–1.5	0.1	+

Qualitative characters. Pectoral fins do not reach beginning of pelvic fins, except for a few males (ca. 7% in total). In most specimens (ca. 70%), the tip of upper lip above the horizontal level of lowest point of the eye, in some specimens (ca. 25%) at the level, and in 5% of the specimens below the level. Origin of the anal fin is mainly behind the vertical of the posterior insertion of the dorsal fin. (ca. 53%), often at the vertical (39%), rarely ahead (8%). Free margin of the dorsal fin mainly straight or slightly convex, anal fin slightly convex or rarely slightly concave. 3rd–6th type of breast scalation (mode 4th type).

Coloration. Live coloration of females outside the spawning period is brown, gray or light golden hues (see Fig. 4). In males, the color is similar, but with a greater dominance of golden or greenish hues. In spawning coloration of females, golden hue increases significantly and the coloration becomes more contrasting, in general. The spawning coloration of males is also more contrasting, with dominance of green color with variations towards yellow-green or black-green. The operculum stains are blue and the suboperculum is yellow in both sexes, but this is much more pronounced in males. Red hues appear in spawning coloration and

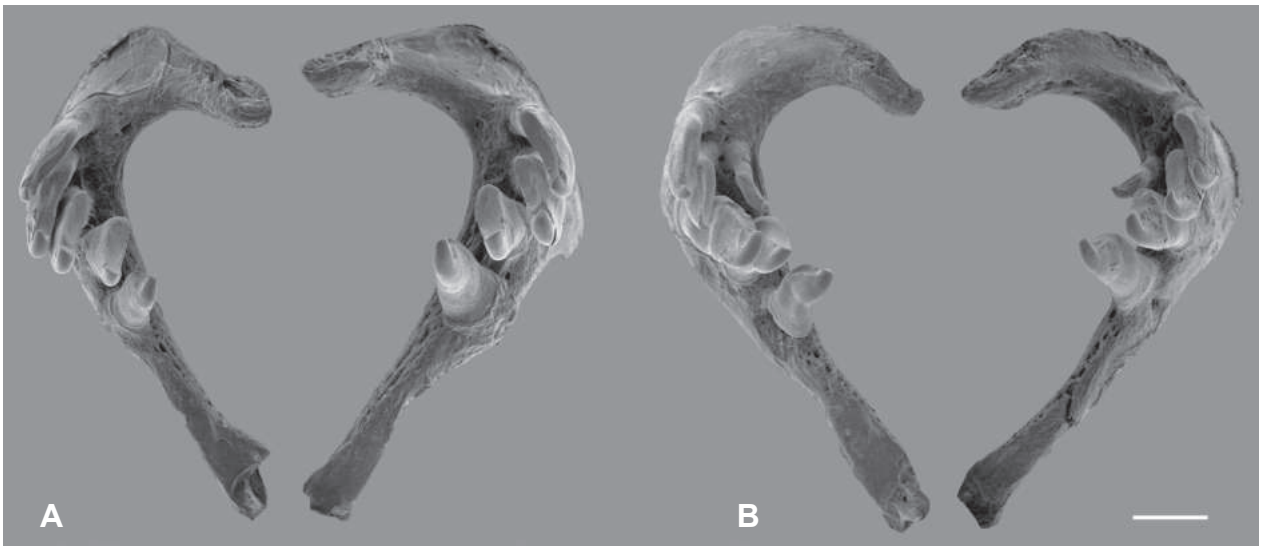

Figure 5. Most frequent variants of formula of pharyngeal bones of *Phoxinus adagumicus* sp. nov.: **A.** Single-row formula 5–4 (in 33% of specimens); **B.** Double-row formula 1.5–4.1 (in 21% of specimens). Scale bar: 0.5 mm.

are concentrated at the base of the pelvic, pectoral and anal fins, as well as around the mouth. The specimens preserved in formalin had a yellowish color, which is somewhat darker with a brown tint in the upper parts.

***Sexual dimorphism*.** Significant differences were observed in 18 out of 41 morphometric characters (Table 2). In addition to some classical sex characteristics in *Phoxinus* minnows (e.g., narrower pectoral fins and less bright colors in females), females of the new species generally have shorter anal and pelvic fins, smaller eye diameter, and a higher ratio of predorsal length to head length.

Table 3. Meristics and scalation pattern of *Phoxinus adagumicus* sp. nov. from type series and additional material from the type locality (primary data see in Suppl. material 2). Additional material from non-type localities is given in Suppl. material 3.

Nos.	Characters	mean	range	SD	n
1	Total number of scales in lateral series (sql)	84.9	81–90	3.0	7
2	Total number of lateralline (pored) scales (llt)	44.2	24–67	17.7	6
3	Number of pored scales in first complete (non-interrupted) section of lateral line (llcs)	29.7	19–57	15.0	7
4	Relative number of total lateral line scales, quotient llt:sql (lltr)	0.5	0.3–0.8	0.2	6
5	Mean number of scale rows on left and right breast patches (BrPScale)	6.4	6–7	0.4	7
6	Number of circumpeduncular scales (cps)	41.1	39–43	1.5	7
7	Scales above lateral line (ScAboveLL)	17.3	15–20	1.6	7
8	Scales below lateral line (ScBelowLL)	11.7	10–13	1.0	6
9	Pattern of scalation on the breast and anterior belly (cstyp)	5	4–6		7
10	Total number of pectoral fin rays (P)	16.6	15–18	1.0	7
11	Total number of pelvic fin rays (V)	8.0	8–8		7
12	Number of branched dorsal fin rays (with 1/2) (D)	7.0	7–7		7
13	Number of branched anal fin rays (with 1/2) (A)	7.0	7–7		7
14	Number of rays in caudal fin (C)	18.9	18–20	0.4	7
15	Total number of vertebrae (tv)	40.4	39–42	0.8	23
16	Number of abdominal vertebrae (abdv)	22.6	21–24	0.7	23
17	Number of caudal vertebrae (caudv)	17.9	17–19	0.7	23
18	Number of predorsal abdominal vertebrae (preDv)	14.8	14–16	0.5	23
19	Number of anal fin pterygiophores in front of the first caudal vertebrae (preAp)	4.5	3–6	0.8	23
20	Difference between numbers of abdominal and caudal vertebrae (dac)	4.6	3–7	1.1	23

Table 4. Frequency of different pharyngeal teeth formulas in *Phoxinus adagumicus* sp. nov., *P. colchicus* and *P. chrysoprasius*.

Species	5–4	1.5–4	5–4.1	5–5.1	1.4–4.2	1.5–4.1	1.5–4.2	1.5–5.1	2.4–4.2	2.5–4.1	2.5–4.2	2.5–5.2	n
P. adagumicus sp. nov.	11	5	6	1	0	7	1	1	0	1	0	0	33
P. chrysoprasius	0	0	0	0	0	0	0	0	0	1	12	2	15
P. colchicus	0	0	0	0	1	1	3	0	1	3	5	1	15

Taxonomic remarks. The presence of *Phoxinus* minnow in the left lower tributaries of the Kuban has been documented since the first half of the 20th century (Malyatsky 1930; Berg 1949; Sukhanova and Troitsky 1949), and all previous researchers have attributed this population to *P. phoxinus*. Emtyl and Ivanenko (2002) used the name '*Phoxinus phoxinus kubanicum* sp. nov.' for the minnows from Trans-Kuban rivers (Aphips, Il, Ubin, Abin, and Adagum) and Lake Abrau (Black Sea basin). Even though the name is accompanied by a comparative description, it cannot be considered as valid because it does not comply with the criteria stipulated in art. 16.4 of the International Code of Zoological Nomenclature (Ride et al. 1999) for species-group names proposed after 1999, as it is not accompanied by an explicit preservation of a holotype or syntypes for the nominal taxon (art. 16.4.1.) and a statement of deposit in a collection (art. 16.4.2.) (Bogutskaya et al. 2023). The names *P. phoxinus kubanicum*, *P. phoxinus kubanicus* [sic], and *P. kubanicus* [sic], after an attempt to describe this species (Emtyl and Ivanenko 2002), were subsequently used several times (Otrishko and Emtyl 2013a, 2013b, 2013c; Karnaukhov 2020); however, according to Bogutskaya et al. (2023), an ICZN commissioner, Nikita Kluge (pers. comm.), taxonomists Pyotr Petrov (pers. comm.) and Boris Kataev (pers. comm.), they cannot be considered as available names.

It is worth noting that the original description of '*P. phoxinus kubanicum*' does not correspond to the

morphological diagnosis of minnows from the Adagum basin rivers obtained in this research. For example, the two-row formula (2.5–4.2) of the pharyngeal teeth is indicated (Emtyl and Ivanenko 2002), but here, none out of 33 examined specimens had such a formula (Table 4). Also, it is necessary to emphasize that the given image of '*P. phoxinus kubanicum*' (fig. 69 in Emtyl and Ivanenko 2002) does not relate to this species but is borrowed from the monograph of L.S. Berg (1949, fig. 447) and refers to the minnows inhabiting Lovozero (Northern Russia), which most probably belong to *Phoxinus* sp. clade 17 of Palandačić et al. (2020). Thus, '*P. phoxinus kubanicum*' should be considered as an *unavailable name*.

Type locality. Pryamaya Shchel River (44.8538°N, 37.8417°E) upstream of Nizhnebakanskaya, Krasnodar Krai, Russia. A tributary of the Bakanka River → Adagum River → Kuban River → Sea of Azov.

Distribution and habitats. An endemic species living in the northwestern Caucasus in the Adagum River basin, a tributary of the Kuban (Fig. 1). The species has a rather limited range with only 55 km between most distant known occurrences. The species has been found only in small streams located in mountainous and foothill areas – in a zone of a width about 15–20 km along the northern slope of the western part of the Main Caucasian Range. Example of habitat for this species (Abin River) is shown in Fig. 6. Habitat of *P. adagumicus* sp. nov. in other parts of the Kuban basin and on the Black Sea coast of the Caucasus (Lake Abrau) indicated according to literature data (Berg 1949; Sukhanova and Troitskiy 1949; Emtyl et al. 1994; Emtyl and Ivanenko 2002; Karnaukhov 2020) was not confirmed by our research and may require additional study (see Discussion).

Morphological comparisons. PCA of morphometric characters shows that *P. adagumicus* sp. nov. is more overlapping with *P. chrysoprasius* than with *P. colchicus* (Fig. 7). The highest loadings for *P. adagumicus* sp. nov. are: head length/caudal peduncle depth, body width at dorsal-fin origin/caudal peduncle depth and eye horizontal diameter (% interorbital width). Sex differences in all three species are divergent in the second component.

The occurrence of single-row pharyngeal teeth, frequent in *P. adagumicus* sp. nov. (Fig. 5, Table 4), is rare in the genus *Phoxinus*. In comparison with the geographically neighboring species, *P. colchicus* and *P. chrysoprasius*, *P. adagumicus* sp. nov. has unique formulas of pharyngeal teeth: 5–4, 1.5–4, 5–4.1, 5–5.1 and 1.5–5.1. According to our data, *P. colchicus* and *P. chrysoprasius* do not show single-row formulae even on one side, while in *P. adagumicus* sp. nov. formula 5–4 is found in 1/3 of all studied specimens. In *P. colchicus* and *P. chrysoprasius*, formula 2.5–4.2 is modal, but this is absent among individuals of *P. adagumicus* sp. nov. Single-row pharyngeal teeth were indicated as a unique feature for *P. apollonicus* Bianco et De Bonis, 2015 from the basin of Lake Skadar in Montenegro (Bianco and De Bonis 2015).

Compared to *P. chrysoprasius* from the rivers of the Crimean Peninsula (Bogutskaya et al. 2023; this study), *P. adagumicus* sp. nov. has a more elongated head – head depth at nape (% HL) 54.1–64.8, mean 60.5 (vs. 58.9–70.7, mean 64.0) in both sexes; larger eyes relative to head height in females – head depth at nape/eye horizontal diameter 2.1–2.6, mean 2.3 (vs. 2.4–3.4, mean 2.7) (Suppl. material 4); less anal fin pterygiophores in front of the first caudal vertebrae (3–7, mean 4.4 vs. 4–8, mean 5.4); less total number of scales in the lateral series (74–94, mean 84.5 vs. 78–104, mean 90.5); less total number of scales in the lateral series (pored) (21–81, mean 58.5 vs. 46–84, mean 70.0); less mean number of scale rows on left and right breast patches (3–9, mean 6.1 vs. 6–11, mean 8.0); less number of circumpeduncular scales (37–44, mean 41.3 vs. 41–55, mean 46.2); and less number of scales below lateral line (8–14, mean 11.8 vs. 11–16, mean 13.8) (Suppl. material 3).

Figure 6. Abin River (44.7210°N, 38.2051°E; 18 Aug. 2016) – example of biotope of *Phoxinus adagumicus* sp. nov.

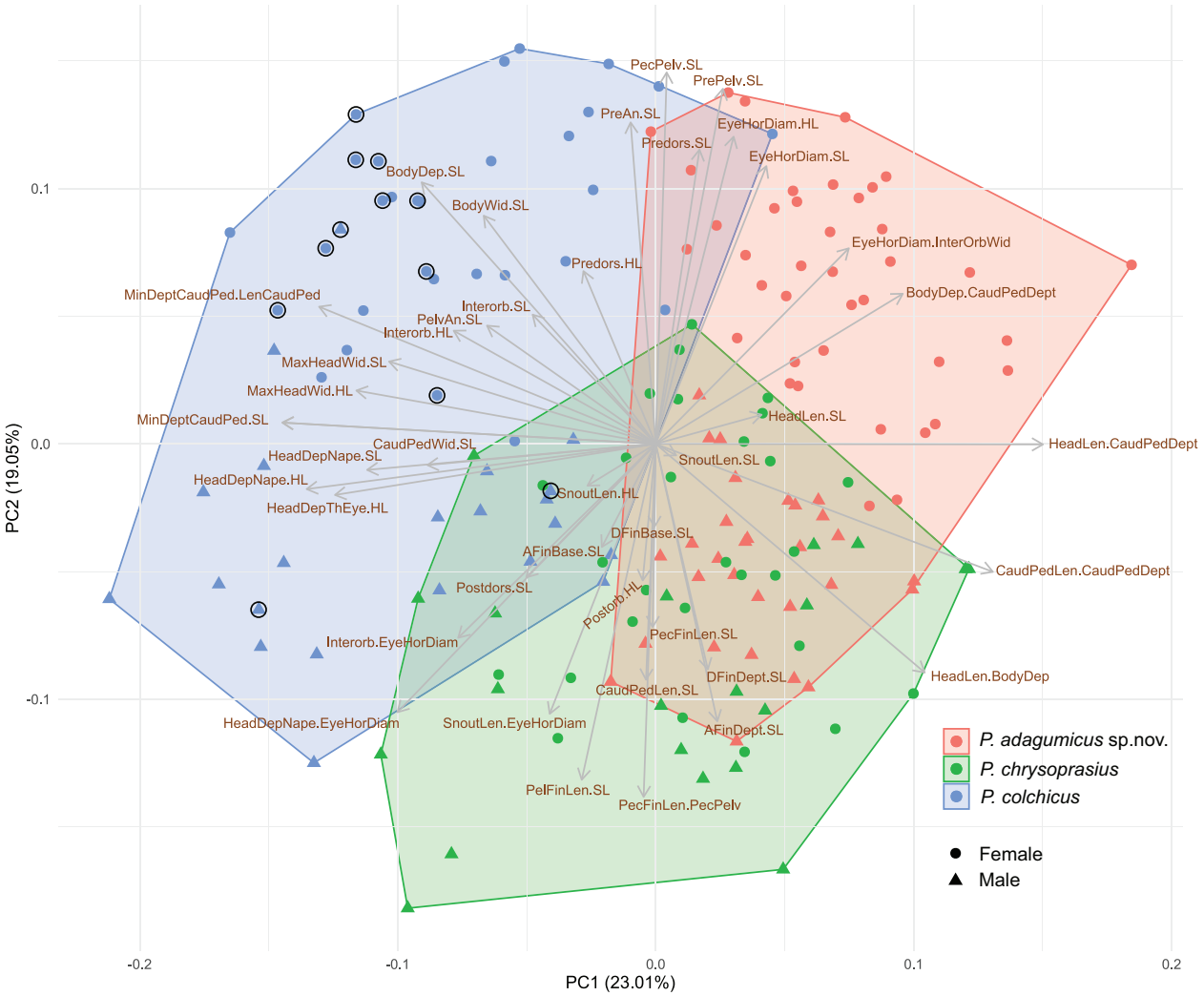

Figure 7. PCA of morphometric characters for *Phoxinus* spp. under comparison and loading plot showing how strongly each character influences principal components. Specimens of *P. colchicus* from the Kuban River basin (Khamyshinka River, a tributary of Belaya River) are encircled by black color.

Compared to *P. colchicus* from the Khamyshinka River (Belaya River drainage, Kuban River basin), Adygea, Russia and the Dyurso, Khotetsai, Dzubga and Pshenaho rivers (Black Sea coast of the Caucasus), Krasnodar Krai, Russia (this study), *P. adagumicus* sp. nov. has lower caudal peduncle – minimum depth of caudal peduncle (% SL) 7.1–10.2, mean 9.1 (vs. 9.6–13.1, mean 11.2) and minimum depth of caudal peduncle (% length of caudal peduncle) 31.3–53.7, mean 40.6 (vs. 42–58.6, mean 49.5); more elongated head – head depth at nape (% HL) 54.1–64.8, mean 60.5 (vs. 61.4–74.7, mean 66.6); caudal peduncle depth in head length 2.7–3.7, mean 3.0 times (vs. 2.1–2.8, mean 2.4 times) (Suppl. material 4); less mean number of scale rows on left and right breast patches (3–9, mean 6.1 vs. 5–11, mean 8.3); 3rd–6th types of scalation pattern of the breast and anterior belly with predominance of 4th type (vs. 3rd–10th, 13th and 14th types with predominance of 6th type); and less number of scales below lateral line (8–14, mean 11.8 vs. 11–17, mean 13.4) (Suppl. material 3).

Compared to *P. csikii* from the Danube River basin, Montenegro and Bulgaria (Bogutskaya et al. 2019, 2023), *P. adagumicus* sp. nov. has a smaller number of anal-fin pterygiophores in front of the first caudal vertebrae (3–7, mean 4.4 vs. 4–8, mean 6.7); and 3rd–6th types of scalation pattern of the breast and anterior belly with predominance of 4th type (vs. 3rd–9th and 11th types with predominance of 7th type) (Suppl. material 3).

Compared to *P. abanticus* Turan, Bayçelebi, Özuluğ, Gaygusuz et Aksu, 2023 from the Lake Abant basin in Turkey (Turan et al. 2023), *P. adagumicus* sp. nov. has scales on the breasts in both sexes (vs. absence of scales on the breast in males); 15–24 scales above lateral line (vs. 11–14 scales); and 18–20 rays in caudal fin (vs. 15–16 rays).

Compared to *P. septimaniae* Kottelat, 2007 from the Herault River, France (Bogutskaya et al. 2019), *P. adagumicus* sp. nov. has more total number of vertebrae (39–43, mean 40.4 vs. 37–41, mean 39.3); less number of anal-fin pterygiophores in front of the first caudal vertebrae (3–7, mean 4.4 vs. 4–7, mean 5.4); and 3rd–6th types of scalation pattern of the breast and anterior belly with predominance of 4th type (vs. 12th–14th types with predominance of 8th type) (Suppl. material 3).

Compared to *P. lumaireul* (Schinz, 1840) clades 1a and 1b from rivers in the Adriatic and Black Sea basins

in Italy, Slovenia, and Croatia (Bogutskaya et al. 2019), *P. adagumicus* sp. nov. has a smaller number of anal-fin pterygiophores in front of the first caudal vertebrae (3–7, mean 4.4 vs. 3–8, mean 5.5 and 3rd–6th types of scalation pattern of the breast and anterior belly with predominance of 4th type (vs. 2nd–7th types with predominance of 3rd type) (Suppl. material 3).

Compared to *P. krkae* Bogutskaya, Jelić, Vucić, Jelić, Diripasko, Stefanov et Klobučar, 2019 from the Krka River, Croatia (Bogutskaya et al. 2019), *P. adagumicus* sp. nov. has more total number of vertebrae (39–43, mean 40.4 vs. 37–40, mean 38.4); more number of abdominal vertebrae (21–24, mean 22.5 vs. 21–22, mean 21.6); more number of caudal vertebrae (16–18, mean 18 vs. 15–18, mean 16.8); more number of predorsal abdominal vertebrae (14–16, mean 14.8 vs. 13–15, mean 14.0)and 3rd–6th types of scalation pattern of the breast and anterior belly with predominance of 4th type (vs. 3rd–7th types with predominance of 5th and 6th types) (Suppl. material 3).

Compared to *P. marsilii* Heckel, 1836 from the Danube River basin, Austria and Croatia (Bogutskaya et al. 2019, 2023), *P. adagumicus* sp. nov. has 3rd–6th types of scalation pattern of the breast and anterior belly with predominance of 4th type (vs. 3rd–8th types with predominance of 6th type) (Suppl. material 3).

Compared to *P. strandjae* from the rivers of the Black Sea basin, Bulgaria and the rivers of the Marmara Sea, Turkey (Bogutskaya et al. 2019, 2023), *P. adagumicus* sp. nov. has a smaller number of anal-fin pterygiophores in front of the first caudal vertebrae (3–7, mean 4.4 vs. 4–8, mean 5.6); and 3rd–6th types of scalation pattern of the breast and anterior belly with predominance of 4th type (vs. 3rd–12th types with predominance of 6th, 7th, 9th and 11th types) (Suppl. material 3).

Discussion

This study clarified the taxonomy, morphology, genetics, and distribution of the *Phoxinus* minnows inhabiting the Caucasus including the Kuban basin, a large riverine system in the Northern Caucasus that is the richest in endemic species compared to fish fauna in remaining European Russia (Abell et al. 2008). Two distinct species, *P. adagumicus* sp. nov. and *P. colchicus*, were identified. Geographic ranges of *P. adagumicus* sp. nov. and *P. colchicus* in the Kuban basin are separated from each other by at least 145 km in a straight line, and also differ in altitude that is ranging within ca. 50–130 m above sea level for *P. adagumicus* sp. nov. and within ca. 280–580 m for *P. colchicus*. *Phoxinus adagumicus* sp. nov. was found only in the Adagum basin, while another species, inhabiting the middle reach of the Belaya River, refers to *P. colchicus* – species widely distributed in the rivers draining the east coast of the Black Sea. *Phoxinus adagumicus* sp. nov. represents deeply divergent lineage that is earlier branched than other European species. Therefore, *P. adagumicus* sp. nov. may represent a relic lineage of European minnows, the ancestors of which were among first colonizers of Europe from the East.

The population of *P. colchicus* in the Belaya River system is apparently a result of the past river capture event. The Kuban population of *P. colchicus* is the single population recorded outside the Black Sea basin. The uniqueness of haplotypes from the Kuban basin may indicate rather long isolation of this population or be a result of founder effect. The upper reaches of the Belaya River system share watershed with upper reaches of the rivers Shakhe, Sochi and Achipse belonging to the Black Sea basin. River captures with naturally translocated fish individuals between the Kuban and Black Sea tributaries might be a common phenomenon. For example, the recent discovery of the Black Sea populations of *Barbus tauricus* Kessler, 1877 in some tributaries of the Lower Kuban might be a result of past colonization through main channel of the Kuban River or be an event of river captures (Levin et al. 2019b).

Large morphological variation and overlap between species are a challenge for *Phoxinus* taxonomy. However, *Phoxinus adagumicus* sp. nov. differs from other closely-related or geographically neighboring species in pharyngeal teeth formula, having reduced number of teeth and rows. The *Phoxinus* spp. usually have two-rowed pharyngeal teeth (Berg 1949) while *P. adagumicus* sp. nov. represents one-rowed formula as strictly dominating over two-rowed. Remarkably, one-rowed teeth formula was found in only one another species – *P. apollonicus* from the basin of Lake Skadar in Montenegro (Bianco and De Bonis 2015), which was suggested to be synonymized with *P. karsticus* Bianco et De Bonis, 2015 (Palandačić et al. 2017). A decrease in the number of teeth (4.2 and 4.1) is also observed in another Western Balkan species – *P. ketmaieri* Bianco et De Bonis, 2015, synonymized subsequently with *P. lumaireul* (Palandačić et al. 2017). Traditionally, the phylogenetic value of pharyngeal tooth numbers and their organization (formula) was high (Chu 1935; Tao et al. 2019) but some recent studies showed great phenotypic plasticity of this character from one side (Shkil et al. 2010; Bolotovskiy and Levin 2011) as well as inheritance of the teeth row numbers from another side (Shkil' and Levin 2008). Nevertheless, in our opinion, future studies should pay more attention to the pharyngeal teeth formula since it is often neglected in the current taxonomical studies.

The geographic distribution of *P. adagumicus* sp. nov. might be wider than its known distribution range in the Adagum River basin. Emtyl et al. (1994) stated that minnows from the rivers Dyurso (Black Sea basin) and Ayuk (tributary of the Psekups River, Kuban basin) are different from "common minnow" (authors did not use Latinian name of species using common name instead, we assume that this is some *Phoxinus* from the European part of the USSR) and "Colchis minnow" (which refers to *P. colchicus*). The habitat of minnows in the Ayuk basin was noted earlier (Sukhanova and Troitskiy 1949), where it was identified as '*P. phoxinus'*. This species was previously reported for the Dyurso River (Luzhnyak 2003). Our examination of the *Phoxinus* material from this river

and nearby (Ozereyka River), only confirmed the presence of *P. colchicus*. Emtyl and Ivanenko (2002), when described '*P. phoxinus kubanicum*', indicated Lake Abrau in the Black Sea basin as the habitat for this species in addition to the rivers of the Kuban basin. The *Phoxinus* was recorded in the lake previously (Malyatsky 1930; Berg 1949), but current studies could not confirm its presence in both Lake (Luzhnyak 2003) and its tributary, the Abrau River (our field survey in 2023). What *Phoxinus* species lived there is unknown, but given the presence of *P. colchicus* in adjacent rivers, one may suggest that this is the same species. In addition, Emtyl and Ivanenko (2002) noted the following locations of the Kuban *Phoxinus* outside the Adagum and Psekups basins: the Aphips and Ubin Rivers. It is worth noting that the Aphips River basin including its left tributary, the Ubin River, are located between the Adagum and Psekups basins (Fig. 1). At the same time, *Phoxinus* was never recorded in the Aphips basin by our numerous field surveys during 2015–2023, or by earlier researchers (Sukhanova and Troitskiy 1949), which also pointed to a large gap in the distributional range between the Adagum and Psekups basins. From all of the above, we can conclude that the entire or the main range of *P. adagumicus* sp. nov. is located within the Kuban River in its sub-basin – the Adagum River system. The taxonomic status of *Phoxinus* from the Ayuk River in the Psekups basin, should be clarified in future research.

We have to consider other peculiarities of the distribution of *P. adagumicus* sp. nov. in the Kuban basin in the light of recent report on its finding (clade 19 by Palandačić et al. 2020) in the Belaya River (tributary of the Kuban). Clade 19 was also reported by Bogutskaya et al. (2023) for "Adagum River at Krymsk, Kuban drainage". Habitat of the *Phoxinus* in the Belaya basin is confirmed by our studies but according to genetic results (Fig. 2) and morphological analysis (Fig. 7), this population belongs to *P. colchicus.* The latter is common in the Belaya River and its tributaries at least from Khamyshki vil. down to Tulsky town along ca. 60 km (Artaev et. al 2021). Thus, we have to conclude that either two species of the genus *Phoxinus* coexist in the Belaya basin, or the coordinates in Palandačić et al. (2020) are indicated incorrectly. We are inclined to the second opinion.

Acknowledgements

The authors are very grateful to Andrey Pashkov and Sergey Reshetnikov for bibliographic assistance; to Maxim Shapovalov, Maxim Saprykin, Alexey Motorin, Alexey Kutuzov, Dmitry Karabanov, Sergey Arefyev, Marina Levina, and Ilya Zabaluev for their help in sampling of material; to Danila Melentev for his help in molecular laboratory; to a member of the International Commission on Zoological Nomenclature – Nikita Kluge, and taxonomists Pyotr Petrov and Boris Kataev for their valuable advice on zoological taxonomy and nomenclature. We are very grateful to Dr. Fatah Zarei and two anonymous reviewers for their valuable comments on this paper. The study was supported partially by the Russian Science Foundation (grant 23-14-00128).

References

Abell R, Thieme ML, Revenga C, Bryer M, Kottelat M, Bogutskaya N, Coad B, Mandrak N, Balderas SC, Bussing W, Stiassny M, Skelton P, Allen GR, Unmack P, Naseka A, Ng R, Sindorf N, Robertson J, Armijo E, Higgins JV, Heibel TJ, Wikramanayake E, Olson D, López HL, Reis RE, Lundberg JG, Sabaj PMH, Petry P (2008) Freshwater ecoregions of the world: A new map of biogeographic units for freshwater biodiversity conservation. Bioscience 58(5): 403–414. https://doi.org/10.1641/B580507

Aljanabi SM, Martinez I (1997) Universal and rapid salt-extraction of high quality genomic DNA for PCR-based techniques. Nucleic Acids Research 25(22): 4692–4693. https://doi.org/10.1093/nar/25.22.4692

Artaev O, Pashkov A, Vekhov D, Saprykin M, Shapovalov M, Levina M, Levin B (2021) Fish occurrence in the Kuban River Basin (Russia). Biodiversity Data Journal 9: e76701. https://doi.org/10.3897/BDJ.9.e76701

Berg LS (1949) Freshwater fishes of the U.S.S.R. and adjacent countries. Part 2. Izdatelstvo Akademii Nauk SSSR, Leningrad, 456 pp. [In Russian]

Bianco PG, De Bonis S (2015) A taxonomic study on the genus *Phoxinus* (Acthinopterigy, Cyprinidae) from Italy and western Balkans with description of four new species: *P. ketmaieri*, *P. karsticus*, *P. apollonicus* and *P. likai*. Researches on Wildlife Conservation 4: 1–17.

Bogutskaya N, Jelić D, Vucić M, Jelić M, Diripasko O, Stefanov T, Klobučar G (2019) Description of a new species of *Phoxinus* from the upper Krka River (Adriatic Basin) in Croatia (Actinopterygii: Leuciscidae), first discovered as a molecular clade. Journal of Fish Biology 96(2): 378–393. https://doi.org/10.1111/jfb.14210

Bogutskaya NG, Diripasko OA, Palandačić A (2023) Novel data support validity of *Phoxinus chrysoprasius* (Pallas, 1814) (Actinopterygii, Leuciscidae). European Journal of Taxonomy 861: 1–20. https://doi.org/10.5852/ejt.2023.861.2061

Bolotovskiy AA, Levin BA (2011) Influence of development rate on pharyngeal teeth formula in *Abramis brama* (L.) bream: Experimental data. Russian Journal of Developmental Biology 42(3): 143–147. https://doi.org/10.1134/S1062360411030039

Chu YT (1935) Comparative studies on the scales and the pharyngeals and their teeth in Chinese cyprinids, with particular reference to taxonomy and evolution. Biological Bulletin of St. John's University 2: 81–221. https://doi.org/10.2307/1436747

Çiçek E, Eagderi S, Sungur S (2018) *Oxynoemacheilus veyseli*, a new nemacheilid species from the upper Aras River drainage of Turkey (Teleostei: Nemacheilidae). Iranian Journal of Ichthyology 5(3): 232–242. https://doi.org/10.22034/iji.v5i3.302

Denys GP, Dettai A, Persat H, Daszkiewicz P, Hautecoeur M, Keith P (2020) Revision of *Phoxinus* in France with the description of two new species (Teleostei, Leuciscidae). Cybium. Revue Internationale d'Ichtyologie 44(3): 205–237. https://doi.org/10.26028/cybium/2020-443-003

Eagderi S, Nikmehr N, Poorbagher H (2020) *Ponticola patimari* sp. nov. (Gobiiformes: Gobiidae) from the southern Caspian Sea. FishTaxa: Journal of Fish Taxonomy 17: 22–31.

Emtyl MKh, Ivanenko AM (2002) Fishes of the South-west of Russia. Kubanskiy Gosudarstvennyy Universitet, Krasnodar, 340 pp. [In Russian]

Emtyl MKh, Plotnikov GK, Reshetnikov SI, Buinov LL, Vishnitskaya L (1994) Clarification of the taxonomy of the common minnow living in the rivers of the Krasnodar region. In: Current issues of nature conservation of steppe ecosystems and adjacent territories. Krasnodar (Russia), 137–141. [In Russian]

Epitashvili G, Japoshvili B, Mumladze L (2023) *Ponticola alasanicus* sp. n. (Gobiiformes, Gobiidae) from the Alazani River Basin, Georgia. Biodiversity Data Journal 11: e101095. https://doi.org/10.3897/BDJ.11.e101095

Esmaeili HR, Sayyadzadeh G, Japoshvili B, Eagderi S, Abbasi K, Mousavi-Sabet H (2020) *Rhodeus caspius*, a new bitterling from Iran (Teleostei: Cypriniformes: Acheilognathidae). Zootaxa 4851(2): 319–337. https://doi.org/10.11646/zootaxa.4851.2.6

Freyhof J, Kaya C, Epitashvili G, Geiger M (2021) *Oxynoemacheilus phasicus*, a new nemacheilid loach from the eastern Black Sea basin with some remarks on other Caucasian *Oxynoemacheilus* (Teleostei: Nemacheilidae). Zootaxa 4952(1): 135–151. https://doi.org/10.11646/zootaxa.4952.1.8

Gadzhiev VD, Kulieva KhG, Vagabov ZV (1979) Flora and vegetation of the highlands of Talysh. Elm, Baku, 149 pp. [In Russian]

Gandlin A, Japoshvili B, Epitashvili G, Mustafaev N, Roubenyan H, Levin B (2022) Phylogeography of the Kura Barbel *Barbus cyri* De Filippi as Inferred from mtDNA Data. Inland Water Biology 15(1): 11–22. https://doi.org/10.1134/S1995082922010047

Geiger MF, Herder F, Monaghan MT, Almada V, Barbieri R, Bariche M, Berrebi P, Bohlen J, Casal-Lopez M, Delmastro GB, Denys GPJ, Dettai A, Doadrio I, Kalogianni E, Kärst H, Kottelat M, Kovačić M, Laporte M, Lorenzoni M, Marčić Z, Özuluğ M, Perdices A, Perea S, Persat H, Porcelotti S, Puzzi C, Robalo J, Šanda R, Schneider M, Šlechtová V, Stoumboudi M, Walter S, Freyhof J (2014) Spatial heterogeneity in the Mediterranean Biodiversity Hotspot affects barcoding accuracy of its freshwater fishes. Molecular Ecology Resources 14(6): 1210–1221. https://doi.org/10.1111/1755-0998.12257

Hammer Ø, Harper DA (2001) Past: Paleontological statistics software package for educaton and data anlysis. Palaeontologia Electronica 4(1): 1–9.

Hill V, Baele G (2019) Bayesian estimation of past population dynamics in BEAST 1.10 using the Skygrid coalescent model. Molecular Biology and Evolution 36(11): 2620–2628. https://doi.org/10.1093/molbev/msz172

Ihaka R, Gentleman R (1996) R: a language for data analysis and graphics. Journal of Computational and Graphical Statistics 5(3): 299–314. https://doi.org/10.1080/10618600.1996.10474713

Imoto JM, Saitoh K, Sasaki T, Yonezawa T, Adachi J, Kartavtsev YP, Miya M, Nishida M, Hanzawa N (2013) Phylogeny and biogeography of highly diverged freshwater fish species (Leuciscinae, Cyprinidae, Teleostei) inferred from mitochondrial genome analysis. Gene 514(2): 112–124. https://doi.org/10.1016/j.gene.2012.10.019

Ivanova NV, Zemlak TS, Hanner RH, Hebert PD (2007) Universal primer cocktails for fish DNA barcoding. Molecular Ecology Notes 7(4): 544–548. https://doi.org/10.1111/j.1471-8286.2007.01748.x

Kalyaanamoorthy S, Minh BQ, Wong TK, Von Haeseler A, Jermiin LS (2017) ModelFinder: Fast model selection for accurate phylogenetic estimates. Nature Methods 14(6): 587–589. https://doi.org/10.1038/nmeth.4285

Karnaukhov GI (2020) Biocenoses of small rivers in the Krasnodar krai. International Scientific Research Journal 10 (100): 71–79. [In Russian] https://doi.org/10.23670/IRJ.2020.100.10.014

Kassambara A (2020) rstatix: Pipe-friendly framework for basic statistical tests. R package version 0.6. 0.

Kolakovskiy AA (1980) Flora of Abkhazia. 2nd edn. 1. Metsniereba, Tbilisi, 211 pp. [In Russian]

Kottelat M (1997) European freshwater fishes. Biologia 52(5): 1–271. https://doi.org/10.5281/zenodo.1311773

Kottelat M (2007) Three new species of *Phoxinus* from Greece and southern France (Teleostei: Cyprinidae). Ichthyological Exploration of Freshwaters 18(2): 145.

Kottelat M, Freyhof J (2007) Handbook of European Freshwater Fishes. Kottelat, Cornol, Switzerland and Freyhof, Berlin, 646 pp.

Kovačić M, Esmaeili HR, Zarei F, Abbasi K, Schliewen UK (2021) A new species of tadpole-goby, *Benthophilus persicus* sp. nov. (Teleostei: Gobiidae) from the southern Caspian Sea. Zootaxa 4980(1): 45–63. https://doi.org/10.11646/zootaxa.4980.1.3

Kuljanishvili T, Epitashvili G, Freyhof J, Japoshvili B, Kalous L, Levin B, Mustafayev N, Ibrahimov S, Pipoyan S, Mumladze L (2020) Checklist of the freshwater fishes of Armenia, Azerbaijan and Georgia. Journal of Applied Ichthyology 36(4): 501–514. https://doi.org/10.1111/jai.14038

Kumar S, Stecher G, Tamura K (2016) MEGA7: Molecular evolutionary genetics analysis version 7.0 for bigger datasets. Molecular Biology and Evolution 33(7): 1870–1874. https://doi.org/10.1093/molbev/msw054

Lanfear R, Calcott B, Ho SY, Guindon S (2012) PartitionFinder: Combined selection of partitioning schemes and substitution models for phylogenetic analyses. Molecular Biology and Evolution 29(6): 1695–1701. https://doi.org/10.1093/molbev/mss020

Lanfear R, Frandsen PB, Wright AM, Senfeld T, Calcott B (2016) PartitionFinder 2: New methods for selecting partitioned models of evolution formolecular and morphological phylogenetic analyses. Molecular Biology and Evolution 34(3): 772–773. https://doi.org/10.1093/molbev/msw260

Levin BA, Simonov EP, Ermakov OA, Levina MA, Interesova EA, Kovalchuk OM, Malinina YA, Mamilov NS, Mustafayev NJ, Pilin DV, Pozdeev IV, Prostakov NI, Roubenyan HR, Titov SV, Vekhov DA (2017) Phylogeny and phylogeography of the roaches, genus *Rutilus* (Cyprinidae), at the Eastern part of its range as inferred from mtDNA analysis. Hydrobiologia 788(1): 33–46. https://doi.org/10.1007/s10750-016-2984-3

Levin BA, Simonov E, Matveyev MP, Artaev ON, Mustafayev NJ, Pashkov AN, Roubenyan HR (2018) DNA barcoding of the fishes of the genus *Alburnoides* (Actinopterygii, Cyprinidae) from Caucasus. Mitochondrial DNA, Part A, DNA Mapping, Sequencing, and Analysis 29(1): 49–55. https://doi.org/10.1080/24701394.2016.1238900

Levin BA, Prokofiev AM, Roubenyan HR (2019a) A new species of algae eaters *Capoeta kaput* sp. nov. (Teleostei, Cyprinidae) from Transcaucasia. Inland Water Biology 12(1): 32–41. https://doi.org/10.1134/S1995082919010139

Levin BA, Gandlin AA, Simonov ES, Levina MA, Barmintseva AE, Japoshvili B, Mugue NS, Mumladze L, Mustafayev NJ, Pashkov AN, Roubenyan HRI, Shapovalov M, Doadrio I (2019b) Phylogeny, phylogeography and hybridization of Caucasian barbels of the genus *Barbus* (Actinopterygii, Cyprinidae). Molecular Phylogenetics and Evolution 135: 31–44. https://doi.org/10.1016/j.ympev.2019.02.025

Levin B, Simonov E, Gabrielyan BK, Mayden RL, Rastorguev SM, Roubenyan HR, Sharko FS, Nedoluzhko AV (2022) Caucasian

treasure: Genomics sheds light on the evolution of half-extinct Sevan trout, *Salmo ischchan*, species flock. Molecular Phylogenetics and Evolution 167: 107346. https://doi.org/10.1016/j.ympev.2021.107346

Luzhnyak VA (2003) Ichthyofauna of rivers and estuaries of the Black Sea coast of Russia. Issues of Ichthyology 43(4): 457–463. [In Russian]

Machordom A, Doadrio I (2001) Evidence of a Cenozoic Betic-Kabilian connection based on freshwater fish phylogeography (*Luciobarbus*, Cyprinidae). Molecular Phylogenetics and Evolution 18: 252–263. https://doi.org/10.1006/mpev.2000.0876

Mahmoudi A, Darvish J, Siahsarvie R, Dubey S, Kryštufek B (2019) Mitochondrial sequences retrieve an ancient lineage of bicolored shrew in the Hyrcanian refugium. Mammalian Biology 95: 160–163. https://doi.org/10.1016/j.mambio.2018.06.006

Malyatsky SM (1930) New relict species of sardelka from Lake Abrau (*Harengula abrau* n. sp.). Proceedings of the Azov-Black Sea Fishery Station 6: 65–74. [In Russian]

Mina MV, Levin BA, Mironovsky AN (2005) On the possibility of using character estimates obtained by different operators in morphometric studies of fish. Journal of Ichthyology 45(4): 284–294.

Minh BQ, Nguyen MA, von Haeseler A (2013) Ultrafast approximation for phylogenetic bootstrap. Molecular Biology and Evolution 30(5): 1188–1195. https://doi.org/10.1093/molbev/mst024

Myers N, Mittermeier RA, Mittermeier CG, Da Fonseca GA, Kent J (2000) Biodiversity hotspots for conservation priorities. Nature 403(6772): 853–858. https://doi.org/10.1038/35002501

Nakhutsrishvili G, Zazanashvili N, Batsatsashvili K, Montalvo CS (2015) Colchic and Hyrcanian forests of the Caucasus: Similarities, differences and conservation status. Flora Mediterranea 25(Special Issue): 185–192. https://doi.org/10.7320/FlMedit25SI.185

Naseka AM (1996) Comparative study on the vertebral column in the Gobioninae (Cyprinidae, Pisces) with special reference to its systematics. Publicaciones Especiales Instituto Espanol de Oceanografia 21: 149–167.

Naseka AM (2010) Zoogeographical freshwater divisions of the Caucasus as a part of the West Asian Transitional Region. Trudy Zoologicheskogo Instituta 314(4): 469–492. https://doi.org/10.31610/trudyzin/2010.314.4.469

Nguyen LT, Schmidt HA, von Haeseler A, Minh BQ (2015) IQ-TREE: a fast and effective stochastic algorithm for estimating maximum-likelihood phylogenies. Molecular Biology and Evolution 32: 268–274. https://doi.org/10.1093/molbev/msu300

Otrishko MP, Emtyl MKh (2013a) History of the formation of the ichthyofauna of the Kuban River basin. Science Prospects 9(48): 19–21. [In Russian]

Otrishko MP, Emtyl MKh (2013b) Current state of the ichthyofauna of the Adagum River. Privolzhskiy Nauchnyy Vestnik 8(24): 21–24. [In Russian]

Otrishko MP, Emtyl MKh (2013c) Preliminary information about ichthyofauna of some left-bank tributaries of the Kuban River. In: Modern problems and prospects of the fishery complex: Materials of the fourth scientific and practical conference of young scientists of the Federal State Unitary Enterprise "VNIRO" with international participation. Moscow, VNIRO Publishing, 68–70. [In Russian]

Palandačić A, Bravničar J, Zupančič P, Šanda R, Snoj A (2015) Molecular data suggest a multispecies complex of *Phoxinus* (Cyprinidae) in the Western Balkan Peninsula. Molecular Phylogenetics and Evolution 92: 118–123. https://doi.org/10.1016/j.ympev.2015.05.024

Palandačić A, Naseka A, Ramler D, Ahnelt H (2017) Contrasting morphology with molecular data: An approach to revision of species complexes based on the example of European *Phoxinus* (Cyprinidae). BMC Evolutionary Biology 17(1): 1–17. https://doi.org/10.1186/s12862-017-1032-x

Palandačić A, Kruckenhauser L, Ahnelt H, Mikschi E (2020) European minnows through time: museum collections aid genetic assessment of species introductions in freshwater fishes (Cyprinidae: *Phoxinus* species complex). Heredity 124(3): 410–422. https://doi.org/10.1038/s41437-019-0292-1

Parvizi E, Keikhosravi A, Naderloo R, Solhjouy-Fard S, Sheibak F, Schubart CD (2019) Phylogeography of *Potamon ibericum* (Brachyura: Potamidae) identifies Quaternary glacial refugia within the Caucasus biodiversity hot spot. Ecology and Evolution 9(8): 4749–4759. https://doi.org/10.1002/ece3.5078

Ramler D, Palandačić A, Delmastro GB, Wanzenböck J, Ahnelt H (2016) Morphological divergence of lake and stream *Phoxinus* of Northern Italy and the Danube basin based on geometric morphometric analysis. Ecology and Evolution 7(2): 572–584. https://doi.org/10.1002/ece3.2648

Reshetnikov YuS, Popova OA, Sokolov LI, Tsepkin EA, Sideleva VG, Dorofeeva EA, Chereshnev IA, Moskvalkova KI Dgebuadze YuYu, Ruban GI, Korolev VV (2003) Atlas of freshwater fishes of Russia in 2 volumes. Vol.1. Nauka, Moscow, 379 pp. [In Russian]

Ride WDL, Cogger HG, Dupuis C, Kraus O, Minelli A, Thompson FC, Tubbs PK (1999) International Commission on Zoological Nomenclature. The Natural History Museum, London, 106 pp.

Roman A, Afanasyev S, Golub O, Lietytska O (2022) *Capoeta svanetica* (Teleostei, Cyprinidae), a new species from the Luchunis River (Rioni River drainage) in Georgia. Zoodiversity 56(2): 117–134. https://doi.org/10.15407/zoo2022.02.117

Rothgänger J, Weniger M, Weniger T, Mellmann A, Harmsen D (2006) Ridom TraceEdit: A DNA trace editor and viewer. Bioinformatics 22(4): 493–494. https://doi.org/10.1093/bioinformatics/btk002

Schönhuth S, Vukić J, Šanda R, Yang L, Mayden RL (2018) Phylogenetic relationships and classification of the Holarctic family Leuciscidae (Cypriniformes: Cyprinoidei). Molecular Phylogenetics and Evolution 127: 781–799. https://doi.org/10.1016/j.ympev.2018.06.026

Shkil' FN, Levin BA (2008) On inheritance of the number of pharyngeal tooth rows in a large African barb *Barbus intermedius*. Journal of Ichthyology 48(8): 686–690. https://doi.org/10.1134/S0032945208080183

Shkil FN, Levin BA, Abdissa B, Smirnov SV (2010) Variability in the number of tooth rows in the pharyngeal dentition of *Barbus intermedius* (Teleostei; Cyprinidae): Genetic, hormonal and environmental factors. Journal of Applied Ichthyology 26(2): 315–319. https://doi.org/10.1111/j.1439-0426.2010.01428.x

Sukhanova ER, Troitskiy SK (1949) Ichthyofauna at the spawning sites of vimba and shemaya in the Psekups River. Proceedings of the fish farming and biological laboratory of Azcherrybvod 1: 151–181. [In Russian]

Tang Y, Horikoshi M, Li W (2016) ggfortify: Unified interface to visualize statistical results of popular R packages. The R Journal 8(2): 474–485. https://doi.org/10.32614/RJ-2016-060

Tao W, Yang L, Mayden RL, He S (2019) Phylogenetic relationships of Cypriniformes and plasticity of pharyngeal teeth in the adaptive radiation of cyprinids. Science China. Life Sciences 62(4): 553–565. https://doi.org/10.1007/s11427-019-9480-3

Taylor WR, Van Dyke GC (1985) Revised procedures for staining and clearing small fishes and other vertebrates for bone and

cartilage study. Cybium 9: 107–109. https://doi.org/10.26028/cybium/1985-92-001

Turan D, Japoshvili B, Aksu İ, Bektaş Y (2016) Description of two new species of the genus *Gobio* (Teleostei: Cyprinidae) from the Black Sea coast of Turkey. Zoology in the Middle East 62(2): 112–124. https://doi.org/10.1080/09397140.2016.1182779

Turan D, Kottelat M, Kaya C (2022) The trouts of the upper Kura and Aras rivers in Turkey, with description of three new species (Teleostei: Salmonidae). Zootaxa 5150(1): 43–64. https://doi.org/10.11646/zootaxa.5150.1.2

Turan D, Bayçelebi E, Özuluğ M, Gaygusuz Ö, Aksu İ (2023) *Phoxinus abanticus*, a new species from the Lake Abant drainage in Türkiye (Teleostei: Leuciscidae). Journal of Fish Biology 102(5): 1157–1167. https://doi.org/10.1111/jfb.15371

Vasil'eva ED, Mousavi-Sabet H, Vasil'Ev VP (2015) *Ponticola iranicus* sp. nov. (Actinopterygii: Perciformes: Gobiidae) from the Caspian Sea basin. Acta Ichthyologica et Piscatoria 45(2): 189–197. https://doi.org/10.3750/AIP2015.45.2.09

Vasil'eva ED, Solovyeva EN, Levin BA, Vasil'ev VP (2020) *Cobitis derzhavini* sp. nova – a new spined loach species (Teleostei: Cobitidae) discovered in the Transcaucasia. Journal of Ichthyology 60(2): 135–153. https://doi.org/10.1134/S0032945220020198

Vucić M, Jelić D, Žutinić P, Grandjean F, Jelić M (2018) Distribution of Eurasian minnows (*Phoxinus*: Cypriniformes) in the western Balkans. Knowledge and Management of Aquatic Ecosystems 11(419): 11. https://doi.org/10.1051/kmae/2017051

Wickham H, Averick M, Bryan J, Chang W, McGowan LDA, François R, Grolemund G, Hayes A, Henry L, Hester J, Kuhn M, Pedersen TL, Miller E, Milton Bache S, Müller K, Ooms J, Robinson D, Paige Seidel D, Spinu V, Takahashi K, Vaughan D, Wilke C, Woo K, Yutani H (2019) Welcome to the Tidyverse. Journal of Open Source Software 4(43): 1686. https://doi.org/10.21105/joss.01686

Xiang CY, Gao F, Jakovlić I, Lei HP, Hu Y, Zhang H, Zou H, Wang GT, Zhang D (2023) Using PhyloSuite for molecular phylogeny and tree-based analyses. iMeta 87(1): e87. https://doi.org/10.1002/imt2.87

Xu W, Chen A, Xia R, Fu C (2014) Complete mitochondrial genome of *Phoxinus tumensis* (Cypriniformes: Cyprinidae). Mitochondrial DNA 25(5): 368–369. https://doi.org/10.3109/19401736.2013.803096

Zarei F, Esmaeili HR, Kovačić M, Schliewen UK, Abbasi K (2022a) *Ponticola hircaniaensis* sp. nov., a new and critically endangered gobiid species (Teleostei: Gobiidae) from the southern Caspian Sea basin. Zootaxa 5154(4): 401–430. https://doi.org/10.11646/zootaxa.5154.4.1

Zarei F, Esmaeili HR, Sadeghi R, Schliewen UK, Kovačić M, Abbasi K, Gholamhosseini A (2022b) An integrative insight into the diversity, distribution, and biogeography of the freshwater endemic clade of the *Ponticola syrman group* (Teleostei: Gobiidae) in the Caucasus biodiversity hotspot. Ecology and Evolution 12(9): e9300. https://doi.org/10.1002/ece3.9300

Zarei F, Esmaeili HR, Schliewen UK, Abbasi K (2022c) Taxonomic diversity and distribution of the genus *Proterorhinus* (Teleostei: Gobiidae) in the Caucasus biodiversity hotspot with conservation implications. Aquatic Conservation 32(1): 129–138. https://doi.org/10.1002/aqc.3728

Zhang D, Gao F, Jakovlić I, Zou H, Zhang J, Li WX, Wang GT (2020) PhyloSuite: An integrated and scalable desktop platform for streamlined molecular sequence data management and evolutionary phylogenetics studies. Molecular Ecology Resources 20(1): 348–355. https://doi.org/10.1111/1755-0998.13096

Supplementary material 1

Additional material on *Phoxinus adagumicus* sp. nov. and comparative material on *Phoxinus chrysoprasius* and *P. colchicus*

Authors: Oleg N. Artaev, Ilya S. Turbanov, Aleksey A. Bolotovskiy, Aleksandr A. Gandlin, Boris A. Levin

Data type: docx

Link: https://doi.org/10.3897/zse.100.115696.suppl1

Supplementary material 2

Primary morphological data of *Phoxinus adagumicus* sp. nov. from type locality (Pryamaya Shchel River)

Authors: Oleg N. Artaev, Ilya S. Turbanov, Aleksey A. Bolotovskiy, Aleksandr A. Gandlin, Boris A. Levin

Data type: xlsx

Link: https://doi.org/10.3897/zse.100.115696.suppl2

Supplementary material 3

Meristic and qualitative characters of *Phoxinus adagumicus* sp. nov., *P. chrysoprasius*, *P. colchicus* and other *Phoxinus* species published in the literature

Authors: Oleg N. Artaev, Ilya S. Turbanov, Aleksey A. Bolotovskiy, Aleksandr A. Gandlin, Boris A. Levin

Data type: xlsx

Link: https://doi.org/10.3897/zse.100.115696.suppl3

Supplementary material 4

Morphometrics of *Phoxinus adagumicus* sp. nov., *P. chrysoprasius*, *P. colchicus* and its comparison

Authors: Oleg N. Artaev, Ilya S. Turbanov, Aleksey A. Bolotovskiy, Aleksandr A. Gandlin, Boris A. Levin
Data type: xlsx

Link: https://doi.org/10.3897/zse.100.115696.suppl4

Supplementary material 5

Material for genetic studies

Authors: Oleg N. Artaev, Ilya S. Turbanov, Aleksey A. Bolotovskiy, Aleksandr A. Gandlin, Boris A. Levin
Data type: xlsx

Link: https://doi.org/10.3897/zse.100.115696.suppl5

Supplementary material 6

The best partition schemes generated by ModelFinder v.2.2.0 (ML) and PartitionFinder v.2.1.1 (BI)

Authors: Oleg N. Artaev, Ilya S. Turbanov, Aleksey A. Bolotovskiy, Aleksandr A. Gandlin, Boris A. Levin
Data type: docx

Link: https://doi.org/10.3897/zse.100.115696.suppl6

Supplementary material 7

ML phylogenetic tree of concatenated COI and cytb mtDNA sequences representing all available species in Genabnk combined with our data set

Authors: Oleg N. Artaev, Ilya S. Turbanov, Aleksey A. Bolotovskiy, Aleksandr A. Gandlin, Boris A. Levin
Data type: docx

Link: https://doi.org/10.3897/zse.100.115696.suppl7

Zoosyst. Evol. 100 (1) 2024, 309–324 | DOI 10.3897/zse.100.116535

PENSOFT

für Natur MUSEUM FÜR NATURKUNDE BERLIN

Bashimyzon cheni, a new genus and species of sucker loach (Teleostei, Gastromyzontidae) from South China

Xiong Gong[1,2], E Zhang[1]

1 *Institute of Hydrobiology, Chinese Academy of Sciences, Wuhan, China*
2 *University of Chinese Academy of Sciences, Beijing, China*

https://zoobank.org/634807EE-E59F-4698-853D-B757C00AEB99

Corresponding author: E Zhang (zhange@ihb.ac.cn)

Academic editor: Nicolas Hubert ♦ **Received** 29 November 2023 ♦ **Accepted** 27 February 2024 ♦ **Published** 20 March 2024

Abstract

Bashimyzon, new genus, is here established for *Erromyzon damingshanensis*, and a new species of the genus is described from the You-Jiang of the Pearl River (=Zhu-Jiang in mandarin Chinese) basin in Guangxi Province, South China. This new genus has a small gill opening above the pectoral-fin base and short pectoral fins extending backwards short of pelvic-fin insertions, both characters combined to separate it from all currently-recognized gastromyzontid genera except *Erromyzon* and *Protomyzon*, but differs from the two genera in having a larger gap between the posterior edge of eye and the vertical through the pectoral-fin insertion and very small fleshy lobes posterior to the maxillary-barbel bases. It is further distinct from its most similar genus *Erromyzon* in having a relatively larger gill opening, fewer branched pectoral-fin rays folded against body, and more posteriorly placed pectoral fins with a shorter fin base. *Bashimyzon cheni*, new species, and *B. damingshanensis*, the single congeneric species, differ in number of lateral-line pored scales, body coloration, and cephalic contour, and also in substantial genetic divergence.

Key Words

Bashimyzon, new genus, new species, taxonomy, Zhu-Jiang basin

Introduction

Species of the family Gastromyzontidae (so-called sucker loaches) are small-sized bottom dwellers, mainly feeding on algae scraped off underwater rocks (Chen 1980a; Chen and Tang 2000; Chen and Zhang 2006). These species are adapted to dwell in rapid-running waters by evolving many morphological traits, such as a depressed head, an inferior mouth, and laterally-expanded pectoral and pelvic fins (Chen 1978; Chen and Zheng 1989; Kottelat 2004). This family is by far among the lesser-known taxonomic freshwater fish groups, and new species are described each year (Kottelat 2012; Zhang and Cao 2021). Numerous unidentified species are waiting for formal descriptions.

There are a total of 20 valid genera currently recognized in the Gastromyzontidae (Fricke et al. 2023). Kottelat (2004) proposed *Erromyzon* to accommodate a Chinese species formerly misplaced in the genus *Protomyzon* Hora, 1932 (*P. sinensis*), and described a new species *E. compactus* from northeastern Vietnam. Subsequently, three new species were described from South China: *E. yangi* by Neely et al. (2007), *E. kalotaenia* by Yang et al. (2012) and *E. damingshanensis* by Xiu and Yang (2017). In Kottelat's (2012) inventory of the loaches (Teleostei, Cypriniformes, Cobitoidei) of the world, 17 valid genera were included in the Gastromyzontidae. Nevertheless, its generic classification remains far from satisfactory mainly due to a poor understanding of the phylogenetic relationships within the family. Following the erection of *Erromyzon*, two new genera were erected: *Yaoshania* by Yang et al. (2012) and *Engkaria* by Tan (2021). *Labigastromyzon* have been elevated to generic status (Chen et al. 2023). *Erromyzon damingshanensis* is reclassified in this study into a new genus of the Gastromyzontidae in China.

Currently, *E. damingshanensis* is found in a stream tributary to the Qingshui-He draining the northeastern slope of the Damingshan Mountain (Xiu and Yang 2017). This stream empties into the Hongshui-He of the middle Xi-Jiang basin. Our recent survey of freshwater fishes, conducted in the Wuming-He (a stream flowing into the You-Jiang) with its source in the southwestern slope of the Damingshan Mountain, yielded many specimens superficially most similar to *E. damingshanensis* but not conspecific with it or all other congeneric species, therefore representing an unrecognized species. Further morphological examination and comparisons demonstrated that these two species have remarkable differences in the length of the gap between the posterior edge of eye and the vertical through the pectoral-fin insertion, gill opening size, number of last branched pectoral-fin rays folded against the flank, and mouth-part structures with the rest of congeneric species, which are sufficient to place both in their own genus. The generic status of *Bashimyzon* gen. nov. is also justified by its substantial genetic divergence (p-distances:10–12%) with phylogenetically allied genera *Erromyzon* and *Yaoshania*. The present study aims to propose a new genus *Bashimyzon*, with *E. damingshanensis* Xiu & Yang, 2017 used as the type species, and then provide a formal description of the unidentified species, here named as *Bashimyzon cheni* gen. et sp. nov.

Materials and methods

Specimen sampling and preservation

All specimens were collected in our field surveys conducted during 2020–2023, in accordance with the Chinese Laboratory Animal Welfare and Ethics animal welfare laws (GB/T35892–2018). Specimens were caught using electrofishing and/or trap nets. After being anaesthetized, all caught individuals were killed by immersion in ethanol or formalin. Some of them were stored in 10% formalin preservative for morphological examination or permanent curation, and the others in 95% ethanol for DNA extraction. The specimens examined in this study are housed in the collection of Kunming Institute of Zoology (**KIZ**), Chinese Academy of Sciences, Kunming City, Yunnan Province, and the Institute of Hydrobiology (**IHB**), Chinese Academy of Sciences, Wuhan City, Hubei Province, P. R. China.

Morphological and geometric morphometric analysis

Measurements, as depicted in Fig. 1, were made point-to-point with digital calipers connected to a data recording computer and recorded to the nearest 0.1mm. Pre-dorsal, pre-pectoral, pre-pelvic and pre-anal lengths were taken from the snout tip to the dorsal-, pectoral-, pelvic- and anal-fin origin or insertion, respectively. Meristic counts were taken with a binocular Zeiss Stereo Discovery V6, following the methods utilized by Kottelat (1990); the last two branched rays of dorsal and anal fins were counted as one when borne by the same pterygiophore. All morphometric measurements and meristic counts were made on the left side of specimens whenever possible. Vertebral count was taken from X-ray photographs. The Weberian apparatus is considered as including four vertebrae. GraphPad Prism 8 (GraphPad Prism Inc.) was used for the basic statistical analysis on morphometric data. Abbreviations utilized here include: **GL** — gill opening length, **G-P** — distance from the lowest extremity of the gill opening to the pectoral-fin insertion, **HD** — head depth, **PPL** — pre-pectoral length, **PBL** — pectoral-fin base length, and **SL** — standard length.

Geometric morphometric (GM) analyses were utilized, targeted at cephalic contour and mouthpart structures to further distinguish *B. cheni* and *B. damingshanensis*. A total of 20 specimens were examined in GM analyses for each of these two species. Individual specimen was photographed for the head in ventral and lateral views using Capture 2.3 connected to the micro-imaging cameras. The software tpsUtil 1.83 (Rohlf 2015) was used to ordinate the digitalized images in the same file under the TPS format. The tpsDig2 software (Rohlf 2015) was used to record landmarks and semi-landmarks. The different sets and descriptions of landmarks and semi-landmarks (curve points) on the digitized image were illustrated in Fig. 2. The tps curve files were converted to landmarks data in tpsUtil 1.83 (Rohlf 2015). Subsequent data analyses were run using MorphoJ 1.07a software (Klingenberg 2011). A generalized Procrustes analysis (GPA) was conducted to scale landmarks of each specimen to a common body size, rotate each specimen to a common alignment and generate a consensus shape. Principal component analysis (PCA) was performed after checking for outliers and constructing a covariate matrix to better assess and visualize shape variation across all individuals.

DNA extraction, amplification and sequencing

Total genomic DNA was extracted from 95% ethanol-stored fin or muscle tissue samples using TIANamp Genomic DNA Kit (Tiangen Biotech Co., Ltd, Beijing, China) following manufactures' instructions. The mitochondrial cytochrome c oxidase subunit I (COI) gene was chosen for phylogenetic analysis. Two new pairs of specific primers were designed for amplification (COI_F: ATCCTACCTGTGGCAATCAC / COI_R: AATAGGGGRAATCAGTGGAC) and sequencing (COI_F1: GCATCWGTAGACCTRACYATYTT / COI_R1: GCATARTATGCYACGACGTGRG) of the COI region in *Bashimyzon* and its close relatives. This gene was amplified by the polymerase chain reaction (PCR) in 25 µl reactions containing 12.5 µl Master mix Taq (Genesand Biotech Co. Ltd., Beijing, China), 1µl of each primer, 1µl template DNA and 9.5µl double distilled water (dd H_2O).

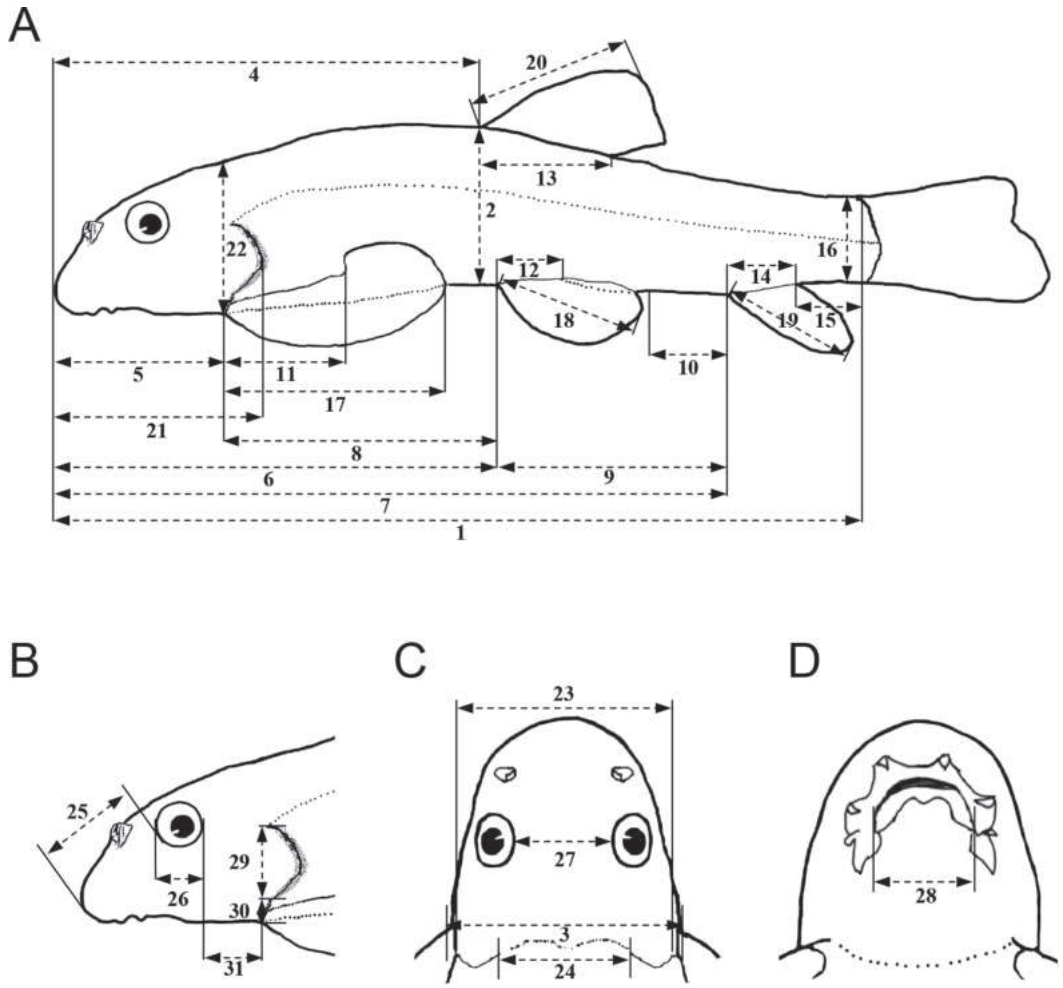

Figure 1. Measurements taken on species of *Bashimyzon* and its relatives. Lateral view of body (**A**), and lateral (**B**), dorsal (**C**) and ventral (**D**) view of head. 1, standard length; 2, body depth; 3, body width crossing pectoral-fin insertions; 4, pre-dorsal length; 5, pre-pectoral length; 6, pre-pelvic length; 7, pre-anal length; 8, distance from pectoral- to pelvic-fin insertion; 9, distance from pelvic-fin insertion to anal-fin origin; 10, distance from anus to anal-fin origin; 11, pectoral-fin base length; 12, pelvic-fin base length; 13, dorsal-fin base length; 14, anal-fin base length; 15, caudal-peduncle length; 16, caudal-peduncle depth; 17, pectoral-fin length; 18, pelvic-fin length; 19, anal-fin length; 20, dorsal-fin length; 21, head length; 22, head depth; 23, head width; 24, width between upper extremities of gill openings; 25, snout length; 26, eye diameter; 27, interorbital width; 28, mouth width; 29, gill opening length; 30, distance from lowest extremity of gill opening to pectoral-fin insertion; 31, distance between posterior edge of eye and vertical through pectoral-fin insertion.

The PCR conditions were given as follows: initial denaturation at 95 °C for 3min followed by 35 cycles of 94 °C for 25s, 54 °C for 25s, and elongation at 72 °C for 45s; and final extension at 72 °C for 5min. Amplified products were stored at 4 °C. The sequencing was done through Aokedingsheng Biotechnology Company (Wuhan, China). All sequences amplified in this study were submitted to GenBank.

Phylogenetic analyses

The amplified 158 gene sequences from six species, namely *E. sinensis* (26), *E. compactus* (two), *E. yangi* (32), *E. kalotaenia* (20), *B. damingshanensis* (43), and *B. cheni* (35), were utilized for molecular phylogenetic analysis along with other seven GenBank-retrieved sequences of the same gene from three outgroups: *Sinogastromyzon tonkinensis* (KY352773), *Vanmanenia pingchowensis* (KP005457) and *Yaoshania pachychilus* (AP012132, KT031050, KX588239, KY352775 and NC030634). Detailed information on specimens used for molecular analysis in this study are given in Table 1. Raw sequences were edited using Seqman in DNAstar (DNAStar Inc., Madison, WI, USA), aligned with Seaview v4.2.5 (Gouy et al. 2010), and checked by eye for some ambiguous alignments. Nucleotide sequences were initially aligned utilizing Clustal X v2.0 (Larkin et al. 2007) with default parameters, and then re-checked visually. The sequence data were translated into amino acids in MEGA v7.0 (Kumar et al. 2016) to confirm the absence of premature stop codons. Then DnaSP v6 (Rozas et al. 2017) was used for genetic diversity analyses and filter the haplotype.

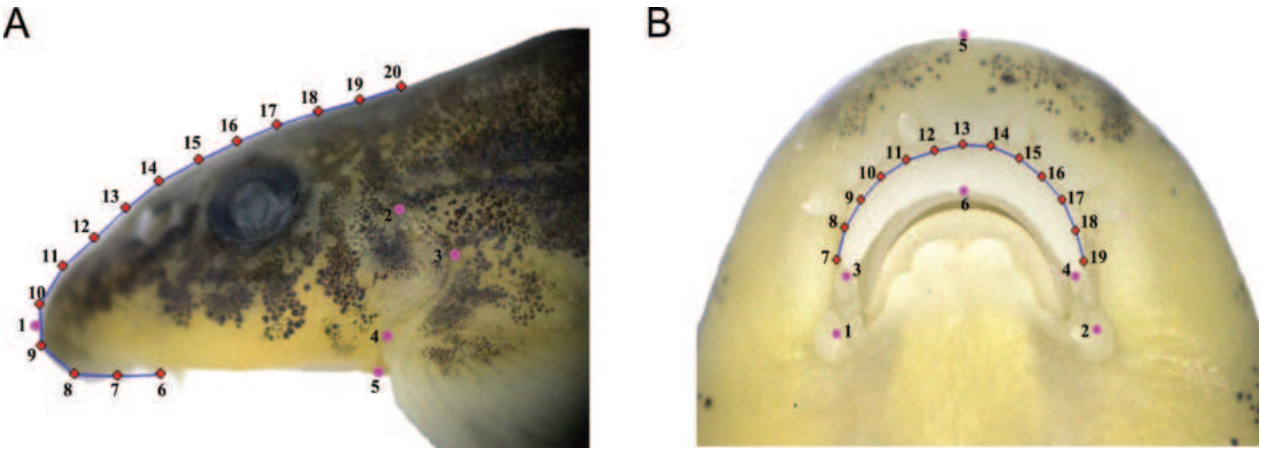

Figure 2. Landmarks (pink dot) and semi-landmarks (red diamond) used in geometric morphometrics. Photographs of *B. cheni*, IHB 202303064716, 42.7 mm SL. **A.** Lateral view of head; 1–5 landmark points (anterior-most tip of snout, topmost, hindmost and lowermost point of gill opening, and pectoral-fin insertion), and 6–20 semi-landmark points to which the curve from the maxillary-barbel root to the posteromedial tip of the supraoccipital was resampled by length; **B.** Ventral view of head; 1–6 landmark points (roots of left and right maxillary barbels, left and right lateral end of upper lip, anterior-most tip of snout, and median point of distal margin of upper lip), and 7–19 semi-landmark points to which the curve between the left and right end of the rostral groove was resampled by length.

Table 1. Detailed information of specimens used for molecular phylogenetic analyses in this study.

Species	N	Specimen voucher	Sampling localities	Haplotypes	GenBank no.
E. sinensis	21	IHB 202203177109, 20, 27–34, 36, 42–46, 51–53, 55–56	Liuding-He, Gui-Jiang, tributary of Zhu-Jiang, Changle Village, Jinxiu County, China	Hap1–6	OR744909–29
	5	IHB 202010049920–24	Lu-Jiang, Gui-Jiang, tributary of Zhu-Jiang, Lujiang Village, Lingchuan County, China	Hap5, 7–9	OR744930–34
E. compactus	2	IHB 01-QN-2023, 02-QN-2023	Ba Che River, Ba Che city, Ba Che District, Quang Ninh Province, Vietnam	Hap10–11	OR744935–36
E. yangi	27	IHB 202203177157–59, 62–85	Meicun-He, Liu-Jiang, tributary of Zhu-Jiang, Meicun Village, Jinxiu County, China	Hap12–15	OR744937–63
	5	IHB 202104053762–66	Shuijing-He, Liu-Jiang, tributary of Zhu-Jiang, Heping Village, Jinxiu County, China	Hap13, 15–16	OR744964–68
E. kalotaenia	18	IHB 202203177107–08, 10–19, 21–26	Liuding-He, Gui-Jiang, tributary of Zhu-Jiang, Changle Village, Jinxiu County, China	Hap17–18	OR744969–86
	2	IHB 202203177160–61	Dishui-He, Gui-Jiang, tributary of Zhu-Jiang, Shibajia Village, Jinxiu County, China	Hap17	OR744987–88
B. damingshanensis	3	IHB 202109136061–63	Qingshui-He, Hongshui-He, tributary of Zhu-Jiang, Shanglin County, China	Hap19	OR744989–91
	40	IHB 202109136064–103	Qingshui-He, Hongshui-He, tributary of Zhu-Jiang, Naxue Village, Dafeng Town, Shanglin County, China	Hap19–20	OR744992–5031
B. cheni	20	IHB 202109136104–23	Wuming-He, You-Jiang, tributary of Zhu-Jiang basin, Xinyang Village, Gulin Town, Mashan County, China	Hap21–22	OR745032–51
	15	IHB 202303064575–89	Wuming-He, You-Jiang, tributary of Zhu-Jiang basin, Jiaobei Village, Liangjiang Town, Wuming District,China	Hap22	OR745052–66

The haplotype sequence matrix was used for subsequent phylogenetic analyses. MrBayes 3.2.2 (Ronquist et al. 2012) was utilized for Bayesian inference (BI) analysis. PartitionFinder v2.1.1 (Lanfear et al. 2017) was used to select the best partitioning strategy and the optimal nucleotide substitution model for the dataset using the Bayesian information criterion (BIC). Three codon partitions and their corresponding substitution model for COI gene sequences were proposed: 1st codon with SYM+I, 2nd with F81+I, and 3rd with GTR+G. Two independent runs were carried out with four Monte Carlo Markov chains (three hot chains and one cold chain) for 20 million generations to calculate posterior probability. Trees were sampled for every 1000 generations. The initial 25% of sampled trees were discarded as burn-in. Convergence of the runs was assessed by the average standard deviation of split frequencies (< 0.01). Partitioned maximum likelihood (ML) analyses were conducted in RAxMLHPC v7.0 (Stamatakis 2006) with the same partitioning strategy as for

Bayesian inference. The more complex model (GTR + I + G) was used for all subsets, and 100 replicates ML inferences were performed with a complete random starting tree. Nodal support for the clades was estimated with 1000 bootstrap pseudoreplicates (Stamatakis et al. 2008). Phylogenetic tree was edited in FigTree v1.4.2 (Rambaut 2009). Additionally, the uncorrected genetic distances (p-distances) between lineages were calculated with MEGA v7.0 (Kumar et al. 2016).

Results

Bashimyzon gen. nov.

https://zoobank.org/1AA6CE02-CC93-4512-9EEC-F9298FF6A3C1
Figs 3D, 5–7

Type species. *Erromyzon damingshanensis* Xiu & Yang, 2017: 893 (type locality: Qingshui-He, tributary to Hongshui-He of Zhu-Jiang basin, in Shanglin County, Guangxi Province)

Diagnosis. *Bashimyzon* is distinct from all currently identified gastromyzontid genera except *Erromyzon* and *Protomyzon* in the presence of a gill opening restricted above pectoral-fin base (vs. gill opening elongate, extending downwards to or beyond the pectoral-fin insertion to the ventral surface of head), and pectoral fins backwards extending away from (vs. close to or beyond) pelvic-fin insertions. This new genus is separated from the two genera in having a larger (vs. small) gap between the posterior edge of eye and the vertical through the pectoral-fin insertion, with the gap length being nearly equal to (vs. less than) eye diameter (Fig. 3; Table 2) and a very small fleshy lobe (vs. a relatively large fleshy lobe or enlarged papillae; see Kottelat 2004: Page 306, figs 4–6, and Yang et al. 2012: Page 176, fig. 3; Table 2) posterior to the maxillary-barbel base.

Other characters useful for distinguishing *Bashimyzon* and *Protomyzon* include: upper and lower lips continuous around the corners of mouth (vs. discontinuous or interrupted by an arched blade-like structure; see Kottelat 2004: Page 306, figs 4–6), lower lip smooth (vs. papillated), and no externally distinct opercle (vs. present) (Table 2).

Bashimyzon is morphologically most similar to *Erromyzo*n, but further differs from it in having a relatively larger (vs. smaller) gill opening (length 46.5–60.7% of HD vs. 25.8–44.9, and the distance from its lower extremity to the pectoral-fin insertion 3.6–16.1% of HD vs. 27.2–43.5; see Figs 3, 4A, B); fewer last branched pectoral-fin rays folded against the flank (3–4 vs. 7–8); and more posteriorly located pectoral fins (pre-pectoral length 17.0–22.3% of SL vs. 12.5–15.8; see Fig. 4C), with a shorter (vs. longer) base (length 8.8–10.8% of SL vs. 13.9–17.4; see Fig. 4D).

Etymology. The generic name is derived from *Bashi* (岜是), the local name of the Damingshan Mountain in Zhuang nationality language, and *myzon*, a common suffix used in the Balitoridae. Gender masculine. The Chinese common generic name is here suggested as "岜是鰍属".

Bashimyzon cheni sp. nov.

https://zoobank.org/8E5656C2-1F1A-4085-962F-45D1594B1D58
Figs 5–7

Type material. ***Holotype*.** IHB 202109064273, 28.3 mm SL; Guangxi Province: Nanning City: Mashan County: Wuming-He, a stream tributary to You-Jiang of Zhu-Jiang basin, at Xinyang Village (23°35'05"N, 108°15'38"E, roughly 237m above sea level) of Gulin Town; collected by X. Gong, D. M. Guo and Y. Liu; 17 September 2021.

***Paratypes*.** IHB 202109064274–78, 5 specimens, 28.3–39.9 mm SL; other data same as holotype. IHB 202303064712–36, 25 specimens, 35.0–42.7 mm SL; Guangxi Province: Nanning City: Wuming District: Wuming-He, a stream tributary to You-Jiang of Zhu-Jiang basin, at Jiaobei Village (23°31'27"N, 108°18'24"E, about 176 m above sea level) of Liangjiang Town; collected by X. Gong, D. M. Guo and P. Shan; 21 March 2023.

Diagnosis. *Bashimyzon cheni* is clearly distinguished from the single congeneric species *B. damingshanensis* in having 8–9 teardrop-shaped black blotches wider than interspaces, with the majority portion of each blotch located above the lateral line on the flank (vs. 12 irregular black bars narrower than interspaces, and located along the lateral line on the flank; see Figs 5, 6); fewer rows of blackish spots

Table 2. Comparison of diagnostic characters among *Bashimyzon* gen. nov. and other related genera.

	***Protomyzon* auct.**	***Erromyzon* s.str.**	***Bashimyzon* gen. nov.**
Gap between posterior edge of eye and vertical through pectoral-fin insertion	small	small	large
Arched blade-like structure between upper and lower lip	present; upper and lower lip interrupted	absent; upper and lower lip continuous	absent; upper and lower lip continuous
Lower lip	papillated (except for *P. aphelocheilus*)	smooth	smooth
Externally opercle	present	absent	absent
Gill opening	restricted to a small slit above pectoral-fin base (except for *P. whiteheadi* and *P. griswoldi*)	restricted to a small slit above pectoral-fin base	larger with its lower extremity stopping short of the pectoral-fin base
Structure posterior to each maxillary barbel	enlarged papillae	a large fleshy lobe	a very small fleshy lobe

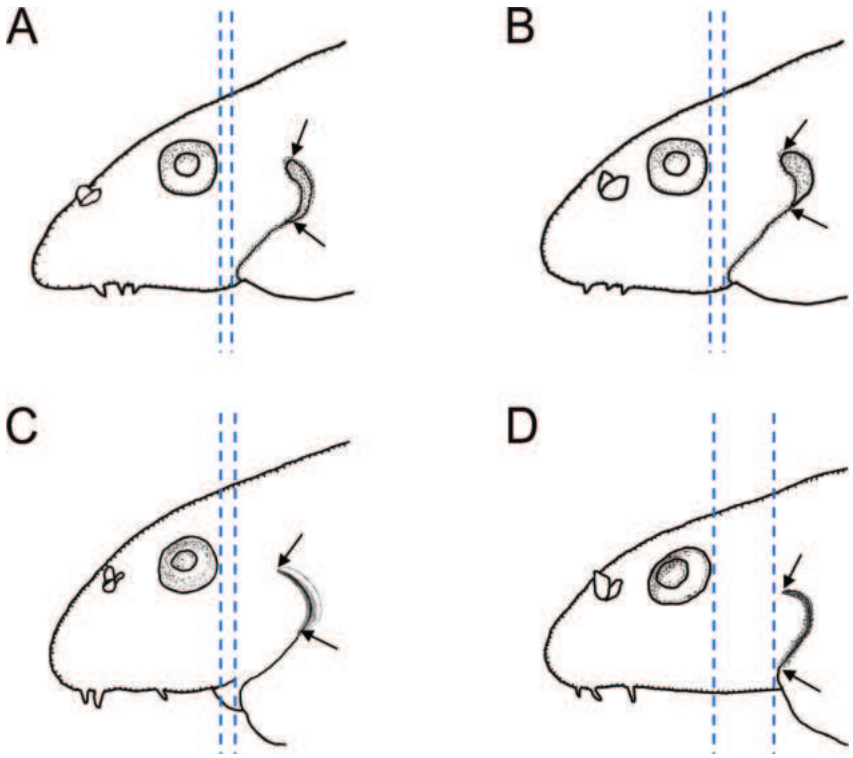

Figure 3. Lateral views of heads for: *Protomyzon aphelocheilus* (**A**), *Protomyzon borneensis* (**B**), *Erromyzon sinensis* (**C**), and *Bashimyzon damingshanensis* (**D**). Arrows indicate extremities of gill openings, and blue dotted lines pass vertically through the pectoral-fin insertion and the posterior margin of eye, respectively.

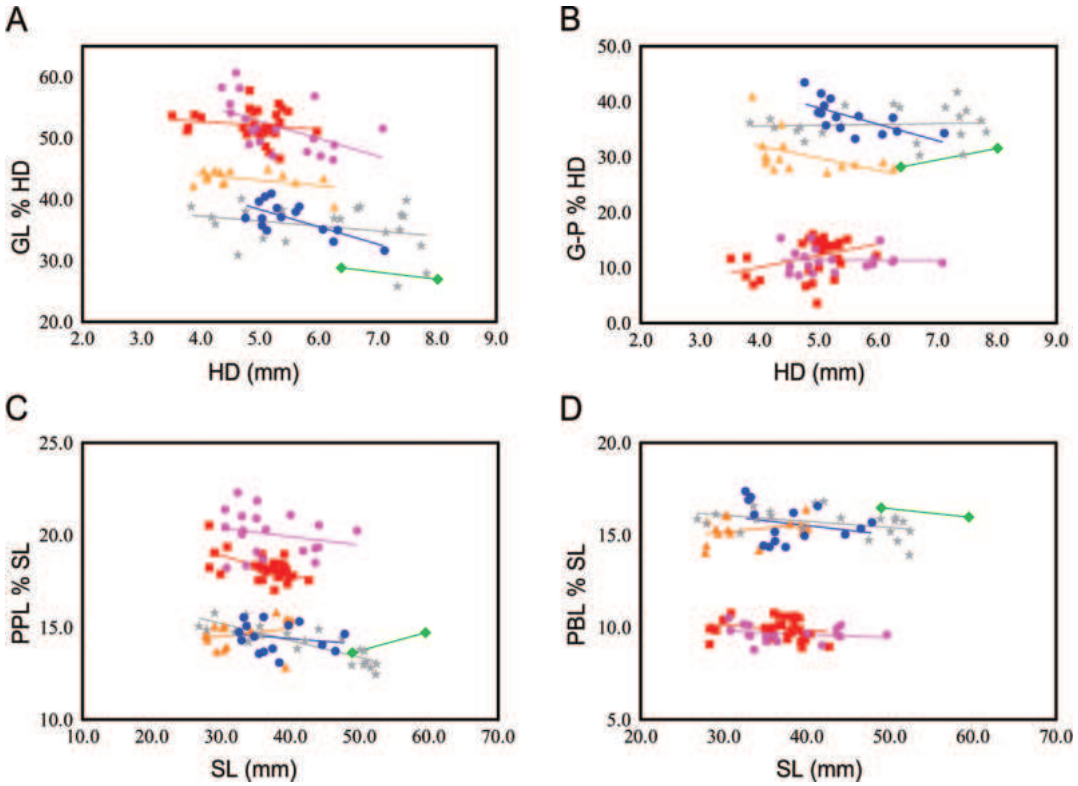

Figure 4. Comparisons (linear regression) of some morphometric measurements between sampled species of *Erromyzon* [*E. sinensis* (blue dot), *E. compactus* (green diamond), *E. yangi* (grey star), and *E. kalotaenia* (yellow triangle)] and *Bashimyzon* [*B. damingshanensis* (ponk dot) and *B. cheni* (red square)]. **A.** Between GL% of HD and HD; **B.** Between G-P% of HD and HD; **C.** Between PPL% of SL and SL; and **D.** Between PBL% of SL and SL. **GL**—gill opening length; **G-P**—distance from the lowest extremity of gill opening to the pectoral-fin insertion; **HD**—head depth; **PPL**—pre-pectoral length; **PBL**—pectoral-fin base length; **SL**—standard length.

Figure 5. Dorsal (top), lateral (middle) and ventral (bottom) views of body in *B. cheni*, IHB 202109064273, holotype, 28.3 mm SL; China: Guangxi Province: Nanning City: Mashan County: Wuming-He, a stream tributary to You-Jiang of Zhu-Jiang basin, at Xinyang Village of Gulin Town.

across dorsal-fin rays (3 vs. 4); fewer lateral-line pored scales (84–86 vs. 88–95); a gradual (vs. abrupt) upward dorsal profile of head in front of nostrils (Fig. 8A); a deeply (vs. slightly) curved rostral groove, or the greater (vs. less) distance from the median point of the distal margin of the upper lip to the anterior-most tip of the snout than half of the mouth width (Fig. 8B), a distinct (vs. indistinct) incision on both side of the fleshy pad of the lower lip (Figs 2B, 7).

Description. General body shape and appearance illustrated in Figs 5, 6 and lateral view of head in Fig. 7. Morphometric measurements and meristic counts provided in Table 3. Body moderately elongate, anteriorly nearly cylindrical, slightly deeper than wide or both equal, and posteriorly compressed laterally, with greatest depth at dorsal-fin origin, and greatest width at middle of pectoral-fin base. Caudal peduncle stout, deeper than long, with minimum caudal-peduncle depth closer to caudal-fin base. Dorsal profile of head gradually rising from anterior-most tip of snout to posterior end of supraoccipital and predorsal body slightly convex or straight; dorsal profile of dorsal-fin base and post-dorsal body slightly concave. Ventral profile of head straight, then slightly convex from pectoral-fin insertion to anal-fin origin, and evenly rising towards caudal-fin base.

Head longer than deep, and shallower than wide. Snout broadly rounded in dorsal view and obtuse in lateral view, nearly equal to postorbital head. Eyes small, situated dorsolaterally in half of head, with broad and slightly flat interorbital space. Anterior and posterior nostrils close together, and short tubular flap on anterior nostril. Mouth small, inferior and arched in ventral view. Rostral fold modified into three rounded, fleshy lobes; median one wider than or equal to two lateral ones, separated from upper lip by distinct shallow groove. Lips fleshy and smooth; upper lip broad and curved, reflected on base of upper jaw; lower lip restricted to corners of mouth.

Table 3. Morphometric data for *Bashimyzon cheni* gen. et sp. nov.

	Holotype	Paratypes (n = 30)			
		Min	Max	Mean	SD
Morphometric measurements					
Standard length (mm)	28.3	28.3	42.7	36.8	3.4
% Standard length					
Pre-dorsal length	48.9	45.7	50.9	48.6	1.4
Pre-pectoral length	18.2	17.0	20.5	18.23	0.69
Pre-pelvic length	50.0	50.3	55.3	52.3	1.2
Pre-anal length	81.3	79.5	85.4	81.6	1.4
Distance between pectoral- and pelvic-fin insertion	33.2	32.0	46.5	34.7	2.7
Distance from pelvic-fin insertion to anal-fin origin	29.7	26.5	31.2	28.9	1.1
Distance from anus to anal-fin origin	8.5	7.3	11.4	9.8	1.0
Body depth	16.5	15.5	21.2	18.3	1.5
Body width	17.9	17.2	19.3	18.2	0.6
Caudal-peduncle length	9.7	8.4	11.7	10.0	0.8
Caudal-peduncle depth	11.4	9.9	12.2	10.9	0.6
Head length	21.3	19.4	23.2	21.3	0.7
Head depth	13.8	12.3	14.9	13.4	0.6
Head width	17.2	14.6	17.9	16.6	0.7
Snout length	9.5	9.4	11.9	10.7	0.5
% Head length					
Snout length	44.5	44.1	56.5	50.3	2.5
Eye diameter	25.7	21.6	29.6	24.7	2.0
Interorbital width	49.0	36.9	49.3	42.8	3.0
Dorsal-fin base length	48.8	47.6	62.6	54.4	3.8
Pectoral-fin base length	46.5	41.7	50.8	46.8	2.7
Pelvic-fin base length	23.2	20.3	26.5	24.1	1.6
Anal-fin base length	19.5	22.7	31.4	28.2	2.3
Dorsal-fin length	84.8	80.7	100.8	93.7	4.2
Pectoral-fin length	123.2	109.8	134.0	123.6	5.5
Pelvic-fin length	78.6	79.4	97.4	87.8	4.4
Anal-fin length	60.6	59.3	77.8	70.3	3.9
Distance between the posterior margin of eye and the vertical through the pectoral-fin insertion	18.4	16.0	22.3	18.6	1.6
% Body width crossing pectoral-fin insertions					
Mouth width	33.6	27.6	38.9	31.4	2.3
Width between upper extremities of gill openings	88.7	79.9	92.8	86.4	3.0
% Caudal-peduncle length					
Caudal-peduncle depth	117.5	100.5	123.7	109.5	6.9
% Head depth					
Distance from lowest extremity of gill opening to pectoral-fin insertion	6.9	3.6	16.1	12.2	3.2
Gill opening length	53.9	46.6	57.8	52.1	2.4
% Eye diameter					
Gill opening length	135.5	109.9	160.3	133.5	11.3
Distance from lowest extremity of gill opening to pectoral-fin insertion	17.4	9.5	43.2	31.4	9.0
Meristic counts					
Dorsal-fin rays	iii, 7	iii, 7			
Anal-fin rays	ii, 5	ii, 5			
Pectoral-fin rays	i, 15	i, 15			
Pelvic-fin rays	i, 7	i, 7–8			
Lateral line scales	85	84–86			
Vertebrae	29	29–30			

Upper and lower lips continuous around corner of mouth, with small notch on confluence between both anterior to corners of mouth. A small papilla present on this notch, but indistinct in some individuals. Postlabial groove widely interrupted, or short and restricted only to corners of mouth, so leaving an anteriorly bilobed median fleshy pad on chin. A distinct incision also on both side of the fleshy pad. Upper and lower jaws bearing thick,

Figure 6. Lateral view of freshly captured individual of **A.** *B. damingshanensis*, IHB 202109064259, topotype, 30.8 mm SL; China: Guangxi Province: Shanglin County: Qingshui-He at Naxue Village of Dafeng Town; and **B.** *B. cheni*, IHB 202109064273, holotype, 28.3 mm SL; China: Guangxi Province: Mashan County: Wuming-He at Xinyang Village of Gulin Town.

flexible horny sheaths on cutting edges. Lower jaw largely exposed. Two pairs of rostral barbels; outer pair larger than inner pair. Maxillary-barbel pair rooted at corners of mouth, longer than rostral-barbel pair. A very small fleshy lobe posterior to maxillary barbel present on lower lip. Gill opening relatively large above pectoral-fin base, with its lower extremity extending away from the pectoral-fin insertion.

Scales minute, cycloid. Lateral line complete, with 84–86 pored scales, slightly curved upwards about half of pectoral-fin length, then downwards to posterior end of anal-fin base, extending along middle of caudal-peduncle to caudal-fin base. No scales on head, abdomen adjacent to ventral midline extending for three-fourths of distance between pectoral- to pelvic-fin insertions, and post-pelvic ventral region in front of anus. Numerous small tubercles densely distributed in suborbital portions of head and sides of snout; not obvious in other areas of body. Vertebrae 4+29–30.

Dorsal fin with three unbranched and seven branched rays; distal margin truncate or straight; origin anterior to pelvic-fin insertion, and closer to caudal-fin base than to snout tip. Pectoral fins with three unbranched and seven branched rays, enlarged and expanded laterally, longer than head; inserted slightly in front of lowest extremity of gill opening; tip of adpressed fin extending away from pelvic-fin insertion; last three or four branched rays folded dorsally against flank, shorter than others. Gap between posterior margin of eye and vertical through pectoral-fin insertion nearly equal to eye diameter. Pelvic fins short and not fused, with one unbranched and seven or eight branched rays; inserted slightly closer to caudal-fin base than to snout tip; tip of adpressed fin reaching anus, but far away from anal-fin origin. Anal fin with two unbranched and five branched rays; distal margin truncate; origin closer to caudal-fin base than to pelvic-fin insertion; and tip of adpressed fin reaching caudal-fin base. Anus located midway from posterior end of pelvic-fin base to anal-fin origin or slightly behind. Caudal-fin emarginated, lower lobe slightly longer than upper lobe.

Coloration. In freshly-captured specimens, background of body yellowish or whitish yellow, with 8–9 vertical brown blotches of variable size on flank, oblong prodorsally and teardrop-shaped below dorsal-fin base and postdorsally (Fig. 6B). In formalin-stored individuals, body faded to lighter brown. Blotches on flank only 2/3 of body depth, wider than interspaces, and interrupted on dorsum. Dorsal surface of body covered

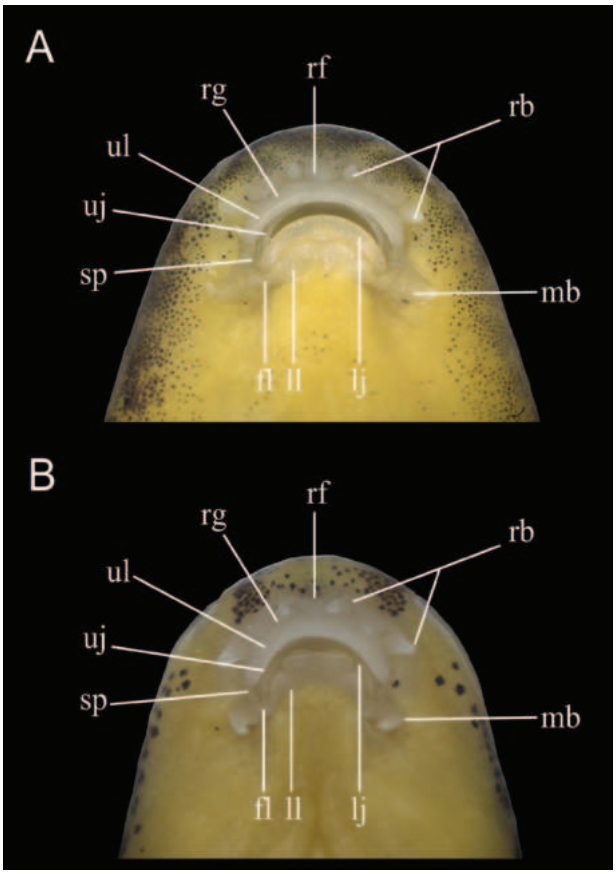

Figure 7. Ventral view of mouth in **A.** *B. damingshanensis*, IHB 202109064259, topotype, 30.8 mm SL; **B.** *B. cheni*, IHB 202109064273, holotype, 28.3 mm SL. **fl**— flesh lobe; **lj**—lower jaw; **ll**—lower lip; **mb**—maxillary barbel; **rg**—rostral groove; **rf**—rostral fold; **rb**—rostral barbels; **sp**—small papilla; **uj**—upper jaw; **ul**—upper lip.

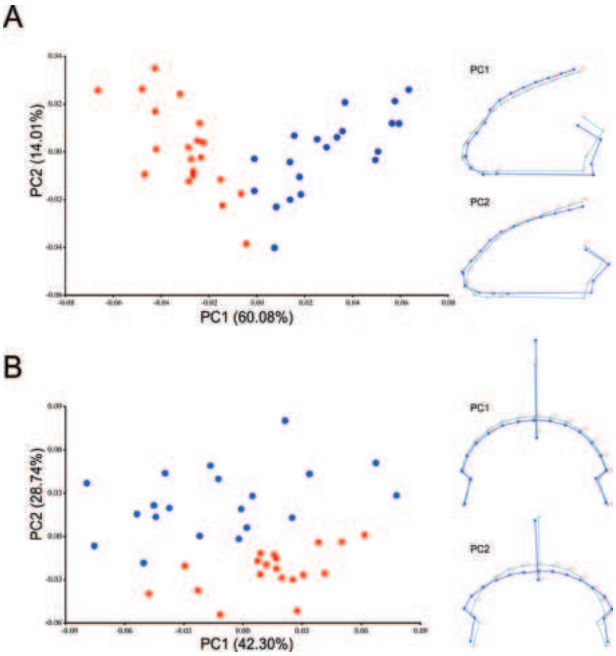

Figure 8. Scatterplots for the first two principal components (PC1 and PC2) of *B. cheni* (red dot) and *B. damingshanensis* (blue dot) principal component analyses for contours of the lateral head (**A**) and mouth-part structures (**B**).

with 7–8 dark elliptical patches along dorsal midline; predorsal patches usually linked to each other. Body pale yellowish-cream on ventral and ventrolateral surfaces, with some small blackish blotches located above pelvic-fin base. Pectoral-fin base lightly speckled with three to four irregular dark brown spots; pelvic fins and anal fin hyaline. Three rows of blackish spots on dorsal-fin rays, and two or three rows on caudal-fin rays; a relatively large black bar at caudal-fin base. Sides of head yellowish brown to black, with dark brown vermiculations visible.

Distribution and habitat. *Bashimyzon cheni* is so far known from the Wuming-He, a stream tributary to the You-Jiang discharging into the Xi-Jiang of the Zhu-Jiang basin, in Guangxi Province, China (Fig. 9). It was caught in shallow fast-flowing waters, at depths of 0.2–0.8 m, with a mixed bottom substrate of boulders, cobbles, and sands (Fig. 10). Coexisting species included *Opsariichthys bidens*, *Osteochilus salsburyi*, *Schistura fasciolata*, *Traccatichthys pulcher*, *Mystus guttatus*, *Glyptothorax fokiensis*, and *Mastacembelus armatus*.

Etymology. The specific epithet is named after Prof. Chen Yi-Yu, a Chinese Academician, in honor for his great contribution to Chinese freshwater fish research. In particular, he discovered and named the type species of *Erromyzon* and *Yaoshania*, which are two close relatives of the genus under description. The Chinese common specific name "陈氏岜是鳅" is here suggested.

Sequence variation and molecular phylogeny

A total of 158 COI gene sequences of 1167 bp (base pair) in length from all four species of *Erromyzon*, and two species of *Bashimyzon* were amplified in this study (Table 1). These sequences were used for molecular phylogenetic analysis together with three outgroups: *Sinogastromyzon tonkinensis* (one), *Vanmanenia pingchowensis* (one), and *Yaoshania pachychilus* (five). Twenty-seven haplotypes (22 and five, respectively for ingroups and outgroups) were detected from the sequences (Table 1). The haplotype sequences matrix consisted of 833 conserved sites, 334 variable sites, 259 parsimony informative sites and 75 singleton sites. The nucleotide frequencies were 25.2% (A), 29.4% (T), 25.8% (C), and 19.5% (G).

Given that BI and ML analyses produced overall identical topologies, only the BI tree with Bayesian posterior probabilities (PP) and bootstrap support (BS) value were presented in Fig. 11. From the tree topologies, samples of *B. cheni* were strongly supported (PP = 1.0 / BS = 100) to group into a lineage further forming a well-supported (PP = 1.0 / BS = 100) clade together with those of *B. damingshanensis*. *Bashimyzon* was weakly supported (PP = 0.57 / BS = 51) to stand as the sister group consisting of sampled species of *Erromyzon* (*E. sinensis*, *E. compactus*, *E. yangi* and *E. kalotaenia*). The two genera together were highly supported (PP = 1.0 / BS = 94) to be sister of *Yaoshania*.

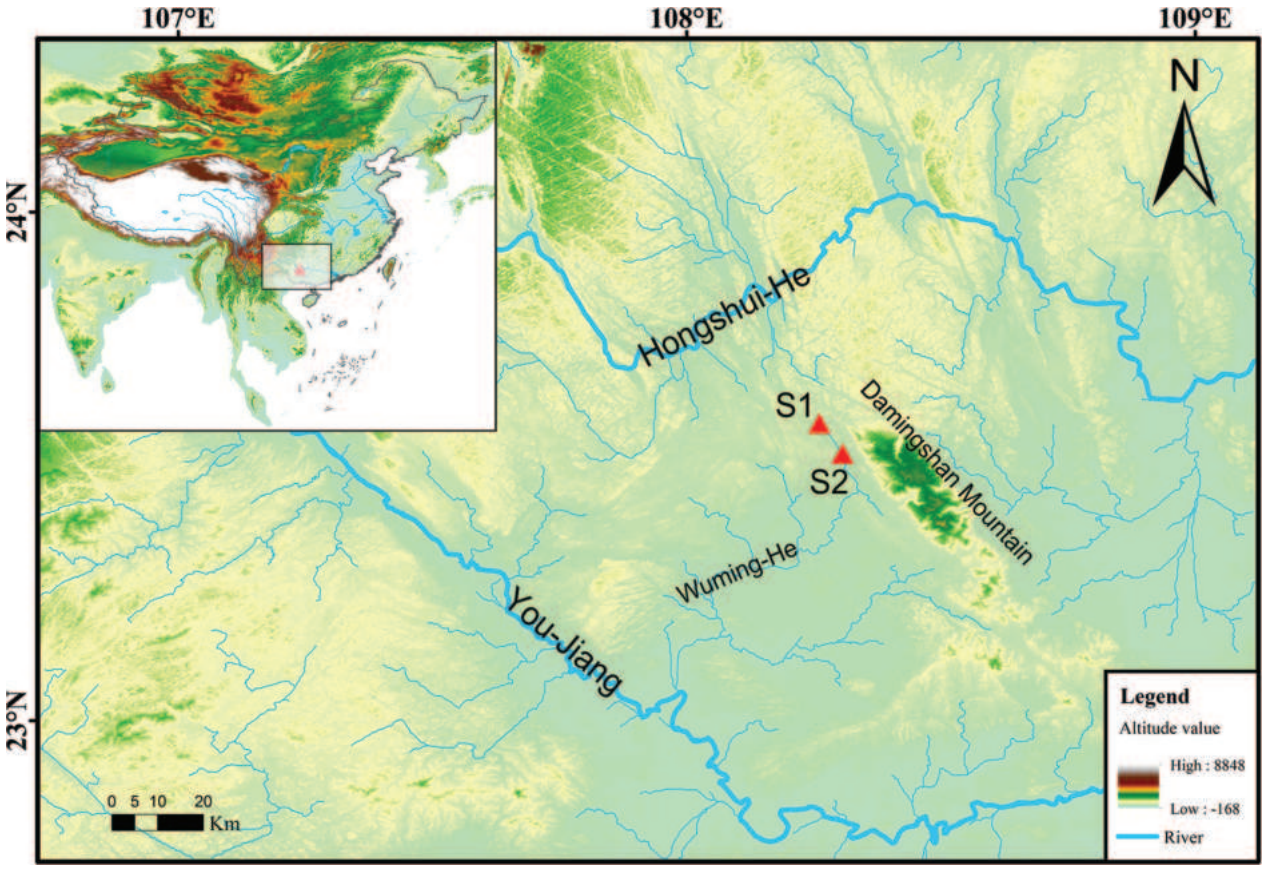

Figure 9. Map showing the two sampling sites of the type specimens of *B. cheni*. S1, Xinyang Village, Gulin Town, Mashan County, and S2, Jiaobei Village, Liangjiang Town, Wuming District, Nanning City, Guangxi Province, P. R. China.

Figure 10. Sampling locality of the holotype (IHB 202109064273) of *B. cheni* in the Wuming-He, tributary to the You-Jiang in Xinyang Village, Gulin Town, Mashan County, Nanning City, Guangxi Province, P. R. China; 17 September 2021, photographed by Yi Liu.

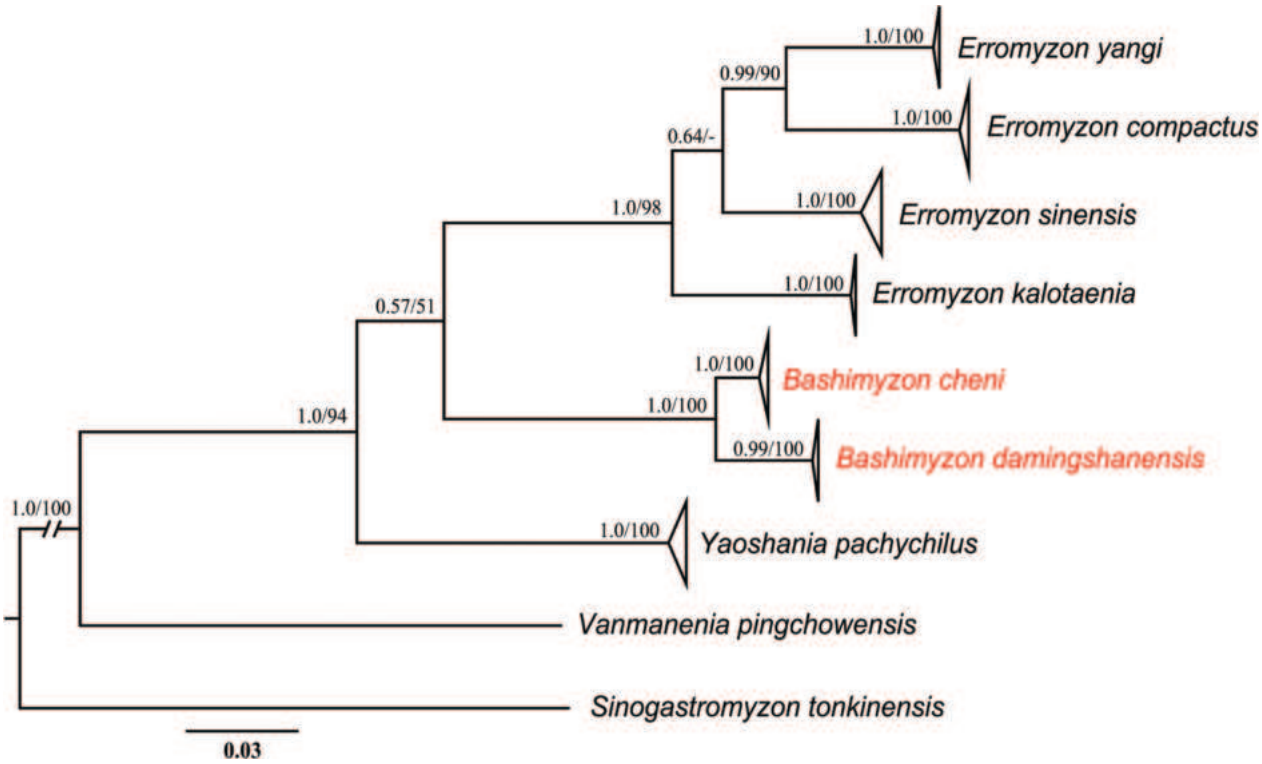

Figure 11. Bayesian Inference tree derived from the mitochondrial COI gene for seven analyzed species of three genera (*Erromyzon*, *Bashimyzon*, and *Yaoshania*). Bayesian posterior probabilities (> 0.5), and maximum likelihood bootstrap values (> 50%) are shown, respectively. Dash represents a node with bootstrap support lower than 50%.

The genetic distances (p-distances) within and between genera were provided in Table 4. Intraspecific genetic distances were 0.03–0.26%, 0.0–0.01%, and 0.19% for sampled species of *Erromyzon*, *Bashimyzon* and *Yaoshania*, respectively. Interspecific genetic distances were 6–8% for *Erromyzon*, 3% for *Bashimyzon* and NA for *Yaoshania* (not available owing to the fact that it is a monotypic genus). The intergeneric genetic distances here calculated were 10–12% (*Bashimyzon* / *Erromyzon*), 10% (*Bashimyzon* / *Yaoshania*), and 11–12% (*Yaoshania* / *Erromyzon*), respectively.

Table 4. Genetic distances (uncorrected p-distance) of COI gene computed by MEGA v7.0 amongst 7 species of *Erromyzon*, *Bashimyzon* and *Yaoshania*.

Species	Within Group	1	2	3	4	5	6
1. *E. sinensis*	0.0021						
2. *E. compactus*	0.0026	0.07					
3. *E. yangi*	0.0008	0.07	0.06				
4. *E. kalotaenia*	0.0003	0.07	0.08	0.07			
5. *B. damingshanensis*	0.0000	0.11	0.12	0.11	0.11		
6. *B. cheni*	0.0001	0.10	0.12	0.10	0.10	0.03	
7. *Y. pachychilus*	0.0019	0.11	0.12	0.12	0.11	0.10	0.10

Discussion

It has been widely recognized that gill-opening size and pectoral-fin extension are of taxonomic importance at the generic level for the Gastromyzontidae (Pellegrin and Fang 1935; Chen 1980b; Kottelat 2004). On the basis of the two characters, the family is subdivided into four groups. The first group is composed of *Annamia* Hora, 1932, *Formosania* Oshima, 1919, *Glaniopsis* Boulenger, 1899, *Katibasia* Kottelat, 2004, *Liniparhomaloptera* Fang, 1935, *Parhomaloptera* Vaillant, 1902, *Plesiomyzon* Zheng & Chen, 1980 and *Vanmanenia* Hora, 1932. These eight genera possess a large gill opening extending downwards beyond the pectoral-fin insertion to the ventral surface of head. The second group, comprising *Paraprotomyzon* s. str. and *Yaoshania*, have an intermediate gill opening extending downwards to but not beyond the pectoral-fin insertion to the ventral surface of head. The third group consists of *Beaufortia* Hora, 1932, *Engkaria* Tan, 2021, *Gastromyzon* Günther, 1874, *Hypergastromyzon* Roberts, 1989, *Labigastromyzon* Tang & Chen, 1996, *Neogastromyzon* Popta, 1905, *Pseudogastromyzon* Nichols, 1925, and *Sewellia* Hora, 1932, all of them having a gill opening restricted only to a very small slit above the pectoral-fin base, and pectoral fins extending backwards beyond or close to pelvic-fin insertions. The fourth group has a relatively small gill opening above the pectoral-fin base and pectoral fins extending backwards away from pelvic-fin insertions, two characters shared with other two genera (*Erromyzon* and *Protomyzon* auct.) and also with *Bashimyzon* herein described.

Only two species are referred to *Bashimyzon*: *B. damingshanensis* (Xiu & Yang, 2017) and *B. cheni* here described. The former was previously placed in *Erromyzon*, a genus

erected to include a Chinese species formerly misidentified in *Protomyzon* and a new species of northeastern Vietnam (Kottelat 2004). Also misplaced in *Protomyzon* was the type species of *Yaoshania* in Chinese literature. From Kottelat's (2004) point of view, the species was unlikely to be the member of either *Protomyzon* or *Erromyzon*. It was later utilized as the type species to erect *Yaoshania* (Yang et al. 2012). Its generic status was confirmed in Shi et al.'s (2018) molecular phylogenetic analysis based on complete mitochondrial genomes for the superfamily Cobitoidea. Our study demonstrated that *Y. pachychilus* had a minimum genetic distance of 11% with *E. kalotaenia* and *E. sinensis* for the COI gene. And the maximum genetic distances of two species of *Bashimyzon* were 12% with *E. compactus*. The congeneric recognition of these species would make the maximum interspecific genetic distance (12%) of *Erromyzon* s.l. slightly greater than the minimum one between *Yaoshania* and *Erromyzon* (11%) (Table 4). Apparently, the generic status of *Bashimyzon* is justified, particularly given its monophyletic nature (see Fig. 11) and the current recognition of *Erromyzon* and *Yaoshania*, two closely allied monophyletic groups, as two distinct genera (Shi et al. 2018).

The erection of *Bashimyzon* as a new genus highlights the need to scrutinize the classification of currently identified species of *Paraprotomyzon* s.l., which was initially erected by Pellegrin and Fang (1935) to accommodate a new species *P. multifasciatus*. The original description of this species stated that it possesses a large gill opening extending downwards close to, but not beyond, the pectoral-fin insertion. However, all other currently identified species of *Paraprotomyzon*, namely *P. bamaensis* Tang, 1997, *P. lungkowensis* Xie, Yang & Gong, 1984, *P. niulanjiangensis* Lu, Lu & Mao, 2005, and *P. yunnanensis* Li, Mao, Lu, Sun & Lu, 1998, have a gill opening only restricted to a small slit above the pectoral-fin base (see Xie et al. 1984; Lu et al. 2005). Moreover, marked differences in mouth-part structures are also found between *P. multifasciatus* and these congeneric species (Tang and Chen 2000). It is more likely that these four species represent their own genus, and *Paraprotomyzon* is actually a monotypic genus.

The constituent species of *Protomyzon* also needs strict scrutiny. The type species of this genus (*P. whiteheadi* Vaillant, 1893) shares with *P. griswoldi* (Hora & Jayaram, 1952) the presence of a relatively large gill opening extending downwards close to but not beyond the pectoral-fin insertion (see Vaillant 1893; Hora and Jayaram 1950, 1952). However, a gill opening restricted to a small slit above the pectoral-fin base is exhibited by the other two congeners: *P. aphelocheilus* Inger & Chin, 1962 and *P. borneensis* Hora & Jayaram, 1952. Given the generic-level taxonomic importance of gill-opening size revealed by Yang et al. (2012) and also in this study, *P. whiteheadi* and *P. griswoldi* likely belong to a distinct genus, and the taxonomy of *Protomyzon* needs further study in the future.

The genetic distance between *B. damingshanensis* and *B. cheni* (3%) is greater than 2%, a threshold used for vertebrates' species delimitation (Avise and Walker 1999; Hebert et al. 2003), thus supporting the recognition of *B. cheni* as a valid species. The discovery of this new species has also conservation implications. As pointed by Tan (2006), the torrent loaches of Borneo usually have a restricted distribution; a single species is often restricted only to a single stream. Their restricted distribution makes these rheophilic fishes susceptible to anthropogenic interferences. This is the case for *B. cheni*. In terms of our observation in the fieldworks, the new species has a large number of individuals currently confined only to a stream tributary to the Wuming-He in Guangxi Province of southern China. The stream drains through two scenic spots—Damingshan Mountain and Jinlun Cave. The rapid development of local tourism industry is predicted to have adverse impacts on species diversity of freshwater fishes and aquatic ecosystem. Due to the construction of many weirs across the Wuming-He for agricultural irrigation, habitats of this new species are fragmented. Its survival is thus put under threat from touristic industry and agriculture. In addition, the new species exhibited an extremely low genetic diversity. Only two haplotypes were detected from a total of 35 COI gene sequences of 1167 bp in length; the haplotype diversity (Hd) was 0.0571 and nucleotide diversity (Pi) was 0.00010 within the Wuming-He population (unpublished data). The presence of this new species, with fragmented populations and low genetic diversity, in a single stream can reduce its evolutionary potential and increase the risk of extinction in the wild. Therefore, conservation efforts should be taken to preserve *B. cheni*.

So far, *B. cheni* occurs in a stream with its source in the southwestern slope of the Damingshan Mountain, and so does *B. damingshanensis* in its northeastern slope. The allopatric distribution of this sister pair suggests that the uplift of the Damingshan Mountain has been acting as the driving force of speciation between both. In such a small scale, mountain build-up plays a crucial role in speciation of these two species. Given that the species of *Erromyzon* also have a montane distribution, it is speculated that the species diversity of the genus in China is underestimated. More in-depth taxonomic research is urgently required for widespread species such as *E. sinensis*.

Comparative material

Erromyzon sinensis: IHB 75-IV-2572–2574, 75-IV-2579, 75-IV-2581, 5 specimens, syntypes, 33.9–53.3 mm SL, Xiuren Town, Lipu County, Guilin City, Guangxi Province, China; IHB 75-V-2804, 1 specimen, syntype, 30.3 mm SL, Lipu County, Guilin City, Guangxi Province, China; IHB 202203064279–88, 10 specimens, 32.63–38.40 mm SL, Liuding-He, Gui-Jiang, tributary of Zhu-Jiang, Changle Village, Jinxiu County, Laibin City, Guangxi Province, China; IHB 202010051119–23, 5 specimens, 39.74–47.85 mm SL, Lu-Jiang, Gui-Jiang, tributary of Zhu-Jiang, Lujiang Village, Lingchuan County, Guilin City, Guangxi Province, China.

Erromyzon compactus: ZRC 49636, holotype, 30.8 mm SL, Ba Che River, a river that flows independently into the sea, Ba Che City, Ba Che District, Quang Ninh Province, Vietnam (photograph examined); IHB 01-QN-2023, 02-QN-2023, 2 specimens, 48.95–59.52 mm SL, other data same as the holotype.

Erromyzon yangi: KIZ 200304423, holotype, 42.8 mm SL, Meicun-He, Liu-Jiang, tributary of Zhu-Jiang, Meicun Village, Jinxiu County, Laibin City, Guangxi Province, China; KIZ 200304422, 2003004424, 2 specimens, paratypes, 36.7–37.1 mm SL, other data same as holotype; IHB 2017056658–61, 2017056678–83, 10 specimens, 26.83–47.47 mm SL, other data same as holotype; IHB 202104052295–99, 202203064413–18, 11 specimens, 41.02–52.45 mm SL, Shuijing-He, Liu-Jiang, tributary of Zhu-Jiang, Heping Village, Jinxiu Town, Jinxiu County, Laibin City, Guangxi Province, China.

Erromyzon kalotaenia: KIZ 200304310, holotype, 41.3 mm SL, Liuding-He, Gui-Jiang, tributary of Zhu-Jiang, Changle Village, Jinxiu County, Laibin City, Guangxi Province, China; KIZ 200304313–14, 200304317, 3 specimens, paratypes, 46.9–47.9 mm SL, other data same as holotype; KIZ 200304049–52, 200304071, 5 specimens, paratypes, 32.4–45.8 mm SL, Dishui-He, Gui-Jiang, tributary of Zhu-Jiang, Shibajia Village, Jinxiu County, Laibin City, Guangxi Province, China; IHB 202203064289–4303, 15 specimens, 27.78–40.13 mm SL, other data same as holotype.

Bashimyzon damingshanensis: KIZ 2014091301, holotype, 48.2 mm SL, Qingshui-He, Hongshui-He, tributary of Zhu-Jiang, Naxue Village, Dafeng Town, Shanglin County, Nanning City, Guangxi Province, China; KIZ2014091302, 2014091304–08, 5 specimens, paratypes, 43.8–47.3 mm SL, same data as the holotype (photograph examined); IHB 202109064253–4272, 20 specimens, 30.57–49.65 mm SL, other data same as the holotype.

Ethics approval and consent to participate

All procedures described in this paper were in accordance with Chinese laws and were licensed by the Ministry of Ecology and Environment of the People's Republic of China.

Availability of data and material

The datasets used and/or analyzed during the current study are available from the corresponding author on reasonable request.

Competing interests

The authors declare that they have no competing interests.

Funding

This work was supported by the special foundation for Natural Science and Technology Basic Research Program of China (2019FY101900) and a grant from the National Natural Science Foundation of China (NSFC No. 31872200).

Authors' contributions

Xiong Gong conceived the study and conducted the data analysis. Xiong Gong led the writing and E Zhang revised the manuscript. All authors contributed to the writing of the paper.

Acknowledgements

Our sincere thanks should be given to Dinh Tao Nguyen, Liang Cao, Chang-Ting An, Wen-Jing Yi, ABELNEH Y. MELAKU, Xiao Chen, Shu-Qing Deng, Wei-Han Shao, Zi-Tong Wang, Dong-Ming Guo, Yi Liu, Man Wang, Chu-Yi Zhang, Peng Shan and Xue Bai for fieldworks and some laboratory analysis. We are grateful to the collection of Kunming Institute of Zoology, Chinese Academy of Sciences for the support and help in examining the collection. This article benefited greatly from insightful comments by the Editors and four anonymous reviewers.

References

Avise JC, Walker D (1999) Species realities and numbers in sexual vertebrates: Perspectives from an asexually transmitted genome. Proceedings of the National Academy of Sciences of the United States of America 96(3): 992–995. https://doi.org/10.1073/pnas.96.3.992

Boulenger GA (1899) Descriptions of two new homalopteroid fishes from Borneo. Annals & Magazine of Natural History 4(21): 228–229. https://doi.org/10.1080/00222939908678188

Chen YY (1978) Systematic studies on the fishes of the family Homalopteridae of China I. Classification of the fishes of the subfamily Homalopterinae. Acta Hydrobiologica Sinica 6(3): 331–348. [in Chinese with English abstract]

Chen YY (1980a) Systematic studies on the fishes of the family Homalopteridae of China II. Classification of the fishes of the subfamily Gastromyzoninae. Acta Hydrobiologica Sinica 7(1): 95–120. [in Chinese with English abstract]

Chen YY (1980b) Systematic studies on the fishes of the family Homalopteridae of China III. Phyletic studies of the Homalopterid fishes. Acta Zootaxonomica Sinica 5(2): 200–211. [in Chinese with English abstract]

Chen YY, Tang WQ (2000) Homalopteridae. In: Yue PQ (Ed.) Fauna Sinica (Osteichthyes: Cypriniformes III). Science Press, Beijing, 438–567. [In Chinese]

Chen M, Zhang CG (2006) Homalopteridae. In: Fisheries Research Institute of Guangxi Zhuang Autonomous Region (Eds) Freshwater Fishes from Guangxi, China (2nd edn.). Guangxi People's Publishing House, Nanning, 357–383. [In Chinese]

Chen YY, Zheng CY (1989) Homalopteridae. In: Zheng CY (Eds) Fishes of the Zhujiang River. Science Press, Beijing, 240–268. [In Chinese]

Chen JC, Chen YY, Tang WQ, Lei HT, Yang JQ, Song XJ (2023) Resolving phylogenetic relationships and taxonomic revision in the *Pseudogastromyzon* (Cypriniformes, Gastromyzonidae) genus: Molecular and morphological evidence for a new genus, *Labigastromyzon*. Integrative Zoology 00: 1–22. https://doi.org/10.1111/1749-4877.12761

Fang PW (1935) Study on the crossostomoid fishes of China. Sinensia 6(1) (1934 [1935]): 44–97. https://doi.org/10.1086/105274

Fricke R, Eschmeyer WN, Van der Laan R (2023) Eschmeyer's catalog of fishes: genera, species, references. Electronic version. http://researcharchive.calacademy.org/research/ichthyology/catalog/fishcatmain.asp [accessed 2 October 2023]

Gouy M, Guindon S, Gascuel O (2010) SeaView version 4: A multiplatform graphical user interface for sequence alignment and phylogenetic tree building. Molecular Biology and Evolution 27(2): 221–224. https://doi.org/10.1093/molbev/msp259

Günther A (1874) Descriptions of new species of fishes in the British Museum. Annals & Magazine of Natural History 14(84): 453–455. https://doi.org/10.1080/00222937408681007

Hebert PD, Cywinska A, Ball SL, DeWaard JR (2003) Biological identifications through DNA barcodes. Proceedings of the Royal Society of London, Series B, Biological Sciences 270(1512): 313–321. https://doi.org/10.1098/rspb.2002.2218

Hora SL (1932) Classification, bionomics and evolution of homalopterid fishes. Memoirs of the Indian Museum 12: 263–330. [pls. 10–12]

Hora SL, Jayaram KC (1950) A note on the systematic position of the two gastromyzonid genera *Protomyzon* Hora and *Paraprotomyzon* Pellegrin and Fang (Fishes: Cyprinoidea). Records of the Indian Museum 48: 61–68. https://doi.org/10.26515/rzsi/v48/i2/1951/162147

Hora SL, Jayaram KC (1952) On two new gastromyzonid fishes from Borneo. Records of the Indian Museum 49: 191–195. https://doi.org/10.26515/rzsi/v49/i2/1952/162103

Inger RF, Chin PK (1962) The fresh-water fishes of North Borneo. Fieldiana. Zoology 45: 1–268.

Klingenberg CP (2011) MorphoJ: An integrated software package for geometric morphometrics. Molecular Ecology Resources 11(2): 353–357. https://doi.org/10.1111/j.1755-0998.2010.02924.x

Kottelat M (1990) Indochinese nemacheilines. A revision of nemacheiline loaches (Pisces: Cypriniformes) of Thailand, Burma, Laos, Cambodia and southern Viet Nam. Pfeil, Munchen, 262 pp.

Kottelat M (2004) On the Bornean and Chinese *Protomyzon* (Teleostei, Balitoridae), with descriptions of two new genera and two new species from Borneo, Vietnam and China. Ichthyological Exploration of Freshwaters 15(4): 301–310.

Kottelat M (2012) Conspectus Cobitidum: an inventory of the loaches of the world (Teleostei: Cypriniformes: Cobitoidei). The Raffles Bulletin of Zoology 26: 1–199.

Kumar S, Stecher G, Tamura K (2016) MEGA7: Molecular evolutionary genetics analysis version 7.0 for bigger datasets. Molecular Biology and Evolution 33(7): 1870–1874. https://doi.org/10.1093/molbev/msw054

Lanfear R, Frandsen PB, Wright AM, Senfeld T, Calcott B (2017) PartitionFinder 2: New methods for selecting partitioned models of evolution for molecular and morphological phylogenetic analyses. Molecular Biology and Evolution 34(3): 772–773. https://doi.org/10.1093/molbev/msw260

Larkin MA, Blackshields G, Brown NP, Chenna R, McGettigan PA, McWilliam H, Valentin F, Wallace IM, Wilm A, Lopez R, Thompson JD, Gibson TJ, Higgins DG (2007) Clustal W and Clustal X version 2.0. Bioinformatics (Oxford, England) 23(21): 2947–2948. https://doi.org/10.1093/bioinformatics/btm404

Li WX, Mao WN, Lu ZM, Sun RF, Lu HS (1998) Two new species of Homalopteridae from Yunnan China. Chinese Journal of Fisheries 11(1): 1–6. [in Chinese with English abstract]

Lu YF, Lu ZM, Mao WN (2005) A new species of *Paraprotomzon* from Yunnan, China (Cypriniformes, Homalopteridae)]. Acta Zootaxonomica Sinica 30(1): 202–204. [in Chinese with English abstract]

Neely DA, Conway KW, Mayden RL (2007) *Erromyzon yangi*, a new hillstream loach (Teleostei: Balitoridae) from the Pearl River drainage of Guangxi Province, China. Ichthyological Exploration of Freshwaters 18(2): 97–102.

Nichols JT (1925) A new homalopterin loach from Fukien. American Museum Novitates 167: 1–2.

Oshima M (1919) Contributions to the study of the freshwater fishes of the island of Formosa. Annals of the Carnegie Museum 12: 169–328. [pls. 48–53] https://doi.org/10.5962/p.34608

Pellegrin J, Fang PW (1935) A new homalopteroid, *Paraprotomyzon multifasciatus*, from eastern Szechuan, China nov. gen. nov. sp. Sinensia 6(2): 99–107.

Popta CML (1905) Suite des descriptions préliminaires des nouvelles espèces de poissons recueillies au Bornéo central par M. le Dr. A. W. Nieuwenhuis en 1898 et en 1900. Notes from the Leyden Museum 25: 171–186.

Rambaut A (2009) FigTree. Version 1.4.3. http://tree.bio.ed.ac.uk/software/figtree

Roberts TR (1989) The freshwater fishes of western Borneo (Kalimantan Barat, Indonesia). Memoirs of the California Academy of Sciences 14: 1–210.

Rohlf FJ (2015) The tps series of software. Hystrix, the Italian Journal of Mammalogy 26: 9–12.

Ronquist F, Teslenko M, Van Der Mark P, Ayres DL, Darling A, Höhna S, Larget B, Liu L, Suchard MA, Huelsenbeck JP (2012) MrBayes 3.2: Efficient Bayesian phylogenetic inference and model choice across a large model space. Systematic Biology 61(3): 539–542. https://doi.org/10.1093/sysbio/sys029

Rozas J, Ferrer-Mata A, Sánchez-DelBarrio JC, Guirao-Rico S, Librado P, Ramos-Onsins SE, Sánchez-Gracia A (2017) DnaSP 6: DNA sequence polymorphism analysis of large datasets. Molecular Biology and Evolution 34(12): 3299–3302. https://doi.org/10.1093/molbev/msx248

Shi LX, Zhang C, Wang YP, Tang QY, Danley PD, Liu HZ (2018) Evolutionary relationships of two balitorids (Cypriniformes, Balitoridae) revealed by comparative mitogenomics. Zoologica Scripta 47(3): 300–310. https://doi.org/10.1111/zsc.12282

Stamatakis A (2006) RAxML-VI-HPC: Maximum likelihood-based phylogenetic analyses with thousands of taxa and mixed models. Bioinformatics 22(21): 2688–2690. https://doi.org/10.1093/bioinformatics/btl446

Stamatakis A, Hoover P, Rougemont J (2008) A rapid bootstrap algorithm for the RAxML web servers. Systematic Biology 57(5): 758–771. https://doi.org/10.1080/10635150802429642

Tan HH (2006) The Borneo suckers. [Revision of the torrent loaches of Borneo (Balitoridae: *Gastromyzon*, *Neogastromyzon*)]. Natural History Publications (Borneo), Kota Kinabalu, 1–21.

Tan HH (2021) *Hypergastromyzon* revisited, with descriptions of a new genus and two new species (Teleostei: Gastromyzontidae). The Raffles Bulletin of Zoology 69: 336–363. https://doi.org/10.26107/RBZ-2021-0056

Tang WQ (1997) A new species of *Paraprotomyzon* from Guangxi, China (Cypriniformes: Homalopteridae). Acta Zoologica Sinica 22(1): 108–111. [in Chinese with English abstract]

Tang WQ, Chen YY (1996) Ultrastructural observation on the chin adhesive apparatus and subgenus division of *Pseudogastromyzon*. Acta Zoologica Sinica 42(3): 231–236. [in Chinese with English abstract]

Tang WQ, Chen YY (2000) Study on taxonomy of Homalopteridae. Journal of Shanghai Fisheries University 9(1): 1–10. [in Chinese with English abstract]

Vaillant L (1893) Contribution à l'étude de la faune ichthyologique de Bornéo. Nouvelles Archives du Muséum d'Histoire Naturelle, Paris, Série 3, 5: 23–114. [pls. 1–2]

Vaillant L (1902) Résultats zoologiques de l'expédition scientifique néerlandaise au Bornéo central. Notes from the Leyden Museum 24: 1–166. [pls. 1–2]

Xie CX, Yang GR, Gong LX (1984) The Homalopterid fishes from Hubei Province, China, with description of a new species and a new subspecies. Journal of Huazhong Agricultural College 3(1): 62–68. [in Chinese with English abstract]

Xiu LH, Yang J (2017) *Erromyzon damingshanensis*, a new sucker loach (Teleostei: Cypriniformes: Gastromyzontidae) from the Pearl River drainage of Guangxi, China. Environmental Biology of Fishes 100(8): 893–898. https://doi.org/10.1007/s10641-017-0579-0

Yang J, Kottelat M, Yang JX, Chen XY (2012) *Yaoshania* and *Erromyzon kalotaenia*, a new genus and a new species of balitorid loaches from Guangxi, China (Teleostei: Cypriniformes). Zootaxa 3586(1): 173–186. https://doi.org/10.11646/zootaxa.3586.1.16

Zhang E, Cao WX (2021) China's Red List of Biodiversity: Vertebrates, Volume V, Freshwater Fishes (II). Science press, Beijing, 655–681. [in Chinese]

Zheng CY, Chen YY (1980) The homalopterid fishes from Guangdong Province, China. Acta Zootaxonomica Sinica 5(1): 89–101. [in Chinese with English abstract]